Yong Shi

Geert Dick van Albada

Jack Dongarra

Peter M.A. Sloot (Eds.)

Computational Science – ICCS 2007

**7th International Conference
Beijing, China, May 2007
Proceedings, Part III**

3 Part III

Springer

Lecture Notes in Computer Science 4489

Yong Shi   Geert Dick van Albada
Jack Dongarra   Peter M.A. Sloot (Eds.)

Computational Science – ICCS 2007

7th International Conference
Beijing, China, May 27 - 30, 2007
Proceedings, Part III

Springer

Volume Editors

Yong Shi
Graduate University of the Chinese Academy of Sciences
Beijing 100080, China
E-mail: yshi@gucas.ac.cn

Geert Dick van Albada
Peter M.A. Sloot
University of Amsterdam, Section Computational Science
1098 SJ Amsterdam, The Netherlands
E-mail: {dick, sloot}@science.uva.nl

Jack Dongarra
University of Tennessee, Computer Science Department
Knoxville, TN 37996-3450, USA
E-mail: dongarra@cs.utk.edu

Preface

The Seventh International Conference on Computational Science (ICCS 2007) was held in Beijing, China, May 27-30, 2007. This was the continuation of previous conferences in the series: ICCS 2006 in Reading, UK; ICCS 2005 in Atlanta, Georgia, USA; ICCS 2004 in Krakow, Poland; ICCS 2003 held simultaneously at two locations in, Melbourne, Australia and St. Petersburg, Russia; ICCS 2002 in Amsterdam, The Netherlands; and ICCS 2001 in San Francisco, California, USA. Since the first conference in San Francisco, the ICCS series has become a major platform to promote the development of Computational Science. The theme of ICCS 2007 was "Advancing Science and Society through Computation." It aimed to bring together researchers and scientists from mathematics and computer science as basic computing disciplines, researchers from various application areas who are pioneering the advanced application of computational methods to sciences such as physics, chemistry, life sciences, and engineering, arts and humanitarian fields, along with software developers and vendors, to discuss problems and solutions in the area, to identify new issues, and to shape future directions for research, as well as to help industrial users apply various advanced computational techniques.

During the opening of ICCS 2007, Siwei Cheng (Vice-Chairman of the Standing Committee of the National People's Congress of the People's Republic of China and the Dean of the School of Management of the Graduate University of the Chinese Academy of Sciences) presented the welcome speech on behalf of the Local Organizing Committee, after which Hector Ruiz (President and CEO, AMD) made remarks on behalf of international computing industries in China. Seven keynote lectures were delivered by Vassil Alexandrov (Advanced Computing and Emerging Technologies, University of Reading, UK) - Efficient Scalable Algorithms for Large-Scale Computations; Hans Petter Langtangen (Simula Research Laboratory, Lysaker, Norway) - Computational Modelling of Huge Tsunamis from Asteroid Impacts; Jiawei Han (Department of Computer Science, University of Illinois at Urbana-Champaign, USA) - Research Frontiers in Advanced Data Mining Technologies and Applications; Ru-qian Lu (Institute of Mathematics, Chinese Academy of Sciences) - Knowledge Engineering and Knowledge Ware; Alessandro Vespignani (School of Informatics, Indiana University, USA) -Computational Epidemiology and Emergent Disease Forecast; David Keyes (Department of Applied Physics and Applied Mathematics, Columbia University) - Scalable Solver Infrastructure for Computational Science and Engineering; and Yves Robert (Ecole Normale Suprieure de Lyon , France) - Think Before Coding: Static Strategies (and Dynamic Execution) for Clusters and Grids. We would like to express our thanks to all of the invited and keynote speakers for their inspiring talks. In addition to the plenary sessions, the conference included 14 parallel oral sessions and 4 poster sessions. This year, we

received more than 2,400 submissions for all tracks combined, out of which 716 were accepted.

This includes 529 oral papers, 97 short papers, and 89 poster papers, spread over 35 workshops and a main track. For the main track we had 91 papers (80 oral papers and 11 short papers) in the proceedings, out of 360 submissions. We had some 930 people doing reviews for the conference, with 118 for the main track. Almost all papers received three reviews. The accepted papers are from more than 43 different countries and 48 different Internet top-level domains.

The papers cover a large volume of topics in computational science and related areas, from multiscale physics to wireless networks, and from graph theory to tools for program development.

We would like to thank all workshop organizers and the Program Committee for the excellent work in maintaining the conference's standing for high-quality papers. We would like to express our gratitude to staff and graduates of the Chinese Academy of Sciences Research Center on Data Technology and Knowledge Economy and the Institute of Policy and Management for their hard work in support of ICCS 2007. We would like to thank the Local Organizing Committee and Local Arrangements Committee for their persistent and enthusiastic work towards the success of ICCS 2007. We owe special thanks to our sponsors, AMD, Springer; University of Nebraska at Omaha, USA and Graduate University of Chinese Academy of Sciences, for their generous support.

ICCS 2007 was organized by the Chinese Academy of Sciences Research Center on Data Technology and Knowledge Economy, with support from the Section Computational Science at the Universiteit van Amsterdam and Innovative Computing Laboratory at the University of Tennessee, in cooperation with the Society for Industrial and Applied Mathematics (SIAM), the International Association for Mathematics and Computers in Simulation (IMACS), the Chinese Society for Management Modernization (CSMM), and the Chinese Society of Optimization, Overall Planning and Economical Mathematics (CSOOPEM).

May 2007   Yong Shi

Organization

ICCS 2007 was organized by the Chinese Academy of Sciences Research Center on Data Technology and Knowledge Economy, with support from the Section Computational Science at the Universiteit van Amsterdam and Innovative Computing Laboratory at the University of Tennessee, in cooperation with the Society for Industrial and Applied Mathematics (SIAM), the International Association for Mathematics and Computers in Simulation (IMACS), and the Chinese Society for Management Modernization (CSMM).

Conference Chairs

Conference Chair - Yong Shi (Chinese Academy of Sciences, China/University of Nebraska at Omaha USA)
Program Chair - Dick van Albada (Universiteit van Amsterdam, The Netherlands)
ICCS Series Overall Scientific Co-chair - Jack Dongarra (University of Tennessee, USA)
ICCS Series Overall Scientific Chair - Peter M.A. Sloot (Universiteit van Amsterdam, The Netherlands)

Local Organizing Committee

Weimin Zheng (Tsinghua University, Beijing, China) – Chair
Hesham Ali (University of Nebraska at Omaha, USA)
Chongfu Huang (Beijing Normal University, Beijing, China)
Masato Koda (University of Tsukuba, Japan)
Heeseok Lee (Korea Advanced Institute of Science and Technology, Korea)
Zengliang Liu (Beijing University of Science and Technology, Beijing, China)
Jen Tang (Purdue University, USA)
Shouyang Wang (Academy of Mathematics and System Science, Chinese Academy of Sciences, Beijing, China)
Weixuan Xu (Institute of Policy and Management, Chinese Academy of Sciences, Beijing, China)
Yong Xue (Institute of Remote Sensing Applications, Chinese Academy of Sciences, Beijing, China)
Ning Zhong (Maebashi Institute of Technology, USA)
Hai Zhuge (Institute of Computing Technology, Chinese Academy of Sciences, Beijing, China)

Local Arrangements Committee

Weixuan Xu, Chair
Yong Shi, Co-chair of events
Benfu Lu, Co-chair of publicity
Hongjin Yang, Secretary
Jianping Li, Member
Ying Liu, Member
Jing He, Member
Siliang Chen, Member
Guanxiong Jiang, Member
Nan Xiao, Member
Zujin Deng, Member

Sponsoring Institutions

AMD
Springer
World Scientific Publlishing
University of Nebraska at Omaha, USA
Graduate University of Chinese Academy of Sciences
Institute of Policy and Management, Chinese Academy of Sciences Universiteit
van Amsterdam

Program Committee

J.H. Abawajy, Deakin University, Australia
D. Abramson, Monash University, Australia
V. Alexandrov, University of Reading, UK
I. Altintas, San Diego Supercomputer Center, UCSD
M. Antolovich, Charles Sturt University, Australia
E. Araujo, Universidade Federal de Campina Grande, Brazil
M.A. Baker, University of Reading, UK
B. Balis, Krakow University of Science and Technology, Poland
A. Benoit, LIP, ENS Lyon, France
I. Bethke, University of Amsterdam, The Netherlands
J.A.R. Blais, University of Calgary, Canada
I. Brandic, University of Vienna, Austria
J. Broeckhove, Universiteit Antwerpen, Belgium
M. Bubak, AGH University of Science and Technology, Poland
K. Bubendorfer, Victoria University of Wellington, Australia
B. Cantalupo, DATAMAT S.P.A, Italy
J. Chen Swinburne, University of Technology, Australia
O. Corcho, University of Manchester, UK
J.C. Cunha, Univ. Nova de Lisboa, Portugal

S. Date, Osaka University, Japan
F. Desprez, INRIA, France
T. Dhaene, University of Antwerp, Belgium
I.T. Dimov, ACET, The University of Reading, UK
J. Dongarra, University of Tennessee, USA
F. Donno, CERN, Switzerland
C. Douglas, University of Kentucky, USA
G. Fox, Indiana University, USA
W. Funika, Krakow University of Science and Technology, Poland
H.J. Gardner, Australian National University, Australia
G. Geethakumari, University of Hyderabad, India
Y. Gorbachev, St. Petersburg State Polytechnical University, Russia
A.M. Goscinski, Deakin University, Australia
M. Govindaraju, Binghamton University, USA
G.A. Gravvanis, Democritus University of Thrace, Greece
D.J. Groen, University of Amsterdam, The Netherlands
T. Gubala, ACC CYFRONET AGH, Krakow, Poland
M. Hardt, FZK, Germany
T. Heinis, ETH Zurich, Switzerland
L. Hluchy, Institute of Informatics, Slovak Academy of Sciences, Slovakia
A.G. Hoekstra, University of Amsterdam, The Netherlands
W. Hoffmann, University of Amsterdam, The Netherlands
C. Huang, Beijing Normal University Beijing, China
M. Humphrey, University of Virginia, USA
A. Iglesias, University of Cantabria, Spain
H. Jin, Huazhong University of Science and Technology, China
D. Johnson, ACET Centre, University of Reading, UK
B.D. Kandhai, University of Amsterdam, The Netherlands
S. Kawata, Utsunomiya University, Japan
W.A. Kelly, Queensland University of Technology, Australia
J. Kitowski, Inst.Comp.Sci. AGH-UST, Cracow, Poland
M. Koda, University of Tsukuba Japan
D. Kranzlmüller, GUP, Joh. Kepler University Linz, Austria
B. Kryza, Academic Computer Centre CYFRONET-AGH, Cracow, Poland
M. Kunze, Forschungszentrum Karlsruhe (FZK), Germany
D. Kurzyniec, Emory University, Atlanta, USA
A. Lagana, University of Perugia, Italy
J. Lee, KISTI Supercomputing Center, Korea
C. Lee, Aerospace Corp., USA
L. Lefevre, INRIA, France
A. Lewis, Griffith University, Australia
H.W. Lim, Royal Holloway, University of London, UK
A. Lin, NCMIR/UCSD, USA
P. Lu, University of Alberta, Canada
M. Malawski, Institute of Computer Science AGH, Poland

M. Mascagni, Florida State University, USA
V. Maxville, Curtin Business School, Australia
A.S. McGough, London e-Science Centre, UK
E.D. Moreno, UEA-BENq, Manaus, Brazil
J.T. Moscicki, Cern, Switzerland
S. Naqvi, CoreGRID Network of Excellence, France
P.O.A. Navaux, Universidade Federal do Rio Grande do Sul, Brazil
Z. Nemeth, Computer and Automation Research Institute, Hungarian Academy
of Science, Hungary
J. Ni, University of Iowa, USA
G. Norman, Joint Institute for High Temperatures of RAS, Russia
B. Ó Nualláin, University of Amsterdam, The Netherlands
C.W. Oosterlee, Centrum voor Wiskunde en Informatica, CWI, The Netherlands
S. Orlando, Università Ca' Foscari, Venice, Italy
M. Paprzycki, IBS PAN and SWPS, Poland
M. Parashar, Rutgers University, USA
L.M. Patnaik, Indian Institute of Science, India
C.P. Pautasso, ETH Zürich, Switzerland
R. Perrott, Queen's University, Belfast, UK
V. Prasanna, University of Southern California, USA
T. Priol, IRISA, France
M.R. Radecki, Krakow University of Science and Technology, Poland
M. Ram, C-DAC Bangalore Centre, India
A. Rendell, Australian National University, Australia
P. Rhodes, University of Mississippi, USA
M. Riedel, Research Centre Juelich, Germany
D. Rodríguez García, University of Alcalá, Spain
K. Rycerz, Krakow University of Science and Technology, Poland
R. Santinelli, CERN, Switzerland
J. Schneider, Technische Universität Berlin, Germany
B. Schulze, LNCC, Brazil
J. Seo, The University of Manchester, UK
Y. Shi, Chinese Academy of Sciences, Beijing, China
D. Shires, U.S. Army Research Laboratory, USA
A.E. Solomonides, University of the West of England, Bristol, UK
V. Stankovski, University of Ljubljana, Slovenia
H. Stockinger, Swiss Institute of Bioinformatics, Switzerland
A. Streit, Forschungszentrum Jülich, Germany
H. Sun, Beihang University, China
R. Tadeusiewicz, AGH University of Science and Technology, Poland
J. Tang, Purdue University USA
M. Taufer, University of Texas El Paso, USA
C. Tedeschi, LIP-ENS Lyon, France
A. Thandavan, ACET Center, University of Reading, UK
A. Tirado-Ramos, University of Amsterdam, The Netherlands

P. Tvrdik, Czech Technical University Prague, Czech Republic
G.D. van Albada, Universiteit van Amsterdam, The Netherlands
F. van Lingen, California Institute of Technology, USA
J. Vigo-Aguiar, University of Salamanca, Spain
D.W. Walker, Cardiff University, UK
C.L. Wang, University of Hong Kong, China
A.L. Wendelborn, University of Adelaide, Australia
Y. Xue, Chinese Academy of Sciences, China
L.T. Yang, St. Francis Xavier University, Canada
C.T. Yang, Tunghai University, Taichung, Taiwan
J. Yu, The University of Melbourne, Australia
Y. Zheng, Zhejiang University, China
W. Zheng, Tsinghua University, Beijing, China
L. Zhu, University of Florida, USA
A. Zomaya, The University of Sydney, Australia
E.V. Zudilova-Seinstra, University of Amsterdam, The Netherlands

Reviewers

J.H. Abawajy
D. Abramson
A. Abran
P. Adriaans
W. Ahn
R. Akbani
K. Akkaya
R. Albert
M. Aldinucci
V.N. Alexandrov
B. Alidaee
I. Altintas
K. Altmanninger
S. Aluru
S. Ambroszkiewicz
L. Anido
K. Anjyo
C. Anthes
M. Antolovich
S. Antoniotti
G. Antoniu
H. Arabnia
E. Araujo
E. Ardeleanu
J. Aroba
J. Astalos

B. Autin
M. Babik
G. Bai
E. Baker
M.A. Baker
S. Balfe
B. Balis
W. Banzhaf
D. Bastola
S. Battiato
M. Baumgarten
M. Baumgartner
P. Beckaert
A. Belloum
O. Belmonte
A. Belyaev
A. Benoit
G. Bergantz
J. Bernsdorf
J. Berthold
I. Bethke
I. Bhana
R. Bhowmik
M. Bickelhaupt
J. Bin Shyan
J. Birkett

J.A.R. Blais
A. Bode
B. Boghosian
S. Bolboaca
C. Bothorel
A. Bouteiller
I. Brandic
S. Branford
S.J. Branford
R. Braungarten
R. Briggs
J. Broeckhove
W. Bronsvoort
A. Bruce
C. Brugha
Y. Bu
K. Bubendorfer
I. Budinska
G. Buemi
B. Bui
H.J. Bungartz
A. Byrski
M. Cai
Y. Cai
Y.Q. Cai
Z.Y. Cai

B. Cantalupo
K. Cao
M. Cao
F. Capkovic
A. Cepulkauskas
K. Cetnarowicz
Y. Chai
P. Chan
G.-L. Chang
S.C. Chang
W.A. Chaovalitwongse
P.K. Chattaraj
C.-K. Chen
E. Chen
G.Q. Chen
G.X. Chen
J. Chen
J. Chen
J.J. Chen
K. Chen
Q.S. Chen
W. Chen
Y. Chen
Y.Y. Chen
Z. Chen
G. Cheng
X.Z. Cheng
S. Chiu
K.E. Cho
Y.-Y. Cho
B. Choi
J.K. Choi
D. Choinski
D.P. Chong
B. Chopard
M. Chover
I. Chung
M. Ciglan
B. Cogan
G. Cong
J. Corander
J.C. Corchado
O. Corcho
J. Cornil
H. Cota de Freitas

E. Coutinho
J.J. Cuadrado-Gallego
Y.F. Cui
J.C. Cunha
V. Curcin
A. Curioni
R. da Rosa Righi
S. Dalai
M. Daneva
S. Date
P. Dazzi
S. de Marchi
V. Debelov
E. Deelman
J. Della Dora
Y. Demazeau
Y. Demchenko
H. Deng
X.T. Deng
Y. Deng
M. Mat Deris
F. Desprez
M. Dewar
T. Dhaene
Z.R. Di
G. di Biasi
A. Diaz Guilera
P. Didier
I.T. Dimov
L. Ding
G.D. Dobrowolski
T. Dokken
J.J. Dolado
W. Dong
Y.-L. Dong
J. Dongarra
F. Donno
C. Douglas
G.J. Garcke
R.P. Mundani
R. Drezewski
D. Du
B. Duan
J.F. Dufourd
H. Dun

C. Earley
P. Edmond
T. Eitrich
A. El Rhalibi
T. Ernst
V. Ervin
D. Estrin
L. Eyraud-Dubois
J. Falcou
H. Fang
Y. Fang
X. Fei
Y. Fei
R. Feng
M. Fernandez
K. Fisher
C. Fittschen
G. Fox
F. Freitas
T. Friesz
K. Fuerlinger
M. Fujimoto
T. Fujinami
W. Funika
T. Furumura
A. Galvez
L.J. Gao
X.S. Gao
J.E. Garcia
H.J. Gardner
M. Garre
G. Garsva
F. Gava
G. Geethakumari
M. Geimer
J. Geiser
J.-P. Gelas
A. Gerbessiotis
M. Gerndt
S. Gimelshein
S.G. Girdzijauskas
S. Girtelschmid
Z. Gj
C. Glasner
A. Goderis

D. Godoy
J. Golebiowski
S. Gopalakrishnan
Y. Gorbachev
A.M. Goscinski
M. Govindaraju
E. Grabska
G.A. Gravvanis
C.H. Grelck
D.J. Groen
L. Gross
P. Gruer
A. Grzech
J.F. Gu
Y. Guang Xue
T. Gubala
V. Guevara-Masis
C.H. Guo
X. Guo
Z.Q. Guo
L. Guohui
C. Gupta
I. Gutman
A. Haffegee
K. Han
M. Hardt
A. Hasson
J. He
J. He
K. He
T. He
J. He
M.R. Head
P. Heinzlreiter
H. Chojnacki
J. Heo
S. Hirokawa
G. Hliniak
L. Hluchy
T.B. Ho
A. Hoekstra
W. Hoffmann
A. Hoheisel
J. Hong
Z. Hong

D. Horvath
F. Hu
L. Hu
X. Hu
X.H. Hu
Z. Hu
K. Hua
H.W. Huang
K.-Y. Huang
L. Huang
L. Huang
M.S. Huang
S. Huang
T. Huang
W. Huang
Y. Huang
Z. Huang
Z. Huang
B. Huber
E. Hubo
J. Hulliger
M. Hultell
M. Humphrey
P. Hurtado
J. Huysmans
T. Ida
A. Iglesias
K. Iqbal
D. Ireland
N. Ishizawa
I. Lukovits
R. Jamieson
J.K. Jan
P. Janderka
M. Jankowski
L. Jäntschi
S.J.K. Jensen
N.J. Jeon
T.H. Jeon
T. Jeong
H. Ji
X. Ji
D.Y. Jia
C. Jiang
H. Jiang

M.J. Jiang
P. Jiang
W. Jiang
Y. Jiang
H. Jin
J. Jin
L. Jingling
G.-S. Jo
D. Johnson
J. Johnstone
J.J. Jung
K. Juszczyszyn
J.A. Kaandorp
M. Kabelac
B. Kadlec
R. Kakkar
C. Kameyama
B.D. Kandhai
S. Kandl
K. Kang
S. Kato
S. Kawata
T. Kegl
W.A. Kelly
J. Kennedy
G. Khan
J.B. Kido
C.H. Kim
D.S. Kim
D.W. Kim
H. Kim
J.G. Kim
J.H. Kim
M. Kim
T.H. Kim
T.W. Kim
P. Kiprof
R. Kirner
M. Kisiel-Dorohinicki
J. Kitowski
C.R. Kleijn
M. Kluge
A. Knüpfer
I.S. Ko
Y. Ko

R. Kobler
B. Koblitz
G.A. Kochenberger
M. Koda
T. Koeckerbauer
M. Koehler
I. Kolingerova
V. Korkhov
T. Korkmaz
L. Kotulski
G. Kou
J. Kozlak
M. Krafczyk
D. Kranzlmüller
B. Kryza
V.V. Krzhizhanovskaya
M. Kunze
D. Kurzyniec
E. Kusmierek
S. Kwang
Y. Kwok
F. Kyriakopoulos
H. Labiod
A. Lagana
H. Lai
S. Lai
Z. Lan
G. Le Mahec
B.G. Lee
C. Lee
H.K. Lee
J. Lee
J. Lee
J.H. Lee
S. Lee
S.Y. Lee
V. Lee
Y.H. Lee
L. Lefevre
L. Lei
F. Lelj
A. Lesar
D. Lesthaeghe
Z. Levnajic
A. Lewis

A. Li
D. Li
D. Li
E. Li
J. Li
J. Li
J.P. Li
M. Li
P. Li
X. Li
X.M. Li
X.S. Li
Y. Li
Y. Li
J. Liang
L. Liang
W.K. Liao
X.F. Liao
G.G. Lim
H.W. Lim
S. Lim
A. Lin
I.C. Lin
I-C. Lin
Y. Lin
Z. Lin
P. Lingras
C.Y. Liu
D. Liu
D.S. Liu
E.L. Liu
F. Liu
G. Liu
H.L. Liu
J. Liu
J.C. Liu
R. Liu
S.Y. Liu
W.B. Liu
X. Liu
Y. Liu
Y. Liu
Y. Liu
Y.J. Liu

Y.Z. Liu
Z.J. Liu
S.-C. Lo
R. Loogen
B. López
A. López García de
    Lomana
F. Loulergue
G. Lu
J. Lu
J.H. Lu
M. Lu
P. Lu
S. Lu
X. Lu
Y.C. Lu
C. Lursinsap
L. Ma
M. Ma
T. Ma
A. Macedo
N. Maillard
M. Malawski
S. Maniccam
S.S. Manna
Z.M. Mao
M. Mascagni
E. Mathias
R.C. Maurya
V. Maxville
A.S. McGough
R. Mckay
T.-G. MCKenzie
K. Meenal
R. Mehrotra
M. Meneghin
F. Meng
M.F.J. Meng
E. Merkevicius
M. Metzger
Z. Michalewicz
J. Michopoulos
J.-C. Mignot
R. mikusauskas
H.Y. Ming

F. Wang

F.L. Wang

H. Wang

H.G. Wang

H.W. Wang

J. Wang

J. Wang

J. Wang

J. Wang

J.H. Wang

K. Wang

L. Wang

M. Wang

M.Z. Wang

Q. Wang

Q.Q. Wang

S.P. Wang

T.K. Wang

W. Wang

W.D. Wang

X. Wang

X.J. Wang

Y. Wang

Y.Q. Wang

Z. Wang

Z.T. Wang

A. Wei

G.X. Wei

Y.-M. Wei

X. Weimin

D. Weiskopf

B. Wen

A.L. Wendelborn

I. Wenzel

A. Wibisono

A.P. Wierzbicki

R. Wismüller

F. Wolf

C. Wu

C. Wu

F. Wu

G. Wu

J.N. Wu

X. Wu

X.D. Wu

Y. Wu

Z. Wu

B. Wylie

M. Xavier Py

Y.M. Xi

H. Xia

H.X. Xia

Z.R. Xiao

C.F. Xie

J. Xie

Q.W. Xie

H. Xing

H.L. Xing

J. Xing

K. Xing

L. Xiong

M. Xiong

S. Xiong

Y.Q. Xiong

C. Xu

C.-H. Xu

J. Xu

M.W. Xu

Y. Xu

G. Xue

Y. Xue

Z. Xue

A. Yacizi

B. Yan

N. Yan

N. Yan

W. Yan

H. Yanami

C.T. Yang

F.P. Yang

J.M. Yang

K. Yang

L.T. Yang

L.T. Yang

P. Yang

X. Yang

Z. Yang

W. Yanwen

S. Yarasi

D.K.Y. Yau

P.-W. Yau

M.J. Ye

G. Yen

R. Yi

Z. Yi

J.G. Yim

L. Yin

W. Yin

Y. Ying

S. Yoo

T. Yoshino

W. Youmei

Y.K. Young-Kyu Han

J. Yu

J. Yu

L. Yu

Z. Yu

Z. Yu

W. Yu Lung

X.Y. Yuan

W. Yue

Z.Q. Yue

D. Yuen

T. Yuizono

J. Zambreno

P. Zarzycki

M.A. Zatevakhin

S. Zeng

A. Zhang

C. Zhang

D. Zhang

D.L. Zhang

D.Z. Zhang

G. Zhang

H. Zhang

H.R. Zhang

H.W. Zhang

J. Zhang

J.J. Zhang

L.L. Zhang

M. Zhang

N. Zhang

P. Zhang

P.Z. Zhang

Q. Zhang

S. Zhang	Z. Zhao	L.G. Zhou
W. Zhang	L. Zhen	X.J. Zhou
W. Zhang	B. Zheng	X.L. Zhou
Y.G. Zhang	G. Zheng	Y.T. Zhou
Y.X. Zhang	W. Zheng	H.H. Zhu
Z. Zhang	Y. Zheng	H.L. Zhu
Z.W. Zhang	W. Zhenghong	L. Zhu
C. Zhao	P. Zhigeng	X.Z. Zhu
H. Zhao	W. Zhihai	Z. Zhu
H.K. Zhao	Y. Zhixia	M. Zhu.
H.P. Zhao	A. Zhmakin	J. Zivkovic
J. Zhao	C. Zhong	A. Zomaya
M.H. Zhao	X. Zhong	E.V. Zudilova-Seinstra
W. Zhao	K.J. Zhou	

Workshop Organizers

Sixth International Workshop on Computer Graphics and Geometric Modelling

A. Iglesias, University of Cantabria, Spain

Fifth International Workshop on Computer Algebra Systems and Applications

A. Iglesias, University of Cantabria, Spain,
A. Galvez, University of Cantabria, Spain

PAPP 2007 - Practical Aspects of High-Level Parallel Programming (4th International Workshop)

A. Benoit, ENS Lyon, France
F. Loulerge, LIFO, Orlans, France

International Workshop on Collective Intelligence for Semantic and Knowledge Grid (CISKGrid 2007)

N.T. Nguyen, Wroclaw University of Technology, Poland
J.J. Jung, INRIA Rhône-Alpes, France
K. Juszczyszyn, Wroclaw University of Technology, Poland

Simulation of Multiphysics Multiscale Systems, 4th International Workshop

V.V. Krzhizhanovskaya, Section Computational Science, University of
    Amsterdam, The Netherlands
A.G. Hoekstra, Section Computational Science, University of Amsterdam,
    The Netherlands

S. Sun, Clemson University, USA
J. Geiser, Humboldt University of Berlin, Germany

2nd Workshop on Computational Chemistry and Its Applications (2nd CCA)

P.R. Ramasami, University of Mauritius

Efficient Data Management for HPC Simulation Applications

R.-P. Mundani, Technische Universität München, Germany
J. Abawajy, Deakin University, Australia
M. Mat Deris, Tun Hussein Onn College University of Technology, Malaysia

Real Time Systems and Adaptive Applications (RTSAA-2007)

J. Hong, Soongsil University, South Korea
T. Kuo, National Taiwan University, Taiwan

The International Workshop on Teaching Computational Science (WTCS 2007)

L. Qi, Department of Information and Technology, Central China Normal University, China
W. Yanwen, Department of Information and Technology, Central China Normal University, China
W. Zhenghong, East China Normal University, School of Information Science and Technology, China

GeoComputation

Y. Xue, IRSA, China

Risk Analysis

C.F. Huang, Beijing Normal University, China

Advanced Computational Approaches and IT Techniques in Bioinformatics

M.A. Pauley, University of Nebraska at Omaha, USA
H.A. Ali, University of Nebraska at Omaha, USA

Workshop on Computational Finance and Business Intelligence

Y. Shi, Chinese Acedemy of Scienes, China
S.Y. Wang, Academy of Mathematical and System Sciences, Chinese Academy of Sciences, China
X.T. Deng, Department of Computer Science, City University of Hong Kong, China

Collaborative and Cooperative Environments

C. Anthes, Institute of Graphics and Parallel Processing, JKU, Austria
V.N. Alexandrov, ACET Centre, The University of Reading, UK
D. Kranzlmüller, Institute of Graphics and Parallel Processing, JKU, Austria
J. Volkert, Institute of Graphics and Parallel Processing, JKU, Austria

Tools for Program Development and Analysis in Computational Science

A. Knüpfer, ZIH, TU Dresden, Germany
A. Bode, TU Munich, Germany
D. Kranzlmüller, Institute of Graphics and Parallel Processing, JKU, Austria
J. Tao, CAPP, University of Karlsruhe, Germany
R. Wissmüller FB12, BSVS, University of Siegen, Germany
J. Volkert, Institute of Graphics and Parallel Processing, JKU, Austria

Workshop on Mining Text, Semi-structured, Web or Multimedia Data (WMTSWMD 2007)

G. Kou, Thomson Corporation, R&D, USA
Y. Peng, Omnium Worldwide, Inc., USA
J.P. Li, Institute of Policy and Management, Chinese Academy of Sciences, China

2007 International Workshop on Graph Theory, Algorithms and Its Applications in Computer Science (IWGA 2007)

M. Li, Dalian University of Technology, China

2nd International Workshop on Workflow Systems in e-Science (WSES 2007)

Z. Zhao, University of Amsterdam, The Netherlands
A. Belloum, University of Amsterdam, The Netherlands

2nd International Workshop on Internet Computing in Science and Engineering (ICSE 2007)

J. Ni, The University of Iowa, USA

Workshop on Evolutionary Algorithms and Evolvable Systems (EAES 2007)

B. Zheng, College of Computer Science, South-Central University for
    Nationalities, Wuhan, China
Y. Li, State Key Lab. of Software Engineering, Wuhan University, Wuhan, China
J. Wang, College of Computer Science, South-Central University for
    Nationalities, Wuhan, China
L. Ding, State Key Lab. of Software Engineering, Wuhan University, Wuhan,
    China

Wireless and Mobile Systems 2007 (WMS 2007)

H. Choo, Sungkyunkwan University, South Korea

**WAFTS: WAvelets, FracTals, Short-Range Phenomena —
Computational Aspects and Applications**

C. Cattani, University of Salerno, Italy
C. Toma, Polythecnica, Bucharest, Romania

Dynamic Data-Driven Application Systems - DDDAS 2007

F. Darema, National Science Foundation, USA

**The Seventh International Workshop on Meta-synthesis and
Complex Systems (MCS 2007)**

X.J. Tang, Academy of Mathematics and Systems Science, Chinese Academy of
    Sciences, China
J.F. Gu, Institute of Systems Science, Chinese Academy of Sciences, China
Y. Nakamori, Japan Advanced Institute of Science and Technology, Japan
H.C. Wang, Shanghai Jiaotong University, China

**The 1st International Workshop on Computational Methods in
Energy Economics**

L. Yu, City University of Hong Kong, China
J. Li, Chinese Academy of Sciences, China
D. Qin, Guangdong Provincial Development and Reform Commission, China

High-Performance Data Mining

Y. Liu, Data Technology and Knowledge Economy Research Center, Chinese
    Academy of Sciences, China
A. Choudhary, Electrical and Computer Engineering Department, Northwestern
    University, USA
S. Chiu, Department of Computer Science, College of Engineering, Idaho State
    University, USA

Computational Linguistics in Human–Computer Interaction

H. Ji, Sungkyunkwan University, South Korea
Y. Seo, Chungbuk National University, South Korea
H. Choo, Sungkyunkwan University, South Korea

Intelligent Agents in Computing Systems

K. Cetnarowicz, Department of Computer Science, AGH University of Science
    and Technology, Poland
R. Schaefer, Department of Computer Science, AGH University of Science and
    Technology, Poland

Networks: Theory and Applications

B. Tadic, Jozef Stefan Institute, Ljubljana, Slovenia
S. Thurner, COSY, Medical University Vienna, Austria

Workshop on Computational Science in Software Engineering

D. Rodrguez, University of Alcala, Spain
J.J. Cuadrado-Gallego, University of Alcala, Spain

International Workshop on Advances in Computational Geomechanics and Geophysics (IACGG 2007)

H.L. Xing, The University of Queensland and ACcESS Major National Research Facility, Australia
J.H. Wang, Shanghai Jiao Tong University, China

2nd International Workshop on Evolution Toward Next-Generation Internet (ENGI)

Y. Cui, Tsinghua University, China

Parallel Monte Carlo Algorithms for Diverse Applications in a Distributed Setting

V.N. Alexandrov, ACET Centre, The University of Reading, UK

The 2007 Workshop on Scientific Computing in Electronics Engineering (WSCEE 2007)

Y. Li, National Chiao Tung University, Taiwan

High-Performance Networked Media and Services 2007 (HiNMS 2007)

I.S. Ko, Dongguk University, South Korea
Y.J. Na, Honam University, South Korea

Table of Contents – Part III

A Novel Description of Multifractal Phenomenon of Network Traffic Based on Generalized Cauchy Process

Ming Li[1], S.C. Lim[2], and Huamin Feng[3]

[1] School of Information Science & Technology, East China Normal University,
Shanghai 200062, P.R. China
`mli@ee.ecnu.edu.cn, ming_lihk@yahoo.com`
[2] Faculty of Engineering, Multimedia University, 63100 Cyberjaya, Selanger, Malaysia
`sclim@mmu.edu.my`
[3] Key Laboratory of Security and Secrecy of Information, Beijing Electronic Science and
Technology Institute, Beijing 100070, P.R. China
`fenghm@besti.edu.cn`

Abstract. Let $D(n)$ and $H(n)$ be the fractal dimension and the Hurst parameter of traffic in the nth interval, respectively. Thus, this paper gives the experimental variance analysis of $D(n)$ and $H(n)$ of network traffic based on the generalized Cauchy (GC) process on an interval-by-interval basis. We experimentally infer that traffic has the phenomenon $\mathrm{Var}[D(n)] > \mathrm{Var}[H(n)]$. This suggests a new way to describe the multifractal phenomenon of traffic. That is, traffic has local high-variability and global robustness. Verifications of that inequality are demonstrated with real traffic.

Keywords: Generalized Cauchy process, Fractal dimension, Hurst parameter, Multifractals, Network traffic, Time series, Variance analysis.

1 Introduction

Network traffic (traffic for short) has multifractal behavior (Taqqu, Teverovsky and Willinger [1]). Multifractional Brownian motion (mBm) is a way to describe the multifractal of a time series by extending the Hurst parameter H to a time-dependent function $H(t)$ on a point-by-point basis, see e.g. Peltier and Levy-Vehel [2], Lim and Muniandy [3]. From a view of networking, however, time-varying H is usually expressed by $H(n)$, where n is the index of the nth interval (see e.g. Willinger, Paxson, Riedi and Taqqu [4], Li [5]), since servers in computer networks usually serve arriving traffic on an interval-by-interval basis. In this paper, we investigate the variances of $H(n)$ and $D(n)$ of real traffic, where $D(n)$ is the fractal dimension of traffic in the nth interval.

A single parameter model, such as the standard Fractional Gaussian noise (fGn for short), is a widely used tool in traffic modeling, see e.g. [6-9,31,35], where H is related to D by the linear expression $D = 2 - H$. However, Tsybakov and Georganas [8, Paragraph 1, Section II] noticed that "the class of exactly self-similar processes (i.e., fGn) is too narrow for modeling actual network traffic." In addition, Paxson and

Floyd [9, Last sentence, Paragraph 4, § 7.4] remarked that "it might be difficult to characterize the correlations over the entire trace with a single Hurst parameter."

Recently, Gneiting and Schlather [12] introduced stationary Gaussian processes indexed by two parameters. A simple one is called the Cauchy class, since the processes in that class can be regarded as an extension of the generalized Cauchy process used in geostatistics [11]. For simplicity, we call a process belonging to such a class as the generalized Cauchy (GC) process as stated in [14]. Li and Lim applied it to traffic modeling in the mono-fractal sense [13] and discussed its properties in [14]. A key point of the GC process is that it has the functionality to separately characterize D and H of a time series with LRD, where H is a measure of LRD while D is a measure of roughness or local irregularity ([12] and Mandelbrot [15,16]). In passing, we note that the linear relation $D = 2 - H$, resulting from fGn, implies that local properties are reflected in global ones for fGn, as can be seen from Mandelbrot [10], [12].

Experimental processing of traffic reveals that traffic is robust at large time scaling [9] but highly irregular at small time scaling (Feldmann, Gilbert, Willinger and Kurtz [17], Willinger, Govindan, Jamin, Paxson and Shenker [18]). This may be a tough issue to explain in traffic analysis from the point of view of a single parameter model such as fGn. Intuitively, such multifractal phenomena of traffic imply $\text{Var}[D(n)] > \text{Var}[H(n)]$, because a high value of $\text{Var}[D(n)]$ represents local high-variability while a small value of $\text{Var}[H(n)]$ implies global robustness. Nevertheless, variance analysis based on fGn results in, due to the relation $D = 2 - H$, $\text{Var}[D(n)] = \text{Var}[H(n)]$, which conflicts with the traffic's multifractal phenomenon experimentally observed in [1,9,17,18].

Now, suppose that H and D of traffic can be decoupled. Then, we can separately characterize $\text{Var}[D(n)]$ and $\text{Var}[H(n)]$ for the goal of investigating multifractal phenomenon of traffic. Recently, we introduced GC to model traffic [13], which provides a useful tool to achieve that goal. It is our belief that this paper is the first attempt at: 1) doing the variance analysis of $D(n)$ and $H(n)$ of traffic based on GC model, and 2) experimentally inferring that traffic has the phenomenon $\text{Var}[D(n)] > \text{Var}[H(n)]$, which may serve as a novel description of the properties that traffic has local high-variability and is globally robust

The rest of this paper is organized as follows. The GC process is briefed in Section 2. The variance analysis of $D(n)$ and $H(n)$ of traffic is discussed in Section 3, which is followed by conclusions.

2   Brief of GC Process

$X(t)$ is called the GC process if it is a stationary Gaussian centered process with the autocorrelation given by $C(\tau) = E\left[X(t+\tau)X(t)\right] = \left(1+|\tau|^{\alpha}\right)^{-\beta/\alpha}$, where $0 < \alpha \leq 2$ and $\beta > 0$ [12-14]. Since $C(\tau)$ is an even function. The following considers $\tau \geq 0$ unless otherwise stated:

$$C(\tau) = (1+\tau^{\alpha})^{-\beta/\alpha}, \quad \tau \geq 0, \tag{1}$$

where $C(\tau)$ is positive-definite for the above ranges of α and β, and it is a completely monotone for $0 < \alpha \le 1$, $\beta > 0$. When $\alpha = \beta = 2$, one gets the usual Cauchy process.

Recall that a self-similar process $X(t)$ with self-similarity index κ requires for $r > 0$,

$$X(rt) \triangleq r^{\kappa} X(t), \tag{2}$$

where $\triangleq$ denotes equality in joint finite distribution. The above equation describes a global property. It is known that a stationary Gaussian random process $X(t)$ that is not an exactly self-similar process may satisfy a weaker self-similar property known as local self-similarity. Taking into account the definition of local self-similarity by Kent and Wood [19], we say that a Gaussian stationary process is locally self-similar of order α if $C(\tau)$ satisfies for $\tau \to 0$,

$$C(\tau) = 1 - \beta' \mid \tau \mid^{\alpha} \{1 + O(\mid \tau \mid^{\gamma})\}, \quad \gamma > 0.$$

For the GC process, $\beta' = \dfrac{\beta}{\alpha}$ and $\gamma = \alpha$. The fractal dimension D of a locally self-similar process of order α is given by (see e.g., [19] and Adler [20])

$$D = 2 - \frac{\alpha}{2}. \tag{3}$$

Note that the local irregularities of the sample paths are measured by α, which can be regarded as the fractal index of the process (Davies and Hall [21], Hall [22], Constantine and Hall [23], Hall and Roy [24], Chan, Hall, and Poskitt [25]). Thus, the behavior of $C(\tau)$ at the origin to a great extent determines the roughness of the random process.

The large time lag behavior of the correlation is given by the following hyperbolically decaying correlation

$$C(\tau) \sim \tau^{-\beta}, \quad \tau \to \infty, \tag{4}$$

which implies LRD for $0 < \beta < 1$. The process becomes short-range dependent if $\beta > 1$. Thus, the index β characterizes LRD. Comparing the large asymptotic value of the correlation $\tau^{-\beta}$ with τ^{2H-2} yields

$$H = 1 - \beta / 2. \tag{5}$$

Therefore, the LRD condition $0 < \beta < 1$ implies $0.5 < H < 1$.

One thing worth noting is that the two parameters α and β can vary independently. Hence, D of the GC process is independent of H. The separate characterization of D and H gives the GC model the flexibility that is lacking in single parameter models like fGn.

At the end of this section, we note that the GC process is non-Markovian since its correlation $C(t_1, t_2)$ does not satisfy the triangular relation given by

$$C(t_1, t_3) = C(t_1, t_2) C(t_2, t_3) / C(t_2, t_2), \quad t_1 < t_2 < t_3,$$

which is a necessary condition for a Gaussian process to be Markovian (Todorovic [26]). In fact, up to a multiplicative constant, the Ornstein-Uhlenbeck process is the only stationary Gaussian Markov process (Lim and Muniandy [27], Wolperta and Taqqu [28]).

3   Experimental Variance Analysis

On an interval-by-interval basis, we write

$$C(\tau; n) = (1 + \tau^{\alpha(n)})^{-\beta(n)/\alpha(n)}, \quad \tau \geq 0. \tag{6}$$

Hence, we have

$$D(n) = 2 - \frac{\alpha(n)}{2}, \tag{7}$$

$$H(n) = 1 - \frac{\beta(n)}{2}. \tag{8}$$

Consider three sets of test data. The first set consists of four traces measured at the Bellcore (BC) in 1989. The second includes traces recorded at Digital Equipment Corporation (DEC) in March 1995. The third contains 4 traces collected by the National Laboratory for Applied Network Research (NLANR) in November 2005. These data are available freely from [29,30]. They have been used in the research of traffic analysis, see e.g. [4,7,9,13,17,31,32]. The third is relatively recent, in comparison with the other two.

Now, we use three test series for demonstrations. They are DEC-PKT-1, BC-Oct89Ext, and AMP-1131669938-1.psize. Denote $x[t(i)]$ a traffic series, indicating the number of bytes in a packet at time $t(i)$ ($i = 0, 1, 2, \cdots$). Then, $x(i)$ is a series, representing the number of bytes in the ith packet. Figs. 1 (a) ~ (c) indicate the first 1024 points of 3 series, namely DEC-PKT-1 at DEC in 1995, BC-Oct89Ext at BC in 1989, and AMP-1131669938-1.psize at NLANR in 2005, respectively.
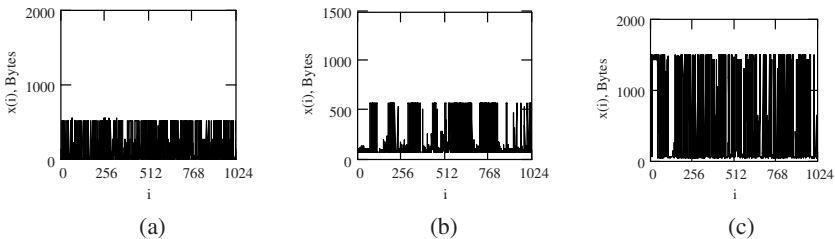
Fig. 1. Real traffic. (a). DEC-PKT-1. (b). BC-Oct89Ext. (c). AMP-1131669938-1.psize.

The computation settings are as follows. Block size L is 1024 and average times N = 10. Sectioning the series as $x(i)$, $i = (n - 1)(L \times N)$, …, $n(L \times N)$ for $n = 1$, …, 30. By computing 30 correlations for each series and using the least square fitting, we

indicate $H(n)$ of those in Fig. 1 by Fig. 2 (a), (b), and (c). Since $H(n)$ appears random, we need investigating its variation statistically. Figs. 3 (a) ~ (c) give their histograms (see [36] for the computation of the histogram of a series). By numeric computation, we have $\text{Var}[H(n)] = 0.073$ for DEC-PKT-1, $\text{Var}[H(n)] = 0.074$ for BC-Oct89Ext, and $\text{Var}[H(n)] = 0.073$ for AMP-1131669938-1.psize.
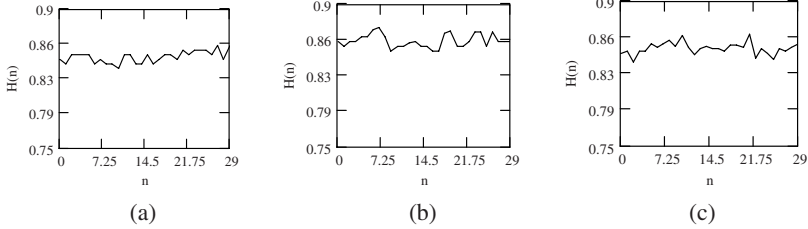
Fig. 2. $H(n)$. (a). For DEC-PKT-1. (b). For BC-Oct89Ext. (c). For AMP-1131669938-1.psize.
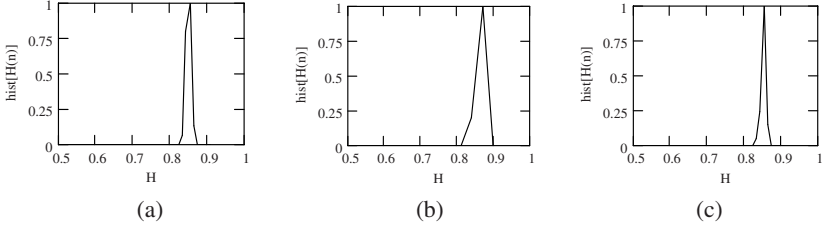
Fig. 3. Histograms of $H(n)$. (a). For DEC-PKT-1: $\text{Var}[H(n)] = 0.073$. (b). For BC-Oct89Ext: $\text{Var}[H(n)] = 0.074$. (c). For AMP-1131669938-1.psize: $\text{Var}[H(n)] = 0.073$.

On the other hand, $D(n)$ of each test series is indicated in Fig. 4 (a), (b), and (c), respectively. Fig. 4 exhibits that $D(n)$ also appears random. Thus, we use the histogram to observe its fluctuation. Figs. 5 (a) ~ (c) show their histograms. According to numeric computation, therefore, we obtain $\text{Var}[D(n)] = 0.298$ for DEC-PKT-1, $\text{Var}[D(n)] = 0.297$ for BC-Oct89Ext, and $\text{Var}[D(n)] = 0.304$ for AMP-1131669938-1.psize. Taking into account $\text{Var}[H(n)]$ and $\text{Var}[D(n)]$ mentioned above, we have

$$\text{Var}[D(n)] = 0.298 > \text{Var}[H(n)] = 0.073 \text{ for DEC-PKT-1}, \tag{9}$$

$$\text{Var}[D(n)] = 0.299 > \text{Var}[H(n)] = 0.074 \text{ for BC-Oct89Ext}, \tag{10}$$

$$\text{Var}[D(n)] = 0.304 > \text{Var}[H(n)] = 0.073 \text{ for AMP-1131669938-1.psize}. \tag{11}$$

Tables 1 ~ 3 give the comparisons of $\text{Var}[H(n)]$ and $\text{Var}[D(n)]$ for 3 sets of test series, respectively. One particular thing worth noting is that $\text{Var}[H(n)]$ is in the order of magnitude of 10^{-2} while $\text{Var}[D(n)]$ is in the order of magnitude of 10^{-1}. Hence, we experimentally infer that traffic has the phenomenon expressed by

$$\text{Var}[D(n)] > \text{Var}[H(n)], \tag{12}$$

which is valid for the test data from the past (1989) to the current (2005) for either Ethernet traffic or WAN one. The mean square errors of the estimations of $D(n)$ and $H(n)$ are in the order of magnitude of 10^{-4}.

(a)   (b)   (c)
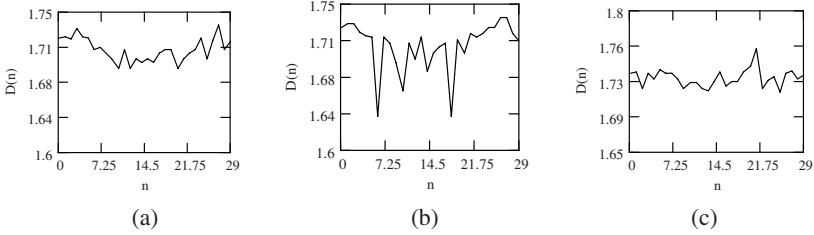
Fig. 4. $D(n)$. (a). For DEC-PKT-1. (b). For BC-Oct89Ext. (c). For AMP-1131669938-1.psize.

(a)   (b)   (c)
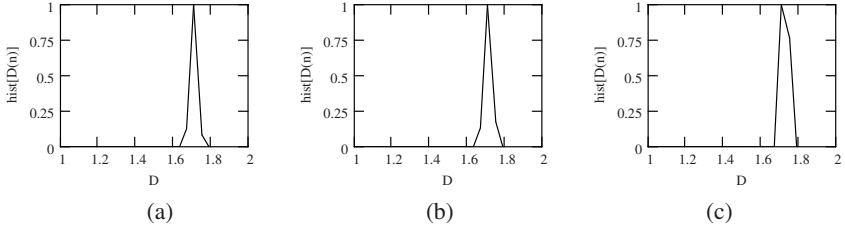
Fig. 5. Histograms of $D(n)$. (a). For DEC-PKT-1: $\text{Var}[D(n)] = 0.298$. (b). For BC-Oct89Ext: $\text{Var}[D(n)] = 0.299$. (c). For AMP-1131669938-1.psize: $\text{Var}[D(n)] = 0.304$.

Table 1. Comparisons of $\text{Var}[H(n)]$ and $\text{Var}[D(n)]$ of traffic at Bellcore

Data series	$\text{Var}[H(n)]$	$\text{Var}[D(n)]$
pAug89	0.074	0.299
pOct89	0.076	0.300
OctExt	0.075	0.298
Octext41	0.077	0.301

Table 2. Comparisons of $\text{Var}[H(n)]$ and $\text{Var}[D(n)]$ of traffic at DEC

Data series	$\text{Var}[H(n)]$	$\text{Var}[D(n)]$
DECPKT1	0.073	0.298
DECPKT2	0.072	0.300
DECPKT3	0.074	0.301
DECPKT4	0.074	0.302

Table 3. Comparisons of Var[$H(n)$] and Var[$D(n)$] of traffic by NLANR

Data series	Var[$H(n)$]	Var[$D(n)$]
AMP-1131409930-1.psize	0.075	0.306
AMP-1131495398-1.psize	0.075	0.305
AMP-1131580868-1.psize	0.075	0.304
AMP-1131669938-1.psize	0.073	0.304

Finally, we note that the generalized GC process provides a new way to investigate or describe the multifractal [phenomenon of traffic. By "new way," we mean that D and H of traffic are separately characterized, which substantially differs from single parameter based models, such as fGn or local Hurst function. We highly appreciate an anonymous referee who proposed a challenging issue of how D statistically correlates H of traffic. Let it be the topic of the future work.

4   Conclusions

We have explained the variance analysis of $D(n)$ and $H(n)$ of traffic based on the GC process. The present result implies that traffic has the property Var[$D(n)$] > Var[$H(n)$], meaning that the variability of $D(n)$ of traffic is greater than that of $H(n)$ in general. This may be a novel description to the multifractal of traffic.

Acknowledgements

References

1. Taqqu, M. S., Teverovsky, V., Willinger W.: Is Network Traffic Self-Similar or Multifractal? Fractals **5** (1997) 63-73
2. Peltier, R. F., Levy-Vehel, J.: Multifractional Brownian Motion: Definition and Preliminaries Results. INRIA TR 2645, 1995
3. Lim, S. C., Muniandy, S. V.: On Some Possible Generalizations of Fractional Brownian Motion. Physics Letters A **226** (2000) 140-145
4. Willinger, W., Paxson, V., Riedi, R. H., Taqqu, M. S.: Long-Range Dependence and Data Network Traffic, in Long-range Dependence: Theory and Applications. Doukhan, P., Oppenheim, G., Taqqu, M. S., (eds.): Birkhauser (2002) 625-715

5. Li, M.: Change Trend of Averaged Hurst Parameter of Traffic under DDOS Flood Attacks. Computers & Security **25** (2006) 213-220

6. J. Beran, J., Shernan, R., Taqqu, M. S., Willinger, W.: Long-Range Dependence in Variable Bit-Rate Video Traffic. IEEE T. Communications **43** (1995) 1566-1579

7. Li, M., Zhao, W., et al.: Modeling Autocorrelation Functions of Self-Similar Teletraffic in Communication Networks based on Optimal Approximation in Hilbert Space. Applied Mathematical Modelling **27** (2003) 155-168

8. Tsybakov, B., Georganas, N. D.: Self-Similar Processes in Communications Networks. IEEE T. Information Theory **44** (1998) 1713-1725

9. Paxson, V., Floyd, S.: Wide Area Traffic: the Failure of Poison Modeling. IEEE/ACM T. Networking **3** (1995) 226-244

10. Mandelbrot, B. B., The Fractal Geometry of Nature. W. H. Freeman, New York (1982)

11. Chiles, J.-P., Delfiner, P.,: Geostatistics, Modeling Spatial Uncertainty. Wiley, New York (1999)

12. Gneiting, T., Schlather, M.: Stochastic Models that Separate Fractal Dimension and Hurst Effect. SIAM Review **46** (2004) 269-282

13. Li, M., Lim, S. C.: Modeling Network Traffic Using Cauchy Correlation Model with Long-Range Dependence. Modern Physics Letters B **19** (2005) 829-840

14. Lim, S. C., Li, M.: Generalized Cauchy Process and Its Application to Relaxation Phenomena. J. Phys. A: Math. Gen. **39** (2006) 2935-2951

15. Mandelbrot, B. B.: Multifractals and 1/*f* Noise. Springer, 1998

16. Mandelbrot, B. B.: Gaussian Self-Affinity and Fractals. Springer (2001)

17. Feldmann, A., Gilbert, A. C., Willinger, W., Kurtz, T.G.: The Changing Nature of Network Traffic: Scaling Phenomena. Computer Communication Review **28** (1998) 5-29

18. Willinger, W., Govindan, R., Jamin, S., Paxson, V., Shenker, S.: Scaling Phenomena in the Internet: Critically Examining Criticality. Proceedings of Natl. Acad. Sci. USA, **99 (Suppl. 1)** (2002) 2573-2580

19. Kent, J. T., Wood, T. A.: Estimating the Fractal Dimension of a Locally Self-Similar Gaussian Process by Using Increments. J. R. Statit. Soc. B **59** (1997) 579-599

20. Adler, R. J.: The Geometry of Random Fields. Wiley, New York (1981)

21. Davies, S., Hall, P.: Fractal Analysis of Surface Roughness by Using Spatial Data. Journal of the Royal Statistical Society Series B **61** (1999) 3-37

22. Hall, P.: On the Effect of Measuring a Self-Similar Process. SIAM J. Appl. Math. **35** (1995) 800-808

23. Constantine, A. G., Hall, P.: Characterizing Surface Smoothness via Estimation of Effective Fractal Dimension. Journal of the Royal Statistical Society Ser. B **56** (1994) 97-113

24. Hall, P., Roy, R.: On the Relationship between Fractal Dimension and Fractal Index for Stationary Stochastic Processes. The Annals of Applied Probability **4** (1994) 241-253

25. Chan, G., Hall, P., Poskitt, D. S., Periodogram-Based Estimators of Fractal Properties. The Annals of Statistics **23** (1995) 1684-1711

26. Todorovic, P.: An Introduction to Stochastic Processes and Their Applications. Springer Verlag, New York (1992) 100-

27. Lim, S. C., Muniandy, S. V.: Generalized Ornstein-Uhlenbeck Processes and Associated Self-Similar Processes. J. Phys. A: Math. Gen. **36** (2003) 3961-3982

28. Wolperta, R. L., Taqqu, M. S.: Fractional Ornstein–Uhlenbeck Lévy Processes and the Telecom Process Upstairs and Downstairs. Signal Processing **85** (2005) 1523-1545

29. On-line available: http://ita.ee.lbl.gov/html/traces.html

30. On-line available: http://pma.nlanr.net/Traces/Traces/daily/

31. Leland, W., Taqqu, M. S., Willinger, W., Wilson, D.: On the Self-Similar Nature of Ethernet Traffic (extended version). IEEE/ACM T. Networking **2** (1994) 1-15
32. Li, M., Jia, W. J., Zhao, W.: Correlation Form of Timestamp Increment Sequences of Self-Similar Traffic on Ethernet. Electronics Letters **36** (2000) 1168-1169
33. http://www.nlanr.net/
34. http://moat.nlanr.net/
35. Li, M., Lim, S. C.: A Rigorous Derivation of Power Spectrum of Fractional Gaussian Noise. Fluctuation and Noise Letters **6** (2006) C33-C36
36. Press, W. H., Teukolsky, S. A., Vetterling, W. T., Flannery, B. P.: Numerical Recipes in C: the Art of Scientific Computing. 2nd Edition, Cambridge University Press (1992)

Rotation Invariant Texture Classification Using Gabor Wavelets

Qingbo Yin[1,2], Jong Nam Kim[1], and Kwang-Seok Moon[1]

[1] Division of Electronic Computer and Telecommunication Engineering, Pukyong National University, 599-1 Daeyeon-dong Nam-gu, Busan, 608-737, Korea
`jongnam@pknu.ac.kr, ksmoon@pknu.ac.kr`
[2] College of Computer Science and Technology, Harbin Engineering University, P.R. China
`yinqingbo@hrbeu.edu.cn`

Abstract. This paper presents a new method for rotation invariant texture classification based on Gabor wavelets. The Gabor representation has been shown to be optimal in the sense of minimizing the joint two-dimensional uncertainty in space and frequency, and the Gabor wavelet can be used to decompose an image into multiple scales and multiple orientations. Two group features, i.e. the global feature vector and local feature matrix, can be constructed by the mean and variance of the Gabor filtered image. The global feature vector is rotation invariant, and the local feature matrix can be adjusted by a circular shift operation to rotation invariant so that all images have the same dominant direction. By the two group features, a discriminant can be found to classify the rotated images. In the primary experiments, comparatively high correct classification rates were obtained using a large sample sets with 1998 rotated images of 111 Brodazt texture classes.

Keywords: Texture Classification, Gabor Wavelet.

1 Introduction

Texture analysis is a fundamental issue in image analysis and computer vision, and has many potential applications, for example, in object recognition, biomedical image analysis and so on. Texture analysis has been an active research topic for more than three decades, but only a limited number of examples of successful exploration of texture exist. A major problem is that textures in the real world are often not uniform due to variations in orientation, scale, or other visual appearance.

Analysis of texture requires the identification of proper attributes or features that differentiate the textures for classification. There are numerous algorithms in the open literature for texture feature extraction and classification. The most common approaches to texture classification assume, either explicitly or implicitly, that all images are captured under the same orientation and the unknown samples to be classified are identical to the training samples with respect to spatial scale and orientation. However, it is unrealistic to control the environment to ensure a zero rotation angle.

In general, the approach towards developing rotation invariant techniques has been to modify successful non-rotation invariant techniques such as statistical methods,

MRF (Markov random fields) and so on [1]. These traditional statistical approaches to texture analysis such as co-occurrence matrices, second order statistics, Gauss-Markov random fields and local linear transforms, are restricted to the analysis of spatial interaction over relatively small neighborhoods on a single scale.

More recently, multi-resolution and multi-channel techniques have gained much attention for texture analysis, such as wavelet transform and Gabor filters. Based on filters with Gabor wavelet or other basis functions, the rotation invariant is realized by computing rotation invariant features from the filtered images or by converting rotation variant features to rotation invariant features. Porter and Canagarajah compared three mainstream paradigms: wavelets, GMRF, Gabor for rotation invariant classification [2]. The wavelet transform decomposes an image into only three orientations, i.e., horizontal, diagonal and vertical detail sub bands in the direction of $0°$, $45°$ and $90°$, respectively, apart from the approximation smooth sub-band. This limits the application of wavelet transform for rotation invariant texture analysis [3].

From two aspects of theory analysis and practices, it is true that Gabor filter has obvious advantages, compared with other methods. For feature-based approaches, rotation invariant is achieved by using anisotropic features. Gabor function can be appropriately considered as an orientation and scale tunable detector. The banks of Gabor filters are a group of wavelet, which one can capture the signal or feature at a specific frequency and a specific orientation. There are some approaches based on Gabor filters, which focus on the rotation invariant texture in [3-8], but most of them only work well on a small database and need a lot of samples for training. Haley and Manjunath used 13 classes of textures to obtain 96.4% correct classification, however only 80.4% on 109 classes of textures [4]. Tan used 15 classes of textures to obtain 89.3% correct classification [5]. Manthalkar and Biswas obtained 81.02% correct classification on 60 classes of textures [6].

The motivation of this paper is to classify rotation invariant textures in a large texture database from the Brodatz album with 1998 rotated texture images derived from them by extracting global and local Gabor wavelet based features. The algorithm discussed in this paper is based on a feature space constructed from Gabor filter responses, in which each texture has the corresponding (unique) global feature and circular shift local feature. Then, a similarity measure, which combined the global and local features, is used to compare the unknown samples with the feature of known textures. The primary experiments have proven that the approach performs well in applications, and only requires one sample of each texture class at $0°$ for training.

2   Gabor Wavelet

A two-dimensional Gabor function consists of a complex sinusoidal plane wave of some frequency and orientations, modulated by a two- dimensional Gaussian envelope. A 'canonical' Gabor filter $g(x, y)$ and its Fourier transform $G(u, v)$ can be written as:

$$g(x, y) = \frac{1}{2\pi\sigma_x\sigma_y}\exp\left[-\frac{1}{2}\left(\frac{x^2}{\sigma_x^2}+\frac{y^2}{\sigma_y^2}\right)\right]\cdot\exp(j2\pi Wx) \tag{1}$$

$$G(u, v) = \exp\left\{-\frac{1}{2}\left[\frac{(u-W)^2}{\sigma_u^2}+\frac{v^2}{\sigma_v^2}\right]\right\} \tag{2}$$

Where $\sigma_u = 1/2\pi\sigma_x$, and $\sigma_v = 1/2\pi\sigma_y$. Gabor functions form a complete but nonorthogonal basis set. Expanding a signal using this basis provides a localized frequency description. A class of self-similar functions, referred to as Gabor wavelets in the following discussion, is now considered. Let $g(x, y)$ be the mother Gabor wavelet, then this self-similar filter dictionary can be obtained by appropriate dilations and rotations of $g(x, y)$ through the generating function [9]:

$$g_{mn}(x, y) = a^{-m}g(x', y'), \ a > 1, \ m, n = \text{integer}$$

$$x' = a^{-m}(x\cos\theta + y\sin\theta), \ y' = a^{-m}(-x\sin\theta + y\cos\theta) \tag{3}$$

Where $\theta = n\pi/K$, k is the total number of orientations, n is the orientation and m is the scale of the Gabor wavelet, respectively. According to the scheme, the space frequency plane is covered nearly uniformly. The scale factor a^{-m} in Eq.(3) ensures that the energy is independent of m.

$$E_{mn} = \int\limits_{-\infty}^{+\infty}\int\limits_{-\infty}^{+\infty}|g_{mn}(x, y)|^2 dxdy \tag{4}$$

Let U_l and U_h represent the lower and upper center frequencies of interest. Let K be the number of orientations and S be the number of scales in the decomposition. Then, the design strategy is to ensure that half peak magnitude cross-section of the filter responses in the frequency spectrum touch each other. This results in the following formulas for computing the filter parameters σ_u and σ_v (and thus σ_x and σ_y).

$$a = \left(U_h/U_l\right)^{1/s-1} \tag{5}$$

$$\sigma_u = \frac{(a-1)U_h}{(a+1)\sqrt{2\ln 2}} \tag{6}$$

$$\sigma_v = \tan(\frac{\pi}{2k})\left[U_h - 2\ln 2\left(\frac{\sigma_u^2}{U_h}\right)\right]\left[2\ln 2 - \frac{(2\ln 2)^2\sigma_u^2}{U_h^2}\right]^{-1/2} \tag{7}$$

Where $W = U_h$, $\theta = \pi/K$, and $m = 0, 1, \ldots, S-1$.

Most Gabor filters have a slight response to the absolute intensity. This results in sensitivity to the background luminance level, which signifies a first order difference between regions. This can be avoided by adding a constant to make them zero mean. Because the Gabor filter is built in the Fourier domain, this same purpose (effect) is achieved by setting G(0,0)=0.

3   Feature Extractions and Classification

3.1 Texture Representation

Given an image $I(x, y)$ of size $M * N$, its discrete Gabor wavelet transform is given by convolution:

$$H_{mn}(x, y) = \sum_{p}\sum_{q} I(x-p, y-q)g^{*}_{mn}(p,q) \tag{8}$$

Where p, q are the filter mask size variables, $g^{*}_{mn}(p,q)$ is the complex conjugate of g_{mn}.

A set of Gabor wavelet of different scale and orientation is convolved with an image to estimate the magnitude of local frequency of the appropriate scale and orientation.

It is assumed that the texture regions are spatially homogeneous. So after applying Gabor filters on the image with orientation at different scale, the 'energy' content is obtained using:

$$E(m,n) = \sum_{M}\sum_{N} |H_{mn}(x, y)| \tag{9}$$

The mean μ_{mn} and standard deviation σ_{mn} of the magnitude of the transform coefficients are used to construct two-group (local and global) features to represent the homogeneous textures.

$$\mu_{mn} = \frac{E(m,n)}{M * N}, \quad \sigma_{mn} = \frac{\sqrt{\sum_{x}\sum_{y}\left(|H_{mn}(x, y)| - \mu_{mn}\right)^{2}}}{M * N} \tag{10}$$

If σ_{mn} and μ_{mn} are combined to a vector $r(W_{m}, \theta_{n}) = (\mu_{mn}, \sigma_{mn})$ as the unique feature at a certain orientation at a specific scale, the first group feature is denoted as the local feature:

$$FG = \begin{pmatrix} r(W_{0}, \theta_{0}) & r(W_{0}, \theta_{1}) & \cdots r(W_{0}, \theta_{K-1}) \\ r(W_{1}, \theta_{0}) & r(W_{1}, \theta_{1}) & \cdots r(W_{1}, \theta_{K-1}) \\ \vdots & \vdots & \vdots \\ r(W_{S-1}, \theta_{0}) & r(W_{S-1}, \theta_{1}) & \cdots r(W_{S-1}, \theta_{K-1}) \end{pmatrix} \tag{11}$$

For convenience, typical matrix indexing is used in FG, $FG(1,1) = r(W_0, \theta_0)$ and $FG_{SK} = r(W_{S-1}, \theta_{K-1})$. Another group of the texture features is obtained from sum of a certain frequency W_m at all orientations:

$$E_m = \sum_n r(W_m, \theta_n) \tag{12}$$

Because the scheme of Gabor filter design have covered all space frequency plane nearly uniformly, a global rotation invariant feature vector can formed as $E = [E_1, E_2, \ldots E_S]$.

3.2   Rotation Invariant Measurement

In this paper, the anisotropic textures are emphasized as which we paid more attentions to them. Because a texture is perfectly homogeneous and isotropic, any texture descriptor would be rotation invariant. So, due to the anisotropic textures, a hypothesis is always correct in saying that there is a dominant pair of orientation and frequency in its Fourier spectrum, which means there is a $r(W_m, \theta_n)$ with highest energy.

Now, a column-wise circular shift of local feature matrix FG can be defined as:

$$FG^k = (FG(1:S, k:K) \quad FG(1:S, 1:k-1)) \tag{13}$$

This column-wise circular shift operation is used to rearrange local feature matrix FG so that its dominant orientation can be in the first column of $FG^{'} = FG^k$.

Now, the direct distance metric can be defined between the query image Q and a target image T in the database as:

$$\left| r(W_m, \theta_n) \right| = \sqrt{(\mu_{mn})^2 + (\sigma_{mn})^2}, \ r(W_m, \theta_n) \in G^{'} \tag{14}$$

$$d_{mn}(Q,T) = \left| r^Q(W_m, \theta_n) - r^T(W_m, \theta_n) \right| = \sqrt{(\mu_{mn}^Q - \mu_{mn}^T)^2 + (\sigma_{mn}^Q - \sigma_{mn}^T)^2} \tag{15}$$

Based on the local feature matrix $FG^{'}$ and global feature vector E, three differential factors can be defined as:

$$df_E = \frac{\sum_{m=1}^{S} (E_m^Q - E_m^T)^2}{\sum_{m=1}^{S} (E_m^T)^2} \tag{16}$$

$$df_{FG} = \frac{\sum\limits_{m=1}^{S}\sum\limits_{n=1}^{K}(d_{mn})^2}{\sum\limits_{m=1}^{S}\sum\limits_{n=1}^{K}\left|r^T(W_m,\theta_n)\right|^2} \qquad (17)$$

$$df_D = \sum\limits_{m=1}^{S}(E_m^Q - E_m^T)^2 + \sum\limits_{m=1}^{S}\sum\limits_{n=1}^{K}(d_{mn})^2 \qquad (18)$$

Actually, in this paper, the texture similarity measurements are accomplished by defining the differentia measurement:

$$df = \min(df_E * df_{FG} * df_D) \qquad (19)$$

This similarity measurement is the rotation invariant, and emphasis that variety ratio of global and local 'energy' between the query image Q and a target image T is smallest if Q is the same as or very similar to T.

4 Experiments

In order to test the efficiency of the proposed method for rotation invariant texture analysis, experiments are carried out on a texture database from the Brodatz texture album, which is comprised of 111 texture images of size 512×512. Each center portion of size 256×256 from the respective texture image of size 512×512 is used in the training phase. In the same way, the samples for testing can be obtained

Table 1. Results of rotated texture classification using the proposed approach with various scale and orientation values

Parameters		Correct classifica-tion rate	Parameters		Correct classifica-tion rate	Parameters		Correct classifica-tion rate
Scale	Orienta-tion		Scale	Orienta-tion		Scale	Orienta-tion	
3	4	85.0%	4	4	91.3%	5	4	93.6%
3	5	87.7%	4	5	92.7%	5	5	92.9%
3	6	88.3%	4	6	94.8%	5	6	95.1%
3	7	88.6%	4	7	92.8%	5	7	92.3%
3	8	90.2%	4	8	95.3%	5	8	95.2%
3	9	89.5%	4	9	92.9%	5	9	91.7%
3	10	91.3%	4	10	95.1%	5	10	95.1%
3	11	92.0%	4	11	92.8%	5	11	92.7%
3	12	90.1%	4	12	96.0%	5	12	95.3%
Mean with scale=3		89.2%	Mean with scale=4		93.7%	Mean with scale=5		93.8%

but rotated in steps of $10°$ up to $180°$. Texture classification is done with a total of 1998 rotated texture images $(111 \times 18 = 1998)$ for various combinations of scale and orientation values of Gabor decomposition (scale is from 3 up to 5; orientation from 4 up to 12). The center frequencies for Gabor filters are 0.05-0.4 and separated by one octave-frequency bandwidth.

The results obtained for various combinations of scale and orientation values of Gabor decomposition are given in Table 1. From Table 1, it can be shown that the lowest mean correct classification rate of 85.0% is obtained at scale=3 and orientation=4 with 28 features (24 features of local feature matrix G plus 4 features of global feature vector E), and the highest mean correct classification rate of 96.0% is obtained at scale=4 and orientation=12 with 100 features (96 features of local feature matrix G plus 4 features of global feature vector E). The next highest mean correct classification rate of 95.3% is at scale=5 and orientation=12 with 125 features (120 features of local feature matrix G plus 5 features of global feature vector E), and at scale=4 and orientation=8 with 68 features (64 features of local feature matrix G plus 4 features of global feature vector E). And it is showed that the correct classification rates increase approximately with scales and orientations increasing. But, when scale is larger than 4, there is no vast difference between the mean classification rate obtained for different combination of scale and orientation values of Gabor decomposition. In practice, the best combination can be decided by taking into account the tradeoff (compromise) of the number of features and the minimum correct classification rate.

5   Conclusions

A rotation invariant texture classification scheme using two group features (global feature vector and local feature matrix) based on the Gabor wavelet is developed for a reasonably large (111 classes) texture databases. Two group features, i.e. the global feature vector and local feature matrix, can be constructed by the mean and variance of the Gabor filtered image. Global feature vector is rotation invariant, and local feature matrix can be adjusted by a circular shift operation to rotation invariant so that all images have the same dominant direction. By the two group features, a discriminant can be found to classify rotated images. The primary experiments have proven that the proposed approach is effective for rotation invariant texture classification.

There are many application areas such as automated inspection, large image database handling, remote sensing and medical image processing. Further research should include its robustness to image noise, and scale invariant texture classification.

Acknowledgements

References

1. Jianguo Zhang, Tieniu Tan.: Brief review of invariant texture analysis methods. Pattern Recognition, Vol. 35(3), (2002) 735-747.
2. Porter, R., Canagarajah, N.: Robust rotation-invariant texture classification: Wavelet, Gabor filter and GMRF based schemes. IEE Proceedings of Image Signal Processing 144 (3), 1997.
3. Arivazhagan, S., Ganesan L., and Padam Priyal, S.: Texture classification using Gabor wavelets based rotation invariant features. Pattern Recognition Letters, Vol.27(16), (2006) 1976-1982
4. Haley, G.M., Manjunath, B.S.: Rotation-invariant texture classification using a complete space-frequency model. IEEE Transactions on Image Processing 8 (2), (1999) 169–255.
5. Tan, T.N.: Rotation invariant texture features and their use in automatic script identification. IEEE Transactions on Pattern Analysis and Machine Intelligence 20, (1998) 751–756.
6. Manthalkar, R., Biswas, P.K. and Chatterji, B.N.: Rotation invariant texture classification using even symmetric Gabor filters. Pattern Recognition Letter, Vol.24(12), (2003) 2061–2068
7. Jianguo Zhang and Tieniu Tan.: New texture signatures and their use in rotation invariant texture classification. Proceedings of Texture 2002 (The 2nd international workshop on texture analysis and synthesis with ECCV 2002)
8. Jianguo Zhang, Tieniu Tan, Li Ma.: Invariant texture segmentation via circular gabor filter. Proceedings of the 16th IAPR International Conference on Pattern Recognition (ICPR), Vol II, (2002) 901-904.
9. Manjunath, B.S., Ma, W.Y.: Texture features for browsing and retrieval of image data. IEEE Transactions on Pattern Analysis and Machine Intelligence, Vol.18(8), (1996) 837 – 842

Harmful Contents Classification Using the Harmful Word Filtering and SVM

Wonhee Lee[1], Samuel Sangkon Lee[2], Seungjong Chung[1], and Dongun An[1]

[1] Dept. of Computer Engineering, Chonbuk National University, South Korea
{wony0603, sjchung, duan}@chonbuk.ac.kr
[2] Dept. of Computer Engineering, Jeonju University, South Korea
samuel@jj.ac.kr

Abstract. As World Wide Web is more popularized nowadays, it is also creating many problems due to uncontrolled flood of information. The pornographic, violent and other harmful information freely available to the youth, who must be protected by the society, or other users who lack the power of judgment or self-control is creating serious social problems. To resolve those harmful words, various methods proposed and studied. This paper proposes and implements the protecting system that protects internet youth user from harmful contents. To effectively classify harmful/harmless contents, this system uses two steps of classification: harmful word filtering and SVM learning based filtering. We achieved result that the average precision of 92.1%.

Keywords: Harmful Word, Content Classification, Filtering, SVM.

1 Introduction

As World Wide Web is more popularized nowadays, the environment is flooded with the information through the web pages. However, despite such convenience of web, it is also creating many problems due to uncontrolled flood of information. The biggest problems are that the users are facing excessive information, making it difficult to search for the right one, and that there is uncontrolled harmful information. Especially, the pornographic, violent and other harmful information freely available to the youth, who must be protected by the society, or other users who lack the power of judgment or self-control is creating serious social problems. There have been many rules and studies of various types to resolve the problem for example PICS, Keyword filtering, research based on image data, intelligent analysis system. However, these methods all have limitation, and their performance levels are very low in actual application [2].

This paper describes the method of filtering using the text data of the web contents. To increase the accuracy of classification, filtering is performed in two steps. First, the system classifies the contents as harmful or harmless using harmful word filtering. In the second step, the harmful contents are rated using SVM based filtering. In Chapter 2, the preceding studies dealing with web contents classification are reviewed and summarized. In Chapter 3, the proposed algorithm and its execution are described. In

Chapter 4, the experiment using the proposed algorithm is described and evaluated. The conclusion is presented in Chapter 5.

2   Related Work

Study of web content filtering can be mainly divided into platform for Internet content selection, URL interception, keyword filtering, artificially intelligent contents analysis and image based filtering [2], [11].

2.1   PICS (Platform for Internet Content Selection)

PICS is a technical standard that allows detecting and classifying the meta data, which describes the web page, using the computer software. RSACi and SafeSurf are generally used for classification of PIC contents. RSACi (Recreational Software Advisory Council) uses four categories of harsh language, nudity, sex and violence. Each category is then further classified into 5 ratings from 0 (harmless) to 4. The classification system of SafeSurf is more detailed. In order to describe harmfulness of web contents to each age group, it uses eleven categories [2], [8], [5], [10].

2.2   Keyword Filtering

This method intercepts the web contents based on the harmful words or phrases contained in the content. The words and phrases in the web page are compared with predefined keyword dictionary, and the content is intercepted if the used of those words and phrases exceed a critical number. This method can quickly determine if the web page potentially contains the harmful content. However, it has the problem of over-blocking the harmless contents due to double meaning of the words or phrases [2], [11], [15].

2.3   Intelligent Content Analysis

A web filtering system can use intelligent content analysis to automatically classify the web contents. One of them is artificial neural network that can learn according to the applied training case. Such learning and adaptation can distinguish the syntax depended words like 'sex' that appears widely in both pornographic and other web pages [10], [11].

3   Implementation

3.1   System Architecture

The system proposed in this paper executes two steps of harmful word filtering and SVM learning to increase the accuracy of classification and shorten the time for evaluation. The system is structured as shown in Fig. 1.
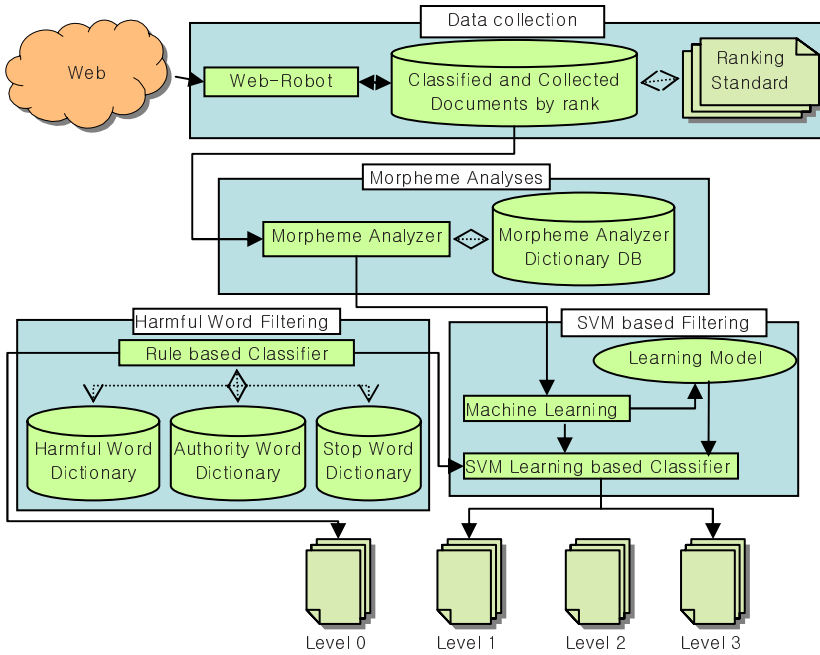
Fig. 1. System Architecture

3.2   Harmful Word Filtering

The harmful word filtering step basically executes keyword filtering. For the filtering work, the harmful word dictionary, authority word dictionary and stop word dictionary are developed and used. If the harmful word dictionary is structured just as a simple list of harmful words, it has the risk of causing the same over-blocking problem as the existing keyword filtering. Therefore, the dictionary adds the information of the words that are used with the harmful words. The added words can lower the fault classification rate due to dual meaning of the words by considering the syntax information of the word. Authority Word dictionary is standard word list for abbreviated or metamorphosed form intentionally or mistakenly by the producer of the content.

3.2.1   Adjacent Word and Non-adjacent Word

A harmful word dictionary consists of the list of the harmful words and the adjacent and non-adjacent words of the harmful word. An adjacent word is defined as the word that can determine the harmfulness level of the harmful word when appearing in the same sentence. A non-adjacent word is the one that appears in the same content as the harmful word, although not in the same sentence, and can still determine the harmful nature of the content. For example, a word 'breast' can be harmful or harmless. In addition, when the word is used in harmful meaning, its level of harmfulness can be very high or little depending on how it is used. If the word 'cancer' appears in the

same sentence as 'breast', then it is very likely that the content is of harmless nature. However, if the word 'tongue' appears, it is likely that the content is of harmful nature. Furthermore, if the word 'rope' appears in the same sentence, the content is likely to be very harmful, containing pervertible nature.

3.2.2 Authority Word Dictionary

When a standard word is presented in abbreviated or metamorphosed form intentionally or mistakenly by the producer of the content, it must be transformed to its standard form. Otherwise, the abbreviated word or metamorphosed word can change the appearance frequency and affect the evaluation of being harmful or harmless.

3.2.3 Harmful Word Filtering

Harmful word filtering is executed in the following procedure:

● Step 1: Tags are removed from the document, and the morpheme analysis is performed.
● Step 2: The list of the morpheme analyzed words is transformed to their standard words.
● Step 3: The harmful word candidates are selected from the word list. The identified word candidates are evaluated of their harmfulness using the adjacent and non-adjacent words. The frequency of the harmful word usage is then calculated. If it is larger than a certain value (α), the document is considered harmful.

The determining function $f(d_i)$ of a document can be expressed as follows:

$$f(d_i) = \frac{FT}{N}, \tag{1}$$

where *FT* is the count of the harmful words in a document and *N* is the total number of harmful words.

3.3 SVM Learning Based Filtering

SVM based filtering consists of the following four steps: (1) Feature Extraction, (2) Indexing, (3) Generation of learning mode, and (4) Classification using the learning model.

3.3.1 Feature Extraction

Feature extraction deals with generating a list of feature to be used for learning based text classification. For the algorithm to extract the feature, DF (Document Frequency), IG (Information Gain), MI (Mutual Information), and CHI-square are tried to determine the best method. DF means the number of documents that a certain word occurs in a set of documents. IG is an algorithm that selects only the feature with high contribution in order to calculate how a word's appearing in the document

contributes to classification of the document. CHI seeks a quantity of term importance by measure the dependence relationship between term t and category c [7].

3.3.2   Indexing

The extracted qualities needed to be weighted according to their importance in the document. For indexing and weighting process, the TF, TF-IDF(Inverse Document Frequency) and TF-ICF(Inverse Category Frequency) algorithms are used [7].

3.3.3   Generation of Learning Model

SVM (Support Vector Machines) are learning systems that use a hypothesis space of linear functions in a high dimensional feature space, trained with a learning algorithm from optimization theory that implements a learning bias derived from statistical learning theory. This learning strategy introduced by Vapnik and co-workers is a principled and very powerful method that in the few years since its introduction has already outperformed most other systems in a wide variety of application [9]. SVM selects the optimum hyperplane from two dimensional classifications and uses it as the decision border surface. The optimum hyperplane identifies two linear separable groups and maximizes the margin. However, since the linear separable case is rare in practical problem, the non-linear space is mapped to the linear space using the kernel function and then classifies using the linear SVM. In this paper, C-SVC and RBF are used as the SVM type and kernel, respectively. The deciding function of C-SVC is

$$\text{sgn}(\sum_{i=1}^{l} y_i \alpha_i K(x_i, x_j) + b)$$
,   (2)

and kernel function is

$$K(x_i, x_j) = \exp(-\gamma \|x_i - x_j\|^2), \quad \gamma > 0$$ (3)

3.3.4   Classification by Using the Learning Model

Classification is the process of rating the document using the generated learning model. The document to be rated creates the feature using the morpheme analysis and goes through indexing and normalization using the created feature. The document data generated through normalization is then rated using the learned model generated through learning.
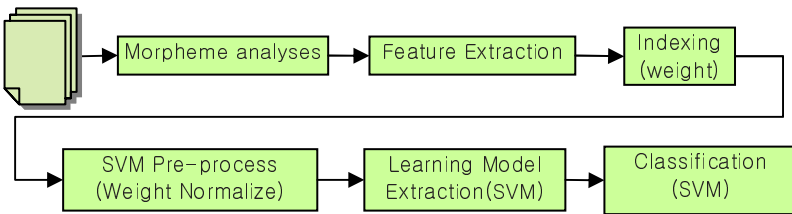
Fig. 2. Processing of Learning and Classification Using SVM

4   Experiment and Evaluation

The environment for the experiment and evaluation is as follows: EHDS-2000 (ETRI Harmful Data Set), which was built as the test based harmful data set, is used. EHDS-2000 is harmful document set built by ETRI(Electronics and Telecommunications Research Institute) in South Korea. EHDS-2000 is composed of Korean Documents and English Documents shown in Table 1. The learning and test data used for the experiment and evaluation are as follows:

Table 1. Data Set

		Collection Documents		Training Documents		Test Documents	
		harmful	harmless	harmful	harmless	harmful	harmless
Languages	Korean	2,572	2,126	1,164	588	509	462
	English	12,250	3,340	936	694	449	533

The experiment was conducted in two steps. First, the optimal algorithm set is determined from the qualifier extraction algorithm (logTF, IG and CHI) and indexing algorithm (TF-IDF and TF-ICF). For the experiment, the qualifier counts between 200 and 800, were adjusted, incrementing by 100. The result of the experiment is shown in Fig. 3. The figure indicates that the combination of CHI and TF-IDF showed the best result at the qualifier count of 800.
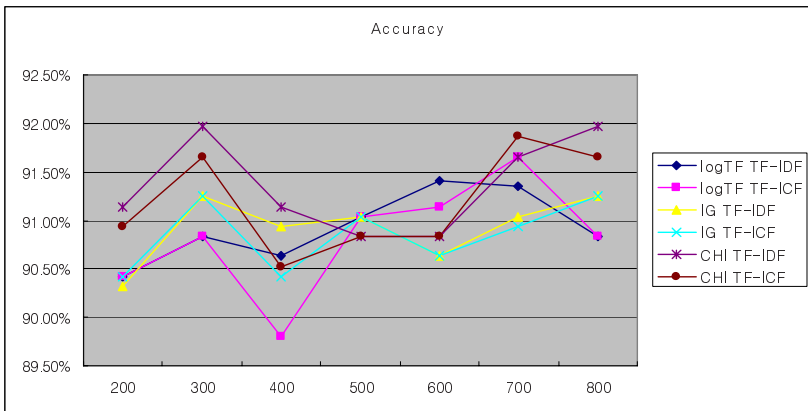
Fig. 3. Comparison of Feature Extracting Algorithm

The second step involved two experiments. One was the classification using harmful word filtering only while the other one was the classification using both harmful word filtering and SVM based filtering. Table 2 shows the result of harmful word filtering only. It indicates that the accuracy level 97.4% for the harmful words. However, the accuracy for the harmless words was only 51.3%. And 48.7% of inaccuracy included the sex advice and medical information document.

Table 2. Result of Classification Using Harmful Word Filtering Only

Non-Harmful(995)		Harmful(958)		Overall Accuracy
correctly	incorrectly	correctly	incorrectly	
511 (51.3%)	484 (48.7%)	933 (97.4%)	25 (2.6%)	74.35%

The inaccuracy was caused by the harmful words in the document. To improve the result, the document sets were separated into three types. First, the harmless documents are divided into type-0 and type-1. Those that contain no harmful words were classified as type-0. And the sex advice or medical information documents that contain the harmful words were classified as type-1. Then the harmful documents were classified as type-2. Table 3 shows the result of the new experiment. It indicates 92.1% accuracy in average. For the harmless documents, the type-0 showed 95.9% accuracy and type-1 90.9%, making the average accuracy of 93.4%, a big improvement. The accuracy of the type-2 (harmful) documents actually was lowered from 97.4%. 7.9% reduction mostly came from the sex advice or medical information contained in the harmful documents. The cases of type-1 or type-2 documents assessed as type-0 were 1.7% and 2.6% for type-1 and type-2, respectively. They were mostly image and the rest of the text was very little.

Table 3. Result of Classification Using both Harmful Word Filtering and SVM based Filtering

Result / Input Data	Type-0	Type-1	Type-2
type-0(524)	503(95.9%)	14(2.7%)	7(1.4%)
type-1(471)	8(1.7%)	428(90.9%)	35(7.4%)
type-2(958)	25(2.6%)	76(7.9%)	857(89.5%)

5   Conclusion

At present, Internet is flooded with information including the harmful contents of pornographic, violent and suicidal nature. To solve the problem, various methods such as the rating system − PICS, keyword filtering, intelligent analysis system are proposed and studied. But these methods all have certain limitations for intercepting the harmful contents.

This paper proposes the system to protect the young Internet users from harmful sites by accurately identifying the harmful contents widely available on the web pages. For effective classification of harmful and harmless contents, the paper proposes a two step system of harmful word filtering and SVM learning based filtering. For harmful word filtering, the syntax information using the adjacent words and non-adjacent words was added to the harmful word dictionary. That improved the classification accuracy. For the quality of the contents, the various algorithms such as logTF, IG, CHI, TF-IDF and TF-ICF were tried to select the optimal extraction and

normalization algorithm. As the result, the accuracy level of 92.1% was achieved. In the future, the accuracy needs to be further improved by analyzing the various content elements such as the image, sound or document structure.

References

1. Chih-Wei Hsu, Chih-Chung Chang, and Chih-Jen Lin. : A Practical Guide to Support Vector Classification, http://www.csie.ntu.edu.tw/~cjlin/libsvm/
2. Christopher D. Hunter : Internet Filter Effectiveness: Testing Over and Underinclusive Blocking Decisions of Four Popular Filters, Proceedings of the Tenth Conference on Computers, Freedom and Privacy: Challenging the Assumptions, (2000) 287-294
3. Dequan Zheng, Yi Hu, Tiejun Zhao, Hao Yu, and Sheng Li : Research of Machine Learning Method for Specific Information Recognition on the Internet, IEEE International Conference on Multimedia Interfaces (ICMI), (2002)
4. Huicheng Zheng, Hongmei Liu, and Mohamed Daoudi : Blocking Objectionable Image: Adult Images and Harmful Symbols, IEEE International Conference on Multimedia and Expo (ICME), (2004) 1223-1226
5. Jae-Sun Lee, and Young-Hee Jeon : A Study on the Effective Selective Filtering Technology of Harmful Website Using Internet Content Rating Service, Communication of KIPS Review, Vol. 9, No. 2, (2002)
6. KwangHyun Kim, JoungMi Choi, and JoonHo Lee : Detecting Harmful Web Documents Based on Web Document Analyses, Communication of KIPS Review, Vol. 12-D, No. 5, (2005) 683-688
7. JH Jeong, WH Lee, SW Lee, DU An and SJ Chung : Study of Feature Extraction Algorithm for Harmful word Filtering, KCC Summer Conference, Vol. 33. No. 01. (2006) 7-9 (in Korean)
8. Mohamed Hammami, Youssef Chahir, and Liming Chen : WebGuard: A Web Filtering Engine Combining Textual, Structural, and Visual Content-Based Analysis, IEEE Transaction on Knowledge and Data Engineering, Vol. 18, No. 2, (2006)
9. Nello Cristianini, and John Shawe-Taylor : An Introduction to Support Vector Machines and Other Kernel-based Learning Methods, Cambridge University Press, (2000)
10. P. Y. Lee, and S. C. Hui : An Intelligent Categorization Engine for Bilingual Web Content Filtering, IEEE Transaction on Multimedia, Vol. 7, No. 6, (2005)
11. P. Y. Lee, S. C. Hui, and A. C. M. Fong : Neural Networks for Web Content Filtering, IEEE Intelligent Systems, (2002) 48-57
12. Yun-Jung Jang, Taehun Lee, Kyu Cheol Jung, and Kihong Park : The Method of Hurtfulness Site Interception Using Poisonous Character Weight, KIPS Spring Conference, Vol. 10, No. 1, (2003) 2185-2188 (in Korean)

HVEM Control System Based on Grid: A Cornerstone of e-Biology

Hyuck Han, Shingyu Kim, Hyungsoo Jung, and Heon Y. Yeom

School of Computer Science and Engineering,
Seoul National University,
Seoul 151-742, Korea
{hhyuck,sgkim,jhs,yeom}@dcslab.snu.ac.kr

Abstract. This paper proposes HVEM Control System, which is the cornerstone for teleinstrumentation infrastructure. The proposed system is oriented for people whose primary work is to get access to a remotely located instrument, a High-Voltage Electron Microscope (HVEM). Our system is implemented to fulfill all the necessary requirements in allowing the user to 1) control every single part of HVEM in a fine-grained manner, 2) check the HVEM and observe various states of sample, and 3) take their high resolution images of the sample. In that aspect, this paper suggests an HVEM Control System designed on the concept of the Grid and Web Service which satisfies various types of user groups, explains novel characteristics of our system.

1 Introduction

Many scientists use computing resources, storage resources and any other resources to perform real-time experiments. This science, which is performed through distributed global collaborations over the Interenet, is called e-Science[1]. Specially, scientists in e-Science need to access or control experimental devices remotely in a fine-grained manner, and this capability is crucial for remote experiments.

High-Voltage Electron Microscope (HVEM) allows scientists to see objects at a magnification greater than the actual sample. The type of HVEM referred in this paper is transmission electron microscopy (TEM), which produces an image that is a projection of the entire object, including the surface and the internal information. When tilt is needed, the Goniometer rotates to change the angle of the sample. When environments inside the HVEM such as voltage and focus are needed to be changed, FasTEM performs such operations which users command. It is the CCD camera that produces an actual image inside the HVEM. HVEM users control the HVEM in a fine-grain manner, observe the sample using the above subcomponents of HVEM, and take high-resolution images using storage resources. Since remote users want to perform the same tasks as offline users, the HVEM-Grid provides remote users with applications for controlling the HVEM, observing the sample, and carrying out other tasks remotely.

The objective of our system is to work towards an implementation of the vision of being able to use the HVEM of the Korea Basic Science Institute

(KBSI)[2] remotely. This typically means that the remote users can carry out the realistically large scale research. Therefore, this requires functions that allow remote users to control subcomponents of the HVEM and to observe the sample. Specially, the functions include requirements of biologists such as memorization of some specific locations and recording/replaying the trace of the sample.

In this paper we describe the HVEM Control System, which has the capabilities listed above. This paper is organized as follows. Section 2 describes background material. Section 3 explains the architecture of our HVEM Control System. Section 4 shows experimental results. Section 5 summarizes our plans for future work and Section 6 concludes the paper.

2   Background and Related Work

2.1   Grid and Web Service

A Grid can be defined as a layer of networked services that allow users single sign-on access to a distributed collection of computing, data, and application resources. The Grid services allow the entire collection to be seen as a seamless information processing system that the user can access from any location. However, the heterogeneous nature of the underlying resources remains a significant barrier. Scientific applications often require extensive collections of libraries that are installed in different ways on different platforms.

Web service is an important emerging distributed computing paradigm that focuses on simple, Internet-based standards to address heterogeneous distributed computing. Web services define a technique for describing software components to be accessed, methods for accessing these components, and discovery methods that enable the identification of relevant service providers.

HVEM Control System utilizes Grid and Web service for the control of HVEM. By doing this, our HVEM Control System can support many other systems. A 3D-image construction service, which we are currently developing, gives us a good example. The service commands the HVEM to tilt the angle of the sample by 1 degree, take an image and repeat this process. Then, it builds a new 3D image out of taken images. Because HVEM Control System is based on Grid and Web service, it can support HVEM Control User Interface as well as other services such the 3D-image construction service.

2.2   Other Research

The National Center for Microscopy and Imaging Research (NCMIR) at the University of California San Diego(UCSD) develops 3D imaging and analysis technologies to help biomedical researchers understand biological structure and function relationships in cells and tissues. Its web-based tool[3] and EMWorkspace[4] are innovative and similar to our system. However, they have some major drawbacks. First, they can not support the HVEM of KBSI, which is really large-scale and newest. Second, GTCP[5] which EMWorkspace uses is not suitable for

asynchronously operated microscopes. When operations are issued to such microscopes, it is needed to poll the status in order to verify success of operations. Although all clients can poll the status of the HVEM, it is to hard to guarantee consistency between clients. Therefore, there exists a Grid service that polls the status of the HVEM and manages the status in our system. Third, they do not have specific functions to biologists such as memorization of interesting locations, recording/replaying traces that remote users are interested in. These functions are necessary because they lead to efficient observation and experiments.

3   Architecture

3.1   HVEM Control System in 3-Tier Architecture

This section of the paper describes the architecture of the HVEM Control System. Our system has a 3-tier architecture[6] which utilizes Grid and Web Service. Grid and Web Service which is based on the XML messaging have many advantages suitable for integration with complex systems: platform independent architecture, interoperability, and flexibility.
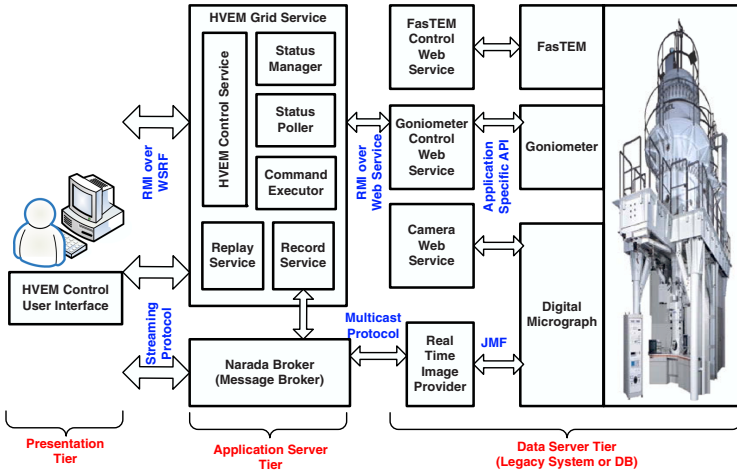
Fig. 1. System Architecture

Figure 1 shows the architecture of the HVEM Control System. HVEM Control User Interface (HVEM Control UI) program corresponds to the presentation tier of the 3-tier architecture. HVEM Grid Service based on Globus Toolkit 4[7] and Narada Broker[8,9] correspond to the application server tier. Remote Method Invocation (RMI) which is based on Web Service Resource Framework(WSRF), is used to communicate between HVEM Control UI and HVEM Grid Service.

HVEM Control Service is responsible of handling control requests from HVEM Control UI. Status Poller polls the overall status of the HVEM such as location

of the angle, voltage value, focus and brightness. Then, it forwards such information to Status Manager, which manages the status of HVEM. Many operations for retrieving specific status are handled by the Status Manager, not corresponding subcomponents of the HVEM. This can alleviate the overhead of FasTEM and Goniometer. Command Executer routes users' operations to related Web services. FasTEM, Goniometer and Digital Micrograph, which are provided by manufacturers, are encapsulated in Web services, and those Web services correspond to data server tier. Applications which control Goniometer and FasTEM are termed Goniometer and FasTEM respectively, and Digital Micrograph is an application to manipulate CCD camera. We encapsulated those application specific APIs in Web services to provide only secure and reliable features.

Record and Replay services are tightly coupled with each other. If the Record service receives a start request, it starts to record real-time images from the Digital Micrograph to a stable storage device. It continues to record them until it receives a stop request. The Replay service transfers the saved video to the HVEM Control UI when it receives a replay request which the HVEM Control UI selects. Record and Replay services provide a good method to biologists because they tend to observe past samples.
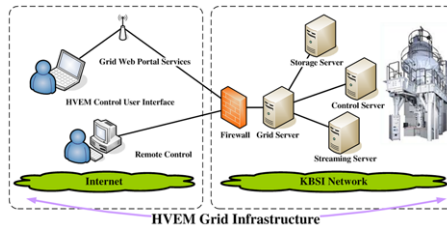
Fig. 2. HVEM Control System Network

Figure 2 outlines the HVEM Control System on the Network. HVEM Control UIs are located on internet, and legacy systems which manipulate HVEM and Web services which encapsulate legacy systems are on KBSI's site, which is protected by firewalls. HVEM Grid Service objects interact with HVEM Control UIs, Web services of HVEM legacy system (encapsulated experimental equipment) and other hardware resources such as storage devices. By doing this, HVEM Control System can be more secure, because unauthorized users are prevented from accessing legacy systems direct.

3.2   Control of Goniometer and FasTEM

Figure 3(a) shows the sequence to move an axis of a sample by HVEM Control UI. HVEM Control UI sends a request message of movements along X-axis to HVEM Control Service by RMI over WSRF, and HVEM Control Service transfers a request message to Goniometer Web service object which encapsulates

(a) Basic Sequence   (b) Optimized Sequence
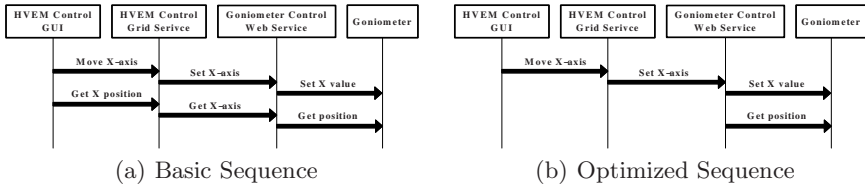
Fig. 3. Sequence to move an axis of a sample by Goniometer

the Goniometer control application. When the response for the request of movements along X-axis is delivered to HVEM Control UI, HVEM Control UI sends another message to request information of current location of a sample. The request message goes through the same way as before. A similar message flow is applied to control of FasTEM.

In general, we can control cameras and microscopes with small number of operations. However, we need many operations to control axis of sample and angle of stand in Goniometer. Usually, biologists start experiments after they complete the whole setting of the HVEM such as brightness, focus and voltage. During observation they move the axis or tilt the angle through the Goniometer to find specific parts of the sample. Then, they take an image. This suggests that most of operations are related to moving or tilting. Therefore, we can get chances to improve performance in that part.

Figure 3(a) shows that we need two operations to move an axis of the sample in Goniometer: changing the axis and reading the location of the sample. Therefore, it could suffer from overload due to too many operations when large number of HVEM Control User Interfaces access to it or moves an axis by trackball. Figure 3(b) shows the optimized sequence of control operations in application level. Unlike Figure 3(a), HVEM Control User Interface can complete two operations, which are operations to change the axis and to read the location, in one RMI call. It could be a useless operation to read the location when you intend to change the axis only. However, biologists look at the samples by changing the axis in most cases. In that case, the operation to read the location of sample is followed by the operation to change the axis. This feature makes the performance improvement larger.

3.3   Control of Camera

Control of camera consists of two parts: Real-Time Streaming Service and Snapshot Service. We begin by introducing Real-Time Streaming Service.

Figure 4(a) shows the sequence for Real-Time Streaming Service. Real-Time Image Provider gets video sources from Digital Micrograph by utilizing Java Media Framework (JMF). It transfers received images to the Narada Broker, which multicasts messages. Then, the Narada Broker delivers them to HVEM Control UI (and Record service if it receives a subscription request).

(a) Sequence of Real-Time Streaming Service

(b) Sequence of Taking Images of an Sample
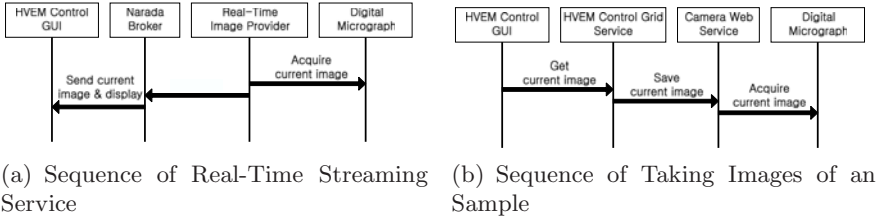
Fig. 4. Sequences of Camera Control

Figure 4(b) shows the sequence of taking images of a sample. This sequence starts from HVEM Control UI. HVEM Control UI sends a request message of taking images of a sample to HVEM Control Service. Next, HVEM Control Service delivers the message to Camera Web service and the message arrives at Digital Micrograph finally. Digital Micrograph has a COM plug-in to process this requests. After plug-in completes the request, the result is delivered to HVEM Control UI through Camera Web service and HVEM Control Service, and HVEM Control UI can download the image.

3.4 Record and Replay

In order to record real-time images, HVEM Control UI sends a start request to Record service. Then, Record service subscribes an appropriate topic to Narada Broker. The topic should be related to real-time images from Digital Micrograph. After the subscription Record service starts and continues to save real-time images into stale storages as an appropriate format until it receives a stop request.

When a remote user wants to replay a specific video, HVEM Control UI sends a replay request to Replay service. Then, it transfers saved images to Narada Broker and Narada Broker delivers them to HVEM Control UI by the same way of the Real-Time Streaming Service. This capability leads to efficient research because many biologists want to watch past experiments during the current observation. Note that sequence diagrams of Record and Replay services are skipped due to the page limit.

4 Evaluation

The machines used in this evaluation were a Pentium IV 2.80GHz PC in Seoul National University (SNU) and two Pentium IV 3.0 GHz PCs in KBSI, running Linux 2.4.18. RMI service server is located in KBSI, and RMI clients are in SNU and KBSI when the experiments run in WAN and LAN environment respectively.

Figure 5 shows latencies of RMI which performs optimized operation of Goniometer Control. We measured latencies when RMI is called 30 times continuously. Figure 5(a) shows all results from first to 30th call. The latency of first call is larger than others, because loading RMI library takes some time in Java VM. Figure 5(b) excluded the first latencies. In this case, the average latencies

(a) Including first RMI call   (b) Except fisrt RMI call
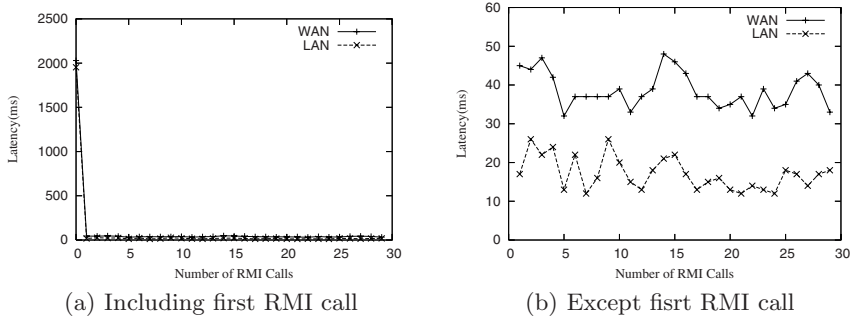
Fig. 5. Latencies of RMI with Optimization in Application Level

are 38ms and 17ms for WAN and LAN respectively. It may take at least 76ms in WAN environment without the optimization because it needs two RMI calls to move axis of sample (changing the axis and reading the location). This is good advantage to reduce the latency to 38ms by the optimization and allows biologists to control the Goniometer with a reasonable speed.

5   Future Work

HVEM Control System is a part of our three-year project, and it is the objective of the first year. Currently, we are developing an image processing system, which is the objective of the second year. It is a kind of workflow systems, which receives a job specification from remote users, carries out the job, and then stores results of the job. Usually, biologists tend to take many images of samples and build 3D images based on the 2D images. To do this, users tilt the angle of samples by some degrees (between 0.5 and 1), focus the lens of the CCD camera, and take a high-resolution 2D image. Until 2D images are enough to construct 3D images, this process is repeated, and then 3D images are built. The objective of the system that we are developing is to automate this workflow. Thus, this system requires to control the Goniometer, the FasTEM, and to take an image through the CCD camera, and our HVEM Control System provides those functionalities.

6   Conclusion

This article has proposed the system to control HVEM at remote site. Our HVEM Control System is implemented based on Grid technology and Web services. Initial version of the system was assembled by basic components, and we optimized flows of messages. Then, we presented reasonable results and our results showed that our system will be a very useful research method to biologists. We are convinced that our HVEM Control System will be a core software infrastructure in research work of scientists at remote stations.

Acknowledgment

References

1. Oxford e-Science Centre: (e-Science Definitions) `http://e-science.ox.ac.uk/public/general/definitions.xml`.
2. Korea Basic Science Institute: (KBSI microscopes & facilitates) `http://hvem.kbsi.re.kr/eng/index.htm`.
3. Hadida-Hassan, M., Young, S.J., Peltier, S.T., Wong, M., Lamont, S., Ellisman, M.H.: Web-based telemicroscopy. Journal of Structural Biology **125** (1999) 235–245
4. National Center for Microscopy and Imaging Research: (Telescience Project) `http://telescience.ucsd.edu`.
5. Globus Alliance: (Globus Teleoperations Control Protocol) `http://www.globus.org/toolkit/docs/development/4.2-drafts/execution/gtcp/`
6. Helal, S., Hammer, J., Zhang, J., Khushraj, A.: A three-tier architecture for ubiquitous data access (2001)
7. Globus Alliance: (Globus Toolkit 4.0 Release Manuals) `http://www.globus.org/toolkit/docs/4.0/`.
8. Fox, G., Pallickara, S., Rao, X.: A Scaleable Event Infrastructure for Peer to Peer Grids. In: Proceedings of the ACM Java Grande ISCOPE Conference. (2002)
9. Uyar, A., Pallickara, S., Fox, G.: Towards an Architecture for Audio Video Conferencing in Distributed Brokering Systems. In: Proceedings of the 2003 International Conference on Communications in Computing. (2003)

Speedup Analysis for Parallel Implementation of Model of Response Accuracy and Response Time in Computerized Testing

Tianyou Wang[1] and Jun Ni[2,3]

[1] Center for Advanced Study in Measurement and Assessment, College of Education
[2] Information Technology Services
[3] Department of Computer Science, College of Liberal Arts
University of Iowa, Iowa City, IA 52242, USA
{tianyou-wang,jun-ni}@uiowa.edu

Abstract. Recently, computerized testing has revolutionized the testing industry by offering an array of benefits for both the examinees and the test users. It potentially enhances the quality of education at all levels. Computerized testing also makes available new types of data such as item-response time and human response at the individual item level. However, the present models of these responses demand much computing time. This paper presents an analysis for a parallel implementation of the models by estimating parallel speedup and efficiency. The model provides an insight into the success of advanced computerized testing study using high performance computing (HPC) technology.

Keywords: social implications of IT, educational and psychological testing, computerized testing, HPC, parallel computing, education measurement.

1 Introduction

In the last two decades, computerized testing has gradually evolved from a research and experimental stage to applications. Large-scale standardized testing programs such as the GRE, TOEFL and GMAT have routinely adopted a computerized testing mode. Computerized testing has revolutionized the testing industry by offering highly flexible testing schedules, instant scoring, and high efficiency. Computerized testing has also been used in assisting classroom learning by offering interactive instruction and instant feedback, which can potentially increase the quality of education at all levels.

Computerized testing generates new dimensions of data that are not available on the traditional paper-and-pencil testing, such as the data of item response time at the individual item level. Such availability of new testing data opens a new door to solve the obstacles to psychometric theory and practice. For example, traditional models of the Item Response Theory (IRT) model, as the basic psychometric tools for computerized testing, focused on modeling response accuracy. In those models, each examinee typically has only one person parameter; i.e., the human personal ability parameter. Recently-proposed models can not only model the accuracy of response

but also account for response time. A general feature of such models is that each examinee has the person parameters (e.g. speed parameter) in addition to the ability parameters. However, due to the extra person parameters, the parameter calibration procedure of an item response model creates a huge demand on the computing power, especially for the calibration of EM algorithm-based item response models. The EM algorithm treats the person parameters as missing data marginalized through an integration of computing the marginal likelihood function. The models that take consideration of person parameters require additional layers of integrations; thus greatly increasing the computation time. For example, in our previous models with two person parameters, even with a small number of items and a relatively small sample size, one calibration takes about several computational hours per PC with 2.8 GHz. The model computation for a large number of items and/or big sample size makes a single calibration unbearably long. In real psychometric applications, simulations are needed to estimate the precision of the calibration procedures and each simulation involves hundreds or even thousands of calibrations, which makes it almost impossible to accomplish computational tasks using conventional computing facilities.

Previous studies indicate that modeling a distribution of response time is quite intriguing and will probably require different sub-models for different testing situations such as different subject materials and testing time constraints. Typically, in an appropriate psychometric model, large-scale simulations are needed to accurately estimate the precision of the calibration procedures. Such simulations usually contain hundreds of calibrations, which make it almost impossible to carry out, based on a single processor computer and its computing capability. This motivates us to consider an alternative approach – to conduct simulations of EM-algorithm-based calibrations using high performance computing (HPC) technology.

The paper presents a speedup analysis for a parallel implementation of a model of response accuracy and response time in computerized testing. The parallel algorithm and its implementation appropriately simulate the joint distributions of response accuracy and response time for different kinds of testing. The analytical model is based on data decomposition and message passing. The model provides insight into large-scale parallel item-response models in computerized testing. The paper is organized in the following sections. Section 1 presents the related work. Section 2 briefly depicts the item response models and the associated numerical algorithms. Section 3 addresses the parallel implementation, domain decomposition, and performance prediction which is followed by a conclusion.

2   Related Work

One of the benefits of computerized testing is that it makes response-time data available at the level of individual items. This new availability, with different dimensions of observable data, opens up new opportunities for the theory and practice of educational measurement. As a result, there has been an increased research interest in how to utilize the response-time data. Schnipke and Scrams [3] provided a comprehensive review on this topic and presented the state-of-the-art research on response time data. Most of the previous models on response time consider the response time as a

dependent variable. These models did not consider the relevance between response accuracy and response time. The few exceptions are by [2,5,7]. The models developed by Verhelst et al and by Roskam were similar in that the probability of correct response approaches 1 as response time goes to infinity. Thus, these models were applicable only to speed measurement tests (i.e., the main purpose is to measurement the examinee's speed) where an unlimited response time is guaranteed to achieve a correct response. Alternatively, Thissen's model [5] applies to power tests (i.e., the main purpose is to measure ability rather than speed). His model used a logistic model for the marginal distribution of response accuracy, and a lognormal model for the marginal distribution of response time. However, this model has a limitation due to the assumption that response accuracy and response time are independent; thus their joint distribution can be expressed as the product of the marginal distributions of response accuracy and response time, although the two marginal distributions share some common parameters. This assumption does not generally hold in realistic testing situations. Recently, Wang and Hanson proposed a four-parameter logistic response-time (4PLRT) model [9] in which the response accuracy and time are modeled correlatively. Besides, the model considers the response time as an independent variable, which impacts the final probability of a correct response. In the model formulation, as response time goes to infinity, the probability of a correct response is consistent with the one described by a regular three parameter logistic (3PL) model. The model is applicable to power tests where an unlimited response time does not guarantee a correct response. The model makes an assumption that the item response time is independent of person parameters. This assumption was given to avoid modeling the distribution of response time and consequently simplifying the calibration procedure. This assumption, however, poses a severe limitation to the applicability of their model. In order to eliminate this limitation, a model of the joint distribution of response accuracy and time is needed. Bloxom [1] presented two different methods to describe such distribution. One way is to model the conditional distribution of response accuracy at a given response time and then to multiply the distribution with the marginal distribution of response time. The other way is to model the conditional distribution of response time with a given response accuracy and then to multiply the distribution with the marginal distribution of response accuracy. In both approaches, there is a variety of methods for modeling the conditional and marginal distributions. Most of these probability distributions have not been thoroughly explored in literature. Wang explored a simple model with the first approach, using a one-parameter Weibull distribution for the marginal distribution of response time [8,10], and achieved limited success in terms of model-data fit and calibration precision. One great obstacle with this line of research is the high demand of computing speed. With only the two person parameters model [8,10], a single calibration for a test of 20 items and 1000 examinees can take more than two hours on a single processor PC. Wang's new model adopted the 4PLRT model as the conditional model, except that it omitted one person parameter in order to avoid three person parameters in the joint distribution because of the infeasibility of computational demand. One possible extension of Wang's new model would be use the 4PLRT model and allow the model for the joint

distribution to have three person parameters. With that extension, people can use HPC technology to increase desired computational power.

2.1 Item Response Models

Below is a description of the first model [8,10] which extends 4PLRT model [9] as the conditional model of response accuracy given response time, without the omission of the person slowness parameter, and using the one-parameter Weibull model for the marginal distribution of response time.

Let y_{ij} be the dichotomous item response variable, with 1 for a correct response, 0 for an incorrect response. Let t_{ij} be the response time variable. In this joint distribution model, the joint distribution of y_{ij} and t_{ij} is expressed as:

$$f(y_{ij},t_{ij}\,|\,\theta_i,\rho_{i},\rho_{2i},\delta_j)=f(y_{ij}\,|\,t_{ij},\theta_i,\rho_{i},\delta_j)f(t_{ij}\,|\,\theta_i,\rho_{2i},\delta_j), \tag{1}$$

The detailed model can be found in [10].

2.2 Model Algorithm

The EM algorithm can be used to find parameter estimates that maximize the likelihood of the observed data based on a sequence of calculations that involve finding parameter estimates that maximize a conditional expectation of the complete data likelihood. In the current model, the maximum likelihood estimates are found for the conditional observed joint likelihood of the item response and the response times. Parameter estimates are found that maximize the following observed data likelihood:

$$L(\mathbf{Y},\mathbf{T}\,|\,\mathbf{D},\mathbf{p}) = \prod_{i=1}^{N}\left(\sum_{k=1}^{K}\sum_{l=1}^{L}\sum_{m=1}^{M}\pi_{kl}\prod_{j=1}^{J}f(y_{ij},t_{ij}\,|\,q_k,u_l,v_m,\mathbf{d}_j)\right), \tag{2}$$

where $\mathbf{D}$ is the set of item parameters for all items $(\mathbf{d}_j,\, j=1,\ldots,J)$. The corresponding likelihood for the complete data is:

$$L(\mathbf{Y},\mathbf{T},\mathbf{q},\mathbf{r}\,|\,\mathbf{D},\mathbf{p}) = \prod_{i=1}^{N}\left(\prod_{j=1}^{J}f(y_{ij},t_{ij}\,|\,\theta_i,\rho_{1i},\rho_{2i},,\mathbf{d}_j)\right)f(\theta_i,\rho_{1i},\rho_{2i},|\,\mathbf{p}), \tag{3}$$

where $f(\theta_i,\rho_i\,|\,\mathbf{p}) = \pi_{kl}$ if $\theta_i = q_k$ and $\rho_i = u_l$. Note that here we do not need to make the simplifying assumption that the joint distribution of θ_i and ρ_i are not independent of response time; that is $f(\theta_i,\rho_i\,|\,t_{ij},\mathbf{p}) = f(\theta_i,\rho_i\,|\,\mathbf{p})$. This assumption was necessary in [9] because in that paper, t_{ij} was treated as a c variable and, without this assumption, the response time distribution would eventually need to be specified. In the current model, t_{ij} is not treated only as a conditioning variable, but rather the joint distribution of y_{ij} and t_{ij} is treated in the first place, and the response time distribution is specified. The details about the log-likelihood can be expressed in [8,10].

$$log[L(\mathbf{Y},\mathbf{q},\mathbf{r}\,|\,\mathbf{T},\mathbf{D},\mathbf{p})] = \sum_{j=1}^{J}\sum_{i=1}^{N}log[f(y_{ij},t_{ij}\,|\,\theta_i,\rho_{1i},\rho_{2i},,\mathbf{d}_j)] + \sum_{i=1}^{N}log[f(\theta_i,\rho_{1i},\rho_{2i},|\,\mathbf{p})]. \tag{4}$$

The computations to be performed in the E and M steps of the EM algorithm are described in the next two sections. Since the E-step dominates most of the computation time, while M-step's computation time is relatively little; therefore, the parallel model, is only focused on the E-step domain decomposition. **E Step**. The E step at iteration $s(s = 0, 1, \ldots)$ consists of computing the expected value of the log-likelihood given in Equation 10 over the conditional distribution of the missing data $(\mathbf{q}, \mathbf{r})$, given the observed data $(\mathbf{Y}, \mathbf{T})$, and the fixed values of the parameters $\mathbf{D}^{(s)}$ and $\mathbf{p}^{(s)}$ obtained in the M step of iteration $s - 1$ (with some type of starting values for the parameters are used for $\mathbf{D}^{(0)}$ and $\mathbf{p}^{(0)}$). The expected complete data log-likelihood is given by (Woodruff and Hanson, 1996):

$$\phi(\mathbf{D}) + \psi(\mathbf{p}) \tag{5}$$

where $\phi(\mathbf{D})$ is the log-likelihood which accounts for item parameter. It dominates the overall computation. It can be expressed as

$$\phi(\mathbf{D}) = \sum_{j=1}^{J}\sum_{i=1}^{N}\sum_{k=1}^{K}\sum_{l=1}^{L}\sum_{m=1}^{M} log[f(y_{ij}, t_{ij} \mid q_k, u_l, v_m, \mathbf{d}_j)]f(q_k, u_l, v_m \mid \mathbf{y_i}, \mathbf{t_i}, \mathbf{D}^{(s)}, \mathbf{p}^{(s)}) \tag{6}$$

The second part, in Equation (11), $\psi(\mathbf{p})$ is the log-likelihood which accounts for the person parameter. It requires less computation time.

$$\psi(\mathbf{p}) = \sum_{i=1}^{N}\sum_{k=1}^{K}\sum_{l=1}^{L}\sum_{m=1}^{M} log\pi_{kl}f(q_k, u_l, v_m \mid \mathbf{y_i}, \mathbf{t_i}, \mathbf{D}^{(s)}, \mathbf{p}^{(s)}) \tag{7}$$

Once the two parts are calculated, one can calculate the joint-distribution function of $f(y_{ij}, t_{ij} \mid q_k, u_l, v_m, \mathbf{d}_j)$.

3   Parallel Implementation

3.1   Domain Decomposition and Message Communication

In the proposed item-response model with EM algorithms, the major computation of parameter estimates is based on the maximization the observed data likelihood, given by Equation (5). The first part is $\phi(\mathbf{D})$. Based on the previous experience, it takes most of the computation time. The second part is $\psi(\mathbf{p})$. It also takes time, but not as much as the first term in Equation (5). There are two approaches we can use.

After task decomposition, we conducted the second-layer data decomposition. On total summation, the domain is decomposed into several sub-domains on which each sub-summation will be performed on a single processor, for example,

$$\phi(\mathbf{D}) = \sum_{np=1}^{NP}\{\sum_{j=1}^{J_{np}}\sum_{i=1}^{N_{np}}\sum_{k=1}^{K_{np}}\sum_{l=1}^{L_{np}} log[f(y_{ij}, t_{ij} \mid q_k, u_l, \mathbf{d}_j)]f(q_k, u_l \mid \mathbf{y_i}, \mathbf{t_i}, \mathbf{D}^{(s)}, \mathbf{p}^{(s)})\} \tag{8}$$

$$(J = \sum_{np=1}J_{np}; N = \sum_{np=1}N_{np}; K = \sum_{np=1}K_{np}; L = \sum_{np=1}L_{np})$$

We may also try to decompose partial summation in different manors such as

$$\phi(\mathbf{D}) = \sum_{j=1}^{J}\{\sum_{np=1}^{NP}\sum_{i=1}^{N_{np}}\sum_{k=1}^{K_{np}}\sum_{l=1}^{L_{np}} log[f(y_{ij},t_{ij}\,|\,q_k,u_l,\mathbf{d}_j)]f(q_k,u_l\,|\,\mathbf{y_i},\mathbf{t_i},\mathbf{D}^{(s)},\mathbf{p}^{(s)})\} \quad (9)$$

We are studying the effects of different data-decomposition in terms of computational time, speedup, and efficiency.

Similarly, we can parallel the computation for the second part. In this domain decomposition algorithm, the load balance between the computations for (D) and $\Psi(\mathbf{p})$ on different HPC clusters should be taken into consideration. However, it should provide significant improvement in the efficiency of computations. In addition, since the computations between $\Phi(D)$ and $\Psi(\mathbf{p})$ are loosely coupled, this computation can be deployed on distributed environments with less concern of network latency. It can be a successful application for a computational grid.

The parallel implementation can be processed using C/C++ with Message Passing Interface (MPI), a parallel library to access the communications between computational processors. Since there is less communication between processors, we can experiment block/non-block communication, and definitely gather/scatter functions to ensure data communication between the master node and the computational nodes. The sub-summation can be operated by computational node and total summation result can be integrated together by master node.

3.2 Analysis of HPC Benchmark Performance and Preliminary Research

The parallel speedup can be estimated by the following simple expression

$$T_{sq} = T_{sq}^{\Phi} + T_{sq}^{\Psi} = T_{input,sq}^{\Phi} + T_{sum(j,i,k,l),sq}^{\Phi} + T_{input,sq}^{\Psi} + T_{sum(i,k,l),sq}^{\Psi}$$
$$T_{pa} = T_{pa}^{\Phi} + T_{pa}^{\Psi} = T_{input,pa}^{\Phi} + T_{sum(j,i,k,l),ps}^{\Phi} + T_{com,ps}^{\Phi} \quad (10)$$

Where T is the time used to accomplish a task. The subscripts *sq* and *pa* stand for sequential and parallel times, and the subscripts *sq* and *pa* stand for sequential and parallel computing; the subscripts *input*, *sum* and *com* refer to stands for input data, summation (major computation), and data or message communication. The parallel speedup can then be calculated as

$$s_{np} = \frac{T_{sq}^{\Phi} + T_{sq}^{\Psi}}{T_{pa}^{\Phi} + T_{pa}^{\Psi}} \approx \frac{T_{sq}^{\Phi} + T_{sq}^{\Psi}}{T_{pa}^{\Phi}} = \frac{T_{input,sq}^{\Phi} + T_{sum(j,i,k,l),sq}^{\Phi} + T_{input,sq}^{\Psi} + T_{sum(i,k,l),sq}^{\Psi}}{T_{input,pa}^{\Phi} + T_{sum(j,i,k,l),ps}^{\Phi} + T_{com,ps}^{\Phi}} \quad (11)$$

We can set $T_{pa}^{\Psi} = \gamma T_{pa}^{\Phi}$, where γ is the ratio of computation time used for item parameter likelihood distribution(s) and the one used for the person parameter distribution. In general, since $\gamma \ll 1$, and if we distribute the computation of T_{pa}^{Ψ} on another HPC system, the speedup can be simplified as

$$s_{np} \approx \frac{T_{sum(j,i,k,l),sq}^{\Phi} + T_{sum(i,k,l),sq}^{\Psi}}{T_{sum(j,i,k,l),ps}^{\Phi} + T_{com,ps}^{\Phi}} = \frac{T_{sum(j,i,k,l),sq}^{\Phi} + T_{sum(j,i,k,l),sq}^{\Phi}/N}{T_{sum(j,i,k,l),sq}^{\Phi}/n_p + T_{com,ps}^{\Phi}} \quad (12)$$

where n_p is the total number of processors of the first HPC Cluster. The estimation of speedup can be expressed as

$$s_{np} \approx \frac{(1+1/N)}{1+\omega n_p} n_p \qquad \omega = T^{\Phi}_{com,ps} / T^{\Phi}_{sum(j,i,k,l),sq} \qquad (13)$$

where the ω is the ratio of time required for data communication and the time used to calculate the total summation in sequential computing. In general, N is in the range of 1000-5000 and $1/N$ is relatively small. The parallel speedup totally depends on the value of n_p and ω. Based on the previous experience, the ratio ω is also very small. The parallel speedup should be in linear increase. Fig. 1(a) plots the speedup vs. the number of processors used when ω takes different values. The smaller the ω value is, the better the performance using parallel computing. Since N ranges from 1000 to 5000, its influence on the parallel performance can be eliminated. The ω strongly influences the parallel performance. Fig. 1(b) plots the corresponding parallel efficiency vs. the number of processors employed. For a low value of ω, the performance is better. In the EM-based algorithm, the communication is relatively low, and data communication does not dominate the computation and computation is very intensive. This is idealized case for parallel computing. That is because the major computation in each simulation of calibration is based on discrete integration. However, the correlation of the distribution function may require extra compensation time.
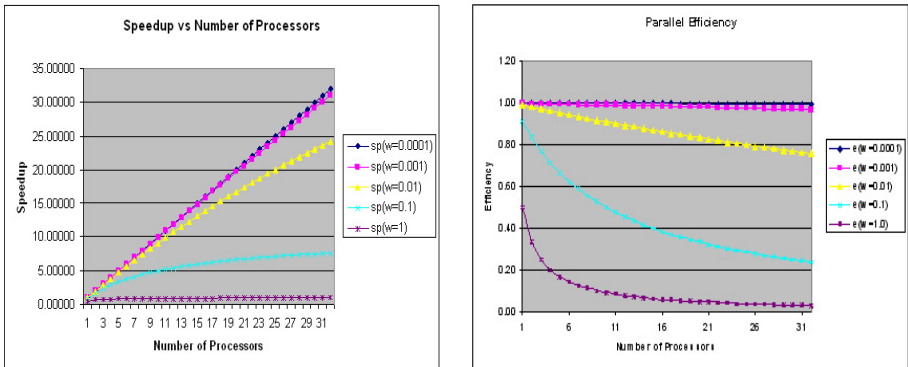
Fig. 1. (a) Estimation of speedup vs. number of processors with N=1000, and =0.0001, 0.001, 0.01, 0.1, 1.0, respectively; (b) Estimation of parallel efficiency vs. number of processors with N=1000, and =0.0001, 0.001, 0.01, 0.1, 1.0, respectively

4 Conclusion

This paper first addresses an interdisciplinary paradigm that integrates computer science and psychometric research that can be applied to computerized testing. The paper presents a parallel analysis of HPC-based the response time data available in computerized testing. Such a model not only improves the measurement precision of

traditional academic ability traits, but also provides valuable information about the examinees' other personality traits such as their problem-solving speed and decision-making strategies. Thus, this line of research and practice can potentially broaden the educational value of computerized testing. One critical phase of developing such item response models is to develop the calibration procedure and evaluate its precision using HPC resources. With the additional person parameters needed to model response time, the simulation of EM algorithm-based calibration procedure can be feasible. The implementation of parallel-algorithm-based simulation in computerized testing studies serves as a pioneer effort in to promote HPC-powered psychometric modeling and computerized testing.

References

1. Bloxom, B.: Considerations in Psychometric Modeling of Response time. Psychometrika. 50. (1985) 383-397
2. Roskam, E. E.: Models for Speed and Time-limit Tests. In W. J. van der Linden & R. K. Hambleton (Eds.). Handbook of Modern Item Response Theory New York: Springer. (1997) 187-208
3. Schnipke, D. L., Scrams, D. J.: Exploring Issues of Examinee Behavior: Insights Gained from Response-time Analyses. In the ETS colloquium on "Computer Based Testing: Building the Foundation for Future Assessment." September 25-26. Philadelphia, PA. (1998).
4. Schnipke, D. L., Scrams, D. J.: Modeling Item Response Times with a Two-state Mixture Model: A New Method of Measuring Speediness. Journal of Educational Measurement, 34, (1997) 213-232
5. Thissen, D.: Timed Testing: An Approach Using Item Response Theory. In New horizons in Testing: Latent Trait test Theory and Computerized Adaptive Testing. D. J. Weiss (Ed.). New York: Academic Press. (1983) 179-203
6. Van Breukelen, G. J. P.: Concentration, Speed, and Precision in Mental Tests. Unpublished Doctoral Dissertation, University of Nijmegen, Netherlands. (1989)
7. Verhelst, N. D., Verstralen, H. H. F. M., Jansen, M. G. H.: A logistic Model for Time-limit Tests. In W. J. van der Linden and R. K. Hambleton (Eds.). In Handbook of Modern Item Response Theory. New York: Springer (1997) 169-185
8. Wang, T. A Model for the Joint Distribution of Item Response and Response Time using a One-Parameter Weibull Distribution. CASMA Research Report, No. 20. Iowa City, IA. CASMA. (2006) (http://www.education.uiowa.edu/casma/documents/20td4plrt.pdf)
9. Wang, T. Hanson, B. A.: Development and Calibration of an Item Response Model that Incorporates Response time. Applied Psychological Measurement. 29 (2005) 323-339
10. Wang, T. Zhang, J.: Optimal Partitioning of Testing Time: Theoretical Properties and Practical Implications. Psychometrika. 71 (2006) 105-120
11. Woodruff, D. J., Hanson, B. A.: Estimation of Item Response Models Using the EM Algorithm for Finite Mixture. ACT Research Report 96-6 Iowa City, IA: ACT, Inc. (1996)

Resource Load Balancing Based on Multi-agent in ServiceBSP Model[*]

Yan Jiang[1], Weiqin Tong[1], and Wentao Zhao[2]

[1] School of Computer Engineering and Science, Shanghai University
[2] Image Processing and Pattern Recognition Institute, Shanghai Jiao Tong University
Shanghai, China
jiangyan2273@hotmail.com, wqtong@mail.shu.edu.cn,
zhaowt1982@hotmail.com

Abstract. Based on ServiceBSP model, a resource load balancing algorithm with Multi-Agent is put forward in this paper which achieves the goal of dynamic load balancing and favorable fault-tolerant. The algorithm calculates the load value according to the status of usage of resources of a node and scheduling tasks relies on the load value, while updating the load information dynamically depending on Multi-Agent. The method also can avoid frequent communications on load information. Furthermore, the paper introduces the function of agents, relations and communications among agents in details. Finally, by comparing response time and distribution of load using proposed method with other available methods such as without no load balancing and load balancing only based on the usage of CPU, the experimental simulation shows that the load balancing based on Multi-Agent possesses superior performance on response time and load balancing.

Keywords: ServiceBSP model , Multi-Agent, Load balancing.

1 Introduction

The problem of load balancing often occurs in some applications of parallel computing. Reasonable load balancing algorithm should be able to improve system throughout and reduce task response time. Many load balancing algorithms designed to support distributed system have been proposed and reviewed in the literature [1][2] [3][4], only a few have been designed or are scalable to support load balancing of all types of resources, which are inclined to cause the occurrence of unbalance of different types of resources in a node(mainly means the computer). In the distributed system, the arrival of task is a dynamic process that sometimes can not be predicted, which indicates that dynamic load balancing is required. Meanwhile, we should know the point that nodes have freedom to join in or leave the queue of providing services. So the method of dynamic load balancing should bear the characteristic of reliability.

ServiceBSP model combines parallel computing model BSP and the concept of service [5]. In the model, we abstract all the resources to services. In the reference [6], the author propounds the ServiceBSP model based on QoS(quality of service) that can satisfy the needs of users. Our method also possesses these advantages.

In this paper, we have developed a load balancing algorithm based on Multi-agent which successfully balances the usage of types of resources. It not only considers the usage ratio of CPU and other types of resources in the precondition of satisfying the needs of users, but also solves the problem of robustness in the process of providing services, avoiding frequent information transfer.

This rest of this paper is organized as follows: ServiceBSP model is shown in Section 2. In Section 3, the load balancing algorithm is proposed and described in details. The application of Multi-agent in load balancing is introduced in Section 4. Section 5 presents experimental simulation results, and Section 6 concludes the paper.

2   ServiceBSP Model

In view of characteristics of distributed system short of providing stable QoS, we advocate ServiceBSP model considering the advantages of BSP model [7][8]. An application is firstly divided into several tasks according to their intrinsic properties because of its loose coupled characteristic and tasks are executed in parallelism.

All the node providing services should publish information of their services to a searchable registry of services description and update it. Such information includes functional performance, physical location, availability and price etc.

Fig.1 shows a superstep of the model.

In the Fig.1, Broker Mediator is responsible to interact with Coordinating Agent. Broker assumes the responsibility to select services satisfying needs of users from the center of service registry while giving consideration to the physical location and
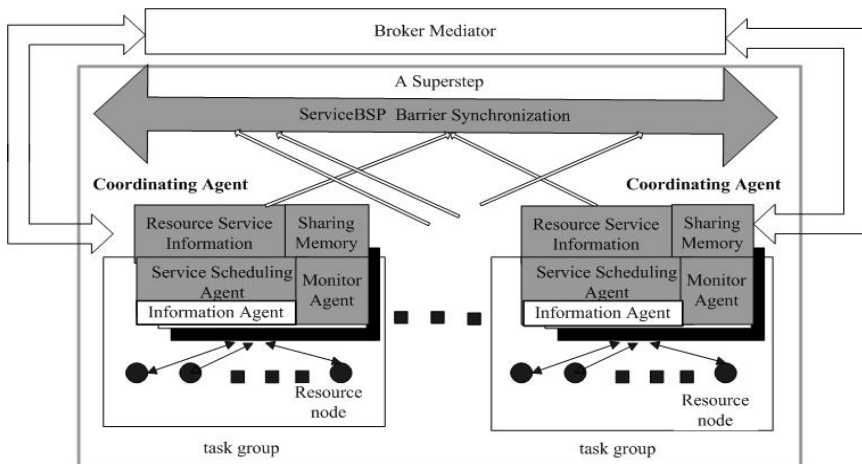
Fig. 1. A superstep of ServiceBSP model

pertinence among services. Then Broker maps the information of selected services to correspondingly initialized Coordinating Agent with the help of Mediator.

3   Load Balancing in ServiceBSP Model

3.1   Resource Load Balancing Algorithm

Load balancing is demand driven issue. The dynamic load balancing we are proposing is based on a load rank of nodes, and then Service Scheduling Agent sends the new task to the currently lightest node. In our method, we assess the load of all the nodes relying on dynamic load value. We calculate the value taking such factors into account as CPU, memory resource, number of current tasks, response time, the number of network link etc.

We define M_j that represents the weight of resource j of a node that a task required, and there$\Sigma M_i=1$. In the view of different types of tasks, the weight of M_j varies according to the features of diverse tasks. For example, task with high weight of memory resource emphases the necessity of memory.

Suppose that we only include above referred attributes. A load value of a node owning only one task can be described by follow formula.

$$V_i = M_1 * V_{cpu} + M_2 * V_{mem} + M_3 * V_{io} + M_4 * V_{tasks} + M_5 * V_{network} + M_6 * V_{response} \qquad (1)$$

V_{cpu}, V_{mem}, V_{io}, V_{tasks}, $V_{network}$, $V_{response}$ respectively represent the usage ratio of CPU, the usage of memory, the number of current tasks, the number of network links, response time. So the load value of a node owning several tasks is V where $V = \Sigma V_i$. Using the current load value V, we can calculate new value when a new task is joining.

The algorithm described above is preferable algorithm with view to the dynamic load balancing of all the nodes in system and types of tasks. In addition, the algorithm is characterized as simplicity and so it would not cause extra cost of system.

3.2   Fault-Tolerant in Load Balancing

We have referred that the nodes have no restrictions to join in or leave the queue of providing services. Therefore ensuring robust and reliable services when we adopt effective method to maintain load balancing is an important issue. Our paper succeeds in solving this issue using Agent technology.

Monitor Agent would discover abrupt change while a node leaves the queue because of fault or other reasons, and then select alternative node ranked as the lightest load from the Resource Information Service. Even with extra time cost, restarting to execute the failed task is preferable to the termination of the task.

4   Application of Multi-agent in Load Balancing

In the Fig.1, we have a general description of Coordinating Agent. The relations among agents and of these agents with other modules in one task group are illustrated in Fig.2.
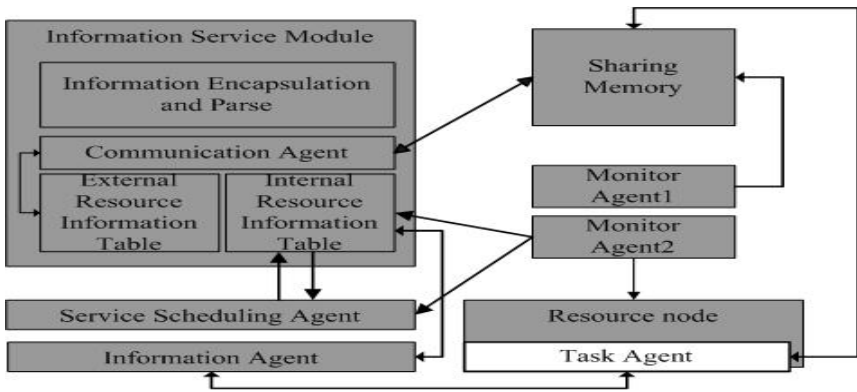
Fig. 2. Relation of Multi-Agent

4.1   Load Balancing Based on Multi-Agent

Fig.2 shows that Coordinating Agent provides such services as node information, monitoring node, communication and scheduling tasks. The interpretation of detailed functions of those modules in Fig.2 is as follows:

External Resource Information Table: The Table stores the information of other Coordinating Agent and makes preparing information of targets for the global communication following a local computation in a superstep.

Internal Resource Information Table: The Table stores the information of all the nodes in a task group including the physical location, logic ID, capability, AgentID, port and load value etc.

Communication Agent: The Communication Agent initializes the interaction with other Coordinating Agent after reading data from Sharing Memory in the end of local computation step. The information sent by Communication Agent can be understood by other Coordinating Agent through Information Encapsulation and Parse Module.

Information Encapsulation and Parse Module: The function of this module is that using XML encodes KQML communication language and describes content in forms of XML documentation after Agent sends message [11]. Similarly, it parses and analyzes the content before Agent receives message.

Task Agent: It is responsible for calculating the dynamic load value for minimizing the frequency of communication between node and Resource Information Service Module. It also reads and writes data in Sharing Memory as representative of node.

Information Agent: The works of receiving the load value of a node and monitoring the information on whether the node is alive or not are assigned to Information Agent. In order to get the valid load value Information Agent should update Internal Resource Information Table timely when monitoring changes.

Service Schedule Agent: It manages to schedule tasks to proper nodes according to the rank of load value by reading the load value from Internal Resource Information Table.

Sharing Memory: Communications in a task group are completed through Sharing Memory rather than the normal direct way. Sharing Memory is also where the data required by global communication are stored.

Monitoring Agent1: It monitors communications occurring in Sharing Memory. For example, Task Agent representative of task A in one node sends data to Sharing Memory, then Monitoring Agent informs Task Agent representative of task B in another node to read these data from Sharing Memory. In addition, it should make sure that a Task Agent has legal right to modify data in Sharing Memory avoiding bringing invalid data.

Monitoring Agent2: Monitoring Agent2 is designed to monitor the status of node for supporting robustness of ServiceBSP model. If nodes encounter abrupt failure or apply to leave the queue of providing services, Monitoring Agent2 would monitor these changes and then update Internal Resource Information Table. Finally, it selects an alternative node with lightest load to execute the discontinued task.

4.2   Agent Communication

In our ServiceBSP model, we suggest two modes of communications among agents [9][10]. One mode concerning agents in the same task group occurs in Sharing Memory. Global communication is attributable to another mode relative to different task groups, meaning direct communication from one point to another point.

The first mode of communication mainly consists of four operations: read data, write data, delete data and modify data. All the operations are supervised by Monitoring Agent.

Up to the point, we have assumed that load value of nodes serves as the criteria for scheduling tasks in order to acquire the goal of load balancing. The load value will update while a new task coming in. The Task Agent of such node that receives a new task assumes the duty to inform the dynamic load value to Internal Resource Information Table immediately, which actually ensures the load balancing.

The second mode of communication adopts the Knowledge Query and Manipulation Language (KQML) to support comparatively massive communications among Coordinating Agents [11]. We argue for an XML encoding of KQML and expressing communications content. It is required that the KQML messages parsed by the Information Encapsulation and Parse Module in Coordinating Agent of target, are separated from XML document, so we can analyze and understand the meaning of these messages.

5   Simulation and Discussion

The experimental simulation is configured with nine task queues, illustrated by the set shown in Table1.These task queues are named *S1……S9* and represent different queues with different characteristics including different number of big, middle and small tasks

giving more or less emphasis to CPU or memory. The characteristics of these task queues are found in Table 1. Three figures in parenthesis are representative of the numbers of big, middle, small tasks orderly. The task with higher CPU value represents the one giving more emphasis on CPU than memory, whereas, the task with higher memory value emphasizes memory.

Table 1. Task queues

Queue NO.	Total numbers of tasks	Numbers of tasks with high CPU value	Numbers of tasks with high memory value
S1	(5,5,5)	(5,5,5)	(0,0,0)
S2	(5,5,20)	(4,3,15)	(1,2,5)
S3	(5,10,15)	(5,5,2)	(0,0,13)
S4	(5,15,10)	(4,5,6)	(1,10,4)
S5	(5,20,5)	(3,6,1)	(2,14,4)
S6	(5,20,20)	(1,13,14)	(4,7,6)
S7	(15,5,15)	(0,0,0)	(15,5,15)
S8	(15,10,10)	(10,7,6)	(5,3,4)
S9	(20,5,5)	(16,3,3)	(4,2,2)

We made several measurements of response time of task execution, which can be divided into three categories: load balancing algorithm only based on CPU, load balancing algorithm based on load value, and no load balancing algorithm. Then we contrast the distribution of load of CPU and memory in a task group including five nodes when respectively adopting load balancing based on load value and no load balancing algorithm. The results of simulation are shown in Fig.3 and Fig. 4.
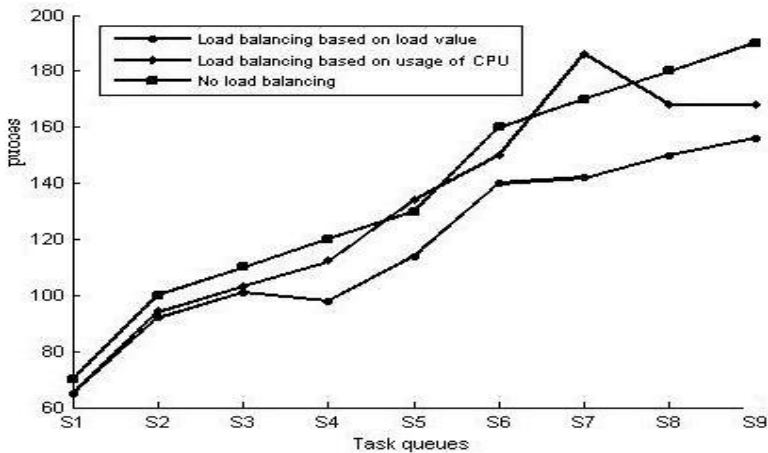
Fig. 3. Contrast of response time
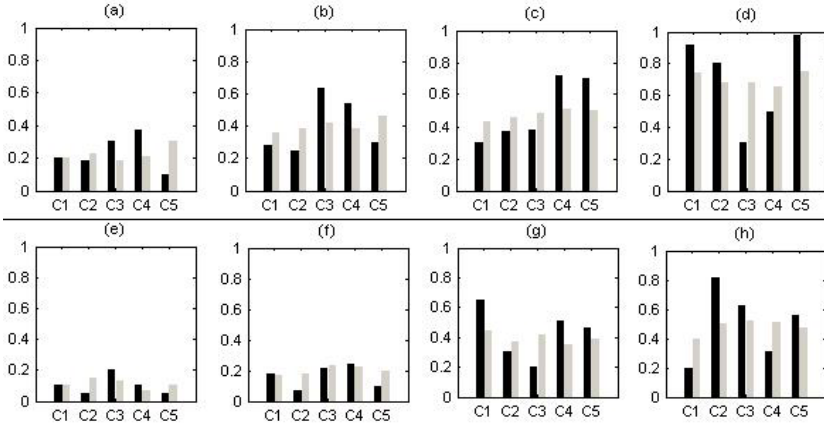
Fig. 4. Contrast of distribution of CPU and memory load

We present results obtained through Fig.3 and Fig.4. Fig.3 illustrates how the load balancing methods performed by contrasting response time. The results obtained in such model with load balancing algorithm based on load value illustrates less response time compared with adopting no balancing algorithm and only based on usage of CPU. Commonly, system with no load balancing algorithm needs longer response time than with load balancing algorithm only based on the usage of CPU. However, if most tasks in task queue with high memory value, sometimes it is better to use no balancing algorithm than the algorithm only based on the usage of CPU.

Fig.4 demonstrates the distribution of memory and CPU load. In the figure, the black and the grey cylinders respectively represent the load distribution in the condition of model with load balancing algorithm based on load value and with no load balancing. (a),(b),(c),(d) represent the distribution of CPU load of a task group including five nodes named C1,C2,C3,C4,C5 in picture while task queues S1,S3,S5,S8 assigning to this task group. (e),(f),(g),(h) present the distribution of memory load. Apparently, a system adopting load balancing algorithm based on load value ensures the balancing distribution of CPU and memory load in five nodes.

6   Conclusion

In this paper, we have proposed a load balancing algorithm based on Multi-Agent in ServiceBSP model. It ensures load balancing and satisfies the needs of users in distributed system. Our method successfully avoids frequent communications between agents when aiming at the goal of dynamic load balancing. The experimental simulation shows that it realizes dynamic load balancing and speed up response time of tasks.

References

1. Wang, Y.T., Morris, R.J.T.: Load sharing in distributed systems. IEEE Trans. Comput., vol. C-34, pp. 204-211, Mar. 1985
2. Fox, G.C.: A review of automatic load balancing and decomposition methods for the hypercube. California Institute of Technology, C3P-385, Nov. 1986
3. Ramamritham, K., Stankovic, J.A., Zhao, W.: Distributed scheduling of tasks with deadlines and resource requirements. IEEE Trans.Comput., pp. 1110-1123, Aug. 1989
4. Baumgartner, K.M., JSling, R.M., Wah, B.W.: Implementation of GAMMON: An efficient load balancing strategy for a local computer system. in Proc. I989 Int. Conf Parallel Processing, vol. 2, Aug. 1989,pp. 77-80
5. Foster, I., Kesselman, C., Nick, J.M., Tuecke, S.: The Physiology of the Grid: An Open Grid Services Architecture for Distributed Systems Integration. Downloadable as: http://www.globus.org/research/papers/ogsa.pdf, 2002
6. Zhu, J.Q., Tong, W.Q., Dong, X.J.: Agent Assisted ServiceBSP Model in Grids. GCC2006
7. Valiant, L.G.: A bridging model for parallel computation. Communications of the ACM, 33(8), (1990) 103~111
8. Song, J., Tong, W.Q., Zhi, X.L.: QOS-BASED PROGRAMMING METHOD IN GRID ENVIRONMENT. Computer application and software. Vol 23.No.10
9. Hyacinth S.N.: Software Agents: An Overview, Knowledge Engineering Review. Vol. 11, No 3, pp. 205-244, October/November 1996
10. Michael, R.G., Steven, P.K.: Softwareagents: Communications of the agent. ACM, 37(7):48–53,147, 1994
11. Yannis, L., Tim, F.: A semantics approach for KQML. In Third International Conference on Information and Knowledge Management, November 1994

Group-Based Key Management for Multicast of Ad Hoc Sensor Network*

Shaobin Cai, Wenbin Yao, NianminYao, Yong Li, and Guochang Gu

Harbin Engineering University, Harbin, China, 150001
Phone: 86-451-82518030
caishaobin@hrbeu.edu.cn

Abstract. In order to protect communication security among sensor nodes, a cryptographic method are needed by ad hoc sensor networks. According to that most ad hoc sensor networks are deployed in groups, a group-based multicast key management scheme is proposed to extend RPS scheme in this paper. Compared with RPS, our scheme improves the probability that a shared key exists between two sensor nodes, and reduce the probability that the shared key is decrypted.

Keywords: Ad hoc sensor networks, Security, Group-based, Key Management.

1 Introduction

The open architectures of ASNs (ad hoc sensor networks) make potential intruder easy to intercept, eavesdrop and fake messages. Therefore, they need strong security services. Most security methods can be realized by message encryption. Therefore, some kinds of cryptographic keys that need to be shared between the communicating parties are needed.

The pre-loaded key management of ad hoc sensor network, proposed by Blom [1], efficiently solves the key management for broadcast and multicast [2-5] of ad hoc sensor network. N-security r-conference key management scheme [6~10] is a typical pre-loaded key management scheme.

Since ad hoc sensor networks are mostly deployed in groups, the communications among nodes are mostly happened among nodes of same group. Therefore, a group-based multicast key management scheme is proposed in this paper to improve the probability that two nodes share at least one key.

The rest of the paper is organized as follow. First, an overview of n-secure r-conference key management scheme is given in section 2. Secondly, a group-based

---

key management for multicast of ad hoc sensor network is proposed in section 3. Thirdly, the performance of group-based scheme is analyzed by mathematical method and simulations in section 4. Finally, we draw a conclusion in section 5.

2   RPS Key Management Scheme

RPS [10] (Random Preloaded Subset key distribution) scheme is proposed as an n-security r-conference key management. RPS determines the public key of each node by a public one way function $F_1()$, which is defined as follow:

$$|I_1 \cdots I_k| = F_1(A) \tag{1}$$

In the above formula, $1 \leq I_1 \cdots I_k \leq P$ is a random permutation of numbers between 1 and P. For instance, it could be obtained by choosing the first k elements of a random permutation of numbers between 1 and P. $I_1 \cdots I_k$ is the index of the keys preloaded in node A. By exchanging their IDs, two nodes can immediately determine their shared indices, and use their shared keys to derive their pair key. For an r-user conference, the r nodes can independently calculate their conference key based on the keys shared by all r nodes.

3   Group-Based n-Security r-Conference Key Management Scheme

In this section, GBKM (Group-Based Key Management) is proposed to extend RPS. In GBKM, keys preloaded in a node are not only tied to its public ID but also to its group ID. Therefore, GBKM not only has a one way public function $F_1()$ but also has a public one way group function $Fm(i)$, which is defined as follow:

$$|I_1 \cdots I_z| = Fm(i) \tag{2}$$

In the above formula, $1 \leq I_1 \cdots I_Z \leq P$ is a random permutation of numbers between 1 and P, and it is a subset A_i of A. When a node acquires its pre-loaded keys, it first calculates out the subset for its group by its group function $F_m()$ with its group ID, and then it calculates out its key from the key subset of group by function $F_1()$.

Therefore, in GBKM, any r nodes of same group can determine whether there exists at least a shared key among them after they exchange their group ID and their public ID. Although, the probability that two nodes of same group share at least one key is improved by the method above, the probability that two nodes of different groups share at least one key is still low. In order to improve the probability that two nodes of different groups share at least one key, they broadcast its received group ID and node ID in its group when two nodes of different groups want to setup a session and do not have any shared key. If one node of its group has shared keys, then it forwards the shared key to the node. Therefore, the probability that two nodes of different groups share at least one key is improved and is equal to that two groups share keys.

4 Analysis

4.1 The Probability That Two Nodes Share at Least One Keys

Let p be the probability that two nodes of same group share at least one key. The probability that two key rings share at least one keys is equal to $1 - \Pr$ [two nodes do not share any key]. Therefore, we first compute the number of the possible key rings. Since each key of a key ring is drawn out of a pool of P keys without replacement, the number of possible key rings is $\dfrac{P!}{k!(P-k)!}$.

After picking out the first key ring, the total number of possible key rings that do not share a key with the first key ring is the number of key rings that can be drawn out of the remaining P-k unused key in the pool, namely $\dfrac{(P-k)!}{k!(P-2k)!}$.

Therefore, the probability that no key is shared between the two rings is the ratio of the number of rings without a match by the total number of rings. Thus, the probability that there is at least a shared key between two key rings is

$$p = 1 - \frac{k!(P-k)!}{P!} \times \frac{(P-k)!}{k!(P-2k)!} = 1 - \frac{((P-k)!)^2}{(P-2k)!P!} \qquad (3)$$

Since P is very large, Stirling's approximation $n! \approx \sqrt{2\pi}\, n^{n+\frac{1}{2}} e^{-n}$ is used to simplify the expression of p, and obtain: $p = 1 - \dfrac{(1-\dfrac{k}{P})^{2(P-k+\frac{1}{2})}}{(1-\dfrac{2k}{P})^{(P-2k+\frac{1}{2})}}$. Since the size of sub-

pool is much smaller than that of pool, the probability that a shared key exists between two sensor nodes of the same group is improved by our scheme.

Figure 1 describes the relationship between the size of ring and the probability that two nodes share at least one key. When pool has 10,000 keys and key ring has 75 keys, the probability of Laurent's scheme that two node share at least one key is only about 0.5. However, the probability of our scheme that two nodes share at least one key is almost about 1 when each sub-pool of our scheme has 1,000 keys.

p' is used to present the probability that a shared key exists between two nodes of different groups, whose sub-pools have P' keys. Each group can draw $\dfrac{P!}{P'!(P-P')!}$ sub-pools from its main pool. Therefore, probability that a shared key exists between two nodes of different groups is

$$p = 1 - \frac{P'!(P-P')!}{P!} \times \frac{(P-P')!}{P'!(P-2P')!} = 1 - \frac{((P-P')!)^2}{(P-2P')!P!} \qquad (4)$$

From the results showed in fig. 1, we can know that the probability, which two nodes of different groups have at least one key, is almost 100% when sub-pool has more than 200 keys. Therefore, GBKM can be improved further by reduce the scope of exchanging group ID and node ID when two nodes belong to different groups. In
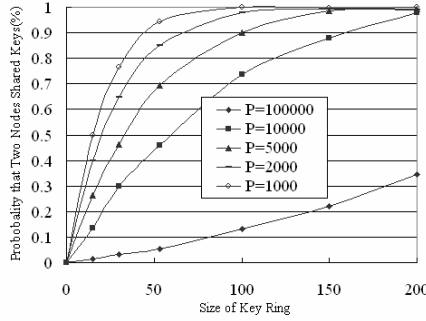
Fig. 1. The relationship between the size of ring and the probability that two nodes share a key

the improved GBMK, the node only exchange group ID and node ID with its neighbors of the same group.

Now, the probability that r nodes share at least one key is calculated. If there is at least a shared key among r nodes, then the intersection $A_k^1 \cap \cdots \cap A_k^r$ is not empty. Therefore, $PS_m^r = \Pr\{|A_k^1 \cap \cdots \cap A_k^r| = m\}$ is first calculated for the probability that $A_k^1 \cap \cdots \cap A_k^r \neq \varnothing$. Therefore, $PS^r \leq (p)^{r-1}$ and r nodes hardly have shared keys when p is small. Therefore, it is necessary to improve the probability that two nodes share at least one key.

4.2 Security

In this section, the security of GBKM is analyzed. The communications among r nodes are safe only when $\exists a \in A_k^1 \cap \cdots \cap A_k^r$ and $a \notin A_k^{r+1} \cup \cdots \cup A_k^{R+n}$. Therefore, $PE_R(P,k,n,r)$ is used to present the probability that r-node communications can be eavesdropped by n nodes, and PS_m^r is calculated first to calculate $PE_R(P,k,n,r)$.

The calculation complexity of PS_m^r increases when r increases and it can not be calculated when r is much larger. Therefore, ϕ_r is used here to present expected m, namely

$$\phi_r = E[m] = \sum_{m=1}^{k} mPS_m^r = k(\frac{k}{P})^{r-1} \tag{5}$$

Therefore, the larger the $\dfrac{k}{P}$ is, the higher probability that r nodes share at least one key. Fig.2 descries the relationship between $\phi_r(r=5)$ and the size of ring. In fig.2, when $\dfrac{k}{P}$ is larger, smaller key ring can guarantee r nodes share at least one key; when $\dfrac{k}{P}$ is smaller, larger key ring is even can not guarantee r nodes share at least one key. Therefore, it is necessary to improve probability that r nodes share at least
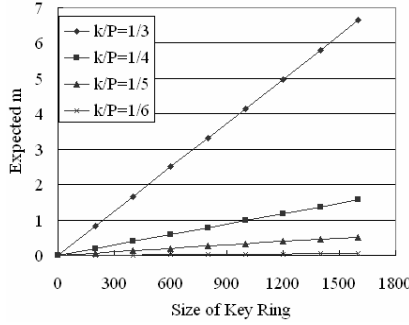
Fig. 2. The relationship between $\phi_r(r = 5)$ and the size of ring

one key by the improvement of $\dfrac{k}{P}$, which is resulted from group-based key management.

Secondly, $PC_{n,k}^q = \Pr\{|A_k^1 \cup \cdots \cup A_k^n| = q\}$ is used here to present the probability that $A_k^1 \cup \cdots \cup A_k^n$ has q keys, where $k \le q \le q_{max} = \min(nk, P)$.

The calculation complexity of PS_m^r also increases when r increases, and PS_m^r cannot be calculated when r is much larger. $\theta_n = E[q] = \sum_{q=k}^{q_{max}} qPC_{n,k}^q$ is used here to present expected q. The value of θ_n can be calculated by recursion, and θ_n is defined as follow:

$$\theta_n = \theta_{n-1} + \frac{k}{P}(P - \theta_{n-1}), \quad \theta_0 = 0 \tag{6}$$

$\theta_n' = \dfrac{\theta_n}{P} = \theta_{n-1}' + \dfrac{k}{P}(1 - \theta_{n-1}')$ is used here to present expected $\dfrac{q}{P}$. Fig.3 descries the relationship between θ_n' and the number of nodes captured by the adversaries. The larger $\dfrac{k}{P}$ is, the lower the security of r nodes communications is, and the easier the adversity can acquire all keys by capturing few nodes. The smaller $\dfrac{k}{P}$ is, the higher the security of r nodes communications is, and the more difficult the adversities acquire all keys by capturing few nodes.

However, from the analysis results in fig3, we know that a higher $\dfrac{k}{P}$ is needed by a key management scheme to guarantee that there is at least one shared keys among r nodes. When adversity does not know the adscription of the nodes, $P = |U_g| (U_g$ presents the sub-pool)in equation (5) mostly, and $\dfrac{k}{P}$ is larger; $P = |U_p|$ in equation
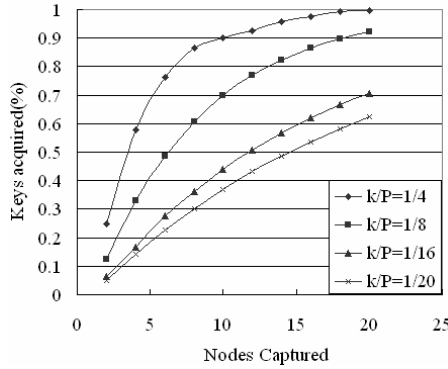
Fig. 3. The relationship between θ_n' and the number of nodes acquired by adversity

(7), and $\dfrac{k}{P}$ is smaller. Therefore, group-based key management not only improves the probability that r nodes share at least one key, but also reduces the probability that the shared keys are decrypted.

Thirdly, $PE_m^q = \Pr\{A_m \subset A_q\}$ is used here to present the probability that $A_m \subset A_q$, where $A_m \subset U_p$ $(|A_m| = m)$ and $A_q \subset U_p$ $(|A_q| = q)$. Therefore,

$$PE_m^q = \frac{\dbinom{P-m}{q-m}}{\dbinom{P}{q}} = \frac{(P-m)!\,q!}{(q-m)!\,P!} \tag{7}$$

$PE_R(P,k,n,r) = \Pr\{G \subset B\}$ is used here to present the probability that $G \subset B$, where $G = A_k^1 \cap \cdots \cap A_k^r$ and $B = A_k^{r+1} \cap \cdots \cap A_k^{n+r}$. Therefore, $PE_R(P,k,n,r)$ can be expressed further as follow

$$PE_R(P,k,n,r) = \sum_{q=k}^{q_{max}} PC_{n,k}^q \sum_{m=0}^{k} PS_m^r PE_m^q \tag{8}$$

$PC_{n,k}^q$ is hardly calculated when $n \geq 3$. Hence, an approximation of $PE_R(P,k,n,r)$ should be calculated, and equitation (8) can be defined further as follow:

$$PE_R(P,k,n) \approx \hat{P}E_R(P,k,n) = \sum_{m=0}^{k} PS_m^r PE_m^{\theta_n} \tag{9}$$

By the method that the approximation of $PE_R(P,k,n,r)$ is calculated when $n \geq 3$, the approximation of $PE_R(P,k,n,r)$ can be acquired when r is larger. Therefore, $PE_R(P,k,n,r)$ can be defined as follow:

$$PE_R(P,k,n,r) \approx \hat{PE}_R(P,k,n,r)$$

$$= \sum_{q=k}^{q_{max}} PC_{m,k}^q PE_{\phi_r}^q \approx \ddot{PE}_R(P,k,n,r)$$

$$= PE_{\phi_r}^{\theta_m} = \frac{(P-\phi_r)!\theta_m!}{(\theta_m-\phi_r)!P!} \tag{10}$$

$\phi_r = i$, and $PE_R^i(P,k,n,r)$ is used to present the probability that the r node communications are eavesdropped. Therefore, $PE_R^1(P,k,n,r) = \theta'_m$, $PE_R^2(P,k,n,r) = \theta'_m \frac{(\theta_m-1)}{(P-1)}$. Hence, the probability that r nodes communications are eavesdropped decreases exponentially when ϕ_r increases because of $1 > \frac{\theta_m}{P} > \frac{(\theta_m-1)}{(P-1)}$.

From the analysis above, a larger ϕ_r and a smaller θ_m is needed to improve the session security among r nodes. When $\frac{k}{P}$ is larger, ϕ_r is larger and θ_m is smaller. When $\frac{k}{P}$ is smaller, ϕ_r is smaller and θ_m is bigger. Therefore, a key management scheme needs a reasonable $\frac{k}{P}$.

When adversity does not know the adscription of the nodes, $P = |U_g|$ in equation (5) mostly, and $\frac{k}{P}$ is larger; $P = |U_p|$ in equation (7), and $\frac{k}{P}$ is smaller. Therefore, group-based key management not only improves the probability that r nodes share at least one key, but also reduces the probability that the shared keys are decrypted.

5   Conclusions

According to that most ad hoc sensor networks are deployed for assigned missions, a group-based key management scheme is proposed in the paper. GBKM divides key pool into some sub-pool according to the relativities of missions, and the numbers of shared keys among missions are determined by the relativities among missions. In ad hoc sensor network, most communications are happened among nodes of same missions. Therefore, the group-based key management not only improves the probability that communicating nodes share at least one key but also reduce the probability that the shared key is decrypted.

References

1. C. Blundo, A. Santi, A. Herzberg, U. Vaccaro, M. Yung. Perfectly-secure Key Distribution for Dynamic Conferences. In Proc. of Crypto'92, Santa Barbara, California, USA, (1992) 471~486
2. A. Fiat, M. Naor. Broadcast Encryption. In Proc. of Crypto'93, Santa Barbara, California, USA, (1994) 480~491

3. D. Halevy, A. Shamir. The LSD Broadcast Encryption Scheme. In Proc. of Crypto'02, Santa Barbara, California, USA, (2002) 47~60
4. R. Kumar, S. Rajagopalan, A. Sahai. Coding Contractions for Blacklisting Problems without Computational Assumptions. In Proc. of Crypto'99, Santa Barbara, California, USA, (1999) 609~623
5. D. Naor, M. Naor, J. Lotspiech. Revocation and Tracing Schemes for Stateless Receivers. In Proc. of Crypto'01, Santa Barbara, California, USA, (2001) 41~62
6. R. Blom. An Optimal Class of Symmetric Key Generation Systems. In Proc. of Santa Barbara, California, USA, (1984) 335~338
7. T. Matsumoto, H. Imai. On the Key Predistribution System: A Practical Solution to the Key Distribution Problem. In Proc. of Crypto'87, Santa Barbara, California, USA, (1987) 185~193
8. T. Leighton, S. Micali. Secret-key Agreement without Public-Key Cryptography. In Proc. of Crypto'93, Santa Barbara, California, USA, (1993) 456~479
9. M. G. Zapata, N. Asokan. Securing Ad-Hoc Routing Protocols. In Proc. of WiSe'02, Singapore, (2002) 1~10
10. H. Chan, A. Perrig, D. Song. Random Key Predistribution Schemes for Sensor Networks. In Proc. of S&P'03, California, US, (2003) 197~215

An Accurate and Fast WLAN User Location Estimation Method Based on Received Signal Strength

Minghua Zhang and Shensheng Zhang

Department of Computer Science and Engineering,
Shanghai Jiao Tong University, China
{zhangmh, sszhang}@sjtu.edu.cn

Abstract. Location estimation is a crucial component of location-aware applications. Positioning based on received signal strength (RSS) in wireless networks is considered a promising and inexpensive solution. Existing techniques only use RSS from some fixed access points (APs) deployed within the area of interest to estimate user location. Through experiments on the properties of RSS, it is found that RSS from far access points can distinguish different locations more easily. In this paper, we propose to introduce RSS from APs outside of the area to increase location estimation accuracy. We also present an online maximum matching method to select the most possible locations first, thus reducing the computational cost incurred by using more RSS values and improving the speed of location estimation. Our new location estimation method is implemented and compared with related work in a practical wireless network. Experimental results illustrate that the proposed method can give a higher degree of accuracy.

Keywords: User location estimation; Received signal strength; Wireless local area network; Maximum matching; Location estimation speed.

1   Introduction

Location estimation is an important task in today's pervasive computing applications [1] that use location information on objects or human beings to provide services without user intervention. A typical positioning system is the Global Positioning System (GPS) [2], yet it doesn't work well in indoor environments or urban areas where high buildings shield the satellite signals. As the proliferation of wireless local area network (WLAN) and the declining cost of mobile devices, great attention have been paid to the received signal strength (RSS)-based location estimation techniques. Such positioning systems build on an already existing, widely available wireless network infrastructure and work indoors as well as outdoors.

RSS-based positioning techniques usually work in two phases: radio map building phase and location determination phase. During the first phase, the received signal strength from observed access points (APs) together with the corresponding sampling position are saved, resulting in a so-called radio map. During the location determination phase, the real-time signal strength measurements are compared to data in the radio map and the nearest match is returned as the estimated user location. In

indoor environments, the propagation of radio signals suffers from severe multi-path effects, noise and interference [3]. RSS-based location estimation techniques need to deal with the noisy characteristics of the wireless channel. Those characteristics cause the real-time signal strength samples measured in the location determination phase to deviate significantly from those stored in the radio map, thereby limiting the accuracy of such systems.

Current RSS-based techniques can be broadly divided into two categories: deterministic techniques [4, 5, 6] and probabilistic techniques [7, 8, 9]. Our work lies in the first category. However, none of the previous positioning systems take into account the role of access points outside the area of interest. The RADAR system [4] uses the k-NNSS (k-nearest neighbor in signal space) algorithm. They collect signals from three fixed access points which can be observed in all predetermined locations. The Horus [8] system improves upon the performance of RADAR by using their Joint Clustering technique. Roos [7] adopts RSS from 10 access points deployed within their testbed. In [10], Kaemarungsi investigated the properties of received signal strength reported by IEEE 802.11b wireless network interface cards. His experimental results indicate that the RSS values from the same AP at two different locations may be difficult to distinguish for positioning purposes when the RSS level is high in which case it tends to have a large degree of variation. To distinguish locations efficiently and improve location estimation accuracy, this finding inspires us to use RSS from the access points deployed not only within the area of interest but also outside of the area. We also propose an online maximum matching method in which the set of observed APs is used to choose possible locations first, alleviating the burden of computation incurred by adopting more RSS values. We test our new location estimation method in a practical wireless network and compare with other work. Experimental results show that the method can achieve a higher degree of accuracy.

The rest of the paper is constructed as follows. Section 2 illustrates the fluctuation of the radio signal strength in WLAN, which is affected by many disturbances. In section 3, we elaborate on our location estimation methodology including the online maximum matching method. We perform experiments and compare our method with others in section 4. Section 5 concludes the paper and describes some potential future work.

2   Propagation of Radio Signals in WLAN

The propagation of radio signals is affected by many disturbances [11]. The IEEE 802.11b standard uses license-free 2.4GHz band to communicate with each other such that other devices using the same band like Bluetooth devices, microwave ovens will be a source of interference. Moreover, 70% part of a human body is water, and the 2.4GHz is the resonance frequency of water. Thus human body is an absorber of radio signals.

Multi-path fading [12, 13] is another common phenomenon in radio signal propagation. A transmitted signal can reach the receiver through different paths, each having its own amplitude and phase. These different components combine and produce a distorted version of the transmitted signal.

Fig. 1 gives a typical example of the normalized histogram of the signal strength received from an access point at a fixed location. People walk in the area, and doors open and close. Such changes in the environment can explain the fluctuation of signal strength shown in the figure.
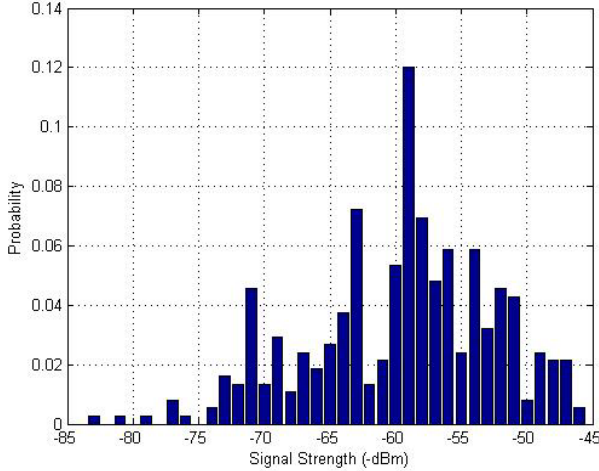
Fig. 1. An example of normalized signal strength distribution

3   Proposed Location Estimation Method

3.1   Radio Map Building Phase

Suppose the location area A has N selected sampling positions, $A = \{position_i \mid 1 \leq i \leq N\}$. A RSS sample in our experiment is a 6-tuple: *(Id, Time, RSS, SSID, BSSID, Position)*, whose elements are explained in detail in Table 1.

Table 1. Explanation of a RSS sample vector

Element name	Explanation	Example
Id	Sequence number of detected access point	1, 2, 3, …
Time	Sampling date	2006-05-23 18:43:03
RSS	Received signal strength in dBm	-76, -81, …
SSID	Service Set Identifier	1x.net.sjtu
BSSID	MAC address of the access point	00-13-C3-59-14-72
Position	2-dimension coordinates and orientation of the sampling location	(12.386, 1.54, south)

In each sampling position *position_i*, several RSS samples are collected in order to represent the fluctuation of radio signal strength. Then the average value of signal strength $avgrss_{ij}$ received from each observed AP, whose MAC address is $bssid_j$, is computed. With the information the radio map is built up. Records in the radio map

can be described in (1), where L is the number of observed APs in each sampling position.

$$r = (position_i, avgrss_{ij}, bssid_j),$$
$$1 \le i \le N,$$
$$1 \le j \le L.$$
(1)

3.2 Location Determination Phase

During the location determination phase, suppose the real-time RSS samples are represented by (2), where L' is the number of access points detected by user.

$$U = \{(m\_avgrss_i, m\_bssid_i) \mid 1 \le i \le L'\}$$
(2)

Before search the nearest location in the radio map, we use an online maximum matching method to choose a subset of radio map containing the possible locations first. As each AP has its own signal's coverage area, the set of observed APs are not totally the same for different locations. Based on the APs in the real-time RSS samples, the positions in the radio map associated with a maximum intersection of the same APs form the sub set P'. It can be described formally as:

$$P' = \{position_i \mid (\forall position_r)(\mid AP_m \cap AP_i \mid > \mid AP_m \cap AP_r \mid)$$
$$\wedge 1 \le i \le N \wedge (position_r \in A - P')\},$$
$$AP_m = \{U_n.m\_bssid \mid 1 \le n \le L'\},$$
$$AP_i = \{r_{xy}.bssid \mid r_{xy}.position = position_i \wedge 1 \le y \le L\},$$
$$AP_r = \{r_{xy}.bssid \mid r_{xy}.position = position_r \wedge 1 \le y \le L\}.$$
(3)

Then the simple and efficient Euclidean distance is selected as matching metric between real-time RSS samples and RSS data saved in the radio map. The position in P', which has a minimum Euclidean distance in signal space is considered as the estimated user location. Euclidean distance is computed by (4):

$$\min(D_j = \sqrt{\sum_{i=1}^{L'} (U_i.m\_avgrss - r_{ij}.avgrss)^2}),$$
$$U_i.m\_bssid = r_{ij}.bssid,$$
$$r_{ij}.position \in P'.$$
(4)

4 Experimental Results and Analysis

4.1 Experimental Testbed

We perform our experiments in the second floor of the third building of the Electronic Information and Electrical Engineering School buildings. The layout of the floor is

shown in Fig. 2. The area has a dimension of 100 meters by 20 meters. It includes a long hallway, a meeting room, lots of offices and labs.

To measure the RSS from different APs, we use an ASUS pocket PC with an embedded wireless Ethernet card to capture the signal. We use WRAPI [14], a third party library for retrieving the signal strength.

There are altogether 30 access points that can be detected. They are deployed not only in the second floor, but also in other floors or in neighboring buildings. For building up the radio map, we take the sampling locations along the hallway on a grid with cells of 5×2 meters (the hallway width is 2 meters). For each location, 10 samples are collected for each orientation.
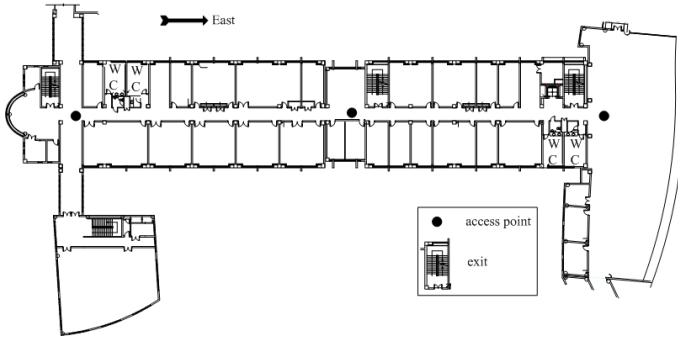
Fig. 2. The layout of the second floor of the third building of the Electronic Information and Electrical Engineering School buildings

4.2 Experimental Results

In this section, we evaluate the performance of our proposed method. An independent test set collected on different time and day from that for the radio map building phase is used. We conduct experiments and compare with other methods. In the first experiment, we only use the RSS values from access points deployed within the testbed. The method is just like the 1-NNSS method in the RADAR system, so we call it the RADAR method in Fig. 3. In the second experiment, we only adopt the RSS data from three strongest APs in each sampling position, which is called as the 3-strongest AP method. This method is similar to the technique in [8] on the selection of RSS data. In the last experiment, we use RSS data from all observed APs.

Experimental results are illustrated in Fig. 3. Location estimation error is defined as the Euclidean distance between the real position and its estimated position. The results of our proposed method are quite positive, for it is more accurate than the other two methods. Fig. 4 gives the cumulative distribution of error distance in the three experiments. Using the proposed method, over 73 percent positions are located within 5 meters, which is higher than the other two methods. This demonstrates that more RSS data can improve the location estimation accuracy.
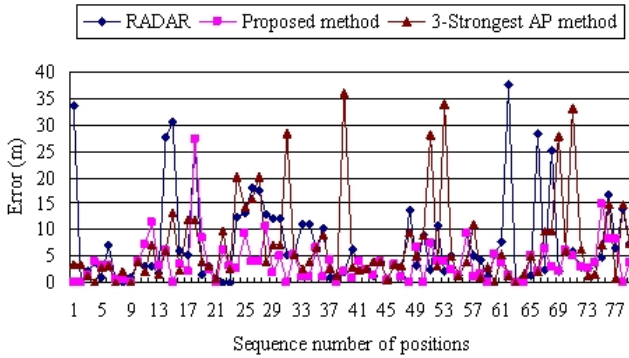
Fig. 3. Comparison of location estimation error in the three experiments
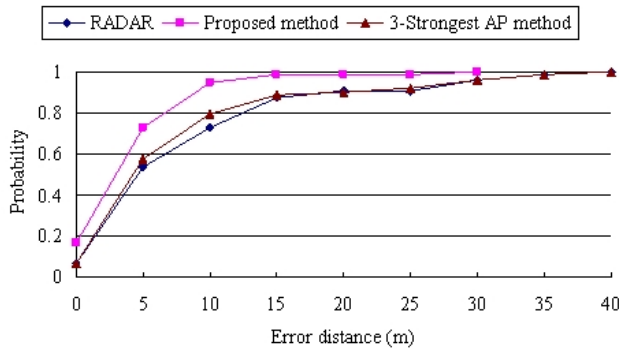
Fig. 4. Error distance CDF of the three experiments

Since we use RSS from more access points to estimate user location, it is possible that the calculating time will increase. Therefore we also perform an experiment to measure the locating time. The personal computer is configured with 512MB of RAM, Intel(R) Pentium(R) M processor 1.5GHz. The three methods are implemented in MATLAB and Table 2 lists the CPU time each method uses. In general, the more access points' signal strength information is used, the more locating time is needed. Although the number of access points used in our method is much more than the RADAR method, yet the difference of CPU time needed is very small (0.13 seconds). However the average error of the RADAR method is about two times that of our proposed method. Therefore it is a tolerable compromise for the improvement of location estimation accuracy. In the Table 2, the tremendous increase of CPU time spent on the 3-strongest AP method is due to the sort operation to choose the first three strongest access points. On the location estimation accuracy, it is very close to the RADAR method.

Table 2. Compare locating time of the three experiments

Comparison Items	Proposed Method	RADAR	3-Strongest AP Method
Number of access points matched	15	3	3
Average error (m)	3.74	7.43	7.29
CPU time (s)	0.86	0.73	1.15

5   Conclusion and Future Work

Mobile user's current location is one of the most important and frequently-used contexts in pervasive computing environments. Positioning based on received signal strength is considered a promising and inexpensive solution. However, received signal strength especially in indoor environments is interfered by many disturbances. This paper proposes a new user location estimation method to improve accuracy, which uses RSS data from access points deployed not only within the area of interest but also outside of the area. RSS data from the far APs are used to better distinguish locations. Moreover an online maximum matching method is presented to quickly get the most possible locations in order to improve the speed of location estimation.

Experimental results show that, with the 2×5 meters sampling grid, our method can estimate user location to within 5 meters with over 73% accuracy. In the same testbed, the proposed method is better than the methods used in other work on accuracy. It is also remarkable that the sampling grid in the proposed method is bigger than that in the related work, which means fewer calibration efforts are needed. Furthermore, through another experiment the increase of locating time by using more access points is negligible relative to the improvement of location estimation accuracy.

In this paper, the proposed method belongs to the deterministic technique. But the idea of using more RSS data from far APs and the online maximum matching method are not limited to it. They can also be used in the probabilistic technique. In the future, we would like to do more extensive experiments, studying the effect of parameters such as the size of sampling grid, the number of access points and try to prove our idea in a formal way.

References

1. Hazas, M., Scott, J., Krumm, J.: Location-Aware Computing Comes of Age. IEEE Computer, Vol. 37, No. 2, (2004) 95-97.
2. Enge, P., Misra, P.: Special Issue on GPS: The Global Positioning System. Proceedings of the IEEE, Vol. 87, No. 1, January (1999) 3-172.
3. Hashemi, H.: The Indoor Radio Propagation Channel. Proceedings of the IEEE, Vol. 81, No. 7, (1993) 943-968.

4. Bahl, P., Padmanabhan, V. N.: RADAR: An In-building RF-based Location and Tracking System. In: Proceedings of the IEEE INFOCOM 2000, Tel-Aviv Israel, March (2000) 775-784.
5. Ahmad, U., Gavrilov, A., Sungyoung Lee, Young-Koo Lee: Modular Multilayer Perceptron for WLAN Based Localization. In: Proceedings of 2006 International Joint Conference on Neural Networks, Vancouver BC, Canada, July (2006) 3465-3471.
6. Smailagic, A., Kogan, D.: Location Sensing and Privacy in a Context-Aware Computing Environment. IEEE Wireless Communications, Vol. 9, No. 5, October (2002) 10-17.
7. Roos, T., Myllymaki, P., Tirri, H., Misikangas, P., Sievanen, J.: A Probabilistic Approach to WLAN User Location Estimation. International Journal of Wireless Information Networks, Vol. 9, No. 3, July (2002) 155-164.
8. Youssef, M., Agrawala, A., Shankar, A. U.: WLAN Location Determination via Clustering and Probability Distributions. In: Proceedings of IEEE International Conference on Pervasive Computing and Communications. IEEE Computer Society (2003) 23-26.
9. Castro, P., Chiu, P., Kremenek, T., Muntz, R.: A Probabilistic Location Service for Wireless Network Environments. In: Proceedings of the International Conference on Ubiquitous Computing. Springer LNCS 2201, Berlin Heidelberg (2001) 18-24.
10. Kaemarungsi, K., Krishnamurthy, P.: Properties of Indoor Received Signal Strength for WLAN Location Fingerprinting. In: Proceedings of the First Annual International Conference on Mobile and Ubiquitous Systems - Networking and Services. IEEE Computer Society (2004) 14-23.
11. Ladd, A. M, et al.: Robotics-Based Location Sensing using Wireless Ethernet. In: Proceedings of the 8th Annual International Conference on Mobile Computing and Networking. ACM Press (2002) 227-238.
12. Stallings, W.: Wireless Communications and Networks. First Edition. Prentice Hall (2002).
13. Youssef, M., Agrawala, A.: Small-Scale Compensation for WLAN Location Determination Systems. In: Proceedings of the IEEE WCNC 2003, Vol. 3. March (2003) 1974-1978.
14. WRAPI. Website: http://ramp.ucsd.edu/pawn/wrapi/.

Optimization of the Switches in Storage Networks

Nianmin Yao[1], Xiuli Zhao, Huimin Meng[2], and Xinlei Jiang[3]

[1] College of Computer Science and Technology,
Harbin Engineering University, Harbin, China
`yaonianmin@hrbeu.edu.cn`
[2] Dalian Institute of Light Industry
[3] China Construction Bank

Abstract. In the Storage Area Network (SAN), the mature network technology is used to substitute for the IO bus. Usually, the common switch is used in the storage network especially in the iSCSI storage system. Because the common switches are not aware of the environment it is used in, it can not make optimization for the storage network. In this paper, an optimization of storage network is presented which can greatly improve the performance and resource utilization of the whole storage system. In this optimization, the IO acknowledgment commands passing through the switch which is used in storage network are transferred in highest priority. This optimization of SAN has been certified by the simulation experiments.

Keywords: SAN, performance, network, switch.

1 Introduction

With the developing of the Internet, a dramatic growth of enterprise data storage capacity can be observed in the last couple of years. Many things including a lot of enterprise data coming onto the internet; data warehouse, e-business and especially the Web contents contribute the growth of storage. People require more and more performance, capacity and manageability of the storage with the time goes by. So the relative slow developing speed of the storage compared to the other parts of the computer system such as CPU, network bandwidth and so on are becoming the bottleneck of IT. Now, the SAN (Storage Area Network) is a popular technology to solve these problems. It can ensure the reliability, serviceability, scalability and availability of the storage. But now it obviously can not satisfy the increasing need of market, so many researchers are working on improving the technology of SAN. There are three main components in an SAN environment such as server systems, storage devices and interconnect devices. So methods to improve the SAN are mainly focused on these three components. For example, many data placement algorithms, for example [1] [2] [3] [4] and so on, which mainly improve the storage devices are proposed to get more performance and scalability of the storage system. In this paper, we focus on the optimization

of the switches which are used to connect the servers and storage devices. So far, there are not many works on improving the switches, because their implementation details are not much clear because they are commercial secrets for the company selling the products. But we may assert that the switches now being sold are not optimized specially for the use of storage networks because most of the switches which can be used to connect the servers can also be used in the storage networks. So the swiches even can not know which environment they are used in, storage network or normal intranet. In fact, there are a lot of properties of switches can be optimized specially for the storage networks. This paper presented a change of the priorities of the routing packages. The theory analysis and simulation tests all ensure that this optimization can improve the response speed of the IO requests and resource utilization. And more, it can be implemented easily in switches being sold.

2   Related Works

There are many works trying to improve the performance of the SAN. But they are most focused on the other two components of the SAN environments such as servers and storage devices. In this paper, we focus on the optimization of the switches which are used as the interconnect devices in the iSCSI storage system. As for switches, they have been well studied in the past two decades. In the traditional method, the switches internally works with fixed-size cells according to which a tremendous amount of scheduling algorithms have been proposed, such as [5] [6] [7] [8]. The packet mode scheduling was first proposed in article[9], in which switches internally operate on variable-length packets and restrict that the packets are transferred without interruption. After then, many packet-based scheduling algorithms have been proposed, such as [10] [11]. In [10], an algorithm which is stable for arbitrary admissible arrival processes was prented. In [11], it showed that making short packets which may preempt the long packets scheduled in high priority can reduce the average waiting time of packet and thus improve the switching performance. All the above works are helpful to promote the performance of the switch when used in normal intranet as well as storage network. But for being used in storage networks, they are too general since they mostly did not take storage networks for granted. In fact, we could do much optimization in the switch specially for the storage network. According to the characteristics of storage networks, we proposed an optimization of scheduling algorithm of switches to improve the performance of the whole storage system.

3   Optimization of the Switches

As mentioned above, the switches which can be used to connect servers can also be used in the storage networks. And more than that, the switches can not get any information about the environments they are in. So we can conclude that the switches being sold in the market must have not been optimized for being used in storage networks. Obviously, not distinguishing the purposes of switches,

being used in normal intranet or storage network, is good for the products costs and applicability. But in fact, when used in the real environments, people always need more performance and the switches are seldom required to connect both servers and storage devices. So, we may do some optimization in the switches when they are specially used in the storage networks.

To illustrate the characteristics of the storage networks which common switches are used in, consider a reading and a writing request in the iSCSI protocol. As for a reading request, it triggers the transmission of iSCSI Command PDU to the target. The target on receiving the command finds the requested data from the buffers and sends out a sequence of Data-In PDUs which contain the data requested. The initiator on receiving the Data-In PDUs, allocates the data into buffers. When all the data for the request have been transferred from the target to the initiator, the target sends an iSCSI Response PDU to the initiator, indicating successful completion of the command. Then both of the initiator and the target release the resources allocated for this request. The interaction of iSCSI Reading Commands is illustrated in fig. 1.
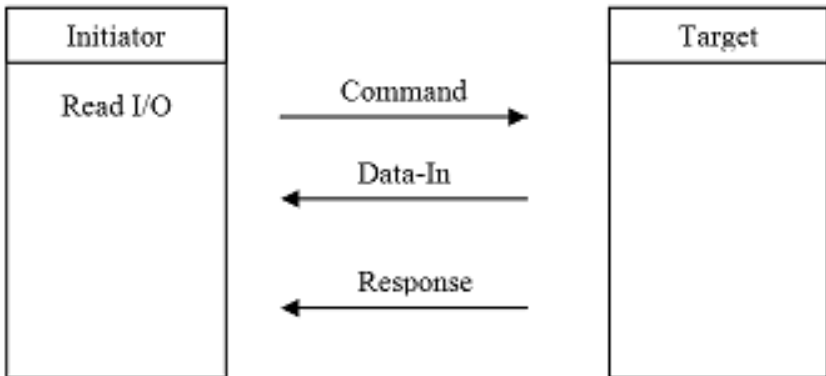
Fig. 1. Interaction of iSCSI Reading Commands

As for a writing request, the initiator transfers an iSCSI Command PDU to the target. After the target receives the command, it allocates buffers for transfer and responds with Ready to Transfer (R2T) PDUs, indicating permission for the initiator to transfer the data. The initiator responds to a R2T PDU by sending out a sequence of Data-Out PDUs which contain the data requested. The target on receiving the Data-Out PDUs, allocates buffer for data. When all the data for the request has been transferred from the initiator to the target, the target sends an iSCSI Response PDU to the initiator, indicating successful completion of the request. Then both of the initiator and the target release the resources allocated for this request. The interaction of iSCSI Writing Commands is illustrated in fig. 2.

From the read and write process of iSCSI protocol described above, we can see that there are two types of iSCSI PDUs transferred between the initiator
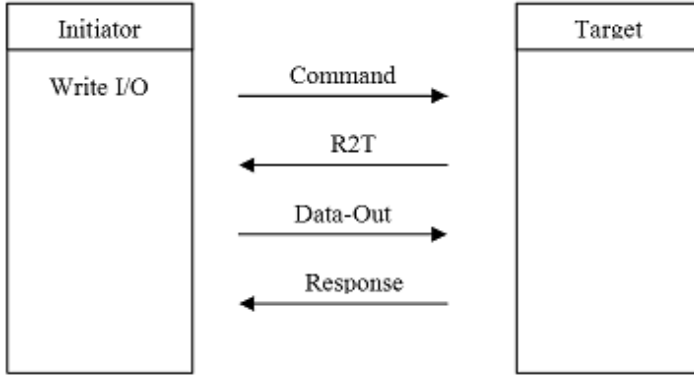
Fig. 2. Interaction of iSCSI Writing Commands

and the target. One type includes the commands which contain the reading or writing data, such as Data-In PDUs and Data-Out PDUs. The other type of the commands are the acknowledgement commands, for example, iSCSI Command PDU, Ready to Transfer (R2T) PDU and iSCSI Response PDU. Were these acknowledgements accepted, the resource allocated for the request would be released. For example, when all the data for the IO request has been transferred between the initiator and the target, the target sends an iSCSI Response PDU to the initiator. Only after the initiator receives this command, both of the initiator and the target can release the resources allocated for the IO request. So by intuition, we can assert that if the second type of commands have higher priority to be transferred, the time waiting for releasing resource will be reduced and the resource utilization will be improved.

We can also conclude that if we give the acknowledgement commands higher priority to be transfered, the performance will be exalted. This is because most of the commands, including the iSCSI command PDU, the Ready to Transfer (R2T) PDU and the iSCSI Response PDU, are so short that they have not extra room for reading or writing data. During the IO commands processing, if these short commands have the higher priority of being transfered, the performance of the system will be improved, which has been tested in other works [11].

4   Simulation Tests

Simpy [12] is used to test the performance promotion of the system with the optimization. Using Simpy, we build a simulation model which is shown in fig. 3. The model for storage networks simulates a closed queueing network, assuming that there are always 1000 requests in the system, 50% of which are reading requests and the others are writing requests. The arrival distribution of the requests is influenced by the time slot which is variable in the simulation model, which means that two requests arrived at the system with a equal time internal. It is assumed that each request takes equal resources of server. As for the switches,
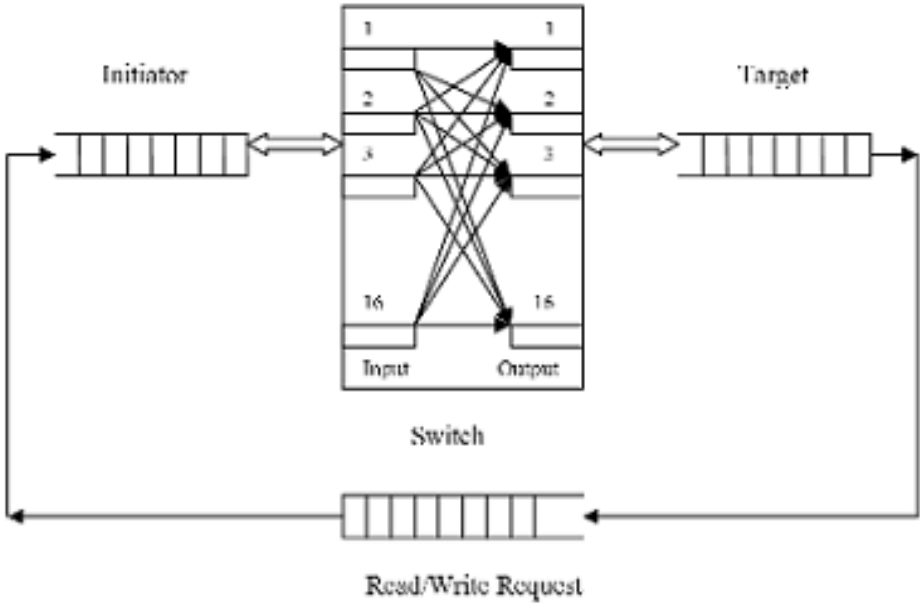
Fig. 3. Simulation Model

they are assumed to have 16 pairs of input and output interfaces and operate on the situation with or without the optimization. The resources of the server are infinite. Some simulation results are showed below.

Fig. 4 shows the comparison of the average processing time of the requests in the two systems. It indicates that when the arrival time slot is less than about 0.3, the processing time of the requts with the optimization is much smaller. When the arrival time slot is more than 0.3, the performance of the two systems is nearly the same. It is because that the system is not busy at that time and there are less requests competing for the resources in the system.

Fig. 5 shows the comparison of the number of the request finished in the two systems. There are much more requests finished in the system with our optimization and the difference between the two systems becomes greater when the arrival time slot is smaller. It can be infered that when there are more competitions happened in the scheduling the optimization will play a dominant role in affecting the performance of the storage networks.

Next, we studied the average resource occupancy in the system whose results were shown in fig. 6. It indicates that the average resource occupancy of the system with optimization is lower when the arrival time slot is smaller. We can get that the busier the system is, the more effectively the resources are used. With the increase of the arrival time slot, the difference is less which nearly none when the arrival time slot is more than 0.3. It is because that there are less requests
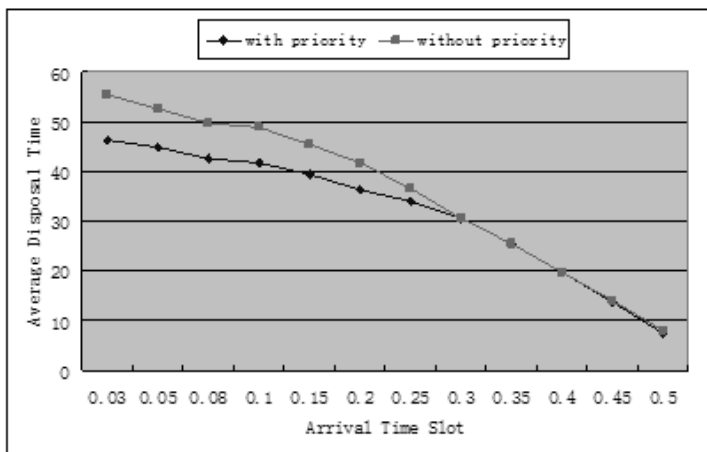
Fig. 4. Comparison of Average Processing Time
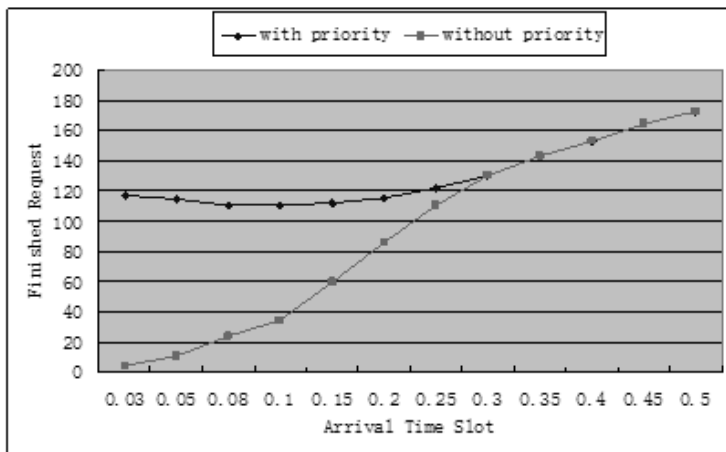
Fig. 5. Comparison of Finished Requests

waiting for being allocated in the server, so there are less requests competing for resources. It can be deduced that our optimiztion can improve the resource utilization of the storage networks.

The results are gained under the assuming that the arrival distribution of the requests is described as the time slot. But in reality, the IO requests happened at random, and the status which indicates in the simulation that two requests are generated more than 0.3 seconds is nearly rare. When there are a great lot of IO requests in the system, the improvement of the performance using the optimization will be more conspicuous.
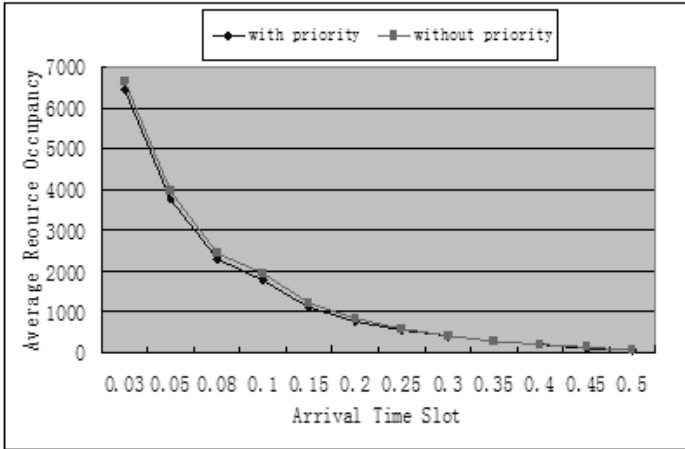
Fig. 6. Comparison of Average Resource Occupancy

5   Conclusions

This paper focused on improving the performance of the storage networks by optimizing the switches which are used as the interconnection devices. Common switches used in intranet can also be used in storage networks, so few optimizations special for the storage networks have been done. The processing steps of iSCSI commands are analyzed, and then based upon that, improving the transferring priority of the acknowledgement commands is proposed. This method can greatly promote the performance of the storage system and improve the resource utilization, for example buffers. Finally, a simulation model implemented by Simpy is constructed to test our conclusion.

Though we take iSCSI as an example, the optimization can also be used in other storage systems, such as FC-SAN. More than that, we wonder that if this optimization could effectively be applied in the whole IO path, including servers, switches, and storage devices. The further theoretical and experimental works are being done.

References

1. Yao Nian-Min, Shu Ji-Wu, Zheng Wei-Min: Improving the Data Placement Algorithm of Randomization in SAN. V.S. Sunderam et al. (Eds.): ICCS 2005, LNCS 3516, pp. 415C422,2005.
2. D. A. Patterson, G. Gibson and R. H. Katz: A case for Redundant Arrays of Inexpensive Disks(RAID). In Proceedings of the 1988 ACM Conference on Management of Data(SIGMOD), pages 109-116, June 1988.

3. G. Weikum, P. Zabback, and P. Scheuermann: Dynamic File Allocation in Disk Arrays. In Proc. of ACM SIGMOD, pp. 406–415, May 1991
4. R. J. Honicky, E. L. Miller: A fast algorithm for online placement and reorganization of replicated data. 17th International Parallel and Distributed Processing Symposium (IPDPS), 2003.
5. N. McKeown, V. Anantharam, and J. Walrand: Achieving 100
6. P. Giaccone, B. Prabhakar, and D. Shah: Toward simple, high-performance schedulers for high-aggregate bandwidth switches. In Proc. IEEE INFOCOM, 2002, pp. 1160-1169
7. C. Partridge et al: A 50-Gb/s IP router. IEEE/ACM Trans. Networking, vol. 6, pp. 237-248, June 1998
8. T. Anderson, S. Owicki, J. Saxe, and C. Thacker: High speed switch scheduling for local area networks. ACM Trans. Comput. Syst., vol. 11, no. 4, pp. 319-352, Nov. 1993
9. M. A. Marsan, A. Bianco, P. Giaccone et al: Packet-mode scheduling in input - queued cell-based switches. IEEE/ACM Trans. Networking, vol. 10, no. 5, pp. 666 - 678. Oct. 2002
10. Y. Ganjali, A. Keshavarzian and D. Shah: Input queued switches: cell switching vs. packet switching. IEEE/ACM Trans. Networking, vol. 13, no. 4, pp. 782 - 789. Aug. 2005
11. Li Wen-Jie, Liu Bin: Preemptive Short-Packet-First Scheduling in Input Queuing Switches. Acta Electronic Sinica, vol. 33, no. 4, pp. 577-583. Apr. 2005
12. Develop group of Simpy: Purpose of the Simpy Laboratory pages. Simpy Homepage [Online]. Available at http://simpy.sourceforge.net

Migration Control of Bio-entities in the Bio-network Middleware

Xiangfeng Zhang[1], Yongsheng Ding[1,2], and Lihong Ren[1]

[1] College of Information Sciences and Technology
[2] Engineering Research Center of Digitized Textile & Fashion Technology, Ministry of Education
Donghua University, Shanghai 201620, P.R. China
ysding@dhu.edu.cn

Abstract. Future Internet applications and services should be autonomous, self-evolutionary, and adaptable to the change of different users and network environments. Inspired by the resemble features between biological neuroendocrine-immune system and future Internet, we introduced some key principles and mechanisms to design a bio-network architecture and its middleware. In this paper, asynchronous migration mechanism is discussed based on the bio-network middleware. A credit-based migration control scheme is proposed. The simulation result shows that the scheme decreases the response time of service bio-entities and reduces the migration frequency. As such, it can ensure that the service bio-entities migrate effectively to provide services for users and minimize their cost. And the desirable requirements of future Internet are further satisfied.

1 Introduction

Internet is evolving into the core of the worldwide information infrastructure and a single integrated platform for computing, data storage, communication, entertainment, e-business, and so on [1]. Future Internet applications and services should be autonomous, self-evolutionary, and adaptable to dynamic network environments. Adopting mobile agent technology is a prospective solution to design the applications and services [2, 3].

Large-scale biological systems have formed a great deal of mechanisms, which can adjust themselves to adaptive and survivable environments. Biological systems are composed of dispersive, autonomous, and mobile biological individuals with self-regulation, adaptability, evolution, and survivability. The biologically inspired information systems have been applied widely to engineering fields. Recent researches in biology show that the biological neuroendocrine-immune system (NEIS) establishes an intelligent system through complicated regulation [4, 5]. We have abstracted an integrated computation framework from the NEIS and developed the NEIS-based bio-network architecture that provides future Internet application environments [6]. The agent-based simulation platform for the bio-network has also been presented [7]. The bio-network can act as a network middleware for complex services and applications on Internet and distributed networks.

In this paper, we discuss migration scheme of bio-entities in the bio-network. Section 2 introduces simply a bio-network middleware and discusses its asynchronous migration mechanism. Section 3 proposes a credit-based migration control scheme. Section 4 simulates the response time and the migration frequency of the bio-entities with or without credit management service. Finally, Section 5 concludes the paper.

2 Macro Migration Model

2.1 Bio-network Middleware and Its Migration Service

The bio-network middleware consists of the bio-network platform, bio-entities and their survivable environment. The bio-network platform is a software framework fully implemented by Java language. The bio-network platform includes bio-network core services and bio-network low-level functional modules established in a network node. The bio-network core service layer provides a set of general-purpose runtime services that are frequently used by bio-entities, such as lifecycle, bio-entities migration, evolution state management, credit management, sustainability management, and security authentication service. The low-level functional modules manage low-level network and system resource and allocate resources to bio-entities. A bio-entity is an autonomous mobile agent and analogous to an individual in the biological system. The bio-entity survivable environment deploys and executes bio-entities and protects the node from being attacked with some security policies.

The bio-network platform runs in an asynchronous distributed system on a network node. Thus an overlay network environment is formed with wide-area bio-network platforms [8]. Several nodes can form a community niche and the niche is a logically defined area where the bio-entities in a community can learn from their surrounding environment. A bio-entity can sense which bio-entities are in the community niche, what services they perform, and which resources it can access to. This helps it create a new application or join an existing community. Physical proximity among network nodes is used to define a community niche in this study.

The bio-network platform provides the bio-entity migration service, which supports the migration behavior of the bio-entities. The migration behavior involves determining where and when to migrate through considering the cost/benefit tradeoff of migrating towards an adjacent community niche. The migration will be used to find useful partner bio-entities and acquire new relationships.

2.2 Asynchronous Migration Mechanism

The bio-network platform reduces network communication throughput and enhances the flexibility, extensibility, and tolerance of the network through a migration mechanism controlled by credits. A bio-entity migrates to another platform in order to provide services to meet user requests. It utilizes network resources after it pays some credits. This method can reduce network delay and provide efficiently network services to obtain more credits from users. A bio-entity also establishes new relationships with other bio-entities after it migrates to another platform and these bio-entities emerge some new services.

The system transfers a bio-entity to a bit-blob using the object serialization method and then sends it to other nodes. The bio-entity may be resumed by the object de-serialization method when the system wants to reuse it. The sustainability management service allows a programmer to store the bio-entity's state into a storage device so that the bio-entity is executed later. It is responsible for storing the serialized codes and states of the bio-entity into the storage material, such as hard disk, to support non-sustainable connection. When a bio-entity waits for non-connection resources, the sustainability management service ensures the lowest costs.

A bio-entity autonomously distributes on a bio-network node. Its behavior is not controlled by network users or other bio-entities. Its migration behavior includes where to migrate, when to migrate, and costs and benefits. It must pay credits for migration and it will die if it has not enough credits. The migration service adopts synchronous or asynchronous migration mechanism (AMM). The bio-entity calls migration service and chooses the migration mechanism. As to synchronous migration mechanism, the platform will immediately execute the migration request from the bio-entity. It will send error information to the bio-entity if the destination node is unreachable. The bio-entity decides how to do next. As to AMM, the platform does not immediately execute the migration request, but insert it into the sequence. The
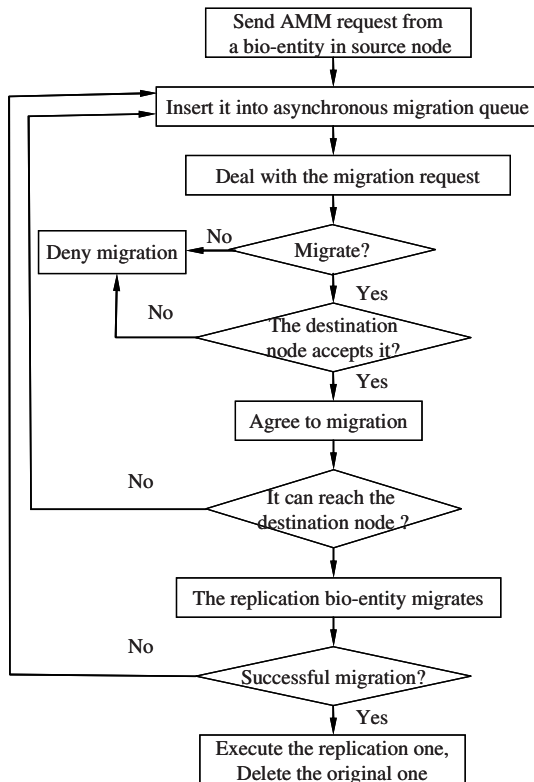
Fig. 1. AMM for a bio-entity

cost of credits is different using these two mechanisms. AMM is adopted when the following case happens:

(1) The chosen destination node is not reached;
(2) The bio-entity is off-line mobile user;
(3) The bio-entity waits a return off-line user on ever-connective node.

Taking AMM as an example, we discuss the migration mechanism based on the credit as shown in Fig. 1. After a bio-entity migrates to asynchronous migration request queue and its migration request is dealt with, the migration service decides whether the bio-entity can migrate according to credits information and migration control algorithm, see section 3.1. Then the migration service judges whether the destination node accepts the request. If the destination node agrees to migration, the platform judges whether it is reached. This causes network delay and reduces quality of service, and thus the bio-entity has to pay many credits for the system resources. Hence, it should balance its cost and benefit. If the destination node is reachable, a replication one migrates to it. After its successful migration, the platform executes the replication one in the destination node and deletes the original one.

3   Credit-Based Migration Control Scheme

Each bio-entity and network resource, such as CPU, memory, and bandwidth, has its own credit-control scheme. A service request (such as a user or a bio-entity) has its own payment scheme, including reward or punishment for acquired service based on quality of service. One or more algorithms implement a bio-entity's state transfer. A set of parameters, such as weights, and a threshold, are included in an algorithm. Take migration operation as an example, we consider how a bio-entity changes from *Dangling* to *Migrating* state. The parameters of migration behavior include:

1) *MigrationBenefit* (*MB*). *MB* is the benefit achieved by a bio-entity when the bio-entity provides service with lower cost and network delay. It is usually a position value.

2) *MigrationCost* (*MC*). *MC* is the cost for either network resource used by the bio-entity or higher resource cost of the destination node. It is a negative value.

3) *MigrationRisk* (*MR*). *MR* includes some uncertain factors. It may be a negative value.

4) *MigrationAsynchronous* (*MA*). *MA* means that the bio-entity adopts the AMM. It may be a negative value.

5) *MigrationThreshold* (*MT*). *MT* determines whether a bio-entity migrates or not.

The bio-entity executes migration operation if the inequation (1) can be met,

$$(MB \ \ MC \ \ MR \ \ MA) \cdot (w_1 \ \ w_2 \ \ w_3 \ \ w_4)^T \geq MT \tag{1}$$

where w_1, w_2, w_3, and w_4 are the weights of MB, MC, MR, MA, respectively. The bio-entity has to pay credit units for environment sensing when the AMM is adopted. The above migration behavior is an incomplete list and a programmer can add other behaviors to it.

A request user gives credits to the bio-entities after it evaluates the acquiring service. This method helps him to decide which bio-entity is worth trusting. We can decide if a bio-entity is reliable based on *TrustCredit*.

The request user return a defray message with a collaboration record and a trust value α ($-\frac{1}{2} \leq \alpha \leq 1$). The trust value α increases for a reward or decreases for a penalty. A bio-entity adjusts the value with its interaction partners based on the level of user satisfaction or preference. Suppose a value α, the *TrustCredit* value V is updated according to the formula (2),

$$V^+ = \begin{cases} V^-(1-\alpha^2)+\alpha^2, & \alpha \geq 0 \\ V^-(2-\dfrac{1}{1+\alpha}), & \alpha < 0 \end{cases} \tag{2}$$

where, V^- and V^+ are the former and new *TrustCredit* value, respectively ($V^- \in [0,1]$). *TrustCredit* value increases with a reward for a high preference and decreases with a penalty for a low preference. The formula (2) ensures that the decrement is faster while the increment is slower. The value α belongs to the interval $[0.5,1]$. Hence, V^+ belongs to the interval $[V^-,1]$ when α is larger than or equal to 0, and V^+ belongs to the interval $[0,V^-]$ when α is less than 0.

4   Simulation and Analysis

4.1 Simulation Model

In our previous work [7], we have implemented the prototype of bio-network service simulation platform, including software, general objects and simulators using Java language. It supports pluggable functions and provides a general easy-to-use programming API. It contributes to implement our approach in real deployment with minimal modifications. The simulation experiment is constructed on Windows 2000 operation system with Intel Pentium 4 processor (2.4 GHz) and 512 MB RAM.

(1) Initial network topology and user requests: A simulated network is a 18×12 topology network with 216 network nodes, and bio-entities are deployed on the platforms. The platforms are initialized on each network node. There are two kinds of bio-entities in the simulation: users request bio-entities and service bio-entities. Request bio-entities do not execute biological behaviors and are arbitrary on the platform. A user sends a request per second. Service bio-entities who are close to user requests have priority.

(2) Behavior mechanisms and credit parameters: In our simulation, a bio-entity has some behaviors, such as creation, service provided, replication, migration, and death, while it has not mutation and crossover behaviors. A user request pays 20 credit units for a service bio-entity. And a service bio-entity can provides 10 services per second

towards a user request. But it need pay 150 credit units for using the resources on the platform, such as CPU, storage, and bandwidth. It should pay its platform 100 credit units for replicating itself and transfer 20,000 credit units to its child bio-entity. It also should pay its platform 200 credit units in order to migrate from the platform to another one.

4.2 Results and Analysis

The bio-network produces initially 60 user requests and 20 service bio-entities. Every service bio-entity has 20,000 credit units. Credit management service asks community niche sensing service to check the resource cost. It also checks resource utilization of each bio-entity on the same platform. And it deducts resource cost from the current credit card of a bio-entity. If the card has not enough credits for resource utilization, credit management service notifies evolution state management service will destroy the bio-entity.
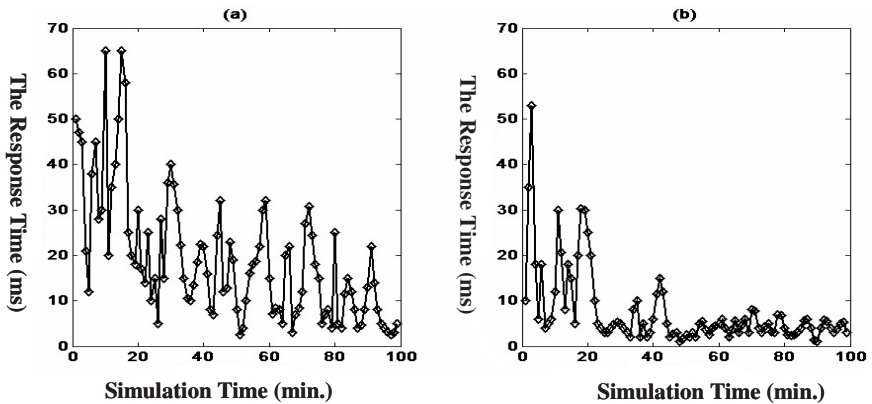
Fig. 2. The response time of the service bio-entity with different environments. (a) without credit management service; (b) with credit management service.

We simulate two kinds of environments with and without credit management service. The request response time and migration frequency of service bio-entities change with the simulation time are as shown in Fig. 2 and Fig. 3.

Without credit management service, the credit flow does not exist among bio-entities so that a request can only be handled by its nearest bio-entities. The bio-entities can only provide service and migrate. The requests are executed more quickly with credit management service than without credit management service in Fig. 2. Credit management service optimizes resource allocation and ensures that service bio-entities are responsible for their behaviors, migrate and replicate according to the number of user requests. The response time decrease quickly with credit management service. From Fig. 3, we can see that the useless migration decreases with credit management service because the service bio-entities will execute carefully their behavior in view of their cost.
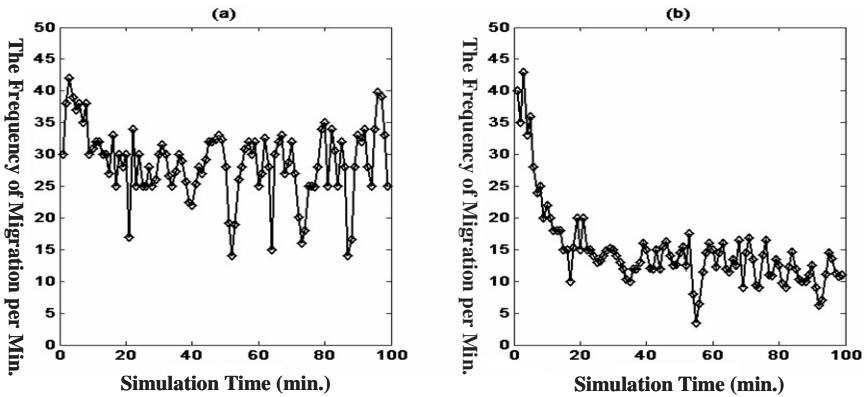
Fig. 3. Migration frequency of the service bio-entity under different simulation environments. (a) without credit management service; (b) with credit management service.

5   Conclusions and Future Work

Inspired by mobile agent technology, we discuss asynchronous migration mechanism of a bio-entity on the bio-network. We propose the migration control scheme based on credit mechanisms. Experiments results show that the proposed scheme ensures that the bio-entities migrate to a neighbor platform to provide services effectively and use their credits reasonably. Network services can adapt and evolve to meet user requests.

The next work is on issue about implementing other services of the bio-network middleware to perfect the bio-network architecture. In addition, in terms of network services and applications, more experiments will be designed to evaluate the performance of the middleware.

Acknowledgments

References

1. McIlraith, S. A., Son, T. C., Zeng, H.: Semantic web services. IEEE Intelligent Systems. 2 (2001) 46-53
2. Chen, W. S. E., Hu, C. L.: A mobile agent-based active network architecture for intelligent network control. Information Sciences. 1-2 (2002) 3-35
3. Kotz, D., Gray, R. S.: Mobile agents and the future of the Internet. ACM Operation Systems Review. 3 (1999) 7-13

4. Besedovsky, H. O., Rey, A. del.: Immune-neuro-endocrine interactions: Facts and hypotheses. Endocrine Reviews. 1 (1996) 64-102
5. Vargas, P., Moioli1, R., Castro, L. N. de, Timmis, J., Neal, M., Zuben, F. J. Von.: Artificial homeostatic system: A novel approach. ECAL 2005, LNAI 3630. (2005) 754-764
6. Ding, Y.-S., Gao, L., Ruan, D.: On the mechanism of communication of ecological network-based grid middleware for service emergence. Information Sciences. in press
7. Ding, Y.-S.: A new scheme for computational intelligence: Bio-network architecture (in Chinese). submitted
8. Zhang, X., Zhang, Q., Zhang, Z., Song, G., Zhu, W.: A construction of locality-aware overlay network: Overlay and its performance. IEEE Journal of Selected Areas in Communications. 1 (2004) 18-28

A Web Portal for Regional Projection of Weather Forecast Using GRID Middleware

A.S. Cofiño, D. San-Martín, and J.M. Gutiérrez

Dept. of Applied Mathematics and Computer Science,
University of Cantabria. Santander, 39005, Spain
{antonio.cofino,daniel.sanmartin,manuel.gutierrez}@unican.es
http://www.meteo.unican.es

Abstract. Weather forecast is a complex multi-disciplinary problem which requires a cascade of different scientific tools, from differential equation solvers to high-dimensional statistical and data-mining algorithms. The demand for high-resolution predictions is continuously increasing due to the multiple applications in hydrology, agronomy, etc., which require regional meteorological inputs. To fill the gap between the coarse-resolution lattices used by global weather models and the regional needs of applications, a number of statistical downscaling techniques have been proposed. In this paper we describe a Web portal which integrates the necessary tools with Grid middleware allowing for distributed data access and computing. The portal is part of the ENSEMBLES EU-funded project and allows end users to interactively downscale weather predictions using a web browser. Both the architecture and the usage of the portal are described in this paper.

Keywords: Grid computing, weather forecast, statistical downscaling, problem-solving environments, data mining, Web portals.

1 Introduction

Weather forecast is a complex interdisciplinary problem which involves several scientific disciplines to model and simulate the atmosphere dynamics in order to predict its future evolution. During the last four decades, several atmospheric circulation models have been developed and successively improved to include new interactions with other main climate components: hydrosphere, cryosphere, listhosphere and biosphere. Nowadays, the resulting Global Circulation Models (GCMs) are numerically solved on coarse-grained resolution grids covering the world, providing a low-resolution description of the future state of the atmosphere (temperature, humidity, geopotential, wind components, etc.) for a particular future period of time (e.g., next week, month, or season). These models are also forced with different future green-house gas emission scenarios to obtain a future estimate of the climate change for the next century. The computational requirements of this problem have recently increased with the adoption of the "ensemble forecast" methodology to deal with uncertainty. Ensemble methods

compute a probabilistic prediction of the atmospheric variables, based on several integrations of the circulation models started from perturbed initial conditions, or perturbed models (see [1] for more details).

The main shortcoming of GCMs is that their spatial resolution is currently constrained by both computational and physical considerations to a scale of hundreds of kilometers; for instance, Fig. 1(a) shows the land-sea mask used by these models with a resolution of one degree (aprox. 100 km at middle latitudes). However, meteorological phenomena such as rainfall, vary on much more local scales, as it can be observed analyzing high-resolution observation databases. For instance, Fig. 1(b) shows the location of 2600 stations in Spain, with records of daily temperature and precipitation during the last 60 years (Fig. 1(c) shows the accumulated precipitation pattern for February 1945, exhibiting high spatial variability). This spatial and temporal high-resolution information is required in different application domains to feed impact models with meteorological information in order to characterize the future evolution of key socio-economic sectors, such as water resources, crop yields, and power consumption.
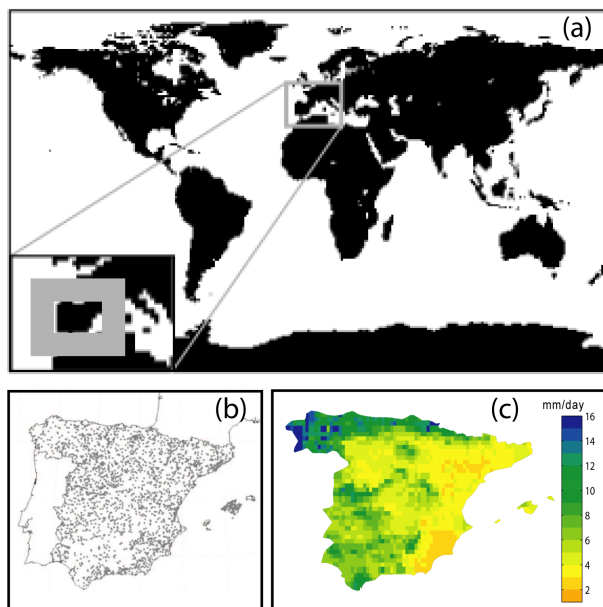
Fig. 1. (a) Land-ocean mask with one degree resolution; the inset shows a magnification of the Iberian peninsula. (b) Network of 2650 stations in Spain with daily records. (c) High-resolution interpolated precipitation (0.2 degrees) for February 1949.

To fill this gap between model outputs and end user requirements, a number of different statistical and machine learning techniques have been developed (downscaling methods). These techniques use the information contained in meteorological databases of GCM simulations in combination with simultaneous historical

high-resolution observations to infer statistical models relating predicted circulation patterns to observations at local points (see [2,3] for an overview). Some of these methods are more efficient than others for different regions and variables. For instance, the STARDEX project intercompared over 20 different statistical downscaling methods. The skill was found to vary depending on the particular method, variable, season and region, with the latter variation dominating [4]. Thus, for each particular application a range of the better statistical downscaling methods should be tested and validated to achieve the maximum skill and a proper representation of uncertainties. This is a complex task for end-users from applied knowledge domains, since it requires an appropriate statistical background to deal with the downscaling methods and certain computing expertise to deal with geographically distributed data in different formats.

The Statistical Downscaling Portal (SDP) described in this paper has been designed and developed in order to facilitate the downscaling task to end-users through a user-friendly Web portal. In this form, users can obtain their downscaled data testing and validating different methods in a transparent form not worrying about the details of the downscaling techniques and the data formats and access. This paper describes both the portal architecture and its application to practical problems. In Sec. 2 we give a brief overview of the ENSEMBLES project and describe the planned climate simulations which will be available from the portal for downscaling purposes. In Sec. 3 we illustrate the use of the portal considering an example of seasonal forecast in the North of Spain. Finally, in Sec. 4 we describe the implementation of the portal using Grid middleware.

2   The ENSEMBLES Project. Seasonal Forecast

The statistical downscaling portal is being developed as a part of the EU-funded ENSEMBLES project (for more details see [5] and `www.ensembles-eu.org`). The goal of this project is to develop an ensemble prediction system based on the principal state-of-the-art global circulation models developed in Europe. These models will be used in different of experiments to provide seasonal forecasts, decadal forecasts, and climate change scenarios. In particular, the seasonal simulations will provide the scientific community with huge amounts of high-dimensional information to explore and validate the skill of these predictions in different regions of the world. This task will require intensive computational effort due to the volume of information and the complexity of the algorithms involved in the analysis. Each seasonal simulation runs for six months, providing the forecasted daily state of the atmosphere for this period.

One of the ENSEMBLES project's aims is maximizing the exploitation of the results by linking the outputs of the ensemble prediction system to a range of applications, including agronomy, energy, water resources, insurance and weather risk management. This requires efficient downscaling tools to fill the gap between model output resolution and user needs. The portal described in this paper was designed for this purpose and provides user-friendly web access to statistical downscaling techniques and simulations produced in ENSEMBLES.

3   The Downscaling Web Portal

Downscaling methods work by obtaining a statistical model which relates predictors (gridded values of atmospheric variables) to predictands (high-resolution surface observations of goal variables; mainly temperature and precipitation). In the so-called Perfect Prog approach the parameters of these models are fitted using long historical data records. For this purpose, there is a number of model simulation databases (called reanalysis) covering long periods (for instance, the ERA40 reanalysis contains daily information for the period 1957-2002) and simultaneous observation networks (for instance, there is a network of over 2600 stations covering Spain with daily information since 1950, see Fig. 1(b)). With these two sources of information a number of different downscaling algorithms can be calibrated for a region and variable of interest. The resulting models can be later applied to regionally project outputs from ENSEMBLES seasonal models. According to this, the downscaling portal has been organized in three sequential steps: selecting the region of interest and the predictors, selecting the predictands and selecting and applying the downscaling method.

3.1   Selecting the Region of Interest

After login as a guest (restricted functionality) or as a registered user, the first step in the downscaling portal is selecting the region of interest and the desired predictors that shall be used to fit the downscaling methods. To this aim, the portal allows the user to visually select a lattice with the desired resolution over a geographical area and to include the desired variables from the reanalysis to be used as predictors (4D cubes of reanalysis information). This process is carried out by clicking and dragging in the "predictors" window (see Fig. 2a) and entering the information such as region, lattice resolution, variables, etc.

Once the zone and predictors have been defined, several internal processes are computed to obtain statistical information needed at a later stage of the downscaling process (principal components, clustering, etc.). This information can be visualized in the lower panels of the window. The defined regions and predictors can be stored in the portal to be used in future sessions. The region manager (see Fig. 2b) allows the user to visualize and load the stored regions.

3.2   Selecting the Stations and the Local Variable of Interest

Once the region of interest and the predictors have been selected, the user can move to the second window ("predictand" tab) and select the network and stations within the region where local forecasts are to be computed. The portal includes some public information such as the Global Station Network (GSN) data, which includes daily observations of precipitation, temperature, etc., for some thousand stations in Europe during the last 50 years. The user can also upload private data to the portal which will be only available for authorized users. The selection of the desired network and the particular stations and the variable to be used in the study is also visually done in a browser window. For
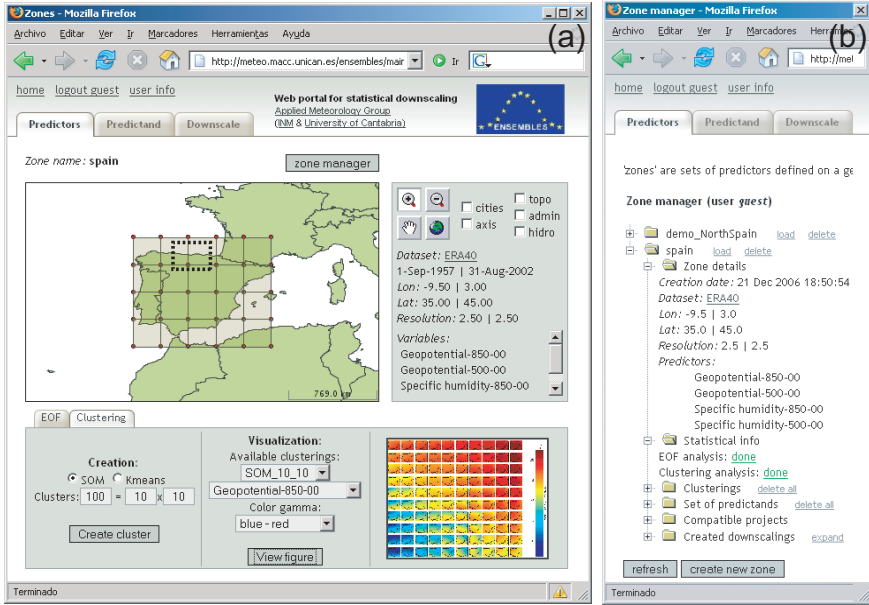
Fig. 2. (a) "Predictors" tab to define the region of interest and the predictors to be used in the downscaling process. (b) Region and predictors manager.
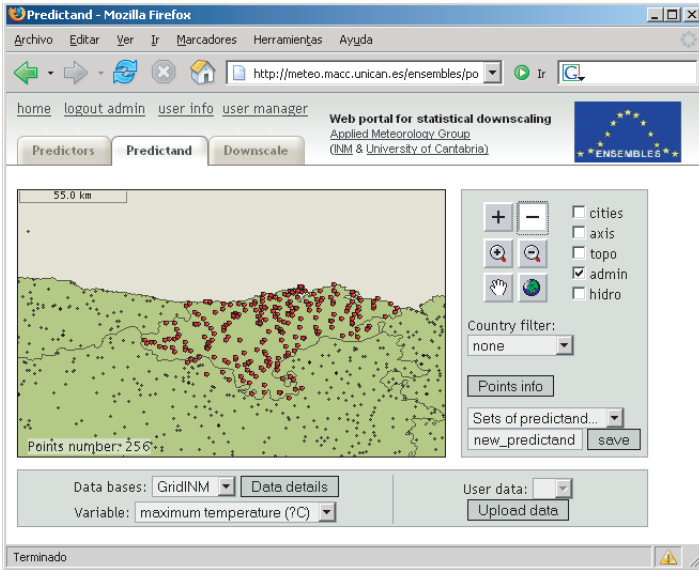
Fig. 3. "Predictand" selector for the desired network and variable

instance, Fig. 3 shows a set of stations in the small region of the North of Spain shown with the dashed box in Fig. 2(a). In this case, maximum temperature is the variable of interest.

3.3 Selecting and Running Downscaling Methods

After selecting the predictors and predictand over a region of interest, the portal allows the user to choose among different downscaling methods from the categories "weather typing", "regression" or "weather generators". These methods can be applied for different seasonal experiments (including the DEMETER project and ENSEMBLES's experiments) selecting the desired models, years and seasons from a matrix containing all the possible combinations to downscale model outputs to local stations (see Fig. 4(a)). This matrix illustrates the complexity of this problem, since each box is a possible downscaling job (the completed jobs are shown in green color). For instance, there is a total of 50 (years) × 12 (seasons) × 3 (models) × 6 (lead time) = 1800 possible downscaling jobs for the DEMETER experiment. Therefore, an efficient design of the computational load is required in order to develop an interactive portal where users can run several jobs simultaneously. In the next section we show how this problem is solved using GRID.

In the near future, this portal will be extended to cover regional projection of climate change scenarios to obtain local estimations of future variables of interest (including an estimation of the associated uncertainty).
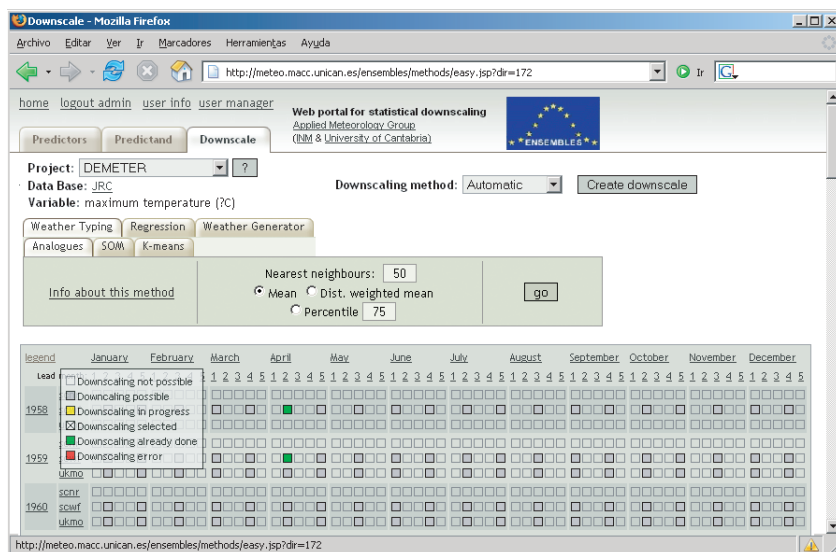
Fig. 4. Downscaling window with the downscaling methods and the matrix of possible downscaling experiments (combining the GCMs, seasons, years and lead times)

4   Implementation with GRID Middleware

GRID computing is a new paradigm for Internet-based distributed computing. It enables the development of interactive problem-solving environments integrating the sharing, selection, and aggregation of geographically distributed autonomous resources, such as computers and databases [6]. The developers of GRIDs applications need to address numerous challenges: security, heterogeneity, resource management, application decomposition, etc. A number of projects around the world are developing technologies (middleware) to run complex applications addressing and testing those challenges. This portal will be implemented in the framework of the 6th EU FP EELA project (see `www.eu-eela.org`) using its infrastructure based on gLite middleware (see `cern.ch/glite`).

Fig. 5 shows the design of the portal, which has been implemented using Java technology. On the one hand, the portal can operate using the local `meteo.unican.es` cluster. In this case, in addition to the local data, the portal can access distributed datasets through OPeNDAP protocol to remote storage servers. OPeNDAP technology (see `www.opendap.org`) allows exposing scientific datasets in the Web (mainly global model outputs) and subsetting this datasets using HTTP protocol. When the necessary information is ready to run a downscaling job requested by a user, the portal send the data and a Matlab script to the local server queue. The scripts to run downscaling jobs are based on the open-source toolbox MeteoLab developed by our group (see `www.meteo.unican.es/MeteoLab` for details).
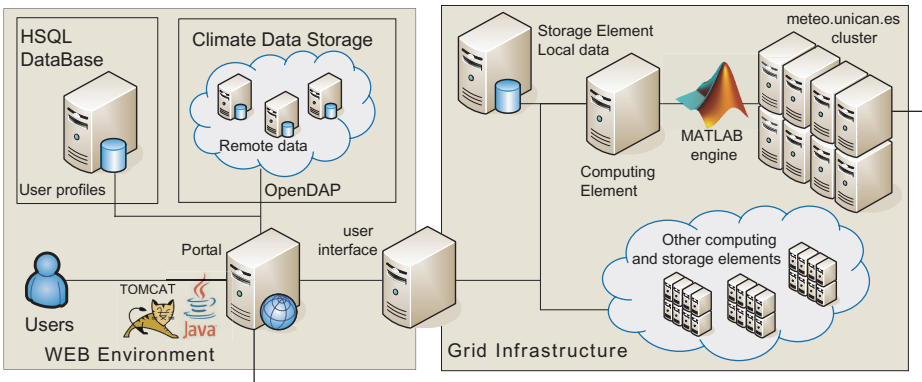
Fig. 5. Scheme of the portal showing the Web and GRID components

On the other hand, the portal will use grid middleware to run the jobs in the GRID using EELA's testbed. In this case, the portal acts as a user interface to the GRID, where a resource broker finds and provides resources to run the job according to the specifications given in the job submission template (in this case, Matlab enabled sites are requested). Apart from the computational resources, the GRID provides distributed data access through the gLite catalog facility

(LFC). Therefore, the datasets stored in the GRID do not need to be submitted, but just conveniently specified the catalog Logical File Name (LFN).

This portal will integrate resources (computing and datasets) from both grid and traditional computing communities, which use heterogeneous authentication methods. Therefore, the portal works with two security alternatives: a local schema based on local authentication and authorization, which is managed by the web portal itself using a database of user profiles, and a second schema which permits the user to configure his profile to use grid security infrastructure (GSI, see `www.globus.org/toolkit/docs/4.0/security/`) based on X.509 allowing the access to the GRID environment resources. The authorization management is based in Virtual Organization Membership (VOMS) provided by the gLite middleware. This configuration allows to the user make a Single Sign-On (SSO) to store (encrypted) different credentials to access multiple external resources.

5   Conclusions

In this paper we have presented a statistical downscaling portal to fill the gap between weather forecast modelers (data producers) and application developers (data consumers). This portal integrates datasets from model outputs and observations datasets and uses statistical modeling tools to project model outputs to local observations, which can be geographically distributed in different regions of interest. To this aim, a GRID approach is presented to make available geographically distributed compute and storage resources using the portal. This work is based in gLite middleware used in EELA project and brings together Europe and Latin-America scientific communities.

References

1. Gneiting, T., Raftery, A.E.: Weather Forecasting with Ensemble. Science **310** (2005) 248-249
2. Wilby, R.L. and T.M.L. Wigley: Downscaling General Circulation Model Output. A Review of Methods and Limitations. Progress in Physical Geography **21** (1977), 530-548.
3. Zorita, E. and H. von Storch: The analog method as a simple statistical downscaling technique: comparison with more complicated methods. Journal of Climate **12** (1999) 2474-2489.
4. Goodess, C. M. *et al.* An intercomparison of statistical downscaling methods for Europe and European regions: Assessing their performance with respect to extreme temperature and precipitation events. Climate change, in press.
5. Hewitt, C.D and Griggs, D.J.: Ensembles-based predictions of climate changes and their impacts. Eos **85** (2004) 566.
6. Foster, I. and Kesselman, C. (2003). *The Grid 2: Blueprint for a New Computing Infrastructure.* Morgan Kaufmann Publishers.

Multi-robot Cooperation Based on Hierarchical Reinforcement Learning

Xiaobei Cheng, Jing Shen, Haibo Liu, and Guochang Gu

College of Computer Science and Technology, Harbin Engineering University,
Harbin 150001, China
adbccxb1306@sina.com.cn, {liuhaibo, shenjing,
guguochang}@hrbeu.edu.cn

Abstract. Multi-agent reinforcement learning for multi-robot systems is a challenging issue in both robotics and artificial intelligence. But multi-agent reinforcement learning is bedeviled by the curse of dimensionality. In this paper, a novel hierarchical reinforcement learning approach named MOMQ is presented for multi-robot cooperation. The performance of MOMQ is demonstrated in three-robot trash collection task.

Keywords: multi-robot, cooperation, hierarchical reinforcement learning.

1 Introduction

Multi-Robot Systems (MRSs) can often be used to fulfil the tasks that are difficult to be accomplished by an individual robot, especially in the presence of uncertainties, incomplete information, distributed control, and asynchronous computation, etc. So MRSs have received considerable attention during the last decade [1][2]. Currently, there has been a great deal of research on multi-agent reinforcement learning (MARL) in MRSs [3]. Multi-agent reinforcement learning allows participating robots to learn mapping from their states to their actions by rewards or payoffs obtained through interacting with their environment. MRSs can benefit from MARL in many aspects. Robots in MRSs are expected to coordinate their behaviors to achieve their goals. These robots can either obtain cooperative behaviors or accelerate their learning speed through learning [4]. But MARL is bedeviled by the curse of dimensionality.

Two methods for combating the curse of dimensionality are function approximation and hierarchical decomposition. Function approximation is aimed at approximating and thereby compacting a value function. Hierarchical approaches use structure in the representation to try to compact the representation and have the potential to reduce the exponential growth in the size of the state space to linear in the number of variables. Hierarchical solution involves multiple levels or stages of decision making that together solve the whole problem. Several alternative frameworks for hierarchical reinforcement learning (HRL) have been proposed [5], including Options [6], HAMs [7] and MAXQ [8]. Ghavamzadeh *et al* [9] extended MAXQ method for single agent HRL to multi-agent cooperative HRL. MAXQ has a number of notable features. MAXQ represents the value of each state in a subtask as a decomposed sum of

completion values. MAXQ allows subtask policies to be reused in different contexts. The final MAXQ feature to be highlighted is the opportunity for state abstraction [8]. State abstraction is key to reducing the storage requirements and improving the learning efficiency. State abstraction means that multiple states are aggregated and one completion value stored for the aggregate state in a subtask. But in the MAXQ framework the ability of state abstraction is limited. For example, in the multi-agent taxi domain [8] and the multi-robot trash collection task [9] the subtask *navigate* cannot be decomposed into more refined MAXQ subtask. On the other hand, the hierarchies are difficult to be discovered automatically.

In this paper, a novel multi-agent hierarchical reinforcement learning approach named MOMQ (Multi-robot Option-MaxQ) by integrating Options into MAXQ is presented for multi-robot cooperation. In the MOMQ framework, the MAXQ framework is used to introduce knowledge into reinforcement learning and the Option framework is used to construct hierarchies automatically.

2   MOMQ Framework

The MOMQ is based on the multi-agent cooperative MAXQ method in [8]. Consider sending a team of robots to pick up trash from trash cans over an extended area and accumulate it into one centralized trash bin, from where it might be sent for recycling or disposed. It is assumed that the robots are homogeneous, i.e., all robots are given the same task hierarchy. At each level of the hierarchy, the designer of the system defines cooperative subtasks to be those subtasks in which coordination among robots significantly increases the performance of the overall task. The set of all cooperative subtasks at a certain level of the hierarchy is called the cooperation set of that level. Each level of the hierarchy with non-empty cooperation set is called a cooperation level. The union of the children of the lth level cooperative subtasks is represented by U_l. Robots actively coordinate only while making decision at cooperative subtasks and are ignorant about the other robots at non-cooperative subtasks. Therefore, cooperative subtasks are configured to model joint-action values. An simulation experiment environment with three robots ($R1$, $R2$, and $R3$) is shown in Fig.1(a). Robots need to learn three skills here. First, how to do each subtask, such as navigate to trash cans $T1$, $T2$, or $T3$ or *Dump*, and when to perform *Pick* or *Put* action. Second, the order to do the subtasks, for instance go to $T1$ and collect trash before heading to *Dump*. Finally, how to coordinate with each other, i.e., robot $R1$ can pick up trash from $T1$ whereas robot $R2$ can service $T2$, and so on. The overall task is decomposed into a collection of primitive actions and temporally extended (non-primitive) subtasks that are important for solving the problem. The non-primitive subtasks in the trash collection task are root (the whole trash collection task), *collect* $T1$, $T2$, and $T3$, *navigate to* $T1$, $T2$, $T3$, and *Dump*. Each of these subtasks has a set of termination states, and terminates when reaches one of its termination states. Primitive actions are always executable and terminate immediately after execution. After defining subtasks, we must indicate for each subtask, which other primitive or non-primitive subtasks it should employ to reach its goal. For example, *navigate to* $T1$, $T2$, $T3$, and *Dump* use four primitive *up*, *down*, *left*, *right*. *Collect* $T1$ should use two subtasks *navigate to* $T1$ and *Dump* plus two primitive actions *Put* and *Pick*, and so on. The problem is how to

navigate efficiently in a large-scale environment. MOMQ framework can now be illustrated according to Fig.1(b). Imagine the robots start to learn the task with same MOMQ graph structure. The robots need to learn the fourth skill, i.e., how to construct the Options automatically.

The MOMQ method decomposes an MDP (Markov decision process) M into a set of subtasks M_0; $M_1...M_n$, where M_0 is the root task and solving it solves the entire MDP M. Each non-primitive subtask is a six tuple $(S_i, I_i, \pi_i, T_i, A_i, R_i)$. S_i is the state space for subtask i. It is described by those state variables that are relevant to subtask i. The range of the state variables describing S_i might be a subset of their range in S, the state space of the overall task MDP M. I_i is the initiation set for subtask i. Subtask i could start only in state $s \in I_i$. π_i is the policy for subtask i can only be executed if the current state $s \in (S_i - T_i)$. The hierarchical policy is executed using a stack discipline similar to ordinary programming languages. Each subtask policy takes a state and returns the name of a primitive action to execute or the name of a subtask to invoke. T_i is the set of terminal states for subtask i. Subtask i terminates when it reaches a state in T_i. A_i is the set of actions that can be performed to achieve subtask i. These actions can either be primitive actions from A (the set of primitive actions for MDP M) or they can be other subtasks. R_i is the pseudo reward function, which specifies a *pseudo-reward* for each transition from a state $s \in (S_i - T_i)$ to a terminal state $s \in T_i$. This *pseudo-reward* tells how desirable each of the terminal states is for this particular subtask. The initial decomposition does not include the Option level. The Options are constructed and inserted into the task graph automatically during learning. Then, the Options play the same roles as other sub-tasks.

Each primitive action a is a primitive subtask in this decomposition, such that a is always executable, it terminates immediately after execution, and it's *pseudo-reward* function uniformly is zero. The projected value function V^π is the value of executing hierarchical policy starting in state s, and at the root of the hierarchy. The completion function $(C^\pi(i, s, a))$ is the expected cumulative discounted reward of completing subtask M_i after invoking the subroutine for subtask M_a in state s. The (optimal) value function $V_t(i, s)$ for doing task i in state s is calculated by decomposing it into two parts as in (1): the value of the subtask which is independent of the parent task, and the value of the completion of the task, which of course depends on the parent task.

$$V^\pi(i,s) = \begin{cases} \max_a Q^\pi(i,s,\pi_i(s)) & \text{if } i \text{ is composite} \\ \sum_{s'} P(s'|s,i)R(s'|s,i) & \text{if } i \text{ is primitive} \end{cases} \tag{1}$$

$$Q^\pi(i,s,a) = V^\pi(a,s) + C^\pi(i,s,a)$$

where $Q_t(i, s, a)$ is the action value of doing subtask a in state s in the context of parent task i.

In cooperative level, The joint completion function for robot j, $C^j(i, s, a^1,..., a^{j-1}, a^{j+1},...a^n, a^j)$, is the expected discounted cumulative reward of completing cooperative subtask i after taking subtask a^j in state s while other robots performing subtasks a^k, $\forall k \in \{1,..., n\}$, $k \neq j$. The reward is discounted back to the point in time where a^j begins execution. $(a^1,..., a^n)$ is a joint-action in the action set of i. More precisely, the decomposition equations used for calculating the value function V for cooperative subtask i of robot j have the forms as in (2),

$$V^j(i,s,a^1,...,a^{j-1},a^{j+1},...a^n) = Q^j(i,s,a^1,...,a^{j-1},a^{j+1},...,a^n,\pi_i^j(s))$$
$$Q^j(i,s,a^1,...,a^{j-1},a^{j+1},...,a^n) = V^j(a^j,s) + C^j(i,s,a^1,...,a^{j-1},a^{j+1},...,a^n)$$
$$(2)$$

3   MOMQ Algorithms

According to prior knowledge, the designer firstly constructs the initial MOMQ task graph manually. Then the MOMQ algorithms construct the completed MOMQ task graph and learn it automatically, which can be outlined as follows:

1) Interact with environment and learn using *MOMQ learning algorithm*.
2) If the MOMQ constructing algorithm was invoked previously, then go to 1).
3) Run *state transition graph constructing algorithm*.
4) If there is no new states being encountered for the last Y episodes (task-dependent), then go to 5), else go to 1).
5) Run *MOMQ constructing algorithm*. Go to 1).

Consider an undirected edge-weighted graph $G=(P, E, W)$, P is the set of nodes, each visited state will become a node in the graph, E is the set of edges, and W is the $(|P| - 1) \times (|P| - 1)$ upper triangular matrix of weights. In the initial phase of the MOMQ learning procedure, The *state transition graph* $G=(\{s_0\}, \Phi, [0])$, where, $s_0 \in S$ is the initial state, Φ means empty set. The *state transition graph constructing algorithm* is shown as follows:

```
For each observed transition sᵢ→sⱼ (sᵢ,sⱼ∈S, sᵢ≠sⱼ) Do
  If sⱼ∉P then
     P ← P ∪ {sⱼ}; E ← E ∪ {(sᵢ, sⱼ)}
     Extend W with [0…0 1 0…0]ᵀ, the ith element is 1.
  Else
     If i>j then   wᵢⱼ=wᵢⱼ+1   else   wⱼᵢ=wⱼᵢ+1   End If
  End If
End For
```

The *MOMQ constructing algorithm* is proposed basing the aiNet, an artificial immune network model proposed in [10]. The aiNet can be defined as an edge-weighted graph, not necessarily fully connected, composed of a set of nodes, called cells, and sets of node pairs called edges. Each connected edge has a number assigned, called weight or connection strength. The aiNet can be used for data clustering. However, it has many drawbacks such as its high number of user-defined parameters, its computational cost per iteration $O(p^3)$ with relation to the length p of the input vectors, and the network sensitivity to the suppression threshold. In this paper, we improve the aiNet by initiating the aiNet with vaccine inoculation, i.e. the node information of the state transition graph, and leaving out the clonal procedure. The Ag-Ab affinity is measured by a topological distance metric (dissimilarity) between them. Oppositely, the Ab-Ab affinity is defined by a similarity metric between them. The *MOMQ constructing algorithm* works as follows:

1) Initiate aiNet with vaccine inoculation: set $C = P$, and $S = W$, where, C is a matrix containing all the network cells, and S is the network Ab-Ab affinity matrix.

2) For each antigen i (responding to $s_i \in P$), do:
   a) Determine Ag-Ab affinity matrix D;
   b) Select $\xi\%$ of the highest affinity cells to create a memory cell matrix M;
   c) Eliminate those cells whose affinity is inferior to threshold σ, yielding a reduction in the size of the M matrix;
   d) Calculate S,
   e) Eliminate $s_{ij} < \sigma$ (clonal suppression);
   f) Concatenate C and M, $(C=[C;M])$;
3) Determine S, and eliminate those cells whose $s_{ij} < \sigma$ (network suppression);
4) Replace $r\%$ of the worst cells;
5) If the network reaches a pre-defined number k of cells then go to 6) else go to 2);
6) $M \leftarrow C$;
7) Each memory cell m_j governs a cluster. The cluster is comprised of the states responding to those antigens of which m_j is their highest affinity cell. One cluster corresponds to an Option.
8) Insert constructed Options into the MOMQ task graph.

In the MOMQ framework, the Q values and the C values can be learned through a standard temporal-difference learning method, based on sample trajectories [7]. One important point to note here is that since subtasks are temporally extended in time, the update rules used here are based on the SMDP (semi-MDP) model. The pseudo code of *MOMQ learning algorithm* is shown as follows, which is similar with the *cooperative HRL algorithm* in [8].

```
Function MOMQ(Robots j, Task i at the lth level, State s)
  Seq ← {}
  If i is a primitive action Then
    Execute action i in state s
    receive reward r(s'| s, i)
    observe state s'
```
$$V_{t+1}^j(i,s) \leftarrow (1-\alpha_t^j(i))V_t^j(i,s)+\alpha_t^j(i)r(s'|s,i) \quad /* \ \alpha_t^j(i) \text{ is the learning rate}*/$$
```
    Push (state s, actions in {U_l| l is a cooperation
    level} being performed by the other robots) onto
    the front of Seq
  Else
    While i has not terminated Do
      If i is a cooperative subtask Then
```
      Choose action a^j according to $\pi_i^j(s,a^1,...,a^{j-1},a^{j+1},...,a^n)$
      `ChildSeq ← MOMQ(j, a^j, s)`
      Observe result state s' and $\hat{a}^1,...,\hat{a}^{j-1},\hat{a}^{j+1},...,\hat{a}^n$
$$a^* \leftarrow \arg\max_{a'\in A_i}[C_t^j(i,s,\hat{a}^1,...\hat{a}^{j-1},\hat{a}^{j+1},...\hat{a}^n,a')+V_t^j(a',s')]$$
      $N \leftarrow 0$
      For each $(s,a^1,...,a^{j-1},a^{j+1},...,a^n)$ in `ChildSeq` from the beginning **Do**
        $N \leftarrow N + 1$

$$C_{t+1}^j(i,s,a^1,...,a^{j-1},a^{j+1},...,a^n,a^j) \leftarrow$$
$$(1-\alpha_t^j(i))C_t^j(i,s,a^1,...,a^{j-1},a^{j+1},...,a^n,a^j)$$
$$+\alpha_t^j(i)\gamma^N[C_t^j(i,s',\hat{a}^1,...,\hat{a}^{j-1},\hat{a}^{j+1},...,\hat{a}^n,a^*)+V_t^j(a^*,s')]$$

```
   /* where γ is discount factor */
   End For
 Else /* i is not a cooperative subtask */
```

Choose action a^j according to $\pi_i^j(s)$

```
   ChildSeq ← MOMQ(j, aʲ, s)
   Observe result state s'
```

$$a^* \leftarrow \arg\max_{a' \in A_i}[C_t^j(i,s,a')+V_t^j(a',s')]$$

```
   N ← 0
   For each s in ChildSeq from the beginning Do
   N ← N + 1
```

$$C_{t+1}^j(i,s,a^j) \leftarrow (1-\alpha_t^j(i))C_t^j(i,s,a^j)+\alpha_t^j(i)\gamma^N[C_t^j(i,s',a^*)+V_t^j(a^*,s')]$$

```
       End For
     End If
     Append ChildSeq onto the front of Seq
     s = s'
   End While
 End If
 Return Seq
End MOMQ
```

4   Simulation Experiments

Consider the three-robot trash collection domain shown as in Fig. 1. Each robot starts in a random location and learns the task of picking up trash from *T*1, *T*2, and *T*3 and depositing it into the *Dump*. There are six primitive actions in this domain: (a) four navigation actions that move the robot one square *Up*, *Down*, *Left*, or *Right*, (b) a *Pick* action, and (c) a *Put* action. Each action is deterministic. The goal state is reached when trash from *T*1, *T*2, and *T*3 has been deposited in *Dump*. The environment space is partitioned into 64 states by grids. The robots do not know the structure of the environment but they can sense their locations. We apply the MOMQ algorithms to this problem, and compare its performance with the *cooperative HRL algorithm* in the multi-agent MAXQ framework [8].

In the experiments, there is a reward of -1 for each action and an additional reward of +20 for successfully depositing the trash into the *Dump*. There is a reward of -10 if the robot attempts to execute the *Put* or *Pick* actions illegally. If a navigation action would cause the robot to hit a wall, the action is a no-op, and there is only the usual reward of -1. The discount factor is set to γ=0.9. The initial Q-values are set to 0 and the learning rate is a constant α=0.1. A ε-greedy exploration is used for both algorithms, with ε=0.3. The constructing algorithm is initiated if no new state is observed in the last *Y*=2 episodes. Set the values of the parameters in the *MOMQ*

constructing algorithm as follows: ξ=20, r=5, σ=0.1, and k=10, experimentally. Each experiment is repeated ten times and the results averaged.

   Using MOMQ framework, we designed the initial task graph, the same as the MAXQ task graph. During learning procedure, the environment is explored and six Options (Opt1,…, Opt6) are automatically constructed for *Navigate* action. The completed MOMQ task graph is shown in Fig.1(b). According to the constructed Options, the state space of the environment is partitioned into six regions as shown in Fig.2(a). The state space of each Option is reduced to below 20% of the whole environment space. As a result, the solving space for the *Navigate* action of the three robots is reduced to about $1/10^{124}$. It is natural that the convergence is sped up in a smaller space. Such advantage is shown in Fig.2.

(a)   (b)
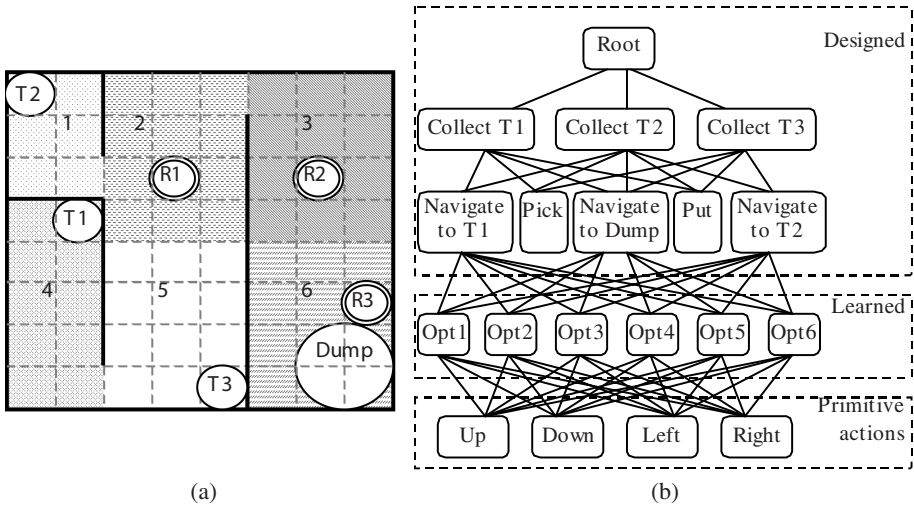
Fig. 1. The constructed results: (a) the constructed Options for *Navigate* action, and (b) the constructed MOMQ task graph
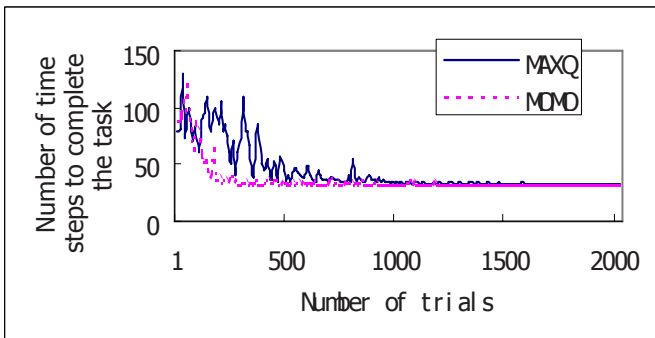
Fig. 2. Performance comparison of MOMQ with MAXQ

5   Conclusions

We described an approach, named MOMQ, for multi-robot cooperation by integrating Options into the MAXQ hierarchical reinforcement learning method. In the MOMQ framework, the MAXQ framework is used to introduce knowledge into reinforcement learning and the Option framework is used to construct hierarchies automatically. The MOMQ is more practical than MAXQ in partial known environment. The advantage performance of MOMQ is demonstrated in three-robot trash collection task and compared with MAXQ. The success of this approach depends of course on providing it with not only a good initial hierarchy but also a good learning ability.

References

1. Cao, Y.U., Fukunaga, A.S., Kahng, A.B.: Cooperative mobile robotics: antecedents and directions. Autonomous Robots, vol.4 (1997) 1-23
2. Fernandez, F., Parker, L.E.: Learning in large cooperative multi-robot domains. International Journal of Robotics and Automation, vol.16, no.4 (2001) 217-226
3. Touzet, C.F.: Distributed lazy Q-learning for cooperative mobile robots. International Journal of Advanced Robotic Systems, vol.1, no.1 (2004) 5-13
4. Yang, E., Gu, D.: Multiagent Reinforcement Learning for Multi-Robot Systems: A Survey. Technical Report CSM-404, University of Essex (2004)
5. Barto, A.G., Mahadevan, S.: Recent advances in hierarchical reinforcement learning. Discrete Event Dynamic Systems: Theory and Applications, vol.13, no.4 (2003) 41-77
6. Sutton, R., Precup, D., Singh, S.: Between MDPs and Semi-MDPs: A framework for temporal abstraction in reinforcement learning. Artificial Intelligence, vol.112 (1999) 181-211
7. Parr, R.: Hierarchical control and learning for Markov decision processes. PhD dissertation, University of California at Berkeley (1998)
8. Dietterich, T.: Hierarchical reinforcement learning with the MAXQ value function decomposition," Journal of Artificial Intelligence Research, vol.13 (2000) 227-303
9. Ghavamzadeh, M., Mahadevan, S., Makar, R.: Hierarchical multiagent reinforcement learning. Journal of Autonomous Agents and Multi-Agent Systems, vol.13 (2006) 197-229
10. de Castro, L.N., Von Zuben, F.N.: An evolutionary immune network for data clustering. Proceedings of the IEEE Brazilian Symposium on Artificial Neural Networks, vol.1, Rio de Janeiro, Brazil (2000) 84-89

Analysis on Spatio-temporal Characteristics of Wintertime Planetary Wave in the Northern Hemisphere Based on 2D FFT

Xiuhong Wang[1] and Weidong Yu[2]

[1] Information Retrieval Office, Jiangsu University, NO.301 Xuefu Road, Zhenjiang, China
[2] Lab of Marine Science and Numerical modeling, First Institute of Oceanography, SOA, China
Lib510@ujs.edu.cn, wdyu@fio.org.cn

Abstract. To describe spatial and temporal characteristics of the activities of wintertime planetary waves in the northern hemisphere, their numbers and periods were precisely calculated, based on NCAR/NCEP reanalysis data. The objective variables include sea level pressure (SLP) and anomaly stream function at 850 hPa, 500 hPa and 200 hPa. 2D FFT and spectral analysis reveal that: (1) The wave numbers 1 and 2 dominate the perturbation pattern at 70º-80 ºN zonal belt. (2) The wave numbers 1, 2 and 3 dominate at 60º-70ºN zonal belt. (3) The wave numbers 1-4 dominate at 50º-60ºN zonal belt. The results accord fairly well with Rossby's classical trough formula and are of potential use for understanding the northern hemisphere large-scale oscillations.

Keywords: Planetary wave, Large-scale oscillations, Northern hemisphere, Wave number.

1   Introduction

According to Rossby's [1] previous work on the relationship between variations in the intensity of the zonal circulation of the atmosphere and the displacements of the semi-permanent centers of action, it is well known that the planetary waves have significant impact on the troposphere circulation. Based on the trough formula, as is often called, Rossby roughly calculated the number of the long stationary waves and their wavelength.

Recent studies reveal that the northern hemisphere climate takes on some kinds of oscillations, including the North Atlantic Oscillation (NAO), the Arctic Oscillation (AO) [2] and the Pacific North American pattern (PNA). These features have close relationship with the planetary wave activities. Cavalieri and Häkkinen [3] reported the variability of SLP planetary waves and related these planetary-scale variations with some changes of climate observed in the Arctic over the last fifty years. Yu [4] proposed a stationary wave-2 frame to relate the NAO, AO and NPO on the basis of

Hoskins' great circle theory. Here the analysis to the higher levels in the troposphere is further extended to demonstrate the planetary wave activities and to show their climate impact.

2   Analysis and Results

The monthly SLP and wind data at 850hPa, 500hPa and 200hPa levels from the NCAR/NCEP Reanalysis Data [5] are used here. Their anomalies are deduced by extracting the corresponding climatologies. The time covers from 1948 to 2003. To examine the characteristics of the planetary-scale wave, only the rotational part of the wind field is kept. It is conducted by decomposing the wind field into non-divergent part $\vec{V}_\psi$ plus an irrotational part $\vec{V}_\phi$ according to the Helmholtz theorem [6]. Thus the stream function ψ is introduced as:

$$\varsigma = \nabla^2 \psi$$

(1)

where the ς is the vorticity. The global stream function corresponding to the rotational part of the wind anomaly is acquired through Eq.(1) with the aid of the Fishpack program package [7]. Then the following analysis is conducted on the basis of SLP and the stream functions at 850 hPa, 500 hPa and 200 hPa levels.

Table 1. Fraction of variance (in percentage) accounted by different wave structures

Field	Latitude	Wave 1	Wave 2	Wave 3	Wave 4	Wave 5
	70°-80°N	71.086	19.787	5.0084	2.0065	0.53583
SLP	60°-70°N	44.529	34.572	9.8977	6.943	1.8271
	50°-60°N	26.601	37.112	16.061	11.722	4.3615
	70°-80°N	62.705	29.641	5.047	2.0109	0.30322
850hPa stream function	60°-70°N	34.058	40.701	15.4	7.3467	1.3215
	50°-60°N	29.592	29.31	20.663	14.185	3.7139
	70°-80°N	52.222	38.733	6.0772	2.4429	0.33537
500hPa stream function	60°-70°N	26.551	42.736	21.062	7.364	1.44
	50°-60°N	25.804	25.823	25.778	16.562	3.8251
	70°-80°N	60.842	33.641	4.5788	0.79062	0.10893
200hPa stream function	60°-70°N	32.834	44.366	17.247	4.6042	0.65593
	50°-60°N	25.658	30.039	25.198	14.434	3.2481

Furthermore, the analysis focuses on three ten-degree latitude bands from 50° N to 80° N latitude, with the January being used as the representative of the wintertime.

We chose 200 hPa, 500 hPa and 850 hPa layers as the representatives of the upper, middle and lower troposphere. The temporal and spatial structure of the planetary-scale wave revealed by the 2D FFT is shown in Fig.1 respectively for the anomalous SLP and the stream functions at upper, middle and lower troposphere. Also the fraction of variance accounted by different waves is shown in Table 1. As for the case of SLP, the wave structure shows different characteristics in three bands. For the 70°-80°N band, the significant fraction of the variance in SLP is carried by wave 1, which accounts for over 71% of the total variance. The energy in shorter waves increases significantly with the decrease of the latitude. The wave 2 in 60°-70°N band and the wave 3 in 50°-60°N band vary significantly, and they account for over 19 % and 5% of the total variance respectively. This tendency also exists in the stream functions, which has the generally similar energy distribution in the wave number space with the intensity of variation increasing from 850 hPa to 200 hPa level. As for the stream functions, the structures of waves 1-2 in70°-80°N band, waves 1-3 in 60°-70°N band and waves 1-4 in 50°-60°N band dominate the variance and explain over 90% of the total variance. From the lower level to the upper level of the troposphere, the perturbation has the similar pattern in the three bands. The result accords well with the qualitative estimate of the stationary wave length given by Rossby's trough formula.

The 2D FFT gives further information on the temporal characteristics of the spatial structure mentioned above. Waves of different length scale have different characteristics of the time evolution. [3] pointed out that the phases of waves 1 and 2 in 70°-80°N band have significant peaks at 3.6, 5.6 and 12.5 years for SLP field. The present analysis focuses on the amplitude of the variation but not on the phase. However, the temporal characteristic can also be seen from Fig. 1. The powers of waves 1, 2 and 3 in 50°-80°N band show concentration peaks at 2.9-, 3.6-, 4.4-, 5.6-, 6.9-, 12.5-, near 14-, near 33-, and near 60-year periods both for SLP and for stream functions. The 3.6-year period is likely related to atmospheric circulation changes with El Nino [8]. The 5.6-year period is probably associated with the variability in Arctic sea ice extent [9]. The reason for the decadal and the interdecadal signals is not clear and needs further exploration. It should be noted that the 5.6-year period is most significantly associated with the wave 2 structure in 60°-70°N band, while the decadal signal is most significantly associated with the wave 1 structure in all the three bands and with the wave 3 structure just in 50°-60° N band. Except for the decadal signal, the interannual (here are 2.9-, 3.6- and 6.9-year periods) signal is also very significantly associated with wave 1 structure in high latitude bands. This may cast some light on their physical interpretation. ENSO has its global influence through the Rossby wave propagation and dispersion on the sphere and thus the signal can be detected at all the three bands. The Arctic
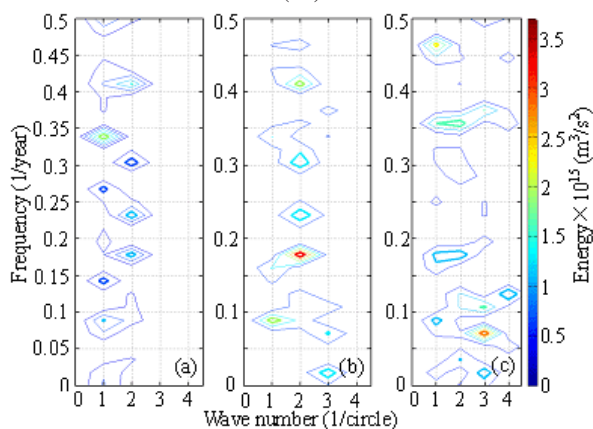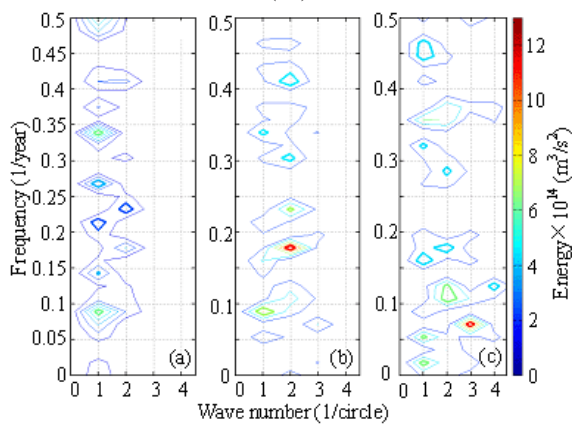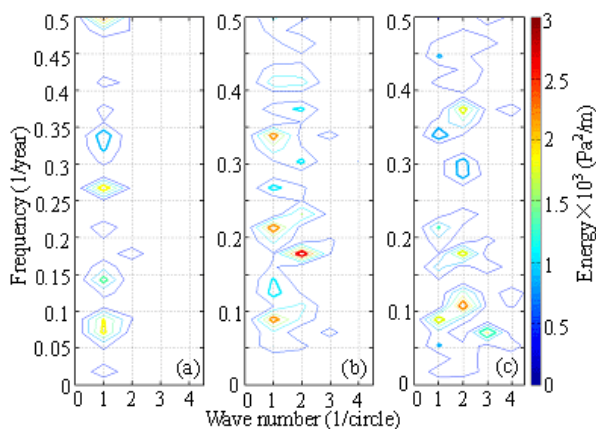
Fig. 1. 2D FFT of the perturbed SLP and stream function
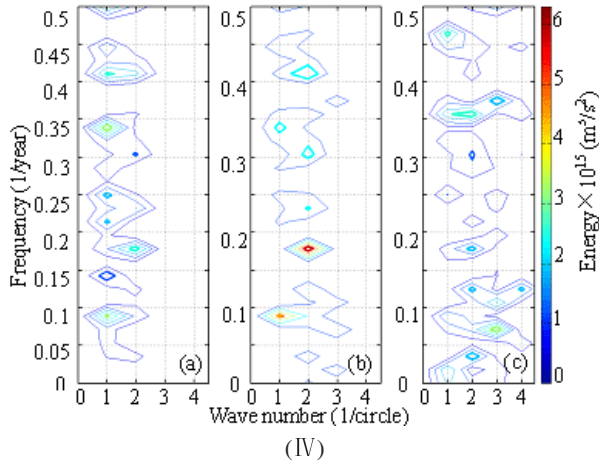
Fig. 1. (*Continued*)

sea ice extent variation can cause the large-scale perturbation, which directly influences the high latitude region because the perturbed long Rossby wave propagates in the zonal and northward direction but not in southward direction according to Hoskins' great circle theory [10].

(I) a. SLP in 70°-80°N band; b. SLP in 60°-70°N band; c. SLP in 50°-60°N band;
(II) a. 850 hPa stream function in 70°-80°N band; b. 850 hPa stream function in 60°-70°N band; c 850 hPa stream function in 50°-60°N band;
(III) a. 500 hPa stream function in 70°-80°N band; b. 500 hPa stream function in 60°-70°N band; c. 500 hPa stream function in 50°-60°N band;
(IV) a. 200 hPa stream function in 70°-80°N band; b. 200 hPa stream function in 60°-70°N band; c. 200 hPa stream function in 50°-60°N band

The spatial-temporal structure is further explored by power spectrum analysis with the time series (1948-2003) of the variances accounting for waves 1-4, as shown in Fig. 2. The fraction of variance is calculated with the FFT of the anomalous quantity subtracted from the zonal average for each calendar January. The time evolution further supports the above conclusion of the wave structure at three latitude bands. It has been known from Table 1 that waves 1 and 2 dominate the variance for 60°-80°N band. An interesting point here is that the waves 1 and 2 in 60°-80°N band vary out of phase, i.e. they alternatively dominate the variance among most of years and only coexist in few years. The out-of-phase evolution of different wave structures exists from the surface to the upper troposphere level. Also the overall wave structures keep well vertically.
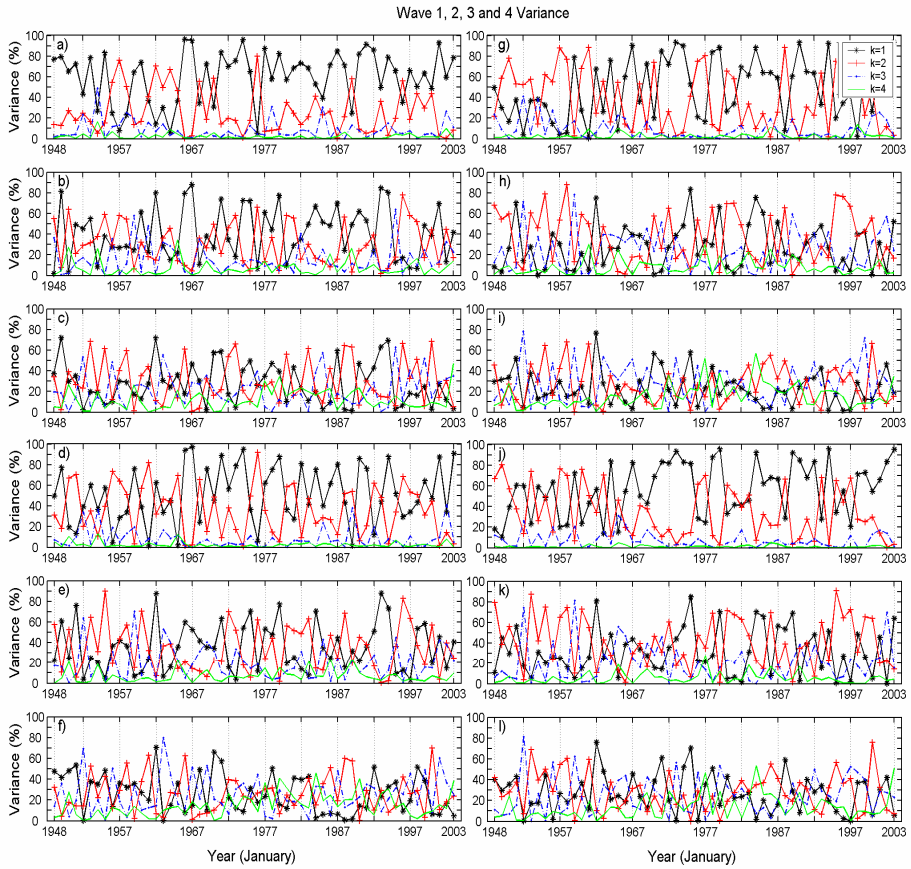
Fig. 2. Time series of the fraction of variance accounted by different wave structure

3   Discussion and Conclusion

It is anticipated from Rossby's pioneering work that the stationary long Rossby wave stands in the northern hemisphere and has close relationship to the intensity of the semi-permanent action center. Based on the NCAR/NCEP reanalysis data, the idea is fully examined and it is shown from the diagnosis that the variation of the perturbed SLP and stream functions from lower to upper troposphere has rather systematic structure. Waves 1-4 dominate the variance pattern at 50°-60°N band, while waves 1-3 and 1-2 dominate it in 60°-70°N band and in 70°-80°N band respectively. The significant wave structure accounts for over 90% of the total variance.

   a. SLP in 70°-80°N band; b. SLP in 60°-70°N band; c. SLP in 50°-60°N band;
   d. 850 hPa stream function in 70°-80°N band; e. 850 hPa stream function in 60°-70°N band;
      f. 850 hPa stream function in 50°-60°N band;

g. 500 hPa stream function in 70º-80ºN band; h. 500 hPa stream function in 60º-70ºN band;
   i. 500 hPa stream function in 50º-60ºN band;
j. 200 hPa stream function in 70º-80ºN band; k. 200 hPa stream function in 60º-70ºN band;
   l. 200 hPa stream function in 50º-60ºN band

According to Hoskins' great circle theory, an important application of the wave structure is that the large scale climate variability in the northern hemisphere can be understood from the point of view of the teleconnection. Large scale Rossby wave can transfer the perturbation information along the ray path around the sphere. Thus the North Atlantic Oscillation, the Arctic Oscillation and the oscillation in the north Pacific are likely to be connected through the wave process. Given the perturbation source at the north Atlantic, the signal can propagate northeastward as the form of planetary wave and cross through the Arctic region to the north Pacific. However, the assumption should be further explored with the data analysis and model works.

References

1. Rossby, C. G., collaborators: Relation between Variations in the Intensity of the Zonal Circulation of the Atmosphere and the Displacements of the Semi-permanent Centers of Action, J. Mar. Res., (1939) 39-55
2. Thompson, D. W. J., J. M. Wallace: The Arctic Oscillation Signature in the Wintertime Geopotential Height and Temperature Fields, Geophys. Res. Lett., 25, (1998) 1297-1300
3. Donald J. Cavalieri, Sirpa Häkkinen: Arctic Climate and Atmospheric Planetary Waves, Geophys. Res. Lett., 28, (2001) 791-794
4. Yu W., M. Ikeda, Z. Liu, M. Xia: A Dynamic View of Arctic Oscillation, its Teleconnection with NAO and PDO. Proceeding of Chinese-Norwegian Symposium on Polar Research, Shanghai (2001)
5. Kalnay E., Co-authors: The NCEP/NCAR Reanalysis 40-year Project, Bull. Amer. Meteor. Soc., 77, (1996) 437-471
6. Holton, J. R.: An Introduction to Dynamic Meteorology, 3rd edn., Academic Press (1992)
7. Adams, J., Swarztrauber, P., Sweet, R.: Fishpack — A package of Fortran Subprograms for the Solution of Separable Elliptic Partial Differential Equations (1980). Available from http://www.netlib.org/fishpack
8. Trenberth, K. E., Hurrel, J. W.: Decadal Atmosphere-ocean Variations in the Pacific, Clim. Dynamics, 9, (1994) 303-319
9. Cavalieri, K. J., P. Gloersen, C. L. Parkinson, J. C. Comiso, H. J. Zwally: Observed Hemispheric Asymmetry in Global Sea Ice Changes, Science, 272, (1997) 1104-1106
10. Hoskins, B. J., Karoly, D. J.: The Steady Response of a Spherical Atmosphere to Thermal and Orographic Forcing, J. Atmos. Sci., 38, (1981) 1179-1196

DECP: A Distributed Election Clustering Protocol for Heterogeneous Wireless Sensor Networks

Xianghui Wang and Guoyin Zhang

College of Computer Science and Technology, Harbin Engineering University, 150001
Harbin, China
Wangxianghui@hrbeu.edu.cn

Abstract. Heterogeneous wireless sensor networks are energy limited and imbalance networks, load balancing and energy efficiency is the most challenging task in these networks. In this paper, we propose a distributed election clustering protocol to prolong the stable region of wireless sensor networks, which is based on remaining energy and communication cost to elect suitable cluster-head nodes. Compared with classical clustering protocol, our protocol can maintain load balancing of networks, and extremely prolong the stable region of network lifetime.

Keywords: wireless sensor networks, cluster, heterogeneous.

1 Introduction

Wireless sensor networks have been envisioned to have a wide range of application in both military and civilian domains [1]. Due to the limitation of sensor node energy, researchers have designed lots of energy-efficient routing protocols to prolong the lifetime of sensor networks. These protocols are mainly for homogeneous sensor networks, and hardly used in heterogeneous environments. In this paper, we propose DECP, a new distributed election clustering protocol for tow-level heterogeneous wireless sensor networks. DECP is heterogeneous-aware, in the sense that election probabilities are weighted by residual energy and communication cost. When energy is imbalance in local area, high energy node is prior to be the cluster head, and when energy is balance, communication cost is considered first. This election mechanism prolong the time interval before the death of the first node (stable region), which is crucial for many applications where the feedback from the sensor network must be reliable. We show by simulation that DECP could implement load balancing and provides long stable region than the classical protocols LEACH [2] and SEP [3].

2 Clustering Parameters

In order to prolong the stable region, DECP attempts to maintain the constraint of well balanced energy consumption. High energy nodes should have more opportunity to

become cluster-head, and low energy nodes should not be the cluster-head until there are no high energy nodes within their detective range. We use Average Power Distinction (APD) to evaluate the power level of node i .

$$APD_i = 1 - \frac{\sum\limits_{j \in NBR_i} E_j^{current}}{|NBR_i| \cdot E_i^{current}} \tag{1}$$

NBR_i is the set of neighbors of node i , which are located in the detective range of nod i , and $|NBR_i|$ is the total number of nodes in NBR_i . $E_i^{current}$ is the current residual energy of node i .

APD_i reflects the power distinction between the node i and its neighbors. If APD_i is more than zero, node i is a high energy node, which means that node i have more energy than his neighbors; if APD_i is less than zero, node i is a low energy node, and should have less opportunity to be the cluster-head node.

In heterogeneous networks, we must both consider the average power distinction and communication cost for cluster-head selection, so we use *mCost* to evaluate communication cost in heterogeneous networks.

$$mCost_i = (1 - APD_i) \cdot \frac{\sum\limits_{j \in NBR_i} d_{i,j}^2}{|NBR_i|} = \frac{\sum\limits_{j \in NBR_i} E_j^{current} \cdot \sum\limits_{j \in NBR_i} d_{i,j}^2}{|NBR_i|^2 \cdot E_i^{current}} \tag{2}$$

$d_{i,j}$ is the distance between node i and node j , and this value should be computed by receiving sensitivity. *mCost* provides a unified criterion for all nodes to select cluster-head nodes, which means that all nodes could use *mCost* to select cluster-head nodes, which is the nodes with high energy and low communication cost.

3   DECP Protocol

A clustered sensor network is partitioned to a number of clusters. Node i working as a cluster-head node is denoted by ch_i . The set of all cluster-head nodes is denoted by CH , $CH \subseteq N$, where N is the set of all nodes including cluster-head nodes and non-cluster-head nodes. Now we describe DECP protocol in detail.

In clustering process, all the nodes broadcast its current energy information **Energy_msg**, and then overhear the energy message from the other nodes. When nodes have sufficient information about its neighbors, such as distance and current energy, nodes calculate **mCost** about itself and broadcast **mCost** to its neighbors. According to **mCost**, each node selects the candidate node which has the minimal **mCost**, and sends **Vote_msg** to the candidate node. The nodes which receive the most **Vote_msg** in neighbors, will announce that the cluster-head nodes are elected, and all non-cluster-head nodes chose one nearest cluster-head to join the cluster.

Table 1. DECP protocol

1. $\forall$ x [node(x).bcast(***Energy_msg***;Dst,all)]
2. if node *i*.hears_from(node *j*)
3.   node *i*.Set_neighbor $\leftarrow$ node *j*
4.   node *i*.Set_energy $\leftarrow$ node *j*.energy
5. $\forall$ x [node(x).bcast(***mCost_msg***;Dst,all)]
6. if node *i*.hears_from(node *j*)
7.   node *i*.Set_mCost $\leftarrow$ node *j*.mCost
8. $\forall$ x, $\exists$ y, y$\in$ node(x).Set_neighbor $\wedge$ node(y).mCost=min(node(x).Set_mCost)
9.   [node(x).send(***Vote_msg***;Dst,node(y))]
10. if node *i*.receive_voteMsg_from(node *j*)
11.   node *i*. ticket = node *i*.ticket+1
12. $\forall$ x [node(x).bcast(***Ticket_msg***;Dst,all)]
13. if node *i*.hear _from(node *j*)
14.   node *i*. Set_ticket $\leftarrow$ node *j*.ticket
15. $\forall$ x , [if node(x).ticket > max(node(x).Set_ticket),
16.   CH $\leftarrow$ node(x)]
17. $\forall$ x, x$\in$ CH [node(x).bcast(***ClustHead_msg***;Dst,all)]
18 if node *i*.hears_from(node *j*)
19.   node *i*.Set_CH $\leftarrow$ node *j*
20. $\forall$ x, x$\in$ N-CH, $\exists$ y, y$\in$ node(x).Set_CH $\wedge$ (y is the nearest cluster-head for x)
21.   [node(x).join(node(y))]

4 Simulation and Evaluation

We simulate a wireless network of 100 nodes in a 100×100 square area using MATLAB, and the sink node is located in the center of the area. We assume that *m* is the percentage of the nodes which are equipped with *a* times more energy than the normal nodes. The initial energy of normal node is 0.1J, so the initial energy of advance node is $0.5(a+1)$ J. In order to measure the energy consumption for data transmission, we used the same energy consumption model introduced in [4], using radio electronics energy $E_{elec} = 50\,nj/bit$, radio amplifier $\varepsilon_{fs} = 10\,pj/bit/m^2$, the consumption of data fusion $E_{fusion} = 5\,nj/bit/message$, 2000 bit-size sensed data package and 50 byte-size broadcast package.
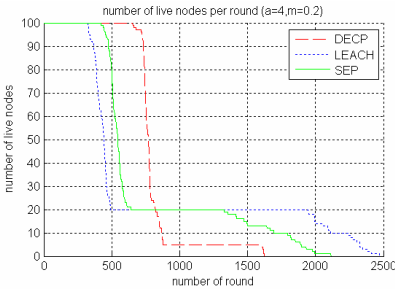
Fig. 1. Number of live nodes   **Fig. 2.** Contrast of APC/APN
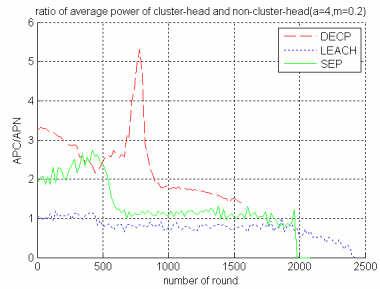
We compare the performance of DECP protocol with LEACH and SEP in the same heterogeneous setting, where m =0.2 and a =4.

Figure1 shows that DECP extremely extend the stable region compared to LEACH by 102.16% and SEP by 49.17%. On the other hand, DECP increase the ratio of stable region in network lifetime. In DECP, the ratio is 40.31%, in LEACH and SEP it is 13.11% and 19.91%. DECP select high energy nodes to be the cluster-head for load balancing, and low energy nodes spend less energy than high energy nodes. So DECP avoid the death of low energy nodes too earlier and prolong the stable region of the wireless sensor networks.

Figure2 shows that the APC/APN of DECP is higher than LEACH and SEP. APC/APN is the ratio of average power of cluster-head nodes and non-cluster-head nodes. If APC/APN more than one, it means that the cluster-head nodes have more average energy than non-cluster-head nodes; if APC/APN is equal one, it means that the cluster-head nodes have the same average energy as non-cluster-head nodes. LEACH use random arithmetic to select cluster-head nodes, so APC/APN is approximately equal one. In SEP, the advance nodes have more opportunity to be the cluster-head, but the arithmetic still use random mechanism to select cluster-head, so the APC/APN is just more than one. DECP has the best performance in APC/APN, because DECP do not use random mechanism for cluster-head selecting, thus DECP could accurately select the high energy node with low communication cost to be the cluster-head, and implement load balancing.

We also analyze the performance of DECP with different m and a , the experiment result show that the stable region of DECP is far more than that of LEACH and SEP, even in the homogeneous networks (a =0).

5   Conclusion

In this paper, we present DECP, a distributed election clustering protocol for tow-level heterogeneous wireless sensor networks. Our protocol does not need any of global energy knowledge at clustering process. As long as nodes exchange local information, cluster-head nodes could be selected. Furthermore, DECP is scalable as it dose not required any of exact position of each node in the filed. Our protocol use local energy information and communication cost for clustering, it is prolong the stable stage of the wireless sensor networks.

References

1. I.F Akyildiz, W. Su, Y. Sankarasubramaniam, E. Cayirci: A survey on sensor networks. IEEE Communications Magazine (2002) 102–114
2. W.R. Heinzelman, A.P. Chandrakasan, H. Balakrishnan: Energyefficient communication protocol for wireless microsensor networks. In Proceedings of the 33rd Hawaii International Conference on System Sciences (2000)
3. Georgios Smaragdakis, Ibrahim Matta, Azer Bestavros: SEP: A Stable Election Protocol for clustered heterogeneous wireless sensor networks. IEEE (2003)
4. W. Heinzelman, A. Chandrakasan, H. Balakrishnan: An Application-Specific Protocol Architecture for Wireless Microsensor Networks. IEEE Trans, Wireless Comm(2002) 660- 670

Catastrophe Prediction of Cnaphalocrosis Medinalis Based on Fuzzy Reasoning

Fei Yu[1,2,3], Yue Shen[1], Guangxue Yue[2,3], Ronghui Wu[3], and Cheng Xu[3]

[1] School of Computer & Information Engineering, Hunan Agricultural University, Changsha 410128, China
{yufei,shenyue}@hunau.edu.cn
[2] State Key Laboratory of Information Security, Graduate School of Chinese Academy of Sciences, Beijing, 100049, China
yufei@hunau.edu.cn
[3] Provincial Key Lab of Image Processing & Imagecom Communication , Nanjing University of Pos & Telecommunications, Nanjing , 210003, China
hunanyufei@126.com

Abstract. The pest catastrophe prediction in ecology catastrophe is one of important part in expert system of intelligence agriculture and also the guarantee for preventing and controlling the pest catastrophe occurrence efficiently. The paper introduces the basic principles and methods of current catastrophe prediction in ecology catastrophe. According to modeling for the dynamic process of population, up-grown and amount of spawn, the paper finds out the trigger point and critical value inducing the pest catastrophe and implements the catastrophe prediction of Cnaphalocrosis Medinalis, which take measures before catastrophe to prevent big population coming into being**.**

1   Introduction

Some mainly pests in crops have regionally migratory, eruptive and destructive characteristics[1][2]. It is very difficult to forecast for the paroxysm in migratory pests. Since "six. five", national science committee have tackled the key problems in forecast of pests, which made the forecast rate has already reached 80 percent. But the remainder other 20 percent which cannot predict by normal methods are just the eruptive increase of pest populations which need forecast precisely. The outbursts of beet webworms in 1980s, cotton bollworm in 1992, rice louses in 1997 and 1991 etc, made people cannot prevent in advance and met the emergency passively, had the disastrous losing.

2   Catastrophe Prediction Module of Cnaphalocrosis Medinalis

Though there are the outside random factors, with the knowledge of pest catastrophe occurrence regular and outside factors physical process deepened little by little, it is possible to divide a part of outside random factors to make them predictable. Since

the un-forecasting proportion decided by outside random factor is more and more little, it improve the forecasting right ratio to the long-term prediction. In essence, the possibility of long-term prediction depends on inherence random of system. The continuity in pest catastrophe occurrence process, dispersion of pest catastrophe occurrence data, un-dynamic evolvement characteristics in pest catastrophe occurrence system result in the complexity of pest catastrophe occurrence system. If the initial conditions or system parameters have little difference, the future state of pest catastrophe occurrence system will be different in essence. However, just uttermost sensitive to initial conditions, the pest catastrophe occurrence represents stability to abnormal. In principle, both the chaos behavior to dissipative nonlinear system and chaos behavior to HARMILTON nonlinear system all can have statistic description by the fix distributed function, which proves the pest catastrophe prediction is possible[3].

3   Implemention of Inference Machine of Catastrophe Prediction

The fuzzy rules of the Oth-order Sugeno model can be expressed as follows[4]:

$$R_i : if \ \ x_1 \ is \ A_1^i \ with \ m_1^i \ and \ x_2 \ is \ A_2^i \ with \ m_2^i \ and \ \dots \ x_n \ is \ A_n^i$$
$$with \ m_n^i \ then \ y_1 \ is \ B_1^i \ and\dots \ y_q \ is \ B_q^i \tag{1}$$

3.1   Automatic Evolution of Fuzzy Rule Base

Through experts' knowledge and experience we can design fuzzy models, however, depending merely on such experience is quite inadequate especially when the target system we are modeling is unacquainted with many uncertainties. Therefore, researchers devoted themselves to designing the fuzzy models automatically based on training the acquired data. By utilizing EP to fuzzy modeling, we can simultaneously evolve the structure and the parameters of fuzzy rule bases for a given task[3]. States are the illuminations of the whole system state inferred by inference machine according to the information base and rules base. The paper defines states like OK, PRE_ATTACK, ATTACKING, ATTACKED.

In the original idea a standard deviation for mutation of the ith component zi, is obtained as a function of the fitness value of the mth individual $\theta(m)$ as follows:

$$z_i' = z_i + \sigma_i * N(0,1), \sigma = \sqrt{(\beta_i * \theta(m)) + \gamma_i} \tag{2}$$

In the design of an optimal fuzzy model, the fitness function usually used can be expressed as follows:

$$F = \frac{1}{E}, E = \frac{1}{num}\left[\frac{1}{q}\sum_{p=1}^{q}\sum_{l=1}^{num}(y_{lp} - y_{lp}^*)^2\right] \tag{3}$$

3.2 Hybrid Learning Rule

Hybrid learning rule can be derived from J. S. Jang's research[3][6]on adaptive network. J. S. Jang observed that the output of a certain adaptive network is linear in some of the network parameters, which thereby can be identified by the least squares method. And then the combination of the gradient method and the LSE forms the so-called hybrid learning rule. For simplicity, assume that the adaptive network under consideration has only one output:

$$Output = F(X,S) \qquad (4)$$

where X is the set of input variables, S is the set of parameters, and F is the whole function of which the adaptive network realizes. If there exits a function H such that the function $H \circ F$ is linear in some of the parameters of S, then these elements can he identified by the least squares method. More formally, if the parameter set can be decomposed into two sets:

$$S = S_1 \oplus S_2 \qquad (5)$$

Remember to submit the psfig or epsf files and further style files and fonts you have used together with your source files.

such that $H \circ F$ is linear in the elements of S2,, then upon applying H to $Output = F(X,S)$, we have:

$$H(F) = H \circ F(BX,S) \qquad (6)$$

4 The Implemention of Rules Base

According to the research results of Cnaphalocrosis Medinalis in recent years and based on the test information of pest test-station of plant prevention in HUNAN farm science academy, the paper described the inference by expert knowledge rules.

Table 1. Predict principle of occurrence period

Condition of Occurrence period	Condition of temperature	Result
the initial period of chrysalis	Larger or equal than 25 °C	initial period of imago after 10-13 days
the initial period of chrysalis	Less than 25°C	initial period of imago after 13-16 days
the fastigium period of chrysalis	Larger or equal than 25 °C	fastigium period of imago after 10-13 days
the fastigium period of chrysalis	Less than 25°C	fastigium period of imago after 13-16 days
the initial period of imago	Larger or equal than 25 °C	initial period of incubation after 6-7 days
the initial period of imago	Less than 25°C	initial period of incubation after 7-8 days
the fastigium period of imago	Larger or equal than 25 °C	fastigium period of incubation after 6-7 days
the fastigium period of imago	Less than 25°C	fastigium period of incubation after 7-8 days

The rules are divided to occurrence trend prediction, occurrence amount prediction, occurrence time prediction and loss rate prediction. The occurrence trend prediction is divided to the whole process of occurrence trend prediction, occurrence trend prediction of Cnaphalocrosis Medinalis in the metaphase of paddy growing and anaphase of paddy growing. The occurrence amount prediction is divided to spawn density and three ages grubs prediction. The occurrence time prediction is divided to the initial period of chrysalis, the fastigium period of chrysalis, the beginning of imago, the fastigium period of imago, the initial period of incubation, the fastigium period of incubation, the initial period of three ages grub, the fastigium period of three ages grub. The least and simplest rule table is as follows.

5   Conclusion

The biology technology and information technology are the mainly basic technologies in modern agriculture. With the geography information used widely in recent years, there are multi-subject intercrossing each other to develop. Compared to the traditional decision system of agriculture, the expert system of ecology catastrophe prediction proposed in paper is a single module, which has many deficiencies. The expert system is built based on the paddy plant information of HUNAN province and the experience of some experts. Our next research will be regarded as whether the system suits other area or not. Meanwhile, if the granularity of rules is too rough, it will effects the exactness of system, else add the overhead of communication between human and computer. How to find the most suitable granularity is the emphasis of next research.

References

1. Zhou Liyang,Zhang Xiaoxi:Prediction Expert System of Rice Leaf Roller in Jianghuai Rice Region. Journal of China Agricultural University,1996,19(3):44-50
2. Ju Baoping: Bio-disaster forecasting: challenges and strategies. Journal of Nanjing Agricultural University,2001,(4):41-45
3. Wang Sishui,Zhang Xiaoxi:Long-time Prediction of Rice Leaf Roller based on Neural Network. Journal of Plant Protect. 2000,27(4):313-316
4. H. V. Jagadish, A. O. Mendelzon, I. S. Mumik. : Managing conflicts between rules. Journal of Computer and System Science,1999, 58 (1):13-28
5. Huang Baohong, Xia Minghai. : Prediction of Rice Leaf Roller in feng-yang county Rice Region. Anhui Agricultural Sciences,1997,17(2):151-152

Preconditioned Krylov Subspace Methods Solving Dense Nonsymmetric Linear Systems Arising from BEM

Zejun Chen and Hong Xiao

College of Mechanical Engineering, Yanshan University, Qinhuangdao 066004, China
chen_zejun@163.com , xhh@ysu.edu.cn

Abstract. Discretization of boundary integral equations leads, in general, to fully populated nonsymmetric linear systems of equations. We research the comparative performances of iterative techniques based on Krylov subspace solvers as GMRES(m), QMR and Bi-CGStab solving linear systems arising from BEM elasticity problems. Several general preconditioners are also considered and assessed. The results of numerical experiments suggest that preconditioned Krylov subspace methods are effective approaches for the solution of dense nonsymmetric linear systems arising from BEM.

Keywords: Krylov Subspace Method; Preconditioner; Dense Nonsymmetric Matrix; Boundary Element Method.

1 Introduction

The Boundary Element Method (BEM) is an important technique in the numerical solution of engineering or scientific problems. The matrix of the system in the BEM is fully populated and nonsymmetric. A fast convergent iterative solution method, which would require the number of iterations much less than the number of DOF, will decrease the computational cost to $O(N^2)$ [1]. The Krylov subspace iterative methods are efficient methods in solving the linear systems arising from BEM formulation [2-4]. On the other hand, the systems obtained from the discretization step are badly conditioned, especially when mixed boundary conditions exist or large scale problems. Thereby, preconditioning is very essential to the successful use of Krylov subspace iterative methods. In this paper, we are primarily concerned with the efficient solution of dense nonsymmetric systems arising from BEM elasticity problems by preconditioned Krylov subspace methods.

2 Preconditioned Krylov Subspace Methods

We are concerned with the solution of dense nonsymmetric linear systems $Ax = b$ arising from BEM formulation. In this paper, three of the most widely used Krylov subspace methods (GMRES, QMR, Bi-CGStab) are considered. Briefly, starting with an initial guess x_0 , iterates $x_i \in x_0 + K_i(A, r_0)$ are produced such that the residuals $r_i = b - Ax_i$ are in some sense small [4]. The Krylov subspace is defined as

$$K_m(A, r_0) = \text{span}\left\{r_0, Ar_0, A^2 r_0, \cdots, A^{m-1} r_0\right\} \tag{1}$$

Note that these subspaces are nested, i.e. $K_m \subseteq K_{m+1}$.

It is well known that the rate of convergence of an iterative method depends greatly on the spectral properties of coefficient matrix. Hence, iterative methods usually involve a matrix that transforms the original coefficient matrix into one having the same solution but more favorable spectral properties. A preconditioner is a matrix that can be used to accomplish such a transformation.

$$M^{-1}Ax = M^{-1}b \tag{2}$$

In practice, the preconditioner should meet the requirement of two characteristics. First, the preconditioned matrix $M^{-1}A$ must be (much) better conditioned than A so that Eq.(2) can be efficiently solved by iterative methods. Secondly, the cost of constructing and applying preconditioner must be cheap. However, the two requirements are contradicting, so there is a trade-off between the cost of constructing and applying the preconditioner, and the improvement of iterative efficiency.

3   Numerical Examples

The experiments with different krylov subspace methods are performed using the iterative solver written in Fortran90 and compiled by Compaq Visual Fortran 6.5. All experiments are performed on a PC with 1GB RAM memory under Windows XP Professional. The computer is equipped with a 2.8GHz Intel Pentium 4 processor and no special software optimization or specialized hardware. A convenient stopping criteria is used the stopping criteria $i > maxit$ or $\left\|r^{(i)}\right\| \leq \varepsilon \cdot \left\|b\right\|$.

Example 1: In this section, we solve the same numerical problem using different preconditioned Krylov subspace methods. The number of DOF is 1806. The initial guess is the zero vector. The convergence histories of Krylov subspace methods are depicted in Figs. 1-3 for different preconditioning techniques gives us some clues as to the numerical behaviors of the proposed schemes. In these figures "JOBI" means Jacobi preconditioning, "BJOB" means Block Jacobi preconditioning, "ILU3" and "ILU5" mean Incomplete LU Factorization Preconditioning with Tri-diagonal and Five-diagonal nonzero structure, respectively.

From these figures, it can be seen that the convergence velocity of Krylov subspace methods can be significantly improved by using the preconditioning techniques. The residual of Jacobi preconditioned Krylov subspace methods tends to decrease very rapidly compared with the ILU preconditioning techniques. Among these Krylov subspace methods, the residues of GMRES methods decrease monotonically and rapidly with the increasing iteration number, the convergence behaviors of other methods are quite irregular, and may even break down.

Example 2: In this section, we choose the three methods to calculate different DOFs of BEM problem. In table 1, we describe the results of experiments on an elasticity
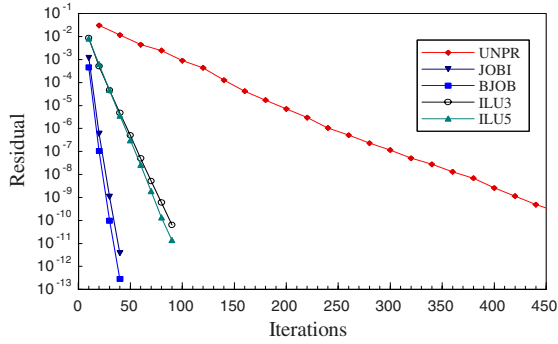
Fig. 1. Convergence histories of GMRES for different preconditioning techniques
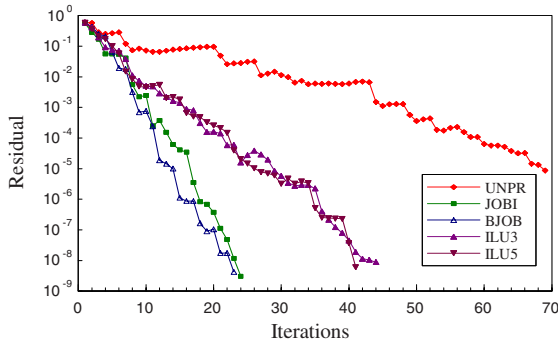
Fig. 2. Convergence histories of QMR for different preconditioning techniques
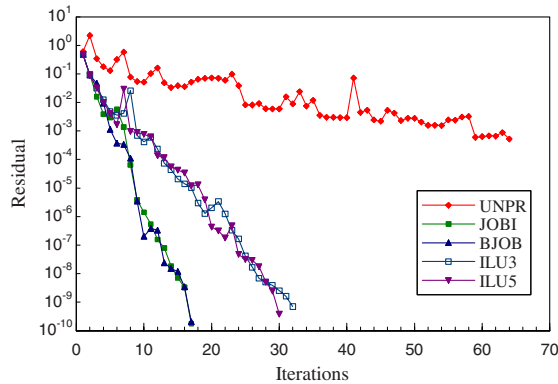
Fig. 3. Convergence histories of Bi-CGStab for different preconditioning techniques

problem with different DOFs for three Krylov subspace methods in conjunct with the Block Jacobi preconditioning scheme. Here, the initial guess is the zero vector, the convergence criterion $\varepsilon = \left\| r^{(i)} \right\| / \left\| b \right\| \leq 1.0 \times 10^{-10}$.

Table 1. The CPU time (in seconds) and iterations of krylov subspace methods

Solvers		DOF				
		1,158	1,806	4,056	4,614	7,206
GMRES(30)	Residual	6.81E-12	5.38E-12	4.13E-11	4.17E-11	7.57E-11
	CPU time	4.78s	10.63s	89.14s	114.25s	293.29s
	Iterations	30	30	30	30	30
QMR	Residual	7.20E-11	3.35E-11	2.72E-11	3.97E-11	8.33E-11
	CPU time	4.85s	11.41s	138.17s	182.40s	514.72s
	Iterations	26	29	31	32	36
Bi-CGStab	Residual	5.85E-11	6.52E-12	8.82E-11	4.62E-10	8.79E-11
	CPU time	4.57s	10.64s	101.51s	126.69s	354.17s
	Iterations	17	19	19	18	21

From the table 1, it can be seen that the performance of GMRES(30) is superior to other iterative methods. On the other hand, we can find that the iteration number increases slowly with the number of DOFs, and the iteration number is fairly small relative to the number of unknowns.

4   Conclusions

Base on the results of numerical experiments we conclude that preconditioned krylov subspace methods are effective solvers for the solution of large scale dense nonsymmetric linear systems. The preconditioning is indispensable to improving the iterative efficiency of large scale problems. There is a trade-off between the cost of the constructing and applying the preconditioner, and the gain of convergence speed.

References

1. H. Wang, Z. Yao, P. Wang.: On the preconditioners for fast multipole boundary element methods for 2D multi-domain elastostatics. Engng. Anal. Bound. Elem. 29 (2005) 673-688
2. Leung CY, Walker SP.: Iterative solution of large three-dimensional BEM analyses using GMRES technique. Int. J. Numer. Methods Eng. 40 (1997) 2227-36
3. Valente FP, Pina HLG.: Conjugate gradient methods for three-dimensional BEM systems of equations. Engng. Anal. Bound. Elem. 30 (2006) 441-449
4. S. Amini, N. D. Maines.: Preconditioned Krylov subspace methods for boundary element solution of the Helmholtz equation. Int. J. Numer. Methods Eng. 41 (1998) 875-898

Research on Bio-inspired Multi-net Paralleling Mechanism Based on Web Application

Ruijuan Zheng, Huiqiang Wang, and Yonggang Pang

College of Computer Science and Technology, Harbin Engineering University,
Harbin 150001, China
rjwo@163.com

Abstract. With the rapid development of network technologies and deteriorating of network environment, traditional single-net security system can't satisfy the security requirement. Excellent security performance of biological systems impels bio-inspired network security theory to be a hot topic currently. We advance Bio-inspired Multi-Net Security (B-MNS) system which implements the functional distributary of different subnets by state transition in Multi-Net Paralleling (MNP) mechanism. Firstly, concept model of B-MNS and MNP mechanism are outlined; secondly, parameter estimation and modifying algorithms are introduced to construct the mathematical model of B-MNS; at last, the practicability and high efficiency are proved by a simulation.

Keywords: bio-inspired; multi-net paralleling; hidden Markov; LoadRunner.

1 Introduction

With the development of network technologies and the deterioration of network entironment, traditional security system can't satisfy the security requirement. Similar security mechanisms between biology and computer network make it possible to solve the network security problems inspired by biology. Bio-inspired research started in the middle of 1990s[1, 2]. In current, bio-inspired research mainly focuses on computer immune system[3], anti-virus immune system[4] and bio-inspired fault tolerance computing[5], which are all limited in the immune system. We are inspired by the "Multi-Net" security mechanism and apply them into the design of B-MNS. The paper is organized as follows: Based on BMNSM[6], section 2 presents the concept model of B-MNS. Section 3 constructs the mathematical model. By a simulation, section 4 compares the performance of B-MNS and traditional security system. Section 5 presents some conclusions and proposes future work on B-MNS.

2 Concept Model for B-MNS

In the intricate and mutable survival environment, biological systems keep high security performance and implement the normal running, which owe to the perfect security system of biology. The key mechanisms can be summarized as follows: (1)

Multi layers. (2) Multi time sequences. (3) Multi nets. Close cooperating with each other, several independent "Nets" complete the security of system. So, the core of security system in specific biological population scale is MNP mechanism.

Inspired by this, B-MNS is divided into three angles: Population Scale, Time Stage and Subnet Type. Monitoring subnet monitors the data transmitted by data transmission subnet and implements precaution, detection and response. Recovery subnet deals with the abnormal information and recovers the network state. Corresponding mechanism takes charge of synchronization and information transfer between three subnets. MNP is embodied as "Three-Net-Paralleling"(Figure 1).
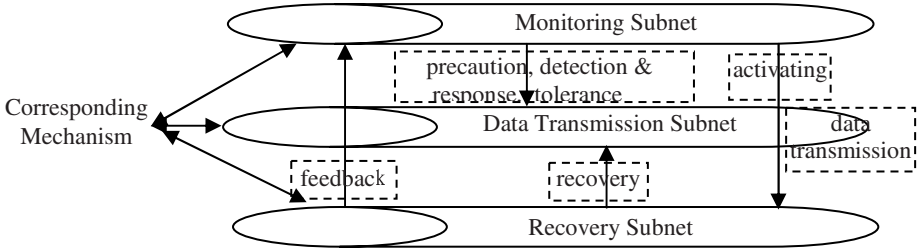
Fig. 1. Three-Net-Paralleling mechanism

3   Mathematical Model

To a given observation sequence $O = O_1, O_2, \ldots, O_T$, Baum-Welch algorithm will find out a $\lambda=(\Pi, A, B)$ which maximizes $P(O/\lambda)$.We select $O=$ (C, C, C) as the example sequence, so the final estimation results are showed in table 1.

Table 1. Estimation results

$P(O/\lambda)$	Π	A				B		
0.33333	(1,0,0,0)	4.46357e-007	0.327284	0.672715	0	0	0	1
		0	1.93327e-007	4.22823e-007	0.999999	0	0	1
		0	0	3.249e-007	1	0	0	1
		0	0	0	1	0	0	1

The modifying procedure is:

a.   Initialization: $\delta_1(i) = \pi_i b_{ii}(O_i), 1 \leq i \leq N$ (1)

$$\varphi_1(i) = 0, 1 \leq i \leq N \tag{2}$$

b.   Recursion: $\delta_t(j) = \max\limits_{1 \leq i \leq N} [\delta_{t-1}(i) a_{ij}] b_{ij}(O_t), 2 \leq t \leq T, 1 \leq j \leq N$ (3)

$$\varphi_t(j) = \operatorname*{argmax}_{1 \leq i \leq N} [\delta_{t-1}(i) a_{ij}], 2 \leq t \leq T, 1 \leq j \leq N \tag{4}$$

c.   Result:
$$P^* = \max_{1 \le i \le N}[\delta_T(i)]$$
(5)

$$q_T^* = \underset{1 \le i \le N}{\operatorname{argmax}}[\delta_T(i)]$$
(6)

d.   Optimal state sequence: $q_t^* = \varphi_{t+1}(q_{t+1}^*), t = T-1, T-2, ..., 1$
(7)

After modifying, we get L= (1/5,1/5,1/5,1/3), U= (1/3,1/3,2/3,3/5).

4   Simulation

Figure 2(a) and 2(b) respectively describes the changing of Hits-Throughput in single-net system and B-MNS. The average Hits and throughput in single-net system respectively is 5.206 times/second (t/s) and 25815.54 Bytes/second (B/s); the average Hits and throughput in B-MNS respectively is 10.851 t/s and 52443.666 B/s.
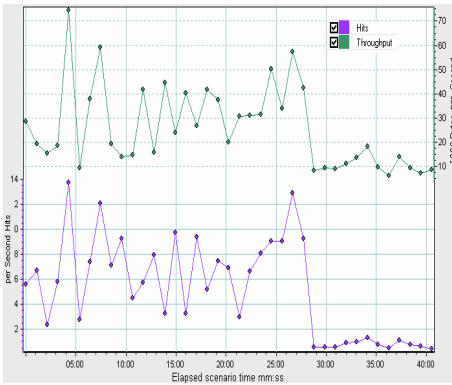
Fig. 2(a). Hits-Throughput per second in single-net system
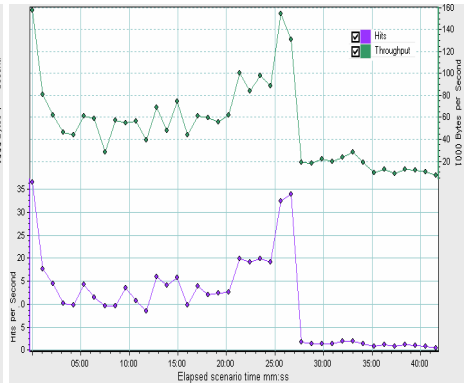
Fig. 2(b). Hits-Throughput per second in B-MNS
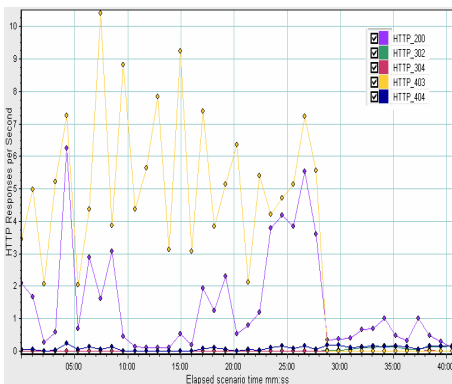
Fig. 3(a). Http responses per second in single-net system
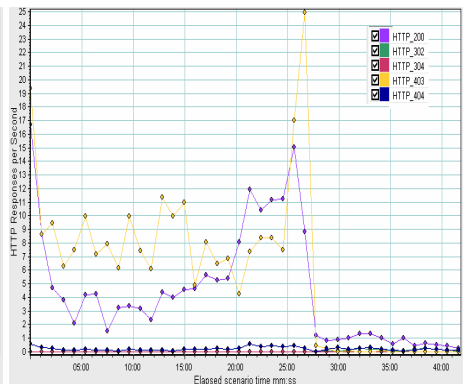
Fig. 3(b). Http responses per second in B-MNS

During the simulation, Http response ability of single-net system is common, which is showed in figure 3(a). In B-MNS, under the help of corresponding mechanism, three subnets in B-MNS implement the functional distributary. The Http response in B-MNS is showed in figure 3(b).

Comparing of Http responses is showed in table 2.

Table 2. Http responses

Responses/s	Http_200	Http_302	Http_304	Http_403	Http_404
single-net	1.455	0.027	0	3.727	0.083
B-MNS	4.569	0.045	0.001	6.168	0.224

5 Conclusion

Traditional single-net security system can't adapt to the increasing user requirement and aggravating network environment. Inspired by multi-net security mechanism of biological system, we advanced MNP mechanism. In this paper, we put forward B-MNS. Simulation results prove that the performance of B-MNS improves 3-4 times than that of single-net system. In the future work, we'll integrate the security methods and technologies in time stages of B-MNS.

References

1. Forrest, S., Perelson, A., Allen, L., et al: Self-nonself Discrimination in a Computer. Proceedings of the IEEE Symposium on Research in Security and Privacy. LOS Alamilos: IEEE Computer Society Press (1994)
2. Kephart, J.O.: A Biologically Inspired Immune System for Computers. Proceedings of the 4th International Workshop on the Synthesis and Simulation of Living Systems and Artificial Life (1994) 130–139
3. Forrest, S., Hofmeyr, S.A., Somayaji, A., Longstaff, T.A., et al: A Sense of Self for Unix Processes. Proceedings of the 1996 IEEE Symposium on Research in Security and Privacy. IEEE Computer Society Press. (1996) 120–128
4. MAO, X.Y., Liang, Y.W.: Research on the Model of Immune Firewall. Computer Engineering. (2004.8), 25(8):1282–1285
5. Bradley, D.W., Ortega-sanchez, C., Tyrrell, A.M., et al: Embryonics + Immunotronics: A Bio-Inspired Approach to Fault Tolerance. Proceedings of the 2nd NASA/DoD Workshop on Evolvable Hardware (2000.7)
6. Wang, H.Q., Zheng, R.J., Li, X.Y., Liu. D.X.: A Bio-inspired Multidimensional Network Security Model. Proceedings of the 2006 International Multi-Symposiums of Computer and Computational Sciences (2006.6) Vol (2):3–7

DRN: A CORBA-Based Distributed Resource Navigation System for Data Grid

Jia-Jia Miao, Ai-Ping Li, Jia Yan, and Quan-Yuan Wu

School of Computer Science, National University of Defense Technology
Changsha 4100073, P.R. China
elanmiao@yahoo.com.cn, apli@x263.net, elanmiao@gmail.com

Abstract. Data grids are becoming increasingly important for sharing distributed data and information in collaborative environments. This paper presents a CORBA-based Distributed Resource Navigation system consisting of Resource Agents and Navigation Service. The former one is a middleware that provides applications with a uniform set of operations to access heterogeneous distributed storage resources including file systems and database systems, and archival storage systems. The latter one is a metadata navigation service which is utilized by DRN to improve data publishing and lookup efficiency. Experiments show that CORBA-based DRN can provide the essential data virtualization services, and that Navigation service and Resource agent have a good performance with concurrent accesses.

Keywords: CORBA, Data intensive computing, Data virtualization.

1 Introduction

Grids [1] are environments that enable software applications to integrate computational and data resources that are managed by diverse organizations in widespread locations. Examples of data-intensive applications include experimental analyses and simulations in several scientific disciplines [2,5], such as high-energy physics, climate modeling, biomedical applications, earthquake engineering, oceanographic systems, and astronomy and so on.

CORBA has emerged as a popular distributed computing standard and meets the necessary requirements for grid computing [3], so as to be adopted by application developers as one kind of the Grid infrastructure. N.A.B. Gray [4] made comparisons of Web Service, Java RMI, and CORBA solutions for demonstration applications.

Work related to the DRN system includes the SRB [7], the SRM [8]. The DRN system differs from those mentioned above in that it provides a file I/O interface to the actual data item, which may reside in a file system or a database system. Thus, the DRN system supports more types of storage resources. Till now, it has been implemented for a variety of storage systems and OS platforms, and the resource providers can implement the data accessing logic in the Resource Agent themselves. Using DRN system, users do not need to care about the communications, which is inter-realm by CORBA mechanism.

2   System Architecture

We propose a novel architecture of Distributed Resource Navigation System. We developed Resource Agents (RAs) to provide seamless access to data stored on a variety of storage resources, including file systems and database systems. Furthermore, we define IDL files with file accessing operations, including readFile, writeFile, makeDir, deleteDir, etc. For each kind of resource, we implemented the object with this kind of IDL. Applications can use the distributed objects' operations to access data stored anywhere of the distributed storage sites. The RA is used to provide the capability to discover the information needed, identify data collections of interest, and select and retrieve data items that may be distributed across a wide network. The application builds on our system can use RAs to access heterogeneous storage resources in a distributed system. The DRN employs a metadata Navigation Service to manage descriptive as well as system metadata associated with data collections and resources. Using the NS, we can store and retrieve metadata about system entities, including RAs' object reference, storage resources, data items and resource access control rules. By providing location transparency, the NS enables attribute-based data accessing. This means that applications can locate the data without providing low-level details or without referencing the data by path names.
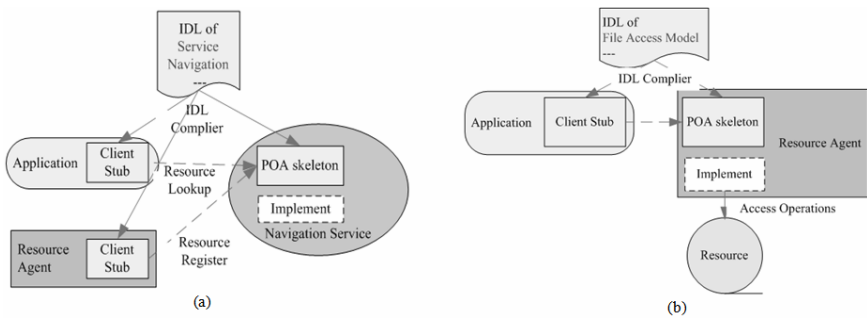
Fig. 1. Client/Server Components of (a) the Navigation Service (b) the Resource Agent

Navigation Service, as shown in Fig. 1-a, a client-side stub is auto-generated from this interface. On the server side, the interface is processed to yield a base class for the implementation class. In our DRN system, the application communicates with Services using CORBA mechanism. The application and RA use the Client Stub to call Navigation Service's functions.

By using Resource Agent, applications can seamless access the data and information stored in the DRN system. The Resource Agent works as a resource wrapper, and it provides the file model operations. From the viewpoint of the resource users, all resources are file systems. As shown in Fig. 1-b, on the client side, applications use the Client Stub, which is auto-generated from the interface, to call the remote service. On the other side, resource providers must accomplish the function implements. As CORBA is a language independent middleware, developers can use their favorite language to accomplish the job.

3   Experiments

In this section we describe our implementations in using the DRN in some applications. In order to demonstrate the features of the DRN system, we present these applications with synthesis data. We also utilize the implementation to illustrate how to deploy the data management system with the DRN system. The total data size of the implementation is 400GB, including about 4,300 files stored in a number of file system servers, and more than 6,100 data items stored in certain number of DBMS.

One of the most important features of this architecture is that the NS must provide data source register and un-register steadily. Then we design an artificial experiment to prove this. In this experiment, that application Register-Machine use number 1 to 400 as the resource register name, it creates 20 threads register and un-register to NS circularly. Then we have application Caller to call for the resources which have registered at NS. Register-Machine will make the NS throw exception named ResAlreadyExist, and Caller will induce exception named ResNotExist. Then we compare two log file to show whether the NS can handle this.

Experimental results are shown in Fig. 2-a. The number of registered RA is the RA which has registered at NS, and the number of Called RA is the RA which has been called from Caller. The results follow our program design. Experimental results show that Navigation Service can handle parallel request steadily.
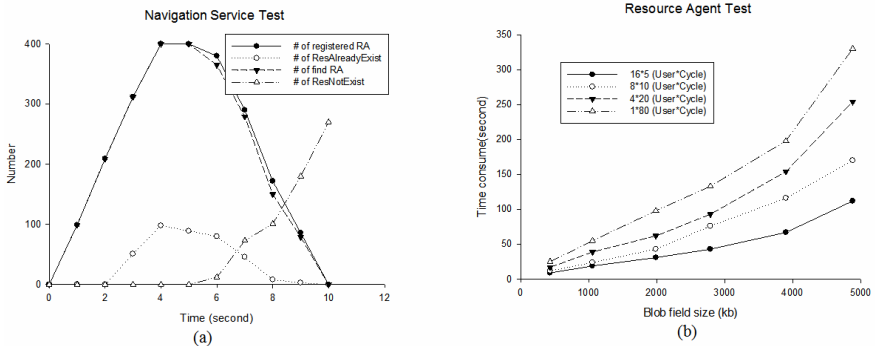
Fig. 2. Experimental Results of (a) NS, (b) RA test

Table 1. Experimental Results of many users concurrent access different blob size

Blob Field Size (kb)	The number of Users	The number of Cycles	Consume Time (second)
434	1	10	1
434	5	10	7
434	10	10	13
434	30	10	37
434	60	10	75
434	100	10	123

We also evaluate data access consume in our system. In this experiment we use a application simulate many users concurrently get the blob field from RA, which wrapped a database resource. We analysis the time consume with different file sizes and the time consume with different number of users.

Experimental results are shown in Fig. 2-b and Table 1, which 16 users with 5 cycles have a sharp reduce its' time consume when compare with 1 user with 80 cycles. According to this, we can conclude that RA supports concurrent access and has a good performance.

4   Conclusion

The DRN system provides the core service for building data management systems that span multiple administration domains, multiple types of storage systems, and multiple types of data access environments. The DRN is currently in release 1.4; we implement it by using CORBA technology, with the platform named StarBus+ [6]. Thus, the client applications and the Resource Agent are implemented for Linux, Sun Solaris, UNIX, and Windows. In order to provide quick implementation of the Resource Agent, some kinds of templates are provided as well.

This paper proposes the first steps to create resources accessing and integration architecture for data-intensive application domains. There are still many interesting issues to be further studied in DRN, such as data replication, aggregating data in containers, and I/O command aggregation via a remote proxy, etc.

References

1. Foster I, Kesselman C, Tuecke S. The anatomy of the grid: Enabling scalable virtual organizations. Int. J. Supercomputer Applications, (2001) 15(3): 200-222
2. M. Antonioletti, A. Krause, N.W. Paton. An Outline of the Global Grid Forum Data Access and Integration Service Specifications. J.-M. Pierson (Ed.): VLDB DMG 2005, LNCS 3836, pp. 71-84, (2005)
3. Snigdha Verma, Manish Parashar, Jarek Gawor, Gregor von Laszewski. Design and Implementation of a CORBA Commodity Grid Kit. GRID (2001): 2-13
4. N.A.B. Gray. Comparison of Web Services, Java-RMI, and CORBA service implementations. Australian Software Engineering Conference, (2004)
5. Reagan W. Moore. Integrating Data and Information Management. Keynote talk of International Supercomputer Conference ISC, (2004)
6. Wang H M, Wang Y F and Tang Y B. StarBus+: Distributed object middleware practice for Internet computing. Journal of Computer Science and Technology, (2005) July, 20(4): 542-551

A Research on Local Mean in Empirical Mode Decomposition

Yong-Ping Huang, Xue-Yao Li, and Ru-Bo Zhang

National Laboratory on Machine Perception, Peking University, Beijing, P.R. China
College of Computer Science and Technology, Harbin Engineering University,
Harbin 150001, P.R. China
{hwangyungping, lixueyao, zrb}@hrbeu.edu.cn

Abstract. The conventional Empirical mode decomposition (EMD) method uses envelope mean interpolated by cubic spline fitting, which is sensitive to extrema. An efficient method for finding the local mean is generated by using support vector regression machines. The analysis results indicate that the proposed algorithm has higher performance in the ability of frequency separation, insensitive to the sampling frequency and can eliminate mode mixing in small-amplitude sine waves intermittence.

Keywords: Empirical Mode Decomposition, Support Vector Regression Machines, Mode Mixing, Local Mean, Hilbert-Huang Transform.

1 Introduction

Empirical mode decomposition (EMD) introduced by Huang [1], is a method for decomposing non-linear and multi-component signals. The intrinsic mode functions (IMFs) resulting from EMD are obtained in the sifting process, which requires that a local mean should be defined [2]. So the critical part of EMD method is how to find the local mean. The conventional EMD proposed by Huang use envelope mean, the mean of upper and lower envelopes which interpolate all the local maxima or minima by the cubic spline, as local mean, but it is not the real one. In addition, the cubic spline fitting suffers overshoot or undershoot.

To find the real local mean, at present there are some solution approaches, such as the stationary-point EMD method (SPEMD) introduced by Zhong [3], a new envelope algorithm using subsection power function proposed by Qin [4], the B-spline approach for empirical mode decomposition adopted by Chen [5].However, all these approaches use curve interpolation, which is sensitive to extrema, calculated by a parameter interpolation equation. This major and serious disadvantage will lead some difficulties when extrema are untrue or corrupted by intermittency.

Therefore, it is necessary to find a better method that is insensitive to extrema and has a robust performance. For the insensitive ability and robustness in interpolation, we introduce SVRM to estimate the local mean in sifting process, and the EMD algorithm based on SVRM is proposed.

2   The Local Mean Based on SVRM

In sifting process, SVRM is trained by local extrema (include local minima and maxima) of time series, then predicts directly the local mean. For the simplicity and the high generalization performance of SVRM, we choose the RBF kernel function and linear ε-insensitive loss function in SVRM. It is well known that SVRM generalization performance depends on a good setting of parameters [6].

For the adaptive and computation of analytical selection method, we adopt the analytical approach to choose the parameters. In the case of a signal $y=f(x)$, the extrema are $(ex_1, ey_1), \cdots, (ex_i, ey_i), \cdots, (ex_n, ey_n)$, where ex_i and ey_i are the coordinates and the corresponding y value of extrema, n is the number of extrema. Note that the extrema should be sorted by coordinate order for computing the information between adjacent extreme. The analytical parameter selections used in sifting process are given as follows, the regularization parameter C:

$$C = \max(\left|\overline{ey} + 3\delta_{ey}\right|, \left|\overline{ey} - 3\delta_{ey}\right|)$$ (1)

here $\overline{ey}$ and δ_{ey} are the mean and the standard deviation of the y value of extrema. In addition, the following RBF kernel parameter γ:

$$\gamma = \max(\left|\overline{dis\_ex} + \delta_{dis\_ex}\right|, \left|\overline{dis\_ex} - \delta_{dis\_ex}\right|)$$ (2)

where $\overline{dis\_ex}$ and δ_{dis_ex} are the mean and the standard deviation of the coordinate distances between adjacent extrema. The parameter of insensitive loss function ε is:

$$\varepsilon = \frac{\overline{dis\_ey}}{2}$$ (3)

where $\overline{dis\_ey}$ is the mean of the y value distances between adjacent extrema.

3   Experiments

To illustrate the behavior of the local mean based on SVRM, we used the conventional EMD introduced by Huang [1] to compare the algorithm using the local mean based on SVRM (hereinafter EMD-SVRM for short). First, we generated a synthetic signal of two superimposed tones:

$$f(x) = a_1 \sin(2\pi f_1 x) + a_2 \sin(2\pi f_2 x), x \in [0, 10\pi]$$ (4)

where both f_1 and f_2 are the frequency of sine tones, respectively. The local mean based on SVRM and the envelope mean are shown in Fig.1. The fluctuation in the SVRM-based local mean is considerable, which implies that the sifting process can separate the tones. As proposed in Ref [10], the conventional EMD can not accurately separate two superimposed tones when the frequency proportion $0.5 < f_2/f_1 < 2.0$. So
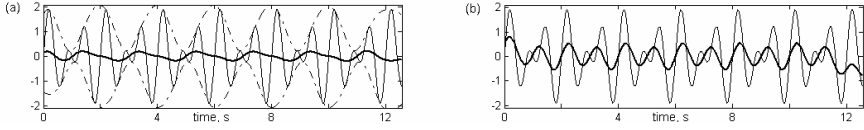
Fig. 1. Illustration of the envelope mean and the local mean using SVRM: (a) the signal in thin solid line, with the upper and lower envelopes in dot-dashed lines and the envelope mean in thick solid line; (b) the signal in thin solid line and the local mean based on SVRM in thick solid line. The signal tested is of the form in Eq.4 with $f_1 = 1$ and $f_2 = 1.5$ with unit amplitude.
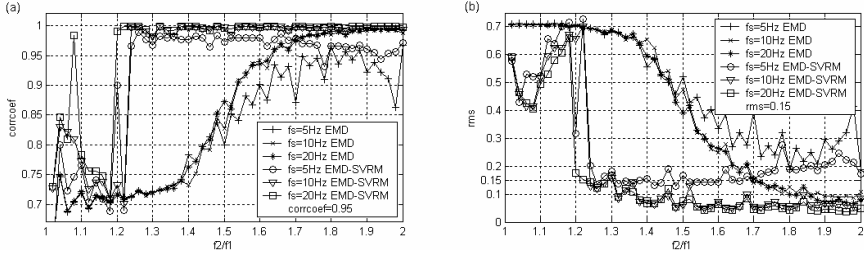
Fig. 2. Comparison of the *corrcoef* and the *rms* between the first IMF and the actual high frequency component: (a) calculated results of *corrocoef*; (b) calculated results of *rms*

we compare the performance in different sampling frequencies and different frequency proportions $f_2/f_1 \in (1.0, 2.0]$.

Fig.2 presents calculated results of the correlation coefficient (corrcoef) and the root mean square error (rms) between the first IMF and the actual high frequency component. No substantial differences in the results of the second IMF, we omit them for the sake of brevity. The measured results show the significant improvement of the proposed algorithm including separate components that are similar in frequency that would be inseparable with conventional one. And the EMD-SVRM algorithm is less insensitive to sampling frequency for the good performance when sampling frequency *fs*=5Hz, while the performance of conventional EMD is unstable and big fluctuation.

In this test, we consider the small-amplitude and high-frequency sine waves intermittent in large-amplitude tones. The signal is given as following:

$$y = \sin(8\pi x) + 0.03\sin(200\pi x)\left[u(x - \tfrac{85}{300}) - u(x - \tfrac{100}{300})\right]$$
$$+ 0.03\sin(200\pi x)\left[u(x - \tfrac{165}{300}) - u(x - \tfrac{180}{300})\right]$$

(5)

where $x \in [0,1]$ and the sample frequency *fs* is 300Hz. Using the conventional EMD, we will obtain the first three components which contain seriously mixed modes especially the first IMF, as shown in Fig.3.a. And with the EMD-SVRM algorithm, the result is given in Fig.3.b. Clearly, the small-amplitude sine wave intermittent was separated from the large-amplitude tones and the amplitude of the third IMF component is very small. The test shows the EMD-SVRM algorithm can eliminate the mode mixing caused by intermittency and do not need the intermittency criterion introduced by Huang [1].
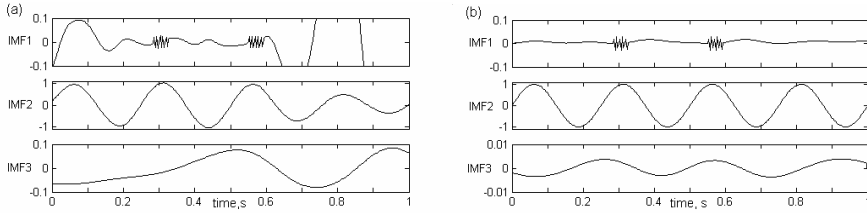
Fig. 3. Comparison of the IMF components between the conventional EMD and the EMD-SVRM for the intermittency tones: (a) the first three IMF components from conventional EMD algorithm; (b) the first three IMF components from EMD-SVRM approach

4   Conclusions

The local mean based on SVRM is designed to overcome the deficiency of sensitivity to extrema, and adopt the generalization performance of SVRM. Compared with conventional one, our approach shows significant improvements over frequency separation and good performance of eliminating mode mixing in intermittency. Future work include finding better model selection especially the analytic parameter selection and using the ν-SVR instead the ε-SVR may get better performance.

References

1. Huang, N.E., Shen, Z.: A new view of nonlinear water waves: the Hilbert spectrum. A. Rev. Fluid Mech, Vol. 31. (1999) 417-457
2. Deering, R., Kaiser, J.F.: The use of a masking signal to improve empirical mode decomposition. ICASSP2005, Vol. 4. (2005) 485-488
3. Zhong, Y.M.: Research on theoretic evidence and realization of directly-mean EMD method. Chinese Journal of mechanical engineering, Vol. 17. (2004) 399-404
4. Qin, S.R., Zhong, Y.M.: A new envelope algorithm of Hilbert–Huang Transform. Mechanical Systems and Signal Processing, Vol. 20. (2006) 1941–1952
5. Chen, Q.H., Huang, N.E., Riemenschneider, S.: A B-spline approach for empirical mode decompositions. Advances in Computational Mathematics, Vol. 24. (2006) 171–195
6. Cherkassy, V., Ma, Y.Q.: Practical selection of SVM parameters and noise estimation for SVM regression. Neural Networks, Vol. 17. (2004) 113-126

An Energy-Efficient Routing Method of Wireless Sensor Networks

Sun Ting[1], Lu Dongxin[2], and Yang Yongtian[1]

[1] College of Computer Science and Technology, Harbin Engineering University, Harbin 150001, China
{sunting, yangyongtian}@hrbeu.edu.cn
[2] ZTE Software Engineering, The Torch Street 999, Nan Chang 330029, China
lu.dongxin@ztenc.com.cn

Abstract. In wireless sensor networks(WSNs), as sensor nodes are characterized by having specific requirements such as limited energy availability, low memory and reduced processing power, energy efficiency is a key issue in designing the network routing. In the existing clustering-based routing protocols for the WSNs, the cluster-heads are usually selected randomly and do a lot of work, which may cause unbalanced energy consumption and thus short network lifetime. Based on this approach, the paper proposes a method that a cluster-head distributes energy load evenly among its members based on their energy usage by chain. With the chain, in a cluster, different node is selected as Agent Node to send the data to cluster-head at different cluster cycle. The new method balances the nodes' power depletion. Simulation results show that it has better power management performance and can prolong the lifetime of the network.

Keywords: Wireless Sensor Networks, Routing Method, Cluster, Chain.

1 Introduction

As a distributed sensing network, wireless sensor networks consist of many small intelligent types of equipment [1]. Since sensor nodes carry limited and generally irreplaceable power source, the routing protocols designed for the WSN must take the issue of energy saving into consideration. Clustering-based routing protocol is a popular protocol proposed for the WSN to minimize the consumption of the energy of the sensors.

There have existed many cluster-based routing protocols [2][3], but they still have many problems. In this paper, based on the cluster-based routing model, we propose a new routing transmission method, with which a cluster-head distributes energy load evenly among its members based on their energy usage by chain.

This paper is organized as follows. Related works are introduced in Section 2. In Section 3, we present the new routing method and its building process. Simulation results are given in Section 4. Finally we summarize the main results and discuss future research direction in Section 5.

2   Related Works

Low Energy Adaptive Clustering Hierarchy (LEACH), described in [2], is probably one of the more referenced protocols in the sensor networks area. The recent researches on the routing with the hierarchical structure such as PEACH [4] and EDACH [5] employ a similar approach as LEACH. As an improved version to LEACH, LEACH-C [6] uses a centralized clustering algorithm to produce better clusters, thus achieves better performance.

The transmission model used in LEACH can lighten the centralized consumption of nodes' energy to a certain extent. However, the randomly election of the cluster-heads can cause unbalance energy consumption in the nodes. On the other hand, in the cluster, the nodes near the cluster-head still need to transfer other nodes' data just like the routers and need more energy. Sub-clustering method [3] improves the LEACH partly, but increases the computation work and management load of the cluster-head. In order to resolve these problems, in this paper we present a new routing method with which a chain is built in every cluster, which can resolve these problems better.

3   Chain in Cluster

Each nodes i maintains a unique identification, ID(i), a cluster identification to which i belongs, CID(i), and its remaining battery power, CRP(i). Its location is L(i). After the clusters are built, the cluster-head check all the member nodes' information and select the node with most residual energy as its' agent node. At the same time the cluster-head broadcasts all nodes location information in the cluster, every node select the closest neighbor to form a chain according to these information. When the cluster-head receives the data collection request from the sink, the agent node transfers the request to the two ends of the chain and the data begin to flow from the two ends to it. At the same time, the middle nodes will aggregate these data and finally the agent node transfers these data to cluster-head and cluster-head transfers them to sink node.

As shown in Figure 1, the method balances the nodes' power consumption.
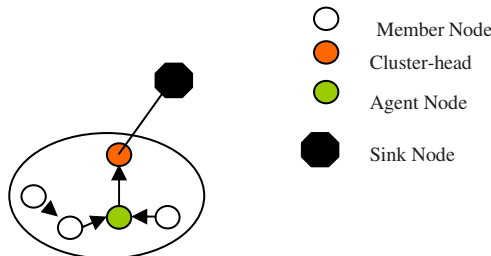
Fig. 1. One Node as Agent Node

As the agent node consumes more energy than other nodes within the chain, the cluster-head elects another node with the most residual power as agent node in next cluster cycle. That is, when a cluster cycle is over, nodes are informed about their newly elected agent node. Nodes within a chain transmit to their newly elected agent node.

4   Simulation Results

For the simulation, we use the OPNET network simulator. The environment consists of 150 nodes distributed randomly in a 100m × 100m area. Each node is equipped with the initial energy of 5 joules. We compare the new method with LEACH routing method and recent research work Sub-cluster routing method.
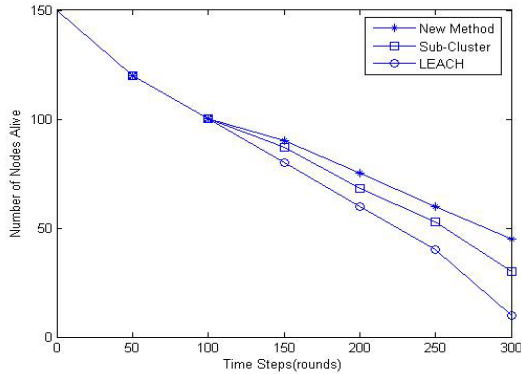
Fig. 2. Number of Nodes Alive

From the Figure 2, we can draw a conclusion that at first new method has the similar performance with other methods. However, with the increase of number of rounds, new approach has better result than conventional approaches. The reason is that, in LEACH, cluster-heads not only transmit the data to sink, but also aggregates all the information that accepted from the member nodes, which need more energy. And in LEACH, the nodes near the cluster-head, as routers to transmit other nodes' data also need more energy. These works can make the nodes die soon. In sub-cluster method, the cluster-head also need to aggregate the information that accepted from the sub-cluster-heads. In our new method, the work is distributed to the member nodes and the data attending cluster-head has been aggregated. With this method, all the nodes in the cluster have more balanced power consumption. The number of nodes alive is larger.

Figure 3 shows us the results of nodes' power consumption with the change of network distribution range. When the distribution range of network is small and the nodes density is high, new model and sub-cluster method have not better performance than traditional model, because they have more computation to form the chain and sub-cluster in the cluster. With the increase of network distribution range, the transmission distance between the nodes increases also. In LEACH, the member nodes of a cluster have to transmit their data to cluster-head with long distance. The sub-cluster method improves it by reducing the overhead of re-clustering and shorter transmission distance. With our method, the nodes of the chain only need forward their data to the nearby neighbor. New method shows us its advantages. It has lower power consumption and will prolong the lifetime of network.
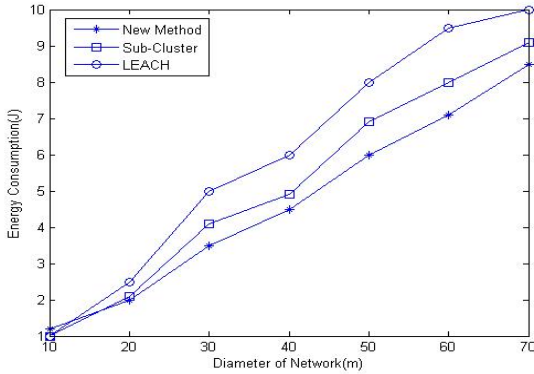
Fig. 3. Energy Consumption

5   Conclusion and Future Works

In this paper, we introduced a new method to prolong the lifetime of WSNs. Simulation results show that the new method has better performance when the network range is increased. But as we all know, the routing protocol of WSNs is application-based. We will study the performance of our approach under various conditions. For example, we will consider nodes' mobility and fault. So, we should do more things to improve the performance of the new method in the future.

References

1. Hill J, Szew Czyk R, Woo A, Hollar S. System architecture directions for networked sensors. Proceedings of the 9th ACM International Conference on Architectural Support for Programming Languages and Operating Systems. 2000, 93-104
2. W. Heinzelman, A. Chandrakasan, Hbalakrishnan. Energy-efficient communication protocol for wireless microsensor networks. The Hawaii Int'l Conf. System Sciences, Hawaii, IEEE Computer Society, 2000
3. Kyung-Won Nam, Jun Hwang, Cheo-Min Park, Young-Chan Kim. Energy-Efficiency Method for Cluster-Based Sensor Networks. ICCSA 2005, LNCS 3480, 2005, pp 1170-1176
4. K.T. Kim and H.Y. Youn.: PEACH: Proxy-Enable Adaptive Clustering Hierarchy for Wireless Sensor network: Proceeding of The 2005 International Conference On Wireless Network, pp. 52-57, June 2005.
5. K.T. Kim and H. Y. Youn.: Energy-Driven Adaptive Clustering Hierarchy (EDACH) for wireless sensor networks: EUC LNCS3823, pp. 1098-1107, 2005.
6. Heinzelman, W., Chandrakasan, A., Balakrishnan, H.: An Application-Specific Protocol Architecture for Wireless Microsensor Networks. IEEE Trans. on Wireless Communications 1(4) (2002) 660-670

Rapid-Response Replication: A Fault Tolerant Algorithm Based on Active Replication

Lingxia Liu, Jingbo Xia, Zhiqiang Ma, and Ruixin Li

The Telecommunication Engineering Institute,
Air Force Engineering University,
710077 Xi'an, China
lingxia_liu@tom.com

Abstract. To the wide area network oriented distributed computing, a slow service is equivalent to an unavailable service. It makes demands of effectively improving the performance of the replication algorithms without damaging the availability. Aim for improving the performance of the active replication algorithm, we propose a new replication algorithm named RRR (Rapid Response Replication). Its basic idea is: all replicas receive request, but only the fastest one sends back the response to the client after it handles the request. Its main advantages are: (1) In the algorithm, the response is sent back directly by the fastest replica after it handles the request; (2) The algorithm avoids agreement; (3) The algorithm avoids the redundant nested invocation problem (the problem may be arisen while using active replication).

Keywords: replication algorithm, performance, fault tolerant.

1 Introduction

Fault tolerance is the ability of an application to continue valid operation after the application, or part of it, fails in some way[1]. Replication[2] [3] is a widely used technique for providing high-availability and fault-tolerance of critical services.

After analyzing the Active Replication algorithm[2], we can find that agreement affects the performance of the algorithm from following aspects: (1) Agreement must be done after the slowest replica handling the request. The response time is decided by the slowest replica; (2) Agreement itself consumes time.

Aim for improving the performance of the active replication algorithm, we propose a new replication algorithm named RRR (Rapid Response Replication). Its basic idea is: all replicas receive request, but only the fastest one sends back the response to the client after it handles the request. Its main advantages are: (1) In the algorithm, the response is sent back directly by the fastest replica after it handles the request; (2) The algorithm avoids agreement; (3) The algorithm avoids the redundant nested invocation problem (the problem may be arisen while using active replication).

The rest of the paper is organized as follows. In Section 2, we set forth the algorithm. Next Section analyzes the performance of the algorithm. Finally, in Section 4, we conclude the paper.

2   RRR Algorithm

We categorize the messages passing in the system into the following five types: C_Req (Client Request): a request message from the client to the service; C_Res (Client Response): a response message from the service to the client; S_Req (Service Request): a request message from one service to the other services; S_Res (Service Response): a response message from one service to the other services; State_Update: a state message from one service to the other services. After processing the message, the state of the service is set to the state in State_Update.

2.1   The Components for the Algorithm

The components for the algorithm are shown in Figure 1.
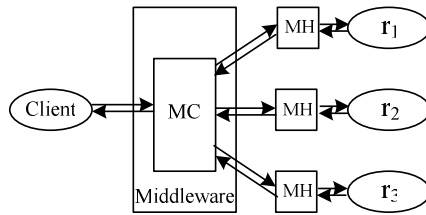
Fig. 1. The components for the algorithm

- Message coordinator (MC)

The MC component is located in the middleware. It assigns a unique identifier (ID) to each request and delivers them to RS. Once RS returns results, MC returns them to clients. It also coordinates RS to decide which replica is the fastest one.

MC assigns and attaches ID to every request message it handles. The generating rule is as follows: All the C_Req are identified with a unique ID; The ID of C_Res is the same as the ID of the corresponding C_Req; The S_Req is generated only when a service sends an invocation to another service. The ID is modified to ID (ID of the corresponding C_Req or S_Req) + URN (URN of the requested service); The ID of S_Res is the same as the ID of the corresponding S_Req; The ID of State_Update is the same as the ID of the corresponding C_Req or S_Req.

- Message handler (MH)

MH is co-located with each member of RS. It is placed in each replica to handler the messages that the replica receives and generates.

MH maintains a buffer for buffering the messages for every member in the group. All messages sending to the members are firstly buffered in the buffer. MH is responsible for scheduling the message in the buffer.

2.2   Overview of the Algorithm

In RRR algorithm, the request message is atomic multicast to every member of RS. The fastest member returns the response message and sends a State_Update to the other members in the group. It is the core idea of the algorithm.

Figure 2 shows a simple flow of the algorithm:

1. A client issues request C_Req to the replicated service.
2. The request is routed to MC (by the middleware). MC assigns a unique ID to C_Req and then multicasts it to the replicated service.
3. C_Req is intercepted and buffered by each MH. Then it waits for scheduling.
4. MH invokes the corresponding replica to handle the request.
5. The replica handles the request and returns response C_Res. C_Res is also intercepted by corresponding MH. MH decides whether the replica is the fastest one to finish handling the request. If the replica is the fastest one, MH sends back C_Res to the client through MC and sends State_Update to other members.
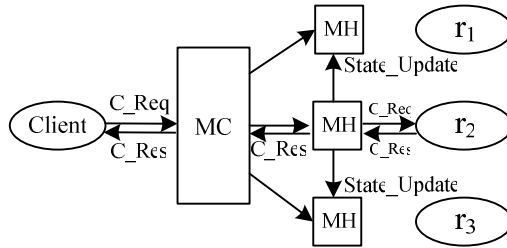
Fig. 2. A simple flow of RRR algorithm

Every member of the group decides whether to process the request or not on the system load and the processing speed of the request. The request doesn't need to be processed by every member and the response can be returned before every member finishes processing the request. They are the main differences from Active Replication.

MC maintains a hash table to ensure that there is only one member to be appointed as the fastest one (the members maybe finish processing the same request message at the same time). If the member can't decide whether it is the fastest one, MH will send an asking message to MC to confirm. MC returns the answer according to the record in the Hash table. Thus two types of messages are increased in the system, namely, Fastest_Query (the asking message from MH to MC) and Fastest_Response (the answer from MC to MH). The ID of the Fastest_Query and Fastest_Response is the same as the ID of the corresponding C_Req or S_Req. The date in the hash table is arranged as (address list, the fastest member's address, time). The address list includes the address of the members that ever sends out the Fastest_Query except the fastest one.

3 Performance Analyze

Experiments are designed to measure the response time of these algorithms. Our measurements were performed on 2.0GHz Intel Pentium4 PCs interconnected by a 100 Mb/sec switched. All machines run on a Windows 2000 operating system and our modified StarWebService 2.0.2. [4]

First we vary the request frequency from 20 requests per second to 100 requests per second to measure the response time on the client side. The result shows that the response time increase as the request frequency increase and the response time of RRR algorithm is shorter than the active replication algorithm. Then we vary the number of the member from 2 to 8 to measure the response time on the client side. The result shows that the response time of the active replication algorithm increases rapidly as the member number increases and the response time of the RRR algorithm hardly increases as the member number increase. Finally we measure the response time of the RRR algorithm with failure occurring. The result shows that the response time hardly change as the number of the failure member changes.

4   Conclusion and Future Work

In this paper, we presented a new algorithm named RRR. In the algorithm, the response is just returned by the fastest member. So it has shorter response time than the active replication algorithm. We prove this by experiments.

The algorithm achieved speed at the expense of communication overhead. Future work is to optimize algorithm to reduce the communication overhead.

References

1. Flavin, C.: Understanding fault-tolerant distributed systems. Comm. of ACM. 2 (1991) 57-58
2. Schneider, F.: chapter 7: Replication Management using the StateMachine Approach. In: Addison, W. (ed.): Distributed Systems. 2nd edn (1993) 169–197
3. Budhiraja, N., Marzullo, K., Schneider, F., Toueg, S.: chapter 8: The Primary Backup Approach. In: Addison, W. (ed.): Distributed Systems. 2nd edn (1993) 199–216
4. StarWebService 2.0.2. Available online at http://www.starmiddleware.net/ws (2004)

An Algorithm for Improving Hilbert-Huang Transform

Song Guo[1], Guochang Gu[1], and Changyou Li[2]

[1] School of Computer Science and Technology, Harbin Engineering University,
Harbin 150001, China
guosong@hrbeu.edu.cn
[2] Department of General Mechanics and Mechanics Foundation, School of Aerospace,
Harbin Institute of Technology, Harbin 150001, China
lichangyou_1980@163.com

Abstract. The Hilbert-Huang transform is viewed as a promising method to process the nonlinear and non-stationary signal. However, it hasn't been a general method in signal processing due to its some deficiencies. In this paper, an algorithm is proposed to resolve one of its deficiencies that the EMD will generate redundant IMFs at the low-frequency region. This deficiency may cause misinterpretation to the result of processing signal. The experimental results show that the proposed algorithm successfully resolves this deficiency.

Keywords: eliminating redundant IMFs; Hilbert-Huang transform; EMD.

1 Introduction

The wavelet transform has become one of the fast-evolving tools for analyzing nonlinear and non-stationary signals in the past decade. However, with the wide application of wavelet transform, some crucial deficiencies are reported. Hence, a new type of time-frequency analysis called Hilbert-Huang transform (HHT) has been proposed by N.E. Huang in 1998[1].

Compared with the wavelet transform, HHT has many advantages which were described in literature [2]. Nevertheless, in practical application, HHT has also some deficiencies, which will be described in detail in section 2. In this paper, an algorithm is proposed to resolve one of them.

2 The Deficiencies of Hilbert-Huang Transform

HHT consists of two main steps, the first step is data "sifting" to generate the intrinsic mode functions (IMFs) and the second step is to apply the Hilbert transform to the IMFs. The Empirical Mode Decomposition (EMD) which is the key part of this method is employed to "sift" data, by means of which any complicated data can be decomposed into a finite number of IMFs. The instantaneous frequency, determined by Hilbert Transform (HT) of IMF, provided much sharper identification of embedded events beyond the limitation of the Uncertainty Principle. HHT is described in detail in literature [1].

HHT seems to be a perfect method to process the nonlinear and non-stationary signal. However, in practice, HHT has some unsolved problems. First, the EMD will generate some undesired low amplitude IMFs at the low-frequency region and raise some undesired frequency components. Second, the first IMF may cover a wide frequency range at the high-frequency region, therefore cannot satisfy the mono-component definition very well. Third, the EMD operation often cannot separate some low-energy components from the analysis signal; therefore those components may not be able to appear in the frequency-time plane. In this paper, all effort is dedicated to resolve the first deficiency because the second and third have been solved in [3] [4].

Now, let's observe the first deficiency according to one example. Let the signal is equal to: $x(t) = \sin(2*\pi*10*t) + \sin(2*\pi*15*t) + \sin(2*\pi*20*t) + \sin(2*\pi*30*t)$ and the results of EMD of $x(t)$ and the FFT of IMFs are described in fig. 1.

There are four mono-components in the signal $x(t)$ so that four IMFs should be acquired by EMD. However, ten IMFs are seen according to the left section of fig. 1 and we can observe that all the redundant IMFs have lower frequency than the lowest frequency of the signal $x(t)$ from the right section.

3   The Proposed Algorithm

In [3], [4], the correlation coefficients of IMFs and the signal is used as a criterion to decide which IMFs should be retained and which IMFs should be eliminated because the author thinks that the real IMF components will have relative good correlation with the original signal and on the other hand, the pseudo-components will only have poor correlation with the signal. However, the analysis is not logical. If the real IMFs have relative good correlation with the original signal, they will be also relative good correlation each other. This is inconsistent with the characteristic of EMD which the IMFs are almost an orthogonal representation for the analyzed signal. In [5], [6], Kolmogorov-Smirnov test is employed to resolve the same problem. Nevertheless, Kolmogorov-Smirnov test is mainly used to check if two independent distributions are similar or different.

According to the theory of EMD, the following equation is obtained

$$v_i(t) = x(t) - h_i(t) = \sum_{j=1}^{i-1} h_i(t) + \sum_{j=i+1}^{n} h_j(t) + r_n(t) \cdot \qquad (1)$$

where, $x(t)$, $h_i(t)$, $r_n(t)$ are the processed signal, IMF and the residual signal respectively.

The redundant IMFs have not only lower frequency than the lowest frequency of the signal $x(t)$ but also less amplitude. This can be explained that the redundant IMFs are generated due to leaking in the decomposing process of EMD. Therefore, if the energy of $v_i(t)$ is almost equal to that of $x(t)$, $h_i(t)$ is viewed as the redundant IMF. The ratio of the energy of $v_i(t)$ to $x(t)$ will be constructed to eliminate the redundant IMFs . It is defined as

$$L_i = \frac{\int v_i^2(t)dt}{\int x^2(t)dt} = \frac{\int (x(t) - h_i(t))^2 dt}{\int x^2(t)dt} \cdot \qquad (2)$$

All L_i make a vector L,

$$L = [L_1, L_2, \cdots, L_n],\tag{3}$$

and D_L is defined as

$$D_L = \left\{ D_i \middle| D_i = |L_{i+1} - L_i|, i = 1, 2, \cdots, n-1 \right\}.\tag{4}$$

If D_m is equal to a local maximum of D_L and L_{m+1} is more than T_0 (in general, $0.95 \leqslant T_0 < 1$), $h_i(t)$ $(1 \leqslant i \leqslant m)$ are viewed as the real IMFs.

There are two reasons why the proposed method is logical to eliminate the redundant IMFs. Firstly, it is based on the fact that the redundant IMFs have lower frequency and less amplitude than the lowest frequency of the signal $x(t)$.

Fig. 1. The results of EMD of $x(t)$ and the FFT of IMFs

Secondly, the frequency of $h_k(t)$ is higher than that of $h_n(t)$ if k is lesser than n. In a word, there is a local maximum of D_L at the boundary between the real IMFs and the redundant IMFs.
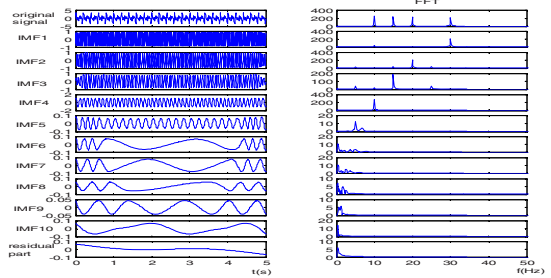
4   Experiment and Analysis

The example of the section 2 is discussed in succession. Above all, all L_i of IMFs are calculated by equation (2). The results are described in table 1. The results of D_L are described in table 2.

Table 1. All L_i of IMFs $(1 \leqslant i \leqslant 10)$

IMFi	1	2	3	4	5
L_i	0.6495	0.5345	0.6406	0.5539	0.9908
IMFi	6	7	8	9	10
L_i	0.9971	0.9987	0.9989	0.9992	0.9989

Table 2. The result of D_L

L_i	1	2	3	4	5
D_i	0.1149	0.1061	0.0867	0.4369	0.0063
L_i	6	7	8	9	--
D_i	0.0016	0.0003	0.0003	0.0003	--

From the table 2, it can be seen that m is equal to four. So, the first four IMFs are viewed as the real IMFs and other are the redundant IMFs. This is consistent with the fact.

The instantaneous frequency estimated by Hilbert-Huang transform without the proposed algorithm is presented in fig. 2 and with the proposed algorithm in Fig. 3. From the two figures, those can be seen that the first deficiency of HHT will cause misinterpretation to the result and the proposed algorithm successfully eliminate the redundant IMFs so that obtain the real instantaneous frequency of the signal $x(t)$.

5   Conclusion

HHT provides a new method for processing the nonlinear and non-stationary signal and has received great attention in various areas, but it is not a perfect tool in practical application due to some deficiencies. In this paper, only one of them, that is, the EMD will generate redundant IMFs at the low-frequency, is discussed. To resolve the problem, an algorithm is proposed which is based on the cause of generating the redundant IMFs and the characteristics of EMD. In the algorithm, a threshold m is calculated which must satisfy some proper conditions, then $h_i(t)$ ($1 \leqslant i \leqslant m$) are viewed as the real IMFs and other the redundant IMFs to be eliminated finally. The results of experiment show that the proposed algorithm is effective on improving HHT.
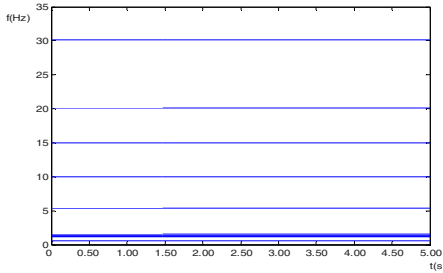
Fig. 1. The instantaneous frequency estimated by HHT without using the proposed algorithm
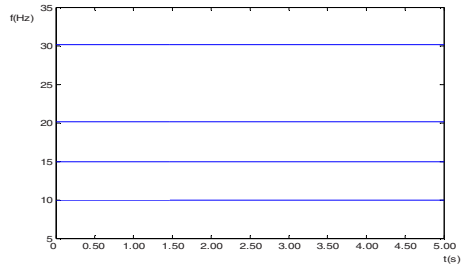
Fig. 2. The instantaneous frequency estimated by HHT with using the proposed algorithm

References

1. N.E. Huang, Z. Shen, S.R. Long, M. Wu, H. Shih, N. Zheng, C. Yen, C.C. Tung, H.H. Liu. The empirical mode decomposition and the Hilbert spectrum for non-linear and non-stationary time series analysis. Proceedings of the Royal Society of London Series A—Mathematical Physical and Engineering Sciences 454 (1998) 903–995.
2. Olivier Adam. The use of the Hilbert-Huang transform to analyze transient signals emitted by sperm whales. Applied Acoustics 67 (2006) 1134–1143
3. Z.K. Peng, Peter W. Tse, F.L. Chu. An improved Hilbert–Huang transform and its application in vibration signal analysis. Journal of Sound and Vibration 286 (2005) 187–205
4. Z.K. Peng, Peter W. Tse, F.L. Chu. A comparison study of improved Hilbert–Huang transform and wavelet transform: Application to fault diagnosis for rolling bearing. Mechanical Systems and Signal Processing 19 (2005) 974–988
5. Liu YB, Wu Q, Ma ZY, Yan KG. An improved Hilbert-Huang transform and its application in faults signal analysis. IEEE ICMA 2006: PROCEEDING OF THE 2006 IEEE INTERNATIONAL CONFERENCE ON MECHATRONICS AND AUTOMATION 1-3(2006) 2426-2431
6. Qi Wu, Yi-bing Liu, Ke-guo Yan. A new approach to improved Hilbert-Huang transform. Sixth World Congress on Intelligent Control and Automation Dalian, China, 21-23 (2006)

Experiment of Event Injection Technology for Network Dependability Evaluation

Yonggang Pang[1], Huiqiang Wang[1], and Ye Du[2]

[1] College of Computer Science and Technology,
Harbin Engeering University 150001 Harbin, China
pangyonggang@hrbeu.edu.cn,
wanghuiqiang@hrbeu.edu.cn
[2] College of Computer, Beijing Jiaotong University, 100044 Beijing, China
mail_dy@163.com

Abstract. Dependability evaluation of computer network is an integrated and complex research problem. Evolving from fault injection, event injection can be better used to evaluate dependability of computer network system. According to the principle of event injection, an experiment model for network dependability evaluation was designed and correlative experiments were carried out. At last, application of event injection for dependability evaluation on computer network was discussed.

Keywords: dependability evaluation; event injection; DDoS; Loadrunner.

1 Introduction

In some important domains, such as national defense, avigation, finance and transportation, dependability of its computer network system is an important problem. Dependability of a system is related to network reliability, availability, security and safety, so how to evaluate the integrated dependability is a problem to be solved urgently [1]. Nowadays, the research on dependability of computer network system concludes important server system, small-size network and web application network, and the conception of dependability is still developing. However, method, model and relative index system of dependability evaluation are lacking, research on these domains sill need to be further carried on.

Event injection technology is introduced to the research on dependability evaluation of network system, by which the integrated dependability of a target system can be tested [2]. Event injection technology adapts better to the experiment in the computer network environment than fault injection. In the event injection experiment, relative characteristic events can be injected into the system to check its reaction according to the relative attributes and characters of dependability evaluation. This paper sequentially dissertates the conception of event injection technology, some event injection experiments and integrated judgment to the experiments. At last, some problems of event injection technology in network experiment are discussed.

2   Dependability of Computer Network

The new conception of dependability[3] was formally advanced by J.C.Laprie in 1985, which included conceptions of reliability, availability, maintainability and safety at that time, that is to say, the reliable computing and fault-tolerance were joined into the conception of dependability. From the medium term of 1980s', fault-tolerance technology was applied to deal with the security threat and a series of exploring researches on hostile failure problems led to a fusion of the two conceptions of security and dependable computing. After that, deep and close discussion of some experts caused the appearance of an academic patent which has further effect [4]. After that, J.C.Laprie deeper illustrated his viewpoint many times at different occasions. After 1995, with the worsening of Internet security, together with the developing of security technologies and changing of attack means, people had to afresh scan the essence of dependable computing and security computing. And the new consideration of dependable computing and security computing by A.Avizienis，J.C.Laprie，Brian Randell, and Carl Landwehr reflected the newest changes.

Correlative conceptions including trusted computing from U.S. military [5] and trustworthy computing advanced by Bill Gates of Microsoft developed. During research on dependability [6], correlative conceptions are developing continuously, but there isn't uniform standard.

3   Event Injection Model

During the dependability evaluation on system, there were not only traditional exact models such as the network hardware reliability problems, but also the non-accurate models, such as the security problem, so event injection evolving from fault injection can solve these problems better.

Event injection technology is an experimental process, in which different kinds of system events including reliability events, availability events, security events of network system are injected into the target system, at the same time, response information of injected events is analyzed or called back by corresponding system, and at last relative results are provided to experimenters. Key technologies affecting the dependability evaluation result by event injection technology mainly are: selection of event model library, statistical event coverage, and experiment comprehensive evaluation.

3.1   Selection of Event Model Library

Event model library should include the events that can influence the service ability of the target system. The injected event model selected is more similar to the events occurred during the actual running of the system or covers them to the greatest extent, the results of the experiment will be more accurate. A suitable event model library should follow two principles: Firstly, it should include a majority of event models that can influence the actual running of the system and cause performance decline of the target computer systems; Secondly, event models in it can detect the vulnerability of the target system.

3.2 Statistical Event Coverage

The events injected into an running system can't include all of the events faced by system applications and injection strategy of one event can't represent entire instances, at the same time, harm extents of different events faced by system are different from each other, so during the dependability evaluation on the target system, the satisfactory degree which is named as statistical event coverage should have a credibility interval.

3.3 Experiment Comprehensive Evaluation

Computer network dependability evaluation includes reliability, availability, safety and security, and so on, moreover the network system can be divided into local area network, distributed network and internet, therefore the network system dependability research is very broad, the corresponding test data will be massive, how to obtain a system' dependability degree is a complex question.

4   Event Injection Experiment

In the network dependability evaluation, the network service performance and security are very important. This article simulates and evaluates the web server in network using event injection technology, use Loadrunner to test the basic performance of the network and use the DDoS attack test to influence the system.

This experiment is to test the operating performance of the target system, Load-Runner8.0 test software is used. The results can then be analyzed in details, to explore the reasons for particular behaviour. the data in Table 1 will be used as the index data in the dependability evaluation to the target server system.

Table 1. Main tesing data of web sever

Measure events	index	min	max	average
connection	Connection shutdowns	0.125	83.063	42.497
rate	New connections	0.107	83.125	42.563
error rate	Error-26628	0	5.438	2.745
Hits per Sec	Hits/s	0.286	153.063	75.377
HTTP Re-	HTTP_200	0.143	91.844	41.775
sponses per	HTTP_403	0	75.75	33.291
Sec_	HTTP_404	0	0.625	0.311
flow speed	B/s	2313	591651	340855

DDoS makes the failure of attacked network server. In Figure 1 and Figure 2, the server average response time increases along with the attack flow increase, the mean flow speed reduces along with the attack flow increase. At the same time, along with the attack duration extension, the server average response time increases, mean flow speed reduces. When the attack computer increases, the server response
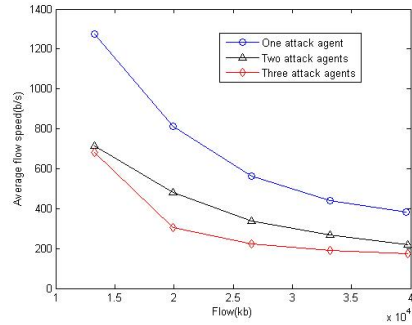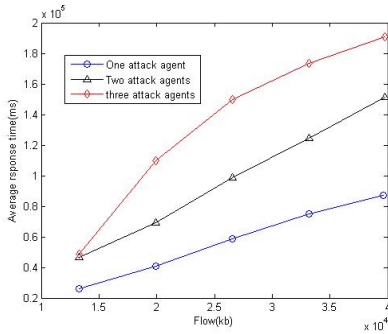
Fig. 1. Average response time curves of server   **Fig. 2.** Average flow speed curves of server

time obviously increases, with the server processing attack request event increases, the server response slows down even in the same flow situation.

5   Conclusions

In the experiment method, event injection technology can preferably solve the problems of network dependability evaluation. Event injection technology can not only analyze the cases when the target system fail but also analyze the cases when the capability of target system performance declines or the system not being able to offer satisfied services to users.

References

1. Yves Deswarte, Karama Kanoun, Jeam-Claude Laprie. Diversity against accidental and deliberate faults. PRDC'99,Hong Kong, 1999.
2. Huiqiang Wang, Yonggang Pang, Ye Du. Evaluation of network dependability using event injection. In: Proc of the APWeb 2006 Int'1 Workshop: XRA, IWSN, MEGA, and ICSE. Berlin: Springer, (2006) 991-998.
3. J.C. Laprie. Dependable Computing and Fault Tolerance: Concepts and Terminology. Proc.15th IEEE Int'l Symp. Fault-Tolerant Computing (FTCS-15), (1985) 2-11.
4. J.C. Laprie, ed. Dependability: basic concepts and terminology-in English, French, German, Italian and Japanese. In Dependable Computing and Fault Tolerance. Springer-Verlag, Vienna, (1992) 265.
5. Department of defense trusted computer system evaluation criteria. http://www.radium.ncsc.mil/tpep/library/rainbow/5200.28-STD.html.
6. Bill Gates. Trustworthy Computing, 2002.

Analysis on Construction of a Sub-sea Tunnel

Wantao Ding, Shucai Li, and Weishen Zhu

Geotechnical & Structural Engineering Research Center of Shandong University , Jinan, 250061, China
{Wantao Ding, Shucai Li, Weishen Zhu, wantaod}@sdu.edu.cn

Abstract. Based on numerical simulation, the construction analysis of a sub-sea tunnel is rewarded. Under the condition that the lateral pressure coefficient is equal to 0.5, two common construction methods that are processes of whole section excavation, schemes of benching excavation are analyzed. The result of that method of benching excavation will slightly disturb the surrounding rock compared the displacements of key-points and the distributions of plastic area on the surface of wall rock. Finally, the conclusion is reached that the reasonable bench pace between benching excavation is around 10 meters is proposed by analyzing tunnel stability under different bench lengths. The conclusion can direct the construction of the tunnel better.

Keywords: sub-sea tunnel, lateral pressure coefficient, plastic area.

1 Introduction

In recent years, experts have done much technical research on the construction of sub-sea tunnels. They researched the minimal rock cover of sub-sea tunnels by means of engineering analogy and numerical simulations. Many valuable results Have been acquired [1],[2]. However, study on the sub-sea tunnels is in the initial steps. In view of construction mechanics, this paper researches the effect of minimal rock cover about crucial profile (K28+800) on different excavation methods and construction sequences [3].

2 Geological Conditions

Geological construction in a tunnel zone is simple and the rock mass is intact. There are a few large faults. A few small faults may exist because of construct of fault around this zone. Most bores show a lot of growth crannies in the part of tunnel zone. The seismic data show that crannies or dikes may exist in eleven places on the shore.

3 Numerical Models

In a numerical model, the z-axis is the direction of the tunnel's axes. The direction vertical to the tunnel axes in the plane is the x-axis. The y-axis is

vertical to the tunnel axes in the profile. The calculation range is between 0 meter and 160 meters on the x-axis. The range is between 0 meters and 10 meters on the y-axis. The range is 50 meters on the z-axis. The distance from the vault of the tunnel cave to the bottom of the numerical model is 80 meters. The horizontal boundaries have been put on both sides of the model. The vertical boundaries are put on the bottom. The top of model is free. The initial stress fields are caused by gravity on the model. Then the construction sequence is simulated. The hydrostatic pressure on the top of the model simulates the effect of seawater. The high level is 4.64 meter up the sea level. Various mechanical parameters of rock mass are shown in Table 1.

Table 1. Mechanical parameters of surrounding rock

Rock & soil	Density (kg/m^3)	Elastic modulus (MPa)	Poisson's ratio	Cohesion (KPa)	Friction angle	Tension strength (KPa)
Silty clay	1720	2.43	0.35	18.5	27	10
Gravel grit	1960	8.8	0.35	15.5	33.3	10
Subclay	1990	7.2	0.35	40.0	23.5	10
Slightly weathering tuff	2500	15000	0.25	1500	40	10
Slightly weathering Sandstone	2680	10000	0.26	8350	48	800
Andesite	2620	6000	0.28	500	35	500
Concrete lining	2500	30000	0.18	2740	55	

4 Result and Analyis Under Different Excavation Methods

The eight key-points on the tunnel wall are picked up. The lateral press coefficient is 0.5 and the excavation methods of whole section as well as benching are chosen. Then the displacement of key-points is computed and compared with each other (Fig.1 & Table 2). The results show the displacement of key-points under benching excavation is smaller than that of the whole section [4], [5].
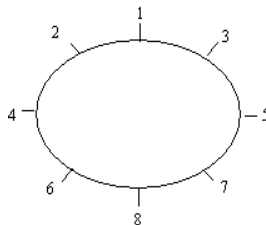
Fig. 1. Key-points on tunnel wall

Table 2. Profile of the displacements of key-points on the surface of wall rock of K28+800

Key-points	Whole section			Upper and down benching		
	x-dis(m)	y-dis(m)	totaldis(m)	x-dis(m)	y-dis(m)	totaldis(m)
1	-5.25E-06	-1.11E-03	1.11E-03	-5.18E-06	-0.92E-03	0.92E-03
2	-2.96E-04	-8.58E-04	9.08E-04	-2.83E-04	-8.46E-04	8.92E-04
3	2.98E-04	-8.56E-04	9.06E-04	2.86E-04	-8.43E-04	8.90E-04
4	-5.72E-04	1.02E-06	5.72E-04	-5.66E-04	1.02E-06	5.66E-04
5	5.74E-04	1.02E-06	5.72E-04	5.69E-04	1.02E-06	5.69E-04
6	-2.97E-04	8.36E-04	8.87E-04	-2.79E-04	8.34E-04	8.79E-04
7	2.94E-04	8.39E-04	8.89E-04	2.82E-04	8.35E-04	8.81E-04
8	-4.98E-06	0.87E-03	0.87E-03	-4.83E-06	0.82E-03	0.82E-03

5   Analysis of Construct Sequence

The step method is used extensively during tunnel construction. But different step lengths may affect tunnel stability in different ways, so it is important to make sure that the step length is reasonable. In view of benching excavation, this paper simulates the excavation effect under different space. Three kinds of step lengths such as 1D, 2D and 3D, are analyzed by numerical simulation [6].

The curvature of different points in the tunnel vault and in the rock cover is rewarded under three different step lengths (Fig.2.).
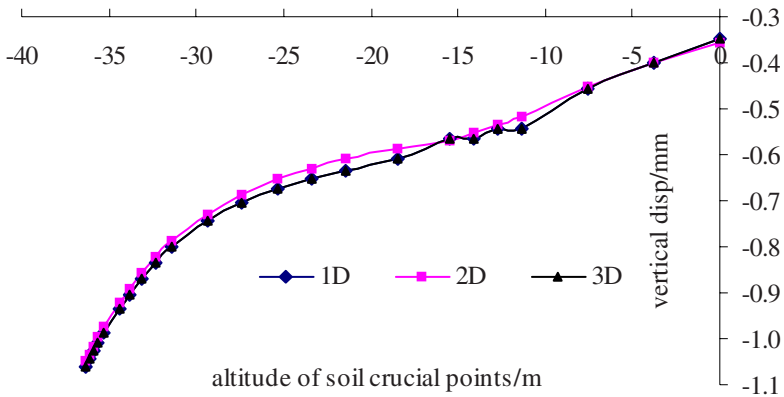
Fig. 2. Displacement compare in tunnel rock cover after excavation

The displacement contrast curve of crucial points in rock cover shows that the different construction sequences affect the final displacement of rock cover. The displacement compare curve of crucial points on tunnel vault shows that the vertical displacement is greatest and the horizontal displacement is small. The displacement movement stabilizes when the distance between frontal step and back step is about 10 meters. So the distance between two steps over about 10 meters is reasonable when using benching excavation.

6 Discussions

According to analysis, engineering experience and excavation methods, the upper and down benching excavation method may decrease the effect of disturbances and protect the stability of rock mass. Meanwhile it can reduce the cost of tunnel excavation.

The different construction sequences slightly affects the final displacement of rock mass. It produces the large displacement near the tunnel face. It affects to choose the reasonable support sequence during construction. The distance between two steps over about 10 meters is reasonable when using upper and down benching excavation. The stable zone of the vault displacement along the z-axis direction is about 10 meters.

References

1. Li Shucai, Li Tingchun, Chen Weizhong: Application of 3D Elastoplastic Fracture Damage Model To Determination of Mininmum Roof Thickness of XiaMen Subsea Tunel, Chinese Journal of Rock Mechanics and Engineering, vol.23. (2004) 3138-3143
2. Li Shucai, Xu Bangshu, Li Shuchen: Lining Structure Type of Subsea Tunnel and Its Support Parameters Optimizing, Chinese Journal of Rock Mechanics and Engineering, vol.24.(2005) 3894-3901
3. Zhu Weishen, Li Shucai, Bai Shiwe etc: Some Developments of Principles For Construction Process Mechanics and Some Case History Studies, Chinese Journal of Rock Mechanics and Engineering, vol.22.(2003) 1586-159
4. Liu Fang, Tang Zhongsheng, Dong Zhiming: Mechanical Analysis on Construction of Metro Station Tunnel of BeiJing, Railway Engineering, (2006) 41-43
5. Zhu Zebing, Liu Xinrong, Zhang Yongxing: Study of Excavation Method For Ultra-shallow-buried Light Railway Station Tunnels With Large Span l, Chinese Journal of Rock Mechanics and Engineering, vol.24.(2005) 290-295
6. Jiang Shuping, Liu Yuanxue, Zhao Shangyi: Finite Element Numerical Simulation of Shallow Buried Biasing Loess Multiple Arch Tunnel Construction Plan, Technology of Highway and Transport. (2006) 95-99

Rotation Invariant Texture Classification Using Circular Gabor Filter Banks

Qingbo Yin[1,2] and Jong Nam Kim[1]

[1] Division of Electronic Computer and Telecommunication Engineering, Pukyong National University, 599-1 Daeyeon-dong Nam-gu, Busan, 608-737, Korea
`Jongnan@pknu.ac.kr`
[2] College of Computer Science and Technology, Harbin Engineering University, Harbin, 150001, P.R. China
`yinqingbo@hrbeu.edu.cn`

Abstract. This paper presents a new method for rotation invariant texture classification based on the circular Gabor wavelets. A circular Gabor filter bank is proposed to decompose an image into multiple scales and be rotation invariant. By the mean and variance of the circular Gabor filtered image, a discriminant can be found to classify rotated images. In the primary experiments, comparatively high correct classification rates were obtained using a large test sample set.

1 Introduction

Texture analysis is a fundamental issue in image analysis and computer vision. The Gabor function can be appropriately considered as an orientation and scale tunable detector. The banks of Gabor filters are a group of wavelets, which one can capture the signal or feature at a specific frequency and a specific orientation. There are several approaches based on Gabor filters, which focus on the rotation invariant texture in [1-3]. But, most of them only work well on a small database and need a lot of samples for training.

The motivation of this paper is to classify rotation-invariant textures in a large texture database. The proposed algorithm is based on circular Gabor filter responses, in which each texture has the corresponding global features. Then, a similarity measure is used to compare the unknown samples with the feature of known textures. The primary experiments have proven this approach performs well in applications.

2 Circular Gabor Wavelet and Classification

For the filter to be rotation invariant, it is necessary that the sinusoidal grating varies in all orientations. In the circular Gabor filter, both Gaussian and grating vary only in a radial direction from origin, such that the filter is completely circularly symmetric. The circular Gabor filter is defined as[1]:

$$Cg(x, y) = \frac{1}{2\pi\sigma^2} \exp\left[-\frac{(x^2 + y^2)}{2\sigma^2}\right] \cdot \exp\left[j2\pi W\left(\sqrt{x^2 + y^2}\right)\right] \qquad (1)$$

Where W is the required centered frequency of the circular Gabor filter, and $\sigma = \sigma_x = \sigma_y$. The frequency domain representation of the circular Gabor filter is given by:

$$CG(u, v) = \frac{\sqrt{2\pi}}{2} \alpha \cdot \exp\left[-\frac{\left(\sqrt{u^2 + v^2} - W\right)^2}{2\alpha^2}\right], \quad \alpha = \frac{1}{2\pi\sigma} \qquad (2)$$

2.1   Circular Gabor Wavelet and Parameter Selection

A class of self-similar functions like the wavelet is considered as the circular Gabor filter bank or circular Gabor wavelet in the following discussion. Let $Cg(x, y)$ be the mother Gabor wavelet, then this self-similar filter dictionary can be obtained by appropriate dilations and rotations of $Cg(x, y)$ through the generating function:

$$Cg_m(x, y) = a^{-m} Cg(x', y'), \ a > 1, \ m = 1, \ldots, S$$
$$x' = a^{-m} x, \text{ and } y' = a^{-m} y \qquad (3)$$

Where a is a scale factor, and the factor a^{-m} is meant to ensure that the energy is independent of m. S is the number of scales in the multiresolution decomposition.

Let W_l and W_h denote the lower and upper center frequencies of interest. Then, the design strategy is to ensure that the half peak magnitude cross-sections of the filter responses in the frequency spectrum touch each other. This results in the following formulas for computing the filter parameters σ and W:

$$a = \left(W_h / W_l\right)^{1/s-1}, \text{ or } W_h = W_l \cdot a^{(S-1)}, \sigma = \left(3\sqrt{2\ln 2}\right) / (2\pi W_h) \qquad (4)$$

2.2   Texture Representation and Rotation Invariant Measurement

Given an image $I(x, y)$ of size $M * N$, its discrete circular Gabor transform is given by convolution:

$$H_m(x, y) = \sum_p \sum_q I(x - p, y - q) Cg_m^*(p, q), \ m = 1, \ldots, S \qquad (5)$$

Where p, q is the filter mask size, $Cg_m^*(p, q)$ is the complex conjugate of Cg_m.

It is assumed that the texture regions are spatially homogeneous. The mean μ_m and standard deviation σ_m of the magnitude of the transform coefficients are used to construct global features to represent the homogeneous textures.

$$\mu_m = \frac{\sum_M \sum_N |H_{mn}(x,y)|}{M * N}, \ \sigma_m = \frac{\sqrt{\sum_x \sum_y (|H_m(x,y)| - \mu_m)^2}}{M * N}, m = 1, \ldots, S \tag{6}$$

Now, the direct distance metric can be defined between the query image Q and a target image T in the database as:

$$d_m^\mu(Q,T) = |\mu_m^Q - \mu_m^T|, \ d_m^\sigma(Q,T) = |\sigma_m^Q - \sigma_m^T| \tag{7}$$

Three differential factors can be defined as:

$$df_\mu = \frac{\sum_{m=1}^S (d_m^\mu)^2}{\sum_{m=1}^S (\mu_m^T)^2}, \ df_\sigma = \frac{\sum_{m=1}^S (d_m^\sigma)^2}{\sum_{m=1}^S (\sigma_m^T)^2}, \ df_D = \sum_{m=1}^S (d_m^\mu)^2 + \sum_{m=1}^S (d_m^\sigma)^2 \tag{8}$$

Actually, the texture similarity measurement is accomplished by defining the differential measurement:

$$df = \min(df_\sigma * df_\mu * df_D) \tag{9}$$

This similarity measurement is rotation invariant, and is smallest if Q is the same as or very similar to T.

3 Experiments

The experiments are carried out on a texture database from the Brodatz texture album, which is comprised of 111 texture images. Each center portion of size 256×256 from each respective texture image is used in the training phase. Texture classification is done with a total of 1998 rotated texture images in steps of $10°$ up to $180°$ for various scale values of Gabor decomposition (scale is from 2 up to 10). The center frequencies for Gabor filters are 0.02-0.48 and are separated by one octave. In Table 1, the results of comparisons with other main methods [2-3] are given. Other schemes need a large training for each class of images. However, the proposed approach only needs a sample of each class for training at 0 angle, then can work well. Nevertheless, the proposed approach can deal with 111 classes with a correct classification rate of more than 97%, only using scale=7 and 14 features.

Table 1. The performance comparisons between the proposed approach and other schemes

Method	Samples			The number of features	Correct classification rate
	Number of classes /total of images	Number of each class for training	Number of each class for testing		
Space-frequency model [3]	109/ (872*2=1744)	8	8	—	80.4%
Arivazhagan's method [2]	112/ (112*36=4032)	1	36	100	93.7%
Proposed approach	111/ (111*18+111=2109)	1	18	14	97.7%

4   Conclusions

A rotation invariant texture classification scheme based on the circular Gabor filter is developed for a reasonably large (111 classes) texture databases. By the mean and variance of the Gabor filtered image, a discriminant can be found to classify rotated images. The primary experiments have proven that the proposed approach is effective for rotation invariant texture classification.

Acknowledgements

References

1. Porter, R., Canagarajah, N.: Robust rotation-invariant texture classification: Wavelet, Gabor filter and GMRF based schemes. IEE Proceedings of Image Signal Processing 144 (3), 1997.
2. Arivazhagan, S., Ganesan L., and Padam Priyal, S.: Texture classification using Gabor wavelets based rotation invariant features. Pattern Recognition Letters, Vol.27(16), (2006) 1976-1982
3. Haley, G.M., Manjunath, B.S.: Rotation-invariant texture classification using a complete space-frequency model. IEEE Transactions on Image Processing 8 (2), (1999) 169–255.

A Clustering Algorithm Based on Power for WSNs*

Kaihua Xu[1], Ya Wang[1], and Yuhua Liu[2]

[1] College of Physical Science and Technology, Central China Normal University, Wuhan, 430079, P.R. China,
Kaihua Xu, Ya Wang, xihuanni3957@sohu.com
[2] Department of Computer Science, Central China Normal University, Wuhan, 430079, P.R. China,
Yuhua Liu, yhliu@mail.ccnu.edu.cn

Abstract. This paper computes the optimum number of cluster heads based on power first, and then proposes the clustering algorithm for WSNs, at last estimates its performances by our emulator. On analysis, clustering time complexity is dependent on the network diameter and it is suitable for small or medium networks. The simulation results show that using this clustering algorithm can generate network topology of optimum number of clusters, the nodes energy is reduced greatly and the lifetime of networks is extended.

Keywords: clustering topology, WSN, generation algorithm, cluster heads, node energy.

1 Introduction

The main goal of the topology management for WSNs is to form an optimal framework based on data transmission by removing unnecessary communication links between nodes, and the prerequisite is to assure network coverage and connectivity [1]. There are two approaches to topology management in WSNs----power control and hierarchical topology organization. Power control mechanisms adjust the power on a per-node basis, so that one-hop neighbor connectivity is balanced and overall network connectivity is ensured; With hierarchical topology control, a subset of the network nodes is selected to serve as the network backbone over which essential network control functions are supported[2]. This approach to topology control is often called clustering, and our study on this paper focuses on the hierarchical clustering algorithm for WSNs.

2 The Clustering Algorithm for WSNs

2.1 The Optimum Number of Cluster Heads Based on Power

To study on the hierarchical clustering algorithm for WSNs, we make the following assumptions:

---

1) The nodes in WSNs are distributed as per a homogeneous spatial Poisson process of intensity λ in a 2-dimensional space which is a square area of side $2a$, and $\lambda = \lambda_0 + \lambda_1$, where the intensity of cluster heads is λ_1, the intensity of non-cluster heads is λ_0; p with mean the probability of cluster heads in a WSN, thus $\lambda_1 = p\lambda$, $\lambda_0 = (1-p)\lambda$;

2) The total number of nodes in this area is n, and the area of this 2-dimensional space is s, n with mean λs, where $s = 4a^2$;

3) Also assume that the origin of coordinates is at the center of the square, and the base station is located at $(0, 2a)$;

4) We assume a simple model for the radio hardware energy dissipation where the transmitter dissipates energy to run the radio electronics and the power amplifier, and the receiver dissipates energy to run the radio electronics [3].

5) In this algorithm, the cluster heads creates a TDMA schedule telling each non-cluster heads when it can transmit message.

According to the assumptions above, We get under the exponent the following expression:

$$p = \sqrt{\frac{10\lambda}{0.0061632025n^2}} \tag{1}$$

The computed values of p and the corresponding values of the number of nodes n and the intensity of nodes λ for WSNs are provided in Table 1.

2.2   Parameters for the Clustering Algorithm

The weighted clustering algorithm (WCA) is an on-demand distributed clustering algorithm proposed for mobile ad hoc networks [4]. It elects a node as a cluster head based on four parameters as follows: the number of neighbors, transmit power, battery-life and mobility rate of the node.

Because the nodes are stationary in WSNs, the considered parameters for the optimizing algorithm of WCA are simple relatively. Consider three parameters as follows: *1)* the battery-life of nodes C_{i_res}; *2)* The nodes degree-difference $\Delta_i = |d_i - E[N]|$, where $E[N] = \lambda_0 / \lambda_1$, and d_i means the neighbors' number of nodes i; *3)* The average distance between node and its neighbors $d_{i\_ave} = D_i / d_i$, where D_i means that the total distance between node i and its neighbors. Consider three parameters above, the combined weight w_i for node i in WSNs can be calculated:

$$w_i = w_1 \cdot \frac{C_t}{C_{i\_res}} + w_2 \cdot \Delta_i + w_3 \cdot d_{i-ave} \tag{2}$$

Where, C_t is defined as the initial energy of nodes, and w_1, w_2, w_3 are defined respectively as the weight of three parameters, where $w_1 + w_2 + w_3 = 1$. When the smaller the weight w_i, the bigger probability of node i being elected as a cluster head.

Table 1. The optimum number of cluster heads p

Number of nodes (n)	Intensity of nodes(λ)	Probability of cluster heads (p)
500	1.25	0.0901
1000	2.5	0.0637
1500	3.75	0.0520
2000	5	0.0450
2500	6.25	0.0403
3000	7.5	0.0368

2.3 The Generation of Clustering

The generation of clustering procedure consists of two processes: cluster heads election phase and cluster Set-Up phase. During cluster heads election phase, the suitable nodes are elected as cluster heads according to some topology control algorithms for WSNs; during cluster Set-Up phase, the cluster heads broadcast their states using the same transmit energy to the non-cluster heads in the networks, after each node has decided to which cluster it belongs, it must inform the cluster head node that it will be a member of the cluster, and then the framework of WSNs forms.

3 Simulation Study and Performance Evaluation

3.1 Simulation Study

The most important goal in WSNs is the effective utilization of energy, so in simulation study, we considered the nexus between the number of cluster heads and the total amplifier energy for WSNs. Figure 1 described the function diagram $e_t(p)$ for 500, 1000 and 2000 nodes in WSNs, where $e_t(p)$ is the total amplifier energy for WSNs. It is evident that the total amplifier energy spent in the network is indeed minimal at the theoretically optimal values of the parameter p computed using (1).
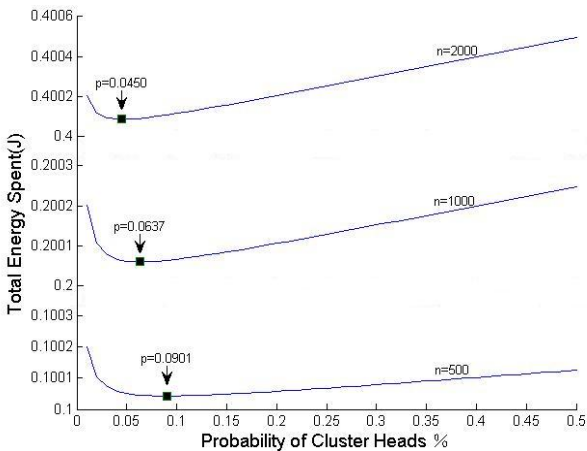
Fig. 1. Total amplifier energy vs. probability of cluster heads in WSNs

3.2 Performance Evaluation

In the clustering algorithm flowchart, its time complexity is $O(n^2)$, where n with mean the number of network nodes. When the size of network is small, the algorithm is simple; when the size of network is large, it is necessary to set more parameters to let it simple. We will study on this research in the future.

4   Conclusion

In this paper, take the optimum number of cluster heads based on power and the optimizing algorithm of WCA into consideration, and generate the clustering topology of WSNs. The simulation results show that because of this clustering algorithm, the nodes energy is reduced greatly. This algorithm is suitable for the small and medium networks. When the size of network is large, it is necessary to set more parameters to let it simple. We will study on this research in the future. At same time, what need study on deeply is how to design a routing protocol of security, QoS and so on based on clustering.

References

1. Akyildiz I F, Su W, Sankarasubramaniam Y, Cayirci E. A survey on sensor networks. IEEE Communications Magazine, 2002, 40: 102~114
2. Bao L, Garcia-Luna-Accves J J. Topology management in ad hoc networks. In: Proc 4th ACM Int'l Symp on mobile Ad Hoc Networking & Computing (MobiHoc 2003), Annapolis, Maryland. 2003. 129~140
3. S Bandyopadhyay and Edward J.Coyle. An energy-efficient hierarchical clustering algorithm for wireless sensor networks[A].Proc.of IEEE INFOCOM[C].San Francisco, USA: IEEE Computer Society, 2003.1713-1723
4. T. Rappaport, Wireless Communications: Principles & Practice. Englewood Cliffs, NJ: Prentice-Hall, 1996
5. Mainak Chatterjee, Sajal K Das, Damla Turgut. WCA: A weighted clustering algorithm for mobile ad hoc networks [J]. Journal of Cluster Computing, Special issue on Mobile Ad hoc Networking, 2002, (5): 193~204

Analysis of Local Route Maintenance for Ad Hoc Network*

Shaobin Cai, Nianmin Yao, Wenbin Yao, Yong Li, and Guochang Gu

Harbin Engineering University, Harbin, China, 150001
Phone: 86-451-82518030
`caishaobin@hrbeu.edu.cn`

Abstract. In ad hoc network, most link ailure recoveries can be localized to a small region along the previous route. However, the theory is not proved by mathematic analysis and simulations. In this paper, we analyze it by mathematical analysis and by simulations.

Keywords: Ad hoc network, Local Route Maintenance, Mathematics Analysis.

1 Introduction

An ad hoc Network [1] is a multi-hop wireless network. According to that most link failure recoveries can be localized to a small region along previous route [2], NSMP [3] and PatchODMRP [4] are proposed to prolong their flooding periods by their local route maintenance. However, none of them mathematically analyze the local route maintenances, and the functions of the local route maintenances are not clearly. Therefore, we analyze local route maintenance by mathematic analysis and simulations in this paper.

2 Local Route Maintenance

NSMP adopts a neighbor supporting local route discovery system to reduce its control overhead. In NSMP, during its forwarding mesh setting up, the nodes, which will transmit data packets, are marked as forwarding nodes, and the nodes, which are neighbors of forwarding nodes, are defined as neighbor nodes. After forwarding mesh has been setup, normal source maintains its forwarding mesh mainly by periodically flooding control packets in the scope of its forwarding nodes and its neighbor nodes.

PatchODMRP extends ODMRP by its local route maintenance. It sets up its forwarding mesh as ODMRP does. During its transmission of data packets, forwarding nodes know the status of their neighbor nodes by BEACON signal of MAC layer. When a forwarding node finds that a link between its upstream node and itself is broken, it does its local route maintenance in two-hop or three-hop.

3 Mathematic Analysis of Local Route Maintenance

In this section, we analyze the characters of local route maintenance by a random graph. The graph presents an ad hoc network, which is formed by n mobile nodes in a square (1000m×1000m), and each node has n' ($n' \leq n$) neighbors.

In ad hoc network, if a link failure is caused by a node failure, then the possibility that the link failure can be amended is equal to the possibility that a i-link path exists between any two un-neighbor nodes.

Statement 1: In ad hoc network, the possibility p'_i that there is only a i ($i > 1$) links path between any two un-neighbor nodes is: $p'_i = \dfrac{(n')^i \times (1 - \dfrac{n'}{n})^{\frac{i(i-1)}{2}}}{n}$, ($i > 1$).

Proof: In ad hoc network, the possibility that a node is a neighbor of another node is $\dfrac{n'}{n}$. A i ($i > 1$) links path between any two un-neighbor nodes, from a source to a destination, consist of two parts:

1. A $i - 1$ links path from the source to one of the neighbors of the destination.
2. A one-link path from the destination to one of its neighbors.

Then, the probability p'_i that only a i-link path exists between any two un-neighbor nodes is a product of the following three fractions:

1. The number of neighbors of the destination.
2. The probability p'_{i-1} that the source reaches one of the neighbors of the destination through a $i - 1$ links path.
3. The probability $(1 - \dfrac{n'}{n})^{i-1}$ that the destination is not a neighbor of the first $i - 1$ nodes on the $i - 1$ links path.

Now, we can know that the probability p'_i that there is a i ($i > 1$) links path between any un-neighbor nodes is:

$$p_i' = p_{i-1}' \times n' \times (1-\frac{n'}{n})^{i-1} = n'^{i-1} \times (1-\frac{n'}{n})^{\frac{i(i-1)}{2}} \times p_1' = n'^{i} \times (1-\frac{n'}{n})^{\frac{i(i-1)}{2}} \times (\frac{1}{n})$$
$(i>1)$ ▪

Statement 2: In ad hoc network, the possibility p_i that there is another i $(i>1)$ links

path between any neighbor nodes is: $p_i = \dfrac{(n')^i \times (1-\dfrac{n'}{n})^{\frac{(i+1)(i-2)}{2}}}{n}$, $(i>1)$

Proof: According to Statement 1, we know the possibility p_i' that there is only a

i $(i>1)$ links path between any two un-neighbor nodes. Then it can be obtained that

the possibility that there is a i $(i>1)$ links path between any two nodes is: $\dfrac{p_i'}{(1-\dfrac{n'}{n})}$.

And thus, the probability that there is a i $(i>1)$ links path between any two neighbor nodes is:

$$p_i = \frac{n'}{n} \times \frac{p_i'}{(1-\frac{n'}{n})} = \frac{(n')^i \times (1-\frac{n'}{n})^{\frac{(i+1)(i-2)}{2}}}{n}, (i>1)$$ ▪

4 Simulations

GloMoSim [5] is used here to realize simulations of PatchODMRP and NSMP protocols. In the simulations, 50 wireless mobile nodes, which move around over a square (1000m×1000 m), form an ad hoc network; the radio transmission power of the mobile nodes is 15dBm. During the 500s simulation period, the nodes move according to the "random waypoint" model without pause time.

Fig1 describes the relationship between local recovery probability and communication radius. From the simulation results, we can know that, when the mobile nodes have the reasonable communication radius, the local route maintenance can amend most link failures. Three-hop PatchODMRP has the strongest local route maintenance; NSMP has a weaker the local route maintenance of than that of PatchODMRP; two-hop PatchODMRP has the weakest local route maintenance.

Fig2 describes the local control overhead of these protocols. In Fig4, the control overhead of global flooding is set 1, and the control overhead of other protocols is related to that of global flooding. From the simulation results, we can know that, the local control overhead of NSMP is the highest; the local control overhead of two-hop PatchODMRP is the lowest. The scope of local route maintenance determines the control overhead of local route maintenance. Therefore, NSMP has the largest local

route maintenance scope; two-hop PatchODMRP has the smallest local route maintenance scope.

Fig3 describes the data delivery ratio of these protocols as a function of sources increases. When there are few sources in group, the ability of their local route maintenances determine the stability of their forwarding mesh; the stability of their forwarding mesh determines their data delivery ratio. Therefore, when there are few sources in group, three-hop PatchODMRP has the highest data delivery ratio; two-hop PatchODMRP has the lowest data delivery ratio. When there are many sources in multicast group, their control overhead determines the wireless bandwidth acquired by data packets for their transmissions, and the wireless bandwidth for data transmissions determines the data delivery ratio. Therefore, when there are many sources in group, two-hop PatchODMRP has the highest data delivery ratio because of its lowest control overhead; NSMP has the lowest data delivery ratio because of its highest control overhead.

From the results of mathematic analysis and simulation, the performance of these local route maintenances is known. The local route maintenances of three-hop PatchODMRP and NSMP is stronger. However, their control overhead is higher. The control overhead of two-hop PatchODMRP is much lower. However, its local route maintenance is weaker, and some link failures can't be amended when the communication radius of mobile nodes is small. Therefore, PatchODMRP outperforms NSMP. However, PatchODMRP still has some shortcomings. Therefore, the local route maintenance scope of PatchODMRP should be reduce further without reducing its functions by some aiding nodes to is improve its scalability when the number of nodes increase.
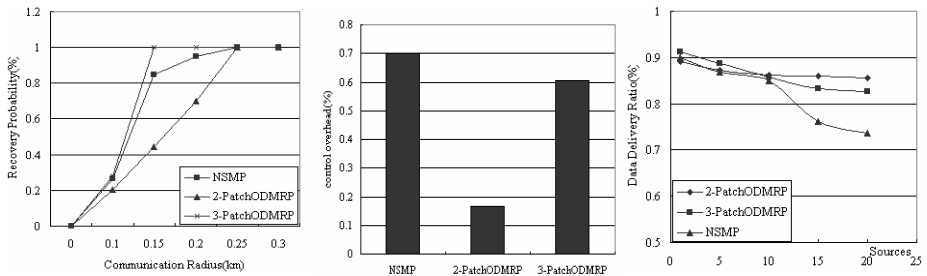
Fig. 1. Relationship between local recovery probability and communication radius

Fig. 2. Control overhead of local route maintenance

Fig. 3. Data delivery ratio as a function of sources

5   Conclusions

In this paper, we analyze the characters of local route maintenance of both NSMP and PatchODMRP by mathematic analysis and simulations. From the mathematic analysis and simulation results, we know that, the overhead of these local route maintenances is

still high, and they scale poor when the number of sources increases. Therefore, we should reduce local route maintenance scope further without affecting its function.

References

[1] Mobile Ad-Hoc Network (MANET) Working Group [Online]. Available http://www.ietf.org/html.charters/ manet-charter.html.

[2] G Aggelou, R Tafazolli, "RDMAR: a bandwidth-efficient routing protocol for mobile ad hoc networks", Proceedings of The Second ACM International Workshop on Wireless Mobile Multimedia (WoWMoM), Seattle, WA, August 1999.

[3] Seungjoon Lee, Chongkwon Kim. "Neighbor supporting ad hoc multicast routing protocol". MobiHOC. 2000 First Annual Workshop on Mobile and Ad Hoc Networking and Computing, 2000.

[4] *Meejeong Lee; Ye Kyung Kim*. "PatchODMRP: an ad-hoc multicast routing protocol" Information Networking, 2001. Proceedings. 15th International Conference on, 2001

[5] Wireless Adaptive Mobility Lab. DEPT of Comp. SCI, UCLA "GloMoSim: A Scalable Simulation Environment for wireless and wired Network System: http://pcl.cs.ucla.edu/projects/domains/glomosim.html

Evaluation of Historic Buildings Based on Structural Equation Models

Qiaohui Tong[1], Tianzhen Liu[2], Hengqing Tong[2], and Zhuoling Ou[2]

[1] School of Urban Design, Wuhan University,
Wuhan, Hubei, 430070, P.R. China
qhtong@whu.edu.cn
[2] Department of Mathematics, Wuhan University of Technology,
Wuhan, Hubei, 430070, P.R. China
tonghq2005@mail.whut.edu.cn

Abstract. This paper proposes a quantitative method for historic buildings evaluation, which is the essential step before conservation decisions. We introduce Structural Equation Models (SEM) in the evaluation of historic buildings making evaluation more objective. We select certain independent variables and dependent variables, including the first degree and the second degree indexes and relationships among them, and put forward an applicable index system which could be spread in all historic sites.[1]

Keywords: Structural equation models, Evaluation, Historic buildings.

1 Introduction

Historic buildings are the most important evidence of the past life style and cannot be regenerated for human being in society. Generally speaking historic buildings include relic, old buildings and outstanding modern architecture in the historical city. Preservation of historic buildings is always the emphasis of research of city planning and architecture, and is also the necessary work of governmental decision-making. For protection of historic buildings, we should classify the grade of buildings and separate different kinds of the buildings. Therefore, evaluation of historic buildings should be put forward and make corresponding settlement for different grade historic buildings.

Compared with other professional field, architecture field lacks for qualitative and quantitative analysis. We need to introduce mathematic method to architecture field, especially to the work of historic buildings evaluation.

There always are index systems in many work of historic buildings evaluation, and these indexes need to be summarized. Traditionally the summarizing coefficients are designated aforehand. However, in this paper we introduce a method in which the summarizing coefficients are calculated by samples, so it is more objective, and could offer more deep analysis for the index systems.

---

2   SEM for Evaluation of Historic Buildings

Structural equation modeling (also SEM) has become a very popular data-analytic technique. It is widely applied in Psychology and Sociology as well as other fields, especially in Customer Satisfaction Index (CSI) model which is required by a series of ISO9000 criterions. The researches of SEM are very plentiful and incessancy (C. Fornell, et al., 1996; S. Auh and M.D. Johnson, 2005).

There are two systems of equations in a SEM. One is a structural system of equations among structural variables, and another is an observation system of equations between structural variables and observed variables. Now we build a SEM for evaluation of historic buildings. The model includes 5 structure variables and 18 observed variables. The variables are in the Table 1 as follows. Notice that the numbers of observed variables corresponding each structure variable are 4,4,4,2,4.

Table 1. Index of Variables

Structure variables		Observed variables			
ξ_1	Historic value	Time of the building	Degree of the integrity	Related famous people and event	Degree of reflection of the local cultural circumstance
η_1	scientific value	Function of building in city planning	Value of technique	Scientific use	Level of the construction
η_2	artful value	Detail and decoration of the art	Value of the landscape near the building	Façade of the building	Interior decoration
η_3	useful value	Quality of the building	Whether can be continually used		
η_4	protective value	Reality of protection	Memorize of being maintained	Value of the landmark	Meaning of protection of the building

Among the structure variables there are some path relationships or causalities. These causalities among the structure variables can be expressed as equations as follows.

$$\begin{pmatrix} \eta_1 \\ \eta_2 \\ \eta_3 \\ \eta_4 \end{pmatrix} = \begin{pmatrix} 0 & 0 & 0 & 0 & 0 \\ \beta_{21} & 0 & 0 & 0 & 0 \\ \beta_{31} & \beta_{32} & 0 & 0 & 0 \\ \beta_{41} & \beta_{42} & \beta_{43} & 0 & 0 \end{pmatrix} \begin{pmatrix} \eta_1 \\ \eta_2 \\ \eta_3 \\ \eta_4 \end{pmatrix} + \begin{pmatrix} \gamma_{11} \\ \gamma_{21} \\ \gamma_{31} \\ \gamma_{41} \end{pmatrix} \xi_1 + \begin{pmatrix} \varepsilon_{\eta 1} \\ \varepsilon_{\eta 2} \\ \varepsilon_{\eta 3} \\ \varepsilon_{\eta 4} \end{pmatrix} \qquad (1)$$

where $\eta_1 \sim \eta_4, \xi_1$ are structural variables, β_{ij} is the path coefficient from dependent variable η_j to η_i, and γ_{ij} is the path coefficient from independent variable ξ_j to dependent variable η_i.

In general, suppose that $\eta_1 \sim \eta_m$ are m dependent variables, arranging them as a vector η by column as (1); and $\xi_1 \sim \xi_k$ are k independent variables, arranging them as a vector ξ by column also. The $m \times m$ square matrix B is the coefficient matrix of η, the $m \times k$ matrix Γ is the coefficient matrix of ξ, ε_η is the residual vector, then SEM (1) may be extended as:

$$\eta = B\eta + \Gamma\xi + \varepsilon_\eta \tag{2}$$

The structural variables are implicit and cannot be observed directly. Each structural variable is corresponding with many observed variables.

Suppose that there are M observed variables and each one has N observed values, then we will get a $N \times M$ matrix. The relationships between the structural variables and the observed variables can also be expressed in equations by two ways of path causality. Let x_{tj}, $j = 1, \cdots, S(t)$ be the observed variables corresponding to ξ_t, $t = 1, \cdots, k$, and y_{ij}, $j = 1, \cdots, L(i)$ be the observed variables corresponding to η_i, $i = 1, \cdots, m$, then the observation systems of equations from observed variables to structural variables are:

$$\xi_t = \sum_{j=1}^{S(t)} \psi_{tj}\, x_{tj} + \varepsilon_{\xi t} \quad , \quad t = 1, \cdots, k \tag{3}$$

$$\eta_i = \sum_{j=1}^{L(i)} \omega_{ij}\, y_{ij} + \varepsilon_{\eta i}, i = 1, \cdots, m \tag{4}$$

where $\sum\limits_{t=1}^{k} S(t) + \sum\limits_{i=1}^{m} L(i) = M$.

We call (2)(3)(4) a SEM, and sometimes we call it path analysis model.

At present, the path causality in popular PLS algorithm for SEM is from observed variables to structural variables as (3)(4), and the iterative initial value vector for ψ_{tj}, ω_{ij} is arbitrary. As we all know, the convergence of the PLS has not been proved well, and its convergence rate may be very slow.

3   The Best Initial Value in PLS Algorithm of SEM

We find that arbitrary initial value is not necessary and PLS can be calculated by a suitable iterative initial value based on the least square estimation in the observation equations.

For this reason, we can write the observation systems of equations from structural variables to observed variables. It is also a linear system of equations with some random errors.

$$\begin{pmatrix} x_{t1} \\ \vdots \\ x_{t\,S(t)} \end{pmatrix} = \begin{pmatrix} v_{t1} \\ \vdots \\ v_{tS(t)} \end{pmatrix} \xi_t + \begin{pmatrix} \varepsilon_{xt1} \\ \vdots \\ \varepsilon_{xtS(t)} \end{pmatrix}, t = 1, \cdots, k \tag{5}$$

$$\begin{pmatrix} y_{i1} \\ \vdots \\ y_{iL(i)} \end{pmatrix} = \begin{pmatrix} \lambda_{i1} \\ \vdots \\ \lambda_{i\,L(i)} \end{pmatrix} \eta_i + \begin{pmatrix} \varepsilon_{y\,i1} \\ \vdots \\ \varepsilon_{y\,i\,L(i)} \end{pmatrix}, i = 1, \cdots, m \qquad (6)$$

where υ_{tj} and λ_{ij} are load items.

Carefully analyzing the relationships among the variables in above equations, we find a series of the least square relationships, and obtain the least square solution of the observation systems of equations from structural variables to observed variables. Our algorithm paper has been accepted by international journal "Mathematical and Computer Modelling" and will be published in 2007. Our algorithm program has been received in DASC software developed by us. More details are omitted here.

4   Conclusion and Discussion

According a group of evaluation data by the observed variables, we complete the computation using DASC software. The data example including data files, figures, and calculation results are offered completely. They can be downloaded from my website: http://public.whut.edu.cn/slx/english/index.htm. We should prove our method is successful.

Having got the solution of SEM in evaluation of historic buildings, the path relationship among the indexes and the path effective coefficients, we can deeply analyze and discuss the effective relationships among the indexes.

References

1. M.S.Waterman: Study on the Evaluation of Indigenous Danger of Architecture Production. Operations Research and Management Science, **16** (2001) 16-18
2. Claes Fornell, Michael D. Johnson, Eugene W. Anderson, Jaesung Cha, Barbara Everitt Bryant: The American Customer Satisfaction Index: Nature, Purpose, and Findings. Journal of Marketing, **60** (4) (1996) 7-18
3. Seigyoung Auh., Michael D. Johnson.: Compatibility Effects in Evaluations of Satisfaction and Loyalty. Journal of Economic Psychology, **26** (1) (2005) 35-57
4. Hengqing Tong: Data Analysis and Statistical Computation(DASC). Electronic publication, Science Press of China, (2005).
5. Chuanmei Wang, Hengqing Tong: Best Iterative Initial Values for PLS in a CSI Model. Mathematical and Computer Modelling, to be published in 2007.

An Adaptive Energy-Efficient and Low-Latency MAC Protocol in Wireless Sensor Networks

Men Chaoguang[1,2], Lu Yongqian[1], Zhang Huajian[1], and Li Guang[1]

[1] Research and Development Center of High Dependability Computing Technology, Harbin Engineering University, Harbin, Heilongjiang, 150001, P.R. China
[2] National Laboratory for Information Science and Technology, Tsinghua University, Beijing 100084, China
{menchaoguang,luyongqian}@hrbeu.edu.cn.

Abstract. In wireless sensor networks, an efficient Medium Access Control (MAC) protocol is critical, especially in terms of energy consumption and message latency. This paper introduces a novel protocol that nodes periodically sleep to conserve energy. When the source node has data packets to send, it uses a wakeup message to awake the sleeping nodes. The protocol needn't take the synchronization which must be achieved in S-MAC. It especially suits to the wireless sensor networks with narrow bandwidth.

Keywords: wireless sensor networks, media access control (MAC).

1 Introduction

Wireless sensor networks have emerged as one of the dominant technology trends of this decade (2000-2010) [1]. A wireless sensor network is comprised of a large number of tiny wireless senor nodes that are capable of sensing the environment and communicating in an ad-hoc fashion to deliver relevant information to the user. The small form factor of these nodes limits the battery life available for their operation. Furthermore, a critical event detected by the sensor network should be delivered to the user as soon as possible. Thus, for sensor networks, energy efficiency and latency both are the important parameters. In this paper, we present a novel medium access control protocol. It not only conserves energy through making the sensor nodes periodically sleep, but also has a low latency.

The rest of this paper is organized as follows: Section 2 analysis the defects of other MAC protocol in sensor networks, and describes our proposed protocol, An Adaptive Energy-efficient and Low-latency MAC Protocol (EL-MAC). Section 3 compares the performance of EL-MAC with existing mechanisms via simulations. Section 4 concludes the paper and presents our future work.

2 An Adaptive Energy-Efficient and Low-Latency MAC Protocol

In S-MAC [2], the periodic sleep may result in high latency, especially for multihop routing algorithms, because all the intermediate nodes have their own sleep schedules.

The disadvantage of LAS-MAC [3] is that the nodes having data to forward must wait for next duty circle when they overhear interference, but the channel may not always be busy in this duty circle. So the throughput is reduced. The disadvantage of TW-MAC [4] is that a busy tone must be transmitted before every data packet, this leads to energy waste and message latency. As mentioned, previous protocols have these defects. So a novel protocol with better performance is proposed in this paper. In our protocol, nodes periodically sleep to conserve energy, and the control messages are reduced on the premise that the reliable transmission is ensured. All of these cause energy conservation, latency decrease and throughput increase.

For brevity, we supposed that the carrier sensing range (radius) is one time larger than the transmission range[5-6]. Radios typically have four power levels corresponding to the following states: transmitting, receiving, listening, and sleeping. Typically, the power required to listen is about the same as the power to transmit and receive. The sleep power is usually one or four orders of magnitude less. Thus, a sensor should sleep as much as possible when it is not engaged in communication. EL-MAC make sensor nodes periodically sleep to conserve energy. Each node can be awaked by the wakeup signal at listen period.
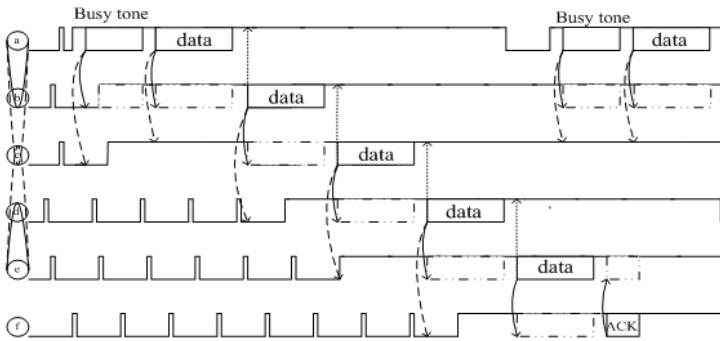
Fig. 1. Overview of EL-MAC

As shown in Fig.1, When a source node (node-a) has data to be sent to the sink node, It first sends a busy tone to wakeup its receiver (node-b). Nodes are not synchronized and, therefore, do not know the phase of each other's listen-sleep cycles in the listen mode. To avoid missing the short time that node-b has its radio on, the busy tone must be long enough to guarantee that all neighbors can sense the wakeup signal. When node-a sends the busy tone, its second hop neighbor (node-c) which is at the carrier sensing zone of node-a also can sense the wakeup signal. So node-b and node-c change their states to listening together. After the busy tone transmission, the source node listens for a short time. If the channel is idle, the data packet will be transmitted in succession. The data packet must be larger than the busy tone. If receiver, node-b, received the data packet successfully and it is not the sink node, it will forward the data packet to the next hop neighbor (node-c). Here, node-c has been waked up, so it can correctly receive that packet. Node-a will consider the data packet sent by node-b as the virtual ACK which denotes the data packet sent by node-a was successfully

received by node-b, if not it repeats to transmit the packet. Then, if the packet needs to be forwarded further, the process is repeated until the sink node receives the data packet successfully and returns an ACK packet.

3   Simulations and Performance Evaluation

We run simulations using opnet. 100 nodes are deployed randomly in an area of 300 * 300m^2. We choose three source nodes and one sink node from the different corner.The radio range (radius) is 30m. We set the bandwidth to 20kbps. Each data packet size is 250bytes, and control packet size is 10 bytes. The busy tone packet size should be 50 bytes.We use the same energy consumption model as in [7] for the radio hardware. The simulation time is one hour.

We compare EL-MAC against S-MAC without the synchronization function. The energy consumption versus duty cycle is plotted in Fig.2. This result exactly demonstrates that EL-MAC can implement energy conservation task successfully.

Fig.3 shows the latency that data packets pass from a source node to a sink node. It shows that EL-MAC performs as better as 802.11 MAC on data packets passing latency. The reason is that the data packet passing of EL-MAC nearly doesn't have the sleep latency expounded in [2].
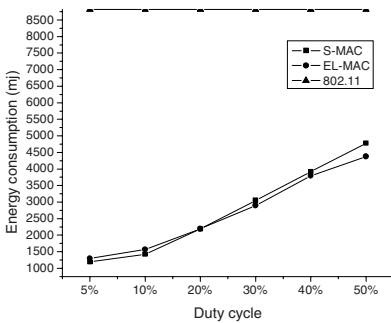
Fig. 2. Energy consumption analysis
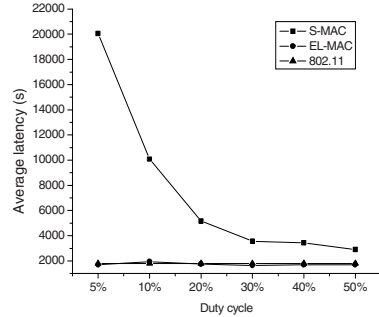
Fig. 3. Data latency analysis
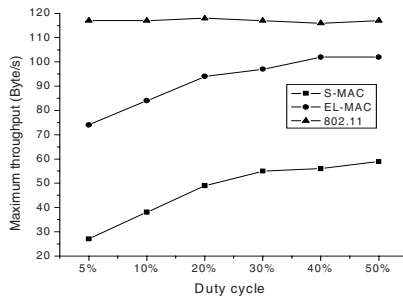
Fig. 4. Throughput analysis

Fig.4 shows the measured throughput for different duty cycle on the sink node. The busy tone becomes small when the duty cycle increases, this diminishes the cost of retransmission, in turn, diminishes the useless load of network. So EL-MAC throughput increases along with the duty cycle. As is shown, the EL-MAC have a much higher throughput than S-MAC.

4 Conclusions and Future Work

This paper presents a novel MAC protocol for wireless sensor networks. Compared to S-MAC, it makes following improvements: minimizing the latency of data passing, increasing the potential space of energy conserving.

Future work includes system scaling studies, parameter analysis and listen time decrease. More simulations will be done for the parameter analysis. The physical layer capability should be improved, so as to decrease the listen time.

References

1. Munee. Ali, Umar Saif, Adam Dunkels: Medium Access Control Issues in Sensor Networks, In: ACM SIGCOMM Computer Communication Review, (2006), 36(2):33-36.
2. Wei Ye, John Heidemann, Deborah Estrin: Medium Access Control with Coordinated Adaptive Sleeping for Wireless Sensor Networks, IEEE/ACM TRANSACTIONS ON NETWORKING, (2004), 12(3):493-506.
3. Jaesub Kim, Keuntae Park, Jeong-Hun Shin, Daeyeon Park: Look-Ahead Scheduling For Energy-Efficiency and Low-Latency in Wireless Sensor Networks, PE-WASUN'06, Spain, (2006), 10:141-144.
4. Matthew J. Miller, Nitin H. Vaidya: A MAC Protocol to Reduce Sensor Network Energy Consumption Using a Wakeup Radio, IEEE TRANSACTION ON MOBILE COMPUTING, (2005), 4(3):228-241.
5. Eun-Sun Jung, Nitin H. Vaidya: A Power Control MAC Protocol for Ad Hoc Networks, In: Proceedings of the IEEE/ACM MobiCom Conference, (2002), 9:36-47.
6. Kamerman A, Monteban L: WaveLAN-II: A High-Performance Wireless LAN for The Unlicensed Band, Bell Labs Technical Journal, (1997), 2(3):118-133.
7. Peng lin, Chunming Qiao, Xin Wang: Medium Access Control With a Dynamic Duty Cycle for Sensor Networks, in WCNC 2004/IEEE Wireless Communications and Networking Conference, (2004), 5(1):1522-1527.

Healthcare Information Management System in Home Environment

Chang Won Jeong[1], Chung Sub Lee[1], and Su Chong Joo[1]

[1] School of Electrical, Electronic and Information Engineering, Wonkwang University, Korea
{mediblue,cslee,scjoo}@wonkwang.ac.kr

Abstract. In this paper, we suggested a healthcare information management system for supporting healthcare home services. Our researching focus in this paper is how to design system and how to use constructed database on the framework for supporting healthcare home services. The healthcare database constructed by using this information for the purpose of healthcare home services is divided into the base information with real schemes and the context based information with view schemes. Finally, for verifying the practical use of healthcare information constructed in this paper, we show an example of healthcare home monitoring service using information, emergency call, home appliance control, and we describes the results of the experimental evaluation between the base and context based information in terms of execution service time for healthcare home applications.

Keywords: Healthcare information system, healthcare home service, distributed object Group Framework.

1 Introduction

Current research in ubiquitous computing focuses on building infrastructures for managing active spaces, connecting new devices, or building useful applications to improve functionality[1]. But, in these researches, integrated management of information is a very important application of healthcare information technology, especially for a u-healthcare home environment. Since existing healthcare information system was constructed independently, there is no interconnection to support total business area such as doctor, nurse, patient and environments. Also, there are a large number of healthcare related applications that effectively support specific needs but are isolated or incompatible. And interfaces are expensive and time-consuming because systems use different platforms, programming languages and data formats[2]

Our system based on the distributed object group framework (DOGF) which enables to easily integrate distributed objects to healthcare home applications[3]. And, we used TMO scheme and TMOSM for interactions between distributed applications. Finally, for verifying the practical use of healthcare database constructed in this paper, via interconnecting this database to framework, we show an example of healthcare home monitoring service, emergency call, appliance control, and so on needed from living activity area for elderly living alone. Also, we show the results of the experimental evaluation between the base and context based information in terms of execution time for healthcare applications.

2   Healthcare Information Management System

Our system used to component of supporting object group management for domain grouping in DOGF, we consider home environments and related services such as location tracking service, healthcare information and titrating environment supporting service. Also, information collection and share in this environment, we adopted the TMO scheme and TMOSM into the development environment of system that we implemented. The architecture of the system is shown in figure 1 and is organized in five layers. The physical layer contains hardware infrastructures such as various sensors, devices, machines etc. Also, healthcare database consists of classification of sensor node, collected sensor data by sensors and user profile included the health, service information and access right information for security and view information for supporting service applications. The framework layer contains a components of DOGF which is supports a logical single view system environment by grouping them. That is, the group manager API supports the execution of application of appropriate healthcare home services on upper layer by using the input information obtained from the individual or grouped physical devices thought sensor manger on the lower layer. The tool layer consists of distributed programming developing-tool(DPD-Tool)and healthcare database management tool(HDM-Tool).
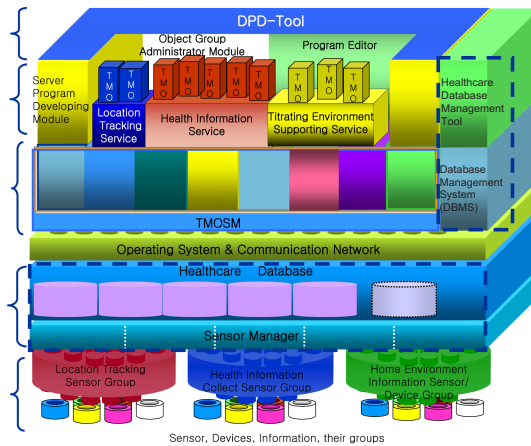
Fig. 1. The architecture for Healthcare Information Management System

We defined the interaction of components which is interacts with the distributed application, database, sensors and components of framework. The process of grouping about distributed object by group manager object. Also, it provides the interaction of distributed application by APIs and service object reference which support collecting real time information from the sensor manager. Also it is support the security service which is security object that is access right information for client through healthcare database. When service object replicated, dynamic

binder object provide the reference of service object by binding algorithm. Distributed application obtains real time information of sensor node through service object reference which enable connect to healthcare database. And, the interaction of objects in distributed application returned the result of service by framework components.

3   Healthcare Database Based Healthcare Home Services

The healthcare database constructed by using this information for the purpose of healthcare home services is divided into the two classes. The base information includes low data obtained from physical sensors relevant to locations, personal health, environments, and the user profiles. And, the context based information that is produced and fused by using the based information. This context based information might be got via various view schemes according to healthcare application services. The context based information constructed by materialized view and save to service schema repository which is manages the view scheme. While programming by using this information, server or client program developers can develop the healthcare application. Figure 2 show, to management of healthcare information, we developed the healthcare database management tool(HDMT) which provides user interface for interaction of healthcare database. The functions of HDMT has a general function for constructed database management such as show the DB List and table data, the query execution by SQL and search of plan by user write SQL, dictionary information management. In addition, it provides the creating function of context based information which is materialization view tables.
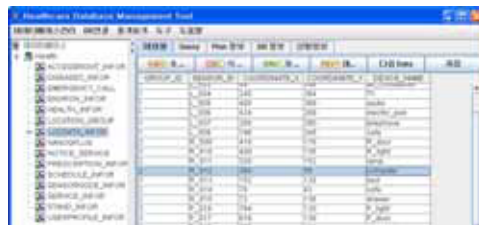
Fig. 2. GUI for Healthcare Database Management Tool

   Figure 3 shows the physical environments for healthcare home Services reflecting real world. From these environments, we verify the executbility of the healthcare home services we constructed. The healthcare home services are home monitoring which provides location tracking, health and environment information for home resident, emergency call as SMS using cell phone and home appliance control based on health, location, standard information specified by user for environments of home such as fan, light, air-conditioner etc.

Fig. 3. The physical environment for healthcare Home services

We analyzed the service time for the base information and the context based information considering applying for the healthcare home services. As a result, we obtained from this experiment. In case of location service is 37.4ms, the health information service is 49.5ms and home auto control service is 20.3ms difference respectively. From above evaluation results, we verified that the context based information could provide the effectively to the healthcare home services.

4   Conclusions

In this paper, our researching focus in this paper is how to design healthcare information management system and how to use constructed database on the Framework for Supporting Healthcare Home Service. And we verified that healthcare related information supporting healthcare home services and the context based information could better impact than base information at healthcare home services.

References

1. Marcela Rodriguez, Jesus Favela, Victor Gonzalez and Miguel Munoz : Agent Based Mobile Collaboration and Information Access in a Healthcare Environment. Proceedings of Workshop of E-Health ISBN: 970-36-0118-9. Cuernavaca, Mexico, December (2003)
2. S.S. Spyrou, P. Bamidis, I. Chouvarda, G. Gogou, S.M. Tryfon, and N, Maglaveras: Healthcare information standards: comparison of the approaches. Health Informatics Journal, Vol. 8. 3 (2002)14 - 19
3. Chang-Won Jeong, Dong-Seok Kim, Geon-Yeob Lee, and Su-Chong Joo,: Distributed Programming Developing Tool Based on Distributed Object Group Framework. Lecture Notes in Computer Science, Vol. 3983, 8-11 May (2006) 853 – 863

Boundary Processing of HHT Using Support Vector Regression Machines

Wu Wang, Xueyao Li, and Rubo Zhang

National Laboratory on Machine Perception, Peking University, Beijing, P.R. China
College of Computer Science and Technology, Harbin Engineering University,
Harbin150001,China
`wangwu131@163.com`

Abstract. In order to better restrain the end effects in Hilbert-Huang Transform, support vector regression machines (SVRM), which have the superiority in the time series prediction, are adopted to extend the data at the both ends. In the application of SVRM, the parameters have a great influence on the performance of generalization. In this paper the influence of parameters is discussed, and then an adaptive support vector regression machine is proposed based on the particle swarm optimization (PSO) algorithm. With the parameters optimized by PSO, SVRM can be characterized as self-adaptive and high generalization performance in applications. Experiments show that this method can solve the problem of selecting parameters properly. Contrast to the neural networks methods and HHTDPS designed by Huang et al., end effects can be restrained better and the Intrinsic Mode Functions have less distortion.

Keywords: End effects, Hilbert-Huang Transform, Support vector regression machines, Particle swarm optimization.

1 Introduction

Hilbert-Huang Transform (HHT) is a powerful data analysis method for nonlinear and non-stationary data[1][2], which is based on empirical mode decomposition (EMD). Although Hilbert-Huang transform is a powerful analysis method for non-stationary signals, but end effects are its unavoidable problem[1][4][5]. If the end effects aren't restrained effectively, it can produce large swings and eventually propagate inward and corrupt the whole data[1]. So it is necessary to restrain the end effects effectively. Many new methods have proposed in recent years, such as time series prediction based on neural networks[3], mirror extending method[4], waveform matching method[5], constructing two periodic series from the original data by even and odd extension[6]. Among these methods, the neural networks have relatively better effects than other methods[7]. The neural networks extending method can work well for non-stationary signals[3], but the local minimum point, over learning and the excessive dependence on experience about the choice of structures and types are its inevitable limitation. A potential solution to the above problems is to use Support vector regression machines (SVRM). In applications, the performance of SVRM is sensitive to its parameters[8], so in this paper the particle swarm optimization (PSO) algorithm is proposed to optimize the parameters. More importantly, with the parameters optimized by PSO, this method can be self-adaptive to nonlinear and non-stationary data.

2   Parameter Selection in SVRM Based on PSO

In the application of Support vector regression machines, there are three important parameters: the regularization parameter C, the tube size ε and the kernel parameter σ^2. All of them have a great influence on the generalization performance of the SVRM. In this paper, PSO is proposed to optimize these parameters. Compared to other parameter selection methods, this approach is simple but faster[9]. In PSO, the potential solutions, called particles, fly through the problem space with a velocity, which is dynamically adjusted according to its own flying experience and its companions' flying experience. Every particle is evaluated by the fitness value. The best previous position of the particle is recorded and represented as *pbest*. The position of the best particle among all the particles in the population is represented by the symbol *gbest*. According to the *pbest* and *gbest*, the particle updates its velocity and position as the following equation:

$$v_{id} = w*v_{id} + c_1*rand()*(pbest_{id} - x_{id}) + c_2*Rand()*(gbest - x_{id})$$
$$x_{id} = x_{id} + v_{id}, i = 1,2,\cdots M \tag{1}$$

where d is the dimension of every particle, which is equivalent to the number of parameters to optimize. Rand ( ) and the Rand ( ) are two random numbers generated independently. w is inertia weight, c_1 and c_2 are learning factors and the M is the population size.

To get better generalization ability, it is necessary to make the SVRM model have lower error rate and a simple structure. Therefore, the fitness function can be defined as follows:

$$F_i = f_{error} + K \times \frac{N_{sv}}{N} \times (1 - f_{error}) \tag{2}$$

where f_{error} is the error rate in the training data sets, N_{sv} is the number of the support vectors(SV) and N is the training data number. $K \in [0,1]$ is used to make a balance between the precision and the complexity.

3   Implementation and Experimental Results

In order to make a comparison between the SVRM and RBF network in forecasting effect, one speech segment of 731 data points and the SNR=5dB was picked as the training samples, which is shown in Fig.1. The data were forecast 150 data points from the back endpoint purposely, but in applications, we only need to forecast very less points. The results by SVRM and RBF neural network are shown in Fig. 2 and Fig. 3, where the dashed line represents the signal forecast by SVRM or RBF network and the solid line represents the actual signal. Figures show the forecasted series by RBF network have a more serious distortion. The mean absolute percentage error (MAPE) of the SVRM and RBF network were 1.1012 and 1.3470. The result also demonstrates that the forecasting method based on SVRM is superior to that based on neural network.
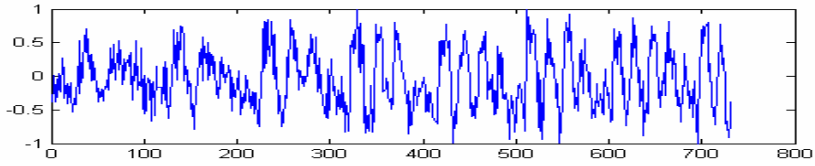
Fig. 1. The noised speech signal with SNR=5dB
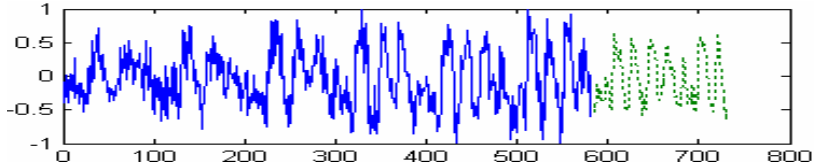
Fig. 2. The noised speech signal after the SVRM predicting
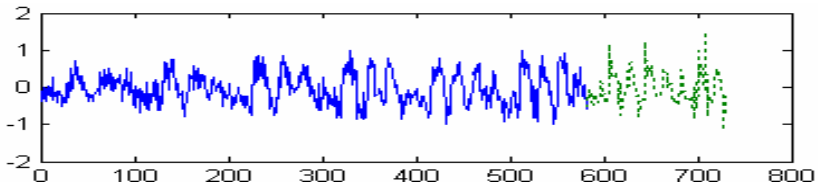
Fig. 3. The noised speech signal after the RBF neural network predicting

(a)   (b)
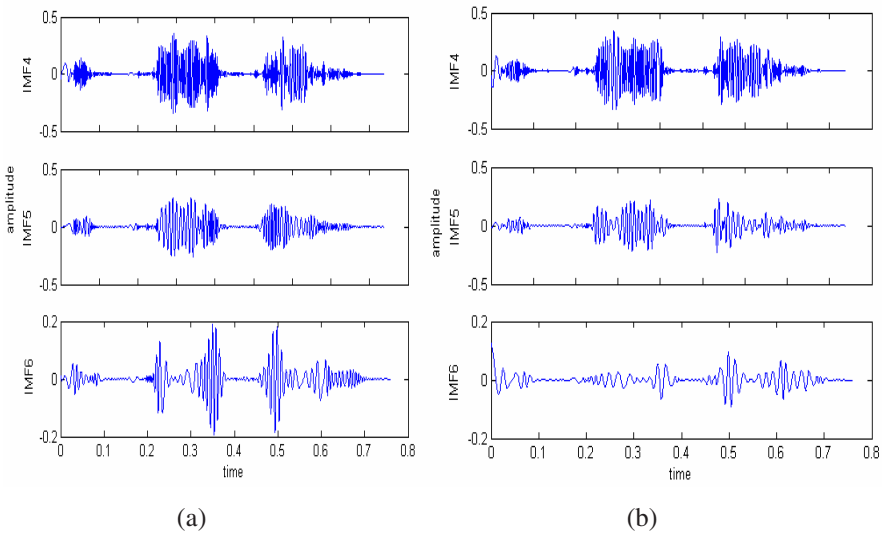
Fig. 4. The EMD decomposition results of the speech signal after being forecast by the SVRM (a) and the HHTDPS (b)

We also conducted our experiments on a speech material of 0.7608s long. Fig.4 shows the IMFs results extracted form our method and decomposed by the HHT Data Processing System (HHTDPS). The HHTDPS is an engineering spectral analysis tool developed at Goddard Space Flight Center (GSFC) of NASA. The HHTDPS used is Version 1.4, which is the latest version of HHT software.

Fig. 4 shows the IMF components after forecasting by SVR and got by HHTDPS respectively. From the Fig.4 (b) we can see the fourth and sixth IMF components in HHTDPS have an explicit distortion at the starting point, while this distortion can be restrained effectively by our algorithm, shown in Fig.4(a).

4   Conclusion

In this paper, we proposed a method to restrain the end effects in HHT by time series prediction based on adaptive support vector regression machine. For the end effects in Hilbert–Huang transform, the original time series can be forecast by SVRM, and the end effects can be released by abandoning the extended data. With the parameters optimized by PSO, SVRM can be self-adaptive to nonlinear and non-stationary data. It is helpful for SVRM to get high generalization performance in time series prediction. Therefore, SVRM is a very suitable forecasting method for the time series. Our experiments show end effects in HHT can be restrained effectively by this method.

References

1. Norden E. Huang .The Empirical Mode Decomposition and the Hilbert spectrum for nonlinear and non-stationary time series analysis J. proc.R.Soc. Lond.A (1998) 454,903-995.
2. Norden E.Huang. A confidence limit for the Empirical Mode Decomposition and Hilbert spectral analysis; J.proc.R.Soc.Lond 2003(459), 2317-2345.
3. Y.J. Deng, W. Wang, Boundary processing technique in EMD method and Hilbert transform, Chinese Science Bulletin 46 (11) (2001) 257–263.
4. J.P. Zhao, D.J. Huang, Mirror extending and circular spline function for empirical mode decomposition method, Journal of Zhejiang University(Science),2001, 2(3) 247-252
5. Q. Gai, X.J. Mao, H.Y. Zhang, et al., New method for processing end effect in local wave method, Journal of Dalin University of Technology, Chinese 42 (1) (2002) 115–117.
6. K. Zeng and M.X. He, A Simple Boundary Process Technique for Empirical Mode Decomposition, IGARSS '04. Proceedings, 6(2004) 4258 – 4261.
7. B.J. Xu, J.M. Zhang, X.L. Xu, J.W. Li, A study on the method of restraining the ending effect of empirical mode decomposition, Transactions of Beijing Institute of Technology, 26(3)(2006) 196-200.
8. C. C. Chuang, S. F. Su, J. T. Jeng, and C. C. Hsiao, Robust support vector regression networks for function approximation with outliers, IEEE Trans. Neural Netw., vol. 13, no. 6, pp. 1322–1330, Nov. 2002.
9. Kennedy, I. and Eberhan, R. C. Paticle swarm optimization. Proceedings of IEEE lnlemational Conference on Neural Networks. Piscalaway, NJ. pp. 1942-1948, 1995.

Water Mine Model Recognition by Immune Neural Network

Haibo Liu, Jing Shen, and Guochang Gu

College of Computer Science and Technology, Harbin Engineering University,
Harbin 150001, China
{liuhaibo,shenjing,guguochang}@hrbeu.edu.cn

Abstract. An immune neural network (INN) is proposed for water mine model recognition. The INN is a two-layer Boolean network whose number of outputs is adaptive according to the task and the affinity threshold. The precision of the recognition results can be controlled through adjusting the affinity threshold. The INN has favorable capability of noise tolerance.

Keywords: water mine model, recognition, immune neural network.

1 Introduction

It is necessary for mine countermeasure systems to recognize the model of a water mine. Most of the previous researches on mine countermeasures [1][2][3] focused main attentions on the detection and classification of water mines. But the previous approaches can only classify the detected object as two classes, i.e., mine-like or not. In this paper, an immune neural network (INN) is constructed based on a modified clonal selection operation for water mine model recognition.

2 Immune Neural Network

Represent the feature data of water mines as an antigen population $A^g=\{A^g_1, A^g_2\ldots A^g_n\}$. An antigen can be represented as l-length bit string. Each bit represents a feature. The antibody repertoire, $A^b=\{A^b_1, A^b_2,\ldots, A^b_m\}$, will be modeled as a Boolean competitive network with l inputs, called INN. Employ an l-dimensional vector w_j represents the weights connecting the inputs to the output unit j. Define the affinity A_{ij} as the Hamming distance between A^g_i and A^b_j. For each A^g_i, v_i indexing the highest affinity antibody. The antigens concentration c_j for A^b_j can be calculated according to Eq.(1),

$$c_j = \sum_{i=1}^{n} \text{iif}(v_i = j, 1, 0),\qquad(1)$$

where, iif($v_i = j$, 1, 0) means that if $v_i = j$ holds then return 1 else 0. Define e as an affinity threshold. For A^g_i and A^b_j, if $l–A_{ij} > e$ then we can say that A^g_i and A^b_j are

matched. Define m_j as an affinity maturation indicator. If m_j is *True* then stop cloning antibody A^b_j. For antibody A^b_j and arbitrary $i \in \{i \mid v_i = j\}$, if $l\text{-}A_{ij} > e$ holds, then set $m_j = \textit{True}$ as Eq.(2),

$$m_j = \bigwedge_{i \in \{i \mid v_i = j\}} (l - A_{ij} > e) .$$

(2)

We developed a modified clonal selection algorithm for constructing an INN:

1) Initiate an INN with n antigens A^g_1, A^g_2... A^g_n and 1 antibody A^b_1. For each integer $i \in [1, n]$, set $v_i = 1$. Set each bit of w_i to 1. Set $c_1 = n$, $m_1 = \textit{False}$. Set e to an appropriate value.

2) Determine the candidate A^b_j to be cloned according to Eq.(3). If j is *null* then stop else continue step 3) to clone A^b_j.

$$j = \arg \max_{j \in O} c_j , \textit{where} \quad O = \{j \mid c_j > 1 \wedge m_j = \textit{False}\}$$

(3)

3) Select the worst matching A^g_i of A^b_j according to Eq.(4),

$$i = \arg \min_{i \in \{i \mid v_i = j\}} A_{ij} .$$

(4)

4) Clone a new antibody A^b_k with the weights w_k of its antibody are the exact complement of A^g_i, then add A^b_k to INN.

5) For each antigen $A^g i$, update v_i. For each antibody A^b_j, update c_j and m_j.

6) If all antibodies are mature then delete the antibodies with $c=0$ and stop, else goto step 2).

When the algorithm (MCSA for short) stops, an INN is constructed, each output of which represents one or several antigen patterns, i.e., water mine models. The number of patterns that an output represents is determined by the affinity threshold e. When $e = 0$, one output corresponds to one pattern. The bigger the value of e is, the more patterns an output represents along with the lower precision.

The process of recognition is very simple. Given an antigen A^g_i as input, the INN computes the antibody being activated according to Eq.(5), then the water mine model can be recognized.

$$j = \arg \max_{j \in O} A_{ij} , \quad \textit{where} \quad O = \{j \mid l - A_{ij} > e\}$$

(5)

There is no output can be activated if $O=\Phi$, which means that A^g_i cannot be recognized, i.e., the water mine is not any known model or may be it is not a water mine at all.

3 Simulation Experiments

For constructing an INN, a water mine data set with models and binary attributes was prepared as shown in Table 1. We applied MCSA to the data set with setting $l=20$, $n=21$, and $e=0$, which means that the MCSA will create a network with antibodies highly specific for each input pattern (antigen). Thus, it would be expected that the

final network was composed of 21 antibodies, but the resultant network contained only 18 antibodies. This is because that the models (e.g., NM103 and WSM210) mapped into the same node are described as the same attribute strings.

Table 1. Water mine data set with their models and binary attributes

	PLARM-1A	PDM-1B	PDM-2B	PDM-1M	PDM-3YA	U/I	MAS/17	MAS/22	VS-RM-30	NM102	NM103	DUM101	DUM102	STORM	WSM110	WSM210	M89A2	MK60	MK65	MK67	MSHM
Shape																					
hemisphere	0	0	0	1	0	1	0	1	0	0	0	0	0	0	0	0	0	0	0	0	0
cylinder	0	0	1	0	0	0	0	0	0	1	0	1	0	1	1	0	0	1	1	1	1
truncated-cone	0	1	0	0	0	0	0	0	0	0	1	0	1	0	0	1	0	0	0	0	0
oblate	0	0	0	0	0	0	0	0	1	0	0	0	0	0	0	0	1	0	0	0	0
clutter	1	0	0	0	1	0	1	0	0	0	0	0	0	0	0	0	0	0	0	0	0
Color																					
green	1	0	0	1	0	0	0	0	0	0	0	0	0	0	0	0	0	0	0	0	0
black	0	0	1	0	0	0	0	0	0	0	0	0	0	0	0	0	0	0	0	0	1
gray	0	0	0	0	0	0	0	1	1	1	1	0	0	1	1	1	1	1	1	1	0
red	0	0	0	0	1	0	0	0	0	0	0	0	0	0	0	0	0	0	0	0	0
orange	0	0	0	0	0	0	0	0	0	0	0	1	1	0	0	0	0	0	0	0	0
yellow	0	1	0	0	0	0	1	0	0	0	0	0	0	0	0	0	0	0	0	0	0
brown	0	0	0	0	0	1	0	0	0	0	0	0	0	0	0	0	0	0	0	0	0
State																					
floating	1	0	0	0	0	0	0	0	0	0	0	0	0	0	0	0	0	0	0	0	0
moored	0	0	1	1	1	1	1	0	0	0	0	0	0	0	0	0	0	1	0	0	1
bottom	0	1	0	0	0	0	0	1	1	0	1	0	1	0	1	1	0	0	1	1	0
navigation	0	0	0	0	0	0	0	0	0	1	0	1	0	1	0	0	0	0	0	0	0
adsorption	0	0	0	0	0	0	0	0	0	0	0	0	0	0	0	0	1	0	0	0	0
Depth																					
deep	0	0	0	0	0	0	0	0	0	1	1	1	1	1	1	1	0	1	1	1	1
shallow	1	1	1	1	1	1	1	1	1	0	0	0	0	0	0	0	1	0	0	0	0
Has																					
antennae	1	1	1	1	1	1	1	1	0	0	0	0	0	0	1	0	0	0	0	0	0

In most cases, the sensor data may be incomplete or inaccurate. The INN can easily deal with these cases by adjusting the value of the affinity threshold e when recognizes, which can be demonstrated by the following experiments. Random noise was inserted into the learning samples in Table 1 by simply reverting a bit 0 into a 1, or vice-versa. We tested eleven different noise levels from 0% to 50%, corresponding to the shift of 0 to 10 bits, respectively. The INN was tested for different values of the affinity threshold e from 0 to 10, and a correct recognition (CR) is assumed when the network maps the corrupted pattern into the same node as the original pattern. Fig.1 depicts the experiment results that are the average taken over ten runs. Fig.1 shows that the CR is affected both by the number of noise bits and the affinity threshold e. Keeping a value of e constant, the CR decreases almost linearly with the noise level increasing. If we keep a constant noise level, the CR increases nonlinearly, i.e., the CR almost keeps constant when the value of e is bigger than the number of noise bits.

In these experiments, we did not take into account the effect of adjusting the affinity threshold e when the INN is constructed. Apparently, the value of e in recognition should be equal to or bigger than that in construction. It is an acceptable strategy to set e in recognition to a bigger value when the noise level is uncertain.
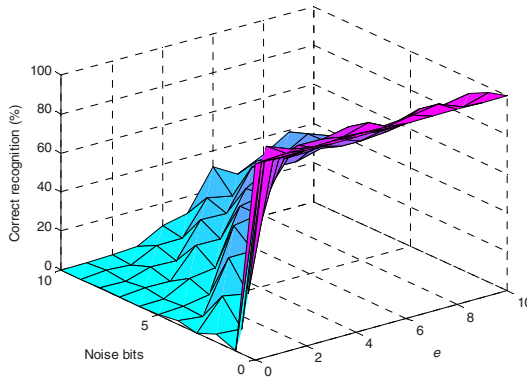
Fig. 1. The correct recognition rate of INN

4 Conclusions

The INN is a two-layer Boolean network whose number of outputs is adaptive according to the task and the affinity threshold, which is significant for solving machine-learning problems, such as knowledge acquisition and classification. The precision of recognition result can be controlled through adjusting the affinity threshold, which endows INN with satisfied noise tolerance capability. In the future, we will apply the INN to underwater minesweepers.

References

1. Tuzlukov, V.P.: Probability of detection of mines and minelike targets in deep water using generalized detector with digital threshold device. Proc. of Detection and Remediation Technologies for Mines and Minelike Targets VI, Orlando, US (2001) 1283-1294
2. Aridgides, T., Fernandez, M., Dobeck G.J.: Improved processing string fusion approach investigation for automated sea mine classification in shallow water. Proc. of Detection and Remediation Technologies for Mines and Minelike Targets IX, Orlando, US (2004) 315-326
3. Ciany, C., Zurawski, W.: Improvements in computer aided detection/computer aided classification (CAD/CAC) of bottom mines through post analysis of a diverse set of very shallow water (VSW) environmental test data. Proc. of Detection and Remediation Technologies for Mines and Minelike Targets IX, Orlando, US (2004) 327-335

Composing Different Models of Computation in Kepler and Ptolemy II

Antoon Goderis[1], Christopher Brooks[2], Ilkay Altintas[3], Edward A. Lee[4], and Carole Goble[5]

[1] School of Computer Science, University of Manchester, UK
goderisa@cs.man.ac.uk
[2] Department of EECS, UC Berkeley, USA
cxh@eecs.berkeley.edu
[3] San Diego Supercomputer Center, UC San Diego, USA
altintas@sdsc.edu
[4] Department of EECS, UC Berkeley, USA
eal@eecs.berkeley.edu
[5] Shool of Computer Science, University of Manchester, UK
carole@cs.man.ac.uk

Abstract. A model of computation (MoC) is a formal abstraction of execution in a computer. There is a need for composing MoCs in e-science. Kepler, which is based on Ptolemy II, is a scientific workflow environment that allows for MoC composition. This paper explains how MoCs are combined in Kepler and Ptolemy II and analyzes which combinations of MoCs are currently possible and useful. It demonstrates the approach by combining MoCs involving dataflow and finite state machines. The resulting classification should be relevant to other workflow environments wishing to combine multiple MoCs.

Keywords: Model of computation, scientific workflow, Kepler, Ptolemy II.

1 The Need for Composing Models of Computation in E-Science

E-scientists design on-line (in silico) experiments by orchestrating components on the Web or Grid. On-line experiments are often orchestrated based on a scientific workflow environment. Scientific workflow environments typically offer support for the design, enactment and provenance recording of computational experiments.

Most workflow environments fix the model of computation (MoC, or the formal abstraction of computational execution) available to an e-scientist. They leave little flexibility to change MoC as the experiment evolves. Different experiments are modeled more cleanly with different MoCs because of their relative expressiveness and efficiency. Different uses of MoCs for scientific workflows include dataflow for pipeline compositions, e.g. gene annotation pipelines; continuous-time ordinary differential equation solvers, e.g. for Lattice-Boltzmann simulations in fluid dynamics; and finite state machines for modelling sequential control logic, e.g. in clinical protocols or instrument interaction.

There are also scenarios where a combination of MoCs is useful, e.g. a mixture of a time dependent differential equation model with dataflow. Most environments do not support experiments that mix multiple MoCs. This interferes with intra and inter-disciplinary collaboration. For example, in genomic biology, gene annotation pipelines provide useful input to systems biology simulation models. Candidates for drug development found in cheminformatics simulations are plugged into bioinformatics annotation pipelines to retrieve the candidates' hazardous interactions within cells. The inability to mix MoCs also makes it more difficult to mix software workflows with physical systems such as sensor networks and electron microscopes, which have continuous dynamics. Moreover, mixing specialized MoCs for visualization (e.g. for animation) with, for example, time-based simulation, makes for more efficient execution and for better models. In addition, if we can mix MoCs, then we can design workflows that manage the execution of models and workflows. Representative use cases include: (i) selective extraction and analysis of proteins from public databases, combining finite state machines and dataflow and (ii) dynamically adapting model control parameters of Lattice-Boltzmann simulations in fluid dynamics by combining finite state machines and continuous-time ODE solvers. In such scenarios, using an integrated environment that supports mixing MoCs enables integrated provenance collection. In the fluid dynamics example, the provenance includes dynamic changes in the overall model as well as parameter sweeps within each model, covering the full range and variability.

2   Paper Contribution and Overview

To date, little is known about how models of computation are joined. Kepler, which is based on Ptolemy II, is a scientific workflow environment that allows for MoC composition. The paper explains how MoCs are combined in Kepler and Ptolemy II, and analyzes which combinations of MoCs are possible and useful. The resulting classification should be relevant to other environments wishing to combine MoCs.

Kepler/Ptolemy II comes with a wide range of MoCs, which are implemented as directors. Section 3 introduces the notion of hierarchy as the key concept for mixing MoCs in a workflows. Section 4 provides an overview of MoCs in Kepler/Ptolemy II. For a scientific workflow developer, determining which MoC combinations are legal is non trivial. Section 5 establishes MoC compatibility, based on the notion of actor abstract semantics and presents a classification of MoCs combinations. Section 6 discusses the validity of the approach and demonstrates successful and unsuccessful combinations of dataflow and finite state machines. We conclude in Section 7.

3   Workflows and Hierarchy

Ptolemy II [2] is a Java-based environment for heterogeneous modeling, simulation, and design of concurrent systems. Ptolemy II forms the core of Kepler [5], an environment for building scientific workflows. The focus of Ptolemy II is to build models based on the composition of components called *actors* [1]. Actors are encapsulations of parameterized actions performed on input tokens to produce output

tokens. Inputs and outputs are communicated through ports within the actors. They provide the common abstraction used to wrap different types of software components, including sub-workflows, Web and Grid services.

The interaction between the actors is defined by a Model of Computation. The MoC specifies the communication semantics among ports and the flow of control and data among actors. *Directors* are responsible for implementing particular MoCs, and thus define the "orchestration semantics" for workflows. By selecting the director, one selects the scheduling and execution semantics of a workflow. Many actors can work with several directors, adapting their behaviors to match the semantics of the director [5]. The models of computation implemented in Ptolemy as directors are described in detail in [2, Vol. 3]. A subset of them, including dataflow, time and event dependent directors, is available in Kepler. Key to mixing MoCs in a workflow is the notion of hierarchical abstraction. Figure 1 shows a Kepler chemistry workflow using the PN director, which implements a process networks MoC [7]. This workflow contains a *composite actor* (a.k.a. sub-workflow) named Babel. The implementation of Babel actor is another workflow that contains another director, the SDF director, which implements a synchronous dataflow MoC. This example mixes two MoCs in a single, hierarchical workflow.
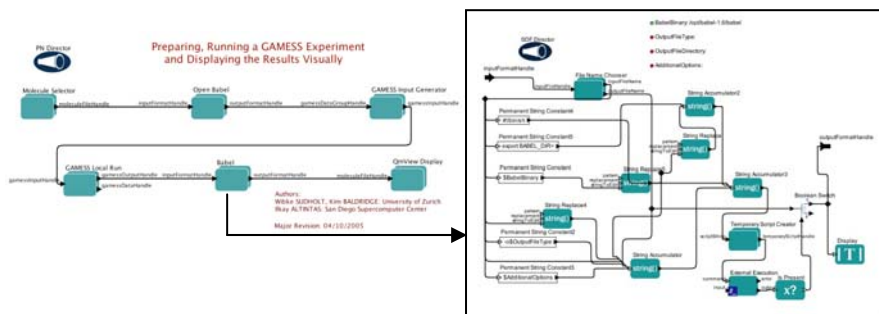
Fig. 1. A Kepler workflow from chemistry combining the PN and SDF director [7]

In Ptolemy/Kepler, hierarchy can serve either of two roles. First, it can be simply an organizational tool in building workflows, permitting a workflow designer to aggregate portions of a workflow and create conceptual abstractions. In this usage, the composite actor does not contain a director, and is called a transparent composite actor. The hierarchy has no semantic consequences; it is just a syntactic device. A second use of hierarchy is to use a workflow to define an actor. The Babel example is of this type. The fact that it has a director makes it function within the top level workflow exactly as if it were an *atomic actor*. A composite actor that contains a director is called an *opaque composite actor*, because its internal structure is neither visible nor relevant to the outside director.

For an opaque composite actor to function externally as if it were an ordinary actor, the director must be able to execute the inside workflow in a manner that emulates an actor. We examine below what that means, but before we can do that, we explain a few of the MoCs in enough detail that they can serve as illustrative examples.

4   Models of Computation in Ptolemy II and Kepler

One of the main objectives of the Ptolemy Project has been the exploration of models of computation. For this reason, many distinct directors have been created by various researchers, some realizing fairly mature and well-understood models of computation, and some that are much more experimental. Kepler has adopted Ptolemy's rich MoC architecture and focused principally on a few of the more mature ones, described here.

Process Networks (PN). In PN, each actor executes in a Java thread, and all actors execute concurrently. An actor can read input data (which is encapsulated in tokens) from input ports, and write data (wrapped in tokens) to output ports. Normally, when it reads from an input port, the read blocks until an input token is available. Writes do not block. The PN director includes sophisticated scheduling policies to ensure that buffers for tokens remain bounded, and also detects deadlock, which is where all actors are blocked attempting to read data. See [3] and [6]. Most of the scientific workflows (composite actors) built with Kepler to date have been based on PN.

Dataflow (DDF and SDF). In dataflow MoCs, instead of having a thread associated with each actor, the director "fires" actors when input tokens are available to them. We discuss two variants of dataflow here, dynamic dataflow (DDF) and synchronous dataflow (SDF). In the case of DDF, the director dynamically decides which actor to fire next, and hence constructs the firing schedule dynamically at run time. In the case of SDF, the director uses static information about the actor to construct a schedule of firings before the workflow is executed, and then repeatedly executes the schedule. SDF is very efficient in that very little decision making is made at run time. PN is semantically a superset of DDF, in that the repeated firings of an actor in DDF can be viewed as (or even implemented as) a thread. Every DDF workflow can be executed using a PN director. DDF in turn is a superset of SDF, in that every SDF workflow can be executed identically with a DDF director. In SDF, a fixed number of tokens are consumed and produced in each firing. The token consumption and production rates allow for the computation of a fixed schedule. In SDF, deadlock and boundedness of communication buffers are decidable. With DDF, actors need not have a fixed token production or consumption rate, the schedule is determined at runtime. In DDF, deadlock and boundedness are not decidable. In a DDF model, an actor has a set of firing rules (patterns) and the actor is fired if one of the firing rules forms a prefix of unconsumed tokens at the actor's input ports.

Continuous Time (CT). In CT, the communication between actors is (conceptually) via continuous-time signals (signals defined everywhere on a time line). The CT director includes a numerical solver for ordinary differential equations (ODEs). A typical actor used in CT is an Integrator, whose output is the integral from zero to the current time of the input signal. The CT director advances time in discrete steps that are small enough to ensure accurate approximations to "true" continuous-time behaviour. For reasons of space we omit discussion of **Discrete Events (DE)** and **Synchronous/Reactive (SR),** two other mature time-based directors.

Finite State Machines (FSM) and Modal Models. An FSM composite actor is very different from the above. The components in an FSM composite actor are not actors, but rather are states. The FSM director starts with an initial state. If that state has a

refinement, then the FSM director "fires" that refinement. It then evaluates guards on all outgoing transitions, and if a guard evaluates to true, then it takes the transition, making the destination state of the transition the new current state. A state machine where the states have refinements is called a Modal Model. A *Modal Model* is an opaque composite actor containing an FSM, each state of which may contain an opaque composite actor. In a modal model, the refinement of the current state defines the current behavior of the state machine. The refinement of a state need not have the same type of director as the workflow containing the modal model.

There are many other MoCs implemented in Ptolemy II, but the above set is sufficient to illustrate our key points. Akin to choosing between programming languages to tackle a problem, often different directors can be chosen to model a given phenomenon. A suitable director does not impose unnecessary constraints, and at the same time is constrained enough to result in useful derived properties (such as efficient execution or deadlock detection). The misinformed use of directors also leads to actors that cannot be embedded in others, as explained in the next section.

5   Composing Models of Computation in Kepler/Ptolemy II

Although prior work has offered formalisms for comparing MoCs, e.g. [4], MoC compositions have not been well treated. To address the void, we develop a classification of valid MoC combinations in Kepler/Ptolemy II.

In the Kepler environment, opaque composite actors can be put into workflows with a different type of director, thereby combining different models of computation in one workflow. In the workflow in Figure 1, the Babel actor is part of a network of actors orchestrated by the PN director. The Babel actor internally uses an SDF director. In the example, SDF is nested inside PN, which is a valid combination, as we will explain below. Nesting PN inside of SDF would have been invalid in most cases, however. The choice of director determines whether a given actor can be put on the inside or outside of other actors.

To determine which combinations are possible, we need to know two things about a director:
1. What properties it assumes of the actors under its control, and
2. What properties it exports via the opaque composite actor in which it is placed.

If a director's exported properties match those assumed by another director, then it can be used within that other director. Otherwise, it cannot. In the example of Figure 1, the SDF director exports properties that match those assumed by the PN director, and hence SDF can be used inside PN. The properties in question can be formulated in terms of actor abstract semantics.

5.1   Actor Abstract Semantics

All models of computation in Kepler and Ptolemy II share a common abstraction that we call the actor abstract semantics. Actors and directors are instances of Java classes

that implement the Executable interface, which defines *action methods*. The action methods include two distinct initialization methods:

1. preinitialize(): invoked prior to any static analysis performed on the workflow (such as scheduling, type inference, checking for deadlock, etc.).
2. initialize(): invoked to initialize an actor or director to its initial conditions. This is invoked after all static analysis has been performed, but it can also be invoked during execution to reinitialize an actor.

The action methods also include three distinct execution methods that are invoked in sequence repeatedly during an execution of the workflow:

3. prefire(): invoked to check whether an actor is ready to fire (for example, an actor may return false if there are not enough input data tokens).
4. fire(): In this method, the actor should read input tokens from input ports and write tokens to output ports, but it should not change its state. That is, if the fire() method is invoked repeatedly with the same input tokens, then the resulting output tokens should be the same.
5. postfire(): In this method, the actor can read input tokens and update its state.

Finally, there is a finalization method:

6. wrapup(): invoked for each actor just prior to finishing execution of a workflow.

All of the methods are required to be finite (they must eventually return).

The method definitions specify a contract, but not all actors obey this contract. Any actor that strictly conforms to this contract is said to be *domain polymorphic*, and the actor may be used by any director that operates on actors (which is all the directors above except FSM, which operates on states).

Actors that do not obey the contract are more specialized, and may only work with specific directors. They are not domain polymorphic (strictly obeying the actor abstract semantics) and come in two flavors. The first flavor obeys a looser version of the abstract semantics where the fire() method provides no assurance that the state of the actor is unchanged. The second is still looser in that it that also provides no assurance that any of these methods is finite. Based on these three levels of conformance to actor abstract semantics, we can now classify the directors.

5.2 Abstract Semantics Assumed by a Director of the Actors Under Its Control

The **PN** director only assumes the loosest of these abstract semantics. It does not require that any method be finite because it invokes all of these methods, in order, in a thread that belongs entirely to the actor. If an actor chooses to run forever in the preinitialize() method, that does not create any problems for the director. The director will let it run. **Dataflow** directors require that actors conform with the loose actor semantics, where all methods are finite. But they do not require that actors leave the state unchanged in the fire() method. **CT** requires that actors obey the strictest form of the semantics. The director iteratively fires actors until some condition is satisfied. The strict actor semantics ensures that the answers will always be the same given the same inputs. **FSM** requires loose actor semantics. A firing of an FSM in Ptolemy II consists of a firing of the refinement of the current state (if there is one), followed by

evaluation of the guards and a state transition. Clearly, the firing of the refinement must be finite for this to be useful.

5.3   Abstract Semantics Exported by a Director Via the Actor in Which It Is Placed

A director also implements the *Executable* interface. If a director conforms to the strict actor semantics, then an opaque composite actor containing that director also conforms to the contract. Such an actor can be used safely within any workflow. In the current version of Ptolemy II (version 6.0), only the **SR** director conforms to the strict actor semantics, although in principle **CT** and **DE** can be made to conform. Currently these and the **dataflow** directors conform to the looser abstract semantics, but still guarantee that all methods return after finite time. **PN** only conforms to the loosest version, providing no guarantees about methods ever returning. The **FSM** director exports whatever the state refinements export.

5.4   Director Compatibility

We classify directors according to two criteria. They require that the actors they control are either *strict*, *looser*, or *loosest*, depending on whether they must conform with the strictest, looser, or loosest form of abstract semantics. They similarly export either *strict*, *looser*, or *loosest*. Ideally, any director should export the same version of the contract it assumes or a stricter version, but this is not the case in currently.

The current status of the directors is given in Table 1. The rule applied to determine director compatibility is that exported abstract semantics should be stricter than or equal to required abstract semantics. The table is on-line and will evolve (see http://www.mygrid.org.uk/wiki/Papers/IccsPaper2007).

Table 1. Rules for hierarchically mixing directors in Kepler and Ptolemy II

Inner director ↓ (**exports X**)	Outer director ↓ (*requires Y*)				
	PN (*loosest*)	SDF (*loose*)	DDF (*loose*)	CT (*strict*)	FSM (*loose*)
PN (**loosest**)	Yes	No	No	No	No
SDF (**loose**)	Yes	Yes	Yes	No	Yes
DDF (**loose**)	Yes	Yes	Yes	No	Yes
CT (**loose**)	Yes	Yes	Yes	No	Yes
FSM (**refinement**)	Yes if the refinement is stricter than or equal to Y				

6   Discussion of PN, Dataflow and FSM Directors

A key question may arise at this point. If actors can be made domain polymorphic by conforming to the strict actor semantics, then why not design all directors to conform?

In some cases, the semantics of the MoC precludes this. In other cases, it would simply be too costly. We examine some of these cases.

PN. The PN director is apparently the least restrictive in the actors it can manage, but also the least useful in an opaque composite actor. The reason for this is very fundamental. If the PN director were to define a finite fire() method, what should that method do? Each of the actors under its control is executing in its own thread of control. How much execution should be performed? One possible answer is "as little as possible," but this would result in nondeterminate execution. If two actors have threads that are able to perform computation, which should be allowed to perform computation? The only other obvious answer is "as much as possible." This can be made determinate, but typical PN workflows can execute forever if given the opportunity. Hence, this yields an infinite execution. PN is sufficiently expressive that determining whether this execution is infinite is equivalent to solving the famous halting problem in computation, and hence is undecidable.

For example, the workflow of Figure 1 with PN on the outside would be hard to reuse inside others. It follows that, when a workflow has potential to be reused inside others, PN should be avoided and, if possible, replaced by a more reusable director.

DDF. DDF is as expressive as PN, and hence potentially suffers from the same limitation. However, DDF has an advantage. It assumes that all actors under its control have finite firings. Thus, it is relatively easy for the designer of a workflow to specify how many firings of the component actors constitute a single firing of the enclosing opaque composite actor. The DDF director assumes a simple default if these numbers are not given by the workflow designer: one firing of a DDF opaque composite actor constitutes at most one firing of each component actor. The actor is fired if possible, and not fired if not, given the available input data. This yields a simple, finite, and determinate notion of a finite firing for the director to export.

SDF. SDF is still simpler in that it is not as expressive as PN, and there is a simple unique finite firing that is natural and easy to define. However, for both DDF and SDF, it is difficult to define a fire() of an opaque composite actor that does not update the state of the workflow because data values stored on buffers change during the firing of the component actors. In order for SDF and DDF to export the strict actor semantics, they would have to backtrack or restore the state of these buffers on repeated invocations of the fire() method.

FSM. A particularly interesting case is FSM and modal models. Modal models always use opaque composite actors as state refinements, and these must at a minimum have finite firings to be useful (given the semantics of an FSM in Ptolemy II discussed before). Hence, it does not make sense to use PN inside the refinement of a state. But any other of the directors described above can be used in a Modal Model.

7   Conclusions

There are scenarios in e-science that rely on composing models of composition. Based on the notion of hierarchy and actor abstract semantics, we give a classification of models of computation available in Kepler and Ptolemy II. The classification shows

which combinations are useful. Notwithstanding several restrictions, many combinations are possible. Time-based simulations can be mixed with dataflow and finite state machines can be combined with almost anything. Our exploration of combinations of models of computation should be useful for other e-science systems.

References

1. G. Agha, *Actors: A Model of Concurrent Computation in Distributed Systems*, MIT Press, Cambridge, MA, (1986).
2. C. Brooks, E. A. Lee, X. Liu, S. Neuendorffer, Y. Zhao, H. Zheng (eds.) "Heterogeneous Concurrent Modeling and Design in Java", Vol. 1-3, Tech. Report UCB/ERL M05/21, University of California, Berkeley. July 15, (2005)
3. G. Kahn and D. B. MacQueen, "*Coroutines and Networks of Parallel Processes*," Information Processing 77, B. Gilchrist, editor, North-Holland Publishing Co., (1977).
4. E. A. Lee and A. Sangiovanni-Vincentelli, "*A Framework for Comparing Models of Computation*," IEEE Transactions on CAD, Vol. 17, No. 12, December (1998).
5. B. Ludäscher, I. Altintas, C. Berkley, D. Higgins, E. Jaeger, M. Jones, E. A. Lee, J. Tao, Y. Zhao, "*Scientific Workflow Management and the KEPLER System*," Concurrency & Computation: Practice & Experience, Special issue on scientific workflows (2005).
6. T. M. Parks, *Bounded Scheduling of Process Networks*, UCB/ERL-95-105, University of California, Berkeley, December (1995).
7. W. Sudholt, I. Altintas, K.K. Baldridge, "*A Scientific Workflow Infrastructure for Computational Chemistry on the Grid*," 1st Int. Workshop on Computational Chemistry and Its Application in e-Science in conjunction with ICCS (2006).

WS-VLAM: A GT4 Based Workflow Management System

Adianto Wibisono, Dmitry Vasyunin, Vladimir Korkhov, Zhiming Zhao,
Adam Belloum, Cees de Laat, Pieter Adriaans, and Bob Hertzberger

Informatics Institute
University of Amsterdam
Kruislaan 403, 1098SJ, Amsterdam, the Netherlands
{wibisono,dvasunin,vkorkhov,zhiming,
adam,pietera,delaat,bob}@science.uva.nl
http://www.science.uva.nl/ii

Abstract. Generic Grid middleware, e.g., Globus Toolkit 4 (GT4), provides basic services for scientific workflow management systems to discover, store and integrate workflow components. Using the state of the art Grid services can advance the functionality of workflow engine in orchestrating distributed Grid resources. In this paper, we present our work on migrating VLAM-G, a Grid workflow engine based on GT2 to GT4. We discuss how we use the rich set of services provided by GT4 in the new design to realize the user interactivity, interoperability and monitoring. The experiment results show that use cases from previous systems can be migrated seamlessly into the new architecture.

1 Background

The Virtual Laboratory for e-Science (VL-e) is a Dutch e-Science project which aims to realise a generic framework for multiple application domains [4]. Workflow management systems are considered as a core service for managing scientific experiments [1]. In VL-e, Virtual Laboratory Amsterdam for Grid (VLAM-G) [5] system is recommended to the VL-e application scientists together with three other workflow systems: Taverna [6], Kepler [9], and Triana [8].

The VLAM-G system was prototyped based on GT2 in an earlier project. Since then, there was a shift of paradigm in the grid community to Service Oriented Architecture. This shift was marked with the Open Grid Service Architecture specification (OGSA) [10] for integrating distributed and heterogeneous grid resources. Globus Toolkit 4 (GT4) is a recent release which implements OGSA and Web Service Resource Framework(WSRF) standards, and provides services for constructing grid services, controlling security issues, and managing distributed data.

To benefit from the rich set of GT4 services, in particular, service oriented integration will provide a standard interface for interoperating with the other workflow systems, a migration of VLAM-G to GT4 is demanded. The paper is organized as follows. First, we describe the design of current VLAM-G prototype

and then discuss the lessons learned from the previous VLAM-G applications, after that a GT4 based architecture called WS-VLAM is presented. We use a test case to demonstrate the migration of previous VLAM-G applications to the new architecture.

2   WS-VLAM: The New Design

VLAM-G provides a synthetic environment for performing grid enabled scientific experiments; it provides graphical user interface for prototyping high level workflows and for steering computing tasks at runtime, and an execution engine for orchestrating experiment processes. On the high level a scientific experiment is described as a data driven workflow in which each component (called *module* in VLAM-G) represents a process or a Grid service in an experiment. In this section we review the design of current VLAM-G prototype, and propose a new design.

2.1   Lessons Learned

The VLAM-G system consists of two core components: a graphical user interface (VL-GUI) and the Run-Time System Manager (RTSM). The RTSM is a GT2 based engine for executing workflows composed by the VL-GUI.

In the initial design, the VL-GUI and RTSM were tightly coupled. The engine handles complex coordination between workflow components; however, the strong dependency between engine and the user interface introduces a number of inconveniences: the user interface has to be up all the time while the workflow is executed remotely, and the RTSM is thus not able to orchestrate Grid components outside the GUI. For lots of data intensive applications in VL-e, these issues become a bottleneck for scientists to perform long running experiments. Decoupling the GUI and workflow engine is highly demanded.

Another lesson we learned from previous design is that VLAM-G has poor interoperability with the other workflow systems. Application scientists often require the integration between workflows developed by different systems, e.g., combining the data streaming based experiments with data statistical computation provided by R or Matlab. Incorporating third party workflows into VLAM-G modules is time consuming, since VLAM-G uses its own defined component architecture.

2.2   A New Design

A new design of VLAM-G, namely WS-VLAM, is proposed. To decouple the GUI from the engine, we wrap the RTSM as a Grid service, which is deployed in a GT4 container, and the original GUI is designed as a client which can talk to the RTSM service. The overall architecture is depicted in Fig 1.

The WS-VLAM client inherits the visual interface from VLAM-G for workflow composition. A user can browse and select proper workflow components from a
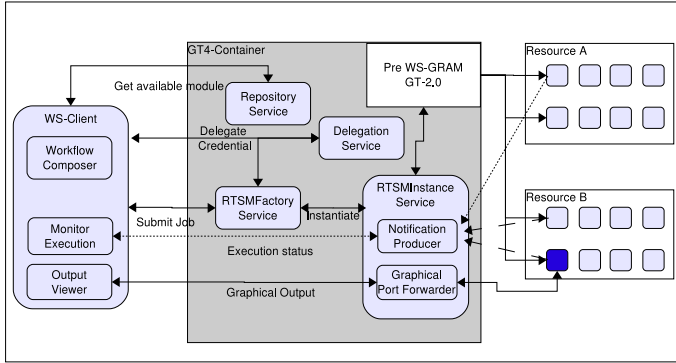
Fig. 1. Overal Architecture

repository according to specific requirements, and he can assemble the selected components by connecting their input or output ports. The workflow can be stored as XML format.

In Fig 1, standard GT4 services e.g., Delegation Service, and a set of WSRF compliant services developed in the VL-e project are deployed in a GT4 container. A repository service stores information about available components, and allows the GUI client to obtain available resources for composition. The original RTSM is wrapped as Grid services: a RTSM Factory Service and a RTSM Instance Service. The factory is a persistent service which instantiates a transient RTSM Instance service when a user submits workflow.

In the rest of this section, we discuss how the new design enacts and executes a workflow, in particular the following issues in detail: workflow execution, workflow monitoring, and user interaction support.

Workflow Execution. To execute a workflow, the RTSM has to do a number of things. Before the execution, the GUI client first contacts the GT4 delegation service to create delegation credential, and retrieves an End Point Reference (EPR), which is used at the execution phase to authenticate and authorize the user. And then, the GUI client contacts the RTSM Factory service to submit the workflow description together with the delegation EPR. After that The RTSM Factory uses the GT4 GRAM to schedule all the workflow components and creates a RTSM instance which monitors the execution of the workflow. After the job has been submitted to Grid, the RTSM Factory returns the EPR of the RTSM instance to the GUI client. The EPR will be used by the GUI client when attaching to and detaching from a remotely running instance of workflow. The basic sequence diagram of the workflow submission mechanism and execution is presented in Figure 2.

By subscribing basic events generated by RTSM, a GUI client can thus obtain the run status of the experiment. A user can subscribe different events from GRAM for monitoring the execution of each workflow component.
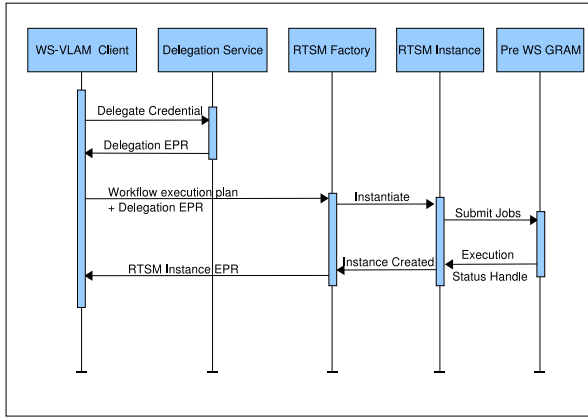
Fig. 2. Workflow Submission and Monitoring

Workflow Monitoring. For long running experiments, monitoring runtime states of the execution is important. In WS-VLAM, monitoring support is using the notification mechanism provided by GT4 Toolkit. Via the standard interface of the notification services, GUI client can be instantiated as multiple instances for subscribing the notification generated by RTSM ResourceProperty for monitoring different execution status. The output and the standard error streams produced by a workflow component are redirected to the RTSM. WSRF notifications are used to inform a client about these updates: if a user subscribes to the WSRF topic associated with these logs, an event generated from the GRAM is propagated to the subscriber (GUI client). This feature will be used to add future provenance functionality.

Graphical Output Forwarding. Human in the loop computing is an important requirement for including expert knowledge in experiment steering. The graphical display generated by the workflow components and the visualization of the entire workflow state is crucial to support the human to interact with workflow at runtime. A key issue is to deliver the remote graphical output to the end user.

Since the current execution environment of VLAM-G is Linux, graphical output of a workflow component is associated with network traffic between graphical application and virtual display to be used for rendering (X-server). A public X-server can cause potential security problem; the privacy of the graphical display will not be protected. Thus, each component has a private X-server instantiated at the same host where the associated module is displayed and executed. This allows to make all network connections between graphical applications (X-clients) and virtual displays (X-servers) local, and be invulnerable for network attacks.

Another technical issue in forwarding graphical output is the common security policy on a grid cluster: direct connection from outside of the cluster to a worker node is often prohibited. To handle this situation, a secure connection
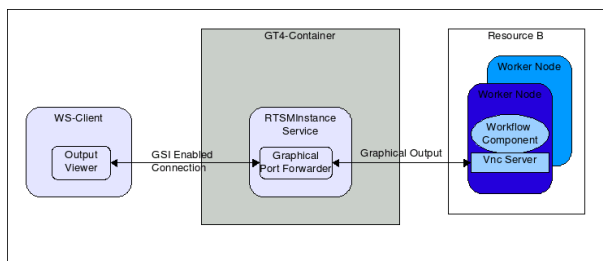
Fig. 3. Graphical Output

forwarding mechanism is used, as shown in Fig 3. The graphical connections from the GUI client are mediated with a port forwarding components at the service side. Since the service resides in the border node of a cluster, we assume that it has bidirectional access to the internal node where graphical output is produced and also access to GUI client which monitors the results. We have enhanced standard VNC X-server with GSI-enabled authorization in order to improve standard VNC authentication/authorization mechanism. This solution provides the same protection level as any other standard Globus component. In the next section, a test case is used to demonstrate how the new WS-VLAM works.

3 A Test Case

We use a VLAM-G application to demonstrate a number of features of the new design: backward compatibility, workflow execution, monitoring, and Graphical display handling.

SigWin-detector [3] use case is in VL-e bio-informatics domain. The goal is to analyze any given sequence of values, spanning from gene expression data to local time series of temperature. The use case has been implemented using the previous VLAM-G environment; the SigWin workflow consists of modules that implement a generalized and improved version of the ridge-o-grammer, a method originally designed to identify regions of increased gene expression in transcriptome maps.

Since the basic architecture for workflow modules remain, thus the previous VLAM-G description can be directly executed by the new RTSM. It allows the high level user continue work with the same workflow without caring for changes in the underlying engine.

Since a GUI client has been adapted; Fig. 4 shows the composition of the SigWin workflow. WS-VLAM client (Fig 4) is now decoupled with the workflow engine, so user can easily detach and re-attach the client to the engine while performing a long running experiment.

We have examined the interoperability between WS-VLAM and other work-flow systems. Since we have a service based workflow engine, such engine can be accessed by other workflow systems which can invoke service based resources.
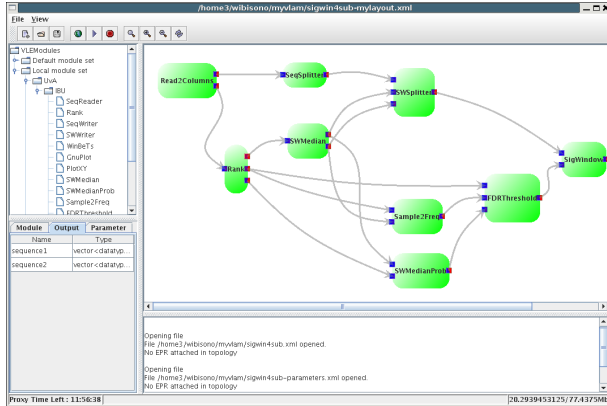
Fig. 4. SigWin Use Case

We attempted to integrate this SigWin workflow with another workflow based on Taverna. Results from this experiment will be reported in a separate paper.

4   Discussion

Compared to the related works, the design of VLAM-G engine has new features. First, the module parameters can be tuned and visualised at runtime, which allows user interaction in the massive computing tasks. Second, the design of the new engine takes the available WSRF services into account, and provides WSRF compliant interface for other types of engine to integrate. We have demonstrated it in the paper. Third, compared to the other Grid service interfaced workflow engines, e.g., GridWorkflow [12], VLAM-G engine takes one step further and makes the implementation based on GT4.

5   Conclusions

In this paper, we discussed our work on scientific workflow systems. We reviewed the design of the previous VLAM-G system, and summarized the lessons learned from applications. We argued that using GT4 services can facilitate the development of workflow engine. A new design of the VLAM-G is presented. From our work, we can at least draw the following conclusions.

1. Decoupling the user interface from the workflow engine allows the execution of the long running experiment to be independent from the user interface. More importantly, it enables workflow monitoring from different nodes.
2. The GT4 release provides rich set of services for realizing workflow engines with considerations of security control, notification, and data management.
3. Finally, the standardized service oriented interface of a workflow engine promotes the interoperability between different workflow systems.

6 Future Work

For future work we will investigate and present further results on the performance and efficiency of the system when applied to other use cases. Especially we will study the usability of this framework for parameter sweep class of applications. This work will also be part of the long term research paradigm in the VL-e context: generic e-Science framework. Currently, the workflow bus [2] is an approach. Integrating WS-VLAM as part of the workflow bus will be another important future research issue.

References

1. E. Deelman, Y. Gil: Managing Large-Scale Scientific Workflows in Distributed Environments: Experiences and Challenges. Proceedings of the 2nd IEEE International conference on e-Science and Grid computing, IEEE CS Press, Amsterdam (2006)
2. Z. Zhao and S. Booms and A. Belloum and C. de Laat and L.O. Hertzberger: VLE-WFBus: a scientific workflow bus for multi e-Science domains. Proceedings of the 2nd IEEE International conference on e-Science and Grid computing, IEEE CS Press, Amsterdam (2006)
3. M.A. Inda, A.S.Z. Belloum, M. Roos, D. Vasunin, C. de Laat, L.O. Hertzberger, T.M. Breit: Interactive Workflows in a Virtual Laboratory for e-Bioscience: the SigWin-Detector Tool for Gene Expression Analysis. Proceedings of the 2nd IEEE International conference on e-Science and Grid computing, IEEE CS Press, Amsterdam (2006)
4. V. Korkhov, A.S.Z Belloum, and L.O. Hertzberger.: Vl-e: Approach to design a grid-based virtual laboratory. In 5th Austrian-Hungarian workshop on Distributed and Parallel systems, (2004)
5. A.S.Z. Belloum, D.L. Groep, Z.W. Hendrikse, L.O. Hertzberger, V. Korkhov, C.T.A.M. de Laat and D. Vasunin: VLAM-G: a grid-based virtual laboratory. Future Generation Computer Systems, Vol. 19. (2003) 209-217
6. T.M. Oinn, R.M. Greenwood, M. Addis, M.N. Alpdemir, J. Ferris, K. Glover, C.A. Goble, A. Goderis, D. Hull, D. Marvin, P. Li, P.W. Lord, M.R. Pocock, M. Senger, R. Stevens, A. Wipat, C. Wroe: Taverna: lessons in creating a workflow environment for the life sciences. Concurrency and Computation: Practice and Experience Vol. 18. (2006) 1067-1100
7. L. Chen, G. Agrawal: A static resource allocation framework for Grid-based streaming applications. Concurrency and Computation: Practice and Experience Vol. 18. (2006) 653-666

8. D. Churches, G. Gombs, A. Harrison, J. Maassen, C. Robinson, M. Shields, I.J. Taylor, I. Wang: Programming scientific and distributed workflow with Triana services. Concurrency and Computation: Practice and Experience, Vol. 18. (2006) 1021-1037

9. I. Altintas and C. Berkley and E. Jaeger and M. Jones and B. Ludäscher and S. Mock: Kepler: An Extensible System for Design and Execution of Scientific Workflows. Proceedings of the 16th International Conference on Scientific and Statistical Database Management, (2004)

10. I. Foster, C. Kesselman, J. Nick and S. Tuecke: The Physiology of the Grid: An Open Grid Service Architecture for Distributed Systems Integration. Global Grid Forum (2002)

11. H. Afsarmanesh, R.G. Belleman, A.S.Z Belloum, A. Benabdelkader, G.B. Eijkel, A. Frenkel, C. Garita, D.L. Groep, R.M.A. Heeren, Z.W. Hendrikse, L.O. Hertzberger, E.C. Kaletas, V. Korkhov, C. de Laat, P.M.A. Sloot, D. Vasunin, A. Visser, H. Yakali: VLAM-G: A Grid-based virtual laboratory. Scientific Programming, Vol. 10. (2002) 173-181

12. S. Hwang, C. Kesselman: A Flexible Framework for Fault Tolerance in the Grid. Journal of Grid Computing Vol. 1. (2003) 251-272

Distributed Applications from Scratch: Using GridMD Workflow Patterns

I. Morozov[1,2] and I. Valuev[1]

[1] Joint Institute for High Temperatures of Russian Academy of Sciences,
Izhorskaya 13/19, Moscow, 125412, Russia
[2] Moscow Institute of Physics and Technology (State University), Institutskii per., 9,
Moscow Region 141700, Russia
`valuev@ihed.ras.ru`

Abstract. A new approach is proposed to generate workflow scenarios of scientific applications such as Molecular Dynamics and Monte-Carlo simulations in a distributed environment. The approach is based on embedding all workflow elements into the source (C++) code of the application as external library (GridMD) function calls. Thus the compiled executable is used both to generate the scenario and to perform computations related to the individual scenario elements. Having the scenario, its execution may be delegated to any resource manager which supports workflows.

1 Introduction

Scientific applications such as simulations using Molecular Dynamics (MD) and Monte-Carlo (MC) methods often require substantial computational resources. Available MD/MC packages (such as NAMD [2] or LAMMPS [1]) provide efficient serial and parallel algorithms for simple execution scenarios, such as to take the system of particles at some initial state and to propagate it through the chain of other states. At higher level the numerical experiment includes statistical averaging [3], parameter sweep, optimal parameter search, etc. While distributed environment looks very promising for these tasks, the researchers face the problem of constructing complicated scenarios and workflows.

Various tools for Grid-enabled workflow management are being developed [4, 5, 7, 8]. They provide both visual interfaces based on direct acyclic graphs [4, 5] and specialized languages [7, 8] for definition of the workflow. However in all cases this definition is to be made by the user of application who must be aware of the execution scenario and the workflow definition software.

Recently GridMD [9] C++ class library was proposed, which is designed for the simulations developers, the programmers who create computational applications. Researchers may use these applications in production runs to obtain physical results. We emphasize here the distinction between users and developers, which for scientific applications are often the same people, to stress the GridMD strategy of delegating the workflow specification entirely to the application developer. The workflow elements are specified in easy and portable way

by the special GridMD function calls inside the application C++ code. Being embedded, the scenario information can be extracted from the executable and passed to the workflow management system at run-time with minimal user intervention. The aim of the library is also to provide specialized mechanisms of submitting the GridMD application jobs to different workflow management systems. The detailed knowledge of these submission mechanisms is not required neither for the application developer nor for the application user. Between the submission mechanisms, the one called "local" where all jobs are executed one-by-one on the same computer is always accessible by any GridMD application. It may be used for testing the distributed application without even having the actual access to the Grid and workflow software. In the following we will analyze the mechanisms of experiment scenario specification in GridMD in more detail.

2   GridMD Workflow Specification Patterns

GridMD has the usual notion of workflow, which may be represented by directed graph consisting of nodes and links (edges of workflow graph). The links represent dependence between nodes, the nodes represent some actions of the program. Unlike other workflow systems, GridMD does not require that *all* actions in the code should be wrapped in workflow elements. Instead, only the parts of the code most important for distributed execution may be specified as nodes.

There are several types of links in GridMD: *logical* or *hard* link from node A to node B means that node B may be executed only by the same process as node A AND only after node A; *data* link between A and B means that either A and B must be executed consecutively by the same process OR B may be executed without executing A provided that the *result data* of node A, associated with this data link, is accessible by the process executing B; *process* link between A and B is a special case of *hard* link assuming that some calculations which are initialized at node A are taking place in node B. Although being a limited subset of possible node dependencies, used by different workflow systems, this system of links provides a sufficient basis for iterative simulation experiments and can be easily extended in the future. Data links are the main sources of distributed capabilities of the code in general. The node result data associated with a link is represented in C++ code as an object of some data type.

The workflow nodes are defined and executed by the same GridMD application, so this application may proceed in two execution modes. *Construction or manager mode* is used for the assembly of the workflow graph and to its subsequent analysis. *Worker mode* is used to execute some subset (subgraph) of the nodes through the invocation of the same application with command line parameters uniquely specifying the subgraph for execution.

3   Example of the Distributed Application

In GridMD, the nodes and links can be created *explicitly*, by associating them with C++ virtual functions and linking them in the graph, or *implicitly*. By

the example in Fig. 1 the use of the implicit mechanism to easy redesigning the existing applications for distributed execution is illustrated. The initial program (Listing 1) is complemented by GridMD calls, and the workflow graph is produced automatically. As it is seen from Listing 2, the implicit node markup patterns have a form of conditional operators with GridMD functions as arguments. All these functions (`bunch.begin()`, `bunch.node_define()`, `bunch.node_process()`, `bunch.end()`, `gmdExperiment.execute()`) return zero in the manager mode and are used simultaneously to specify the nodes and to conditionally bypass the time consuming parts of node execution. The bypassed parts are in fact the actions, associated with defined nodes. They are performed only in worker mode and only if corresponding GridMD functions return nonzero, i.e. when the execution of specific node is requested.

The `gmdSweep` object implements branching where a data link can be put in the middle of the branch (see Fig 1). This data link is bound with an object of some data type (this type is a C++ template parameter, double for the example). The object for the current branch may be accessed by `node_result()` function both in the source node of the link (marked by `node_define`) and in the target node (marked by `node_process`). If these nodes are executed by different processes, the data transfer according to this link (including file creation) is managed by GridMD through type-specific I/O operations.
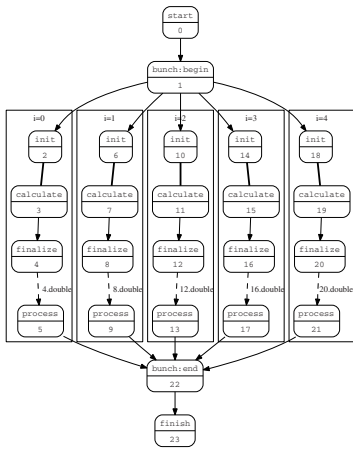
Listing 1:
```
1  double s=0;
2  for(int i=0;i<5;i++){
3    s+=long_calculation(i);
4  }
5  printf("The result is: %lf\n",s);
```

Listing 2:
```
1  gmdExperiment.init(argc,argv);
2  gmdSweep<double> bunch("bunch");
3  bunch.mark_begin();
4  double s=0;
5  for(int i=0;i<5;i++){
6    if(bunch.mark_node_define(strfmt("i=%d",i)))
7      bunch.node_result()=long_calculation(i);
8    if(bunch.mark_node_process())
9      s+=bunch.node_result();
10 }
11 bunch.mark_end();
12 if(gmdExperiment.execute())
13   printf("The result is: %lf\n",s);
```

Fig. 1. Execution graph (left part) automatically generated from the code presented in Listing 2 (right part). Logical links are represented by solid lines with arrows, data links by dashed lines with names of transferred files indicated, process links are shown by thick lines. The numbers are node unique identifiers which are assigned to the nodes in the order of creation. Visualized by graphviz.

After the workflow graph is created, an iterative graph analysis algorithm is used to determine which branches (subgraphs) may be used concurrently. In order for the workflow defined by GridMD markings to be consistent, there must

be no implicit logical links between nodes except those known from the work-flow graph. This has to be checked by the application code developer, because GridMD is unable to analyze this in advance in construction mode and will only report an error in worker mode when the actual execution does not conform to the defined graph.

Distributed execution can be controlled by the GridMD application itself or it can be delegated to the external execution manager which supports work-flows (NIMROD [10], Kepler [4]). In the later case GridMD application first generates the workflow definition file (plan file or script). The script (external Perl submission) for starting all the tasks of example in Fig. 1 is shown below:

```
# Generator: appl.exe -plscript -engine=submit.pl
require "submit.pl";
# distributed subgraph submission
submit("appl.exe -w0-4","","4.double");
submit("appl.exe -w0-1:6-8","","8.double");
submit("appl.exe -w0-1:10-12","","12.double");
submit("appl.exe -w0-1:14-16","","16.double");
submit("appl.exe -w0-1:18-20","","20.double");
wait_for_queue();    # wait till all subgraph tasks finished
# distributed subgraph submission
submit("appl.exe -w5:9:13:17:21-23","4.double 8.double 12.double 16.double 20.double","");
wait_for_queue();    # wait till all subgraph tasks finished
```

Acknowledgements

References

1. http://www.ks.uiuc.edu/Research/namd/
2. http://lammps.sandia.gov/
3. Kuksin, A.Yu., Morozov, I.V., Norman, G.E., Stegailov, V.V., Valuev, I.A.: Standards for Molecular Dynamics Modelling and Simulation of Relaxation. Molecular Simulation **31** (2005) 1005–1017
4. http://www.kepler-project.org
5. http://pegasus.isi.edu
6. Pytlinski, J., Skorwider, L., Benedyczak, K., Wronski, M., Bala, P., Huber, V.: Uniform Access to the Distributed Resources for the Computational Chemistry Using UNICORE. In: Sloot, P.M.A., et al (eds.): Lecture Notes in Computer Science, Vol. 2658. Springer-Verlag, Berlin Heidelberg New York (2003) 307–315
7. W.M.P. van der Aalst: The Application of Petri Nets to Workflow Management: The Journal of Circuits, Systems and Computers, Vol. 8, No. 1 (1998) 21–66.
8. Lee, E.A., Parks, T.M.: Dataflow process networks. Proc. of the IEEE **83** (1995) 773–799

9. Valuev, I.: GridMD: Program Architecture for Distributed Molecular Simulation. In: Hobbs, M., et al (eds.): Lecture Notes in Computer Science, Vol. 3719. Springer-Verlag, Berlin Heidelberg New York (2005) 307–315

10. Sudholt, W., Baldridge, K., Abramson, D., Enticott, C., Garic, S.: Parameter Scan of an Effective Group Difference Pseudopotential Using Grid Computing: New Generation Computing **22** (2004) 125–135

Heterogeneous Workflows in Scientific Workflow Systems

Vasa Curcin, Moustafa Ghanem, Patrick Wendel, and Yike Guo

Department of Computing, Imperial College London

Abstract. Workflow systems are used to model a range of scientific and business applications, each requiring a different set of capabilities. We analyze how these heterogeneous approaches can be resolved, look at how existing workflow systems address this and present the solution in Discovery Net, which combines three levels of workflows, control, data and grid, at different levels of abstraction.

1 Introduction

A disctinction is often drawn between workflow systems based on their intended aim. Typically, the two types isolated are dubbed business and scientific workflows, with the former concentrating on increasing efficiency within an organization, while the latter are concerned with the fostering of innovation in scientific environments. While the two are not neccessarily in direct conflict and even share some common areas of interest such as automation, provenance tracking and collaboration, they do branch into different fields. The business workflow field revolves around issues such as messaging protocols, process optimization, and sophisticated patterns involved in component interaction. Scientific workflows, on the other hand include technologies which help bring the usability of the workflow abstraction in scientific research up to the level of a research scientist, by investigating interactive analysis creation, process knowledge capture, dissemination and reusability, and harnessing complex computational infrastructures within simple graphical metaphors. In addition to this separation, there are several perspectives from which a workflow model can be observed [2]. *Control flows* describe the flow of execution control between tasks, *data flows* represent a functional programming perspective, in which tasks are data transformations, while some other perspectives, such as *resource* and *operational* are also possible.

Workflow technologies have also been used in the context of Grid computing, mainly automating the submission and execution of user tasks on distributed computing resources. The level of details captured in such workflows varies between different systems. For example, within the Globus GT3 [3] project, GridAnt provides a workflow language with conditional, sequential, and parallel constructs that are used to describe the detailed steps required for submission and execution of user tasks on high performance resources. In contrast, within the Pegasus [4] system, the VDL language is used to define workflows as dependency graphs between user tasks, and the Pegasus system then automatically

maps the abstract workflows down to executable ones based on the available grid resources.

The Discovery Net system [1] was designed primarily to support the analysis of scientific data based on a distributed Web Service/Grid Service composition methodology. Within this framework, computational services executing at remote locations can be treated as black boxes with known input and output interfaces. Such services are connected together into acyclic graphs or workflows defined as sequences of operations where the outputs of one service act as inputs for other services. To initiate an execution, the user defines the termination node in the workflow and data is pulled through the preceding nodes in a demand driven fashion. Data passed between the nodes can be either atomic or a collection (e.g. a table of values), and in the latter case, each node will implicitly iterate over the input contents. That original paradigm is best suited to capture the semantics of a data flow model of computation. Although the system allowed the definition of parallel branches within a workflow to be formed (e.g. through the availability of multiple output ports in a service), it supported no explicit control flow constructs (e.g. conditionals) or explicit iteration operations. Despite these restrictions, the system has been extremely successful in enabling end users to create complex data analysis applications in various fields, including Life Sciences [6], Environmental Monitoring [5] and Geo-hazard Modelling [7]. Some of the key features that enabled its wide uptake were rooted in its support for a fully interactive model of workflow construction and deployment.

In this paper we describe the introduction of new extended features for supporting control flow semantics within the Discovery Net system. The paper is organized is follows. Section 2 reviews the main features of the scientific workflow systems that were described in the literature since the design of the original Discovery Net system. In Section 3, we present and describe the notion of workflow embedding as a generic solution to heterogeneous workflow composition, demonstrating it in Discovery Net through two new layers: a control flow layer and Grid control layer. Section 4 presents the conclusion and lays out the future research directions.

2   Heterogeneity in Existing Workflow Systems

There are numerous criteria which we can use to characterize the workflow execution semantics: atomic vs. streaming, push vs. pull, single vs. multiple starting/ending points, implicit or explicit iterations over data sets etc. The important thing to note is that *all* of these have their uses in some workflow scenarios. However, we argue that the correct way of modelling systems with multiple requirements is by implementing the heterogeneity in different semantic levels, rather than providing all of the functionality as different components in the same environment. In this section, we will investigate how some popular workflow systems address this issue.

2.1   Taverna

Taverna [8] is a graphical workflow authoring and execution environment, using SCUFL as its workflow language, and Freefluo as its enactment engine. SCUFL (Simple Conceptual Unified Flow Language) was developed for the purposes of the Taverna project, and can integrate any Java executable code as a component. The basic unit of execution in SCUFL is a processor, which has associated with it input and output ports. The processor may be regarded as a function from input data to output data, with possible side effects on the execution environment.

Data links between the components have a source processor and output port name, a sink processor and an input port name. This type of link ensures the basic consistency in pure dataflow execution. However, due to possible effects on the execution environment which are separate from inputs and outputs, explicit ordering constraints are introduced, which are not based on the data dependency between processors. These control constraints are useful when execution ordering must be imposed between two processors but when there is no dataflow between them. The execution of a SCUFL workflow will start from the nominated starting points, *sources*, and finish when all end points, *sinks*, have either produced their outputs or failed. Whether the workflow can execute partially (ie. if one sink failed, should the others complete) is configurable by the user.

In addition to control constraints and data links SCUFL also has an indirect conditional construct, which corresponds to *if/else* or *case* structure in procedural programming languages. This construct consists of a single input being passed to multiple nodes, which are all connected downstream to the same component. The user has to ensure that only one of them will succeed and continue the execution. If, however, for some reason multiple nodes execute and produce output, the downstream node will only process the first input received. The generic iteration construct is not supported, but one special case is the *implicit iteration*. This form of execution happens when a single-item processor receives a data collection, then the processor is executed once for each item in the collection. This behaviour is equivalent to the *map* construct in functional programming languages.

2.2   Triana

Triana [9] is a visual workflow-based problem solving environment, developed at Cardiff University. The functional component in Triana is called a *unit*. Units are connected through *cables* to form workflows. The notion of hierarchical workflows is supported through grouping connected components into a higher-level group unit. The created group unit implicitly has an associated control structure, another unit, which can coordinate its executional behaviour.

In addition to numerous functional components, Triana provides control flow units that operate on the same level as the data flow, and can be freely combined with them. The looping is achieved through a dedicated Loop component, that has two output ports. One typically connects to a functional unit, while the other provides the final output once the iteration is over. The Loop component

receives input data, evaluates its exit condition, and then passes the data either to the exit port or to its functional unit. Also, Triana posseses a number of *trigger* units, which can be used to send a signal on user action, at a fixed time or after a certain delay. Streaming execution is achieved using dedicated units for blocking, merging, splitting, pausing, etc. There is no explicit distinction between data and control components, placing them all on the same level. Semantics are left for the user to design, using the large number of specialized units provided. This design is opposed to languages such as YAWL and Kepler, which try to minimize the number of control nodes, the former through formalizing them into a minimum neccessary set, and the latter by separating control from the nodes altogether.

2.3   YAWL

YAWL (*Yet Another Workflow Language*) has its origins in theoretical work on workflow patterns [2] comparing a number of (mostly business) workflow systems. and was not developed for the purposes of an application project. Realizing that all the patterns described can be implemented in high-level Petri nets, albeit with some difficulty in cases of patterns with multiple process instances, advanced synchronization and cancellation, YAWL was based on high-level Petri nets, in order to preserve their benefits, but with extensions to help direct support of the special cases mentioned. YAWL's formal semantics are in contrast with other languages which either have no formal semantics (Triana, XPDL) or they constructed post hoc (Taverna). While the control flow perspective of YAWL is the most investigated one, the language also supports the data and resource perspective by allowing input and output parameters in the components to be connected to global variables.

The core component concept in YAWL is derived from the Petri Nets, with the workflow being a set of tasks, conditions and flows between them. Unlike Petri Nets, tasks can be connected to each other directly, without a condition inbetween (or an implicit condition that automatically succeeds). A task in a workflow can be either atomic or composite, with composite tasks containing another workflow (*extended workflow net* in YAWL terminology) within them. This corresponds exactly to the grouping concept present in Discovery Net, Taverna, Kepler, Triana and some other systems. There are six explicit branching constructs: three splits (AND, XOR and OR) and three joins (AND, XOR and OR), which model every legal data routing through the workflow. Due to the nature of splits the execution path through the workflow is determined dynamically at runtime, as opposed to being apriori statically determined. Both looping and conditional constructs are achieved using explicit conditions which evaluate the state of the workflow and direct the execution accordingly. So, there are no *if/else* or *while* components but the structure of the graph can create such behaviour.

The data flow in YAWL is achieved via variables, and can be split into internal and external data transfers. Internal transfers are always performed between the tasks and their workflows, since all variables inside tasks are internal to that task. So, in order to communicate some data between tasks A and B, task A

has to register its variable as the output parameter, and pass it to some global workflow variable N, which task B will take as its input parameter. External transfers occur between global variable and the user or an external component, such as a web or Grid service.

2.4 Kepler

Kepler [11] is a scientific workflow construction, composition, and orchestration engine, focusing on data analysis and modelling. This focus influenced the design in that it is suitable for modelling a wide variety of scientific domains, from physics via ecosystems to bioinformatics web services. Instead of trying to provide a generic semantic for all possible types of processes encountered in these domains, Kepler externalizes the execution engine from the workflow model, and assigns one *director* to each model, that then coordinates the model execution.

The workflow components in Kepler are represented by *actors* with ports that can be input, output, or mixed. Tokens are basic data containers, and they are passed from the output port of one actor to another through the relation connections. The number of tokens consumed and produced depends on the node used. *Directors* are the key concept in Kepler. While actors and relations together constitute a workflow model, the directors form the execution model, or the model of computation. In this setup, actors' intelligence stretches as far as knowing its inputs, the operation to be performed on them and what outputs to produce. The decision when to schedule the execution of each actor is left to the director. Therefore, depending on the director used, the actors may have separate threads of control, or they may have their executions triggered by the availability of new input, in a more conventional dataflow manner. The architecture in which components are agnostic to the manner in which they are executed is formalized as *behavioural polymorphism*.

Kepler supports four director types. **SDF - Synchronous Dataflow** is characterized by fixed token production and consumption rates per firing. The actor is invoked as soon as all inputs have data, which is possible to know since all actors have to declare their token production before the execution. Therefore, the order of execution is statically determined from the model, and components cannot change the routing of tokens during execution. **PN - Process Network** is a derestricted variant of SDF, in that the actor is invoked when the data arrives. However, there is no requirement that *all* data has to be present, which results in a more dynamic environment, where actors are executing in parallel and sending each other data when and if needed. The tokens are created on output ports whenever input tokens for an actor are available and the outputs can be calculated. The output tokens are then passed to connected actors where they are held in a buffer until that next actor can fire. The workflow is thus driven by data availability. **CT - Continuous Time** introduces the notion of time that is affixed to tokens in order to perform system simulations. The system is typically based on differential equations, and start conditions, which are then used to predict the state at some specified future time. The data tokens that are passing through the system then have a timestamp that the director is using

to determine the step and the stop condition. **DE - Discrete Event** director is working with timestamps, however, they are not used to approximate functions and schedule executions, but to measure average wait times and occurrence rates.

3   Discovery Net Workflow Embedding

The key new feature of Discovery Net 3.0 is the layered approach for definition, embedding and execution of scientific workflows. The top, control flow, layer is introducing new control operators for the coordination of the traditional data flow operations. This layer enables the execution of distributed applications with scheduling dependencies more advanced than the simple data availability criteria, and where the data passing between components need to be restricted due to volume or costs associated with transfers. The middle layer corresponds to the traditional Discovery Net data flow layer enabling data integration, transformation and processing using distributed services. The bottom layer, Grid Control, enables the access and control of Grid resources.
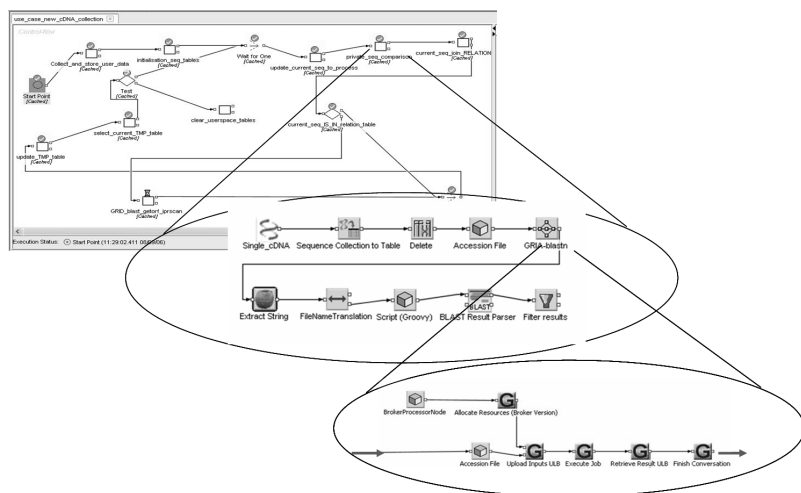
Fig. 1. Hierarchical workflow composition

3.1   Control Flow Layer

This layer includes a range of control flow elements such as branching synchronisation, conditional branching and looping. The control flow mechanisms use a different execution scheme to the standard workflow execution engine; hence the control flow components cannot be connected to data flow components, but rather they orchestrate data flows, specifying which will be the next data flow

to run based on the control decision. The key new control flow operations introduced in Discovery Net include:

- **Test** Generic condition construct, where the user specifies the condition, and indicates which branch is to be executed, depending on the outcome.
- **Wait for All** Provides synchronisation allowing waiting for all arriving tasks to be completed before a workflow can proceed.
- **Wait for One** Similar to Wait for All, except that it executes the node, once the first of the arriving tasks is complete.
- **For** Explicit looping construct, which loops through activities a specified number of times - a syntactic shortcut for a generic loop implementable using the former three components.
- **While** Loops through activities while a variable is true, also a syntactic shortcut.

Firstly, a notion of *token* was introduced, in which each component may receive a token, which will cause an execution of its instance. Multiple tokens may exist in the workflow at any one time, and even in a single component. Secondly, the execution switched from the pull-based model to a push-based one, with a dynamic flow of control – nodes making runtime decisions about the direction which the execution will take. Furthermore, tokens have access to the component that produced them, thereby giving a link to the result of a previous execution, if needed.

Interestingly enough, even though the control flow does not fit into the workflow-as-service model, so strongly upheld on the dataflow level, it utilizes it in order to have a uniform execution paradigm for its components. Namely, the execution node in the control flow is the only component which can perform an action outside of the scope of the flow being executed. The way it operates is by executing an internal dataflow, with a nominated output, which is used to produce and fire a token once the execution is complete. The output is nominated by declaring it as the output of the service created from the inner workflow. So, the atomic unit of execution inside the control flow is actually a dataflow-based service.

3.2   Grid Control Layer

The role of the bottom layer is to enable access and control of remote Grid computing resources. Specifically, within this layer, sub-workflows are used to control selection of resources as well as authentication, job submission, job invocation, collection of results as well as session management. An example implementation of these operations for the GRIA middleware is described in details in [10].

4   Summary

This paper discussed the need for heterogeneity in workflow systems, reviewed the approaches different scientific workflow systems take, and introduced the hierarchical approach to combining control and data structures in Discovery Net.

Discovery Net adopts a conservative approach to its dataflow semantic, insisting on a single-output static execution model, corresponding to a function call, with no non-determinism in the execution flow. All non-deterministic elements, such as conditional and looping structures, are implemented in a separate level, as well as strategies for GRID execution which involve scheduling and service discovery. This is in sharp contrast to other systems analyzed, which are either enriching a dynamic control flow structure with global variables (YAWL), introducing dataflow-flavoured control elements (Taverna), placing all the combinations of functionality/semantics into separate nodes (Triana). The Kepler approach of letting the user determine the hierarchical composition of different semantics, is the closest to the one presented here, but it allows for some distinctly non-workflow systems to be built. In the future work, we plan to analyze how multiple execution semantics interact in a hierarchical model, by looking at error handling, user interaction and process provenance. The complete picture of the Discovery Net model will then allow us to compare and contrast workflow executions with other scientific workflow systems, producing formal notions of equivalences between these systems.

References

1. AlSairafi et al: The Design of Discovery Net: Towards Open Grid Services for Knowledge Discovery, High Performance Computing Applications, vol 17, no 3, (2003) 297–315
2. Aalst van der et al: Advanced Workflow Patterns, 7th International Conference on Cooperative Information Systems, vol 1901, Lecture Notes in Computer Science (2000) 18–29
3. Ian T. Foster: Globus Toolkit Version 4: Software for Service-Oriented Systems, NPC (2005) 2–13
4. Deelman, E. et al: Pegasus: Mapping Scientific Workflows onto the Grid, Lecture Notes in Computer Science : Grid Computing, (2004) 11–20
5. Richards et al: Grid-based analysis of air pollution data, Ecological Modelling, vol 194, no 1–3 (2006) 274–286
6. Rowe et al: The discovery net system for high throughput bioinformatics, Bioinformatics, vol 19, no 90001, (2003) 225–231
7. Guo et al: Bridging the Macro and Micro: A Computing Intensive Earthquake Study Using Discovery Net, Proceedings of SC2005 ACM/IEEE (2005)
8. Hull et al: Taverna: A tool for building and running workflows of services, Nucleic Acids Research, Web Server Issue, vol 34, (2006) W729–W732
9. Taylor, Ian et al: Visual Grid Workflow in Triana Journal of Grid Computing, vol 3, no 3-4, (2005) 153–169,
10. Ghanem, M. et al.: Grid-enabled workflows for industrial product design, 2nd IEEE International Conference on e-Science and Grid Computing (2006)
11. Ludaescher, B. et al.:Scientific Workflow Management and the Kepler System, Concurr. Comput. : Pract. Exper., vol 18, no 10, (2006) 1039–1065

A Multi-agent System for Cross-Organizational Workflows Management Based on Process-View*

Ping Jiang, Xinyu Shao, Liang Gao, and Zhenfeng Yang

Department of Industrial & Manufacturing System Engineering,
Huazhong University of Science & Technology, 430074, Wuhan, China
gaoliang@mail.hust.edu.cn

Abstract. Workflow interoperability across enterprises boundaries presents a significant challenge recently. Process-view provides a promising way to cross-organizational workflows design. A multi-agent system combined with Petri net based process-view approach is proposed to facilitate cross-organizational workflows management. Within this multi-agent system, a Petri net algebra model and a character string mapping algorithm are proposed to automate the mapping from a Petri net workflow model to a process-view workflow model; the synchronization points are added to integrated process-view workflow models to coordinate the execution of cross-organizational workflow instances.

Keywords: Cross-organizational workflows management; Process-view; Petri net; Multi-agent system; Mapping.

1   Introduction

The existing Workflow Management Systems (WMS) are commonly developed for stable and long-running business processes in individual enterprises, which are always rigid and centralized. But in cross-organizational business collaboration, cooperative processes are highly dynamic and the execution of collaborative activities are distributed, the required WMS should support dynamic and flexible business collaboration across enterprises boundaries while maintaining privacy and autonomy of participant enterprises. Facilitating interoperability among existing WMS provides a promising way for realizing efficient cross-organizational workflows collaboration, which avoids spending time and cost on developing new WMS.

A process-view is an abstract process derived from an implemented base process [1]. In the process-view approach, an enterprise can realize business processes integration with various partner enterprises by reusing its internal processes, which saves much time to remodeling. Our previous work [2] proposed a Petri net based process-view approach for workflow modeling in virtual enterprises. This paper proposes a Multi-Agent System (MAS) combined with the previous approach to facilitate interoperability among existing WMS.

---

2   Background and Related Work

The Workflow Management Coalition (WfMC) has developed specifications to enable interoperability between heterogeneous workflow systems [3]. W.M.P. van der Aalst [4] adopted Petri net to model interorganizational workflow. Liu and Shen [1] proposed an order-preserving process-view approach to business-to-business (B2B) workflow interoperability. Martin A. et al [5] utilized Petri net refinement paradigm to simplify the handling of complex and large-scale workflows. The MAS offers a distributed and open platform architecture for dynamically changing systems. In this paper, we propose a MAS combined with the Petri net based process-view approach to manage cross-organizational workflows, which can automate the mapping from a Petri net workflow model to a process-view workflow model and coordinate the execution of cross-organizational workflow instances.

3   A MAS for Cross-Organizational Workflows Management

The MAS combined with Petri net based process-view approach (PVMAS) is described in Fig. 1. It provides a mediator architecture to facilitate distributed WMS interoperability.
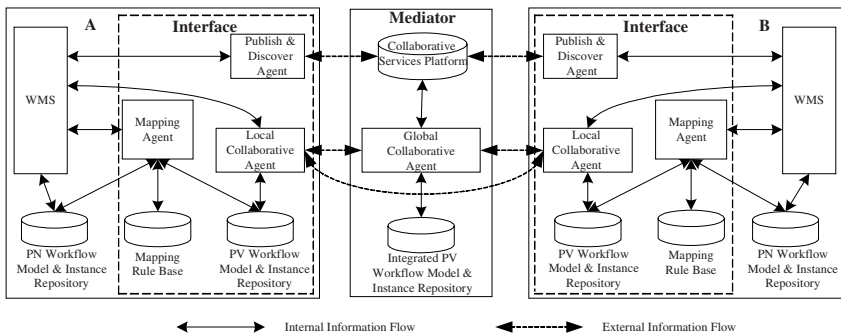
Fig. 1. The PVMAS for cross-organizational workflows management

3.1   Mapping Agent

The Mapping Agent automates the mapping from a Petri Net (PN) workflow model to a Process-View (PV) workflow model. A PN algebra model is proposed to automate the mapping.

Definition 1. A PN algebra model is a character string L consists of Pi, Aj, Tk, Lm, +, -, *, /, [ ], ( ) and F, Where:

(1) Pi, Aj, Tk and Lm are the starting and ending characters representing base place, *abstract place*, base transition and *logic transition* respectively, where i, j, k and m are the sequence number;

(2) +, -, *, / represent the order structures of Or-Join, Or-Split, And-Join and And-Split respectively;

(3) [ ] represents the Loop structure, the places and transitions included in it are executed repeatedly;

(4) ( ) represents the parallel branch;

(5) F represents nothing.

The Mapping Agent can realize the automation of mapping by intelligently processing character strings. We use "{ }" to denote the sub-models must be hidden. Fig. 2 describes the mapping, and the mapping steps are as follows:

(1) Build the PN workflow model described in Fig. 2.(a);

(2) Get the corresponding PN algebra model L described in Fig. 2.(b);

(3) Select the sub-models needed to be hidden in the PN workflow model. In Fig. 2.(c), the sub-models {P02, T02, P03} and {T05, P06, T06, P07} surrounded by curving dashed line are the selected ones;

(4) Add "{ }" to the PN algebra model to denote the selected sub-models, and get the middle character string L` described in Fig. 2.(d);

(5) Process L` by character string mapping algorithm, the PN algebra model L`` of the PV workflow model can be obtained described in Fig. 2.(e), in which sub-models {P02-(T02P03)} and {[T05P06T06P07]} in L` are replaced by *abstract places* A01 and A02 respectively;

(6) Get the PV workflow model from the character string L`` described in Fig. 2.(f).
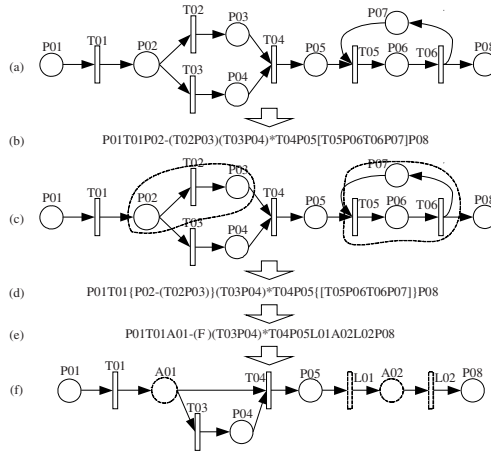
Fig. 2. The mapping from a PN workflow model to a PV workflow model.(a) The PN workflow model; (b) the PN algebra model L; (c) the PN workflow model with sub-models needed to be hidden; (d) the PN algebra model L`; (e) the PN algebra model L``; (f) the PV workflow model.

The core of the character string mapping algorithm is graph reducing theory. The main procedures of the character string mapping algorithm are as follows:

```
input >> PN1;           // Input initial character string
PN1 = find_nodes(PN1);  // Find out all nodes
out_in_way(PN2);        // Search the split and join nodes
```

```
creat_graph(PN2);        // Transform the character string to a matrix
combine_graph(PN1);   // Replace the nodes needed to be hidden with necessary
                                        abstract place nodes
insert_L( );                    // Add some necessary logic transition nodes
ans = output_graph( );   // Transform the matrix into a character string
output(ans).                   // Output the last character string
```

3.2 Local and Global Collaborative Agent

In order to coordinate the execution of cross-organizational workflow instances, we designate the *synchronization points* (SP) in the integrated PV workflow models.

Definition 2. SP are some base transitions in integrated PV workflow models, which can facilitate the exchange of workflow status information and the coordination of the workflow progress among the corresponding workflow instances.

When the integrated PV workflow instance execute to SP, the SP will trigger the Global Collaborative Agent to inquire the status information of corresponding PV workflow instances from Local Collaborative Agents of participant enterprises. If there exist some delayed or abnormal information, the responsible Local Collaborative Agents will be triggered to synchronize the execution of corresponding PN workflow instances of participant enterprises.

4   Conclusion

The PVMAS for cross-organizational workflows management has the following advantages: Different WMS can finish a common business collaboratively across enterprises boundaries and keep autonomy; enterprises can adopt different PV workflow models mapped from the same PN workflow model to quickly construct cross-organizational workflows.

Our future work will mainly address two themes. First, extending PN to Timed Colored Petri Net (TCPN) to enhance the modeling ability of our system. Second, developing the PVMAS and validating the availability of the system.

References

1. Duen-Ren L., Minxin S.: Workflow modeling for virtual processes: an order-preserving process-view approach. Information Systems 28 (2003) 505-532
2. Xinyu S., Ping J., Haobo Q., Liang G.: Workflow Modeling for Virtual Enterprise: a Petri Net Based Process-View Approach. Proceedings of the 10th International Conference on Computer Supported Cooperative Work in Design 2(2006) 1213-1218
3. Workflow Management Coalition.: Interface 1: Process definition interchange process model. Technical report WfMC TC-1016-P (1998)
4. Van der Aalst. W.M.P.: Loosely coupled interorganizational workflows: modeling and analyzing crossing organizational boundaries. Information & Management 37 (2000) 67-75
5. Martin A., Sergei G., Andreas, H., Hans-Werner, P.: Using High-Level Petri Nets for Hierarchical Grid Workflows. Proceedings of the Second IEEE International Conference on e-Science and Grid Computing (2006)

Towards a Formal Foundation for Aggregating Scientific Workflows

Frank Terpstra, Zhiming Zhao, Wico Mulder, and Pieter Adriaans

Informatics Institute
University of Amsterdam
Kruislaan 419, 1098VA, Amsterdam, The Netherlands
{ftrpstra,zhiming,wicomul,pietera}@science.uva.nl

Abstract. In e-Science, scientific workflow systems are used to share data and knowledge in collaborative experiments. In recent work we discussed the concepts of a workflow bus [1], allowing multiple workflow systems to be coupled in a meta-workflow system with multiple execution models. In this paper we propose an approach for a formal model to perform the task of reasoning of about the execution models of such workflow systems. We propose that I/O Automata can be used as a formalism to prove the correctness of complicated workflows involving multiple workflow engines and execution models.

Keywords: I/O Automata, formalism, workflow design.

1 Introduction

In scientific workflow research many different implementations of workflow systems exist [2,3,4,5]. These systems vary in the formal models by which workflows are described and execution semantics are interpreted, sometimes even allowing multiple execution models within one system [2]. This is in part a result of the different types of applications they try to support, which can have very different requirements. It is also in part due to a lack of standards, each system having its own workflow definition language. The execution models in the Business Process community control easily map onto Petri Nets and thus formal reasoning about workflows is mostly done using Petri Nets [6]. But where business workflows are about describing actual business processes, scientific experiments are more constrained and need to be exactly reproducible. Within e-science not only are there more diverse execution models, there also is a need to use different models within one application. This can be catered for by systems such as Kepler [2]. Furthermore, the need to combine different workflow management systems within one scientific experiment is emerging. Solutions such as the workflow bus [1] are being developed within our research group to suit these needs.

Working with different execution models within one experiment can seriously complicate the design procedure. A way to prove the correctness of these complicated experiments is needed, as well as assistance in exploring the workflow design space. Therefore we need a formal model to reason about the associated

design issues. In previous work we used Turing machines as a formal model to reason about workflow design [7]. One of the advantages to this approach was that we could isolate the execution model in our formal description, allowing us to reason about every possible type of workflow. Being able to reason on this level can give a formal basis for studying meta workflow problems such as the workflow bus [1].

In this paper we introduce an existing formal model called Input Output Automata [8](abbreviated to I/O Automata), to perform the task of reasoning about workflow design.

2 Workflow Design Problem

To reason about workflow design one needs a formal model to represent workflows. One often employed formalism is petri-nets. They are well suited to study control flow in workflows [6]. There are more issues involved in workflow design:

– Connectivity, are two workflow components compatible both in data type and runtime behavior.
– Workflow Provenance, can the experiment be exactly reproduced using the provenance data recorded by a workflow system.
– Workflow representation, what level of detail is desired in a workflow description.

For our research into a workflow bus where multiple (sub) workflows with different execution models are connected, these other issues play a more important part. We propose the use of I/O automata as a formal representation for reasoning about workflow representation and runtime behavior.

I/O Automata were first introduced by Lynch and Tuttle [8], and have been used for the study of concurrent computing problems. They form a labeled state transition system consisting of a set of states, a set of actions divided into input- internal- and output actions(as illustrated in figure 3) and a set of transitions which consists of triples of state, action and state. This allows us to study the inherently concurrent nature of workflow systems. One of the characterizing properties of I/O Automata is that input actions are "input enabled", they have to accept and act upon any input. Figure 4 illustrates both that the "input enabled" property defines connections between automata as well as one I/O automaton being computationally equivalent to a composition of several automata.

We study reasoning about representation as a hierarchical problem. Here abstract descriptions should be computationally equivalent to detailed low level descriptions of workflows. This requirement is satisfied by a property called compositionality. In figure 4 compositionality for I/O automata is illustrated.

The composition of a workflow representation starts with a desired input and output as well as a set of available building blocks. The representation of a workflow needs to strike a balance between generality and specificness, resulting in an ideal workflow which is neither to abstract nor to detailed. This idea is illustrated in figure 2, both a top down and bottom up approach are possible.

In the first, the initial input and output requirements are refined into multiple workflow steps. In the second, existing resources are combined (automatically) until they satisfy requirements. The design process can be formalized in a lattice as we did in our previous work [7]. This lattice is set up between the most abstract and most detailed representations of the computational process that a workflow satisfies. In other words, in this design lattice only the representation differs. All different representations within this lattice are computationally equivalent.
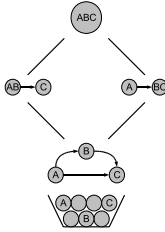
Fig. 1. Workflow design lattice
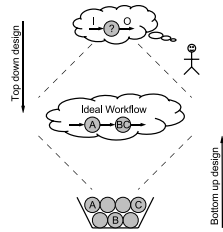
Fig. 2. Workflow design problem
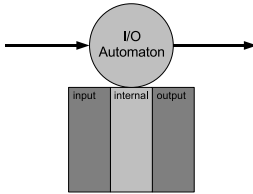
Fig. 3. I/O Automaton
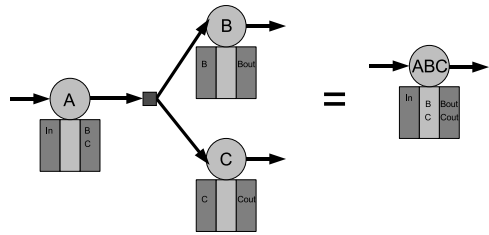
Fig. 4. Illustration of compositionality principle

Workflow components are very general computational elements, which can be modeled as an I/O Automaton. Workflow systems in practice use different execution models based on either data-flow or control flow. To model these execution models I/O Automata representing workflow components need constraints placed on them. In [9] it is shown how the Kahn principle, used as a basis for some data-flow execution models, can be modeled using I/O Automata. The main constraints are that the automata have to be deterministic and all connections are one to one.

3   Conclusions and Future Work

I/O Automata may not provide the answer to all problems involved in creating a workflow bus and other formalisms may be needed. However I/O Automata are suitable for reasoning about workflow representation as well as the runtime

behavior of complicated workflows involving multiple workflow engines and execution models. Using I/O Automata as a formalism, automatic workflow composition can be easily modeled and studied. In future work we plan to give a detailed overview of which formalisms are best suited to what part of workflow design. Furthermore we will show how existing tools for I/O Automata can be used to provide practical support in the workflow design process.

References

1. Zhao, Z., Booms, S., Belloum, A., de Laat, C., Hertzberger, B.: Vle-wfbus: a scientific workflow bus for multi e-science domains. In: E-science 2006, 2nd IEEE International Conference on e-Science and Grid Computing, Amsterdam Netherlands. (2006)
2. Ludascher, B., Altintas, I., Berkley, C., Higgins, D., Jaeger-Frank, E., Jones, M., Lee, E., Tao, J., Zhao, Y.: Scientific workflow management and the kepler system. Concurrency and Computation: Practice and Experience, Special Issue on Scientific Workflows **18**(10) (08 25 2006)
3. Majithia, S., Shields, M.S., Taylor, I.J., Wang, I.: Triana: A Graphical Web Service Composition and Execution Toolkit. In: Proceedings of the IEEE International Conference on Web Services (ICWS'04), IEEE Computer Society (2004) 514–524
4. Afsarmanesh, H., Belleman, R., Belloum, A., Benabdelkader, A., van den Brand, J., Eijkel, G., Frenkel, A., Garita, C., Groep, D., Heeren, R., Hendrikse, Z., Hertzberger, L., Kaandorp, J., Kaletas, E., Korkhov, V., de Laat, C., Sloot, P., D.Vasunin, Visser, A., Yakali., H.: Vlam-g: A grid-based virtual laboratory. Scientific Programming (Special issue on Grid Computing) **10** (2002) 173–181
5. Oinn, T., Addis, M., Ferris, J., Marvin, D., Senger, M., Greenwood, M., Carver, T., Glover, K., Pocock, M.R., Wipat, A., Li, P.: Taverna: A tool for the composition and enactment of bioinformatics workflows. Bioinformatics Journal. **online** (June 16, 2004)
6. Aalst, W.M.P.V.D., Hofstede, A.H.M.T., Kiepuszewski, B., Barros, A.P.: Workflow patterns. Distrib. Parallel Databases **14**(1) (2003) 5–51
7. Terpstra, F.P., Adriaans, P.: Designing worklfow components for e-science. In: E-science 2006, 2nd IEEE International Conference on e-Science and Grid Computing, Amsterdam Netherlands. (2006)
8. Lynch, N.A., Tuttle, M.R.: An Introduction to Input/Output Automata. CWI Quarterly **2**(3) (1989) 219–246
9. Lynch, N.A., Stark, E.W.: A proof of the kahn principle for input/output automata. Information and Computation **82**(1) (1989) 81–92

Autonomic Workflow Management in the Grid

Guangsheng Zhang[1, 2], Changjun Jiang[1], Jing Sha[1], and Ping Sun[1]

[1] College of Electronic & Information Engineering Tongji University
201804 Shanghai, P.R. China
`Zhanggstide@hotmail.com`
[2] The Public Security Bureau of Jinan 250001 Jinan, Shandong, P.R. China

Abstract. The autonomic workflow engine enables workflow to be dynamically specified and adapted using Event-Condition-Action rules. A new approach to autonomic execution of workflow processes based on matrix-based formulation was adopted that, together with the Petri net marking transition equation, provides a full dynamical description of a workflow system. We have built a workflow that models Traffic-information-grid-based Mobile Navigation Service to illustrate the quality of self-management using DEC through awareness of the computational environment.

Keywords: Grid, Workflow, Petri net, Discrete-event controller.

1 Introduction

In order to support complex scientific experiments and applications, grid services including computational devices, data, applications, and scientific instruments need to be orchestrated and composed while managing the application workflow operations within Grid environments. Thus grid workflow faces many uncertain factors such as unavailability, incomplete information and local policy changes. The complexity of workflow management in a grid context has sparked a great deal of interest in autonomic systems designed to run on the grid platform.

Autonomic computing [1] is touted as the means to realizing grid workflow systems capable of managing themselves with minimum human intervention. Bae J et al [2] propose a new approach to the automatic execution of business processes using ECA rules that can be automatically triggered by an active database. [3]presents a novel approach of using ECA rules to realize the workflow modeling and implementation for service composition. However, there are still many challenges that must be addressed by the research community. At runtime, as the execution proceeds, new components might be added to the application workflow and/or old components might be deleted. How can we dynamically add, delete, and change the algorithm used to implement each component at runtime?

Another issue in grid workflow is the balance between centralized and decentralized control.There are already many distributed business workflow management systems in the market. In [4], the Grid Workflow Execution Services is the dynamic and interactive execution of distributed workflows which coordinates the

composition and execution process of grid workflows. As far as we know, most workflow systems employ a centralized structure (see GridAnt and Condor). Dynamic SWMS [5] includes a human user in the runtime loop of a flow execution, and allows an engine to flexibly orchestrate a workflow according to the human decision and the runtime states of the environment. Some significant results in a supervisory control have also been obtained using Petri nets(PN) [6]. However, PN based workflow is hard to model uncertainty. There is a lack of supervisory-control techniques that can dynamically sequence different processes in the Autonomic Workflow Engine(AWE) according to the scenario and reformulate the process if some of the grid services fail.

In this paper, we propose the use of the matrix-based DEC as a central planner to produce high level missions for AWE. The DEC allows for tailored combinations of centralized and decentralized control by using the properties of block-matrix structures.   This paper presents the AWE that enables self-managing Grid applications. It extends the service-based grid computing paradigm to relax static (defined at the time of instantiation) application requirements and system/application behaviors and allows them to be dynamically specified via ECA rules. **A** new approach to autonomic execution of workflow processes based on matrix-based formulation was adopted that, together with the PN marking transition equation, provides a full dynamical description of a grid workflow system.

The rest of the paper is organized as follows. Section 2 describes the design and implementation of the AWE architecture. Section 3 illustrates self-managing behaviors enabled by DEC using Traffic-information-grid-based Mobile Navigation Service(TigMNS). Section 4 presents a conclusion.

2   Autonomic Workflow Engine Architecture (AWEA)

The AWEA focuses on setting up the application execution environment and then maintaining its requirements at runtime. As shown in Fig.1, the AWEA main modules include Workflow Runtime Manager, Autonomic Service Component(ASC) and Policy engine. The users can specify the requirements using an Application Strategies Editor. Each application(or mission) can be expressed in terms of the Policy engine which creates and manipulates policies. These policies are stored in the policy repository so they can be reused if the user comes back later in order to avoid renegotiation and redefinition of previously generated policies.

The Workflow Runtime Manager can be further divided into several parts: Online Monitoring and Analysis(OMA), DEC, Event server and Autonomic Execution. The OMA performs online *monitoring* to collect the status and state information using ASC sensors and *analyzes* ASC behaviors and detects any anomalies or state changes [1]. The DEC generates the appropriate control and management *plans*. The plan generation process involves triggering the appropriate rule from the list of rules (for the appropriate service) in the knowledge repository.

An ASC is the fundamental service building block .It is a simple computational cell(service agent) with encapsulated rules, constraints and mechanisms for self-management and dynamic interactions with other cells. It also extends autonomic cell defined in [1].The ASC implements two interfaces for importing/exporting the functionalities of the services component (functional port),sensing and changing the runtime state of the component(sensor port).For example in TigMNS, map service(S_2)

is a agent which produces a desired background digital map on a geographical data query formula. On receipt of a relevant event from sensor port, S_2 will be able to produce and listen for specific event types and content via local policy database to proper manage its sub-workflow processes such as data prefetching increase the display speed and to eliminate screen shake for thin terminal while PAD terminal need to filter out unsuitable ones. This is the sub-workflow autonomic management.
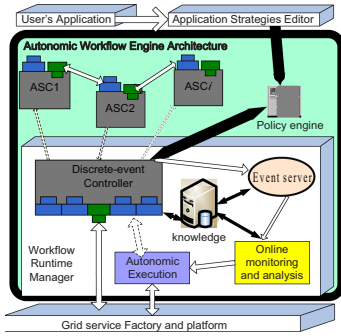
Fig. 1. AWE architecture
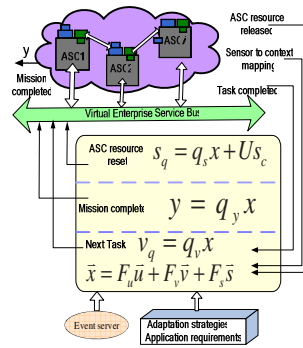
Fig. 2. System Level control architecture

2.1   Discrete-Event Controller (DEC)

A matrix-based DEC gives a very direct and efficient technique for both computer simulation and actual online supervisory control of DE systems[7,8]. In complex workflow systems, the interdependence of ASCs generates multiple events when a single change happens causing multiple rules to be triggered. The order of execution of rule actions determines the system behavior necessitating reasoning about execution order. For coordination problems of workflow systems we can write down a set of ECA rules to define **the mission planning** of the AWE, such as: **on** *event* **if** *condition* **do** *action*. The matrix-based DE controller allows one to easily represent these linguistic rules in a rigorous fashion. Let *s* be the vector of ASCs, *v* the vector of tasks that the services can perform, and *u* the vector of input events (occurrence of sensor detection events or content-based event notification[9], node failures, etc.). We define a mission as a prescribed sequence of tasks programmed into the Planer database. Let *y* be the vector of completed missions (outputs). Finally, let *x* be the state logical vector of the rules of the DE controller, whose entry of "1" in position *i* denotes that rule *i* of the supervisory-control policy is currently activated.

The DEC is based on formal equations that allow computation of the next tasks and ASCs to be assigned in the grid services pool. As shown in Fig.1, the DEC reads information from the Event server about sensor events, node failures, and ASCs availability. Then, it computes which tasks to start and which ASCs to assign or release, which are commands sent to the ASCs. In the following, all matrix operations are defined to be in the or/and algebra, where + denotes logical *or* and 'times' denotes logical *and*. The main equation is the controller-state equation

$$\bar{x} = F_u \bar{u} + F_v \bar{v} + F_s \bar{s} \tag{1}$$

where F_v is the task-sequencing matrix, F_s is the ASCs matrix, and F_u is the input matrix. F_v has element (i, j) set to "1" if the completion of task v_j is an immediate prerequisite for the activation of logic state x_i. The F_s has element (i, j) set to "1" if the availability of service (ASC $_j$) is an immediate prerequisite for the activation of logic state x_i. The overbar in equation (1) denotes logical negation so that tasks complete or resources released are represented by '0' entries.On the grounds of the current status of the workflow system, (1) calculates the logical vector x, i.e., which rules are currently activated. The activated rules determine the commands that the DEC has to sequence in the next iteration, according to the following equations:

$$v_q = q_v x \tag{2}$$

$$s_q = q_s x + U s_c \tag{3}$$

$$y = q_y x \tag{4}$$

Where q_v : task-start matrix and has element (i, j) set to "1" if logic state x_j determines the activation of task i. q_y : output matrix and has element (i, j) set to "1" if activation of logic state x_j determines the completion of mission i. q_s : ASC matrix and has element (i, j) set to "1" if the activation of logic state x_j determines the release or resetting of ASC_i ; U is any user-defined matrix of n x m dimensions (m can be equal to n but not smaller). n will assume the number of elements in the s_q column vector. Equation (3) can be read as follows: s_q can only be released if the relevant conditions (determined by q_s) are satisfied and the relevant user-defined service(s) is/are inactive. It is worth noting that the presence of the s_c element in the latter part of the equation serves only as an added validity check since the status of s_c is already present in x. Regardless of whether the engine has co-scheduled the entire workflow or incrementally scheduled specific services(q_s), the engine must know which services are currently active (executing), and which services are not yet active. For services that are active, the engine can (a) synchronously wait for them to complete, or (b) asynchronously terminate them. These can be used in any replanned workflow[9].It is noted that (2) and (4) are inspired by [8,7]. Equations (1)-(4) represent the rule base of the supervisory control of the workflow system, where the DEC equations are efficiently implemented using a software such as MATLAB [7].

2.2 Dynamical Description and Rules Termination Analysis

In complex grid systems, the interdependence of ASCs generates multiple events when a single change happens causing multiple rules to be triggered. The order of execution of rule actions determines the system behavior necessitating reasoning about execution order. However, the behavior of ECA rule set is complicated and it is difficult to analyze its termination property. We introduce a new notion called enforcement semantics that provides guarantees about rule ordering based on Conditional Color Petri net(CCPN)[10]. With CCPN, it can better express the behavior of ECA rules. The termination property of ECA rule set can be analyzed via

reachability graph or T-invariants[10]. The incidence matrix of the PN equivalent to the DE controller is obtained by defining the activity completion matrix and the activity start matrix as: $F = [F_u, F_v, F_s, F_y]; S = [S'_u, S'_v, S'_s, S'_y]$. The PN incidence matrix is then given by $M = S' - F$. A PN marking transition equation can be written as

$$M_{k+1} = M_k + M' x_k \qquad (5)$$

To put the DEC eqs. into a format convenient for simulation, one may write (1) as

$$\bar{x} = F\bar{m} \qquad (6)$$

The combination of the DEC (6) and PN marking eq. (5) provides a complete dynamical description of the system, which is inspired by[7,8].

3   Self-managing for TigMNS

At present, a mobile navigation system faces a lot of challenges, including: the universality and compatibility are poor; real time information service and dynamic navigation are weak; service personalization is insufficient. To overcome above problems, TigMNP was finished successfully(see Fig.3). It has four primary submodels: Personal service configuration, Mobile map generation, Individual QoS and DEC. Because different mobile terminals have different processing ability, and different wireless network has different capacity as well;this requires workflows that can be dynamically reconfigured on-the-fly on the receipt of important events from both external physical systems such as heterogenous terminals request through multiple wireless communications, and from other computational systems such as: real time transportation status on the whole route network based on STIG[11].
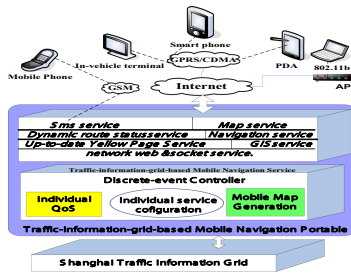
Fig. 3. Workflow Management for Traffic-information-grid-based Mobile Navigation Portable

Self-configuring behavior : self-configuring occurs on two levels. On one level, the AWE allows for a dynamic online assignment of tasks and ASCs based on Personal Service Configuration, given fixed DEC matrices F_v, F_s, q_v, and q_s. These matrices contain the task-sequencing and ASC-assignment information for fixed prescribed missions. In TigMNP, there are seven ASCs[11]:*Sms service(S_1) Map service(S_2),*

Dynamic route status service(S_3), Navigation service(S_4), Up-to-date Yellow Page Service(S_5), GIS service(S_6), and *network web &socket service(S_7).* Therefore, on a second higher level, self-configuring requires a modification of the DEC matrices as mission change, nodes fail, or additional nodes are deployed.

Self-optimizing behavior: a dynamic reallocation of the ASCs to missions can be performed by rearranging the "1"s in the matrices F_s and q_s when new missions are added. Some possible criterion could be the balance of workload of the ASCs, the minimization of circular waits and deadlock risks, the maximization of throughput (mission-completion time),Thanks to the matrix representation of the plans, these objectives can be governed via computationally efficient algorithms[7,8].

3.1   Implementation of a Mission

The procedure for implementing the supervisory-control policy consists of four different steps. (1) define the vector of S present in the system and the tasks they are able to perform. Here the ASC vector is $S = [s_1, s_2, s_3, s_4, s_5, s_6, s_7]$.(2) for each mission *i*, we define the vector of inputs u^i,of outputs y^i and of tasks v^i, and the task sequence of each mission. Then, we write down the ECA rules representing the supervisory coordination strategy to sequence the programmed missions (Tables 1 and2 for the mission1).(3) translate the linguistic description of the coordination rules into a more convenient matrix representation, suitable for computer implementation. (4) the formulation proposed in section 2.2 can be used to represent a CCPN. The termination property of ECA rules set can be analyzed using reachability graph[10].(5) if termination is satisfied then dispatch the command and the end else goto (2).

Table 1. Task Sequence of the Mission1

Mission1	description
Input(u)	S_7 connect DEC get Service Detail Code
T1	S_3 gives the traffic status report on given route
T2	S_4 provides a real-time dynamic navigation
T3	S_4 gives users a dynamic travel scheme
T4	S_5 provides GIS services to find a specific place
T5	generate answer message output y
Output(y)	Mission completed

Example: Given the Mission1: thin client with a connection to wireless network by CDMA 1x or GPRS **has request to get the best route between start point and destination.** Here, 'thin' means an application has to be installed locally and exchange information with background platform by a Socket connection[11]. We give the rule-base of Mission1 (Table 1) and the planer of services composition sequences(Table 2).We can easily write down the F_v, F_s as follows:

$$F_v = \begin{array}{c|ccccc} & T1 & T2 & T3 & T4 & T5 \\ X_1 & 0 & 0 & 0 & 0 & 0 \\ X_2 & 1 & 0 & 0 & 0 & 0 \\ X_3 & 0 & 1 & 0 & 0 & 0 \\ X_4 & 0 & 0 & 1 & 1 & 0 \end{array} \qquad F_s = \begin{array}{c|ccccccc} & S_1 & S_2 & S_3 & S_4 & S_5 & S_6 & S_7 \\ X_1 & 0 & 0 & 0 & 0 & 0 & 0 & 1 \\ X_2 & 0 & 1 & 0 & 1 & 0 & 0 & 0 \\ X_3 & 0 & 1 & 0 & 0 & 1 & 0 & 0 \\ X_4 & 0 & 0 & 1 & 1 & 0 & 0 & 1 \end{array}$$

With reference to (2),(3).we also get q_s, q_v (we omit them for limited space). Fig. 4 shows the Petri Net sequence of the task with its respective autonomic service components. There is no cyclic path in the CCPN. The termination of the CCPN is guaranteed according to the algorithm in [10]. This provides a feasibility check to ensure if the task, given the request and resource assignments and the planning process, will actually be executable or not.

Table 2. Mission1-Rule Base

Rule	Mission1-operation sequence
X_1	On u occurs if S_7 available then act T1
X_2	On T1 completed if S_4 and S_2 available then act T2 and T3
X_3	On T2 completed if S_5 available then act T4
X_4	On T3 and T4 completed if S_7 connected then act T5

Table 3. Testing results of thin clinets and SMS service using Autonomic Workflow Engine

	Service content	Response time (s)
thin clients	get the best route between start point and destination	10.5
SMS service	query for the real-time traffic status about the route segment	5.6
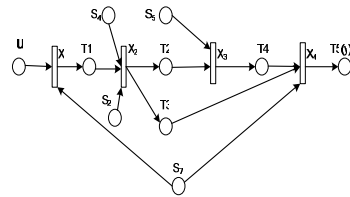
Fig. 4. CCPN representation of the mission1

3.2 Actual Running Effect

With the integration of our model to the Grid architecture, both sensor ports and functional ports of the autonomic service cell are implemented as WSDL documents. The publication/subscription structure is used for interactions between DEC and ASCs. The details of service selection and mappings of ECA rules to workflows are abstracted from the user and handled by the system itself.Fig.5 shows the result of the Mission1using AWE. When the event server(Individual Service Configuration)detects the thin terminal changes,it generates a new SDD code for DEC. Thus the AWE reconfigures the workflow (here deactive the GIS service) and dispatch S_2. To adapt to new context of service composition, the map server agent are customized for PDA (see Fig.6). Table 3 is the testing result of service answering speed for these two applications and better performance is achieved than [11].
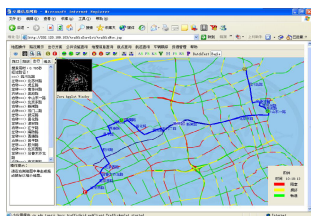
Fig. 5. Query result for thin client
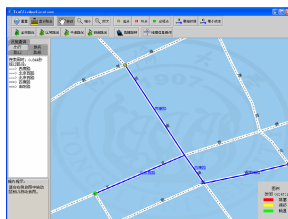
Fig. 6. Query result for PDA

4   Conclusion

The architecture enables grid workflow to be dynamically specified and adapted using ECA rules. In this architecture, enactment services can be added or removed on demand. Therefore, the whole engine will have high performance and high availability. Given the presence of such shared resources, simultaneous activation of conflicting rules may arise. That is, several tasks (possibly from different missions) may simultaneously request the same set of resources.

References

1. S. Hariri., et al., The Autonomic Computing Paradigm, Cluster Computing. 9(1), (2006) 5-17.
2. Bae J, Bae H, Kang SH, Kim Y., Automatic control of workflow processes using ECA rules. IEEE Trans. on Knowledge and Data Engineering,,16(8), (2004) 1010-1023.
3. L.Chen, et al., ECA Rule-Based Workflow Modeling and Implementation for Service Composition, IEICE Transactions on Information and Systems, E89-D(2) (2006) 624-630.
4. http://www.gridworkflow.org/kwfgrid/gwes/docs
5. Z.Zhao, et al., Dynamic Workflow in a Grid Enabled Problem Solving Environment, In proc. of CIT (2005) 339-345 .
6. Falk Neubauer, Andreas Hoheisel, Joachim Geiler., Workflow-based Grid Applications. Future Generation Computer Systems, Volume 22, Number 1-2, pp. 6-15.
7. J. Mireles, F. Lewis, Intelligent material handling: Development and implementation of a matrix-based discrete event controller, IEEE Trans.Ind. Electron., 48(6) (2001) 1087–1097.
8. V. Giordano et al, Supervisory control of mobile sensor networks: math formulation, simulation, implementation, IEEE Transactions on Systems, Man and Cybernetics, Part B,36(4) (2006) 806-819.
9. Craig A. Lee, et al, The Event-Driven Workflows towards A Posteriori Computing, Future Generation Grids, Springer-Verlag, (2006):3-29.
10. L. Baba-hamed, et al., Termination Analysis Approach and Implementation, Journal of Applied Sciences.,6 (8)(2006) 1738-1744.
11. FANG Yu, et al. A Mobile Navigation Service Platform Based on Traffic Information Grid. International Journal of Services Operations and Informatics, Vol.1 (2006) 23-37.

Framework for Workflow Parallel Execution in Grid Environment

Lican Huang

Institute of Network & Distributed Computing,
Zhejiang Sci-Tech University,
Hangzhou,P.R.China
Ministry's intelligent virtual research center, Zhejiang University
{huang_lican@}@yahoo.co.uk

Abstract. This paper presents a framework for Web Service based workflow optimisation in Grid environment. In this framework, parallel service is introduced as adaptor and container of parallel block of workflow. In parallel service, workflow is divided into multi sub-workflows, which are dispatched and executed in parallel at different workflow engines in different grid nodes. By this strategy, the performance of workflow can be enhanced greatly. In this paper, we also give a strategy how to guarantee the correctness in complicated network environment by redundant computing.

Keywords: workflow optimisation,Grid, e-Science,workflow Parallelization.

1 Introduction

Web service technologies are widely used in industry and research institutes. This brings in a variety of Web service composition languages and a variety of workflow engines available, some of which implement the same description language, but differ in their configuration, specific deployment description, and performance[1]. Grid[2] aims to solve resource and information sharing problems between virtual organizations. A variety of workflow management systems for Grid computing have been reported in literature. These range from portal-based interface for users to connect components together, to complete systems that allow composition and deployment of a set of services. Often these systems are categorized as being a Problem Solving Environment(PSE)[3]. In many ways, a PSE is seen as a mechanism to integrate different software construction and management tools and application specific libraries, within a particular problem domain. Often PSE and Grid Computing Environment are interchangeable – as PSE research predates the existence of Grid infrastructure. A key element within a PSE is therefore the provision of a workflow engine that enables a set of services (provided by one or more scientist) to be executed, in the context of a particular application. Workflow in PSE often is called as scientific workflow[4]. Scientific workflow is the workflow technology used by scientists to access and analyze

data in scientific research. Scientific workflow often requires support for large data volumes, high throughput computation or high performance computation.

Scientific workflow usually takes long time to execute, from several hours to several months. Therefore, scientific workflow optimisation is an important issue. There are several kinds of workflow optimisation: Static optimisation by re-order of workflow[5], Dynamic optimisation by selecting optimal service from multi semantic Web Services based on machine's status such as CPU speed, CPU load monitored just before the service is executed[6] and Workflow parallelization by dividing workflow into sub workflows which are executed in multi workflow engines.

Workflow parallelization for optimisation in Grid environment is a challenge issue. We need to discover the optimal workflow engines to execute sub-workflows. The workflow engines are differ in workflow languages, configuration, auto-deployment, etc. And the performance of workflow engines are differ in the quality and workload of host machines at the pre-execution point. We also need to solve fault-resistance in the complex network environment.

We present a framework for workflow optimisation in Grid environment. The discovery of suitable workflow engines is based on domain specific P2P - VIRGO [7], which is hybrid of structural and un-structural P2P technologies. We use parallel service as a container of sub workflows, which contains workflow parallelization, workflow engine discovery,dispatcher of sub workflows, collector of sub results, and integration of sub results into final result. The fault-resistance is solved by executing multi copies of sub-workflows in Grid environment.

The structure of this paper is as follows: Section 2 describes framework for workflow parallel execution in Grid environment; Section 3 presents implementation of prototype; and finally we give conclusions.

2   Framework for Workflow Parallel Execution in Grid Environment

In the workflow applications, the parallel blocks are re-written as parallel service as Figure 1 shows. Parallel service serves as adaptor and container of parallel block in workflow script. The script describing workflow block and parameters of the block are input into parallel service as parameters. After sub workflows are dispatched and executed in multi workflow engines, the results are collected and integrated into final result, and output as parameters into the successive Web service in the workflow script.

The parallel service contains workflow parallelization, workflow engine discovery, dispatcher,collector,and integrator shown in Figure 2. Workflow parallelization parallelizes the parallel block of workflow into multi blocks of sub workflows, which can be auto-deployed and executed in workflow engines. Workflow engine discovery discovers suitable workflow engines, which are active, support for corresponding workflow languages and lightweight workload, etc. Dispatcher dispatches sub workflows into multi Grid nodes which host workflow engines. Collector collects the results sent by the Grid nodes which have executed these sub workflows. Integrator integrates these results into a whole.
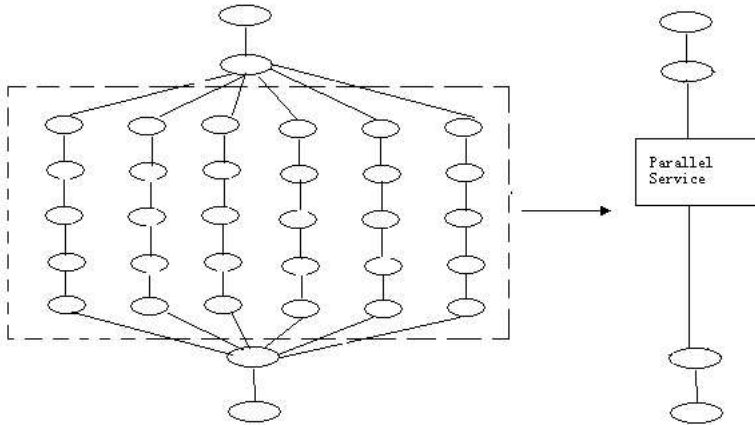
Fig. 1. workflow parallelization
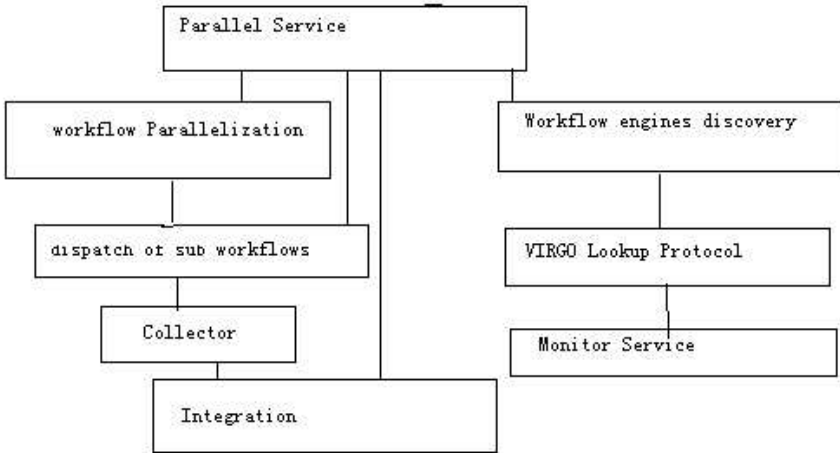
Fig. 2. The components of parallel service

Figure 3 shows the sequence of the framework of workflow parallel execution. The parallel blocks of workflow are transformed into parallel services in the workflow scripts at design time. Then the scripts are deployed. When client invokes workflow engine, the workflow engine will invoke services according to the script. When it encounters the parallel blocks, the engine will invoke parallel service. The parallel service first divides the parallel block into several sequential sub workflow scripts. Then, the parallel service discovers the suitable workflow engines, and then dispatches these sub workflow scripts into the Grid nodes which host the suitable workflow engines. After that, the parallel service collects the executed results by the Grid nodes and integrates these results into a whole. Finally, the parallel service sends the result to the workflow engine.
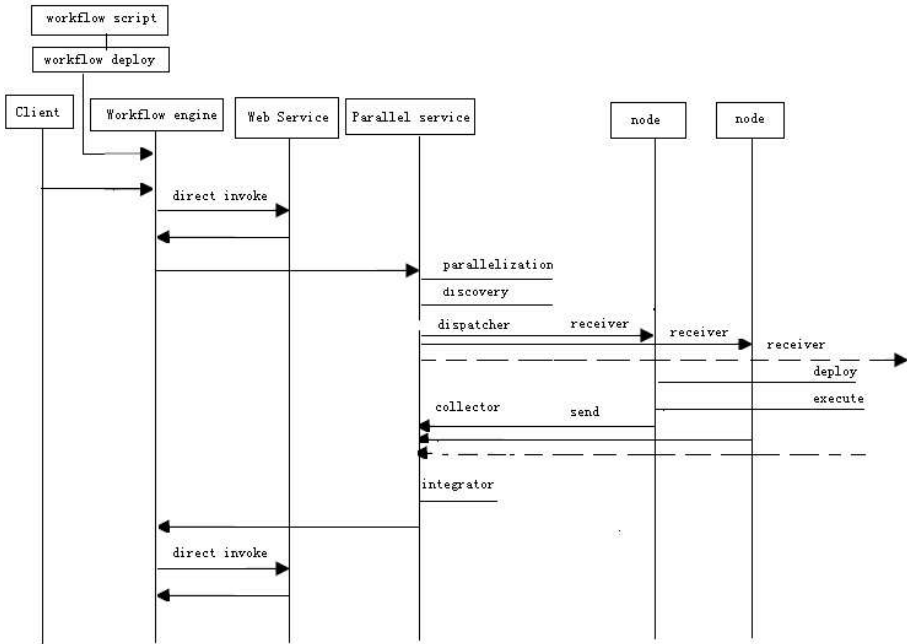
Fig. 3. The sequence of workflow parallelization

2.1   Workflow Parallelization

This module parallelizes workflow as multi sub workflow blocks. As Figure 1 shows, the block of workflow is parallelized as six sub blocks. This module also adds input and output parameters into sub workflow scripts. It concerns about analysis of workflow dependence graph. It may involve with the strategies for parallelism at multiple levels of workflow granularities in order to optimize workflow execution[8].

2.2   Workflow Engine Discovery

In the cluster of workflow engines, to find out the most suitable engine for a specific task is an important issue. Workflow engines are different in workflow languages, in the vendors and in performance, etc. The process of workflow engine discoverer is as follows: When workflow engine discoverer discovers the locations of workflow engines according to properties of required workflow engines (see Table 1) such as supported workflow languages, auto-deploy,operation system of hosts, etc., the host machines will invoke the processes of Ganglia[9] to get their performance data such as host workload, CPU speed, etc. Then workflow engine discoverer will collect information of suitable workflow engines which lists the locations, language, performance, availability, active time, failure frequency and so on for workflow engines. These workflow engines are optimally re-ordered by

their performance data. Finally dispatcher of parallel service will dispatch the
workflow sub blocks into those suitable workflow engines by the rule that the
workflow sub blocks are dispatched into those optimal workflow engines.

Table 1 shows some terminologies about workflow engine.

Table 1. Workflow engine description terminologies

workflow language
workflow engine
workflow engine stability
whether workflow engine is auto-deployed?
performance of workflow engine
host performance
Operation system of workflow engine host
etc.

Compared with discovering Web services with UDDI, there are no existed
standards to discover the workflow engines. We here use VIRGO P2P network
to discover workflow engines. VIRGO is a domain-related hierarchical structure
hybriding un-structural P2P and structural P2P technology. VIRGO consists of
prerequisite virtual group tree, and connections cached by least-recently used and
minimum distance replacement strategies. The workflow properties are published
into the nodes of VIRGO network which are the hosts of the workflow engines.
The workflow engines are classified as domain catalogues. The nodes containing
workflow engines join VIRGO network as the same domains as the classifica-
tions of workflow engines. The discovery of workflow engine uses VIRGO lookup
protocol[7][10] to find the suitable workflow engines. The main advantage using
VIRGO based distributed workflow engines discovery are that all hosts of suit-
able workflow engines can concurrently get performance data by Ganglia and
the discovery is effective when there are a large amount of Grid nodes.

2.3   Dispatcher

When workflow parallelization has divided workflow into many sub workflows,
the dispatcher dispatches these sub workflows to the suitable workflow engines.
The suitable workflow engines are chosen based on the strategies as following:

1. sub workflows are dispatched into different workflow engines.

2. the workflow engines which host many Web services of sub workflow prefer
to those which invoke Web service remotely.

3. the highest performance of workflow engines are preferred to be chosen. The
workload, CPU speed, etc of workflow engines are obtained by monitor such as
Ganglia.

4. the key sub workflows are dispatched into several copies of workflow engines
to solve the fault-resistance problems.

2.4   Collector

After dispatcher dispatched sub workflows to the workflow engines, and all workflow engines deployed and executed these sub workflows, the collector will receive the results sent by the sender of those workflow engines.

2.5   Integrator

When all results are collected by collector, the integrator will integrate the results into a whole. It will produce the parameters of output as the input parameters of the successor Web services.

3   Implementation of Prototype

We have implemented the prototype of parallel service. The parallel service is a standard Web service taking as adaptor of parallel blocks of workflow. We use XML document to represent the parallel block of workflow. In this XML document, the script of workflow block and the output interfaces of parameters are described.

We have implemented two classes –MasterNode, which dispatches subworkflow , and ExecuteNode, which executes subworkflow.

Class MasterMode includes functions of parallelization, which divides parallel block into subworkflows, discoveryWorkflowEngine, which discovers the optimal workflow enignes, Dispather, which dispatches subworkflows into the optimal workflow engines, Collector, which collects the results from workflow engines, and Integrater, which integrates the results into the whole result.

Class ExecuteNode includes functions of Receiver, which receives the message containing subworkflow script from Master Node , deployer, which automatically deploys the subworkflow script in workflow engine, Executer, which invokes subworkflow and get the result, and Sender, which sends the result to Master Node.

The following is pseudo code of parallelServiceProxy service:

```
public String[]parallelServiceProxy(String
XMLparallelXML,String[]parameters)
{
  subworkflowList =
     masternode.parallelization(XMLparallelXML,parameters);
  workflowEngines =
     masternode.discoveryWorkflowEngine(XMLparallelXML);
  masternode.Dispatcher(subworkflowList, workflowEngines);
  collectResults= masternode.Collector( message);
  results = masternode.Integrater(collectResults );
  return  results;
}
```

In the above, discoveryWorkflowEngine has following pseudo code:

```
public String[] discoveryWorkflowEngine( String XMLparallelXML )
{
   WorkflowEngineMeta = parse(XMLparallelXML);
   Send WorkflowEngineMeta to virgo-lookup protocol;
   workflowEnginesXML = get_response_of_virgo-lookup;
   workflowEnginesList=DecisionWorkflowEnigne(workflowEnginesXML);
      /*re-order optimally workflow engines by performance data*/
   return workflowEnginesList;
}
```

The pseudo code of Receiver in Execute Node is as following:

```
public void  Receiver(Message msg)
{
   subworkflowscript =  parse_workflowscript(msg);
   parameters =  parse_paremeters(msg);
   WebServiceURL = deployer(subworkflowscript,parameters);
   result = Executer(WebServiceURL);
   msg = modifyMessage(result);
   Sender(msg) to Master Node;
}
```

Every host machine of workflow engine installed virgo software. The functions of discoveryWorkflowEngine, Dispatcher and Collector in MasterNode class and functions of Receiver,Sender in ExecuteNode use virgo socket port to send and receive messages. The VIRGO node uses Tomcat as Web Server and Axis as Web service container. Every node implements Lookup protocol and VIRGO structure maintenance, and matchmaker and Register for Web Service and workflow engine. The messages are XML formed. The message type in the message is used to distinguish kinds of messages and indicates how to handle these messages.

We use BPEL4WS as experimental workflow language and Activebpel as workflow engines. The operation system for host machines of workflow engine is Linux. We have used simple example to do the experiments.

4   Conclusions

We have presented a framework for workflow parallel execution for workflow optimisation in Grid environment. In this framework, parallel workflow block is divided into multi sub-workflows, which are dispatched and executed in parallel at different workflow engines in different grid nodes. We also give a strategy how to guarantee the correctness in complicated network environment by redundant computing. We use parallel service as adaptor and container of parallel block of workflow. We insert parallel services into workflow script at design time as agents which execute multi sub workflows in parallel. Workflow engine discovery

is based on VIRGO protocol to effectively find suitable workflow engines. We also implemented the prototype of the framework. In the near future, we will use a real optimal workflow example from Bioinformatics to demonstrate the enhance effectiveness of Research via the strategy presented in this paper.

Acknowledgments

References

1. L. Huang, D. W. Walker, O. F. Rana and Y. Huang, "Dynamic Invocation, Optimisation and Interoperation of Service-oriented Workflow", CCGRID2005 WIP section, Cardiff 2005
2. I. Foster, and C. Kesselman, "Globus: A Metacomputing Infrastructure Toolkit", *International Journal of Supercomputer Applications*, 11(2): 115-128, 1997
3. O. Bunin, Y. Guo, and J. Darlington, "Design of Problem-Solving Environment for Contingent Claim Valuation", Proceedings of EuroPar, LNCS 2150, Springer Verlag, 2001
4. Bertram Ludascher, et.al, "Scientific workflow management and the Kepler system: Research Articles", Concurrency and Computation: Practice & Experience, 18(10): 1039 - 1065 , 2006
5. Yash Patel, Andrew Stephrn McGough and John Darlington, "Grid Workflow Scheduling In WOSE", UK e-Science Programme All Hands Meeting 2006 (AHM2006)
6. L. Huang, D. W. Walker, Y. Huang and O. F. Rana , "Dynamic Web Services Selection for Workflow Optimization", UK e-Science Programme All Hands Meeting 2005 (AHM2005)
7. L. Huang, "VIRGO: Virtual Hierarchical Overlay Network for Scalable Grid Computing", Proc. European Grid Conference (EGC2005), in LNCS 3470, pp911-921, February 14-16, 2005, Amsterdam, Netherlands
8. Michael J Pan and Arthur W Toga, "Multi-granularity parallelization for scientific workflow management", http://www.loni.ucla.edu/twiki/pub/Pipeline/ Research-Publications/parallelStrategies.pdf
9. Ganglia, 2006 http://ganglia.sourceforge.net/
10. L. Huang, "A P2P service discovery strategy based on content catalogues", the 20th CODATA International Conference, Beijing, China, 23-25 October

Toward Dynamic Adoption for a User's Situation Information in a Context-Aware Workflow System[⋆]

Yongyun Cho, Kyoungho Shin, Jongsun Choi, and Jaeyoung Choi

School of Computing, Soongsil University,
1-1 Sangdo-dong, Dongjak-gu, Seoul 156–743, Korea
{yycho,delio,jschoi}@ss.ssu.ac.kr, choi@comp.ssu.ac.kr

Abstract. Recently, there are many studies to adopt the workflow model, which has been successively applied to traditional computing environments, into ubiquitous computing environments for context-aware and autonomous services. A service in the ubiquitous computing environments must be executed according to a user's situation information, which is generated dynamically from sensors. However, such existing workflow systems as FollowMe and uFlow to support context-aware services through workflow models, can't immediately adopt changes of a user's situation into a already on-going service workflow. In this paper, we propose a context-aware workflow system, for ubiquitous computing environments, which can apply changes of user's service demand or situation information into an on-going workflow without breaking its operation. To do this, the proposed system represents contexts described in a workflow as a RDF-based DItree (Document Instance tree). The system uses the tree information to recognize a exact position to be changed in the on-going workflow for user's situation changes, and to reconstruct only the position under the influence of the changes in the DItree. Therefore, the suggested system can quickly and efficiently apply a change of user's new situation into a on-going workflow without a lot loss of the time and the space, and can offer a context-aware service continuously, according to a new workflow.

1 Introduction

A workflow model for business services in traditional distributed computing environments can be applied as a service model to connect services with others related in ubiquitous computing environments and express service flows [1]. Compared with traditional distributed computing environments, workflow services in ubiquitous computing environments must decide a service transition according to the user's situation information that is dynamically generated from various sensors in ubiquitous environments [4]. For that, a workflow system in ubiquitous environments must consider the user's situation information in service

executions of workflows. Workflow systems such as FollowMe and uFlow can supply context-aware services through workflows, which express user's situation services as service's execution conditions. Usually in the ubiquitous computing environments, the information dynamically occurs, and frequently changes initial conditions to execute a service. However, the existing workflow systems cannot apply the dynamically occurred changes into an on-going service workflow. Therefore, when changes of a user's service request or his situation information happen dynamically, we need a method that can re-apply the changes in a scenario and supply a context-aware service correspondent with the changes.

In this paper, we propose a context-aware workflow service system that uses contexts in a workflow service scenario as conditions of service execution, and dynamically derives service transition according to a user's situation information generated from real environments. To do this, the suggested system represents contexts described in the scenario as rule-based context subtrees. When a change of a user's situation information happens, the suggested system can dynamically reconstructs a workflow by modifying only the subtrees under the effect of ethe change. It means that the suggested system does not obstruct a flow of an earlier on-going context-aware service. Therefore, the suggested system uses the modified sub-tree's node information in comparison with user's situation information, and can support context-aware service continuously without stopping a on-going workflow.

2   Related Work

2.1   Workflow Languages for Context-Aware Services

From the studies to adopt workflow models to ubiquitous computing environments, we know that a workflow in a ubiquitous computing environment should consider not only result values but also context information as transition constraint for service execution. Unlike such workflow languages as BPEL4WS [5], WSFL [6], and XLANG [7], which do not consider a context information as transition conditions of services, uWDL [3] can describe context information as transition conditions of services through the <context> element consisting of the knowledge-based triplet - subject, verb, and object. uWDL reflects the advantages of current workflow languages such as BPEL4WS, WSFL, and XLANG, and also contains rule-based expressions to interface with the DAML+OIL [8] ontology language.

2.2   Workflow Systems for Context-Aware Services

WorkSco [10] is an situation-adaptable workflow system that can support service demands generated dynamically in a business process. It is based on a micro workflow model, a dynamic evolution and an open-point adaptation techniques to dynamically handle user's requests, which may be generated in various business domains. However, even though WorkSco considers dynamic handling for user's requests in a workflow system, it does not yet give an explicit method

to do that in ubiquitous computing environments. FollowMe [11] is an OSGi framework that unifies a workflow-based application model and a context model based on ontology. FollowMe uses a scenario-based workflow model to handle user's service demands from various domains. However, it does not support a method to handle user's service demands during service processing. uFlow [3] is a ubiquitous workflow framework to support a context-aware service based on a uWDL workflow scenario. Because uFlow is also based a workflow scenario like FollowMe, it does not yet consider a method to handle the changes of user's demands or user's situation information, such as user's position or user's doing, which can be dynamically generated during service processing.

3   A context-Aware Workflow Service System

3.1   A System Architecture

Figure 1 shows a architecture of a suggested context-aware workflow system, which is aware of dynamic changes of user's situation information in ubiquitous computing environments.
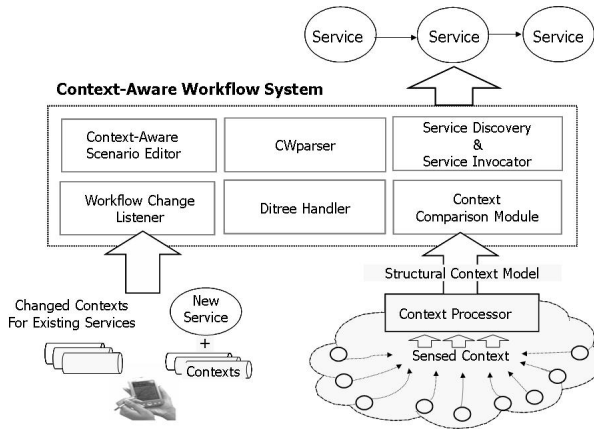
Fig. 1. An architecture of a suggested context-aware workflow system

As shown in Figure 1, a suggested system supports context-aware workflow services using a uWDL document. After a service developer or an end-user writes an uWDL workflow service scenario, the scenario is transmitted to the CWparser in Figure 1. The CWparser (Context Workflow scenario parser) represents contexts described in an uWDL scenario as RDF-based context subtrees through parsing. The CWparser constructs the RDF-based context subtree by using the structural context model [3]. And, the suggested system uses the model to objectify contexts, which is actually sensed from environments as the entities. The service discovery module searches a service appropriate to objectified contexts from an available service lists, and the service invocation module invokes the service.

3.2   A Context Comparison for Contex-Aware Workflow Services

The suggested system uses uWDL as a workflow language to compose a workflow scenario for context-aware workflow service. In Figure 1, the context comparison module compares contexts described in a uWDL workflow as transition conditions for a service in a context subtree with contexts objectified as entities through the structural context model for contexts sensed from ubiquitous environments. In the comparison, the suggested system drives an execution process of the service only if the context comparison module finds objectified contexts suitable as transition conditions of a service. Figure 2 shows a context comparison algorithm.

```
Boolean MatchContext(UC A, OCS B) {
  int j; /* For the index of context in B each context set */
  for each j in OCS B { /* Repeatedly comparing contexts in A, B context set */
    if ((A.UCs_type == Bj.OCs_type && A.UCs_value == Bj.OCs_value) &&
       (A.UCv_type == Bj.OCv_type && A.UCv_value == Bj.OCv_value) &&
       (A.UCo_type == Bj.OCo_type && A.UCo_value == Bj.OCo_value))
          return TRUE /* Found context match */
  } /* End for */
  return FALSE; /* Return matchresult */
}
```

Fig. 2. An algorithm for comparing UC A with OCS B

In Figure 2, OC means a context objectified with the structural context model, and it consists of OCs, OCv, and OCo, which mean subject, verb, and object entities, respectively. UC means a context described in a uWDL scenario. An OC consists of (OCs_type, OCs_value), (OCv_type, OCv_value), (OCo_type, OCo_value), and an UC consists of (UCs_type, UCs_value) (UCv_type, UCv_value), (UCo_type, UCo_value). UCs, UCv, and UCo mean subject, verb, object entities, respectively. A context consists of a pair of type and value. Also, OCS and UCS that mean each set of OC and UC can be defined as OCS = $(OC1, OC2, OC3, ..., OCi)$ and UCS = $(UC1, UC2, UC3, ..., UCi)$.

3.3   A Dynamic Adoption for Changes of User's Demands or Contexts

In ubiquitous environments, a user can meet the kaleidoscope of situations, and will want a new context-aware service for the changes. However, existing context-aware workflow systems , which are almost based on a context-aware workflow scenario including contexts as transition conditions of service, cannot adopt the changes of situations into already on-going workflows. The change may be a new service demand with new contexts as transition conditions for execution of the service. And, it may be modifying of contexts, which may be used as transition conditions for a service by an on-going workflow. If a user through hand-held equipments such as PDA, or PCS raises a change, the workflow change listener instantly catches the change and throws it to the DItree handler. Then,

the DItree handler finds parts influenced in a DItree of an on-going workflow scenario by the change and modifies only the subtrees around the parts. Figure 3 shows changes in a DItee for a sample uWDL workflow, after a user makes a new service demand including contexts as execution conditions of the service.
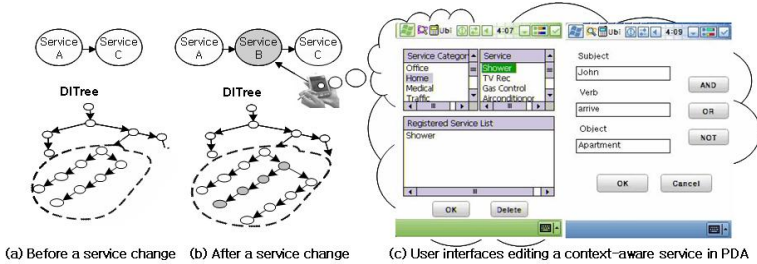
Fig. 3. Changes in a DItree when a user makes a new service and edit windows in PDA

In Figure 3(a), the suggested system will individually and automatically processes the service A and C according to contexts described as their execution conditions in a uWDL workflow. The dotted area in (a)'s DItree expresses RDF-based subtrees for the service A and C. Figure 3(b) represents the partial change of the DItree, when a user makes a new service, which may has to be between the service A and C orderly. A user needs interfaces to input a new service or modify a existing service through a his hand-held device. Figure 3(c) shows the workflow edit window that the suggested system offers. The workflow edit window consists of a service select window, which includes a usable service list and a registered service window, and a pop-up window to input RDF-based context information. For modifying contexts of a existing service, a user selects the service from the registered service lists in Figure 3(c). Then, he just modifies contexts through the RDF-based input fields. Now, to make a new service, a user selects a service, which he wants, from the service category window and the service list window. In the context information window of Figure 3(c), 'AND', 'OR', and 'NOT' buttons are for a composite context. Then, he has to input contexts, which are needed to execute the selected service. Figure 4 shows a demand process algorithm to adopt the changes into an on-going workflow and to do the dynamic reconstruction.

In Figure 3, because the service A and C are affected by a new service including its contexts as execution conditions, the DItree handler will re-constructs only the subtrees of the dotted area by using the demand process algorithm. The DItree's reconstruction happens partially and incrementally only in the part [12], which is influenced by workflow's changes. Therefore, the suggested system can quickly and efficiently make a new DItree including new demands or changes, with re-using the remaining parts of the DItree.

```
Input : An initial DItree and a user's new demand
Output : A DItree reconstructed against the changes

Method :

start demand_Process()
1.  Checks whether the demand is for a new service or for context
    modification of services, which exist already in the DItree.
2.  In the case of the former, calls make_Subtree() function, in the case of
    the latter, calls modify_Subtree() function.

    In make_Subtree(param1:DItee, param2:service, param3:contexts)
      1.  Makes a service node for the new service.
      2.  Makes a RDF-based subtree for execution conditions of the new
          service through the structural context model in Figure 2.
      3.  Calls a function find_Placeholder() to find a exact position that the
          subtree can be attached in the DItee.
      4.  Attaches the subtree onto the placeholder, that the
          find_placeHolder() returns.

        In find_Placeholder(param1:DItee, param2:subtree)
          1.  Traverses the DItee to find a position in which the subtree has
              to be inserted among service nodes of the DItee.
          2.  When the position is found, return the point of it.

    In modify_Subtree(param1:service, param2:contexts)
      1.  Moves the root node of subtree for a service, which will be
          modified.
      2.  Modifies the structures or contents of the subtree according to the
          contexts, which a user inputs to change.
end
```

Fig. 4. An demand process algorithm to adopt changes of contexts to a DItree

4   Experiments and Results

For an experiment with the suggested system, we develop a workflow scenario for smart home services in ubiquitous environments, and show how the suggested system can efficiently handle service demands generated dynamically from a user, and continuously support a context-aware workflow service. The scenario was developed in a uWDL editor [3]. The example scenario is as follows: John has a plan to go back his home at 10:00 PM, take a warm bath, and then watch a recorded TV program, which he wants to see after a bath. When John arrives in his apartment, an RFID sensor above the apartment door transmits John's basic context information (such as name and ID number) to the smart home server. If the conditions, such as user location, situation, and current time, are satisfied with contexts described in the workflow service scenario, then the server will prepare warm water. When he sits on the sofa in the living room after he finishes his bath, the service engine will turn on the power of the TV in the living room and play the TV program that was recorded earlier.

Now, let's again suppose that, as John is driving to his home, he needs a new service, which is a meeting preparation service with Tom at his home. The new service is to download files for meeting from John's PC in his office. That is a migration service about job environments.

If John arrives in front of his home's door with Tome, the sensed context OCs are not only for John but also for Tom. For example, the OCs may be John and Tom's locations, IDs, and Times. If John gave a priority to the meeting service during coming back to his home, the reserved bath service will be postponed after the meeting service. That is, the sensed context OCs, which are suitable
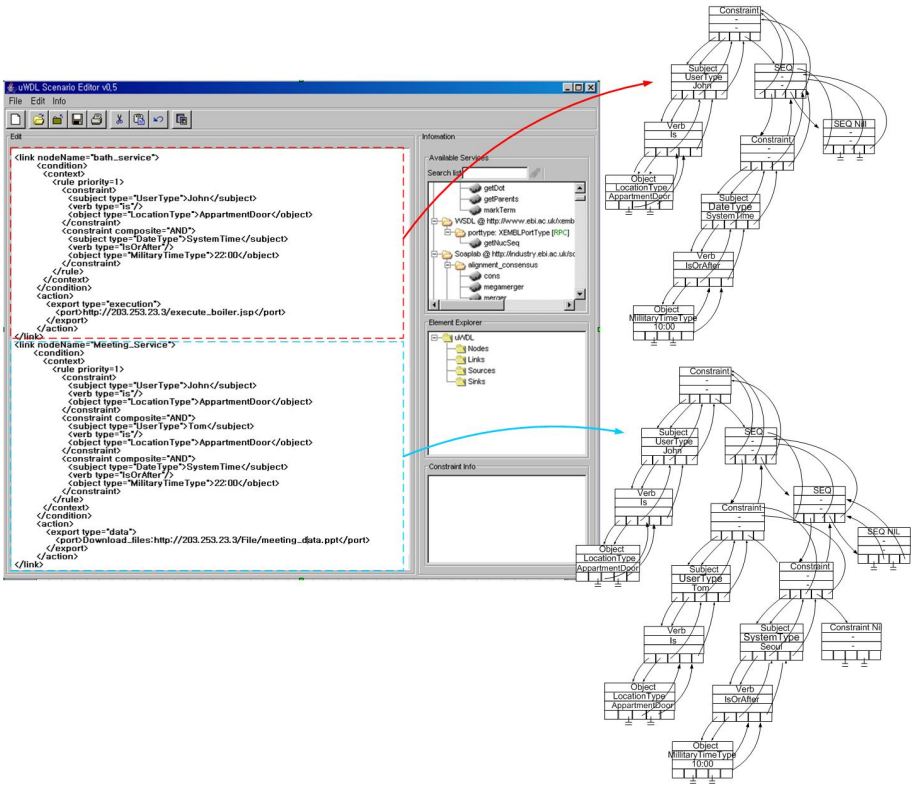
Fig. 5. The changes of the workflow scenario and its DItree

for both the bath service and the meeting service, will be applicable to the new service, not the bath service due to the priority. Figure 5 shows changes of the workflow scenario and its DItree after the DItree handler did dynamically adopt the new service to the initial workflow.

The bath service will be re-operated after Tom finishes the meeting with John, if John does not retract the bath service itself. In that time, the contexts as execution conditions of the bath service will be Tom's location and the meeting's situation. For example, if Tom locates out of John's house door and a value of the meeting's situation is over, the bath service will re-operate. After that, the suggested system executes remaining services in the workflow scenario according to contexts transmitted from the context processor.

5   Conclusion

In this paper we propose a context-aware workflow system dynamically to support user's service demands, by adopting changes of services or contexts into an initial workflow without interrupting the workflow. Through experiments, we

showed that the suggested system represented contexts described in the workflow scenario as RDF-based subtrees and a process of reconstructing a DItree. The proposed system uses an demand process algorithm to support context-aware services without interrupting through recognizing exactly the place holder that have to be changed in a workflow scenario and reconstructing only the part under the influence of the changes. Through an experiment with an example workflow scenario, we showed how the suggested system can reconstruct DItree for a user's new service demand. With the suggested system, a user can easily and efficiently apply his new service demands into a scenario document regardless of the time and the space. Therefore he can be served a continuous context-aware service according to a new workflow scenario adopted with the new service demands.

References

1. Workflow Management Coalition: The Workflow Handbook 2002, Future Strategies Inc. and Lighthouse Point, FL, USA., (2002)
2. Anind k. Dey: Understanding and Using Context, Personal and Ubiquitous Computing, Vol 5, Issue 1, pp.69-78 (2001)
3. Joohyun Han, Yongyun Cho, Jaeyoung Choi: Context-Aware Workflow Language based on Web Services for Ubiquitous Computing, ICCSA 2005, LNCS 3481, pp. 1008-1017, (2005)
4. Anand Ranganathan, Scott McFaddin: Using Workflows to Coordinate Web Services in Pervasive Computing Environments, Proceedings of the IEEE International Conference on Web Services, ICWS'04, pp. 189-197, (2004)
5. Tony Andrews, Francisco Curbera, Yaron Goland: Business Process Execution Language for Web Services, BEA Systems, Microsoft Corp., IBM Corp., Version 1.1 (2003)
6. Frank Leymann: Web Services Flow Language (WSFL 1.0). IBM (2001)
7. Satish Thatte: XLANG Web Services for Business Process Design, Microsoft Corp. (2001)
8. R. Scott Cost, Tim Finin: ITtalks: A Case Study in the Semantic Web and DAML+OIL, University of Maryland, Baltimore County, IEEE (2002) 1094-7167
9. W3C: RDF/XML Syntax Specification, W3C Recommendation (2004)
10. Pedro Vieira, Antonio Rito-Silva: Adaptive Workflow Management in WorkSCo, 16th International Workshop on Database and Expert Systems Applications (DEXA'05), pp. 640-645, 2005.
11. Jun Li, Yingyi Bu, Shaxun Chen, Xianping Tao, Jian Lu: FollowMe: On Research of Pluggable Infrastructure for Context-Awareness, 20th International Conference on Advanced Information Networking and Applications(AINA'06), Volume 1, pp. 199-204, 2006
12. C. Ghezzi and D. Mandrioli: Incremental Parsing, ACM Transactions on Programming Languages and Systems, 1(1):58-70, 1979.

A Dataflow-Oriented Atomicity and Provenance System for Pipelined Scientific Workflows[*]

Liqiang Wang[1], Shiyong Lu[2], Xubo Fei[2], and Jeffrey Ram[3]

[1] Dept. of Computer Science, University of Wyoming, USA
wang@cs.uwyo.edu
[2] Dept. of Computer Science, Wayne State University, USA
{shiyong, xubo}@wayne.edu
[3] Dept. of Physiology, Wayne State University, USA
jeffram@med.wayne.edu

Abstract. Scientific workflows have gained great momentum in recent years due to their critical roles in e-Science and cyberinfrastructure applications. However, some tasks of a scientific workflow might fail during execution. A domain scientist might require a region of a scientific workflow to be "atomic". Data provenance, which determines the source data that are used to produce a data item, is also essential to scientific workflows. In this paper, we propose: (*i*) an architecture for scientific workflow management systems that supports both provenance and atomicity; (*ii*) a dataflow-oriented atomicity model that supports the notions of commit and abort; and (*iii*) a dataflow-oriented provenance model that, in addition to supporting existing provenance graphs and queries, also supports queries related to atomicity and failure.

1 Introduction

Scientific workflow systems are increasingly used to execute scientific data management and analysis in many disciplines, such as biology, medicine, chemistry, physics, and astronomy. In contrast to traditional business workflows, which are task-centric and control-flow oriented, scientific workflows are data-centric and dataflow oriented. More specifically, in a business workflow model, the design of a workflow focuses on how execution control flows from one task to another (sequential, parallel, conditional, loop, or event-condition-action triggers), forming various "control-flows". In a scientific workflow model, the design of a workflow focuses on how the input data are streamlined into various data analysis steps using data channels to produce various intermediate data and final data products, forming various "dataflows".

Atomicity is an important transactional property, which requires that a transaction either runs in completion or has no partial effect (all-or-nothing). In scientific workflows, some task might fail during execution due to either the failure of the task itself or inappropriate input to a task. Despite the failure of tasks, a

---

[*] The first two authors contributed equally to this paper.

domain scientist might require a region of a scientific workflow to be "atomic" in the sense that either the execution of all the tasks in that region run to completion or none of them has any effect at all. However, traditional techniques for atomicity in transaction processing systems are inappropriate for complex long-running processes in distributed and heterogeneous environments. Compensation is generally considered as a proper way to handle rollback in business workflows [6], as it can eliminate effects of already committed transactions. The atomicity techniques based on compensation in business workflows [8,5] are not suitable for scientific workflows. They often require the explicit definitions of transaction boundaries which are obscured in our case due to the data dependency introduced by pipelined execution of workflows. Moreover, since scientific workflows are often computation-intensive, traditional rollback techniques are inefficient because the intermediate results of aborted transactions, which might be reusable in the future, are discarded.

Data provenance is closely related to the data lineage problem [3] studied in the database community, which determines the source data that are used to produce a data item. However, in scientific workflows, datasets are not necessarily contained in a relational or XML database and data processing cannot necessarily be accomplished by a database query. Therefore, existing approaches to the data lineage problem are not sufficient for solving the data provenance problem in scientific workflows. Moreover, although several provenance models (such as [2]) have been proposed for scientific workflows, none of them supports the notion of atomicity.

This paper proposes a novel dataflow-oriented atomicity and provenance system for scientific workflows. To the best of our knowledge, our system is the first one that supports both atomicity and provenance. It captures dataflows in scientific workflows, where data communications between tasks are modeled as enqueue and dequeue operations of a recoverable queue [1]. Transaction boundaries are not necessarily defined, instead, data dependencies are tracked and logged. Our system consists of two subsystems: atomicity management subsystem, which performs commit and abort, and provenance subsystem, which infers data dependencies and processes queries. The former is contained in the workflow engine; the latter can be outside. Although our system is based on the Kepler scientific workflow management system [9], our approach is general and can be extended to other systems.

2   Background

2.1   The Kepler Scientific Workflow Management System

The Kepler system [9] is an open source application to provide generic solutions to scientific workflows. In Kepler, a workflow consists of a set of "nodes" (called *actors*), which represent components or tasks, and a set of "edges" (called *dataflow connections*), which connect actors. Actors have *input ports* and *output ports* that provide the communication interfaces to other actors. Actors communicate by passing *data tokens* (called *token* for short) between their ports.

Each token is unique in the whole workflow. A unique feature of Kepler is that the overall execution and component interactions are coordinated by a separate component called *director* instead of implicitly defined in actors. Kepler provides a variety of directors that implement different computation models. In the process network model, each actor is an independent process or thread, and each dataflow connection is an asynchronous and unidirectional channel with unbounded buffers. Such scientific workflows execute in a pipelined fashion; our atomicity and provenance System is based on such a pipelined workflow model.

2.2   A Scientific Workflow in Biology

We implemented a scientific workflow in Kepler for a biological simulation project which analyzes the response of male worms to pheromone. The movement of a male worm is affected by chemical stimuli produced by female worms. Fig. 1 shows the workflow in Kepler. The actors `SampleFactory`, `EnvironmentFactory`, and `ModelFactory` provide parameters for simulations of male worms, environment, and their interactions, respectively. The actor `Simulation` repeatedly calculates the movement of worms over a time interval and the dispersion of the chemical. The actor `ImageDisplay` is used to show the result. The actor `StatisticalAnalysis` analyzes the simulations.
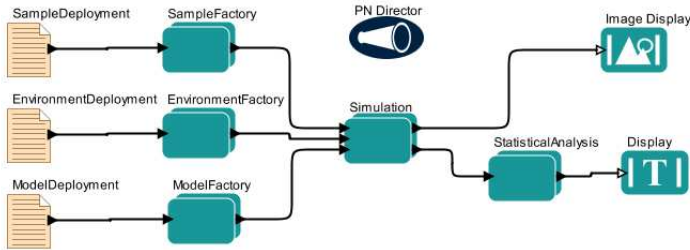
Fig. 1. A biological simulation scientific workflow in Kepler

3   The Atomicity Management Subsystem

We first define a formal model for scientific workflows adapted from the Kepler system [9] introduced in Section 2.1.

This paper makes some assumptions about the scientific workflows that we analyze. First, each actor is "white", *i.e.*, data dependencies between input tokens and output tokens are observable. Second, message-send-response relationships between actors and services are known. Third, each retriable Web service is modeled as a local actor (this is how it is done by Kepler), which calls the remote Web service on behalf of the user. Thus, the execution of all tasks are performed in a local machine except the execution of Web or Grid Services.

A workflow $W = \langle A, E \rangle$ consists of a set A of actors, and a set E of dataflow connections. Each actor $a \in A$ has a set of associated data ports, each of which

is either an input or output port. A dataflow connection bridges a set of output ports with a set of input ports.

3.1   Round and Data Dependency

In our atomicity model, a workflow execution invokes a series of actors to run. Each actor maintains a state which stores intermediate results computed from previous input tokens. A state indicates some data dependencies between the output tokens and the input tokens.

For example, Fig. 2 shows how the actors in Fig. 1 consume and produce tokens, and the data dependencies between tokens (which is shown in Fig. 2(d)). In Fig. 2(a), actor SF (*i.e.*, SampleFactory) consumes tokens f1 (number of males) and f2 (parameters for males), then produces token s1 (a sample of males). When SF calls reset(), its state is flushed. Then SF consumes tokens f3 (number of females) and f4 (parameters for females), and produces token s2 (a sample of females). Actors EnvironmentFactory and ModelFactory work similarly, which are not shown. In Fig. 2(b), actor S (*i.e.*, Simulation) consumes s1, s2, e1 (a set of environment parameters) and m1 (interaction model), saves s1 and s2 into its state, then produces a1 (a result). Next, S consumes e2 then produces a2. Before the next simulation starts, reset() is called to flush the state. In Fig. 2(c), actor A (*i.e.*, StatisticalAnalysis) produces an analysis result for each simulation. In the meanwhile, it saves the intermediate results in its state and finally performs a full analysis based on its state. This procedure continues after reset() is called.
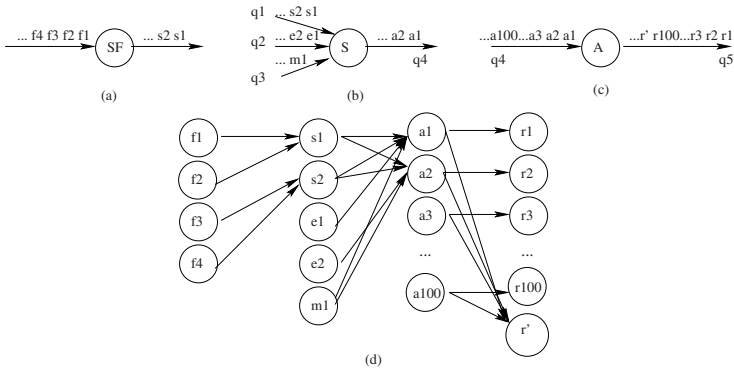
Fig. 2. Actors and data dependencies between tokens

A *round* on an actor is the whole events that happen between two consecutive (*i.e.*, no other reset events in the middle) reset events. Each round has a unique identifier in the workflow. Thus, an invocation of a workflow contains a series of actor invocations; each invocation of an actor contains one or more rounds. Round is decided by each actor itself. When an actor calls reset(), it tells the

workflow engine that the current round has completed. The call of `reset()` is a non-blocking operation. A reset event terminates the current round of data dependencies, and starts a new round of data dependencies. For each output token in a round, we assume that the actor can tell what input tokens that it depends on. Note that these dependent tokens might be some of the input tokens read so far (not the whole), as shown in Fig. 2(b), `a2` does not depend on `e1`. For a round $a.r$ on an actor a, let $input(a.r)$ and $output(a.r)$ denote its input and output tokens, respectively.

For two tokens t_1 and t_2, if t_2 is computed from t_1, we call t_2 *depends* on t_1, denoted $t_1 \rightarrow t_2$. For two rounds $a.r$ and $a'.r'$, if $\exists t.(t \in output(a.r) \wedge t \in input(a'.r') \wedge a \neq a')$, *i.e.*, $a'.r'$ consumes the tokens produced by $a.r$, we call $a'.r'$ *depends* on $a.r$, denoted $a.r \Rightarrow a'.r'$. Data dependencies are transitive: for token dependencies, if $t_1 \rightarrow t_2$ and $t_2 \rightarrow t_3$, then $t_1 \rightarrow t_3$; for round dependencies, if $a.r \Rightarrow a'.r'$, $a'.r' \Rightarrow a''.r''$, and $a \neq a''$, then $a.r \Rightarrow a''.r''$. Note that we do not allow cyclic transitive data dependencies on rounds. It is assumed that the workflows do not contain cyclic dataflows.

Let $depd\text{-}ancestors(a.r) = \{a'.r'|a'.r' \Rightarrow a.r\}$ (*i.e.*, all rounds that a round $a.r$ depends on) and $depd\text{-}descendents(a.r) = \{a'.r'|a.r \Rightarrow a'.r'\}$ (*i.e.*, all rounds that depend on a round $a.r$). They can be easily computed from the log introduced in Section 4.

3.2   Commit and Abort

Formally, we define the *atomicity* of a round as follows: the execution of a round $a.r$ is atomic if either it and all the rounds that depend on $a.r$ run to completion or none of them has any effect. Thus, users do not need to explicitly define transaction boundaries as in business workflows and database systems. Atomicities in the whole workflow are ensured automatically by our atomicity management subsystem. Although the atomicity granularity is based on one "round" of execution of a task in this paper, the technique can be readily extended for various granularities.

For two rounds $a.r$ and $a'.r'$, and $a.r \Rightarrow a'.r'$, if $a'.r'$ consumes only some early output tokens of $a.r$, $a'.r'$ might finish by calling `reset()` even when $a.r$ is still running. Thus, "reset" does not mean "commit" of the round, because we have to rollback both $a.r$ and $a'.r'$ if $a.r$ fails. A round $a.r$ *commits* if $a.r$ has been reset and every round in $depd\text{-}ancestors(a.r)$ has committed. If $depd\text{-}ancestors(a.r)$ is empty, $a.r$ commits once it is reset. Intuitively, a reset event indicates the ending of the current round and the starting of the next round, and a commit event makes the results of the round be observable to the users. The left column of Fig. 3 shows how the atomicity management subsystem commits a round $a.r$. When a round $a.r$ calls `reset()`, the atomicity management subsystem writes a reset event in a log, then repeatedly checks the log to see whether all rounds that $a.r$ depends on have committed. If the commit condition is satisfied, it commits $a.r$ by writing a commit event in the log.

In our system, each dataflow connection is modeled and implemented as an extended recoverable queue adapted from [1]. An extended recoverable queue

Commit algorithm for a round $a.r$
  while ($a.r$ has not been reset) **continue**;
  while (**true**)
    boolean toCommit = **true**;
    for all $a'.r' \in depd\text{-}ancestors(a.r)$
      if ($a'.r'$ has not committed)
        toCommit = **false**;
    if (toCommit)
      commit($a.r$);
      return;

Abort algorithm for a round $a.r$
  if ($a.r$ has already committed)
    print("cannot abort.");
    return;
  Stop the execution of $a.r$ if running;
  while (**true**)
    boolean toAbort = **true**;
    for all $a'.r' \in depd\text{-}descendents(a.r)$
      if ($a'.r'$ has not aborted)
        toAbort = **false**;
    if (toAbort)
      for all $t \in$ output($a.r$)
        getRecoveryQueue(t).$\neg enq(t)$;
      for all $t \in$ input($a.r$)
        getRecoveryQueue(t).$\neg deq(t)$;
      abort($a.r$);
      return;

Fig. 3. Commit algorithm and abort algorithm for a round $a.r$

is a reliable and fault-tolerant queue which supports the following operations: *enqueue* pushes a token at the head; *dequeue* removes a token from the end and returns the token; ¬*enq* undoes the operation of enqueue, *i.e.*, deletes an enqueued token; ¬*deq* undoes the operation of dequeue, *i.e.*, recovers a token that has been dequeued. After a round commits, its associated enqueue and dequeue operations cannot be undone.

When the atomicity management subsystem detects crashing of a round $a.r$, it will send *failure* messages to all actors that execute rounds in *depd-descendents* $(a.r)$ to abort the corresponding rounds, which are not necessarily the on-going rounds. A round $a.r$ *aborts* if all rounds in *depd-descendents*$(a.r)$ have aborted. The abort of a round will delete all output tokens, then recover all input tokens. Note that the "failure" event occurs only on the actor where $a.r$ runs, and "abort" events occur on each actor in *depd-descendents*$(a.r)$ and $a.r$ itself. The right column of Fig. 3 shows how the atomicity management subsystem aborts a round $a.r$. The atomicity management subsystem first checks whether $a.r$ has already committed, if not, tells the actor to stop the execution of $a.r$ if it is still running. Then, repeatedly check the log to see whether all rounds that depend on $a.r$ have aborted. During the abortion, the atomicity management subsystem looks up the log to find the corresponding recoverable queue for a given token t (*i.e.*, by calling `getRecoveryQueue`(t)); then it commands the recoverable queue to undo the previous operations. Finally, it writes an abort event in the log.

One optimization for the abort algorithm is: if both $a.r$ and $a'.r'$ are going to abort and $a.r \Rightarrow a'.r'$, during aborting $a'.r'$, we do not need to recover the tokens that are the output of $a.r$ and input of $a'.r'$ because they will be deleted again during aborting $a.r$.

4 The Event Log

Our atomicity & provenance system records the following events for supporting atomicity: *enqueue* (*enq*) a token; the counter-operation of *enq*, *i.e.*, ¬*enq*; *de-*

queue (*deq*) a token; the counter-operation of *deq*, *i.e.*, ¬*deq*; *reset* (*rst*) a state; *failure* of an actor; *commit* (*cmt*) a round; and *abort* (*abt*) a round. These events are stored in a sequential event log. Each row in an event log contains: *event identifer*; *time stamp*; *workflow identifier*; *round identifier* (which contains actor identifier); *queue identifer*, if the event is an *enq*, *deq*, ¬*enq*, or ¬*deq* operation; *event type*, which is one of event types listed above; *token identifier*, if the event is related with a token (such as enqueue or dequeue); and *dependent tokens*, which denote all source tokens used for producing the current token, if the event produces a token.

evt	tm	wf	rnd	que	type	tok	depdToks
01	-	-	$S.r$	q_1	deq	s_1	-
02	-	-	$S.r$	q_1	deq	s_2	-
03	-	-	$S.r$	q_2	deq	e_1	-
04	-	-	$S.r$	q_3	deq	m_1	-
05	-	-	$S.r$	q_4	enq	a_1	$\{s_1, s_2, e_1, m_1\}$
06	-	-	$A.r$	q_4	deq	a_1	-
07	-	-	$S.r$	-	$fail$	-	-
08	-	-	$A.r$	q_4	¬deq	a_1	-
09	-	-	$A.r$	-	abt	-	-
10	-	-	$S.r$	q_4	¬enq	a_1	-
11	-	-	$S.r$	q_3	¬deq	m_1	-
12	-	-	$S.r$	q_2	¬deq	e_1	-
13	-	-	$S.r$	q_1	¬deq	s_2	-
14	-	-	$S.r$	q_1	¬deq	s_1	-
15	-	-	$S.r$	-	abt	-	-

evt	tm	wf	rnd	que	type	tok	depdToks
01	-	-	$S.r$	q_1	deq	s_1	-
02	-	-	$S.r$	q_1	deq	s_2	-
03	-	-	$S.r$	q_2	deq	e_1	-
04	-	-	$S.r$	q_3	deq	m_1	-
05	-	-	$S.r$	q_4	enq	a_1	$\{s_1, s_2, e_1, m_1\}$
06	-	-	$A.r$	q_4	deq	a_1	-
07	-	-	$A.r$	q_5	enq	r_1	$\{a_1\}$
08	-	-	$S.r$	q_2	deq	e_2	-
09	-	-	$S.r$	q_4	enq	a_2	$\{s_1, s_2, e_2, m_1\}$
10	-	-	$S.r$	-	rst	-	-
11	-	-	$A.r$	q_4	deq	a_2	-
12	-	-	$S.r$	-	cmt	-	-
13	-	-	$A.r$	q_5	enq	r_2	$\{a_2\}$
14	...	...	...	...	...	...	...
15	-	-	$A.r$	q_5	enq	r'	$\{a_1, ..., a_{100}\}$
16	-	-	$A.r$	-	rst	-	-
17	-	-	$A.r$	-	cmt	-	-

Fig. 4. A log for an execution of the workflow in Fig. 2

Fig. 4 shows a part of the log file for a run of the workflow in Fig. 2. The left column shows an aborted workflow run. Round $S.r$ first dequeues s_1, s_2, e_1, and m_1 from queues q_1, q_1, q_2, and q_3, respectively. $S.r$ then enqueues a_1 (which is produced by S based on s_1, s_2, e_1, and m_1) into q_4. After round $A.r$ dequeues a_1 from q_4, $S.r$ crashes. Thus, we first abort $A.r$ by recovering a_1, then abort $S.r$ by deleting a_1 and recovering m_1, e_1, s_2, and s_1. The right column shows a successful run, where $A.r$ does not commit until $S.r$ commits.

5   The Provenance Subsystem

Based on the event log, we can build *token dependency graph*, *object dependency graph*, *round dependency graph* as in [2], and *token usage graph*, which are represented as directed acyclic graphs (DAG). The event log produced by our system contains all information of the event log in [2]. Therefore, our system can support all provenance queries listed in [2]. In addition, our system can support the atomicity and failure related queries, which are illustrated in the following examples.

– **What actors ever aborted rounds?**
  $q_1 := \{a | e \in log(\tau) \wedge type(e) = abort \wedge actor(e) = a\}$,

where the expression $e \in log(\tau)$ selects an event from the log τ, the expression $type(e) = abort$ checks that the event is an abort, and the expression $actor(e) = a$ obtains the actor that executes the event.

– **When a round $a.r$ runs, what actors simultaneously execute the rounds that depend on $a.r$?**
$q_2(a.r) := \{a'.r' | e \in log(\tau) \wedge a'.r' \in depd\text{-}descendents(a.r) \wedge round(e) = a'.r' \wedge time(e) < reset\text{-}time(a.r)\}$, where $reset\text{-}time(a.r)$ denotes the time when $a.r$ is reset, which is easily obtained based on the log.

6   Related Work

In recent years, scientific workflows have gained great momentum due to their roles in e-Science and cyberinfrastructure applications. There are a plethora of scientific workflows covering a wide range of scientific disciplines. A survey of various approaches for building and executing workflows on the Grid has been presented by Yu and Buyyaby [12].

Bowers et al. [2] propose the Read-Write-State-Reset (RWS) provenance model for pipelined scientific workflows within the Kepler framework [9]. The RWS model assumes that each output token depends on all tokens input so far in the current round, whereas our model refines this by assuming actors can tell what input tokens each output token depends on.

Although several provenance models [7,11,2,4,10] have been proposed for scientific workflows, there has been no work on the provenance system that supports the notion of atomicity.

Finally, although atomicity is a well studied topic in the context of databases in transaction processing and business workflows, there has been no work on atomicity in the context of "dataflows" and "pipelined execution" in scientific workflows. The read committed assumption that existing atomicity techniques are based on does not hold in pipelined scientific workflows, where both task parallelism and pipelined parallelism are present.

7   Conclusions and Future Work

We have proposed an architecture for scientific workflow management systems that supports both provenance and atomicity. We have shown that, while our atomicity system can support the notion of atomicity, currently at the round level that does not contain cyclic transitive data dependencies, our provenance system has added value to existing provenance systems as we support atomicity and failure related queries.

In the future, we will extend current atomicity and provenance models to various granularities of atomicity and for different models of computations. We will also investigate the atomicity problem for multilevel, distributed, parallel, and heterogeneous scientific workflows.

References

1. P. A. Bernstein, M. Hsu, and B. Mann. Implementing recoverable requests using queues. In *Proc. of the 1990 ACM SIGMOD international conference on Management of data*, pages 112–122. ACM Press, 1990.

2. S. Bowers, T. McPhillips, B. Ludascher, S. Cohen, and S. B. Davidson. A model for user-oriented data provenance in pipelined scientific workflows. In *Proc. of the International Provenance and Annotation Workshop (IPAW'06)*, Chicago, Illinois, USA, May 2006.

3. P. Buneman, S. Khanna, and W.-C. Tan. Why and where: A characterization of data provenance. *Proc. of the International Conference on Database Theory (ICDT)*, 1973:316–330, 2001.

4. S. Cohen, S. C. Boulakia, and S. B. Davidson. Towards a model of provenance and user views in scientific workflows. In *Data Integration in the Life Sciences*, pages 264–279, 2006.

5. W. Derks, J. Dehnert, P. Grefen, and W. Jonker. Customized atomicity specification for transactional workflows. In *Proc. of the Third International Symposium on Cooperative Database Systems for Advanced Applications(CODAS'01)*, pages 140–147. IEEE Computer Society Press, 2001.

6. H. Garcia-Molina and K. Salem. Sagas. In *SIGMOD '87: Proceedings of the 1987 ACM SIGMOD international conference on Management of data*, pages 249–259. ACM Press, 1987.

7. P. Groth, S. Miles, W. Fang, S. C. Wong, K.-P. Zauner, and L. Moreau. Recording and using provenance in a protein compressibility experiment. In *Proc. of the 14th IEEE International Symposium on High Performance Distributed Computing (HPDC'05)*, Research Triangle Park, North Carolina, U.S.A., July 2005.

8. F. Leymann and D. Roller. *Production workflow: concepts and techniques.* Prentice Hall, 2000.

9. B. Ludascher, I. Altintas, C. Berkley, D. Higgins, E. Jaeger, M. Jones, E. A. Lee, J. Tao, and Y. Zhao. Scientific workflow management and the kepler system: Research articles. *Concurr. Comput. : Pract. Exper.*, 18(10):1039–1065, 2006.

10. S. Miles, P. Groth, M. Branco, and L. Moreau. The requirements of recording and using provenance in e-science experiments. *Journal of Grid Computing*, 2006.

11. Y. L. Simmhan, B. Plale, and D. Gannon. A framework for collecting provenance in data-centric scientific workflows. In *Proc. of the IEEE International Conference on Web Services (ICWS'06)*, pages 427–436, Washington, DC, USA, 2006.

12. J. Yu and R. Buyya. A taxonomy of scientific workflow systems for grid computing. *SIGMOD Record*, 34(3):44–49, Sept. 2005.

Dynamic Workflow Management for P2P Environments Using Agents

Wallace A. Pinheiro[1,3], Adriana S. Vivacqua[1], Ricardo Barros[1],
Amanda S. de Mattos[1], Nathalia M. Cianni[1], Pedro C.L. Monteiro Jr.[1],
Rafael N. De Martino[1], Vinícius Marques[1], Geraldo Xexéo[1,2], and Jano M. de Souza[1,2]

[1] COPPE/UFRJ, Graduate School of Engineering
[2] DCC-IM, Dept. of Computer Science, Institute of Mathematics
Federal University of Rio de Janeiro, Brazil
PO Box 68.511 - ZIP code: 21945-970 – Rio de Janeiro, RJ – Brazil
[3] IME, Military Institute of Engineering
Pr. General Tibúrcio, 80 - ZIP code: 22290-270 - Rio de Janeiro, RJ – Brazil
{awallace, avivacqua, rbarros, amandasm, nathalia, calisto,
rmartino, vgmarques, xexeo, jano}@cos.ufrj.br

Abstract. Traditional workflow systems don't handle dynamic scenarios well, as they are centralized and pre-defined at the start of the project. In this paper, we present a P2P framework to support dynamic workflows, which uses contracts to deal with unexpected changes in the flow of activities. DynaFlow is an agent based framework, where agents take action when exceptions occur. DynaFlow could provide adequate support for E-Science experiments mapped into workflows instances, with tasks operating in distributed environments and diverse types of computational resources and data.

Keywords: P2P Systems, Dynamic Workflows, Workflow Flexibility, Agents.

1 Introduction

In-silico experiments are scientific processes in which structured activities can be designed to address questions that arise in scientific problem-solving [1]. These experiments can be mapped to scientific workflows that automate these processes, managing various interconnected tools and large scale data in multiple data formats, distinct environments, algorithms, applications and services. E-Science areas can benefit from workflow technologies, data parallelism and distributed environments to minimize execution time and enable collaboration, regardless of locations.

In these environments, problems such as node failure or unexpected participant changes have to be managed on the fly, creating a need for more flexibility. Furthermore, lengthy processes may have to be executed and any changes during workflow execution need to be handled so as not to lose work already done.

In order to support dynamic workflows, management tools should deal with two types of flexibility: a priori and a posteriori. The first one focuses on flexible behavior specification in order to achieve a behavior more precise and less restrictive in terms

of flow advance. The second one enables changes in the specification. In this case, it must be defined when and in what states these changes should be allowed, to guarantee consistency of the experiment throughout its life cycle.

Centralized coordination causes problems such as vulnerability, loss of flexibility and no guarantee of availability. The adoption of peer-to-peer (P2P) technology enables the construction of a system that decentralizes workflow control and management [2], adopting a low coupling structure with no central data repository, to increase workflow flexibility. Some example of E-Science workflows systems are Taverna [3], Kepler [4] and GridOneD [5].

The goal of our research is to analyze the main problems inherent to the definition and execution of dynamic workflows in environments characterized by flexibility and distribution. We adopt a P2P agent based environment, because they are decentralized, heterogeneous and dynamic. Besides, they enable spontaneous group formation by physically dispersed participants, leading to added flexibility in workflows. This paper is organized as follows: the next section presents the DynaFlow architecture and is followed by a brief discussion.

2   DynaFlow: Agents to Handle Workflows

DynaFlow is a peer-to-peer, agent based, framework to support dynamic workflows, which uses contracts to deal with unexpected changes in the flow of activities. Each peer can assume the role of workflow publisher or executor. The publisher peer will be responsible for the definition and publication of activities to the neighboring peers, and the executor peers are the peers that volunteer to execute at least one of the available activities. Each peer is supported by a group of agents that handles contracts and task assignment and execution, to enable dynamic adjustment of the system.

2.1   System Architecture

DynaFlow defines two applications built on top of the COPPEER framework [6], one Publisher and one Executor, each running on one peer. The following agents are implemented to control the workflow:

- Publisher – is the agent responsible for publishing workflows activities. This agent is started when a workflow has to be published or republished
- ActivityListener – is constantly waiting for new published activities. When it receives an activity that demands the same competence manifested by the executor, it inserts this activity on an activity list.
- Negotiation – the goal of this agent is to move contracts from executor to publisher and vice-versa.
- ContractReceiver – this agent receives contract proposals send by the Executor for the time established by the Chronometer Agent.
- Chronometer – controls system timeouts.
- ContractAnalyser – analyses contract proposals sent from the Executors. This agent can use several strategies to select which Executor will undertake an activity. For example, it can consider the minimum of time and cost.

- ApprovedContractListener – this agent receives approved contracts from the Publisher. It creates a list with the approved contracts. The Executor uses this list to confirm a contract to the Publisher.
- ConfirmedContractReceiver – this agent receives confirmed contracts (send by the Executor) and sends them to the Foreman Agent.
- Foreman – manages the execution orders. It sends the orders to Executors in the correct sequence and, when an activity depends of other activity, it waits the conclusion of its predecessor.
- ExecutionOrderListener – receives execution orders and shows to the Executor.

The publisher defines the activities, their structure and flow manually. From there on, all remaining actions will be executed autonomously by agents: contract receipt and analysis, activity republication, task result receipt, activity execution order definition, and so on. At the executor side, agents will receive available activities, approved contracts and execution orders. There are also agents to send notifications to the publisher. These notifications can propose, confirm or finalize a contract.

2.2 Contract

DynaFlow uses contracts to establish rewards and punishments that can be converted into a measure of reputation. These can be used to handle issues such as change in activity specification or incomplete execution. In this case, upon fulfillment of a contract, a peer increases its reliability degree, while a peer that breaks a contract has its reliability reduced. Table 1 shows typical contract terms.

Table 1. Contract Terms

Contract Terms
Publisher Reputation Grade and *Executor Reputation Grade*
Number of Evaluations (received by the publisher and executor)
Approval Limit Date (for the publisher to accept the contract proposal made by the executor)
Execution Order Limit Date (for the publisher to order the task execution)
Signature Date
Execution Period (after this, the executor pays a delay punishment)
Execution Period Extension (after this, the contract is rescinded)
Task Cost (processing time, trustworthiness, etc)
Period of Result Availability (after this, the executor can discard the result)
Subtasks Delivery (flag that indicates if the subtasks will be delivered after concluded)
Task Description, Subtask Descriptions and Subtask Weights to the Task
Status Check Period (for the executor)
Delay Punishment Value (processing time, trustworthiness, etc)
Rescission Conditions and Punishment Value (processing time, trustworthiness, etc)

Reputation can be a fundamental factor to decide whether a peer is trustworthy or not. Reputation systems provide a summarized (perhaps imperfect) history of another peer's transactions. Users use this information to decide to what extent they should trust an unknown peer before they themselves have interacted with it [7]. The initial

calculation of a peer's reputation is based on criteria adopted by schools to evaluate students: calculating the arithmetic mean of grades received by their evaluators.

Thus, each executor peer, after it has participated of a workflow, is evaluated and receives a grade for its participation. A new average will be calculated whenever a new grade is received. The publisher peer receives a grade calculated from the grades given by the executors. Historical grades (grades given and received) are stored by the executor as well by the publisher, and are composed by the workflow identification and the peer grade.

3 Discussion and Future Work

The possibility of task assignment and renegotiation provides new opportunities for handling events in E-science workflows. Revising a workflow after execution has begun is important for dynamic workflow control.

More efficient structures to handle the contract and its negotiation need to be defined. A good definition of the relevant contract metadata (e.g., time to execution, reliability of results, time to provision of results, etc.) enables appropriate task distribution and workflow adjustment. The definition of rules to handle events is also very important: if a result comes in that is not what was expected, how should the rest of the workflow be handled? Should the process be aborted? Can alternative results be obtained? Can these results be verified by other sources? Should the experiment be rerun? These actions will depend on the situation, but need to be addressed.

References

1. Singh, M. P.; Vouk, M. A.: Scientific Workflows: Scientific Computing Meets Transactional Workflows. Proceedings of the NSF Workshop on Workflow and Process Automation in Information Systems: State-of-the-Art and Future Directions, Univ. Georgia, Athens, GA, USA; 1996, pp.SUPL28-34.
2. Fakasa, G.J.; Karakostasb, B., 2004. A peer to peer (P2P) architecture for dynamic workflow management. In Information and Software Technology, Vol. 46, No. 6, pp. 423-431.
3. Goble, C., Wroe, C., Stevens, R., and the myGrid consortium, "The myGrid Project: Services, Architecture and Demonstrator", Proceedings UK e-Science All Hands Meeting 2003 Editors - Simon J Cox, p. 595-603, 2003.
4. Kepler , Kepler: Distribueted Kepler Visited July 27, 2006 http://www.kepler-project.org/Wiki.jsp?page=DistributedKepler
5. Taylor, I , Shields, M. , Philip, R. 2002, GridOneD: Peer to Peer visualization using Triana: A Galaxy formation Test Case In *UK eScience All Hands Meeting*, September 2-4.
6. Miranda, M.; Xexeo, G. B.; Souza, J. M, 2006. Building Tools for Emergent Design with COPPER. Proceedings of 10th International Conference on Computer Supported Cooperative Work in Design, Nanjing, v. I. p. 550-555.
7. Marti, S., 2005. Trust And Reputation In Peer-To-Peer Networks. A dissertation submitted to the Department of Computer Science and the Committee on Graduate Studies of Stanford University.

Analyzing Data Dependence Based on Workflow Net⋆

Yu Huang, Hanpin Wang⋆⋆, Wen Zhao, and Jiaqi Zhu

School of EECS, Peking University, Beijing, China, 100871
huangyu1979@gmail.com, whpxhy@pku.edu.cn

Abstract. Workflow management systems (WfMSs) frequently use data to coordinate the execution of workflow instances. A WfMS makes routing decisions according to data constraints. This paper presents an extended workflow net which has its business form and portrays data constraints among tasks which act as the decision condition. Data constraint is expressed by pre-condition and post-condition which formalize a task's input and output conditions. After introducing the model, we give an important definition of consistence related to data dependance. Then, we proposes a domain computation method during reduction to verify the consistence. The method considers data operation during reduction. In the end, a case study is analyzed by our method.

1 Introduction

Workflow has become an essential technology in e-business, providing a flexible and appropriate environment for development and maintenance of next-generation component-oriented information systems for enterprise applications [1]. Nowadays, workflow management systems have been widely deployed in the domains of administration, production, and scientific research in order to ensure high efficiency of business process.

There exist many formal models mainly aiming at control flow and resource perspective, e.g. [1][2][3], but few concerning data perspective. Data perspective mainly handles business documents and other objects which flow between activities, and local variables of the workflow. Data perspective is crucial for the correctness of a workflow execution, because routing decisions depend on it. There are a series of concepts that apply to the representation and utilization of data within workflow systems. [4] integrated workflow model with production data model to support production development. [5] proposed data guard to guarantee significant changes in data. Nevertheless, no articles have given formal models linking the business form with data dependence and verification methods to check the soundness related to data.

[2] proposed a subclass of Petri nets called the workflow net (WF-net) which models the control flow perspective of a workflow. Tasks are represented by transitions, and procedure logic is modeled by places and arcs. Some papers extended WF-net to model resource perspective, critical section, etc. [3] [7]. This paper gives an extended workflow net describing the data dependence. Then we introduce the inconsistent problem after adding data constraint. Therefore, we give the definition of data consistency. Furthermore, we propose a new method to verify its property.

The structure of the remainder is: section 2 states basic definitions about workflow and its extension. Section 3 discusses the conditional expressions and some new reduction rules for analyzing data consistency. This paper concludes in section 4.

2   Basic Workflow Definitions

In this section, we give the basic notions of workflow net and its extension.

Definition 1 (Petri net). *A Petri net is a triple (P, T, F) where:*

- *P is a finite set of places.*
- *T is a finite set of transitions, and $P \cap T = \varnothing$.*
- *$F \subseteq (P \times T) \cup (T \times P)$ is a set of edges.*

Given a Petri net (P, T, F), we will use the following notations: $^\bullet p = \{t| < t, p > \in F\}, p^\bullet = \{t| < p, t > \in F\}, ^\bullet t = \{p| < p, t > \in F\}, t^\bullet = \{p| < t, p > \in F\}$.

Definition 2 (Workflow net (WF-net)). *A Petri net $N = (P, T, F)$ is a WF-net if and only if:*

- *N has two special places: i and o where $^\bullet i = \varnothing$, $o^\bullet = \varnothing$.*
- *If we add a transition t^* to N, connecting place o with i so that $^\bullet t^* = i$, the Petri net N^* obtained is strongly connected. where t^* represents a transition which connects the output to the input.*

Definition 3 (Soundness). *A WF-net $N = (P, T, F)$ is sound if and only if:*

- *For every state or marking M reachable from state i, there exists a firing sequence leading from state M to state o. Formally:*
  $\forall_M (i \xrightarrow{*} M) \Rightarrow (M \xrightarrow{*} o)$
- *State o is the only state reachable from state i. Formally:*
  $\forall_M (i \xrightarrow{*} M \wedge M \geq o) \Rightarrow (M = o)$
- *There are no dead transitions in (N,i). Formally:*
  $\forall_{t \in T} \exists_{M,M'} i \xrightarrow{*} M \xrightarrow{t} M'$

Examples of the business process include insurance claim, visa application, goods ordering and goods transportation, etc. All these processes share three qualities: case-driven, process-essential and a predefined explicit procedure. Every process has a predefined (or predesigned) business form(B-form) or document, like a

visa application form, an order form of goods. Therefore, B-form is the key to define a workflow process. A B-form(document) is a view for an information set required to support a task which is the unit consisting of a workflow. A B-form is filled up and its content is changed when it is passed from task to task.

Definition 4 (B-form). *B-form is a set of typed variables which have been evaluated.*

Definition 5 (Domain Expression). *Domain expression is the following form:* $\{(variable_1, variable_2, \cdots, variable_n), (valueRange_1, valueRange_2, \cdots, valueRange_n)\}, n \in \mathbb{N}$. *E represents that all variables can be evaluated into arbitrary values which are allowed in their type. $\varnothing$ denotes that all variables cannot be valuated into any values.*

Domain expression is divided into two parts: one represents the variables, the other represents the respective evaluated ranges.

Definition 6 (Data Constraint). *The data constraint of a task indicates its precondition and postcondition. When a transition is fired, the B-form in this moment must satisfy its data constraint. Data constraint is composed of two parts: data constraint={precondition, postcondition}.*

The precondition and postcondition are represented by domain expressions which describe the constraint of variables in the B-form. The variables which aren't included in the precondition or postcondition represent that the fired transition does not care them. We call $\{precondition, postcondition\}$ bi-domain.

Definition 7 (Data Dependence Workflow net (DDWF-net)). *A DDWF-net is Five tuples $N = (P, T, F; \varphi, B)$, satisfying the followings:*

1. *(P,T,F) is a WF-net.*
2. *B is a B-form which is dealt with in the workflow. The initial values in B are null. And B_0 represents the initial B-form which means initial marking $M_0 = \{i = B_0\}$.*
3. *φ is a function from tasks to the set of data constraints.*

Figure 1 is an example of **application of leaving** in government affair processing. In the DDWF-net, B-form is represented by token. The variables in B-form is changed or copied by tasks which can be fired. Since every task has data constraint, there exists consistency between the B-form and data constraint. When
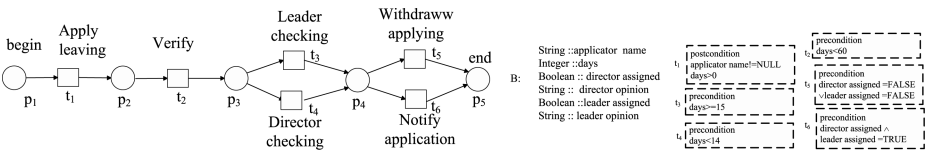
Fig. 1. An Example of DDWF-net

a task can be fired, we must evaluate whether the B-form satisfies its precondition. For example, in Figure 1, if t_2 can be fired and $days > 60$, then there exists conflict with the constraint of t_2. What is more, at the point of choice or parallel, we must judge whether the preconditions of following tasks have the relationship of choice or parallel. Actually, the decision-making must be consistent with the control relation. If p_3 has one token and the $days = 14$, dead state occurs. Therefore, we must give one method to solve these problems. Next, we define the property of consistency.

Definition 8 (Data Consistency of DDWF-net). *A DDWF-net $N = (P, T, F; \varphi, B)$ is consistent, satisfying the followings:*

1. *For every marking M which can be reachable from i, if every p in P and $M(p) \neq 0$, domain of every variable in B-form of $M(p)$ is in the union of respective variables in preconditions of $p^\bullet$.*
2. *For every place p, the intersection of every variable of preconditions in $p^\bullet$ is empty.*

According to the definition, place p_2 in Figure 1 dissatisfies item 2, since the intersection of variable days in the preconditions of t_3, t_4 is not empty. Therefore, data consistency is an import property.

3   Domain Computation Analysis Based on Reduction

Workflow process model is a description and specification model of business process. Structural and data conflict of process model is hard to be detected without computer aid. Therefore, an automatic mechanism is essential to discover errors in the model quickly, and the analysis of workflow has gradually become a hot yet difficult spot in the current workflow research. In [2], Aalst WMP made use of the analytical method of Petri nets to verify the soundness of Wokflow net(WF-net). Many scholars share in common with the idea of reduction which can be used to detect conflicts in models. The earliest is Sadiq who proposed several reduction rules to reduce workflow graph(acyclic graph) for detecting structural conflict[1]. However, there are no researches based on data dependence. How to verify the data consistency of a workflow model is a complex problem. In the following, we introduce a domain computation method based on reduction.

Definition 9 (Domain Operation). *Domain operation gives all the operators in domain expression.*

1. *divide(/): a/b means removing the variables in b from a and the result acts as the return of a/b.*
2. *symmetry substraction($\otimes$):$a \otimes b$ return the common variables and the commutative substraction of their ranges. For example: $((x, y), (\{1, 2\}, \{2, 3\})) \otimes ((x, z), (\{0, 2\}, \{1, 3\})) = ((x), (\{0, 1\}))$.*

3. *intersect($\cap$): $a \cap b$ return not only the common variables and the intersection of their ranges but also the different variables. For example: $((x, y), (\{1, 2\}, \{2, 3\})) \cap ((x, z), (\{0, 2\}, \{1, 3\})) = ((x, y, z), (\{2\}, \{2, 3\}, \{1, 3\}))$.*
4. *union ($\cup$): $a \cup b$ return not only the common variables and the union of their ranges but also the different variables. For example: $((x, y), (\{1, 2\}, \{2, 3\})) \cup ((x, z), (\{0, 2\}, \{1, 3\})) = ((x, y, z), (\{0, 1, 2\}, \{2, 3\}, \{1, 3\}))$.*

The intersect and union satisfy commutative laws and distributive laws:

1. *$a \cup b = b \cup a$, $a \cap b = b \cap a$.*
2. *$(a \cup b) \cap c = (a \cup c) \cap (b \cup c)$.*
3. *$(a \cap b) \cup c = (a \cap c) \cup (b \cap c)$.*

In order to relate data constraint to control flow, we define some conditional expressions to describe the computation of data constraint. We use the form $(pre_1, post_1)$ to represent data constraint.

Definition 10 (conditional expression(bi-domain computation)).
First, we introduce the basic operators.

1. *OR: $(pre_1, post_1) \vee (pre_1, post_2) = ((pre_1 \cup pre_2), post_1)$ if $post_1 = post_2$. Its semantics is if two elements have choice relationship and the same postcondition then the unitary precondition is the union of their preconditions.*
2. *AND: $(pre_1, post_1) \wedge (pre_2, post_2) = ((pre_1, post_1 \cup post_2))$ if $pre_1 = pre_2$. Its semantics is if two elements have parallel relationship and the same precondition then the unitary postcondition is the union of their postconditions.*
3. *ADD: $(pre_1, post_1) + (pre_2, post_2) = (pre_1 \cap (pre_2/post_1), post2 \cap (post_1/(pre_2 \cup post_2)))$ if $post_1 \subseteq pre_2$ that means the range of each variable in $post_1$ is a subset of the rang of respective variable in pre_2. This operation expresses the simple connection. If $\neg post_1 \subseteq pre_2$, then the expression would return to an error because of the occurrence of dead lock. Therefore, through estimating the condition, we can judge whether the model has the property of data consistency.*

Then, we introduce distributive laws in operators.

1. *$((pre_1, post_1) \vee (pre_2, post_2) \cdots \vee (pre_n, post_n)) + (pre, post) = ((pre_1 \cap (pre/post_1)) \cup (pre_2 \cap (pre/post_2)) ... \cup (pre_n \cap (pre/post_n)), post \cap ((post_1/(pre \cup post)) \cup (post_2/(pre \cup post)) \cdots (post_n/(pre \cup post))))$ if $post_1 \cup post_2 \cup \cdots post_n \subseteq pre$, otherwise $\neg post_1 \cup post_2 \cup \cdots post_n \subseteq pre$ would lead to deadlock and an error would be thrown. Therefore, according to this operator, we can judge the data consistency.*
2. *$((pre_1, post_1) \wedge (pre_2, post_2) \cdots \wedge (pre_n, post_n)) + (pre, post) = (pre_1 \cap pre_2 \cdots \cap pre_n \cap pre/post_1 \cap pre/post_2 \cdots \cap pre/post_n, post \cap (post_1/(pre \cup post)) \cap (post_2/(pre \cup post)) \cdots \cap (post_n/(pre \cup post)))$ if $post_1, post_2, \cdots post_n \subseteq pre$, otherwise dead lock would occur and an error would be thrown which dissatisfies the data consistency.*

3. $(pre, post) + ((pre_1, post_1) \vee (pre_2, post_2) \cdots \vee (pre_n, post_n)) = ((pre \cap (pre_1/ post)) \cup (pre \cap (pre_2/post)) \cdots \cup (pre \cap (pre_n/post)), post_1 \cap ((post/(pre_1 \cup post_1)) \cup (post_2 \cap (post/(pre_2 \cup post_2))) \cdots \cup (post_n \cap (post/(pre_n \cup post_n))))))$ if $pre_1 \cup pre_2 \cup \cdots pre_n \subseteq post$ and $\forall i, j, pre_i \otimes pre_j = E(i \neq j)$, *otherwise dead lock would occur and an error would be thrown which dissatisfies the data consistency.*

4. $(pre, post) + ((pre_1, post_1) \wedge (pre_2, post_2) \cdots \wedge (pre_n, post_n)) = (pre \cap pre_1/post \cap pre_2/post \cdots \cap pre_n/post, post_1 \cap post_2 \cdots \cap post_n \cap (post/(pre_1 \cup post_1)) \cap (post/(pre_2 \cup post_2)) \cdots \cap (post/(pre_n \cup post_n)))$ if $post_1, post_2, \cdots post_n \subseteq pre$, *otherwise dead lock would occur and an error would be thrown which dissatisfies the data consistency.*

Theorem 1 (Expression Consistency). *If a conditional expression can be computed to the form of one bi-domain and the precondition of the respective bi-domain is E, then the expression is data consistent. And during computing, if an error is thrown, the expression is data inconsistent.*

Because all computations of expressions keep the data consistency, the theorem naturally comes into existence.

After introducing the conditional expression or domain computation, we must solve the problem of how to construct the expression in order to compute whether the DDWF-net has consistent data constraints. We use the reduction rules to build the conditional expression. The following reduction rules keep soundness in control flow based on [1]. For the simpleness of reducing procedure, every place also has the (pre,post) constraint. In the beginning, the constraint of every place is (E, E) representing no restriction, i.e., all variables can be their typed values.

Reduction 1. *The sequential structure which is composed of two places and one transition can be reduced into a* ADD *conditional expression. Figure 2 shows the procedure.*

Fig. 2. Rule One

Fig. 3. Rule Two

Reduction 2. *The sequential structure which is composed of two transitions and one place can be reduced to a ADD conditional expression. Figure 3 shows the procedure.*

Reduction 3. *This rule describes the merging of xor-split and xor-join. Figure 4 shows the procedure.*

Reduction 4. *This rule describes the merging of and-split and and-join. Figure 5 shows the procedure.*
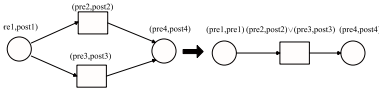
Fig. 4. Rule Three
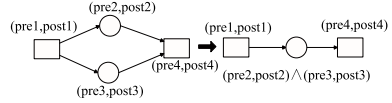
Fig. 5. Rule Four

Theorem 2 (Soundness and Data Consistency). *If a DDWF-net can be reduced to one place without any error and the precondition of the respective bi-domain is E, then DDWF-net is data consistent.*

According to [1], that one model can be reduced to one place means the model is sound. Due to theorem 1, that the conditional expression can be computed to one bi-domain denotes the model is data consistent. Therefore, this theorem comes into existence.

We give a DDWF-net which is sound but data inconsistent through applying reduction rules. Figure 6 shows the example. Its B-form has only three variables $x \in \{1,2,3,4,5,6\}, y \in \{0,1,2,3\}, z \in [0,1]$. And the respective data constraints are: $g_1 = (E,E), g_2 = (x > 2, E), g_3 = (x \leq 2, E), g_4 = (y > 2 \wedge x > 4, E), g_5 = (y \neq 3, E), t_1 = (E, (z > 0.5)), t_2 = (E, (y > 2)), t_3 = (E, (x > 4)), t_4 = (E, (z < 0.3 \wedge y = 3)), t_5 = (E, (x > 4)) t_6 = (E, (z > 0.2)), t_7 = (E,E)$, other places are equal to (E,E).
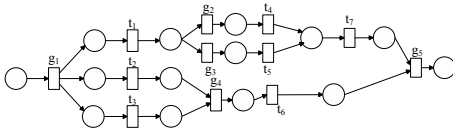
Fig. 6. DDWF-net with Data Inconsistent
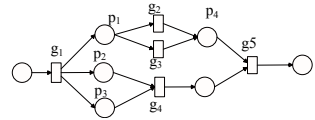
Fig. 7. DDWF-net After First Reduction

Furthermore, we construct the conditional expression through the reduction rules. Firstly, we apply the rule one and two to construct conditional expression which is shown in Figure 7. The respective data constraints are: $p_1 = t_1, p_2 = t_2, p_3 = t_3, p_4 = t_7, g_2 = (x > 2, (z < 0.3 \wedge y = 3)), g_3 = (x \leq 2, (x > 4)), g_4 := (y > 2 \wedge x > 4, (z > 0.2))$, others remain intact. Secondly, we apply the rule three and four shown Figure 8. The respective data constraints are: $g_6 = g_2 \vee g_3 = (x > 2, (z < 0.3 \wedge y = 3)) \vee (x \leq 2, (x > 4)), p_5 = p_2 \wedge p_3$. Thirdly, Figure 9 shows the third reduction. The respective data constraints are: $p_6 = p_1 + g_6 + p_4 = (E, (z > 0.5)) + ((x > 2, (z < 0.3 \wedge y = 3)) \vee (x \leq 2, (x > 4))) + (E,E) = (E, (z < 0.3 \wedge y = 3 \wedge x > 4)), p_7 = p_5 + g_4 = (E, (z > 0.2))$. At last, we reduce the model into one place, get one conditional expression, and judge whether it can be computed into one bi-domain. The conditional expression is $g_1 + (p_6 \wedge p_7) + g_5$. It is obvious that $(p_6 \wedge p_7) + g_5$ can throw an error. Actually, postcondition of $(p_6 \wedge p_7)$ satisfies $y = 3$, but the precondition of g_5 dissatisfies $y = 3$. Though the example is small, it shows that our method is correct and usable.
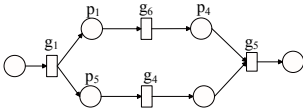
Fig. 8. DDWF-net After Second Reduction
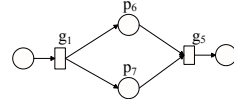
Fig. 9. DDWF-net After Third Reduction

4   Conclusion

This paper presents an extended workflow net which can describes business form and data constraints among tasks acting as the decision conditions. Data constraint is expressed by bi-domain, and we give an important definition of consistency related to data dependence. Then, we propose some domain operators and conditional expressions. During the reduction, we construct the conditional expression in order to analyze the data consistency. This paper also analyzes an example to confirm our methods. For further study, we will do more extended work on verification of our workflow model and implement a tool based on our method.

References

1. Wasim Sadiq, Maria E. Orlowska. Applying Graph Reduction Techniques for Identifying Structural Conflicts in Process Models. In M.Jarke and A. Oberweis, editors, Proceedings of the 11th International Conference on Advanced Information Systems Engineering (CAiSE '99), *Lecture Notes in Computer Science* vol. 1626: 195-209. Springer-Verlag, Berlin, 1999.
2. W.M.P. van der Aalst, The Application of Petri Nets to Workflow Management. *Journal of Circuits, Systems and Computers*, vol. 8, pp. 21-66, 1998.
3. Kees van Hee, Alexander Serebrenik, Natalia Sidorova, and Marc Voorhoeve, Soundness of Resource-Constrained Workflow Nets. *Lecture Notes in Computer Science* vol. 3536, pp. 250-267, 2005.
4. Nigel Baker, Alain Bazan, G. Chevenier, Florida Estrella, Zsolt Kovacs, T. Le Flour, Jean-Marie Le Goff, S. Lieunard, Richard McClatchey, Steve Murray, Jean-Pierre Vialle, An Object Model for Product and Workflow Data Management. *Proceedings of Ninth International Workshop on Database and Expert Systems Applications*, pp. 731-738, 1998.
5. Johann Eder and Marek Lehmann, Workflow Data Guards, *Lecture Notes in Computer Science* vol. 3760, pp. 502-519, 2005.
6. Bartosz Kiepuszewski. Expressiveness and Suitability of Languages for Control Flow Modelling in Workflows. PHD thesis, 2002.
7. Yehia Thabet Kotb, Andre Stephan Baumgart. An Extendted Petri net for modeling workflow with critical secitons. *Proceedings of the 2005 IEEE International Conference on e-Business Engineering*.
8. Jaeho Kim, Woojong Suh, Heeseok Lee. Document-based workflow modeling: a case-based reasoning approach. *Expert Systems with Applications* vol. 23, pp. 77-93, 2002.

Knowledge-Based Grid Workflow System

Marian Babik, Michal Laclavik, Zoltan Balogh, Ladislav Hluchy,
and Ondrej Habala

Department of Parallel and Distributed Computing, Institute of Informatics,
Slovak Academy of Sciences
Marian.Babik@saske.sk, Ondrej.Habala@savba.sk, Ladislav.Hluchy@savba.sk,
Michal.Laclavik@savba.sk

Abstract. In this paper we present design and development of the grid
workflow system based on the semantic grid services. We will highlight
the process of the discovery and composition of grid and web services
into workflows and semantic technologies supporting the users during
the workflow composition and evaluation of the results [13]. We will
describe in detail the challenges of the design and development of the
semantic grid service model, which is based on the Web Service Resource
Framework (WSRF) and the Web Service Ontology (OWL-S). Semantic
descriptions of the WSRF services as well as mapping of such descriptions
to the workflow model will be presented. Further, we will demonstrate
how experience management solutions can help in the process of service
discovery and user support. The system provides a unique bottom-up
approach in the Semantic Grids by combining the advances of semantic
web services and grid architectures [1].

1 Introduction

Recently, knowledge-based technologies are gaining importance in the imple-
mentation of the distributed systems and grids. Especially interesting is the
design and development of the service-oriented workflow systems, which tries to
automate the process of discovery, composition and execution of the services.
One such example is the semantic web services effort, showing the potential of
how ontological modeling can improve the shortcomings of the service-oriented
computing. In this paper we present a user-friendly knowledge-based workflow
system, which can support complex user interactions during the composition of
the workflow, e.g. automated composition of dynamic workflows based on the
user queries, storage and retrieval of the past workflows and results based on the
current user context. The system is based on our previous work [18] and tries
to reduce the complexity of the grid-based workflow systems by exploiting the
semantic descriptions of services, user context and experience.

The structure of the paper is follows: In Sections 2 and 3 we described the
underlying semantic and workflow technologies used in the system. Section 4
presents our approach in mapping the workflow model to the semantic web ser-
vices and the semantic descriptions of user context and experience. We conclude
with a flood-forecasting application scenario demonstrating the benefits of the
system and description of related work.

2   Web Ontology of Services (OWL-S)

OWL-S is an ontology-based approach to the semantic web services [9]. The structure of the ontology consists of a *service profile* for advertising and discovering services, a *process model* which supports composition of services, and a *service grounding*, which associates profile and process concepts with underlying service interfaces. Service profile (*OWL-S profile*) has functional and non-functional properties. The functional properties describe the inputs, outputs, preconditions and effects (IOPE) of the service. The non-functional properties describe the semi-structured information intended for human users, e.g. service name, service description, and service parameter. Service parameter incorporates further requirements on the service capabilities, e.g. security, quality-of-service, geographical scope, etc. Service grounding (*OWL-S grounding*) enables the execution of the concrete Web service by binding the abstract concepts of the OWL-S profile and process to concrete messages. Although different message specifications can be supported by OWL-S, the widely accepted *Web Service Description Language* (WSDL) is preferred. In the following we will denote the WSDL operations as O_i and input and output messages as M_{in}^j, M_{out}^j respectively.

3   Workflow Model

The services and the middleware for discovery, composition and execution is based on the Web Service Resource Framework (WSRF) [10], a recent standard for the grid services. Since we do not rely on the single service, but on the set of services, it is necessary to describe the application in terms of the *workflow*, which represents a control and data flow of the corresponding services. The representation of the workflow should be easy to use and intuitive, however it should also be able to cope with the complexity of the Grid, i.e. large number of services, dynamic scheduling, automatic handling of resource properties, etc.

We have relied on the workflow model based on the High-level Petri Nets (HLPN), which allows to compute the output tokens of a transition from the input tokens [17]. In this model service operations are represented as transitions. Each service operation is represented by the *transition T_i*, denoted by a thick vertical line. The variables of the formal parameters are represented as input, output *places*, P_{in}^j, P_{out}^j, shown as empty circles. Each place can hold a number of *tokens*, which represent the data items of the parameters. The input and output parameters of the operation are shown as input and output *edge expressions*, respectively. Additionally, each transition can have a set of Boolean *condition* functions. Firing transition and thus calling the service operation is only allowed if all of its conditions evaluate to true. Given the individual service representation, we can describe the complex workflows by connecting the output places of one transition with input places of another transition. All of the mentioned concepts and relations are defined in the form of an XML-Schema as Grid Workflow Description Language (GWorkflowDL). A detailed description of the

GWorkflowDL and High-level Petri Nets is beyond the scope of this document and can be found in [17].

4 Semantics

4.1 Overview

In order to support the complex user interactions, automated discovery, composition and execution of service operations, it is necessary to provide a mechanism for semantically describing the set of services, users, application domains and grid environment [6]. Semantic descriptions together with the related Semantic Web technologies can then allow to automatically discover services based on the user query, compose the services into the workflow, optimize the execution of the service operations and present the results in a clear and understandable way. Further, it can support collaboration among users, possibility to store and re-use the important results and workflows gathered by previous runs.

The knowledge captured by the semantic descriptions in the form of ontologies has two major areas: semantic description of services allowing to discover, compose and execute the workflows and semantic description of user context and experience. In the area of semantic service descriptions we have used the upper ontology of services OWL-S [9]. In the area of the user context and experience we have relied on the ontological descriptions and mechanism defined by the knowledge and experience management. In the next section we will describe the service descriptions and its mappings to the workflow model as well as the issues we faced during the extension of the OWL-S standard to the grid services. In Section 4.3 we will present our approach in describing the system context and experience.

4.2 Semantic Description of Grid Services

Our description of services has three layers: *grid layer*, represented by the WSDL operations and messages, *workflow layer*, represented by the GWorkfloDL elements and *ontological layer*, represented by the OWL-S and OWL ontologies (see Fig. 1). The corresponding mapping between grid and workflow layer is quite straightforward. Each workflow transition T_i represents one WSDL operation O_i, whose input/output messages $M_{in/out}^j$ are mapped to input/output tokens $P_{in/out}^j$. Ontological layer provides semantic description of services in terms of service *profile* and *grounding*. Service *process* is atomic thus leaving the workflow description to the *workflow layer*. Service *profile* functional properties, i.e. inputs, outputs, preconditions and effects, are described by the corresponding domain concepts, e.g. flood-forecasting concepts - river, basin, location, watershed. Non-functional properties are described by service name, service providers, quality of service metrics and service classes (hierarchy of services). Service *grounding* maps the functional properties to the actual WSDL messages. Since we already have such information in the *workflow layer*, we provide service *grounding* descriptions only for compatibility purposes. This means, that based on the service
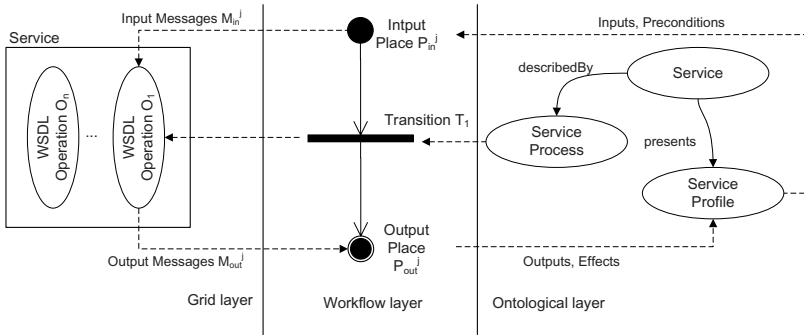
Fig. 1. Layers of the service description with corresponding mapppings

profiles, we can infer whether it is possible to connect inputs and outputs of any two services and thus create workflow [12]. Since OWL-S is based on the OWL-DL we can use any OWL-DL capable reasoner for this task. Another benefit of such approach is that we have a direct mapping between workflow transitions and service *profile*. [1]

4.3   Semantic Description of User Context and Experience

Capability to store and re-use knowledge is presented in several system requirements such as possibility to store and re-use previous workflows and results, guide the users during the workflow composition according to previous experience or creating workflows based on user queries. These requirements reflect the fact that in the system with many services and users, everyone can benefit from the previous cases experienced by others. An example of such functionality is creation of a workflow from a simple query such as, flood-forecasting for tomorrow for the basin of Danube river. The answer to such query is a list of services together with list of notes describing each service an its suitability for the requested area and time. Upon selection of the concrete service the system should be able to either compose the workflow or show all fitting workflows computed previously by other users. It should also suggest the location of available results for the given query. In order to provide such functionality it is necessary to find a suitable technology, which can semantically describe the user context and experience.

  Semantic description of user context and experience allows to determine similarity and relations among different contexts experienced by other users. This is the domain of the knowledge and experience management [19], where such functionality is defined as a capability to collect lessons from the past associated to cases. Experience of the user is modeled as a Case-Lesson pair (C, L), where C denotes the *Case Space* and L denotes the *Lesson Space*. The Case Space C

---

[1] The described mapping is implemented by the tool available under EDG license at: http://http://www.tuke.sk/fei-cit/babik/wsrf2owls/

is usually represented as a set of vectors c, whose elements determine the user context. The Lesson Space L is a set of notes (i.e. free text), workflows and results, which have the form of some global URI. The elements of the user context vector c are simply instances of the ontological concepts, i.e. instances of the domain concepts such as concrete time, city, basin or instances of the service concepts, i.e. service descriptions.

Given the Case-Lesson pair database and the current user context vector c_u, the system can compare its similarity to the previous cases and list the most relevant Lessons L to the user. The similarity of the two vectors c, c_u is determined by using an ontological similarity metric based on similarity graphs [20].

The actual build-up of the current user context vector c_u is based on user queries and actions in the user interface, e.g. user query: "Flood-forecasting for tomorrow in Bratislava" would result in the context having the following instances ($DaveF2DVisualization, Bratislava, Danube, 241206$); the vector contains instances of the concepts Service, City, River, Date, which were determined from the user query. As previously described, evaluating the current user context vector c_u results in the list of lessons from previous cases. Based on the user actions in this list, the user context can be further extended/updated, e.g. by clicking on the note describing the service $DaveF2DVisualization$, the system can present other similar services and update the context based on next user decisions. If the user is interested in the concrete workflow or result, its URI is then used to enact the workflow engine and either run the workflow or present its results. A special case is the possibility to compose the workflow based on the identified service (as was described in Section 2).[2]

5   Application Scenario

In this section we present a scenario which showcases the functionality described in previous sections[3]. The scenario is hosted by the K-WfGrid user portal shown in Fig. 2 [13]. The portal has only three main components: control panel, user assistant and workflow panel. The *user assistant* guides the user throughout the composition and execution of the workflow, which is shown in the *workflow panel*. The workflow can be started, stopped or suspended at any time by using the *control panel*, which also provides a list of tasks that the user needs to accomplish in order to make progress (e.g. provide input data).

The system allows the user to type a free text query, e.g. flood forecasting in Bratislava. The *user assistant* parses the query and determines the user context, e.g. in this case the list of services appropriate for the region and concepts reflecting the location and basin. This context is presented as a list of clickable concepts, which the user can select. Based on the user selection the *user assistant* displays the list of relevant lessons, e.g. past workflows, results and notes

---

[2] An implementation of the described approach is available at http://www.ikt.ui.sav.sk/?page=software.php

[3] A captured demo session can be found at http://www.gridworkflow.org/kwfgrid/distributions/movie-09-ffsc-red.avi
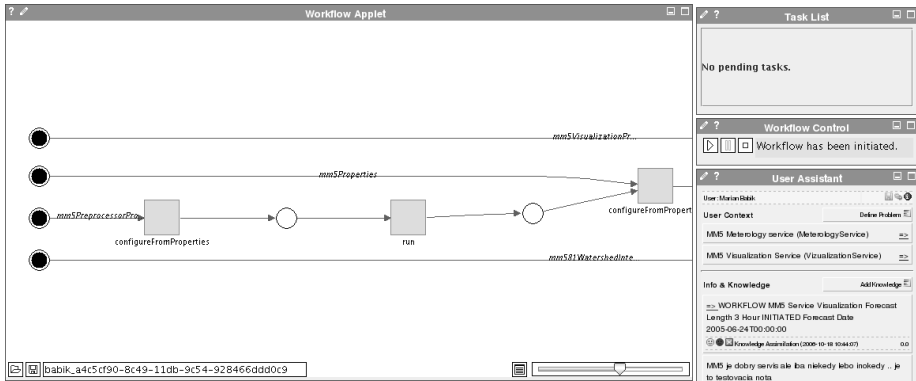
Fig. 2. K-Wf Grid portal with *control panel* (top right), *user assitant* (bottom right) and *workflow panel* left. A sample workflow for wheather prediction is shown; grey boxes denoting the transitions/service operations; circles denoting places/service parameters.

submitted by previous users. The next steps vary based on the user actions. The user can browse through existing notes, workflows and results to see if someone has already computed any similar results or workflows. Based on the user selection the system will display the results and notes describing each service. By clicking on the workflow the system will load it into the *workflow panel* and the user can restart it with his/her data by using the *control panel*. Generally, the process of user guidance is based on the semantic descriptions of user context and experience as described in Section 4.3.

Another alternative path is followed when the user selects a concept, which describes a flood-forecasting method, e.g. DaveF2DVisualization. Such concept is related with the semantic description of the service hosting the method. Based on the semantic description of the service the system can automatically compose an abstract workflow and present it to the user. This process is based on the semantic description of services as described in Sec.4.2. This abstract workflow is then analyzed, relevant services capable of creating the solution are found, and a more concrete workflow is created, where the abstract transition is replaced by several classes of services. The user is presented by a list of tasks that he/she needs to fulfil in order to continue execution the workflow, e.g. specifying time and date for the forecast. The user can then start the workflow through *control panel*. Consequently, the system looks for real service instances and executes them. The process of instance lookup and execution is visualized in real-time in the *workflow panel*. After the workflow finishes the user can get the results by clicking on the corresponding output place in the *workflow panel*, e.g. in this case it would display an animation of the possible flooding in the region. The workflows and results can be annotated by the user during the whole process. The overall process of composition and execution is captured by the semantic

description of context and experience is stored by the system for later retrieval. The benefits of the approach are mainly user-friendly interface with possibility to compose workflow based on user query, as well as user support and guidance throughout the process of composition and execution.

6   Related Work

There are many existing workflow-based graphical problem solving environments such as [3,5,4]. Our approach differs mainly in the exploitation of the user context and experience, which enables storing and re-using past workflows and results, creation of workflows based on queries and complex support for user interactions during the process.

In the domain of Semantic Grid there are many projects, which are trying to develop an architecture for the Semantic Grid applications such as [2,7,8]. Unlike our approach the mentioned projects are trying to address the Grid semantics by a top-down approach, creating reference architectures, which should cover a broad range of applications and requirements. On the contrary, our approach can be seen as a bottom-up approach, which is trying to leverage as much as possible from the existing Semantic Web Service technologies. A similar approach can be seen in the ^{my}Grid, which is a pioneering Semantic Grid project, providing a set of tools and services to enable workflow composition in biological domain [7]. It is, however, more focused on the support for the OGSA and OGSA-DAI, while we aim at supporting WSRF and OWL-S, which have shown to be more suited for the domain of our applications.

In the context of the *Semantic Web Services*, WSMO, WSMX and IRS-III provide an industry scale framework for discovery, composition and execution of web services [14]. A similar approach to ours is taken by the WSDL-S and METEOR-S, which attempts to add semantics to the basic web service descriptions [15]. Generally, none of the existing semantic web service frameworks provide support for composition and execution of the grid services or any possibility for user assistance based on experience or knowledge re-use.

7   Conclusions

We have described a working flood-forecasting system based on the semantic grid services. We have shown how it can compose and execute workflows while supporting complex user interactions and assisting technologies. The system is currently tested and evaluated by the Slovak Hydrometeorological Institute on the datasets of the major Slovak river basins.

References

1. Goble, C., De Roure, D., The Semantic Grid: Myth Busting and Bridge Building, in Proceedings of the 16th European Conference on Artificial Intelligence (ECAI-2004), Valencia, Spain, 2004
2. Alper, P., Corcho, O., Kotsiopoulos, I., Missier, P., Bechhofer, S., Goble, C., S-OGSA as a Reference Architecture for OntoGrid and for the Semantic Grid, GGF16 Semantic Grid Workshop. Athens, Greece. February 2006
3. Taylor, I., Shields, M., Wang, I., Harrison, A., Visual Grid Workflow in Triana, Journal of Grid Computing, pp. 153-169, vol. 3, September 2005
4. Deelman, E., et.al., Pegasus: Mapping Scientific Workflows onto the Grid, Grid Computing, 2004, Springer, LNCS
5. Hategan, M., von Laszewski, G., Amin, K., Karajan: A Grid Orchestration framework, Supercomputing 2004, Pittsburgh, 6-12 November 2004.
6. Kryza, B., Slota, R., Majewska, M., Pieczykolan, J., Kitowski, J.: Grid organizational memory-provision of a high-level Grid abstraction layer supported by ontology alignment, Future Generation Computer Systems, Volume 23, Issue 3, March 2007, Pages 348-358
7. C. Wroe, C. A. Goble, M. Greenwood, P. Lord, S. Miles, J. Papay, T. Payne, and L. Moreau, Automating Experiments Using Semantic Data on a Bioinformatics Grid, IEEE Intelligent Systems, vol. 19, pp. 48-55, 2004.
8. Li Zha, Wei Li, Haiyan Yu, Xianghui Xie, Nong Xiao, Zhiwei Xu: System Software for China National Grid. NPC 2005: 14-21
9. A. Ankolekar et.al, OWL-S: Semantic Markup for Web Service, 2003, http://www.daml.org/services/owl-s/1.1
10. Web Service Resource Framework, http://www.globus.org/wsrf/
11. Globus Toolkit, http://www-unix.globus.org/toolkit/
12. Gubala, T., Bubak, M., Malawski, M., Rycerz, K., Semantic-based Grid Workflow Composition, In: Proc. of 6-th Intl. Conf. on Parallel Processing and Applied Mathematics PPAM'2005, R.Wyrzykowski et.al. eds., 2005, Springer-Verlag, Poznan, Poland
13. The Knowledge-based Workflow System for Grid Applications FP6 IST project. http://www.kwfgrid.net
14. Fensel D. and Bussler C., The Web Service Modeling Framework WSMF, Eletronic Commerce: Research and Applications, 1, 2002
15. P. Rajasekaran and J. Miller and K. Verma and A. Sheth, Enhancing Web Services Description and Discovery to Facilitate Composition, International Workshop on Semantic Web Services and Web Process Composition, 2004
16. Motta E. and Domingue J. and Cabral L. and Gaspari M., IRS-II: A Framework and Infrastructure for Semantic Web Services, 2nd International Semantic Web Conference (ISWC2003), Sundial Resort, Sanibel Island, Florida, USA, 2003
17. F. Neubauer, A. Hoheisel, J. Feiler: Workflow-based Grid application, Future Generation Computer Systems 22 (2006) 6-15
18. Hluchy, L., et.al., Flood Forecasting in CrossGrid project. In: Grid Computing, 2nd European Across Grids Conference, Nicosia, Cyprus, January 28-30, 2004, LNCS 3165, 2004
19. Ralph Bergmann, Experience Management: Foundations, Development Methodology, and Internet-Based Applications, Lecture Notes in Artificial Intelligence, ISBN 3540441913, 2002
20. Laclavik, M., Babik, M., Balogh, Z., Hluchy, L., AgentOWL: Semantic Knowledge Model and Agent Architecture. In: CAI journal,. Vol. 25, no. 5 (2006), p. 419-437.

Building Scientific Workflows for Earth System Modelling with Windows Workflow Foundation

Matthew J. Fairman[1], Andrew R. Price[1], Gang Xue[1], Marc Molinari[1], Denis A. Nicole[2], Timothy M. Lenton[3], Robert Marsh[4], Kenji Takeda[1], and Simon J. Cox[1]

[1] Microsoft Institute for High Performance Computing,
School of Engineering Sciences, University of Southampton, Southampton, UK
`{mjf, andrew, gx, mm, ktakeda, sjc}@soton.ac.uk`
[2] School of Electronics and Computer Science, University of Southampton, UK
`dan@ecs.soton.ac.uk`
[3] School of Environmental Sciences, University of East Anglia, Norwich, UK
`t.lenton@uea.ac.uk`
[4] National Oceanography Centre, University of Southampton, Southampton, UK
`rma@noc.soton.ac.uk`

Abstract. The GENIE project has built a Grid enabled framework that facilitates the integration, execution and management of component models for the study of the Earth system over millennial timescales. The existing framework supports collaborative study of GENIE models across heterogeneous compute grids through scripted workflows in the Matlab environment. In this paper, Windows Workflow Foundation technologies are applied to demonstrate the benefits of an environment that provides rapid composition, event driven logic and reliable hosting of scientific workflows. These improvements are demonstrated through a parametric study of bi-stability of the oceanic thermohaline circulation in a GENIE model.

Keywords: Workflow, GENIE, Windows Workflow Foundation.

1 Introduction

E-Science applications are usually composite systems that involve collaborations among various computational resources and software components in a distributed, heterogeneous environment. Workflow technologies have become a key element to e-Science systems, which help to orchestrate interactions with services so that they are seamlessly knitted together to implement the desired behaviour of the system.

A typical example of such an e-Science system can be found in GENIE [1]. The GENIE project has developed a framework for the composition, execution and management of integrated Earth system models. Component codes (e.g. ocean, atmosphere, land surface, sea-ice, ice-sheets, biogeochemistry, etc.) of varying resolution and complexity can be flexibly coupled together to form a suite of efficient climate models capable of simulation over millennial timescales. The project brings

together a distributed group of environmental scientists with a common interest in developing and using GENIE models to understand the Earth system. Grid computing technology supports the virtual organization to collaboratively study the models from the framework.

Earth system simulations are both computationally and data intensive processes, often consisting of a discrete series of steps. The GENIE framework has been designed to support running of such simulations across multiple distributed data and computing resources over a lengthy period of time. It has therefore put rigorous requirements on the selection of workflow technologies for GENIE.

The recently released Microsoft Windows Workflow Foundation (WF) [2] is a general, extensible framework for developing workflow solutions. As an integral part of the .NET Framework 3.0 [3], WF provides a common development model for creating workflows, a set of tools that facilitate workflow design, and a robust workflow hosting environment. It also allows seamless integration with other .NET technologies to provide support for distributed communication and rich user experiences. We have therefore applied WF to the GENIE framework to provide a solid base for the design and running of Earth system simulations.

In this paper we discuss and demonstrate how the WF technologies are applied to build efficient and flexible workflows for running Earth system simulations based on the GENIE framework. In section 2 we describe the functions of the GENIE workflows and explain why the attempt has been made to adopt WF technologies. Section 3 gives a detailed summary of the features of WF. Section 4 describes the design and running of our WF based GENIE workflow. Results from a scientific study of bi-stability in the thermohaline circulation (THC) in a GENIE model, undertaken using our WF based system, are presented in section 5. We draw our conclusions in section 6.

2   Workflow in the GENIE Framework

The GENIE framework has been designed to facilitate collaboration between a distributed team of environmental scientists to perform large ensemble studies of Earth system models that would be impossible for a single user. In contrast to system likes GridSolve [4] and Nimrod/G [5], in which a central manager controls all available resources and makes decisions about where to assign work units, the GENIE framework devolves responsibility for the management of work units to the client side, and pools compute resources contributed by members of the project to carry out large parametric studies. A central shared database accessible from all clients has been set up to provide the means to upload model configurations and experiment definitions, and be queried against to find available work units.

A GENIE workflow running at the client side is therefore responsible for the following tasks when contributing to a particular study:

-   Querying the central database for available work units.
-   Submitting the work units to the compute resources specified by the user.

- Monitoring the status of the submitted jobs; retrieving and checking the results once jobs are finished.
- Post-processing the results and saving them in the database.

The workflow runs until there is no work available, or it is terminated by the user.

Presently, the GENIE workflow is implemented using the Matlab scripting language and is hosted in the Matlab environment. While simplicity and flexibility are achieved through scripting, a few problems remain. The scripting approach for workflow tends to be less efficient when dealing with external events. When running a GENIE simulation, the user needs to keep running the script all the time and query the central database periodically to find work items, submit and monitor jobs, and post-process data from completed work items. Time intervals between two scheduled tasks can only be set in a speculative mode. Events such as new work units being added and compute tasks completing are unlikely to be handled efficiently. Callback mechanisms or publish/subscribe mechanisms would be an optimal choice for improvement. For example, the database could publish new work as it becomes available and the clients would subscribe for these events. However, it is difficult to make such modifications in the current scripting environment.

Another problem with hosting workflows in the scripting environment is the lack of support for persisting state of the workflow. While it is possible for the users to manually save some of the state information, restoring the running of a workflow in the cases of a system or network failure is always difficult. The GENIE system is robust to such failures since the experiment status is always defined in the shared repository but resumption of a study can only be achieved by restarting the workflow.

Finally, implementing the GENIE workflow in the Matlab script ties the system to a single user environment. It is very difficult to migrate existing workflows to other systems. Workflows in scripting languages are also less well-structured and might require individual human knowledge to interpret or modify. This makes it hard to maintain or to try to reuse the workflow activities.

As an attempt to address these problems, we have exploited the WF technologies to develop a dynamic and robust workflow implementation which actively manages the operations of the GENIE simulations with improved efficiency and stability.

3   Windows Workflow Foundation

Windows Workflow Foundation (WF) [2] is a Microsoft technology for quickly building workflow enabled applications. It consists of a programming model, a host engine and tools for defining, executing, and managing workflows. WF significantly enhances a developer's ability to model and support sophisticated science and engineering processes. Being part of the recently released .NET Framework 3.0, WF can be seamlessly integrated with other .NET technologies to provide a solid base for the design and running of Earth system simulations.

3.1   Workflow Design with WF

WF supports two built-in workflow styles, i.e. sequential workflows, which carry out a series of operations in a pre-defined pattern, and state machine workflows, which

are driven by external events. This enables WF to accommodate both the well structured, automated system workflows and the loosely defined, flexible human workflows. WF adopts a component like approach, where each step of a workflow can be implemented by a specific piece of software called 'activity'. A base activity library is supplied which contains a group of pre-defined activities most commonly used in both sequential and state machine workflows. Users are also allowed to build their own customised activities, build new activities by aggregating existing ones, and reuse activities in different workflows.

WF is a general framework not limited to a single language or a single tool. Workflows can be created using any programming language that is compliant with the .NET Framework's Common Language Specification, such as C#, Visual Basic and Visual C++. In addition, WF supports defining workflows in XAML (eXtensible Application Markup Language) [6], an XML based object initialization language, so that different workflow designers can be used to generate or parse WF workflows. WF also provides its own graphical designer, usually hosted in Visual Studio 2005, to support visual design of workflows.

3.2   Workflow Hosting with WF

WF workflows can be hosted in any Windows process ranging from simple console applications to large, sophisticated enterprise services. The workflow execution is carried out within the WF runtime engine, which provides important services, such as persisting workflow state, tracking the execution, and supporting transactions. The WF runtime can make decisions to unload long-running workflows that have been inactive for a period of time, and load them back when necessary. It also works as a proxy for all interactions between the workflow and external software, including Web services, in an asynchronous style.

Being an integrated part of the .NET Framework, it is possible for WF workflows to take advantage of other Microsoft technologies including Windows Communication Foundation (WCF) [7], Windows CardSpace [8] and MS SQL Server 2005 [9] to address problems such as communication in a distributed environment, federated security control and data access. Application of some of these technologies together with WF can be found in our work on the Earth system modelling workflows, which is discussed in the following section.

4   A Composite Workflow for GENIE Simulations

A number of key components have been developed for the GENIE project to facilitate the running of Earth system simulations. These include a shared database hosted in Oracle 10g which contains the definitions, states and results of the experiments, a number of gateway systems to integrate compute resources from different HPC platforms including Microsoft Cluster Computing Server [10], Condor [11] and Globus [12], and a shared file store managed by using the Geodise Toolkit [13]. In order to bring these components together in a single system that manages the Earth system simulations, a composite workflow has been implemented using the WF technologies. Figure 1 shows the structure of the WF based Genie system.
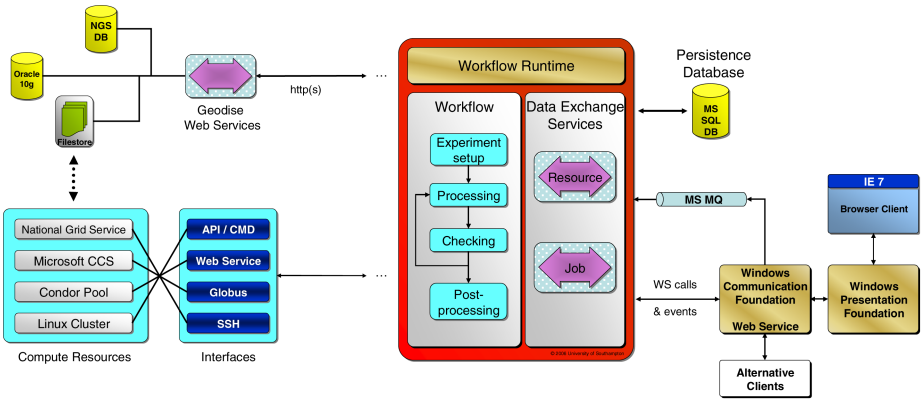
Fig. 1. The Complete Structure of the WF based GENIE Simulation System
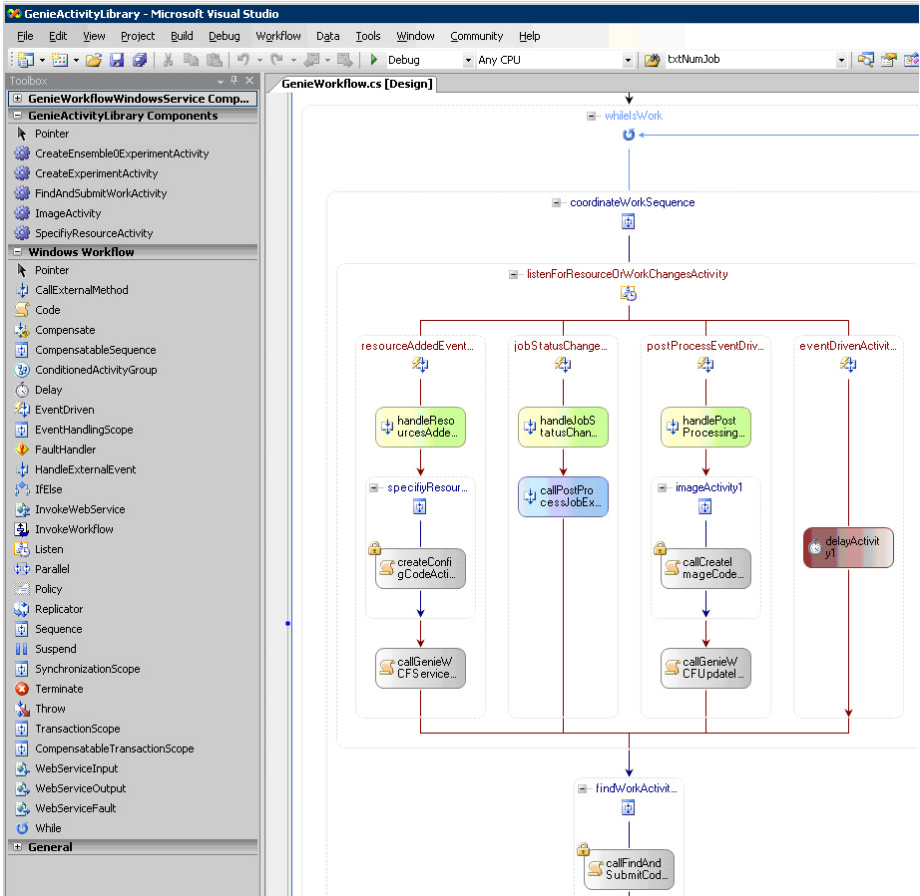
Fig. 2. Design of the GENIE workflow in the WF Designer with Visual Studio

The Genie WF workflow implementation automates the operations and interactions on the system components. It is a sequential workflow that consists of a while loop activity which contains a single parallel asynchronous event listening activity that waits for the following changes in the state of an experiment: newly specified resources, changes of job states and completion of work item post-processing. This not only provides a more responsive solution than the scripting based approach of polling, but also achieves better efficiency and robustness of the system by allowing the runtime to persist workflow instances in a database and unload them during periods of idleness. All of the asynchronous events are indications that either compute resources have become available or subsequent work items are now available. Consequently, a find work activity is performed after any one of these events has occurred. Figure 2 shows the main part of the design of the GENIE workflow.

The Genie workflow employs a set of external data exchange services that run within the workflow runtime. These services provide the means by which events occurring within the experiment system are passed into the workflow. When compute jobs are submitted, the workflow registers their identifiers with the Job Service which is responsible for monitoring the jobs' running statuses. The Job Service notifies the workflow instance of changes to the job status by firing a batched 'jobStatusChanged' event. In addition, the Job Service also performs asynchronous post-possessing of results from completed jobs when the workflow receives a 'jobStatusChanged' event of either 'Completed' or 'Failed'. Another external data exchange service, the Resource Service, allows the users to instruct the workflow to create new experiment work units by registering additional compute resources with it.

5   Earth System Simulation with WF

To demonstrate the WF based GENIE system, we repeat a systematic 2-parameter study of bi-stability in the Atlantic thermohaline circulation [14] using a higher resolution version of the GENIE model. The study investigates the C-GOLDSTEINcomposition referred to as *genie_ea_go_gs* in the GENIE framework nomenclature, which consists of a 3D frictional geostrophic ocean coupled to a simple 2D energy-moisture balance model and a 2D sea-ice component. The study seeks to investigate the properties of the Atlantic Thermohaline Circulation as a function of two of the key parameters that dominate atmospheric moisture transport in the model:

- FW_x: Zonal moisture transport from the Atlantic to the Pacific.
- K_q: Atmospheric moisture diffusivity - principally controls meridional moisture transport between the equator and poles.

A systematic sweep over a range of values for these parameters was undertaken. Each simulation was integrated over 4000 years to ensure an equilibrium state was achieved. The individual model runs each required approximately 2 hours compute time on a typical desktop. With the benefit of knowledge of the behaviour of the model at a lower resolution we chose to perform a coarser sampling of the parameter space (11x11 as opposed to 31x31) than the original study. The initial parameter sweep therefore required approximately 242 hours of compute time.

The WF based GENIE system has been used to repeat the study of Marsh et al. using a 16-level seasonal version of the *genie_ea_go_gs* model. Having provided a coarse mapping of the behaviour of the Atlantic THC in the model, the study proceeded by performing two further identical parameter sweeps using models with different boundary conditions. These secondary ensembles performed identical model runs initializing the models using particular end-states from the initial ensemble. Such runs are designed to investigate whether there are points in the parameter space of the atmospheric water transport properties for which the equilibrium THC state of the model is dependent upon its initial conditions. In Marsh et al. nine end-states were taken from the extremes of the parameter space to search for bi-stability. In this study we perform just two secondary ensembles using the end-states from the "top-left" and "bottom-right" points (Figure 3 (c)) which represent the extreme "off" and "on" states in the THC respectively. Following the coarse initial mapping the parameter space was further refined through the addition of another 100 (10x10) members to each ensemble. An interactive plot of the results was then exploited to add further ensemble members in the emerging regions of bi-stability in the THC to focus further work in the most appropriate locations.
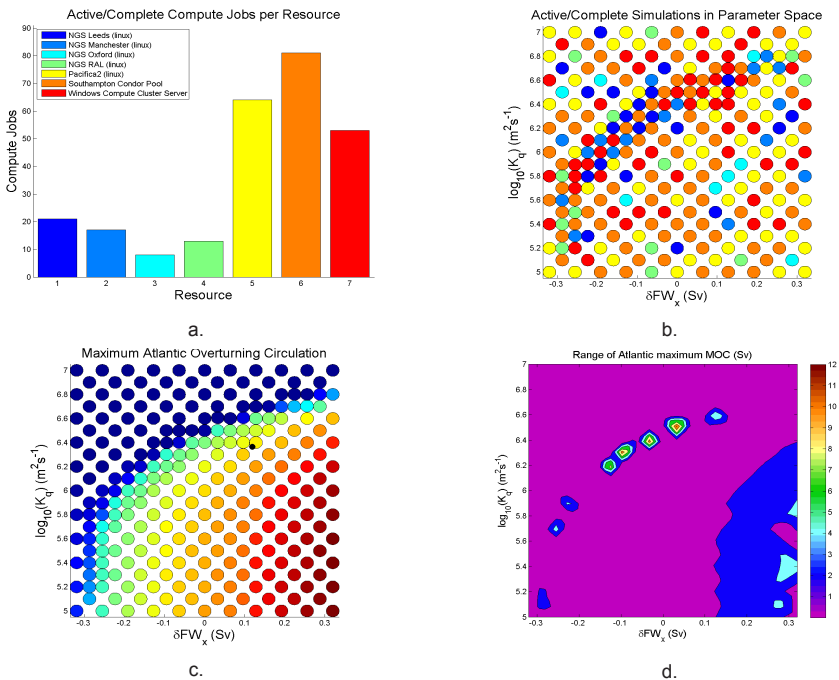
Fig. 3. Study of bi-stability in the Atlantic Thermohaline Circulation. a) Summary of distribution of compute jobs across the computational grid, b) distribution of compute jobs in the parameter space, c) Strength of maximum Atlantic Overturning Circulation in the initial parameter sweep and d) narrow region of bi-stability in the parameter space.

The results of the bi-stability study are presented in Figure 3. Figure 3 (a) summarises the resource usage in performing the initial ensemble. The distribution of compute jobs broadly reflects the relative numbers of single concurrent compute tasks that the schedulers on each system allow to a single user. The distribution of simulations across the resource pool is plotted in the parameter space in Figure 3 (b). The user additions of model runs are focused along the "cliff-edge" of THC collapse (Figure 3 (c)) where a narrow region of bi-stability emerges (Figure 3 (d)). It is evident that further runs will be required to fully resolve the extent of the bi-stable region. First indications are that the newly tuned 16-level model has a narrower region of bi-stability than the original 8-level model [14]. A more detailed study of the parameter space and analysis of the results will be the subject of future work.

6   Summary

In this paper we discussed and demonstrated how the Windows Workflow Foundation technologies can be exploited to implement scientific workflows for e-Science systems such as GENIE. We reviewed features of WF technologies and explained how they have been deployed in the GENIE framework to facilitate coordinated operations among various distributed components. A collaborative study of bi-stability in the thermohaline circulation of an efficient climate model has been performed to demonstrate the running of the WF based GENIE system.

References

1. Gulamali, M.Y., et al., GENIE: Delivering e-Science to the environmental scientist. UK e-Science All Hands Meeting, pp. 145-152, Nottingham, UK, 2003. ISBN 1-904425-11-9.
2. Shukla, D., Schmidt, B., Essential Windows Workflow Foundation. Addison Wesley Professional. ISBN-10: 0-321-39983-8
3. Microsoft .NET Framework 3.0. http://msdn2.microsoft.com/en-gb/netframework/
4. YarKhan, A., Seymour, K., Sagi, K., Shi, Z. and Dongarra, J., Recent Developments in Gridsolve. Int. J. of High Performance Computing Applications, 20 (2006), 131-141
5. Buyya, R., Abramson, D. and Giddy, J. Nimrod/G: An Architecture of a Resource Management and Scheduling System in a Global Computational Grid, HPC Asia 2000, May 14-17, 2000, pp 283 289, Beijing, China.
6. Microsoft, XAML Overview. http://msdn2.microsoft.com/en-us/library/ms752059.aspx
7. Microsoft, Windows Communication Foundation Architecture Overview.
8. http://msdn.microsoft.com/library/en-us/dnlong/html/wcfarch.asp
9. Chappell, D., Introducing Windows CardSpace. http://msdn.microsoft.com/library/en-us/dnlong/html/introinfocard.asp
10. Microsoft, SQL Sever 2005 Books Online. http://www.microsoft.com/technet/
11. prodtechnol/sql/2005/downloads/books.mspx
12. Microsoft, Windows Compute Cluster Server 2003 Product Overview.
13. http://www.microsoft.com/windowsserver2003/ccs/overview.mspx
14. The Condor Project. http://www.cs.wisc.edu/condor/
15. The Globus Project. http://www.globus.org
16. The Geodise project. http://www.geodise.org
17. Marsh, R., *et al.*, Bistability of the thermohaline circulation identified through comprehensive 2-parameter sweeps of an efficient climate model. Clim. Dyn. 23 (2004) 761-777

Balancing Quality and Performance of Task Distribution in Workflow Based on Resource Aptitude

Renê Rodrigues Veloso[1] and Autran Macêdo[2]

[1] FACIT - College of Science and Technology, Department of Computer Engineering,
Brazil
[2] Federal University of Uberlandia, School of Computing, Brazil

Abstract. The distribution of tasks in a workflow system, in general, does not consider resource aptitude. Resources that share the same role in a workflow can have different degrees of aptitude to a task. This work proposes an extension to task distribution strategies and presents the use of this extension in the selection of resources to tasks. The experiments presented here demonstrate the effectiveness of the extension. A comparison with traditional strategies has shown gains in terms of time and quality of tasks executed.

Keywords: Workflow, Performance, Quality, Aptitude, Task distribution.

1 Introduction

Task distribution to resources is one of the critical functions of Workflow Management Systems (WfMS) [1,2] and is directly related to time of completion and quality of the execution process [3,4,5].

Task distribution mechanisms based on aptitude can be used in the prevention of workflow bottlenecks. Being resource oriented, theses mechanisms are able to use the information found in the capacities and abilities of available resources. With this, it is possible to safeguard against inadequate and/or busy resources receiving tasks, therefore avoiding the occurance of bottlenecks.

There are proposals of hybrid approaches between Push and Pull [2,6,7,8,9]. In this case, resources have individual queues of tasks that are filled by an heuristic that moves tasks of a shared queue to individual queues. This heuristic is batch-based with the purpose of minimizing flowtime, i.e., the difference between the beginning and the end of a task. It create groups of tasks based on their process time. However, none of this related research is worried about maximizing quality, maintaining a satisfactory execution time of the business process.

The research of Kumar et al. [4], proposes distribution mechanisms that, beyond considering the aptitude of resources, tries to balance quality and performance through rules that restricts the visibility of resources to tasks. However, as the mechanisms there proposed are strongly based on the Pull mechanism, the

choice of tasks are made by resources, which can facilitate the occurance of bot-tlenecks. Apart from the Kumar et al. research, the mechanisms proposed and explored in this paper are implemented as Push mechanisms, where the system chooses the resources at the moment of distribution. Permitting the system to totally guide the distribution can improve the quality and performance goals of balancing, because these goals are controlled and leveled according to resource availability and aptitude to each delivered task.

1.1   Solution Approach

Resource aptitude can be surveyed by means of metrics, which indicate the degree of adequacy of resources to the completion of tasks ([4]). In other words, the degree of adequacy measures the level of competence of resources for the realization of the tasks of the workflow. keeping to the context of this paper, resources with high degree of adequacy to a given task has greater aptitude for the execution of the tasks. So the fact that these resources perform tasks more efficiently than those less adequate to the tasks is to be expected.

The metrics of allocation are defined as a systematic solution to dynami-cally create equilibrium between quality and performance. This equilibrium is obtained through the construction of a model directionally toward better dis-tribution. In this way, the systems should know how to choose the most apt resources to do tasks in any given process which one desires to automate.

Therefore, the purpose of this paper has two approaches: (i) to develop effi-cient task distribution mechanisms to apt resources, which may be applied to various types of businesses. (ii) to make a comparative study of existing tradi-tional mechanisms. These implemented mechanisms should be able to facilitated gains in work execution efficiency of workflow systems, taking in to consideration the resource aptitude to the task and the workload already allocated. To realize this goal, section 2 describes the metrics used by the distribution mechanisms to allocate resources and also to measure the quality of the execution processes, as well as their respective parameters. The section 3 shows mechanisms based on resource aptitude and describes the proposal *Sel-push* e *Sel-push-10*, to bal-ance both quality and performance. In the section 4, a computer experiment to compare the performance and quality of mechanisms is detailed, and the results analyzed considering various kinds of problems. In the end, the conclusion is commented on, followed by the bibliographical references used in this paper.

2   Allocation Metrics

The allocation metric presented in [4] was originally propose as criteria of com-mitment between quality and performance for a workflow system. This proposal relates resources and tasks by means of parameters such as adequacy and avail-ability. [1]

---

[1] Other parameters are defined by Kumar *et al.* as being urgent to the execution of tasks and degree of violation of restriction in the modeled process. These were dis-considered in this paper (the tasks are equally urgent and do not exist restrictions).

The parameters are combined in a metric which determines the allocation of the task to a resource. This metric called a *absolute allocation factor* or, simply, *abs_alloc*, is defined by:

$$abs\_alloc(w, rs) = adequacy(w, rs) \times availability(rs). \tag{1}$$

The adequacy parameter is about the aptitude of a resource in relation to a given task. This parameter is given by the function $adequacy(w, rs) \in [0, 1]$, in w is a workflow task and rs is a workflow resource. The lower the adequacy value, the lower aptitude rs possesses to execute w.

Availability indicates how available a resource is to perform a task. This parameter is expressed by the function $availability(rs) \in [0, 1]$. Values lower than 1 indicates that the resource in question is already allocated to some task. A value equal to zero indicates that the resource is unavailable.

The metric *abs_alloc* depends only on a task and a resource isolatedly. This metric assumes a value between 0 and 1, which is an absolute measure of adequacy to a resource to perform a task immediately. The higher the value of *abs_alloc* of a resource, more adequate it will be to execute the task. [2]

3 Distribution Mechanisms Based on Aptitude

The distribution of tasks in workflow systems, in general, occurs through the Push and Pull mechanisms [10]. However, neither of these mechanisms considers the resource aptitude to the tasks.

In this sense, Kumar et al. [4] defines three mechanisms based on Pull. These mechanisms are practically based on the definited adequacy thresholds that increase or decrease the amount and the quality of the involved resources. These thresholds are as follows:

– *Typical*: one task w is visible to resource rs if, and only if, *abs_alloc(w, rs)* exceeds a value 0.5. This represents a typical resource.
– *Receptive*: one task w is visible to resource rs if, and only if, *abs_alloc(w, rs)* exceeds a lesser value than the typical one, e.g., 0.4. This indicates a more receptive resource .
– *Selective*: one task w is visible to a resource rs if, and only if, *abs_alloc(w, rs)* exceeds a value higher than the typical one, e.g., 0.6. This indicates a more selective resource than the typical resource.

The proposal of this paper involves an extension to the mechanisms of distribution cited previously. Also taking as base the values of absolute allocation, the differential of this extension is in the form which the tasks are delivered to the resources. Before the resources receive the tasks, their availability values are verified. When receiving tasks, the resources are less available in the context of the system. In this way, a resource that has a high workload will not have to receive more tasks, these being repassed to other resources that are apt and have availability to execute them. Based on Push, the extension is implemented as two other mechanisms are: the Sel-Push and the Sel-Push-10.

---

[2] In the equation 1 the disconsidered parameters both assume a value equal to one.

3.1   The Sel-Push Distribution Mechanism

In a simplified manner, the distribution mechanism Sel-Push is called to action whenever the task queue (ready) is not empty and continues until the tasks of the queue are allocated, or until the resources are no longer available. In this case, the mechanism goes into waiting mode until some resource becomes available. An choice of the resource with greatest *abs_alloc* occurs guided by a dynamic threshold. This means, a resource which is initially found inside a margin of selective threshold, depending on how much this resource is being attributed tasks, its value of *abs_alloc* suffers a decrease, going to the typical threshold and after that, to the receptive threshold. The Sel-Push verifies beforehand if the resources most apt to the task are selective, and if they are not, others are sought for within the boundaries of inferior thresholds.

Of similar working to the mechanism Sel-Push, the Sel-Push-10 mechanism tries to pass tasks to the most apt resources. Therefore, besides choosing the resource with greater *abs_alloc*, it also considers the neighborhood of this resource. The neighborhood of a resource are all the resources within a certain numerical distance from adequacy value of this resource. In the case of Sel-Push-10 the neighborhood is within a radius of 10% of *abs_alloc* of the most adequate resource.

4   Computational Study

Considering the little information available about other solutions to the problem of task distribution in workflow systems, an analytical evaluation of all other existing mechanisms go far beyond the scope of this paper. Therefore, a computational study was done to compare the performance and quality of seven mechanisms, i.e., Push, Pull, Selective, Typical, Receptive, Sel-Push and Sel-Push-10. It is important to stress that the mechanism Push in this study, attributes the tasks to always the same resource with the greatest adequation value. In this section, the procedures used to simulate and presents the statistics based on the results of simulation are described.

4.1   Workload Generation

To control the workload of the computational study, a model proposed by Zeng and Zhao [2] is used. The idea of this model is centralized mainly in the evaluation of quality and performance of the mechanisms under study of varying business work environments. The parameters which characterize these scenarios of environments and their adjustments examined in this study are presented in the Table 1. Only a small number of resources were used (3 and 6), which is sufficient for the simulation of a organizational workflow environment.

In the model, the medium system load measures the number of tasks that arrive. This number is related to the capacity of the resource. Therefore, the control of the dynamic generation of tasks and the process used by Zeng and Zhao is detailed as following. With the processing time of each task fixed in

Table 1. Simulation Parameters

Resource number	3 and 6
Medium system load	0.2(low), 0.6(medium), 1.0(high)
Variability of tasks	20(low), 80(medium), 140(high)
Variability of resources	20(low), 80(medium), 140(high)

10 units of time, the medium capacity of a resource for each unit time is $1/10$. Assuming that n resources are presented in the system, the total capacity of resources per unit of time is $n/10$. In this way, a medium system workload l, the number of tasks which arrive during each unit of time follows a Poisson distribution with $\lambda = l \times n/10$.

Two other parameters of the table, the variability of tasks and of resources control the time adjustment of processing of the task p_{ij}. In this study, this time is generated in two steps:

- Step 1. For the task j, the average processing time $\overline{p_j}$ is generated based on the normal distribution with average of 10 (average time of each task) and standard deviation $varTask$. Therefore, $\overline{p_j} \approx N(10, (10 \times varTask)^2)$. For example, considering a process with three tasks and a low variability of tasks, we have a processing time varying between 8 and 12 units.
- Step 2. The processing time of task j by resource i expressed by p_{ij}, is obtained after the average $\overline{p_j}$. So $varTask$, the resource variability $varResource$ indicates the percentage standard deviation of the individual processing of a task. Therefore, p_{ij} is generated from a normal distribution where: $p_{ij} \approx N(\overline{p_j}, (\overline{p_j} \times varResource)^2)$.

All of the values of average time generated by the model were rounded out to whole numbers and negative values to the value 1.

4.2   Execution of the Simulation

The Table 1 represents a total of $2 \times 3 \times 3 \times 3 = 54$ experimental conditions. For each condition, 20 instances of problems had been generated randomly and then the seven mechanisms were applied to the these instances. In the total, 7560 instances had been simulated. For the proposed study, a simulator able to execute the instances under any one of the described mechanisms of distribution was implemented [11]. Writing in Java(TM) language, the program is based on the analysis of charts and concepts of the Scheduling area ([12]), to compute the times of execution and the allocations of the tasks for the resources.

Among the data that is generated by the simulator after the execution of the instances is the total execution time of the processes and the value of quality, resultant of the attributions made for the distribution mechanisms. This data was collected and is analyzed later in order to make possible the identification of the mechanism with greater commitment to performance and quality. For reasons of space, only the results based on the execution average of the 3 system load types, i.e., low load (20%), average (60%) and high (100%) will be presented. In

the same way, each data point on the result graphs is the average of 20 instances with the same system load and processing time variation of only 3 different resources concurring for each task.

In the simulated model, two independent parameters exist, i.e., task variability and resource variability, each one with three different possible values (low, medium and high) resulting in nine different combinations. However, only four of the possible representative combinations are shown. Thus $(varTask, varResource) \in \{(Low, Low), (Low, High), (Medium, Medium), (High, High)\}$ is seen to be enough for the intention of the paper. The target process of the simulations contains three tasks. Initially all of the resources possess high availability. The adequation values of each resource are empiric and generated randomly.

4.3   Total Execution Time and Quality of the Processes

The behavior of seven mechanisms was evaluated in terms of total execution time and quality of the processes. It is also observed that the execution times and quality of the processes of the Push mechanism surpasses the others mechanisms in all variations of task and resource. The Selective mechanism, with similar behavior, also has high time and quality indices. These results occur due to the fact that these mechanisms are very restrictive, delivering tasks always to a single resource or to a small group of resources. However, in consequence, waiting queues occur for more adequate resources, accumulating tasks and increasing the completion time of processes. The mechanisms Pull and Typical result in less time and quality in execution because they are very liberal, i.e., they make it difficult to accumulate tasks because they involve a greater number of resources. The mechanisms based on Sel-push, combine the characteristics of both the liberal and restrictive mechanisms distributing tasks better.

Table 2. Comparison of mechanisms for execution time and quality

	Sel-Push	Sel-push-10
Push	-/+	-/+
Pull	+/-	+/-
Selective	-/=	-/+
Typical	=/-	=/-
Receptive	+/-	+/-
Sel-push		-/+

The observations shown previously are confirmed by the execution of some statistical tests. For example, the Table 2 contains comparisons proceeding from a statistical test called *pairwise t-test*, used to see if the results of each mechanism can be considered statistically equal to each other. In this table there are three symbols: the symbol "+", the symbol "-" and the symbol "=". These symbols, in each column, are in the format *symbol/symbol* representing *time/quality*. The symbol "+" means that the mechanism that is in the row on the table is statistically better than the mechanism which is in its respective column, with

95% of confidence. The symbol "-", contrary to the symbol "+", means that the mechanism which is in the row is statistically worse than the mechanism in the column. In the case of the symbol "=", also demonstrating the same 95% of confidence, confirms that there is no significant difference between the corresponding row and column of the table.

It is observed that through testing, that the mechanisms behave in a constant manner regarding task variation, resources and system load. The more restrictive mechanisms elevate the time necessary to conclude processes due to task accumulation. Although, for the same reason, the mechanisms raise the average quality of executed process. On the other hand, while the more liberal mechanisms spend less time in the execution of processes because they have more resources receiving tasks, at the same rate favor the decreasing service quality. Therefore, the mechanisms Sel-Push and Sel-Push-10, englobe the best of these two worlds, because besides guaranteeing a average time of execution of the processes similar to the processes dealt with by the liberal mechanisms, they keep a high level of quality, equaling the more restrictive mechanisms.
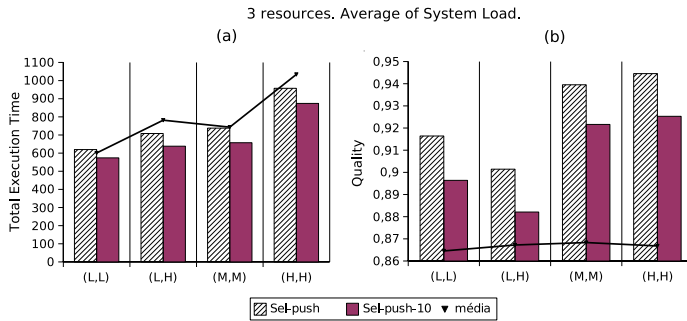
Fig. 1. Average Curve of (a) execution time and (b) quality of processes

The graph of the Figure 1 resumes the behavior of the Sel-Push and Sel-Push-10 mechanisms in relation to the average curves of execution time and quality of executed processes with Push, Pull, Selective, Typical and Receptive mechanisms. Conforming to the graph, the mechanism Sel-push has an average behavior in relation to execution time and quality better than the other analyzed mechanisms. This betterment becomes more evident as the variation of processing time of tasks increases.

5   Conclusions

The task distribution, besides being a key toward dynamically attributing task which arrive individually for resources, directly affects the service quality and the resource productivity. It also is an integral part of decisions of the strategical level of the organizations [2].

Two task distribution mechanisms were proposed. Their performance was studied by simulation. The results were compared to other mechanisms which reflect the current practice in workflow. The study done concentrated on analysis of two factors of performance: quality and execution time of work. The impact of variation of individual processing time of tasks, the number of resources involved and the system load of these performance factors were evaluated under the seven evaluated mechanisms.

It was observed that the proposed based on *Push* mechanisms obtained effective gains in average quality and execution time in simulated scenarios.

References

1. Stohr, E.A., Zhao, J.L.: Workflow automation: Overview and research issues. Inform. Systems Frontiers **3** (2001) 281–296
2. Zeng, D.D., Zhao, J.L.: Effective role resolution in workflow management. INFORMS journal on computing **17**(3) (2005) 374–387 ISSN: 1091-9856.
3. Governatori, G., Rotolo, A., Sadiq, S.: A model of dynamic resource allocation in workflow systems. In: XV Australasian Database Conference. Volume 27., Dunedin, New Zealand (2004)
4. Kumar, A., van der Aalst, W.M., Verbeek, E.M.: Dynamic work distribution in workflow management systems: How to balance quality and performance? Journal of Management Information Systems **18**(3) (2001) 157–193
5. Momotko, M., Subieta, K.: Dynamic changes in workflow participant assignment. In: ADBIS Research Communications. Volume 2., Bratislava, Slovakia, Slovak University of Technology, Bratislava (setembro 2002) 175–184
6. Alt, R., Klein, S., Kuhn, C.: Service task allocation as an internal market. In: Proc. of the Second European Conf. on Information Systems. (1994) 424–432
7. Harker, P.T., Ungar, L.H.: A market-based approach to workflow automation
8. Tan, J.C., Harker, P.T.: Designing workflow coordination: centralized versus market-based mechanisms. Technical report, Department of Systems Engineering, University of Pennsylvania, Philadelphia (1997)
9. Shen, M., Tzen, G.H., Liu, D.R.: Multi-criteria task assignment in workflow management systems. In: Proc. Thristysixth Hawaii Internat. Conf. System Sci., Big Island, Hawaii 202
10. van der Aalst, W.M.P., van Hee, K.M.: Workflow Management: Models, Methods, and Systems. MIT Press (2002)
11. Veloso, R.R., Macêdo, A.: Lambari: Simple workflow test environment. Technical report, Department of Computer Science, Federal University of Uberlandia, MG, Brazil (2005)
12. Brucker, P.: Scheduling Algorithms. Springer-Verlag New York, Inc., Secaucus, NJ, USA (1998)

A Process Meta Model to Support Policy Based Management in Workflow System

Song Ouyang and Hao Xu

School of Information Science and Engineering, Central South University, Changsha,
Hunan, P.R. China 410083
ouyangsong@yahoo.com,
xuhao916@gmail.com

Abstract. Policy-based management and process-based management are two main management paradigms that are widely used in information management systems. The foundation of traditional WfMS is process-based management. In this paper we present a process meta model to support policy based management in WfMS. With the new meta model the system has better flexibility in workflow design time and higher adaptability at run-time. It can also keep the business rules consistent across the whole enterprise and provide a uniform method to deal with business rules, resources and security in workflow system.

Keywords: Workflow, WfMS.

1 Introduction

With the increase of complexity, traditional workflow management systems (WfMS) are facing many challenges in meeting the requirements of flexibility and adaptability and implementing resource management and security control [2]. To improve flexibility and adaptability, a Petri net formalism is presented to analyze structural change in the workflow process modeling [3]. A new workflow modeling method is proposed to improve flexibility and adaptability of system [4]. A meta-model is proposed in [5] to support dynamic changes of workflow process and enable the dynamic characteristics. Similar approach can be found in [6]. To address various software and/or hardware resources management issues, a resource management system that can handle a large number of workflow resources is proposed [7].

The foundation of a traditional WfMS is process-based management. The features of this management method are: the execution of each step of a task is based on an instruction and its parameters; the description of the instruction is imperative and it invokes execution components directly; after one instruction completed, another pre-defined instruction is initiated based on the pre-defined rules and conditions. The controlling mechanism between steps is accurate. In some workflow systems, better flexibility and adaptability in flow control are achieved through expanding the types of activities and adding more collaboration between activities. For the applications with comprehensive requirements in resources management and security control,

however, it is difficult to improve the flexibility and adaptability by using similar methods that are used in control flow since the requirements are more complicated.

Another management paradigm widely used in information management systems is policy-based management. The features of this management method are: the execution of each step of a task is based on the objective or behavior constraints; the description of instruction is declarative and it can not invoke execution components directly in most cases; after one step completed the subsequence step will be executed based on the analysis of active policies and the state of whole system.

Although some workflow systems used policies to deal with resources and security control, it is not real policy-based management system. The distinct features of policy-based management from process-based management are: declarative instruction, a centralized policy repository, dynamic policy transformations and looking up for policies, independent policy engine, and decision-making based on policies.

To meet the challenges we proposed to integrate the policy-based management in a WfMS [1]. This paper presents a process meta model to support policy based management in a WfMS. With the new meta model the system has better flexibility in workflow design time and higher adaptability at run-time.

2 Process Meta-model to Support Policy Based Management

Workflow process meta-model is the base for process definition modeling. A new process meta-model to support policy management is shown in Fig.1.
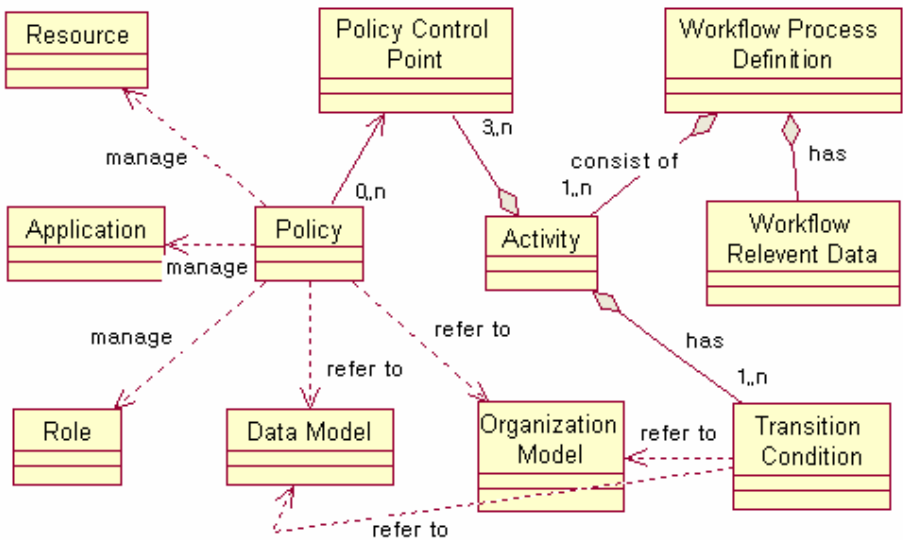
Fig. 1. A process meta-model to support policy based management

The main elements in the model are described as follows.

Process Activity: A logical step or description of a piece of work that contributes toward the achievement of a process.

Workflow Relevant Data: Data that is used by a WfMS to determine the state transition of a workflow instance.

Transition Condition: Criteria for moving, or state transitioning, from the current activity to the next activity(s) in a process instance.

Organization Model: The model of an enterprise's organizational structures.

Resource/Application/Role: They are managed through late-bound components (Subjects) to perform the specific behavior described by a policy.

Policy Control Point: The proper point defined in workflow to apply policies.

The new meta model has some new features:

(1) It provides more means to develop a process definition in workflow system. Using policies the complicated business rules, the local activity goals, and the constraints for resources can be described in a straight way. The flexibility in workflow design time is much better than that in a traditional process-based system.
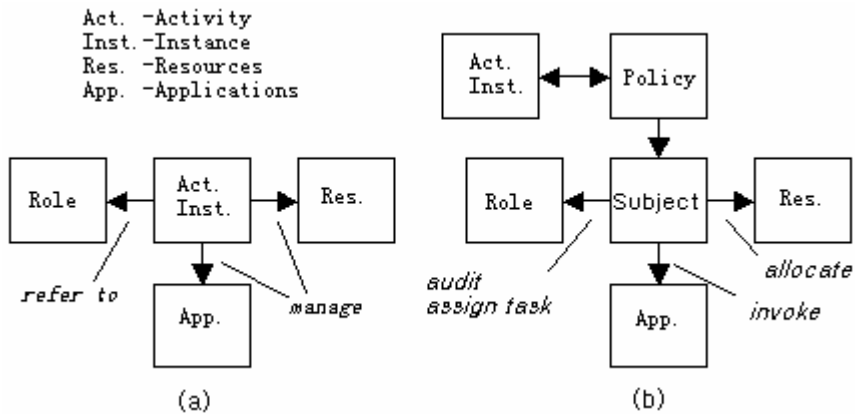
Fig. 2. Relations of activities, roles/participant, resources, and applications

(2) It makes it possible to separate the activities of process from the operations on roles, resources, and the applications. In the traditional process-based system, the relations between activities, roles, resources, and applications are shown in Fig.2 (a). It can be seen that workflow engine needs to deal with them directly. It results in some difficult in system design and system maintenance. Fig. 2(b) shows the new relations. All the operations on resources, roles and the applications are done by policy engine through the late-bound components. The separation benefits the system design and the enterprise administration.

3   Advantages of New Approach

Integrate the policy-based management in traditional WfMS has many advantages:

Firstly, it improves flexibility and adaptability. For example, a loan application usually has many business rules to deal with. This can be done by a traditional process based workflow system. For some business rules such as determine whether the supplied information is complete, credit scoring and other risk assessment, execute the required level of approval and ensure regulatory compliance it is better using policy-based management. With policy-based management, business managers can specify only the policies or local objectives for these business rules. Policies can also describe much complex requirements of resources and security control. So it has better flexibility in design time. At the run-time the active policies in policy repository can be changed dynamically, a policy and the components to execute this policy can be late bound to achieve higher adaptability.

Secondly, a centralized policy repository and an independent policy engine to execute policies make it possible to keep the business rules consistent across the whole enterprise.

Lastly, it is possible to use a uniform method to deal with resources and security controls and business rules. This benefits the system design.

4   Conclusion and Future Work

The new process meta model described in this paper defines new elements to support policy-based management in WfMS. Based on the model a workflow system has better flexibility and adaptability. We have some experience on developing the policy engine in network management systems. The future work is to make expansions to the traditional workflow engine to achieve close collaboration with the policy engine.

References

1. Song Ouyang, "Integrate Policy based Management and Process based Management—A New Approach for Workflow Management System", IEEE proceedings of CSCWD2006, Nanjing, China (2006).
2. Shi MeiLin, Yang GuangXin, Xiang Yong, Wu ShangGuang, "Workflow Management Systems: A Survey", Proceedings of IEEE Intl Conf on Communication Technology, Beijing (1998)
3. CA Ellis, K. Keddara, G. Rozenberg., "Dynamic change within workflow systems", Proceedings of International, ACM Conference, COOCS '95, Milpitas, CA, August. (1995)
4. Fan YuShun, Wu Cheng, "Research on a Workflow Modeling Method to Improve System Flexibility", Journal of Software, Vol. 13 (2002)
5. Sun ReiZhi, Shi MeiLin, "A Process Meta-Model Supporting Dynamic Change of Workflow", Journal of Software, Vol. 14 (2003)
6. Zhao Wen, Hu WenHui, Zhang ShiKun, Wang LiFu, "Study and Application of a Workflow Meta-Model", Journal of Software, Vol. 13 (2003)
7. Weimin Du, Ming-Chien Shan: "Enterprise Workflow Resource Management". RIDE (1999)

Using Gavish-Grave LP to Formulate the Directed Black and White Traveling Salesman Problem

He Jiang[1], XianChao Zhang[1], MingChu Li[1], and HaoYang Che[2]

[1] School of Software, Dalian University of Technology, Dalian 116621, China
{xczhang, jianghe, mingchul}@dlut.edu.cn
[2] Institute of Software, The Chinese Academy of Sciences, Beijing 100080, China
grandiose11@msn.com

Abstract. The black and white traveling salesman problem (BWTSP) is a new class of NP-hard problem arising from work on airline scheduling and telecommunication fiber networks. The existing Ghiani LP for the undirected BWTSP contains an exponential number of constraints. For a special case of the directed BWTSP whose $L = +\infty$, the LP with polynomial number of constraints could be obtained by transforming it to an asymmetric traveling salesman problem with replenishment arcs (RATSP), whereas there exists no LP for the directed BWTSP in its general form. This paper proposes a LP with $3n^2 + 2n$ constraints only for the directed BWTSP in such a way that, by reducing the problem to an asymmetric traveling salesman problem (ATSP), we add n^2 cardinality constraints and n^2 length constraints to the existing Gavish-Grave LP for the ATSP. The new LP is also valid for the undirected BWTSP when viewed as a special case of the directed BWTSP.

Keywords: Black and white traveling salesman problem, Linear programming, Gavish-Grave LP.

1 Introduction

The black and white traveling salesman problem (BWTSP) is a generalization of the well known traveling salesman problem (TSP) and is therefore NP-hard. Given a directed graph $G = (V, A)$ or an undirected graph $G = (V, E)$ with vertex set $V = \{1, \cdots, n\}$, arc set $A = \{(i, j) : i, j \in V, i \neq j\}$ or edge set $E = \{(i, j) : i, j \in V, i \neq j\}$, and costs on the arcs $c \in R^{|A|}$ or costs on the edges $c \in R^{|E|}$, the BWTSP is to find a shortest Hamiltonian tour on G. However the tour must satisfy additional constraints i) cardinality constraints: the vertex set V is partitioned into black vertices, denoted by B ($|B| \geq 2$) and white vertices, denoted by $W = V \setminus B$, the number of white vertices between two consecutive black vertices on the tour does not exceed a positive integer Q, and ii) length constraints: the length of any path or chain between two consecutive black vertices does not exceed a positive value L.

An application of the BWTSP arises in the design of telecommunication fiber networks using the SONET technology [1, 2]. When designing survivable fiber

networks using the SONET technology, one seeks a shortest Hamiltonian cycle comprising hubs (white vertices) and ring offices (black vertices) with upper bounds on both the number of hubs and chain length between consecutive ring offices. Aside the above-mentioned application, the scheduling of airline operations that incorporate maintenance connections [3] can also be modeled as a BWTSP.

Ghiani et al. have shown a linear programming (LP) with exponential constraints for the undirected BWTSP, whereas no LP exists for the directed BWTSP in its general form. With the special case of the directed BWTSP whose $Q = L = +\infty$ is associated extensive existing LPs by reverting to the usual ATSP (see [5]). Dantzig et al. [6] introduced a conventional LP with $2^{n-1} - n - 1$ constraints in 1954. Miller et al. [7] presented a sequential LP with $n^2 - n + 2$ constraints in 1960. A single commodity flow based LP with $n(n+2)$ constraints was proposed by Gavish et al. [8] in 1978. In 1983 Finke et al. [9] developed a two-commodity flow based LP with $n(n+4)$ constraints. Wong [10] and Claus [11] described the multi-commodity flow based LP with $n^3 + n^2 + 6n - 3$ constraints, respectively, in 1980 and 1984. Besides a time staged LP with $2n^2 - n + 3$ constraints by Vajda [12] in 1961, Fox et al. [13] showed two time staged LPs in 1980, one with $4n - 1$ constraints, the other with $n(n+2)$ constraints.

When $L = +\infty$, the directed BWTSP reduced to an asymmetric traveling salesman problem with replenishment arcs (RATSP). The natural arc LP for the RATSP was developed by Zhu [14] based on the DFJ formulation for the ATSP in 1994. Boland et al. [15] proposed a path LP for the same problem in 2000. Both of the previously mentioned LPs involve exponentially many variables and constraints. Vicky [16] strengthened the LP by Zhu, and proposed a polynomial-size LP.

In this paper we propose a new LP with polynomial constraints for the directed BWTSP in its general form. The directed BWTSP reduces to an ATSP when $Q = L = \infty$, thus we can derive our LP from the Gavish-Grave LP [8] for the ATSP. The new n^2 formulations of cardinality constraints are obtained in such a way that, by introducing cardinality flow representing the number of white vertices quota remaining, we investigate the conditions that the arcs on the tour should be subject to. Similarly, we obtain n^2 formulations of length constraints. Therefore, we establish the new LP with $3n^2 + 2n$ constraints for the original problem. The new LP is also valid for the undirected BWTSP when viewed as a special case of the directed BWTSP. The results of the paper can promote the complete algorithm design of the BWTSP.

The remainder of this paper is organized as follows. In section 2, we describe the Gavish-Grave LP for the ATSP. Cardinality constraints and length constraints are presented in section 3 and in section 4, respectively, followed by conclusions in section 5.

2   Gavish-Grave LP for the ATSP

As mentioned before, the directed BWTSP reduces to an ATSP when $Q = L = \infty$, thus any solution to the directed BWTSP is feasible for the ATSP, and all inequalities

for the ATSP are also valid for the directed BWTSP. Therefore, we are able to derive our LP from the Gavish-Grave LP.

We define x_{ij} as a binary variable equal to 1 iff arc (i, j) belongs to the solution. To eliminate subtours, we introduce y_{ij} as a continuous variable which represents the commodity flow in arc (i, j). The Gavish-Grave LP for the ATSP can be described as follows.

$$\min \sum_{i \neq j} c_{ij} x_{ij} \tag{1}$$

$$\text{s.t. } \sum_{i \neq j} x_{ij} = 1 \qquad\qquad \forall j \in B \bigcup W \tag{2}$$

$$\sum_{j \neq i} x_{ij} = 1 \qquad\qquad \forall i \in B \bigcup W \tag{3}$$

$$x_{ij} = 0 \text{ or } 1 \qquad\qquad (i, j) \in A \tag{4}$$

$$0 \leq y_{ij} \leq (n-1) x_{ij} \qquad\qquad \forall i, j \in B \bigcup W, i \neq j \tag{5}$$

$$\sum_{j \neq 1} y_{1j} = n-1 \tag{6}$$

$$\sum_{i \neq j} y_{ij} - \sum_{z \neq j} y_{jz} = 1 \qquad \forall j \in B \bigcup W - \{1\} \tag{7}$$

In this LP, constraints (2)-(4) are degree constraints which insure that exactly one arc enters and leaves each vertex. Whereas constraints (5)-(7) are called arc constraints which guarantee that the solution contains exactly one loop. Assume that the solution contains more than one loop, all of them distinct. Consider a loop $t = (i_0, i_1, ..., i_k, i_0)$ which does not contain vertex 1. From (5) and (7) it follows that $y_{i_{j-1} i_j} - y_{i_j i_{(j+1) \bmod (k+1)}} = 1$ for all $j = 1, ..., k$, therefore we have $y_{i_0 i_1} = y_{i_k i_0} + k$, nevertheless from (7) it follows that $y_{i_k i_0} - y_{i_0 i_1} = 1$. No loops can exist that do not contain vertex 1; since vertex 1 is contained in exactly one loop, thus at most one loop is generated.

The Gavish-Grave LP consists of $n(n+2)$ constraints, $n(n-1)$ 0-1 variables and $n(n-1)$ continuous variables.

3   Cardinality Constraints

We define $p = (i_0, i_1, ..., i_k)$ as a black-to-black path with $(i_{j-1}, i_j) \in A$ for all $j = 1, ..., k$, $i_j \neq i_l$ for all distinct $j, l \in \{0, ..., k\}$, and $i_0, i_k \in B, i_j \in W$ for all $j = 1, ..., k-1$. We also define $V(p) = \{i_0, i_1, ..., i_k\}$ as the vertices on p, $A(p) = \{(i_0, i_1), (i_1, i_2), ..., (i_{k-1}, i_k)\}$ as the arcs on p, and $f(p) = c_{i_0 i_1} + c_{i_1 i_2} + ... + c_{i_{k-1} i_k}$ as the length of p. A black-to-black path p is said to be feasible if the number of white

vertices on it does not exceed Q, i.e. $|V(p)| - 2 \leq Q$, and the length of it does not exceed L, i.e. $f(p) \leq L$. Otherwise it is said to be infeasible. Obviously, a feasible solution of the BWTSP consists of alternating feasible black-to-black paths.

To eliminate cardinality violation, we introduce extra cardinality flow q_{ij} for each $(i, j) \in A$, which represents the number of white vertices quota remaining after visiting arc (i, j). Then our cardinality constraints can be derived as follows.

The total cardinality flow into a white vertex $j \in W$ will be 1 more than that out of j. Therefore, we have the following constraint:

$$\sum_{i \neq j} q_{ij} - \sum_{z \neq j} q_{jz} = 1 \qquad \forall j \in W \qquad (8)$$

And the total cardinality flow out of each black vertex $j \in B$ should not exceed Q in order to guarantee that, the number of white vertices on the black-to-black path starting with vertex j does not exceed Q.

$$\sum_{i \neq j} q_{ji} \leq Q \qquad \forall j \in B \qquad (9)$$

Last of all, q_{ij} is bounded according to:

$$0 \leq q_{ij} \leq Q x_{ij} \qquad \forall i, j \in B \bigcup W, i \neq j \qquad (10)$$

Constraints (8), (9) and (10) are formulations of cardinality constraints which impose the maximum number restriction of white vertices between consecutive black vertices. These formulations consist of n^2 constraints and $n(n-1)$ new continuous variables.

Proposition 1. Constraints (8), (9) and (10) are valid for the directed BWTSP.

Proof. Assume that a solution of the directed BWTSP subject to constraints (8), (9) and (10) violates the cardinality constraints. Thus, there must be a black-to-black path $p = (i_0, i_1, ..., i_k)$ on the solution subject to $k - 2 \geq Q$. From (8) and (10) it follows that $q_{i_r i_{r+1}} = q_{i_{r+1} i_{r+2}} + 1$ for all $r = 0, ..., k - 2$. Therefore, we have $q_{i_0 i_1} = q_{i_{k-1} i_k} + k - 1 > Q$, which contradicts with constraint (9). Thus, no solution subject to (8), (9) and (10) could exist that does not satisfy cardinality constraints.

To show that a feasible solution of the directed BWTSP satisfies (8), (9) and (10), assume that $p = (i_0, i_1, ..., i_k)$ is a feasible black-to-black path on the solution; (8), (9) and (10) hold by assigning $q_{i_r i_{r+1}} = k - 1 - r$, $q_{i_r z} = 0$ for all $(i_r, z) \notin A(p)$, $r = 0, ..., k - 1$. □

4   Length Constraints

To eliminate length violation, we introduce length flow l_{ij} for each $(i, j) \in A$, which represents the length quota remaining after visiting arc (i, j). Our length constraints are derived as follows.

If arc $(i, j) \in A$ ($i \in W$) belongs to the solution, i.e. if $x_{ij} = 1$, the total length flow out of vertex i will be c_{ij} less than that into it. To guarantee this is satisfied, we require that if $x_{ij} = 1$, then $\sum_{z \neq i} l_{iz} = \sum_{s \neq i} l_{si} - c_{ij}$. Therefore, we have the following constraint:

$$\sum_{z \neq i} l_{iz} = \sum_{s \neq i} l_{si} - \sum_{z \neq i} c_{iz} x_{iz} \qquad \forall i \in W \qquad (11)$$

If arc $(i, j) \in A$ ($i \in B$) belongs to the solution, i.e. if $x_{ij} = 1$, the total length flow out of vertex i will be considered "refreshed" after visiting i and l_{ij} will be set to $L - c_{ij}$. Thus, we obtain the following constraint:

$$\sum_{z \neq i} l_{iz} = L - \sum_{z \neq i} c_{iz} x_{iz} \qquad \forall i \in B \qquad (12)$$

Last of all, l_{ij} is bounded according to:

$$0 \leq l_{ij} \leq x_{ij} L \qquad \forall i, j \in B \cup W, i \neq j \qquad (13)$$

Constraints (11), (12) and (13) are formulations of length constraints which impose the maximum length restriction between consecutive black vertices. These formulations consist of n^2 constraints and $n(n-1)$ new continuous variables.

Proposition 2. Constraints (11), (12) and (13) are valid for the directed BWTSP.

Proof. Assume that a solution subject to constraints (11), (12) and (13) violates the length constraints. Thus, there must be a black-to-black path $p = (i_0, i_1, ..., i_k)$ on the solution subject to $\sum_{0 \leq r \leq k-1} c_{i_r i_{r+1}} > L$ and $x_{i_r i_{r+1}} = 1$ for all $r = 0, \cdots, k-1$. From (11) it follows that $l_{i_{r+1} i_{r+2}} = l_{i_r i_{r+1}} - c_{i_{r+1} i_{r+2}}$ for all $r = 0, ..., k-2$. Therefore, we have $l_{i_{k-1} i_k} = l_{i_0 i_1} - \sum_{1 \leq r \leq k-1} c_{i_r i_{r+1}}$. From (12) it follows that $l_{i_0 i_1} = L - c_{i_0 i_1}$; hence, we have $l_{i_{k-1} i_k} = L - \sum_{0 \leq r \leq k-1} c_{i_r i_{r+1}} < 0$, which contradicts with constraint (13). Thus, no solution subject to (11), (12) and (13) can exist that does not satisfy length constraints.

We can show that a feasible solution of the directed BWTSP satisfies (11), (12) and (13) in a similar way as given in the proof of Proposition 1. Given a feasible black-to-black path $p = (i_0, i_1, ..., i_k)$ on the solution, (11), (12) and (13) hold by assigning $l_{i_r i_{r+1}} = L - \sum_{0 \leq s \leq r} c_{i_s i_{s+1}}$, $l_{i_r z} = 0$ for all $(i_r, z) \notin A(p)$, $r = 0, ..., k-1$.   □

5   Conclusion

In this paper, we have introduced a new LP for the directed BWTSP. Compared to the Ghiani LP with exponential constraints for the undirected BWTSP, our LP involves $3n^2 + 2n$ constraints only. The new LP is derived from the Gavish-Grave LP by

defining two classes of flows: one represents the number of white vertices quota remaining, the other represents the length quota remaining.

References

1. Wasem OJ. An algorithm for designing rings in survivable fiber networks. IEEE Transactions on Reliability (1991) 40:428-32
2. Cosares S, Deutsch DN, Saniee I, Wasem OJ. SONET toolkit: a decision support system for designing robust and cost-effective fiber-optic networks. Interfaces (1995) 25(1):20-40
3. Talluri KT. The four-day aircraft maintenance routing problem. Transportation Science (1998) 32:43-53
4. Mak V, Boland N. Heuristic approaches to the asymmetric traveling salesman problem with replenishment arcs. International Transactions in Operation Research (2000) 7:431-47.
5. Orman AJ, Williams HP. A survey of different integer programming formulations of the travelling salesman problem. Working Paper No: LSEOR 04.67, The London School of Economics and Political Science (2004)
6. Dantzig GG, Fulkerson DR and Johnson SM. Solutions of a large scale traveling salesman problem. Operations. Research (1954) 2:393-410
7. Miller CE, Tucker AW and Zemlin RA. Integer programming formulation of traveling salesman problem. Journal of ACM (1960) 3:326-329
8. Gavish B and Graves SC. The traveling salesman problem and related problems. Working Paper OR-078-78, Operations Research Center, MIT, Cambridge, MA (1978)
9. Finke KR, Gavish B and Graves SC. A two-commodity network flow approach to the traveling salesman problem. Combinatorics, Graph Theory and Computing, Proc. 14th South Eastern Conf., Atlantic University, Florida (1983)
10. Wong RT. Integer programming formulations of the traveling salesman problem. Proc. IEEE Conf. On Circuits and Computers (1980) 149-152
11. Claus A. A new formulation for the traveling salesman problem. SIAM Journal of Algorithm and Discrete Mathematics (1984) 5:21-25
12. Vajda S. Mathematical Programming. Addison-Wesley, London (1961)
13. Fox KR, Gavish B and Graves SC. An n-constraint formulation of the (time-dependent) traveling salesman problem. Operations Research (1980) 28:1018-1021
14. Zhu, Z. The aircraft rotation problem. PhD thesis, Georgia Institute of Technology (1994)
15. Boland NL, Clarke LW, Nemhauser GL. The asymmetric traveling salesman problem with replenishment arcs. European Journal of Operations Research (2000) 123:408-427
16. Vicky M. On the asymmetric traveling salesman problem with replenishment arcs. Department of Mathematics and Statistics, University of Melbourne, PhD thesis (2000)

Semicomplete Multipartite Digraphs Whose Every Arc Is Contained in a Hamiltonian Path

Wei Meng[*] and Shengjia Li

School of Mathematical Sciences, Shanxi University,
030006 Taiyuan, P.R. China
{alfred.hofmann,ursula.barth,ingrid.beyer,christine.guenther,
frank.holzwarth,anna.kramer,erika.siebert-cole,lncs}@springer.com
http://www.sxu.edu.cn

Abstract. A semicomplete multipartite digraph is obtained by replacing each edge of a complete multipartite graph by an arc or by a pair of two mutually opposite arcs. In 2002, L.Volkmann [5] raised a problem: determine some sufficient conditions for semicomplete multipartite digraphs such that every arc is contained in a Hamiltonian path. In this paper, we give a new sufficient condition and describe some semicomplete multipartite digraphs demonstrating that this sufficient condition is independent and in some sense, it is best possible.

Keywords: Semicomplete multipartite digraph, Hamiltonian paths, Semi-partition complete digraphs.

1 Terminology and Introduction

In this paper all digraphs are finite without loops and multiple arcs. The vertex set and the arc set of a digraph are denoted by $V(D)$ and $A(D)$, respectively. The number of vertices in D is called the *order* of D. A digraph obtained by replacing each edge of a complete n-partite graph by an arc or a pair of mutually opposite arcs is called a *semicomplete n-partite* or *multipartite digraph*. Obviously, a tournament is a semicomplete multipartite digraph without cycles of length 2 where each partite set contains exactly one vertex.

If xy is an arc of a digraph D, then we say that x *dominates* y and write $x \to y$. More generally, for disjoint subsets A and B of $V(D)$ or subdigraphs of D, if every vertex of A dominates every vertex of B, then we say that A *dominates* B, denoted by $A \to B$. In the case when there is no arc from B to A, we write $A \Rightarrow B$. If both of $A \to B$ and $A \Rightarrow B$ hold, then we say that A *strictly dominates* B, denoted by $A \mapsto B$. Furthermore, if for all $a \in A$ and

---

$b \in B$, either a, b are not adjacent or $a \to b$, then we denote this relationship between A and B by $A \hookrightarrow B$. For $S \subseteq V(D)$ and for any vertex $x \in V(D)$, we define $d^+(x, S)$ $(d^-(x, S))$ to be the number of out-neighbours (in-neighbours) of x in S. If $S = V(D)$, we also write $d^+(x, D) = d^+(x)$ $(d^-(x, D) = d^-(x))$. Furthermore, $N^+(S)$ $(N^-(S))$ is the set of out-neighbours (in-neighbours) of S.

By a cycle (path) we mean a directed cycle (directed path). A path $P = x_1 x_2 ..... x_k$ starts with the arc $x_1 x_2$, or $x_1 x_2$ is the *initial arc* of P. A cycle of length m is an m-cycle. A cycle in a digraph D is *Hamiltonian* if it includes all the vertices of D. A digraph D is *Hamiltonian* if it contains a Hamiltonian cycle. If x is a vertex on a cycle, then x^+ (x^-) denotes the successor (predecessor) of x on C. If a cycle (path) Q contains a subpath from x to y, then we denote it by $Q[x, y]$. A subdigraph F of a digraph D which contains all the vertices of D and which consists of a set of vertex-disjoint cycles is called a 1-*regular factor*. F is said to be *minimal* if there is no 1-regular factor F' of D consisting of less cycles than F.

For a vertex set X of digraph D, we define $D[X]$ as the subdigraph induced by X. A set $X \subseteq V(D)$ is *independent* if the induced subdigraph $D[X]$ has no arcs. The *independent number* $\alpha(D) = \alpha$ is the maximum size among the independent sets of vertices of D. A digraph D is *strong connected* or *strong* if, for each pair of vertices u and v, there is a path in D from u to v. A digraph D with at least $k + 1$ vertices is k-*connected* if for any set A of at most $k - 1$ vertices, the subdigraph $D - A$ obtained by deleting A is strong. The *connectivity* of D, denoted by $\kappa(D)$, is then defined to be the largest value of k such that D is k-connected.

Some first observation on semicomplete multipartite digraphs can be found in Moon's book [3]. In the following decades graph theorists began to study multipartite semicomplete digraphs more extensively. Excellent sources for more information in this area are found in recent book by Bang-Jensen and Gutin [1]. In 2002, L.Volkmann [5] discussed the longest paths through an arc in strong semicomplete multipartite digraphs and gave a sufficient condition such that all arcs are contained in a Hamiltonian path.

Theorem 1 [5].   Let D be a semicomplete multipartite digraphs with $\kappa(D) > \alpha(D)$, then every arc is contained in a Hamiltonian path.

In addition, L.Volkmann [5] posed the following problem:

Problem 1 [5]. Determine some sufficient conditions for semicomplete multipartite digraphs such that every arc is contained in a Hamiltonian path.

In this paper, we give a new sufficient condition in term of this problem. Furthermore, through examples we illustrate the independence of this sufficient condition and the best possibility in some sense. Moreover, a new class of semicomplete multipartite digraphs are introduced and we present a sufficient condition for these digraphs to be Hamiltonian.

2   Preliminaries

The following results play an important role in our investigation. First the definition of semi-partition complete digraphs which was first introduced by Guo [2] and some properties of these digraphs are given.

Definition 1. Let D be a semicomplete multipartite digraph with the partite sets V_1, V_2,...,V_k. If $d^+(x_i, V_j), d^-(x_i, V_j) \geq |V_j|/2$ for every vertex $x_i \in V_i$ and for every $1 \leq i, j \leq k$, $j \neq i$, then D is called a semi-partition complete digraph.

Theorem 2 [2]. Let D be a semi-partition complete digraph of order n with $\alpha(D) \leq n/2$. Then D is Hamiltonian or there exists two vertex-disjoint cycles C_1 and C_2 in D such that $V(C_1) \cup V(C_2) = V(D)$ and $|V(C_1) \cap V_j| = |V(C_2) \cap V_j| = |V_j|/2$ for all $1 \leq j \leq k$, where $V_1, V_2, ..., V_k$ are the partite sets of D.

Now we state a shorten version of Yeo's [6] result about the structure of semicomplete multipartite digraphs with a 1-regular factor.

Theorem 3 [6]. Let D be a semicomplete multipartite digraph containing a 1-regular factor. Then there exists a 1-regular factor F in D whose cycles can be labeled, $C_1, C_2, ..., C_t$, such that the following holds:

There exists a partite set V^* in D such that whenever $x_j \to x_1$ where $x_j \in V(C_j)$, $x_1 \in V(C_1)$ and $1 < j \leq t$, we have $\{x_j^+, x_1^-\} \subseteq V^*$.

In particular, if F is minimal, then it has the properties described above.

3   Main Results

Theorem 4. Let D be a semicomplete multipartite digraph with partite sets $V_1, V_2, ..., V_k$. If $d^+(x_i, V_j), d^-(x_i, V_j) \geq (|V_j| + 1)/2$ for every vertex $x_i \in V_i$, for each $1 \leq i, j \leq k$, $j \neq i$, and $\alpha(D) \leq (n-1)/2$, then every arc is contained in a Hamiltonian path.

Proof. Let xy be any arc of D. From the assumption we see that $D - x$ is a semi-partition complete digraph which satisfies $\alpha(D - x) \leq \alpha(D) \leq (n-1)/2 = |V(D-x)|/2$. According to Theorem 2, $D-x$ is either Hamiltonian or there exists two vertex-disjoint cycles C_1 and C_2 in $D-x$ such that $V(C_1) \cup V(C_2) = V(D-x)$ and C_i contain exactly half of the vertices of every partite set of $D-x$, for $i = 1, 2$.

If $D - x$ has a Hamiltonian cycle, denoted by $yy_2y_3...y_{n-1}y$, then xy lies on such a Hamiltonian path of D $xyy_2y_3...y_{n-1}$. Then we are done.

Now, we assume that there exists two vertex-disjoint cycles C_1 and C_2 in $D-x$ satisfying the condition described as above. Assume without loss of generality that $y \in C_1 \cap V_1$. Since x and y^- are both adjacent to y, x and y^- do not belong to V_1. Note that $C_2 \cap V_1 \neq \emptyset$, we claim that there exists at least one vertex $z \in C_2 \cap V_1$ such that $y^- \to z$. In fact, if this is not true, then we have $C_2 \cap V_1 \mapsto y^-$. Hence, $N^+(y^-, V_1) \subseteq C_1 \cap V_1$ holds. Recalling x does not belong to V_1, we have $|C_1 \cap V_1| = |V_1|/2$. This contradicts the assumption

$d^+(y^-, V_1) \geq (|V_1| + 1)/2$. Now, the arc xy is on such a Hamiltonian path $xyC_1[y^+, y^-]zC_2[z^+, z^-]$. This completes the proof. □

An example will show that conditions in Theorem 4 are independent to Theorem 1.

Example 1. Let $V_1 = \{v_1, v_2, v_3\}$, $V_2 = \{v_4, v_5, v_6\}$, and $V_3 = \{v_7\}$ be the partite sets of a semicomplete 3-partite digraphs D. The arcs between v_1, v_2, v_3, v_4 are $v_1 \rightarrow v_4 \rightarrow v_2 \rightarrow v_4 \rightarrow v_3$, and the other arcs between two vertices of different partite sets are two mutually opposite arcs. It is not difficult to check that this digraph D satisfies all conditions in Theorem 4 and hence, every arc is contained in a Hamiltonian path.

Note that the vertices $\{v_5, v_6, v_7\}$ is a separating set of D. So $\kappa(D) \leq 2$, but $\alpha(D) = 3$. Therefore, D does not satisfy the conditions in Theorem 1.

In addition, at the proof of Theorem 4, we actually showed that every arc is not only on a Hamiltonian path, but also the arc is exactly the initial arc of the Hamiltonian path. In this sense, the degree-condition in Theorem 4 is best possible. See the following example.

Example 2. Let $V_1 = \{x_1, x_2, x_3, x_4\}$, $V_2 = \{y_1, y_2, y_3, y_4\}$ and $V_3 = \{z_1, z_2, z_3, z_4\}$ be the partite sets of a semicomplete 3-partite digraphs D. The arcs between any two vertices in $S_1 = \{x_1, y_1, z_1, x_2, y_2, z_2\}$, which belong to different partite sets are defined by two mutually opposite arcs. Similarly, we define the arcs in $S_2 = \{x_3, y_3, z_3, x_4, y_4, z_4\}$. Moreover, $S_1 \hookrightarrow S_2$.

It is easy to see that D is a semicomplete 3-partite digraph with order 12, $\alpha(D) = 4$ and $d^+(x_3, V_2) = 2$. But every arc in S_2 is not on any Hamiltonian path which starts with this arc.

In the following we abstract the conditions in Theorem 4 and define a new class of semicomplete multipartite digraphs. Furthermore, we will present a sufficient condition for these digraphs to be Hamiltonian.

Definition 2. Let D be a semicomplete multipartite digraph with partite sets $V_1, V_2, ..., V_k$. If $d^+(x_i, V_j), d^-(x_i, V_j) \geq (|V_j| + 1)/2$ for every vertex $x_i \in V_i$ and for every $1 \leq i, j \leq k$, $j \neq i$, then D is called a quasi-semi-partition complete digraph.

Remark 1. According to Definition 2, Theorem 4 can be stated as: Let D be a quasi-semi-partition complete digraph with order n and $\alpha(D) < n/2$, then every arc of D is contained in a Hamiltonian path.

Remark 2. Clearly, quasi-semi-partition complete digraphs are also semi-partition complete digraphs.

Theorem 5. Every quasi-semi-partition complete digraph is strong.

Proof. Let D be a quasi-semi-partition complete digraph with partite sets $V_1, V_2, ..., V_k$, and x, y any two distinct vertices of D.

If $x, y \in V_i$ for some $i \in \{1, 2, ..., k\}$, then for any $j \neq i$, and $1 \leq j \leq k$, let $A_j = \{a \in V_j | x \mapsto a\}$, $B_j = \{b \in V_j | x \to b, b \to x\}$, and $C_j = \{c \in V_j | c \mapsto x\}$. Obviously, A_j, B_j, C_j are pairwise disjoint and $A_j \cup B_j \cup C_j = V_j$. Because of $d^+(x, V_j) \geq (|V_j|+1)/2$, we know $|A_j \cup B_j| \geq (|V_j|+1)/2$ and then, $|C_j| < |V_j|/2$. Also note that $d^-(y, V_j) \geq (|V_j|+1)/2$, so there is at least one vertex in $A_j \cup B_j$ which dominates y, say u. According to the definitions of A_j and B_j, xuy is a path in D from x to y. Similarly, we can show that there is also a path from y to x.

Now we suppose that $x \in V_i$, $y \in V_j$ for some $i, j \in \{1, 2, ..., k\}$ and $i \neq j$. Since x and y are adjacent, we assume without loss of generality that $x \to y$. If $y \to x$ also holds, then there is nothing to prove. Otherwise, we have $x \mapsto y$. Let $A = \{a \in V_i | a \mapsto y\}$, $B = \{b \in V_i | y \to b, b \to y\}$, $C = \{c \in V_i | y \mapsto c\}$, $L = \{d \in V_j | x \mapsto d\}$, $M = \{e \in V_j | x \to e, e \to x\}$ and $N = \{f \in V_j | f \mapsto x\}$. Clearly, L, M, N are pairwise disjoint, $L \cup M \cup N = V_j$ and $B \neq \emptyset$. Because of $d^-(x, V_j) \geq (|V_j|+1)/2$, we know $|M \cup N| \geq (|V_j|+1)/2$ and then, $|L| < |V_j|/2$. Now we claim that there is at least one arc uv in D from B to $M \cup N$. In fact, if this is not true, then $M \cup N \mapsto B$ and for any vertex b of B, we have $N^+(b, V_j) \subseteq L$. So $d^+(b, V_j) \leq |L| < |V_j|/2$, a contradiction ! By the definitions of B, M and N, we see that $y \to u$ and $v \to x$ hold. Hence, $yuvx$ is just a path in D from y to x.

In summary, D is strongly connected. $\qquad\square$

By using Theorem 5, we obtain a sufficient condition for a quasi-semi-partition complete digraph to be Hamiltonian.

Theorem 6. Let D be a quasi-semi-partition complete digraph with $\alpha(D) \leq n/2$. Then D is Hamiltonian.

Proof. From Remark 2 and Theorem 2, D is either Hamiltonian or there exists two vertex-disjoint cycles C_1 and C_2 in D such that $V(C_1) \cup V(C_2) = V(D)$ and $|V(C_1) \cap V_j| = |V(C_2) \cap V_j| = |V_j|/2$ for all $1 \leq j \leq k$, where $V_1, V_2, ..., V_k$ are the partite sets of D. We only need to consider the latter case. Obviously, C_1, C_2 is the minimal 1-regular factor. Thus, according to Theorem 3, we may assume that C_1, C_2 and V^* just satisfies Theorem 3. Theorem 5 ensue that D is strong, hence there are vertices $u \in C_1$ and $v \in C_2$ such that $v \to u$. Furthermore, $u^- \in V^*$ and $u^- \mapsto V(C_2) \cap (V - V^*)$. In fact, u^- is adjacent to any vertex of $V(C_2) \cap (V - V^*)$. If there exists a vertex in $V(C_2) \cap (V - V^*)$ which dominates u^-, then again by Theorem 3, we deduce $u^{--} \in V^*$, but this is clearly not impossible. For any partite set V' different from V^*, we have $d^-(u^-, V') \leq |C_1 \cap V'| = |V'|/2$. This contradicts the definition of quasi-semi-partition complete digraphs. Therefore, D is Hamiltonian. $\qquad\square$

References

1. Bang-Jensen,J., Gutin,G.: Digraphs: Theory, Algorithms and Applications. Springer, London (2000)
2. Guo,Y., Tewes,M., Volkmann,L., Yeo,A.: Sufficient conditions for semicomplete multipartite digraphs to be Hamiltonian. Discrete Math. **212** (2000) 91-100
3. Moon,J.W.: Topics on Tournaments. Holt, Rinehart and Winston, New York (1968)
4. Ore,O.: Theory of graphs. Amer. Soc. Colloq. Publ., Vol. 38. (1962)
5. Volkmann,L.: Longest paths through an arc in strong semicomplete multipartite digraphs. Discrete Math. **258** (2002) 331–337
6. Yeo,A.: One-diregular subgraphs in semicomplete multipartite digraphs. J. Graph Theory **24** (1997) 175–185

The Roman Domination Problem in Unit Disk Graphs*

Weiping Shang and Xiaodong Hu

Institute of Applied Mathematics, Chinese Academy of Sciences
P. O. Box 2734, Beijing 100080, China
{shangwp, xdhu}@amss.ac.cn

Abstract. Unit disk graphs are the intersection graphs of equal sized disks in the plane, they are widely used as a mathematical model for wireless ad-hoc networks and some problems in computational geometry. In this paper we first show that the Roman domination problem in unit disk graphs is NP-hard, and then present a simple linear time approximation algorithm and a polynomial-time approximation scheme for this problem, respectively.

Keywords: Domination, approximation algorithm, unit disk graph.

1 Introduction

Let $G = (V, E)$ be a simple and undirected graph. A set $D \subseteq V$ is a *dominating set* if every vertex in $V \setminus D$ is adjacent to at least one vertex in D. The *domination number*, denoted $\gamma(G)$, is the minimal cardinality of a dominating set in G. The *minimum dominating set problem* is to compute a dominating set of minimal cardinality for any given graph G. A *Roman dominating function* [1] of a graph G is defined as a function $f : V(G) \to \{0, 1, 2\}$ satisfying the condition that every vertex u with $f(u) = 0$ is adjacent to at least one vertex v with $f(v) = 2$. The *weight* of a Roman dominating function is $f(V) = \sum_{v \in V} f(v)$. The *Roman domination number*, denoted $\gamma_R(G)$, is the minimum weight of Roman dominating functions in G. The minimum Roman domination problem is to compute a minimum weight dominating function for any given graph G.

Minimum Roman domination problem is introduced in [1] as one of variants of classical dominating set problem. It comes with a nice story: The Roman Empire needs to defence itself by positioning some legions on the various parts of the Empire in such a way that either (1) a specific region v is also the location of at least one legion or (2) one region u neighboring v has two legions, so that u can afford sending off one army to the region v (in case of an attack) without loosing self-defence capabilities. Since it is expensive to maintain a legion at a location, the Emperor would like to station as few legions as possible, while still defending

the Roman Empire. Roman domination problem has not only historical but also mathematical interests, particularly in the field of server placements [3].

In reality, it is desired that dispatching a legion from one location to another location should not take too much time; In particular, it is desirable that a legion from one location could be dispatched to another location if the Euclidean distance between the two corresponding points is no more than a specified bound. Unit disk graphs satisfy such a property. A undirected graph $G = (V, E)$ is a *unit disk graph* (UDG) if its vertices can be put in one-to-one correspondence with disks of equal radius in the plane in such a way that two vertices are joined by an edge if and only if the corresponding disks intersect. In other words, G is a UDG if there exists a map $f : V \to R^2$ such that $(u, v) \in E$ if and only if $\|f(u) - f(v)\| \leq 1$, where $\|.\|$ denotes the Euclidean norm. *Grid graphs* compose a subclass of unit disk graphs under such an intersection model that all the disks have centers with integer coordinates and radius $1/2$.

It has been shown in [7] that many graph related problems in unit disks graphs are NP-hard, including the independent set problem, the dominating set and connected dominating set problems; In fact, the dominating set problem is NP-hard even for grid graphs. Polynomial-Time Approximation Schemes (PTASs) for these problems in unit disk graphs are presented in [10, 11]. Roman domination problem in general graphs is proved to be NP-hard in [2], $(2+2ln(n))$-approximation algorithms and a PTAS are proposed in [3] for general graphs and for minimum planar Roman domination problem, respectively.

In this paper, we consider the Roman domination problem in unit disk graphs. We will first give some preliminaries about the problem in Section 2, and then we will prove that the Roman domination problem in unit disk graphs is NP-hard in Section 3, after that we will propose a simple linear-time approximation algorithm and a polynomial-time approximation scheme for the problem in Section 4. In Section 5 we conclude the paper.

2   Preliminaries

Let G be a graph with vertex-set $V(G)$ and edge-set $E(G)$. For any vertex $v \in V$, the *closed neighborhood* of v is denoted and defined by $N(v) \equiv \{u \in V(G) : uv \in E(G)\} \cup \{v\}$. For a subset S of V, let $N(S) = \bigcup_{v \in S} N(v)$, and for a natural number r, define the $r-th$ *neighborhood* of $v \in V$ as $N^r(v) \equiv N(N^{r-1}(v))$, where $N^1(v) = N(v)$.

A subset $U \subseteq V$ is an *independent set* (IS) of G if all vertices in U are pairwise non-adjacent, and a *maximal independent set* (MIS) U of G is such an IS that each vertex $V \setminus U$ is adjacent to at least one vertex in U. Clearly, an MIS $I(G)$ of G is also a dominating set of G. Thus any minimum dominating set $D(G)$ of G has size no more than that of an MIS $I(G)$. In addition, a subset S of $V(G)$ is called a *2-packing* if $N(u) \cap N(v) = \emptyset$ for every pair of vertices $u, v \in S$.

Some useful facts on Roman dominating functions were proved in [1], which will be used in our following discussions.

Proposition 1. *For any graph G, $\gamma(G) \leq \gamma_R(G) \leq 2\gamma(G)$.*

Proposition 2. *Let f be a minimum Roman dominating function of a graph G without isolated vertices. Let V_i be the sets of vertices v with $f(v) = i$ for $i = 0, 1, 2$. Let $f = (V_0, V_1, V_2)$ be such a function that $|V_1|$ is minimal. Then V_1 is a 2-packing and there is no edge between V_1 and V_2.*

Proposition 3. *For any non-trivial connected graph G, $\gamma_R(G) = min\{2\gamma(G \setminus S) + |S| : S$ is a 2-packing$\}$.*

Clearly, a function $f = (V_0, V_1, V_2)$ is a *Roman dominating function* if the set V_2 dominates the set V_0, and the weight of f is $f(V) = \sum_{v \in V} f(v) = 2|V_2| + |V_1|$. Moreover, a Roman dominating function $f = (V_0, V_1, V_2)$ defines a Roman dominating set $D_R = (V_1, V_2)$ since, for each vertex $v \in V$, we have either $v \in V_1 \cup V_2$ or v is dominated by some node in V_2. The weight of a Roman dominating set D_R is $W(D_R) = 2|V_2| + |V_1|$. If D_R is a minimum Roman dominating set (MRDS) of graph G, then $W(D_R) = \gamma_R(G)$.

3   Complexity Study of Roman Domination Problem

Let $V = \{v_1, v_2, \cdots, v_n\}$ be the set of points located in the Euclidean plane. Denote the coordinates of v_i by (x_i, y_i) for $i = 1, 2, \cdots, n$. For each vertex $v_i \in V$, there is a vertex u_i with coordinates $(x_i + \frac{1}{10}, y_i)$, and let $U = \{u_1, u_2, \cdots, u_n\}$ denote the set associated with V. Now construct a graph $G' = (V', E')$ with vertex-set $V' = V \cup U$ and edge-set $E' = \{(u, v) : u, v \in V'$ and $\|uv\| \leq 1 + \frac{1}{10}\}$. It is clear that G' is a unit disk graph, and $N(v_i) = N(u_i)$ in graph G'. Moreover, the following lemmas give some other properties of graph G'.

Lemma 1. *Let $f' = (V_0', V_1', V_2')$ be a minimal Roman dominating function of $G' = (V', E')$. Then $|\{u_i, v_i\} \cap V_2'| \leq 1$, for $i = 1, 2, \cdots, n$.*

Proof. Suppose, by contradiction, that there exists a j such that $\{u_j, v_j\} \subseteq V_2$. Let $V_0'' = V_0' \cup \{u_j\}$, $V_1'' = V_1'$ and $V_2'' = V_2' \setminus \{u_j\}$. It is easy to verify that function $f'' = (V_0'', V_1'', V_2'')$ is a Roman dominating function satisfying $f''(V') < f'(V')$, a contradicting that f' is minimal. □

Lemma 2. *Let $f' = (V_0', V_1', V_2')$ be a minimal Roman dominating function of $G' = (V', E')$. Then there exists a minimal Roman dominating function $f'' = (V_0'', V_1'', V_2'')$ satisfying $f''(V') = f'(V')$ such that $V_1'' = \emptyset$ and $V_2'' \cap \{u_1, u_2, ..., u_n\} = \emptyset$.*

Proof. Suppose that $V_1' \neq \emptyset$. Then let $v_j \in V_1'$ for some j. Thus we have $N(v_j) \cap V_2' = \emptyset$ and $N(u_j) \cap V_2' = \emptyset$ since $N(v_j) = N(u_j)$, which implies $u_j \in V_1'$. Hence we have either $|\{u_i, v_i\} \cap V_1| = 0$ or 2 for each i. Let $V_1' = \{v_{i1}, u_{i1}, v_{i2}, u_{i2}, ..., v_{ik}, u_{ik}\}$ for some $1 \leq k \leq n$, $V_0'' = V_0' \cup \{u_{i1}, u_{i2}, ..., u_{ik}\}$, $V_1'' = \emptyset$, and $V_2'' = V_2' \cup \{v_{i1}, v_{i2}, ..., v_{ik}\}$. Clearly, $f'' \equiv (V_0'', V_1'', V_2'')$ is a Roman dominating function satisfying $f''(V') = f'(V')$.

Now suppose that $V_2' \cap \{u_1, u_2, \cdots, u_n\} \neq \emptyset$. Assume, without loss of generality, that $V_2' \cap \{u_1, u_2, \cdots, u_n\} = \{u_1, u_2, \cdots, u_m\}$ for some $1 \leq m \leq n$. Since $|\{u_i, v_i\} \cap V_2'| \leq 1$ for each i, then $\{v_1, v_2, \cdots, v_m\} \subseteq V_0'$. Let $V_0'' = (V_0' \setminus \{v_1, v_2, \cdots, v_m\}) \cup \{u_1, u_2, \cdots, u_m\}$, $V_1'' = V_1'$ and $V_2'' = (V_2' \setminus \{u_1, u_2, \cdots, u_m\}) \cup \{v_1, v_2, \cdots, v_m\}$. It is easy verify that $f'' \equiv (V_0'', V_1'', V_2'')$ is a Roman dominating function satisfying $f''(V') = f'(V')$ and $V_2'' \cap \{u_1, u_2, ..., u_n\} = \emptyset$. The lemma is then proved. $\square$

Theorem 1. *The minimum Roman dominating set problem in unit disk graphs is NP-hard.*

Proof. The reduction is from the minimum dominating set problem in grid graphs, which is known to be NP-hard. Given a grid graph $G = (V, E)$, we will construct a unit disk graph $G' = (V', E')$ such that G has a dominating set D with $|D| \leq k$ if and only if G' has a Roman dominating set D_R with $W(D_R) \leq 2k$.

Given any grid graph $G = (V, E)$ with vertex-set $V = \{v_1, v_2, ..., v_n\}$, where each v_i has integral coordinates (x_i, y_i) and $(v_i, v_j) \in E$ if and only if $\|v_i v_j\| = 1$. For each vertex $v_i \in V$, we add a new vertex u_i with coordinates $(x_i + \frac{1}{10}, y_i)$. Now construct the graph $G' = (V', E')$ with vertex-set $V' = \{v_1, u_1, v_2, u_2, ..., v_n, u_n\}$, and for any two vertices $u, v \in V'$, $(u, v) \in E'$ if and only if $\|uv\| \leq 1 + 1/10$. It is clear that G' is a unit disk graph, and for each $1 \leq i \leq n$, v_i and u_i have the same neighborhood $N(v_i) = N(u_i)$, and the same degree $d_{G'}(u_i) = d_{G'}(v_i) = 2d_G(v_i) + 1$.

Let D_R be a minimal Roman dominating set of G'. Then by Lemma 2, we can assume, without loss of generality, that $D_R = (\emptyset, V_2)$ and $V_2 \cap \{u_1, u_2, \cdots, u_n\} = \emptyset$. Suppose that D is a dominating set of G with $|D| \leq k$. Let $D_R = (\emptyset, D)$, then D_R is a Roman dominating set with $W(D_R) \leq 2k$. Conversely, suppose that G' has a Roman dominating set $D_R = (\emptyset, V_2)$, $V_2 \cap \{u_1, u_2, ..., u_n\} = \emptyset$ and $W(D_R) \leq 2k$. Then V_2 is also a dominating set of G, $|V_2| = \frac{1}{2}W(D_R) \leq k$. Let $D = V_2$, then G has a dominating set D with $|D| \leq k$. Therefore, G has a dominating set D with $|D| \leq k$ if and only if G' has a Roman dominating set D_R with $W(D_R) \leq 2k$. The proof is then completed. $\square$

4   Approximation Algorithms

It is well known that any maximal independent set D is also a dominating set. Thus $D_R = (\emptyset, D)$ is a Roman dominating set. One method of finding a Roman dominating set in a graph is to find a maximal independent set. A straightforward method of finding a maximal independent set is as follows: Select an arbitrary vertex $v \in V$, add v to the current independent set D, which is initially set to be an empty set, and delete $N(v)$ from the current graph G, and then repeat the process until all vertices in $V(G)$ have been deleted.

Algorithm A. 5-Approximation Algorithm for MRDS

Input: A unit disk graph $G = (V, E)$
Output: A Roman dominating set D_R

1. $S := V$, $D := \emptyset$
2. **while** $S \neq \emptyset$ **do**
3.   Choose $v \in S$
4. $D := D \cup \{v\}$, $S := S \setminus N(v)$
5. **end-while**
6. **return** $D_R = (\emptyset, D)$

Theorem 2. *Let $G = (V, E)$ be a unit disk graph, Algorithm A returns a Roman dominating set in time of $O(|E|)$ whose size is at most five times that of the minimum Roman dominating set.*

Proof. It is clear that the algorithm returns a Roman dominating set in time of $O(|E|)$. Let $D_R^* = (V_1^*, V_2^*)$ denote an optimal Roman dominating set of G such that V_1^* is a minimal. By Proposition 2 we have V_1^* is a 2-packing and there is no edge between V_1^* and V_2^*. Note that G is a unit disk graph and the returned set D is an independent set. Moreover, no vertex in V_2^* can dominate more than 5 vertices in $D \setminus V_1^*$, and each vertex in V_1^* only can dominate itself. Hence we have

$$|V_2^*| \geq \frac{|D| - |V_1^* \cap D|}{5},$$

and

$$\gamma_R(G) = f(V) = 2|V_2^*| + |V_1^*| \geq \frac{2|D|}{5} = \frac{W(D_R)}{5},$$

and then the theorem follows. □

In the following we will show that there exists an algorithm that can return a better approximation solution at the expenses of increasing the time complexity. For this purpose, we first show the following lemma.

Lemma 3. *If the maximum independent set $I(G)$ of graph $G = (V, E)$ has cardinality $|I(G)|$ no greater than a constant c. Then $\gamma_R(G)$ can be computed in polynomial time.*

Proof. By $|I(G)| \leq c$, we have $\gamma(G) \leq c$ since any maximal independent set is also a dominating set. As $\gamma_R(G) = \min\{2\gamma(G - S) + |S| : S \text{ is a 2-packing}\}$, $\gamma(G \setminus S)$ and $|S|$ both are at most c. Thus to compute $\gamma_R(G)$ we can first choose a 2-packing set S in G, and then find a minimum dominating set in $G \setminus S$, finally choose the set S such that $|S| + 2\gamma(G - S)$ is minimal. Clearly we can compute $\gamma_R(G)$ by a brute-force method in time of $O(|V|^c)$. □

The basic idea of our polynomial time approximation scheme is as follows: First, compute a local Roman dominating set for a neighborhood of a vertex, and

then expand this neighborhood until we have formed some sets that satisfy the desired bound. Secondly, eliminate the current neighborhoods and repeat the same operation for the remaining graph.

Algorithm B PTAS for MRDS

Input: A unit disk graph $G = (V, E)$, $\varepsilon > 0$
Output: $(1 + \varepsilon)$-approximation MRDS D_R

1. $V := V$, $D_R := \emptyset$
2. **while** $V \neq \emptyset$ **do**
3.   choose a vertex $v \in V$
4.   **while** $W(D_R(N^{r+2}(v))) > (1 + \varepsilon)W(D_R(N^r(v)))$ **do**
5.   compute $D_R(N^r(v))$
6.   **end-while**
7.   compute $\overline{r} = min\{r : W(D_R(N^{r+2}(v))) \leq (1 + \varepsilon)W(D_R(N^r(v)))\}$
8. $V := V \setminus N^{\overline{r}+2}(v)$
9. $D_R := D_R \cup D_R(N^{\overline{r}+2}(v))$
10. **end-while**
11. **Return** D_R

Let k be the total number of executed iterations by Algorithm B. Let $v_1, v_2, \cdots, v_k$ be the vertices chosen in step 3, and $N_i, i = 1, 2, \cdots, k$, denote the corresponding neighborhoods, i.e., $N_i = N^{\overline{r}_i+2}(v_i)$. By the rules of Algorithm B, it is easy to verify that the returned set $D_R = \bigcup_{i=1}^{k} D_R(N_i)$ is a Roman dominating set of G. Moreover, we have the following lemma.

Lemma 4. *Let $G = (V, E)$ be a unit disk graph. Then $W(D_R(N^r(v))) \leq 8(r + 1/2)^2$ for every $v \in V$ and any positive integer r.*

Proof. From the definition of a unit disk graph, we know that for any $w \in N^r(v)$, the Euclidean distance between w and v is at most r. Let $I(N^r(v))$ denote an independent set in $N^r(v)$. Then the sets of unit-diameter disks centered at the nodes in $I(N^r(v))$ are disjoint and their convex hull is contained in the disk of radius $r + 1/2$. Then $|I(N^r(v))| \leq 4(r + 1/2)^2$, and $W(D_R(N^r(v))) \leq 2|D(N^r(v))| \leq 2|I(N^r(v))|$. Thus the lemma follows. $\square$

Lemma 5. *The obtained $\overline{r}$ in Step 7 of Algorithm B is no greater than constant $c = O(\frac{1}{\varepsilon^2}ln\frac{1}{\varepsilon})$.*

Proof. Note that $W(D_R(N^0(v))) = 1$ and $W(D_R(N^1(v))) = 2$ since vertex v dominates itself and all its neighbors. For an arbitrary value $r < \overline{r}$, consider the following two cases.

Case (1) r is an even number. By the rules of Algorithm B and Lemma 4 we have

$$8(r + \frac{1}{2})^2 \geq W(D_R(N^r(v)))$$

$$> (1+\varepsilon)W(D_R(N^{r-2}(v)))$$
$$> (1+\varepsilon)^{\frac{r}{2}}W(D_R(N^0(v)))$$
$$= (1+\varepsilon)^{\frac{r}{2}}.$$

Case (2) r is an odd number. In this case we have

$$8(r+\frac{1}{2})^2 \geq W(D_R(N^r(v)))$$
$$> (1+\varepsilon)W(D_R(N^{r-2}(v)))$$
$$> (1+\varepsilon)^{\frac{r-1}{2}}W(D_R(N^1(v)))$$
$$= 2(1+\varepsilon)^{\frac{r-1}{2}}.$$

In both cases the above inequalities will not hold for sufficiently large r, the bound on $\overline{r}$, which is achieved when these inequalities are violated the first time, only depends on ε and not on the order of graph G. By applying a similar argument used in [10], we can show $\overline{r} \leq c$, where $c = O(\frac{1}{\varepsilon^2}ln\frac{1}{\varepsilon})$. The proof is then proved. $\qquad \square$

The number of independent sets in $N^{\overline{r}}(v)$ is polynomially bounded in $\overline{r}$, and $\overline{r}$ is also polynomially bounded. By Lemma 3, a minimum Roman dominating set $D_R(N^{\overline{r}}(v))$ can be computed in polynomial time $O(|V|^{c^2})$, where $c = O(\frac{1}{\varepsilon^2}ln\frac{1}{\varepsilon})$. The following theorem shows the correctness and approximation guarantee of the algorithm.

Theorem 3. *Algorithm B returns a Roman dominating set $D_R = \bigcup_{i=1}^k D_R(N_i)$ whose weight is no more than $(1+\varepsilon)\gamma_R(G)$.*

Proof. Let D_R^* denote the optimal Roman dominating set. It is clear that $N(N^{\overline{r}_i}(v_i))$ and $N(N^{\overline{r}_j}(v_j))$ are mutually disjoint in G for $i \neq j$, and $N(N^{\overline{r}_i}(v_i)) \cap D_R^*$ dominates $N^{\overline{r}_i}(v_i)$. Thus by Lemma 5 we have

$$\gamma_R(G) = W(D_R^*) \geq \sum_{i=1}^k W\big(D_R^* \cap N(N^{\overline{r}_i}(v_i))\big)$$
$$\geq \sum_{i=1}^k W\big(D_R(N^{\overline{r}_i}(v_i))\big)$$
$$\geq \sum_{i=1}^k \frac{1}{1+\varepsilon}W\big(D_R(N^{\overline{r}_i+2}(v_i))\big)$$
$$\geq \frac{1}{1+\varepsilon}W\big(\cup_{i=1}^k D_R(N^{\overline{r}_i+2}(v_i))\big)$$
$$= \frac{1}{1+\varepsilon}W(D_R).$$

Hence the theorem holds. $\qquad \square$

5   Conclusion

In this paper we first show that the Roman domination problem in unit disk graphs is NP-hard, and then present a 5-approximation algorithm of linear time and a polynomial-time approximation scheme for this problem, respectively.

Grid graphs compose a subclass of unit disk graphs. However, hardness results for the Roman domination problem in grid graphs are still unknown (to the best knowledge of the authors). This raises an interesting problem for future work.

References

[1] E. J. Cockayne, P. A. Dreyer, S. M. Hedetniemi, and S. T. Hedetniemi: Roman domination in graphs, Discrete Mathematics. **278** (2004) 11-22

[2] P. A. Dreyer: Applications and Variations of domination in graphs, PhD Thesis, Rutgers University, New Jersey. (2000)

[3] A. Pagourtzis, P. Penna, K. Schlude, K. Steinhofel, D. Taylor, and P. Widmayer: Server placements, Roman domination and other dominating set variants, In Proceedings of the Second International Conference on Theoretical Computer Science. (2002) 280-291

[4] M. A. Henning: A characterization of Roman trees, Discuss. Math. Graph Theory. **22** (2) (2002) 325-334

[5] M. A. Henning and S. T. Hedetniemi: Defending the Roman Empire - A new strategy, Discrete Mathematics. **266** (2003) 239-251

[6] I. Stewart: Defend the Roman Empire!, Scientific American. December (1999) 136-138

[7] B. N. Clark, C. J. Colburn, and D. S. Johnson: Unit disk graphs, Discrete Mathematics. **86** (1990) 165-177

[8] H. B. Hunt III, M. V. Marathe, V. Radhakrishnan, S. S. Ravi, D. J. Rosenkrantz, and R. E. Stearns: NC-approximation schemes for NP-and PSPACE-hard problems for geometric graphs, Journal of Algorithms. **26** (2) (1998) 238-274

[9] M. V. Marathe, N. Breu, H. B. Hunt III, S. S. Ravi, and D. J. Rosenkrantz: Simple heuristics for unit disk graphs, Networks. **25** (1995) 59-68

[10] T. Nieberg, J. Hurink, and W. Kern: A robust PTAS for maximun independent sets in unit disk graphs, In Proceedings of the Thirtieth Workshop on Graph Theoretic Concepts in Computer Science. (2004) 214-221

[11] T. Nieberg and J. Hurink: A PTAS for the minimum dominating set problem in unit disk graphs, In Proceedings of the Third Workshop on Approximation and Online Algorithms. (2005) 6-7

Binding Number and Connected
$(g, f + 1)$-Factors in Graphs

Jiansheng Cai*, Guizhen Liu, and Jianfeng Hou

School of Mathematics and system science,
Shandong University, Jinan 250100, P.R.China
healthcai@163.com

Abstract. Let G be a connected graph of order n and let a, b be two integers such that $2 \le a \le b$. Let g and f be two integer-valued functions defined on $V(G)$ such that $a \le g(x) \le f(x) \le b$ for every $x \in V(G)$. A spanning subgraph F of G is called a $(g, f + 1)$-factor if $g(x) \le d_F(x) \le f(x) + 1$ for every $x \in V(F)$. For a subset X of $V(G)$, let $N_G(X) = \bigcup_{x \in X} N_G(x)$. The binding number of G is defined by $bind(G) = min\{\frac{|N_G(X)|}{|X|} \mid \emptyset \ne X \subset V(G), N_G(X) \ne V(G)\}$. In this paper, it is proved that if $bind(G) > \frac{(a+b)(n-1)}{an}$, $f(V(G))$ is even and $n \ge \frac{(a+b)^2}{a}$, then G has a connected $(g, f + 1)$-factor.

1 Introduction

In this paper, we consider only finite undirected graphs without loops and multiple edges. The set of vertices of graph G is denoted by $V(G)$; the set of edges by $E(G)$. We use $\nu(G)$ to denote the cardinality of $V(G)$. If H is a subgraph of G and S is a subset of $V(G)$, we denote by $N_H(S)$ the set of vertices in H which are adjacent to some vertex in S, and set $\mid N_H(S) \mid = d_H(S)$. In particular, when $H = G$ and $S = u$, then let $N_G(u) = N(u)$ and let $d_G(u) = d(u)$. The binding number of G is defined by $bind(G) = min\{\frac{|N_G(X)|}{|X|} \mid \emptyset \ne X \subset V(G), N_G(X) \ne V(G)\}$. We write $E_G(X, Y) = \{xy \in E(G) \mid x \in X, \ y \in Y\}$, and $e_G(X, Y) = \mid E_G(X, Y) \mid$. As usual, we use δ for the minimum degree of G. For other definitions and notations not defined here, we refer the readers to [1]. Let G be a connected graph of order n and let a, b be two integers such that $2 \le a \le b$. Let g and f be two integer-valued functions defined on $V(G)$ such that $a \le g(x) \le f(x) \le b$. A spanning subgraph F of G is called a $(g, f + 1)$-factor if $g(x) \le d_F(x) \le f(x) + 1$ for every $x \in V(F)$. If F is connected, we call it a connected $(g, f+1)$-factor. The purpose of this paper is to present a sufficient condition which guarantees the existence of connected $(g, f+1)$-factors in graph G related to the binding number of graph G. For convenience, we write $d_{G-S}(T) = \sum_{x \in T} d_{G-S}(x), f(S) = \sum_{x \in S} f(x)$ and $f(T) = \sum_{x \in T} f(x)$.

---

* Corresponding author.

Many authors have investigated factors, connected factors and factorizations [3,5,7]. In this paper, we study conditions on the binding number and the order of a graph G which guarantee the existence of a connected $(g, f + 1)$-factor in G. We begin with some known results.

There is a well-known necessary and sufficient condition for a graph G to have a (g, f)-factor which was given by Lovász.

Theorem 1 ([6]). *A graph G has a (g, f)-factor if and only if*

$$\delta(S, T) = f(S) + d_{G-S}(T) - g(T) - h(S, T) \geq 0$$

for any disjoint subsets S and T of $V(G)$, where $h(S, T)$ denotes the number of components C of $G - (S \bigcup T)$ such that $g(x) = f(x)$ for all $x \in V(C)$ and $e_G(T, V(C)) + \sum\limits_{x \in V(C)} f(x)$ is odd. Furthermore, if $g(x) = f(x)$ for every $x \in V(G)$, then $\delta(S, T) = f(V(G))(mod\ 2)$.

M. Kano gave a result which shows the relation of binding numbers and existence of f-factors.

Theorem 2 [2]. *Let G be a connected graph of order n and let a and b be integers such that $1 \leq a \leq b$ and $2 \leq b$. Let f be an integer-valued function defined on $V(G)$ such that $a \leq f(x) \leq b$ for every $x \in V(G)$. Suppose that $n \geq \frac{(a+b)^2}{a}$ and $\sum\limits_{x \in V(G)} f(x) \equiv 0(mod\ 2)$. If*

$$bind(G) > \frac{(a + b - 1)(n - 1)}{an - (a + b) + 3},$$

and for any nonempty independent subset X of $V(G)$

$$N_G(X) \geq \frac{(b - 1)n+ \mid X \mid -1}{a + b - 1},$$

then G has an f-factor.

The following two results are essential to the proof of our main theorem.

Theorem 3 [4]. *Let G be a graph and let g and f be two positive integer-valued functions defined on $V(G)$ such that $g(x) \leq f(x) \leq d_G(x)$ for all $x \in V(G)$. If G has both a (g,f)-factor and a Hamiltonian path, then G contains a connected (g,f+1)-factor.*

Theorem 4 [8]. *If $bind(G) \geq \frac{3}{2}$, then G has a Hamiltonian cycle.*
Liu and Zhang proposed the following problem.

Problem [5]. *Find sufficient conditions for graphs to have connected [a,b]-factors related to other parameters in graphs such as binding number, neighbor union and connectivity.*

We now give our theorem which partially solve the above problem.

Theorem 5. *Let G be a connected graph of order n, and let a and b be two integers such that $2 \leq a \leq b$. Let g and f be two integer-valued functions defined on $V(G)$ such that $a \leq g(x) \leq f(x) \leq b$ for every $x \in V(G)$ and $f(V(G))$ is even. If $n \geq \frac{(a+b)^2}{a}$, $bind(G) > \frac{(a+b)(n-1)}{an}$, then G has a connected $(g, f+1)$-factor.*

2 Proof of the Theorem 5

In this section, we assume that G satisfies the conditions of Theorem 5. Since $bind(G) > \frac{(a+b)(n-1)}{an} > \frac{3}{2}$, according to Theorem 4, graph G has a Hamiltonian cycle. Hence by Theorem 3, to prove Theorem 5, we need only to prove that graph G has a (g, f)-factor. At first, we need some lammas.

Lemma 1. *Suppose that G satisfies the conditions of Theorem 5. Then $\mid N_G(X) \mid > \frac{bn+|X|-1}{a+b}$ for all nonempty subset X of $V(G)$ with $N_G(X) \neq V(G)$ and $\delta(G) > \frac{bn}{a+b}$.*

Proof. Let $bind(G) > l$, and $Y = V(G) \setminus N_G(X)$. Since $N_G(Y) \subseteq V(G) \setminus X$, we obtain $(n- \mid X \mid) \geq \mid N_G(Y) \mid > l \mid Y \mid = l(n- \mid N_G(X) \mid)$. Therefore we have $\mid N_G(X) \mid > ((l-1)n+ \mid X \mid)/l$, and $\delta(G) > ((l-1)n+1)/l$.

Then replace l by $\frac{(a+b)(n-1)}{an-b}$, we have

$$\delta(G) > \frac{bn}{a+b}. \tag{1}$$

Since $n \geq \frac{(a+b)^2}{a}$, similarly we obtain

$$\mid N_G(X) \mid > \frac{(an + bn - a - b - an)n + an \mid X \mid}{(a+b)(n-1)}$$
$$= \frac{bn(n-1) - an + an \mid X \mid}{(a+b)(n-1)}$$
$$\geq \frac{bn+ \mid X \mid -1}{a+b}.$$

So

$$\mid N_G(X) \mid > \frac{bn+ \mid X \mid -1}{a+b}. \tag{2}$$

∎

We begin to prove that graph G has a (g, f)-factor. By contradiction, we suppose that G has no (g, f)-factors. Then according to Theorem 1, there exist disjoint subsets S and T of $V(G)$ satisfying

$$f(S) + d_{G-S}(T) - g(T) - h(S, T) < 0. \tag{3}$$

Let $s = |S|$ and $t = |T|$. Then by Theorem 1 and (3) we have

$$as + d_{G-S}(T) - bt - \omega \leq -1, \tag{4}$$

where ω denotes the number of components of $G - (S \cup T)$. Obviously,

$$\omega \leq n - s - t. \tag{5}$$

Let m denote the minimum order of components of $G - (S \cup T)$. Then we know that

$$m \leq \frac{n - s - t}{\omega}. \tag{6}$$

By the definition of m, it is obvious that

$$\delta(G) \leq m - 1 + s + t. \tag{7}$$

The following Claims hold.

Claim 1. $T \neq \emptyset$.

Proof. Otherwise $T = \emptyset$.

Case 1. $S = \emptyset$.
Since G is connected and $\delta(S, T) < 0$, $h(S, T) = 1$. So obviously $f(x) = g(x)$ for every $x \in V(G)$ by the definition of $h(S, T)$. Hence $\delta(S, T) = -1$. On the other hand, since $f(V(G))$ is even, according to Theorem 1, $\delta(S, T)$ is even. This is a contradiction.

Case 2. $S \neq \emptyset$. Then by (4) and (5), we get

$$as + 1 \leq \omega \leq n - s. \tag{8}$$

So from (1), (6), (7) and (8) we know that

$$\frac{bn}{a+b} < \delta(G) \leq m - 1 + s \leq \frac{n-s}{\omega} - 1 + s$$
$$\leq \frac{n-s}{as+1} - 1 + s$$
$$\leq \frac{n-1}{a} - \frac{(n-1-as-s)(s-1)}{as+1}.$$

Since $n - 1 - as - s \geq 0$ by (8), it follows that

$$\frac{n}{2} \leq \frac{n-1}{a}.$$

This is a contradiction since $a \geq 2$. So $T \neq \emptyset$. ∎

Since $T \neq \emptyset$ by Claim 1, let $h = min\{d_{H-S}(x) \mid x \in T\}$.
Then obviously

$$\delta(G) \leq h + s. \tag{9}$$

Claim 2. $h \neq 0$.

Proof. If $h = 0$, let $X = \{x \in T \mid d_{G-S}(x) = 0\}$. Then $\mid X \mid \neq 0$. From (2) we get

$$s \geq \mid N_G(X) \mid > \frac{bn+ \mid X \mid -1}{a + b}. \tag{10}$$

On the other hand, from (4),(5) we get

$$as - b \mid X \mid +(1 - b)(t- \mid X \mid) - (b - 1)(n - s - t) \leq -1.$$

Thus

$$s \leq \frac{(b - 1)n+ \mid X \mid -1}{a + b - 1}.$$

From (10) and the above inequality, we get

$$\frac{bn+ \mid X \mid -1}{a + b} < \frac{(b - 1)n+ \mid X \mid -1}{a + b - 1},$$

which means $\mid X \mid > an + 1$. This is a contradiction. So $h \neq 0$. ∎

Claim 3. $h < b$.

Proof. Otherwise, $h \geq b$. We consider two cases.

Case 1. $h > b$.
Then by (4),

$$as + (h - b)t - \omega \leq -1. \tag{11}$$

And so

$$\omega \geq as + t + 1 \geq s + t + 1. \tag{12}$$

Since $T \neq \emptyset$ by Claim 1, $\omega \geq 2$.
    First suppose that $m \geq 2$. Then from (7) and (12) we get

$$\frac{bn}{a + b} < \delta(G) \leq m - 1 + s + t \leq m + \omega - 2$$
$$\leq m + \omega - 2 + \frac{(m - 2)(\omega - 2)}{2}$$
$$= \frac{m\omega}{2} \leq \frac{n}{2}.$$

This is a contradiction. Hence we may assume $m = 1$. Then from (12) and (5) we have

$$s + t \leq \frac{n-1}{2}.$$

Let C_1 be the least component of $G - (S \cup T)$. Then C_1 contains only one vertex x. Hence

$$\frac{bn}{a+b} < \delta(G) \leq d(x) \leq s + t \leq \frac{n-1}{2}.$$

This also is a contradiction. ∎

Case 2. $h = b$.
From (4) we have

$$\omega \geq as + 1. \tag{13}$$

So by (6) and (13)

$$m \leq \frac{n-s-t}{\omega} \leq \frac{n-s-1}{as+1}.$$

From (1) and (9) it is obvious that

$$\frac{bn}{a+b} \leq \delta(G) \leq h + s = b + s.$$

So

$$s > \frac{bn}{a+b} - b = \frac{b(n-a-b)}{a+b}.$$

Let $f(s) = \frac{n-s-1}{as+1}$. Then $f'(s) = \frac{-1-an+a}{(as+1)^2}$. Namely, $f'(s) < 0$.
Hence,

$$m < \frac{n - \frac{b(n-a-b)}{a+b} - 1}{a\frac{b(n-a-b)}{a+b} + 1}.$$

Since $n \geq \frac{(a+b)^2}{a}$, it follows that $m < 1$. This is a contradiction. Therefore, from Case 1 and Case 2 we have known that $h < b$. ∎

Hence, by Claim 2 and Claim 3 we have $1 \leq h \leq b - 1$.
By (4),(5) and $b - h \geq 1$, we obtain

$$as + (h - b)t - (b - h)(n - s - t) \leq -1,$$

which implies

$$s \leq \frac{(b-h)n - 1}{a+b-h}. \tag{14}$$

Then from (1),(9) and (14) we obtain

$$\frac{bn}{a+b} \le \delta(G) \le s + h \le \frac{(b-h)n-1}{a+b-h} + h. \tag{15}$$

Let $f(h) = \frac{(b-h)n-1}{a+b-h} + h$. Then by $n \ge \frac{(a+b)^2}{a}$,

$$f'(h) = \frac{-an - 1 + (a+b-h)^2}{(a+b-h)^2}$$
$$< \frac{-1}{(a+b-h)^2} < 0.$$

Hence the maximum value of $f(h)$ is $\frac{(b-1)n-1}{a+b-1} + 1$.
So by (1) and (15) we have

$$\frac{bn}{a+b} < \frac{(b-1)n-1}{a+b-1} + 1,$$

which implies

$$an < (a+b)^2 - 2(a+b).$$

Thus $n < \frac{(a+b)^2}{a}$. This contradicts the assumption that $n \ge \frac{(a+b)^2}{a}$. Hence we get the desired contradiction and conclude that G has a (g, f)-factor. Since G has both a Hamiltonian path and a (g, f)-factor, according to Theorem 3, graph G has a connected $(g, f+1)$-factor. ∎

The possible further problem in this topic is the following.

Question. *Find the proper binding number and order of G which guarantees the existence of connected k-factors in G.*

References

1. Bondy, J. A., Murty, U. S. R.: Graph Theory with Applications. Macmillan, London (1976).
2. Kano, M., Tokushige, N.: Binding number and f-factors of graphs. J. Combin. Theory Ser. B 54(1992) 213-221
3. Kouider, M., Vestergaard, P. D.: Connected factors in graphs - a survey. Graphs and Combinatorics 21 (2005) 1-26
4. Li, G., Xu, Y., Chen, C., Liu, Z.: On connected $(g, f+1)$-factors in graphs. Combinatorica 25 (4) (2005) 393-405
5. Liu, G., Zhang, L.: Factors and factorizations of graphs(in Chinese). Advances in Math. 29(2000) 289-296
6. Lovász, L.: Subgraphs with prescribed valencies. J. Combin. Theory 8 (1970) 391-416
7. Plummer, M. D.: Graph factors and factorization. Chapter 5.4 in Handbook on Graph Theory Eds.: J. Gross and R. Yellen CRC Press , New York (2003) 403-430
8. Woodall, D. R.: The binding number of a graph and its Anderson number. J. Combin. Theory Ser. B 15 (1973) 225-255

Some Results on List Total Colorings of Planar Graphs[*]

Jianfeng Hou[**], Guizhen Liu, and Jianliang Wu

Department of Mathematics, Shandong University, Jinan, Shandong, P.R. China
houjianfeng@mail.sdu.edu.cn

Abstract. Let G be a planar graph with maximum degree Δ. In this paper, it is proved that if $\Delta \geq 9$, then G is total-$(\Delta+2)$-choosable. Some results on list total coloring of G without cycles of specific lengths are given.

Keywords: planar graph, total coloring, list total coloring, cycle.

1 Introduction

We consider finite simple graphs. Any undefined notation follows that of Bondy and Murty [2]. We use $V(G)$, $E(G)$, $\delta(G)$ and $\Delta(G)$ to denote the vertex set, the edge set, the minimum degree and the maximum degree of a graph G, respectively. Let $d(v)$ denote the degree of vertex v.

A *total k-coloring* of a graph G is a coloring of $V(G) \cup E(G)$ using k colors such that no two adjacent or incident elements receive the same color. The *total chromatic number* $\chi''(G)$ is the smallest integer k such that G has a total k-coloring. Total colorings were introduced by Vizing [16] and Behzad [1]. They both, independently, conjectured that $\chi''(G) \leq \Delta(G) + \mu(G) + 1$ holds for multigraphs, where $\mu(G)$ denotes the (edge) multiplicity of G. This conjecture became known as the Total Coloring Conjecture. The conjecture has been verified for multigraphs of sufficiently small maximum degree. Rosenfeld [13] and Vijayaditya [15] independently proved that the total chromatic number for multigraphs of maximum degree 3 is at most 5. Kostochka in [10,11] proved that the total chromatic number of multigraphs of maximum degree 4 (respectively 5) is at most 6 (respectively 7). It is also easy to see that for a bipartite multigraph G, we have $\chi''(G) \leq \Delta(G) + 2$. For planar graphs, the conjecture only remains open for $\Delta(G) = 6$ [3,20,14].

The mapping L is said to be a *total assignment* for the graph G if it assigns a list $L(x)$ of possible colors to each element $x \in V \cup E$. If G has a total coloring ϕ such that $\phi(x) \in L(x)$ for all $x \in V(G) \cup E(G)$, then we say that G is *total-L-colorable*. Let $f : V \cup E \longrightarrow \mathbb{N}$ be a function into the positive integers. We say that G is *total-f-choosable* if it is total-L-colorable for every total

---

assignment L satisfying $|L(x)| = f(x)$ for all elements $x \in V(G) \cup E(G)$. The *list total chromatic number* $\chi_l''(G)$ of G is the smallest integer k such that G is totally-f-choosable when $f(x) = k$ for each $x \in V(G) \cup E(G)$. The *list chromatic number* $\chi_l(G)$ of G and the *list edge chromatic number* (or *list chromatic index*) $\chi_l'(G)$ of G are defined similarly in terms of coloring vertices alone, or edges alone, respectively; and so are the concepts of *vertex-f-choosability* and *edge-f-choosability*.

List colorings were introduced by Vizing [17] and independently by Erdös, Rubin, and Taylor [6]. Probably the most well-know conjecture about list colorings is the List Coloring Conjecture which states that every (multi)graph G is edge-$\chi'(G)$-choosable, where $\chi'(G)$ is the usual chromatic index of G. This conjecture has been proved for special cases, such as bipartite multigraphs [7], complete graphs of odd order [8], multicircuits [19], outerplanar graphs [18], and graphs with $\Delta(G) \geq 12$ which can be embedded in a surface of nonnegative characteristic [5].

As far as list total colorings are concerned, Juvan, Mohar and Škrekovski [9] posed the following conjecture which is the generalization of the Total Coloring Conjecture:

Conjecture 1.1. $\chi_l''(G) \leq \Delta(G) + \mu(G) + 1$, *where $\mu(G)$ is the multiplicity of G.*

In [9], Juvan et al. proved that the conjecture is true for bipartite multigraphs and mutigraphs of maximum degree 3. They also proved that the total-choosability of a graph of maximum degree 2 is equal to its total chromatic number.

In Section 2, we show that Conjecture 1.1 is true for planar graph G with $\Delta(G) \geq 9$. In Section 3, we consider planar graphs without cycles of specific lengths and get some related results on Conjecture 1.1. In Section 4, open problems for future research are given.

2   Planar Graphs with Maximum Degree at Least 9

First, let us introduce some notations and definitions. Let $G = (V, E, F)$ be a planar graph. A vertex v is called a *k-vertex* or *k^+-vertex* if $d(v) = k$ or $d(v) \geq k$, respectively. For $f \in F$, we use $b(f)$ to denote the closed boundary walk of f and write $f = [u_1 u_2 ... u_n]$ if $u_1, u_2, ..., u_n$ are the vertices on the boundary walk in the clockwise order, with repeated occurrences of vertices allowed. The degree of a face f, denoted by $d(f)$, is the number of edges-steps in $b(f)$. Note that each cut-edge is counted twice. A *k-face* or a *k^+-face* is a face of degree k or of degree at least k, respectively. Let $\delta(f)$ denote the minimum degree of vertices incident with f. When v is a k-vertex, we say that there are k faces incident to v. However, these faces are not required to be distinct, i.e., v may have repeated occurrences on the boundary walk of an indent face. Let $n_k(v)$ or $n_{k^+}(v)$ denote the number of k-faces or k^+-faces incident with vertex v with repeated occurrence of faces allowed, respectively.

Following theorem is our main result in this section.

Theorem 2.1. *Let G be a planar graph with maximum degree $\Delta \geq 9$. Then G is total-$(\Delta + 2)$-choosable.*

Proof. Let $G = (V, E, F)$ be a minimal counterexample to the theorem. Then G has the following properties.

(a) G is connected.

(b) G contains no edge uv with $\min\{d(u), d(v)\} \leq \lfloor \frac{\Delta+1}{2} \rfloor$ and $d(u) + d(v) \leq \Delta + 2$.

(a) is obvious. We will show (b). Suppose it does contain such edge $e = uv$. Without loss of generality, let $d(u) = \min\{d(u), d(v)\}$. We can list total color $G - e$ by the minimality of G and then erase the color on u. Thus e touches at most $(\Delta+1)$ colors and can be colored from its list. Now u is adjacent or incident to at most $2d(u) \leq \Delta + 1$ colors and it too can be colored. This contradicts the choice of G as a counterexample and shows that (b) holds.

It is easy to verify $\delta(G) \geq 3$ by (b). Let G_3 be the subgraph induced by the edges incident with the 3-vertices of G. Clearly, G_3 does not contain odd cycles by (b). Thus G_3 is a bipartite graph with partite sets V_1, V_2, so that $V(G_3) = V_1 \cup V_2$ and for any vertex $v \in V_1$, $d_G(v) = 3$, for any vertex $v \in V_2$, $d_G(v) = \Delta$. Since G is a minimal counterexample, we have

(c) G_3 contains a bipartite subgraph $G' = (V_1', V_2', E(G'))$, such that $V_1' = V_1$ and for any vertex $v \in V_1'$, $d_{G'}(v) = 2$; for any vertex $v \in V_2'$, $d_{G'}(v) = 1$. If $uv \in E(G')$ and $d_G(u) = 3$, then v is called the 3-*master* of u and u is called the *dependent* of v.

Before prove (c), we first show that G contains no even cycle $v_1v_2...v_{2t}v_1$ such that $d(v_1) = d(v_3) = ... = d(v_{2t-1}) = 3$. Suppose it does contain such an even cycle C. Total color all elements of $G - E(C)$ from their lists, which is possible by the minimality of G. Then erase the colors on $v_1, v_3, ..., v_{2t-1}$. If e is an edge of C, then e now effectively has a list $L'(e)$ with $|L'(e)| \geq \Delta + 2 - (2 + \Delta - 1) = 2$. Thus the edges of C can be colored from their lists. Finally, if we are coloring vertices $v_1, v_3, ..., v_{2t-1}$, then each vertex $v_{2k-1} \in C$, $1 \leq k \leq t$, is now adjacent or incident to at most 6 colors and so there is at least one color in its list that we can give to v_{2k-1}. Thus we obtain the required contradiction.

The mentioned result above implies that G_3 does not contain even cycles. Thus G_3 is a forest. For any component of G_3, we can select a vertex u with $d_G(u) = 3$ as the root of the tree. We denote edges of distance i from the root to be at level $i+1$, where $i = 0, 1, ..., d$, and d is the depth of tree. Since G does not contain two adjacent 3-vertices, the distance from any leaf to the root is even. We can select all the edges at even level to form a 3-path v_1vv_2 such that $d_G(v) = 3$ in this component. Thus we can find a bipartite subgraph $G' = (V_1', V_2', E(G'))$, such that $V_1' = V_1$, for any vertex $v \in V_1'$, $d_{G'}(v) = 2$ and for any vertex $v \in V_2'$, $d_{G'}(v) = 1$. It completes the proof of (c).

Note that each 3-vertex has exactly two 3-masters and each vertex of degree Δ can be the 3-master of at most one 3-vertex.

Since G is a planar graph, by Euler's formula, we have

$$\sum_{v \in V}(d(v) - 4) + \sum_{f \in F}(d(f) - 4) = -4(|V| - |E| + |F|) = -8 < 0.$$

Now we define the initial charge function $w(x)$ for each $x \in V \cup F$. Let $w(x) = d(x) - 4$ for $x \in V \cup F$. It follows that $\sum_{x \in V \cup F} w(x) < 0$. The discharging method distributes the positive charge to neighbors so as to leave as little positive charge remaining as possible. This leads to $\sum_{x \in V \cup F} w(x) \geq 0$. A contradiction follows.

To prove the theorem, we are ready to construct a new charge $w^*(x)$ on G as follows.

R_1: Each 3-vertex receives $\frac{1}{2}$ from each of its 3-master.

R_2: Each 9^+-vertex transfer $\frac{1}{2}$ to each of its incident 3-face.

R_3: Each k-vertex, where $5 \leq k \leq 8$, transfer $\frac{k-4}{k}$ to each of its incident 3-face.

Let $\gamma(x \rightarrow y)$ denote the amount transferred out of an element x into another element y according to the above rules.

Clearly, $w^*(f) = w(f) \geq 0$ if $d(f) \geq 4$. Assume that $f = [v_1 v_2 v_3]$ is a 3-face with $d(v_1) \leq d(v_2) \leq d(v_3)$. If $d(v_1) = 3$, then $d(v_2) = d(v_3) = \Delta$ by (c). So $w^*(f) = w(f) + 2 \times \frac{1}{2} = 0$. If $d(v_1) = 4$, then $d(v_2) \geq 8$ and $d(v_3) \geq 8$. So $\gamma(v_2 \rightarrow f) = \frac{1}{2}$ and $\gamma(v_3 \rightarrow f) = \frac{1}{2}$. Thus $w^*(f) = w(f) + 2 \times \frac{1}{2} = 0$. If $d(v_1) = 5$, then $d(v_2) \geq 7$ and $d(v_3) \geq 7$. So $\gamma(v_1 \rightarrow f) = \frac{1}{5}$, $\gamma(v_2 \rightarrow f) \geq \frac{3}{7}$, and $\gamma(v_3 \rightarrow f) \geq \frac{3}{7}$. Thus $w^*(f) \geq w(f) + \frac{1}{5} + 2 \times \frac{3}{7} > 0$. If $d(v_1) = 6$, then $\gamma(v_i \rightarrow f) \geq \frac{1}{3}$ for $i = 1, 2, 3$. So $w^*(f) \geq w(f) + 3 \times \frac{1}{3} = 0$.

Let v be a k-vertex. If $k = 3$, then there are two vertices, say v_1, v_2, such that v_i, $i = 1, 2$, is the 3-master of v. So $\gamma(v_i \rightarrow v) = \frac{1}{2}$ for $i = 1, 2$. Thus $w^*(v) \geq w(v) + 2 \times \frac{1}{2} = 0$. If $k = 4$, then $w^*(v) = w(v) = 0$. If $5 \leq k \leq 8$, then $w^*(v) = w(v) - k \times \frac{k-4}{k} = 0$. If $k \geq 9$, then v can be the 3-master of at most one 3-vertex. So $w^*(v) \geq w(v) - \frac{1}{2} - \frac{k}{2} = \frac{k-9}{2} \geq 0$. $\square$

3   Planar Graphs Without Cycles of Specific Lengths

In this section, we consider planar graphs without certain cycles. Note notations and definitions are the same as those in Section 2. Following result is our main theorem in this section.

Theorem 3.1. *Let G be a planar graph with maximum degree Δ such that G is free of k-cycles, where $k \geq 3$. Then G is total-$(\Delta + 2)$-choosable, if*

(1) $\Delta \geq 5$ *and* $k = 3$, *or*

(2) $\Delta \geq 5$ *and* $k = 4$, *or*

(3) $\Delta \geq 6$ *and* $k = 5$, *or*

(4) $\Delta \geq 6$ *and* $k = 6$.

Proof. Let $G = (V, E, F)$ be a minimal counterexample to the theorem. Then G has the following proprieties.

(a) G is connected.

(b) G contains no edge uv with $\min\{d(u), d(v)\} \leq \lfloor\frac{\Delta+1}{2}\rfloor$ and $d(u) + d(v) \leq \Delta + 2$.

(c) $\delta(G) \geq 3$ and for any 3-vertex $v \in V$, v has exactly two 3-masters. For each vertex v of degree Δ, v can be the 3-master of at most one 3-vertex.

(a) is obvious. The proofs of (b) and (c) are the same as the above in Theorem 2.1, so we omit.

Since G is a planar graph, by Euler's formula, we have

$$\sum_{v \in V}(d(v) - 4) + \sum_{f \in F}(d(f) - 4) = -4(|V| - |E| + |F|) = -8 < 0.$$

Now we define the initial charge function $w(x) = d(x) - 4$ for each $x \in V \cup F$. It follows that $\sum\limits_{x \in V \cup F} w(x) < 0$.

In order to prove (1), we are ready to construct a new charge $w^*(x)$ on G as follows.

R_1 : Each 3-vertex receives $\frac{1}{2}$ from each of its 3-master.

Clearly, $w^*(f) = w(f) \geq 0$ for any face $f \in F$. If v is a 3-vertex by (c), then v has exactly two 3-masters . So $w^*(v) = w(v) + 2 \times \frac{1}{2} = 0$. If v is a 4-vertex, then $w^*(v) = w(v) = 0$. If v is a 5^+-vertex, then v can be the 3-master of at most one 3-vertex. So $w^*(v) \geq w(v) - \frac{1}{2} > 0$.

We will prove the following claim before we proof (2).

Claim 3.2. If $\Delta \geq 5$, then G contains no 3-face $f = uvw$ such that $d(u) = d(v) = d(w) = 4$.

Proof. Suppose on the contrary, such 3-face does exist. Thus $G - \{uv, uw, vw\}$ has a list total coloring ϕ by the minimality of G, then erase the colors on u, v and w. For each element x incident with f, we define a reduced total list $L'(x)$ such that $L'(x) = L(x) \setminus \{\phi(x')|x'$ is incident or adjacent to x and x' is not incident with $f\}$. Then $|L'(u)| \geq 3, |L'(v)| \geq 3, |L'(w)| \geq 3, |L'(uv)| \geq 3, |L'(uw)| \geq 3$ and $|L'(vw)| \geq 3$. It follows from $\chi_l''(C_3) = \chi''(C_3) = 3$ that uncolor elements incident with f in G can be colored from its total lists L'. This contradicts the choice of G as a counterexample. □

To prove (2), we are ready to construct a new charge $w^*(x)$ on G as follows:

$R_{2.1}$: Each 3-vertex receives $\frac{3}{10}$ from each of its 3-master.

$R_{2.2}$: For a k-face f, where $k \geq 5$, and each occurrence of a vertex $v \in b(f)$, transfer the amount $\frac{k-4}{k}$ from f to v.

$R_{2.3}$: From each 4-vertex to each of its incident 3-face, transfer $\frac{1}{5}$.

$R_{2.4}$: From each 5^+-vertex v to each of its incident 3-face, transfer $\frac{3}{5}$.

Clearly, $w^*(f) = w(f) - k \times \frac{k-4}{k} = 0$ if $k \geq 5$. Let f be a 3-face. If f is incident with a 3-vertex, then the other vertices f incident with are 5^+-vertices. So $w^*(f) = w(f) + 2 \times \frac{3}{5} = \frac{1}{5} > 0$. Otherwise, f is incident with at least one 5^+-vertex by Claim 3.2. So $w^*(f) \geq w(f) + 2 \times \frac{1}{5} + \frac{3}{5} = 0$.

Let v be a k-vertex. If $k = 3$, then v has exactly two 3-master by (c) and v is incident with at least two 5^+-faces since G is C_4-free. So $w^*(f) \geq w(f) + 2 \times \frac{3}{10} + 2 \times \frac{1}{5} = 0$. If $k = 4$, then v is incident with at most two 3-faces. So $w^*(f) \geq w(f) + 2 \times \frac{1}{5} - 2 \times \frac{1}{5} = 0$. If $k = 5$, then v can be the 3-master of at most one 3-vertex and v is incident with at most two 3-faces. So $w^*(f) \geq w(f) + 3 \times \frac{1}{5} - 2 \times \frac{3}{5} - \frac{3}{10} = \frac{1}{10} > 0$. If $k \geq 6$, then v is incident with at most $\lfloor \frac{k}{2} \rfloor$ 3-faces, since G is C_4-free. So $w^*(f) \geq w(f) + \frac{1}{5} \times \frac{k}{2} - \frac{k}{2} \times \frac{3}{5} - \frac{3}{10} > 0$.

To prove (3), we are ready to construct a new charge $w^*(x)$ on G as follows.

$R_{3.1}$: Each 3-vertex receives $\frac{1}{2}$ from each of its 3-master.

$R_{3.2}$: For a k-face f, where $k \geq 6$, and each occurrence of a vertex $v \in b(f)$, transfer the amount $\frac{1}{3}$ from f to v.

$R_{3.3}$: From each 4-vertex to each of its incident 3-face, transfer $\frac{1}{3}$.

$R_{3.4}$: From each 5^+-vertex to each of its incident 3-face, transfer $\frac{1}{2}$.

Clearly, $w^*(f) = w(f) = 0$ if $d(f) = 4$. Assume that $d(f) = 3$. If $\delta(f) = 3$, then f is incident with two 6^+-vertices by (b). So $w^*(f) = w(f) + 2 \times \frac{1}{2} = 0$. Otherwise, $w^*(f) \geq w(f) + 3 \times \frac{1}{3} = 0$. If f is a 6^+-face, then $w^*(f) = w(f) - d(f) \times \frac{1}{3} = \frac{2d(f)}{3} - 4 \geq 0$.

Let v be a k-vertex. If $k = 3$, then $w^*(v) \geq w(v) + 2 \times \frac{1}{2} = 0$. Assume that $k = 4$. If v is incident with no 3-faces, then $w^*(v) = w(v) = 0$. Otherwise, v is incident with at least two 6^+-faces, since G is C_5-free, so $w^*(v) \geq w(v) + 2 \times \frac{1}{3} - 2 \times \frac{1}{3} = 0$. Assume that $k = 5$. If v is incident with no 3-faces, then $w^*(v) \geq w(v) = 1 > 0$. Otherwise, v is incident with at most three 3-faces and if v is incident with exactly three 3-faces, then the other faces f incident with are 6^+-faces. So $w^*(v) \geq w(v) + \min\{-2 \times \frac{1}{2}, -3 \times \frac{1}{2} + 2 \times \frac{1}{3}\} = 0$. Let $k = 6$. Then v can be the 3-master of at most one 3-vertex. If v is incident with at most three 3-faces, then $w^*(v) \geq w(v) - \frac{1}{2} - 3 \times \frac{1}{2} = 0$. Otherwise, v is incident with exactly four 3-faces since G is C_5-free, and the other faces f incident with are 6^+-faces. So $w^*(v) \geq w(v) - \frac{1}{2} - 4 \times \frac{1}{2} + 2 \times \frac{1}{3} = \frac{1}{6} > 0$. If $k \geq 7$, then v is incident with at most $(k - 2)$ 3-faces since G is C_5-free. So $w^*(v) \geq w(v) - \frac{1}{2} - (k - 2) \times \frac{1}{2} = \frac{k-7}{2} \geq 0$.

In order to proof (4) in the theorem, we need the following claim.

Claim 3.3. *If $\Delta \geq 6$ and G contains a 3-face $f = uvw$ such that $d(u) = d(v) = 4$, then $d(w) \geq 6$.*

Proof. Otherwise, $d(w) \leq 5$. We can list total color $G - \{uv, uw, vw\}$ by the minimality of G, then erase the colors on u, v and w. For each element x incident with f, we define a reduced total list $L'(x)$ similar to Claim 3.2. Then $|L'(w)| \geq 2$, $|L'(u)| \geq 4$, $|L'(v)| \geq 4$, $|L'(uw)| \geq 3$, $|L'(vw)| \geq 3$ and $|L'(uv)| \geq 4$. If there is a color $\alpha \in L'(wu) \setminus L'(u)$, then color wu with color α and color w, wv, v, uv and u successively. So $L'(wu) \subseteq L'(u)$. If there is a color $\beta \in L'(u) \setminus L'(v)$, then color u with β and color w, uw, wv, uv and v successively. So $L'(u) \subseteq L'(v)$. This implies that $L'(wu) \subseteq L'(v)$. Choose a color $\gamma \in L'(wu)$ and color wu

and v with color γ, then color w, wv, uv and u successively. Thus we obtain the required contradiction. $\qquad\square$

We are ready to construct a new charge $w^*(x)$ on G as follows.

$R_{4.1}$: Each 3-vertex receives $\frac{1}{2}$ from each of its 3-master.

$R_{4.2}$: For a k-face f, where $k \geq 5$, and each occurrence of a vertex $v \in b(f)$, transfer the amount $\frac{k}{k-4}$ from f to v.

$R_{4.3}$: From each 4-vertex v to each of its incident 3-face f, transfer

    0, if $n_3(v) \geq 3$.

    $\frac{3}{7}$, if $n_{7+}(v) \geq 2$.

    $\frac{1}{5}$, otherwise.

$R_{4.4}$: From each 5-vertex v to each of its incident 3-face, transfer

    $\frac{1}{2}$, if $\delta(f) = 4$.

    $\frac{1}{3}$, if $\delta(f) \geq 5$.

$R_{4.5}$: From each 6^+-vertex v to each of its incident 3-face, transfer

    $\frac{1}{2}$, if $\delta(f) = 3$.

    $\frac{3}{5}$, if $\delta(f) = 4$.

    $\frac{1}{3}$, otherwise.

Clearly, $w^*(f) = w(f) = 0$ if $d(f) = 4$ and $w^*(f) = w(f) - k \times \frac{k-4}{k} = 0$ if $k \geq 5$. Let $f = [u_1 u_2 u_3]$ be a 3-face with $d(u_1) \leq d(u_2) \leq d(u_3)$. If $d(u_1) = 3$, then $d(u_2) = d(u_3) = \Delta$. So $w^*(f) \geq w(f) + 2 \times \frac{1}{2} = 0$. If $d(u_1) \geq 5$, then $w^*(f) \geq w(f) + 3 \times \frac{1}{3} = 0$. Assume that $d(u_1) = 4$. If $d(u_2) = 4$, then $d(u_3) \geq 6$ by Claim 3.3. So $\gamma(u_3 \to f) = \frac{3}{5}$. In this case, without loss of generality, we suppose that $\gamma(u_1 \to f) \leq \gamma(u_2 \to f)$. If $\gamma(u_1 \to f) = 0$, then u_1 is incident with at least three 3-faces. This implies that u_2 is incident with at least two 7^+-faces. So $\gamma(u_2 \to f) = \frac{3}{7}$. Thus $w^*(f) \geq w(f) + \frac{3}{7} + \frac{3}{5} > 0$. If $\gamma(u_1 \to f) = \frac{1}{5}$, then $\gamma(u_2 \to f) \geq \frac{1}{5}$. So $w^*(f) \geq w(f) + 2 \times \frac{1}{5} + \frac{3}{5} = 0$. If $\gamma(u_1 \to f) = \frac{3}{7}$, then $w^*(f) \geq w(f) + \frac{3}{7} + \frac{3}{5} > 0$. If $d(u_2) \geq 5$, then $\gamma(u_2 \to f) \geq \frac{1}{2}$ and $\gamma(u_3 \to f) \geq \frac{1}{2}$. So $w^*(f) \geq w(f) + 2 \times \frac{1}{2} = 0$.

Let v be a k-vertex. If $k = 3$, then $w^*(v) \geq w(v) + 2 \times \frac{1}{2} = 0$. Let $k = 4$. If $n_3(v) = 0$, then $w^*(v) \geq w(v) = 0$. If $n_3(v) \geq 3$, then $w^*(v) = w(v) = 0$. If $n_{7+}(v) \geq 2$, then v is incident with at most two 3-faces. So $w^*(v) \geq w(v) + 2 \times \frac{3}{7} - 2 \times \frac{3}{7} = 0$. Otherwise, let f be a 3-face incident with v. Then $\gamma(v \to f) = \frac{1}{5}$. In this case, if $n_3(v) = 1$, then v is incident with at least 5^+-faces since G is C_6-free. So $w^*(v) \geq w(v) + \frac{1}{5} - \frac{1}{5} = 0$. If $n_3(v) = 2$, then v is incident with at least one 7^+-faces. So $w^*(v) \geq w(v) + \frac{3}{7} - 2 \times \frac{1}{5} > 0$. Let $k = 5$. Then v is incident with at most three 3-faces. If $n_3(v) \leq 2$, then $w^*(v) \geq w(v) - 2 \times \frac{1}{2} = 0$. If $n_3(v) = 3$, then v is incident with at least one 7^+-face. So $w^*(v) \geq w(v) - 3 \times \frac{1}{2} + \frac{3}{7} > 0$. Let $k = 6$. Then v is incident with at most four 3-faces. If $n_3(v) \leq 2$, then $w^*(v) \geq w(v) - 2 \times \frac{3}{5} - \frac{1}{2} = \frac{3}{10} > 0$. If $n_3(v) = 3$, then v is incident with at least one 7^+-face. So $w^*(v) \geq w(v) - 3 \times \frac{3}{5} - \frac{1}{2} + \frac{3}{7} > 0$. If $n_4(v) = 4$, then the other face f incident with are 7^+-faces. In this case, if v is not adjacent to a 3-vertex, then $w^*(v) \geq w(v) - 4 \times \frac{3}{5} + 2 \times \frac{3}{7} > 0$. Otherwise, v is adjacent to a 3-vertex. This implies that v is incident with at least one

3-face f with $\delta(f) = 3$. So $w^*(v) \geq w(v) - \frac{1}{2} - \frac{1}{2} - 3 \times \frac{3}{5} + 2 \times \frac{3}{7} > 0$. If $k \geq 7$, then $n_3(v) \leq k - 2$. If $n_3(v) \leq k - 3$, then $w^*(v) \geq w(v) - \frac{1}{2} - (k-3) \times \frac{3}{5} > 0$. If $n_3(v) = k - 2$, then the face v incident with are 7^+-faces. So $w^*(v) \geq w(v) - \frac{1}{2} - (k-2) \times \frac{3}{5} + 2 \times \frac{3}{7} > 0$. $\qquad\square$

4   Open Problems for Future Research

Following conjecture was posed by Borodin, Kostochka, and Woodall [5] which is stronger than Conjecture 1.1.

Conjecture 4.1. *If G is a multigraph, then $\chi_l''(G) = \chi''(G)$.*

Problem 4.2. *Consider Conjecture* 4.1 *for planar graphs. Especially, when planar graphs without cycles of specific lengths.*

References

1. Behzad, M.: Graphs and their chromatic number. Doctoral Thesis. Michigan State University 1965
2. Bondy, J.A., Murty, U.S.R.: Graph Theory with Applications. Macmillan Press, London (1976)
3. Borodin, O.V.: On the total coloring of planar graphs. J. Reine Angew. Math. 394 (1989) 180-185
4. Borodin, O.V.: An extension of Kotzig theorem and the list edge coloring of plane graphs. Matem. Zametki 48 (1990) 22-48 (in Russian)
5. Borodin, O.V., Kostochka, A.V., D.R. Woodall, D.R.: List edge and list total colorings of multigrahs. J. of Combin. Theory Series B 71 (1997) 184–204.
6. Erdös, P., Rubin, A., Taylor, H.:, Choosability in graphs. Congr. Number. 26 (1980) 125-157
7. Galvin, F.:, The list chromatic index of a bipartite multigraph. J. Combin. Theory Ser. B 63 (1995) 153-158
8. Häggkvist, P., Janssen, J.: New bounds on the list-chromatic index of the complete graph and othe simple graphs, Combin., Probab. and Comput. 6 (1997) 295-313
9. Juvan, M., Mohar, B., Škrekovski, R.: List total colorings of graphs. Combin., Probab. and Comput. 7 (1998) 181-188
10. Kostochka, A. V.: The total coloring of a multigraph with maximum degree 4. Discrete Math. 17 (1977) 161-163
11. Kostochka, A. V.: Exact upper bound for the total chromatic number of a graph (in Russian). In Proc. 24th Int. Koll. Tech. Hochsch. Ilmenau (1979) 33-36
12. Kostochka, A. V.: Upper bounds of chromatic functions on graphs (in Russian). Doctoral Thesis, Novosibirsk (1978)
13. Rosenfeld, M.: On the total coloring of certain graphs. Israel J. Math. 9(1971) 396-402
14. Sanders, D.P., Zhao, Y.: On total 9-coloring planar graphs of maximum degree seven. J. Graph Theory 31 (1999) 67-73
15. Vijayaditya, N.: On total chromatic number of a graph. J. London Math. Soc. (2) 3 (1971) 405-408

16. Vizing, V.Z.: Some unsolved problems in graph theory (in Russian). Uspekhi Mat. Nauk 23 (1968) 117-134
17. Vizing, V.G.: Coloring the vertices of a graph in prescribed colors (in Russian). Diskret. Anal. 29 (1976) 3-10
18. Wang, W.F. , Lih, K.W.: Choosability, edge-choosability and total choosability of outerplane graphs. European J. Combin. 22 (2001) 71–78
19. Woodall, D.R.: Edge-choosability of multicircuits. Discrete Math. 202 (1999) 271-277
20. H. P. Yap, H.P.: Total-coloring of graph. Lecture note in Mathematics 1623 (1996)

Linear Polynomial-Time Algorithms To Construct 4-Connected 4-Regular Locally Connected Claw-Free Graphs[*]

MingChu Li[1], Liming Xiong[2], and Hong Liu[3]

[1] College of Science, Chongqing Technology and Business University,
Chongqing, P.R. China
School of Software, Dalian University of Technology
Dalian 116620, China
[2] Department of Mathematics, Beijing Institute of Technology
Beijing 100081, P.R. China
[3] School of Software, Dalian University of Technology
Dalian 116620, China

Abstract. A vertex of a graph is locally connected if its neighborhood is connected. A graph G is locally connected if every vertex of G is locally connected. A graph is called claw-free if it does not contain a copy of $K_{1,3}$ as an induced subgraph. In this paper, we provide a constructive characterization of 4-connected 4-regular locally connected claw-free graphs. From its proof, we can give a linear polynomial-time algorithm to construct a 4-connected 4-regular locally connected claw-free graph.

Keywords: constructive characterization, linear polynomial-time, claw-free graph.

1   Terminology and Notation

We will consider the class of undirected finite graphs without loops or multiple edges, and use [1] for terminology and notation not defined here. Let $G = (V, E)$ be a graph. For a subgraph H of a graph G and a subset S of $V(G)$, we denote by $G - H$ and $G[S]$ the induced subgraphs of G by $V(G) - V(H)$ and S, respectively. A clique of G is a complete subgraph of G. A clique with k vertices is called a k-clique. We say that a vertex is adjacent to a clique if it is adjacent to at least one vertex of the clique. A subgraph K and a subgraph B are disjoint if the vertices of K and the vertices of B are disjoint. For any vertex v, $N(v)$ denotes the neighborhood of v. For S in V, let $N(S) = \cup_{x \in S} N(x)$, and $\bar{N}(S) = N(S) - S = \{x \in N(S) \text{ but } x \notin S\}$. A vertex v of G is locally connected if its neighborhood $N(v)$ is connected otherwise v is locally disconnected. A graph G is locally connected if every vertex of G is locally connected. A graph is called claw-free if it does not contain a copy of $K_{1,3}$ as an induced subgraph. Whenever

$\{v, v_1, v_2, v_3\}$ denotes an induced claw, then the leftmost vertex v is meant to be the center of the claw.

2 Results

There are a lot of results on algorithms and their complexity analysis (see [2], [3], [4], [5]). In this paper, we will provide a constructive characterization of 4-connected, 4-regular, locally connected, claw-free graphs. From its proof, we can give a linear polynomial-time algorithm to construct a 4-connected 4-regular locally connected claw-free graph. In order to explore our main results, we first prove the following result.

Lemma 1. *Let G be a 4-connected 4-regular claw-free graph on n vertices. If G contains a 4-clique, then every vertex of G is contained in a 4-clique, and all 4-cliques are disjoint if $n \geq 6$.*

Proof. Let K be a clique in G. If there is a vertex in G such that it is not contained in any 4-clique, then there is at least one vertex w in G adjacent to some clique such that w is not contained in any 4-clique. Without loss of generality assume that K is such a 4-clique adjacent to w. Let $V(K) = \{v_1, v_2, v_3, v_4\}$ and $wv_1 \in E(G)$. Then $N(v_1) = \{v_2, v_3, v_4, w\}$. Let w' be a neighbor of w and $w' \neq v_1$. If $w' \in \{v_2, v_3, v_4\}$ (say $w' = v_2$), then $N(v_2) = \{v_1, v_3, v_4, w'\}$. If $n = 5$, then G is K_5 and so we are done. So $n \geq 6$. It follows that $G - \{v_3, v_4, w\}$ is not connected. Thus G is not 4-connected. This contradiction shows that $w' \notin \{v_2, v_3, v_4\}$ and $(N(w) - \{v_1\}) \cap \{v_2, v_3, v_4\} = \emptyset$. For any two vertices w_1, w_2 in $N(w) - \{v_1\}$, we have $w_1 w_2 \in E(G)$ since $G[w, v_1, w_1, w_2] \neq K_{1,3}$ and $d(v_1) = 4$. It follows that $G[(N(w) \cup \{w\}) - \{v_1\}]$ is a 4-clique. This contradiction shows that every vertex of G is contained in a 4-clique. Since G is 4-regular, all 4-cliques are disjoint. So the proof of Lemma 1 is completed.

Lemma 2. *Let G be a 4-connected 4-regular claw-free graph on $n \geq 7$ vertices and v a vertex of G. If v is locally connected, then $G[N(v)]$ is an induced hamiltonian path in $G[N(v)]$.*

Proof. Let v be a vertex in G and $N(v) = \{v_1, v_2, v_3, v_4\}$ such that $G[N(v)]$ is connected. If G contains a 4-clique, then, by Lemma 1, every vertex of G is contained in a 4-clique K. Assume that $v \in V(K)$ and $G[(N(v) \cup \{v\}) - \{v_4\}]$ is a 4-clique, then v_4 is adjacent to at least one vertex of $\{v_1, v_2, v_3\}$ since $G[N(v)]$ is connected. Let $v_4 v_1 \in E(G)$. Then $N(v_1) = \{v, v_2, v_3, v_4\}$ and $G - \{v_4, v_3, v_2\}$ is not connected. Thus G is not 4-connected. This contradiction shows that G does not contain a 4-clique. It follows that $G[N(v) - \{v_i\}]$ is not a clique for $i = 1, 2, 3, 4$. Assume that $v_1 v_2 \notin E(G)$. Since $G[N(v)]$ is connected, there is a path P with three or four vertices connecting v_1 and v_2 in $G[N(v)]$. Thus we consider two cases to prove that $G[N(v)]$ is an induced path on 4 vertices with internal vertices of degree 2 and two end-vertices of degree 1 in $G[N(v)]$.

Case 1. $|V(P)| = 3$.

Assume that $V(P) = \{v_1, v_3, v_2\}$. Since $G[v, v_1, v_2, v_4] \neq K_{1,3}$, $v_4v_1 \in E(G)$ or $v_4v_2 \in E(G)$ (say $v_4v_2 \in E(G)$). Note that $v_3v_4 \notin E(G)$ since otherwise $G[v, v_2, v_3, v_4]$ is a 4-clique. We have that $v_4v_1 \notin E(G)$ since otherwise $G[v_1, v_4, v_3, v_1'] \neq K_{1,3}$, $v_1'v_3 \in E(G)$ or $v_1'v_4 \in E(G)$, where $v_1' \in N(v_1) - \{v_3, v_4, v\}$. Let $A = \{v_1', v_2, w'\}$, where $w' = v_3$ if $v_4v_1' \in E(G)$ and $w' = v_4$ if $v_3v_1' \in E(G)$. It easy to see that $G - A$ is not connected since $n \geq 7$. Thus G is not 4-connected. This contradiction shows $v_4v_1 \notin E(G)$. Thus $G[N(v)]$ is just an induced hamiltonian path $P = v_1v_3v_2v_4$ with internal vertices of 2 degree and two end-vertices of degree 1 in $G[N(v)]$.

Case 2. $|V(P)| = 4$.

Assume that $P = v_1v_3v_4v_2$. Then $v_1v_4, v_3v_2 \notin E(G)$ since otherwise, say $v_1v_4 \in E(G)$, $G - \{v_1, v_2, v_3\}$ is not connected since $\bar{N}(\{v, v_4\}) = \{v_1, v_2, v_3\}$, a contradiction. Thus $G[N(v)]$ is just an induced hamiltonian path $P = v_1v_3v_4v_2$ with internal vertices of 2 degree and two end-vertices of degree 1 in $G[N(v)]$. It follows that the proof of Lemma 2 is completed.
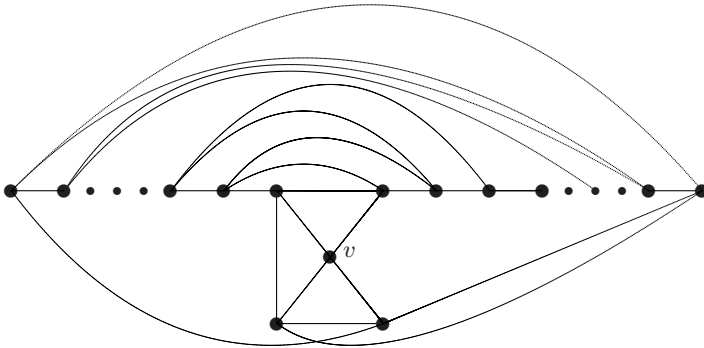
Fig. 1.

Theorem 3. *Every 4-connected 4-regular locally connected claw-free graph G on at least 7 vertices is isomorphic to a graph of the depiction in Figure 1.*

Proof. Assume that G is not isomorphic to a graph of the form in Figure 1, and v is any vertex of G. Then v is locally connected. By Lemma 2, $N(v)$ is just an induced hamiltonian path in $G[N(v)]$. We construct the graph starting from v. Let $N(v) = \{v_1, v_2, u_1, u_2\}$ and $G[N(v)] = v_2v_1u_1u_2$. Let $W_1 = \{v_1, v_2\}$ and $W_2 = \{u_1, u_2\}$ and let W be the closed neighborhood of v (i.e., $W = W_1 \cup W_2 \cup \{v\}$) and $H = G[W]$. Note that $v_2u_1, v_1u_2, v_2u_2 \notin E(G)$. Then

$N(v_1) \cap N(u_1) = \{v\}$ since otherwise, let $u \in N(v_1) \cap N(u_1) - \{v\}$. Then $\bar{N}(\{v_1, u_1, v\}) = \{u, v_2, u_2\}$. Thus $\{u, v_2, u_2\}$ is a cut set of G with three vertices, a contradiction. Let $N(v_1) = \{v_2, v, u_1, v_3\}$. Then $v_3 u_1 \notin E(G)$. Adding v_3 to W_1. Since $|V(G)| \geq 7$ but $|W| = 6$, $V(G) \neq W$. We have from Lemma 2 that $v_3 v_2 \in E(G)$. We further have the following fact.

Claim 1. $v_3 \notin N(W_2)$.

Recall that $v_3 u_1 \notin E(G)$. Now we prove $v_3 u_2 \notin E(G)$. If $v_3 u_2 \in E(G)$, let $N(v_2) = \{v, v_1, v_3, v_4\}$. Then we have from $G[v_2, v_4, v, v_3] \neq K_{1,3}$ that $v_4 v_3 \in E(G)$. Since $G[v_3, v_4, v_1, u_2] \neq K_{1,3}$ and $v_1 v_4, v_1 u_2 \notin E(G)$, $u_2 v_4 \in E(G)$. If $V(G) \neq W \cup \{v_4\}$, then $\{v_4, u_1\}$ is a cut-set of two vertices since v_1, v_2, v_3, u_2 are of degree 4 in $G[W \cup \{v_4\}]$, a contradiction. Thus $V(G) = W \cup \{v_4\}$ and add v_4 into W_1, it follows that $u_1 v_4 \in E(G)$ since only v_1, u_1, v_4 are of degree 3 in $G[W]$. So G is isomorphic to a graph of the depiction in Figure 1, a contradiction. Thus Claim 1 is true.

Note that v_2 is of degree 3 and v_3 is of degree 2 and v_1 is of degree 4 in H. Consider the vertex v_3 of degree 3 in H. By Claim 1, we have $V(G) \neq W$. Let $N(v_2) = \{v, v_1, v_3, v_4\}$ and add v_4 into W_1. From Lemma 2, $v_i v_{i-1} \in E(G)$, where $i = 4$. We further have the following fact.

Claim 2. If $V(G) \neq W$, then $v_4 \notin N(W_2)$.

If $v_4 u_2 \in E(G)$, let $N(v_3) = \{v_1, v_2, v_4, v_5\}$. Then $v_5 v_4 \in E(G)$ since $G[v_3, v_5, v_4, v_1] \neq K_{1,3}$. Since $G[v_4, v_2, v_4, u_2] \neq K_{1,3}$ and $v_2 v_5, v_2 u_2 \notin E(G)$, $v_5 u_2 \in E(G)$. Thus $d_H(v_4) = 4$. If $V(G) \neq W \cup \{v_5\}$, then $\{v_5, u_1\}$ is a cut set of two vertices, a contradiction. Thus $V(G) = W \cup \{v_5\}$, and add v_5 into W_1. Since $d_H(v_5) = d_H(u_1) = 3$, $u_1 v_5 \in E(G)$. Thus G is isomorphic to a graph of the depiction in Figure 1, a contradiction. So $v_4 u_2 \notin E(G)$. If $v_4 u_1 \in E(G)$, then $G[u_1, u_2, v_1, v_4] = K_{1,3}$. This contradiction shows that Claim 2 is true.

From the above, we have established the following claim.

Claim 3. v_i is of degree 2, v_{i-1} is of degree 3, and v_j is of degree 4 in H for $j = 1, 2, ..., i - 2$, where $i = 4$.

Now we return to the proof of Theorem 3. If $V(G) = W$, then we have from $d_H(u_2) = 2$ that $u_2 v_4, u_2 v_3 \in E(G)$. Thus $u_1 v_4 \in E(G)$. It follows that G is isomorphic to Figure 1. We assume that $V(G) \neq W$. Then, by Claim 3, consider the vertex v_3 of degree 3 in H and add the neighbor v_5 of v_4 outside W into W_1. By Lemma 2, $v_5 v_4 \in E(G)$. Then v_5 has similar properties in Claim 2 and Claim 3 ($i = 5$). But G is finite, we must have $V(G) = W$ and $W_1 = \{v_1, v_2, ..., v_{n-3}\}$. And Claim 3 is true for $i = n - 3$. It follows that G is isomorphic to a graph of the depiction in Figure 1. Therefore, the proof of Theorem 3 is completed.

Algorithm 4. *Construction of a 4-connected 4-regular locally connected claw-free graph G on $n \geq 7$ vertices.*

1. Pick up any vertex v.
2. Find 4 neighbors of v. Let $v_2 v_1 u_1 u_2$ is a hamiltonian path in $N(v)$ and $W_1 = \{v_1, v_2\}$ and $W = \{v, u_1, u_2\} \cup W_1$, and set $i = 1$.
3. Find a neighbor v_{i+2} of v_i. Set $W_1 = (W_1 \cup \{v_{i+2}\}) - \{v_i\}$ and $W = W \cup \{v_i\}$
4. If $|W| = |V(G)|$, go to Step 5. Otherwise, set $i = i + 1$ and go to 3.
5. Check whether u_2 is adjacent to all vertices of W_1 and u_1 is only adjacent to v_{n-3}.

We now analyze time in Algorithm 4. Note that n is the number of vertices.

Step 1 needs $O(1)$. Step 2 needs $O(n)$. Step 3 needs $O(n)$ and Step 4 needs $O(1)$. By Theorem 3, such a graph is 4-connected 4-regular locally connected claw-free. Thus we obtain a linear polynomial time algorithm to construct a 4-connected 4-regular locally connected claw-free graph.

References

1. J. A. Bondy and U.S.R. Murty, Graph Theory with its applications, MacMillan, New York,1976
2. M.R. Garey and D.S. Johnson, Computers and Intractability-A Guide to the theory of NP-completeness, Freeman, New York, 1979.
3. M. R. Garey, D.S. Johnson and R.E. Tarjan, The planar hamiltonian circuit problem is NP-complete, SIAM J. Computing, 5(1976), 704-714.
4. M. Li, D.G. Corneil and E. Mendelsohn, Pancyclicity and NP-completeness in planar graphs, Discrete Applied Math., 98(2000) 219-225.
5. L. G. Valiant, The complexity of computing the permanent, Theor. Computer Sci., 8(1979), 189-201.

Connectivity of Connected Bipartite Graphs with Two Orbits

Xiaodong Liang and Jixiang Meng[*]

College of Mathematics and System Sciences,Xinjiang University
Urumqi,Xinjiang 830046, People's Republic of China
liangxd-1970@163.com,
mjx@xju.edu.cn

Abstract. Let $X = (V, E)$ be a simple connected graph, the connectivity $\kappa(X)$ of X is the minimum cardinality of all vertex cut sets in X. Let $x \in V(X)$, the set $\{x^g : g \in Aut(X)\}$ is called an orbit of $Aut(X)$, the automorphism group of X. In this note, we prove that the connectivity of a connected bipartite graph with two orbits attains its minimum degree.

Keywords: Connectivity, Bipartite graph, Orbit.

1 Introduction

Let $X=(V, E)$ be a simple connected graph, with $V(X)$ the set of vertices and $E(X)$ the set of edges. A *vertex cut* of X is a subset U of V such that the subgraph $X\backslash U$ induced by $V\backslash U$ is either trivial or not connected. The *connectivity* $\kappa(X)$ of a nontrivial connected graph X is the minimum cardinality of all vertex cut sets of X. If we denote by $\delta(X)$ the minimum degree of X, then $\kappa(X){\leq}\delta(X)$.

We denote by $Aut(X)$ the automorphism group of X. The graph X is said to be *vertex transitive* if for any two distinct vertices of X there is an automorphism mapping one to the other. Let $x \in V(X)$, we call the set $\{x^g : g \in Aut(X)\}$ an *orbit* of $Aut(X)$. Clearly, $Aut(X)$ acts transitively on each orbit of $Aut(X)$.

In [3], Mader proved that the connectivity of a connected vertex transitive graph, which is $K_4{-}free$, attains its minimum degree. It arouses us to consider the relation between the connectivity and the number of orbits. In this note, we prove that the connectivity of a connected bipartite graph with two orbits attains its minimum degree.

In the next, we introduce some terms and theorems which will be used in proving our main results.

Let $X = (V, E)$ be a connected graph and F be a non-empty subset of $V(G)$. Set $N(F) = \{x{\in}V(X)\backslash F : \exists y{\in}F, st. \quad xy{\in}E(X)\}$, $C(F) = F \cup N(F)$ and $R(F) = V(X) \backslash C(F)$. Clearly, $N(F)$ is a vertex cut set if $R(F){\neq}\emptyset$. A subset $F{\subset}V(X)$ is said to be a *fragment* if $|N(F)|{=}\kappa(X)$ and $R(F){\neq}\emptyset$. A fragment of minimum cardinality is called an *atom* of X. An *imprimitive block* for a group

U of permutations on a set T is a proper, nontrivial subset A of T such that if $\sigma \in U$ then either $\sigma(A) = A$ or $\sigma(A) \cap A = \emptyset$. A subset A of $V(X)$ is called an imprimitive block for X if it is an imprimitive block for $Aut(X)$ on $V(X)$.

Theorem 1. *[8] Let $X=(V, E)$ be a nontrivial connected graph which is not a complete graph.*
(i) $\kappa(X) = \delta(X)$ if and only if every atom of X has cardinality 1;
(ii) if $\kappa(X) < \delta(X)$, then each atom has cardinality at most $[(|V| - \kappa(X))/2]$ and induces a connected subgraph of X.

Theorem 2. *[5] If $X=(V, E)$ is a nontrivial connected graph which is not a complete graph, then distinct atoms of X are disjoint. Thus if $\kappa(X) < \delta(X)$, the atoms of X are imprimitive blocks of X.*

Theorem 3. *[5] Let $X=(V, E)$ be a nontrivial connected graph. If W is a minimum vertex cut set and A an atom of X, then $A \cap W = \emptyset$ or $A \subseteq W$.*

2   Main Results

Let $X=(V, E)$ be a connected bipartite graph with two orbits. Clearly, it is semiregular. In this section, we use X_0 and X_1 to denote the two orbits of $Aut(X)$. Without loss of generality, we may assume that $m = d(u)$ for any $u \in X_0$, $n = d(v)$ for any $v \in X_1$, and $m \le n$. So we have $\delta(X) = m$. Let A be an atom of X. Set $A_0 = A \cap X_0$ and $A_1 = A \cap X_1$, then $A = A_0 \cup A_1$.

Lemma 1. *Let $X=(V, E)$ be a connected bipartite graph with two orbits, and A be an atom of X. If $\kappa(X) < \delta(X)$, then $A_i=A \cap X_i(i = 0, 1)$ are nontrivial.*

Proof. By Theorem 1, the induced subgraph $Y=X[A]$ is a nontrivial connected subgraph of X, which is a bipartite graph, thus $A_i=A \cap X_i \neq \emptyset(i = 0, 1)$. Suppose that one of these two vertex subsets is trivial.

Case 1: $|A_0|=1$. Thus, $|A_1| \le m$ since Y is connected. Set $F = N(A)$.

Subcase 1.1: $|A_1|=m$. So we have $|F| \ge n - 1$. If $|F|=n - 1$, then the induced subgraph $Y'=X[A \cup F]$ is a connected component of X, which is impossible since X is connected. Thus $|F|>n - 1$, namely $|F| \ge n \ge m = \delta(X)$, a contradiction.

Subcase 1.2: $|A_1|=p \le m - 1$. Thus $|N(A_0) \setminus A_1|=m - p$. Let $q=|N(A_1) \setminus A_0|$, we have $q \ge n - 1$. Since

$$|F| = |N(A)| = |N(A_0) \setminus A_1| + |N(A_1) \setminus A_0| = m - p + q \ge m + n - p - 1$$

and $|F| = \kappa(X) < m$, we have $n < p + 1 \le m$, a contradiction.

Case 2: $|A_1|=1$. Thus, $|A_0| \le n$ since Y is connected. Set $F = N(A)$.

Subcase 2.1: $|A_0|=n$. So we have $|F|\geq m-1$. Since $|F|=\kappa(X) < m$, $|F|\leq m-1$. Namely, $|F| = m-1$. Thus we have that the induced subgraph $Y'=X[A\cup F]$ is a connected component of X, a contradiction.

Subcase 1.2: $|A_0|=p\leq n-1$. Thus $|N(A_0)\backslash A_1|=n-p$. Let $q=|N(A_1)\backslash A_0|$, then $q \geq m-1$. Since

$$|F| = |N(A)| = |N(A_0) \setminus A_1| + |N(A_1) \setminus A_0| = n - p + q \geq n + m - p - 1$$

and $|F| = \kappa(X) < m$, we have $n < p+1 \leq n$, a contradiction.

The result follows. $\qquad\square$

Lemma 2. *Let $X=(V,E)$ be a connected bipartite graph with two orbits, and A be an atom of X, and $Y=X[A]$. If $\kappa(X) < \delta(X)$, then Aut(Y) acts transitively on $A_i = A \cap X_i(i = 0,1)$.*

Proof. By Lemma 1, $A_i=A \cap X_i(i=0,1)$ are nontrivial. For any $u, v\in A_0$, there exists an automorphism φ of X with $\varphi(u) = v$ and so $\varphi(A)\cap A \neq \emptyset$. By Theorem 2, $\varphi(A) = A$. Since A_0 and A_1 are contained in different orbits, we have $\varphi(A_0) = A_0$ and $\varphi(A_1) = A_1$. Thus the restriction of φ on A induces an automorphism of Y, and then $Aut(Y)$ acts transitively on A_0. Similarly, $Aut(Y)$ acts transitively on A_1. The result follows. $\qquad\square$

Lemma 3. *Let $X=(V,E)$ be a connected bipartite graph with two orbits, and A be an atom of X. If $\kappa(X) < \delta(X)$, then*
(i) Every vertex of X lies in an atom;
(ii) $|A| \leq \kappa(X)$.

Proof. (i) By Lemma 1, the induced subgraph $Y=X[A]$ is a nontrivial connected subgraph of X, thus at least one vertex of $X_i(i = 0, 1)$, respectively, lies in an atom. By the transitivity of X_i, every vertex of X lies in an atom.

(ii) Let $F=N(A)$. By (i), for any $u \in F$, u lies in an atom A' of X. By Theorem 3, $A'\subseteq F$, then $|A| = |A'| \leq |F| = \kappa(X)$. $\qquad\square$

Theorem 4. *If $X=(V,E)$ is a connected bipartite graph with two orbits, then $\kappa(X) = \delta(X)$.*

Proof. Suppose to the contrary that $\kappa(X) < \delta(X)$. By Theorem 1 and Lemma 3, $V(X)$ is a disjoint union of distinct atoms. Let A be an atom of X, then there exist $\sigma_i \in \mathrm{Aut}(X)(i = 1, \cdots, k)$, such that

$$V(X) = \bigcup_{i=1}^{k} \sigma_i(A) . \tag{1}$$

By Lemma 1, the induced subgraph $Y=X[A]$ is a nontrivial connected subgraph of X, and $A_i=A\cap X_i(i = 0, 1)$ are nontrivial. Since $\mathrm{Aut}(X)$ has two orbits X_0, X_1, for any $1 \leq i, j \leq k$ and $i \neq j$, $\sigma_i(A_0) \cap \sigma_j(A_0) = \emptyset$ and $\sigma_i(A_0), \sigma_j(A_0) \subseteq X_0$.

Thus, we have $X_0 = \bigcup_{i=1}^{k} \sigma_i(A_0)$, $X_1 = \bigcup_{i=1}^{k} \sigma_i(A_1)$, and $|A_i| \mid |X_i| (i = 0, 1)$. Since $|X_0|/|X_1| = n/m$, we have $|A_0|/|A_1| = n/m$.

By Lemma 2, the induced subgraph Y is semi-regular. Let $d = \delta(Y) = \delta_{A_0}$ and $F = N(A)$, we have $\delta_{A_1} = nd/m$. Since every vertex of A_0 has $m - d$ neighbours in F and every vertex of A_1 has $n - nd/m$ neighbours in F, we have $|F| = \kappa(X) \geq m - d + n - nd/m = m + n - (m+n)d/m$. By $\kappa(X) < \delta(X) = m$, we have $d > mn/(m+n)$. Thus, $|A| = |A_0| + |A_1| \geq d + nd/m = (m+n)d/m > n \geq m > \kappa(X)$. By Lemma 3, we deduce a contradiction.

The theorem then follows.   □

Acknowledgements

References

1. Hamidoune, Y.O.: Sur les atomes d'un graphe orienté. C.R.Acad. Sc. Paris Ser. A 284 (1977) 1253–1256
2. Liang, X., Meng, J.: Connectivity of Bi-Cayley Graphs. accepted by Ars. Comb.
3. Mader, W.: Über den Zusammenhang symmetricher Graphen. Arch. Math. 21 (1970) 331–336
4. Mader, W.: Minimale n-fach kantenzusammenhängende Graphen. Math. Ann. 191 (1971) 21–28
5. Mader, W.: Ein Eigenschaft der Atome endlicher Graphen. Arch. Math. 22 (1971) 331–336
6. Meng, J.: Connectivity of vertex and edge transitive graphs. Discrete Appl. Math. 127 (2003) 601–613
7. Tindell, R.: Connectivity of Cayley digraphs. In: Du D.Z., Hsu D.F.(Eds.): Combinatorial network theory. Kluwer Academic Publishers, The Netherlands (1996) 41–64
8. Watkins, M.E.: Connectivity of transitive graphs. J.Comb. Theory 8 (1970) 23–29

Heavy Cycles in 2-Connected Weighted Graphs with Large Weighted Degree Sums

Bing Chen[1], Shenggui Zhang[1,2], and T.C. Edwin Cheng[2]

[1] Department of Applied Mathematics, Northwestern Polytechnical University,
Xi'an, Shaanxi 710072, P.R. China
[2] Department of Logistics, The Hong Kong Polytechnic University,
Hung Hom, Kowloon, Hong Kong

Abstract. In this paper, we prove that a 2-connected weighted graph G contains either a Hamilton cycle or a cycle of weight at least $2m/3$ if it satisfies the following conditions: (1) $\sum_{i=1}^{3} d^w(v_i) \geq m$, where v_1, v_2 and v_3 are three pairwise nonadjacent vertices of G, and two of them are nonadjacent vertices of an induced claw or an induced modified claw; (2) In each induced claw and each induced modified claw of G, all edges have the same weight. This extends several previous results on the existence of heavy cycles in weighted graphs.

Keywords: Hamilton cycle, weighted graph, induced claw (modified claw.)

1 Terminology and Notation

We use Bondy and Murty [3] for terminology and notation not defined here and consider finite simple graphs only. Let G be a graph. G is called a *weighted graph* if each edge e is assigned a nonnegative number $w(e)$, called the *weight* of e. For a subgraph H of G, $V(H)$ and $E(H)$ denote the sets of vertices and edges of H, respectively. The *weight* of H is defined by $w(H) = \sum_{e \in E(H)} w(e)$. For a vertex $v \in V$, $N_H(v)$ denotes the set, and $d_H(v)$ the number, of vertices in H that are adjacent to v. We define the *weighted degree* of v in H by $d_H^w(v) = \sum_{h \in N_H(v)} w(vh)$. When no confusion occurs, we will denote $N_G(v)$, $d_G(v)$ and $d_G^w(v)$ by $N(v)$, $d(v)$ and $d^w(v)$, respectively.

An unweighted graph can be regarded as a weighted graph in which each edge is assigned weight 1. Thus, in an unweighted graph, $d^w(v) = d(v)$ for every vertex v, and the weight of a subgraph is simply the number of its edges.

The number of vertices in a maximum independent set of G is denoted by $\alpha(G)$. If G is noncomplete, then for a positive integer $k \leq \alpha(G)$ we denote by $\sigma_k(G)$ the minimum value of the degree sum of any k pairwise nonadjacent vertices, and by $\sigma_k^w(G)$ the minimum value of the weighted degree sum of any k pairwise nonadjacent vertices. If $k > \alpha(G)$, then both $\sigma_k(G)$ and $\sigma_k^w(G)$ are defined as ∞.

An (x, y)-*path* is a path connecting the two vertices x and y. A y-*path* is a path which has y as one of its end-vertices. The *distance* between two vertices

x and y, denoted by $d(x, y)$, is the length of a shortest (x, y)-path. We call the graph $K_{1,3}$ a *claw*, and the graph $K_{1,3} + e$ (e is an edge between two nonadjacent vertices in the claw) a *modified claw*. For a graph G, if there exist three pairwise nonadjacent vertices in which two of them are nonadjacent in an induced claw or an induced modified claw, then by $\overline{\sigma}_3^w(G)$ we denote the minimum value of the weighted degree sum of such three pairwise nonadjacent vertices. Otherwise, $\overline{\sigma}_3^w(G)$ is defined as ∞. Clearly we have $\overline{\sigma}_3^w(G) \geq \sigma_3^w(G)$.

2 Results

In [8], Pósa gave a degree sum condition for the existence of long cycles in graphs. This result was generalized by the following two theorems along different lines.

Theorem A (Fan [5]). *Let G be a 2-connected graph such that $max\{d(x), d(y)|$ $d(x, y) = 2\} \geq c/2$. Then G contains either a Hamilton cycle or a cycle of length at least c.*

Theorem B (Fournier & Fraisse [6]). *Let G be a k-connected graph where $2 \leq k < \alpha(G)$, such that $\sigma_{k+1}(G) \geq m$. Then G contains either a Hamilton cycle or a cycle of length at least $2m/(k + 1)$.*

Bondy *et al.* [2] generalized the result of Pósa to weighted graph. In [10], it was showed that if one wants to give a generalization of Theorem A to weighted graphs, some extra conditions cannot be avoided. By adding two extra conditions, the authors gave a weighted generalization of Theorem A. Motivated by this result, by adding two same extra conditions, Zhang *et al.* [9] gave a weighted generalization of Theorem B in the case $k = 2$.

Theorem 1 (Zhang *et al.* [9]). *Let G be a 2-connected weighted graph which satisfies: (1) $\sigma_3^w(G) \geq m$; (2) $w(xz) = w(yz)$ for every vertex $z \in N(x) \cap N(y)$ with $d(x, y) = 2$; (3) In every triangle T of G, either all edges of T have different weights or all edges of T have the same weight. Then G contains either a Hamilton cycle or a cycle of weight at least $2m/3$.*

Theorem A was further extended by the following result.

Theorem C (Bedrossian *et al.* [1]). *Let G be a 2-connected graph. If max $\{d(x), d(y)\} \geq c/2$ for each pair of nonadjacent vertices x and y, which are vertices of an induced claw or an induced modified claw of G, then G contains either a Hamilton cycle or a cycle of length at least c.*

By adding one extra condition, Fujisawa [7] gave a weighted generalization of Theorem C.

Theorem 2 (Fujisawa [7]). *Let G be a 2-connected weighted graph which satisfies: (1) For each induced claw and each induced modified claw of G, all its nonadjacent pair of vertices x and y satisfy $max\{d^w(x), d^w(y)\} \geq s/2$; (2) For each induced claw and each induced modified claw of G, all of its edges have the same weight. Then G contains either a Hamilton cycle or a cycle of weight at least s.*

Clearly, Conditions (2) and (3) of Theorem 1 imply Condition (2) of Theorem 2. In a previous paper [4], the authors proved that Conditions (2) and (3) of Theorem 1 can be replaced by Condition (2) of Theorem 2. Here we will further show that Condition (1) of Theorem 1 can also be replaced by a weaker one.

Theorem 3. *Let G be a 2-connected weighted graph which satisfies the following conditions: (1) $\overline{\sigma}_3^w(G) \geq m$; (2) For each induced claw and each induced modified claw of G, all of its edges have the same weight. Then G contains either a Hamilton cycle or a cycle of weight at least $2m/3$.*

3   Proof of Theorem 3

We call a path P a *heaviest longest path* of a graph G if P has the following properties

- P is a longest path of G, and
- $w(P)$ is maximum among all longest paths in G.

Proposition 1. *Let G be a non-hamiltonian 2-connected weighted graph which satisfies conditions (1) and (2) of Theorem 3. Then G contains a heaviest longest path $P = v_1 v_2 \cdots v_p$, such that $d^w(v_1) + d^w(v_p) \geq 2m/3$.*

We prove this proposition in the next section. Theorem 3 can be proved by combining Proposition 1 and the following lemma. The proof of Lemma 1 is implicit in [2].

Lemma 1 (Bondy *et al.* [2]). *Let G be a non-hamiltonian 2-connected weighted graph and $P = v_1 v_2 \cdots v_p$ be a heaviest longest path in G. Then there is a cycle C in G with $w(C) \geq d^w(v_1) + d^w(v_p)$.*

Proof of Theorem 3. Suppose that G does not contain a Hamilton cycle. Then by Proposition 1 and Lemma 1, we can find a cycle of weight at least $2m/3$.

4   Proof of Proposition 1

In the proof of Proposition 1, we need the following two lemmas.

Lemma 2 (Fujisawa [7]). *Let G be a weighted graph satisfying Condition (2) of Theorem 3. If $x_1 y x_2$ is an induced path with $w(x_1 y) \neq w(x_2 y)$ in G, then each vertex $x \in N(y) \backslash \{x_1, x_2\}$ is adjacent to both x_1 and x_2.*

Lemma 3 (Fujisawa [7]). *Let G be a weighted graph satisfying Condition (2) of Theorem 3. Suppose $x_1 y x_2$ is an induced path such that $w_1 = w(x_1 y)$ and $w_2 = w(x_2 y)$ with $w_1 \neq w_2$, and $y z_1 z_2$ is a path such that $\{z_1, z_2\} \cap \{x_1, x_2\} = \emptyset$ and $x_2 z_2 \notin E(G)$. Then the following (i) and (ii) hold:
(i) $\{z_1 x_1, z_1 x_2, z_2 x_1\} \subseteq E(G)$, and $y z_2 \notin E(G)$. Moreover, all edges in the subgraph induced by $\{x_1, y, x_2, z_1, z_2\}$, other than $x_1 y$, have the same weight w_2.*

(ii) Let Y be the component of $G - \{x_2, z_1, z_2\}$ with $y \in V(Y)$. For each vertex $v \in V(Y) \backslash \{x_1, y\}$, v is adjacent to all of x_1, x_2, y and z_2. Furthermore, $w(vx_1) = w(vx_2) = w(vy) = w(vz_2) = w_2$.

Proof of Proposition 1. Choose a heaviest longest path $P = v_1 v_2 \cdots v_p$ in G such that $d^w(v_1) + d^w(v_p)$ is as large as possible. It is clear that $N(v_1) \cup N(v_p) \subseteq V(P)$. And it is not difficult to prove that there exists no cycle of length p.

Suppose $d^w(v_1) + d^w(v_p) < 2m/3$. Without loss of generality, we may assume $d^w(v_1) < m/3$.

Claim 1. Let P_1 and P_2 be two heaviest longest paths such that P_1 has v' and v_p as its end-vertices, and P_2 has v'' and v_p as its end-vertices. Then v' and v'' cannot be nonadjacent vertices of an induced claw or an induced modified claw.

Proof. Suppose v' and v'' are nonadjacent vertices of an induced claw or an induced modified claw. Since P_1 and P_2 are heaviest longest paths, $v'v_p \notin E(G)$ and $v''v_p \notin E(G)$. By the choice of the path P in (b), $d^w(v') \le d^w(v_1)$ and $d^w(v'') + d^w(v_p) < 2m/3$. So we have $d^w(v') + d^w(v'') + d^w(v_p) < m$, contradicting Condition (1) of Theorem 3. $\square$

Since G is 2-connected, v_1 is adjacent to at least one vertex on P other than v_2. Choose $v_k \in N(v_1)$ such that k is as large as possible. It is clear that $3 \le k \le p - 1$.

Case 1. $N(v_1) = \{v_2, \cdots, v_k\}$.

Since P is longest and $N(v_1) = \{v_2, \cdots, v_k\}$, $N(v_i) \subseteq V(P)$ for every i with $i = 2, \cdots, k - 1$; Since G is a non-hamiltonian 2-connected graph, $k + 2 \le p$; Since $G - v_k$ is connected, there must be an edge $v_j v_s \in E(G)$ with $j < k < s$.

We assume that such an edge $v_j v_s$ was chosen so that: (i) s is as large as possible; (ii) j is as large as possible, subject to (i). Clearly we have $s \le p - 1$.

Claim 2. $w(v_1 v_{j+1}) = w(v_j v_{j+1})$.

Proof. Suppose $j \le k - 2$. By the choices of v_k, v_j and v_s, we have $v_1 v_s \notin E(G)$ and $v_{j+1} v_s \notin E(G)$. So $\{v_j, v_1, v_{j+1}, v_s\}$ induces a modified claw, which implies that $w(v_1 v_{j+1}) = w(v_j v_{j+1})$.

Suppose $j = k - 1$ and $s \ge k + 2$. By the choices of v_k and v_s, we have $v_1 v_s \notin E(G)$, $v_1 v_{s+1} \notin E(G)$ and $v_j v_{s+1} \notin E(G)$. If $v_k v_{s+1} \in E(G)$, then $\{v_k, v_1, v_{k-1}, v_{s+1}\}$ induces a modified claw. So $w(v_1 v_k) = w(v_{k-1} v_k)$. If $v_k v_s \notin E(G)$, then $\{v_{k-1}, v_1, v_k, v_s\}$ induces a modified claw. So $w(v_1 v_k) = w(v_{k-1} v_k)$. If $v_k v_{s+1} \notin E(G)$ and $v_k v_s \in E(G)$, then $\{v_k, v_1, v_{k+1}, v_s\}$ induces a claw or a modified claw. So $w(v_1 v_k) = w(v_k v_s)$; On the other hand, $\{v_s, v_{k-1}, v_k, v_{s+1}\}$ induces a modified claw. So $w(v_k v_s) = w(v_{k-1} v_k)$; Then $w(v_1 v_k) = w(v_{k-1} v_k)$.

Suppose $j = k - 1$ and $s = k + 1$. Since P is longest, $N(v_k) \subset V(P)$; Since $G - v_{k+1}$ is connected, there exists an edge $v_k v_t \in E(G)$ with $t \ge k + 2$. Choose $v_k v_t$ such that t is as small as possible. So $\{v_k, v_1, v_{k-1}, v_t\}$ induces a modified claw. Then $w(v_1 v_k) = w(v_{k-1} v_k)$. $\square$

Claim 3. $s = k + 1$.

Proof. Suppose $s \geq k + 2$. Let $P' = v_{s-1}v_{s-2}\cdots v_{j+1}v_1\ v_2\cdots v_jv_sv_{s+1}\cdots v_p$. If $v_jv_{s-1} \in E(G)$, then $\{v_j, v_1, v_{s-1}, v_s\}$ induces a modified claw, so $w(v_{s-1}v_s) = w(v_jv_s)$. By Claim 2, now P' is a heaviest longest v_p-path different from P, contradicting Claim 1. If $v_jv_{s-1} \notin E(G)$, then $\{v_s, v_j, v_{s-1}, v_{s+1}\}$ induces a claw or a modified claw. Thus $w(v_{s-1}v_s) = w(v_jv_s)$. By Claim 2, both $v_jv_{j-1}\cdots v_1$ $v_{j+1}v_{j+2}\cdots v_p$ and P' are heaviest longest v_p-paths, contradicting Claim 1. $\square$

As in the proof of Claim 2, since $s = k + 1$ and $G - v_{k+1}$ is connected, there exists an edge $v_kv_t \in E(G)$ with $k + 2 \leq t \leq p - 1$. Choose v_kv_t such that t is as small as possible.

Case 1.1. $t \geq k + 3$.

By the choices of v_s and v_t, $v_jv_{k+2} \notin E(G)$ and $v_kv_{k+2} \notin E(G)$. So $\{v_{k+1}, v_j, v_k, v_{k+2}\}$ induces a claw or a modified claw. Thus $w(v_kv_{k+1}) = w(v_jv_{k+1})$.

Suppose $v_kv_{t+1} \notin E(G)$. By the choice of v_t, $v_kv_{t-1} \notin E(G)$. So $\{v_t, v_k, v_{t-1}, v_{t+1}\}$ induces a claw or a modified claw. Thus $w(v_{t-1}v_t) = w(v_kv_t)$. By Claim 2, both $v_kv_{k-1}\cdots v_{j+1}v_1\cdots v_jv_{k+1}\cdots v_p$ and $v_{t-1}v_{t-2}\cdots v_{k+1}v_jv_{j-1}\cdots v_1v_{j+1}\cdots$ $v_kv_tv_{t+1}\cdots v_p$ are heaviest longest v_p-paths, contradicting Claim 1. Suppose $v_kv_{t+1} \in E(G)$. By the choice of v_k, $v_1v_t \notin E(G)$ and $v_1v_{t+1} \notin E(G)$. So $\{v_k, v_1, v_t, v_{t+1}\}$ induces a modified claw. Thus $w(v_kv_{t+1}) = w(v_tv_{t+1})$. By Claim 2, $v_tv_{t-1}\cdots v_{k+1}v_jv_{j-1}\cdots v_1v_{j+1}\cdots v_kv_{t+1}v_{t+2}\cdots v_p$ is a heaviest longest v_p-path different from P, contradicting Claim 1.

Case 1.2. $t = k + 2$.

By the choice of v_k, now $\{v_k, v_1, v_{k+1}, v_{k+2}\}$ induces a modified claw. So we get $w(v_kv_{k+1}) = w(v_kv_{k+2}) = w(v_{k+1}v_{k+2}) = w(v_1v_k)$.

Since $G - v_t$ is connected, there exists an edge $v_{k+1}v_{t'} \in E(G)$ with $t' \geq k+3$. By the choice of v_s, $v_jv_t \notin E(G)$ and $v_jv_{t'} \notin E(G)$. So $\{v_s, v_j, v_t, v_{t'}\}$ induces a claw or a modified claw. In this case $s = k + 1$ and $t = k + 2$, thus we have $w(v_jv_{k+1}) = w(v_{k+1}v_{k+2})$. By Claim 2, now $v_{k+1}v_jv_{j-1}\cdots v_1v_{j+1}v_{j+2}\cdots v_kv_{k+2}$ $\cdots v_p$ is a heaviest longest v_p-path different from P. At the same time, v_1 and v_{k+1} are nonadjacent vertices in the modified claw induced by $\{v_k, v_1, v_{k+1}, v_{k+2}\}$, contradicting Claim 1.

This completes the proof of Case 1.

Case 2. $N(v_1) \neq \{v_2, \cdots, v_k\}$.

Choose $v_r \notin N(v_1)$ with $2 < r < k$ such that r is as large as possible. Then $v_1v_i \in E(G)$ for every i with $r < i \leq k$. Let j be the smallest index such that $j > r$ and $v_j \notin N(v_1) \cap N(v_r)$. Since $v_{r+1} \in N(v_1) \cap N(v_r)$, we have $j \geq r + 2$. On the other hand, it is obvious that $j \leq k + 1$. By the choice of v_r and v_j, now v_1 and v_r are nonadjacent vertices of a claw or a modified claw induced by $\{v_{j-1}, v_1, v_r, v_j\}$. By Claim 1 and the choice of P, we have the following claim.

Claim 4. *There exists no heaviest longest v_p-path with v_r as it's another end-vertex.*

Claim 5. $w(v_1v_{r+1}) \neq w(v_rv_{r+1})$.

Proof. If $w(v_1v_{r+1}) = w(v_rv_{r+1})$, then $v_rv_{r-1}\cdots v_1v_{r+1}v_{r+2}\cdots v_p$ is a heaviest longest v_p-path different from P, contradicting Claim 4. □

Claim 6. $v_{r+1}v_j \notin E(G)$.

Proof. By the choice of v_r, $v_1v_r \notin E(G)$. So, if $v_{r+1}v_j \in E(G)$, then by the choice of v_j, we know that $\{v_{r+1}, v_1, v_r, v_j\}$ induces a claw or a modified claw. Thus $w(v_1v_{r+1}) = w(v_rv_{r+1})$, contradicting Claim 5. □

By Claim 6, we have $r + 3 \le j \le k + 1$. Let n be the largest index such that $r + 1 \le n \le j - 2$ and $v_nv_j \notin E(G)$. Then $v_iv_j \in E(G)$ for every i with $n + 1 \le i \le j - 1$.

Claim 7. *If $r + 3 \le j \le k$, then $w(v_1v_{n+1}) = w(v_nv_{n+1})$.*

Proof. By the choice of v_n, $v_{n+1}v_j \in E(G)$. So $\{v_{n+1}, v_1, v_r, v_j\}$ induces a modified claw. Thus $w(v_1v_{n+1}) = w(v_{n+1}v_j)$. Since $v_rv_j \notin E(G)$ and $v_nv_j \notin E(G)$, $\{v_r, v_n, v_{n+1}, v_j\}$ induces a modified claw. Thus $w(v_nv_{n+1}) = w(v_{n+1}v_j)$. So $w(v_1v_{n+1}) = w(v_nv_{n+1})$. □

Case 2.1. $r + 3 \le j \le k - 1$.

Suppose $v_{r+1}v_{j+1} \notin E(G)$. By Claim 6, $v_{r+1}v_j \notin E(G)$, so $\{v_1, v_j, v_{j+1}, v_{r+1}\}$ induces a modified claw. Thus $w(v_1v_{j+1}) = w(v_jv_{j+1})$. Suppose $v_{r+1}v_{j+1} \in E(G)$. By Claim 5 and the choice of v_j, applying Lemma 3 (i) to $\{v_1, v_{r+1}, v_r, v_{j+1}, v_j\}$, we get $w(v_1v_{j+1}) = w(v_jv_{j+1})$.

By Claim 7, both $v_nv_{n-1}\cdots v_1v_{n+1}v_{n+2}\cdots v_p$ and $v_jv_{j-1}\cdots v_1v_{j+1}v_{j+2}\cdots v_p$ are heaviest longest v_p-paths. Furthermore, v_n and v_j are nonadjacent vertices in the modified claw induced by $\{v_r, v_n, v_{n+1}, v_j\}$, contradicting Claim 1.

Case 2.2 $j = k$.

Since $\{v_{j-1}, v_1, v_r, v_j\}$ induces a claw or a modified claw and $j = k$, we have

Claim 8. $w(v_1v_{k-1}) = w(v_1v_k) = w(v_{k-1}v_k)$.

Claim 9. $v_{r+2}v_k \notin E(G)$.

Proof. Suppose $v_{r+2}v_k \in E(G)$. Applying Lemma 3 (ii) to $\{v_1, v_{r+1}, v_r, v_{r+2}, v_k\}$ and the vertex v_2 (which is adjacent to v_1), we get $v_2v_{r+1} \in E(G)$ and $w(v_1v_2) = w(v_2v_{r+1}) = w(v_1v_k) = w(v_rv_{r+1})$. By Claim 8, $v_rv_{r-1}\cdots v_2v_{r+1}v_{r+2}\cdots v_{k-1}v_1 v_kv_{k+1}\cdots v_p$ is a heaviest longest v_p-path, contradicting Claim 4. □

Now, we have $v_{r+1}v_{k-1} \notin E(G)$. Since otherwise, applying Lemma 3 (ii) to $\{v_1, v_{r+1}, v_r, v_{k-1}, v_k\}$ and the vertex v_{r+2} (which is adjacent to v_{r+1}), we get $v_{r+2}v_k \in E(G)$, contradicting Claim 9. By Claim 6, v_{k-1} and v_{r+1} are nonadjacent vertices in the modified claw induced by $\{v_1, v_{r+1}, v_{k-1}, v_k\}$.

By Claims 6 and 9, now $\{v_1, v_{r+1}, v_{r+2}, v_k\}$ induces a modified claw. Then $w(v_1v_{r+2}) = w(v_{r+1}v_{r+2})$. By Claim 8, both $v_{k-1}v_{k-2}\cdots v_1v_kv_{k+1}\cdots v_p$ and $v_{r+1}v_r\cdots v_1v_{r+2}\cdots v_p$ are heaviest longest v_p-paths, contradicting Claim 1.

Case 2.3 $j = k + 1$.

Since $\{v_{j-1}, v_1, v_r, v_j\}$ induces a claw or a modified claw, we have

Claim 10. $w(v_1 v_k) = w(v_k v_{k+1}) = w(v_r v_k)$.

Claim 11. $v_{r+1} v_k \notin E(G)$.

Proof. Suppose $v_{r+1} v_k \in E(G)$. Applying Lemma 3 (ii) to $\{v_1, v_{r+1}, v_r, v_k, v_{k+1}\}$ and the vertex v_{r-1} (which is adjacent to v_r), we get $v_{r-1} v_{k+1} \in E(G)$ and $w(v_{r-1} v_r) = w(v_{r-1} v_{k+1})$. By Claim 10, we get a heaviest longest v_p-path $v_r v_{r+1} \cdots v_k v_1 v_2 \cdots v_{r-1} v_{k+1} v_{k+2} \cdots v_p$, contradicting Claim 4.   □

Claim 12. $v_i v_{k+1} \notin E(G)$ for every $v_i \in N(v_1) \cap N(v_r) \setminus \{v_k\}$.

Proof. Suppose there exists a vertex $v_i \in N(v_1) \cap N(v_r) \setminus \{v_k\}$ such that $v_i v_{k+1} \in E(G)$. If $w(v_1 v_{r+1}) \neq w(v_1 v_k)$, then applying Lemma 3 (i) to $\{v_{r+1}, v_1, v_k, v_i, v_{k+1}\}$, we get $w(v_1 v_{r+1}) = w(v_k v_{k+1})$. So $w(v_1 v_k) \neq w(v_k v_{k+1})$, contradicting Claim 10. So we get $w(v_1 v_{r+1}) = w(v_1 v_k)$. Similarly, we can prove that $w(v_r v_{r+1}) = w(v_r v_k)$. By Claim 10, we get $w(v_1 v_{r+1}) = w(v_r v_{r+1})$, contradicting Claim 5.   □

Claim 13. $w(v_1 v_{k-1}) = w(v_{k-1} v_k)$.

Proof. By the choice of v_k and Claim 12, we get $v_1 v_{k+1} \notin E(G)$ and $v_{k-1} v_{k+1} \notin E(G)$. So $\{v_k, v_1, v_{k-1}, v_{k+1}\}$ induces a modified claw and $w(v_1 v_{k-1}) = w(v_{k-1} v_k)$.   □

Case 2.3.1. $w(v_r v_{r+1}) \neq w(v_r v_k)$.

By Claim 11, $v_{r+1} v_k \notin E(G)$. Furthermore, $v_r v_{k+1} \notin E(G)$, since otherwise it follows from Lemma 2 that $v_{r+1} v_{k+1} \in E(G)$, which contradicts Claim 6.

Applying Lemma 2 to the induced path $v_{r+1} v_r v_k$ and the vertex $v_{r-1} \in N(v_r) \setminus \{v_{r+1}, v_k\}$, we get $v_{r-1} v_{r+1} \in E(G)$ and $v_{r-1} v_k \in E(G)$. By Claim 5, $w(v_1 v_{r+1}) \neq w(v_r v_{r+1})$. Applying Lemma 2 to the induced path $v_1 v_{r+1} v_r$ and the vertex $v_{r-1} \in N(v_{r+1}) \setminus \{v_1, v_r\}$, we get $v_1 v_{r-1} \in E(G)$. This implies that $v_{r-1} \in N(v_1) \cap N(v_r)$. By Claim 12, we have $v_{r-1} v_{k+1} \notin E(G)$. Then $\{v_k, v_{r-1}, v_r, v_{k+1}\}$ induces a modified claw, so $w(v_{r-1} v_r) = w(v_{r-1} v_k)$. Therefore, by Claim 13, $v_r v_{r+1} \cdots v_{k-1} v_1 v_2 \cdots v_{r-1} v_k v_{k+1} \cdots v_p$ is a heaviest longest v_p-path, contradicting Claim 4.

Case 2.3.2. $w(v_r v_{r+1}) = w(v_r v_k)$.

By Claim 5 and Claim 10, we can get that $w(v_1 v_{r+1}) \neq w(v_1 v_k)$.

Claim 14. $v_2 v_k$, $v_2 v_{r+1}$ and $v_2 v_r \in E(G)$.

Proof. By Claim 11, $v_{r+1} v_k \notin E(G)$. Applying Lemma 2 to the induced path $v_{r+1} v_1 v_k$ and the vertex $v_2 \in N(v_1) \setminus \{v_{r+1}, v_k\}$, we get $v_2 v_k \in E(G)$ and $v_2 v_{r+1} \in E(G)$. By Claim 5, $w(v_1 v_{r+1}) \neq w(v_r v_{r+1})$. Applying Lemma 2 to the induced path $v_1 v_{r+1} v_r$ and the vertex $v_2 \in N(v_{r+1}) \setminus \{v_1, v_r\}$, we get $v_2 v_r \in E(G)$.   □

Claim 15. $v_r v_{k+1} \notin E(G)$.

Proof. Suppose $v_r v_{k+1} \in E(G)$. By Claim 14, we get $v_2 \in N(v_1) \cap N(v_r)$, $v_2 v_k$ and $v_2 v_{r+1} \in E(G)$. By Claims 6 and 12, we get $v_{r+1} v_{k+1} \notin E(G)$ and $v_2 v_{k+1} \notin E(G)$. Thus both $\{v_r, v_2, v_{r+1}, v_{k+1}\}$ and $\{v_k, v_1, v_2, v_{k+1}\}$ induce modified claws. Then we have $w(v_2 v_{r+1}) = w(v_r v_{r+1}) = w(v_1 v_2) = w(v_1 v_k)$. By Claim 13, we get $w(v_1 v_{k-1}) = w(v_{k-1} v_k)$. So, $v_r v_{r-1} \cdots v_2 v_{r+1} v_{r+2} \cdots v_{k-1} v_1 v_k$ $v_{k+1} \cdots v_p$ is a heaviest longest v_p-path, contradicting Claim 4.   □

Suppose $v_1 v_{r-1} \in E(G)$. Then by applying Lemma 2 to the induced path $v_k v_1 v_{r+1}$ and $v_{r-1} \in N(v_1) \backslash \{v_k, v_{r+1}\}$, we get $v_{r-1} v_k \in E(G)$ and $v_{r-1} v_{r+1} \in E(G)$. By Claims 12 and 15, we get $v_{r-1} v_{k+1} \notin E(G)$ and $v_r v_{k+1} \notin E(G)$. Then $\{v_k, v_{r-1}, v_r, v_{k+1}\}$ induces a modified claw. Thus $w(v_{r-1} v_r) = w(v_{r-1} v_k)$. Therefore, by Claim 13, we have $v_r v_{r+1} \cdots v_{k-1} v_1 v_2 \cdots v_{r-1} v_k v_{k+1} \cdots v_p$ is a heaviest longest v_p-path, contradicting Claim 4.

Suppose $v_1 v_{r-1} \notin E(G)$. Then by Claim 5 and Lemma 2, we have $v_{r-1} v_{r+1} \notin E(G)$. Furthermore, $v_2 v_{r-1} \notin E(G)$, since otherwise, applying Lemma 3 (ii) to $\{v_r, v_{r+1}, v_1, v_2, v_{r-1}\}$ and the vertex v_k (which is adjacent to v_r), we get $w(v_1 v_{r+1}) = w(v_1 v_k)$, a contradiction. By Claims 12 and 14, $v_2 v_{k+1} \notin E(G)$. Then, both $\{v_r, v_{r+1}, v_2, v_{r-1}\}$ and $\{v_k, v_1, v_2, v_{k+1}\}$ induce modified claws. Thus $w(v_2 v_{r+1}) = w(v_r v_{r+1})$ and $w(v_1 v_2) = w(v_1 v_k)$. By Claim 13, we know that $v_r v_{r-1} \cdots v_2 v_{r+1} v_{r+2} \cdots v_{k-1} v_1 v_k$ $v_{k+1} \cdots v_p$ is a heaviest longest v_p-path, contradicting Claim 4.

The proof of the theorem is complete.

Acknowledgements

References

1. Bedrossian, P., Chen, G., Schelp, R.H.: A generalization of Fan's condition for Hamiltonicity, pancyclicity, and Hamiltonian connectedness, Discrete Math. **115** (1993) 39-50
2. Bondy, J.A., Broersma, H.J., van den Heuvel, J., Veldman, H.J.: Heavy cycles in weighted graphs, Discuss. Math. Graph Theory **22** (2002) 7-15
3. Bondy, J.A., Murty, U.S.R.: Graph Theory with Applications, New York: Macmillan London and Elsevier, 1976
4. Chen, B., Zhang, S.: A new σ_3-type condition for heavy cycles in weighted graphs, Accepted by Ars Combinatoria.
5. Fan, G.: New sufficient conditions for cycles in graphs, J. Combin. Theory Ser. B **37** (1984) 221-227
6. Fournier, I., Fraisse, P.: On a conjecture of Bondy, J. Combin. Theory Ser. B **39** (1985), 17-26.

7. Fujisawa, J.: Claw conditions for heavy cycles in weighted graphs, Graphs & Combin. **21** (2) (2005) 217-229
8. Pósa, L.: On the circuits of finite graphs, Magyar Tud. Math. Kutató Int. Közl. **8** (1963) 355-361
9. Zhang, S., Broersma, H.J., Li, X.: A σ_3 type condition for heavy cycles in weighted graphs, Discuss. Math. Graph Theory **21** (2001) 159-166
10. Zhang, S., Broersma, H.J., Li, X., Wang, L.: A Fan type condition for heavy cycles in weighted graphs, Graphs & Combin. **18** (2002) 193-200

Componentwise Complementary Cycles in Almost Regular 3-Partite Tournaments

Zhihong He[1],[*], Guojun Li[1] Dawei Ding[2], and Quanhui Liu[3]

[1] School of Mathematics and System Sciences, Shandong University,
Jinan, 250100, China
`zhihhe@126.com`
[2] Opto-Electronic Information, Yantai University, Yantai, 264005, China
[3] College of Mathematics and Information, Ludong University, Yantai,
264005, China

Abstract. The vertex set of a digraph D is denoted by $V(D)$. A c-partite tournament is an orientation of a complete c-partite graph. Let $V_1, V_2, \ldots, V_c$ be the partite sets of D. If there exist two vertex disjoint cycles C and C' in D such that $V_i \cap (V(C) \cup V(C')) \neq \emptyset$ for all $i = 1, 2, \ldots, c$, then D is cycle componentwise complementary. The global irregularity of D is defined by $i_g(D) = \max\{\max(d^+(x), d^-(x)) - \min(d^+(y), d^-(y))|x, y \in V(D)\}$ over all vertices x and y of D ($x = y$ is admissible), where $d^+(x)$ and $d^-(x)$ are the outdegree and indegree of x, respectively. If $i_g(D) \leq 1$, then D is almost regular. In this paper, we consider a special kind of multipartite tournaments which are almost regular 3-partite tournaments, and we show that each almost regular 3-partite tournament D is cycle componentwise complementary, unless D is isomorphic to $D_{3,2}$.

Keywords: almost regular, componentwise complementary cycles, tournament.

1 Terminology and Preliminary Results

We shall assume that the reader is familiar with the standard terminology on directed graphs and refer the reader to [1]. In this paper all digraphs are finite without loops or multiple arcs. The vertex set and the arc set of a digraph D are denoted by $V(D)$ and $E(D)$, respectively. For a vertex set X of D, we define $D[X]$ as the subdigraph induced by X. If xy is an arc of a digraph D, then we write $x \rightarrow y$ and say x *dominates* y.

A c-partite or multipartite tournament is an orientation of a complete c-partite graph. A tournament is a c-partite tournament with exactly c vertices. A semicomplete multipartite digraph is obtained by replacing each edge of a complete multipartite graph by an arc or by a pair of two mutually opposite arcs with the same end vertices. Let $V_1, V_2, \ldots, V_c$ be the partite sets of a c-partite tournament or semicomplete c-partite digraph D and $|V_1| \leq |V_2| \leq \ldots \leq |V_c|$. If

[*] Corresponding author.

the vertex x of D belongs to the partite set V_i, then we define $V(x) = V_i$ and define $\gamma(D) = V_1$.

If X and Y are two disjoint subsets of $V(D)$ or subdigraphs of D such that every vertex of X dominates every vertex of Y, then we say that X *dominates* Y, denoted by $X \to Y$. If there is no arc from Y to X, but $x \to y$ for all $x \in X$ and $y \in Y$ which are in different partite sets, then we denote this by $X \Rightarrow Y$ which denotes the property that there is no arc from Y to X.

The *out-neighborhood* $N_D^+(x) = N^+(x)$ of a vertex x is the set of vertices dominated by x, and the *in-neighborhood* $N_D^-(x) = N^-(x)$ is the set of vertices dominating x. The number $d_D^+(x) = d^+(x) = |N^+(x)|$ and $d_D^-(x) = d^-(x) = |N^-(x)|$ are the *outdegree* and *indegree* of x, respectively. The *minimum outdegree* and the *minimum indegree* of D are denoted by $\delta^+(D) = \delta^+$ and $\delta^-(D) = \delta^-$, and $\delta(D) = \delta = \min\{\delta^+, \delta^-\}$. The irregularity $I(D)$ of a digraph is $\max |d^+(x) - d^-(y)|$ over all vertices x and y of D ($x = y$ is admissible). In addition, the *local irregularity* is defined by $i_\ell(D) = \max |d^+(x) - d^-(x)|$ over all vertices x of D and the *global irregularity* of a digraph D is defined by $i_g(D) = \max\{\max(d^+(x), d^-(x)) - \min(d^+(y), d^-(y)) | x, y \in V(D)\}$ over all vertices x and y of D ($x = y$ is admissible). Clearly, $i_\ell(D) \leq I(D) \leq i_g(D)$. If $i_g(D) = 0$, then D is *regular* and if $i_g(D) \leq 1$, then D is *almost regular*.

A cycle of length m is an *m-cycle*. A cycle or a path in a digraph D is *Hamiltonian* if it includes all the vertices of D. A set $X \subseteq V(D)$ of vertices is *independent* if the induced subdigraph $D[X]$ has no arcs. The *independence number* $\alpha(D) = \alpha$ is the maximum size among the independent sets of vertices of D.

A digraph D is *strongly connected* or *strong* if, for each pair of vertices u and v, there is a path from u to v in D. A digraph D with at least $k + 1$ vertices is *k-connected* if for any set A of at most $k - 1$ vertices, the subdigraph $D - A$ obtained by deleting A is strong. The *connectivity* of D, denoted by $k(D)$, is then defined to be the largest value of k such that D is k-connected. A set S of vertices of a digraph D is a *separating set* if $D - S$ is not strong.

If we replace every arc xy of D by yx, then we call the resulting digraph, denoted by D^{-1}, the *converse digraph* of D.

A digraph D is *cycle complementary* if there exist two vertex-disjoint cycles C and C' such that $V(D) = V(C) \cup V(C')$.

The following results play important roles in the proof of our main result.

Lemma 1 ([2]). *Let D be a c-partite tournament with the partite sets $V_1, V_2, \ldots, V_c$. Then $||V_i| - |V_j|| \leq 2I(D) \leq 2i_g(D)$ for $1 \leq i \leq j \leq c$.*

Theorem 1 ([3]). *If D is a multipartite tournament, then*

$$k(D) \geq \frac{|V(D)| - 2i_\ell(D) - \alpha(D)}{3}.$$

Theorem 2 ([14]). *Let D be a regular 3-partite tournament with $|V(D)| \geq 6$. Then D contains two complementary cycles of length 3 and $|V(D)| - 3$, unless D is isomorphic to $D_{3,2}$. ($D_{3,2}$ is shown in Fig. 1.)*
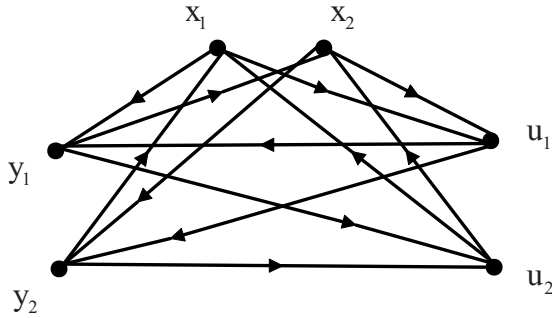
Fig. 1. The 2-regular 3-partite tournament $D_{3,2}$

Theorem 3 ([4] 1994). *Let D be a strong c-partite tournament with $c \geq 3$. Then at least one vertex of every partite set of D is contained in an m-cycle for each $m \in \{3, 4, \ldots, c\}$.*

Lemma 2 ([2]). *If D is an almost regular multipartite tournament, then for every vertex x of D we have*

$$\frac{|V(D)| - \alpha(D) - 1}{2} \leq d^+(x), d^-(x) \leq \frac{|V(D)| - \gamma(D) + 1}{2}.$$

Proposition 1 ([2]). *Let D be an almost regular c-partite tournament with the partite sets $V_1, V_2, \ldots, V_c$ such that $r = |V_1| \leq |V_2| \leq \ldots \leq |V_c| = r + 2$. Then $|V(D)| - r$ is even.*

2 Main Result

The problem of complementary cycles in tournaments was almost completely solved by Reid [5] in 1985 and by Song [6] in 1993. These authors proved that every 2-connected tournament D on at least 8 vertices has complementary cycles of length t and $|V(D)| - t$ for all $t \in \{3, 4, \ldots, |V(D)| - 3\}$. Later, Guo and Volkmann [7], [8] extended this result to locally semicomplete digraphs. In addition, there are some results on complementary cycles on bipartite tournaments by Z. Song, K. Zhang, J. Wang and Manoussakis. See [9], [11], [10], [12].

Volkmann [13] confirmed that each regular multipartite tournament is cycle complementary, unless D is isomorphic to $T_7, D_{4,2}, D_{4,2}^*, D_{3,2}$. But the problem about the existences of complementary cycles in multipartite digraphs which are not tournaments or bipartite tournaments or locally semicomplete digraphs or regular digraphs is still open. It seems that the problem of complementary cycles in semicomplete n-partite digraphs with $n \geq 3$ is difficult. In the following, we give the definition of *componentwise complementary cycles* in multipartite digraphs.

Definition 1. *(componentwise complementary cycles) Let $V_1, V_2, \ldots, V_c$ be the partite sets of D. If there exist two vertex disjoint cycles C and C' in D such that $V_i \cap (V(C) \cup V(C')) \neq \emptyset$ for all $i = 1, 2, \ldots, c$, then C and C' are two componentwise complementary cycles of D.*

Clearly, a pair of componentwise complementary cycles of D is a pair of complementary cycles of D, if it contains all vertices of D.

If D contains a pair of componentwise complementary cycles, then D is *cycle componentwise complementary.*

Our main result is the following theorem.

Theorem 4. *If D is an almost regular 3-partite tournament with $|V(D)| \geq 6$, then D is cycle componentwise complementary, unless D is isomorphic to $D_{3,2}$.*

Example 1. Let $V_1 = \{x_1, x_2\}$, $V_2 = \{y_1, y_2\}$, $V_3 = \{u_1, u_2\}$ be the partite sets of the 2-regular 3-partite tournament $D_{3,2}$ presented in Fig. 1. Then it is a simple matter to verify that $D_{3,2}$ contains no componentwise complementary 3-cycles (and of course no complementary cycles).

3   Proof of Theorem 4

Let V_1, V_2, V_3 be the partite sets of D such that $|V_1| \leq |V_2| \leq |V_3|$. By Theorem 1 and $i_\ell(D) \leq i_g(D)$,

$$k(D) \geq \frac{|V(D)| - 2i_\ell(D) - \alpha(D)}{3} \geq \frac{|V(D)| - 2i_g(D) - \alpha(D)}{3}. \quad (1)$$

If $|V_1| = r$, then because of $i_g(D) \leq 1$ we deduce from Lemma 1 that $|V_3| = r + l$ for some $l \in \{0, 1, 2\}$. Since $|V(D)| \geq 6$, $r \geq 2$.

Clearly, if $l = 0$, then D is a regular 3-partite tournament. By Theorem 2, D contains a pair of complementary cycles, i.e. D contains a pair of componentwise complementary cycles, unless D is isomorphic to $D_{3,2}$. In the following, we consider the case $l \neq 0$. According to (1), we have $k(D) \geq 1$. In view of Theorem 3, there exists a 3-cycle C_3 in D. If we define the 3-partite tournament H by $H = D - V(C_3)$, then $i_\ell(H) \leq i_g(H) \leq 3$. We distinguish five cases.

1. $|V_1| = r$, $|V_2| = r$, $|V_3| = r + 1$.
2. $|V_1| = r$, $|V_2| = r + 1$, $|V_3| = r + 1$.
3. $|V_1| = r$, $|V_2| = r$, $|V_3| = r + 2$.
4. $|V_1| = r$, $|V_2| = r + 1$, $|V_3| = r + 2$.
5. $|V_1| = r$, $|V_2| = r + 2$, $|V_3| = r + 2$.

According to Proposition 1, we have case 4 is impossible.

Since the proofs of the cases above are similar, we give the proof of case 1 only.

Let $V_1 = \{x_1, x_2, \ldots, x_r\}$, $V_2 = \{y_1, y_2, \ldots, y_r\}$, $V_3 = \{u_1, u_2, \ldots, u_{r+1}\}$, and let $C_3 = x_1 y_1 u_1 x_1$. By Lemma 2, we have $r - 1 \leq d_D^+(x), d_D^-(x) \leq r + 1$, for

$x \in V(D)$. If H contains a cycle C, then we have $V(C_3) \cap V(C) = \emptyset$ and $(V(C_3) \cup V(C)) \cap V_i \neq \emptyset$ for all $i = 1, 2, 3$. Otherwise, let $P = v_1 v_2 \ldots v_p$ be a longest path of H. Clearly, $v_1 \Rightarrow V(D - V(C_3))$ and $V(D - V(C_3)) \Rightarrow v_p$. Hence, we have

$$d_D^+(v_1) \geq 3r + 1 - 3 - r = 2r - 2, \quad \text{and}$$

$$d_D^-(v_1) \leq 2.$$

If $r \geq 4$, then $d_D^+(v_1) \geq 2r - 2 > r + 1$. The contradiction to the almost regular of D.

If $r = 3$, then $d_D^+(v_1) \geq 2r - 2$. Since $d_D^-(v_1) \leq 2$, we have $d_D^+(v_1) - d_D^-(v_1) \geq 2r - 4 = 2$, a contradiction to $i_g(D) \leq 1$.

If $r = 2$, then $|V_1| = 2$, $|V_2| = 2$, and $|V_3| = 3$. If $p < 3$, i.e. $p = 2$, then there is one vertex u such that it is adjacent with y for all $y \in V(P)$. Since P is a longest path in H, $v_1 \to u$ and $u \to v_2$. Then H has a path $x_1 u x_2$, a contradiction. Therefore, $p = 3$ or $p = 4$. If there exists V_i such that $V_i \cap V(P) = \emptyset$ for some $i \in \{1, 2, 3\}$, then there is a vertex $z \in V_i$ such that it is adjacent with y for all $y \in V(P)$. Since P is a longest path in H, $v_1 \to z$ and $z \to v_p$. Then there is an integer $j \in \{1, 2, \ldots, p\}$ such that $v_{j-1} \to z \to v_j$. Therefore, H has a $(p+1)$-path, a contradiction. We consider two cases.

(1) Let $p = 3$. Then $P = v_1 v_2 v_3$.

If $v_2 \in V_3$, then there is one vertex $x \in V_3$ such that $v_1 \to x \to v_3$. Let, without loss of generality, $v_1 \in V_1$ and $v_3 \in V_2$. Since $i_g(D) \leq 1$, $\{y_1, u_1\} \to v_1$, $v_3 \to \{x_1, u_1\}$. If $y_1 \to v_2$, then $v_2 \to x_1$ and we obtain the componentwise complementary cycles $x_1 y_1 v_2 x_1$ and $u_1 v_1 x v_3 u_1$. If $v_2 \to y_1$, then $x_1 \to v_2$. Furthermore, if $x_1 \to x$, then we have the componentwise complementary cycles $x_1 x v_3 u_1 x_1$ and $y_1 v_1 v_2 y_1$; if $x \to x_1$, then $y_1 \to x$ and we obtain the componentwise complementary cycles $x_1 y_1 x x_1$ and $u_1 v_1 v_2 v_3 u_1$.

Let $v_3 \in V_3$. If $v_1 \in V_3$, then we consider D^{-1}. Let, without loss of generality, $v_1 \in V_1$ and $v_2 \in V_2$. Since P is a longest path in H, $|V_1| = 2$, $|V_2| = 2$, and $|V_3| = 3$, there is one vertex $x \in V_3$ such that $\{v_1, v_2\} \to x$. Since $i_g(D) \leq 1$, $\{v_3, x\} \to \{x_1, y_1\}$, $\{y_1, u_1\} \to v_1$, and $x_1 \to v_2$. If $v_2 \to u_1$, then we have the componentwise complementary cycles $x_1 v_2 u_1 x_1$ and $y_1 v_1 v_3 y_1$. If $u_1 \to v_2$, then we have the componentwise complementary cycles $x_1 v_2 x x_1$ and $y_1 u_1 v_1 v_3 y_1$.

(2) Let $p = 4$. Then $P = v_1 v_2 v_3 v_4$.

Note that $|V_1| = 2$, $|V_2| = 2$, and $|V_3| = 3$.

First we assume that $V(v_1) = V(v_4)$, i.e. $V(v_1) = V(v_4) = V_3$. Let, without loss of generality, $v_2 \in V_1$ and $v_3 \in V_2$. Since $i_g(D) \leq 1$, $\{x_1, y_1\} \to v_1$ and $v_4 \to \{x_1, y_1\}$.

If $v_3 \to x_1$ and $u_1 \to v_2$, then we obtain the componentwise complementary cycles $x_1 v_1 v_3 x_1$ and $y_1 u_1 v_2 v_4 y_1$.

If $v_3 \to x_1$ and $v_2 \to u_1$, then we have $y_1 \to v_2$ and $u_1 \to v_3$. This leads to the componentwise complementary cycles $y_1 v_2 v_4 y_1$ and $x_1 v_1 v_3 x_1$.

If $x_1 \to v_3$, then we have $v_3 \to u_1$ and $u_1 \to v_2$. Furthermore, if $v_2 \to y_1$, then we obtain the componentwise complementary cycles $y_1 u_1 v_2 y_1$ and $x_1 v_1 v_3 v_4 x_1$;

if $y_1 \rightarrow v_2$, then we obtain the componentwise complementary cycles $y_1 v_2 v_4 y_1$ and $x_1 v_1 v_3 u_1 x_1$.

Now we assume that $V(v_1) \neq V(v_4)$. Let, without loss of generality, $\{v_2, v_4\} \subset V_3$. If $\{v_1, v_3\} \subset V_3$, then we consider D^{-1}. Let, without loss of generality, $v_1 \in V_1$ and $v_3 \in V_2$. Since $i_g(D) \leq 1$, $\{y_1, u_1\} \rightarrow v_1$ and $v_4 \rightarrow \{x_1, y_1\}$.

If $y_1 \rightarrow v_2$, then we have $v_2 \rightarrow x_1$, $x_1 \rightarrow v_3$, and $v_3 \rightarrow u_1$. This leads to $x_1 v_3 u_1 x_1$ and the componentwise complementary cycle $y_1 v_1 v_4 y_1$.

If $v_2 \rightarrow y_1$, then $x_1 \rightarrow v_2$. Furthermore, if $v_3 \rightarrow u_1$, then we obtain the componentwise complementary cycles $u_1 x_1 v_2 v_3 u_1$ and $y_1 v_1 v_4 y_1$; if $u_1 \rightarrow v_3$, then $v_3 \rightarrow x_1$ and the componentwise complementary cycles $x_1 v_2 v_3 x_1$ and $y_1 u_1 v_1 v_4 y_1$.

The proof is complete.

Acknowledgements

References

1. J.A.Bondy, Diconnected orientation and a conjecture of Las Vergnas, *J. London Math. Soc.,* **14**(1976), 277-282.
2. A.Yeo. Diregular c-partite tournaments are vertex-pancyclic when $c \geq 5$. *J. Graph Theory,* **32** (1999), 137-152.
3. A.Yeo, Semicomplete multipartite digraphs, Ph.D. thesis, *Odense University,* 1998.
4. Y. Guo, L. Volkmann. Cycles in multipartite tournaments. *J. Combin. Theory Ser.B*, **62** (1994), 363-366.
5. K. B. Reid, Two complementary circuits in two-connected tournaments, *Ann. Discrete Math.,* **27**(1985): 321-334.
6. Z. M. Song, Complementary cycles of all lengths in tournaments, *J. Combin. Theory Ser.B,* **57**(1993): 18-25.
7. Y. Guo and L. Volkmann, On complementary cycles in locally semicomplete digraphs, *Discret Math.* **135**(1994), 121-127.
8. Y. Guo and L. Volkmann, Locally semicomplete digraphs thar are complementary m-pancyclic, *J. Graph Theory* **21** (1996), 121-136.
9. Z. Song, Complementary cycles in bipartite tournaments, *J. Nanjing Inst. Tech.* **18**(1988): 32-38.
10. K. Zhang, Y. Manoussakis, and Z. Song, Complementary cycles containing a fixed arc in diregular bipartite tournaments, *Discrete Math.* **133** (1994), 325-328.
11. K. Zhang and Z. Song, Complementary cycles containing a pair of fixed vertices in bipartite tournaments, *Appl. J. Chin. Univ.* **3** (1988), 401-407.
12. K. Zhang and J. Wang, Complementary cycles containing a fixed arc and a fixed vertex in bipartite tournaments, *Ars Combin.* **35** (1993), 265-269.
13. L. Volkmann, Complementary cycles in regualr multipartite tournaments, where one cycle has length four, *Kyungpook Math.,J.,* **44**(2004), 219-247.
14. L. Volkmann, All regualr multipartite tournaments that are cycle complementary, *Discrete Math.,* **281**(2004), 255-266.

Sharp Bounds for the Oriented Diameters of Interval Graphs and 2-Connected Proper Interval Graphs

Jing Huang[1] and Dong Ye[2]

[1] Department of Mathematics and Statistics, University of Victoria,
P.O. Box 3045, Victoria, B.C., Canada, V8W 3P4
`jing@math.uvic.ca`
[2] School of mathematics and Statistics, Lanzhou University,
Lanzhou, Gansu, 730000, People's Republic of China
`dye@lzu.edu.cn`

Abstract. The diameter $diam(H)$ of a (directed) graph H is the maximum value computed over the lengths of all shortest (directed) paths in H. Given a bridgeless connected graph G, the oriented diameter $OD(G)$ is given by $OD(G) = \min\{diam(H) : H$ is an orientation of $G\}$. In this paper, we show that $OD(G) \leq \lceil \frac{3}{2} diam(G) \rceil + 1$ for every connected bridgeless interval graph G. Further, for every 2-connected proper interval graph G, we show $OD(G) \leq \lceil \frac{5}{4} diam(G) \rceil + 1$ if $diam(G) \leq 3$ and $OD(G) \leq \lceil \frac{5}{4} diam(G) \rceil$, otherwise. All the bounds are sharp and improve earlier estimations obtained by Fomin et al.

Keywords: Diameter, orientation, oriented diameter, interval graph, proper interval graph.

1 Introduction

Given a (directed) graph H, the *distance* from a vertex x to a vertex y in H, denoted by $d_H(x, y)$, is the length of a shortest (directed) path from x to y in H. The maximum value of distances, denoted by $diam(H)$, is called the *diameter* of H. When H is a graph, $diam(H)$ is finite if and only if H is connected; when H is a directed graph, $diam(H)$ is finite if and only if H is strongly connected.

Let G be a graph. An *orientation* of G is a directed graph obtained from G by assigning a direction to each edge of G. The *oriented diameter* of G, $OD(G)$, is given by

$$OD(G) = \min\{diam(H) : H \text{ is an orientation of } G\}.$$

Clearly if G is not connected or has a bridge (i.e., a cut-edge) then $OD(G)$ is not finite. A celebrated theorem of Robbins [11] asserts $OD(G)$ is finite if G is both connected and bridgeless. Any orientation H of G with $diam(H) = OD(G)$ is called a *minimum diameter orientation* of G. The problem of evaluating the

value $OD(G)$ for an arbitrary graph G is very difficult. In fact it is NP-complete to determine whether a graph G satisfies $OD(G) \leq 2$, [2].

Chvátal and Thomassen [2] initiated the investigation of the relation of the two parameters $OD(G)$ and $diam(G)$. They proved that $OD(G) \leq 2(diam(G))^2 + 2diam(G)$ for every connected bridgeless graph G. Minimum diameter orientations of various families of graphs have already been studied by Gutin [6], Koh and Tan [7], Soltés [12], Plesnik [10], Boesch and Tindell [1], and others. We direct the reader to the survey of Koh and Tay [8] for a comprehensive discussion on the minimum diameter orientations of graphs.

A graph G is an *interval graph* if there is a family of intervals I_v, $v \in V(G)$, in a real line such that two vertices u, v are adjacent in G if and only if I_u, I_v overlap. If such a family of intervals can be chosen so that no interval is completely contained in another, then the graph G is called a *proper interval graph*. Recently, Fomin et al. [3] proved that, for every connected bridgeless interval graph G, $OD(G) \leq \frac{3}{2}diam(G) + \frac{25}{2}$ and, for every 2-connected proper interval graph G, $OD(G) \leq \frac{5}{4}diam(G) + \frac{29}{2}$.

The purpose of this paper is to sharpen these two upper bounds. More precisely, we show that $OD(G) \leq \lceil \frac{3}{2}diam(G) \rceil + 1$ for every connected bridgeless interval graph G. There are (proper) interval graphs of arbitrarily larger diameter achieving this bound. Further, we show that, for every 2-connected proper interval graph G, $OD(G) \leq \lceil \frac{5}{4}diam(G) \rceil + 1$ if $diam(G) \leq 3$ and $OD(G) \leq \lceil \frac{5}{4}diam(G) \rceil$, otherwise. Again the bounds can be attained by appropriate 2-connected proper interval graphs.

2   Connected Bridgeless Interval Graphs

Interval graphs can be characterized in many ways, cf. [5]. According to Gilmore and Hoffman [4], a graph G is an interval graph if and only if the maximal cliques of G can be linearly ordered so that, for every vertex v of G, the maximal cliques containing vertex v occur consecutively in the ordering.

Let G be a connected bridgeless interval graph and let $\mathcal{C} : C_1, C_2, \ldots, C_r$ be an ordering of the maximal cliques of G that satisfies the above-mentioned property. Since G is bridgeless, every C_i has at least 3 vertices. When $r = 1$, G is a complete graph, i.e., $G = K_n$ where n is the number of vertices of G. Plesnik [10] has proved that $OD(K_4) = 3$, and $OD(K_n) = 2$ for all $n \geq 3$ and $n \neq 4$ (cf. also [1,9]). A minimum diameter orientation of K_4 is depicted in Figure 1.
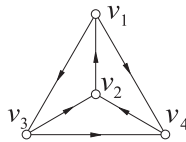
Fig. 1. K_4 and its minimum diameter orientation

Suppose that G is not a complete graph, i.e., $r \geq 2$. Let $\mathcal{C}' : C_{i_1}, C_{i_2}, \ldots, C_{i_d}$ with $1 = i_1 < i_2 < \cdots < i_d = r$ be chosen such that $C_{i_j} \cap C_{i_{j+1}} \neq \emptyset$ and $C_{i_j} \cap C_{i_{j+1}+1} = \emptyset$ for $1 \leq j \leq d-1$. Clearly, $d = diam(G)$. Denote $S_j = C_{i_j} \cap C_{i_{j+1}}$, $1 \leq j \leq d-1$. Then S_j is contained in C_m for $i_j \leq m \leq i_{j+1}$. Since $C_{i_j} \cap C_{i_{j+1}+1} = \emptyset$, $S_j \cap S_{j+1} = \emptyset$ for $1 \leq j \leq d-1$.

When $|S_j| = 1$, denote by z_j the only vertex in S_j; otherwise when $|S_j| \geq 2$, choose arbitrarily two vertices z_j, z'_j in S_j. Call C_{i_j} *bad* if $|S_{j-1}| = |S_j| = 1$ ($2 \leq j \leq d-1$), and *good* otherwise. Denote by ℓ the number of bad maximal cliques (in $\mathcal{C}'$). Then $\ell \leq d-2 = diam(G) - 2$.

We orient G using the following steps:

(1) If $|S_1| = 1$, arbitrarily choose a vertex $w \in C_1 - \{z_1\}$ let $w \to x \to z_1 \to w$ for all $x \in C_1 - \{w, z_1\}$; if $|S_1| \geq 2$, let $z_1 \to z'_1 \to x \to z_1$ for all $x \in C_1 - \{z_1, z'_1\}$. Note that this gives a partial orientation of C_1. Similarly, if $|S_{d-1}| = 1$, arbitrarily choose a vertex $w \in C_r - \{z_{d-1}\}$ let $w \to x \to z_{d-1} \to w$ for all $x \in C_r - \{w, z_{d-1}\}$; if $|S_{d-1}| \geq 2$, let $z_{d-1} \to z'_{d-1} \to x \to z_{d-1}$ for all $x \in C_r - \{z_{d-1}, z'_{d-1}\}$. Again this gives a partial orientation of C_r.

(2) For the first $\lfloor \frac{\ell}{2} \rfloor$ bad cliques C_{i_j}, orient $v \to z_{j-1} \to z_j \to v$ for $v \in C_{i_j} - \{z_{j-1}, z_j\}$ and for the remaining $\lceil \frac{\ell}{2} \rceil$ bad maximal cliques C_{i_j}, orient $v \to z_j \to z_{j-1} \to v$ for $v \in C_{i_j} - \{z_{j-1}, z_j\}$;

(3) For each good clique C_{i_j} with $|S_{j-1}| = 1$ and $|S_j| \geq 2$, orient $v \to z_j \to z'_j \to v$ for any $v \in C_{i_j} - \{z_j, z'_j\}$. For each good clique with $|S_j| = 1$ and $|S_{j-1}| \geq 2$, orient $v \to z_{j-1} \to z'_{j-1} \to v$ for $v \in C_{i_j} - \{z_{j-1}, z'_{j-1}\}$;

(4) For each good clique C_{i_j} with $|S_{j-1}| \geq 2$ and $|S_j| \geq 2$, we let $z_{j-1} \to z'_{j-1}$, $z_{j-1} \to z_j \to z'_j \to z'_{j-1}$, and $\{z'_{j-1}, z'_j\} \to v \to \{z_{j-1}, z_j\}$ for all $v \in C_{i_j} - \{z_j, z'_j, z_{j-1}, z'_{j-1}\}$;

(5) For each $C_m \in \mathcal{C} - \mathcal{C}'$, we must have $i_j < m < i_{j+1}$ for some j. (Note that the ordering of maximal cliques ensures that C_m contains S_j and in particular z_j and z'_j.) When $|S_j| \geq 2$, for each $v \in C_m - (C_{i_1} \cup C_{i_2} \cup \ldots \cup C_{i_d})$, let $v \to z_j \to z'_j \to v$. When $|S_j| = 1$, we select a vertex $w \in C_m - \{z'_j\}$ in such a way that the preference is given to a vertex in $C_{i_j} \cup C_{i_{j+1}}$. Note that the edge wz_j may or may not be oriented by the previous steps. If it has not been oriented, then we orient it arbitrarily. Now for each vertex $v \in C_m - (C_{i_1} \cup C_{i_2} \cup \ldots \cup C_{i_d})$, we assign directions to edges vw, vz_j in such a way that v, w, z_j form a directed triangle;

(6) Finally, for each edge which has not been oriented by the above steps, we assign arbitrarily a direction to it.

Lemma 1. *Let G be a connected bridgeless interval graph which is not complete and let H be an orientation of G obtained using the above steps. Then*

$$diam(H) \leq \lceil \tfrac{3}{2} diam(G) \rceil + 1.$$

Proof. Let v be a vertex of G. Then $v \in C_i$ for some $1 \leq i \leq r$. Assume $i_j \leq i \leq i_{j+1}$, i.e., $v \in C_{i_j} \cup C_{i_j+1} \cup \cdots \cup C_{i_{j+1}}$. When $|S_j| = 1$, it follows from
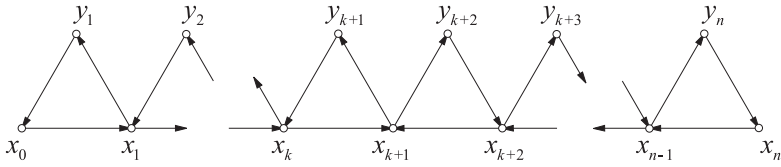
Fig. 2. A minimum diameter orientation of an interval graph G of diameter n showing $OD(G) = \lceil \frac{3}{2}n \rceil + 1$, where $k = \lfloor \frac{n}{2} \rfloor$

steps 1, 2, 3, and 5 that $d_H(v, z_j) \leq 2$ and $d_H(z_j, v) \leq 2$; when $|S_{j+1}| \geq 2$, by steps 1, 3, 4, and 5, $d_H(v, z_j) \leq 1$, $d_H(z_j', v) \leq 1$, and $d_H(z_j, z_j') = 1$.

Let u, v be any two vertices of G. Then $u \in C_a$ and $v \in C_b$ for some $1 \leq a, b \leq r$. If $i_j \leq a, b \leq i_{j+1}$ for some $j = 1, 2, \ldots, d - 1$, then

$$d_H(u, v) \leq \begin{cases} d_H(u, z_j) + d_H(z_j, v) \leq 4 & \text{if } |S_j| = 1; \\ d_H(u, z_j) + d_H(z_j, z_j') + d_H(z_j', v) \leq 3 & \text{if } |S_j| \geq 2. \end{cases}$$

Suppose that $i_j \leq a < i_{j+1} \leq i_k \leq b < i_{k+1}$ where $1 \leq j < k \leq d - 1$. By step 2, $d_H(z_j, z_k) \leq diam(G) - 2 + \lceil \frac{\ell}{2} \rceil$ and $d_H(z_k, z_j) \leq diam(G) - 2 + \lfloor \frac{\ell}{2} \rfloor$. Hence

$$d_H(u, v) \leq d_H(u, z_j) + d_H(z_j, z_k) + d_H(z_k, v) \leq 2 + diam(G) - 2 + \lceil \frac{\ell}{2} \rceil + 2$$

$$\leq 2 + diam(G) + \lceil \frac{diam(G) - 2}{2} \rceil = \lceil \frac{3}{2}diam(G) \rceil + 1,$$

and

$$d_H(v, u) \leq d_H(v, z_k) + d_H(z_k, z_j) + d_H(z_j, u) \leq 2 + diam(G) - 2 + \lfloor \frac{\ell}{2} \rfloor + 2$$

$$\leq 2 + diam(G) + \lfloor \frac{diam(G) - 2}{2} \rfloor \leq \lceil \frac{3}{2}diam(G) \rceil + 1.$$

Therefore $diam(H) \leq \lceil \frac{3}{2}diam(G) \rceil + 1$. □

Theorem 1. *Let G be a connected bridgeless interval graph. Then*

$$OD(G) \leq \lceil \frac{3}{2}diam(G) \rceil + 1.$$

Proof. The statement follows from Lemma 1 and the fact that $OD(K_n) \leq 3$. □

The sharpness of the upper bound given in Theorem 1 is shown by Figure 2, where an orientation of diameter $\lceil \frac{3}{2}n \rceil + 1$ is given for an interval graph of diameter n.

3   2-Connected Proper Interval Graphs

In this section, we focus on the minimum diameter orientations of 2-connected proper interval graphs G. We shall adopt the same notations as in Section 2.

In particular, $C_1, C_2, \ldots, C_r$ is an ordering of the maximal cliques of G in the sense of Gilmore and Hoffman. Since G is a proper interval graph, the ordering is essentially unique. We also let $C_{i_1}, C_{i_2}, \ldots, C_{i_d}$ be the cliques as defined in Section 2. We begin with the lemma (which does not assume G is 2-connected).

Lemma 2. *Let G be a connected proper interval graph. Then for $1 \leq j \leq d-1$ and $i_j < m < i_{j+1}$, $C_m \subseteq C_{i_j} \cup C_{i_{j+1}}$.*

Proof. Suppose that C_m contains a vertex w that is not in $C_{i_j} \cup C_{i_{j+1}}$. Since w is not in $C_{i_j} \cup C_{i_{j+1}}$, w is not adjacent to a vertex $x \in C_{i_j}$ and not adjacent to a vertex $y \in C_{i_{j+1}}$. Let z be any vertex in $C_{i_j} \cap C_{i_{j+1}}$. Since $C_{i_j} \cap C_{i_{j+1}} \subseteq C_m$, z is in C_m and hence adjacent to w. So z is adjacent to w, x, and y. Since G is a proper interval graph, it does not contain an induced $K_{1,3}$. This implies that x and y are adjacent (as otherwise the vertices w, x, y, z induce a $K_{1,3}$). In particular, x, y, z are pairwise adjacent.

Consider a maximal clique $C_{m'}$ containing x, y, z. Note $C_{m'}$ is distinct from C_{i_j}, C_m and $C_{i_{j+1}}$. If $m' > m$, then x is must be in C_m and hence adjacent to w, a contradiction. On the other hand, if $m' < m$, then y is in C_m and adjacent to w, also a contradiction. $\square$

From now on, we assume G is a 2-connected proper interval graph. Lemma 2 implies that $V(G) = C_{i_1} \cup C_{i_2} \cup \cdots \cup C_{i_d}$. As in Section 2, if $|S_j| = |C_{i_j} \cap C_{i_{j+1}}| \geq 2$, let z_j, z_j' be any two fixed vertices in S_j, and if $|S_j| = 1$, let z_j be the only vertex in S_j. Since G is 2-connected, in the case when $|S_j| = 1$, there exist $x_j \in C_{i_j} - \{z_j\}$ and $x_{j+1}' \in C_{i_{j+1}} - \{z_j\}$ such that x_j and x_{j+1}' are adjacent.

We next show how to orient G and to do so we consider several cases. In each case, we only give a partial orientation of G and the orientations of the remaining edges may be given arbitrarily.

Case 1. $diam(G) = 2$.
  – (1) If $|S_1| = 1$, let $x_2' \to x_1$, $v \to z_1 \to w$ for all $v \in C_{i_1} - z_1$ and $w \in C_{i_2} - z_1$, $x_1 \to v$ for all $v \in C_{i_1} - \{x_1, z_1\}$, and $w \to x_2'$ for all $w \in C_{i_2} - \{x_2', z_1\}$.
  – (2) If $|S_1| \geq 2$, let $v \to z_1 \to z_1' \to v$ for all $v \in V(G) \setminus \{z_1, z_1'\}$.
Case 2. $diam(G) = 3$.
  – (1) Suppose $|S_1| = |S_2| = 1$. Note that it is possible to select x_2', x_2 from $C_{i_2} - \{z_1, z_2\}$. Let $x_1 \to z_1 \to x_2' \to x_1$, $z_1 \to z_2$, and $x_2 \to x_3' \to z_2 \to x_2$. For all $u \in C_{i_1} - \{x_1, z_1\}$ let $x_1 \to u \to z_1$, for all $v \in C_{i_2} - \{z_1, z_2, x_2', x_2\}$ let $z_2 \to v \to z_1$, and for all $w \in C_{i_3} - \{z_2, x_3'\}$ let $x_3' \to w \to z_2$.
  – (2) Suppose that exactly one of $|S_1|$ and $|S_2|$ equals 1. Assume $|S_1| = 1$ (the case when $|S_2| = 1$ can be handled in a similar way). Let $v \to z_1 \to x_1 \to v$ for $v \in C_{i_1} - \{z_1, x_1\}$, $u \to z_2 \to z_2' \to u$ for $u \in C_{i_2} \cup C_{i_3} - \{z_2, z_2'\}$.
  – (3) Suppose $|S_1| \geq 2$ and $|S_2| \geq 2$. Let $z_1 \to z_2$ and $z_2' \to z_1'$. Let $v \to z_1 \to z_1' \to v$ for $v \in C_{i_1} - \{z_1, z_1'\}$, and $u \to z_2 \to z_2' \to u$ for $u \in C_{i_2} \cup C_{i_3} - S_1 - \{z_2, z_2'\}$.

Case 3. $diam(G) \geq 4$.

Let C_{i_k} be a bad clique with $3 \leq k \leq d - 3$. Call C_{i_k} *2-bad* if $C_{i_{k+1}}$ is also bad. Choose a set $\mathcal{L}$ of 2-bad cliques $C_{i_{j_1}}, C_{i_{j_2}}, \ldots, C_{i_{j_\eta}}$ so that the following properties are satisfied:

(P1) the set contains as many 2-bad cliques as possible;

(P2) $i_{j_k+1} \neq i_{j_k+1}$;

(P3) $i_{j_1} + i_{j_2} + \cdots + i_{j_\eta}$ is minimum.

Note that $\mathcal{L}$ does not contain all 2-bad cliques. For instance, if $C_{i_{k-1}}$ is in $\mathcal{L}$, then C_{i_k} cannot be in $\mathcal{L}$ even though it may be 2-bad. Denote by $\mathcal{M}$ be the set of all bad but not 2-bad cliques C_{i_k} with $3 \leq k \leq d - 2$ such that $C_{i_{k-1}}$ is not in $\mathcal{L}$ and $|\mathcal{M}| = \ell$. Then the number of good cliques in $\mathcal{C}' - \{C_{i_1}, C_{i_2}, C_{i_{d-1}}, C_{i_d}\}$ is $d - 4 - 2\eta - \ell$. When $C_{i_k} \in \mathcal{M}$, we have $C_{i_{k+1}}$ is either good or $C_{i_{d-1}}$ and hence $\ell \leq (d - 4 - 2\eta - \ell) + 1$.

– (1) If $|S_1| = 1$, let $x_2' \to x_1 \to z_1$, $x_1 \to v \to z_1$ for all $v \in C_{i_1} - \{z_1, x_1\}$, and $u \to x_2' \to z_1 \to u$ for all $u \in C_{i_2} - \{z_2, x_2'\}$; If $|S_1| \geq 2$, let $z_1' \to v \to z_1$ for all $v \in C_{i_1} - \{z_1', z_1\}$, and $u \to z_1' \to z_1 \to u$ for all $u \in C_{i_2} - S_1$.

– (2) If $|S_{d-1}| = 1$, let $x_{d-1} \to x_d' \to z_{d-1}$, $v \to x_{d-1} \to z_{d-1} \to v$ for all $v \in C_{i_{d-1}} - \{z_{d-1}, x_{d-1}'\}$, and $x_d' \to u \to z_{d-1}$ for all $u \in C_{i_d} - \{z_{d-1}, x_d'\}$; If $|S_{d-1}| \geq 2$, let $v \to z_{d-1}' \to z_{d-1} \to v$ for all $v \in C_{i_{d-1}} - \{z_{d-1}, z_{d-1}'\}$ and $z_{d-1}' \to u \to z_{d-1}$ for all $u \in C_{i_d} - S_{d-1}$.

– (3) Suppose $C_{i_j} \in \mathcal{L}$. We only show how to give orientations of the edges in C_{i_j} and $C_{i_{j+1}}$ for $i_{j_1} \leq i_j \leq i_{j_{\lceil \frac{\eta}{2} \rceil}}$. (When $i_{j_{\lceil \frac{\eta}{2} \rceil}} < i_j \leq i_{j_\eta}$, the edges are oriented reversely.) Let $x_{i_{j+1}}' \to x_{i_j}$, $v \to z_{j-1} \to z_j \to v$ for all $v \in C_{i_j} - \{z_j, z_{j-1}\}$, and $u \to z_j \to z_{j+1} \to u$ for all $u \in C_{i_{j+1}} - \{z_j, z_{j+1}\}$.

– (4) For the first (with respect to the order of $\mathcal{C}$) $\lfloor \frac{\ell}{2} \rfloor$ cliques C_{i_k} in $\mathcal{M}$, let $v \to z_{k-1} \to z_k \to v$ for all $v \in C_{i_k} - \{z_{k-1}, z_k\}$; for the other cliques in $\mathcal{M}$, we orient the edges reversely.

– (5) Suppose that C_{i_j} with $3 \leq j \leq d - 2$ is a good clique. If $|S_{j-1}| = 1$ and $|S_j| \geq 2$, let $v \to z_j \to z_j' \to v$ for any $v \in C_{i_j} - \{z_j, z_j'\}$; if $|S_j| = 1$ and $|S_{j-1}| \geq 2$, let $v \to z_{j-1} \to z_{j-1}' \to v$ for $v \in C_{i_j} - \{z_{j-1}, z_{j-1}'\}$; if $|S_{j-1}| \geq 2$ and $|S_j| \geq 2$, let $z_{j-1} \to z_{j-1}'$, $z_{j-1} \to z_j \to z_j' \to z_{j-1}'$, and $\{z_{j-1}', z_j'\} \to v \to \{z_{j-1}, z_j\}$ for all $v \in C_{i_j} - \{z_j, z_j', z_{j-1}, z_{j-1}'\}$.

Theorem 2. *Let G be a 2-connected proper interval graph. Then*

$$OD(G) \leq \begin{cases} \lceil \frac{5}{4} diam(G) \rceil + 1 \text{ if } diam(G) \leq 3; \\ \lceil \frac{5}{4} diam(G) \rceil \quad \text{ if } diam(G) \geq 4. \end{cases}$$

Proof. When G is complete, $OD(G) \leq 3 \leq \lceil \frac{5}{4} diam(G) \rceil + 1$ by Theorem 1. When G is not complete and satisfies $diam(G) \leq 3$, it can be verified easily from the orientations given in Case 1 and Case 2 that $OD(G) \leq \lceil \frac{5}{4} diam(G) \rceil + 1$. So suppose that $diam(G) \geq 4$.

Let u, v be any two vertices of G. Without loss of generality assume $u \in C_{i_j}$ and $v \in C_{i_k}$ for some $j \leq k$. When $k - 1 \leq j \leq k$, according to steps 1 and 2 in Case 3, $d_H(u, v) \leq 5$ if $j = k = 1$ or $j = k = d$ and, according steps 3, 4, and 5 in Case 3, $d_H(u, v) \leq 3$ if $j = k \neq 1, d$. When $j = k - 1$, $d_H(u, v) \leq 4$ according to steps 1-5 in Case 3.

Suppose now $j < k - 1$. Let $u' \in C_{i_1} - \{z_1, x_1\}$ if $|S_1| = 1$ and $u' \in C_{i_1} - S_1$ if $|S_1| \geq 2$, and let $v' \in C_{i_d} - \{z_{d-1}, x'_d\}$ if $|S_{d-1}| = 1$ and $v' \in C_{i_d} - S_{d-1}$ if $|S_{d-1}| \geq 2$.

Claim: $d_H(u, v) \leq d_H(u', v')$ and $d_H(v, u) \leq d_H(v', u')$.

Proof of Claim: We only prove $d_H(u, v) \leq d_H(u', v')$ as the proof of the other inequality is similar. Denote $P''_t = C_{i_t} \cup C_{i_{t+1}}$ with $C_{i_t} \in \mathcal{L}$. If u does not lie in P''_t for any t, then $d_H(u, z_j) \leq 2 \leq d_H(u', z_j)$; If u lies in P''_t for some t, then $3 \leq t \leq d - 3$ and either $t = j$ or $t = j - 1$, so $d_H(u, z_{t+1}) \leq 3 \leq d_H(u', z_{t+1})$.

If v does not lie in P''_t for any t, then $d_H(z_{k-1}, v) \leq 2 \leq d_H(z_{k-1}, v')$; If v lies in P''_p for some p, then $3 \leq p \leq d - 3$ and either $p = k$ or $p = k - 1$, so $d_H(z_{p-1}, v) \leq 3 \leq d_H(z_{p-1}, v')$. So

$$d_H(u, v) \leq d_H(u, z_r) + d_H(z_r, z_m) + d_H(z_m, v)$$
$$\leq d_H(u', z_r) + d_H(z_r, z_m) + d_H(z_m, v') = d_H(u', v')$$

where $r = t + 1$ if u lies in P''_t for some t, and $r = j$ otherwise; $m = p - 1$ if v lies in P''_p for some p, and $m = k - 1$ otherwise. $\square$

To estimate $d_H(u', v')$ and $d_H(v', u')$, first we have

$$d_H(u', v') = d_H(u', z_2) + d_H(z_2, z_{d-2}) + d_H(z_{d-2}, v')$$
$$\leq 2 + 2\lfloor \frac{\eta}{2} \rfloor + 3\lceil \frac{\eta}{2} \rceil + \lceil \frac{\ell}{2} \rceil + 2\lfloor \frac{\ell}{2} \rfloor + (d - 4 - 2\eta - \ell) + 3$$
$$= 1 + \lceil \frac{\eta}{2} \rceil + \lfloor \frac{\ell}{2} \rfloor + d.$$

Since $\ell \leq (d - 4 - 2\eta - \ell) + 1$, we have

$$d_H(u', v') \leq 1 + \lceil \frac{\eta}{2} \rceil + \lfloor \frac{d - 3 - 2\eta}{4} \rfloor + d \leq 1 + \lceil \frac{\eta}{2} \rceil + \lceil \frac{d}{4} \rceil - \lceil \frac{3}{4} + \frac{\eta}{2} \rceil + d = \lceil \frac{5}{4} diam(G) \rceil.$$

Similarly, $d_H(v', u') \leq 1 + \lfloor \frac{\eta}{2} \rfloor + \lceil \frac{\ell}{2} \rceil + d$ and hence

$$d_H(v', u') \leq 1 + \lceil \frac{\ell}{2} \rceil + \lfloor \frac{d - 3 - 2\ell}{4} \rfloor + d \leq 1 + \lceil \frac{\ell}{2} \rceil + \lceil \frac{d}{4} \rceil - \lceil \frac{3}{4} + \frac{\ell}{2} \rceil + d = \lceil \frac{5}{4} diam(G) \rceil.$$

$\square$

When $diam(G) = 1$, the upper bound of $OD(G)$ in Theorem 2 is achieved by a minimum diameter orientation of K_4 (see Figure 1). The following proposition from [3] shows that the upper bound in Theorem 2 is sharp for $diam(G) \geq 4$.

Proposition 1. [3] For $d \geq 3$, there is a 2-connected proper interval graph G with $diam(G) \geq d$ and $OD(G) \geq \frac{5}{4} diam(G)$. $\square$

The sharpness of upper bounds of $OD(G)$ for the cases when $2 \leq diam(G) \leq 3$ is given by Propositions 2 and 3 below. Indeed, it can be verified that the digraphs in Figures 3 and 4 are the minimum diameter orientations of their underlying graphs. Therefore we have
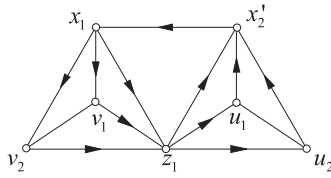
Fig. 3. A minimum diameter orientation of a 2-connected proper interval graph of diameter two, where unoriented edges may be oriented arbitrarily
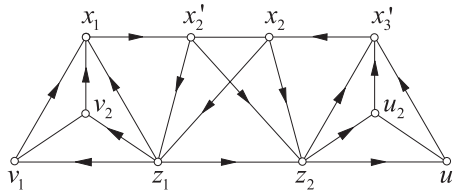
Fig. 4. A minimum diameter orientation of 2-connected proper interval graph of diameter three, where unoriented edges may be oriented arbitrarily

Proposition 2. *Let G_1 be the underlying graph of the digraph in Figure 3. Then $OD(G_1) \geq 4$.*   □

Proposition 3. *Let G_2 be the underlying graph of the digraph in Figure 4. Then $OD(G_2) \geq 5$.*   □

References

1. F. Boesch and R. Tindell, Robbins' theorem for mixed multigraphs, Amer. Math. Monthy 87 (1980) 716-719.
2. V. Chvátal and C. Thomassen, Distances in orientations of graphs, J. Combin. Theory Ser. B 24 (1978) 61-75.
3. F.V. Fomin, M. Matamala, E. Prisner and I. Rapaport, AT-free graphs: linear bounds for the oriented diameter, Discrete Appl. Math. 141 (2004) 135-148.
4. P.C. Gilmore and A.J. Hoffman, A characterization of comparability graphs and of interval graphs, Canadian J. Math. 16(3) (1964) 539-548.
5. M.C. Golumbic, **Algorithmic Graph Theory and Perfect Graphs**, Academic Press, New York, 1980.
6. G. Gutin, Minimizing and maximizing the diameter in orientations of graphs, Graphs Combin. 10 (1994) 225-230.
7. K.M. Hoh and B.P. Tan, The minimum diameter of orientations of complete multipartite graphs, Graphs Combin. 12 (1996) 333-339.
8. K.M. Koh and E.G. Tay, Optimal orientations of graphs and digraphs: a survey, Graphs Combin. 18 (2002) 745-756.
9. S.B. Maurer, The king chicken theorems, Math. Mag. 53 (1980) 67 - 80.

10. J. Plesnik, Diametrically critical tournaments, Pest. Matem. 100 (1975) 361 - 370.
11. H. E. Robbins, Theorem on graphs with an application to a problem of traffic control, Amer. Math. Monthy 46(5) (1929) 281-283.
12. L. Sotles, Orientations of graphs minimizing the radius or the diameter, Math. Slovaca 38(3) (1986) 289-296.

A Class of Graphs of f-Class 1*

Xia Zhang** and Guizhen Liu

School of Mathematics and System Science, Shandong University, 250100, P.R. China
xzhang@math.sdu.edu.cn

Abstract. An f-coloring of a graph G is an edge-coloring of G such that each color appears at each vertex $v \in V(G)$ at most $f(v)$ times. The minimum number of colors needed to f-color G is called the f-chromatic index of G, and denoted by $\chi'_f(G)$. Any simple graph G has f-chromatic index equal to $\Delta_f(G)$ or $\Delta_f(G)+1$, where $\Delta_f(G) = \max_{v \in V(G)}\{\lceil \frac{d(v)}{f(v)} \rceil\}$. If $\chi'_f(G) = \Delta_f(G)$, then G is of f-class 1; otherwise G is of f-class 2. In this paper, we show that if $f(v)$ is positive and even for all $v \in V_0^*(G) \cup N_G(V_0^*(G))$, then G is of f-class 1, where $V_0^*(G) = \{v \in V(G) : \frac{d(v)}{f(v)} = \Delta_f(G)\}$ and $N_G(V_0^*(G)) = \{v \in V(G) : uv \in E(G), u \in V_0^*(G)\}$. This result improves the simple graph version of a result of Hakimi and Kariv [4].

Keywords: Edge-coloring, simple graph, f-coloring, f-chromatic index.

1 Introduction

Our terminologies and notations will be standard, except where indicated. The reader is referred to [1] for the undefined terms. Throughout this paper, a *graph* G allows multiple edges but no loops and has a finite nonempty vertex set $V(G)$ and a finite edge set $E(G)$. If G has neither loops nor multiple edges, we will call G a *simple graph*.

An *edge-coloring* of G is an assignment of colors to all the edges of G. A *proper edge-coloring* of G is an edge-coloring of G such that no two adjacent edges are assigned the same color. The minimum number of colors for which such a proper edge-coloring of G exists is called the *chromatic index* of G, and denoted by $\chi'(G)$. Hakimi and Kariv [4] generalized the proper edge-coloring and obtained many interesting results. Let G be a graph and f be a function which assigns a positive integer $f(v)$ to each vertex $v \in V(G)$. An *f-coloring* of G is an edge-coloring of G such that each vertex v has at most $f(v)$ edges colored with the same color. The minimum number of colors needed to f-color G is called the *f-chromatic index* of G, and denoted by $\chi'_f(G)$. If $f(v) = 1$ for all $v \in V(G)$, the f-coloring problem, which is to determine $\chi'_f(G)$ of a given graph G, is reduced to the proper edge-coloring problem.

f-colorings have many applications in scheduling problems such as the file transfer problem in a computer network (see [2, 3, 6]). Since the proper edge-coloring problem is NP-complete [5], the f-coloring problem is also NP-complete. Hakimi and Kariv [4] studied the f-coloring problem and obtained some upper bounds on $\chi'_f(G)$. Nakano et al. [8] obtained another upper bound on $\chi'_f(G)$.

In the proper edge-coloring, one of the most celebrated results, which is due to Vizing [9], is that $\chi'(G) = \Delta(G)$ or $\Delta(G) + 1$ for any simple graph G. This result naturally partitions all simple graphs into two classes. We say that simple graph G is of *class* 1 if $\chi'(G) = \Delta(G)$, and of *class* 2 otherwise. Significantly, we have a similar result to simple graphs on f-colorings. We define

$$\Delta_f(G) = \max_{v \in V(G)} \{\lceil \frac{d(v)}{f(v)} \rceil\},$$

where $\lceil \frac{d(v)}{f(v)} \rceil$ is the smallest integer not smaller than $\frac{d(v)}{f(v)}$. It is trivial that $\chi'_f(G) \geq \Delta_f(G)$.

Lemma 1. *[10, 11] Let G be a simple graph. Then*

$$\Delta_f(G) \leq \chi'_f(G) \leq \max_{v \in V(G)} \{\lceil \frac{d(v) + 1}{f(v)} \rceil\} \leq \Delta_f(G) + 1.$$

For the sake of self-completeness, a proof of Lemma 1 can be obtained by Lemma 3 later. Similarly, we can classify simple graphs into two classes according to their f-chromatic indices. We say that simple graph G is of f-*class* 1 if $\chi'_f(G) = \Delta_f(G)$, and of f-*class* 2 otherwise. Zhang and Liu [10, 11], Zhang, Wang and Liu [12] studied the classification of complete graphs, simple regular graphs and some other special classes of simple graphs on f-colorings. Liu, hou and Cai [7] studied the properties of f-critical graphs (i.e. connected simple graphs G of f-class 2 satisfying that $\chi'_f(G - e) < \chi'_f(G)$ for any edge $e \in E(G)$).

In Section 2 we present a useful lemma, by which we can easily deduce two results of Hakimi and Kariv [4]. In Section 3, we give a new sufficient condition for a simple graph to be of f-class 1, which generalizes the simple graph version of a result of Hakimi and Kariv [4]. In Section 4 we conclude that this condition is best in a sense, and briefly discuss some problems for further research.

2   A Useful Lemma

Let G be a graph, $Q \subseteq E(G)$ and $Q \neq \emptyset$. We use $G[Q]$ to denote the subgraph of G induced by Q. A *partial edge-coloring* of G is an edge-coloring of a subgraph $G[Q]$ of G. When $Q = E(G)$, a partial edge-coloring of G is exactly an edge-coloring of G. Let C denote the set of colors available to color the edges of a graph G. An edge colored with color $\alpha \in C$ is called an α-*edge*. We denote by $|\alpha(v)|$ the number of α-edges of G incident with the vertex $v \in V(G)$. Given a partial edge-coloring of G with the colors in C, a vertex v of G is called f-*proper* if $|c(v)| \leq f(v)$ for each $c \in C$. All vertices of G are f-proper if and only if G is

given a partial f-coloring. Note that any subgraph G' of G has $f_{G'}(v) = f_G(v)$ for all $v \in V(G')$.

A *circuit* is a connected graph in which each vertex has even degree. Denote $|E(G)|$ by $\varepsilon(G)$. A circuit G is *even*, or *odd*, if $\varepsilon(G)$ is even, or odd, respectively. A *walk* W is a sequence of distinct edges $v_0 v_1, v_1 v_2, \ldots, v_{k-1} v_k$, where the vertices $v_0, v_1, \ldots, v_k$ are not necessarily distinct. An *Eulerian circuit* of a graph G is a closed walk (i.e. $v_0 = v_k$) that traverses every edge in G. It is well known that every circuit has an Eulerian circuit. Given a partial edge-coloring of graph G, we call a connected subgraph H of G an *obstruction* (to a partial f-coloring), if $\varepsilon(H)$ is odd and $d_H(v) = 2f(v)$ for each $v \in V(H)$. Clearly, any obstruction is an odd circuit. Denote by $G(v; \alpha, \beta)$ the component containing v of the subgraph of G induced by all α-edges and all β-edges.

Lemma 2. *Let G be a graph and $w \in V(G)$. Let $C = \{c_1, c_2, \ldots, c_{\Delta_f(G)}\}$. Suppose that G is given a partial edge-coloring with the colors in C such that all vertices but w are f-proper. Let $\alpha, \beta \in C$ such that $|\alpha(w)| = \max_{c \in C}\{|c(w)|\}$ and $|\beta(w)| = \min_{c \in C}\{|c(w)|\}$. Also, suppose that the vertex w has*

$$\begin{cases} |\alpha(w)| = f(w) + 1, \\ |c(w)| \le f(w) \qquad \text{for each } c \in C \text{ and } c \ne \alpha. \end{cases}$$

If $H = G(w; \alpha, \beta)$ is not an obstruction, then we can recolor H such that all vertices of G are f-proper.

Proof. By the choice of β, we claim that $|\beta(w)| \le f(w) - 1$. Otherwise, the number of the edges colored and incident with w is $(\Delta_f(G) - 1)f(w) + f(w) + 1$. Clearly, $(\Delta_f(G) - 1)f(w) + f(w) + 1 > \Delta_f(G)f(w) \ge d(w)$. A contradiction.

Let m' represent the set m with respect to the new partial edge-coloring of G after recoloring H. We will recolor H with α and β. Obviously, all vertices in $V(G) \setminus V(H)$ remain f-proper, and the edges colored with colors other than α and β remain unchanged.

Next, we consider three cases as follows.

Case 1. H is not a circuit.
Then it has even vertices with odd degree. Pair off the vertices with odd degree, and join the two vertices of each pair by an extra edge. The graph H^* so formed is a circuit, and then it has an Eulerian circuit. Starting with an extra edge and following an Eulerian circuit, we color the edges of H^* with α and β alternately. Restrict H^* to H. Obviously, we have $||(\alpha(v))'| - |(\beta(v))'|| \le 1$ for all $v \in V(H)$. $||(\alpha(v))'| - |(\beta(v))'|| = 1$ if and only if $d_H(v)$ is odd. So $||(\alpha(v))'| - |(\beta(v))'|| \le ||\alpha(v)| - |\beta(v)||$ for all $v \in V(H)$. Then we have $\max\{|(\alpha(v))'|, |(\beta(v))'|\} \le \max\{|\alpha(v)|, |\beta(v)|\}$ for all $v \in V(H)$. So all vertices but w are still f-proper. For vertex w, since $|\alpha(w)| - |\beta(w)| \ge 2$, we have $||(\alpha(w))'| - |(\beta(w))'|| \le 1 < |\alpha(w)| - |\beta(w)|$. Then $\max\{|(\alpha(w))'|, |(\beta(w))'|\} < |(\alpha(w))| = f(w) + 1$. So w is f-proper now.

Case 2. H is an even circuit.
Then it has an Eulerian circuit. Starting at w and following an Eulerian circuit, color the edges of H with α and β alternately. Now we have $|(\alpha(v))'| = |(\beta(v))'|$,

i.e. $|(\alpha(v))'| - |(\beta(v))'| = 0$, for all $v \in V(H)$. Note that $|\alpha(w)| - |\beta(w)| \geq 2$. we can see that all vertices of G are f-proper now.

Case 3. H is an odd circuit, but not an obstruction.

By the assumption about H, there is at least one vertex in it, say v_1, at which $|\alpha(v_1)| + |\beta(v_1)| \leq 2f(v_1) - 2$. Find an Eulerian circuit and color the edges in it with α and β alternately starting at v_1. Then we have $||(\alpha(v_1))'| - |(\beta(v_1))'|| = 2$ and $|(\alpha(v))'| = |(\beta(v))'|$ for each $v \neq v_1$ in $V(H)$. For vertex v_1, $\max\{|(\alpha(v_1))'|, |(\beta(v_1))'|\} \leq f(v_1)$. Then all vertices of G are f-proper now. $\square$

We define $M(v) = \{c \in C : |c(v)| < f(v)\}$ and $E_j = \{e_1, e_2, \ldots, e_j\}$ $(1 \leq j \leq \varepsilon(G))$. By Lemma 2, we have the following theorem.

Theorem 1. *Let G be a graph. If there is no obstruction in G, then $\chi'_f(G) = \Delta_f(G)$.*

Proof. To see this point, we present an f-coloring of G with colors in $C = \{c_1, c_2, \ldots, c_{\Delta_f(G)}\}$ by coloring the edges of G in an arbitrary order $e_1, e_2, \ldots,$ $e_{\varepsilon(G)}$. For the first edge $e_1 = w_1v_1$, there are $M(w_1) = M(v_1) = C$. Thus $G[E_1]$ can be f-colored with an arbitrary color in C. Suppose that $G[E_{j-1}]$ is f-colored so far, $2 \leq j \leq \varepsilon(G)$. When color the jth edge $e_j = w_jv_j$, we consider two cases. If $M(w_j) \cap M(v_j) \neq \emptyset$, color e_j with a color in $M(w_j) \cap M(v_j)$, and then $G[E_j]$ is f-colored. If $M(w_j) \cap M(v_j) = \emptyset$, then color e_j with a color $\alpha \in M(v_j)$. Now, all vertices but w_j are f-proper. In particular, for vertex w_j, we have $|\alpha(w_j)| = f(w_j) + 1$ and $|c(w_j)| \leq f(w_j)$ for each $c \in C$ and $c \neq \alpha$. By Lemma 2, we can obtain an f-coloring of $G[E_j]$ with colors in C, $2 \leq j \leq \varepsilon(G)$. So $\chi'_f(G) = \Delta_f(G)$. $\square$

Obviously, a bipartite graph contains no odd circuit. A graph G, in which $f(v)$ is positive and even for all $v \in V(G)$, contains no obstruction. The reason is that, for any circuit H of G with $d_H(v) = 2f(v)$ for each $v \in V(H)$, $\varepsilon(H) = (\sum_{v \in V(H)} 2f(v))/2 = \sum_{v \in V(H)} f(v)$ is even. Therefore, two results of Hakimi and Kariv [4] are immediately derived from Theorem 1.

Corollary 2. [4] *Let G be a bipartite graph. Then $\chi'_f(G) = \Delta_f(G)$.*

Corollary 3. [4] *Let G be a graph. If $f(v)$ is positive and even for all $v \in V(G)$, then $\chi'_f(G) = \Delta_f(G)$.*

3   Main Results

We denote the neighbor set of vertex set S in G by $N_G(S)$ for $S \subseteq V(G)$. Let

$$V_0^*(G) = \{v \in V(G) : \frac{d(v)}{f(v)} = \Delta_f(G)\}.$$

Then $N_G(V_0^*(G)) = \{v \in V(G) : uv \in E(G), u \in V_0^*(G)\}$. The f-*core* of a graph G is the subgraph of G induced by the vertices of $V_0^*(G)$ and is denoted by G_{Δ_f}.

There has been great interest in properties of the f-core G_{Δ_f} of a simple graph G, which would guarantee that G is of f-class 1. For example, if G_{Δ_f} is a forest, then G is of f-class 1 [11]. The *quasi-f-core* of a graph G is the subgraph of G induced by the vertices of $V_0^*(G) \cup N_G(V_0^*(G))$. In fact, the f-chromatic index of a simple graph G has very close relations with the quasi-f-core of G. Later, we can see that if the quasi-f-core of G can be f-colored with $r(\geq \Delta_f(G))$ colors, then the following Lemma 3 guarantees that G can be f-colored with r colors.

Before proceeding, we need some new notations and definitions.

We define $m(v, \alpha) = f(v) - |\alpha(v)|$ for each $v \in V(G)$ and each $\alpha \in C$. Clearly, given an edge-coloring of G with the colors in C, G is f-colored if and only if $m(v, \alpha) \geq 0$ for each $v \in V(G)$ and each $\alpha \in C$. Color α is *available* at vertex v if $m(v, \alpha) \geq 1$. Obviously $M(v) = \{\alpha \in C : m(v, \alpha) \geq 1\}$ for each $v \in V(G)$. Walk W is often denoted simply by $v_0 v_1 \ldots v_k$. We call v_0 the *start vertex* of W and v_k the *end vertex*. The *length* of W is the number k of edges in W, and denoted by $|W|$.

We now describe two tools commonly used for f-colorings of simple graphs.

(1) *ab-alternating walks*

For two distinct colors $a, b \in C$, a walk W of length one or more is called an *ab-alternating walk* if W satisfies the following conditions:

(a) The edges of W are colored alternately with a and b, and the first edge of W is colored with b;

(b) $m(v_0, a) \geq 1$ if $v_0 \neq v_k$,
    $m(v_0, a) \geq 2$ if $v_0 = v_k$ and $|W|$ is odd;

(c) $m(v_k, b) \geq 1$ if $v_0 \neq v_k$ and $|W|$ is even,
    $m(v_k, a) \geq 1$ if $v_0 \neq v_k$ and $|W|$ is odd.

Note that any closed walk W of even length whose edges are colored with a and b alternately is an ab-alternating walk. If G is given a partial f-coloring and W is an ab-alternating walk in G, then interchanging the colors a and b of the edges in walk W yields another partial f-coloring of G. This operation is called *switching W*. When W is switched, $m(v_i, a)$ and $m(v_i, b)$ remain as they were if $i \neq 0, k$, while $m(v_0, b) \geq 1$ if W is not a closed walk of even length. We denote by $W(a, b; v_0)$ an ab-alternating walk which starts with vertex v_0.

(2) Fan Sequences

Let $e_0 = w v_0$ be an uncolored edge of G. Then a *fan F* is a sequence of distinct edges $e_0, e_1, \ldots, e_k$ incident with the vertex w such that there is a sequence of distinct colors $\alpha_0, \alpha_1, \ldots, \alpha_{k-1}$ satisfying the following conditions (a) and (b), where w is called the *pivot* of F, v_i ($0 \leq i \leq k$) is the end of e_i other than w and $c(e)$ is the color assigned to the edge e.

(a) $\alpha_i \in M(v_i)$, $0 \leq i \leq k - 1$;
(b) $c(e_i) = \alpha_{i-1}$, $1 \leq i \leq k$.

When G is a simple graph, vertices $v_0, v_1, \ldots, v_k$ are distinct. *Shifting a fan F* means to recolor e_i with α_i for each i, $0 \leq i \leq k - 1$, and erase the color α_{k-1} of e_k. If G is given a partial f-coloring, then shifting F yields another partial

f-coloring of G in which e_k instead of e_0 is uncolored. A *maximal fan* is the one whose length k cannot be increased.

Lemma 3. *Let C denote the set of colors available to color the edges of a simple graph G. Suppose that $e_0 = wv_0$ is an uncolored edge in G, and graph $G - \{e_0\}$ is f-colored with the colors in C now. If every neighbor v of either w or v_0 has $M(v) \neq \emptyset$, then we can f-color e_0 with a color in C.*

Proof. Without loss of generality, we assume that all neighbors v of w have $M(v) \neq \emptyset$. If $M(w) \cap M(v_0) \neq \emptyset$, clearly e_0 can be f-colored with a color in $M(w) \cap M(v_0)$. Otherwise, construct a fan $F = e_0, e_1, \ldots, e_m$ with a sequence of distinct colors $\alpha_0, \alpha_1, \ldots, \alpha_{m-1}$. If $M(w) \cap M(v_i) \neq \emptyset$ for some $i \in \{1, 2, \ldots, m\}$, then there exists a color $\gamma \in M(w) \cap M(v_i)$ such that γ is available at vertices w and v_i. By shifting the subfan $F' = e_0, e_1, \ldots, e_i$ and subsequently coloring e_i with γ, we f-color e_0 with a color in C. Thus one can assume that $M(w) \cap M(v_i) = \emptyset$ for all $i \in \{0, 1, \ldots, m\}$. Furthermore, assume that F is a maximal fan. Obviously, F has $M(v_m) \subseteq \{\alpha_0, \alpha_1, \ldots, \alpha_{m-1}\}$.

Let $\beta \in M(w)$ and $\alpha_m \in M(v_m)$. With the assumptions above, F does not have a β-edge and has exactly one $\alpha_m(=\alpha_j)$-edge e_{j+1}, $0 \leq j \leq m-1$. Note that $\alpha_0, \alpha_1, \ldots, \alpha_{m-1}$ are all distinct. Thus any $\alpha_m \beta$-alternating walk $P = W(\alpha_m, \beta; v_m)$ of G passes through none of edges of F except for the α_m-edge e_{j+1}. We consider four cases depending on the end vertex of P.

Case 1. If P ends at $v \in V(G) \setminus \{w, v_j, v_m\}$, then switch P and subsequently shift $F = e_0, e_1, \ldots, e_m$. Since β becomes an available color at both ends of the uncolored edge $e_m = wv_m$, we can color e_m with β.

Case 2. If P ends at w, then switch P and subsequently shift the subfan $F' = e_0, e_1, \ldots, e_j$. Since $\alpha_m = \alpha_j$ becomes an available color at both ends of the uncolored edge $e_j = wv_j$, we can color e_j with α_m.

Case 3. If P ends at v_j, then switch P and subsequently shift the subfan $F' = e_0, e_1, \ldots, e_j$. Since β becomes an available color at both ends of the uncolored edge $e_j = wv_j$, we can color e_j with β.

Case 4. If P ends at v_m, then P is a closed $\alpha_m \beta$-alternating walk and $|P|$ is odd because $\beta \notin M(v_m)$. Furthermore, $m(v_m, \alpha_m) \geq 2$. Switching P and subsequently shifting the fan $F = e_0, e_1, \ldots, e_m$ make β an available color at both ends of the uncolored edge $e_m = wv_m$. We can color e_m with β.

In any case, e_0 can be f-colored with a color in C. $\square$

Let $q(G) = \max_{v \in V(G)} \{\lceil \frac{d(v)+1}{f(v)} \rceil\}$. For any $v \in V(G)$, since $f(v)q(G) > d(v)$, there are always $M(v) \neq \emptyset$. By Lemma 3, we can obtain an f-coloring of G with $q(G)$ colors by coloring the edges of G one by one. Hence Lemma 1 is proved. Similarly, when $V_0^*(G) = \emptyset$, there are also $M(v) \neq \emptyset$ for all $v \in V(G)$. Hence an earlier result of the authors [11] can be derived from Lemma 3.

Theorem 4. *[11] Let G be a simple graph. If $V_0^*(G) = \emptyset$, then G is of f-class 1.*

Holding above result, we only need to consider the situation with $V_0^*(G) \neq \emptyset$. Now we give the main result as follows, which improves Corollary 3 on simple graphs.

Theorem 5. *Let G be a simple graph. Suppose that $V_0^*(G) \neq \emptyset$. If $f(v)$ is positive and even for all $v \in V_0^*(G) \cup N_G(V_0^*(G))$, then G is of f-class 1.*

Proof. We will give an f-coloring of G with $\Delta_f(G)$ colors. Let C denote the set of $\Delta_f(G)$ colors available to color the edges of G.

Here we denote the quasi-f-core of G by G^*. Simply, we write $E(G^*)$ as E^*. First, we color the edges in E^*. By Corollary 3, we know that G^* is of f-class 1. Also, by $\Delta_f(G^*) = \Delta_f(G)$, we have $\chi'_f(G^*) = \Delta_f(G)$. Hence we can f-color G^* by the colors in C.

Let $\overline{E^*} = E(G) \setminus E^*$. Next, we color the edges in $\overline{E^*}$. Clearly, for any edge $e \in \overline{E^*}$, both ends of e are not in $V_0^*(G)$. Furthermore, at least one end of e is not in $N_G(V_0^*(G))$. (Otherwise, $e \in E^*$.) That is to say, for any edge $e \in \overline{E^*}$, there is at least one end of e which is not adjacent to the vertices in $V_0^*(G)$. Note that, for any vertex $v \in V(G) \setminus V_0^*(G)$, we always have $M(v) \neq \emptyset$. Let $e = wu$. Thus every neighbor v of either w or u has $M(v) \neq 0$. e can be f-colored with a color in C by Lemma 3. □

In fact, a more general sufficient condition can be obtained in the similar way. Obviously, it is necessary also.

Theorem 6. *Let G be a simple graph. Suppose that $V_0^*(G) \neq \emptyset$. G is of f-class 1 if and only if the quasi-f-core of G is of f-class 1.*

4   Conclusion and Further Research

Let G and H be disjoint graphs. We use $G + H$ to denote the graph with vertex set $V(G) \cup V(H)$ and edge set $E(G) \cup E(H)$. The *join* $G \vee H$ of disjoint graphs G and H is the graph obtained from $G + H$ by joining each vertex of G to each vertex of H. Let G_1 be a subgraph of G. We use $G - G_1$ to denote the graph with vertex set $V(G)$ and edge set $E(G) \setminus E(G_1)$. If $k \geq 3$ and $v_0, v_1, \ldots, v_{k-1}$ are distinct, then we call a closed walk $v_0 v_1 \ldots v_{k-1} v_0$ a *cycle* and denote it by C_k.

In this paper, we give a new sufficient condition for a simple graph G to be of f-class 1 based on vertex set $V_0^*(G) \cup N_G(V_0^*(G))$. We attempt to find a more general sufficient condition based on $V_0^*(G)$. However, the condition that $f(v)$ is positive and even for all $v \in V_0^*(G)$ is not sufficient for a simple graph G to be of f-class 1. A counterexample is $G = (K_{14} - C_{14}) \vee K_1$, in which each vertex v with $d(v) = 12$ has $f(v) = 4$ and the unique vertex w with $d(w) = 14$ has $f(w) = 5$. It is easy to see that $\Delta_f(G) = 3$ and all vertices but w belong to $V_0^*(G)$. Let $C = \{c_1, c_2, c_3\}$. We say that G is of f-class 2, for otherwise, there will exist some color $\gamma \in C$ such that the number of edges colored with γ, i.e. $(4 \times 14 + 5)/2$, is not an integer.

In the further research, we may try to find new even conditions on function f for a simple graph to be of f-class 1 based on some other special vertex subsets. Also, we may study that which classes of simple graphs G are of f-class 1 when $f(v)$ is positive and even for all $v \in V_0^*(G)$. In many edge-coloring problems, some special subgraphs such as obstructions in f-colorings are rather difficult to deal with. Therefore, we often seek some techniques to avoid them. Applying even conditions on function f to other edge-coloring problems, e.g. equitable edge-coloring problem, maybe we can obtain some interesting results.

References

1. Bondy, J. A., Murty, U. S. R.: Graph Theory with Applications. Macmillan, London, 1976
2. Choi, H., Hakimi, S.L.: Scheduling file transfers for trees and odd cycles. SIAM J. Comput. **16(1)** (1987) 162-168
3. Coffman, Jr E.G., Garey, M.R., Johnson, D.S., LaPaugn, A.S.: Scheduling file transfers. SIAM J. Comput. **14(3)** (1985) 744-780
4. Hakimi, S.L., Kariv, O.: A generalization of edge-coloring in graphs. J. Graph Theory **10** (1986) 139-154
5. Holyer, I.J.: The NP-completeness of edge-coloring. SIAM J. Comput. **10** (1981) 718-720
6. Krawczyk, H., Kubale, M.: An approximation algorithm for diagnostic test scheduling in multicomputer systems. IEEE Trans. Comput. **C-34** (1985) 869-872
7. Liu, G.Z., Hou, J.F., Cai, J.S.: Some results about f-critical graphs. Networks (accepted)
8. Nakano, S., Nishizeki, T., Saito, N.: On the f-coloring of multigraphs. IEEE Trans. Circuit and Syst. **35(3)** (1988) 345-353
9. Vizing, V.G.: On an estimate of the chromatic class of a p-graph. Discret Analiz **3**, (1964) 25-30 (Russian)
10. Zhang, X., Liu, G.Z.: The classification of complete graphs K_n on f-coloring. J. Applied Mathematics & Computing **19(1-2)** (2005) 127-133.
11. Zhang, X., Liu, G.Z.: Some sufficient conditions for a graph to be C_f 1. Applied Mathematics Letters **19** (2006) 38-44.
12. Zhang, X., Wang, J.H., Liu, G.Z.: The classification of regular graphs on f-colorings. Ars Combinatoria (to appear)

The Vertex-Neighbor-Integrity of Digraphs

Jiangyan Guo and Elkin Vumar⋆

College of Mathematics and System Sciences, Xinjiang University,
Urumqi 830046, P.R.China
vumar@xju.edu.cn

Abstract. In this paper, as an extension of the concept of vertex-neighbor-integrity of graphs, we introduce the notion of vertex-neighbor-integrity of digraphs. Let $D = (V, A)$ be a digraph. The open and closed out-neighborhoods of a set $S \subseteq V$ are denoted by $N^+(S) = \{v : uv \in A(D), u \in S, v \in V \setminus S\}$ and $N^+[S] = N^+(S) \bigcup S$, respectively. The vertex-neighbor-integrity of the digraph D is defined as $VNI(D) = \min_{S \subseteq V} \{|S| + m(D/S^+)\}$, where $D/S^+ := D - N^+[S]$ and $m(D/S^+)$ denotes the order of a maximum strong component of D/S^+. We first discuss some basic properties of the vertex-neighbor-integrity of digraphs, and then using these properties we study the maximum vertex-neighbor-integrity which can be obtained by orienting the edges of K_n and $K_{s,t}$.

Keywords: Vertex-neighbor-integrity, directed vertex-neighbor-integrity, orientation.

1 Introduction

Among several graph parameters, is the integrity introduced by Barefoot, Entringer, and Swart [1], [2] as an alternative measure of the vulnerability of graphs to disruption caused by the removal of vertices. In 1996, modeling a spy network by a graph whose vertices represent the agents and whose edges represent the lines of communication, Cozzens and Wu [3], [4] introduced a new graph parameter called "vertex-neighbor-integrity". In a spy network, if a spy is betrayed or arrested, then the espionage agency can no longer trust any of the spies with whom he or she was in direct communication. Clearly this means that the vertex representing the discovered spy and all its neighbors become efficiently useless to the network as a whole. Hence one way of measuring the robustness of such spy network is to consider the effect of removing a set of vertices and all of its neighbors from the graph.

Let $G = (V, E)$ be a graph and $m(G)$ be the order of a maximum component of G. The integrity $I(G)$ and the edge-integrity $I'(G)$ are defined respectively as $I(G) = \min_{S \subseteq V} \{|S| + m(G - S)\}$ and $I'(G) = \min_{T \subseteq E} \{|T| + m(G - T)\}$. A vertex subversion strategy S of G is a set of vertices in G whose closed neighborhood

---

⋆ Corresponding author. The project sponsored by SRF for ROCS, REM.

is deleted from G. The survival graph is denoted by G/S. The vertex-neighbor-integrity of G, $VNI(G)$, is defined as

$$VNI(G) = \min_{S \subseteq V}\{|S| + m(G/S)\}\ .$$

For the results on the vertex-neighbor-integrity of graphs see [3], [4], [5] and [8].

Until quite recently, the studies of the vulnerability parameters of networks have focus on undirected graphs. Since many situations can be modeled by directed graphs, it is quite natural to consider such vulnerability parameters for digraphs as well. Based on this idea, Goddard and Vandell [9] extended the concept of integrity to digraphs and Vandell [10] extended edge-integrity to digraphs. They introduced in [9] and [10] respectively the integrity and the arc-integrity of digraphs. The integrity and the arc-integrity of a digraph $D = (V, A)$ are defined respectively as $I(D) = \min_{S \subseteq V}\{|S| + m(D - S)\}$ and $I'(D) = \min_{T \subseteq A}\{|T| + m(D - T)\}$, where $m(H)$ stands for the order of a maximum strong component of H. In [9] and [10], after some basic properties of $I(D)$ and $I'(D)$, the authors studied the maximum (arc-)integrity which can be obtained by orienting the edges of graphs.

Motivated by the above work of Goddard and Vandell, we extend the concept of vertex-neighbor-integrity to digraphs and introduce the directed vertex-neighbor-integrity of graphs. The idea behind our extension is the following. Consider a spy network modeled by a simple digraph $D = (V, A)$ whose vertices represent agents and whose arcs represent directed line of communications, where an arc uv means that u is a superior of v, and in operations v receives orders from his or her superior u, but never knows who u is. Hence when the agent u is discovered, all the subordinates of u can no longer be trusted, but the superiors of u are still safe for the whole network. Such a betrayals are clearly equivalent to the removal of the closed out-neighborhood of u in the modeling digraph.

Let $D = (V, A)$ be a simple digraph and $u \in V(D)$. The open and closed out-neighborhoods of u are defined as $N^+(u) = \{v \in V(D) : uv \in A(D)\}$ and $N^+[u] = N^+(u) \cup \{u\}$, respectively. For a subset S of V, the open and closed out-neighborhoods are defined as $N^+(S) = \bigcup_{v \in S} N^+(v) - S$ and $N^+[S] = N^+(S) \cup S$, respectively. The open and closed in-neighborhoods of a vertex v and a set $S \subseteq V$ are defined similarly. Let $d^+(v) = |N^+(v)|$ and $d^-(v) = |N^-(v)|$. We say that a vertex u dominates v if $uv \in A(D)$. A set $S \subseteq V$ is called a *dominating set* if $N^+[S] = V$. In particular, when $S = \{u\}$ is a dominating set we call u a dominating vertex.

Following Cozzens and Wu, we introduce the concept of vertex subversion strategy in digraphs. A vertex u is said to be subverted from D, if the closed out-neighborhood $N^+[u]$ is deleted from D. A set of vertices S in D is called a vertex subversion strategy of D, if the closed out-neighborhood of S is deleted from D, i.e., each of the vertices in S has been subverted from D. Let D/S^+

denote the subgraph left after the closed out-neighborhood $N^+[S]$ has been deleted from D. The vertex-neighbor-integrity of D, $VNI(D)$, then is defined as

$$VNI(D) = \min_{S \subseteq V(D)} \{|S| + m(D/S^+)\} .$$

And the directed vertex-neighbor-integrity, $\overline{VNI}(G)$, of a graph G is defined as

$$\overline{VNI}(G) = \max_{D} \{VNI(D) : D \text{ is an orientation of } G\} .$$

A set $S \subseteq V(D)$ is called an *optimal subset* of V if $VNI(D) = |S| + m(D/S^+)$.

2   Some Basic Properties of Vertex-Neighbor-Integrity of Digraphs

In this section we present some basic properties of the vertex-neighbor-integrity of digraphs.

Property 1. It is easy to see that there exist digraphs D_1 and D_2 and two subdigraphs $H_1 \subset D_1$ and $H_2 \subset D_2$ such that $VNI(D_1) > VNI(H_1)$ and $VNI(D_2) < VNI(H_2)$.

Property 2. $VNI(D) = 1$ if and only if D has no directed cycle or there exists a dominating vertex in D.

Proof. The sufficiency is obvious. Suppose that $VNI(G) = 1$ and D has a directed cycle. Let S be a subset of V such that $VNI(D) = |S| + m(D/S^+) = 1$. Since D has a directed cycle necessarily $|S| = 1$ and $m(D/S^+) = 0$, hence D has a dominating vertex. □

Property 3. If D^* is a digraph obtained from a digraph D by reversing one arc of D, then $VNI(D) - 1 \leq VNI(D^*) \leq VNI(D) + 1$.

Proof. By symmetry, it suffices to show that $VNI(D^*) \leq VNI(D) + 1$. Suppose that $uv \in A(D)$ and D^* is obtained from D by reversing uv. Then $d_{D^*}^+(u) = d_D^+(u) - 1$ and $d_{D^*}^-(u) = d_D^-(u) + 1$. Let S be a subset of V such that $VNI(D) = |S| + m(D/S^+)$. Note that S may be empty. Let $S_1 = S \cup \{v\}$. Then $m(D^*/S_1^+) \leq m(D/S^+)$, consequently $VNI(D^*) \leq |S_1| + m(D^*/S_1^+) \leq |S| + 1 + m(D/S^+) = 1 + VNI(D)$. □

Property 4. Let u be a vertex of D with $d^+(u) = 0$. If $D - u$ has no dominating vertex, then $VNI(D - u) = VNI(D)$.

Proof. If D is acyclic, then too is $D - u$. In this case, since $D - u$ has no dominating vertex, we have $VNI(D - u) = VNI(D) = 1$. Assume that D contains a directed cycle. Since $d^+(u) = 0$, u is not in any directed cycle of D. If $S \subseteq V$ such that $VNI(D) = |S| + m(D/S^+)$, then $u \notin S$. For otherwise, $v \notin S$ for any $v \in N^-(u)$. But then $m(D/S_1^+) = m(D/S^+)$ for $S_1 = S - u$, and hence

$|S_1| + m(D/S_1^+) = |S| - 1 + m(D/S^+) = VNI(D) - 1$, a contradiction. If $S \cap \{u\}^- \neq \emptyset$, then clearly $VNI(D-u) = VNI(D)$. Finally suppose that $S \cap \{u\}^- = \emptyset$ for every optimal subset S of V. Then we have $m((D-u)/S^+) = m(D/S^+)$ and $VNI(D-u) \leq |S| + m((D-u)/S^+) = |S| + m(D/S^+) = VNI(D)$. Let T be an optimal subset of $V(D-u)$. Then $m(D/T^+) = m((D-u)/T^+)$, as $d^+(u) = 0$. Now $VNI(D) \leq |T| + m(D/T^+) = |T| + m((D-u)/T^+) = VNI(D-u)$. Hence $VNI(D) = VNI(D-u)$.   □

Remark 1. Let $u \in V(D)$. If $d^+(u) = 0$ and $D - u$ has no dominating vertex, then no optimal subset S of V contains u.   □

Property 5. Let D be a digraph with $\delta^-(D) > 0$ and contain a directed cycle. Then $VNI(D) = 2$ if and only if at least one of the following holds.
(i) $m(D) = 2$;
(ii)   there exists u in D such that $D/\{u\}^+$ is acyclic;
(iii) there exist distinct u and v in D such that $N^+[u] \cup N^+[v] = V(D)$.

Proof. By the assumption D has a directed cycle and has no dominating vertex. By *Property 2* we have $VNI(D) \geq 2$. If one of $(i), (ii)$ and (iii) occurs, then certainly we have $VNI(D) \leq 2$ and hence $VNI(D) = 2$. Suppose $VNI(D) = 2$, and let S be a subset of V such that $VNI(D) = |S| + m(D/S^+) = 2$. The possible values of $(S, m(D/S^+))$ are $(0,2), (1,1)$ and $(2,0)$, which imply that at least one of $(i), (ii)$ and (iii) holds.   □

3   Directed Vertex-Neighbor-Integrity of K_n and $K_{s,t}$

In this section, we first present bounds for the directed vertex-neighbor-integrity of K_n, and then we determine the directed vertex-neighbor-integrity of $K_{s,t}$ ($s \leq t$) for $s = 3, 4$.

We give an orientation, denoted by D_n, of a complete graph K_n. Let $V(D_2) = \{v_1, v_2\}$ and $A(D_2) = (v_1, v_2)$. Suppose D_n has been defined. Then D_{n+1} is orientated according to the following regulations.

When $n + 1$ is odd, $V(D_{n+1}) = V(D_n) \cup \{v_{n+1}\}$ and $A(D_{n+1}) = A(D_n) \cup \{(v_i, v_{n+1})$ *when* $d^-(v_i) \geq \frac{n}{2}$, *and* (v_{n+1}, v_i) *otherwise*$\}$.

When $n + 1$ is even, $V(D_{n+1}) = V(D_n) \cup \{v_{n+1}\}$ and $A(D_{n+1}) = A(D_n) \cup \{(v_i, v_{n+1})$ *when* $i \leq \frac{n+1}{2}$, *and* (v_{n+1}, v_i) *otherwise*$\}$.

Theorem 1. *Let* $D_n(n \geq 2)$ *be the orientation of* K_n *defined as above. Then*

$$VNI(D_n) = \begin{cases} 1, & n = 2, \\ 2, & n \text{ is odd or } n \text{ is even with } 4 \leq n \leq 10, \\ 3, & n \text{ is even with } n \geq 12. \end{cases}$$

Proof. Suppose n is odd. By the definition of D_n, the vertex v_n dominates the vertices u with $d^+(u) - d^-(u) = 1$. In D_n, as $n - 1$ is even, v_{n-1} dominates the vertices v_j for $\frac{n-1}{2} + 1 \leq j \leq n, j \neq n - 1$, and there are arcs (v_i, v_{n-1}) for $i \leq \frac{n-1}{2}$. In D_n the vertex v_n dominates the vertices v_i for $i \leq \frac{n-1}{2}$. Hence

$N^+[v_{n-1}] \cup N^+[v_n] = V(D_n)$, and $VNI(D_n) \leq 2$. On the other hand, since D_n contains directed cycles, we have $VNI(D_n) \geq 2$. Thus $VNI(D_n) = 2$.

Now let $n \in \{4, 6, 8, 10\}$. It is easy to check that $\{v_1, v_2\}, \{v_2, v_3\}, \{v_1, v_4\}$ and $\{v_2, v_5\}$ are dominating sets in D_n for $n = 4, 6, 8, 10$, respectively. Hence in this case $VNI(D_n) = 2$ by *Property 5*.

Let n be even with $n = 2k \geq 12$. It is not difficult to see that $D_{2k}/S^+ = \{v_k\}$ for $S = \{v_{2k-1}, v_{2k}\}$, and consequently $VNI(D_{2k}) \leq 3$. Since D_{2k} is strongly connected, we have $m(D_{2k}) > 2$. Hence to prove $VNI(D_{2k}) \geq 3$, by *Property 5*, it suffices to show

(a)   there is no vertex v_i such that $D_{2k}/\{v_i\}^+$ is acyclic, and
(b)   there are no two vertices v_i and v_j $(i \neq j)$ in D_{2k} such that $N^+[v_i] \cup N^+[v_j] = V(D_{2k})$.

We first show (a). By the definition of D_{2k}, $d^+(v_i) - d^-(v_i) = 1$ for $v_i \in \{v_1, ..., v_k\}$ and $d^+(v_j) - d^-(v_j) = 1$ for $v_j \in \{v_{k+1}, ..., v_{2k}\}$. Since all vertices in $\{v_1, ..., v_k\}$ ($\{v_{k+1}, ..., v_{2k}\}$) have equal positions in D_{2k}, it suffices to check $D_{2k}/\{v_1\}^+$ and $D_{2k}/\{v_{2k}\}^+$, respectively. Again by the definition of D_{2k}, v_1 dominates v_{2j} for $j = 1, 2, ..., \frac{k}{2}$, so we have $D_{2k}/\{v_1\}^+ = \{v_3, v_5, ..., v_{2k-1}\}$ and $v_3 v_5 v_7 v_3$ is a cycle in $D_{2k}/\{v_1\}^+$. Similarly, $v_1 v_2 v_3 v_1$ is a cycle in $D_{2k}/\{v_{2k}\}^+$.

We prove (b) by induction on n. When $n = 12$, it is easy to see that D_{12} contains no vertices u and v such that $N^+[u] \cup N^+[v] = V(D_{12})$. Suppose that (b) holds for D_{2l} with $6 \leq l < k$.

Now suppose that D_{2k} contains u and v such that $N^+[u] \cup N^+[v] = V(D_{2k})$. Then $\{u, v\} \cap \{v_{2k-1}, v_{2k}\} \neq \emptyset$, for otherwise $N^+[u] \cup N^+[v] = V(D_{2k-2})$, contradicting the induction hypothesis. In D_{2k}, as $N^+(v_{2k-2}) = \{v_k, ..., v_{2k-3}\}$ and $N^+(v_{2k-1}) = \{v_1, v_2..., v_{k-1}\}$, we have $\{v_{2k-2}, v_{2k-1}\} \cap \{u, v\} = \emptyset$. So we may assume $u = v_{2k}$ and $v \in \{v_1, ..., v_{2k-3}\}$. Since in D_{2k} the vertex v_{2k} dominates v_i with $k + 1 \leq i \leq 2k - 1$, the vertex v must dominate v_j with $1 \leq j \leq k$. But then in D_{2k-2}, we would have $N^+(v) \cup N^+(v_{2k-1}) = V(D_{2n-2})$, contradicting the induction hypothesis.

Hence (b) is proved and this completes the proof of the theorem.   □

Theorem 2. *If n is an integer not less than 2, then $\overline{VNI}(K_n) \leq \lceil \log_2 \frac{n}{2} \rceil + 1$.*

Proof. Suppose D is a tournament with n vertices. In the following, to get the upper bound we shall determine a subset S of V such that $|S| + m(D/S^+)$ can not excess the upper bound.

For technical reason we denote $D_1 = D$ and $n_1 = n$. D_1 has a vertex u_1 such that $d_{D_1}^+(u_1) \geq \lfloor \frac{n_1}{2} \rfloor$. Set $D_2 = D_1/\{u_1\}^+$ and $n_2 = n_1 - |N_{D_1}^+[u_1]| \leq n_1 - \lfloor \frac{n_1}{2} \rfloor - 1 \leq \lfloor \frac{n_1}{2} \rfloor$. And D_2 has a vertex u_2 such that $d_{D_2}^+(u_2) \geq \lfloor \frac{n_2}{2} \rfloor$. We continue this process until some D_{k+1} has at most 2 vertices. Then by the construction, we have $n_{k+1} \leq \lfloor \frac{n_k}{2} \rfloor$. For simplicity, we assume that $n_{i+1} \leq \frac{n_i}{2}$ for $i = 2, ..., k - 1$ and $\frac{n}{2^k} \leq 2$. Then we have $n_{k+1} \leq \frac{n}{2^k} \leq 2$, consequently $k \geq \log_2 \frac{n}{2}$. The minimum value of k is $\lceil \log_2 \frac{n}{2} \rceil$. We set $S = \{u_1, u_2, ..., u_k\}$ with $k = \lceil \log_2 \frac{n}{2} \rceil$. Then $m(D/S^+) \leq 1$, and consequently $VNI(D) \leq |S| + m(D/S^+) \leq \lceil \log_2 \frac{n}{2} \rceil + 1$. Having chosen D arbitrarily, we have obtained the upper bound.   □

Corollary 1. *Let n be an integer not less than 2. Then*
(i) $2 \leq \overline{VNI}(K_n) \leq \lceil \log_2 \frac{n}{2} \rceil + 1$, *if n is odd or $n \in \{4, 6, 8, 10\}$;*
(ii) $3 \leq \overline{VNI}(K_n) \leq \lceil \log_2 \frac{n}{2} \rceil + 1$, *if n is even with $n \geq 12$.*

Let D be an orientation of $K_{s,t}$ ($s \leq t$) with bipartition (X, Y). We label $X = \{x_1, \ldots, x_s\}$ and $Y = \{y_1, \ldots, y_t\}$.

Proposition 1. $\overline{VNI}(K_{3,t}) = 2$, *where $t \geq 3$.*

Proof. We prove the proposition by using *Property 5*. Clearly $\overline{VNI}(K_{3,t}) \geq 2$. Let D be an orientation of $K_{3,t}$. We consider the out-degrees of vertices in Y.
  If $N^+(Y) = \bigcup_{y_i \in Y} N^+(y_i) \neq X$, then there exists a vertex $x_k \in X$ such that $N^+(x_k) = Y$, and $D/\{x_k\}^+$ is acyclic. So in this case $VNI(D) \leq 2$. Next suppose $\bigcup_{y_i \in Y} N^+(y_i) = X$. If there exists, in addition, $y_k \in Y$ with $d^+(y_k) \geq 2$, then $D/\{y_k\}^+$ is acyclic, and again $VNI(D) \leq 2$. If $d^+(y_i) \leq 1$ for every $y_i \in Y$ then, by *Property 4*, we only need to consider the vertices y_j with $d^+(y_j) = 1$. And in this subcase, $D/\{x_i\}^+$ is acyclic for every $x_i \in X$, consequently again we have $VNI(D) \leq 2$. Hence $\overline{VNI}(K_{3,t}) \leq 2$. □

Proposition 2. $\overline{VNI}(K_{4,t}) = 3$, *where $t \geq 4$.*

Proof. First we show $\overline{VNI}(K_{4,t}) \geq 3$. Let D be an orientation of $K_{4,t}$ defined as follows. For a vertex $y_i \in Y$, we define $N^+(y_i) = \{x_1, x_2\}$ when $i = 1 \ (mod \ 4)$; $N^+(y_i) = \{x_1, x_3\}$ when $i = 2 \ (mod \ 4)$; $N^+(y_i) = \{x_2, x_4\}$ when $i = 3 \ (mod \ 4)$ and $N^+(y_i) = \{x_3, x_4\}$ when $i = 0 \ (mod \ 4)$, and the remaining edges are oriented on the opposite direction. Let S be a subset of $V(D)$. Since we want to prove $VNI(D) \geq 3$, we may assume that $|S| < 3$. If S contains only the vertices in X, then since $d^+(y_i) = 2$ for every vertex $y_i \in Y$, we infer that S must contain at least two vertices to make D/S^+ be acyclic, so in this case $|S| + m(D/S^+) = 3$. If S contains the vertices in both X and Y, then S consists of one vertex in X and one vertex in Y, by construction obviously S is not a dominating set and D/S^+ is acyclic. Thus $|S| + m(D/S^+) = 3$. Suppose S contains only the vertices in Y. If $|S| = 1$, then obviously $|S| + m(D/S^+) = 5$. Hence we assume $|S| = 2$, say $S = \{y_1, y_2\}$, then also $|S| + m(D/S^+) = 3$. So from all cases above, $|S| + m(D/S^+) \geq 3$ for any $S \subseteq V(D)$. Hence $VNI(D) = 3$ and $\overline{VNI}(K_{4,t}) \geq 3$.
  Next we show $\overline{VNI}(K_{4,t}) \leq 3$. Let D be an arbitrary orientation of $K_{s,t}$. If $N^+(Y) = \bigcup_{y_i \in Y} N^+(y_i) \neq X$, then there exists a vertex $x_k \in X$ such that $N^+(x_k) = Y$, and consequently $VNI(D) \leq 2$ in this case.
  Now suppose $\bigcup_{y_i \in Y} N^+(y_i) = X$.

Case 1. There exists $y_k \in Y$ with $d^+(y_k) \geq 3$.

In this case $m(D/S^+) = 1$ for $S = \{y_k\}$, hence $VNI(D) \leq |S| + m(D/S^+) \leq 2$.

Case 2. There exists a vertex $y_k \in Y$ such that $d^+(y_k) = \max_{y_i \in Y} d^+(y_i) = 2$.

If there exists a vertex $x_l \in X$ with $d^-(x_l) = 1$ then $D/\{x_l\}^+$ is acyclic and $VNI(D) \leq |\{x_l\}| + m(D/\{x_l\}^+) = 2$. In the remaining subcase we choose an $x_j \in X - N^+(y_k)$, and set $S = \{y_k, x_j\}$. Then $m(D/S^+) = 1$, and again $VNI(D) \leq 3$.

Case 3. $d^+(y_i) \leq 1$ for every $y_i \in Y$.

Setting $S = \{x_j\}$ for arbitrary $x_j \in X$, we have $m(D/S^+) = 1$ since all vertices y_i in D/S^+ have no out-neighbors to X. Hence $VNI(D) \leq |S| + m(D/S^+) = 2$.
From all above we have $\overline{VNI}(K_{4,t}) \leq 3$, and hence $\overline{VNI}(K_{4,t}) = 3$.   □

Acknowledgements

References

1. Barefoot, C.A., Entringer. R., Swart, H.: Vulnersbility in graphs - a comparative survey, J. Combin. Math. Combin. Comp. **1** (1987) 13-22.
2. Barefoot, C.A., Entringer. R., Swart, H.: Integrity of trees and powers of cycles, Congr. Numer. **58** (1987) 103-114.
3. Cozzens, M.B., Wu, S.-S.Y.: Vertex-neighbor-integrity of trees, Ars. Combin. **43** (1996) 169-180.
4. Cozzens, M.B., Wu, S.-S.Y.: Vertex-neighbor-integrity of powers of cycles, Ars. Combin. **48** (1998) 257-270.
5. Cozzens, M.B., Wu, S.-S.Y.: Relations between vertex-neighbor-integrity and other parameters, Ars. Combin. **55** (2000) 271-282.
6. Cozzens, M.B., Wu, S.-S.Y.: Edge-neighbor-integrity of trees, Australas. J. Combin.**10** (1994) 163-174.
7. Cozzens, M.B., Wu, S.-S.Y.: Bounds for edge-neighbor-integrity of graphs, Australas. J. Combin.**15** (1997) 71-80.
8. Gambrell, M.J.: Vertex-neighbor-integrity of magnifiers, expanders, and hypercubes, Discrete Math. **216** (2000) 257-266.
9. Goddard, W.G., Vandell, R.C.: The integrity of a directed graph and the directed integrity of a graph, to appear.
10. Vandell, R.C.: Maximum arc-integrity of tournaments and bipartite tourments, to appear in : Proceedings of the ninth quadrennial international conference in graph theory, combinatorics, algorithm, and applications.
11. Wu. S.-S.Y., Cozzens, M.B.: The minimun size of critically m-neighbor-connected graphs, Ars. Combin. **29** (1990) 149-160.

Hamiltonian Connected Line Graphs⋆

Deng-Xin Li[1], Hong-Jian Lai[2], Ye-Hong Shao[3], and Mingquan Zhan[4]

[1] College of sicence, Chongqing Technology and
Business University, Chongqing, P.R. China 400067
sx-ldx@ctbu.edu.cn
[2] Department of Mathematics, West Virginia University,
Morgantown, WV 26506-6310
[3] Arts and Science, Ohio University
Southern, Ironton, OH 45638
yshao@math.wvu.edu
[4] Department of Mathematics, Millersville University,
Millersville, PA 17551

Abstract. Thomassen conjectured [8] that every 4-connected line graph is hamiltonian. An hourglass is a graph isomorphic to $K_5 - E(C)$, where C is a cycle of length 4 in K_5. In [2], it is shown that every 4-connected line graph without an induced subgraph isomorphic to the hourglass is hamiltonian connected. In this note, we prove that every 3-connected, essentially 4-connected hourglass-free line graph is hamiltonian connected.

Keywords: Line Graph, Hourglass, Hourglass-Free, Hamiltonian Connected.

1 Introduction

Graphs considered here are finite and loopless. Unless otherwise noted, we follow [1] for notations and terms. A graph G is **nontrivial** if $E(G) \neq \emptyset$. For a vertex v of a graph G, $d_G(v)$ denotes the degree of v in G and $E_G(v)$ denotes the set of edges incident with v in G. For an integer $i > 0$, $D_i(G) = \{v \in V(G) : d_G(v) = i\}$.

The **line graph** of a graph G, denoted by $L(G)$, has $E(G)$ as its vertex set, where two vertices in $L(G)$ are adjacent if and only if the corresponding edges in G are adjacent. Thomassen [8] conjectured that every 4-connected line graph is hamiltonian. This conjecture is still open.

An hourglass is a graph isomorphic to $K_5 - E(C)$, where C is a cycle of length 4 in K_5. A graph is hourglass-free if it does not have an induced subgraph isomorphic to the hourglass.

Theorem 1.1. (Broersma, Kriesell and Ryjáček, [2]) Every 4-connected hourglass-free line graph is hamiltonian connected.

A vertex (edge, respectively) cut X of a connected graph G is *essential* if $G - X$ has at least two nontrivial components. A graph G is essentially k-connected (essentially k-edge-connected, respectively) if G does not have an essential vertex cut (essential edge cut, respectively) X with $|X| < k$. In this note, we shall improve Theorem 1.1 in the following form.

Theorem 1.2. Every 3-connected, essentially 4-connected hourglass-free line graph is hamiltonian connected.

Since adding edges will not decrease the connectivity and the essential connectivity, applying the line graph closure of Ryjáček [6], Theorem 1.2 has the following corollary.

Corollary 1.3. Every 3-connected, essentially 4-connected, claw-free graph without hourglass is hamiltonian.

2   Mechanism

Let G be a graph. An edge $e \in E(G)$ is *subdivided* when it is replaced by a path of length 2 whose internal vertex, denoted by $v(e)$, has degree 2 in the resulting graph. This process is called *subdividing e*. For a graph G with $e', e'' \in E(G)$, let $G(e')$ denote the graph obtained from G by subdividing e', and let $G(e', e'')$ denote the graph obtained from G by subdividing both e' and e''. Then,

$$V(G(e', e'')) - V(G) = \{v(e'), v(e'')\}.$$

For vertices $u, v \in V(G)$, an (u, v)-*trail* is a trail that starts with u and ends with v.

Theorem 2.1. ([4]) If G is essentially 4-edge-connected such that for every vertex $v \in V(G)$ of degree 3, G has a cycle of length at most 3 containing v, then for every pair of edges $e', e'' \in E(G)$, $G(e', e'')$ has a spanning $(v(e'), v(e''))$-trail.

Let G be a graph such that $\kappa(L(G)) \geq 3$ and $L(G)$ is not complete. The **core** of this graph G, denoted by G_0, is obtained from $G - D_1(G)$ by contracting exactly one edge xy or yz for each path xyz in G with $d_G(y) = 2$.

Lemma 2.2. ([5], [7]) Let G be a connected nontrivial graph such that $\kappa(L(G)) \geq 3$, and let G_0 denote the core of G. If $\forall e', e'' \in E(G_0)$, $G(e', e'')$ has a spanning $(v(e'), v(e''))$-trail, then $L(G)$ is hamiltonian connected.

3   Proof of Theorem 1.2

Let G_0 be the core of G. Then as $\kappa(L(G)) \geq 3$, $\kappa'(G_0) \geq 3$. Let X be an essential edge cut of G_0. Suppose that $|X| \leq 3$. If one side of $G_0 - X$ has only one edge, then by $\delta(G_0) \geq 3$, we must have $|X| \geq 4$, a contradiction. Therefore, both

sides of $G - X$ must have a pair of adjacent edges, and so X corresponds to an essential vertex cut of $L(G)$. Since $L(G)$ is assumed to be essentially 4-connected, $|X| \geq 4$, a contradiction. Thus we proved the claim:
(3.1) G_0 is essentially 4-edge-connected.
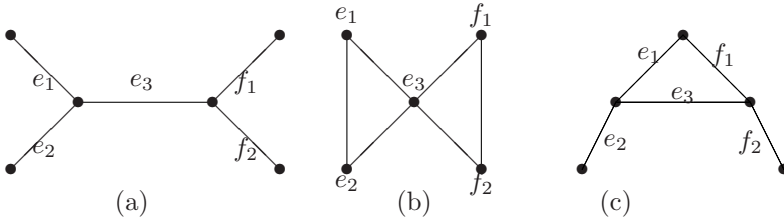
Fig. 1. $G[\{e_1, e_2, e_3, f_1, f_2\}]$ and $L(G)[\{e_1, e_2, e_3, f_1, f_2\}]$

We shall prove the next claim:
(3.2) $\forall v \in D_3(G_0)$, G_0 has a cycle of length at most 3 intersecting $E_{G_0}(v)$.

By contradiction. Let $v \in D_3(G_0)$ with $E_{G_0}(v) = \{e_1, e_2, e_3\}$ such that no edge in $E_{G_0}(v)$ lies in a cycle of length at most 3. Let v_1, v_2, v_3 denote the vertices of G_0 adjacent to v such that $e_i = vv_i$, $(1 \leq i \leq 3)$. Since $\delta(G_0) \geq 3$, we can assume that $\{f_1, f_2\} \subseteq E_{G_0}(v_3) - \{e_3\}$ (see Figure 1(a)). By the definition of a core, either $e_3 \in E(G)$ or e_3 is a new edge replacing a path of length 2 in G (see Figure 2).
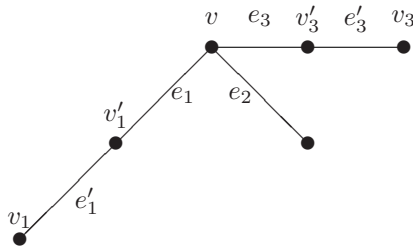
Fig. 2. The edge cut $\{e'_1, e_2, e'_3\}$ in G

If $e_3 \in E(G)$, and if neither e_1 nor e_2 is adjacent to f_1 or f_2 (see Figure 1(a) and (b)), then $L(G)$ would have an induced hourglass, contrary to the assumption that $L(G)$ is hourglass-free. Hence we may assume that $e_1 f_1 \in E(L(G))$ (see Figure 1(c)). Then $f_1 \in E_{G_0}(v_1)$, and so $G_0[\{e_1, e_3, f_1\}] \cong K_3$, contrary to the choice of v.

By symmetry, we may assume that $\forall i \in \{1, 2, 3\}$, e_i is a new edge which replaces a path with edges $\{e_i, e'_i\}$ in G, where we also use e_i to denote the edge adjacent to v in G. Then $\{e'_1, e_2, e'_3\}$ corresponds to an essential vertex

cut of $L(G)$ (see Figure 2), contrary to the assumption that $L(G)$ is essentially 4-connected. This proves Claim (3.2).

By (3.1), (3.2) and by Theorem 2.1, $\forall e', e'' \in E(G_0)$, $G_0(e', e'')$ has a spanning $(v(e'), v(e''))$-trail, and so by Lemma 2.2, $L(G)$ is hamiltonian connected.

References

[1] J. A. Bondy and U. S. R. Murty, Graph Theory with Applications. Elsevier, New York, (1976).

[2] H. J. Broersma, M. Kriesell and Z. Ryjáček, On Factors of 4-Connected Claw-Free Graphs, J. Graph Theory 37 (2001), 125-136.

[3] P. A. Catlin, A reduction method to find spanning eulerian subgraphs, J. Graph Theory 12 (1988), 29-44.

[4] H.-J. Lai, X. Li, Y. Ou and H. Poon, Spanning trails joining given edges, Graphs and Combinatorics, accepted.

[5] H.-J. Lai, Y. Shao, G. Yu and M. Zhan, Hamiltonian connectedness in 3-connected line graphs, submitted.

[6] Z. Ryjáček, On a closure concept in claw-free graphs, J. Combin. Theory Ser. B, 70 (1997), 217-224.

[7] Y. Shao, Hamiltonian claw-free graphs, PhD dissertation, West Virginia University, (2005).

[8] C. Thomassen, Reflections on graph theory, J. Graph Theory, 10 (1986), 309-324.

A Degree-Condition for (s, t)-Supereulerian Graphs⋆

Bin Wang, Xiao-Min Li, and Lan Lei

The faculty of science, Chongqing Technology
and Business University, Chongqing, P.R. China 400067
wb@ctbu.edu.cn

Abstract. For two integers $s \geq 0$, $t \geq 0$, G is (s, t)-superlerian, if $\forall X$, $Y \subset E(G)$ with $X \cap Y = \phi$, where $|X| \leq s$, $|Y| \leq t$, G has a spanning eulerian subgraph H such that $X \subset E(H)$ and $Y \cap E(H) = \phi$. It is obvious that G is supereulerian if and only if G is (0, 0)-supereulerian. In this note, we have proved that when G is a $(t + 2)$-edge-connected simple graph on n vertices, if $n \geq 21$ and $\delta(G) \geq \frac{n}{5} + t$, then G is (3, t)-supererlerian or can be contracted to some well classified special graphs.

Keywords: (s, t)-supereulerian; Collapsible; Reduced Graph; Edge-disjoint Spanning Trees.

1 Introduction

Graphs in this note are simple, finite and loopless. Undefined terms and notations are from [2]. We use $H \subseteq G$ to denote the fact that H is a subgraph of G. For a graph G, $O(G)$ denotes the set of all vertices of odd degree in G. A graph G is called an *even* graph if $O(G) = \phi$, and a connected even graph is an *eulerian* graph. A graph is *supereulerian* if it has a spanning eulerian subgraph. The collection of all supereulerian graphs will be denoted by SL. For the literature on the subject of supereulerian graphs, see Catlin's excellent survey [4]. As indicated by the authors in [1], characterizing supereulerian graphs appears very difficult. Pulleyblank in [8] pointed out that the problem of determining if a graph G is supereulerian is $NP - complete$.

In [7] Jaeger proved Theorem 1.1 below.

Theorem 1.1(Jaeger [7]). If G has two edge-disjoint spanning trees, then G is in SL.

Let $F(G)$ be the minimum number of edges that must be added to G so that the resulting graph has 2 edge-disjoint spanning trees. Thus Theorem 1.1 says that if $F(G) = 0$, then $G \in SL$. In [5] , Catlin showed that Theorem 1.1 can be improved.

Theorem 1.2(Catlin [5]). If $F(G) \leq 2$, then either G is in SL, or G can be contracted to K_2 or $K_{2, t}$, where t is odd natural number.

In [3], Catlin got a degree condition for supererlerian graphs.

Theorem 1.3(Catlin [3]). Let G be a 2-edge-connected simple graph on n vertices. If $\delta(G) \geq \frac{n}{5}$, then G is supereulerian.

In this note, we want to improve the Theorem 1.3. We need the following concept. For two integers $s \geq 0$, $t \geq 0$, G is (s, t)-superlerian, if $\forall X, Y \subset E(G)$ with $X \cap Y = \phi$, where $|X| \leq s$, $|Y| \leq t$, G has a spanning eulerian subgraph H such that $X \subset E(H)$ and $Y \cap E(H) = \phi$. It is obvious that G is supereulerian if and only if G is $(0, 0)$-supereulerian. The Theorem 1.3 then says G is $(0, 0)$-supereulerian if $\delta(G) \geq \frac{n}{5}$ with edge-connectivity≥ 2. In section 2, we shall display some preliminaries and in section 3, we shall extend the Theorem 1.3 to its (s, t)-supererlerian version.

2   Preliminaries

In [3], Catlin defined the *collapsible* graphs. Let $R \subseteq V(G)$, a graph H of G is called an $R - subgraph$ if both $G - E(H)$ is connected and $v \in R$ if v has odd degree in H. A graph G is *collapsible* if for any even subset R of $V(G)$, G has an R-subgraph. Catlin showed in [4] that every vertex of G is lying in a unique maximal collapsible subgraph of G. The collection of all collapsible graphs is denoted by CL. Clearly $CL \subseteq SL$.

The contraction G/H is obtained from G by contracting each edge of H and deleting the resulting loops. The *reduction* of G is obtained from G by contracting all maximal collapsible subgraphs, and is denoted by $G\prime$. A graph G is reduced if G is the reduction of some graph.

Theorem 2.1(Catlin [3]). Let G be a graph. Each of the following holds:
(1)G is reduced if and only if G has no nontrivial collapsible subgraphs;
(2)If G is reduced, then G is simple and contains no K_3, $\delta(G) \leq 3$;
(3)If G is reduced and $|V(G)| \geq 3$, then $F(G) = 2|V(G)| - |E(G)| - 2 \geq 2$;
(4)If H is a collapsible subgraph of G, then $G \in CL$ if and only if $G/H \in CL$;
(5)If H is a collapsible subgraph of G, then $G \in SL$ if and only if $G/H \in SL$.

Let G be a graph and let $X \subseteq E(G)$. The graph G_X is obtained from G by replacing each edge $e \in X$ with ends u_e and v_e by a (u_e, v_e)-path P_e of length 2, where the internal vertex w_e of the path P_e is newly added.

Lemma 2.2. Let G be a graph and let $X \subset E(G)$, $Y \subset E(G)$ with $X \cap Y = \phi$, then G has a spanning eulerian subgraph H such that $X \subset E(H)$ and $Y \cap E(H) = \phi$.

Lemma follows from the definitions.

We need the following definition. The Peterson graph is denoted by P.

Let $\mathcal{F}=\{K_1, K_2, k_{2, t}, K_{2, t}', K_{2, t}'', K_{1, 3}(s, s', s''), S(m, l), J(m, l), J'(m, l), P\}$, where t, s, s', s'', m, l are nonnegative integers. The definitions of $K_{2, t}'$, $K_{2, t}''$, $K_{1, 3}(s, s', s'')$, $S(m, l)$, $J(m, l)$, $J'(m, l)$, please see the reference [6].

Theorem 2.3(Chen and Lai [6]). If G is a connected reduced graph with $|V(G)| \leq 11$ and $F(G) \leq 3$, then $G \in \mathcal{F}$.

Let $\mathcal{F}^*=\{\ G \in \mathcal{F}$: G is 2-edge-connected$\}\cup\{$ G: the subdivision of $K_{2, t}$, t is odd natural number$\}\cup F_1 - SL$, here F_1 denotes the graph obtained from a $K_{2, 3}$ and C_4 by identifying a vertex of degree 2 in $K_{2, 3}$ with any one in C_4.

3   Main Result

Theorem 3.1. G is a $(t + 2)$-edge-connected simple graph on n vertices, where t is a nonnegative integer. If $n \geq 21$ and $\delta(G) \geq \frac{n}{5} + t$, take any two edge-disjoint subsets of $E(G)$, X and Y, where $|X| \leq 3$ and $|Y| \leq t$, then G is $(3, t)$-supereulerian or $(G - Y)_X'$ is in $\mathcal{F}^*$.

Note that in Theorem 3.1, G need to be $(2 + t)$-edge-connected because that $G - Y$ is supereulerian only when $G - Y$ is 2-edge-connected. Before the proof of the theorem 3.1, we need the following lemma:

Lemma 3.2. G is a connected simple graph on n vertices. G' is the reduction of G. $V_5 = \{v \in V(G')|d_{G'}(v) < 5\}$. If $\delta(G) \geq 5$, then $|V_5| \leq 4$.

Proofs of Theorem 3.1 and Lemma 3.2 are omitted because of the length.

References

1. F. T. Boesch, C. Suffel, R. Tindell, The spanning subgraph of Eulerian graphs, J. Graph Theory 1(1977)79–84.
2. J. A. Bondy, U. S. R. Murty, Graph Theory with Applications, American Elsevier, Amsterdan, 1976.
3. P. A. Catlin, A reduction method to find spanning eulerian subgraphs, J. Graph Theory 12(1988)29–45.
4. P. A. Catlin, Supereulerian graphs: A survey, J. Graph Theory 16(1992)177–196.
5. P. A. Catlin, Z. Han, H. J. Lai, Graphs without spanned closed trails, Discrete Math. 160(1996)81–91.
6. Z. H. Chen, H. J. Lai, Supereulerian graphs and the Petersen graph II, ARS COM-BINAORIA 48(1998)271–282.
7. F. Jaeger, A note on sub-Eulerian graphs, J. Graph Theory 3(1979)91–93.
8. W. R. Pulleyblank, A note on graphs spanned by eulerian graphs, J. Graph Theory 3(1979)309–310.

On (s, t)-Supereulerian Locally Connected Graphs*

Lan Lei, Xiao-Min Li, and Bin Wang

The faculty of science, Chongqing Technology
and Business University, Chongqing, P.R. China 400067
leilan@ctbu.edu.cn

Abstract. For two integers $s \geq 0, t \geq 0$, a graph G is (s,t)-*supereulerian*, if $\forall X, Y \subset E(G)$, with $X \cap Y = \emptyset, |X| \leq s, |Y| \leq t$, G has a spanning eulerian subgraph H with $X \subset E(H)$ and $Y \cap E(H) = \emptyset$. We prove that if G is $(t+2)$-edge-connected and locally connected, then G is $(2,t)$-supereulerian, or G belongs to a well characterized class of graphs.

Keywords: (s,t)-supereulerian, Collapsible graph, Locally connected graphs, Reduction.

1 Introduction

Graphs in this note are simple and finite. We follow the notation of Bondy and Murty [2] unless otherwise stated. For a graph G, $O(G)$ denotes the set of all vertices of odd degree in G. A graph G with $O(G) = \emptyset$ is an *even graph*, and a connected even graph is an *eulerian graph*. A graph is *supereulerian* if it has a spanning eulerian subgraph. The collection of all supereulerian graphs will be denoted by SL. For a graph G with a subgraph H, the contraction G/H is the graph obtained from G by replacing H by a vertex v_H, such that the number of edges in G/H joining any $v \in V(G) - V(H)$ to v_H in G/H equals the number of edges joining v in G to H. v_H is *nontrivial* if $E(H) \neq \emptyset$. As in [2], the edge-connectivity and the minimum degree of G are denoted by $\kappa'(G)$ and $\delta(G)$. For an integer $i \geq 1$, define $D_i(G) = \{v \in V(G) | d_G(v) = i\}$. A vertex $v \in G$ is called a *locally connected* vertex if $G[N_G(v)]$ is connected. A graph is a locally connected if every $v \in G$ is a locally connected.

For two integers $s \geq 0$, $t \geq 0$, G is (s,t)-*supereulerian*, if $\forall X, Y \subset E(G)$, with $X \cap Y = \emptyset$, $|X| \leq s$, $|Y| \leq t$, G has a spanning eulerian subgraph H with $X \subset E(H)$ and $Y \cap E(H) = \emptyset$. Clearly, G is supereulerian if and only if G is $(0, 0)$-supereulerian. Since every supereulerian graph must be 2-edge-connected, it is necessary that any (s,t)-supereulerian graph must be $(t+2)$-edge-connected. We consider the problem of $s = 2$ and shall prove that if G is $(t+2)$-edge-connected and locally connected, then either G is $(2,t)$-supereulerian or G belongs to a well characterized class of graphs. In [3], Catlin proved the following.

---

* Research is supported in part by Natural Science Foundations of Chongqing municipality, China.

Theorem 1 (Catlin [3]). If G is connected and locally connected, then $G \in SL$.

The main purpose of this paper is to improve this theorem of Catlin on $(0,0)$-supereulerian graphs to $(2, t)$-supereulerian graphs.

2 Collapsible Graphs and Reduced Graphs

A graph is *collapsible* if for every set $R \subset V(G)$ with $|R|$ even, there is a spanning connected subgraph H_R of G, such that $O(H_R) = R$. Thus K_1 is both supereulerian and collapsible. Denote the family of collapsible graphs by CL. Let G be a collapsible graph and let $R = \emptyset$. Then by definition, G has a spanning connected subgraph H with $O(H) = \emptyset$, and so G is supereulerian. Therefore, we have $CL \subset SL$.

In [3], Catlin showed that every graph G has a unique collection of pairwise disjoint maximal collapsible subgraphs $H_1, H_2, ..., H_c$. The contraction of G obtained from G by contracting each H_i into a single vertex $(1 \le i \le c)$, is called the *reduction* of G. A graph is *reduced* if it is the reduction of some other graph.

Theorem 2 (Lai [9]). Let G be a 2-edge-connected triangle-free simple graph on $n > 30$ vertices, if $\delta(G) > \frac{n}{10}$, then $G \in SL$.

Theorem 3 (Catlin, Theorem 8 of [3]). Let H be a collapsible subgraph of a graph G, then $G \in SL$ if and only if $G/H \in SL$.

Let $F(G)$ denote the minimum number of extra edges that must be added to G so that the resulting graph has 2-edge-disjoint spainning trees.

Theorem 4 (Catlin, Han and Lai, Lemma 2.3 of [6]). If G is reduced with $|V(G)| \ge 3$, then $F(G) = 2|V(G)| - |E(G)| - 2$.

Theorem 5 (Catlin, Theorem 7 of [4], Catlin, Han and Lai, Theorem 1.3 of [6]). Let G be a connected reduced nontrivial graph. If $F(G) \le 1$, then $G \cong K_2$; if $F(G) \le 2$, then $G \in \{K_1, K_2, K_{2,t} \ (t \ge 1)\}$.

Theorem 6 (Caltin, Theorem 8 and Lemma 5 of [3]). If G is reduced, then G is simple and contains no K_3. Moreover, if $\kappa'(G) \ge 2$, then $\sum_{i=2}^{4} |D_i(G)| \ge 4$, and when $\sum_{i=2}^{4} |D_i(G)| = 4$, G must be eulerian.

3 Main Result

Let G be a graph and let $X \subset E(G)$. Define G_X to be the graph obtained from G by replacing each edge $e \in X$ with end u_e and v_e by a (u_e, v_e)-path P_e of length 2, where the internal vertex $w(e)$ of the path P_e is newly added. We call this process of replacing e by P_e an elementary subdivision of G on the edge e. Lemma 7 below follows from the definitions.

Lemma 7. Let G be a graph and let $X \subset E(G)$, $Y \subset E(G)$ with $X \cap Y = \emptyset$, then G has a spanning eulerian graph H such that $X \subset E(H)$ and $Y \cap E(H) = \emptyset$ if and only if $(G - Y)_X \in SL$.

Let G_0 be the reduction of $(G - Y)_X$. Let D_2^1 denote the set of those vertices of degree 2 newly created from subdividing edges of X, and let $D_2^2 = D_2(G_0) - D_2^1$. Let $d_2^1 = |D_2^1|$, $d_2^2 = |D_2(G_0)| - d_2^1$.

Lemma 8. Let G be $(t+2)$-edge-connected, then $d_2^2 \leq 2$.

Proof: Let $v \in D_2^2$ and the two edges incident with v in G_0 is an edge-cut in $(G - Y)_X$. Since G is $(t+2)$-edge-connected, so at least t edges incident with v are removed. Since in order to get three vertices that belong to D_2^2, at least $\frac{3}{2}t$ edges must be removed, by $|Y| \leq t$, $d_2^2 \leq 2$.

Lemma 9. (Catlin, Lemma 1 of [7]) $K_{3,3} - e$ is collapsible.

Theorem 10. Let $s \leq 2$ and $t \geq 0$ be two integers. G is a $(t+2)$-edge-connected locally connected graph on n vertices. For any $X, Y \subset E(G)$ with $X \cap Y = \emptyset$, $|X| \leq s$, $|Y| \leq t$, exactly one of the following holds:
  (i) G has a spanning eulerian graph H, such that $X \subset E(H)$ and $Y \cap E(H) = \emptyset$. (e.g. G is $(2,t)$-supereulerian).
  (ii) The reduction of $(G - Y)_X$ is a member of $\{K_1, K_2, K_{2,t} \ (t \geq 1)\}$.

Proof: Let G_0 be the reduction of $(G - Y)_X$. We consider these cases.

Case 1. $F(G_0) \geq 3$.

If $|V(G_0)| \geq 3$, then by Theorem 4, we have

$$F(G_0) = 2|V(G_0)| - |E(G_0)| - 2 \geq 3. \tag{1}$$

Let $d_j = |D_j(G_0)|, j = 1, 2, \cdots$. Since G is $(t+2)$-edge-connected, G_0 must be 2-edge-connected, and so

$$|V(G_0)| = \sum_{j \geq 2} d_j, \ 2|E(G_0)| = \sum_{j \geq 2} jd_j.$$

By (1)

$$4\sum_{j \geq 2} d_j - \sum_{j \geq 2} jd_j - 4 \geq 6.$$

By algebraic manipulation, we have,

$$2d_2 + d_3 - \sum_{j \geq 5}(j - 4)d_j - 10 \geq 0,$$

and so

$$2d_2^1 + 2d_2^2 + d_3 - \sum_{j \geq 5}(j - 4)d_j - 10 \geq 0.$$

As $s \leq 2$, we have

$$4 + 2d_2^2 + d_3 - \sum_{j \geq 5}(j-4)d_j - 10 = 2d_2^2 + d_3 - \sum_{j \geq 5}(j-4)d_j - 6 \geq 0. \quad (2)$$

For any $v \in D_2^2 \cup D_3$, by Lemma 8, we have $d_2^2 \leq 2$. By (2), $(d_2^2, d_3) \notin \{(2,1), (1,1), (1,2), (1,3)\}$. In the following we will proceed our proof by considering the possible values of t.

Subcase 1.1. $t \geq 3$.
Then, $|Y| = t \geq 3$. Take $v \in D_3$, as shown in the Lemma 8, the three edges incident with v is an edge-cut of $(G-Y)_X$. Since G is $(t+2)$-edge-connected, at least $t-1$ edges incident with v are removed. Since in order to get three vertices in D_3, at least $\frac{3}{2}(t-1)$ edges must be removed, by $|Y| \leq t$ and $\frac{3}{2}(t-1) \geq t$ while $t \geq 3$, $d_3 \leq 3$.

When $d_3 = 3$, at least $\frac{3}{2}(t-1)$ edges are removed. As $\frac{3}{2}(t-1) \geq t$ (the equal sign holds if and only if $t = 3$), we have $d_2^2 = 0$. By (2), it is a contradiction.
    Similarly, $d_3 = 2$ implies $d_2^2 \leq 1$. It contradicts to (2).
    If $d_3 = 1$, by Lemma 8, $d_2^2 \leq 2$, (2) can't hold.
    So, when $F(G_0) \geq 3$ and $\kappa'(G) \geq 5$, $|V(G_0)| \leq 2$. If $|V(G_0)| = 2$, G_0 is simple, and so we must have $G_0 \cong K_2$. So at least $t+1$ edges are removed. It contradicts to $|Y| \leq t$. Thus $|V(G_0)| = 1$, $G_0 \in SL$.

Subcase 1.2. $t = 2$.
Similarly, if $D_3 \geq 5$, then at least $\frac{5}{2}(t-1)$ edges must be removed, and so $2 = t \geq |Y| \geq \frac{5}{2}(t-1)$, contrary to the fact that $t = 2$. This shows that $d_3 \leq 4$.

If $d_3 = 2$, by (2), $d_2^2 \geq 2$. But by Lemma 8, when $d_2^2 = 2$, we must remove t edges in Y. This contradicts to $d_3 = 2$. So, $d_3 = 2$ is impossible.
    Similarly, if $d_3 = 3$, by (2), $d_2^2 \geq 2$. As the discussion above, that contradicts to $d_3 = 3$. Hence $d_3 = 3$ is impossible.
    Note that when $d_3 = 4$, $d_2^2 = 0$. And by (2), $d_2^2 \geq 1$, another contradiction. This shows that $d_3 = 4$ is impossible.
    As the shown in the Subcase 1.1, $|V(G_0)| = 1$, then $G_0 \in SL$.

Subcase 1.3. $t = 1$.
Since G is locally connected, and $\kappa'(G) \geq 3$, so any v in G, there is a path connecting its neibouring verties. Thus any v is in a triangle. By Theorem 6, G_0 has no K_3. So a locally connected graph will be reduced to K_1. Hence any $v \in D_3$, any e in $(G[N(v)])$ is either divided or removed. Thus when $s = 2, t = 1$, $d_3 = 2$, G_0 must be depicted as the graph in Figure 1.
    Clearly, this gragh is $(2,1)$-supereulerian.
    When $d_3 = 3$, since G is locally connected, G_0 must have $K_{3,3} - e$. This contradicts to Lemma 9. Thus $d_3 = 3$ is impossible.
    When $d_3 = 4$, by Lemma 9, G_0 has no $K_{3,3}$-e. So G_0 must be depicted as the graph in Figure 2. But $v_3 \in D_3$, the edge in $(G[N(v_3)])$ incident with a and
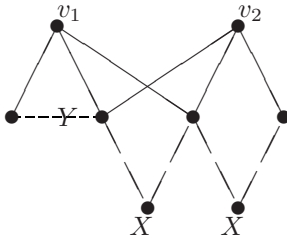
Fig. 1.
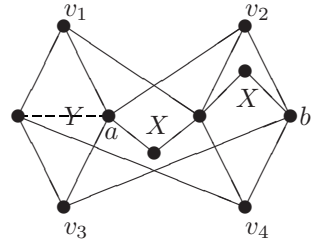
Fig. 2.

b can't be divided or removed. So, we get a contradiction. So $G_0 \in CL$, thus $G \in SL$.

If $d_3 > 4$, $K_{3,3} - e$ will appear. So, $d_3 \leq 4$.

Case 2. $F(G_0) \leq 2$.

By Theorem 5, $G_0 \in \{K_1, K_2, K_{2,t} \ (t \geq 1)\}$. This proves Theorem 10.

References

1. F. T. Boesch, C. Suffel, R. Tindell, The spanning subgraph of Eulerian graphs, J. Graph Theory 1 (1977) 79–84.
2. J. A. Bondy, U. S. R. Murty, Graph Theory with Applications, American Elsevier, Amsterdan, 1976.
3. P. A. Catlin, A reduction method to find spanning eulerian subgraphs, J. Graph Theory 12 (1988) 29–45.
4. P. A. Catlin, Supereulerian graphs: a survey, J. Graph Theory 16 (1992) 177–196.
5. P. A. Catlin, Suppereulian graphs, collapsible graphs and four-cycles, Congressus Numerantium, 58 (1987) 233–246.
6. P. A. Catlin, Z. Han, H.-J. Lai, Graphs without spanned closed trails, Discrete Math. 160 (1996) 81–91.
7. Z. H. Chen, H.-J. Lai, Supereulerian graphs and the Petersen graph, Ars Combinatoria 48 (1998) 271–282.
8. F. Jaeger, A note on sub-Eulerian graphs, J. Graph Theory 3 (1979) 91–93.
9. H.-J. Lai, Contractions and Hamiltonian line graphs, J. Graph Theory 1 (1988) 11-15.
10. H.-J. Lai, Eulerian subgraphs containing given edges, Discrete Math. 230 (2001) 63-69.

A Linear Algorithm for Edge-Face Coloring Series-Parallel Graphs[*]

Jian-Liang Wu[1] and Ping Wang[2]

[1] Department of Mathematics, Shandong University, Jinan, Shandong, P.R. China
`jlwu@math.sdu.edu.cn`
[2] Dept. of Math., Stats. and Computer Science, St. Francis Xavier University,
Antigonish, NS, Canada, B2G 2W5

Abstract. Let G be a series-parallel graph. In this paper, we present a linear algorithm of constructing an **oriented binary decomposition tree** of G. We use it to find 33 unavoidable subgraphs of G. Based on these 33 avoidable subgraphs, we can determine the edge-face chromatic number, denoted by $\chi_{ef}(G)$, of G where G is 2-connected and $\Delta(G) = 5$. This completes the literature of determining $\chi_{ef}(G)$ for 2-connected series-parallel graphs.

Keywords: edge-face coloring, decomposition tree, series-parallel graph.

1 Introduction

In this paper all graphs are simple, undirected and plane. A plane graph G is a particular drawing of a planar graph on the Euclidean plane. Let G be a plane graph with vertex set $V(G)$, edge set $E(G)$ and face set $F(G)$. An edge-face coloring of a plane graph G is a coloring of $E(G) \bigcup F(G)$ such that no two adjacent or incident elements receive the same color. A 2-*terminal simple series-parallel graph*, denoted by SP-**graph**, is a graph with two distinguished vertices (the terminals) that is obtained as follows:

Base case A single edge uv is a 2-terminal SP-graph with terminals u and v.
Recursive step Let G_1 be a SP-graph with source $u(G_1)$ and terminal $v(G_1)$, and let G_2 be a SP-graph with source $u(G_2)$ and terminal $v(G_2)$.
-A graph G obtained from G_1 and G_2 by identifying $v(G_1)$ and $u(G_2)$ is a SP-graph with source $u(G) = u(G_1)$ and terminal $v(G) = v(G_2)$. Such a connection is called *a series connection*.
-A graph G obtained from G_1 and G_2 by identifying $u(G_1)$ and $u(G_2)$ and $v(G_1)$ and $v(G_2)$ is a SP-graph with source $u(G) = u(G_1) = u(G_2)$ and terminal $v(G) = v(G_2) = v(G_2)$ where $u(G_1)v(G_1)$ and $u(G_2)v(G_2)$ can not be both edges simultaneously in G_1 and G_2. Such a connection is called *a parallel connection*. It is well-known that the following statements are equivalent if G is a 2-connected graph:

Figure 1-a   Figure 1-b   Figure 1- c
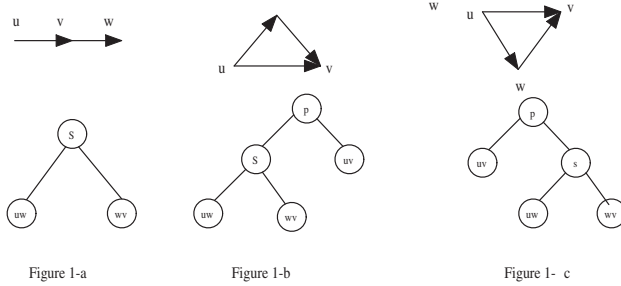
Fig. 1. Examples of series and parallel connections

(1) G does not contain K_4 as a minor;
(2) G is a 2-terminal SP-graph;
(3) G is a partial 2-tree.

The family of SP-graphs is a distinguished family of plane graphs which is particularly interesting to computer scientists. For example, the problem of determining chromatic index is NP-complete. On the other hand, for plane graphs G, it is not known whether determining $\chi'(G)$ is NP-hard. However, there is a linear algorithm to find $\chi'(G)$ if G is a series-parallel graph [12]. Fast algorithms have been found on the SP-graphs for min-max matching problem, Steiner subgraph and dominating set problems (see [3]). Graph theorists also use SP-graphs in an attempt to solve problems on plane graphs. For example, Seymour's conjecture on chromatic index, if G is a plane graph then $\chi'(G) = \max\{\Delta(G), \lceil \Gamma(G) \rceil \}$, was first proven on outerplane graphs, then on series-parallel graphs (see [5]) where $\Gamma(G) = \max\{\frac{2\bar{X}}{|X|-1} : X \subset V(G), |X| \geq 3$ and odd $\}$ and $\bar{X}$ denotes the set of edges with both ends in X.

In 1975, Mel'nikov [2] conjectured that $\Delta(G) \leq \chi_{ef}(G) \leq \Delta(G) + 3$ for any plane graph G. Waller [7] (independently by Sanders and Zhao [4]) proved the conjecture by using the Four Color Theorem. Wang and Lih [10] recently proved the conjecture without using the Four Color Theorem. Borodin [1] proved that for any plane graph G, $\chi_{ef}(G) \leq \max\{11, \Delta(G) + 1\}$. Wang [8] proved that for any outerplane graph G, $\chi_{ef}(G) \leq \max\{7, \Delta(G) + 1\}$ and $\chi_{ef}(G) = \Delta(G)$ if G is 2-connected and $\Delta(G) \geq 6$. In [9], Wang and Zhang further improved Wang's result and obtained the edge-face chromatic number of outerplane graphs with $\Delta(G) \geq 5$. Wu and Wang [11] extend the previous result to SP-graphs and proved that $\chi_{ef}(G) = \Delta(G)$ if G is a 2-connected SP-graph with $\Delta(G) \geq 6$. This result provides a better upper bound than the one in Borodin's result and encompasses a larger family of plane graphs than the one given by Wang and Zhang in [9]. In the following theorem, we will prove the remaining case where $\Delta(G) = 5$. This is the only case which is still open for these types of theorems in which $\chi_{ef}(G) = \Delta(G)$ with $\Delta(G) \geq c$ because of the following example. Let abc and xyz be two triangles. We form a new graph G by identifying vertices c and x and add a P_2 between a and z. Clearly, $\chi_{ef}(G) = 5$ and $\Delta(G) = 4$. In

fact, a family of graphs constructed similarly with any two odd cycles has the same property. This completes the literature of edge-face coloring of 2-connected SP-graphs.

Theorem 1. *If G is a 2-connected SP-graph, then $\chi_{ef}(G) = 5$ if $\Delta(G) = 5$.*

2   Subgraph Identification

It is well-known that a SP-graph G can be represented by a binary decomposition tree [6]. This technique has been used very successfully to design linear time algorithms to obtain different parameters of SP-graphs (see [12] [13]). In order to apply the binary decomposition tree technique successfully to the face coloring problem, we not only need to construct a binary decomposition tree to represent G but we also require this representation to provide further information about the allocation of faces with respect of its adjacent edges. In the following we shall use the left child and the right child of a node to distinguish whether a face is on the left side or the right side of a particular subgraph. Next we will define an oriented binary decomposition tree of G, denoted by T_O, according to the binary decomposition tree of G, denoted by T, where T is constructed by the algorithm provided by by Takamizawa et.al. in [6].

Lemma 1. *Let G be a 2-terminal SP-graph with terminals u and v. Then there exists an acyclic edge orientation of G such that u is the only source and v is the only terminal.*

This can be easily showed by using induction to the connection steps in the definition of a 2-terminal simple SP-graph. By Lemma 1, we can assign an acyclic edge orientation to G from the source to the sink of G. Let G_1 be a SP-graph with source $u(G_1)$ and terminal $v(G_1)$, and let G_2 be a SP-graph with source $u(G_2)$ and terminal $v(G_2)$. For any S node in the binary decomposition tree of T, we assign G_1 as its left child and G_2 as its right child in T_O if $v(G_1) = u(G_2)$. For example, Figure 1-a shows a binary decomposition tree which represents a series connection of two oriented edges. For any P node in the binary decomposition tree of T, we assign G_1 as its left child and G_2 as its right child in T_O if G_1 is on the left side of G_2 when facing from the source to the terminal in G_2. Otherwise we assign G_2 as its the left child and G_1 as its right child in T_O if G_1 is on the right side of G_2 when facing from the source to the terminal in G_2. For example, Figure 1-b and Figure 1-c show two binary decomposition trees which represent two possible parallel connections for the case where $G_1 = uv$ and $G_2 = uwv$.

Clearly, all internal nodes are either S or P nodes and all leaves are edges of G. We shall use a sequence SXY (PXY) to denote a subtree of T_O where X and Y are the left child and the right child of S (P) which can be either a subtree or a leaf ($e \in E(G)$). Since we have to color faces of G, PXY and PYX might be different. By the symmetry of subgraphs, most of SXY and SYX are the same.

Theorem 2. *Let G be a 2-connected SP-graph. Then G must contain at least one of the following 33 unavoidable subgraphs (see Figure 2).*
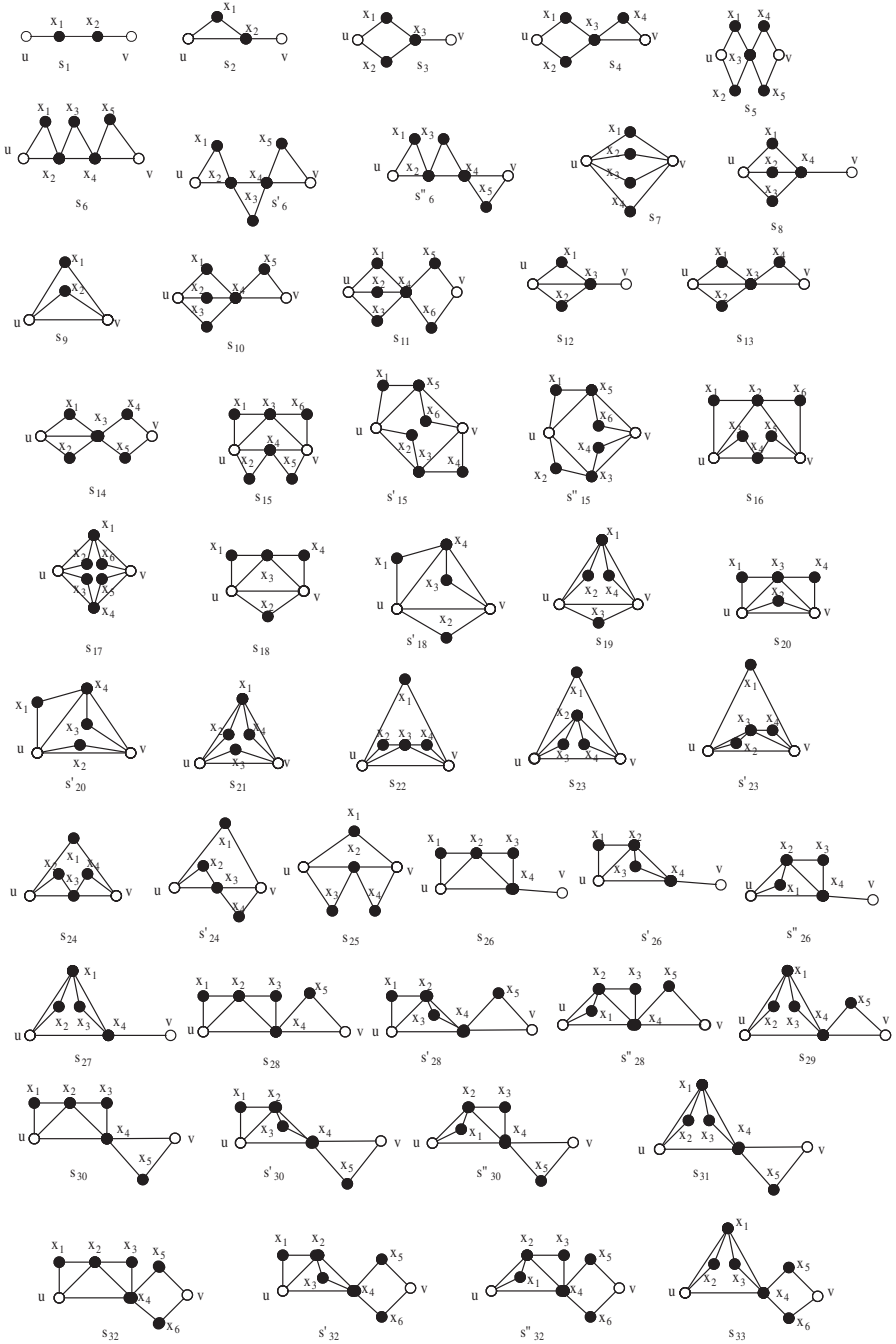
Fig. 2. 33 unavoidable subgraphs

Proof. Let $P\{t_k, t_{k-1}, ..., t_1, t_0\}$ be the longest path in T_O where $t_0 = e$ is a leaf node and t_k is the root node. Since G is a simple graph, the last internal node t_1 must be a S node. For convenience, let $A_0 = See$ (see Figure 3). In the following, we shall move up on the longest path P and find all the desired subgraphs. Since the nodes t_0 and t_1 have been discussed above, we shall start from t_i where $i \geq 2$ in the following cases.

Case 1. $i = 2$

If $t_2 = S$, then one of its two children of t_2 must be A_0 and the other can be either A_0 or a leaf node. In all three cases, s_1 is found. If $t_2 = P$, then there are three possible combinations and we call the three resulting subgraphs $A_1 = PA_0e$, $A'_1 = PeA_0$ and $A_2 = PA_0A_0$ (see Figure 3).
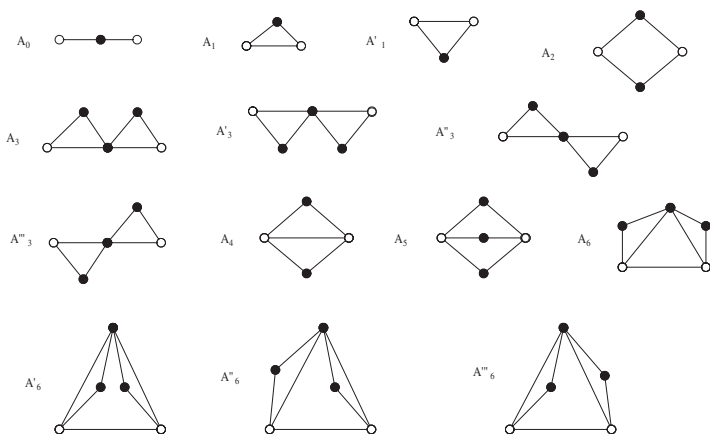
Fig. 3. A_i for $i = 1, 2, ..., 6$

Case 2. $i = 3$

One of the children of t_3 must be in $\{A_1, A'_1, A_2\}$.

Subcase 2.1. $t_3 = S$

SA_1A_2 and SA'_1A_2 leads $s_4 \subseteq G$. SA_1e leads to $s_2 \subseteq G$. SA_2e leads $s_3 \subseteq G$. Let $A_3 = SA_1A_1$, $A'_3 = A'_1A'_1$, $A''_3 = A_1A'_1$ and $A'''_3 = A'_1A_1$ (see Figure 3).

Subcase 2.2. $t_3 = P$

It is impossible to have PXY where X and $Y \subseteq \{e, A_1, A'_1\}$ because G is a simple graph. PeA_2, PA_2e, PA_1A_2, PA_2A_1, PA'_1A_2, $PA_2A'_1$, PA_0A_1 and PA'_1A_0 lead to $s_9 \subseteq G$. PA_2A_2 leads to $s_7 \subseteq G$. Let $A_4 = PA_0A'_1 = PA_1A_0$ and $A_5 = PA_0A_2 = PA_2A_0$ (see Figure 3).

Case 3. $i = 4$

One of the children of t_4 must be in $\{A_3, A'_3, A''_3, A'''_3, A_4, A_5\}$. Since $\Delta(G) = 5$, we will not consider the combinations of A_4 and A_4, A_4 and A_5, and, A_5 and A_5.

Subcase 3.1. $t_4 = S$

SXY leads to $s_2 \subseteq G$ if $X \in \{e, A_0\}$ and $Y \in \{A_3, A_3', A_3'', A_3'''\}$. SXY implies that one of $\{s_6, s_6', s_6''\}$ is a subgraph of G if $X \in \{A_1, A_1', A_3, A_3', A_3'', A_3'''\}$ and $Y \in \{A_3, A_3', A_3'', A_3'''\}$. SA_2Y leads to $s_4 \subseteq G$ if $Y \in \{A_3, A_3', A_3'', A_3'''\}$. SA_4Y leads to $s_{13} \subseteq G$ if $Y \in \{A_3, A_3'\}$. SA_5Y leads to $s_{10} \subseteq G$ if $Y \in \{A_3, A_3'\}$. SA_4Y leads to $s_{12} \subseteq G$ if $Y \in \{e, A_0\}$, to $s_{13} \subseteq G$ if $Y \in \{A_1, A_1'\}$, and to $s_{14} \subseteq G$ if $Y = A_2$. SA_5Y leads $s_8 \subseteq G$ if $Y \in \{e, A_0\}$, to $s_{10} \subseteq G$ if $Y \in \{A_1, A_1'\}$, and to $s_{11} \subseteq G$ if $Y = A_2$.

Subcase 3.2. $t_4 = P$

Let $A_6 = PA_3 e = PeA_3'$, $A_6' = PA_3' e = PeA_3$, $A_6'' = PA''e = PeA_3'''$ and $A_6''' = PA_3''' e = PeA_3''$ (see Figure 3). $PA_3 A_0$ and $PA_3' A_0$ lead to $s_{25} \subseteq G$. $PA_0 A_3$ and $PA_3' A_0$ lead to $s_{24} \subseteq G$. PXY and PYX lead to $s_{24}' \subseteq G$ if $X = A_0$ and $Y \in \{A_3', A_3'''\}$. $PA_3 A_1$ and $PA_1' A_3'$ lead to $s_{20} \subseteq G$, $PA_1 A_3$ and $PA_3' A_1'$ lead to $s_{19} \subseteq G$, $PA_3 A_1'$ and $PA_1 A_3'$ lead to $s_{18} \subseteq G$, and $PA_3' A_1$ and $PA_1' A_3$ lead to $s_{21} \subseteq G$. PXY and PYX lead to either $s_{18}' \subseteq G$ or $s_{20}' \subseteq G$ if $X \in \{A_1, A_1'\}$ and $Y \in \{A_3'', A_3'''\}$. PXA_2 and $PA_2 X$ lead to $s_4 \subseteq G$ if $X \in \{A_3, A_3', A_3'', A_3'''\}$. $PA_3 A_3$ and $PA_3' A_3'$ lead to $s_{16} \subseteq G$. $PA_3 A_3'$ leads to $s_{15} \subseteq G$. And $PA_3' A_3$ leads to $s_{17} \subseteq G$. $PA_3'' A_3''$ and $PA_3''' A_3'''$ lead to $s_{15}' \subseteq G$. $PA_3'' A_3'''$ and $PA_3''' A_3''$ lead to $s_{15}'' \subseteq G$. PXA_4 and $PA_4 X$ lead to either $s_{20} \subseteq G$ or $s_{21} \subseteq G$ if $X \in \{A_3, A_3'\}$. PXA_4 and $PA_4 X$ lead to $s_{20}' \subseteq G$ if $X \in \{A_3, A_3'\}$. PXA_5 and $PA_5 X$ lead to $s_{10} \subseteq G$ if $X \in \{A_3'', A_3'''\}$. It is impossible to have PXA_4 and $PA_4 X$ where $X \in \{e, A_1\}$ because G is a simple graph. $PA_4 A_2$ and $PA_2 A_4$ lead to $s_9 \subseteq G$. $PA_5 e$ and PeA_5 lead to $s_9 \subseteq G$. $PA_5 X$ and PXA_5 lead to $s_7 \subseteq G$ if $X \in \{A_0, A_2\}$. $PA_5 A_1$ and $PA_1' A_5$ lead to $s_7 \subseteq G$. $PA_5 A_1'$ and $PA_1 A_5$ lead to $s_9 \subseteq G$.

Case 4. $i = 5$

One of the children of t_5 must be in $\{A_6, A_6', A_6'', A_6'''\}$. Since $\Delta(G) = 5$, we will not consider the subtrees SXY, PXY and PYX where $X \in \{A_6, A_6', A_6'', A_6'''\}$ and $Y \in \{A_4, A_5, A_6, A_6', A_6'', A_6'''\}$.

Subcase 3.1. $t_5 = S$

$SA_6 Y$ leads to $s_{26} \subseteq G$ if $Y = \{e, A_0\}$, to either $s_{28} \subseteq G$ or $s_{30} \subseteq G$ if $Y \in \{A_1, A_1', A_3, A_3'\}$, and to $s_{32} \subseteq G$ if $Y = A_2$. $SA_6' Y$ leads to $s_{27} \subseteq G$ if $Y \in \{e, A_0\}$, to either $s_{29} \subseteq G$ or $s_{31} \subseteq G$ if $Y \in \{A_1, A_1', A_3, A_3'\}$, and to $s_{33} \subseteq G$ if $Y = A_2$. $SA_6'' Y$ and $SA_6''' Y$ lead to either $s_{26}' \subseteq G$ or $s_{26}'' \subseteq G$ if $Y \in \{e, A_0\}$, to either $s_{28}' \subseteq G$ or $s_{28}'' \subseteq G$ if $Y \in \{A_1, A_3\}$, to either $s_{30}' \subseteq G$ or $s_{30}'' \subseteq G$ if $Y \in \{A_1', A_3'\}$, and to either $s_{32}' \subseteq G$ or $s_{32}'' \subseteq G$ if $Y = A_2$.

Subcase 3.1. $t_5 = P$

Since G is a simple graph, we will not consider the subtrees PXY and PYX where $X \in \{A_6, A_6', A_6'', A_6'''\}$ and $Y \in \{e, A_1, A_1'\}$.

$PA_6 A_0$ and $PA_6 A_2$ lead to $s_{18} \subseteq G$. PXY and PYX lead to either $s_{28} \subseteq G$ or $s_{30} \subseteq G$ if $X = A_6$ and $Y \in \{A_3, A_3', A_3'', A_3'''\}$. $PA_0 A_6$ and $PA_2 A_6$ lead $s_{22} \subseteq G$. $PA_6' A_0$ and $PA_6' A_2$ lead to $s_{19} \subseteq G$. PXY and PYX lead to either $s_{29} \subseteq G$ or $s_{31} \subseteq G$ if $X = A_6'$ and $Y \in \{A_3, A_3', A_3'', A_3'''\}$. $PA_0 A_6'$ and $PA_2 A_6'$ lead to

$s_{23} \subseteq G$. PXY leads to $s'_{18} \subseteq G$ and PYX leads $s'_{23} \subseteq G$ if $X \in \{A''_6, A'''_6\}$ and $Y \in \{A_0, A_2\}$. PXY and PYX lead to either $s'_{30} \subseteq G$ or $s''_{30} \subseteq G$ if $X \in \{A''_6, A'''_6\}$ and $Y = A_3$, and to either $s'_{28} \subseteq G$ or $s''_{28} \subseteq G$ if $X\{A''_6, A'''_6\}$ and $Y = A'_3$. This completes the proof.

Since the algorithm we used to construct T given by Takamizawa et.al. in [6] is a linear algorithm in terms of $|E(G)|$ and we traverse T once to construct T_O. We may traverse the whole tree T_O once in the worst case to find one of the 33 unavoidable subgraphs in G. Therefore, one can find one of the 33 unavoidable subgraphs in G in $O(|E(G)|)$. This technique of constructing an oriented binary decomposition tree from any SP-graph can be applied to future research on the problems that are related to the faces and edges of any SP-graph. As an example, we will use it to prove Theorem 1 in the next section.

3   Proof of Theorem 1

Proof. We shall prove the theorem by induction on $|V(G)|+|E(G)|$. Clearly, the result is obvious if $|V(G)| \leq 4$. Let $G' \subset G$ and ϕ be an edge-face coloring of G' where $\phi : (EF(G)) \to C = \{1, 2, ..., 5\}$. We shall extend ϕ to an edge-face coloring σ of G with t colors. For convenience, we denote $T(v) = C\backslash\{\phi(vv') : v' \in N(v)\}$, the set of colors missing at vertex v. In Figure 2, let f denote the face on the left side of uv and f' denote the face on the right side of uv when facing from u to v, and, without loss of generality, let $\phi(f) = 1$ and $\phi(f') = 2$.

For s_1, let G' be the result graph by identifying vertices x_1 and x_2 in G. Then ϕ can be easily extend to G since $d(x_1) = d(x_2) = 2$ and $|C| \geq 5$. For s_2, let $G' = G\backslash\{x_1\}$ and $c_1 \in T(u)$. If $c_1 = 1$, then we assign $\sigma(ux_2) = 1, \sigma(ux_1) = 2, \sigma(vx_2) = \sigma(ux_1x_2) = 4$, and $\sigma(x_1x_2) = 5$. If $c_1 \neq 1$, we can assign $\sigma(ux_2) = 3$, $\sigma(vx_2) = 4$, $\sigma(ux_1) = c_1$; $\sigma(x_1x_2) = 2$ and $\sigma(ux_1x_2) = \{4, 5\} - c_1$ if $c1 \neq 2$ or $\sigma(x_1x_2) = 5$ and $\sigma(ux_1x_2) = 4$ if $c1 = 2$.

For s_3, let $G' = G\backslash\{x_1, x_2\} + ux_3$ and $c_1 \in T(u)$. If $c_1 = 1$, then we assign $\sigma(ux_2) = 1, \sigma(ux_1) = \sigma(x_2x_3) = 3$, $\sigma(vx_3) = \sigma(ux_1x_3x_2) = 4$ and $\sigma(x_1x_3) = 5$. If $c_1 \neq 1$, we can assign $\sigma(ux_1) = c_1$, $\sigma(x_2x_3) = 1$, $\sigma(ux_2) = \sigma(x_1x_3) = 3$, $\sigma(vx_3) = 4$ and $\sigma(ux_1x_3x_2) = \{4, 5\} - c_1$.

For s_4, let $G' = G\backslash\{x_1, x_2, x_4\} + ux_3$. Without lose of generality, we may assume that $\phi(ux_3) = 3$ and $\phi(x_3v) = 4$. Let $c_1 \in T(u)$ and $c_2 \in T(v)$. If $c_1 = c_2 = 1$, then we can assign $\sigma(ux_2) = \sigma(vx_3) = 1, \sigma(x_3x_4) = 2, \sigma(ux_1) = \sigma(x_2x_3) = 3, \sigma(vx_4) = \sigma(ux_1x_3x_2) = 4$, and $\sigma(vx_3x_4) = \sigma(x_1x_3) = 5$. Now consider the case where $c_1 = 1$ and $c_2 \neq 1$. We can assign $\sigma(ux_2) = 1$, $\sigma(ux_1) = \sigma(x_2x_3) = 3$, $\sigma(vx_3) = \sigma(ux_1x_3x_2) = 4$, $\sigma(vx_4) = c_2$; $\sigma(x_1x_3) = 2, \sigma(x_3x_4) = 5$ and $\sigma(vx_3x_4) = 3$ if $c_2 = 2$ or $\sigma(x_1x_3) = 5, \sigma(x_3x_4) = 2$ and $\sigma(vx_3x_4) = \{3, 5\} - c_2$. Note that the case where $c_1 \neq 1$ and $c_2 = 1$ can be solved similarly. Finally, we consider the case where $c_1 \neq 1$ and $c_2 \neq 1$. We assign $\sigma(ux_1) = c_1, \sigma(x_4v) = c_2, \sigma(ux_2) = \sigma(x_3x_1) = 3, \sigma(vx_3) = 4, \sigma(x_2x_3) = 1$, and $\sigma(ux_1x_3x_2) \in \{4, 5\}\backslash c_1$; $\sigma(x_3x_4) = 5, \sigma(vx_3x_4) = 3$ if $c_2 = 2$ or $\sigma(x_3x_4) = 2, \sigma(vx_3x_4) \in \{3, 5\}\backslash c_2$ if $c_2 \neq 2$.

The rest of proof is similar with these cases. We shall leave it on the following website www.stfx.ca\people\pwang\restproof.pdf.

Remarks. The process of coloring these 33 unavoidable subgraphs takes a constant time. Hence, one can color the edges and faces of G with 5 colors in $O(|E(G)|)$ time.

References

1. Borodin, O. V.: Simultaneous coloring of edges and faces of plane graphs. Discrete Math. 128 (1994) 21-33
2. Mel'nikov, L. S.: Problem in recent advances in graph theory. Proc. International Symposium, Prague, 1974, Academic Praha (1975) 543
3. Richey, M.B., Parker, R. G.: Minimum-maximal matching in series-parallel graphs. Euro. J. of Operation Research 33 (1987) 98-103
4. Sanders, D.P., Zhao, Y.: On simultaneous edge-face colorings of plane graphs. Combinatorica no. 3 17 (1997) 441–445
5. Seymour, P. D.: Colouring Series-Parallel graphs. Combinatoria 10(4) (1990) 379-392
6. Takamizawa, K., Nishizeki, T., Saite, N.: Linear-time computability of combinatorial probelms on series-aprallel graphs. J. Assoc. Comput. Mach. 29 No. 4 (1982) 1382-1389
7. Waller, A.O.: Simultaneously coloring the edges and faces of plane graphs. J. Combinatorial Theory, Series B 69 (1997) 219-221
8. Wang, W.F.: On the colorings of outerplane graphs. Discrete Math. 147 (1995) 257-269
9. Wang, W.F., Zhang, K.M.: Δ-matchings and edge-face chromatic numbers. (Chinese) Acta Math. Appl. Sinica 22(2) (1999) 236-242
10. Wang, W.F., Lih, K.W.: A new proof of Melnikov's conjecture on the edge-face coloring of plane graphs. Discrete Math. 253 (2002) 87-95
11. Wu, J.L., Wang, P.: Simutaneous coloring of edges and faces of series-parallel graphs. Adavnces in Mathematics, No.4, Vol.34 (2005) 461-467
12. Zhou, X., Suzuki, H., Nishizeki, T.: A Linear Algorithm for Edge-coloring Series-Parallel Multigraphs. J. of Algorithms 20 (1996) 174-201
13. Zhou, X., Nishizeki, T.: Multicoloring of Series-Parallel Graphs. Algorithmica 38 (2004) 271-294

Even Factors with Degree at Most Four in Claw-Free Graphs

Qiuxin Wu[1], Liming Xiong[2,*], and Tingzeng Wu[3]

[1] College of Science Beijing Institute of Machinery
Beijing 100085, P.R. China
qxwu@263.net
[2] Department of Mathematics, Beijing Institute of Technology
Beijing 100081, P.R. of China
lmxiong@eyou.com
[3] Department of Mathematics, Qinghai Nationalities College
Qinghai, 810007, P.R. China

Abstract. In this paper we will prove that every simple claw-free graph G with the minimum degree at least two such that each of its odd branch-bonds contains a branch of length one has an even factor of degree 2 or 4. Some examples showed the conclusion can not be replaced by "2-factor" even for 2-connected graphs.

Keywords: even factor, claw-free graph, branch-bond.

1   Introduction

All graphs considered in this paper are simple graphs. For the notations or terminologies not defined here, see [1].

A *factor* of a graph G is a spanning subgraph. A connected spanning subgraph is called a *connected factor*. A *even factor* of a graph G is a spanning subgraph of G such that it has only even positive degree vertices. A *2-factor* of a graph G is a spanning subgraph such that it has only degree 2 vertices. An even factor of G is called an *even* $[2,4]$-*factor* if the degree of every vertex is either 2 or 4. Clearly, a hamiltonian graph has a 2-factor with exactly one component. There are many results on the existence of the factors with some properties, for the connected factors, see the updated survey papers [5] and [6].

From the results of Choudum and Paulraj [2], and Egawa and Ota [3], one can deduce that every claw-free graph with minimum degree at least 4 has a 2-factor. Very recently, Yoshimoto show that the minimum degree can be reduced if we increase its connectivity.

Theorem 1. *(Yoshimoto, [11]) Every 2-connected claw-free graph G such that $\delta(G) \geq 3$ has a 2-factor.*

A nontrivial path is called a *branch* if it has only internal vertices of degree two and end vertices of degree not two. The *length of a branch* is the number of its edges. Note that a branch of length one has no internal vertex. A set $\mathcal{B}$ of branches of G is called a *branch cut* if the subgraph of G obtained from $G[E(G) \setminus \bigcup_{B \in \mathcal{B}} E(B)]$ by deleting all internal vertices in any branch of $\mathcal{B}$ has more components than G. A minimal branch cut is called a *branch-bond*. A branch-bond is called *odd* if it has an odd number of branches. The idea of branch-bond is from [9] which has also been applied in [4] and [10].

If G is a graph such that it has an odd branch-bond with a shortest branch of length 2, then clearly G has no even factor. However our result shows that every graph in which every branch-bond has a shortest branch of length one has an even factor.

Theorem 2. *Let G be a claw-free graph with $\delta(G) \geq 2$ such that every odd branch-bond of G contains a branch of length one. Then G has an even $[2, 4]$-factor.*

Let G_0 be the graph in Figure 1. Then G_0 has no 2-factor since the two vertices of degree 2 in the cycle of length 8 must be in the same cycle of a possible 2-factor but then the vertices of degree 2 having distance 2 must be in a component of maximum degree 4. Note that G_0 satisfies the condition of Theorem 2. This shows that Theorem 2 is best possible in a sense that the conclusion in Theorem 2 can not be replaced by "2-factor". Note that G_0 is 2-connected. This shows that Theorem 2 is best possible even if the graph is 2-connected.
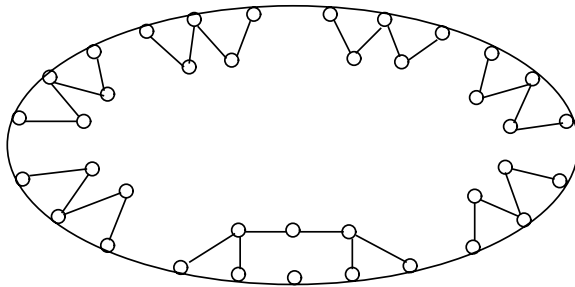
Fig. 1. The graph G_0

2   Proof of Theorem 2

We start with the following lemma which is a special case of a result in [8].

Lemma 3. *(Li and Xiong [8], Lai, Li, Shao and Xiong [7]) Let G be a claw-free graph. If G has a connected even factor H, then G has a connected even $[2, 4]$-factor.*

For subgraphs $H \subset F$, let $\text{Int}_F H = \{u \in V(H) \mid d_F(u) \neq 1\}$. A *circuit* is a connected graph with at least three vertices in which every vertex has even degree.

Proof of Theorem 2. Let G be a graph in Theorem 2. Then we have the following fact.

Claim 1. G has a set of vertex-disjoint circuits containing all branches of length not 1.

Proof of Claim 1. Let $C_1, C_2, \ldots, C_t$ be vertex-disjoint circuits in G such that $C = \bigcup_{i \leq t} C_i$ contains branches of length not equal to one as many as possible. Let $F = G - V(C)$, and suppose F contains a branch of G with length not one, say P. Hence P has no end-vertex of degree one in G. Since $\text{Int}_G(P) \subset V(F)$, $E(P) \subset E(G) \setminus E(C)$. Let T be a maximal tree such that $P \subset T$ and

if there is an edge e in $T \cap C$, then e is in a branch of G with length one. (2.1)

If we remove all edges and the internal vertices of P from T, then two trees T_1 and T_2 remain. Let $\mathcal{B}$ be a branch-bond of G joining T_1 and $G - V(T_1) \cup \text{Int}_P(P)$ in which P is one of branches.

We choose a branch B of G in $\mathcal{B}$ as follows. If $\mathcal{B} \setminus P$ has a branch of G which is edge-disjoint to C, then let B be the branch. In the case that $\mathcal{B} \setminus P$ has no such a branch, $\mathcal{B}$ is an odd branch-bond, and so $\mathcal{B}$ has a shortest branch of length one. We choose the shortest branch as B. Notice that if $E(B) \cap E(C) \neq \emptyset$, then B is a branch of length one. In either case, because of the maximality of T, B is joining T_1 and T_2, and so $T \cup B$ contains a cycle D. Then

$$C' = ((C \cup D) \setminus E(C \cap D)) - \text{Int}_{C \cap D}(C \cap D)$$

is a set of circuits. Because $P \subset C'$ and any vertex in $\text{Int}_{C \cap D}(C \cap D)$ is contained in a branch of length one by (2.1), the set C' of the circuits contains more branches of length not equal to one than C, a contradiction. This completes the proof of Claim 1.

By Claim 1, we can choose vertex-disjoint circuits $C_1, C_2, \cdots, C_k$ such that

1. $C = \bigcup_{i \leq k} C_i$ contains all edges in any branch of length not equal to one;
2. Subject to 1, $|V(C)|$ is maximal;
3. Subject to the above, k is as small as possible.

We claim that C is a spanning subgraph of G. First we claim that $G - C$ has no cycle for otherwise we will obtain a set of circuits contains bigger k after adding a cycle of $G - C$. Now it suffices to prove that C contains all vertices of G. We will prove this by contradiction. If possible, suppose that $x \in V(G) \setminus V(C)$. By Claim 1, $d_G(x) \geq 3$. Let y_1, y_2 and y_3 be three vertices in $N_G(x)$. Since G is claw-free, there exists an edge between two of $\{y_1, y_2, y_3\}$, say, $y_1 y_2 \in E(G)$.

We obtain a new C' from C by replacing y_1y_2 with y_1xy_2 if $y_1y_2 \in E(C)$ and by adding y_1y_2x otherwise. Note that C' satisfies 1. But C' contains more vertices than C, a contradiction.

Since G is claw-free, $G[C_i]$ is also claw-free. Note that it has an connected even factor C_i. By Lemma 3, $G[C_i]$ has a connected even $[2,4]$-factor. Hence G has an even factor with degree at most 4. This completes the proof of Theorem 2.

References

[1] J.A. Bondy and U.S.R. Murty, Graph Theory with Applications, American Elsevier (1976).

[2] S.A. Choudum and M.S. Paulraj, *Regular factors in $K_{1,3}$-free graphs*, J. Graph Theory **15** (1991) 259-265.

[3] Y. Egawa and K. Ota, *Regular factors in $K_{1,n}$-free graphs*, J. Graph Theory **15** (1991) 337-344.

[4] J. Fujisawa, L. Xiong, K. Yoshimoto and S. Zhang, *The upper bound of the number of cycles in a 2-factor of a line graph*, J. Graph Theory, 55 (2007) 72-82.

[5] R. Gould, *Advance on the hamiltonian problem-a survey*, Graphs and Combinatorics, **19** (2003) 7-52.

[6] M. Kouider and P.D. Vestergaard, Connected factors in graphs-a Survey, Graphs and Combinatorics, **21** (2005) 1-26.

[7] H.-J. Lai, M. Li, Y. Shao and L. Xiong, Spanning eulerian subgraphs in N^2-locally connected claw-free graphs, Ars Combinatoria, To appear.

[8] M. Li and L. Xiong, *Connected even factors in claw-free graphs*, Preprint, 2003.

[9] L. Xiong, H.J. Broersma, X. Li and M. Li, *The hamiltonian index of a graph and its branch-bonds*, Discrete Math. **285** (2004) 279-288.

[10] L. Xiong and M. Li, *On the 2-factor index of a graph*, Discrete Math.(2007), DOI:10.1016/j.disc.2006.11.012.

[11] K. Yoshimoto, On the number of components in 2-factors of claw-free graphs, Discrete Math. (2007) doi: 10.1016/j.disc.2006.11.022.

Finding the $(n, k, 0)$-Extendability in Bipartite Graphs and Its Application

Yueping Li and Dingjun Lou

Department of Computer Science, Sun Yat-sen University
Guangzhou 510275, P.R. China
maplezsu@gmail.com, issldj@sysu.edu.cn

Abstract. We study the problem of finding the $(n, k, 0)$-extendability in bipartite graphs. Let G be a graph with vertex set $V(G)$. Let n, k, d be non-negative integers such that $n + 2k + d \leq |V(G)| - 2$ and $|V(G)| - n - d$ is even. A matching which saturates exactly $|V(G)| - d$ vertices of G is called a *defect-d matching* of G. If when deleting any n vertices in $V(G)$ the remaining subgraph contains a matching of k edges and every k-matching can be extended to a defect-d matching, then G is said to be (n, k, d)-extendable. We present an algorithm to find the $(n, k, 0)$-extendability for bipartite graphs. This problem finds application in the circuit design of allocating jobs to processors while some jobs require specified machines to process and some machines are not available. In addition, the connectivity of $(n, k, 0)$-extendable graphs is also discussed.

Keywords: perfect matching, matching extendability, algorithms.

1 Introduction and Terminology

The graphs studied in this paper will be finite and simple. Let $G = (V, E)$ be a simple graph with vertex-set $V(G)$ and edge-set $E(G)$. A *matching* M is a subset of $E(G)$ of which the edges are disjoint. A vertex is said to be *saturated* with respect to a matching if it is covered by the matching and *unsaturated*, otherwise. The *cardinality* of matching is the number of edges it contains. A matching with k edges is called to be a k-matching. A matching is said to be *maximum* if its cardinality is the maximum in all matchings. Furthermore, a matching is called a *defect-d* matching if it it covers exactly $|V(G)| - d$ vertices of G. Let M be a matching of G. If there is a matching M' of G such that $M \subset M'$, then M' is called an *extension* of M.

Let G be a graph with at least $2k + 2$ vertices. If G has a k-matching and every k-matching is contained in a perfect matching, then G is said to be k-extendable.

The concept of extendability was introduced firstly by Heytei in 1964. The extendability of graphs plays an important role in the decomposition theory by means of maximum matchings. For the historic evolution and detailed results on extendability, we refer the reader to [5][6].

Let G be a graph with vertex set $V(G)$. Let n, k, d be non-negative integers such that $n + 2k + d \leq |V(G)| - 2$ and $|V(G)| - n - d$ is even. If when deleting

any n vertices in $V(G)$ the remaining subgraph contains a k-matching and every k-matching can be extended to a defect-d matching, then G is said to be an (n, k, d)-graph. The (n, k, d)-*extendability* is the maximum of value k_0 such that the graph G is a (n, k_0, d)-graph where n, d are constants.

The concept of (n, k, d)-graph was introduced by Liu and Yu [3]. And they gave a characterization of (n, k, d)-graphs and investigated several properties (such as connectivity, minimum degree, etc.).

It is straightforward that a bipartite graph cannot be (n, k, d)-extendable where $n > 0$. Thus, we amend the definition of (n, k, d)-graph with respect to bipartite graphs. Let $G = (U, W)$ be a bipartite graph with bipartitions U and W. Without loss of generality, suppose $|V(U)| \leq |V(W)|$. Let n, k, d be non-negative integers such that $n + k + d \leq |V(W)| - 1$ and $k \leq |V(U)| - 1$. If when removing any n vertices in $V(W)$ the remaining subgraph contains a k-matching and every k-matching can be extended to a defect-d matching, then G is said to be (n, k, d)-extendable.

For a vertex x, let $\Gamma(x)$ denote the set of vertices that are adjacent to x. A complete graph of order n is denoted by K_n. Therefore, K_1 stands for a vertex. And cK_1 denotes a graph which consists of c isolated vertices, where c is a natural number.

2 Preliminary Results

Lemma 1 (Plummer [7]). *Let k be an integer such that $0 < k < |V(G)|/2$. If G is k-extendable then it is $(k-1)$-extendable. And if G is a connected k-extendable graph, then G is $(k+1)$-connected.*

Corollary 1. *A graph G is k-extendable where $1 < k < |V(G)|/2$. For every $(k-1)$-matching M, $G - V(M)$ is 1-extendable.*

Lemma 2 (Liu, Yu [3]). *A graph G is an $(n, k, 0)$-graph if and only if for any $S \subset V(G)$ where $|S| = n$, $G - S$ is k-extendable.*

Let G be a bipartite graph with a perfect matching M. The vertices of G can be colored white and black such that no adjacent vertices has the same colors. An orientation is defined as follows: orient all edges of M from the white vertices to the black ones and orient the other edges of G from the black vertices to the white ones. The resulting directed graph is denoted by $\overrightarrow{G}(M)$.

Lemma 3 (Zhang, Zhang [8]). *Let G be a connected bipartite graph with a perfect matching M. Then G is 1-extendable if and only if $\overrightarrow{G}(M)$ is strongly connected.*

A general result is given in the following lemma.

Lemma 4 (Lakhal, Litzler [2]). *Let G be a connected bipartite graph with a perfect matching M. Then the extendability of G equals the strong connectivity of $\overrightarrow{G}(M)$.*

Independently, the equivalent result of Lemma 5 was given in [1][4].

3   Our Results

Theorem 1. *Let G be a graph which has a perfect matching. The graph G is k-extendable if and only if for every connected component H of G, one of the following propositions holds:*
(a) When $2k < |V(H)|$, H is a k-extendable graph.
(b) When $2k \geq |V(H)|$, H is a $(|V(H)|/2 - 1)$-extendable graph.

Proof. Necessity, first. Suppose G is a k-extendable graph. Let H be a connected component of G. Since G is k-extendable, there is a perfect matching of G (denoted by M). Furthermore, $M \bigcap E(H)$ is a perfect matching of H. Then, we have $|V(H)|$ is even.

If $2k < |V(H)|$, let M' be any k-matching of H. Since H has a perfect matching, the k-matching M' exists. And M' is also a k-matching of G. Then, there is a perfect matching of G containing M' (denoted by M_G), by the definition of k-extendability. We have $M_G \bigcap E(H)$ is perfect matching of H which contains M'. It follows.

If $2k \geq |V(H)|$, let M' be any $(|V(H)|/2 - 1)$-matching of H. Let $k' = |V(H)|/2 - 1$. Since H has a perfect matching, the k'-matching M' exists. We have $k' < k$, so G is k'-extendable, by Lemma 1. Furthermore, M' is also a k'-matching of G, there is a perfect matching of G containing M' (denoted by M_G), since G is k'-extendable. Then, $M_G \bigcap E(H)$ is perfect matching of H which contains M'. It follows.

Sufficiency. Let $H_1, H_2, \ldots, H_j$ be the connected components of G such that $G = H_1 \bigcup H_2 \bigcup \ldots \bigcup H_j$. Let M be a perfect matching of G, by the assumption.

Let M' be any k-matching of G. The existence of a k-matching can be concluded by the assumption. For every H_i where $1 \leq i \leq j$, we assign the perfect matching in H_i (denoted by M_i) as follows:

- If $M' \bigcap E(H_i) = \emptyset$, let $M_i = M \bigcap E(H_i)$;
- If $M' \bigcap E(H_i) \neq \emptyset$ and $|V(M' \bigcap E(H_i))| = |V(H_i)|$, let $M_i = M' \bigcap E(H_i)$;
- If $M' \bigcap E(H_i) \neq \emptyset$ and $|V(M' \bigcap E(H_i))| < |V(H_i)|$, let $k' = |M' \bigcap E(H_i)|$. Since H_i is k'-extendable, by the assumption, $M' \bigcap E(H_i)$ can be extended to a perfect matching of H_i. Let M_i be this perfect matching.

Finally, we have that $M_1 \bigcup M_2 \bigcup \ldots \bigcup M_j$ is a perfect matching of G which contains the k-matching M'. □

Different from k-extendable graphs, $(n, k, 0)$-graphs have high connectivity. The following theorem was given by Liu and Yu in [3]. Their proof does not cover all the situations. We complete the remained parts as follows:

Theorem 2. *Every connected $(n, k, 0)$-graph G is $(n + k + 1)$-connected where $k \geq 1$.*

Proof. Suppose G is not $(n + k + 1)$-connected. Let S be a cut set of G with minimum cardinality, then $|S| \leq n + k$.

If $|S| > n$, choose $S' \subset S$ such that $S' = n$. Then, by the Lemma 2. $G - S'$ is k-extendable graph. S' is not a cut set of G, by the minimum of S. Thus,

$G - S'$ is connected. Therefore, its connectivity is at least $k + 1$, by Lemma 1. But $S - S'$ is a cut set of $G - S'$ and $|S - S'| < k + 1$, a contradiction.

If $|S| = n$, let u be a vertex of S and H_1, H_2 be two connected components in $G - S$. Then, H_1 and H_2 have positive even order, by Lemma 2. Let v be a vertex adjacent with u in H_1. We choose any vertex of $H_1 - v$ (denoted by v'). $v' \bigcup \{S - u\}$ is a vertex set whose cardinality is n. Then $G - \{v' \bigcup \{S - u\}\}$ is k-extendable, by Lemma 2. Let H' be the connected component of $G - \{v' \bigcup \{S - u\}\}$ which v lies in. Since v and H_2 are adjacent with u, it can be concluded that u and H_2 lie in H'. Therefore, $|V(H')| \geq 4$. The connected component H' is at least 1-extendable, by Lemma 1 and Theorem 1. Thus, H' is 2-connected. It indicates that v and H_2 is connected in $H' - u$, a contradiction.
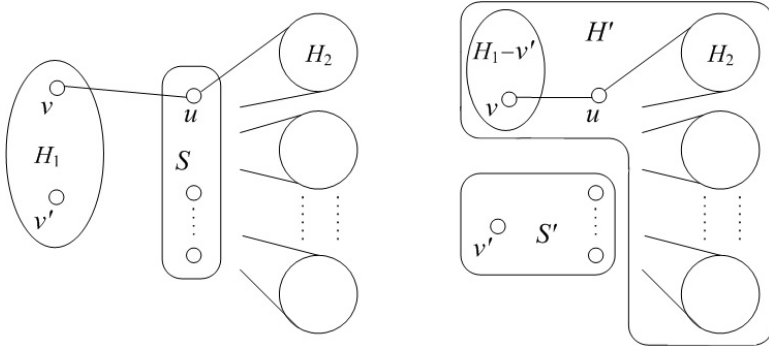
Fig. 1. The situation when $|S| = n$

If $|S| < n$, let H_1' be a connected components in $G - S$. Then, H_1' has positive even order, by Lemma 2. If $n - |S| \leq |V(G - S - H_1')|$, choose a set of vertices (denoted by S') such that S' consists of a vertex (denoted by v) in H_1' and $n - |S| - 1$ vertices in $G - S - H_1'$. Then, we have $|S \bigcup S'| = n$. Thus, $G - \{S \bigcup S'\}$ is k-extendable, by Lemma 2. But $H_1' - v$ is a connected components with odd order in $G - \{S \bigcup S'\}$, contradicting.

If $n - |S| > |V(G - S - H_1')|$, let H_2' be a connected components in $G - S$ such that H_2' is different from H_1'. Similarly, H_2' has positive even order. Furthermore, we have $n - |S| \geq |V(H_2')|$. Let S' be a set of vertices such that S' consists of $|V(H_2')| - 1$ vertices in H_2' and $n - |S| - (|V(H_2')| - 1)$ vertices in $G - S - H_2'$. Since $|S \bigcup S'| = n$, $G - \{S \bigcup S'\}$ is k-extendable, by Lemma 2. But $H_2' \setminus S'$ is a component which contains exactly one vertex in $G - \{S \bigcup S'\}$, contradicting. $\square$

Since the determination of k-extendability is highly efficient in bipartite graphs [2], our investigation arises from the problem: for bipartite graph, is there any relationship between $(n, k, 0)$-graphs and k-extendable graphs? We want to search a necessary and sufficient condition. If such condition exists, we could

obtain the $(n, k, 0)$-extendability by means of finding k-extendability. Moreover, how this operation can be done?

First, a necessary construction is given. For a bipartite graph $G = (U, W)$ where $|U| \leq |W|$. Let $n = |W| - |U|$. Add n isolated vertices (i.e. nK_1) into $V(U)$ and connect them with every vertex in $V(W)$. The resulting graph is denoted by $\widetilde{G}$.

Theorem 3. *Let $G = (U, W)$ be a connected bipartite graph where $|U| \leq |W|$. Let $n = |V(W)| - |V(U)|$. Then G is $(n, k, 0)$-extendable if and only if $\widetilde{G}$ is $(n + k)$-extendable where $0 < k < |V(W)| - n$.*

Proof. Let $m = |V(U)|$ and the new added vertices nK_1 in $\widetilde{G}$ be $v_1, v_2, \ldots, v_n$ (denoted by U').

Assume that G is $(n + k)$-extendable. Since G is connected, we have $\widetilde{G}$ is connected, according to the construction of $\widetilde{G}$. For any $S \subset V(W)$ with $|S| = n$ and any k-matching M of $G - S$, we need to show M can be extended to a perfect matching of $G - S$.

First, we point out that $G - S$ has a k-matching. Assume that $S = \{w_1, w_2, \ldots, w_n\}$. Then, the edges $\{(v_1, w_1), (v_2, w_2), \ldots, (v_n, w_n)\}$ is an n-matching (denoted by M_1) in $\widetilde{G}$, since $v_i \neq v_j$ and $w_i \neq w_j$ for any $i \neq j$ where $1 \leq i, j \leq n$. Then, the graph $\widetilde{G}$ is n-extendable, by Lemma 1. Thus, there is a perfect matching (denoted by M_2) of $\widetilde{G}$ containing M_1. Then, $M_2 - M_1$ is a perfect matching in $\widetilde{G} - V(M_1)$. It indicates that there is a perfect matching in $G - S$. Hence, $G - S$ has a k-matching where $0 < k < |V(W)| - n$.

Note that $M \bigcup M_1$ is an $(n + k)$-matching in $\widetilde{G}$. Similarly, there is a perfect matching (denoted by M') of $\widetilde{G}$ containing $M \bigcup M_1$. Then, $M' - M_1$ is a perfect matching in $G - S$ which contains the k-matching M. It follows.

Conversely, suppose that G is $(n, k, 0)$-extendable. First, we need to show that $\widetilde{G}$ has an $(n + k)$-matching. For any set $S' \subset V(W)$ such that $|S'| = n$, assume that $S' = \{w_1, w_2, \ldots, w_n\}$. Note that $G - S'$ has a k-matching (denoted by M_a), by the definition of $(n, k, 0)$-graph. Similarly, the edges $\{(v_1, w_1), (v_2, w_2), \ldots, (v_n, w_n)\}$ is an n-matching (denoted by M_b) in $\widetilde{G}$. Thus, $M_a \bigcup M_b$ is an $(n + k)$-matching of $\widetilde{G}$.

For any $(n + k)$-matching of $\widetilde{G}$ (denoted by $\widetilde{M}$), let $\widetilde{M_1} = \{(v'_1, w'_1), (v'_2, w'_2), \ldots, (v'_i, w'_i)\}$ be the matching edges in $\widetilde{M}$ which have an end-vertex in $V(U')$ where $1 \leq i \leq n$ and let $\widetilde{M_2} = \{(u_1, w_1), (u_2, w_2), \ldots, (u_j, w_j)\}$ be the matching edges in $\widetilde{M} - \widetilde{M_1}$. We have $i + j = n + k$. Let $S_1 = \{w'_1, w'_2, \ldots, w'_i, w_1, w_2, \ldots, w_{n-i}\}$. Since the graph G is $(n, k, 0)$-graph, $G - S_1$ is k-extendable. Furthermore, $\{(u_{n-i+1}, w_{n-i+1}), (u_{n-i+2}, w_{n-i+2}), \ldots, (u_j, w_j)\}$ is a k-matching in $G - S$ (denoted by $\widetilde{M_3}$). Hence, the matching $\widetilde{M_3}$ can be extended to a perfect matching of $G - S_1$ (denoted by $\widetilde{M'}$). Let $\{(u_1, w'_{i+1}), (u_2, w'_{i+2}), \ldots, (u_{n-i}, w'_n)\}$ be the matching edges in $\widetilde{M'}$ which have an end-vertex in $V(\widetilde{M_2})$. It can be concluded that $\{w'_{i+1}, w'_{i+2}, \ldots, w'_n\} \bigcap \{w_{n-i+1}, w_{n-i+2}, \ldots, w_j\} = \emptyset$; that is $\{w'_{i+1}, w'_{i+2}, \ldots, w'_n\} \bigcap V(\widetilde{M_3}) = \emptyset$.

Let $\{v'_{i+1}, v'_{i+2}, \ldots, v'_n\}$ be the vertices in $V(U')\backslash V(\widetilde{M_1})$. Finally, we can obtain a perfect matching which is $\{\widetilde{M'}\backslash\{(u_1, w'_{i+1}), (u_2, w'_{i+2}), \ldots, (u_{n-i}, w'_n)\}\}$ $\bigcup \{(v'_{i+1}, w'_{i+1}), (v'_{i+2}, w'_{i+2}), \ldots, (v_n, w'_n)\} \bigcup \widetilde{M}$. It is straightforward that the matching $\widetilde{M}$ is contained in this perfect matching. □

An example is illustrated in Figure 2. The wavy lines stand for the edges in $\widetilde{M}$. The solid lines shows the edges in $\widetilde{M'}$.
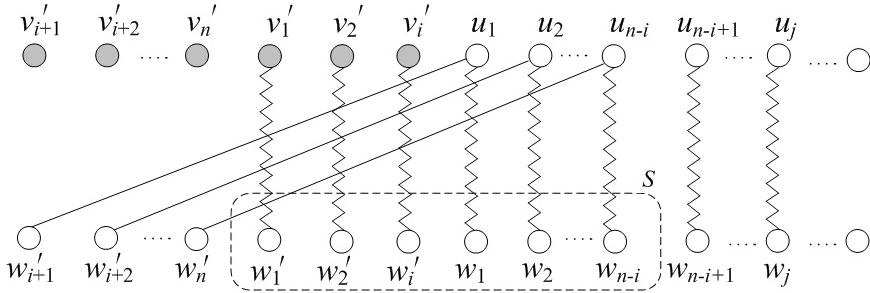
Fig. 2. An example displays the edge in $\widetilde{M}$ and $\widetilde{M'}$

The graphs we discuss in the following theorem are not necessary bipartite. To be different, denote a general graph by graph H. And we focus on the connected graphs. The results for not connected graphs can be obtained easily.

Theorem 4. *A connected graph H is k-extendable where $k < |V(H)|/2 - 1$. Add a new vertex u to $V(H)$ such that $\Gamma(u) \neq \emptyset$. The resulting graph, denoted by H', is $(0, k, 1)$-extendable.*

Proof. For any k-matching M in H', if M does not saturate the vertex u, then M is also a k-matching in H. Since H is k-extendable, M is contained in a perfect matching of H, denoted by M'. Furthermore, M' is a defect-1 matching in H', which just misses the vertex u. It follows in this situation.

If M covers the vertex u, let the matching edge be (u, v). H is $(k-1)$-extendable by Lemma 1. Since $M\backslash(u, v)$ is a $(k-1)$-matching in H, there is a perfect matching of H, denoted by M', containing $M\backslash(u, v)$. In M', let the matching edge covering v be (v, v'). We have $v' \neq u$. And $\{M'\backslash(v, v')\}\bigcup\{(u, v)\}$ is a defect-1 matching of H', which only misses the vertex v'. □

The following theorem can be proved by means of similar technique.

Theorem 5. *A connected graph H is k-extendable where $k < |V(H)|/2-1$. Add a set of vertices to $V(H)$ (denoted by S) such that $\Gamma(u) \neq \emptyset$, for every $u \in S$. The resulting graph is $(0, k, |S|)$-extendable.*

Theorem 5 implies that the connectivity of $(0, k, d)$-graphs can be very small where $d \geq 1$. Furthermore, the connectivity is independent from the value k.

Thus, we cannot construct a $(0, k, d)$-graph to obtain a k-extendable graph by means of similar method described in Theorem 3. We find that this property also holds for bipartite graphs.

4   Application

Since matching extension has many applications, our results will be useful. For example, we find that our results help to design the assignment circuit between channels and processing machines. Suppose there are c jobs coming from c parallel channels which demand simultaneous processing. The same as the classical job assignment, each job requires only a single machine for processing and every machine can serve only one job at the same time. We study the problem of checking whether the circuit supports the assignment when some jobs specifies some machines to operate. Different from the job scheduling problem, we consider assignment rather than scheduling. Moreover, our goal is verifying the circuit design instead of the minimization of the total processing time.
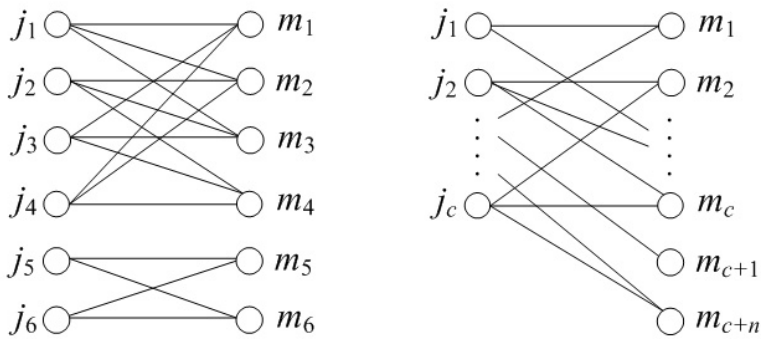
Fig. 3. Two examples

Denote a instance of the problem by a bipartite graph $G = (J, M)$ where $V(J) = \{j_1, j_2, \ldots, j_c\}$ are the jobs and $V(M) = \{m_1, m_2, \ldots, m_c\}$ are the machines. In addition, if one job can be assigned to the machine, i.e. a job can be processed by a machine, then there is an edge connecting them. It is straightforward that the k-extendability of G is the maximum number (denoted by k_0) such that when any k_0 jobs specify k_0 distinct machines to process, the other jobs can be assigned to the remaining machines. For instance, a 2-extendable graph is presented on the left side of Figure 3. Thus, when any two jobs require the desire distinct machines, the other jobs can find machines to process. Lakhal and Litzler [2] presented an algorithm to find the k-extendability of connected bipartite graphs. By Theorem 1, the improved algorithm for not connected bipartite graphs can be developed.

In order to obtain higher robusty, more machines are deployed such that the jobs can be processed even when some machines fail to work. Next, we focus

on this situation. Suppose there are n more machines of which an example is illustrated on the right side of Figure 3. Then, it is natural to determine the $(n, k, 0)$-extendability of the graph whose instance is the circuit. The algorithm is given as follows:

Input: A bipartite $G = (U, W)$
Output: k_0 /* the $(n, k, 0)$-extendability of G where $n = ||W| - |U||$
          $k_0 = 0$ means that G is not $(n, 1, 0)$-extendable */
1) Suppose $|U| < |W|$. Let $n = |W| - |U|$
2) Construct $\widetilde{G}$ by adding n new isolated vertices (denoted by S) to $V(U)$
   such that $\Gamma(u) = V(W)$, for every $u \in S$.
3) Find the extendability of $\widetilde{G}$ and store it in k'
4) if $k' > n$, then $k_0 = k' - n$; else $k_0 = 0$. endif

Step 1) and 4) require $O(1)$ time. Step 2) needs $O(|V|)$ time. Step 3) can be done in $O(|E| \cdot \min(k_0^3 + |V|, k_0|V|))$. The corresponding algorithm is presented in [2]. So our algorithm runs in $O(|E| \cdot \min(k_0^3 + |V|, k_0|V|))$ time. It is superior to the algorithm developed basing on the definition. The latter algorithm needs to enumerate n vertices in the partition $V(W)$, first. This enumeration demands $\frac{m!}{n!(m-n)!}$ time where $m = |V(G)|$. It is clear that the whole running time is even larger.

5   Conclusions

We investigate the property of not connected k-extendable graphs and the connectivity of $(n, k, 0)$-graphs. For bipartite graphs, a necessary and sufficient condition which illustrates the relation between $(n, k, 0)$-extendability and k-extendability is presented. Basing on the condition, we develop an algorithm to find the $(n, k, 0)$-extendability of bipartite graphs. Our result is applicable in many fields. For instance, it helps the design the circuit of the job assignment. However, we notice that our method does not work for the (n, k, d)-extendability where n, d are constants and $d > 0$. But we can determine $(0, 1, 1)$-extendable general graphs efficiently using similar technique which will be given in subsequent paper.

References

1. Aldred, R., Holton, D., Lou, D., Saito, A.: M-alternating Paths in n-extendable Bipartite Graphs. Discrete Math. **269** (2003) 1–11
2. Lakhal, J., Litzler, L.: A Polynomial Algorithm for the Extendability Problem in Bipartite Graphs. Information Processing Letters **65** (1998) 11–16
3. Liu, G., Yu, Q.: Generlization of Matching Extensions in Graphs. Discrete Math. **231** (2001) 311–320
4. Lou, D., Saito, A., Teng, L.: A Note on Internally Disjoint Alternating Paths in Bipartite Graphs. Discrete Math. **290** (2005) 105–108

5. Plummer, M.: Extending Matchings in Graphs: a Survey. Discrete Math. **127** (1994) 277–292
6. Plummer, M.: Extending Matchings in Graphs: an Update. Congr. Numer. **116** (1996) 3–32
7. Plummer, M.: On n-extendable Graphs. Discrete Math. **31** (1980) 201–210
8. Zhang, F., Zhang, H.: Construction for Bicritical Graphs and k-extendable Bipartite Graphs. Discrete Math. **306** (2006) 1415–1423

An Algorithm to Solve the Partition into Perfect Matchings Problem in Halin Graphs

Yunting Lu and Dingjun Lou

Department of Computer Science, Sun Yat-sen University
Guangzhou 510275, P.R. China
lu-yunting@163.com, issldj@sysu.edu.cn

Abstract. In this paper, we consider whether the vertices of graph G can be partitioned into K subsets V_1, V_2, ... V_K so that for each $i \in \{1,\dots,K\}$, the subgraph induced by V_i is a perfect matching where $K \leq |V|$. It is known that it is an NP complete problem in general graphs. In this paper, we restrict the problem in Halin graphs and give an algorithm to find the minimum value of K ($2 \leq K \leq 4$) in Halin graphs. The time complexity is $O(n)$.

Keywords: Halin Graph, Perfect matching, Algorithm.

1 Introduction and Terminology

Let M be a matching of graph G and $v \in V(G)$. If v is incident with an edge in M, v is called M-saturated. If every vertex of G is M-saturated, then M is a perfect matching of G. If edges in graph G share a common vertex or adjacent to a same edge, these edges are said to be connected. A perfect matching M in G is called k-colored if at least k colors are used to color the edges in M such that any two connected edges in M have different colors, and k is called the chromatic number of M. If the minimum chromatic number of all the perfect matchings in graph G is k, G is called k perfect matching colored (PMC).

A Halin graph $H = T \cup C$ is obtained by embedding a tree T having no nodes of degree 2 in the plane, and then add a cycle C to join the leaves of T in such a way that the resulting graph is planar. If T is a star, that is, a single vertex joining to the other vertices, then $H = T \cup C$ is called a wheel. Suppose T has at least two non-leaves. Let w be a non-leaf of T which is adjacent to only one non-leaf of T. Then the set of leaves of T adjacent to w, which we denote by $C(w)$, comprises a consecutive subsequence of the cycle C. We call the subgraph of H induced by $\{w\} \cup C(w)$ a fan and call w the center of the fan. An edge cutset of a connected graph $G = (V, E)$ is a set of edges whose removal leaves a disconnected graph. If it consists of exactly k edges, then we call it a k-edge cutset. Given a fan F of H, the three edges connecting $V(F)$ to $V(H - F)$ compose a 3-edge cutset of H. We denote the 3-edge cutset by $EC_3(F)$.

In the following sections, we use $H = T \cup C$ to denote a Halin graph and K to denote the minimum integer satisfying that $V(H)$ can be partitioned into K sets, say $V_1, ..., V_K$, such that $H[V_i]$ is a perfect matching for all $i \in \{1, \dots, K\}$.

2   Preliminary Results

Lemma 1. *The chromatic number of a planar graph is 4.*

3   Main Results

Theorem 1. *Let H and K be as defined as above. And H has even order. Then $2 \leq K \leq 4$.*

Proof. Halin graphs have hamilton cycles and if any node is deleted, the resulting graph still has a hamilton cycle [2]. So H has a perfect matching. Assume M is a perfect matching in H. Let H' be a graph by contracting each edges in M. Let $e(v)$ be the edge in M such that v is the vertex constructed in H' after contracting $e(v)$. Obviously H' is planar, so by Lemma 1, H' is 4-colored. Assume 1, 2, 3, 4 are the four colors used to color H', W_i are all the vertices in H' which are colored color i and $U_i = \{e(v): v \in W_i\}$ where $1 \leq i \leq 4$. Let $e(v_1)$ and $e(v_2)$ be any two edges in U_i, then v_1, $v_2 \in W_i$. Then $e(v_1)$ and $e(v_2)$ are not connected, otherwise v_1 and v_2 have different colors, contradicting v_1, $v_2 \in W_i$. So let $T_i=\{v: v \in V(e)$ and $e \in U_i\}$ where $1 \leq i \leq 4$ and then $H[T_i]$ is a matching in H. Since $\cup_{i=1}^{4}U_i = M$, then $\cup_{i=1}^{4}T_i = V(H)$. So $K \leq 4$. K can not be 1. So $2 \leq K \leq 4$.

Theorem 2. $K = k$ *if and only if H is k PMC.*

Proof. Suppose $K=k$. Assume H is k' PMC. Then the vertices of a Halin graph H can be partitioned into k subsets, say V_1, V_2, $\ldots$,V_k, such that the subgraph induced by V_i is a perfect matching, say M_i, where $1 \leq i \leq k$. So $M = M_1 \cup M_2\cup\ldots\cup M_k$ is a perfect matching in H. Obviously, M is k-colored because if edges in M_i are colored with a same color c_i where $1 \leq i \leq k$ and $c_x \neq c_y$ (if $x \neq y$ and $1 \leq x, y \leq k$), then no adjacent edges in M have a same color. So $k' \leq k$. Suppose $k' < k$. Then there is a perfect matching M' in H such that M' is k'-colored. Let M_i be all the edges in M that have one same color where $1 \leq i \leq k'$. Then $V(V_1)\cup V(V_2)\cup\ldots\cup V(V_{k'})=V(H)$, $H[V_1]=M_1$, $H[V_2]=M_2$ $\ldots$ and $H[V_{k'}]=M_{k'}$. The subgraph induced by V_i is a perfect matching, so $k \leq k'$. A contradiction with $k' < k$. That is $k' = k$, H is k PMC.

Now we prove sufficiency. If H is k PMC, then there exists a perfect matching, say M, such that M is k-colored. Let M_i are all edges in M that have one same color where $1 \leq i \leq k$. $V_1 = V(M_1)$, $V_2 = V(M_2)$ $\ldots$ and $V_k = V(M_k)$. Then $V(V_1) \cup V(V_2)\cup\ldots\cup V(V_k) = V(H)$. The subgraph induced by V_i is a perfect matching, so $K \leq k$. Suppose $K < k$, Then the vertices of a Halin graph H can be partitioned into K subsets, say V_1, V_2, $\ldots$, V_K, such that the subgraph induced by V_i is a perfect matching, say M_i, where $1 \leq i \leq K$. So $M = M_1\cup M_2\cup\ldots\cup M_K$ is a perfect matching in H. Hence M is K-colored, so $k \leq K$. A contradiction with $K < k$. That is $K = k$. So $K = k$ if and only if H is k PMC.

Since all the vertices in V_i are colored with the same colors, an edge coloring about the Halin graph H is obtained. It obeys that the colored edges must

cover all the vertices of H and if two edges are connected, they are colored with different colors. So we convert the problem to the edge coloring in Halin graphs.

4   Description of the Algorithm

Firstly we briefly describe the method of shrinking fan firstly appeared in [3]. Let F be a fan. We use $H \times F$ to denote the graph obtained from H by shrinking F to a new "pseudo-vertex", say v_F; that is, $V(H \times F) = \{v_F\} \cup \{V(H) \backslash V(F)\}$ and the edges of $H \times F$ are defined as follows:

1. An edge with both ends in F is deleted;
2. An edge with both ends in $H - F$ remains unchanged;
3. An edge with one end-vertex in $H - F$ and the other in F now joins the incident vertex of $H - F$ and v_F.

By Theorem 1, K is 2, 3 or 4. Firstly we check whether $K = 2$. If $K \neq 2$, check whether $K = 3$. If $K \neq 3$, $K = 4$. We discuss it in the following two cases.

4.1   Case 1: Check Whether $K = 2$

By Theorem 2, in order to check whether $K = 2$, we only need to check whether there is a perfect matching in H which is 2-colored. Let F be a fan of H, M be a perfect matching of H and $EC_3(F) = \{k, j, l\}$. Let $k = u_k v_k$, $j = u_j v_j$ and $l = u_l v_l$ such that $u_k, u_j, u_l \in V(F)$, $v_k, v_j, v_l \in V(H - F)$, $j, l \in C$ and the direction v_j, u_j, u_l, v_l is anti-clockwise in the cycle C.

Since M is a perfect matching of H, each vertex of H is saturated by M. If $k \in M$, we say the vertex u_k is externally saturated in F; otherwise, internally. The denotations are the same to u_j and u_l. Only the situation of $\{u_k, u_j, u_l\}$ affects the situation of $M \cap (H - F)$. In the following we use $Pos(v)$ to denote whether the vertex v is internally or externally colored where $Pos(v) \in \{externally, internally\}$, $Color(v)$ to denote which color vertex v is colored where $Color(v) \in \{c_1, c_2\}$, and $X(v)$ to denote the coloring state of vertex v. We define the following four situations respectively:

$X(v) = 1$ means $Pos(v) =$ internally and $Color(v) = c_1$;
$X(v) = 2$ means $Pos(v) =$ externally and $Color(v) = c_1$;
$X(v) = 3$ means $Pos(v) =$ internally and $Color(v) = c_2$;
$X(v) = 4$ means $Pos(v) =$ externally and $Color(v) = c_2$;

We use a triple $(X(u_k), X(u_j), X(u_l))$ to denote one situation of u_k, u_j, u_l. And $T(F)$ is a set of all the triples to F in all the colorings . After shrinking a fan F to a pseudo vertex v_F, we set $T(v_F) = T(F)$.

We regard an original vertex on the cycle C as a special fan. Let C be the cycle of H and u be an original vertex on C. Let $j = uv_j$, $l = uv_l$ and $k = uv_k$ such that $v_j, v_l \in V(C)$, $v_k \in V(H - C)$ and the direction of v_j, u, v_l is anti-clockwise in the cycle C. If $k \in M$, we say the vertex u is externally
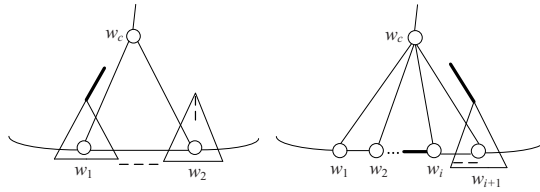
Fig. 1. Two examples of computing $T(PF_2)$ and $T(PF_i)$ (Thick lines are colored color c_1 and broken lines are colored color c_2)

saturated and use a triple $(X(u), 0, 0)$ where $X(u) = 2$ or 4 to denote a possible situation. If $j \in M$, we use a triple $(0, X(u), 0)$ to denote this situation. If $l \in M$, similarly. So for each leaf v in H, we relate v with a set of triples $T(v) = \{(2,0,0), (4,0,0), (0,2,0), (0,4,0), (0,0,2), (0,0,4)\}$.

Now we describe how to get all the triples in a certain fan F. Dynamic programming is used here. Let F be a fan of H. Let w_c be the center of F and $w_1, w_2 \ldots w_r$ be the vertices on the cycle C in anti-clockwise order. Each w_i $(1 \leq i \leq r)$ can be either an original vertex or a pseudo-vertex. We denote the induced subgraph $H[\{w_c, w_1, w_2, \ldots, w_k\}]$ by pseudo-fan PF_k of F $(2 \leq k \leq r)$. Note that if $w_c w_i \in M$ $(k + 1 \leq i \leq r)$, then vertex w_c is said to be externally saturated according to the pseudo-fan PF_k in M. Hence $T(PF_i)$ is a set of all the triples to the pseudo-fan PF_i. We calculate the situation of $k = 2$ first.

$T(PF_2) = \{t_1 \bullet s_1 | t_1 \bullet s_1 \neq NULL$ and $t_1 \in T(w_1)$ and $s_1 \in T(w_2)\}$.
Let $y, z \in \{1, 2, 3, 4\}$. $t_1 \bullet s_1 = NULL$ except the following situations:
$(2,y,1)\bullet(3,3,z)=(1,y,z)$, $(2,y,3)\bullet(3,1,z)=(1,y,z)$, $(2,y,2)\bullet(3,2,z)=(1,y,z)$
$(2,y,4)\bullet(3,4,z)=(1,y,z)$, $(3,y,1)\bullet(2,3,z)=(1,y,z)$, $(3,y,3)\bullet(2,1,z)=(1,y,z)$
$(3,y,2)\bullet(2,2,z)=(1,y,z)$, $(3,y,4)\bullet(2,4,z)=(1,y,z)$, $(2,0,0)\bullet(0,0,4)=(1,1,4)$
$(0,4,0)\bullet(2,0,0)=(1,4,1)$, $(2,0,0)\bullet(3,3,z)=(1,1,z)$, $(3,y,3)\bullet(2,0,0)=(1,y,1)$
$(3,y,1)\bullet(3,3,z)=(2,y,z)$, $(3,y,3)\bullet(3,1,z)=(2,y,z)$, $(3,y,2)\bullet(3,2,z)=(2,y,z)$
$(3,y,4)\bullet(3,4,z)=(2,y,z)$, $(0,4,0)\bullet(3,1,z)=(2,4,z)$, $(0,0,4)\bullet(3,4,z)=(2,3,z)$
$(3,y,1)\bullet(0,0,4)=(2,y,4)$, $(3,y,4)\bullet(0,4,0)=(2,y,3)$, $(0,0,4)\bullet(0,4,0)=(2,3,3)$
$(4,y,3)\bullet(1,1,z)=(3,y,z)$, $(4,y,1)\bullet(1,3,z)=(3,y,z)$, $(4,y,4)\bullet(1,4,z)=(3,y,z)$
$(4,y,2)\bullet(1,2,z)=(3,y,z)$, $(1,y,3)\bullet(4,1,z)=(3,y,z)$, $(1,y,1)\bullet(4,3,z)=(3,y,z)$
$(1,y,4)\bullet(4,4,z)=(3,y,z)$, $(1,y,2)\bullet(4,2,z)=(3,y,z)$, $(4,0,0)\bullet(0,0,2)=(3,3,2)$
$(0,2,0)\bullet(4,0,0)=(3,2,3)$, $(4,0,0)\bullet(1,1,z)=(3,3,z)$, $(1,y,1)\bullet(4,0,0)=(3,y,3)$
$(1,y,3)\bullet(1,1,z)=(4,y,z)$, $(1,y,1)\bullet(1,3,z)=(4,y,z)$, $(1,y,4)\bullet(1,4,z)=(4,y,z)$
$(1,y,2)\bullet(1,2,z)=(4,y,z)$, $(0,2,0)\bullet(1,3,z)=(4,2,z)$, $(0,0,2)\bullet(1,2,z)=(4,1,z)$
$(1,y,3)\bullet(0,0,2)=(4,y,2)$, $(1,y,2)\bullet(0,2,0)=(4,y,1)$, $(0,0,2)\bullet(0,2,0)=(4,1,1)$

Suppose w_1, w_2 are pseudo vertices. Let u_c (the center), $u_1, u_2 \ldots u_r$ be all the vertices in H after restoring the pseudo vertex in w_1 and u'_c (the center), $u'_1, u'_2 \ldots u'_r$ be all the vertices in H after restoring the pseudo vertex in w_2. If $(X(u_c), X(u_1), X(u_r)) = (2, y, 4)$ and $(X(u'_c), X(u'_1), X(u'_r)) = (3, 4, z)$, then

the triple $(X(w_c), X(w_1), X(w_2))$ in $T(PF_2)$ equals $(1, y, z)$, that is $(2, y, 4)\bullet(3, 4, z) = (1, y, z)$. See Fig.1 (The left).

Once we have the set $T(PF_i)$, we can calculate $T(PF_{i+1})$.

$T(PF_{i+1}) = \{t_1 \bullet s_1|\ t_1 \bullet s_1 \neq NULL$ and $t_1 \in T(PF_i)$ and $s_1 \in T(w_{i+1})\}$ $(2\leq i \leq r$-1$)$, Similarly, we present the formulas to the calculation as following:

$t_1 \bullet s_1 = NULL$ except the following situations:
(1,y,1)$\bullet$(3,3,z)=(1,y,z), (1,y,3)$\bullet$(3,1,z)=(1,y,z), (1,y,2)$\bullet$(3,2,z)=(1,y,z)
(1,y,4)$\bullet$(3,4,z)=(1,y,z), (1,y,1)$\bullet$(0,0,4)=(1,y,4), (1,y,4)$\bullet$(0,4,0)=(1,y,3)
(3,y,3)$\bullet$(1,1,z)=(3,y,z), (3,y,1)$\bullet$(1,3,z)=(3,y,z), (3,y,4)$\bullet$(1,4,z)=(3,y,z)
(3,y,2)$\bullet$(1,2,z)=(3,y,z), (3,y,3)$\bullet$(0,0,2)=(3,y,2), (3,y,2)$\bullet$(0,2,0)=(3,y,1)
(2,y,1)$\bullet$(2,3,z)=(1,y,z), (2,y,3)$\bullet$(2,1,z)=(1,y,z), (2,y,2)$\bullet$(2,2,z)=(1,y,z)
(2,y,4)$\bullet$(2,4,z)=(1,y,z), (2,y,3)$\bullet$(2,0,0)=(1,y,1)
(4,y,3)$\bullet$(4,1,z)=(3,y,z), (4,y,1)$\bullet$(4,3,z)=(3,y,z), (4,y,4)$\bullet$(4,4,z)=(3,y,z)
(4,y,2)$\bullet$(4,2,z)=(3,y,z), (4,y,1)$\bullet$(4,0,0)=(3,y,3)
(2,y,1)$\bullet$(3,3,z)=(2,y,z), (2,y,3)$\bullet$(3,1,z)=(2,y,z), (2,y,2)$\bullet$(3,2,z)=(2,y,z)
(2,y,4)$\bullet$(3,4,z)=(2,y,z), (2,y,1)$\bullet$(0,0,4)=(2,y,4), (2,y,4)$\bullet$(0,4,0)=(2,y,3)
(4,y,3)$\bullet$(1,1,z)=(4,y,z), (4,y,1)$\bullet$(1,3,z)=(4,y,z), (4,y,4)$\bullet$(1,4,z)=(4,y,z)
(4,y,2)$\bullet$(1,2,z)=(4,y,z), (4,y,3)$\bullet$(0,0,2)=(4,y,2), (4,y,2)$\bullet$(0,2,0)=(4,y,3)
Once the set $T(PF_r)$ is obtained, we can calculate $T(F) = T(PF_r)$.

Suppose w_{i+1} is a pseudo vertex. Let u_c (the center), $u_1, u_2 \ldots u_r$ be all the vertices in H after restoring the pseudo vertex in w_{i+1}. If one triple in $T(PF_i)$ is $(X(w_c), X(w_1), X(w_i)) = (2, y, 1)$ and $(X(u_c), X(u_1), X(u_r)) = (2, 3, z)$, then the triple $(X(w_c), X(w_1), X(w_{i+1}))$ in $T(PF_{i+1})$ equals $(1, y, z)$, that is $(2, y, 1)\bullet(2, 3, z) = (1, y, z)$. See Fig.1 (The right).

Firstly, our algorithm picks a non-leaf vertex r as the root of T such that r is adjacent to a leaf f of T and perform a postorder scan of T. When a vertex is scanned there are three possibilities: (I) v is a leaf, it is simply bypassed, (II) v is a non-leaf different from r, v and all its children constitute a fan F. We shrink F to v_F and get $T(F)$. Let $T(v_F) = T(F)$, (III) $v = r$, then H has been reduced to a wheel. Let $F \equiv H - f$. We consider F as a fan and shrink F to a pseudo vertex r' and get $T(r') = T(PF_{k-1})$, then H is reduced to a graph as Fig.2.
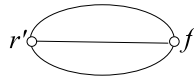
Fig. 2. The graph after shrinking all fans in H

$T(r')$ and $T(f)$ can match if and only if there is a triple (x, y, z) in $T(r')$ and a triple (x', y', z') in $T(f)$ such that they can match in a legal 2 coloring, that is, they satisfy the following conditions:
  (1) If $x' = 2$, then $x = 2, y = z = 3$ else if $x' = 4$, $x = 4, y = z = 1$.
  (2) If $y' = 2$, then $z = 2, x = y = 3$ else if $y' = 4$, $z = 4, x = y = 1$.
  (3) If $z' = 2$, then $y = 2, x = z = 3$ else if $z' = 4$, $y = 4, x = z = 1$.

Theorem 3. *Let r' be the vertex after applying the shrinking operations on fans in H recursively and $T(r')$, $T(f)$ as defined above. Then $T(r')$ and $T(f)$ can match if and only if H is 2 PMC.*

Proof. To prove this theorem, it is sufficient to prove the following claim.

Claim. Let H be a Halin graph and F be a fan in H. Let w_c be the center of F and let $w_1, w_2 \ldots w_r$ for $r \geq 2$ be the vertices of F belong to C. $T(PF_i)$ includes all the possible triples in a pseudo fan PF_i where $2 \leq i \leq r$.

Proof. It is sufficient to prove $T(PF_i)$ includes all the possible triples in a pseudo fan PF_i where $2 \leq i \leq r$. We use induction on i.
(1)When $i = 2$, the table $T(PF_2)$ includes all the possible triples according to $T(w_1)$ and $T(w_2)$.
(2)When $i < m$, suppose Claim holds.
(3)When $i = m$, suppose $T(PF_i)$ does not include all the possible triples, that is there exits one triple $(X(w_c), X(w_1), X(w_i))$ is not in $T(PF_i)$, but $(X(w_c), X(w_1), X(w_i))$ is one situation of w_c, w_1, w_i in a fan PF_i actually.
(3.1) If w_i is an original vertex
(3.1.1) $(x, 0, 0) \in T(w_i)$, $x \in \{2, 4\}$.
    By the structure of $T(PF_{m-1})$, we know it must include the triple $(X(w_c)'$, $X(w_1), X(w_{i-1}))$ such that $X(w_{i-1})$ MOD $2 = 1$, $X(w_{i-1}) \neq X(w_i)$, $X(w_c)' = x$ and $X(w_c)' = X(w_i) + 1$. Then after $(X(w_c)', X(w_1), X(w_{i-1}))\bullet(x, 0, 0)$ we can get the triple $(X(w_c), X(w_1), X(w_i))$ in $T(PF_i)$. A contradiction.
(3.1.2) $(0, y, 0) \in T(w_i)$, $y \in \{2, 4\}$. Similarly.
(3.1.3) $(0, 0, z) \in T(w_i)$, $z \in \{2, 4\}$. Similarly.
(3.2) If w_i is a pseudo-vertex. Suppose we get w_i after shrinking F, let v_0 be the center of F and $v_1, v_2 \ldots v_m$ be the vertices on the cycle C in that order. $\forall$ $(x, y, z) \in T(w_i)$, (x, y, z) is equal to $(X(v_0), X(v_1), X(v_m))$,$x, y, z \in \{1, 2, 3, 4\}$
(3.2.1) If $Pos(v_0) =$ externally and $Pos(v_1) =$ externally
    By the structure of $T(PF_{m-1})$, it must include one triple $(X(w_c)', X(w_1), X(w_{i-1}))$ such that $X(w_c)' = X(w_c) + 1 = X(v_0)$ and $X(w_{i-1}) = X(v_1)$. Then after $(X(w_c)', X(w_1), X(w_{i-1}))\bullet(x, y, z)$ we can get the triple $(X(w_c), X(w_1), X(w_i))$ in $T(PF_i)$. A contradiction.
(3.2.2) If $Pos(v_0) =$ externally and $Pos(v_1) =$ internally. Similarly.
(3.2.3) If $Pos(v_0) =$ internally and $Pos(v_1) =$ externally. Similarly.
(3.2.4) If $Pos(v_0) =$ internally and $Pos(v_1) =$ internally. Similarly.
    So when $i = m$, $T(PF_i) = T(F)$ includes all the possible triples.

After applying shrinking operations recursively, H is reduced to the graph in Fig.2. Let $V_1 = \{$all vertices in H after restoring each pseudo vertex in $r'\}$, $V_2 = \{f\}$, $\{e_1, e_2, e_3\}$ are the three edges joining V_1 to V_2, H_1 and H_2 are subgraphs constructed by adding $\{e_1, e_2, e_3\}$ to subgraphs $H[V_1]$ and $H[V_2]$ respectively. Then each $t \in T(r')$ corresponds a legal 2 coloring of a matching in H_1 covering all the vertices in V_1 and so does each $s \in T(f)$. By Claim, $T(r')$ contains all the possible coloring situations in H_1 and $T(f)$ contains all the possible coloring situations in H_2. Then by definition $T(r')$ and $T(f)$ can match if and only if

there exists a triple t in $T(r')$ and a triple s in $T(f)$ such that the coloring in H_1 that t corresponds and the coloring in H_2 that s corresponds can match together in a legal 2 coloring of H. So if $T(r')$ and $T(f)$ can match, H is 2 PMC.

Now we prove sufficiency. Suppose H is 2 PMC, there must exist C which is a legal 2 coloring of H. C contains a legal 2-coloring C_1 of H_1 and a legal 2-coloring C_2 of H_2. By Claim, C_1 corresponds a triple t in $T(r')$ and C_2 corresponds a triple s in $T(f)$. Hence t and s can match together in a legal 2 perfect matching coloring of H. By definition, $T(r')$ and $T(f)$ can match. Thus the Theorem holds.

4.2   Case 2: Check Whether $K=3$

Similar to Case 1.

5   Procedure of the Algorithm

Algorithm to Solve the partition into Perfect Matchings problem in Halin Graphs $K(H)$
1. Choose a non-leaf vertex of T, denoted by v_{root}, such that v_{root} is adjacent to a leaf of T, denoted by v_{leaf}.
2. Perform a postorder scan of T, for each fan F has been found do
3. If the centre of $F \neq v_{root}$ then
    begin
      calculate $T(F)$ as Case 1, shrink F to v_F, let $T(v_F) = T(F)$;
    end
Let H_w be the wheel we finally get and k be the edge joining v_{root} and v_{leaf}.
Let j, l be the two edges in C adjacent to v_{leaf} such that the direction of j, v_{leaf}, l is anti-clockwise. Let $F_w \equiv H_w - v_{leaf}$.
4. Calculate the set $T(F_w)$.
5. Shrink the fan F_w to the pseudo-vertex v_w, let $T(v_w) = T(F_w)$.
6. If $T(v_w)$ and $T(v_{leaf})$ can match.
7. return $K = 2$
8. else
9. Perform a postorder scan of T, for each fan F has been found do
10. If the centre of $F \neq v_{root}$ then
    begin
      calculate $T(F)$ as Case 2, shrink F to v_F, let $T(v_F) = T(F)$;
    end
Let H_w be the wheel we finally get and k be the edge joining v_{root} and v_{leaf}.
Let j, l be the two edges in C adjacent to v_{leaf} such that the direction of j, v_{leaf}, l is anti-clockwise. Let $F_w \equiv H_w - v_{leaf}$.
11. Calculate the set $T(F_w)$.
12. Shrink the fan F_w to the pseudo-vertex v_w, let $T(v_w) = T(F_w)$.
13. If $T(v_w)$ and $T(v_{leaf})$ can match.
14. return $K = 3$
15. else
16. return $K = 4$
17. end
18. end

6   An Example

We apply the algorithm to a given Halin graph. Illustrated in Fig.3. $v_{root} = a$. (2,3,3) in $T(a')$ and (2,0,0) in $T(l)$ can match, so $K = 2$.

T(PF₂)	T(e)	T(PF₃)
(4,1,1)	(4,0,0)	(3,1,3)
(2,3,3)	(2,0,0)	(1,3,1)
(3,3,2)	(0,2,0)	(3,3,1)
(1,1,4)	(0,4,0)	(1,1,3)
(1,4,1)	(0,0,4)	(1,4,4)
(3,2,3)	(0,0,2)	(3,2,2)

T(PF₂)	T(k)	T(PF₃)
(4,1,1)	(4,0,0)	(3,1,3)
(2,3,3)	(2,0,0)	(1,3,1)
(3,3,2)	(0,2,0)	(3,3,1)
(1,1,4)	(0,4,0)	(1,1,3)
(1,4,1)	(0,0,4)	(1,4,4)
(3,2,3)	(0,0,2)	(3,2,2)

T(f)	T(i')	T(PF₂)
(0,2,0)	(1,3,1)	(4,2,1)
(0,4,0)	(3,1,3)	(2,4,3)
(0,0,2)	(1,4,4)	
(0,0,4)	(3,2,2)	
(2,0,0)	(3,3,1)	(1,1,1)
(4,0,0)	(1,1,3)	(3,3,3)

T(a')	T(l)
(2,3,3)	(0,2,0)
(4,1,1)	(4,0,0)
	(2,0,0)
	(0,4,0)
	(0,0,2)
	(0,0,4)

T(b')	T(g')	T(PF₂)
(3,3,1)	(3,3,3)	(2,3,3)
(1,1,3)	(1,1,1)	(4,1,1)
(3,2,2)	(4,2,1)	
(1,4,4)	(2,4,3)	
(1,3,1)		
(3,1,3)		
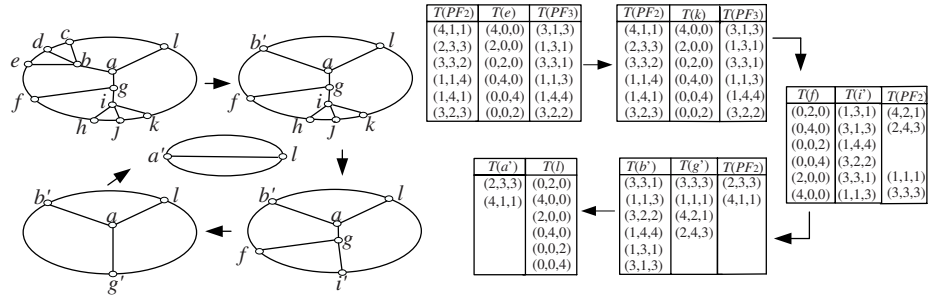
Fig. 3. The procedure of the calculation

7   The Correctness and the Time Complexity

Theorem 4. *The algorithm $K(H)$ returns K.*

Proof. The algorithm firstly checks whether K equals 2. In step 2), it finds a fan F. In step 3), it returns all the possible triples to F by Theorem 3. After applying shrinking operations repeatedly, H is reduced to a graph as Fig.2. In the algorithm, if $T(r')$ and $T(f)$ can match, it returns 2. So it returns the right K by Theorem 3. If they cannot match, the algorithm checks whether K equals 3 from 9)-14). Similar to Case 1, if $T(r')$ and $T(f)$ can match, it returns 3. Otherwise, $K(H)$ returns 4.

In the algorithm, step 1) needs $O(1)$ time. Step 3) is the operation of shrinking fans in H. If a fan F contains $r+1$ vertices, then it is verified that the time of the shrinking operation is $O(r)$. Moreover, shrinking F reduces the number of vertices of the graph by r. Thus, the total time of the shrinking operation is $O(|V|)$. The time of the postorder scan without shrinking is bounded by $O(|V|)$. The steps 4)-7) need $O(1)$ time. The time of steps 9)-14) is the same as the steps 2)-7). Therefore, the total time for this algorithm is $O(|V|)$.

References

1. Bondy, J.A., Murty, U.S.: Graph Theory with Applications.1976
2. Bondy, J.A.: Pancyclic Graphs: Recent Results. Colloq. Math. Soc. Janos Bolyai. **10**(1975) 181–187
3. Cornuejols, G., Naddef, D., Pulleyblank, W.: Halin Graphs and the Travelling Salesman Problem. Mathematical programming. **26**(1983) 287–294

4. Horton, S.B., Parker, R.G.: On Halin Subgraphs and Supergraphs. Discrete Applied Mathematics. **56**(1995) 19–35
5. Lou, D.: Hamiltonian Paths in Halin graphs. Chinese Mathematica Applicata. **8**(1995) 158–160

A Graph-Theory Algorithm for WCET Estimation

Guowei Wu[1] and Kai Yao[2]

[1] Software College of Dalian University of Technology, Dalian 116023,China
wgwdut @dlut.edu.cn
[2] Library Information Center of Shenyang University of Technology, Shenyang
150001, China
frantodd2002@yahoo.com.cn

Abstract. The complexity of modern program increases the difficulty to compute the upper bound worst case execution time fast and accurately. A new estimation method for WCET estimation is presented that uses graph theory to solve the program complexity problem. In this method, program basic blocks are represented as vertices in an undirected graph. The resulting graph can be partitioned into connected subgraphs with no edges between them. These subgraphs can in turn be broken into biconnected components. The combinational problem is reduced to finding the maximum energy of these small biconnected components and combining the results to identify the global maximum energy information, that is the worst case execution time. This algorithm will allow to analyze more complex program and can makes the execution time upper bound more accurate.

1 Introduction

The worst-case execution time (WCET) estimation of a program remains a difficult challenge. Software for today's large embedded real time system is very complex, consisting of many intercommunicating components for various devices and control functions. The field of execution time analysis is both broad and deep. There are many complimentary techniques that can be used to calculate the value of the WCET for a complex system. However each technique assume that there is no interaction between components. To deal with this intractable problem, the researchers trade off prediction accuracy for computational complexity by proposing different pessimistic heuristics, which results in fast but less accurate analysis. Different pessimistic methods are thus proposed to cope with this complexity[1],[2],[3],[4],[5], and they result in loose estimated WCET. Another severe drawback is that they cannot handle any user annotations describing infeasible program paths, which are essential in tightening the estimated WCET. In this article, we will present a new algorithm based on graph theory, which enable to deal with programs that have interaction. A graph G=[V,E] consists of an ordered pair, where V represents a nonempty set of vertices and E symbolizes a set of edges. When V represents the program basic block and E represents the set of program flows, graph G becomes a program control flow graph.

The rest of the paper arranges as follows. Section 2 describe the proposed estimation method, section 3 gives the experiment results ,the conclusions and future work are presented in section 4.

2 Graph-Theory Algorithm for WCET Estimation

Given that each instruction takes a constant time to execute, the total execution time can be computed by summing the product of instruction counts by their corresponding instruction execution times. Since all instructions within a basic block must have the same execution counts, they can be considered as a single unit. If we let x_i be the execution count of a basic block M_i and c_i be the execution time of the basic block, then given that there are N basic blocks, the total execution time of the program is given as:

$$T = \sum_{i}^{N} c_i x_i \qquad (1)$$

The possible values of x_i are constrained by the program structure and the possible values of the program variables. If we can represent these constraints as linear inequalities, then the problem of finding the estimated WCET of a program will become an ILP problem.

The linear constraints can be divided into two parts: **program structural constraints**, which are derived from the program's control flow graph (CFG), and **program functionality constraints**, which are provided by the user to specify loop bounds and other path information.

The accuracy of program control flow information effect the accuracy of WCET estimation. In our algorithm, we can represent the program basic block in terms of graph theory by making each residue a vertex in an undirected graph. If at least one basic block of residue i interacts with at least one basic block of residue j, then there is an edge between vertices i and j of the graph. The active residues can be represented as a graph, the active residues can therefore be grouped into interacting clusters. Residues in different clusters do not have contacts with one another. Each cluster is a connected subgraph of the entire graph. The problem is therefore to enumerating the combinations of the basic block for the residues in each connected graph. Assuming each residues has the same number of basic block n_{blk}. The graph in Figure 1 has one residue labeled as a dark gray vertex that breaks the graph into two pieces when removed. The global maximum of the execution time can be found by identifying the maximum execution time configuration for each subgraph once for each basic block of the keystone residues. The solution is the one that finds the maximum execution time using equation (2), where EL is the largest execution time combination of basic block in the left subgraph, ER is the right subgraph, Eself is the execution time of interaction of the basic blocks. According to different programs, give the constraints, all the constraints are passed with the goal of maximizing cost function (2). The solver will return the estimated WCET.

To improve the process speed, we break up clusters of interacting basic block into

$$E = \max_{r_i}\{E_L(r_i) + E_R(r_i) + E_{self}(r_i)\}$$

(2)

biconnected components of an undirected graph. Biconnected graphs are those that cannot be broken apart by removal of a single vertex. Biconnected graphs are cycles,nested cycles, or a single pair of residues connected by an edge. Vertices that appear in more than one biconnected component are called "repoint". Removing a repoint from a graph breaks the graph into two separate subgraphs. Finding biconnected components and their repoints is easily accomplished by using standard depth-first search algorithm from graph theory contained in many computer science textbooks. For each biconnected component with only one repoint, we find the maximum execution time over all combinations of basic blocks of the residues in the component. This execution time includes all interactions among these residues and between these residues. The worst case execution path is the path that has the most bidirect line path. In Figure 1 ,the worst case execution path is (1,2,3,4,5,…12).
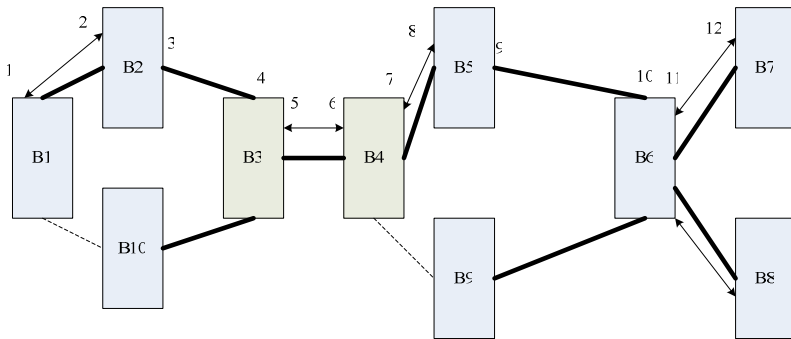
Fig. 1. Flow graph using graph theory for software worst case execution time estimation

Algorithm 1.
Input: A new program sequence.
Output: Print the fixed basic block and the maximum execution time.
1. Rotamers: for each residue,read in rotamer dihedral angles and probabilities to determine which pairs of basic block may be interact.
2. Disulfides: if desired, determine likely disulfide pairings.Fix the basic block that are designated disulfides for the rest of the calculation.
3. Dead-end elimination: perform a DEE of rotamers that cannot be part of the global maximum execution configuration by using the "Goldstein criterion". The Goldstein criterion is the simplest version of DEE. If the total execution time for all basic blocks is expressed as the sum of self and pairwise execution time, see equation (3). The execution time of interaction of these fixed basic blocks with any unfixed basic blocks is added to the self-execution of the unfixed basic blocks. That is equation (4).

4. Residue graph: define residues that have more than one rotamer left after the DEE step as "active residues". That is, determine which sets of residues form connected graphs, given the list of edges.

5. Biconnected components:for each cluster, determine the set of biconnected components and repoints in the graph by using a depth-first search procedure. The order of each repoint is defined.

6. Solve clusters: find the maximum execution time for each connected graph(cluster) in turn, for each biconnected component of the cluster with only one repoint,find the maximum execution time of the residues in the component for each rotamer of the repoint each connected graph. A branch-and-bound backtracking algorithm is used for this purpose, in which the residues in the component are sorted from lowest to highest number of rotamers.

$$E = \sum_{i=1}^{N} E_{self}(r_i) + \sum_{i=1}^{N-1} \sum_{j>i}^{N} E_{pair}(r_i, r_j) \tag{3}$$

$$E_{self}(r_i) = \sum_{i=1}^{N} E_{bb}(r_i) + \sum_{j \in fixed} E_{pair}(r_i, r_j) \tag{4}$$

The maximum execution time is the maximum execution time of the self residues plus the maximum execution time pairwise of these residues. The bound is defined as:

$$E_{bound}(i) = \sum_{j>i}\left\{ \max_{r_j} E_{self}(r_j) \right\} + \sum_{j>i} \sum_{k<j}\left\{ \max_{r_j, r_k} E_{pair}(r_j, r_k) \right\} \tag{5}$$

3 Experimental Results

To verify the proposed method, we use Motorola MMC2107 development board as target platform which is containing a 40MHz Motorola MMC2107 processor, 128KB of main memory and several I/O peripherals. The M2107 processor contains an on-chip 8KB direct-mapped instruction cache organized as 32-16-byte lines.

We select the set of benchmark programs from [1] for our evaluation. Since it is impractical to simulate all the possible program input data and all initial system states, a program's actual WCET cannot be computed. We use the measured WCET in [1] as the actual WCET, We assume that the measured WCET of a program is very close to its actual WCET. Table 1 is the experimental results, time unit is clock period counts, it shows that the proposed method give a more accurate WCET estimation than Wu's method[6]. By using graph theory can extract accurate program flow graph, and thus make the estimation more accurate, and the results prove that the method we give is right and feasible. The result is more accurate than the result in our previous work[6]. So it is an effective approach to use graph theory for embedded real time software WCET estimation.

Table 1. WCET estimation experimental result

Function	Measured WECT	Proposed method	Wu's method
FFT	$1.25*10^6$	$1.21*10^6$	$1.18*10^6$
DES	$2.42*10^5$	$2.41*10^5$	$2.38*10^5$
Stats	$1.65*10^4$	$1.63*10^4$	$1.59*10^4$
DCT	$1.15*10^5$	$1.14*10^5$	$1.1*10^5$

4   Conclusion

In this paper, we present a new method to find a tight bound on the worst case execution time of real-time software. This approach combines graph-theory to extract program flow graph and can deal with the program that have interaction between components. Experimental results show that the estimated WCET is much closer to the measured WCET. Our next research work will focus on combining data cache and TLB cache analysis into graph-theory algorithm analysis, thus the WCET estimation result will get more accurate.

Acknowledgment

References

1. Liu,J.C.,Lee,H.J.:Deterministic Upperbounds of Worst-case Execution Times of Cached Programs. In: Proceeding of the 15th IEEE Read-Time Systems Symposium,Vol.30,New York(1998)182-191.
2. Lim,S.S.,Young,H.B.,Gu,T.J.:An Accurate Worst Case Timing Analysis Technique for RISC Processors. In: Proceeding of the 15th IEEE Real-Time Systems Symposium,Vol.30, New York(1998)97-108.
3. Alan,C.S.:Reasoning about Time in Higher-level Language Software. IEEE Transactions on Software Engineering, Vol.15,No.7,pp.875-889,July 1999.
4. Robert, A.: Bounding Worst-case Instruction Cache Performance. In: Proceeding of the 15th IEEE Real-Time Systems Symposium,Vol.30, New York(1998)172-181.
5. Li,Y.S.,Malik,S., Wolfe, A.: Cache Modeling for Real-Time Software Beyond Direct Mapped Instruction Caches. In: Proceeding of the 17th IEEE Real-Time Systems Symposium, Vol.35, New York (2002)35-42.
6. Wu ,GW.,Yao,lin.: A New WCET Estimation Algorithm based on Instruction Cache and Prefetching Combined Model. Lecture Notes in Computer Science ,Vol (3605). Springer-Verlag, Berlin Heidelberg New York (2005) 557-562.

Context-Aware Optimal Assignment of a Chain-Like Processing Task onto Chain-Like Resources in M-Health

Hailiang Mei and Ing Widya

Architecture and Services for Networked Applications Group, Department of Computer Science, University of Twente, The Netherlands
{H.Mei, I.Widya}@utwente.nl

Abstract. This paper focuses on the optimal assignment of a chain-structured medical task onto a chain of networked devices, a need identified in context-aware mobile healthcare applications. We propose a graph-based method to compute the assignment which has the minimal end-to-end process and transfer delay. In essence, the method transforms the assignment problem to a shortest path problem in a graph representing all possible assignments. Compared to earlier work, our method relaxes a so-called contiguity constraint, which is a necessity in the earlier case but unnecessarily constraining in the healthcare applications. The proposed method reduces the time and space complexity in case it is adapted to include the contiguity constraint.

Keywords: graph-based, task assignment, contiguity constraint, M-health.

1 Introduction

In recent years, mobile healthcare (M-health) applications have received more and more attentions due to its ability to satisfy today's society demands, like patient self-management, continuous and anywhere tele-monitoring and tele-treatment ([1-3]). In M-health, sensed biosignals of mobile patients need to be processed and transferred to healthcare professionals via several handheld or body-worn devices. On the other hand, a biosignal processing task often consists of cascaded processing units, which have to be configured onto the previously mentioned devices. A challenge in M-health is therefore to study the dynamic assignments of the processing units to devices such that the performance of the processing task can be guaranteed despite the resource changes or fluctuations in the mobile environment. In this paper, we address the optimal assignment to minimize the *end-to-end process and transfer delay*. This measure suits our intended M-health applications which require timely responses.

This assignment problem is similar to an industrial case in the area of parallel computing studied earlier by Bokhari ([4]). In order to find the optimal assignment of *m* task units connected in a chain onto *n* processors also connected in a chain, Bokhari presented a graph-based solution using a layered assignment graph to find an optimal assignment with minimal *bottleneck processing time*. In this assignment graph, any path connecting two distinguished nodes represents a possible assignment. Therefore, the assignment problem is translated into a path-search problem which can be solved

with time complexity of $O(m^3n)$ and space complexity of $O(m^2n)$ ([4]). Some improved algorithms are further reported in [5-7].

Since the objective is to minimize the bottleneck processing time, the previous solutions have to obey a so-called *contiguity constraint*, i.e. any device should be assigned with at least one task unit. However, this constraint unnecessarily rules out several potential solutions for the M-health applications. In this paper, we propose a more general graph-based method to compute the optimal assignment, where it is possible that some devices are not assigned with a processing unit but only forward the processed biosignal data from the precedent device to the next device, for example to save battery power or to avoid complex processing on the particular device. With a slight modification, the proposed method is also applicable to problems with contiguity constraint while reducing the time and space complexity by a factor of m^2 and m respectively compared to Bokhari's original approach.

This paper is organized as follows: Section 2 describes a context-aware M-health application scenario for predicting epileptic seizures. Section 3 gives the problem formulation. Section 4 presents the graph-based method on finding the optimal assignment. Section 5 illustrates the result of performance measurement. Section 6 concludes the work.

2   Background

An epilepsy prediction task developed in ([8]) consists of six biosignal processing units (BSPU) as shown in Fig. 1. First, the patient's raw Electro Cardio Gram (ECG) data is filtered to remove signal artifacts and environment noise. Thereafter, beat-to-beat heart rate (HR) is derived and heart rate variability (HRV) in the frequency domain is calculated. The frequency spectrum of the HRV is then used to calculate the probability of an upcoming or occurring seizure. To reduce the chance of false alarms, the patient's activity information is monitored as well and correlated with the analyzed spectrum in the final stage.
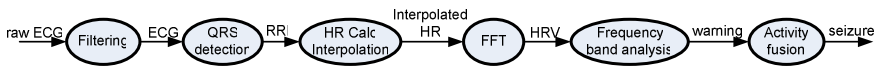
Fig. 1. Epilepsy prediction task consisting of six BSPUs

The studied M-health platform ([9]), which facilitates the sensing, processing and transporting of the biosignals, consists of the following devices: a set of body-worn sensorboxes, a handheld Mobile Base Unit (MBU), a back-end server and an end-terminal (Fig. 2). The sensorboxes collect the biosignals of the patient, sense other data like location or activity, and send the data to the MBU over wireless short-range connections, e.g. a Bluetooth connection. As a gateway, the MBU sends the data to the back-end server over a WiFi, GPRS or UMTS connection. Thereafter, the data can be streamed to or accessed by a healthcare professional using his end-terminal, e.g. his laptop or desktop PC.

Like other applications running in a mobile environment, the usability of M-health applications are seriously affected by the fluctuations and scarcity of the environment's resources, e.g. network bandwidth, battery power and computational power of handhelds, etc. In order to deliver dependable healthcare services, M-health applications should embed context-aware features. For example, if a patient is outdoor and GPRS performance severely suffers from the GSM calls in the cell, transfer of raw ECG data to the back-end server may be impeded unacceptably if seizure forecasting or detection is completely processed at the server. Dynamically reassigning the processing units to the available devices may solve the problem: If the QRS detection can be assigned to the MBU, the GPRS channel bandwidth may be sufficient for smooth transfer of the derived heart rate signal, the patient's activity data and optionally one of the adequately downscaled ECG signal to conform to medical protocols. To realize this desired adaptation, two major topics should be addressed: computation of a better assignment of BSPUs and distribution of BSPUs across the devices according to this new assignment. We focus on the first topic in this paper and formulate the research problem in the next section.
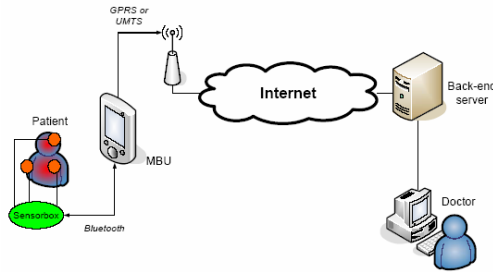
Fig. 2. M-health platform

3   Problem Formulation

We formulate the problem of optimally assigning a BSPU chain onto a device chain as:

- Given: a directed BSPU chain containing m BSPUs increasingly indexed by $i \in \{1,2,\ldots m\}$, a directed device chain containing n devices increasingly indexed by $j \in \{1,2,\ldots n\}$ and a performance measure τ, where τ denotes the end-to-end process and transfer delay for a particular configuration of BSPUs across devices.
- Goal: To find an assignment function Ψ_{opt} among all possible $\Psi: \{i\} \rightarrow \{j\}$ such that $\tau(\Psi_{opt})$ is the minimal one among all $\tau(\Psi)$.
- Subject to: the following *ordering-* and *local-constraints*.

The *ordering constraint* is that for every pair of BSPU i and BSPU i', if $i < i'$, then $\Psi(i) \le \Psi(i')$. This constraint therefore reflects the consistency of directions of the two chains. It is a more relaxed constraint compared to the *contiguity constraint* discussed earlier (cf. [5-7]). The *local constraint* is that for every BSPU i, its hosting device $\Psi(i)$

should satisfy the BSPU i's system requirement (e.g. CPU speed and library support) and user preference (e.g. this BSPU i has to run on device $\Psi(i)$).

We define the computation time for BSPU i to process one frame of biosignal data at device j as $p_{i,j}$ and the communication time for transferring one frame of BSPU i's output biosignal data over the link between device j and $j+1$ as $c_{i,j}$. The variable $c_{0,j}$ denotes the communication time for transferring one frame of raw sensor output over the link between device j and $j+1$. We neglect intra-device communication time, e.g. if both BSPU i and $i+1$ are located on the same device. We further assume there is no additional computation time overhead for executing several BSPUs on the same device. Since the values of $p_{i,j}$ and $c_{i,j}$ could be known a prior, e.g. based on analytical benchmarking or task profiling ([10]), the end-to-end delay τ of a particular configuration of BSPUs across devices can be calculated. In Fig. 3, we illustrate a 6-BSPU-4-device assignment of the epilepsy prediction task on the networked M-health devices. In this example, BSPU 1 and 2 are assigned to device 1, BSPU 3, 4 and 5 are assigned to device 3, etc. Based on our definitions, its end-to-end process and transfer delay can be calculated as:

$$\tau = p_{1,1} + p_{2,1} + p_{3,3} + p_{4,3} + p_{5,3} + p_{6,4} + c_{2,1} + c_{2,2} + c_{5,3}$$
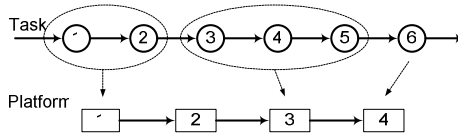
Fig. 3. An example of assigning a directed BSPU chain (m=6) onto a directed device-chain (n=4)

4   Optimal Assignment Computation Procedure

In order to find the optimal assignment of m BSPU (indexed by i) onto n devices (indexed by j), we first build a layered assignment graph consisting $mn+2$ nodes (Fig. 4). In this graph, each row (excluding nodes <S> and <T>) corresponds to a BSPU and each column corresponds to a device. The label <i,j> on each node corresponds to a possible (i.e. satisfying the local constraint) assignment of BSPU i to device j. A node labeled <i,j> is connected by edges to all nodes <$i+1,j$>, <$i+1,j+1$> … <$i+1,n$> in the layer below (ordering constraint). All nodes in the first (last, respectively) layer are connected to the node <S> (<T>, respectively). Therefore, any path connecting nodes <S> to <T> corresponds to an assignment of BSPUs to devices fulfilling the earlier mentioned constraints (e.g. the thick path in Fig. 4 which corresponds to the assignment shown in Fig. 3).

Each edge of this layered assignment graph is then labeled with the sum weight of computation time and communication time appropriately: (1) the edges connecting node <S> to node <$1,1$> till <$1,n$> are weighted with the communication time of transfer the raw sensor data as 0, $c_{0,1}$, $c_{0,2}$ … $c_{0,n-1}$. (2) In layer i (except for the last layer), each edge connecting node <i, j> to the layer below is first weighted with the computation time for BSPU i to process one frame at device j, i.e $p_{i,j}$. Then, to the

weight on the edge from $<i, j>$ to $<i+1,j+1>$, $<i+1,j+2>$ … $<i+1,n>$ in the layer below, a communication time required to transfer BSPU i's output data, $c_{i,j}$, $c_{i,j}+c_{i,j+1}$, …, $c_{i,j}+c_{i,j+1}+…+c_{i,n-1}$ is added respectively. (3) For the last layer, each edge connecting node $<m,j>$ to node $<T>$ is first weighted with the computation time for BSPU m to process one frame at device j, i.e. $p_{m,j}$. Then, to the edge from $<m,j>$ (except for $<m,n>$) to $<T>$, a communication time required to transfer BSPU m's output data, $c_{m,j}+c_{m,j+1}…+c_{m,n-2}+c_{m,n-1}$ is added. As an illustration, the weights associated with the thick edges are shown in Fig. 4.
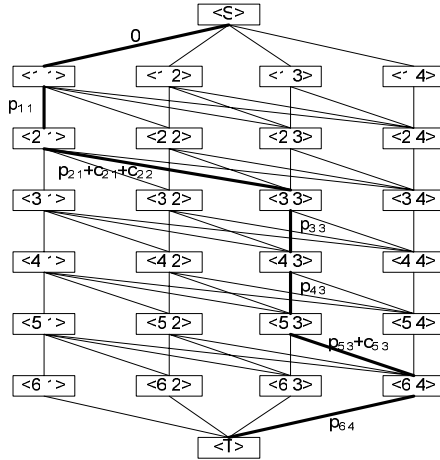
Fig. 4. The 6-BSPU-4-device assignment graph without contiguity constraint

In the last step, by applying a shortest-path search algorithm (e.g. Dijkstra algorithm), we can identify a path connecting $<S>$ and $<T>$ in this weighted graph which corresponds to an optimal assignment (Ψ_{opt} with the minimal τ).

The space complexity (defined as the number of nodes in the assignment graph) of this method is $O(mn)$. Thus the time complexity of shortest-path search step is $O(m^2n^2)$ if the Dijkstra algorithm is used. If a labeling method as proposed by Bokhari ([4]) is used for search, the time complexity can be reduced to $O(mn)$.

It is easy to convert our procedure to tackle the assignment problem with the contiguity constraint. We only need to remove all the edges which are "cutting a vertical edge", i.e. the assignment of two adjacent BSPUs onto two non-adjacent devices and all the edges connecting nodes $<S>$ and $<T>$ except for the ones connecting $<1,1>$ and $<m,n>$. This simplified assignment graph is shown in Fig. 5. It is obvious that the two triangle areas (the grey area in Fig. 5) can not be part of the optimal path. Therefore, they can be removed from the assignment graph as well in order to reduce the space complexity. Following the similar weighting and search steps, the optimal assignment with the contiguity constraint can be obtained. This new assignment graph has some sort of relation with an earlier proposed assignment graph or ([5, 11, 12]): the nodes matrix in our solution is the transpose of the nodes matrix proposed earlier with the contiguity constraint.
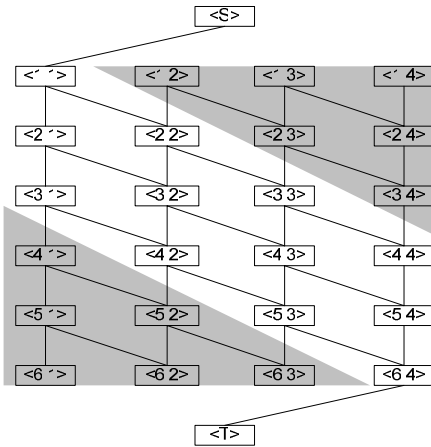
Fig. 5. The 6-BSPU-4-device assignment graph with contiguity constraint

5   Performance

We implement the proposed assignment method in Java to get more in-depth understanding. This is, to the best our knowledge, the first experimental study based on series of theoretical studies on chain-to-chain assignment problem. We record the CPU time of two computation steps in this method: the weighted assignment graph construction and the shortest-path search. For the "search" step, we use an open source library[1] which implements the Dijkstra shortest-path algorithm. The program is tested on a Windows XP machine with Intel Pentium 2.4G CPU and 1.5G RAM. Different pairs of m and n, e.g. (20,10), (40,10), … (100,20), are tested and the number of assignment graph nodes ranges from 200 to 2000. Both the assignment with the contiguity constraint and the assignment without are tested (Fig. 6).
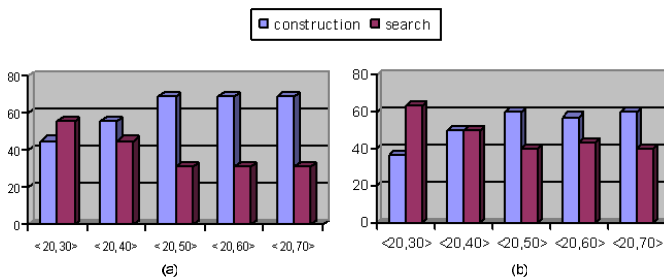
Fig. 6. The percentage of CPU time spending on each of two steps in assignment with contiguity constraint (a) and assignment with ordering constraint (b)

---

[1] http://rollerjm.free.fr/pro/graphs.html

One observation we could make is that the "construction" step is more time consuming than the actual "search" step in most of cases, which suggests that the evaluation on this kind of graph-based method should based on the time complexity of the entire method instead of the "search" step only ([4-7]).

On the other hand, we also implement a program based on the optimal assignment approach proposed by Bokhari ([4]) and tested against our method with the contiguity constraint. Again, the CPU time of graph construction and shortest-path search are measured separately. Several pairs of m and n are tested and the results are shown in Table 1. Due to the reduced time and space complexity, our method outperforms the original Bokhari's method. For a m-BSPU-n-device assignment, our method requires an assignment graph with $mn+2$ nodes compare to a Bokhari's graph with $(m-n+2)*(m-n+1)*(n-2)/2+(m-n+1)*2+2$ nodes. For example, for the 60-BSPU-30-device assignment, an assignment graph with 14952 nodes will be constructed if Bokhari's method is used. Because the adjacent matrix is used to represent the graph, which implies heavy memory requirement, the program runs out of memory before the completion.

Table 1. CPU time (in millisecond) comparison between Bokhari's original method and our proposed method on chain-to-chain assignment with the contiguity constraint

| Setting		CPU time of Bokhari's method			CPU time of our method		
# BSPU	# device	Construction	Search	Total	Construction	Search	Total
20	10	94	63	157	16	47	63
30	10	392	172	564	31	47	78
40	10	985	673	1658	32	46	78
30	20	250	94	344	63	78	141
40	20	1017	563	1570	94	78	172
50	20	3996	2690	6686	141	94	235
40	30	360	156	516	172	94	266
50	30	2112	939	3051	235	109	344
60	30	Out of memory	Out of memory	Out of memory	282	110	392

6 Conclusion

In this paper, we study the problem of assigning a chain-structured biomedical signal processing task across several devices connected in a chain based on the context information. We present a graph-based method to search for an optimal task assignment which minimizes the end-to-end process and transfer delay. Our solution differs from earlier work by means of a different objective and the relaxation of a so-called contiguity constraint, which is a necessity in the earlier case but unnecessarily constraining in the healthcare applications. The proposed method also reduces the time and space complexity in case it is adapted to include the contiguity constraint.

However, we are aware that more complex M-health tasks can not be modeled by a chain of processing units. On the other hand, the involvement of other devices may also complicate the model of M-health platform, e.g. adding a home gateway into the configuration (Fig. 2) can create a second path between the MBU and the backend

server. Therefore, in the future work, we plan to address a more general model, i.e. (Directed Acyclic Graph) DAG-tasks-to-DAG-resources assignment problem. Since, very likely, no algorithms with polynomial time complexity will be ever found to solve the general problem, our future work will be focused on heuristic approaches, e.g. *Branch-and-Bound* ([13]) and *Genetic Algorithms* ([14]).

Acknowledgement

References

1. Hung, K. and Z. Yuan-Ting, *Implementation of a WAP-based telemedicine system for patient monitoring.* Information Technology in Biomedicine, IEEE Transactions on, 2003. **7**(2): p. 101.

2. Yuan-Hsiang, L., et al., *A wireless PDA-based physiological monitoring system for patient transport.* Information Technology in Biomedicine, IEEE Transactions on, 2004. **8**(4): p. 439.

3. Halteren, A.v., et al., *Mobile Patient Monitoring: The MobiHealth System.* The Journal of Information Technology in Healthcare, 2004. **2**(5).

4. Bokhari, S.H., *Partitioning problems in parallel, pipelined, and distributed computing.* IEEE Transactions on Computers, 1988. **37**(1): p. 48-57.

5. Sheu, J.-P. and Z.-F. Chiang, *Efficient allocation of chain-like task on chain-like network computers.* Information Processing Letters, 1990. **36**(5): p. 241 - 246.

6. Nicol, D.M. and D.R. O'Hallaron, *Improved Algorithms for Mapping Pipelined and Parallel Computations.* IEEE Transactions on Computers, 1991. **40**(3): p. 295-306.

7. Woeginger, G.J. *Assigning chain-like tasks to a chain-like network.* in *Proceedings of the twelfth annual ACM-SIAM symposium on Discrete algorithms.* 2001.

8. Tönis, T., H.J. Hermens, and M. Vollenbroek-Hutten, *Context aware algorithm for discriminating stress and physical activity versus epilepsy.* 2006, AWARENESS deliverables (D4.18).

9. AWARENESS, *Freeband AWARENESS project webpage.* 2005, http://www.freeband.nl/project.cfm?id=494&language=en.

10. Braun, T.D., et al. *A Taxonomy for Describing Matching and Scheduling Heuristics for Mixed-Machine Heterogeneous Computing Systems.* in *17th IEEE Symposium on Reliable Distributed Systems.* 1998.

11. Hansen, P. and K.-W. Lih, *Improved Algorithms for Partitioning Paroblems in Parallel, Pipelined, and Distributed Computing (Correspondence).* IEEE Transactions on Computers, 1992. **41**(6): p. 769-771.

12. Yeh, C.-C. *On the Power-Aware Resource Allocation for Linear-Pipelined Real-Time Tasks.* in *19th International Conference on Advanced Information Networking and Applications.* 2005.

13. Ma, Y.-C., T.-F. Chen, and C.-P. Chung, *Branch-and-boundtask allocation with task clustering-basedpruning.* Journal of Parallel and Distributed Computing, 2004. **64**: p. 1223-1240.

14. Wang, L., et al., *Task Matching and Scheduling in Heterogeneous Computing Environments Using a Genetic-Algorithm-Based Approach.* Journal of Parallel and Distributed Computing, 1997. **47**: p. 8-22.

On Efficiency Group Multicasting Algorithm with Multiple Minimum Steiner Trees

Moonseong Kim[1], Minseok Kang[2], Hyunseung Choo[1],
Jong S. Yang[3], and Young-Cheol Bang[2],*

[1] School of Info. and Comm. Engineering, Sungkyunkwan University, Korea
{moonseong, choo}@ece.skku.ac.kr
[2] Dep. of Computer Engineering, Korea Polytechnic University, Korea
{k19m81s, ybang}@kpu.ac.kr
[3] Korea Institute of Industrial Technology Evaluation and Planning, Korea
yjs@mail.itep.re.kr

Abstract. In this paper, we study the problem of constructing minimum cost group multicast trees with bandwidth reservations. Our algorithm uses multiple candidate paths to select a path from source to each destination member in each multicast tree construction. We show that our proposed algorithm performs better in terms of total tree cost for real life networks over well-known algorithm GKMB. The enhancement is up to about 10% ∼ 25% in terms of normalized surcharge for the GKMB tree cost.

Keywords: Group Multicast Routing Algorithm, Minimum Steiner Trees, Group KMB (GKMB) Algorithm, and Minimum Cost Multicast Tree (MCMT) Algorithm.

1 Introduction

With the emergence of real-time applications, such as video conferences and online games, and peer-to-peer (P2P) applications, and other content distribution networks, a group of entities may exchange data among themselves. A network layer may provide support for these applications by creating a set of multicast routing trees simultaneously. The problem of finding a set of multicast trees where every member in a group is a terminal as well as a source node is called the Group Multicast Routing Problem (GMRP). The routing algorithm must construct a multicast tree for each member node with each tree rooted at the member and spanning all other member nodes simultaneously.

Jia and Wang proposed a group multicast routing algorithm, Group KMB (GKMB) [1], that is based on KMB algorithm. The KMB heuristic was proposed by Kou, Markowsky, and Berman [2]. KMB applies Prim's minimum spanning tree algorithm to the complete distance graph, where the complete distance graph is a graph that contains Steiner points (multicast members) and has an

---

* Corresponding author.

edge between every pair of nodes representing the shortest path between them. KMB is very well-known heuristic algorithm in minimum Steiner tree problem.

Recently, Bang *et al.* proposed the Minimum Cost Multicast Tree (MCMT) algorithm [3] to create minimum Steiner tree. MCMT is proved that it has the nearest optimal tree cost than other algorithms, are known to be the best heuristic. Although KMB algorithm has the nearest optimal solution, we strongly believe that MCMT outperforms KMB in terms of tree cost. Therefore, in this paper, we propose an algorithm, called Group MCMT (GMCMT), that is based on the adaptation of MCMT algorithm. Also, simulation studies show that our algorithm outperforms GKMB.

The subsequent sections of this paper are organized as follows. In Section 2, the network model and previous algorithms are described. Section 3 presents details of our algorithm. Section 4 shows the results of simulation studies. This paper is finally concluded in Section 5.

2   Preliminaries

2.1   Network Model

The source node of a multicasting is assumed to know all the information needed to construct the multicast tree. A network is modeled as a directed weighted graph $G = (V, E)$ with node set V and edge (link or arc) set E. An edge $e \in E$ from $u \in V$ to $v \in V$ is represented by $e = (u, v)$. We define a path as sequence of links such that $(v_0, v_1), (v_1, v_2), \ldots, (v_{i-1}, v_i)$, belongs to E. Let $P(v_0, v_i) = \{(v_0, v_1), (v_1, v_2), \ldots, (v_{i-1}, v_i)\}$ denote the path from node v_0 to node v_i. The path contains the nodes $v_0, v_1, \ldots, v_i$ and the edges $(v_0, v_1), (v_1, v_2), \ldots, (v_{i-1}, v_i)$. Each link $e = (u, v) \in E$ is associated with two parameters, namely link cost $c(e) \geq 0$ and available link bandwidth $b(e) \geq 0$. They are asymmetric in general. The cost of a link can be associated with the utilization of the link. A higher utilization is represented by a higher link cost. The path cost of path $P(s, m)$ is $\phi_C(P) = \sum_{e \in P} c(e)$ and the tree cost of tree T is given by $\phi_C(T) = \sum_{e \in T} c(e)$.

For a given a network graph $G(V, E)$, let a multicasting group be $D \subset V$. $D = \{m_1, m_2, \ldots, m_k\}$ is a group of nodes in G, where $|D| = k$. For each node $m_i \in D$, multicast member node m_i has a bandwidth requirements of B_i units. The bandwidth requirement B_i of each node in D is specified by the user. The GMRP is that of finding a set of directed routing trees $\{T_1, T_2, \ldots, T_k\}$, one for each member of group D which satisfy the follows:

$$minimize \left\{ \sum_{i=1}^{k} \sum_{e \in T_i} c(e)\, \chi_e^i \,, \quad {}^\forall e \in E \right\}$$

subject to

$$\sum_{i=1}^{k} B_i\, \chi_e^i \leq b(e) \,, \quad \text{where } \chi_e^i = \begin{cases} 1 & \text{if } e \in E_i \\ 0 & \text{otherwise} \end{cases} \tag{1}$$

for each tree $T_i = (V, E_i)$, where $E_i \subset E$, represents the tree rooted at node $m_i \in D$ that spans all members in D.

The objective function ensures that the total cost of generated trees is minimized under constraint (1) is to ensure that the total bandwidth utilized on each link does not exceed its available bandwidth. A set of trees $\{T_1, T_2, \ldots, T_k\}$ which satisfy constraint (1) is called a feasible solution to the GMRP. A link is called to be saturated if the difference between its available bandwidth and its allocated bandwidth is less than the amount of bandwidth required by a user.

Variations of the GMRP have been investigated in the literature, including GMRP under bandwidth constraints, GMRP under delay constraints, GMRP protocols, and the static and dynamic GMRP. GMRP under QoS constraints has drawn attention with the increasing development of real-time multimedia applications, such as video-conference and on-line games. In this paper, we focus on the bandwidth constrained GMRP.

2.2   Group KMB Algorithm

Jia and Wang proposed Group KMB (GKMB) [1] using KMB [2] as the single source multicast routing algorithm. This algorithm constructs the set of multicast trees by sequentially invoking a single source multicast tree algorithm over the multicast member nodes. If any links in the network become saturated, *i.e.*, overloaded, in the process, it implies that some multicast trees constructed previously which use these links have to release them and take alternative paths.

The algorithm KMB by Kou, Markowsky, and Berman is a minimum spanning tree based algorithm. Doar and Leslie report that KMB usually achiving 5% of the optimal for a large number of realistic instances [4]. KMB algorithm is illustrated in Fig. 1. To find a tree, KMB starts with constructing the complete distance network $G' = (V', E')$ induced by D where, V' contains source node and destination nodes D only, and E' is a set of links connecting nodes in V' for each other. In next step, a minimum spanning tree T of G' is determined. After then, a subgraph G_s is constructed by replacing each link (i, j) of T with its actual corresponding minimum cost path from i to j in G. If there exist several minimum cost paths, pick an arbitrary one. Next step is to find the minimum spanning tree T' of G_s. In final step, delete from T' all unnecessary nodes and corresponding links. Then the resulting tree is a KMB tree. Fig. 1(b) shows the complete graph from the given network Fig. 1(a) and the minimal spanning tree. Fig. 1(c) represents KMB tree by replacing each edge in the spanning tree by its corresponding shortest path in the given network.

In GKMB algorithm, a multicast tree rooted at v is constructed for each $v \in D$ using KMB algorithm. When two or more trees compete for a saturated link, it would simply imply that some of these trees would have to use alternative links to get to the other member nodes in the trees. The difference in cost between the original tree and the alternative tree is known as the alternative overhead. The tree with the least alternative overhead will be forced to give up this link and take the alternative link. GKMB has shown that the algorithm runs in time $O(k^3 n^2)$ with $|D| = k$ and $|V| = n$.

(a) A given network

(b) The   complete (c) A multicast tree based on
graph and the minimal KMB
spanning tree
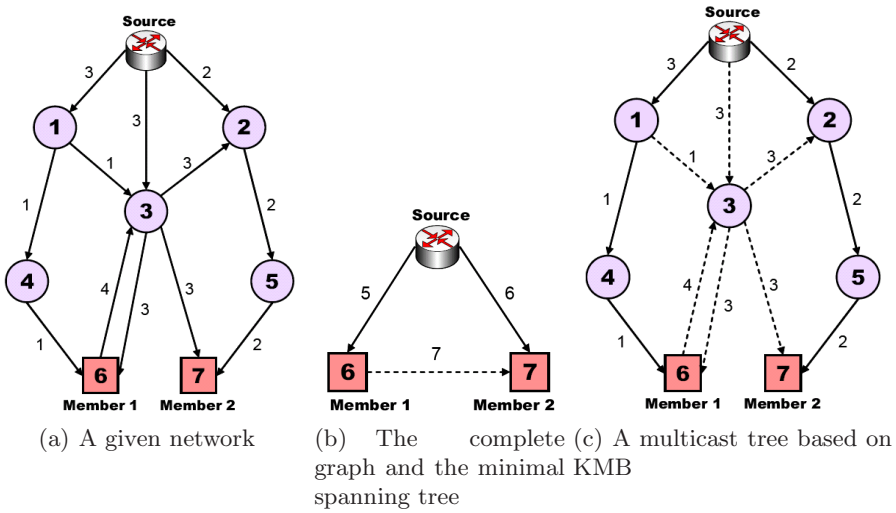
Fig. 1. *e.g.*, KMB algorithm

3   The Proposed Algorithm

3.1   MCMT Algorithm

Recently, Bang *et al.* proposed the Minimum Cost Multicast Tree (MCMT) algorithm [3] to create Steiner tree. MCMT is based on the Modified Dijkstra's Shortest Path (MDSP) algorithm to select all the minimum cost paths from source to each destination in G [5] and Prim's minimum spanning tree [6].

In Fig. 2, the sub-graph $G^{\alpha}_{m_j}$ such that $G^{\alpha}_{m_j}$ is constructed by merging all the shortest paths from $\alpha \in V$ to each $m_j \in D$, where $G^{\alpha}_{m_j}$ can be constructed using MDSP. Thus, any path of $G^{\alpha}_{m_j}$ is a minimum cost path, also $G^{\alpha}_{m_j}$ is an acyclic graph. Let T be a set of nodes that constitute a tree we want to define, and be empty initially. Let $G' = (V', E')$ be sub-graph of G with $V' \subseteq V$ and $E' \subseteq E$, where $G' = G' \cup G^{\alpha}_{m_j}$ with $G' = \emptyset$ initially. Then, the conceptual main idea of MCMT is as follows; select (s, m_k) pair, called $(s, m_k)_{min}$ such that $\phi_C(P(s, m_k))$ is minimum among all (s, m_i) pairs with $m_i \in D$ where, s is a source of the multicast communication at initial step. If $G' \neq \emptyset$, find $(\alpha, m_j)_{min}$ pair with $\alpha \in V'$ and $m_j \in D$. If α is not in T that is empty initially, we select single minimum cost path P_{min} of $G^{s}_{m_k}$ that contains a node α. Once P_{min} via α is selected, nodes of P_{min} are added to T, and all other redundant nodes and links are pruned from $G^{s}_{m_k}$. When α is in T, then we just add $G^{\alpha}_{m_j}$ to the set G'. We repeat this process until all $G^{\alpha}_{m_j}$ with $\alpha \in V'$ and $m_j \in D$ are considered. At the end of process, if there exist $G^{\alpha}_{m_j}$ of which P_{min} is not selected, single path from such $G^{\alpha}_{m_j}$ selected and all redundant nodes and links

(a) MCMT basic concept   (b) A multicast tree based on MCMT
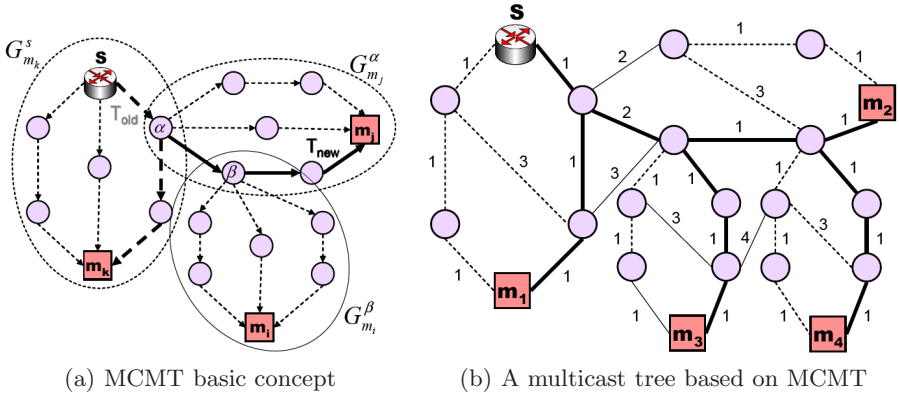
Fig. 2. *e.g.*, MCMT algorithm

are removed. Then, the final sub-graph, G', is a tree, and spans all destinations. We strongly believe MCMT outperforms KMB in terms of tree cost. Therefore, in this, we propose an algorithm, Group MCMT (GMCMT), that is based on the adaptation of MCMT algorithm.

3.2 Group MCMT Algorithm

According to GKMB algorithm, which is based on KMB algorithm, it only considers the shortest paths between the destination nodes in multicast members set D in the construction of each multicast tree. In particular, the selection of the least cost link in each iteration of the greedy strategy is made from the set of shortest paths between the multicasting members. However, if we increase the set for the greedy strategy, the final multicast trees may lead to lower cost solution for GMRP. The proposed algorithm is based on MCMT algorithm [3] and we call this algorithm Group MCMT (GMCMT). Since the MCMT algorithm finds multiple shortest paths and also considers the nodes between the group members and the relay nodes, we strongly believe that the proposed algorithm GMCMT is better than the performance of GKMB.

The GMCMT algorithm constructs a multicast tree T_d, rooted at $d \in D$, using the MCMT algorithm. If saturated edges occurs in a tree T_d, then it may imply that some trees which uses these edges will have to release them and use other alternative edges. In this case, the goal is to obtain a feasible solution with least cost possible. Since the problem of finding feasible solution for the GMRP is NP-complete, however, the determination of which set of trees to throw up the saturated edges will be a non-trivial task. In GMCMT algorithm, the alternative overhead of the current tree T_d is compared with the alternative overhead of the most recently built tree that uses the saturated edges. The party that has the smaller alternative overhead will have to give up the saturated edges and use alternative links to get to other member nodes of D. The GMCMT algorithm runs in time $O(k^3 n^2)$ with $|D| = k$ and $|V| = n$.

4 Performance Evaluations

4.1 Random Real Network Topology

Random graphs of the acknowledged model represent different kinds of networks, communication networks in particular. There are many algorithms and programs, but the speed is usually the main goal, not the statistical properties. In the last decade the problem was discussed, for examples, by B. M. Waxman (1993) [7], M. Doar (1993, 1996) [8,9], C.-K. Toh (1993) [10], E. W. Zegura, K. L. Calvert, and S. Bhattacharjee (1996) [11], K. L. Calvert, M. Doar, and M. Doar (1997) [12], R. Kumar, P. Raghavan, S. Rajagopalan, D. Sivakumar, A. Tomkins, and E. Upfal (2000) [13]. They have presented fast algorithms that allow the generation of random graphs with different properties, in particular, these are similar to real communication networks. However, none of them have discussed the stochastic properties of generated random graphs. A. S. Rodionov and H. Choo [14] have formulated two major demands for the generators of random graph: attainability of all graphs with required properties and uniformity of distribution. If the second demand is sometimes difficult to prove theoretically, it is possible to check the distribution statistically. The method uses parameter Pe, the probability of link existence between any node pair. We use the method by Rodionov and Choo.

4.2 Simulation Results

We now describe some numerical results with which we compare the performance of the proposed schemes. We generate 100 different random networks for each size of 25, 100, 150, and 200. Each node in network has the probability of link existence $P_e = 0.3$. The algorithms, GKMB and GMCMT, are implemented in C. The destination nodes are picked uniformly from the set of nodes in the network topology (excluding the nodes already selected for the destination). Moreover, the destination nodes in the multicast group, D, are occupied $5\% \sim 50\%$ of the overall nodes on the network. The link cost values in our computer experiment are selected uniformly between 1 and 10. We simulate 1000 times ($10 \times 100 = 1000$) for each $|V|$. For the performance comparison, we implement GKMB and GMCMT in the same simulation environments.

Fig. 3 are described that GMCMT is always better than GKMB. We use the normalized surcharge, introduced in [15], of the algorithm with respect to our method defined as follows:

$$\delta_C = \frac{\phi_C(T_{GKMB}) - \phi_C(T_{GMCMT})}{\phi_C(T_{GMCMT})}$$

The enhancement is up to about $10\% \sim 25\%$ ($|V|$: 200) in terms of normalized surcharge for the GKMB tree cost.
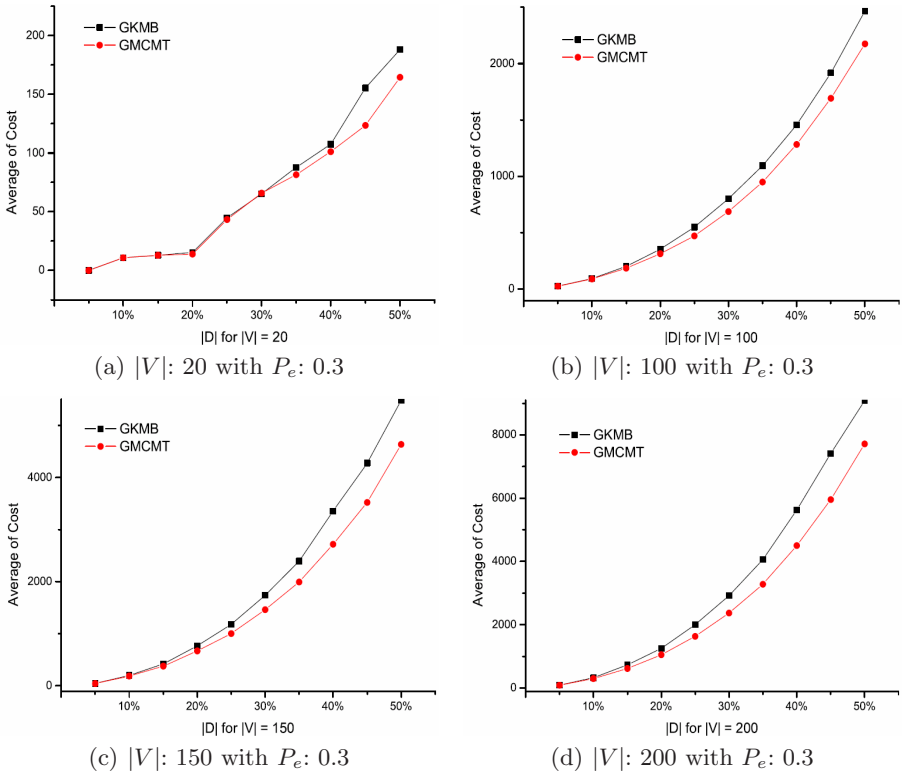
Fig. 3. Total tree costs

5   Conclusion

In this paper, we study the problem of constructing minimum cost group multicast trees with bandwidth reservations. Following that we propose a new efficient heuristic algorithm, called GMCMT, for finding low cost solutions for GMRP. Results from our computer simulation show that GMCMT algorithm performs better than GKMB algorithm in terms of total tree cost. For future work, we intend to investigate GMRP under dynamic group multicast routing. Any change of the group membership (*i.e.*, a process quits or joins the group) would incur the re-computation of the routing trees of the group if keeping the network cost optimal after the group membership change is the primary goal. Furthermore, another future research direction is to extend the algorithm to GMRP under other kinds of constraints.

Acknowledgment

References

1. X. Jia and L. Wang, "A group multicast routing algorithm by using multiple minimum Steiner trees," Elsevier Computer Communications, vol. 20, pp. 750-758, 1997.
2. L. Kou, G. Markowsky, and L. Berman, "A fast algorithm for Steiner trees," Acta Informatica, vol. 15, pp. 141-145, 1981.
3. Y.-C. Bang, S.-T. Chung, M. Kim, and S.-S. Joo, "On Multicast Communications with Minimum Resources," Springer-Verlag Lecture Notes in Computer Science, vol. 3726, pp. 4-13, September 2005.
4. M. Doar and I. Leslie, "How Bad is Naive Multicast Routing?," In Proceeding of IEEE INFOCOM 93, pp. 82-89, 1993.
5. R. K. Ajuja, T. L. Magnanti, and J. B. Orlin, *Network Flows: Theory, Algorithms, and Applications*, Prentice-Hall, 1993.
6. R. C. Prim, "Shortest Connection Networks And Some Generalizations," Bell System Techn. J. 36, pp. 1389-1401, 1957.
7. B. W. Waxman, "Routing of multipoint connections," IEEE Journal on Selected Areas in Communications, vol. 6, no. 9, pp. 1617-1622, December 1988.
8. M. Doar, "Multicast in the ATM environment," Ph.D dissertation, Cambridge University, Computer Lab., September 1993.
9. M. Doar, "A Better Mode for Generating Test Networks," In Proceeding of IEEE GLOBECOM 96, pp. 86-93, 1996.
10. C.-K. Toh, "Performance Evaluation of Crossover Switch Discovery Algorithms for Wireless ATM LANs," In Proceeding of IEEE INFOCOM 96, pp. 1380-1387, 1996.
11. E. W. Zegura, K. L. Calvert, and S. Bhattacharjee, "How to model an Internetwork," In Proceeding of IEEE INFOCOM 96, pp. 594-602, 1996.
12. K. L. Calvert, M. Doar, and M. Doar, "Modelling Internet Topology," IEEE Communications Magazine, pp. 160-163, June 1997.
13. R. Kumar, P. Raghavan, S. Rajagopalan, D. Sivakumar, A. Tomkins, and E. Upfal, "Stochastic Models for the Web Graph," In Proceeding of the 41th IEEE Symposium on Foundations of Computer Science 2000.
14. A. S. Rodionov and H. Choo, "On Generating Random Network Structures: Connected Graphs," Springer-Verlag Lecture Notes in Computer Science, vol. 3090, pp. 483-491, September 2004.
15. V. P. Kompella, J. C. Pasquale, and G. C. Polyzoa, "Multicast routing for multimedia communications," IEEE/ACM Transactions on Networking, vol. 1, no. 3, pp. 286-292, 1993.

The Edge Connectivity of Circuit Graphs of Matroids[*]

Ping Li[**] and Guizhen Liu

Department of Mathematics, Shandong University, Jinan 250100, P.R. China
liping@math.sdu.edu.cn

Abstract. Let G be the circuit graph of any connected matroid and let $\kappa'(G)$ and $\delta(G)$ be the edge connectivity and minimum degree of G. It is proved that $\kappa'(G) = \delta(G)$.

Keywords: Matroid, circuit graph of matroid, edge connectivity.

1 Introduction

We shall assume familiarity with graph theory and matroid theory. For terms that are not defined in this note, see [2] for graphs, and [8] for matroids. Let $\mathscr{C}$ be the family of circuits of a matroid M. It satisfies the following two axioms:

(**C1**) A proper subset of a member of $\mathscr{C}$ is not a member of $\mathscr{C}$.

(**C2**) If $a \in C_1 \cap C_2$ and $b \in C_1 - C_2$ where $C_1, C_2 \in \mathscr{C}$ and $a, b \in E$, then there exists a $C_3 \in \mathscr{C}$ such that $b \in C_3 \subseteq (C_1 \cup C_2) - \{a\}$.

Now we give a new concept as follows. The circuit graph of a matroid M is a graph $G = G(M)$ with vertex set $V(G)$ and edge set $E(G)$ such that $V(G) = \mathscr{C}$ and $E(G) = \{CC' \mid C, C' \in \mathscr{C}, \mid C \cap C' \mid \neq 0\}$, where the same notation is used for the vertices of G and the circuits of M.

Maurer discussed the relationship of bases of matroids and graphs and defined the base graph of a matroid [6,7]. Liu studied the connectivities of base graph of matroids [3,4]. Other related results can be found in [1,5]. In this paper we study the edge connectivity in the circuit graphs of matroids.

In this paper we will prove that the edge connectivity of the circuit graph of any connected matroid is equal to its minimum degree $\delta(G)$.

2 Preliminary Results

Lemma 1 [8]. *A matroid M is connected if and only if for every pair e_1, e_2 of distinct elements of E, there is a circuit containing both e_1 and e_2.*

Lemma 2 [8]. *If M is a connected matroid, then for every $e \in E$, either M/e or $M \backslash e$ is also connected.*

Lemma 3 [8]. *Let C and $C^\star$ be any circuit and co-circuit of a matroid M. Then $|C \cap C^\star| \neq 1$.*

Lemma 4 [8]. *If M is a matroid and if X and Y are two disjoint sets of elements of M, then $(M\backslash X)/Y = (M/Y)\backslash X$.*

3   Main Results

A matroid M is trivial if it has no circuits. In the following all matroids will be nontrivial.

Next we will discuss the properties of the matroid circuit graph. To prove the main results we firstly present the following lemmas which are clearly true.

Lemma 5. *Let M be any nontrivial matroid on E and $e \in E$. If G and G_1 are circuit graphs of M and $M\backslash e$, respectively, then G_1 is a subgraph of G induced by $V_1 = V(G) - V_2$ where $V_2 = \{C \mid C \in \mathscr{C}, e \in C\}$.*

Obviously the subgraph G_2 of G induced by V_2 is a complete graph. By Lemma 5, G_1 and G_2 are induced subgraphs of G and $V(G_1)$ and $V(G_2)$ partition $V(G)$.

Lemma 6. *For any matroid $M = (E, \mathscr{C})$ which has a 2-cocircuit $\{a, b\}$, the circuit graph of M is isomorphic to that of M/a.*

Lemma 7. *Suppose that $M = (E, \mathscr{C})$ is a connected matroid with two distinct circuits C_1, C_2 such that $|E - (C_1 \cup C_2)| \geq 2$ and for any $e \in E - (C_1 \cup C_2)$, $M\backslash e$ is disconnected. Then M has a co-circuit of cardinality two.*

Proof: We shall prove the theorem by induction on $|E-(C_1\cup C_2)|$. Suppose that $E - (C_1 \cup C_2) = \{e_1 \cup e_2\}$ and $M\backslash e_i$ $(i = 1, 2)$ is disconnected. If C_1 and C_2 are in the same component of $M\backslash e_1$, and $\{e_2\}$ is the other component of $M\backslash e_1$, then any circuit containing e_2 contains e_1. $\{e_1, e_2\}$ is a co-circuit of M because by (**C2**), if there is a circuit containing e_1 does not contain e_2 then there is a circuit containing e_2 does not contain e_1, which is a contradiction. If C_1 and C_2 are not in the same component of $M\backslash e_1$ and e_2 is in the same component with C_1, then $M\backslash e_2$ cannot be disconnected because there is a circuit containing e_1 intersects both C_1 and C_2 but does not contain e_2. Thus $\{e_2\}$ is another component of $M\backslash e_1$. Therefore $\{e_1, e_2\}$ is a co-circuit of M.

Suppose the result is true for $|E-(C_1\cup C_2)| = n-1$. We prove that the result is also true for $|E-(C_1\cup C_2)| = n > 3$. Let e_1 be an element of $E-(C_1\cup C_2)$ and $M\backslash e_1$ is disconnected. Hence, by Lemma 2, M/e_1 is connected. Now if e_2 is any element of $E - (C_1 \cup C_2 \cup \{e_1\})$, the matroid $(M\backslash e_2)/e_1$ is disconnected unless $\{e_1\}$ is a component of $M\backslash e_2$. If $\{e_1\}$ is a component of $M\backslash e_2$, then $\{e_1, e_2\}$ is a co-circuit of M. If $(M\backslash e_2)/e_1$ is disconnected for each $e_2 \in E - (C_1 \cup C_2 \cup \{e_1\})$, by Lemma 4, $(M/e_1)\backslash e_2 = (M\backslash e_2)/e_1$, we have $(M/e_1)\backslash e_2$ is disconnected for all $e_2 \in E - (C_1 \cup C_2 \cup \{e_1\})$. By induction, M/e_1 has a co-circuit of cardinality two. A co-circuit of M/e_1 is also a co-circuit of M. We prove the Lemma.   □

Now we give the main theorem of this paper.

Theorem 1. *Suppose that $G = G(M)$ is the circuit graph of a connected non-trivial matroid $M = (E, \mathscr{C})$ and C_1 and C_2 are distinct vertices of G. Then C_1 and C_2 are connected by $d = min\{d(C_1), d(C_2)\}$ edge-disjoint paths where $d(C_1)$ and $d(C_2)$ denote the degree of vertices C_1 and C_2 in G, respectively.*

Proof: We shall prove the theorem by induction on $|E(M)|$. When $|E(M)| = 3$, each element in M is parallel to another. It is easy to see that $G(M) = K_3$. The theorem is clearly true. Suppose that the result is true for $|E(M)| = n - 1$. We prove that the result is also true for $|E(M)| = n > 3$. Let C_1 and C_2 be any two vertices in G.

There are two cases to distinguish.

Case 1: $(C_1 \cup C_2) = E(M)$. It is easy to see that C_1 and C_2 are both adjacent to any circuit in $\mathscr{C} - \{C_1 \cup C_2\}$ and the conclusion is obviously true.

Case 2: $(C_1 \cup C_2) \neq E(M)$.
There are two subcases to distinguish.

Subcase 2.1: There is an element $e \in E(M) - (C_1 \cup C_2)$ such that $M \backslash e$ is connected. Let $G_1 = G(M \backslash e)$ be the circuit graph of $M \backslash e$ and G_2 be the subgraph of G induced by V_2 where $V_2 = \{C \mid C \in \mathscr{C}, e \in C\}$. Thus C_1 and C_2 are in G_1. By induction, in G_1, C_1, C_2 are connected by $d_1 = min\{d_1(C_1), d_1(C_2)\}$ edge-disjoint paths where $d_1(C_1)$ and $d_1(C_2)$ denote the degree of vertices C_1 and C_2 in G_1, respectively. Let $\mathscr{P}_1 = \{P_1, P_2, \ldots, P_{d_1}\}$ be the family of shortest edge-disjoint paths connecting C_1 and C_2 in G_1. Without loss of generality, we may assume that $d_1(C_1) \geq d_1(C_2)$. There are two subcases to distinguish.

Subcase 2.1a: $d_1(C_1) = d_1(C_2)$. The conclusion is obvious because G_2 is a complete graph.

Subcase 2.1b: $d_1(C_1) > d_1(C_2)$. By induction, in G_1 there are $d_1 = min\{d_1(C_1), d_1(C_2)\} = d_1(C_2)$ edge-disjoint paths connecting C_1 and C_2. Let $\mathscr{P}_1 = \{P_1, P_2, \ldots, P_{d_1(C_2)}\}$ be the family of shortest edge-disjoint paths connecting C_1 and C_2 in G_1. It is obvious that each $P_i (i = 1, 2, \ldots, d_1(C_2))$ contains exactly one vertex adjacent to C_1 and one vertex adjacent to C_2. Let $A_1, A_2, \ldots, A_{d_1(C_1)-d_1(C_2)}$ be the vertices in G_1 that are adjacent to C_1 but not contained in d_1 edge-disjoint paths. By Lemma 1, for any element e' in A_i $(i = 1, 2, \ldots, d_1(C_1) - d_1(C_2))$ there is a circuit A_i' in G_2 containing e and e', thus $A_i A_i'$ is an edge in $G(M)$. Let $D_1, D_2, \ldots, D_m$ denote the vertices in G_2 that is adjacent to C_2. G_2 is a complete graph, so A_i' is adjacent to $D_j (i = 1, 2, \ldots, d_1(C_1) - d_1(C_2); j = 1, 2, \ldots, m)$. If $m \leq d_1(C_1) - d_1(C_2)$, $C_1 A_i A_i' D_i C_2$ are m edge-disjoint paths connecting C_1 and C_2 where A_i' can be D_i $(i = 1, 2, \ldots, m)$. Here it is possible that $A_i' = A_j' (i \neq j; i, j = 1, 2, \ldots, d_1(C_1) - d_1(C_2))$. But it is forbidden that $D_i = D_j (i \neq j; i, j = 1, 2, \ldots, m)$. $d(C_2) = d_1(C_2) + m \leq d_1(C_1) < d(C_1)$, thus $d = min\{d(C_1), d(C_2)\} = d(C_2)$. $\mathscr{P} = \mathscr{P}_1 \cup \{C_1 A_1 A_1' D_1 C_2, C_1 A_2 A_2' D_2 C_2, \ldots, C_1 A_m A_m' D_m C_2\}$ are d edge-disjoint paths connecting C_1 and C_2 in G (see Fig.1).

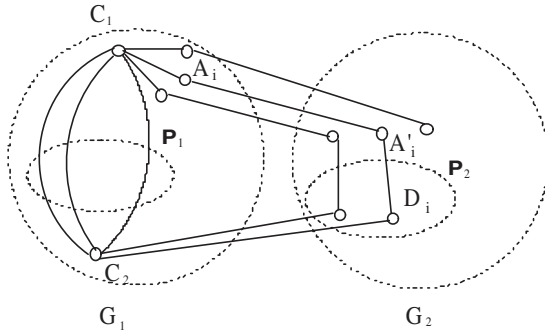If $m > d_1(C_1) - d_1(C_2)$, The proof is similar to that above.

Fig. 1.

Subcase 2.2: There is no element $e \in E(M) - (C_1 \cup C_2)$ such that $M \backslash e$ is connected. If $E(M) - (C_1 \cup C_2) = \{e\}$ and $M \backslash e$ is disconnected, it is easy to see that $C_1 \cap C_2 = \emptyset$ and C_1, C_2 are the two components of $M \backslash e$. Thus any circuit of M intersecting both C_1 and C_2 contains e, then C_1 and C_2 are both adjacent to any circuit in $\mathscr{C} - \{C_1 \cup C_2\}$ and the conclusion is obviously true. Suppose that $|E(M) - (C_1 \cup C_2)| \geq 2$ and for any $e \in E(M) - (C_1 \cup C_2)$, $M \backslash e$ is disconnected. By Lemma 7, M has a 2-cocircuit $\{a, b\}$. By Lemma 6, the circuit graph of M/a is isomorphic to that of M. By induction hypothesis, the result holds.

Thus the theorem follows by induction. $\qquad \square$

By Theorem 1 and Menger's Theorem, we can get the following corollary.

Corollary 2. *Suppose that $G = G(M)$ is the circuit graph of a connected matroid M with minimum degree $\delta(G)$. Then the edge connectivity $\kappa'(G) = \delta(G)$.*

References

1. Alspach, B., Liu, G.: Paths and Cycles in Matroid Base Graphs, Graphs and Combinatorics, **5**(1989), 207-211
2. Bondy, J. A., Murty, U. S. R.: Graph Theory With Applications, Macmillan, New York, (1976)
3. Liu, G.: A Lower Bound on Connectivities of Matroid Base Graphs, Discrete Mathematics, **64**(1988), 55-66
4. Liu, G.: The Proof of a Conjecture on Matroid Basis Graphs, Science in China, **6(A)**(1990), 593-599
5. Liu, G., Zhang, L.: Forest Graphs of Graphs, Chinese Journal of Engineering Mathematics, **22(6)**(2005),1100-1104
6. Maurer, S. B.: Matroid basis graphs 1, Journal of Combinatorial Theory Series B, **14**(1973), 216-240
7. Maurer, S. B.: Matroid basis graphs 2, Journal of Combinatorial Theory Series B, **15**(1973), 121-145
8. Oxley, J. G.: Matroid Theory, Oxford University Press, New York, 1992.

An Incremental Learning Algorithm Based on Rough Set Theory⋆

Yinghong Ma⋆⋆ and Yehong Han

School of Management, Shandong Normal University, Jinan, 250014, P.R. China
yinghongma71@163.com

Abstract. A decision table is a pair $S = (U, A)$, where U and A are nonempty finite sets called the universe and primitive attributes respectively. In order to computing the minimal rule sets on the decision table in which a new instance is added, a classification of the new instances and a criteria for the minimum recalculation are given, an incremental learning algorithm is presented and this algorithm is proved that can be used to the consistent and the inconsistent decision tables. The complexity of this algorithm is also obtained.

Keywords: rough sets, incremental learning, algorithm.

AMS Subject Classifications: TP18.

1 Introduction and Notations

Rough set theory was introduced by Z. Pawlak in 1982, it has been used in a variety of domains [1] [2] [3], such as machine learning, pattern recognition, decision support system and expert systems and so on. The incremental learning is a branch of machine learning. One of the main researches on rough sets theory is how to compute the attribute's reduction on a decision table, but those research is limited by the static data, but in real life, it is not such case, a new instance is allowed to put in S. Computing a minimal rule set on a decision table when the new instance is added, all the data in the decision table will be recalculated by the classical method [4]. In [5], there are three cases when a new instance x is added to S, x confirms the actual knowledge; x contradicts to the actual knowledge; x is completely new. But this category is not a partition of $S \cup \{x\}$. In [6] , a new category method based on decision logical was introduced, unfortunately, it isn't including all the cases.

Knowledge representation system is a pair $S = < U, A >$, where U and A are all nonempty finite sets called the universe and primitive attributes respectively. Every primitive attribute $a \in A$ is a total function $a : U \to V_a$, where V_a is the set of values of a, called the domination of a. Let $C, D \subset A$ be the condition and

---

⋆ This work is carried out under the Taishan Scholar project of Shandong China and the Doctor Foundation of Shandong(2006BS01015).
⋆⋆ Corresponding author.

decision attributes of A respectively. A KR-system with distinguished condition and decision attributes will be viewed as a decision table, denoted by $S = (U, A)$, the decision table often is often called a decision logic. Using the decision logic language(DL-language), the following notations are defined.

The set of formulas in decision logic language is a set satisfying the following conditions: (1) The expression of the forms (a, v) (in short a_v called elementary formulas) are formulas of the DL-language for any $a \in A$ and $v \in V_a$; (2) If θ, ψ are formulas of the DL-language, then $\neg\theta, \theta \vee \psi, \theta \wedge \psi, \theta \to \psi$ and $\theta \equiv \psi$ are formulas too. If $x \in U$ satisfies formula θ in $S = (U, A)$, denoted by $x \models_S \theta$. If θ is a formula, then the set $|\theta|_S$, defined as $|\theta|_S = \{x \in U : x \models_S \theta\}$, is called the meaning of the formula θ in S. Let $P = \{a_1, a_2, \cdots, a_n\}$ and $P \subseteq A$. Then $(a_1, v_1) \wedge (a_2, v_2) \wedge \cdots \wedge (a_n, v_n)$ is called a P-basic formula. If θ is a P-basic formula and $R \subseteq P$, we denote the R-basic formula obtained from the formula θ by removing all elementary formulas (a, v_a) such that $a \in P - R$ by θ/R. The other notation and definition not be given here can be find in [5].

2   An Algorithm for Incremental Learning

The Category of New Instances. Denoted the new instance by x and the new decision table by S', let M', R' be a minimal decision rule-set and a condition attribute reduction set of S' respectively. The new definitions and notations are given.

x is called matching M, if and only if all the rules $\theta \to \psi$ such that $\theta_x \to \theta$ in M imply $\psi_x \equiv \psi$, denote the set of thus x by I_m. The set $M_x = \{i|i \in U, \theta_x \to \theta_i, \psi_x \equiv \psi_i\}$ is called the matching domain of x, where $\theta_i \to \psi_i$ is the RD-rule reduction of object i. x is called totally contradicts to M if and only if all the rules $\theta \to \psi$ such that $\theta_x \to \theta$ in M imply $\psi_x \neq \psi$. x is partially contradicts to M if there exist a rule in M satisfying $\theta_x \to \theta$ such that $\psi_x \equiv \psi$ and there exist an other rule in M satisfying $\theta_x \to \theta$ such that $\psi_x \neq \psi$. Denote the set of those x by I_c. The set $C_x = \{i|i \in U, \theta_x \to \theta_i, \psi_x \neq \psi_i\}$ is called the contradict domination of x. If there is no rule $\theta \to \psi$ such that $\theta_x \to \theta$ in M, then x is called completely new in M. Denote the set of thus x by I_n.

By the above definitions, the following property holds.

Proposition 1. *Let I denote all the new instances for a decision table. Then $\{I_m, I_c, I_n\}$ is a partition of I.*

Proposition 2. *Let x be a new instance. If there is no an object $y \in C_x$ such that $y \models_S \theta_x/R$ in S. Then the reduction of condition attributes of S' is R.*

Proof: There is no an object $y \in C_x$ such that $y \models_S \theta_x/R$ in S, therefore, there is no any RD-rule $\theta \to \psi$ such that $\theta_x/R \equiv \theta$ and $\psi_x \neq \psi$ in S. Set $U' = U \bigcup\{x\}$ and $S' = (U', A)$. Then $POS_R(D)' = POS_R(D) \bigcup\{x\}$ and $POS_C(D)' = POS_C(D) \bigcup\{x\}$, where $POS_R(D)'$ and $POS_C(D)'$ are R-Positive region and C-Positive region of D on U' respectively. Hence $POS_C(D)' = POS_R(D)'$ since $POS_C(D) = POS_R(D)$. Therefor the reduction of condition attributes of S' is R because R is the D-independent subfamily of C in U'.   □

Proposition 3. *If there is an object $y \in M_x$, $y \models_S \theta_x$ in decision table S, then the decision table $S' = S$, and its reduction of attributes and minimal set of rules will not change.*

The proof of the above proposition is obvious.

Proposition 4. *If there is an object $y \in C_x$ such that $y \models_S \theta_x$ and there is no other object $i \in C_x (i \neq y)$ such that $i \models_S \theta_x/R$. Then There is a condition attributes reduction R' of S' such that $R' \subseteq R$.*

Proof: If there is unique $y \in C_x$ such that $y \models_S \theta_x$ in S, then $POS_C(D)' = POS_C(D) - \{y|y \models_S \theta_x\}$. There is no any other $i \in C_x$ such that θ_x/R, then $POS_R(D)' = POS_R(D) - \{y|y \models_S \theta_x\}$. Hence, $POS_C(D)' = POS_R(D)'$. Because the size of positive region is reduced when the new instance is add to S, R may be not the D-independent subfamily of C in U'. There is a reduction R' of condition attributes of S' such that $R' \subseteq R$.   □

Proposition 5. *If there are two objects $y \in C_x$ satisfying $y \models_S \theta_x$ at least, then R is still a condition attributes reduction of S'.*

Proof: If there are two objects $y_1, y_2 \in C_x$ satisfying $y_i \models_S \theta_x$ $(i = 1, 2)$, then $POS_R(D)' = POS_R(D)$ and $POS_C(D)' = POS_C(D)$. Hence $POS_C(D)' = POS_R(D)'$. The positive region doesn't change in S', R is the D-independent subfamily of C in U'. So a condition attribute reduction S' is still R.   □

Proposition 6. *Let $\theta_i \rightarrow \psi_i$ be a RD-rule reduction of object i in S, and $i \overline{\in} C_x \bigcup \{j|\theta'_j \equiv \theta'_h, h \in C_x, j \in M_x\}$ (where θ'_h and θ'_j are C-basic formulas of h and j respectively). Let W be the set of all minimal rule sets of S'. If an attribute reduction R in S is also an attribute reduction in S'. Then there is a minimal rule-set $M' \in W$ such that $\theta_i \rightarrow \psi_i \in M'$.*

Proof: because $i \overline{\in} C_x \bigcup \{j|\theta'_j \equiv \theta'_h, h \in C_x, j \in M_x\}$ (where θ'_h and θ'_j are C-basic formulas of h and j respectively). Clearly, there is no $\theta_x \rightarrow \theta_i$ nor $\psi_x \neq \psi_i$. Hence there is a minimal rule-set $M' \in W$ such that $\theta_i \rightarrow \psi_i \in M'$.   □

According to the above propositions, the following corollaries can be got.

Corollary 1. *If a new instance x matches to M, then M is also a minimal decision rule-set of S'.*

Corollary 2. *If a new instance x is completely new in M, then R is a condition attributes reduction of S' and a minimal set of rules of S' is $M \bigcup \{\theta'_x \rightarrow \psi_x | \theta'_x \rightarrow \psi_x$ is a reduction of $\theta_x/R \rightarrow \psi_x\}$.*

3   Algorithm for Incremental Learning

The algorithm for incremental learning
Input: $S = (U, A)$, R, M, x and its CD-basic rule $\theta_x \rightarrow \psi_x$.
Output: M' (the minimal rule set of S').

Algorithm: Set $M_1 = M_2 = M_3 = \emptyset$;

$\forall \theta \rightarrow \psi$ in M

    If $\theta_x \rightarrow \theta$ is false, then $M_1 = M_1 \bigcup \{\theta \rightarrow \psi\}$

    Else if $\psi_x \equiv \psi$, then $M_2 = M_2 \bigcup \{\theta \rightarrow \psi\}$

       Else $M_3 = M_3 \bigcup \{\theta \rightarrow \psi\}$.

    If $M_2 = M_3 = \emptyset$, then $M' = M \bigcup \{\theta'_x \rightarrow \psi_x\}$.

    Else if $M_3 = \emptyset$, then $M' = M$.

       Else compute $C_x = \{i | i$ is an object which rule is in $M_3\}$.

       If $\exists y \in M_x$ such that $y \models_S \theta_x$, then $M' = M$;

       Else if $\nexists y \in C_x$ such that $y \models_S \theta_x / R$, then $R' = \{R\}$

         else, $\exists y_i \in C_x$ $(i \geq 2)$ such that $y_i \models_S \theta_x$, then $R' = \{R\}$;

         if there is unique $y \in C_x$ such that $y \models_S \theta_x$, then compute R';

         Else compute R'.

       If $R \in R'$, then compute $C_{C_x} = \{\theta_j \rightarrow \psi_j |$ for all $i \in C_x$, $j \in M_x$, $\theta_i \equiv \theta_j\}$

       and M''. Set $M' = M'' \bigcup M_1 \bigcup M_2 - C_{Cx}$.

       Else simply the rules in S', then minimal rule set is M'.

    End for

OUTPUT M'.

Let m and n be the size of C and U respectively. If x matches to M or is completely new in M, the time-complexity of the algorithm is $O(mn)$. If x is contradicts to M and there no any object in C_x such that $y \models_S \theta_x / R$ or there are two objects $y_i \in C_x$ such that $y_i \models_S \theta_x$ $(i = 1, 2)$, the time-complexity of the algorithm is $O(mn^2)$. Those two cases are the best cases of the algorithm. But in other situations, the efficiency of this algorithm is $O(2^m n^2)$.

Acknowledgements

References

1. Mollestad T, *A rough set approach to data mining, extracting a logic default rules from data*, Norwegian University of Science and Technology, 1997.
2. Tong Linyun, An Liping, *Incremental learning of decision rules based on rough set theory*, Proceedings of the 4th World Congress on Intelligent Control and Automation, Shanghai, Press of East China University of Science and Technology, 2002: 420-425.
3. Liping An, Jianyong Zhang, Lingyun Tong, *Knowledge acquisition, incremental modification and reasoning based on rough set theory in expert systems*, Computer engineering and design, 25(1)(2004): 42-45.
4. Z. Pawlak, *Rough sets and intelliegent data analysis*, Information Sciences, 147(2002): 1-12.
5. Z. Pawlak, *ROUGH SETS: Theoretical Aspects of Reasoning about Data*, Kluwer Academic Publishers, 1991.
6. Ning Shan, Wojciech Ziarko, *Data-based acquisition and incremental modification of classification rules*, Computational Intelligence, 11(2)(1995): 357-370.

On f-Edge Cover-Coloring of Simple Graphs[*]

Jihui Wang[1,**], Sumei Zhang[1], and Jianfeng Hou[2]

[1] School of Science, University of Jinan, Jinan, 250022, P.R. China
wangjh@ujn.edu.cn
[2] Department of Mathematics, Shandong University, Jinan, 250100, P.R. China

Abstract. Let $G(V, E)$ be a simple graph, and let f be an integer function on V with $1 \leq f(v) \leq d(v)$ to each vertex $v \in V$. An f-edge cover-coloring of a graph G is a coloring of edge set E such that each color appears at each vertex $v \in V$ at least $f(v)$ times. The f-edge cover chromatic index of G, denoted by $\chi'_{fc}(G)$, is the maximum number of colors such that an f-edge cover-coloring of G exists. Any simple graph G has f-edge cover chromatic index equal to δ_f or δ_f-1, where $\delta_f = \min_{v \in V}\{\lfloor \frac{d(v)}{f(v)} \rfloor\}$. If $\chi'_{fc}(G) = \delta_f$, then G is of C_f I class; otherwise G is of C_f II class. In this paper, we give some sufficient conditions for a graph to be of C_f I class, and discuss the classification problem of complete graphs on f-edge cover-coloring.

Keywords: Simple graph, Edge-coloring, f-edge cover-coloring.

1 Introduction

Our terminology and notation will be standard. The reader is referred to [1] for the undefined terms. Graphs in this paper are simple, unless otherwise stated, i.e., they have no loops or multiple edges. We use V and E to denote, respectively, the vertex set and edge set of a graph G. Let $N_G(v)$ denote the neighborhood of v and let $d(v) = |N_G(v)|$ be the degree of v in G. We write δ for the minimum degree of G. We associate positive integer $1, 2, \cdots$ with colors, and we call C a k-edge coloring of G if $C : E \rightarrow \{1, 2, \cdots, k\}$. Let $C_i(v)$ denote the number of edges of G incident with vertex v that receive color i by the coloring C. Assume that a positive integer $f(v)$ with $1 \leq f(v) \leq d(v)$ is associated with each vertex $v \in V$. We call C an f-edge cover-coloring of G if for each vertex $v \in V$, $C_i(v) \geq f(v)$ for $i = 1, 2, \cdots, k$, that is each color appears at each vertex $v \in V$ at least $f(v)$ times. Let $\chi'_{fc}(G)$ denote the maximum number of colors for which an f-edge cover-coloring of G exists. We call $\chi'_{fc}(G)$ the f-edge cover chromatic index of G. In our daily life many problems on optimization and network design, e.g., coding design, the file transfer problem on computer networks, schedule problems and

so on, are related to the f-edge cover-coloring which was first presented by Song and Liu [5].

Let $\delta_f = \min\limits_{v \in V}\{\lfloor \frac{d(v)}{f(v)} \rfloor\}$, in which $\lfloor \frac{d(v)}{f(v)} \rfloor$ is the largest integer not larger than $\frac{d(v)}{f(v)}$. It is easy to verify that $\chi'_{fc}(G) \leq \delta_f$. Song and Liu studied the bound of f-edge cover chromatic index of a graph and obtained the following result.

Theorem 1. [5] *Let G be a graph. Let $f(v)$, $d(v)$ and δ_f be as defined earlier. Then*

$$\delta_f - 1 \leq \min_{v \in V}\{\lfloor \frac{d(v)-1}{f(v)} \rfloor\} \leq \chi'_{fc}(G) \leq \delta_f.$$

From the above theorem we can see that the f-edge cover chromatic index of any graph G must be equal to δ_f or δ_f-1. This immediately gives us a simple way of classifying graphs into two types according to $\chi'_{fc}(G)$. More precisely, we say that G is of C_f I class if $\chi'_{fc}(G) = \delta_f$, and that G is of C_f II class if $\chi'_{fc}(G) = \delta_f$-1.

Song and Liu also obtained the following two results.

Theorem 2. [5] *Let G be a bipartite graph. Let $f(v)$ and δ_f be as defined earlier. Then $\chi'_{fc}(G) = \delta_f$.*

Theorem 3. [5] *Let G be a graph. Let $f(v)$ and δ_f be as defined earlier. If $f(v)$ is positive and even for all $v \in V$, then $\chi'_{fc}(G) = \delta_f$.*

If $f(v) = 1$ for all $v \in V$, the classification problem on f-edge cover-coloring is reduced to the classification problem on the ordinary edge cover-coloring which was studied by Miao [4] and Wang [6]. Hilton [2] studied the f-edge cover-coloring of multigraph G with $f(v) = j \geq 2$ for all $v \in V$. In this paper, we study the f-edge cover chromatic index of simple graphs. In section 2, we give some sufficient conditions for a simple graph to be of C_f I class. In section 3, we discuss the classification problem of complete graphs on f-edge cover-coloring.

2 The Classification of Graphs on f-Edge Cover-Coloring

In this section, we give some sufficient conditions for a graph to be of C_f I class.

Let $V^* = \{v : \delta_f = \lfloor \frac{d(v)}{f(v)} \rfloor, \quad v \in V\}$, then we have the following important theorem.

Theorem 4. *Let G be a graph. Let $f(v)$ and V^* be as defined earlier. If $f(v^*) \nmid d(v^*)$ for all $v^* \in V^*$, then G is of C_f I class.*

Proof. By Theorem 1, it is enough to prove that $\min\limits_{v \in V}\{\lfloor \frac{d(v)-1}{f(v)} \rfloor\} \geq \delta_f$. For $\delta_f = \min\limits_{v \in V}\{\lfloor \frac{d(v)}{f(v)} \rfloor\}$, we have $\lfloor \frac{d(v)}{f(v)} \rfloor > \delta_f$ for each vertex $v \in V \setminus V^*$. So $\lfloor \frac{d(v)-1}{f(v)} \rfloor \geq \delta_f$.

On the other hand, for each vertex $v^* \in V^*$, $f(v^*) \nmid d(v^*)$ implies that $\frac{d(v^*)}{f(v^*)} > \lfloor \frac{d(v^*)}{f(v^*)} \rfloor = \delta_f$. So $\frac{d(v^*)-1}{f(v^*)} \geq \lfloor \frac{d(v^*)}{f(v^*)} \rfloor = \delta_f$, then we have $\min\limits_{v \in V}\{\lfloor \frac{d(v)-1}{f(v)} \rfloor\} \geq \delta_f$. Thus $\chi'_{fc}(G) = \delta_f$, this completing the proof. □

Let k be a positive integer and the k-core of G be the subgraph of G induced by the vertices v of G such that $k \mid d(v)$. The following lemma is given by Hilton and de Werra.

Lemma 1. [3] *Let G be a graph and let $k \geq 2$. If the k-core of G is a set of isolated vertices, then G has a k-edge coloring such that for each vertex $v \in V$ and each $i, j \in \{1, \cdots k\}$, $|C_i(v) - C_j(v)| \leq 1$ holds.*

Theorem 5. *Let G be a graph. Let $f(v)$, $d(v)$,δ_f and V_0^* be as defined earlier. If $V_0^* = \{v : \delta_f = \frac{d(v)}{f(v)}, \quad v \in V\}$ is a set of isolated vertices in graph G, then G is of C_f I class.*

Proof. If $\delta_f = 1$, obviously, G is of C_f I class. Assume that $\delta_f \geq 2$. Let $V_0 = \{v : \delta_f | d(v), \quad v \in V\}$ and $S = V_0 \setminus V_0^*$. It is easy to prove that for each vertex $v \in S$, $\frac{d(v)}{f(v)} > \delta_f$, that is $\frac{d(v)}{\delta_f} > f(v)$. Since $f(v)$ and δ_f are both integer, and $\delta_f | d(v)$. Then $\frac{d(v)}{\delta_f} \geq f(v) + 1$.

We shall form graph G' by adding a pendant edge to each vertex of S on graph G. Clearly, $\delta_f \nmid d(v)$ for each vertex $v \in S$, and V_0^* is the δ_f-core of G' which is a set of isolated vertices. By Lemma 1, G' has a δ_f-edge coloring such that for each vertex $v \in V(G)$ and $\forall\, i, j \in \{1, \cdots \delta_f\}$, $|C_i(v) - C_j(v)| \leq 1$ holds. Since for each vertex $v \in S$, we notice that $\lfloor \frac{d_{G'}(v)}{\delta_f} \rfloor \geq \lfloor \frac{d(v)}{\delta_f} \rfloor \geq f(v) + 1$, and $|C_i(v) - C_j(v)| \leq 1$ ($\forall\, i, j \in \{1, \cdots \delta_f\}$). That is, every color of $\{1, 2, \cdots \delta_f\}$ is represented at least $f(v) + 1$ times at v. By restricting the δ_f-edge coloring of G' to G, we obtain an f-edge cover-coloring of G with δ_f colors. That is, G is of C_f I class. This proves the Theorem. $\qquad\square$

3   The f-Edge Cover-Coloring of Complete Graphs

In this section, we discuss the classification problem of complete graphs on f-edge cover-coloring. Our main result is Theorem 6, in order to prove it, we need the following useful lemma which appears in [3].

Lemma 2. [3] *Let C be a k-edge coloring of graph G. If $|C_\alpha(v_0) - C_\beta(v_0)| > 2$ for some pair α, β of colors and some vertex v_0. Then G must be recolored with k colors such that*

$$\max_{1 \leq i < j \leq \delta} |C_i'(v_0) - C_j'(v_0)| \leq 2.$$

And for each $v \in V$, the number of colors appears on vertex v would not reduce.

A k-*factor* of a graph G is a k-regular spanning subgraph. Let G be an mk-regular graph. If $H_1, H_2, \ldots, H_m$ are edge-disjoint k-factors of G, then which is called a k-*factorization* of G.

Theorem 6. *Let G be a complete graph K_n. If k and n are odd integers, $f(v) = k$ and $k \mid d(v)$ for all $v \in V$, then G is of C_f II class. Otherwise, G is of C_f I class.*

Proof. If $\delta_f = 1$, obviously, G is of C_f I class. Assume that $\delta_f \geq 2$. Let $f^* = \max_{v \in V}\{f(v)\}$. If $f^* \nmid (n-1)$, then by Theorem 4, G is of C_f I class. Next suppose $f^* \mid (n-1)$, we consider the following two cases.

Case 1: n is even, suppose $n = 2t$, where t is a positive integer. Then $f^* \mid (2t-1)$. It is well-known that G has a 1-factorization, and we can give an f-edge cover-coloring of G with δ_f colors. G is of C_f I class.

Case 2: n is odd. Let $n = 2t + 1$, where t is a positive integer. There are three subcases.

Subcase 2.1. f^* is even, let $f^* = 2m$. It is well-known that $G = K_{2t+1}$ has a 2-factorization, and we also can give an f-edge cover-coloring of G with δ_f colors. So G is of C_f I class.

Subcase 2.2. If $f(v) = k$, $k \mid 2t$ and k is odd for all $v \in V$. We show that G is of C_f II class. Because $\delta_f = \min_{v \in V}\{\lfloor \frac{d(v)}{f(v)} \rfloor\}$, we have $\delta_f = \frac{d(v)}{k} = \frac{2t}{k}$. Suppose that $G = K_{2t+1}$ is of C_f I class. Thus $c_i(v) = k$ for each $i \in \{1, 2, \ldots, \delta_f\}$ and each $v \in V$. The number of edges colored with a color of δ_f colors is $\frac{k(2t+1)}{2}$. Obviously, $\frac{k(2t+1)}{2}$ is not an integer. This contradicts to our assumption. So $G = K_{2t+1}$ is of C_f II class when $f(v) = k$ is odd and $k \mid d(v)$ for all $v \in V$.

Subcase 2.3. f^* is odd and there exists at least a vertex $v \in V$ such that $f(v) < f^*$. Clearly, $\delta_f = \frac{2t}{f^*}$. We will give an f-edge cover-coloring of G with δ_f colors as follows. Suppose v' is the vertex of graph G such that $f(v') \leq f^* - 1$. Let $G' = G \setminus \{v'\}$. Obviously, $G' = K_{2t}$, and let $H = \{H_1, H_2, \ldots, H_{2t-1}\}$ is a 1-factorization of G'. Partition H into δ_f subsets $A_1, A_2, \ldots, A_{\delta_f}$, in which $|A_{\delta_f}| = f^* - 1$ and $|A_i| = f^*, 1 \leq i \leq \delta_f - 1$. Assign color i to the edges in A_i, for each $i \in \{1, 2, \ldots, \delta_f\}$. Clearly, $C_i(v) = f^*$ for all $v \in V(G')$ and all $i \in \{1, 2, \ldots, \delta_f - 1\}$, but $C_{\delta_f}(v) = f^* - 1$ for all $v \in V(G')$. Let $E_{v'} = \{v'u : u \in V(G')\}$, and we color the edges in $E_{v'}$ with color δ_f. Then $C_i(v) = f^* \geq f(v)$ for all $v \in V(G')$ and all $i \in \{1, 2, \ldots, \delta_f\}$, and $C_{\delta_f}(v') - C_i(v') = 2t$ for all $i \neq \delta_f$. We apply Lemma 2 successively to vertex v' for each color of $\{1, 2, \ldots, \delta_f - 1\}$ and color δ_f, until we ultimately obtained a δ_f-edge coloring C' of graph G such that for each vertex $v \neq v'$ and for all $i \in \{1, \cdots, \delta_f\}$, $C_i'(v) = C_i(v) = f^* \geq f(v)$ and $|C_i'(v') - C_j'(v')| \leq 2$ for all $i, j \in \{1, \cdots, \delta_f\}$. It implies $C_i'(v') \geq \lfloor \frac{2t}{\delta_f} \rfloor - 1 = f^* - 1 \geq f(v')$ for each $i \in \{1, \cdots, \delta_f\}$. Then C' is an f-edge cover-coloring of G. Graph G is of C_f I class. This completes the proof of the theorem. $\square$

References

1. J.Bondy and U.Murty, *Graph theory with applications*, MacMillan,London (1976).
2. A.Hilton, *Coloring the edges of a multigraph so that each vertex has at most j, or at least j edges of each color on it*,J. London Math. Soc. **12**(1975), 123-128.
3. A.Hilton and D.Werra, *A sufficient condition for equitable edge-colouring of simple graphs*, Discrete Math. **128** (1994),179-201.

4. L.Miao and S.Pang,*The Classification of Graphs on Edge Covering coloring*, Journal of Matheticas. **21** (2001),368-372.
5. H.Song and G.Liu, *on f-Edge Cover-coloring of graphs*, Acta Math. Sinica. **48** (2005),919-928.
6. J.Wang,X.Zhang and G.Liu, *Edge Covering Coloring of Nearly Bipartite Graphs,* J. Appl. Math. and Comput. **22** (2006),435-440.

Upper Bounds on the $D(\beta)$-Vertex-Distinguishing Edge-Chromatic Numbers of Graphs*

Tian Jing-jing[1,2], Liu Xin-sheng[1], Zhang Zhong-fu[1], and Deng Fang-an[1]

[1] Department of Mathematics, Shaanxi University of Technology,
Hanzhong, Shaanxi 723001, China
[2] College of Mathematics and Information Science, Northwest Normal University,
Lanzhou, Gansu 730070, China
tianjj_1225@yahoo.com.cn

Abstract. In this paper, let d be the maximum degree of G, we study the upper bounds for the $D(\beta)$-vertex-distinguishing edge-chromatic number by probability method and prove that

$$\chi'_{\beta-vd}(G) \leq \begin{cases} 2\sqrt{2(\beta-1)}d^{\frac{\beta+2}{2}}, & d \geq 4, \beta \geq 4; \\ 8d^{\frac{5}{2}}, & d \geq 6, \beta = 3; \\ 32d^2, & d \geq 4, \beta = 2. \end{cases}$$

It is well known to compute the chromatic number of a graph is NP-Hard in graph theory. In the past, the people have some results about it by combined methods, see [1, 2, 3].At ICM2002, Noga Alon advanced a new theory that graph coloring could studied by probability methods. For instance, some conclusions have been gotten by probability methods, see[4][5][6][7]. In 2006, Zhang Zhongfu present a new concept of the α-$D(\beta)$-*vertex-distinguishing proper edge-coloring* and conjecture, see [8]. In this paper, let d be the maximum degree of G, we study the upper bounds for the $D(\beta)$-vertex-distinguishing edge-chromatic number by probability method

All the graphs $G = G(V,E)$ discussed in this paper are finite, undirected, simple and connected. Let d be the maximum degree of G and δ be the minimum degree of G.

Definition 1. α-$D(\beta)$-*vertex-distinguishing proper edge-coloring $D(\beta)$-vertex-distinguishing edge-chromatic number, see [8].*

Definition 2. *dependency digraph, see [10].*

Lemma 1 ((The General Local Lemma)). *see[9][10]*

Please refer to [11] for other terminologies and notations.

Theorem 1. *Let d be the maximum degree of G, then*

$$\chi'_{\beta-vd}(G) \leq \begin{cases} 2\sqrt{2(\beta-1)}d^{\frac{\beta+2}{2}}, & d \geq 4, \beta \geq 4; \\ 8d^{\frac{5}{2}}, & d \geq 6, \beta = 3; \\ 32d^2, & d \geq 4, \beta = 2. \end{cases}$$

Proof. We only give the proof for the case that $\beta \geq 4, d \geq 4$, the other cases can be proved similarly. The proof consists of five steps. We assign to each edge of G a uniformly random coloring from $\{1, 2, \ldots, 2\sqrt{2(\beta-1)}d^{\frac{\beta+2}{2}}\}$ named this new coloring f. We will use Lemma 3 to show that a positive probability, f is a $D(\beta)$-vertex-distinguishing proper edge-coloring.

Step 1. The following bad events are defined :
$< 1 >$For each pair of incident edges e, f, let $A_{e,f}$ be the event that both e and f are colored with the same color;
$< 2 >$ For each edge $e = uw$, such that $deg(u) = deg(w) \geq \delta(G)$, let B_e be the set of all edges which are connected u or w, then E_{B_e} is the events that the edges which are adjacent to u and w are colored properly, and $C(u) = C(w)$;
$< 3 >$ For each path whose length is 2, $P_{uv} = uewfv$, such that $deg(u) = deg(v) \geq \delta(G)$, let P_{uv} be the set of all edges which are connected u or v, then $E_{P_{uv}}$ is the event that the paths which are adjacent to u and v are colored properly, and $C(u) = C(v)$;
$\ldots$ $\ldots$ $\ldots$
$< \beta + 1 >$ For each path whose length is β, $P_{u(\beta)} = uewfv\ldots, \beta$, such that $deg(u) = deg(\beta) \geq \delta(G)$ let $P_{u\beta}$ be the set of all edges which are connected u or β, then $E_{P_{u\beta}}$ be the event that the edges which are adjacent to u and β are colored properly, and $C(u) = C(\beta)$.
It remains to show that with positive probability none of these events happen, then f is a $D(\beta)$-VDPEC of G. Let us construct dependency graph H whose nodes are all the events of two nodes E_X and E_Y are adjacent if and only if X and Y contain at least one common edge. Since the occurrence of each event E_X depends only on the edges of X, H is dependency graph for our events. In order to apply The General Local Lemma, we need estimates for the probability of each event and the number of nodes of each type in H which are adjacent to any give node.These estimates are given in the two steps below.

Step 2. Estimate the probability of each event:

$$\Pr(A_{e,f}) = \frac{1}{2\sqrt{2(\beta-1)}d^{\frac{\beta+2}{2}}};$$

$$\Pr(E_{B_e}) = \frac{1}{\binom{2\sqrt{2(\beta-1)}d^{\frac{\beta+2}{2}}}{1}} + \binom{2\sqrt{2(\beta-1)}d^{\frac{\beta+2}{2}}}{2} + \ldots + \binom{2\sqrt{2(\beta-1)}d^{\frac{\beta+2}{2}}}{d-1}}$$

$$< \frac{1}{(d-1)2\sqrt{2(\beta-1)}d^{\frac{\beta+2}{2}}};$$

$$\Pr(E_{P_{uv}}) = \Pr(E_{P_{ur}}) = \ldots = \Pr(E_{P_{u(\beta-1)}}) = \Pr(E_{P_{u\beta}})$$

$$= \frac{1}{(2\sqrt{2(\beta-1)}d^{\frac{\beta+2}{2}})^d} \frac{1}{(2\sqrt{2(\beta-1)}d^{\frac{\beta+2}{2}})^d}$$

$$= \frac{1}{(2\sqrt{2(\beta-1)}d^{\frac{\beta+2}{2}})^{2d}}.$$

Step 3. Estimate the dependency events number, in the following table:

event	< 1 >	< 2 >	< 3 >	< 4 >	. .	< $\beta+1$ >
$A_{e,f}$	$4d-5$	$3d-2$	$2(d-1)^2+$ $d(d-1)$	$2(d-1)^3$ $+d(d-1)^2$	...	$2(d-1)^\beta$ $+d(d-1)^{\beta-1}$
E_{B_e}	$(2d-1)(2d-2)$	$(2d-2)d$ $+1$	$(2d-1)d(d-1)$	$(2d-1)d(d-1)^2$	...	$(2d-1)d(d-1)^{\beta-1}$
$E_{P_{uv}}$	$2d(2d-1)$ $+1+2(d-2)$	$2d^2$ $+d-2$	$2(d-1)^3$ $+d(d-1)$	$2(d-1)^4+d(d-1)^2$	...	$2(d-1)^{\beta+1}$ $+d(d-1)^{\beta-1}$
$E_{P_{ur}}$	$2(d-1)(2d-1)$ $+2+4(d-2)$	$2d^2+2d$ -3	$2d(d-1)^2$ $+2d(d-1)-3$	$2d(d-1)^3$ $+2d(d-1)^2-3$	...	$2d(d-1)^\beta+$ $2d(d-1)^{\beta-1}-3$
...	...	...	...	...	...	...
$E_{P_{u\beta}}$	$2(d-1)(2d-1)$ $+(\beta-1)+$ $2(\beta-1)(d-2)$	$2d^2$ $+(\beta-1)d$ $-\beta$	$2d(d-1)^2+$ $(\beta-1)d(d-1)-\beta$	$2d(d-1)^3+$ $(\beta-1)d(d-1)^2-\beta$	...	$2d(d-1)^\beta+$ $(\beta-1)d(d-1)^{\beta-1}-\beta$

Step 4. Find the real constant $x_i(0 \le x_i \le 1)$ for applying Lemma 3. Let

$$\sqrt{2(\beta-1)}d^{\frac{\beta+2}{2}}, (d-1)\sqrt{2(\beta-1)}d^{\frac{\beta+2}{2}}, (\sqrt{2(\beta-1)}d^{\frac{\beta+2}{2}})^{2d}, \ldots, (\sqrt{2(\beta-1)}d^{\frac{\beta+2}{2}})^{2d}$$

be the constants associated with events of Type $< 1 >, < 2 >, \ldots, < \beta+1 >$.

Step 5. Conclude that with positive probability no events of Type $< 1 >, < 2 >, < 3 >, \ldots, < \beta+1 >$ provided that:
Let $m = \sqrt{2(\beta-1)}d^{\frac{\beta+2}{2}}$.
(1)

$$\frac{1}{2m} \le \frac{1}{m}(1-\frac{1}{m})^{4d-5}(1-\frac{1}{(d-1)m})^{3d-2} \cdot (1-\frac{1}{m^{2d}})^{d(d-1)+2(d-1)^2}$$

$$\cdot(1-\frac{1}{m^{2d}})^{2(d-1)^3+d(d-1)^2} \cdot \ldots \cdot (1-\frac{1}{m^{2d}})^{d(d-1)^{\beta-1}+2(d-1)^\beta};$$

(2)

$$\frac{1}{2(d-1)m} \le \frac{1}{(d-1)m}(1-\frac{1}{m})^{(2d-1)(2d-2)} \cdot (1-\frac{1}{(d-1)m})^{(2d-2)d+1}$$

$$\cdot(1-\frac{1}{m^{2d}})^{(2d-1)d(d-1)} \cdot (1-\frac{1}{m^{2d}})^{(2d-1)d(d-1)^2} \cdot \ldots \cdot (1-\frac{1}{m^{2d}})^{d(d-1)^{\beta-1}(2d-1)};$$

(3)

$$\frac{1}{(2m)^{2d}} \le \frac{1}{m^{2d}}(1-\frac{1}{m})^{2d(2d-1)+2(d-2)+1} \cdot (1-\frac{1}{(d-1)m})^{2d^2+d-2}$$

$$\cdot (1-\frac{1}{m^{2d}})^{2(d-1)^3+d(d-1)} \cdot (1-\frac{1}{m^{2d}})^{2(d-1)^4+d(d-1)^2}$$

$$\cdot \ldots \cdot (1-\frac{1}{m^{2d}})^{2(d-1)^{\beta+1}+d(d-1)^{\beta-1}};$$

$(4-\beta+1)$

$$\frac{1}{(2m)^{2d}} \le \frac{1}{m^{2d}}(1-\frac{1}{m})^{2(d-1)(2d-1)+(t-1)+2(t-1)(d-2)} \cdot (1-\frac{1}{(d-1)m})^{2d^2+(t-1)d-t}$$

$$\cdot (1-\frac{1}{m^{2d}})^{2d(d-1)^2+(t-1)d(d-1)-t} \cdot (1-\frac{1}{m^{2d}})^{2d(d-1)^3+(t-1)d(d-1)^2-t}$$

$$\cdot \ldots \cdot (1-\frac{1}{m^{2d}})^{2d(d-1)^{\beta}+(t-1)d(d-1)^{\beta-1}-t} \cdot (t=3,\ldots,\beta)$$

Now, since $(1-\frac{1}{z})^z \ge \frac{1}{4}$ for all real $z \ge 2$, and $(\sqrt{2(\beta-1)}d^{\frac{\beta+2}{2}})^{2d} \ge (\sqrt{2(\beta-1)}d^{\frac{\beta+2}{2}})^2$, we can prove that the inequalities $(1), (2), \ldots, (\beta+1)$ are true, when $d \ge 4, \beta \ge 4$, Using Lemma 3, G has $(2\sqrt{2(\beta-1)}d^{\frac{\beta+2}{2}})$-$D(\beta)$-VDPEC,when $d \ge 4, \beta \ge 4$.

This completes the proof.

References

1. Zhang Zhongfu, Liu Linzhong, Wang weifan, Adjacent strong Edge Coloring of Graphs, Applied Mathematics Letters, **5**(2002) 623-626.
2. Wang Weifan, Equitable total coloring of graphs with maximum degree 3, Graphs and Combinatorics, **18**(2002) 677-85.
3. Bazgan C., Harkat-Benhamdine A., Li Hao and et al, On the Vertex-distinguishing Proper Edge-colorings of Graphs, J. Combin Theory(Ser. B), **75**(1999) 288-301.
4. Alon N, Sadakov B, Zaks, A. Acyclic Edge Coloring of Graphs, Journal of Graph Theory, **37**(2001)157-167.
5. Sun yirong, Yan Jingzhi, Relationship Between Girth and Acyclic Edge Chromatic Numbet of Graphs, Journal of Mathematical Study Series B, **95**(2005)246-256.
6. H. Hatami, $\Delta+300$ is a bound on the adjacent vertex distinguishing edge Chromatic Numbet of Graphs, Journal of Combinatorial Theory, **36(2)**(2003)135-139.
7. Liu Xinsheng, An Mingqiang, Chen Xiang'en, An Upper Bound for the Adjacent Vertex-distinguishing Acyclic Edge Chromatic Number, sumbitted.
8. Zhang Zhongfu, Li Jinwen, $D(\beta)$-Vertex edge coloring of graph, Journal of Mathematical, **49(3)**(2006) 703-708.
9. M. Michael, R. Bruce, Graph Coloring and the Probabilistic Method, Springer, 2002.
10. A. N. Spencer, J. H. Erdos, Paul, The Probabilistic Method, 1992.
11. J. A. Bondy, U. S. R. Marty, Graph Theory with Applications, The Macmillan Press Ltd, New York, 1976.

The Equitable Edge-Coloring of Series-Parallel Graphs[*]

Huimin Song[1], Jianliang Wu[2], and Guizhen Liu[2]

[1] Department of Applied Mathematics, Shandong University at Weihai, Weihai, 264209, P.R. China
[2] School of Mathematics and System Science, Shandong University, Jinan, 250100, P.R. China

Abstract. An edge-coloring of a graph G is *equitable* if, for each vertex v of G, the number of edges of any one color incident with v differs from the number of edges of any other color incident with v by at most one. A graph G is called equitable if G has an equitable edge-coloring with k colors for any integer $k \geq 1$. A plane graph is series-parallel graph if it contains no subgraphs homeomorphic to K_4. In the paper, we prove that any simple and connected series-parallel graph is equitable if and only if it is not an odd circuit.

Keywords: edge-coloring; equitable, series-parallel graph.

1 Introduction

Throughout the paper, all graphs are finite, simple and undirected. Let G be a graph, $V(G)$ and $E(G)$ denote the set of vertices and the set of edges of G, respectively. We associate positive integer $1, 2, \ldots$ with colors, and call C a k-edge-coloring of G if $C : E \rightarrow \{1, 2, \ldots, k\}$. Let $C_v^{-1}(i)$ denote the number of edges of G incident with vertex v that receive color i by the coloring C. We call C an equitable k-edge-coloring of G if for each vertex $v \in V$

$$|C_v^{-1}(i) - C_v^{-1}(j)| \leq 1 \quad (1 \leq i < j \leq k) .$$

A graph G is called *equitable* if G has an equitable k-edge-coloring for any integer $k \geq 1$. It is an interesting problem to determine whether a graph is equitable or not. If a graph is equitable, then its edge chromatic index is equal to its maximum degree Δ and its edge cover chromatic index equal to its minimum degree δ (refer to [1] for the definition of edge cover chromatic index).

A plane graph is series-parallel graph if it contains no subgraphs homeomorphic to K_4, denoted by SP graph briefly. A series-parallel graph is a kind of very interesting graph which has many good properties and is well applied in electricity networks.

A circuit is a connected graph in which each vertex has even degree. A circuit is odd, or even, if the number of edges is odd, or even, respectively. It is stated in

[2] that a connected graph G has an equitable 2-edge-coloring if and only if it is not an odd circuit. Hilton and Werra [3] gave a sufficient condition for equitable edge-coloring of simple graphs. Werra[2] has proved that all bipartite graphs are equitable. Wu Jian-liang [4] has proved that a connected outerplanar graph is equitable if and only if it is not an odd circuit.

2   The Main Result

In this paper, we consider the equitable edge-coloring of simple series-parallel graphs and obtain the following result.

Theorem 1. *Any simple and connected series-parallel graph is equitable if and only if it is not an odd circuit.*

Firstly we discuss the properties on the structure of series-parallel graphs. Wu Jian-liang has made many researchs on the structure of series-parallel graphs and gained some results by which some problems on the list edge-coloring and the linear arboricity of series-parallel graphs are successfully solved (see [5,6]). We will discuss the structure of series-parallel graphs more meticulously by new methods. Our result on the structure of series-parallel graphs will be more appropriate for the discussion of the equitable edge-coloring of series-parallel graphs.

A 2-connected series-parallel graph can be gained from K_2 by iteratively using the following operations: Replace an edge with a path of length 2 (denoted by S-operation briefly) or duplicate an edge (denoted by P-operation briefly). For every 2-connected series-parallel graph, we can express the operation process with a complete binary tree. For we always begin constructing a SP graph with K_2, let an isolated point denote the only edge in K_2 at the beginning. If an S-operation is performed on an edge, call the point representing the edge S-node and join two son nodes to the S-node each of which represents one of the two edges on the path of length 2 respectively; If a P-operation is performed on an edge, call the point representing the edge P-node and join two son nodes to the P-node which represent the edge and its duplicate respectively. By the above process, every 2-connected series-parallel graph G corresponds to a complete binary tree T.

By discussing the corresponding complete binary trees in detail, we obtain the properties on the structure of simple SP graphs which are described in the following lemma. In the following, $N_G(v)$ denotes the set of vertices adjacent to a vertex v in G, without confusion, $N(v)$ briefly. A vertex v is called a k-vertex if $|N_G(v)| = k$.

Lemma 1. *Let G be a simple and 2-connected series-parallel graph of order at least 5. Then one of the following conditions holds:*

1. *G has two adjacent 2-vertices x and y;*
2. *G has two different 2-vertices x and y and $N(x) = N(y)$;*
3. *G has a 4-vertex z adjacent to two 2-vertices x and y such that $N(z)\backslash\{x, y\} = \{N(x) \cup N(y)\} \backslash \{z\}$;*

4. G has a 3-vertex w with $N(w) = \{x, y, z\}$ such that both x and y are 2-vertices, $N(x) = \{z, w\}$ and $yz \notin E(G)$;

5. G has two adjacent 3-vertices x and y such that $N(x) \cap N(y) = \{z\}$ and $N(z) = \{x, y\}$;

6. G has two adjacent 3-vertices w_1 and w_2 such that $N(w_1) = \{x, z_1, w_2\}$, $N(w_2) = \{y, z_2, w_1\}$, $N(x) = \{z_1, w_1\}$ and $N(y) = \{z_2, w_2\}$;

7. G has a 3-vertex w with $N(w) = \{x, y, z\}$ such that $N(z) = \{w, y\}$ and $xy \in E(G)$;

8. G has two nonadjacent 3-vertices w_1 and w_2 such that $N(w_1) = \{x, y, z_1\}$, $N(w_2) = \{x, y, z_2\}$, $N(z_1) = \{x, w_1\}$ and $N(z_2) = \{y, w_2\}$;

9. G has two nonadjacent 3-vertices w_1 and w_2 such that $N(w_1) = \{x, y, z_1\}$, $N(w_2) = \{x, y, z_2\}$, $N(z_1) = \{x, w_1\}$ and $N(z_2) = \{x, w_2\}$;

10. G has a 3-vertex w with $N(w) = \{x, z_1, z_2\}$ such that there is a 2-vertex $y \in N(z_1) \cap N(z_2)$ and $N(x) = \{z_1, w\}$.

Let C denote color set $\{1, 2, \cdots, k\}$. Given a edge-coloring φ of G in which k colors in C are used. For each vertex $v \in V(G)$, let $\varphi_v^{-1}(i)$ denote the number of edges of G incident with vertex v that receive color i by the coloring φ, and let $C_\varphi(v) = \{i | \varphi_v^{-1}(i) = \min_{1 \leq j \leq k} \varphi_v^{-1}(j)\}$. Obviously, $|C_\varphi(v)| \geq 1$.

Now we will give the main idea for the proof of our theorem. It is known that a connected graph G has an equitable 2-edge-coloring if and only if it is not an odd circuit. So it is only to prove that any simple and connected SP graph G has an equitable k-edge-coloring for any integer $k \geq 3$. We prove the result by induction on $|G|$, the number of vertices of G.

When $|G| \leq 4$, the result is obvious. Assume that p $(p \geq 5)$ is an integer and that the theorem holds for all simple SP graphs with less than p vertices. Let G be a simple and connected SP graph of order p. If G is not 2-connected, there is a cut vertex $v \in V(G)$ such that $G - v$ is not connected. Select a component of $G - v$ arbitrarily, let S denote its vertex set, $\bar{S}$ denote the set of vertices in $G - v$ which do not belong to S. Let G_1 denote the subgraph of G induced by $S \cup \{v\}$, G_2 denote the subgraph of G induced by $\bar{S} \cup \{v\}$. It is obvious that $E(G) = E(G_1) \cup E(G_2)$ and $V(G) = V(G_1) \cup V(G_2)$. Because both G_1 and G_2 are SP graphs of order less than p, then G_1 and G_2 have equitable k-edge-colorings φ_1 and φ_2 respectively. Let $k_1 = k - |C_{\varphi_1}(v)|$, $k_2 = |C_{\varphi_2}(v)|$. By interchanging the colors used, an equitable k-edge-coloring φ_1' of G_1 and an equitable k-edge-coloring φ_2' of G_2 will be gained such that $C \backslash C_{\varphi_1'}(v) = \{1, 2, \cdots, k_1\}$, $C_{\varphi_2'}(v) = \{1, 2, \cdots, k_2\}$. Combine coloring φ_1' in G_1 with coloring φ_2' in G_2, an equitable k-edge-coloring of G will be gained.

In the following we suppose that G is 2-connected. According to Lemma 1, the proof can be divided into ten parts. In every case as described in Lemma 1, we always obtain a simple SP graph G^* of order less than p. By the induction hypothesis, G^* has an equitable k-edge-coloring φ. On the basis of φ, we always can construct an equitable k-edge-coloring σ of G using the same set of k colors. By the induction, the theorem is true.

3   Concluding Remarks

An outerplanar graph is a graph which contains no subgraphs homeomorphic to K_4 or $K_{2,3}$. That is to say, an outerplanar graph is also a series-parallel graph. From this point of view, our result generalizes the result in [4].

References

1. Miao lianying, Liu Guizhen: Edge covered coloring and fractional edge covered coloring. J. of Systems Science and Complexing **15(2)**(2002) 187-193.
2. D. de Werra: Equitable colorations of graphs. Revue francaise d'Informatique et de Recherche Operationelle, **R-3**(1971) 3-8.
3. A. J. W. Hilton, D. de Werra: A sufficient condition for equitable edge-coloring of simple graphs. Discrete Math. **128** (1994) 179-201.
4. Wu Jianliang: The equitable edge-coloring of outerplanar graphs. JCMCC **36:1** (2001) 247-253.
5. Wu Jianliang: List edge-coloring of series-parallel graphs. Journal of Shandong University(Natural Science) **35(2)** (2000) 144-149.
6. Wu Jianliang: The linear arboricity of series-parallel graphs. Graphs and Combinatorics **16**(2000) 367-372.

A Low Complexity Intrusion Detection Algorithm

Lin Yao[1] and Kai Yao[2]

[1] Software College of Dalian University of Technology, Dalian 116023, China
lin_yao@eyou.com
[2] Library Information Center of Shenyang University of Technology, Shenyang 150001, China
frantodd2002@yahoo.com.cn

Abstract. A low complexity clustering algorithm for intrusion detection based on wavecluster is presented. Using the multiresolution property of wavelet transforms, we can effectively identify arbitrarily shaped clusters at different scales and degrees of detail, moreover, applying wavelet transform removes the noise from the original feature space and make more accurate cluster found. Experimental results on KDD-99 intrusion detection dataset show the efficiency and accuracy of this algorithm. A detection rate above 98% and a false alarm rate below 3% are achieved. The time complexity of the wavecluster algorithm is $O(N)$, which is comparatively low than other algorithms.

1 Introduction

Network Intrusion detection is the process of monitoring the events occurring in a computing system or network and analyzing them for signs of intrusions, defined as attempts to compromise the confidentiality, integrity, availability, or to bypass the security mechanism of a computer or network. Recently, many researchers turned into data mining techniques to attack the problem. Data mining can improve variants detection rate, control false alarm rate, and reduce false dismissals. A wide variety of data mining techniques has been applied to intrusion detections. In data mining, clustering is the most important unsupervised learning process used to find the structures or patterns in a collection of unlabeled data. Until now, the clustering algorithms can be categorized into four main groups: partitioning algorithm, hierarchical algorithm, density-based algorithm and grid-based algorithm[1],[2],[3]. Gholamhosein proposed wavecluster approach, which is a grid-based approach, and successfully used in image processing[4].We extend wavecluster to use in intrusion detection, but traffic in a network is never stagnant, for example, new services can be activated, work patterns can change as projects start or finish, and so on. Consequently, an intrusion detection system needs to be able to adapt to these changing traffic patterns while still maintaining a high level of detection accuracy. To deal with these issues, we modify wavecluster and develop a low complexity wavecluster algorithm with little prior knowledge, the proposed method allows the discovery of clusters of any shape and can detect timely not only the known intrusion types, but also their variants.

The rest of the paper is organized as follows. Section 2 discusses the low complexity wavecluster method, in section 3, we present the experimental evaluation of the wavecluster method using KDD-99 intrusion detection dataset. Finally, we present concluding remark and suggestions for future study.

2   Low Complexity Wavecluster Algorithm

Given a set of spatial objects, the goal of the adaptive algorithm is to detect cluster and assign labels to the objects based on the cluster that they belong to, thus it can detect whether there is intrusion exists. Applying wavelet transform to transform the original feature space and then find the dense regions in the new space. It yields sets of clusters at different resolutions and scales, which can be chosen based on user needs. The main step of adaptive wavecluster algorithm are shown in Algorithm 1.

Algorithm 1.
Input: Multidimendional data objects feature vectors
Output: clustered objects
1. Quantize feature space, then assign objects to the cells.
2. Apply wavelet transform on the quantized feature space.
3. Find the connected components in the subbands of transformed feature space.
4. Assign labels to the cells
5. Map the objects to the clusters

The first step of the adaptive wavecluster algorithm is to quantize the feature space, where each dimension A_i in the d-dimensional feature space will be divided into m_i intervals. Then, corresponding cell for the objects will be determined based on their feature values. A cell $C_i=[c_{i1},c_{i2},...c_{id}]$ contains an object $O_i=[o_{k1},o_{k2},...o_{kd}]$.

We recall that c_{ij} is the right open interval in the partitioning of A_j. For each cell, we count the number of objects contained in it to aggregation of the objects. The quantization m_i effect the performance of this algorithm, we set the correct value of m_i for intrusion detection dataset by simulation. In the second step, discrete wavelet transform will be applied on the quantized feature space. Applying wavelet transform on the cells in $\{C_j:1<j<h\}$ results in a new feature space, that is new cells. Given the set of new cells, wavecluster detects the connected components in the transformed feature space. Each connected component is a set of new cells and is considered as a cluster. For finding the connected components, we define that a new neighborhood for intrusion detection application, that is ,the neighborhood is defined in Euclidean space, a significant cell a in the transformed feature space is neighbor of another cell b if a lies within one of the four grid cells surrounding cell b,with the shortest Euclidean distances is defined to be its nearest neighbors. With an indexing scheme such as an R-tree, it is very easy to find the neighborhoods in short time.

Each cluster w will have a cluster number w_n, the adaptive wavecluster algorithm labels the cells in each cluster in the transformed feature with its cluster number. Calculate the mean of every cluster, remark as x_n. The clusters that are found are in the transformed feature space and are based on wavelet coefficients. Thus, they cannot be directly used to define the clusters in the original feature space. We make a lookup table to map the cells in the original feature space. Each entry in the table

specifies the relationship between one cell in the transformed feature space and the corresponding cell in the original feature space. Finally, the algorithm assigns the label of each cell in the feature space to all the objects whose feature vector is in that cell, and thus the cluster as determined.

When the objects are assigned to the cells of the quantized feature space at step 1 of the algorithm, the final content of the cells is independent of the order in which the objects are presented performed on these cells. Hence, the algorithm will have the same results for any different order of input data, so it is order insensitive with respect to input objects.

3 Experimental Results

In order to evaluate the low complexity wavecluster algorithm, we test the algorithm on a benchmark dataset, the network traffic data from the KDD Cup 1999 dataset. In the experiments, the values of each features are normalized with the minimum and maximum values of that features so that they fall in the range of [0,1]. In our experiment, beside the normal instances, instances of three popular attacks are involved: ipsweep, smurf, neptune. For each type, only one seed point is labeled at the beginning, and four nearest neighbors are defined as the nearest neighborhood of each instance. As shown in Table I, most attacks can be distinguished from the normal activities and the detection rate is as high as 98.3%. At the same time, the false alarm rate is approximately 1.8%. Assuming m cells in each dimension of feature space, there would be $K=m^d$ cells. Complexity of applying wavelet transform on the quantized feature space will be $O(dK)$.Since we assume that the value of d is low, we can consider it as a constant, thus $O(dK)=O(K)$.Making the lookup table requires $O(K)$ time. The time complexity of last step of our low complexity wavecluster algorithm is $O(N)$. Since this algorithm is applied on very large databases with a low number of dimensions, we can assume that $N>K$.Thus, based on this assumption, the overall time complexity of the algorithm will be $O(N)$.

Table 1. Experiment Result

Experiment	Detection Rate	False Alarm Rate
First	98.3%	1.8%
Second	98.7%	1.7%

4 Conclusion

In this paper, we present a low complexity wavecluster algorithm for intrusion detection, which can adapt to changes in normal traffic. Experimental results on a subset of KDD-99 dataset showed the stability of efficiency and accuracy of the adaptive wavecluster algorithm. With different setting, the detection rate stayed

always above 98% while the false alarm rate was below 3%. The time complexity of adaptive wavecluster is low, which is $O(N)$, N is the number objects in the database.

Acknowledgment

References

1. Pauwels EJ, Fiddelaers P,Van Gool L. DOG-based unsupervised clustering for CBIR. In Proceedings of the 2nd International Conference on Visual Information Systems, Vol.2, San Diego,Calif (2003) 137-145.
2. Wang W, Yang J,Muntz R.STING: A Statistical Information Grid Approach to Spatial Data Mining. In Proceedings of the 23rd VLDB Conference, Athens, Vol.30, Greece(2000) 186-195.
3. Xu X,Ester M,Kriegel H. A distribution-based clustering algorithm for mining in large spatial database. In Proceedings of the 14th International Conference on Data Engineering, Vol.41,Orlanda,Fla.(2002)324-331.
4. Gholamhosein S. et al, WaveCluster: a wavelet-based clustering approach for spatial data in very large databases. Journal of VLDB(2000) Vol.33, 289-294.

Most Power Reliable Paths Algorithm for Maximizing the Lifetime of Energy Constrained Sensor Networks

Moonseong Kim, Hyunseung Choo⋆, and Won Kim

School of Information and Communication Engineering
Sungkyunkwan University, Korea
{moonseong, choo, wonkim}@skku.edu

Abstract. In wireless sensor networks, maximizing battery life (network lifetime), and thus the number of messages the networks can support (network capacity), is a key issue. In this paper, we propose an algorithm, called **Mo**st **Po**wer **Re**liable **Pa**ths (MoPoRePa), for online message routing in energy constrained wireless sensor networks. The time complexity of MoPoRePa is significantly lower than the well-known max min zP_{min} algorithm. Moreover, simulation studies show that MoPoRePa about 14.75 % and 8.05 % improvement over the max min zP_{min} algorithm in terms of network capacity and the network lifetime, respectively.

Keywords: Wireless Sensor Networks, Network Capacity, and Network Lifetime.

1 Introduction

Wireless sensor networks (WSNs) are composed of low cost sensors. Since low cost sensors typically have short battery life, conserving battery energy is of primary importance [1]. Li *et al.* [2,3] proposed an online message routing algorithm, called max min zP_{min}, with the view to maximizing the lifetime of WSNs. To maximize the network lifetime and/or the network capacity, they balance the energy consumed by a route and the minimum residual energy at the nodes along the chosen route. The max min zP_{min} algorithm selects a unicast path that uses at most zP_{min} energy, where z is a parameter to the algorithm and P_{min} is the energy required by the minimum energy unicast path. The algorithm achieves over 80 % of the optimal in terms of network lifetime. However, the time complexity of max min zP_{min} is very high. The reason is that the algorithm involves several invocations of the shortest path computation. The algorithm also requires a lot of time to obtain the z parameter.

In this paper, we propose an algorithm called the **Mo**st **Po**wer **Re**liable **Pa**ths (MoPoRePa) for online message routing in energy constrained WSNs. Our objectives are as follows. One is to maximize the total number of messages

---

⋆ Corresponding author.

successfully carried by the network (or the network capacity) without making any assumptions on future message arrivals. Another is to increase the network lifetime when the message sequence is not known. We model the lifetime as the earliest time at which communication fails. The MoPoRePa algorithm is very simple, as it requires only one shortest path computation. Further, its performance is better than three previously proposed algorithms in terms of both network capacity and network lifetime. The rest of this paper is organized as follows. Section 2 presents the MoPoRePa algorithm. Section 3 shows the results of simulation studies. Section 4 concludes the paper.

2 Most Power Reliable Paths Algorithm

The ad hoc sensor network can be modeled as a directed weighted graph $G = (V, E)$ with node set V and edge (link or arc) set E. The energy consumed for transmitting a unit message along link $(u, v) \in E$ is associated with $e_{uv} \geq 0$. Let P_u denote the power of node $u \in V$. Formally, we wish to maximize the number of messages in the system subject to the following constraints: 1) the total power used to send all messages from node u does not exceed P_u and 2) the number of messages from u to all other nodes is the same as the number of messages from all other nodes to u. We assume that our algorithm has knowledge of the topology of the network and the current energy utilization at all nodes in the network. The topology of the network includes all the nodes and links in the network as well as the energy used to transmit a unit message on each link. The network topology can be learned by a node at the time it joins a network.

Using a low energy path frequently leads to energy depletion of the nodes along that path and in the worst case leads to a network partition. We propose an algorithm called **Mo**st **Po**wer **Re**liable **Pa**ths (MoPoRePa) algorithm. The main idea is to increase the *reliability of a path* [4]. The *potential reliable probability* that the transmission along the link $(u, v) \in E$ is fault free is $\wp(u, v) = (P_u^T - e_{uv})/P_u^T$, where P_u^T is the power of the node u at time T. Let π_{sd} be a path from source s to destination d. The reliability of path $s - d$ is $R(\pi_{sd}) = \prod_{(u,v) \in \pi_{sd}} \wp(u, v)$. π_{sd} is called a most power reliable $s - d$ path if $R(\pi_{sd})$ is maximum among all $s - d$ paths. The *link cost function* for transmitting a unit message along link $(u, v) \in E$, is defined as $C_{uv} = -\log \wp(u, v)$. Then computing a most power reliable path is equivalent to computing a shortest path using the link cost function C. The following summarizes the MoPoRePa algorithm:

MoPoRePa Algorithm

```
1. Associate the potential reliable probability with each link.
2. Associate the link cost function with the probability.
3. Find the shortest path from source to destination with the cost.
```

Generally, the logarithm function changes the multiplicative routing measure into an additive routing measure as in equation (1).

$$-\log \prod_{(u,v)\in \pi_{sd}} \wp(u,v) \;=\; \sum_{(u,v)\in \pi_{sd}} C_{uv} \tag{1}$$

Hence, a most power reliable path can be computed in $O(m + n \log n)$ time complexity ($|V| = n$, $|E| = m$) using the algorithm of Fredman and Tarjan [5]. In contrast, max min zP_{min} involves performing as many as m shortest path computations. The running time is at most $O(m(m + n \log n))$. Using binary search, the running time can be reduced to $O(\log m(m + n \log n))$ [2,3].

3 Performance Evaluation and Discussion

For simulation studies of the MoPoRePa algorithm, we generated random networks by modifying the Rodionov and Choo's mechanism [6] to include properties of ad hoc networks. We implemented in C our method of setting up the paths. We generated 100 different networks with 50 nodes and placed the nodes randomly with density of $0.005 \sim 0.03 \; nodes/m^2$. We set the transmission radius of each node as $30m$. The power consumption weights for transmitting a message were $e_{uv} = 0.001 \cdot d_{uv}^3$ [7], where d is a distance, and the initial power of each node is 30. We generated 1000 messages between all possible pairs of nodes and distributed them evenly.
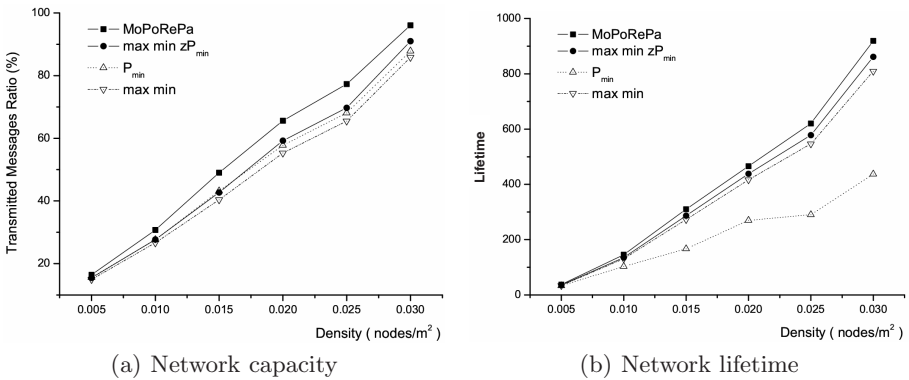

(a) Network capacity   (b) Network lifetime

Fig. 1. Simulation results

We compared the MoPoRePa algorithm with three existing algorithms in terms of the network capacity and the network lifetime. For the P_{min} algorithm, a message was routed on a path that consumes minimum total energy; *i.e.*, z is 1 in the max min zP_{min} algorithm. For the max min algorithm, a message was routed along a path such that minimum residual energy fraction of nodes on

that path is the maximum among all paths; *i.e.*, z is ∞ in the max min zP_{min} algorithm.

Fig. 1(a) shows the simulation results with respect to network capacity. The performance of MoPoRePa algorithm is better than those of the other three algorithms. The improvement is up to about 14.75 % compared to max min zP_{min}. As indicated in Fig. 1(b), the lifetime of MoPoRePa is longer than that of the other three algorithms. MoPoRePa is longer by up to 5.98 $\sim$ 8.05 % compared to max min zP_{min}.

4   Conclusion

In this paper, we reported the results of our work on maximizing the lifetime and capacity of energy-constrained wireless sensor networks. In particular, we proposed and validated an online message routing algorithm, called MoPoRePa. The algorithm is worthy because its time complexity is much lower than the best-known algorithm, the max min zP_{min} algorithm. Moreover, simulation studies showed that the algorithm is better than the max min zP_{min}, and a few others, with respect to both network lifetime and network capacity.

Acknowledgment

References

1. Chang, J.-H., Tassiulas, L.: Energy Conserving Routing in Wireless Ad-hoc Networks. Proceeding of INFOCOM, Vol. 1. IEEE (2000) 22-31
2. Li, Q., Aslam, J., Rus, D.: Online Power-aware Routing in Wireless Ad-hoc Networks. Proceeding of MobiCom. ACM (2001) 97-107
3. Aslam, J., Li, Q., Rus, D.: Three Power-aware Routing Algorithms for Sensor Networks. Wireless Communications and Mobile Computing, Vol. 3. John Wiley & Sons (2003) 187-208
4. Xue, G.: End-to-End Data Paths: Quickest or Most Reliable?. Communications Letters, Vol. 2, No. 6. IEEE (1998) 156-158
5. Fredman, M. L., Tarjan, R. E.: Fibonacci Heaps and Their Uses in Improved Network Optimization Algorithms. Journal of the ACM, Vol. 34, Issue 3. ACM (1987) 596-615
6. Rodionov, A. S., Choo, H.: On Generating Random Network Structures: Connected Graphs. Lecture Notes in Computer Science, Vol. 3090. Springer-Verlag (2004) 483-491
7. Heinzelman, W. R., Chandrakasan, A., Balakrishnan, H.: Energy-Efficient Communication Protocol for Wireless Microsensor Networks. Proceeding of the 33rd Hawaii International Conference on System Sciences. IEEE (2000)

From Mathematics to Software Engineering: Introducing Category Theory into the Computer Science Curriculum⋆

Yujun Zheng[1,2,3], Haihe Shi[1,2], and Jinyun Xue[1,2]

[1] Institute of Software, Chinese Academy of Sciences, 100080 Beijing, China
`yujun.zheng@computer.org`
[2] Coll. Computer Inf. & Eng., Jiangxi Normal University, 330027 Nanchang, China
[3] Graduate University of the Chinese Academy of Sciences, 100080 Beijing, China

Abstract. Category theory, with its increasing role in computer science, has proved useful in the investigation of programming languages and other theoretical aspects of software engineering. As a bridge-building exercise, we introduce the category theory course into the computer science curriculum, the purpose of which includes building a unified framework to generalize the discrete structures of mathematical courses and providing an environment for formulating concepts of other software engineering courses. We develop a teaching schema, summarize our experiences, and give some suggestions for pedagogical techniques for the course.

1 Introduction

Category theory has developed rapidly, and its influence is being felt in many parts of computer science including the design and implementation of programming languages, models of concurrency, type theory, polymorphism, specification language, constructive logic, automata theory, and the development of algorithms [1]. Nevertheless, as a relatively young branch of pure mathematics, category theory is mainly incorporated into the mathematical curriculum for postgraduate education in a handful of universities, and it is widely supposed that the subject could only be understood by those with nontrivial facts in algebraic topology.

The motivation for this paper derives from our experience in introducing the category theory course for graduates in computer science over the last three years. Its aim is not to work through the mathematical derivations and proofs of the abstract theory, but to provide a high-level, categorial understanding of mathematical constructions in various aspects of computer science and software engineering. The key role of the course in the curriculum can be divided into two parts:

---

1. Building a sound, unified framework that generalizes the structures learned from the preceding mathematical courses such as discrete mathematics, set theory and graph theory.
2. Providing a mathematical environment to formulate uniform definitions of the preceding, following, or concurrent software engineering courses including data structures and algorithms, object-oriented design, programming languages and formal methods.

The above two parts are described respectively in Section 2 and Section 3. Section 4 proposes some strategies and suggestions for teaching the category theory course, and Section 5 concludes with discussion.

2   Generalization of Mathematical Structures

The introductory category theory course usually starts with a review of discrete mathematics, from which students have learned a number of fundamental discrete structures and gained a basic knowledge of the mathematical foundations for computer science. First, elementary definitions in category theory should be introduced in terms of ordinary set theory: *collections* are sets, *operations* are set-theoretic functions, and *equalities* are set-theoretic identities. Second, the fundamental notions of category theory is that of a monoid: a set with a binary operation of multiplication that is associative and that has a unit; a category itself can be regarded as a sort of generalized monoids [2]. In this way, students can quickly have a self-contained and structural understanding of categories.

Alternatively, category theory deals in an abstract way with structures, i.e., offers a highly formalized language for expressing general properties and analyzing relations between classes of mathematical structures. By presenting a variety of categories of familiar structures, we can give students a unified, categorial understanding of mathematical structures. Those typical categories include:

- **N** with natural numbers as objects and ordering $n \to n + 1$ as morphisms.
- **Rel** with sets as objects and relations as morphisms.
- **Set** with sets as objects and total functions between sets as morphisms.
- **Poset** with pre-ordered sets as objects and monotonic functions as morphisms. A pre-order is a category where there is at most one arrow between any two objects.
- **Mon** with monoids as objects and morphisms of monoids as (categorial) morphisms. A monoid is a category with one object.
- **Grp** with groups as objects with morphisms of groups. A group is a category with one object in which each arrow has an inverse under composition.
- **Ab** with additive abelian groups as objects with morphisms of such.
- **Rng** with rings as objects with the ring morphisms preserving units.
- K-**Mod** with modules over the communicative ring K as objects and K-linear maps as morphisms.
- **Top** with topological spaces as objects and continuous functions as morphisms.

Next, we can show how to use the categorial approach to achieve the generality of various concepts; that is, many different formalisms and structures may be proposed for what is essentially the same concept [3] in the language of categories. For example, the coproduct of any two objects exists in many categories, where it has various names as follows:

- **Set**: disjoint union of sets.
- **Grp**: free product.
- **Ab**: direct sum $A \bigoplus B$.
- **Top**: disjoint union of topological spaces.

3 Theoretical Standardization of Software Engineering Methods

3.1 Data Structures

After a generalization of mathematical structures, we should move towards data structures frequently used in computer programming. While the traditional set theory generally considers concrete implementations, category theory describes objects more as abstract data types, or specifications that are independent of particular implementations. Category localization semantics for specifications by Goguen [4][1] need to be introduced, followed by the exploration of category theory as a framework for designing, understanding, manipulating and evolving data structures. For example, specifications of data structures *Preorder* and *Antisymmetry* can be defined as follows:

Preorder: sort E
op $\leq$: $E, E \rightarrow Boolean$
axiom reflexivity: $x \leq x$
axiom transitivity: $x \leq y \wedge y \leq z \Rightarrow x \leq z$

Antisymmetry: sort E
op $\leq$: $E, E \rightarrow Boolean$
axiom antisymmetry: $x \leq y \wedge y \leq x \Rightarrow x = z$

An initial object in the category *SPEC* can be worked out as a specification that shares the properties of above two specification:

BinaryRelation: sort E
op $\leq$: $E, E \rightarrow Boolean$

---

[1] In brief, a specification is the finite presentation of a theory, and a signature provides the vocabulary of a specification; *SPEC* is a category with specifications as objects.

By constructing the morphisms $f : BinaryRelation \rightarrow Preorder$ and $g : BinaryRelation \rightarrow Antisymmetry$ and computing the colimit of f and g, the composition of *Preorder* and *Antisymmetry* can be mechanically generated:

Partial Order: sort E

op $\leq: E, E \rightarrow Boolean$

axiom reflexivity: $x \leq x$

axiom transitivity: $x \leq y \wedge y \leq z \Rightarrow x \leq z$

axiom antisymmetry: $x \leq y \wedge y \leq x \Rightarrow x = z$

In a word, under the categorial framework, the basic principle to specify a system is to build the structures for each component separately, and then use the colimit operation to compose these specifications [5]. This also provides an oriented direction from structured design to component-based software engineering (CBSE).

3.2   Programming Languages

Based on the categorial understanding of data structures that constitute the theoretic background of language design, we can lead students to relate category theory with widely used programming methodologies and to investigate mathematical semantics of programming languages.

A simplest example is given by (deductive) logic programming languages as categories, in which propositions are objects and proofs are morphisms. Such categories can be easily constructed and understood in the presence of the identical proof: $a \rightarrow a$ and the associative compositions of proofs: $(a \rightarrow b) \wedge (b \rightarrow c) \Rightarrow (a \rightarrow c)$.

We can also show how to construct categories corresponding with functional programming languages. Consider a simple language with four primitive types *Boolean*, *Integer*, *Double*, and *Element*, the corresponding category contains primitive types as objects and constants and built-in operations as morphisms, as illustrated in Fig. 1.
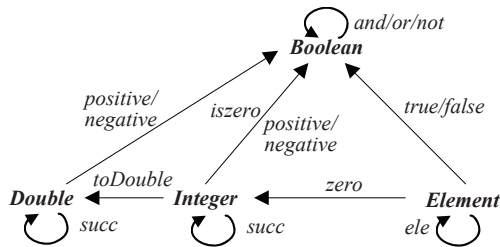

Fig. 1. A category representing a funtional programming language

Given the facility of category theory to defined more structured categories out of simper ones, many other features of modern functional languages, including formal and concrete parameters of functions, parameterized data types,

polymorphic functions and recursive functions, can be addressed by stepwise introducing more properties of category theory, such as principle morphisms, exponentiation, and natural transformation [1]. Afterwards, we can go deep into extra topics including type-free and second order lambda-calculus.

3.3   Object-Oriented Design

As mentioned above, category theory studies "objects" and "morphisms" between them: any immediate access to the internal structure of objects is prevented, and all the concepts must be defined by their relations with other objects. This is quite similar to ideas of object-oriented design. Therefore we can guide students to construct object-oriented categories step by step (the process of which abstracts the transition from structured programming to object-oriented programming). Such a underlying categorial framework for object-oriented design can be summarized as follows:

- **OBJ-SIG** is a category with object signatures $\theta =< \Sigma, A, \Gamma >$ (where $\Sigma =< S, \Omega >$ is a universe signature, A is an $S^* \times S$-indexed family of attribute symbols, and Γ is an S^*-indexed family of action symbols) as objects, and an object signature morphism is a consistent mapping from one signature to another.
- **OBJ-SPEC** is a category with object specifications $OSP =< \theta, \Phi >$ (where Φ is a finite set of θ-axioms) as objects and a morphism between specification $< \theta_1, \Phi_1 >$ and specification $< \theta_2, \Phi_2 >$ is a mapping of signature θ_1 into signature θ_2 such that all the axioms in Φ_1 are translated to theorems in Φ_2.
- Let D_1, $D_2 \ldots D_n$ be ω-diagrams in *OBJ-SPEC* and COL_i be colimits for $D_i (i = 1, 2, \ldots n)$, then **CLS-SPEC** is a category with COL_i as objects, and a class morphism between COL_1 and COL_2 is the colimit of all morphisms in *OBJ-SPEC* that between an object in D_1 and an object in D_2.
- **I-FRM-SPEC** is a category with diagrams in *OBJ-SPEC* as objects, and a morphism between two (implemented) object frameworks, namely $I\text{-}FRM_1$ and $I\text{-}FRM_2$, is the colimit of morphisms in *OBJ-SPEC* that between an object of $I\text{-}FRM_1$ and an object of $I\text{-}FRM_2$.

Morphisms in *OBJ-SPEC* may represent object relationships such as message connection, whole-part, generalization/specialization, etc., which are upgraded to morphisms in *CLS-SPEC* including association, aggregation, and inheritance [6]; functors from *CLS-SPEC* to *OBJ-SPEC* can be treated syntactically as instantiations or refinements, and functors from *OBJ-SPEC* to *I-FRM-SPEC* as compositions. In a similar way, categories *M-CLS-SPEC* (of meta-classes), *MM-CLS-SPEC* (of meta-meta-classes), *FRM-SPEC* (of class frameworks), *M-FRM-SPEC* (of meta-frameworks), and *MM-FRM-SPEC* (of meta-meta-frameworks) can also be constructed [7]. As illustrated in Fig. 2, the left refinement process of class-based specifications is brought to the right refinement process of framework-based specifications through compositions at different levels of abstraction.
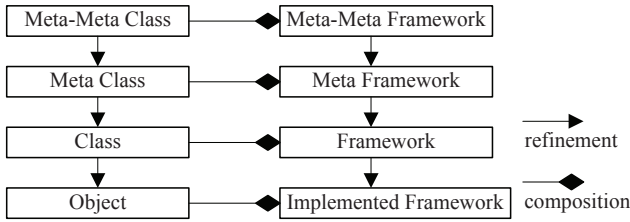
Fig. 2. Constructing object-oriented categories

As a typical paradigm of object-oriented design framework, design patterns can be employed to illustrate the application of theory-based approach in large-scale and mechanizable software reuse [8]. In detail, a design pattern is a (category) object in *M-FRM-SPEC*, and one of its refinement pathes to *I-FRM-SPEC* can be implemented rigorously and saved; when encountering another problem within the same pattern context, we can utilize the "standard" refinement to generate a new implementation via category theoretic computations. For example, suppose the *Observer* pattern [9] has been refined into an object framework (i.e., an executable program), namely FRM_1, where two observers *DigitalClock* and *AnalogClock* query the subject *Timer* to synchronize their time with the *Time*'s state. As shown in Fig. 3, to work out a new framework (namely FRM_2) representing the underlying dataset in separate forms of interface, we just construct a functor H_1[2] from FRM_1 and generate the program $I\text{-}FRM_2$ without refining $G_2 \circ G_1$ manually: G_1 is the composition $H_1 \circ F_1$, while G_2 and H_2 are obtained by computing the colimit of H_1 and F_2.

4   Guiding Strategies and Suggestions

Arising in algebraic topology as a way to explain in what sense the passages from geometry to algebra are "natural" in the sense of reflecting underlying geometric reality [10], category theory would be considered esoteric by many students in computer science. Based on our lessons and experiences, we propose the following strategies and suggestions for improving the pedagogical effectiveness of the course:

- **Utilizing diagrams.** Diagrams are an important tool in the practice of category theory, especially for describing equational reasoning. From beginning, we should help students learn how to go back and forth from diagrams to equations, and use diagrams as possible for stating and proving properties of categorial constructions.
- **Informal explanation.** Many category theoretic formalizations are too abstract and heavily notational for students. To avoid the expense of devious

---

[2] Which is the colimit of the four morphisms: $f_0 \to g_0$; $f_1 \to g_1$; $coequalizer(f_2, f_3) \to coequalizer(g_2, g_3, g_4)$; $coequalizer(f_4, f_5) \to coequalizer(g_5, g_6, g_7)$.
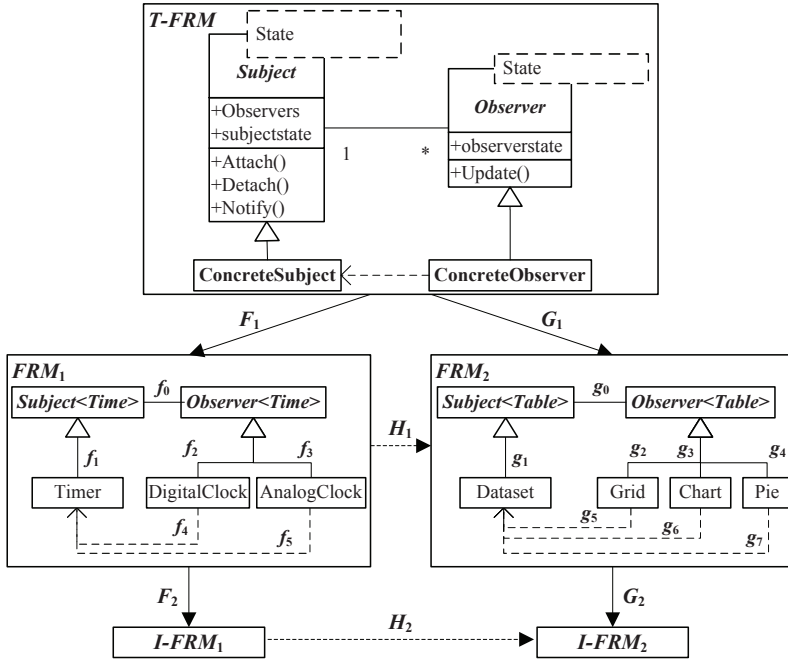
Fig. 3. Mechanization of deign patterns via category theoretic computations

circumlocutions, most lectures should begin with a clear definition, prefaced with an informal explanation of the construction, and followed by accessible examples illustrating the methodological connection and applications in computer science.

– **Avoid misleading.** Connection between category theory and set theory is helpful to introduce many categorial concepts, but we should be careful because sometimes it can be misleading. For example, a morphism that is both epic (surjective) and monic (injective) does not need to be isomorphic, and in a Cartesian closed category a reflexive object a is given by $a^a < a$, which are clearly impossible in ordinary set theory.

– **Guide to computation.** For students in computer science, we should give more emphasis on the presentation of ideas and methods than mathematical notions and proofs, exhibit the intriguing advantages of formalizing and mechanizing computations in categorial principles, and help students learn to model and reason *categorically*.

– **Orientation to specific research.** Within limited credit hours, it is impossible to work through the constructions, derivations and proofs of all important propositions and theorems. Category theory is, by and large, a self-contained discipline and one can go a long way without mentioning the traditional mathematical examples [11]. The course is just a doorstep, and

its main purpose is to give a familiarity with the category theory and make the students prepared to approach further researches applying the theory to various aspects of computer science.

5   Conclusions

As a "theory of functions", category theory offers a highly formalized language which is suitable for focusing concerns on various areas of computer science and software engineering. The paper summarizes our efforts and experiences in introducing the category theory course into the computer science curriculum, the role of which includes building a unified framework that generalizes the structures of preceding mathematical courses and providing a mathematical environment to formulate uniform definitions of the other software engineering courses. The main purpose is not to work through the mathematical derivations and proofs, but to give students a structural understanding of categorial constructions and improve their mathematic literacy for further researches in computer science.

References

1. Pierce, B.C.: Basic Category Theory for Computer Scientists. MIT Press, Cambridge, London (1991)
2. Saunders, M.L.: Categories for the Working Mathematician. Springer-Verlag, New York (1998)
3. Asperti, A and Longo, G.: Categories, Types and Structures: an introduction to category theory for the working computer scientist. MIT Press, Cambridge (1991)
4. Goguen, J.A.: A Categorical Manifesto. Mathematical Structures in Computer Sciences, vol. 1 (1991) 49-67
5. Wiels, V. and Easterbrook, S.: Management of Evolving Specifications Using Category Theory. In Proceedings of 13th IEEE Conference on Automated Software Engineering, Hawaii (1998) 12-21
6. Kung, D.C., Gao, J., Hsia, P., Toyoshima, Y., and Chen, C.: On Regression Testing of Object-Oriented Programs. Journal of Object-Oriented Programming, vol. 8, no. 2 (1995) 51-65
7. Zheng, Y.J., Xue, J.Y., and Liu,W.B.: Object-Oriented Specification Composition and Refinement via Category Theoretic Computations. In Proceedings of 3rd International Conference on Theory and Applications of Models of Computation, Beijing, China, 2006. Lecture Notes in Computer Science, vol. 3959 (2006) 601-610
8. Zheng, Y.J., Shi, H.H., and Xue, J.Y.: Formalization and Mechanization of Design Patterns. In Proceedings of 1st International Conference on Computer Science and Education, Xiamen, China (2006) 892-897
9. Gamma, E., Helm, R., Johnson, R., and Vlissides J.: Design Patterns: Elements of Reusable Object-Oriented Systems. Addison-Wesley, Reading MA (1995)
10. Rydeheard, D.E. and Burstall, R.M.: Computational Category Theory. Prentice Hall, New York (1988)
11. Turi, D.: Category Theory Lecture Notes. Laboratory for Foundations of Computer Science, University of Edinburgh (2001)

Avatar Augmented Annotation Interface for e-Learning

Won-Sung Sohn[1], Jae-Kyung Kim[2], and Jaeho Lee[1]

[1] Department of Computer Education, Gyeongin National University of Education,
Gyesan-Dong, Gyeyang-Gu, 407-753, Incheon, Korea
{sohnws, jhlee}@ginue.ac.kr
[2] Department of Computer Science, Yonsei University,
Shinchon-dong, Seodaemoon-gu, Seoul, Korea
ki187cm@gmail.com

Abstract. Creating avatar-augmented presentations that extend gesture and annotation to distance education is laborious and time-consuming. We present Avatar Augmented Annotation (AAA), a project to design and share web based e-Learning materials using an animated avatar and digital inking. Using AAA, the instructor can create a presentation, using freehand annotations that include high-level teaching behavior without doing any programming. The AAA then generates a script expressed in XML and augments the presentation with an animated avatar following each annotation. We found that AAA provides positive educational effectiveness and usability compared to previous online courseware.

1 Introduction

Today e-Learning, web-based teaching (WBT), and distance learning techniques are common in university classrooms[1],[2],[3]. These approaches enable students to learn in their own spaces and times[2],[3]. However another issue offset this advantage: interactions between students and teachers provide more educational effect[2],[3],[7]. If online teaching systems can't provide any interactions, students become bored with online coursework. Many students who take online coursework print out all web materials as exam period approaches in our experiences.

To address this problem, some interaction techniques are proposed. Many commercial online coursewares provide video and animation clips that have advantages over static web courseware. Several recent systems provide a Cyber Teaching Assistant (CTA) to improve the educational effect of static WBT material. The main advantage of classroom instruction over distance education is that students can easily observe gestures and annotations performed in live instruction. Shindo[2] developed CTA for a programming class that includes an animated avatar and scenario markup language. CTA responds to student questions and calls using previously defined scenario files from a database. Ray[3] makes a course that uses an animated agent to guide students and emphasize specific teaching material. Ray found that students overwhelmingly preferred the animated lecture courses over other online courses they

had taken. Mash[4] generates a script to control an MS-Agent avatar[6] without requiring the user to do any programming. In Mash, the user simply chooses gestures, types in the accompanying script, and saves the file.

Surprisingly, avatars may be a better approach than live video[7] – for example, this approach enables an instructor to update a presentation over time, without needing to keep the same suit of clothes in the closet! However, a key limitation of such systems is that the content provider must build avatar movement and interaction into web material manually using a script or other programming language. Creating these avatar-augmented presentations is usually laborious and time consuming. Mash used a parameter box to control the avatar, in which the user enters the physical parameter in the 'X', 'Y' field even though it doesn't require programming. Mash generates script for MS product and mash's format which can't be shared in other system.

Annotation can minimize such effort. Annotation (digital inking) is an important feature of a digital lecture or presentation system[1],[9]. Digital inking can capture the knowledge between student and teacher and easily share and reuse material[1],[9]. Webtour[5] allow to web document designer augmenting the contents with digital ink. Webtour records a user's drawing and supports playback with web media. This scenario is useful and cost effective. But, Webtour can only synchronize annotation itself without any animated agent.

Thus we believe that avatar augmented annotation tool for e-Learning, can enhance learning effects of distance education and usability. We present the Avatar Augmented Annotation (AAA) interface, which supports a method to design teaching scenarios and augment them using an animated avatar in web based learning materials. The instructor first creates a presentation, and then marks up the presentation using freehand annotations such as underlining, circling, and selects teaching behavior such as introduce, exit which be done by animated avatar. The AAA then generates XML based script to control the avatar movement. Finally AAA augments the presentation with an animated avatar that follows the annotations sequentially, drawing attention to the content that the instructor indicated.

2   Overview of Avatar Augmented Annotation

The overview of AAA interface shown in Figure 1.

As shown in Figure 1, AAA includes an authoring interface to make a scenario with avatar and annotation interface to allow a student to add his or her own knowledge or perspective.

On the authoring interface side, the key components are:

- Annotation recognizer to allow freeform drawing from scenario designer and determine its type.
- Script generator to control avatar movement and create avatar control markup language (XML) that includes high-level teaching behavior.
- Synchronizer to interpret the script and map avatar behavior to low-level avatar movement. Then synchronizer plays avatar lecturing on the HTML/XML document.

On the annotation interface side, the key modules are:

- Annotation recognizer to determine marking type such as line, circle, note annotation from the student.
- Annotation integrator to store marking as the markup language and print out annotation to the screen.

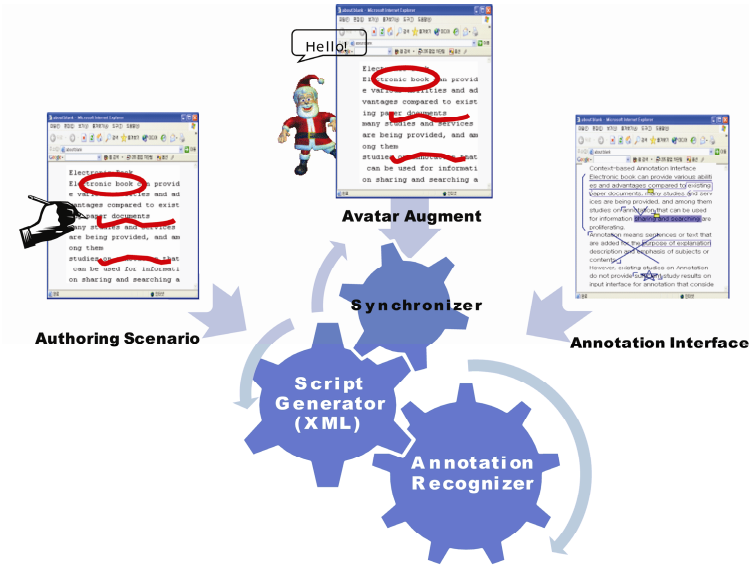We describe each interface in detail in the following sections.

Fig. 1. Overview of AAA interface

3   Avatar Annotation Markup Language

We define Avatar Annotation Markup Language (AAML) to express annotation and control animated avatar on web document. In AAA, instructor draws freehand annotations and adds comments. Then system creates annotation and avatar motion information represented in XML form. This approach allows users to more easily control the avatar behaviors, compare to previous efforts[2],[3],[8]. Creating scenarios using digital inking in the HTML/XML document requires that graphic information of the markings and context information of the original document be presented in the form of external links[9]. Through external linking, markings are saved independently from the original document and can be shared by multiple users. The overall structure of AAML is shown in Figure 2 (A).

AAML includes 'meta' and 'annotationList' elements. A 'meta' element includes attributes for lecturer, lecture name, date and note. The annotationList element includes each annotation elements (Figure 2 (B)). Annotation has 'type', 'behavior',

'context', 'comment' and 'avatar' elements. The type element of an annotation expresses one of nine marking types, for example 'line', 'ellipse', 'highlight' and others. The behavior element describes a high-level motion set for describing avatar behavior in the teaching material.
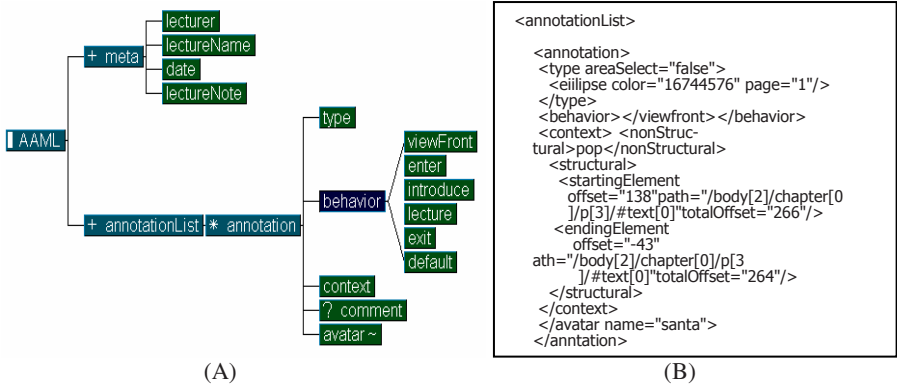

Fig. 2. Overall structure of AAML and an example of AAML document

We define 5 kinds of behavior including 'viewFront', 'enter, 'introduce', 'lecture' and 'exit' behavior. If the instructor does not select any behavior, the system selects 'default' behavior. Context elements include 'nonstructural' and 'structural' sub elements. A non-structural context has target (anchor) text. A structural context describes a point and offset within the annotated part such as Xlink and Xpointer.

4   Authoring Interface

In the authoring interface, the instructor first marks on the web content and then selects the teaching behavior of AAML such as introduce, exit, and others. The system generates a teaching scenario with AAML and web contents. The interpreter analyzes scenario information saved as XML and maps high-level motion of teaching behavior to low-level motion of avatar movement. Lastly, the authoring interface augments the animated teaching avatar to follow the annotation.

Figure 4 and shows a scenario for a data-structure course lesson on simple stack operations. Our prototype is based on a Window XP and XML document. This supports 3D-based avatar motion renderer (Figure 3(A)) or 2D-based MS-Agent[6] (Figure 3 (B)) and we will describe each interface in detail next.

Figure 3 shows a screen shot of marking procedure by the instructor. The instructor draws free-form annotation and selects teaching behavior defined in AAML. In Figure 4 (A), instructor draws annotation on his interesting point. User draws marking on 'push' and 'pop' context with 'Viewfront' behavior selection in Figure 4 (B). He can add a comment that the avatar will pronounce when the avatar presents the lecture on the push and pop concepts.
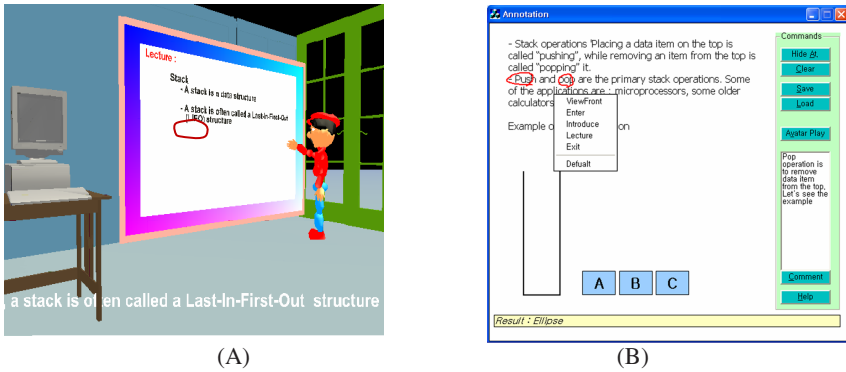
Fig. 3. Screen shot of authoring interface

The AAA system generates a scenario script based on AAML after the user pushes the save button. The system recognizes the free-form marking type and analyzes the context behind the marking, which consists of element and physical position.
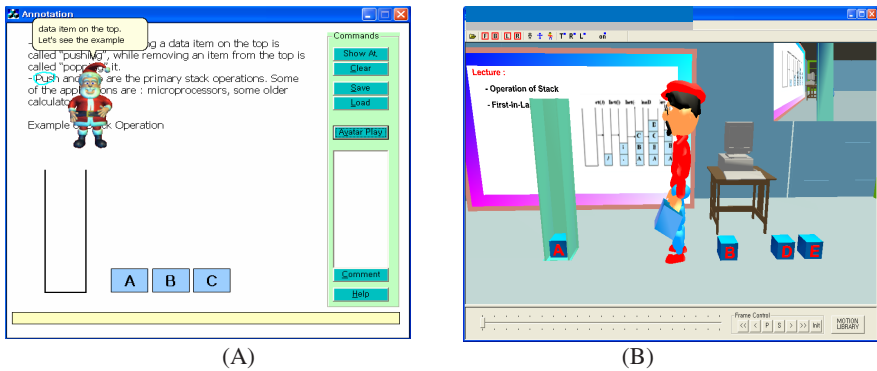

Fig. 4. Presents 'push' and 'pop' concept

Figure 4 shows the avatar augmenting procedure after the user pushes the 'avatar play' button. Subsequently the system interprets high-level behavior of AAML and sends it to the avatar motion generator to generate low-level avatar movement. The motion-generator traces the positions of annotation anchors and creates a physical path to each annotation, in order to play back the avatar animation. This approach enables the instructor to design a teaching scenario without having to know a script language or to understand the system architecture in detail.

AAA supports synchronization between an animated avatar and a multimedia object. In Figure 5 (A), instructor moves each box to show the concept of pushing an element onto the stack. After that, AAA synchronizes the movement between a box and an avatar using internal rules (Figure 5 (B)).
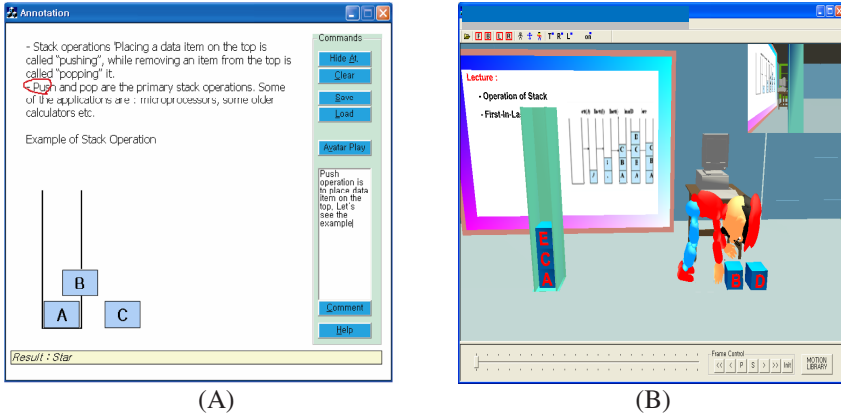
(A)   (B)

Fig. 5. An example of synchronization process

5   Annotation Interface

AAA's Annotation interface is enables students to add questions, comments, critiques, and more using several annotation types. We used a context-based annotation engine[9] which include reorganization and integration modules for the HTML/XML document. Figure 6 (A) shows our annotation interface; students have added line, circle, and note annotations.

AAA provides interaction techniques that enable students to ask questions instructors to reply (Figure 6 (B)). To ask questions, students draw marks and type their question in a text input box. The system recognizes the marking type and extracts the context under the marking area to produce an image screen and send it to the instructor along with the question. Hence instructor doesn't need to check the annotation notes on the web site.
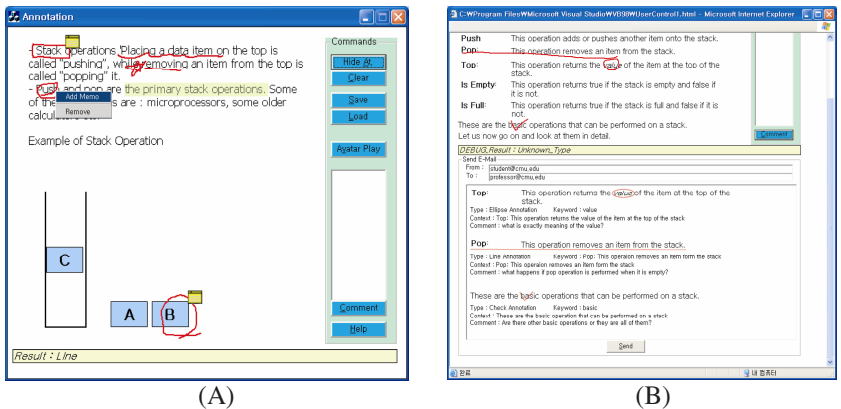

(A)   (B)

Fig. 6. Annotation Interface Interaction between instructor and student in AAA

6   Summary of Usability Inspection

We conducted a usability inspection on our prototype using heuristic evaluation[11] with five instructors and seven university students. We built a small data-structure lesson using AAA to augment existing university online coursework[10]. We surveyed the instructor and students who had previously taken online data structure courses. The instructors were asked to design scenario. We demonstrated the AAA lecturing to the students and ask to add annotation. After the tests, a survey was done with 5 principles and 6 heuristics which include severity from 1 to 6. For items with severity less than 3, an empirical study was performed through separate survey. In the chapter, only the most important items from test results are summarized.

All five instructors commented that our approach was very interesting and they were satisfied with AAA's easy authoring interface. Four instructors suggested incorporating more real-world teaching behavior into AAA. One instructor pointed out if we would support synchronization functions between annotation and multimedia objects, it would takes too a great deal of time to build on existing material. For this reason, they recommended adding or substituting Flash or Java applets in AAA rather programming the synchronization.

All seven students preferred animated online courses to previous static web courses. Most students were satisfied that they could clearly understand the key point of the page they were shown. However some students disliked the necessity of animated teaching assistant in online courseware. They have to watch the avatar lecturing even though they can grasp the key point quickly. They commented that they would prefer to be able to choose watching the avatar or not.

7   Conclusions and Future Works

We have built an avatar augmented annotation (AAA) interface and investigated its effectiveness and usability. Our authoring interface enables an instructor to create a teaching scenario using digital inking annotation on 2D and 3B based web material. AAA generates a script for avatar lecturing which includes high-level teaching behavior. To do this, we define an avatar annotation markup language and support annotation techniques to lecture material. We found that AAA presents positive educational effectiveness and usability compared with previous static online courseware.

We acknowledge that there are significant technical issues with some of the features and methods as indicated from the user study. Our study applies to e-Learning, IETM (Interactive Electronic Technical Manual), Intelligent Tutoring System, and eBook. In future work we plan to develop a plug-in program to add our lecturing interface on existing web document.

Acknowledgement

References

1. Anderson R.J., Hoyer C, Wolfman S A., Ruth A.: "A study of digital ink in lecture pres-
   entation," Proceedings of the Human factors in computing systems, Vienna, Aus-
   tria.(2004) 567-574
2. Shindo Y., Matsuda H.:"Prototype of Cyber Teaching Assistant," Proceedings of IEEE In-
   ternational Conference on Advanced Learning Technology (ICALT2001), IEEE, USA
   (2001) 70-73,
3. Ray August: "Animating Web Lectures with Agent Technology," http://juri-st
   .law.pitt.edu/lessons/lesfeb01.htm.
4. Mash, http://www.bellcraft.com/mash.
5. Chellury R. Sastry, Darrin P. Lewis, Arturo Pizano.: "Webtour: a system to record and
   playback dynamic multimedia annotations on web document content," Proceedings of the
   seventh ACM international conference on Multimedia (Part 2)Orlando, Florida, United
   States. (1999)175-178
6. MS Agent, "http://www.microsoft.com/msagent"
7. Elisabeth A., Thomas R. and Jochen M., "WebPersona: A Life-Like Presentation Agent
   for Educational Applications on the WWW," Proceedings of the workshop "Intelligent
   Educational Systems on the World Wide Web", Kobe, Japan, (1997)
8. Kshirsagar, S., Guye-Vuilleme.A., Kamyab. K., Magnenat-Thalmann N. D., Thalmann E.,
   Mamdani. :"Avatar Markup Language", Proceedings of the Eurographics Workshop on
   Virtual Environments (EGVE'02) Spain. (2002) 169-177
9. Sohn W. S., et al.: Context-based Free-form Annotation in XML Documents. In Interna-
   tional Journal of Human Computer Studies , Academic Press (2003)257-285
10. YSCEC, http://yscec.yonsei.ac.kr/
11. Useit.com: Jakob Nielsen's Website http://useit.com.

Education–Oriented Virtual Environment for Clothing Thermal Functional Performance

Xiaonan Luo[1], Wenbang Hou[1], and Yi Li[2]

[1] Computer Application Institute, SUN YAT-SEN University,
Guang Zhou 510275, China
[2] Institute of Textiles and Clothing, The Hong Kong Polytechnic University,
Hung Hom, Hong Kong
`lnslxn@zsu.edu.cn, houwenbang@yahoo.com.cn,`
`tcliyi@inet.polyu.edu.hk`

Abstract. This paper presents a simulation environment for the education of clothing thermal function. It allows learners in a virtual environment to learn the clothing thermal comfort theory and identify the most important factors that influence clothing thermal functional performance. The virtual wearing case is defined with primary parameters and the numerical simulation results are visualized with 3D virtual environment and 2D animation, which provide virtual reality based interpretation of the thermal state and the dynamic thermal processes of the human-clothing system. This system can also be used as an effective visualization tool by textile researchers.

Keywords: Visualization; education oriented; clothing thermal functional performance; virtual environment.

1 Introduction

The thermal functional performance is a critical aspect that is highly concerned in clothing design. Especially during bad thermal conditions, the thermal protection of clothing relates to the health and survival of human beings. Even in ordinary living conditions, there are more and more consumers begin to concern the thermal comfort performance of clothing.

To explore the factors and mechanisms that affect the thermal functional performance of clothing, many advances have been achieved. In recent years, researchers have made great efforts to develop numerical models such as the thermoregulation of human body, the heat and moisture transfer behaviors of clothing material, as well as the dynamical interaction between human, clothing and environment system [1], [2], [3]. Based on the numerical models, Li et al proposed a virtual system for clothing thermal functional design [4], which can design clothing and analyze its thermal functional performance effectively. Although this system provides GUI interface and good 3D visualization for the result dataset, it's still very difficult and inconvenient for education of students and young engineers in clothing industry because of so many kinds of professional terms and intrinsic

complexity of numerical solver. It's would be valuable to develop a learning tool that can educate people for a dedicated clothing, what will the thermal effect like in different wearing cases, how does the thermal processes interact in human-clothing system, how does the temperature and dampness distribute in every clothing layers, and what are the key factors that decide the thermal function of clothing.

In most cases, simulation environments are powerful learning tools and have been used in many engineering fields successfully [5-7]. Such systems are generally based on sophisticated didactical concepts and have used the modern technical possibilities include 3D visualization and virtual reality technique. They can enable exploration by allowing learners to manipulate parameters and visualize results in a virtual reality environment. In general there are two basic kinds of such systems: inanimate (off-line) and live (on-line, real-time) [8]. Inanimate simulators are used to evaluate complex equations and models. They do not simulate real-time operations of physical systems; therefore the user interaction is limited. While live simulators are highly interactive and allowing learners to explore, they are always very complicated and time-consuming. To overcome their shortcuts, it's necessary to find an appropriate approach that allows the utmost manipulation options and decreases the complexity and time consumption simultaneously.

In this paper, we present a simulation based learning tool for clothing thermal functional performance. It could be called "half-live" simulation because the simulation is completed in advance and the result dataset is stored in database. By reorganizing the input data of simulation cases, user can manipulate parameters and explore situations in a more instinct and simple way as if by imitating a simulation case. This program can visualize simulation datasets in a virtual environment, and special attention is given to the design of a user interface being easy to learn and to use. The rest of the paper is organized as follows: Section 2 describes the numerical model for clothing thermal function simulation, and section 3 presents the details of the "half-live" simulation design. The visualization techniques are described in Section 4, and examples are presented in Section 5. Finally, we conclude and point out the future works.

2   Numerical Model for Clothing Thermal Function Simulation

The key factors that influence the thermal functional performance include the thermal properties of clothing materials (Fiber, membrane, PCM et al.), and the structure features of clothing assemblies. In the virtual design system, all materials can be designed and stored in database, even include the human body and environment conditions [4]. The specified human body, clothing and environment together consist a simulation scenario, and one or more scenarios with respective phase time comprise a simulation case. After all definition completed, the thermal processes in human body-clothing-environment system, as shown in Fig. 1, are simulated, and the dynamic thermal state of human body and clothing are calculated as the result datasets.
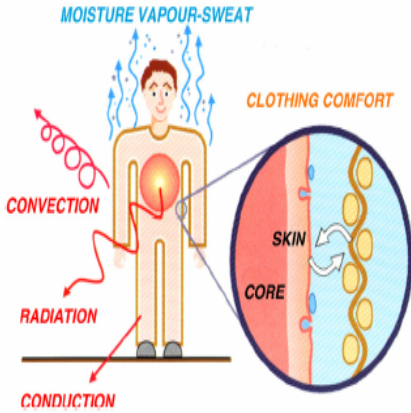
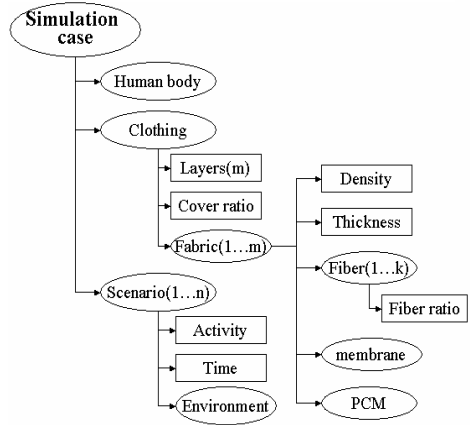**Fig. 1.** Thermal processes in Human-Clothing-Environment system

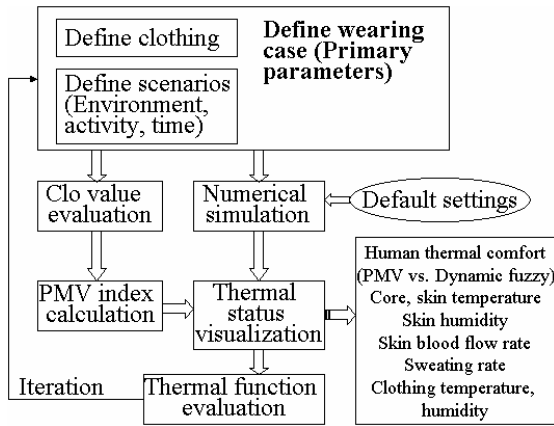**Fig. 2.** Primary parameters used to define simulation case

Fig. 3. System architecture of the half-live simulation

3   The Half-Live Simulation

As hereinbefore analysis, the numerical models have many kinds of parameters and most of them are professional nomenclatures that are difficult and impossible to give an instinct perception. To make the virtual environment as realistic as possible, only the primary and perceptual parameters are used to construct the simulation cases. These primary parameters are input by graphical icons to enhance the virtual environment. To retrieve the relative simulation dataset with the input primary parameters, the definition data of simulation cases are well organized. The primary parameters and the simulation case definition are shown as in Fig. 2.

Because this half-live simulation is based on the existed simulation result, it's significant to assure that all reasonable simulation cases can be retrieved. Considering the fact that the available clothing materials, the effect clothing assemblies, the human body properties and the typical environment conditions are all limited and predictable, most of the meaningful simulation cases can be designed and calculated preliminarily. In case that no exact matched cases can be found, it always can find the nearest case and would not lead any big impact for learning purpose. The system is also designed to be able to collect such case definitions for appending its simulation result afterwards. The system architecture is shown as in Fig. 3.

4   Visualization Overview

4.1   Virtual Environment

In order to visualize the thermal state of a clothed human being as realistic as possible, 3D real geometrical models are used to construct a virtual scene, and the 2D animation as a supplement. Human bodies and clothing sets models exported from Poser@ 5 are used to visual the clothed people. They can express some important parameters such as body mass, surface area, clothing cover ratio and clothing style approximately. The male character model is realistic enough with about 35,000 triangular faces. For environment visualization, a virtual climate chamber is designed with wall color representing the air temperature, lighting on the wall representing the radiant temperature, a hygrometer on the wall to reflect the relative humidity, and the waving window curtain for air velocity.

The thermal state of a clothed human being include many kinds of parameters such as human thermal comfort, body temperature, skin humidity, sweating rate, metabolic rate and blood flow rate, as well as the temperature and humidity of each clothing layer. It's necessary to display these parameters simultaneously to explore the thermal processes and thermal state more accurately. To achieve this aim, the 2D animation and cross section view are provided additionally.

4.2   Perceptual Colormap

Visualization is a process of mapping data onto graphical primitives like colored sets of lines or polygons. A proper selection of colormap is important to produce an effective visualization. The most common rainbow colormap is typically the default map. Although it has the problem that the minimum perceivable increment varies widely over the range of the map [10,11], it is still ubiquitous in scientific visualization for following reasons: It is attractive, colorful, with easy to discriminate "regions" of the data which can then be associated with specific data values given a colorbar key (low values with blue, medium-low with cyan, medium with green, etc.) [12]. Therefore the rainbow colormap is used to map the temperature data with improvement from 2 respects. One is the correction of using several piecewise linear maps instead of a single linear map between blue-green-red color space. The other is by fixing the scale points of temperature that reflect the human thermal sensations such as hot, warm, cool and cold. In general, red is for hot, yellow to green for warm,
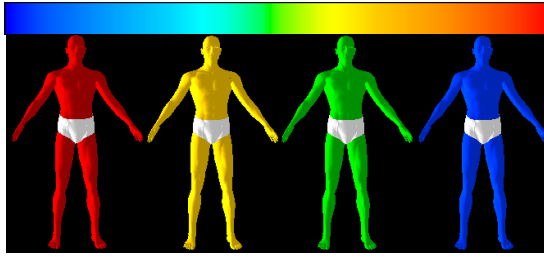
Fig. 4. Colormap examples, top – the improved rainbow colormap for temperature; bottom-from left to right, color maps for hot, warm, cool and cold

green to light blue for cool, and blue for cold. For humidity, a luminance blue colormap is used. The designed colormap examples are shown as in Fig. 4.

4.3 Adaptive Exploring for Time-Varied Data

In order to generate the virtual environment with maximum realistic, it's necessary to realize the real-time animation of the dynamic thermal processes in human-clothing system, thereby it can help learners to sense the change speed of body thermal state in a defined wearing case. On the other hand, the actual time period of the simulation case maybe too long to wait, it's will helpful to provide a flexible control on animation speed.

Real-time animation. To realize real-time clock step, the clock event of windows Timer control is used. The calculation formula for real time is

$$t = t_0 + (T - T_0) * n . \tag{1}$$

where:

   t – real simulation time.
   t_0 – previous end simulation time (considering the pause operation).
   T – current computer system time.
   T_0 – computer system time when start.
   n – animation speed, n = 1 means real time.

Adaptive time-varied data exploring. In most situations, the analysis may care more on quick varying data zone instead of whole simulation period. To automatically display those remarkable data zone, an adaptive algorithm is used. For a given parameters, first a valve value is set, then for each time step the datum is compared with this value, and is displayed only if it's larger than the valve value.

5   Example

In order to illustrate the system functions and the evaluation process of clothing thermal functional performance, a wearing case with contrastive definitions are introduced. The dynamical thermal states are visualized and the traditional thermal

comfort index – PMV index is calculated for reference. As shown in Fig. 5, the wearing case definition interface consists of a tree structure navigator and a tree-node context-sensitive detail form. Each wearing case is the root node, and some of the sub-nodes can be added or deleted dynamically. When a sub-node is selected, the relative detail definition form will be activated.
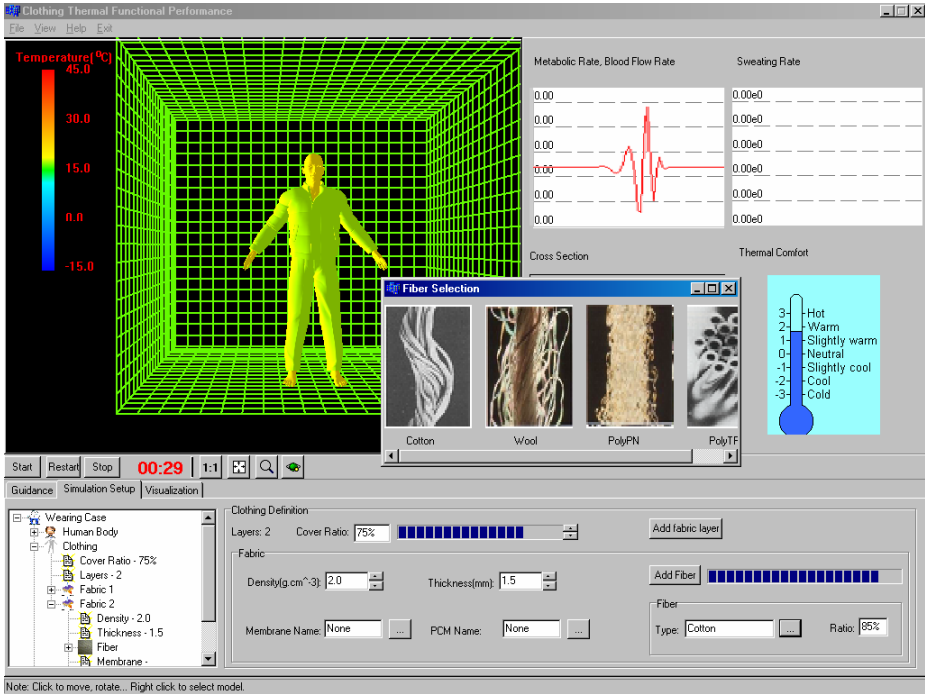

Fig. 5. Wearing case definition: left is the wearing case definition tree, right is a detailed definition page that related to the selected tree node

The wearing case is for summer outdoor walking with three clothing layers, the definition is as follows:

Human body specification: Resting (1 Met), walking (2 Met).
Environmental specification: 35 ^{o}C and 80% relative humidity, air conditional room is 25 ^{o}C and 60% relative humidity.
Clothing design: three cotton fabrics layer.
Scenario: rest for 15 min. in room, then walking for 15 min.

Figure 6 shows snap shot from the thermal processing animation for summer wearing case. Temperatures of body skin and the outside fabric layer are visualized in virtual scene, the cross section view for displaying detail temperature distribution, and the 2D animation for body thermal physiological parameters. It's evident that the clothing with three layers has hot thermal functional performance when walking in summer thermal condition.
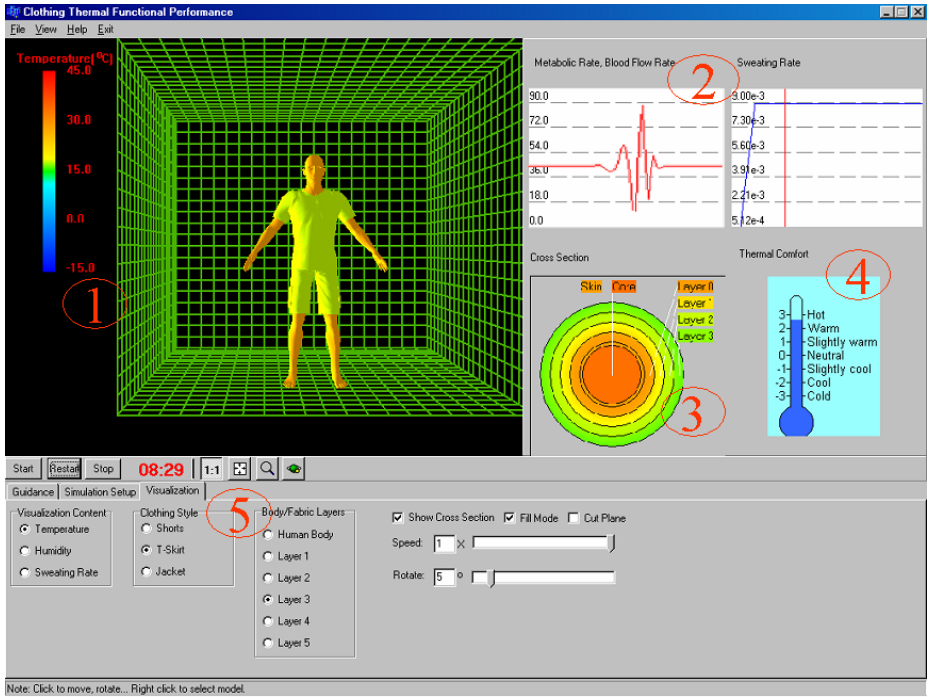
Fig. 6. Thermal state visualization: region 1 – 3D virtual scene; region 2 – 2D animation; region 3 – cross section; region 4 – thermal comfort index; and region 5 – visualization control

6   Conclusions and Future Work

This paper reports the development of a virtual environment for the education of clothing thermal function. The virtual wearing case is defined with primary parameters and the numerical simulation results are visualized with 3D virtual environment and 2D animation, which interpret the thermal state and the dynamic thermal processes of the human-clothing system in a vivid mode. It allows learners in a virtual environment to learn the clothing thermal comfort theory and identify the most important factors that influence clothing thermal functional performance. This virtual environment system is specially developed to help teaching clothing thermal functional design for students and new designers, and it can also be used as a visualization tool by textile researchers. The trial use proves that this system can provide good demonstration of clothing thermal function model numerical simulation result, giving user an intuitive and insightful understanding of clothing thermal function and thermal comfort.

Further works are to implement the virtual reality scene and behavior animation, and to develop an Internet application version using VRML models.

References

1. Wang, Z., Li, Y.: An Integrative Adaptive Model for Simulating Human Dynamic Thermal Comfort in the Body-Clothing-Environment System. Psychophysiology (2003)
2. Li, Y., Li., F., Liu, Y.X., Luo, Z.X.: An integrated model for simulating interactive thermal processes in human-clothing system. Journal of Thermal Biology 29 (2004) 567-575
3. Gagge, A.P., Stolwilk, J.A.J., Nishh, Y.: An Effective Temperature Scale Based on a Simple Model of Human Physiological Regulation Response. ASHRAE Trans. 77 (1971) 247-262
4. Li, Y. et al.: P-smart—a virtual system for clothing thermal functional design. Computer-Aided Design 38 (2006) 726–739
5. Jentsch, M., Reimann, K.: E-Learning for Structural Analysis. Proceedings of the 20th CAD-FEM Users' Meeting 2002 International Congress on FEM Technology, Germany (2002)
6. Ostermann, T. et al.: eLearning Platform with Microelectronic Contents. Proceedings of the IASTED International Conference on WEB-BASED EDUCATION - WBE 2004, Innsbruck, Austria (2004)
7. Mokhtar, A., Khan, M.: Education – oriented visualization model for buildings cross ventilation. Proceedings of the 2nd international conference on Computer graphics and interactive techniques in Australasia and South East Asia, Singapore (2004) 71-73
8. Nahvi, M.: Dynamics of student-computer interaction in a simulation environment: Reflections on curricular issues. Proceedings of Frontiers in Education'96, IEEE, 1383-1386
9. ISO: ISO 7730 Moderate Thermal Environments - Determination of the PMV and PPD indices and specification of the conditions for thermal comfort. 2nd ed. International Organization for Standardization, Geneva, Switzerland (1995)
10. Rogowitz, B.E., Treinish, L.: Data Visualization: The End of the Rainbow. IEEE Spectrum 35 (1998) 52-59
11. Bergman, L.D., Rogowitz, B.E., Treinish, L.A.: A rule-based tool for assisting colormap selection. Proceedings of IEEE Visualization (1995) 118-125
12. Kalvin, A. D., Rogowitz, B. E., Pelah, A., Cohen, A.: Building perceptual color maps for visualizing interval data. Proceedings of SPIE Conference on Human Vision and Electronic Imaging, San Jose, CA. (2000) 323–335

A Question Understanding Model Based on Knowledge Points for Chinese Question Answering Service in E-Learning

Zheng-Hong Wu[1], Ming Li[1], and Huamin Feng[2]

[1] School of Information Science & Technology, East China Normal University, Shanghai 200062, P.R. China
wzh_hongzheng@hotmail.com, mli@ee.ecnu.edu.cn,
ming_lihk@yahoo.com
[2] Key Laboratory of Security and Secrecy of Information, Beijing Electronic Science and Technology Institute, Beijing 100070, P.R. China
fenghm@besti.edu.cn

Abstract. Question answering service in e-learning environment is an important issue. Chinese semantic analysis is a key bottleneck for question answering service to understand question's content. This paper proposes a question understanding model to understand and process syntactic and semantic structure. In this paper, we analyzed a lot of questions from students, and clustered questions based on knowledge points. The question understanding model is made to get question focus and question type. According to question focus and question type, the question answering service can precisely know the question's answer by locating knowledge point's attribute. This method could more perfectly understand semantic content of questions than using pure Chinese semantic analysis. It is very useful for students to study in a self-learning environment.

Keywords: Question Answering, Knowledge Point, E-Learning.

1 Introduction

Nowadays, question answering (Q&A) has become an important research field with the rapid development of the Internet. However, current Q&A systems are far below human expectations. This is because natural language is not easy to process and interactive Q&A is even harder to model. Q&A research is a multidisciplinary field, and systems are usually integrated from many techniques and resources. Information Retrieval (IR), Natural Language Processing (NLP), Information Extraction (IE), Machine Learning, and even Software Engineering techniques are all needed to build a Q&A system. Most Q&A system would be an ideal way for people to search for information. Since 1999, many international question answering contests have been held, such as TREC (Ellen M. Voorhees 2003, 2004, 2005), CLEF, and NTCIR. Results from the TREC evaluations ((Kwok et al., 2000) (Radev et al., 2000) (Allen et al., 2000)) showed that Information Retrieval (IR) techniques alone are not sufficient

for finding answers with high precision. The Webclopedia project at the USC Information Sciences Institute (Hovy 2000, 2001) pursued a semantics-based approach to answer pinpointing that relies heavily on parsing. They want to provide much more accurate answers for users. Some researchers were working on designing the Q&A methodologies, such as Debra T. Burhans (2005), Dan Moldovan (2005), and Humphreys (2000), etc. Some researchers researched the question stem, e.g. who, where or how much and eventually one of the question concepts. But the stem is ambiguous (for example what), as described in (Harabagiu et al., 2000) (Radev et al., 2000) (Srihari and Li, 2000). There are only a handful research teams working on Chinese QA, which may explain why the first Chinese QA contest was only held at this year's NTCIR workshop (2005). New Chinese question taxonomy respectively from approach and semantic viewpoints was presented (Youzheng Wu et al.). Hybrid architecture for answering Chinese factoid questions from news documents was proposed (Cheng-Wei Lee et al.).

Frequently, question reformulations use different words, but imply the same answer. Moreover, many equivalent answers are phrased differently. That is the main trouble in solving Q&A. Current Q&A systems are far below human expectations. This is because natural language is not easy to process and interactive Q&A is even harder to model. Since natural language is full of noise, it is important to deal with real data. Noisy or inconsistent information could be filtered out to achieve better performance. Q&A also has the same features in e-learning. And Q&A is an important part in e-learning for students. But, Chinese semantic analysis is a key bottleneck in Q&A field.

How to solve these difficulties is very important for Q&A system. Firstly, we collected a lot of questions from students and textbooks. Then, we analyzed these question samples. We found that a question from students in e-learning course always asks content about some knowledge point. Moreover, each question's answer is connected with one attribute of knowledge point. Knowledge is composed by knowledge points. Attributes of knowledge point are the followings: knowledge name, definition, characteristic, function, and so on. The same attribute can reformulate question use different words, namely different question types, but simply the same answer. So, questions have some special features from students in e-learning. Every question has two important features. One is that a question is almost related with some knowledge points. This feature is named question focus. The other is that the question's answer is some attributes of one or more knowledge points. This second feature is named question type or knowledge attribute. At the same time, we found another key feature. Though different questions, they are always related with one or more knowledge points. And their answers are these knowledge points' attributes. So questions can be classified into simple question and complex question based on the number of knowledge points involved in one question sentence. If the question focus relates to one knowledge point, it is called simple question. And its answer can be found from an attribute of the knowledge point. Complex question is defined that its question focus is connected with several knowledge points. Complex question is divided into several kinds according to the relationship of knowledge points (Zheng-Hong Wu et al., 2004). Then, Knowledge base is constructed by ontology. Each

attribute of knowledge point can be found by linking this knowledge point. If these two features are determined, the answer can be retrieved from knowledge base.

Combining early research (Zheng-Hong Wu et al., 2005), we modeled question item from two novel angels based on knowledge points. One is question focus. The other is knowledge attribute. Two novel angels are helpful in locating answer in this paper. Section 2 gives the overview of the architecture of Q&A service. According to Neural Network Classifier (NNC) and knowledge base, Section 3 describes process of generating question understanding model including question item and question panel, and gives the experiment system. Finally, Section 4 makes a simple conclusion and describes some possible future works.

2　Question Answering Service

Figure 1 shows how the question answering service works. The first part is inputting questions by interface. This part classifies question type and question focus through question item. Question item is constructed by Neural Network Classifier (NNC).The second part is setting up knowledge point base, synonymy base and answer base. And, the third part is mining answer.
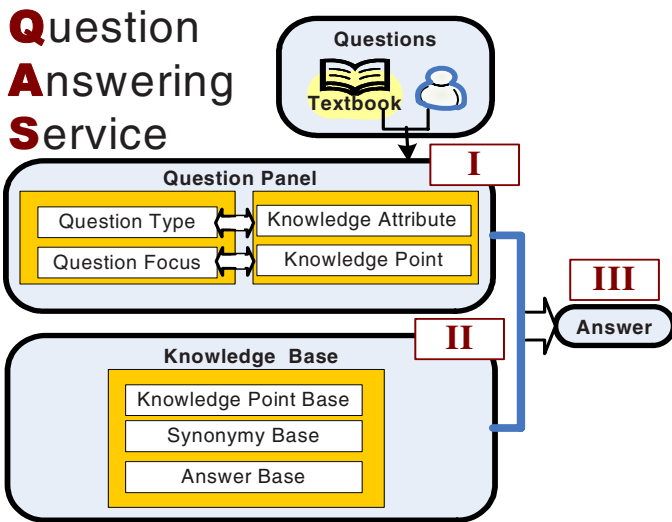

Fig. 1. Question Answering Service

In the beginning, the service retrieves question from the interface. And, question focus and question type could be created (step I) according to the question item. Then, the service uses data mining to locate the knowledge point in knowledge base (step II). Finally, the service is to generate answer (step III). Students then would be able to see the answer item by simply using their web browser.

3   Operation Flow of Generating Question Panel

This section goes through the question item by clustering abundant question examples. From the knowledge point, Table 1 details question focus and question type. There are three sub-sections in this section, and each sub-section represents a key for different parts in the service architecture as Figure 2 shows. The three keys are the knowledge base (step I-2), question item modeling (step I-3) and question panel (step I-4).
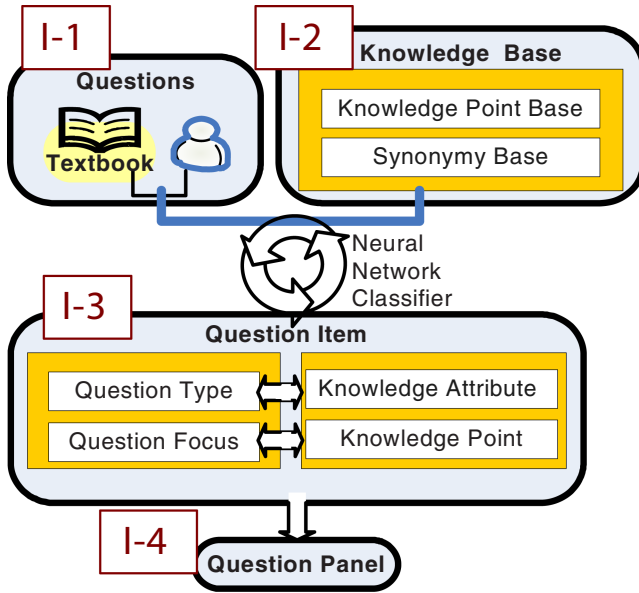

Fig. 2. Flow of Question Panel

Figure 2 shows the flow of generating question panel. The architecture of question panel could be seen as four parts: the first part is sampling questions from students and textbooks (step I-1); the second part is setting up synonymy base (step I-2); and, the third part is to model question item by classing question type and question focus on the base of the synonymy base and Neural Network Classifier (step I-3); the fourth part is generating question panel (step I-4). The repeated flow indicates the question item would be changed from time to time. Finally question panel is made by question item. Students then would be able to see the question panel by simply using their web browser.

3.1   Modeling Question Item

In the beginning, we collected thousands of questions from students and textbooks. Then, we concluded that student inputting a question is to know some content about one or some knowledge points, which is the attribute of knowledge point. Additionally,

a question is composed by question focus and question type. The question focus is knowledge point. The question type is to know attribute of one or more knowledge points. Finally, we found that questions could be modeled according to the number of knowledge points. Therefore, we can classify questions from two angels. One is the number of knowledge. The other is the attribute involved in questions.

Table 1. Question Attribute Clustering and Statistics

Q.C.	**Q.T. (K.A.)**	**Example of question**	**Q.F. (K.P.)**
Simple	What…(Definition/Concept…)	What (*definition*) is *optical fiber communication*?	*Optical fiber communication*
	What/How…(Function/Use/Meaning/…)	What is the meaning of developing intelligent network?	*intelligent network*
	How/What…(Mechanism/Theory/…)	How (*mechanism*) to avoid *disturber from the same frequency*?	*disturber from the same frequency*
	How/What…(Application…)	Describe the method that realizes the *global communication using synchronous satellite*.	*global communication using synchronous satellite*
	What/How…(Feature/…)	What are the features of *satellite communications*?	*satellite communications*
	What/How…(Structure/Component/Kind…)	What components compose the *optical fiber communication*?	*optical fiber communication*
	…	…	…
Complex	What/How…(Difference/Comparison/Relating…)	What is the difference between *transmission* and *convection*?	*Transmission, convection*
	What/How…(Reason/Influence/…)	What special demand for *modem* in *mobile communication*? What is the influence from *waste* and *chromatic dispersion of optical fiber* in *optical fiber communication system*?	*Modem, mobile communication waste, chromatic dispersion of optical fiber, optical fiber communication system*
	…	…	…

Q.C.: Question Class; Q.T.: Question Type; Q.A.: Question Attribute; Q.F.: Question Focus; K.P.: Knowledge Point;

Taking questions in Modern Communication Technology for example, Table 1 shows the question type and question focus. The model of question item could be seen as two parts: the first part is simple question (from Q.C.) which involves one knowledge point (from Q.F. (K.P.)); the second part is complex question (from Q.C.) which involves two or more knowledge points (from Q.F. (K.P.)).

As we can see within Table 1, any question is about some attribute of knowledge points. One attribute may be expressed by similar words. For instance, mechanism, theory and other synonymy standard the same attribute for knowledge point, e.g.

Q1: How does the signal microwave communication work?
Q2: What is the working mechanism/theory of microwave communication?
Q1 and Q2 use different words, but imply the same answer, namely the same attribute of knowledge point.

So, synonymy words are ranged (Table 1) to express the same attribute after studying those question examples. Using sampling more questions, more synonymy words could be found by clustering. And more exact attribute kinds could be set up.

Simple question is focused on one knowledge point's attribute. These are several attributes in a knowledge point, including concept, function, feature, and others. The answer of question mainly aims at these attributes (from Q.T. (K.A.)).

Complex question's answer focused on the attribute among several knowledge points regarding one knowledge point as prerequisite. Complex question can be classified into two main sub-classes. One is the comparison of these knowledge points to know the difference or respective strongpoint. The other is that which influences one knowledge point to other knowledge points, or how does one knowledge point function at others.

According to the above features, NNC is introduced in this paper to set up question item. NNC implemented through neural network method. During a learning session, each example of the question, representing a single question feature vector, must be pre-classified by a human expert. The NNC processes training examples and induces rules for extracting question features from further unclassified examples, to be used by the question item. According to the synonymy base, NNC can discriminate question focus and question type from questions for the question item.

3.2 Knowledge Base

Knowledge base is built based on ontology. It includes knowledge point base, synonymy base and answer base. Knowledge point base is designed according to question's focus. Synonymy base is designed according to question's type. Answer base is designed by knowledge attribute.

First, the question is put. Use logic calculation to get question item. Question focus and question type are determined. According to question focus, the service could know exact knowledge point. Then the knowledge attribute is determined by question type. Finally, the service matches the answer by pitching the attributes of knowledge point.

3.3 Question Understanding Model

Based on question item and knowledge base, we set up a question panel using Visual Studio.NET to implement the question answering service. Figure 3 shows the question panel. When a student logs on and asks a question, the service can present this question panel for the student.

In this question panel, if you click knowledge attribute, a new windows will tell you the examples of attribute, such as definition, mechanism etc. If the question includes several knowledge points, you should input underline among several knowledge point names. For instance, the question: What (definition) is optical fiber communication? This question is generated in Figure 3. Through the panel, the service can precisely know his/her question's content to avoid trouble from semantic analysis using Natural Language Understanding. This question panel is very simple and effective for students in Q&A.
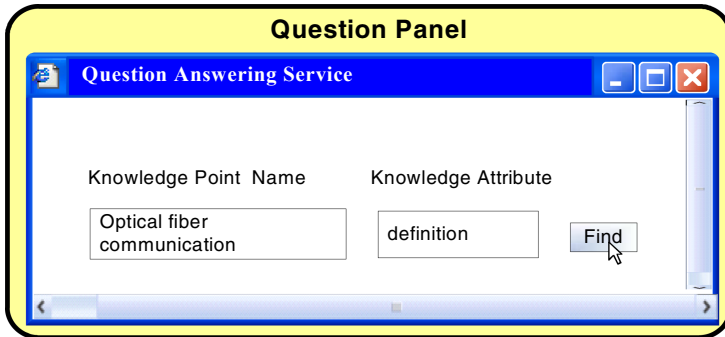

Fig. 3. Question Panel for Students

4   Conclusions and Future Directions

This paper focuses on setting up a question understanding model to support question answering for self-learning in e-learning course. To reach the goal, we collected a lot of questions and analyzed them from the number of knowledge point and attribute of that. Questions were clustered by using NNC. Subsequently, question panel was built to get question focus and question type. Then, knowledge base was set up. Finally, the question could be precisely understood through question understanding model. The service could provide the student answer. This model was tested in the network college in CCNU. This method has some efficiency in Q&A, especially in simple question. But this model should be improved in deal with complex question.

Question answering service becomes more and more important in e-learning field. We should have a more accurate method to reach accurately and adaptively present answer. Furthermore, because the clustering attributes should be more precise, we have to improve the method of clustering question type, knowledge attribute and synonymy base. Besides, we also need to establish a perfect and friendly question model.

References

1. Voorhees, E. M.: Overview of the TREC 2005 Question Answering Track. Proc., the Thirteenth Text Retrieval Conference (TREC 2005), 2006
2. Voorhees, E. M.: Overview of the TREC 2004 Question Answering Track. Proc., the Thirteenth Text Retrieval Conference (TREC 2004), (2005) 52–62
3. Voorhees, E. M.: Overview of the TREC 2003 Question Answering Track. Proc., the Twelfth Text Retrieval Conference (TREC 2003), (2004) 54–68
4. Burhans, D. T., Shapiro, S. C.: Defining Answer Classes using Resolution Refutation. Special Issue of the Journal of Applied Logic on Questions and Answers: Theoretical and Applied Perspectives, Available online 18 Jan. 2006, (2006) 279–295
5. Shapiro, S. C.: A Logic of Arbitrary and Indefinite Objects, in: Principles of Knowledge Representation and Reasoning. Proc., the Ninth International Conference (KR-2004), AAAI Press, (2004) 565–575
6. Fleischman, M., Hovy, E., Echihabi, A.: Offline Strategies for Online Question Answering: Answering Questions Before They Are Asked. Proc., 41st Annual Meeting of the Association for Computational Linguistics, (2003) 1–7
7. Ferret, O., Grau, B., Hurault-Plantet, M., Illouz, G., Jacquemin, C., Masson, N., Lecuyer, P.: QALC- the Question-Answering System of LIMSI-CNRS. Proc., the Text Retrieval Conference (TREC-9), (2000) 316–326
8. Moldovan, D., Rus, V.: Logic Form Transformation and its Applicability to Question Answering. Proc., ACL 2001
9. Moldovan, D., Pasca, M., Harabagiu, S., Surdeanu, M.: Performance Issues and Error Analysis in an Open-Domain Question Answering System. Proc., ACL 2002
10. Wu, Y.-W., Wu., Z.-H., et al.: Generating Personalized Answer by Constructing Question Situation. Springer LNAI, (2006) 731–739
11. Wu, Y.-W., Wu., Z.-H., et al.: Personalized Intelligent Question Answering Algorithm in E-learning. The Fourth International Conference on Machine Learning & Cybernetics (ICMLC-2005) 3299–3303
12. Wu, Y.-Z., Zhao, J., Xu, B.: Chinese Question Classification from Approach and Semantic Views. Information retrieval technology (Second Asia Information Retrieval Symposium, AIRS 2005, Jeju Island, Korea, Oct. 2005, proceedings) Asia Information Retrieval Symposium No2, (2005) vol. 3689, 485–490
13. Lee, C.-W., et al.: Perspectives on Chinese Question Answering Systems. Proc., the Workshop on the Sciences of the Artificial (WSA 2005), Taiwan, (2005)
14. Lee, C.-W., et al.: ASQA: A Hybrid Architecture for Answering Chinese Factoid Questions. http://www.iis.sinica.edu.tw/~thtsai/paper/Rocling2005_Demo.pdf

Focus and Attitude in Computer-Mediated Peer Assessment: ePortfolios Methods in Chinese Context

Youmei Wang

Dept. of Educational Technology, Wenzhou University, China
ymwang@wzu.edu.cn

Abstract. Peer-assessment has become more popular in the instructional assessment area.Eportfolios was used as an important tool to facilitate computer-mediated peer assessment in online instruction. This study adopted quantitative approaches to explore the focus and attitude of onymous or anonymous peer-assessment with WePS (Web-based ePortfolios System) in Chinese context. Findings showed that Onymous group members paid attention to the response of their learning peers,that the onymous group had more confidence in peer-assessing and they thought that their assessment was more effective than anonymous groups,and that Onymous groups members recognized peer's assessment on their learning more than the anonymous one.Compared with the realted studies in western context this findings is different in some aspects.

Keywords: Computer-Mediated Peer Assessment. ePortfolios. Focus. Attitude.

1 Introduction

Eportfolios is a collection of authentic and diverse evidence, drawn from a larger archive representing what a person or organization has learned over time on which the person or organization has reflected, and designed for presentation to one or more audiences for a particular rhetorical purpose (NLII, 2003; Barrett, 2003). And now eportfolios is being an approach to assess learning performance of students in many educational institution. Eportfolios assessment belongs to authentic assessment and formative assessment, aiming to break through the traditional assessment ways such as quantification assessment and paper test (Wang, 2003), and it is a trend to build the web-based eportfolios assessment system to evaluate performance of online learning, which depended on the implementation of peer-assessment and self-assessment(Barrett, 2003). Online learners tend to play a hidden role, and identity of learner will affect on the performance of learning (He, 2002), so it is an important issue to study the problems of onymous or anonymous learner in the process of assessment and learning. Based on the previous studies, this study carried out an experimental method to discuss the quality and effectiveness of peer-assessment with different anonymities with computer-mediated eportfolios system in Chinese context.

2   A Review of Relevant Literature

2.1   On Peer-Assessment

Topping (1998) put forward a definition regarding peer-assessment. According to his definition, Peer-assessment is that students attempt to play the role as teacher to give assessment on their classmates at the same grade. After studying 109 articles on peer-assessment in the ERIC database, Topping pointed out that some scholars had already used this kind of assessment technique in various subjects including science, information and social study, and that the peer-assessment has reached a certain level of reliability and effectiveness. Peer-assessment technique can be used to improve the high-order thinking and learning motivation of students, which is a good assessment model for adult learners.

Jack McGourty had also found that there were consistency between self-assessment and peer-assessment; and some learning outcomes that cannot be tested in traditional assessment may be reflected in peer-assessment. Peer-assessment can not only engage students better in study, but also improve the quality of students learning and students' ability of criticism and provide them with opportunities to take part in the assessment. And students could help each other and improved their learning performance (Falchikov, 1995). Topping (1998) analyzed 31 studies about applying peer-assessment into various projects in higher education during the year of 1980 to 1996, which was related to the reliability of peer-assessment. By calculating the correlation coefficient between peer-assessment and professionals assessment, Topping (1998) found 25 among 31 research articles showed that peer-assessment has high reliability.

2.2   Computer-Mediated Peer-Assessment

Yong Zhao (1998) systematically summarized anonymous computer-mediated assessment. He took on a research to study aspects of assessment such as attention focus, critical and cognitive slack of students. His experimental courses were educational introduction to students and Spanish, which is an important course in two American universities. His experiment chose 22 and 23 students as samples respectively; he studied the influence of anonym on students' cooperative learning and discussed the anonymous peer-assessment. It was found that anonym has double-side function, it can make the testees more critical but it also lowers the quality of assessment in the process of peer-assessment. However, the framework of this study came from western culture for its experimental background, and it still needs validating whether it can be analogized to eastern thoughts and learning environment, about which I talked with the famous expert on eportfolios——Dr. Helen Barrett. Based on her work experience in Singapore, She thought there is an obvious difference in self-reflection and peer-assessment between western and eastern students, which is the root of the framework for our study.

3 Method

3.1 Learning Environment

The study was carried out by the WePS online, which was a web-based eportfolios system developed by us (Wang, 2004). WePS is different from other eportfolios systems in that it is integrated learning eportfolios、course portfolios and teaching course portfolios(Fig.1).In practice we look upon eportfolios as a kind of aggregation in which learner can represent their learning objectives, activities, outcomes, performance, efforts, progress and reflection about learning process and result under an eportfolios learning environment. So each student had a learning space online; actually it was a portal for student to learning. Students can collect the learning artifacts, assess himself and others, write the reflection on learning and development, and there are powers for everyone to access others eportfolios with teachers accredit.
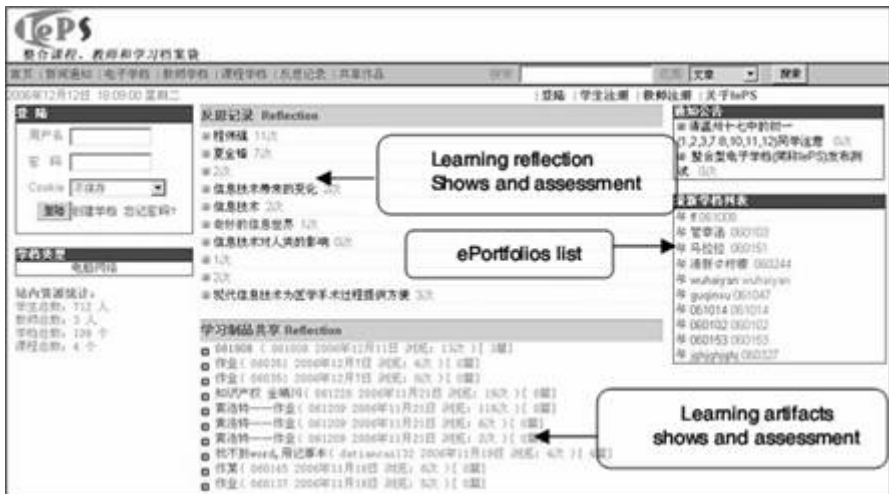

Fig. 1. Web-based ePortfolios System Interface

3.2 Task and Design

The time of study span was two years. And we took 40 students majored educational technology coming from Wenhou university in China. They learned with WePS1.0 and took on eportfolios-based assessment each other for a long time. The experimental course was systematically instructional design and project management. In this study we choose one time randomly (this time is mid-term assessment) to analyse and test. Without being told the purpose of the experiment, 40 students were required to finish the eportfolios task including analyzing, designing and concluding constructivist cases after web-based learning the same as before. The scale for eportfolios was provided to them before learning. After finishing the task, they were to post their artifacts online with the requirements and carry through self-assessment and peer-assessment, which included qualitative and quantitative assessment, and then

complete the questionnaires (38 of which were valid) provided by the teacher, the questions in which are all Likert's scale.

3.3   Sample and Design

The samples were organized in such way as is shown in the following table 1, based on the partition of anonymous and onymous peer-assessment:

Table 1. Sample and design

Group definition	Random grouping	Onymous requirement	eportfolios task	Assessment requirement
Anony-ous group	Choose 20 students randomly in terms of seats	Register; hand in works and assessment without real name. All the information is anonymous.	Complete tasks combining consultation with self-doing.	Assess at least one anonymous and onymous peer
Onym-us group	The same as above	Register and hand in works and assessment with real name	Complete tasks combining consultation with self-doing.	Assess at least one anonymous and onymous peer

3.4   Research Questions

(1)Difference of focus in the process of assessment between two groups.

(2)Difference of attitude in the process of assessment between two groups.

3.5   Data Collection and Processing

The experimental data came from three aspects: the first was from the questionnaires on online learning, which was an attitudinal scale and converted into 5 scored statistically; the second from the score of eportfolios assessment (including self-assessment and peer-assessment) (max.100-score); the third from the quantitative assessment from teacher on assessors' qualitative assessment, taking a 5-scale (5=Strongly agree and 1=Strongly disagree). Finally SPSS11.0 and EXCEL2003 were used to analyze the data.

4   Data Analysis and Results

The main purpose of this study was to discuss the attitude to and effect of different onymous peer-assessment in eportfolios. For the samples were not many, it was reasonable to adopt the methods of comparison of effect size and t-test, and we were mainly concerned difference of effect size to explore the impact that different onymous peer-assessment has on learning.

4.1   Difference of Focus in the Process of Assessment Between Two Groups

Referencing the scale proposed by Yong Zhao (1998), we set two questions to discuss the difference of focus in the process of assessment between two groups. The first question was: "I have thought of how the author will respond to my assessment when I assess others' eportfolios", the result indicated that comparatively, as the assessors, onymous group paid more concerns about the response of the assessees to their assessment during the process. As to the second question: "when assessing others, I pay more attention to the quality of the peers' task and content rather than author themselves or other aspects". Both two groups thought they paid more attention to the quality of the peers' task and content rather than author themselves. But it was obvious that more testees of onymous group agree on this view than the other group(Fig. 1 and Fig.2 shows the results).
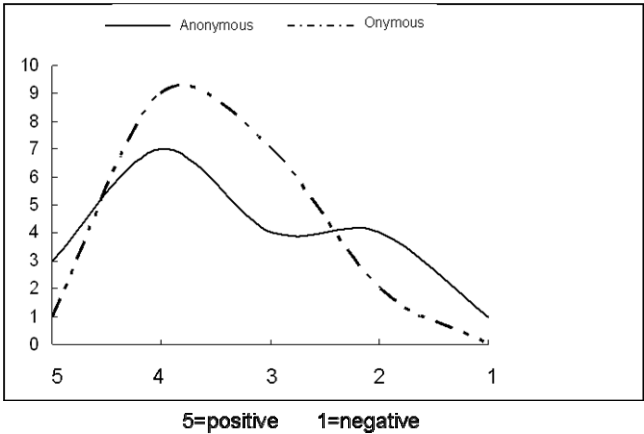

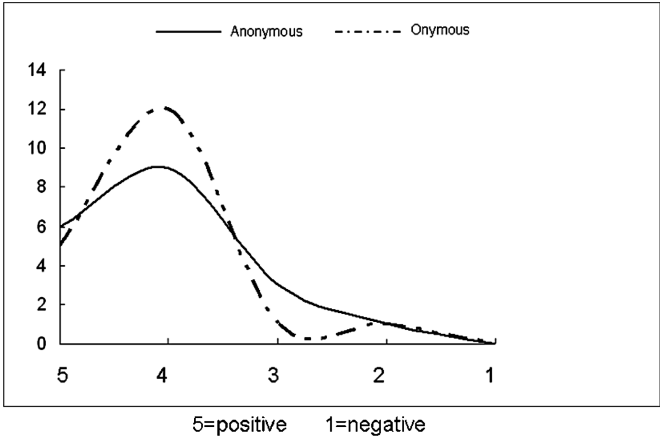**Fig. 2.** Distribution of response on question one

Fig. 3. Distribution of response on question two

When converting the qualitative table into 5-score scale and conducting single-sample t-test (two-tailed test, df=36, the same as follows), we found that the answers of two groups on the two questions had no "significance of difference" (Q1:p=.17>.05;Q2:p=.10>.05).

4.2   Difference of Attitude in the Process of Assessment Between Two Groups

In the web-based collaborative peer-assessment process, were there any differences in assessors' attitude to assessment between two groups? We designed two questions to test and found that the onymous group members had more confidence in their assessment for their companions and their assessment were more effective than the anonymous group, and there were "significance of difference" (P<.05) .However, both the two groups thought that they were diligent and responsible in this process, and there were no "significance of difference" (P>.05).

Table 2. Self-cognition of the two groups on their assessment on their peers

groups	"my assessment can promote the peer's learning"		"I fulfill the responsibility of peer-assessment seriously"	
	M	SD	M	SD
Anonymous group	3. 26	0. 73	3. 89	0. 57
Onymous group	3. 84	0. 60	3. 95	0. 52
t-value	2. 66（P<.05）		0.297（P>.05）	

5   Comparison with Other Researches

As mentioned above, there were few studies in the field of peer-assessment with eportfolios. We mainly compared this one with the experimental results of Yong Zhao (1998), which were conducted in the CMC learning environment. The results were identical in the anonymous assessment that anonymous assessment was helpful to improve criticality but had lower quality. However, our study showed that on the focus during the process of assessment there were significance of difference between onymous and anonymous assessment, comparatively, more members of onymous groups were more concern of the author's response on their assessment and more about the content of eportfolios rather than the author himself, but there were no significance of difference between two groups. In contrast, the conclusion of Yong Zhao was that in the condition of anonymous assessment, the assessors concern more of content. The difference may be caused by different attitude of western and oriental students on collaborative learning and their comprehension of collaborative assessment, at the same time it may be related with teachers' direction of the experiments. Certainly, it was a very important factor that the supporting environment of these two experiments was different. Yong Zhao adopted e-mail assessment in the CMC, and we adopted independent web-based eportfolios system supporting assessment and study.

6 Conclusion

Based on a two-year experimental research, the following conclusions were drawn:

- Onymous group members paid attention to the response of their learning peers when conducting assessment, and they argued that they paid more attention on portfolio content per se and there were no obvious differences between the two groups;
- The onymous group had more confidence in peer-assessing and they thought that their assessment was more effective than anonymous groups. Both onymous and anonymous groups thought they were responsible in their assessment on others;
- Onymous groups members recognized peer's assessment on their learning more than the anonymous one;

At last we must pointed out that, in this kind of studies, many factors such as samples、course and experiment platform will affect the results. So we think this experimental data and conclusions are correct in a specifically context. And it provides a kind of thought and can be used as a reference for the implement of e-learning and online instruction in the future. We hope that it can be of some help for the development of web-based instruction and its evaluation.

References

1. Barrett, H. Presentation at First International Conference on the e-Portfolio, Poiters, France (2003), October 9, 2003. http://electronicportfolios.org/portfolios/eifel.pdf,2005-12-10
2. Barrett, H. "Electronic Portfolios as Digital Stories of Deep Learning: Emerging Digital Tools to Support Reflection in Learner-Centered Portfolios." (2005) http://electronicportfolios.org/digistory/epstory.html,2006-5-4
3. Belanoff, Pat & Dickson, Marcia (eds.). Portfolios: Process and Product. Poutsmouth: Heinemann (1991).
4. Falchikov, N. Peer feedback marking: Developing peer assessment. Innovations in Education & Training International(1995), 32, 175-187
5. He Kekang, Instructional system design, Beijing Normal University Press (2002), Beijing, China
6. Keith Topping, Peer assessment between students in colleges and universities. Educational Research(1998), 68(3), 249-276.
7. Wang Youmei, Web-based eportfolios system in e-learning environment, Open Education Research(2004), 51(5), 56-58
8. Yong Zhao.The Effects of Anonymity on Computer-mediated Peer Review. International Journal of Educational Telecommunications (1998), 4(4), 311-345.

eCSM: Semantic Classification Model for Educational Repositories

Dongwon Jeong[1], Myounghoi Choi[1], and Keunhwan Jeon[2]

[1] Dept. of Informatics & Statistics, Kunsan National University
San 68, Miryoung-dong, Gunsan, Jeollabuk-do, 573-701 Korea
`{djeong, cmh775}@kunsan.ac.kr`
[2] Dept. of Internet Media Information, Kunjang College
608-8, Seongsan-Myoen, Gunsan, Jeollabuk-do, 573-709
`khjeon@kunjang.ac.kr`

Abstract. This paper proposes a new classification model for management of resources in an educational repository. To facilitate usability of educational resources, a proper classification model should be provided. If no classification model, it causes several issues such as inefficient management of educational resources, incorrect retrieval, and low usability. To achieve the goal of this paper, the model should support a classification mechanism in multiple viewpoints. The proposed model enables more precise and systematic management of implementation resources, and also increases the ease of usability.

Keywords: Semantic Classification, Educational Repositories, Classification Model.

1 Introduction

An educational repository is intended to manage efficiently and systematically a variety of resources generated in the educational course so that learning effects are maximized and qualitatively improved educational systems are developed. However, there have been few studies on educational repository system, especially, on classification scheme absolutely required to manage diverse and enormous educational resources and materials. An accurate classification scheme is required to store and manage systematically resources generated and to ensure accurate retrieval and maximized application.

Until now, in many other disciplines, multiple studies on classification schemes designed to manage efficiently and systematically their generated and used resources and apply correctly and exactly them have been conducted [1,2,3]. Although various classification schemes have been defined, most of them target commercial goods or services, and are inappropriate to the resource management for educational repository.

The classification scheme for educational resources is essentially similar to that for scientific technologies. Of the current scientific technology classification schemes in Korea, the most commonly used schemes are those suggested by Korea Science and Engineering Foundation (KOSEF) and Korea Research Foundation (KRF) [4,5,6].

These classification schemes pose the problem that they are based upon static classification models, i.e., static classification management models. In addition, a same subclass may be redundant with several other super-classes. Above all, since the relationship among the classes within a certain scheme is not clarified, it is difficult to interpret and understand their significance and implication, as well as impossible to define the associations among classification schemes and given careful consideration to the relationship between different resources. Importantly, if relying only on such classification schemes, it is impossible to classify and manage correctly and accurately the resources in an educational repository, because their classes were defined just from the viewpoint of scientific technologies. To the contrary, for resources to be managed in an educational repository, their classification scheme should be defined from the viewpoint of applications as well as simply scientific technologies [7].

In another aspect, the conventional classification schemes involve simple code-based classification models with tree structures or classification codes. In a code-based classification scheme, a super-class code (e.g., A10) becomes the prefix notation of its subclass code (e.g., A1011, A1012). Information - that is, the conceptions of classes, the relationship among the conceptions, integrity constraints, etc. – is expressed primarily rather implicitly than explicitly. For the reason, as any systematic processing is unavailable, guidelines are prepared and maintained merely via documentation. The above-mentioned problems of the logical models for code-based classification schemes may cause several problems including lack of consistency and flexibility attributed to classification criteria and levels mixed up in a same classification scheme [8].

The purpose of this paper is to define a classification scheme for educational repository and suggest a model designed to manage dynamically the defined classification scheme. A dynamic classification model, i.e., dynamic classification scheme management model enable add, merge and split operations in the defined scheme, and defining and managing the relationship between the classes to do so. In particular, it helps make classes significant and thereby define even the relationship among the classes, instead of defining the classes simply with codes in order to define and manage significantly the classification scheme.

2   Definition of the Classification Model

The matter of how to classify resources in an educational repository depending upon their generating subjects is of little importance. Regarding definition of classification model, one of the critically important characteristics of such the resources is that they may be generated for a wide range of disciplines. In addition, classification according to educational courses should be also taken into consideration. In this paper, classification according to developed language should be also considered owing to the nature of the specified resource range. First, let us give an example concerning educational course. "Database" and "Algorithm" courses should be definitely classified and each of them can be defined as a class. The resources generated in the individual courses become the resource objects belonging to the classes called either "database" or "algorithm".

As a result, this paper supposes that in consideration of the three viewpoints, a resource classification scheme is to be defined. Fig. 1 shows the schematic diagram of a classification scheme considering the three viewpoints. Considering the three viewpoints suggests that an integrated classification scheme is completely composed of the three types of classification schemes. Further, it represents that a resource belongs to a certain class in the three different classification schemes according to the three viewpoints. In particular, the viewpoint of applications can be regarded as that of application user. In other words, it indicates the viewpoint for users who are familiar with or want to search and apply data under different classification schemes – e.g., "personal information management system" or "video management system" – from scientific technology classification scheme or language classification scheme. Defined in this paper, all the three viewpoints for classification are intended not to meet the universal needs for all applied fields, but to perform a case paper concerning the said multiple viewpoints and dynamic classification model for the purpose of this paper. In this light, the classification viewpoints and classes for each viewpoint should be defined by target fields. However, the concept of the classification scheme management, and its basic architecture and operations suggested by this paper are applicable to all kinds of fields.
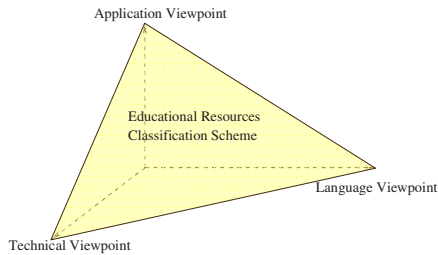

Fig. 1. Classification scheme & its multiple viewpoints

The purpose of this paper is to define a classification model for educational repository resources, named eCSM (Educational Classification Scheme Management Model), and eCSM is defined as follows:

Definition 1. A classification scheme for resources R, called eCSM consists of 5-tuple <R, C, C_R, P, OP>, where

- R: the group of target resources to be classified. Composed of 3-tuple <R_{source}, R_{doc}, R_{u_guide}>, where
    - R_{source}: Actually implemented resources, i.e., implemented sources
    - R_{doc}: Reporter on and interface with implemented resources
    - R_{u_guide}: User guide covering implementation settings, installation and so on.
- C: All classification schemes; C={$C_S \cup C_A \cup C_L$ }, where in order denoting schemes for science technology, application, and language viewpoint.
- C_R: Root classes of each classification scheme; C_R= {c_{RS}, c_{RA}, c_{RL}}, where each element indicates the root class of C_S, C_A, and C_L.

- P: P represents the relationships between classes and the suggested classification scheme has not a tree structure but a graph model.
- OP: The set of operations depending on changes in the classes. Operations are classified largely into the operations for classes, OP_{class} and the operations related to resource allocation depending on changes in the classes, $OP_{instance}$.

In Definition 1, resources R is grouped by classification scheme C, while the relationship among the classes corresponding to elements of C is expressed by P. If a new class is added, the values C, R and P are modified by an operation of OP.

In order to implement a more intelligent and versatile classification scheme, the inter-class relationship or class-resource relationship should be defined. Relationship means the relation between two entities. In this paper, largely three types of relationship exist. Additionally, the term relationship stated in this paper is used as the same meaning with Predicate or Property in other similar research fields. This paper doesn't define all the significant relationships available in the selected target field. If required in future, the relationship can be defined and applied in a dynamic manner. The types of relationship defined in this paper include threes – inter-class (class-class) relationship, class-resource relationship and inter-resource (resource-resource) relationship. In eCSM, the relationship P is defined as Definition 2.

Definition 2. Assuming that the groups of inter-class, class-resource and inter-resource relationships are expressed as PCC, PCR and PRR, respectively, the relationship P of eCSM consists of 3-tuple <PCC, PCR, PRR>.

First, inter-class relationship means the relationship between two classes in the classification scheme and its typical examples include parentOf(superClassOf) and childOf(subClassOf). Class-resource relationship is a simple relation of is_a, which represents that resources belong simply to the relevant terminal classes and are subject to grouping. This paper targets primarily the short-term project outputs generated in the departments of computer science, in universities or colleges. Accordingly, the generated resources include outcomes of development (implemented data, programming sources), reporters, and user guides such as development settings. Thus, there are the inter-resource relationship, for example, sourceOf, documentOf and userGuideOf. Additionally, the proposed classification model can define new types of relationship, other than the above-mentioned ones.

Fig. 2 illustrates the case where the above-mentioned relationship exists. c_R represents the parent class of c_1; if the direction is reversed, the meaning is also reverse. That is, there seems to be the relationship between c_4 and c_2 that the former is the child class of the latter. It is seen that there is just is_a relationship between the class and the resource. For inter-resource relationship, r_1 represents the user guide of r_2, which suggests that the two resources are the outputs from a same short-term project.

OP represents the group of operations depending on changes in the classes and is divided largely into the operations for classes and the operations for resource reallocation depending upon changes in the classes. The followings are the main operations for the classes.

- GENERATE: Generate a new class. This operation is associated with other operations such as ADD, GENERALIZE, MERGE and SPLIT. GENERATE operation is divided into twos: one is GENERATE operation (associated directly with ADD or GENERALIZE) without any change in the existing classes and the other is the operation (associated with MERGE or SPLIT) with any change in the existing classes.
- ADD NODE: Add a class as either terminal node or non-terminal node after GENERATE operation.
- ADD RELATIONSHIP: Add the relationship between classes.
- MERGE: Merge classes according to the attributes of newly generated or existing classes. Integrate classes with similar attributes and if merging terminal classes, their resources also belong to the new class.
- GENERALIZE: Generalize subclasses to a single super class, unlike MERGE.
- SPLIT: Split in details depending upon the attributes of class.
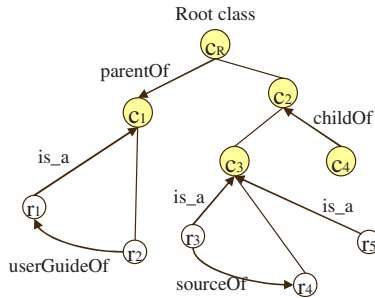- DELETE: Delete the classes which have failed to be merged or split.

Fig. 2. An example of the expression of relationship in eCSM

3   Metamodel for Data Management in eCSM

Fig. 3 shows a metamodel intended to implement eCSM. View defines the information on the viewpoint, and Classification_Class is used to define each class in the classification scheme. All the groups of Classification_Class involving a certain View form a classification scheme derived from the viewpoint. Thus, in this paper, the followings can be defined substantially.

Fig. 4 illustrates the case where class-resource relationship and inter-resource relationship are substantially expressed. In this figure, the resource with resource_ID of "R0101" belongs to class "C0001" and the relationship is "is_a". This relationship is expressed in PCR. The inter-resource relationship is expressed in PRR, which represents the relationship that resource "R0101" is the source to implement another resource "R1100".

There are many ways to define physically a class and an instance, and their relationship. Typically, the methods of defining them with a programming language or with description language such as XML [9], RDF [10] or DAML [11] are used. Recently, OWL (Web Ontology Language)-based approaches have attracted public
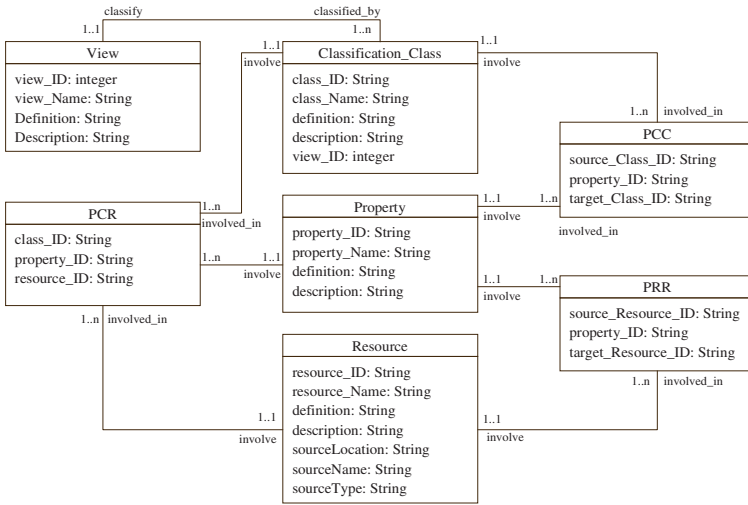
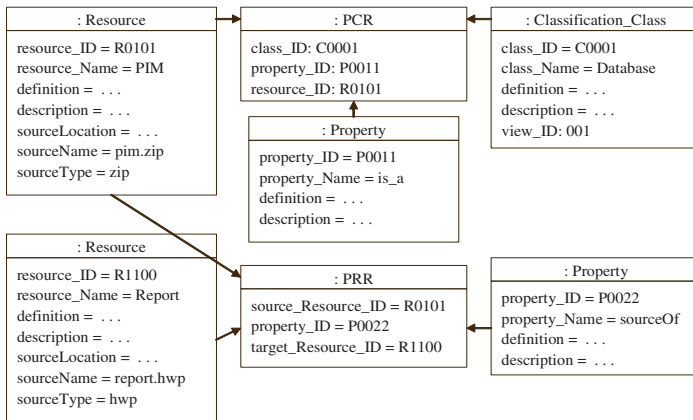**Fig. 3.** Metamodel intended to implement eCSM

Fig. 4. An example of relationship expression

attention. OWL is a more intelligent language than XML and has been recognized as a next-generation description language integrating RDF or DAML [12,13].

4   Implementation Prototyping of eCSM

Fig. 5 shows the system architecture intended to develop an educational repository system based on eCSM.

Resource Management Agent is responsible for user authentication and interfacing including resource registration and retrieval. If the user registers a resource, Relationship Management Agent generates and adds its relationship.

Once registration event occurs, first Relationship Management Agent generates the inter-resource relationship, and subsequently, the class-resource relationship is automatically generated through the index table located in Resource Management Agent according to the classification information selected by the user. Any additional relationship, that is, relationship which cannot be automatically generated is manually generated by the administrator. In this paper, the phrase "automatically generated" means not that the system automatically generates and manages classes, but that the resource-class relationship is spontaneously generated and managed on the basis of the classification information defined by the user (customized) as well as the system resources.

As one of the most important modules, Classification Class Management Agent plays the role of generating and managing the classification scheme. Various operations (GENERATE, ADD, SPLIT, MERGE, GENERALIZE and DELETE) are performed. Once an event concerning class operations occurs, Relationship Management Agent generates or modifies the inter-class relationship. Further, if class-resource relationship is to be changed, the relevant jobs are performed. In connection with these jobs, some operations not affecting the relationship with resources can be automatically executed, while other operations affecting the relationship are difficult to execute automatically. For the reason, they are either manually operated or semi-automatically performed via an efficient interface.

At last, Storage Management Agent stores information through interlocking with database, and if needed, delivers appropriate information to other individual agents. Interlocking with database can be readily implemented by means of database connector such as ODBC or JDBC, which is already a well-known technique.
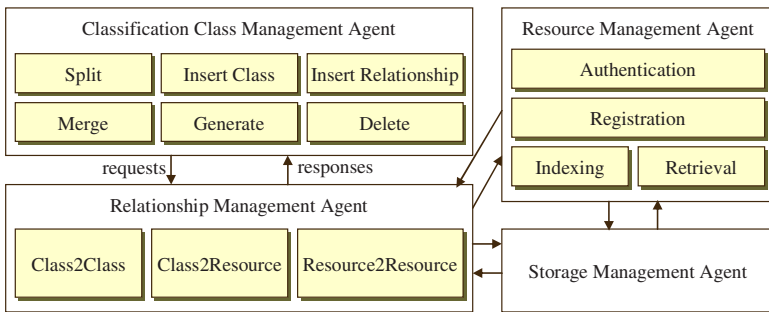

Fig. 5. System Architecture for eCSM-based educational repository system

As previously mentioned, this paper targets short-term projects in computer science field at the level of university or college. The purpose of this paper is to develop a classification model capable of managing dynamically and defining a classification scheme from various viewpoints in order to ensure more efficient management of educational repository resources. Thus, this paper doesn't attempt to define a perfect classification scheme for educational repository. Instead, it attempts to define partially the classification scheme as required for prototype development.

5   Conclusion

This paper suggested eCSM, a classification model designed to manage consistently resources in an educational repository system and to improve their applications. Furthermore, it analyzed the science technology classification scheme adopted by KOSEF and Korea Research Foundation and defined additionally some classes in order to develop an appropriate classification scheme for the management of educational repository resources. Especially, the suggested eCSM takes multiple viewpoints – i.e., of users (applications) and of languages as well as simply of scientific technologies – into consideration, and thus, facilitates applications among the users. In addition, it defined how to manage dynamically classification scheme and the involved main operations, and the model to be implemented with the classification scheme, and presented the results of implementation.

The proposed eCSM first suggests an efficient resource management model intended to develop an educational repository management system. In order to manage and use efficiently resources, an efficient classification scheme and its management are absolutely essential. eCSM comes up with a solution for this requirement. Further, it can not only function as the fundamentals for developing a classification scheme for the still poorly studied field of educational resource management, but also facilitate to develop a better educational repository management system.

Further studies need to define more perfect classification schemes in discussion and collaboration with many researchers and experts engaging in the relevant fields. Further, they need to analyze fully the limitations of the suggested eCSM by expanding the target range and thereby developing more practical systems.

References

1. UNDP (United Nations Development Programme), United Nations Standard Products and Service Code, White Paper, http://www.unspsc.org (2001)
2. Harmonized System Committee, Harmonized System Convention (2004)
3. UNDP (United Nations Development Programme), Better Supply Management with UNSPSC, White Paper, http://www.unspsc.org (2006)
4. KRF (Korea Research Foundation), http://www.krf.re.kr/ (2006)
5. KOSEF (Korea Science and Engineering Foundation), http://www.kosef.re.kr/ (2006)
6. KISTI (Korea Institute of Science and Technology Information) (2006)
7. KCS (Korean Chemical Society), http://newkcsnet.kcsnet.or.kr/ (2006)
8. Kim, D., Lee, S.-g., Chun, J., and Choi, D.-H.: A Semantic Classification Model for e-Catalogs," Korea Information Science Society, Journal of KISS: Databases, Vol. 33, No. 1 (2006) 102~116
9. Yergeau, F., Cowan, J., Bray, T., Paoli, J., Sperberg-McQueen, C.M., and Maler, E.: Extensible Markup Language (XML) 1.1, W3C Recommendation, W3C (2004)
10. Beckett D.: RDF/XML Syntax Specification (Revised), W3C Recommendation, W3C (2004)
11. The DARPA Agent Markup Language, About DAML, http://www.daml.org/ (2003)
12. McGuinness, D.L., and van Harmelen F.: OWL Web Ontology Language Overview, W3C Recommendation, W3C (2004)

Distance Geographic Learning Based on Collaborative Virtual Environment

Wenhang Li, Jianhua Gong, Daojun Wang, Mingxiang Huang, and Jieping Zhou

State Key Laboratory of Remote Sensing Science,
Institute of Remote Sensing Applications, Chinese Academy Sciences, Beijing 100101, China
mylihang@163.com, jhgong@sina.com.cn,
{wangdaojun1980,hmx780202,janepencil}@163.com

Abstract. Although collaborative e-learning has been applied in many fields, it is rarely reported in geographic education. This paper describes one prototype of collaborative virtual geographic education environment (CVGEE). The prototype, developed using Java and Java 3D, provides one immersive 3-dimensional environment and many virtual teaching methods including virtual geographic environment, virtual geographic process. Teachers and learners can discuss with each other in a social way by combination virtualization and reality. Group learning and normal teacher-learner relationship can then be realized in CVGEE. An experiment was conducted to test the functions of the CVGEE prototype.

Keywords: collaborative virtual geographic education environment (CVGEE), geography, e-learning, group learning, collaborative virtual environment (CVE).

1 Introduction

Education theories have been evolved from traditional teacher-centered theories to learner-centered theories and group learning theories. Collaborative E-learning (CEL) has been one of the most significant education trends recent years based on such theories, as well as virtual reality and web technologies [1]. Educations based on CEL are no longer confined to fixed place and learners, which makes public education and individual education possible. CEL always provides a friendly, immersive, 3-dimensional virtual environment and several real-time intercommunication ways for knowledge sharing and question discussion. Many CEL prototype systems have been developed, for example, INVITE[1], VES[2], VRLEARNER[3], and other systems. Some researchers have applied CEL in various fields such as bio-education [4], medical training [5], and geometric spatial training [6].

Although CEL has been applied in many subjects mentioned above, it is still rare for application in geographic education. Contrast to other subjects, geographic education needs more help from CEL, because (1) Geographic education emphasizes students' experience. But in reality, it seems impossible for teacher to take students out to all geographic environments due to funding, time, and other factors like safety. (2) The content of geographic education is complicate. Geographic knowledge covers physics,

chemistry, mathematics and other subjects. It's a good idea for students studying together to manage these complex knowledge. New tools are suggested to help geographic education solve such problems. It is noteworthy that the innovative Google Earth has been developed and evolved rapidly [7]. Google Earth can display virtual terrain covered with remote sensing images for any place of the world. Some geography teachers have applied it in teaching. But Google Earth is not designed specifically for education, it is still necessary to explore CEL for geography.

Collaborative Virtual Geographic Education Environment (**CVGEE**) is such a system to help explore new ideas for geographic education. This paper introduces the prototype. Section 2 focuses on its development, including the architecture, server, and client. Section 3 presents the prototype and an experiment on tornado. Features of CVGEE, such as VGE and VGP simulation and their experience, social intercommunication, virtual teacher-learner relationship, as well as virtual teaching methods are discussed based on the experiment. Section 4 gives summary of current work, as well as prospects for future work.

2 Development of CVGEE

2.1 The Architecture

One framework of CVGEE is proposed here (Fig.1). It is based on a three-layer structure, including *data layer*, *communication layer* and *representation layer*. The *data layer* contains all resources for geography teaching and collaborations. The
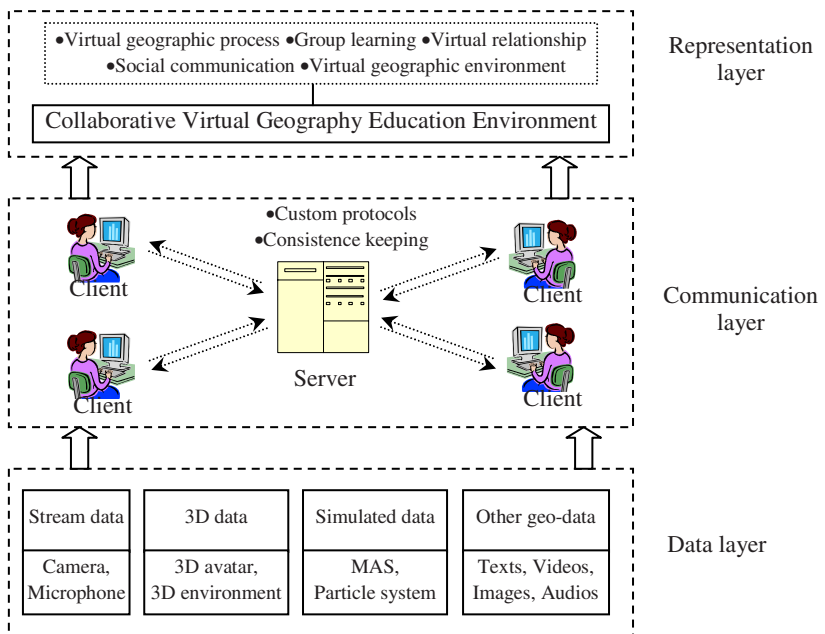

Fig. 1. The three-layer based architecture of CVGEE

communication layer is one C/S mode Collaborative Virtual Environment (CVE), consisting of server and clients. Its purpose is to transfer data of the *data layer*, as well as collaboration messages via server to realize social communications, distance teaching, and group learning. The representations of *data layer* and *communication layer* are participants' social communication, geographic group learning, and collaborative e-learning, that is, CVGEE.

2.2 Implementation of CVGEE

The server is responsible for data and message transfer among clients, to keep all clients consistent. Five services, named "*Message ServiceAgent*", "*Chat ServiceAgent*", "*Video ServiceAgent*", "*Audio ServiceAgent*", and "*File ServiceAgent*" are deployed on the server. Each service is one multi-thread *Java ServerSocket*, responsible for one specific kind of data transfer. The service behavior is as follows: when new request arrives, the service will derive a new thread instance to transfer specific data. When data transfer finished, the thread will destroy itself automatically. The behavior is something like *agent*, so CVGEE calls these services "*ServiceAgent*".

Client program is the visual interface for teachers and learners to take part in the virtual education. It's a 3-dimensional virtual environment developed using *Java 3D*. The virtual scene is on a tree structure. The root node is a "*SimpleUniverse*" which has many child branches, termed "*BranchGroup*". These children branchGroups are classified according to their functions into "avatar branchGroup", "studyobject branchGroup", and "environment branchGroup". Child branchGroup may have its sub-child branchGroups. All virtual data are organized and virtual scene is then built up by this way. The virtual scene is rendered by a *Canvas3D* instance, who responses to the keyboard events, and menu events.

All actions of the clients are captured as *commands* and transferred to all others by the server. When one *command* arrives, the client will carry out a corresponding action to modify the virtual scene for consistency. Collaborations are then accomplished. All are done based on custom protocols (Table 1).

Table 1. Example custom collaboration protocols

Action	Parameters		
JOIN	User Name	Avatar Figure	Avatar Location
MOVEAVATAR	User ID	User Name	New Avatar Location
SENDVIDEO	User ID		Video Data
TALK	User ID	User Name	Message Content

3 Experiment of CVGEE

3.1 Brief Description on the Experiment

One CVGEE prototype has been developed. As an experiment, the prototype was applied in Beijing Qianfeng middle school. The subject was on tornado, one dangerous

(a) teacher in experiment

(b) student in experiment

(c) snapshot of teacher's viewpoint

(d) snapshot of one student's viewpoint

Fig. 2. These pictures are demonstrations of the experiment. The numbers' meanings are: ① virtual classroom, ②remote sensing image, ③chat text, ④student's avatar and captured video, ⑤VRML sand-table, ⑥list of participants, ⑦playing geo-video, ⑧teacher's avatar and her captured video, ⑨dynamic tornado process model (particle system), and ⑩geo-slides.

geographic process. Teacher and students entered into the virtual classroom at different places via Internet. The teacher taught in voice, slides, and videos. Figure 2 gives some demonstrations of the experiment.

3.2 VGE and VGP Simulation and Experience

Hong Kong (Zhujiang delta) encountered with tornado was simulated during the experiment. The "terrible" event "happened" on the desk. The ground was the VRML-format Hong Kong terrain overlaid with the remote sensing image (Fig. 2 ⑤). Tornado was simulated with particle system (Fig. 2 ⑨). The simulation demonstrated the process that tornado came into being on the sea and moved towards the mainland.

There are two alternatives for students to experience VGE and VGP. One is to study or view as outsiders (Fig. 3 a). Another is to shrink the avatar, together with the viewpoint, into VGE or VGP to experience (Fig.3 b A). In the latter mode, participants can walk along the virtual mountains, or float across the virtual sea. It's similar to the reality. The simply changes are participants to avatars, and realistic environments to VGE and VGP.
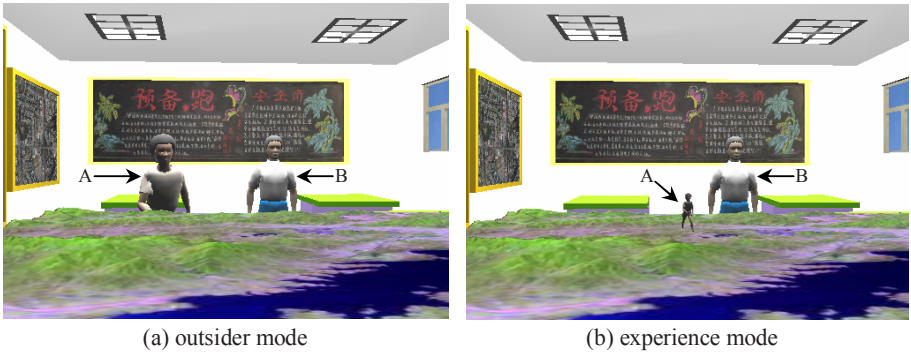
(a) outsider mode   (b) experience mode

Fig. 3. VGE and VGP experience modes

3.3 Social Intercommunication and Group Learning

Education is one inter-communication activity between teachers and learners, which needs sight, voice, gesture, and even emotional expression to achieve mutual recognition. Referring to this mode, in the experiment, CVGEE proposed one "virtual-and-reality-mixed" method (Fig. 4 a). In virtual environment, participants have avatars. Their real figure, actions, as well as expression are captured real-time by digital cameras to "transplant" upon their virtual avatars, and their voices are broadcast through microphones. By this way, when two avatars meet in virtual classroom they (participants) can see and hear each other. Social face to face inter-communication is then simulated in CVGEE (Fig. 4 b).
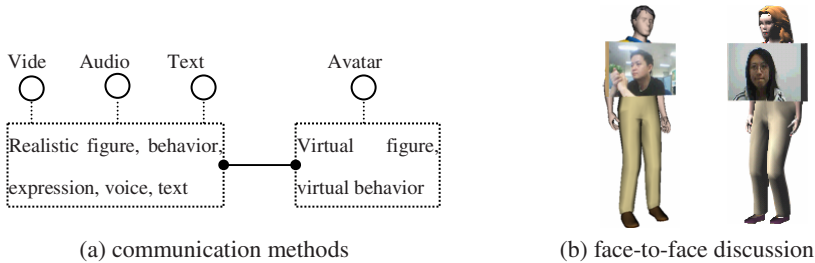

(a) communication methods   (b) face-to-face discussion

Fig. 4. Participants' realistic figures are "transplanted" on their avatars. When the avatars meet, participants can see and talk with each other. It seems nearly face-to-face communication.

Based on the above communication methods, the experiment realized *group learning*. They saw each other, talked with each other, or used texts to discuss on geo-materials such as slides, pictures, videos, or models. They could exchange their cognation and knowledge, or even their own geo-materials. CVGEE turned to be a platform for group discussion.

3.4 Virtual Teacher-Learner Relationship and Virtual Teaching Methods

CVGEE respects learner-centered theories and group learning theories. But in the experiment, we found that most of the students, especially younger students, still could not teach themselves. So, CVGEE regards that the virtual education should not develop all by learners themselves, but follow certain supervision. So, the function of teachers should not be ignored in virtual education, and they were still the knowledge disseminator, course designers and teaching organizers. However, one significant change is teachers' status: they are not central any more but learners' helpers. Education in CVGEE is students' actively learning under guidance of teachers.

CVGEE also reserved successful traditional teaching methods in reality such as slides, geo-videos and geo-images. Students could gain geographic knowledge from various ways. Teaching methods in the experiment are list as table 2.

Table 2. Teaching methods in CVGEE

Classification	Features	Purpose
Environment	3D environment、3D avatar	Providing one real-like education environment
Virtual simulations	VGE,VGP	Achieving virtual experience of geographic environment and geographic process
Traditional methods	Slides, video, audio, images	Inheriting the successful realistic education methods
Group learning methods	Captured video, captured audio, text chat	Simulating virtual face-to-face inter-communication

4 Conclusion and Future Work

In this paper, we discussed the collaborative virtual geographic education environment and its prototype. Contributions of this paper to geographic education can be summarized as following: (1) CVGEE turns geographic education into the virtual one based on a distributed collaborative virtual environment. Distance teaching, distance learning and group learning can be carried out in CVGEE; (2) CVGEE helps solve the puzzle of experience by introducing virtual geographic environments and virtual geographic processes; (3) CVGEE appreciates socially face-to-face participants' communication in virtual education activities; and (4) CVGEE indicates a normal virtual teacher-learner relationship for virtual geographic education.

But further contributions can be achieved in future work, not only for geographic education but also for education itself: (1) Educations have been carried out in virtual space. Since present education theories are based on realistic education behaviors, then one question should be asked: are they fit for the virtual ones? How about the relationship between teachers and learners in the virtual world? They're rarely seen in literature. Maybe new theories should be proposed. (2) One more thing needs to be pointed out that virtual educations including CVGEE are not substitute for the realistic ones. They are supplements for each other. So it will be interestingly innovative to integrate the virtual education with the realistic one. Nevertheless, it is a worthwhile field of study CVGEE for geographic education.

Acknowledgements

References

1. Kuljis J.: A Distributed Virtual Collaborative Learning Environment. In Proceedings of the IASTED International Conference, Applied Informatics, Innsbruck, Austria (2002) 464-469
2. Bouras C., Fotakis D., Kapoulas V.,Koubek A., Mayer H., Rehatscheck H.: Virtual European School-VES. In Proceedings of the IEEE Multimedia Systems'99, Special Session on European Projects, Florence, Italy (1999) 1055-1057
3. Kladias N., Pantazidis T., Avagianos M., Kalamas I., Kopidakis Y., Labbri M.: The VRLEARNERS project: development of a Virtual Reality learning environment providing access to digital museums. http://www.vrlearners.iis.gr/vrlearners/vrlearn.RTF
4. Okada M., Tarumi H., Yoshimura T.: Distributed virtual environment realizing collaborative environment education. In Proceedings of the 2001 ACM symposium on Applied computing, Las Vegas, USA (2001) 83-88
5. Bernhard J., Abdul A., Matthias W.: The Affective Virtual Patient: An E-Learning Tool for Social Interaction Training within the Medical Field. http://isnm.de/~aahad/Downloads/AVP_TESI.pdf
6. Liu D., Wang T. M.: A virtual reality training system fro robot assisted neurosurgery. In Advances in Artificial Reality and Tele-Existence, ICAT 2006, Hangzhou, China (2006) 457-466
7. Declan B.: Virtual globes: The web-wide world. Nature, 439(16) (2006) 776-778

A Distance Learning System for Robotics

Soon Hyuk Hong, Ji Hwan Park, Key Ho Kwon, and Jae Wook Jeon

School of Information and Communication Engineering, Sungkyunkwan University
Chunchun-Dong, Jangan-Gu, Suwon City, Korea 440-746
jwjeon@yurim.skku.ac.kr

Abstract. In order to help students to understand robotics concepts, various types of materials are needed, in addition to real robots. It is difficult for all students to perform actual experiments because of the lack of real robots. In order to solve these problems, this paper describes the development of a web-based distance learning system for robotics, which consists of multimedia contents and a 3D (3-dimensional) robot simulator. Students can easily access the multimedia contents and, in this way, understand the concept of robotics. Also, they can use a 3D robot simulator to perform virtual experiments using a virtual robot which can be connected to a real robot.

Keywords: robot, learning, learning system, 3D robot simulator, simulator.

1 Introduction

Many theoretical concepts are described in a robotics course, and in order to understand them easily, various types of materials and many experiments are needed. However, the amount of robotics material available remains insufficient and not enough real robots are available to allow for every student to perform robot experiments, due to a lack of resources. Therefore various types of materials need to be developed, in order to make it easier to understand robotics. Also, virtual robot experiments need to be made available, which are similar to experiments with real robots. Thus, a web-based distance learning system that can enable students to conveniently access these materials and perform virtual experiments needs to be developed.

In general, existing distance learning systems only provide learning materials using NRT (Non-Realtime Teleteaching), BBS (Bulletin Board System) or VOD (Video On Demand) techniques. This means that the students can study what they need to using the received material, but cannot perform experiments. If the distance learning system allowed them to perform real or virtual experiments that were similar to the real ones, it would be much easier to understand the learning materials. In order to accomplish this, a 3D (3-dimensional) robot simulator needs to be developed that is connected to a real robot.

Existing graphic robot simulators have been developed to make simulation programs for robots, to check manufacturing system software in advance, and to control remote systems efficiently. In previous studies, in order to make a robot program, virtual robots were developed using the VR (virtual reality) technique [1, 2]. In order to check manufacturing software, a virtual simulator was developed [3]. In a remote

control system, the VR technique is used to predict the result of a robot command before sending it to the remote robot. In a previous study, remote robot tasks were performed using a task sequence script that was used to control the sequences of robot behavior [4]. A virtual robot and its environment were designed using the VR technique and this virtual robot was used instead of a remote real robot to send the information, in order to reduce the time delay [5, 6].

A remote robot system using the internet appeared in Goldberg's Mercury project and Taylor's Australia's Telerobot project [7, 8]. Since previous remote robots were controlled through a dedicated line, it was only possible to control them within a fixed area. In these two projects, however, multiple users were able to control the robots through the internet without any limit as to their location. Research into the sharing of robotic devices through the internet has also been performed in various universities and research institutes [9, 10]. A remote robot controlled through the internet is called an internet robot or internet-based robot. If a web browser is used as the user interface, the internet robot is referred to as a web robot or web-based robot.

In this study, we prepared multimedia contents for robotics materials and developed a 3D robot simulator for the purpose of building a web-based distance learning system for robotics. The multimedia contents and 3D robot simulator can be accessed through a web browser. The proposed web-based distance learning system can be used to access the robotics multimedia contents and to perform virtual robot experiments having similar effects to real robot experiments without any limit of time and location. Also, the 3D robot simulator can be connected to a real robot through the internet, thereby allowing the virtual robot experiments to be compared with the real robot experiments.

In sections 2 and 3, the structure of the proposed web-based distance learning system for robotics and its contents are explained. In section 4, various experiments are performed, including the connection of a real robot. Finally, the conclusion is presented in section 5.

2   Structure of the Proposed Web-Based Distance Learning System for Robotics

The proposed web-based distance learning system for robotics consists of lecture materials, complementary materials, and a 3D robot simulator, as shown in Fig. 1. Both the lecture and complementary materials are organized in the form of multimedia contents that can be inserted in a webpage. A multimedia tool, Authorware of Macromedia, is used to develop these multimedia contents. The web-based 3D robot simulator was developed using Java Applets to allow for its insertion into a web browser and a Java3D API is used to provide the 3D effect. Because all of the materials and the robot simulator are viewed in a webpage, students can conveniently connect to the web site through a browser to peruse the contents and to use the robot simulator.

The web-based 3D robot simulator used as a training tool is designed to allow several students to access it through the internet in the form of a client/server application. A student can connect to the web server as a client and download the executable

interface through a web browser. The user interface is a Java Applet application program that can show 3D robot motions and control real robots using the motion results. As shown in Fig. 2, a real robot can be controlled by transmitting robot commands to the robot control server. That is, the robot server receives robot commands from a student and drives the real robot. Fig. 2 shows the internet based remote control system using the web-based 3D robot simulator.

The remote system consists of a web-server, a camera server, a robot control server, and a robot. Using a mouse and keyboard, a student can perform virtual robot experiments and remotely control a real robot. Before sending commands to the real robot, the student can check the robot motions by performing virtual robot experiments using the simulator. When the real robot moves after receiving commands from one student, the camera server obtains images of its motion and sends them to the other students. The virtual robot in the simulator was developed using the 3D graphic API Java3D and the real robot is a FARA SM3 of Samsung electronics.
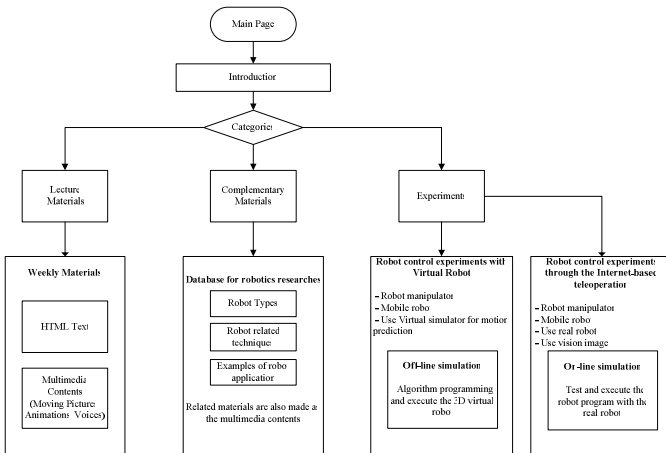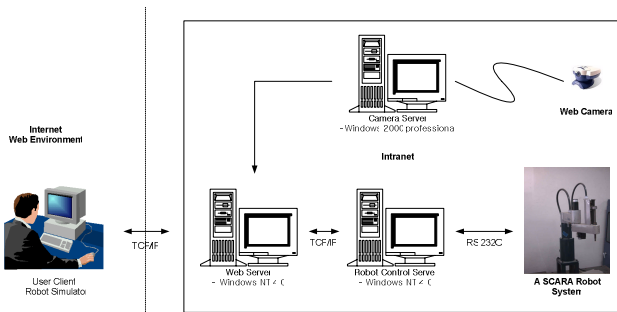

Fig. 1. Web-based distance learning system

Fig. 2. Web-based distance learning system

3   A Web-Based Distance Learning System for Robotics

3.1   Lecture Material

The robot lecture materials in the distance learning system for robotics consist of multimedia contents that comprise a moving picture, animation, and synthesized voice. These multimedia contents are inserted in the webpage so that students can peruse the lecture materials through a web browser. The sixteen week lecture materials include robot related vector theory, robot kinematics, and robot dynamics [11].

Fig. 3 shows a screen capture of the 'Introduction to Robotics' section, that makes up the first week lecture materials. Each page of the lecture materials contains text, clip art, video, or multimedia material such as animations and synthesized voices that are used to explain the lecture. In order to download the lecture materials from the web server, the web page indicates the necessary metadata and it is organized so as to download data by using the streaming service of the web server and to execute some of lecture materials.

It is difficult to express robotics theory efficiently using only algebraic expressions and text data. Thus, the IGRIP (Interactive Graphical Robot Instruction Program) software package is used to make the lecture materials, which consist of 3D animations that help the students to easily understand robotics theory. IGRIP can show robot motions based on 3D graphic animation using robot kinematics, robot dynamics, and many robot parameters. For example, to explain the structure and motion of a Cartesian robot, IGRIP can show each axis motion and task space of a Cartesian robot in the form of a 3D animation.

3.2   Web-Based 3D Robot Simulator

In this study, a 3D robot simulator is developed using the 3D graphic API, Java3D, and it is shown in Fig. 4. This 3D robot simulator allows students who have studied web-based robot lecture materials to perform virtual tasks by using a virtual robot. Also, this 3D robot simulator can be used as a user interface for controlling a remote robot. Since the 3D robot simulator is web-based, it can be used anywhere.

Since a function allowing for the visualization of the image from a remote camera is included in this simulator, it is possible to watch the motion of a remote robot.
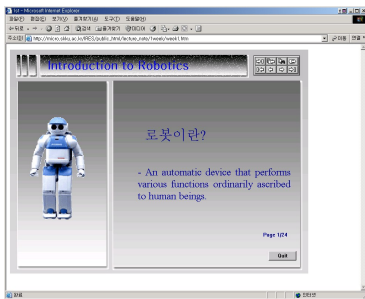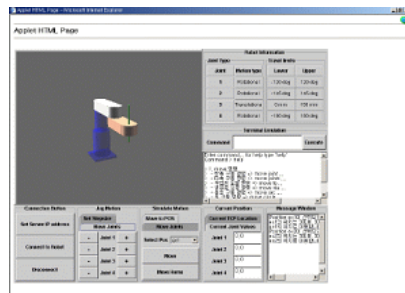

Fig. 3. Lecture material on the web page

Fig. 4. Web-based 3D robot simulator

Also, the students can easily watch the virtual environment, since the simulator allows its view to be rotated, translated, expanded, and contracted.

The simulator includes a user interface for robot simulation, a robot information display, and a connection to a real robot, as shown in Fig. 4. The students can access all of the functions that are provided using a mouse or send commands to the virtual robot using text input.

4 Experiment

Students can study robotics related lecture materials and perform real experiments using the system developed in this paper. In the experiments we performed using the web-based 3D robot simulator, an offline simulation is performed first. Then, the 3D robot simulator is linked to a real remote robot in order to remotely control it.

Students can understand robotics concepts, such as dynamics and kinematics, by performing offline simulations using a virtual robot. Fig. 5 shows an offline simulation in the web-browser, in which a robot moves an object along a straight line.

The simulator provides three modes which allow the robot to be moved and shows the resultant robot motion: jog mode, simulation mode, and virtual terminal mode. Fig. 6 shows the panels used to control the robot in these three modes. In the jog
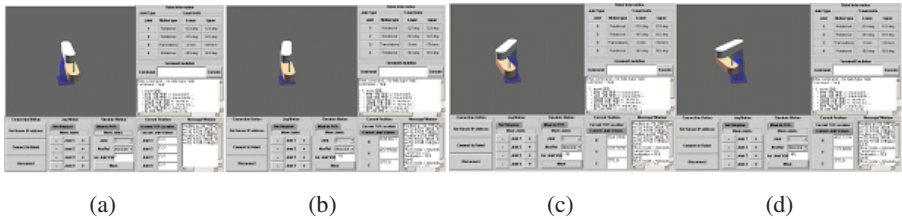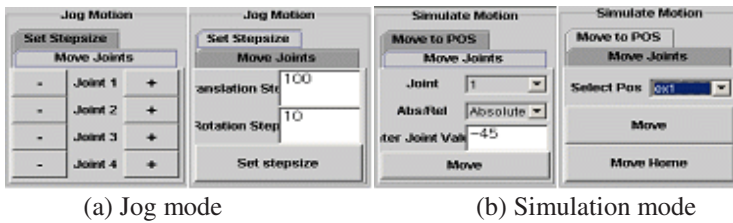

(a)   (b)   (c)   (d)

Fig. 5. An offline simulation

(a) Jog mode   (b) Simulation mode

(c) Virtual terminal mode

Fig. 6. Robot control panel

mode, it is possible to make one joint of the robot move without moving the other joints. As shown in Fig. 6-(a), the displacement amount of one joint can be adjusted by varying the stepsize, in order to perform more precise tasks. In the simulation mode shown in Fig. 6-(b), students can enter a displacement value, either for one joint or for the robot end-effector, and make the robot move to the designated position. In virtual terminal mode, as shown in Fig.6-(c), students can move the virtual robot by using robot commands. Some explanations in Korean are included in this figure.

As shown in Fig. 7, the execution results obtained using the simulator can be checked with the present position of the robot and the messages provided by the simulator. As shown in Fig. 8, the displacement range of each joint is displayed, in order to prevent input errors related to the joint displacement.

Students can use the graphic functions of the simulator to execute the virtual robot and check its action. In this way, the students can understand the commands and parameters of the robot. In order to control a remote real robot using the simulator, robot commands must be sent through the internet. Fig. 5 shows the motion of a virtual robot when it executes the commands: Move joints -10 10 0 0, Move joints -30 45 0 0, and Move joints -45 70 0 0. The operation codes and necessary parameters for these robot commands are converted into network messages which are sent through the internet. The robot control server shown in Fig. 2 receives these network messages and translates them into a form which is understandable by the controller of the real robot, in order to control it.

After observing the motion of a virtual robot in the offline simulation, an online simulation can be performed to check the motion of the corresponding real robot. In the online simulation, the virtual robot shows the same motion as that observed in the offline simulation and the virtual robot communicates with the corresponding real robot.

During the online simulation, the virtual robot and its corresponding real robot show synchronized motions. Since this synchronization is performed using robot commands and their motion result, continuous communication is not required between the virtual robot and the corresponding real robot.

During the online simulation shown in Fig. 9, the real robot shows the same motion as that shown by the virtual robot during the offline simulation illustrated in Fig. 5. A camera is used to obtain the images, as shown in Fig. 9, and these images can be watched on the web. Thus, many students can see the motion of the real robot without connecting to the additional vision server.

Fig. 7. Robot position information and simulator message

Fig. 8. Robot information display

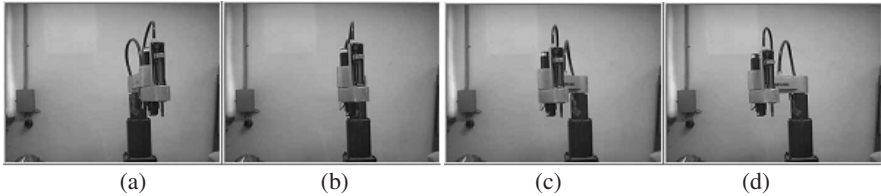(a)   (b)   (c)   (d)

Fig. 9. Online Simulation

5   Conclusion

In this study, we developed robot lecture materials and a web based 3D robot simula-
tor system. Students can study the robot lecture materials through the internet and
perform experiments related to them using a virtual robot. Since the web-based 3D
robot simulator can be connected to a real robot through the internet, the programs of
the virtual robot can be sent to the real robot in order to execute them, so that the
students can compare the motion results of the virtual robot with those of the corre-
sponding real robot.

In contrast to previous robot simulators, the robot simulator developed in this study
consists of Java Applet software modules that are executable in a web browser and,
therefore, it can be used as a web-based user interface for remote control.

Acknowledgement

References

1. W. Strommer, J. Neugebauer, and T. Flaig, : Transputer-based virtual reality workstation
   as implemented for the example of industrial robot control. Proceedings of Interface Real
   Virtual World Conference Montpellier, France, March (1993) 137-146
2. T. Flaig, K. Grefen, and D. Neuber, : Interactive graphical planning and design of spacious
   logistic environments. Proceedings of Conference in FIVE Working Group, Scuola Supe-
   riore S. Anna, Italy, (1996) 10-17

3. Ju-Yeon Jo, Yoohwan Kim, Andy Podgurski, and Wyatt S. Newman, : Virtual Testing of Agile Manufacturing Software Using 3D Graphical Simulation. Proceedings of the 1997 IEEE International Conference on Robotics and Automation, April (1997) 1223-1228

4. T. T Blackmon and L. W Stark, : Model-based supervisory control in telerobotics. Presence: Journal of Teleoperators and Virtual Environments, vol. 5, no. 2, (1996) 205-223

5. F. Arai, M. Tanimoto, T. Fukuda, K. Shimojima, H. Matsura, and M. Negoro, : Multimedia Tele-surgery Using High Speed Optical Fiber Network and Its Application to Intravascular Neurosurgery - System Configuration and Computer Networked Robotic Implementation. Proceedings of the 1996 IEEE International Conference on Robotics and Automation, (1996) 878-883

6. R. Oboe, P. Fiorini, : A Design and Control Environment for Internet-based Telerobotics. Journal of Robotics Research, vol. 17, no. 4, (1998) 433-449

7. Ken Goldberg, Michael Marscha, Steve Gentner, Nick Rothenberg, Carl Sutter, and Jeff Wiegley, : Desktop Teleoperation via the World Wide Web. Proceedings of the 1995 IEEE International Conference on Robotics and Automation. (1995) 654-659

8. K. Taylor and J. Trevelyan, : Australia's telerobot on the web. 26th International Symposium on Industrial Robotics. Singapore, (1987) 39-44

9. Song You, Tianmiao Wang, Roy Eagleson, Cai Meng, Qixian Zhang, : A low-cost internet-based telerobotic system for access to remote laboratories. Artificial Intelligence in Engineering, (2001) 265-279

10. A. Bicchi, A. Coppelli, F. Quarto, L. Rizzo, F. Turchi, A. Balestrino, : Breaking the Lab's Walls Tele-Laboratories at the University of Pisa," Proceedings of the 2001 IEEE International Conference on Robotics & Automation. Seoul Korea, May (2001) 1903-1908,

11. K. S. Fu, R. C. Gonzalez, and C. S. G. Lee, ROBOTICS: Control, Sensing, Vision, and Intelligence, McGraw-Hill Book Co., Singapore, (1987)

Personalized Recommendation Service System in E-Learning Using Web Intelligence

Xinye Li[1], Qi Luo[2,3], and Jinsha Yuan[1]

[1] Department of Electronic and Communication Engineering, North China Electric
Power University, Baoding 071003, China
[2] Information Engineering school,
Wuhan University of Science and Technology and Zhongnan Branch,
Wuhan 430223, China
[3] College of Engineering and Technology, Southwest University,
Chongqing 400715, China
`yljh654@sina.com, ccnu_luo2008@yahoo.com.cn`

Abstract. Personalized education is a very hot topic in distant research. To realize personalized E-learning, a personalized recommendation service system was proposed and realized. Web technologies of personality and adaptive filtering were applied in the system. The structure of system, workflow and key technologies of realizing feature selection module, user interest module, personalized teaching resources filtering module were introduced in the paper.

Keywords: E-Learning, Data Mining, Web Intelligence, Personality.

1 Introduction

Nowadays, personalized education is a very hot topic in E-learning research. The importance of E-Learning has been transferred from how to solve the limitation of space-time problem in traditional teaching to build up the personalized learning environment, and offer a kind of personalized service based on modern pedagogy and psychology theories[1]. The learners are different in age level, sex, and social role, their culture, education background, attention, interest hobby are also exist a great difference. Giving corresponding learning contents and tactics to realize teaching according to learners' needs is very difficult [2]. The investigation indicates that personalized service system for E-Learning is imperfect. The validity and accuracy of providing information are low, which makes learners feel unconfident and suspicious in E-learning. If E-learning wants to attract more learners, the idea of personalized design should be needed. It means that the personalized knowledge and information service should be provided according to learners' needs. The key of personalized design is how to recommend teaching resources based on their interests by using web intelligence technology.

Web intelligence has been recognized as a new direction for scientific research and development to explore the fundamental roles as well as practical impacts of artificial intelligence and advanced information technology on the next generation of

web-empowered products, systems, services, and activities. It is one of the most important as well as promising IT research fields in the era of web and agent intelligence [3].

Basing on it, web technologies of personality and adaptive filtering are applied in the paper [4], while the model of personalized E-learning recommendation service system (PERSS) is proposed.

2   System Structure

Personalized E-learning recommendation service system (PERSS) is showed in Fig.1
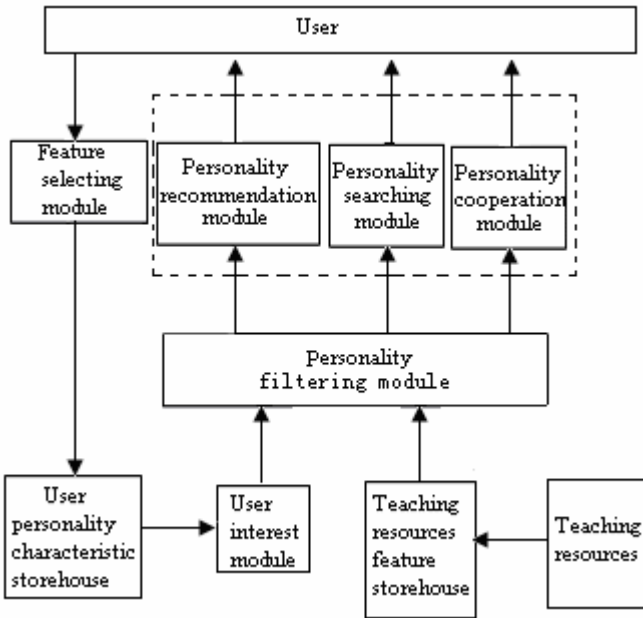

Fig. 1. Personalized recommendation service system

The main function of PERSS is to help users to find out teaching resources quickly and accurately according to their interests.

Feature selecting module selects users' interested teaching resources information according to browsing and feedback of teaching resources. Then, the information is stored in user personality characteristics storehouse that is tracked and updated promptly.

User personality characteristics storehouse saves user personality information such as name, age, occupation, purchasing interest, hobby and so on. It tracks users' interests dynamically. The key words of user personality characteristics are selected and recorded; it can also provide user characteristics for constructing the module of user interest model.

The module of user interest model selects key words from user personality characteristics storehouse and constructs user interest model.

The filtering module of personality teaching resources filters teaching resource according to user model.

Personality recommendation module realizes automatic recommendation and request recommendation. Request recommendation is realized by calling the management module of teaching resources and the filtering module of teaching resources.

Personality searching module accepts user requests. Personality searching result is obtained through filtering module.

Personality cooperation module makes user get help immediately and accurately when they have problems of learning.

The work process of model is as follows: firstly, user interest feature information of teaching resources is selected by feature selecting module. The information is saved in user personality characteristics storehouse. Personality characteristics storehouse is tracked and updated promptly. Then, user interest model is constructed by user personality characteristics information. Furthermore, teaching resources are filtered by filtering module of personality teaching resources according to user model. Finally, personality searching service, personality recommendation service and personality cooperation service are realized by the module of personality searching, personality recommendation and personality cooperation, which according to the filtering results.

3   Key Technologies

3.1   User Interest Model

The process of establishing user interest model is the process of knowledge acquisition. There are two ways of knowledge acquisition such as user obvious feedback and user hiding feedback [5].

In order to fully utilize the advantages of the two ways, user interest initial model is established according to user register information and user interest model is updated according to web server log. A web server log records user's IP address, visiting time, visiting page, visiting way, requested the document URL ,HTTP version, return codes, transmission byte, protocol, wrong codes and so on.

3.1.1   Establishing User Interest Model
User initial interest model is established according to user register information. User register information is submitted to the system server though Web inputting. When user register, the Web may let the user reply some questions such as research orientation, interests and so on. Different people' answers are formed different personalized vectors which express user interests.

Supposed user interest model vector is Q_i, the number of interest feature item is n, and the interest number is m, then user initial interest model U may be represented as a vector matrix $U = (Q_1, Q_2, \cdots Q_m)$, interest vectors $Q_i = (q_{i1}, q_{i2}, \cdots q_{in})$.

3.1.2 Updating User Interest Model

Because user interest is variable, user interest model is updated through observing user's behavior in web server log. When website has been visited one time, log database increases corresponding records; these records are arranged from visiting time. Mining these log documents may discover what the user has browsed and how long the user has browsed the page.

Generally speaking, the user may visit interesting pages, if the user browses the page repeatedly, then it shows that user is interested in this page. Therefore, mining this page could find out user interests and interest degree. $Q_1, Q_2, \cdots Q_m$ represent all interest vectors in user interest model, supposed vectors $X_1, X_2 \cdots X_d$ represent all content pages that user has visited. If page X_j approaches to user interest Q_i namely, $Q_i X_j / |X_j|$ is bigger than the thresholds a, then page X_j vector is add to the user interest Q_i

$$Q_i = Q_i + \frac{m^2 X_j XJ(j)T(j)}{\sum_{k=1}^{m} XJ(k) \sum_{k=1}^{m} T(k)} \tag{1}$$

$XJ(j)$ represents the frequency of visiting the page, $T(j)$ represents the time of visiting the page, $j = 1, 2, \cdots m$.

If page X_j does not approach to user's any interest Q_i, then X_j is regarded as user new interest. But the category of user interest increases massively, then we must establish the thresholds b, if the mold of user interest vector is smaller than b, pushing correlative pages don't consider this interest.

Page browsing also is random and regular. If user is interested in the page, then the user will consume more time when browsing it, simultaneously also visit this page repeatedly. The following formula 2 is used to calculate user interest degree.

$$F = (\frac{n}{N} + \frac{t}{T})\frac{k}{K} \tag{2}$$

Where F is interest degree of visiting the node, n is the number of times in visiting the node, N is the total number of times in this visit, t is the consuming time in visiting the node, T is the total time in visiting website, k is number of node in this visit, K is the total number of node in visiting website.

3.2 Filtering Module for Teaching Resources

Adaptive filtering algorithm for teaching resources based on vector space model is composed of three steps such as training, adaptive filtering and modifying thresholds adaptively.

Step1: training phase. According to assigned training texts, initial filtering profiles and thresholds are generated [6].

Step2: adaptive filtering phase. For each text in teaching resources, we judge whether it is related with initial filtering profiles or not.

Step3: modifying thresholds adaptively. Users' feedback is utilized to modify the profiles and thresholds adaptively.

3.2.1 Training

Fig.2 is the flow of training algorithm. Firstly, topics are converted to vector forms. Then feature vectors are separately obtained from user interest model, positive samples and pseudo positive samples. So, initial profiles vectors are composed of positive samples vectors, pseudo positive samples vectors, user interest vectors and topic vectors. Then the similarity between initial profiles vectors and all training samples is computed, so we can obtain the best initial thresholds.
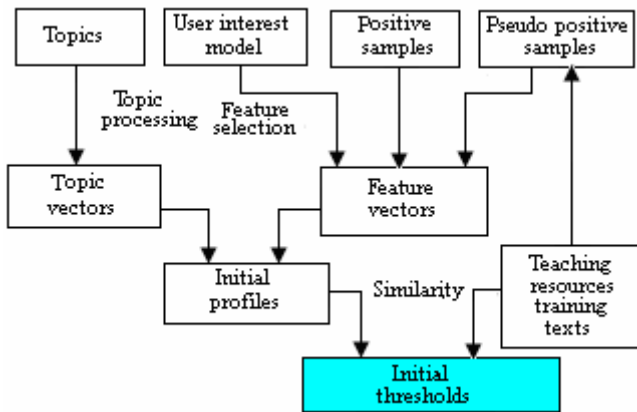

Fig. 2. The flow of training algorithm

3.2.2 Adaptive Filtering

After Initial filtering profiles are set up and initial thresholds are selected, the process of filtering is to modify filtering profiles and thresholds adaptively. It is just the process of machine learning that improves filtering performance. Fig.3 is the flow of adaptive filtering algorithm. For each text in the teaching resources, the similarity between it and profiles vectors is computed. If the similarity is bigger than the thresholds, then it is regarded as the related texts. Whether the texts are really related to the topics or not is judged by users. Profiles and thresholds are modified according to user' results.

3.2.3 Modifying Thresholds Adaptively

The proportion of related texts in teaching resources is very low, so it is necessary to modify thresholds adaptively. The goal of elevating thresholds is to filter less positive samples and increase precision. The goal of lowering thresholds is to filter more positive samples. Probability density distribution is proposed in the paper. If probability density distribution of positive samples currently surpasses the expectation of distribution scope, then the thresholds would be elevated. Otherwise, thresholds would be lowed.
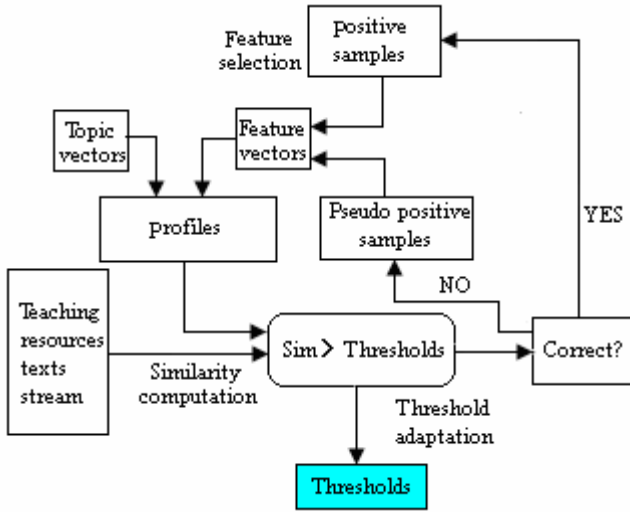
Fig. 3. The flow of training algorithm

Definition 1. n is the serial number of filtering texts in teaching resources. D is the expectation of positive samples distribution density.

Definition 2. S (n) is the number of total documents which the documents' serial number is up to n.

Definition 3. SR (n) is positive samples which the documents' serial number is up to n

Definition 4. O (n) is thresholds which the documents' serial number is up to n.

Definition 5. DR (n_t, n_{t+1}) is probability density distributing of previous thresholds.

$$DR(n_t, n_{t+1}) = \frac{SR(t+1) - SR(t)}{S(t+1) - S(t)} \tag{3}$$

Thresholds adjusting algorithm is as follows:

(1) If $DR(n_t, n_{t+1}) > \max(D, 0.3)$ and $SR(n) < 0.3\ S(n)$, then $O(n+1) = O(n)*1.3$. If precision is lower excessively and the number of filtering texts is not too few, then thresholds are elevated rapidly.

(2) If $DR(n_t, n_{t+1}) > D$, then $O(n+1) = O(n)*1.2$. If the number of filtering texts is more than what we need, then thresholds are elevated.

(3) If $DR(n_t, n_{t+1}) < D$, then $O(n+1) = O(n)*0.8$. If the number of filtering texts is less than what we need, then thresholds are lowered.

4 Conclusion

Based on the above research, the author constructs a system website recommending personalized courses service .In order to obtain the contrast experimental results,
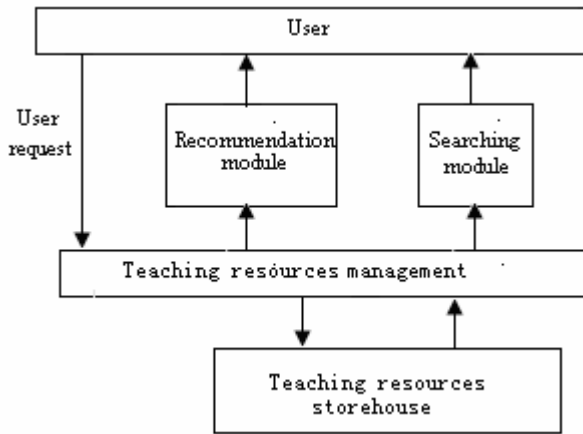
Fig. 4. Contrast system

feature selection module, user interest module, personalized teaching resources filtering module are removed from PERSS, and the contrast system is formed. The contrast system is Fig.4.

Evaluation metrics as follows [7]:

$$\Pr ecision = \frac{number\ of\ \inf ormation\ correctly\ filtered}{number\ of\ \inf ormation\ filtered} \tag{4}$$

$$\mathrm{Re}\, call = \frac{number\ of\ \inf ormation\ correctly\ filtered}{number\ of\ \inf ormation} \tag{5}$$

$$F_{\beta} = \frac{(\beta^2 + 1) \times Precision \times \mathrm{Re}\, call}{Precision + \mathrm{Re}\, call} \tag{6}$$

There are 150 people register in this system. 150 personality characteristics storehouse are established. The interest group is 41; there are 341 texts in teaching resources.12 texts that have the biggest correlation in teaching resources are provided to the corresponding user. Through the experiment, table 1 shows the results:

Table 1. The experiment results

System	Avg.Precision	Avg.Recall	F_{β}
PERSS	0.34	0.23	0.28
Contrast System	0.13	0.11	0.12

From the table1, we discover that the filtering average precision of PERSS is higher than the contrast system.

In summary, the model of personalized E-learning recommendation service system using web intelligence is proposed and realized in the paper. Web intelligence of adaptive filtering algorithm is also used in personalized E-learning recommendation service system.

References

1. Luo Q.: Research on Application of Association Rule Mining Algorithm in Learning Community. Proceedings of CAAI-11, Wuhan, 2005, 1458-1462.
2. Yanwen W. and Zhonghong W..:Knowledge Adaptive Presentation Strategy in E-Learning. Proceedings of Second International Conference on Knowledge Economy and Development of Science and Technology, Beijing, 2004, pp.6-9.
3. Feng Shicong.: Research of personalization technologies based on web mining.Computer Engineering and Design.No.1, 2004.
4. Yu Li, Liu Lu.:Comparison and Analysis on E-Commence Recommendation Method in china. System Engineering Theory and Application, 2004(8), 96-98.
5. Nie Xin.:Take about the Digital Individualized Information Service of Library. Information Science Journal, vol.23, 2005, 1-5.
6. Robertson S, Hull DA.:The TREC-9 filtering track final report. Proceedings of the 9th Text Retrieval Conference. Gaithersburg, 2001, 25-40.
7. Hu Tian, Xia Yingju and Huang Xuanjing. : A Web-based Chinese Information Filtering System Base on VSM. Computer engineering, Beijing, vol.29, 2003, 25-27.

Mobile Peer-to-Peer Technology Used in Mobile Education Field

Liang Ye and Ci Lin-lin

School of Computer Science and Engineering, Beijing Institute of Technology, Beijing
100081, China
Liang_ye@sohu.com,cilinlin@263.net

Abstract. Mobile Education is a new way of using wireless and mobile
technologies for education, and it usually applies to nature-based field
study. However, the fee of use is so high that few people could accept this
new learning method. But we take note of that the message, required by
users coming from the same group with wireless communication equip-
ments, usually focuses on a certain area. So, we could use the mobile
peer-to-peer (MP2P) technology to resolve this confliction. MP2P net-
work can let messages be transferred in the group instead of in the whole
communication system, and this could save the messages in the group
and meet the need of other users through storage and transmitting. So
the users could cut down the fee of using mobile education system.

Keywords: Mobile P2P, Mobile Education, Wireless Communication.

1   Introduction

Mobile Education, or M-Education, is a new way of using wireless and mobile
technologies for education by extending access to a desktop-based online virtual
environment called MOOsburg [1] to handheld devices used as part of a mobile
collaborative community. That means, we can get knowledge all over the time,
and be not limited by where we are. In mobile education field, the handheld
mobile devices, i.e. mobile phone, could help us to get information. At the same
time, numerous schools begin to build resource servers and provide education re-
sources for their students, especially the resources which may be used in the field
study. When the students take part in a nature-based field study, for example,
the geology field course, they usually come to be perplexed by a lot of nature
phenomena. And they also want to share their discovery with their classmates,
so that they could collaborate with each other. In this case, they need use the
phones to download or upload the message with the fixed server in the school.

But we know that, the fee of using those mobile equipments is very high, so
we couldn't use them for all things we want, and this may affect the effect of this
geology field course. In order to reduce the fee for communication, the mobile
peer-to-peer (MP2P) technology is proposed. Using MP2P technique, we can
reduce the rate of communication. That is, the fee for communication is low,
and we can use mobile devices for study on a larger scale.

This paper is organized as follows. In Section 2, we briefly summarize related work. In Section 3 we present the technique of organizing a MP2P network. Comparing results and conclusions are reported in Section 4.

2   Related Work

Numerous efforts are being made in the direction of using handheld mobile devices for the purposes of sharing educational resource. Some technologies simply store the shared educational resources in the database server, and distribute these resources through browser / server (B/S) mode or client / server (C/S) mode to users' handheld devices. Other technologies plan to realize the function of sharing resources by means of the third generation mobile phone. By examining a few related applications and concepts, we shall see how MP2P makes mobile education technologies using wireless and mobile devices one step further.

Now, most people get information using the traditional network technique, which base on B/S or C/S network mode. But there are two disadvantages to this technique: On the one hand, the bandwidth of wireless link is a major performance bottleneck. The more users want to get the similar resource from server at the same time, the more response time is needed for each user. On the other hand, wireless communication is very expensive, and the burden of fee would fell to the users after they use this kind of application for a long time.

There are some technologies designed for the third general mobile phone. These technologies mainly concentrate on how to use P2P technique in the mobile communication field. But yet, P2P technique can't be used on the mobile phone of 2.5G networks generation, in which an IP address, unlike the third generation mobile phone, can't be distributed for each, the research on P2P for mobile phone only has theoretic value.

In the interest of the users, we propose a new technique, MP2P technique, for mobile education. Through the MP2P technique, we can get the education resource we need with shorter response time and lower fee via our mobile phone.

3   Organizing a MP2P Network

In mobile environment, handheld mobile devices are always moving; signal might break off frequently; the bandwidth of wireless link is narrow[2]. As a result, we need to design a new network organizing technique to suit for it. It consists of group management technique, resource management technique, and pipe technique.

3.1   Group Management Technique

Group management technique includes creating, entering, and exiting group.

At first, all the handheld mobile devices use Bluetooth module or Ad hoc module to connect with each other and buildup a local MP2P network, and all

of them makeup a basic group. When a task, for instance, downloading a map all about them, is brought forward in the basic group, a device which could do it immediately is selected to buildup a new sub-group by the mobile agent running in the MP2P network, and this device is called leader of the new group.

After the leader device builds up a new group, the devices which maybe use the same resource join into the group one by one. But how to decide whether a device needs to enter the group? In order to explain the regulation in detail, we put forward some definitions.

Definition 1 Relativity: Suppose there are two devices named N_A and N_B respectively, the aggregate of attributes for N_A is $A_{attribute}$, and for N_B is $B_{attribute}$, the correlation coefficient could be expressed by R_{AB} , then $R_{AB} = (A_{attribute} \cap B_{attribute})/(A^{attribute} \cup B_{attribute})$. According to the definition, $R_{AB} \in [0, 1]$, if the value of R_{AB} is high, the attributes of N_A and N_B are similar.

Definition 2 Threshold: When a device wants to join into a group, it need calculate the correlative degree with the devices in the group. If all values are higher than a certain value, it will be allowed to enter the group, and this certain value is called Threshold(T). So, if the leader device N_A creates a new group G, and all the devices in the group G are denoted as N_G, that is $N_G \geqslant 1$. When a new device N_B want to enter the group, if $N_G > 1$, and $|N_C|R_{BC} \geq T, N_C \in N_G| \geq 2$, or $|N_G| = 1$, and $R_{AB} \geq T$, the new device could enter this group.

If a device doesn't need the sharing resource again, and it wants to get a new kind of resource from another group, it could apply to exit current group. If the leader device needs to exit the group, the mobile agent of managing group must select a new leader for the group.

3.2   Resource Management Technique

After creating a group, the mobile agent needs to control the distribution of resource. To describe the resource management technique better, we put forward some definitions and theorems.

Definition 3 Atomic resource message: It is also called atomic message (AM) for short. It is the minimum block of message which could be cut into, but still could be used in the future. Only AM could be allowed to transfer in the group at MP2P network. We use the mark R^* to denote it.

Definition 4 Combinative resource message: It is also called combinative message (CM) for short. It makes up of a serial of AM. The method of combination concludes combination on different dimension, combination on the same dimension, and both of above. We use the mark R to denote it. Then R=nR^*($n \geq 2$).

Definition 5 Resource binary tree (RBT): It is used to record a certain resource of group. In binary tree, the node represents the handheld mobile device, and the branch represents the two devices with a direct communication link. The leaf of tree represents the AM of group at a certain device.

In RBT, there is a branch between two nodes. This represents they could share resource with greater efficiency and speed, and the nodes connected by left branch are better than the nodes connected by right branch. According to

the definition, only the AM could be represented by RBT, but we usually need CM as we work. So we must ensure that they could transform into each other.

Theorem 1: In MP2P network, CM could be combined by AM.

Proof. Let A, B, C, D are AMs, A, B at the same dimension, C, D at the different dimension, and A, B could not be combined with C, D, Then $R_{AB} = R_A^* + R_B^*$, $R_{CD} = R_C^* \cup R_D^*$. So, $R_{ABCD} = R_{AB} + R_{CD} = (R_A^* + R_B^*) + (R_C^* \cup R_D^*)$ That is the AMs could transform into a CM.

Theorem 2: In MP2P network, AM could be transformed by CM and AMs.

Proof. Let A, B, C, D are AMs, R_{ABCD} is a CM, which is combined by A, B, C, D. With theorem 1, we know:$R_{ABCD} = (R_A^* + R_B^*) + (R_C^* \cup R_D^*)$. If we want to get A or B, Then, $R_A^* = R_{ABCD} - R_B^* - (R_C^* \cup R_D^*)$ or $R_B^* = R_{ABCD} - R_A^* - (R_C^* \cup R_D^*)$. We obtain that A or B could be transformed. If we want to get C or D, Then, $(R_C^* \cup R_D^*) = R_{ABCD} - R_A^* - R_B^*$. That is $R_C^* = (R_{ABCD} - R_A^* - R_B^*)/R_D^*$ or $R_D^* = (R_{ABCD} - R_A^* - R_B^*)/R_C^*$. We obtain that C or D could be transformed. So, AM could be transformed by a CM and the other AMs.

Using the RBT, according to theorem 1 and 2, we can buildup a route from the user to the resource or part of the resource meeting the request.

3.3　Pipe Technique

Definition 6 Pipe technique: In MP2P network, pipe technique is that a device could get a resource from another group directly.

In MP2P network, pipe technique is a core technique of mobile education field, and we will introduce it in next paper in detail.

4　Conclusions

In geology field course, the resources only are saved on the server, so anything must be got from it. In MP2P network, we suppose the server is a number of the group, and call it A0. A1, A2, A3, A4 all could get the resources from A0 through the index of RBT if they need. So, no matter which method is used to get the map, the fee is equal. However, after anyone of them gets the map from A0, the others don't need get the map from A0, and they could get it via the MP2P network, so the fee for communication is descended.

With MP2P, any group that requires a collaborative channel for achieving an educational goal could be brought to success with less time and money. So, the MP2P technique has a broad prospect at M-Education field.

References

1. Carroll, J.M. Rosson, M.B. Isenhour P.L. : Designing Our Town: MOOsburg, International Journal of Human-Computer Studies, Vol.54, No.5, pp. 725-751.
2. Liang, Y. Ci, L. Su, F. : Dynamic Location Service Based on Measurement of Moving Regularity in Mobile Computing Environment[C]. 6th International Symposium on Test and MeasurementVol. 8, Jul. 2005: pp.7987-7990.

A Model of Facial Expression for 3D Avatar

Zhen Liu

Faculty of Information Science and Technology, Ningbo University,
315211, China
liuzhen@nbu.edu.cn

Abstract. Modeling 3D avatar is very useful in e-learning software, a believable 3D avatar can have complex facial expression, and how to construct complex facial expression is a very interesting topic. The concept of emotion vector is presented. Emotion state of a 3D avatar can be transformed to an emotion vector that is calculated by basic emotion vector. The concept of expression vector is established, expression can be transformed to expression vector that is calculated by basic expression vector. Emotion mapping is set up from emotion vector space to expression vector space. A preliminary experiment is carried on microcomputer.

Keywords: emotion, emotion vector, emotion synthesis.

1 Introduction

Modeling 3D avatar is very useful in e-learning software, a believable 3D avatar can have complex facial expression, and how to construct complex facial expression is a very interesting topic.

Parke first presented the research paper on facial animation [1], and there are many methods of facial animation in now days. The prior research mainly concentrated on driving some local movements of face effectively, and little on whole movement of face. For example, the physical model is an effective method of controlling muscle's movement on face, the relation between muscle movement and facial expression's semantic information is not clear. Some methods emphasized on synthesis of facial expression by local movement, Ekman first proposed the famous FACS system that can describe facial expression by Action Units [1], but the method has many limitations for synthesis of complex expression. Noh et al. presented an ingenious technique to clone expression vector from one character to another, the purpose utilizes existing expression information, but it cannot create new expression [2]. However, the interpolation technique of facial expression can utilize whole information of the face effectively [3], it only produces little new expression and lacks the quantitative description of the emotion meaning.

A synthesis model of emotion is presented on basic emotion in this paper, the model attempts to set up a formal description of complex emotion according to each intensity of basic emotion.

2   A Computational Model of Emotion Synthesis

For a certain 3D avatar, $\boldsymbol{BE}$ is a basic emotion class set, $\boldsymbol{BE}=\{be_1, \ldots\ldots ,be_N\}$, $i\in$ [1, N], be_i is a basic emotion (such as happiness). N is the number of basic emotion class. $EI_i(t)$ is the intensity of be_i. $EI_i(t)\in$ [0, 1], t is time variable. $\boldsymbol{be}_i$ is the unit vector of be_i. For example, $\boldsymbol{be}_1=\{1,\ldots,0\}$, $\boldsymbol{be}_N=\{0,\ldots,1\}$. Let E is emotion state, $\boldsymbol{E}$ is represented emotion vector of E, the projection length of $\boldsymbol{E}$ on $\boldsymbol{be}_i$ is $EI_i(t)$. $\boldsymbol{E}$ can be represented as formula (1):

$$E = \sum_{i=1}^{N} EI_i(t)\, \boldsymbol{be}_i \, . \tag{1}$$

Let $\boldsymbol{E}_1$ and $\boldsymbol{E}_2$ are two emotion vectors, the synthesis of $\boldsymbol{E}_1$ and $\boldsymbol{E}_2$ is represented as $\boldsymbol{E}_1 + \boldsymbol{E}_2$. There is a formula (2).

$$E_1 + E_2 = \sum_{i=1}^{N} [EI_{i1}(t)\, \boldsymbol{be}_{i1} + EI_{i2}(t)\, \boldsymbol{be}_{i2}]. \tag{2}$$

Let $\boldsymbol{EP}$ is the set of all emotion vectors, if any element of $\boldsymbol{EP}$ satisfies to formula (1)(2), $\boldsymbol{EP}$ is called emotion vector space, $\boldsymbol{be}_i$ is called the basic emotion vector.

A face's geometry model is described by polygons, the location of any vertex can be represented as vector $\boldsymbol{v}_k$, $k \in$ [0, L], L is the number of all vertex. Let $\boldsymbol{V}$ is a vector for all vertex, $\boldsymbol{V}$ is called expression vector. $\boldsymbol{V}$ is represented as formula (3).

$$V =(\boldsymbol{v}_1 ,\ldots\ldots,\boldsymbol{v}_L) \, . \tag{3}$$

In general, there are some expression vector, pn is the number of expression vector, $\boldsymbol{V}_i$ is an expression vector, $i\in$ [0, pn], SY is an synthesis function among all $\boldsymbol{V}_i$, $\boldsymbol{FV}$ is calculated by formula (4):

$$FV \; = SY \; (\boldsymbol{V}_1,\ldots\ldots, \boldsymbol{V}_{pn}). \tag{4}$$

In general, $\boldsymbol{EP}$ is emotion vector space, $\boldsymbol{FV}$ is called expression vector space, T is a emotion function from $\boldsymbol{EP}$ to $\boldsymbol{FV}$, for any $\boldsymbol{E}\in \boldsymbol{EP}$, $T\,(\boldsymbol{E}) \in \boldsymbol{FV}$. Let $\boldsymbol{be}_i$ is a unit vector, $i\in$ [1, N], $T\,(\boldsymbol{be}_i)$ is called base expression vector. If $pn=$N, $\boldsymbol{FV}$ is calculated by formula (5):

$$FV \; = SY \; (T\,(\boldsymbol{be}_1)_1,\ldots\ldots, T\,(\boldsymbol{be}_N)). \tag{5}$$

In order to simplify the formula (5), let SY is linear function, λ_i is the corresponding interpolation function of V_i, the sum of all λ_i is equal to 1, let $\lambda_i= EI_i$, $\boldsymbol{FV}$ is calculated by formula (6):

$$FV \; = \sum_{i=1}^{N} (EI_i)\, T\,(\boldsymbol{be}_i). \tag{6}$$

3 A Demo of Complex Facial Expression

A demo of synthesis on expression by formula (6) is realized on pc, the programming tools are Visual c++ language and Direct3D API. In the demo, only six basic facial expressions are selected. Six basic facial expressions are shown in Fig.1, some of synthesis results are shown in Fig. 2. For example, in Fig. 2(1), "1/2 happiness+1/2 sadness" is represented the synthesis of happiness and sadness, each emotion intensify is equal to 1/2.
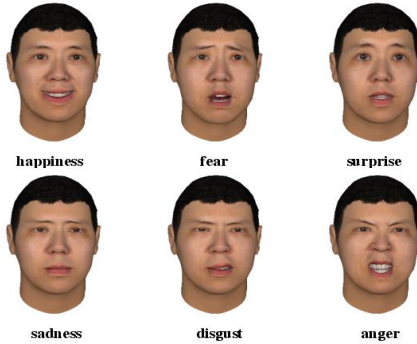

Fig. 1. Six basic facial expressions
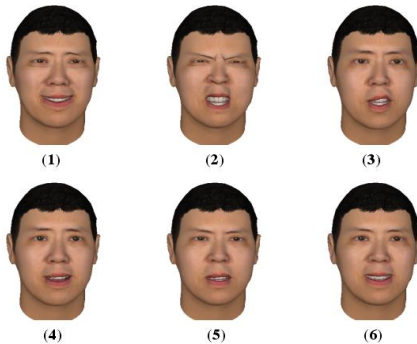
Fig. 2. (1)1/2happiness+1/2sadness;(2)1/2sadness+1/2anger;(3)1/2surprise+1/2disgust;(4)1/3happiness +1/3fear+1/3disgust;(5)1/3sadness+1/3disust+1/3anger;(6)1/3happiness+1/3sadness+1/ 3anger

4 Conclusion and Future Work

A model of facial expression for 3D avatar is presented in this paper. The paper improves the interpolation technique of facial expression. The concept of emotion vector space is introduced, and a basic emotion can be regarded as a unit vector in emotion vector space. The concept of expression vector space is also introduced, and an expression vector can describe a facial expression. An emotion function can transform a basic emotion to a base vector in expression vector space. In order to simplify an

emotion function, an expression vector can be described by linear combination of base vector. A preliminary experiment indicates that basic emotion can produce many new emotions.

Acknowledgements

References

1. Parke, F.I., Waters,K.: computer facial animation, Wellesley, Boston, USA: AK Perters (1996)
2. Noh, Jun-yong, and Ulrich Neumann. Expression Cloning, In Proceedings of ACM SIGGRAPH2001 Conference (2001) 277-288
3. Blanz, V., Vetter, T.: A Morphable Model for the Synthesis of 3D Faces, In Proceedings of ACM SIGGRAPH 99 Conference (1999) 187–194

Investigation on E-Learning Adoption Intention Among Chinese Undergraduates Via Innovation Adoption Theory

Zetian Fu, Xiaoshuan Zhang, Weisong Mu, Lingxian Zhang[*], and Yajie Gao

College of Information & Electrical Engineering, China Agricultural University, Beijing, China
zlx131@163.com

Abstract. E-learning, as an innovative and alternative way of distance learning, provides a strong challenge to the traditional learning with its unique advantage. The paper, for the diffusion of e-learning adoption in China, investigates people's perceptions and attitudes toward adopting e-learning, and explores the factors affecting the e-learning adoption behavior from innovation adoption perspective. Based on the model of Rogers' innovation adoption theory, the factors in each of "perceived innovative attributes" that affect the individual adoption behavior will be analyzed to test the relationship between these attributes and e-learning adoption. The result shows that the four perceived innovative attributes, namely "perceived relative advantage", "perceived compatibility", "perceived trialability" and "percieved observability", have certain influences on peoples' adoption of e-learning.

Keywords: Adoption intention; E-Learning; Adoption behavior; Perceived innovation attributes; Innovation adoption theory; China.

1 Introduction

E-learning can offer potential learners an alternative and innovative learning environment compared with the traditional learning [1]. As e-learning is still a new concept for many people, their attitudes towards its application have not been fully studied, especially in China [2]. It is believed that a better understanding of e-learning adoption behavior would enable e-learning providers to offer courses more likely accepted by future e-learners [1]. The innovation diffusion theory developed by Rogers, is clarified five perceived attributes of the innovation, and has the influence on the innovation adoption [3]. Based on extensive study on many different innovations, the theory provides the basic model of how perceived attributes affect the adoption of innovation. In the original framework proposed of Rogers, the adoption of innovation was regarded as the dependent variable. Without breaking the consistency of the original framework, some researchers had regarded the adoption of the

---

[*] Corresponding author.

innovation as the dependent variable instead [4]. It appears that the importance of issues related to the adoption of e-learning in China has not been fully recognized [2]. No previous studies have been conducted to analyze the perceptions of e-learning adopters and e-learning adoption intention of non-adopters in China [2] [5]. Thus, this research tries to explore the acceptance and intention of e-learning in China based on the model of Rogers' innovation adoption theory.

2   Methodology

2.1   Theoretical Framework of Assessment Method

Rogers has identified five attributes of an innovation that are key influencers on innovation acceptance. According to Rogers, these characteristics include relative advantage, compatibility, complexity, trialability, and observability [3]. This research will try to explore what the relationships between perceived attributes and the adoption intention of e-learning by Chinese undergraduates as a case. The theoretical framework of the paper regards five perceived innovation characteristics above as independent variables, and the e-learning adoption intention as a dependent variable whether or not to have influence on the e-learning adoption intention.

2.2   Research Hypothesis

Based on Rogers's original model, the research hypotheses are as followings.
Hypothesis I: Higher level of perceived relative advantage will positively affect the level of the intention of e-learning adoption (LIEA).

Hypothesis II: Higher level of perceived compatibility will positively affect LIEA.
Hypothesis III: Higher level of perceived complexity will negatively affect LIEA.
Hypothesis IV: Higher level of perceived trialability will positively affect LIEA.
Hypothesis V: Higher level of perceived observability will positively affect LIEA.

3   Results and Discussion

A total of 154 questionnaires are distributed and collected, 134 of which are valid responses. All valid respondents said they had not ever obtained a formal qualification through an e-learning course in the past or are currently engaged in an e-learning course. 97 percent of respondents are between 18 and 22, and only 3 percent between 23 and 25. Similarly, all respondents are full-time undergraduates.

3.1   Respondents' Perception on Innovative Attributes

With regard to the questions on each of the five components of the theoretical framework, the respondents were asked their opinions on various statements. In order to analyze the respondents' information, the scales of answers are coded and divided into five groups of Strongly Agree (5), Agree (4), Uncertain (3), Disagree (2), and Strongly Disagree (SD, 1).

As a result, there is not more difference between the individual answers in each of the eleven questions. The highly perceived relative advantage of e-learning is "pricing, flexibility, personal control, access (time) and access (place)" (around 4). SD in compatibility indicates that there are not more differences (around 3 except question 7). Students have generally a higher level perception on the complexity of e-learning adoption except "access to technology". Perceptions on trialability are quite high comparing other innovative attributes(above 3.50). Except "opportunities to observe other e-learners experiences", the other three questions are between 3.10 and 3.34.

3.2 Summary of Respondents' Perception vs. Intention

Analyzing table 1 horizontally, the value points on relative advantage, compatibility, trialability and observability are all descending with the decrease of intention degrees. That is the same situation as the hypothesis above that the higher perception of relative advantage, compatibility, trialabililty and observability be, the higher level of intention on adopting e-learning be. However, except complexity, respondents who are unlikely or very unlikely to try e-learning have similar levels of perceived complexity as these who choose "likely" or "very likely", as indicates that complexity hypothesis in Roger's theory is not true in China's case.

Table 1. A summary of respondents' perceptions from different e-learning intention groups

Variables	Very likely (9)		Likely (24)		Not sure (35)		Unlikely (46)		Very unlikely (20)	
	Mean	SD	Mean	SD	Mean	SD	Mean	SD	Mean	SD
Relative Advantage	3.89	0.41	3.68	0.44	3.41	0.42	3.26	0.56	2.83	0.60
Compatibility	3.44	0.51	3.33	0.53	3.26	0.43	3.01	0.43	2.76	0.59
Complexity	3.37	0.42	3.33	0.68	3.31	0.54	3.40	0.47	3.36	0.78
Trialability	4.22	0.52	3.64	0.68	3.55	0.67	3.51	0.61	3.29	0.59
Observability	3.83	0.71	3.32	0.65	3.20	0.67	2.95	0.57	2.75	0.47

3.3 Hypothesis Tests

Collecting required information from respondents to test research hypotheses, the correlation analysis has been conducted by the relationships established between respondents' intention to adopt e-learning and their perceptions on different innovation attributes (Table 2). Hypothesis I is accepted. The results show that the level of intention to adopt e-learning is significantly related to the perceived relative advantage. It suggests that the higher the perceived level of relative advantage over traditional learning, the more likely students would adopt e-learning method. Hypothesis II is accepted. According to the correlation analysis, perceived compatibility is found to have significant positive influence on e-learning adoption. Hypothesis III is rejected (not significant). The results show that the perceived complexity of e-learning has no significant negative influence on students' adoption intention, as seems inconsistent with previous studies on innovation adoptions.

Hypothesis IV is accepted. There is significant positive relationship between perceived trialability and e-learning adoption. Hypothesis V is accepted. The more visible the results of an innovation, the more likely the innovation will be adopted. To Chinese students, whether they are aware of benefits and advantages demonstrated by other e-learners will affect their adoption decisions.

Table 2. The correlation analysis between the intention to adopt e-learning and five innovation

Variables	Mean	Correlation Coefficient	Significance
Relative advantage	3.351	0.491**	0.000
Compatibility	3.124	0.389**	0.000
Complexity	3.354	-0.031	0.362
Trialability	3.558	0.270**	0.001
Observability	3.110	0.401**	0.000

Note: ** Is significant at $P < 0.01$.

4   Conclusion

The study suggests that Rogers' innovation adoption theory provide useful framework to examine e-learning acceptance behavior as a case. Findings help to gain valuable insights into the factors of e-learning adoption decision and how e-learning benefits perceived affect adoption intention. However, the paper has certain limitations due to its sample selection, sample size and respondents profile; Moreover, using cross-sectional survey, the changes of perception in a long term could be ignored.

References

1. S.S. Liaw, H. M. Huang, G. D. Chen. An activity-theoretical approach to investigate learners' factors toward e-learning systems. Computers in Human Behavior (2006) (in press)
2. van Raaij, E.M., Schepers, J.J.L.. The acceptance and use of a virtual learning environment in China. Computers & Education (2006) (in press)
3. Rogers M. E.: Diffusion of Innovations, New York: The Free Press (1995)
4. Agarwal, R., Prasad, J.:"The Role of Innovation Characteristics and Perceived Voluntariness in the Acceptance of Information Technologies", Decision Sciences, Vol. 28, No. 3(1997) 557-582
5. Yajie Gao: A Study of E-learning Adoption and Diffusion in Higher Education in China. China Agricultural University, 2004

E-Learning Assistant System Based on Virtual Human Interaction Technology

Xue Weimin[1,2] and Xia Wenhong[1]

[1] Institute of Information Technology, Beijing Union University, Beijing 100101
[2] Department of Computer Science & Technology, Tsinghua University, Beijing 100084
xuewm@mail.tsinghua.edu.cn

Abstract. The virtual human affective interaction is one of the hotspots in information science and cognitive science today. The importance of emotions in learning process is more and more acknowledged. This paper introduces a new virtual human interaction module based on multi-agents. The affective interactive model is built according to the human cerebrum control pattern. The multimodal detection agents are able to help tutor to better understand the emotional and motivational state of the learner throughout the learning process. The results of the practical application virtual human interaction in E-Learning system indicate that virtual human technology can improve the interactivity and entertainment for the E-learners.

Keywords: E-Learning, virtual human, multi-agents model.

1 Introduction

The virtual human with affection is challenging project facing to modern scientists, especially when those characters interact with real people possessing real affection. In biological systems, the existence of emotions can have both advantageous and detrimental effects on the cognitive process [1]. Now a growing amount of studies support the claim that affection plays a critical role in decision-making and learning performance as it influences cognitive processes [2]. For example, as suggested by Goleman [3] "the extent to which emotional upsets can interfere with mental life is no news to teachers. Students who are anxious, angry or depressed don't learn; people who are caught in these states do not take information efficiently or deal with it very well". So it is obviously that the user's affective state plays an important role in improving the effectiveness of e-learning. The emotional unawareness has been con-sidered one of the main limits of the traditional e-learning tools. In fact, while skilled teachers can modify the learning path and their teaching style according to the feedback signals provided by the learners, e-learning platforms cannot generally take account of these feedbacks resulting often too rigid and weakened [4].This paper presents our studies on affective interaction between real human and virtual human. The virtual human can perceive real human affection by recognition of his voices and facial expressions, and the virtual human can generate his simple affective behavior autonomously [5].

2   The Virtual Human Affective Interaction Theory

2.1   The Characters of Virtual Human

Affective virtual human is to make virtual human has certain characteristics and emotion interactive ability (to identify and express emotions and affections), to endow it with artificial psychological model and the ways to identify and express emotions and affections. It is the application of artificial psychology theory in the field of virtual reality. It researches how virtual human recognizes natural human's emotion and how virtual human expresses the object's affection based on its artificial psychology model. The virtual human can study human interactive skills through communication with human, and have the same value criterions as human. Its intelligence is not the intelligence in narrow sense, but it is the intelligence in broad sense, which is not only including certain intelligence quotient, but also including certain affection quotient [5]. The virtual human uses an internal model of the agent's affective state to guide the conversational dialogue between virtual human and user.

2.2   The Model of Virtual Human

Traditional human machine interaction is normally based on passive instruments such as keyboard, mouse, etc. It's impossible for them to understand and express emotions. Without the ability of emotion processing, the virtual human cannot be expected to be a human-like agent in the virtual environment, and also cannot be expected to communicate with humans in a natural and harmonious way.

(1) BDI Agent Architectures

The basic BDI agent architecture designed for the virtual human is presented in Fig.1. The inputs to the agent are events from the environment and the outputs are the agent's actions. The interpreter loops and generates an action in each cycle. External and internal events are always added to an event queue. The agent's beliefs are adjusted according to those events.
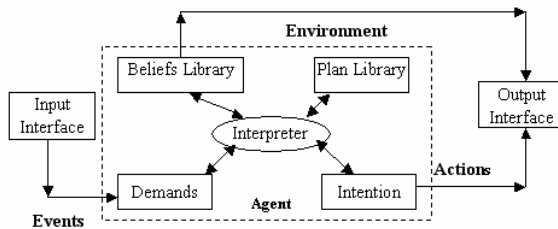

Fig. 1. This shows a basic BDI Agent Architecture

At the beginning of a cycle, plans are chosen from the plan library that specifies courses of action that may be undertaken in order to achieve the agent's goals. Next, the deliberator, a component of the interpreter, selects a subset of these plans to be adopted and adds them to the intention structure. The agent then executes one action from one plan in the intention structure. The intention and demand structures are

modified by dropping successful goals and satisfied intentions, as well as impossible goals and unrealizable intentions. Hence, due to new external events, the agent can reactively choose to drop intended plans and/or adopt others.

(2) Affective interaction model

According to the virtual human characters, we adopted the composed structure of reactive agent and deliberative agent as the basic structure (Fig.2 shows the structure). The system structure includes two emotional information channels. The deliberative agent has affective reasoning engine for affective state recognition and modeling. The reactive agent subsystem can make reaction to the apperception results without complicated reasoning.
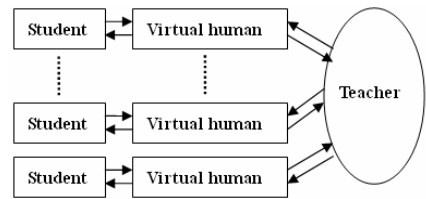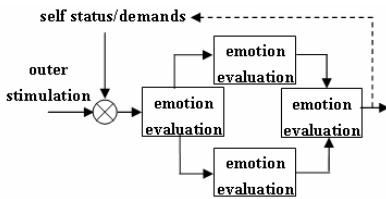
Fig. 2. The Structure of Interaction System

Fig. 3. The structure of the E-Learning system

3   E-Learning System Structure

In the e-learning process there is often one teacher for most students. To promote effectiveness of learning for the students, each student is assigned to have one virtual human. The E-Learning system structure is shown as the Fig.3. The virtual human is represented as a teacher in the e-learning platform. Except for the animate agent supplied by Microsoft Corporation, we can design a likely character or use the character from the third one. Each character has supplied a lot of interface function. It can dialog to the student face to face through the facial expression recognition system and the voice recognition system. The virtual human can change his facial expression emotion according to the learner's emotion state.   Thus the e-learning process is making more and more personalized and humanized.

In the e-learning interactive system, extracting and validating emotional cues through analysis of users' facial expressions is very important. The process of the facial expression subsystem is generally carried out according to following stages: detection of the face, the automatic extraction of contours of the permanent features of the face to knowing: the eyes, the eyebrows and the lips. Extracted contours being sufficiently realistic, we then according to the changes of the facial expression character points to recognize the six universal emotions on the face (joy, surprise, fear, disgust, anger and sadness).The video frequency facial expression character point track and recognition technology is presented in reference [8]. A speech emotion recognition algorithm was developed based on the statistical and temporal features of the acoustic parameters for discriminating between emotions. The process of the speech emotion recognition subsystem is carried out in reference [9, 10].

4   Conclusion and Future Work

This paper simply reports our exploratory approach in the teaching computation. The virtual human interaction has been used in the e-learning system in order to realize the harmonious emotion interaction. Some technologies and effective arithmetic are used in the system. This system is able to recognize the emotional state of the learner according to his facial expression. As a result, it has realized the personalized and humanized human-machine interactive function. However the virtual human interactive technology is not mature, especially the facial expression recognition rate is relatively low, so the system is only an original one. There are many aspects in the system needing to be improved. In the future we will improve and better our system, especially in facial expression track speed, recognition rate. With the development of the virtual human interaction, the virtual human will not only be used in learning in interaction ,but also capable of direct psychological enrichment tasks, such as mental therapy and entertainment.

References

1. Picard R. Affective Computing. Cambridge, MA: MIT Press, 1997
2. Kinard, E. M.:. Perceived and actual academic competence in maltreated children. Child Abuse and Neglect, Vol. 25, 1 (2001) 33-45
3. LeDoux, J..The emotional brain: The mysterious underpinnings of emotional life. Weiden¬feld & Nicholson, London (1998)
4. Goleman, D.: Emotional intelligence. Bantam Books, New York (1995)
5. Weimin Xue, Zhiliang Wang, Zhehua Wei. A new method for simulating human emotions[J]. Journal of university of science and technology Beijing. Vol.10, No. 2, April. 2003,10（2）：72-74
6. Picard, R. W., Papert, S., Bender, W., Blumberg, B., Breazeal, C., Cavallo, D., Machover, T., Resnick, M., Roy, D., Strohecker, C.: Affective Learning - A Manifesto. BT Technology Journal Vol. 22, 4 (2004) 253-269
7. Luigi Anolli,etc The Potential of Affective Computing in E-Learning: MYSELF project experience". Proceedings of INTERACT 2005 Conference - Workshop on eLearning and Human-Computer Interaction: Exploring Design Synergies for more Effective Learning Experiences, Rome, 12-15 September 2005.
8. Weimin Xue. Facial Expression Recognition Based on Gabor Filter and SVM. Chinese Journal of Electronics [J]. October.2006, 15(4A):809~812.
9. Xue Weimin. Research on Speech Interaction of Affective Robot. Proceedings of the 7th International Conference on Electronic Measurement and Instruments, ICEMI'2005. 16-18 Aug., 2005, Beijing, China, (7) :344~347.
10. Jiang Danning, Cai Lianhong. Speech emotion recognition using acoustic features. Journal of Tsinghua University (Science and Technology).2006, 46(1):86-89

Research on Speech Emotion Recognition System in E-Learning

Ken Chen[1], Guangxue Yue[2], Fei Yu[1,3], Yue Shen[1], and Aiqing Zhu[4]

[1] School of Computer & Information Engineering, Hunan Agricultural University,
Changsha, 410128, China
`{shenyue,yufei}@hunau.edu.cn`
[2] College of Information Engineering, Jiaxing University, 314000 China
`guangxueyue@yahoo.com.cn`
[3] Jiangsu Provincial Key Laboratory of Computer Information Processing Technology,
Province, Suzhou University, Suzhou, 2150063, China
`hunanyufei@126.com`
[4] College of Urbanand Environment Science, Central China Normal
University, Wuhan, China, 430079
`zhuaiqin1982@yahoo.com.cn`

Abstract. Aiming at emotion deficiency in present E-Learning system, a lot of negative effects were analyzed and corresponding countermeasures were proposed. Basing on it, we combined affective computing with the traditional E-Learning system. The model of E-Learning system based on affective computing was constructed by using speech emotion, which took speech feature as input data. Our simulation experiment results showed that neural networks was effective in emotion recognition, and we achieve a recognition rate of approximately 50% when testing eight emotions .besides, other key techniques of realizing the system such as tracking the change of emotion state and adjusting teaching strategies were also introduced.

Keywords: E-learning, Affective computing, Speech emotion, Teaching strategies.

1 Introduction

E-Learning uses modern educational technologies to implement an ideal learning environment through integrating the information technology into curriculum, which can embody the learning styles of students' main-body function, reform the traditional teaching structure and the essence of education thoroughly [1].

Although the current E-Learning systems have many merits, many of them only treat advanced information technology as simple communication tools, and release some learning contents and exercises in the network [2]. This kind of movable textbook or electronic textbook is indifferent to the learners, which lacks of the interaction of emotion. Besides, this kind of learning materials without using of the superiority of interactive multimedia technology and displaying the function of network effectively, which leads to the phenomenon of emotion deficiency in the current E-Learning system.

Emotion deficiency refers to the separation among students and teachers, students and students, which make students and teachers, students and students can't carry on face to face communicating promptly like conventional education. Thus, some learning problems of the learners in the learning process can't be solved and perplexity of the psychology can't get help. If students gaze at indifferent computer screens for a long time, they do not feel the interactive pleasure and emotion stimulation, and they may have antipathy emotion.

2   Model of E-Learning System Based on Affective Computing

In the learning process, language of learners is abundant. When they understand and accept the learning content, their emotion is high and displays as cheerful spoken language. Otherwise, their emotion is low.
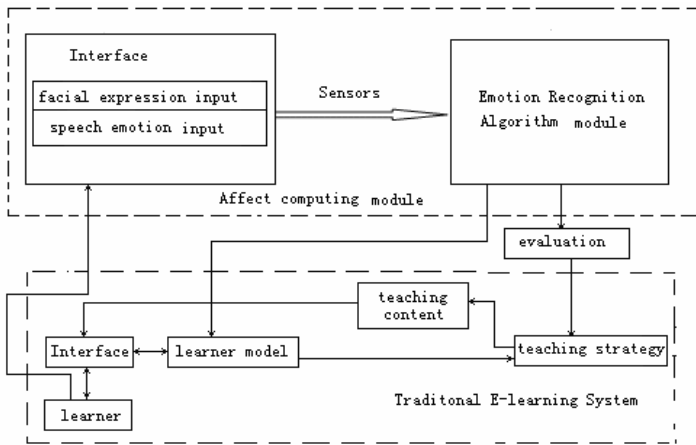

Fig. 1. The model of E-learning system based on affective computing

These emotional behaviors are quite important feedback signals of learners. We may use these feedback signals effectively and adjust teaching strategies to serve personalized learning. Basing on it, the traditional E-Learning model is added the affective computing module. The model of E-learning system based on affective computing is Fig.1.

3   Emotion Recognition Module

Consciously expressed emotions are easier for humans to recognize, and significantly easier to gather data on. Therefore, this study is limited itself to the recognition of emotions that are consciously and purposefully expressed by the speaker. We expect to be able to expand our methodology to unconscious or concealed emotions as well in future work.

3.1   Classification of Emotions

How to classify emotions is an interesting but difficult issue. Researchers on emotion recognition differ on the number of categories and the kinds of categories to use. Some classification systems that have been used include

> Neutrality, joy, boredom, Sadness, anger, fear, indignation[3]
> Neutrality, happiness, sadness, anger, fear, boredom, disgust[4]

We dealt with four emotional states (anger, sadness, happiness and cheerfulness) in our previous study; based on examining these examples, and on the consideration that increasing the number of recognizable emotional states is effective for achieving interaction between humans and computers, we have selected the following eight emotional states to use in this study: joy, teasing, fear, sadness, disgust, anger, surprise, neutral.

3.2   Speaker and Context Independence

Speaker independence is an important part of speech and emotion recognition. A speaker-dependent system requires a training period for each new speaker before the system is able to function at a reasonable level. On the other hand, a speaker-independent system will tend to have a lower level of accuracy, since it is not finely tuned for each speaker. However, eliminating the need for training sessions with each new speaker seems well worth the resultant loss in accuracy. By carrying out initial training using a number of different speakers, our system has become speaker-independent. Context independence is also a desirable quality in emotion recognition systems. A system that can determine the emotion in an utterance regardless of the context or text of the utterance is considered context-independent. A context-dependent system would require language understanding in order to determine the context. Our system achieves context independence by using a large set of phoneme balanced words as its training set.

Of course, there are other important factors, such as the effect of social and cultural differences. However, these are difficult issues that will require long term research. Therefore, in this research, we deal with emotions contained in the utterances spoken only by Chinese speakers. Under this restriction, we tried to achieve speaker-independent and context independent emotion recognition.

4   Tracking the Change of Emotion State

In the E-Learning environment, tracking psychological state change of cognition process is always neglected. When the learners cannot understand and accept the learning contents, they will generate worried, disagreeable, fearsome emotion. Therefore, it is necessary to track emotion state in the E-Learning environment. Thus, when learner's state is not fine, the learning process can also carry on under healthy state though adjusting teaching strategies and intervening emotion.

The change of learners' emotion is more complex in the learning process. The learner contacts with a new knowledge point, two kinds of attitudes such as interested

state ① and indifferent state may appear. Interested state is to explain the change process of learner's emotion, and learner's emotion state is divided into four categories approximately in the paper.

①surprise ②puzzle, bewilderment ③depression, despair ④self-confidence. With the learning process advancing, learner's emotion is changed. For instance, the learner has an idea to solve this problem. If the learner defeated repeatedly, he will suspect himself and changes into the state ③, this kind of state is disadvantageous to learning. The system should apperceive this kind of emotional change and carry on emotion intervening, which let him turn to self-confident state ④. When he contacts with a new knowledge point, the emotion turns to state ① and ② too.

5   Conclusion

The results obtained in this study demonstrate that emotion recognition in speech is feasible, and that neural networks are well suited for this task.

There is still more work that needs to be done in the field of emotion recognition in speech. An examination of the speech features used in this study may allow the number of features to be reduced. In addition, further trials with different topologies of neural networks may also help improve performance. And multi-module emotion recognition including facial, speech, and other features such as gesture will be studied. I wish that this article's work could give some references to certain people.

References

1. Kekang H.:E-Learning Essence- information technology into curriculum. E-education Research(2002)3-4
2. Wang J.J.: Emotion deficiency and compensation in distance learning. Chinese network education(2005) 117-120.
3. Picard R.W.: Affective Computing, Challenges, Cambridge. International Journal of Human Computer studies(2003)55-64.
4. Klasmeyer G, Sendlneier W.: Objective voice parameters to characterize the emotional content in speech. Proceedings of Processing(1995)

A General-Purpose Mobile Framework for Situated Learning Services on PDA

Seong Baeg Kim, Kyoung Mi Yang, and Cheol Min Kim

Department of Computer Education, Cheju National University,
66 Jejudaehakno, Jeju-si, Jeju-do, 690-756, Korea
`{sbkim,kmyang,cmkim}@cheju.ac.kr`

Abstract. Recently, as ubiquitous technology has been developed rapidly, a specific application service considering users' situations has been becoming the focus of attention. As a field of a typical situation-based application, we focus on situated learning using a mobile device. A u-learning system can provide learners with individualized learning at any time in any place. In this paper, we propose a general-purpose mobile framework suitable for situated learning on PDA with RFID mobile system. Specially, we examine three aspects in making the framework. First, we investigate how learners obtain and access customized learning contents suitable for them. Second, we construct a mobile middleware for RFID on PDA. Finally, we devise the application-specific system for situated learning.

Keywords: RFID, Situated Learning, Mobile middleware, Framework.

1 Introduction

In recent years, the development of information technology has encouraged the spread of various mobile devices. Thus, the attention to a ubiquitous system has been increasing. In general, a u-learning using a mobile device is more suitable for customized learning. Furthermore a u-learning can be used to bring situated learning for each learner. It has been recognized that web-based education systems enable learners to have self-directed learning. However, they have still limits on making possible customized learning reflecting differences such as degrees of knowledge, learning capability and learning goals. For this reason, the systems have activities made based just on inexact learning preferences of the learner and without doubt aren't supporting effectively the learner for active and individualized learning.

There has been research regarding customized learning for each learner [1][2][4][5]. However, there has been little research on personalized learning considering situation. Also, the previous research on middleware system has focused on constructing a middleware system on a desktop or server [3]. However, it is also essential to construct a mobile middleware platform for developing the mobile applications. The platform would be small volume, which includes minimal APIs required for developing an application. From the viewpoint of situated learning theory [7], the learning effect of using traditional learning methods is not good, because it are mostly failed for learners to apply the knowledge in an actual situation that is

obtained from learning without consideration of an actual situation. To solve it, the situated learning theory has been studied [7].

2 Profiling Scheme

The profile data collected from a mobile device are sent using an encoding scheme the form of the variable HTTP_USER_AGENT in order to provide customized learning based on situation. Fields composed of the encoded values are divided into 4 main parts:PDA Profile, Learner Information, GPS Information and RFID Information. They are split by a semicolon.

We encoded the values of the device manufacturer field with 15 mobile device makers we have studied so far. When known the manufacturer and model of a PDA, such hardware specifications of the PDA as CPU, RAM, and ROM etc. can be extracted from a server. This information would be used in providing the customized learning at right time in right place on the PDA that each learner has. Learner information is composed of learner's age, learning time, learning subject, learning type, and learning motive.

In case of GPS information, it enables the system to find the exact location and the moving direction of the learner at a certain time. Also, in case of RFID information, it enables the system to identify an exact situation given. We encoded the RFID information based on EPC (Electronic Product Code) that is currently used in popular. The standard EPC consists of header, EPC manager, object class, and serial number [6].

3 Mobile RFID Middleware

In addition to our profiling system, there is a mobile RFID middleware developed in order to support situated learning based on RFID. The structure of the mobile RFID
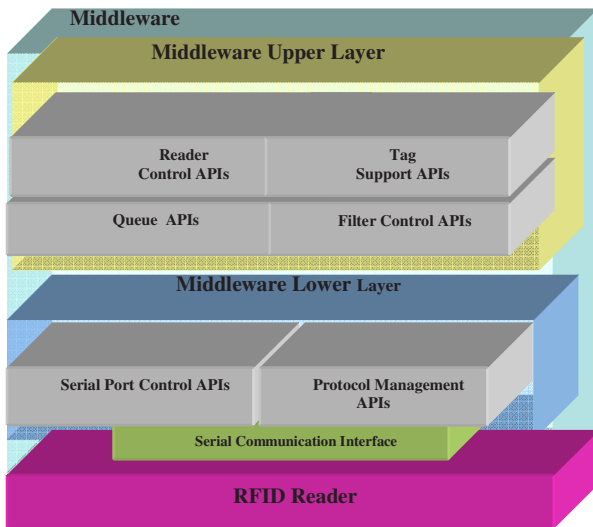

Fig. 1. The Structure of the Mobile RFID Middleware

middleware is shown in Figure 1. The middleware consists of two layers: upper layer, lower layer. The upper layer provides APIs for supporting applications. The lower layer has functions for various RFID readers. The APIs of the lower layer consists of the serial port control APIs and the protocol management APIs.

4   Situated Learning

The situated learning theory based on constructivism explains that learning can be effective when knowledge is provided in the meaningful context. The overall architecture for situated learning on PDA is shown in Figure 2. The application
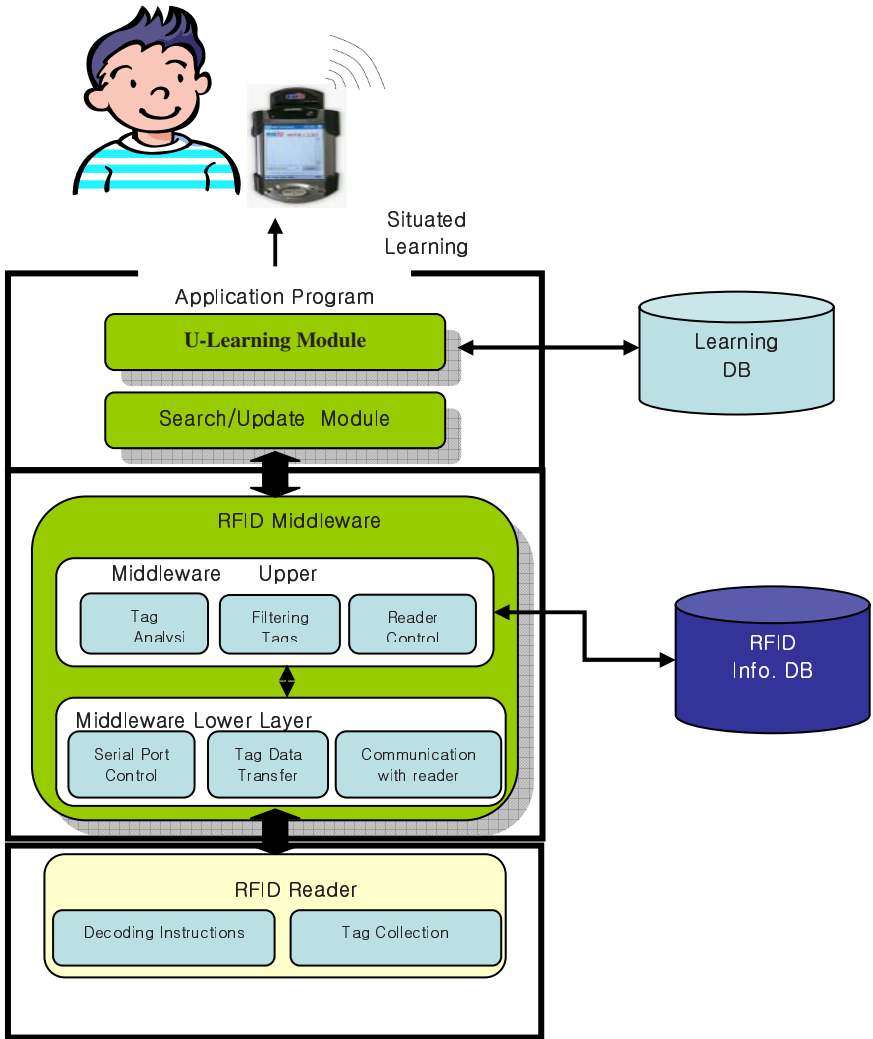
Fig. 2. The Overall Structure for Situated Learning

program consists of U-learning module and Search/Update module. U-learning module is implemented using U-learning APIs. Search/Update module provides the function to search and update databases that serve RFID and learning information.

5 Conclusion

We suggested a general-purpose mobile framework for enabling situated learning services under ubiquitous environment. In the framework, we described how to encode learner's profiling information considering the characteristics of a mobile device and each learner, which is required for providing personalized learning at the right time in the right place. That is to come up with a way of providing a best-suited learning environment for each learner who uses a mobile device. Also, we proposed the mobile RFID middleware, which is largely composed of two parts:upper layer and lower layer. Finally, we presented the overall structure of application for situated learning using RFID reader, which is attached to a mobile device PDA.

We're optimizing the mobile RFID middleware modules and tuning it to improve performance and reliability.

References

1. Tan-Hsu Tan, Tsung-Yu Liu: The Mobile-Based Interactive Learning Environment (MOBILE) and A Case Study for Assisting Elementary School English Learning", In Proceedings of the 4th IEEE International Conference on Advanced Learning Technologies, (2004).
2. Phivos Mylonas, Paraskevi Tzouveli, Stefanos Kollia: Towards a Personalized e-learning scheme for Teachers, In Proceedings of the 4th IEEE International Conference on Advanced Learning Technologies, (2004).
3. T. Jung, Y. Kim, Y. Lee: The Platform Technology of RFID Middleware, Telecommunications Review, Vol. 15, No. 2, (2005).
4. Abbattista, F., Degemmis, M., Fanizzi, N., Licchelli, O., Lops, P., Semeraro, G., and Zambetta, F.: Learning User Profiles for Content-Based Filtering in e-Commerce, In Proceedings of AI Workshop su Apprendimento Automatico: Metodi e Applicazioni. (2002).
5. Ricardo Carreira, Jaime M. Crato,Daniel Gonçalves, Joaquim A Jorge: Evaluating Adaptive User Profiles for News Classification, In proceedings of IUI'04, (2004).
6. S. Sarma, D. Brock, and D. Engels: Radio Frequency Identification and the Electronic Product Code, IEEE Micro, Vol. 21, (2001).
7. S. Kim: Good Ideas to Foment Educational Revolution, Communications of Korea Educational Technology Research Association, Vol. 38, No. 1, (1998).

Construction of Virtual Learning Environments of Lushan Mountain

Weijun Yang[1], Jianhua Gong[1], Lihui Zhang[1], and Hongli Fan[2]

[1] Institute of Remote Sensing Applications, Chinese Academy of Sciences,
P.O.Box9718, Beijing, 100101, P.R. China,
`wjy172@163.com`
[2] Institute of Automotive Industry
ShiYan, HuBei, 442002, P.R. China

Abstract. Organizing a fieldwork in LuShan Mountain consumes much money and time, but the result is not effective. This demands a virtual learning environment of LuShan Moutain. Some methods of data collection based on mobile equipments are adopted. The data collection system constructs a collaborative 3D modeling environment, in which students can do goecollaboration. In this paper, some technologies to support data collection are discussed.

Keywords: Virtual Learning Environment, Virtual Geographic Environment, Virtual Geographic Fieldwork, Data Collection, Collaborative 3D Modeling.

1 Introduction

A virtual geographic environment (VGE) is a multi-user shared, intelligent, and virtual environment representing the real geographic environment to conduct geo-spatial analysis, to carry out geo-visualization, to support collaborative work, planning and decision making, as well as to serve training, geographic education, and entertainment [2]. VGE can represent the natural world and enables a person to explore and interact with objects in cyberspace.

In this paper, some technologies such as collaborative 3D modeling between multi PCs or mobile equipments are discussed.

2 Virtual Geographic Fieldwork

Virtual learning environment uses the combination of long-distance communication tools and multimedia technologies such as VR to provide an online learning path for students. Virtual learning environment (VLE), not only provides rich teaching patterns and teaching contents, but also helps improve learners' ability of analyzing problems and exploring new concepts [5]. VR is the most feasible technology for us to create VLE. Virtual geographic fieldwork is a key application of VGE in the field of geographic fieldwork. It also forms a virtual learning environment of Lushan Mountain.

Lushan Mountain, situated in the north of Jiangxi Province, at 115°52'-116°08E'29°26-29°41'N, occupies an area of 302 square kilometers. Lushan Mountain is famous for its beautiful natural landscape. Not just so, because of its special terrain, geology, etc, it has become a perfect fieldwork place for students of many majors, such as GIS, Geology, Remote Sensing, etc. Why a virtual geographic fieldwork is necessary?

First, organizing such a fieldwork consumes so much money and time. And students often complain that the result is not effective. The data collection became a mess because of no trim and no accumulation. It's like a travel more than a fieldwork. Second, the data collection will certainly do some destroy to the environment of Lushan Mountain. This is also a problem in the outdoor fieldwork. Third, the information stored in the computer can be permanent, but specimens, such as plants, cannot last a long time.

These all call for a virtual fieldwork system, students can explore in the virtual geographic environment and acquire knowledge in a virtual 3D scene. Above disadvantages can be avoided. So, at the first, we need a data collection system, which can be applied to the data collection of virtual fieldwork. It forms an environment in which many modelers can do collaborative 3D modeling.

3   Data Classification and Structure

The data of outdoor fieldwork can be classified to six categories, such as plant, rock, soil, terrain, geology and artificial object.

Dem and image objects are the information of the terrain. Point, linear, surface, body objects are base types of CyberCity GIS. Point object is implemented to afford the ability to integrate with CAD models. The point object can describe such features as trees, annotations, static CAD models. Trees are represented by transparent textures [3]. Some artificial objects can be represented by CAD models of point object and inserted to the scene.

The virtual geographic fieldwork is required to afford the ability of spatial analysis. So the data structure is very important. Similar to the formal data structure (FDS) [1] [4] [6], the CyberCity models are grouped into six different object types: DEM object, image object, point object, linear object, surface object, and body object. 3D point object, the cube object, has the simplest spatial extension (the 3D position, the azimuth and the box size) and sometimes special attributes such as CAD models in 3DS format.

4   Offline Data Collection Though PDA

The first method is offline data collection though PDA. Students can collect the text and picture information though PDA. The position information is acquired by GPS. After coming back, they transport the data to the PC and build the 3D models. The data collection and modeling are separate. So an environment of offline data collection is constructed.

In the process of data collection, a linkage file is created. In this file, the relationship of the information such as pictures, texts, videos and position is recorded. After the students come back, they can add the data to the database in a collaborative 3D modeling environment. Some support technologies must be adopted to support it. The most important one is to integrate some theories of 3D interactive visualization to the collaborative 3D modeling environment, such as dynamic loading by data page, view frustum culling, etc.

5   Online Data Collection Though Mobile Phone

The second method is online data collection though mobile phone. The students collect the information though mobile phone and GPS. After some simple data handling in mobile phone, they can send the data to the database server directly after simple handling. At the same time, the 3D scene is built. After data collection, the 3D data is created at the same time. So an environment of online data collection is constructed.

J2ME is Sun Microsystems' answer to a consumer wireless device platform. J2ME allows developers to use Java language and the J2ME wireless toolkit to create applications and programs for wireless and mobile devices. The Connected Limited Device Configuration (CLDC) is the J2ME configuration for smaller handheld devices that are usually battery operated and low in memory with limited processing power and low bandwidth. CLDC defines the base set of application programming interfaces and a virtual machine for resource-constrained devices like mobile phones, pagers, and mainstream personal digital assistants. When coupled with a profile such as the Mobile Information Device Profile (MIDP), it provides a solid Java platform for developing applications to run on devices with limited memory, processing power, and graphical capabilities.

In MIDP, there are two methods to communicate between MIDlet and Servlet. The first method is using Java Server Pages as server component. The second method is communicating with Servlet directly. Java Server Pages are mainly applied in the representation layer of WEB applications. Servlet is more adapted to handle logic or communicate with client as a control. HTTP protocol is adopted to visit web data and service.

6   Collaborative 3D Modeling

6.1   Collaborative Modeling Between PCs

Integrating interactive visualization to 3D modeling is a revolutionary change to traditional 3D modeling method based on subareas. It forms an environment in which many modelers can carry collaborative work. Some technologies, such as network, 3D interactive visualization, etc, are used to establish this environment. Many modelers can create 3D models in a large scene with great amount of data. Thus, a collaborative 3D modeling environment is constructed to support 3D modeling for 3DGIS, CyberCity GIS, virtual reality, VGE, 3D game, etc.

6.2 Collaborative Modeling Between Mobiles

Because there is no 3D graphic interface on mobile equipments, the theories of collaborative modeling between PCs are not used on them. But if there is a demand of graphic interface on mobile equipments in the future, the theories are also useful.

6.3 Collaboration Between Mobiles and PCs

In some applications, the PCs and mobiles may be both needed. So the collaboration between PCs and mobile equipments must be considered. Four communication patterns are put forward. These are S2S (Static to Static), M2S (Mobile to Static), S2M (Static to Mobile), and M2M(Mobile to Mobile). S2S means the communication between the persons using different computers in the rooms. M2S means the outdoor person with mobile equipment communicates with the person using computer in the room. S2M means the person using computer in the room communicates with the outdoor person with mobile equipment. M2M means the communication between the outdoor persons with mobile equipments. In the collaborative modeling between mobiles, only the pattern M2S is implemented. But in other applications, some other patterns may be used.

Acknowledgements

References

1. Gong, J., Li, D.: Object-oriented and Integrated Spatial Data Model for Managing Image, DEM, and Vector Data, Photogrammetric Engineering & Remote Sensing (2000), 66(5):619-623.
2. Gong, J., Lin, H.: A geographical perspective on online virtual reality (2001), pp.62-63.
3. Jurgen, D.: An object-oriented approach for integrating 3D visualization systems and GIS, Computers & Geosciences, 26 (2000) 67-76
4. 4.Molenaar, M.: A topology for 3D vector maps, ITC Journal (1992), (1): 25-33.
5. Pan, Z., Cheok, A., Yang, H.: Virtual reality and mixed reality for virtual learning environments. Computers & Graphics (2005)
6. Wang, X.: A Hybrid GIS for 3-D City Models, In: International Archives of Photogrammetry and Remote Sensing (2000). Vol. XXXIII, Part B4, pp. 1165-1172.

A Collaborative Teaching Approach
Using Integrated Electronic Environments
for Information Security

Yu-An Tan, Zuo Wang, and Xu-Bo Wu

School of Computer Science and Engineering
Beijing Institute of Technology, 100081 Beijing, P.R. China
`victortan@yeah.net, qiushui@bit.edu.cn, wuxubo@bit.edu.cn`

Abstract. Rapid advancement and new information sources in many academic fields offer expanded opportunities for collaborative teaching. In this paper, we propose a collaborative teaching approach using integrated electronic environments for information security. Taking the security problem of implicit type conversion of C++ program as instance, we present the learning goals & objectives, course content, student assignments and discussion of the collaborative teaching approach using integrated electronic environments. The teaching performances suggest that this new proposed teaching approach is very efficacious.

Keywords: collaborative teaching approach; integrated electronic environments; information security; safety vulnerability.

1 Introduction

There is a growing call for competency-based education in educational contexts. Competencies can be construed as abilities that enable learners to recognize and define new problems in their domain of study as well as solve these problems [1]. According to Keen [2], competencies are a combination of complex cognitive and higher-order skills, highly integrated knowledge structures, interpersonal and social skills, and attitudes and values. Acquired competencies enable learners to apply these skills and attitudes in a variety of situations and over an unlimited time span [3].

In educational circles, educational designers are moving from cognitive, often rule based instructional design for efficient and effective teaching towards constructivist instructional design for competency based learning. The problem is that this is not a question of adaptation of the design methodology used, but is a question of beginning anew. For this reason, we proposed a collaborative teaching approach using integrated electronic environments for information security in this paper.

This paper is organized as following. Section 2 presents the proposed collaborative teaching approach using integrated electronic environments for information security. Finally, the conclusions of this study are drawn in section 3.

2   The Proposed Collaborative Teaching Approach

In this section, we will present the proposed collaborative teaching approach using integrated electronic environments for information security. Taking the security problem of implicit type conversion of C++ program as instance, we present the learning goals & objectives, course content, student assignments and discussion of the collaborative teaching approach using integrated electronic environments.

2.1   Teaching Background

The business information plays an extremely important role in most organizations today, and efforts to protect such business information should be of the utmost importance. Information security is more often than not viewed only as a technical concern [4], and hence seems to lack the attention of top management and boards of directors. According to the current popular viewpoints, information security awareness should switch to a better program [5-6]. For this reason, the security problem of implicit type conversion of C++ program is adopted as an instance in this paper.

2.2   Learning Goals and Objectives

The learning goals and objectives can be characterized as follows.

(1) Teach advanced techniques for searching data.
(2) Make students aware of information security awareness.
(3) Emphasize the importance of evaluating research findings.
(4) Provide individual assistance as necessary to ensure that all students achieve a "comfort level" result.

2.3   Course Content

The course contents can be described as following.

Session 1: searching technology. We will spend 10 minutes to explain the searching technology and approach, for example, Internet, BBS, library, etc.

Session 2: information security awareness. We will spend 10 minutes to explain the information security awareness. In this session, we should emphasize following two points: (1) business information plays an extremely important role today, and efforts to protect such business information should be of the utmost importance; (2) information security awareness should switch to a better program.

Session 3: The security problem of implicit type conversion of C++ program. We will spend 20 minutes to explain the security problem of implicit type conversion of C++ program. In this session, we will apply a material example to explain this content.

<div align="center">

Conversion between Pointer & Citing

</div>

A pointer which points to any type object can be evaluated to the variable with the *void** type. It can convert the *void** type to another type with an evident way. This *void** object can evaluate to that *void** object. Two *void** objects can

be compared each other. Besides the above basic operation, other operation to the *void** object is insecure. In the following, we will give a material example of this kind of security problem. In this example, *pv* points to an integer object (achieved by *pi* in the third line). In the sixth line, this pointer was evaluated to the *pd2* after its conversion. As you know, this conversion is not secure.

Example of a Computer Program about Conversion Between Pointers

```
1: int main(int *pi)
2: {
3:     void *pv = pi;
4:     int *pi2 = (int *)pv;
5:     double *pd1 = (double *)pv;
6:     double *pd2 = pv;
7:     return 0;
8: }
```

Session 4: task arrangement. We will spend 10 minutes to arrange the subsequent tasks. There are four major tasks should be finished for these students. The first one is to get together some accidents about information security. The second one is to collect some examples about the security problem of implicit type conversion in C++ program. The third one is to design or implement some solutions for security problem of implicit type conversion in C++ program. The forth one is to design and execute the evaluation for research findings.

Session 5: Student's presentation. We will spend 100 minutes for student's presentation. Each group of students can present their research findings with their own freeform presentation methods, but the presentation time should be limited to 20 minutes.

Session 6: Evaluating research findings. We will spend 10 minutes for evaluating research findings. The Evaluating group will estimate the presentation of each group according to their proposed index system, and they will notify the final evaluating result at this session.

2.4 Student Assignments

All the students were assigned as follows (Table 1).

Table 1. The student assignments

Group	Major Task	Group Scale
1	Collect some accidents about information security	3-5
2	Collect some examples about the security problem of implicit type conversion in C++ program	3-5
3	Design or implement some solutions for security problem of implicit type conversion in C++ program	6-8
4	Evaluate the research findings	4-8

2.5   Discussion

The teaching performances of this class can be characterized as follows.

(1) Abundant teaching content. There are 3 accidents about information security, 8 examples about the security problem and 5 solutions for security problem were collected and presented by the students.

(2) Equitable evaluation for research findings. The evaluating group designed a practical and efficacious evaluation index system, and their evaluation is equitable and evenhanded on the whole.

(3) Collaborative learning approach using integrated electronic environments. All the students learned, prepared and presented their course contents with a collaborative way, and they applied many electronic types of equipment for their learning. Through this way, all the students can learn the course contents with an initiative way.

3   Conclusions

The contribution of this paper can be characterized as follows: it proposed a collaborative teaching approach using integrated electronic environments for information security. We present the learning goals & objectives, course content, student assignments and discussion of the collaborative teaching approach using integrated electronic environments. The teaching performances suggest that this new proposed teaching approach is very efficacious.

References

1. Kirschner, P.A., Van Vilsteren, P., Hummel, H., et al.: A Study Environment for Acquiring Academic and Professional Competence. Studies of Higher Education, 22(2): 151-171. (1997).
2. Van Merrienboer, J.J.G.: Cognition and Multimedia Design for Complex Learning. Inaugural address available from the Educational Technology Expertise Center of the Open University of the Netherlands, (1999).
3. Keen, K.: Competence: What Is It and How Can It Be Developed? In J. Lowyck, P. de Potter, & J. Elen (Eds.), Instructional design: Implementation issues. Brussels, Belgium: IBM International Education Center, (1992) 111-122.
4. Birman K.P.: The Next-generation Internet: Unsafe at Any Speed. IEEE Computer, 33(8): 54-60(2000).
5. Johnson E.C.: Security Awareness: Switch to a Better Programme. Network Security, 2(2): 15-18(2006).
6. Kovacich G.L.: Establishing a Network Security Programme. Computer & Security, 15(6): 486-498(1996).

Research on Advanced Distributed Learning by Using SCORM

Ronghui Wu[1], Renfa Li[1], Fei Yu[1,2,3], Guangxue Yue[1], and Chen Xu[1,2,3]

[1] College of Computer & Communication, Hunan University, Changsha 410082, China
wrh@hnu.cn
[2] Jiangsu Provincial Key Laboratory of Computer Information Processing Technology, Province, Suzhou University, Suzhou, 2150063, China
hunanyufei@126.com
[3] Guangdong Province Key Lab of Electronic Commerce Market Application Technology, Guangdong University of Business Studies, Guangzhou,510320, China
Yufei@hunau.edu.cn

Abstract. The Sharable Content Object Reference Model (SCORM) was created to assist the e-learning industry in standardizing the best approaches to creating, storing, transferring and deploying learning content. The Advanced Distributed Learning Initiative(ADL) provides these guidelines consequent to a survey of authoring tools that support SCORM. In this paper, we us SCORM Sequencing Definition model to construct adaptive courseware. At first introduces the architecture of the whole system; Then introduces the way to build adaptive courseware, Finally gives a conclusion.

1 Introduction

The SCORM introduces technical changes in the way authoring tools prepare and package learning content. Beyond the technical changes, the SCORM affects the overall relationship between authoring tools and other key e-learning elements, such as Learning Management Systems (LMSs) and content repositories. This paper is primary to provide insights to authoring tool vendors about key aspects of SCORM.

2 Architecture

Before we utilize SCORM into our courseware , we should make a brief cognition of how it works. As we described in section 1, SCORM 1.3 is mainly consisted of two parts: SCORM Content Aggregation Model and SCORM Run-Time Environment.

2.1 SCORM Content Aggregation Model

SCORM Content Aggregation Model: not only defines the content components of a learning experience but also how to represent the intended behavior of a learning experience (Content Structure) and how to aggregate activities of learning resources

for movement between different environments (Content Packaging). Furthermore, it provides a mechanism for describing specific instances of the components of the content model named meta-data. The basic content objects in SCORM are categorized as Asset and Sharable Content Object (SCO).

The SCORM Version 1.2 Content Aggregation Model, describes three types of SCORM Meta-data: Content Aggregation, SCO and Asset. Any or all of these three types may be contained in two different XML documents: as standalone meta-data (i.e., a single XML document that describes one thing), or embedded in a SCORM manifest. A manifest allows for meta-data to be represented in two ways: in-line or referenced to a file. Meta-data that is part of a manifest is referred to as "in-line" meta-data in the SCORM Content Packaging Information Model.
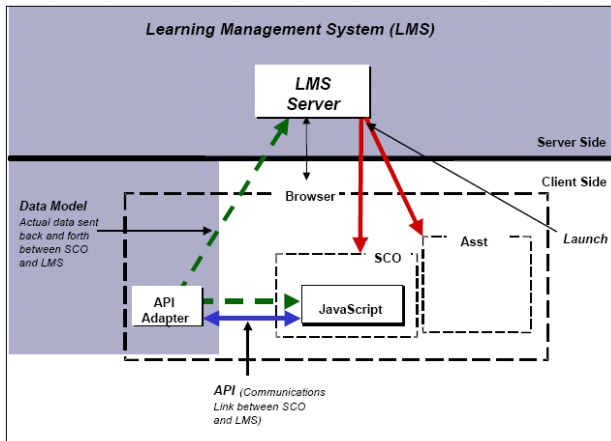
Fig. 1. Shows the system architecture of the SCORM Run-Time Environment and demonstrates how the system is worked

2.2 SCORM Run-Time Environment

SCORM Run-Time Environment defines a common content object launch mechanism, a common communication mechanism between content objects and LMSs, and a common data model for tracking a learner's experience with content objects.

In SCORM 1.3, the SCORM RTE is constructed based on a JSP&Java Servlet-enabled jakarta-tomcat-4.1.24 Servlet Engine and Web server. On the server side , a JSP component is used to dynamically analysis and render the content aggregation file of one specific courseware into a navigation menu which will appears as a series of hyperlinks whose targets contain the corresponding launch locations of SCOs. What's more, there are also several Java Servlet components that are responsible for controlling actual sequencing of SCOs and handling communication between RTE and SCO. While on the client side, a non-face Java Applet is implement as the SCORM RTE API Adapter, which provides the communication to the RTE server-side Servlet components.

3   Construct the Adaptive Courseware

While the ADL provides several useful SCORM utilities and testing tools that are freely available to the public, ADL does not provide a means to directly test authoring tools for SCORM conformance. The following step is to design the activity tree of the whole courseware to achieve the goal of adaptive capacity. Fig.2 shows our design of activity tree of CIS courseware.
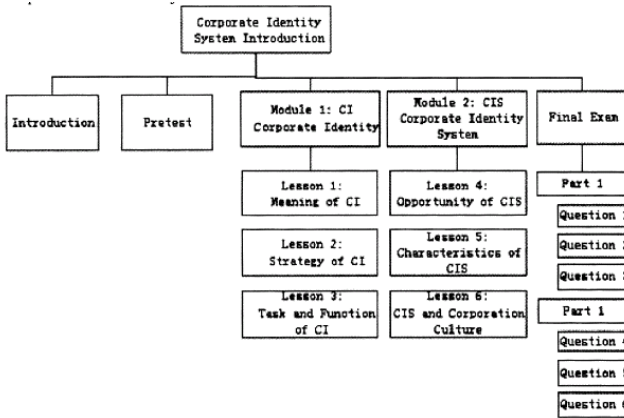

Fig. 2. The activity tree of the CIS courseware

4   System Analysis

The adaptive capacity of a Web-based course is probably the next main issue of the individuals and organizations using E-learning standards to develop coursewares after achieving the goal of reusability and interoperability of the coursewares. This paper introduces a method of constructing courseware by using SCORM Sequencing Model, and shows how to use this model to define required content organizations.

Being conformant with the E-learning standard, it can be reusable and interoperable through the internet which greatly meets the need of exchanging some newly accumulated experience between different organizations. By using the SCORM Sequencing Definition Model, the courseware realizes the adaptive capacity, that is different learners view different content according to their acknowledge level.

5   Conclusion

By using the Sequencing Definition Model, we define more complicated organization of the courseware with the adaptive feature according to various instructional needs. Furthermore, we plan to develop a SCORM-conformant intelligent tutoring system to improve the adaptive characteristics of our Web-based coursewares.

References

[1] Charlton J P,Birkett P E. : An Integrative Model of Factors Related to Computing Course Performance.Education Computing Research,1999,20(3) :237～257

[2] Valverde-Albacete, F.J. Pedraza-Jimenez, R, Cid-Sueiro, J. : An environment for instructional content design based on competences.Proceedings of the ACM Symposium on Applied Computing, 2003

[3] Jun-Ming Su,Shian-Shyong Tseng,Jui-Feng Weng. : An Object Based Authoring Tool for Creating SCORM Compliant Course. Proceedings of Advanced Information Networking and Applications(AINA'2005)

Research on Affective State Recognition in E-Learning System by Using Neural Network

Egui Zhu[1], Qizhen Liu[1], Xiaoshuang Xu[2], and Tinan Lei[1]

[1] Faculty of Education, Hubei University, Wuhan 430062, China
[2] College of Computer Science & Technology, Huazhong University of Science and Technology, Wuhan 430000, China
zhuergui@yahoo.com.cn

Abstract. Aiming at current E-Learning system was not able to estimate the affective state of the users , an intelligent affective state recognizer that used facial expression as input was proposed and implemented in the paper. The recognizer system consists of two neural network classifiers and a fuzzy logic facial analysis module. The recognizer system had been used in an E-Learning system to recognize the emotion state. The results manifested that the recognizer system was effective. However, other bio-signals such as heartbeat, skin resistance and voice tone could also be used for affective state recognition.

Keywords: E-Learning, Neural Network, Affecting Computing, Emotion Deficiency.

1 Introduction

E-Learning uses modern educational technologies to implement an ideal learning environment through integrating the information technology into curriculum, which can embody the learning styles of students' main-body function, reform the traditional teaching structure and the essence of education thoroughly [1].

Although the current E-Learning systems have many merits, many of them only treat advanced information technology as simple communication tools, and release some learning contents and exercises in the network [2]. This kind of movable textbook or electronic textbook is indifferent to the learners, which lacks of the interaction of emotion. Besides, this kind of learning materials without using of the superiority of interactive multimedia technology and displaying the function of network effectively, which leads to the phenomenon of emotion deficiency in the current E-Learning system.

Emotion recognition is one of the most fundamental and important modules. It is always based on facial and audio information. At present, many scholars have carried on a great of researches on facial emotion recognition method. For example, face detection, face recognition, facial feature extraction, and some attempts at automatic facial expression analysis have been made [3] [4]. It is only recently that researchers are starting to integrate these techniques into systems that can make use of the affective state of the user.

The goal of the work presented in this paper is the analysis of people's facial expressions from an image using a combination and extension of existing algorithms. Algorithms for face detection, feature extraction and face recognition were integrated and extended to develop a facial expression analysis system that is used in current E-learning systems. The new facial expression analysis system uses a neural network and fuzzy approach to interpret facial expressions. Although recognizing people's facial expression is a challenging task, it can lead to many exciting developments in human-computer interaction.

2   System Framework

Fig.1 shows the overall framework of the intelligent affective state recognizer. The affective state recognizer is composed of image Grabber, Pre-processing, classification, feature extraction, and interpretation.
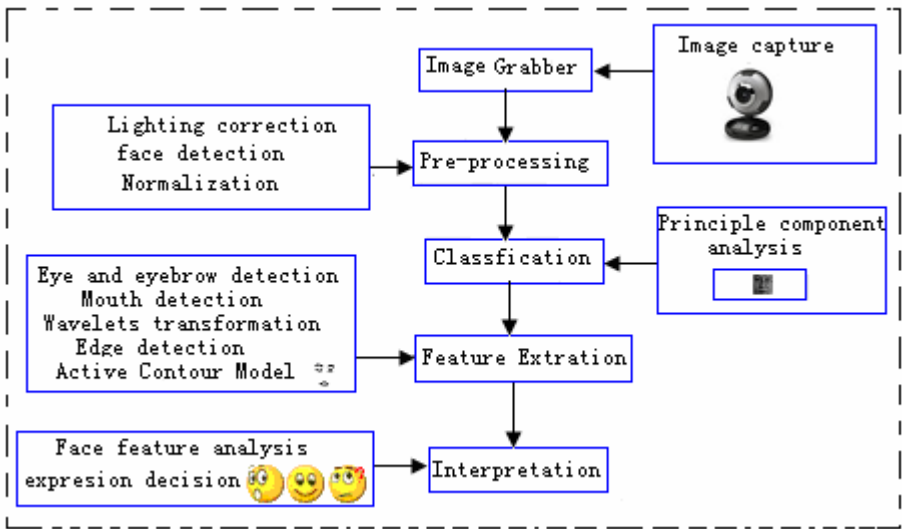
Fig. 1. System Framework

The workflow of system is as follows
The image of the user is captured by a web cam which is then preprocessed by a neural network so that the position of the face in the image is identified. The next phase identifies the user based on the database of known users using principle component analysis. The final two stages consist of a facial feature extraction system based on. Neural networks and an affective state estimator based on fuzzy logic. All of the processing is completed at the client application side of the system. This means that any online implementation of this system will only send the final affective state of the user to the server side of the system providing only a small overhead. This

chapter discusses in detail the two neural network classifiers used for face detection and facial feature location and the fuzzy logic based affective state recognizer.

3 Key Technologies

3.1 Neural Network Based Face Detection

A sixteen by sixteen pixel sub-sample of the web cam image is selected and examined to see if it is the region of the face. This is repeated for all sub-samples choosing the best candidate face for further processing. A neural network approach is adopted, in which the 256 pixel sub-sample image is given as input to a neural network that has been trained to identify face images. There are 256 neurons as input, 40 neurons in hidden layer one, 16 neurons in hidden layer two, and one output neuron. The transfer functions are tan-sigmoid functions. The training data is taken from standard face databases so that it is robust to variations in race, gender and age.

3.2 Eye Detection

Similar to face detection, a neural network was used to detect people's eyes. An eye database was extracted from the face database that was use for face detection. The eyes were normalized to the same size and with the iris in the centre of the eye image. A feed-forward back-propagation network was created for face detection. The network is a 3 layers-structure. It has 2 hidden layers and 1-output layer. It also has 1 layer for input. Each eye image is 18 pixels in width by 12 pixels in height forming a rectangular image. So, there are 216 neurons as input, 8 neurons in hidden 216 inputs 8 hidden neurons 4 hidden neurons 1 output layer 1, 4 neurons in hidden layer 2, and 1 output neuron. The transfer functions are tan-sigmoid function. Using this approach the exact position of the eyes in the image can be identified as well as the candidate point for the eyebrows since they are invariably above the eye for an upright full frontal image of the face.

3.3 Mouth Detection

Mouth detection is challenging because of the difficulty in modeling the shape of mouth. Firstly, the lighting of the mouth region is corrected locally. Secondly, noise in the mouth region of the image is eliminated using a wavelet transformation algorithm. Thirdly, Sobel edge detection combined with Laplacian edge detection is used followed by a morphing logic operation to fill in the holes. The largest blob found by this procedure is the mouth. Once the mouth has been identified candidate points for the mouth outline are available[5] [6].

4 Conclusion

An intelligent affective state recognizer that used facial expression as input was proposed in the paper. The facial expression analysis system implemented is based on a fuzzy approach. Six expressions, namely, happiness, anger, surprise, sadness, puzzled

and disgusted are detected. Fig.2 shows the affective state recognition software. The bars in the boxes to the right of the image show the result of the intelligent expression analysis. The longest bar is the best value and if it is significantly larger the other remaining values a conclusive decision on the affective state of the user can be estimated.
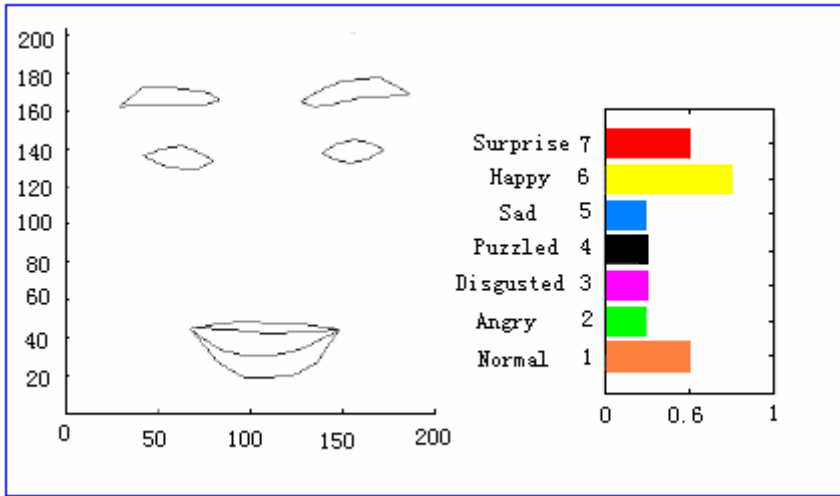

Fig. 2. Affective State Recognition Software

References

1. He Kekang.: E-Learning Essence- information technology into curriculum. E-education Research, 105, 1, 2002, 3-4.
2. Wang Jijun.: Emotion deficiency and compensation in distance learning. Chinese network education, 2005.
3. R.W.Picard.: Affective Computing. Cambridge. MIT Press, 1997.
4. R.W.Picard.: Affective Computing, Challenges. Cambridge. International Journal of Human Computer studies, 59(1), 2003, 55-64.
5. X. Li and Q. Ji.: Active Affective State Detection and User Assistance with Dynamic Bayesian Networks. Proceedings of Bayesian Modeling Applications Workshop, 2003.
6. M. Pantic and L.J.M. Rothkrantz.: Automatic Analysis of Facial Expressions, the State of the Art. IEEE Transactions on Pattern Analysis and Machine Intelligence, vol. 22, 2000, 1424-1445.

One Learning and Teaching Tool for Preliminary Virtual Instrument Course

Yongkai Fan[1], Tianze Sun[1], Xiaolong Fu[1], Jun Lin[2], and Yangyi Sui[2]

[1] Computer and Information Management Center, Tsinghua University, Beijing 100084,
Haidian District, China
{fyk, stz,fuxiaolong}@cic.tsinghua.edu.cn
[2] Instrument Science and Electronic Engineering College, Jilin University, Changchun 130026,
Jilin, China
{lin_jun, syy}@jlu.edu.cn

Abstract. This paper presents one teaching and leaning assistant tool with the purpose of reinforcing both teaching process and learning process for introductory virtual instrument course. This tool has two main ends: from the teacher's viewpoint, the tool gives preliminary introductory information and foundational theory related the course which will help reinforce lecture and laboratory session, therefore, teacher can save time to pay more attention to personalized education for different student; from the students' viewpoint, it providing a leaning environment which equipped with help, collaborative learning group, communication tool, all of those which can facilitate their personal work and make them more motivated to involved in course session.

Keywords: Teaching and leaning assistant tool; Preliminary Virtual Instrument Course; Leaning environment.

1 Introduction

The importance of virtual instrument in measurement and instrument filed results in it as a compulsory course appeared in engineering students' curriculum. Virtual instrument programming environment, tool, and even graphic languages rush to support the process of learning virtual instrument. However, students still find learning and programming a virtual instrument is a difficult subject, especially for the beginner. It is said that practice is the best "teacher" for beginner. This Paper describes an experimentation practice platform to meet the needs. The platform is such an e-learning platform for providing test and measurement experimentation, which is based on some distributed measurement hardware resources, and for providing experience sharing means. The end of this platform is to providing student one tool to study virtual instrument and teacher one tool to teaching. This platform consists of four parts: the manager server, the web server, experiment resources, and client software for students. The platform is described in terms of its architecture and an example is illustrated. Further work is outlined in corresponding parts and the conclusions are given in the end.

2   Platform Architecture

The architecture of e-learning platform is showed in Fig. 1. The architecture is mainly composed of four parts: the manager server, the web server, experiment resources, client software and other accessories part.

   The manager server: special software runs on the manager server act as a connector between client software and experiment resources. It is the vital part of the e-learning platform, which acts as the gap between client software and experiment resources. It hides the technical details from the users and provides users a transparent connection to experiment resources. On the one hand, the manager server software receives experiment resources registration information and stored information into database. On the other hand, the manager server software broad those experiment resources' information when new experiment resource joining in or the manager server send those experiment resources' information when a user connect to it. Also, the manager server software is a central server responsible for responding to events, such as registration, requiring, data receiving, translating, dispatching and etc, and performs the controlling functionalities and manipulating the underlying logic connection. The screen snapshot is shown as fig 2.
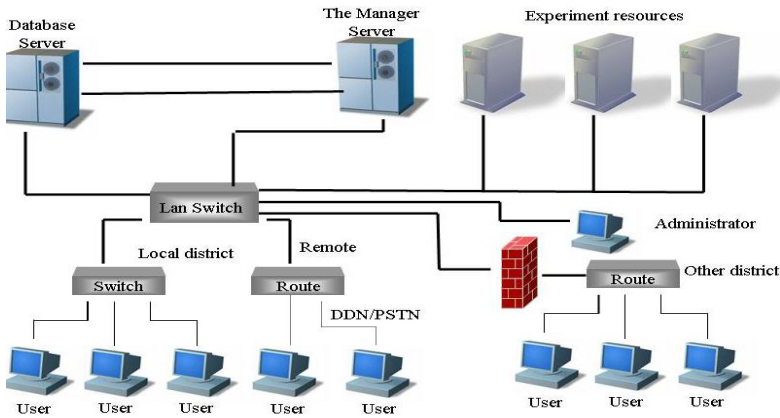
Fig. 1. The architecture of e-learning platform. The web server and the software for manager server share same computer.

   Experiment resources: experiment resource is an extensive concept. It refers instrument-equipped computer. The most common used measurement instrument is one data acquisition device. Various sensors connected to the data acquisition device can be treated as one type of experiment resource. The instrument equipped computers are directly connected to instruments in order to measure physical quantities. From the manager server's viewpoint, different experiment resource is the different computer connection. Experiment resources can be located everywhere on the network, but physical connections and access authorizations are given to every legal user.

   Client software: with the intention of offering greater convenience to the user, including three different levels user (on-campus user, off-campus users, and distance

users), client software offers user a friendly and convenient entry to experiment resources. This allows any user to easily install client software in his client computer, connect international network and then can access the instrumentation components (data acquisition devices) from the experiment resources without taking any pains.

The web server: the web server mainly possesses two functions. The first one is electronic forum in which users, whether on campus, off campus or distance user, can login and join to discuss problem they meted met during the process of experiment, the second one, also is the most important one, is sharing experience and normal knowledge. The web server is an assistant for user who wants to get some instruction or documents.

Others: There are special users who are responsible for the maintaining and managing the platform or experiment resources presented as administrator in this architecture, the administrator run corresponding administrator software to monitor and mange the e-learning platform. Firewall and gateway is used to protect server, user operations are controlled through verification of the password or the IP address either of the client or the gateway through which the client connects to the server; Database server is deployed for modeling and storing information needed.

Fig. 2. Screen snapshot of software run on the manager server

3 Process of Doing Experiment and Experience Sharing

To explain the practice process, a simple measurement process is provided by a step-by-step explanation.

1. Firstly, the platform's database should start up and prepare for the whole system, the software running on manager server initializes itself and gets ready to receive event from client connection or experiment resources connection.

3. When experiment resources are ready for providing instrument connection, they advertise their IP address and functionalities to the manager server for registration.

4. A user with client software runs client software on his/her own personal computer in which a client workbench is presented on screen, showing in fig. 3.

5. The manager server will receive a login-request event with a data packet in which user's information and then begin verify process. If authorized, user can select a data acquisition component, for example, on receiving this packet, the manager

server first assure user's access privilege to the experiment resource to which user want and then decided whether sending user's request to homogenous experiment resource or declining user's request with reasons.

6. When an experiment resource server received a request, it will accept and build a connection with the user. After acquiring data from equipped measurement instrument, experiment resource delivers the sampled data directly to the user who send request. User can do some analysis and process through corresponding software components.
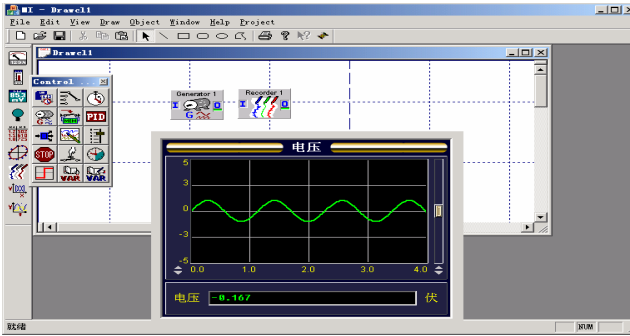
Fig. 3. Screen snapshot of client workbench

4   Evaluation and Conclusion

Hands-on experiments have become an important consideration in measurement technologies education. In this paper, one e-learning platform based on distributed measurement hardware resources is presented for education and experience sharing purposes. Though there are many problems, which were found in test phase, should be tackled with, the platform as an accessory experimentation environment provides an effective approach for measurement technologies education according to the test results from individual students. Also, the comparison result of studying effect between students who use this tool before attending virtual instrument class and students who without using this tool indicates that this tool is effective.

Research on Personalized Community E-Learning Recommendation Service System by Using Adaptive Filtering Algorithm

Liang Zhao[1] and Qi Luo[2,3]

[1] School of Mechanical and Electronic Engineering, Wuhan University of Technology,
Wuhan 430070, China
[2] Information Engineering school,
Wuhan University of Science and Technology and Zhongnan Branch,
Wuhan 430223, China
[3] College of Engineering and Technology, Southwest University,
Chongqing 400715, China
Hejm2000@163.com, Ccnu_luo2008@yahoo.com.cn

Abstract. To meet the needs of education in the learning community, an adaptive filtering algorithm for teaching resources based on vector space model was proposed in the paper. First, feature selection and pseudo feedback were used to select the initial filtering profiles and thresholds through training algorithm. Then user feedback was utilized to modify the profiles and thresholds adaptively through filtering algorithm. The algorithm had two advantages, the first was that it could carry on self-study to improve the precision; the second was that the execution did not need massive initial texts in the process of filtering. The result manifested that the algorithm was effective.

Keywords: Adaptive Filtering Algorithm, Vector Space Model, Personalized Community E-learning Recommendation Service.

1 Introduction

With the increase of computers and network, people pay more and more attention in community E-learning. E-learning can break through the limit of space and time, reduce learning cost and improve learning efficiency. Therefore, many community websites based on E-learning have also been constructed; community residents can get some information or some study courses. But the application of these websites is difficult to attract community resi-dents' initiative participation [1]. The investigation indicates that personalized recommendation service system is imperfect. If the community E-learning wants to attract residents, the idea of personalized design should be needed. It means that the personalized knowledge and information service should be recommended according to residents' needs.

At present, many scholars have carried on a great deal of researches on filtering algorithms, such as traditional batch filtering algorithm [2].But those algorithms have some disadvantages, For example, it needs massive initial training texts, yet the preci-

sion and the recall is low [3]. According to this, an adaptive filtering algorithm for teaching resources based on vector space model is proposed in the paper. It has improved the traditional algorithm and introduced adaptive feedback study mechanism in intelligence control. The advantage of the algorithm is that it can carry on self-study to improve the precision, and the execution does not need massive initial texts in the process of filtering.

2 Adaptive Filtering Algorithm

Adaptive filtering algorithm based on vector space model is composed of two steps.

Step1: training phase. The task of training stage is to get the initial filtering profile and set the initial threshold.
Step2: adaptive filtering phase. In adaptive filtering, the main task is to modify the profile and threshold adaptively.

2.1 Training Stage

Fig.1 shows the architecture of the training stage. At first, feature vectors are extracted from positive and pseudo-positive documents. The pseudo-positive documents are those that have high similarity with the topic but haven't been labeled as positive documents in the training set. The pseudo-positive documents can be obtained by several ways. We can get pseudo-positive documents by pseudo feedback. We also can get the pseudo-positive documents by using the hierarchy of categories: a topic's pseudo-positive documents are those that have the same high-level categories provided by the training set.

To get the feature vectors, we first remove stop-words and do morphological analysis on remaining words. Then, we compute the logarithm mutual information between words and topics [4]. The formula 1 is shown as follows:

$$\log MI(w_i . T_j) = \log(\frac{p(w_i/T_j)}{p(w_i)}) \tag{1}$$

Where w_i is the i-th word and T_j is the j-th topic. Higher logarithm mutual information means w_i and T_j are more relevant. $p(w_i/T_j)$ and $p(w_i)$ are estimated by maximal likelihood method.

After gotten the feature vectors of positive and pseudo-positive documents, we merged them into the initial profile. The initial profile is the weighted sum of positive and pseudo-positive feature vectors. Then we should set initial threshold for each topic. The initial threshold is set based on the similarity of each document in the training set . The similarity between a profile and training document is computed by the cosine formula 2.

$$Sim(d_i, p_j) = \cos\theta = \frac{\sum_k d_{ik} p_{jk}}{\sqrt{\sum_k d_{ik}^2 \sum_k p_{jk}^2}} \tag{2}$$

Where p_j is the profile vector of the j-th topic and d_i is the vector representation of the i-th document. d_{ik} is the weight of the k-th word in d_i. d_{ik} is computed as formula 3.

$$d_{ik} = 1 + \log(tf_{ik} avdl / dl)$$ (3)

Where tf_{ik} is the term frequency of the k-th word in the i-th document, the dl is the document length counted by tokens in the document after morphological processing and stop-words removal, the $avdl$ is the average document length gotten from training set. According to the similarities of training documents, each initial threshold is set to get the best filtering performance.
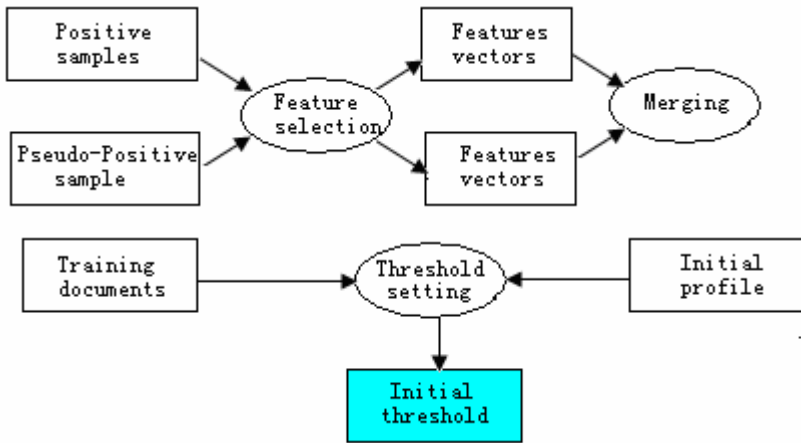
Fig. 1. Architecture of the training stage

2.2 Adaptive Filtering Architecture

Fig.2 shows the architecture of adaptive filtering. When a document arrives, its similarity with the topic profile is calculated. If its similarity is higher than the current threshold, then this document is retrieved and the user's relevance judgment is gotten.

   If the document is really relevant to the topic, it will be considered as positive sample, otherwise negative sample. The vectors of positive and negative samples will be used to modify the topic's profile, which is shown in formula 4.

$$p_j' = p_j + \alpha p_j(pos) + \beta p_j(neg)$$ (4)

Where p_j' is the topic's profile after modification, p_j is the topic's profile before modification, $p_j(cos)$ is vector of positive samples gotten at this updating interval while $p_j(neg)$ is vector of negative samples; α and β are the weight of positive and negative vectors respectively.
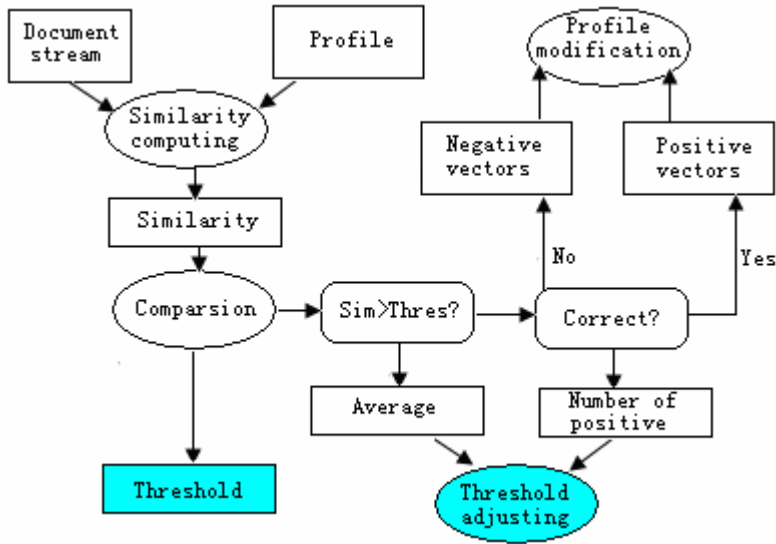
Fig. 2. Architecture of the adaptive filtering

3   Conclusion

In summary, a new adaptive filtering algorithm for community E-learning based on vector space model is proposed in the paper. The results manifest that the algorithm is effective through testing in personalized recommendation service system based on community E-learning.

References

1. Yanwen W. and Zhonghong W.: Knowledge Adaptive Presentation Strategy in E-Learning. Proceedings of Second International Conference on Knowledge Economy and Development of Science and Technology, Beijing, 2004, 6-9.
2. Lawrence R D, Almasi G S, Kotlyar V, et al.: Personalization of Supermarket Product Recommendations. Special Issue of the International Journal Data Mining and Knowledge Discovery, Vol.5, 2001, 11-32.
3. Nie Xin.: Take about the Digital Individualized Information Service of Library. Information Science Journal, vol.23, 2005, 1-5.
4. Robertson S and Hull DA.: The TREC-9 filtering track final report. Proceedings of the 9th Text Retrieval Conference. Gaithersburg, 2001, 25-40.

Research on Personalized E-Learning System Using Fuzzy Set Based Clustering Algorithm

Feng Lu[1,2], Xin Li[1,2], Qingtang Liu[1], Zongkai Yang[1], Guoxin Tan[1], and Tingting He[1]

[1] Engineering & Research Center for Information Technology on Education, Huazhong Normal University Wuhan 430079, China
[2] Science and Technology of Education Department, Hunan University Of Science and Engineering Yongzhou 425100, China
lufengmaster@126.com

Abstract. Personalized service is becoming increasingly important, especially in E-learning field. Most personalized E-learning systems only take learners preferences, interests and browsing behaviors into consideration. These systems usually neglect considering whether the learners ability and the difficulty level of recommended learning materials are matched to each other or not. This paper proposes a personalized E-learning system using fuzzy set based clustering algorithm which considers both course materials' difficulty and learners' ability to provide appropriate learning stuffs for learners individually, to help learners learn more efficiently and effectively.

Keywords: Difficulty level; Learner ability; Fuzzy clustering algorithm.

1 Introduction

As the Internet gains wide popularity around the world, high diversity of the learners on the Internet brings new challenges to the traditional "one-size-fit-all" learning model [1]. So it's of great importance to provide a personalized system which can automatically adapt to the interests and levels of learners' ability.

Cluster analysis is a technique to divide the data set in such a way that cases assigned to the same cluster should be as similar as possible whereas two objects from different clusters should be as dissimilar as possible[2]. In the proposed system, we strive to model learners' ability to group similar learners into homogeneous classes, and the fuzzy clustering algorithm is a good choice which we adopt.

2 Personalized E-Learning System

2.1 System Architecture

In the proposed personalized E-learning system, there are five layers. Database layer consists of user account, course and user profile databases. The user account database records the basic information. The user profile database contains learners' trajectory. The course database contains the course materials and their corresponding difficulty

levels. Users' feedback acquisition layer consists of questionnaire, quiz and behavior record. Through the questionnaire and quiz after each material, system can collect the main information of the learners' ability and the materials' difficulty level. Through the record of the learners' behavior, it can provide the system with the proof of the feedback and the information of the learners' ability and preferences. Data mining and inference layer is to extract and infer the materials' difficulty level and the learners' ability from the data of database layer. Recommend and push layer uses the learners' new abilities to select appropriate course materials for learners individually. Presentation layer provides a register, login, searching and browsing interface to let the users become registered ones, help learners retrieve specified course materials.

2.2 The Key Techniques and Algorithms

2.2.1 Calculate Difficulty Parameters of Course Materials Dynamically

The course materials' difficulty level is classified into five points: {very hard, hard, moderate, easy, and very easy}, depicted as Dif_1, Dif_2, Dif_3, Dif_4, Dif_5 [3]. D_{exp} denotes the experts' decision of material difficulty level, which can be calculated in formula (1).

$$D_{exp} = \sum_{n=1}^{5} \frac{C_n}{C_{experts}} D if_n \cdot \tag{1}$$

Where C_n denotes the number of experts that select the difficulty level of Dif_n, $C_{experts}$ denotes the fixed number of experts, as a constant here.

The materials difficulty parameters assessed by the learners and teachers can be calculated by formula (2), marked as D_{stu} and D_{tea} respectively.

$$D_{stu} = \sum_{m=1}^{5} \frac{C_m}{C_{learners}} D if_m \; , \; D_{tea} = \sum_{j=1}^{5} \frac{C_j}{C_{teachers}} D if_j \cdot \tag{2}$$

Where C_m/C_j denotes the number of learners/teachers that select the difficulty level of Dif_m/Dif_j, $C_{learners}$/$C_{teachers}$ denotes the number of learners/teachers who have already studied/used the course material.

The adjusted difficulty parameter of a certain material is calculated by formula (3):

$$D = w_1 \times D_{exp} + w_2 \times D_{tea} + (1 - w_1 - w_2) \times D_{stu} \cdot \tag{3}$$

Where w_1 and w_2($0<1-w_1-w_2<w_2<w_1<1$) denote the weight of the course difficulty parameters the experts recommend and the teacher users decide respectively.

2.2.2 Estimate the Level of Learner Abilities

In E-learning systems, there are many variables that determine the learners' ability. Herein, we just consider the most important ones. We form a factor set for the system, which is depicted as: $U=\{u_1,u_2,u_3,u_4,u_5\}$, in which u_1 denotes the time spent on each material, u_2 denotes questionnaire feedback after each material, u_3 denotes quiz feedback after each material, u_4 denotes times clicking on antecedent material links, u_5 denotes random mouse move and click. The weight set can be depicted as: $W=\{w_1,w_2,w_3,w_4,w_5\}$, which we adopts the value as $W=\{0.2, 0.35, 0.3, 0.1, 0.05\}$.

(1) u_1: the time spent on each material, with the weight w_1.

The assessment set of u_1 is depicted as V_1= {very long, long, moderate, short, very short}, the corresponding weight set is depicted as A={a_1,a_2,a_3,a_4,a_5}. T_i represents a learner's browsing time on a certain material. We compute the learners' average browsing time on a certain material [4], depicted as formula (4).

$$\overline{T} = \frac{T_1 + T_2 + \cdots + T_n}{n} = \frac{\sum_{i=1}^{n} T_i}{n} \quad . \tag{4}$$

Where n represents the total number of learners that has browsed the certain material. Notably, the T_is which are too big and too small are excluded.

Then we can use statistic method to calculate the ratio of each assessment element in assessment set V_1 for a certain material. We defined the time range as formula (5):

$$T_{range} = (1+b) \times \overline{T} , \quad (b = \frac{T - \overline{T}}{\overline{T}}) \tag{5}$$

The variable b denotes the bias of the time period. The membership degree of different time range corresponding to V_1 is defined as formula (6):

$$a_1 = \frac{1_{T_1} + 1_{T_2} + \cdots + 1_{T_i}}{n}, (c_1 \le b \le c_2, (T_{range} \mid b = c_1) \le T_i \le (T_{range} \mid b = c_2)) . \tag{6}$$

Where a_1 denotes one of the assessment set element {very long}, $T_1, T_2,\ldots, T_i$ denote the learners that consume the time between $T_{range}|b=c_1$ (computing T_{range} when $b=c_1$) and $T_{range}|b=c_2$, the numerator $1_{T_1} + 1_{T_2} + \cdots + 1_{T_i}$ denotes the number of a group of learners of fore mentioned kind, n denotes the total learners that has browsed the material. Notably, the constant c_1 and c_2 in formula (6) are as cutoff point; their values are acquired through experiment. The other weight calculation method resembles a_1's, where the value b is differentiated every time.

(2) u_2: questionnaire feedback after each material, with the weight w_2.

The assessment set of u_2 is depicted as V_2={completely understand, understand, moderate, little of understanding, completely not understand}, and its corresponding weight set is depicted as B={b_1,b_2,b_3,b_4,b_5}. We use the statistic method to calculate the ratio of each assessment element in assessment set V_2 for a certain material.

(3) u_3: quiz feedback after each material, with the weight w_3.

The assessment set of u_3 is described as V_3={very good, good, moderate, bad, very bad}, and its corresponding weight set is depicted as C={c_1,c_2,c_3,c_4,c_5}. The calculation method of the weight set of C resembles the B's fore mentioned.

(4) u_4: times clicking on antecedent material links, with the weight w_4.

The assessment set of u_3 is described as V_4={very many, many, moderate, few, very few}, and its corresponding weight set is depicted as D={d_1,d_2,d_3,d_4,d_5}. The calculation method of the weight set of D resembles the one of B fore mentioned.

⑸ u_5: random mouse move and click, with the weight w_5.

The assessment set of u_3 is described as V_5={very many, many, moderate, few, very few}, with its weight set E={e_1,e_2,e_3,e_4,e_5}. The calculation method of E resembles the ones of u_1 and u_4. Herein, we don't mention any more about the algorithm.

Now, we can calculate the learners' abilities. Just take one group of data for example. The factor weight set W={0.2, 0.35, 0.3, 0.1, 0.05}, assume that we have the result data of a learner X, whose vector set is calculated already, his/her vector set result is v_x=(0.9,0.5,0.8,0.8,0.8). The learner X's ability is calculated as formula (7):

$$X_{ability} = W \times v_x = 0.715 \ . \tag{7}$$

Before we rank the learner X's ability level, we have to classify the number 0～1 into five points: {Very high ability, high ability, moderate ability, low ability, very low ability}. Herein, X's ability result is 0.715, is between the {high ability} thresholds from the system inference.

After reevaluates learners' abilities and recalculates the course materials difficulty levels, the system can recommend materials to learners based on learners' ability.

3   Conclusion

The system provides personalized learning according to course materials visited by learners and their responses, the experiment results show that the proposed system precisely provides personalized course material recommendations based on learners ability, and moreover accelerate learners' learning efficiency and effectiveness.

Acknowledgement

References

1. Li X, et al.:A Personalized E-learning System Based on User Profile Constructed Using Information Fusion. DMS'2005
2. Döing C, Lesot M.J, Kruse R. :Data analysis with fuzzy clustering methods. Computational Statistics & Data Analysis 51(2006)192 – 214
3. Chen C.M., et al.: Personalized E-learning system using Item Response Theory. Computers & Education 44 (2005) 237–255
4. Huang C.J., et al. :Implementation and performance evaluation of parameter improvement mechanisms for intelligent E-learning systems. Computers & Education (2005)

Building a Fuzzy Ontology of Edutainment Using OWL

Hua-Mao Gu[1,2], Xun Wang[2], Yun Ling[2], and Jin-Qin Shi[3]

[1] College of Computer Science, Zhejiang University, 310027 Hangzhou, China
[2] College of Information, Zhejiang Gongshang University, 310018 Hangzhou, China
[3] College of Food, Zhejiang Gongshang University, 310018 Hangzhou, China
{ghmsjq, wx, yling, shijinqin}@ mail.zjgsu.edu.cn

Abstract. OWL Web Ontology Language is a W3C recommended Language for representing machine-readable knowledge with more facilities than other knowledge representation languages. In this paper, we present a Use-Case based Fuzzy Ontology Constructing (UFOC) methodology for the building of edutainment ontology, which is encoded with OWL. Besides, a solution of representing fuzzy relation in OWL is also provided. In the edutainment ontology, two fuzzy relations, DE and AE are discovered, both playing vital roles in property calculation among online computer game.

Keywords: Fuzzy Ontology; Edutainment; OWL; Ontology Building.

1 Introduction

Computer games have gained great popularity in recent years, especially within teenagers. Along with prevalence of games, some intelligent scholars realized the significant influence of games on teenagers, and hoped for the combination of game and education. Under such situation, the project "Educational Game for Middle & Primary School Students" (EGMPSS) was carried out, aiming at making students "Learning in playing".

As a widely accepted knowledge representation model, ontology has been used and taken a key role in many software applications. An increasing number of researchers realized, however, the difficulty of describing uncertainty knowledge in ontology. To approach this problem, some pioneers incorporated fuzzy logic into ontology in some domains [1] [2].

Although there are already some papers concerning Ontology building [3], no paper describes how to build Fuzzy Ontology so far. And as a way of representation of knowledge, Ontology has not been applied to game domain yet, not to speak of edutainment. So, the main goal of this paper is providing not only a methodology of building Fuzzy Ontology, but also the Fuzzy Ontology of edutainment itself.

The rest of this paper is organized as following. Section 2 presents some related definitions of Edutainment Fuzzy Ontology. Section 3 gives the way of representing Fuzzy Relation in OWL. Section 4 introduces the UFOC methodology. Section 5 provides a simplified case study. Finally, section 6 concludes this paper and discusses some future work.

2   Fuzzy Ontology of Edutainment

Firstly, we give some formal definitions related to Edutainment Fuzzy Ontology based on Fuzzy Set theory [4] and our research before going ahead.

Definition 1: Fuzzy Relation. A Fuzzy Relation R is a set of triples $\{<x, y, \mu_R(x,y)>$ | $x \in X, y \in Y\}$. The $\mu_R(x,y)$ is a membership function mapping from universe of discourse $X \times Y$ to real number region [0,1]. For every $x \in X, y \in Y$, $\mu_R(x,y)$ denotes the membership degree of relation R between x and y.

Definition 2: Damage Effectiveness. Damage Effectiveness (DE) is a Fuzzy Relation between Intelligence and Strength, which means the degree of fitness of the proportion among them. In EGMPSS, the damage to monster is affected by the player's Intelligence and Strength, and vice versa.

Definition 3: Armor Effectiveness. Armor Effectiveness (AE) is a Fuzzy Relation between Intelligence and Dexterity, which means the degree of fitness of the proportion among them. In EGMPSS, the defense against attack is affected by the player's Intelligence and Dexterity, and so does Monster.

Definition 4: Fuzzy Ontology. Fuzzy Ontology in EGMPSS is an extended Domain Ontology, denoted as $\{C, I, R_{ex}\}$. Here, $C = \{C_1, C_2, \ldots, C_m\}$. I is a set of instances of the concepts in C. $R_{ex} = R_n \cup \{DE, AE\}$ where R_n is a set of binary relations among C and I of the domain.

3   Representation of Fuzzy Relation in OWL

According to the above definition, Fuzzy Ontology is an extension of domain ontology. Then, how to represent the membership degree in OWL (or other representation languages) will be an urgent problem to be solved before Fuzzy Ontology could be put to use.

   First thought is to extend owl:DatatypeProperty to allow for two domains at the same time. It, however, is impractical. A feasible solution is to build a concept of Fuzzy Relation, which includes two owl:ObjectPropertys: "domain-1" and "domain-2", and one owl:DatatypeProperty: "hasFuzzy_Degree". The two domains denote two universes of discourse in Fuzzy Relation, and "hasFuzzy_Degree" means the corresponding membership degree. Whenever there is a need of an element of Fuzzy Relation, create an instance of this concept and assign specific values for each property.

4   Use-Case Based Fuzzy Ontology Constructing Methodology

There are many suggestions for building domain ontology [5]. Fuzzy Ontology, however, is an extended domain ontology, which involves Fuzzy Information processing. For this purpose, we present a Use-Case based constructing methodology.

The main processes of this methodology are explained as follows.

(1) Use-Case: the basis for guiding ontology construction.
(2) Objects Enumeration: enumerating all objects that may occur in domain.
(3) Categorization: categorizing objects into different concepts.
(4) Concept Tree: reorganizing concepts with "is-a" relation.
(5) Attributes Discovery: discovering appropriate attributes for each concept.
(6) Pruning: eliminating those unnecessary concepts and attributes.
(7) Relations Discovery: finding other right relations among concepts.
(8) Instances Creating: creating necessary individuals for ontology.
(9) DE, AE: building elements of DE and AE from relative individuals.

5   Case Study: The EGMPSS Ontology

In this section, we just give the Use-Case diagram and the hierarchy of core concepts in the EGMPSS due to the restriction of page in length. Both of them may cooperate to present a full picture of the EGMPSS ontology.

5.1   Use-Case Diagram of EGMPSS

In EGMPSS, there are three actors: PC, NPC and Monster. According to the requirements of EGMPSS, we present a Use-Case diagram in Fig. 1.
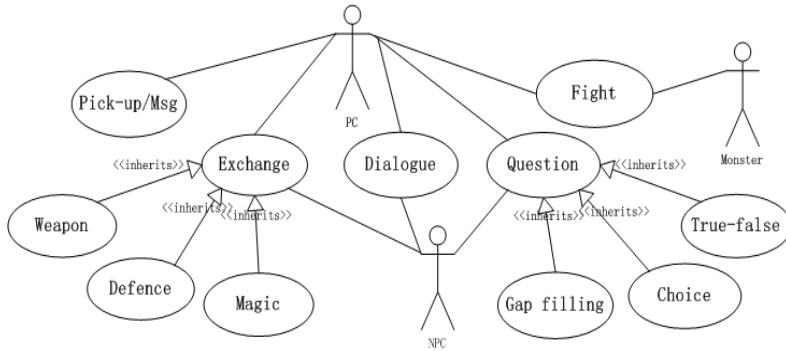
Fig. 1. The Use-Case diagram of EGMPSS

From this diagram, we know that (1) PC can talk to NPC by dialogue to learn knowledge, (2) PC may pick up treasures and read some messages (some knowledge points), and (3) NPC may ask questions in the form of gap-filling, choice and true-false. Questions, dialogues and messages provide full knowledge appeared in the textbooks of middle and primary school, and etc.

5.2   Core Concepts Hierarchy

As EGMPSS is an educational game, naturally, there should be two main series of concepts, one for game, and the other for education. Reflected in concept tree, there are two branches from the top concept, as shown in Fig. 2.
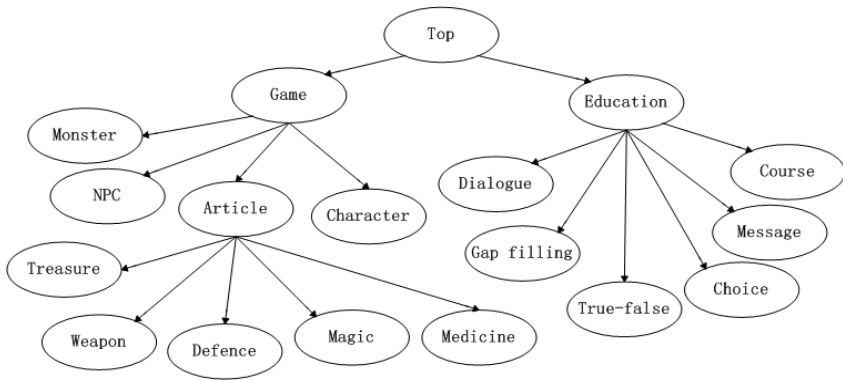
Fig. 2. The hierarchy of Core concepts in EGMPSS Ontology

In the Game branch, all leaves are not the ends of concept tree. They all should be derived out more special concepts. For instance, there are certainly some kinds of monsters, each kind being a concept. And so do other leaves. While in the education branch, each concept leaf means one mode for providing knowledge. There is no need to be further subdivided.

6   Conclusions

In this paper, we have proposed a Use-Case based methodology for constructing Fuzzy Ontology, and provided a Fuzzy Ontology that has come into use in EGMPSS. Besides, representation Fuzzy Relation in OWL is also introduced. All these work would be much useful for guiding Fuzzy Ontology building to engineers.

However, there are still some problems to be solved. For example, establishing inference rules on Fuzzy Ontology to enable intelligent query and making the Fuzzy Ontology well accepted are all important and beneficial work.

References

1. Lee C.S, Jian Z.W., Huang L.K: A Fuzzy Ontology and Its Application to News Summarization. IEEE Transactions on Systems, Man and Cybernetics. 35 (2005) 859 – 880
2. Quan T.T, Siu C.H, Cao T. H: Automatic Fuzzy Ontology Generation for Semantic Web. IEEE Transactions on Knowledge and Data Engineering. 18 (2006) 842 – 856
3. Stevens R., Goble C., Horrocks I., Bechhofer S.: Building a Bioinformatics Ontology Using OIL. IEEE Trans. Inf. Technol. Biomed. 6 (2002) 135– 141
4. Zadeh L. A.: Fuzzy sets. Information and Control. 8 (1965) 338 – 353
5. Jones D., Bench-Capon T., Visser P.: Methodologies for ontology development. In : Proc. IT&KNOWS Conference, XV IFIP World Computer Congress. Chapman-Hall London (1998) 62 – 75

A Modeling and Assessing Method Based on Bayesian Networks

Zhi Liu and Jie Jiang

Software College, Zhejiang University of Technology
Hangzhou, China, 310032
`lzhi@zjut.edu.cn`

Abstract. In order to give adaptive instruction to the learner, it needs to know what knowledge the learner has and what goals the learner is trying to archive. This paper proposes a method to build a model based on Bayesian networks in order to assess the learner's knowledge level. An overlay student model based on Bayesian networks is presented. This student model built on knowledge relationships with prediction ability is discussed in details. In this model, an assessing method based on Logistic model in IRT with three parameters is provided to evaluate student's performance. A case study in the course of Data Structure is illustrated in this paper.

Keywords: Modeling, Assessing, Bayesian networks.

1 Introduction

In the e-learning field, many researchers have focused on how to instruct the learners in order to support them adaptive learning. Because the learners' backgrounds are different and what goals they are trying to archive are different, they need to be instructed individually in the e-learning system. In order to assess the learner, we propose an effective student modeling method using overlay model to represent the beliefs for the student's knowledge. In this model, the student's knowledge is regarded as the subset of expert's knowledge. The expert's knowledge can be divided into various knowledge items in different levels. The student model is used to represent the understanding degrees on those knowledge items. The teaching goal is to reduce the difference between the expert's knowledge and student's knowledge.

2 Student Modeling Method

In this paper, we analyze and build the student model in the course of Data Structure. Each type of data structures has its various applications based on its characteristics. Here, we describe the various knowledge items in the unit of Binary Tree in table 1.

There are two kinds of relationships between knowledge items: organization relationships and dependency relationships. Combining these two structures, we can build the student model based on knowledge relationships in figure 1.

Table 1. The knowledge items in the unit of Binary Tree

Node	Knowledge item	Node	Knowledge item
BTKU	Binary Tree Knowledge Unit	BTT	Binary Tree Traversal
BTC	Binary Tree Concept	LT	Binary Tree Level Traversal
BTE	Binary Tree Establish	LA	Level Traversal Application
CBT	Complete Binary Tree	PIPT	Pre/In/Post order Traversal
BTCH	Binary Tree Character	PIPA	Pre/In/Post order Traversal App
BTD	Binary Tree Definition	QUU	Queue Knowledge Unit
BTSS	Binary Tree Sequential Storage	STU	Stack Knowledge Unit
BTCS	Binary Tree Chained Storage	CHU	Chain Knowledge Unit
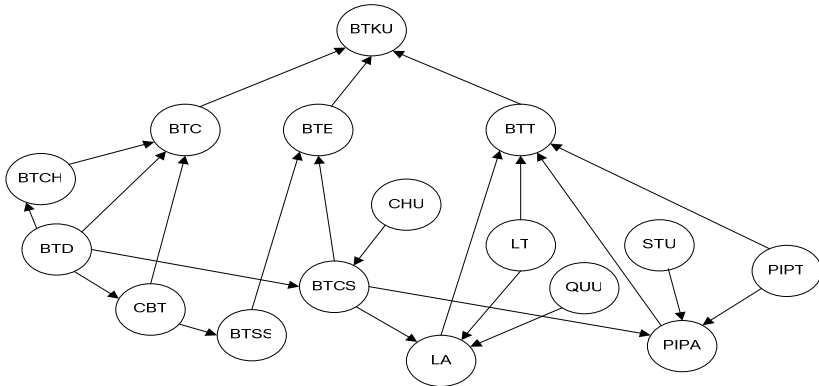
Fig. 1. The student model based on knowledge relationships

In the organization relationships, the item at the beginning of an arrow is the parent item to the item at the end point. The items in the topological structure have different importance levels and difficulty levels. They also have different influences to their parent items. We define the different weights of the knowledge item I_i to influence its parent in different status: High, Medium, Low, and UMaster. For each item I_i, its weight to its parent is defined as w_i. The θ is defined as $\theta_{I_i} \in \{High, Medium, Low, UMaster\}$. Its updated weigh will be given in formula 1:

$$
w_i' = \begin{cases}
w_i & if \quad \theta_{I_i} = High \\
\dfrac{2}{3} w_i & if \quad \theta_{I_i} = Medium \\
\dfrac{1}{3} w_i & if \quad \theta_{I_i} = Low \\
0 & if \quad \theta_{I_i} = UMaster
\end{cases}
\tag{1}
$$

Under the expert's help, we could decide the weight distributions. So we could calculate the conditional probability among the items in the organization relationships. The dependency relationships in the student model could be used to predict the related mastered status based on status of other item. Here, we use the

parameter learning algorithm, which was proposed by Heckerman[2], to identify these conditional probabilities. The hypothesis is described in the formula 2:

$$p(K_{N+1} \mid D_s, S^s) = \prod_{i=1}^{n} \frac{\alpha_{ijk} + N_{ijk}}{\alpha_{ij} + N_{ij}} \tag{2}$$

In which $\alpha_{ij} = \sum_{k=1}^{r_i} \alpha_{ijk}$, $N_{ij} = \sum_{k=1}^{r_i} N_{ijk}$. Where N_{ijk} is the number of cases in domain D, in which $X_i = x_i^{\ k}$ and $Pa_i = pa_i^{\ i}$. Here, we use D_s as the student assessing sample. S^s is the topological structure in the student model. K_{N+1} is some knowledge item.

3   Assessing Method

Here we add the testing nodes in the student model in order to get the student's responses as evidences[3]. The assessing parameter is the prior probability between the knowledge item and testing node and can be described by the item characteristic curve(ICC) with three parameters[1]. The model can be written as formula 3:

$$P(T = 1 \mid I = \theta) = P(\theta) = c_i + (1 - c_i)\frac{1}{1 + e^{-1.7a_i(\theta - b_i)}} \tag{3}$$

In which, the parameter a, b and c could be decided by the experts. We use four statuses, such as H, M, L, and UMaster. They are defined as $P(\theta_H)=1-s$, $P(\theta_M)=2*(\theta_H - \theta_U)/3$, $P(\theta_L)=(\theta_H - \theta_U)/3$, and $P(\theta_U)=c$. Here s is the probability of misplay. Then we could predigest the formula as formula 4:

$$\begin{cases} \theta_H = \dfrac{\log \dfrac{s}{1 - s - c_i}}{-1.7a_i} + b_i \\[2ex] \theta_M = \dfrac{2}{3}\theta_H \\[2ex] \theta_L = \dfrac{1}{3}\theta_H \end{cases} \tag{4}$$

So we could assess the student's ability according to his answer with this assessing method. The student model can be described as the set of KnowledgeItem-Value, in which the KnowledgeItem is the knowledge unit, and Value is the examinee's mastery level θ. The value of θ belongs to the range of (High, Medium, Low, UMaster). So we can calculate the value of meta-knowledge item I_a in the formula 5:

$$V_{Ia} = \theta \quad\quad \text{if} \quad\quad \exists\ P(I_a = \theta') < P(I_a = \theta) \tag{5}$$

In which $\theta' \in \{S-\theta\}$, S={High, Medium, Low, UMaster}. Here, we define the maximal marginal probability (MP) of the student's knowledge level as the student's mastery ability. $\{I_a\}$ represents the whole knowledge items included in the composed knowledge item I_o and minMP is the minimum marginal probability. We can calculate the value of the composed knowledge item in formula 6:

$$\theta_{I_o} = \begin{cases} High & minMP + 2/3(1-minMP) < P(I_o = Master) < 1 \\ Medium & 2/3minMP + 1/3(1-minMP) < P(I_o = Master) < minMP + 2/3(1-minMP) \\ Low & 1/3minMP < P(I_o = Master) < 2/3minMP + 1/3(1-minMP) \\ UMaster & 0 < P(I_o = Master) < 1/3minMP \end{cases} \quad (6)$$

So we can get the final student model based on the marginal probability (MP) coming from the updated Bayesian networks.

4 Conclusions

In this paper, we propose an effective student modeling method built on organization relationships and dependency relationships among the knowledge items based on Bayesian networks. The dependency relationships among the knowledge items are reflected in this overlay model. In order to assess student's performance, we adopt Logistic model with three parameters in IRT model to calculate the conditional probability distribution among the testing items. In the further work, we will improve and apply this method in the whole process of the course of Data Structure.

References

1. Collins, J.A.,Greer, J.E., Huang, S.X.: Adaptive Assessment Using Granularity Hierarchies and Bayesian Nets. In: Frasson, C., Gauthier, G., Lesgold, A. (eds.): Intelligent Tutoring Systems. Third International Conference, ITS '96, Canada, Proceedings. Lecture Notes in Computer Science, Vol. 1086. Springer(1996) 569-577
2. Heckerman, D.: A Tutorial on Learning with Bayesian Networks. In: Jordan, M. (ed.): Learning in Graphical Models. MIT Press, Cambridge, MA (1999)
3. Hambleton, R.K.: Principles and Selected Applications of Item Response Theory. In: Linn, R. L. (ed.): Educational measurement (3rd edn.). New York: American Council on Education and Macmillan (1989) 147–200

Research on Affective Computing Model in E-Learning System

Ruiming Zhao[1], Zhenhui Ren[1], Li Zhang[1], and Ruiguo Qin[2]

[1] Mechanical and Electrical College, Hebei Agriculture University, Baoding
071001, China
[2] Hebei Baoding TV, Baoding 071050, China
`powerzrm@yahoo.com.cn`

Abstract. Emotion deficiency was a hot topic research in current E-learning system. A lot of negative effects were analyzed and corresponding counter-measures were proposed in the paper. Basing on it, affective computing model was set up and used in the traditional E-learning system. Affective computing model was constructed by using audiovisual emotion, which took both facial and audio features as input data. Rough set theory was used in audiovisual emotion recognition. Our simulation experiment results showed that Rough set theory was effective in emotion recognition, and a high recognition rate was resulted.

Keywords: Affective Computing, Emotion recognition, Rough Set, Feature Selection.

1 Introduction

With the development and widespread of network, E-learning has become one of most important ways of educating and researching. E-learning can break through the limit of space and time, reduce learning cost and improve learning efficiency [1]. People pay more and more attention to it.

Although the current E-learning systems have many merits, the phenomenon of emotion deficiency in the current E-learning system is existed. How to measure cognitive emotion of learners in the E-learning system and realize harmonious emotion interaction becomes an important research topic in the distance education [2]. Aiming at the problem of emotion deficiency in E-learning, domestic and abroad scholars bring forward some strategies as follows:

(1) Designing the emotional network curriculums.
(2) Implementing exploring and cooperative learning.
(3) Implementing blended learning.
(4) Improving learning supporting service system.

The application of above strategies have avoided emotion deficiency in certain degree, but learner's emotion state cannot be tracked accurately, the corresponding emotional encouragement and compensation also cannot be provided according to specific emotion state, which cannot help the learner to solve emotion deficiency fundamentally.

Affective computing is a hot topic in Artificial intelligence, it is computing that related to, arise from, or deliberately influence emotion [3], which is firstly proposed by Professor Picard at MIT in 1997.Affective computing consists of recognition, expression, modeling, communicating and responding to emotion [4].in this components, emotion recognition is one of the most fundamental and important modules. It is always based on facial and audio information.

Basing on it, affective computing model was set up and used in the traditional E-learning system. Both facial expression recognition and speech emotion recognition are used to construct affective computing model. Rough set theory was used in audiovisual emotion recognition.

2   Affective Computing Model

The affective computing model is Fig.1. The system model is composed of several modules as follows:
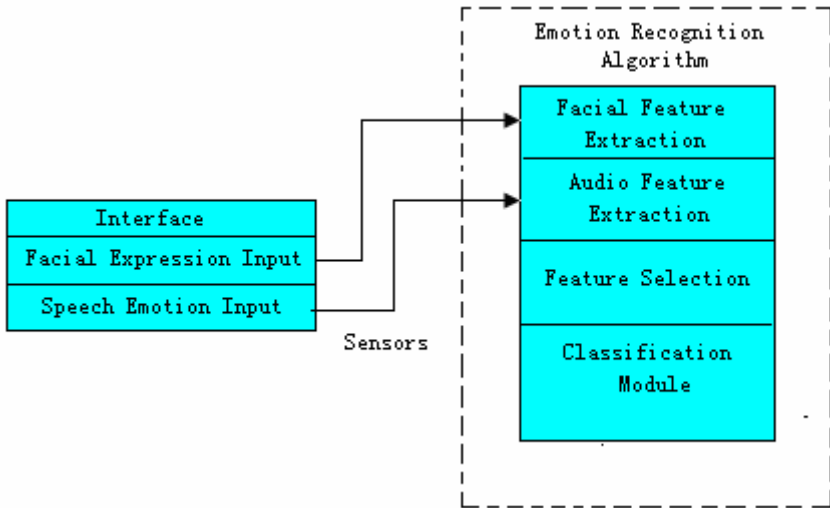
Fig. 1. Affective Computing Model

Interface module: affective computing input will be added to human machine interface of traditional E-learning system (both facial expression recognition input and emotion recognition of speech input), which collects learners' emotion feedback information primarily, thus emotion compensation is realized.

Emotion Recognition algorithm module: emotion recognition algorithm module is composed of input, pre-processing, feature extraction, feature selection, classification and output. Firstly, facial image and audio information of human are taken as input data through some relevant sensors. Then, audio feature and facial feature are extracted from input data. Furthermore, valuable features from all features are

selected for emotion recognition. Finally, the overall emotion is recognized by using emotion recognition algorithm based on Rough Set theory.

3   Emotion Recognition Algorithm

3.1   Audio Feature Extraction

The 37 secondary (statistical) speech features listed in table 3 are often used in speech emotion recognition systems, and the 37 features are taken in our emotion recognition module [5].

3.2   Facial Feature Extraction

In this paper, AAM is adopted to locate feature points. On the other hand, the MPEG-4 standard is a popular standard for feature point selection. It extends FAGS to derive Facial Definition Parameters (FDP) and Facial Animation Parameters (FAP). FAP has been used widely in facial animation for its good performance on compression in recent years. Besides, the FDP and low level FAP constitute a concise representation of a face. They are adequate for basic emotion recognition because of the varieties of expressive parameter. In FAP, 66 low level parameters are defined to describe the motion of a human face. Among 66 parameters, 52 parameters are chosen to represent emotion in our recognition system as shown in Fig.2, because some parameters have not much impact on emotion. Thus, a feature point set including 52 feature points is defined in the image sequence. Based on the feature points, feature distance can be calculated as the features for emotion recognition.
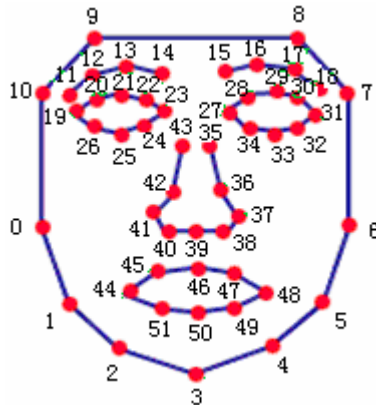
Fig. 2. Feature points

3.3   Feature Selection

Feature selection is the key part of emotion algorithm recognition module. The purpose of feature selection is to select valuable features for emotion recognition from

all features. In this module, features for emotion recognition are decreased. Thus, the complexity and cost for the following classification procedure are reduced. It would improve the efficiency of the whole system.

In our emotion algorithm recognition module, feature selection is based on the rough set theory. The attribute reduction algorithm adopted to select features is introduced in RSFSA, and results of experiment shows the algorithm is effective.

3.4 Classification Module

The classification techniques used in existing emotion recognition algorithm module include template-based classification, rule-based classification, ANN-based classification, HMM-based classification, Bayesian classification, SVM-based classification, etc.

In our emotion recognition algorithm module, classification rules created according to rough set reduction algorithm are taken as the classifier.

4 Conclusion

In this paper, affective computing model was set up and used in the traditional E-learning system. Both facial expression recognition and speech emotion recognition are used to construct affective computing model. Rough set theory was used in audiovisual emotion recognition. Depending on these features, an average recognition rate of 79.2% is achieved. In the future, based on the selected features, other effective classification method will be used. And multi-module emotion recognition including facial, audio, and other features such as gesture will be studied [6].

References

1. Luo Qi.: Research on Application of Association Rule Mining Algorithm in Learning Community. Proceedings of CAAI-11, Wuhan, 2005, 1458-1462.
2. Ma Xirong.: Research on harmonious man-machine interaction model. Computer science, 2005.
3. R.W.Picard.: Affective Computing. Cambridge. MIT Press, 1997.
4. R.W.Picard.: Affective Computing, Challenges. Cambridge. International Journal of Human Computer studies, 59(1), 2003, 55-64.
5. D.Ververidis, et al.: Automatic emotion speech classification. Proceedings of the ICASSP2004, 2004, 593-596.
6. Q.Cai, A.Mitche and J.K.Aggarwal.:Track Human Motion in an Indoor Environment. Proceedings of 2nd international conference Image Processing, 2003.

Learning Assessment Model in Web-Learning Based on Rough Set

Yan Li[1] and Chen Yang[2]

[1] School of Physics & Information Engineering, Jianghan University, Wuhan 430056,
P.R. China
junlzeng@126.com
[2] Engineering Research Center for Information Technology on Education, Center China
Normal University, Wuhan 430079, P.R. China
ly_lj1975@sina.com

Abstract. Assessment is a powerful technique for improving Web-Learning achievement. In this paper we outline a learning assessment model to assessment learning effect for improving learning efficiency. This learning assessment model is based on the rough set theory. In Web-Learning process, learners' data are collected. And, the model used attribute reduction to reduce many factors that in the learning process. It found the key factors which affect the learning effect. Then, the association rules among factors have been concluded. Finally, this learning assessment model is experimented at Jianghan University.

Keywords: Learning Procedure Assessment; Rough Set; Attribute Reduction.

1 Introduction

Learning assessment is a powerful technique for learners to improving Web-Learning achievement. There are some methods for assessment, such as fuzzy and probability, which need accessional information. Moreover, this is difficult to get such accessional information. So, we find rough set is a better method for learning assessment. This paper constructed a learning assessment model based on rough set. The learning assessment model used rough set to assess Web-Learning. The reason is that rough set doesn't need any accessional information. It directly discovers connotative knowledge [1]. We used rough set to analyze every learner's learning characteristics in the process of Web-Learning. It had reduced many factors in the learning process. And it found the key factors which affect the learning effect. Then it concluded the association rules between factors. Finally, the paper evaluated the learners' learning process using the rule according to the learning assessment model. Therefore, learners could get personal learning assessment and improve his or her learning efficiency.

2 Learning Assessment Framework

2.1 Knowledge Express

Learning assessment is not only to assess the learning result, but also to assess all the influential factors in learning process. These factors which affect the learning effect

can be divided into subjective factors and objective factors. This system mainly assess the learning process from the factors: learning background, learning time, learning content, learning difficulty, teaching pattern, presentation style. Followings are the concrete description.

The learning assessment model uses decision table $S=(U, C\cup\{d\}, V, f)$ to represent the knowledge system. $U=\{x_1, x_2, x_3, \ldots, x_m\}$ is composed by learning process. x_i ($1\leq i\leq m$) is the learning process of knowledge point i. $C=\{C_1, C_2, C_3, C_4, C_5, C_6\}$ is the condition attribute set. It is corresponding to {learning background, presentation style, learning content, learning difficulty, teaching pattern, learning time}. d is the decision attribute, which represents the learning effect degree. In V, the value range of each condition attribute is defined as the followings: learning background $C_1=\{1, 2, 3\}=\{$excellent, generic, poor$\}$ reflects learner's learning status; presentation style $C_2=\{1, 2, 3\}=\{$video, text, animation$\}$; learning content $C_3=\{1, 2, 3\}=\{$concept, rule, advanced rule$\}$; learning difficulty $C_4=\{1, 2, 3\}=\{$easy, mezzo, difficult$\}$; teaching pattern $C_5=\{1, 2, 3\}=\{$prelection pattern, drilling pattern, exploring pattern$\}$; learning time $C_6=\{1, 2, 3\}=\{$long, mezzo, short$\}$; learning effect $D=\{1, 2, 3\}=\{$excellent, generic, poor$\}$.

2.2 Learning Assessment Model

Learning assessment model is information module, data pretreatment module, decision table, attribute reduction, rule reduction and learning assessment. Figure 1 gives the flow structure.
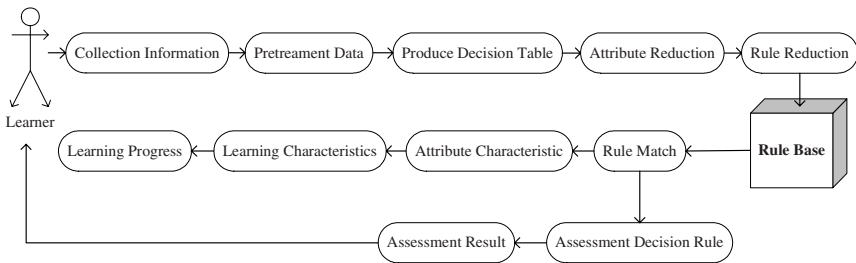
Fig. 1. Flow Structure of Learning Assessment Model

Information module mainly collects learning characteristic data, such as learning path, learning content and so on. Data pretreatment module deals with documents or other data from database. It eliminates redundant information. According to the value range of attribute, it converts consecutive and semantic data to characteristic value. Then initialization decision table. Attribute reduction is to avoid irrelevant or weak relevant attribute. And it gets the key factor which affects the learning result. Now, there are many attribute reduction methods, such as partition matrix, extendibility principle[2]. This model uses the heuristic arithmetic based on partition matrix. That makes core as start. Attribute frequency $p(c_k)$ stands the heuristic formula to reduce condition attribute. $p(c_k)$ is the times of c_k in T. Figure 2 is the arithmetic flow.
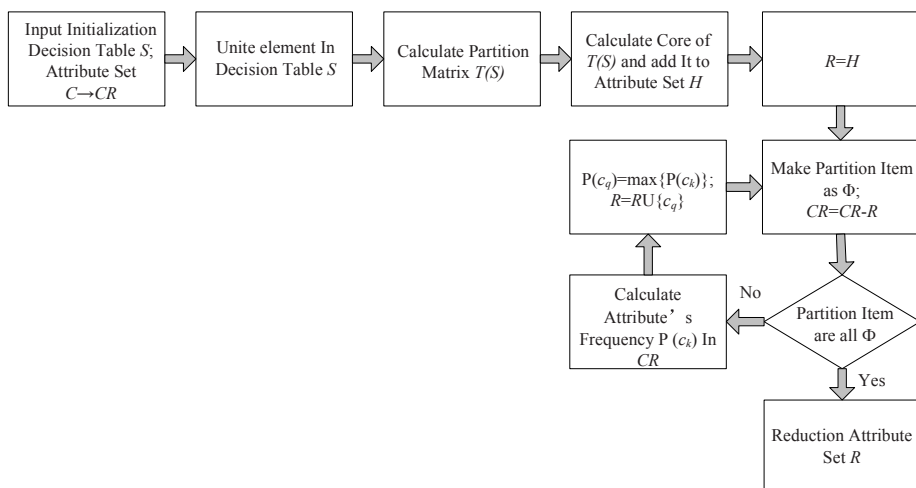
Fig. 2. Arithmetic Flow of Attribute Reduction

If there are several least attribute reduction set. The learning assessment model will have a better standard to make the best attribute reduction set. The standard is from difficult or easy degree of test and control. Condition attribute set R is the key factors which affect learner's efficiency. The condition attribute set R is one of the attribute assessment indexes in the assessment model.

Decision rule reduction: attribute reduction reduces condition attribute, but it is not necessary to each decision rule. Decision rule reduction uses decision making logic to eliminate the needless reduction attribute. Then a high performance decision rule is produced. These rules reflect the associated relation between learning characteristic factor and learning efficiency. This module reduces decision rule according to decision table of reduced attribute set and produces assured rules to form rule base.

Learning assessment: First it analyses attribute reduction set R to help Web-Learning system decide teaching tactic and teach course. The influential degree of every attribute index is confirmed by the concept of attribute importance in rough set. Secondly, learning process is assessed on the basis of rules base. The concrete method is to match between the characteristic factor and associated rules in rules base. According to matched rule, learner's learning process is evaluated. And learner can be given his or her advantage and shortcoming. Learner may be told the appropriate advice to get efficient learning. There are some situations in the rule match.

- No matched rule
- Only one matched rule
- Many matched rules, and consistent conclusion
- Many matched rules, but no consistent conclusion

If there is no matched rule, that is to say the knowledge is not enough to make a believable assessment. If there is only one matched rule or consistent conclusion, it shows that conclusion of matched rule is output firstly, then give corresponding assessment according to importance of attribute. If there is no consistent conclusion, it

will have a synthetical assessment and select the best assessment rule. For example, d_1, d_2, … d_r are different assessment conclusions. And r_1, r_2, … r_m are the decision rules which support d_i. Then formula 1 is the assessment function of d_i.

$$V(d_i) = \sum \text{cov}_j / \sum (\text{cov}_j / con_j) \tag{1}$$

In the above formula: $\text{cov}_j = |X_i \cap Y_j|/|Y_j|$ is the coverage of assessment rule $r_j(1 \leq j \leq m)$, and $con_j = |X_i \cap Y_j|/|X_i|$ is the confidence of assessment rule r_j. The coverage reflects the coverage degree in the equivalent decision class. The confidence reflects the probability of the trueness conclusion based on this decision rule. According to assessment function, $v(d_1)$, $v(d_2)$,…, $v(d_r)$ can be calculated. The biggest function value is selected as the best assessment for learner's learning.

This model was experimented on network teaching course of data structure in the Electronic Information Department, we found this method is welcome.

3   Conclusion

This paper has set up a learning assessment model on the basis of rough set. The model analyzes learning characteristics in the learning process. And the model finds association rule among factors which affect the learning efficiency. Then the model uses these rules to realize learning assessment. The model's functions are as follow: One is to clear the irrelevant or weak relevant attributes to get the key attributes. The other is finding association rule between learning characteristics and learning efficiency to get optimum teaching tactic and teaching pattern. At the end, assess the learning behavior in learning process to help Web-Learning decide next teaching activity. In the end, it improves teaching efficiency.

References

1. Pawlak, Z., Grzymalw-Busse, J., Slowinski, R., Ziarko, W.: Rough sets. Communications of the ACM. 11 (1995) 89-95
2. Keyun Hu, Yuchang LU, Chunyi SHI: Advances in rough set theory and its applications. Journal of Tsinghua University(Science and Technology). 1 (2001) 64-68
3. Greco, S., Matarazzo, B., Slowinski, R.: Rough sets methodology for sorting problems in presence of multiple attributes and criteria. European Journal of Operational Research.138 (2002) 247-259
4. Rasmussen, K. L., Davidson, G.: Hypermedia and Learning Styles: Can Performance Be Influenced. J of Education Multimedia and Hypermedia. 4 (1998) 291-308

Computational Sciences Learning Project
for Pre-university Students

Mustafa Murat Inceoglu[1] and Burak Galip Aslan[2]

[1] Ege University, Computer Education and Instructional Technology,
35100 Bornova, Izmir, Turkey
mustafa.inceoglu@ege.edu.tr
[2] Izmir Institute of Technology, Department of Computer Engineering,
35430 Gulbahce, Urla, Izmir, Turkey
bgaslan@ieee.org

Abstract. It is quite useful for high school students to study on computational sciences, especially for those who are planning to have a higher education in engineering. This paper proposes a pilot study on 9th and 10th grade students for teaching them the basic aspects of computer sciences. This study focuses on a schedule consisting two consecutive courses – first one theoric and the second one is applied – for student volunteers from science high schools.

Keywords: pre-engineering education, computational sciences education, parallel computing, MPI.

1 Introduction and Motivation

Pre-university engineering education is introducing the notion of engineering to high school students who are inclined to engineering education. Such an engineering education is crucial for; graduation of destined engineers, preparing the students for the competitive field of engineering following their graduation, and making them gain experience on critical decisions and creativity. 2-day pre-university design course of Kanazawa University [1], and pre-engineering project design studies of the University of West Florida over selected 4-year high school graduates [2, 3, 4] are interesting examples of pre-engineering education projects.

Computer engineering and electrical engineering are essential areas of engineering in developing countries like Turkey. Parallel computing lays the foundation of computational sciences. Engineering students are expected to solve complex problems via parallelization in this field.

2 Computational Sciences Education for High-School Students

Computer clusters are perfect tools for parallel computing education. Today, clusters are very cost-effective for education units in teaching parallel computing education. The students are learning the concept of *coarse grain parallelism* easily by using clusters [5]. There are also several studies in literature for teaching parallel computing to both undergraduate and graduate students [6-9].

3   Project Setup

The implementation of the project consists of 5 steps; teacher selection, student selection, orientation seminars, courses, and evaluation.

Teacher Selection: Five different teachers required for different stages of project are chosen from the high schools of volunteer students by informing them about the project and discussion. Four of these teachers are assigned to prepare the math, physics, chemistry and biology questions of a selection exam for volunteer students. Same teachers are also assigned to evaluate the exam results. *Blind-evaluation* technique is used for the evaluation of exams. One of the teachers who has a background of mathematics is assigned to teach basic matrix algebra in program.

Student Selection: All of the selected students are studying in science high schools which are education grounds of science and technology. The project has started in 2003-2004 academic year and only 9th grade students are enrolled in the project in order to achieve continuity. The selected 9th grade students are invited for the second stage of the project in the 10th grade. The project is finalized as of November 2006. Some information about the selected high-schools and students are given in Table-1. The students have been asked a total of ten questions from mathematics, physics, chemistry, and biology in the selection exam for better education of pre-university students in the field of computational sciences. The students who are preparing for the Olympics of computer and mathematics have been given higher priority. The willingness of students has been the most important criteria during the student selection process.

Academic year	2003 2004	2004 2005	2005 2006	TOTAL
Selected High-Schools (A)	2	3	3	8
Student volunteers who have taken selection exam (B)	11	17	19	57
Student volunteers who have passed the selection exam (C)	7	14	11	32
Selected students (D)	5	9	7	21
Ratio of selected students (D/B)*100	45%	53%	37%	

Table. 1. Information about the selected high-schools and students in project

Orientation Seminars: Three orientation seminars have been organized so as to introduce the students the concept of computational sciences. The first seminar was based on introducing the basic concepts of engineering. The second seminar followed as giving information about computer engineering, electrical engineering, and professional organizations such as Institute of Electrical and Electronical Engineers (IEEE) and Society for Industrial and Applied Mathematics (SIAM). The last seminar was about parallel computer systems, parallel applications, and some applications from daily life.

Courses: The project is planned to be completed in 3 years. Table. 2. shows the number of selected students, the number of drop-outs, and their corresponding ratios in relation with the academic year. Combining the information from Table.1. and Table.2., it can be seen that there is an increase in both the number and the continuity of students during the three-year project.

Academic Year	2003 2004	2004 2005	2005 2006	End of Project
Selected students (A)	5	9	7	---
The students who did not continue in the second year (B)	---	2	3	1
The ratio of drop-out students (B/A)*100	---	40.0%	33.3%	14.3%
The students who have completed their education plan (C)	---	3	6	6
The ratio of students who completed their education (C/A)*100	---	60.0%	66.7%	85.7%

Table. 2. The attendance information about enrolled students in the project

The project of computational sciences education has been planned as a 2-year program. There will be two semesters in an academic year, 15 weeks in a semester, and 3 hours of lesson for each week so that there will be a total of 90-hour program.

First year covers; Algorithms and C programming (40 hours), and parallel computing (15 hours) courses are given by professors from university, while basic matrix algebra (15 hours) course is given by high-school mathematics teachers. Parallel applications (20 hours) are realized within the supervision of university professors in the applied course. Second year covers; Parallel algorithms (30 hours) course where five algorithms are introduced in this course. Namely; parallel vector addition, parallel sorting, parallel matrix addition, parallel matrix multiplication, and parallel solving of linear systems. Laboratory (60 hours) is about basic knowledge about Message Passing Interface (LAM/MPI) installation, and MPI programming is introduced to students in this course.

Evaluation: *Academic year evaluation* covers the first year evaluation of enrolled 9th grade students in the project has been handled by the university professors and high-school math teachers who have given the courses during the academic year. This stage evaluates the correspondence between project targets and achieved results. The criticisms of students are examined thoroughly by both one-to-one and group discussions. *Semester evaluation* covers the 10th grade students who have completed the first year of the project and continuing the second year are evaluated in two stages. The first stage of evaluation is the evaluation of laboratory applications as an ongoing task. The five parallel algorithm applications are run within the supervision of university professor who gave the course, and the results are discussed. The second stage of evaluation is one-to-one and group discussion with the enrolled students.

4   Results and Discussion

Most of the enrolled students who completed the 2-year project clarified their positive comments on the education project. Considering that science high-schools education is based on science and technology, the students did not show much of resistance; quite the contrary, the students sometimes gave new comments on what could be done in the following years.

Teaching concepts of basic matrix algebra, open-source software such as Linux and MPI, C programming could be very useful for high-school students could be very useful if they continue their higher education in engineering departments. These courses mentioned above lay foundations of several university courses such as differential equations, linear algebra, computer programming which are usually being given in the first years of engineering education. It has been realized that, it is quite advantageous for a future engineering student to know how to program an important parallel library, MPI.

References

[1] Matsuishi, M., Kitamura, T.: Introductory Pre-College Engineering Design Course Based upon Collaborative Learning to High School Students, IEEE International Conference on Sensor Networks, Ubiquitous, and Trustworthy Computing, Vol. 2 (2006) 138 – 142

[2] Harrell D., Bataineh M., El-Sheikh E., Spolski J.: The Development of A Pre-College Engineering Curriculum for High School Students: Design and Implementation, 34th ASEE/IEEE Frontiers in Education Conference, Savannah, GA (2004)

[3] Hirsch, L., S., et al: High School Student's Attitudes To and Knowledge About Engineering, , 33rd ASEE/IEEE Frontiers in Education Conference, Boulder, CO (2003)

[4] Todd R.: A New Paradigm for Pre-Engineering Education: Design and Technology Education K-12, 1993 Frontiers in Education Conference (1993)

[5] Prins P.: Teaching Parallel Computing Using Beowulf Clusters: A Laboratory Approach, Journal of Computing Sciences in Colleges. 20 (2004) 55-61

[6] Fung Y., F., Ercan M., F., Chong, Y., S., Ho, T., K., Cheung, W., L., Singh, G: Teaching Parallel Computing Concepts with A Desktop Computer, International Journal of Electrical Engineering Education. 41 (2004) 113-125

[7] Bernreuther, M., Brenk, M., Bungartz, H., J., Mundani, R., P., Muntean, I., L.: Teaching High-Performance Computing on A High-performance Cluster, Lecture Notes in Computer Science. 3515 (2005) 1-9

[8] Aloisio, G., Cafaro, M., Epicoco, I., Quarta, G.: Teaching High Performance Computing Parallelizing A Real Computational Science Application. Lecture Notes in Computer Science. 3515 (2005) 10-17

[9] Apon, A., Mache, J., Buyya, R., Jin, H.: Cluster Computing in the Classroom and Integration with Computing Curricula 2001. IEEE Transactions on Education. 47 (2004) 188-195

A Study on Fast Preparation of Electron Microscope Biological Specimens

Guo Huashan, Yao Hongjun, Wu Yang, Yang Tian, Zhang Wei, and Guo Jianjun

College of Life Science, Huazhong Normal University, Wuhan 430079, China
guohuashan1982@sohu.com

Abstract. The electron microscope is widely used in chemistry, physics and biology fields, especially in biomedicine ultrastructure research. Using the ultrasonic waves, the time that we spend in preparing the biological specimen will be decreased from 5~10 days to 3~5 hours. A few investigation and discussion of fast preparation was proposed in the paper. This work is very significant to biomedicine research and clinic pathology diagnoses aspects. It is better to choose amplitude with low frequency for the purpose of fast preparation.

Keywords: Electron Microscope, Biology Samples, Preparation, Specimen.

1 Introduction

The electron microscope is widely used in chemistry, physics and biology fields, especially in biomedicine ultrastructure research. It is very important to know alternation of morphological structure to detail, but preparations of biology samples require cockamamie procedure before they can be observed by electron microscope. Routine preparation costs at least 5 days, even 10 days long or longer. In order to save time, reduce work, and improve working efficiency, the author has engaged in electron microscope technology for more than twenty years. A few investigation and discussion of fast preparation was proposed in the paper. This work is very important to biology science research and clinic pathology diagnoses aspects.

2 Materials and Methods

2.1 Laboratory Apparatus and Reagents

(1) Apparatus ultrasonic cleaner: An output of 50 watts, vibration frequency of 40 KHz.
(2) Reagents. Paraform+glutaraldehyde mixed fixation, 0.2mol PBS, 1% osmium tetroxide，30%，50%, 60%, 70%, 80%, 90%, 95%, 100% ethanol, acrylic propane，Epon812 acrylic resin.

To ensure that the reproduction of your illustrations is of a reasonable quality, we advise against the use of shading. The contrast should be as pronounced as possible.

If screenshots are necessary, please make sure that you are happy with the print quality before you send the files.

2.2 Preparation

Before preparation, two-thirds volume of ice water is infused to flume of ultrasonic cleaner as driving medium. Glass vials containing specimens are placed into the flume. Here, taken the treatment of myocardium tissue of M.m.albula, kidney cortex, liver tissue, leaf tissue of photinia serrulata as an example.

(1) Pre-fixation
First, cutting material into 1mm3 or smaller pieces, putting them in vial containing fixation solution as soon as possible, and then placing them into 4℃ freezer.

Choosing fast-penetrating fixation solution, such as paraform+glutaraldehyde mixture, acrolein+glutaraldehyde mixture. After 20 minutes, putting vials containing specimens into flume of ultrasonic cleaner and start ultrasonic cleaner for 10 minutes.

(2) Washing
Discarding fixation solution, washing by 0.1mol PBS to remove the fixation solution leaving on the surface of specimens, treating by ultrasonic for 4-6 minutes.

(3) Post-fixation
Post-fix specimens by 1% osmium tetroxide after washing, placing them into 4℃ freezer for20 minutes, and then treating by ultrasonic for 10 minutes. This step should add ice to flume to keep the temperature down or cold-cycle water.

(4) Washing
Method is as same as (2).

(5) Dehydratation and staining
Dehydrating by ethanol in grads. Treating by 50%, 70%(containing 2% uranylacetate), 80%, 90%, 95%, 100% ethanol, each concentration for 3 minutes, and then treating by acrylic propane for 3 minutes.

(6) Permeance
The ratio of acrylic propane to Epon812 acrylic resin is 1:1. Treating by ultrasonic for 10 minutes, and then treating by pure Epon812 for 10 minutes. This step is important for embedding reagent to penetrate specimens fast.

(7) Embedding and polymerization
The specimens after permeance are better placed on warm table, put into capsules, and then embed in pure Epon812. Polymerizing specimens after placing them in 90-100℃ incubator for 1 hour.

It can be concluded that the whole process costs less than 4 hours from fixation to polymerization. After polymerizing, embedded specimens can be used for trimming and sectioning, staining, observing and taking photos by electron microscope.

3 Results

Compared ultrasonic prepared specimens with routine prepared specimens, according to the electron microscopic pictures, structure of kidney cortex and liver cell of M.m.albula, mitochondrion and myofibril in myocardium cell are preserved perfectly. Similarly, cell wall, plasmodesmatas of plant cells, especially grana and stroma of chloroplasts, have a normal configuration. In conclusion, this is an improved and efficient method to prepare electron microscope specimens of both plant and animal cell (Fig.1, Fig.2).
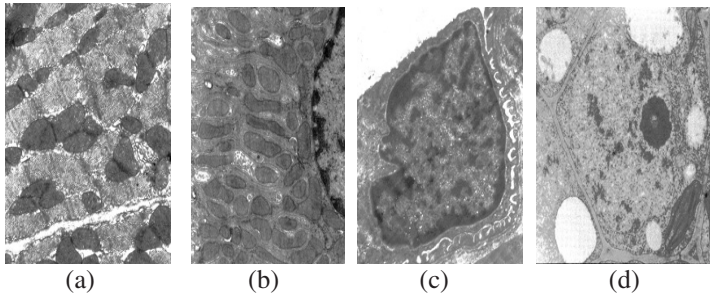
(a) (b) (c) (d)

(a).Cardiac muscle of M.m albula（Bar=10μm） (b).liver of M.m albula（Bar=10μm）
(c).Kidney cortex of M.m albula（Bar=10μm）   (d).leaf of photinia scrrulata（Bar=10μm）

Fig. 1. Ultrasonic prepared specimens
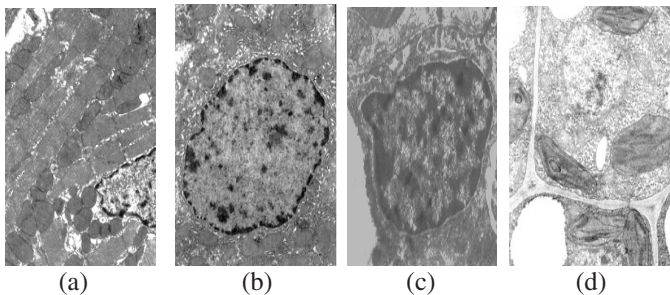
(a) (b) (c) (d)

(a).Cardiac muscle of M.m albula（Bar=10μm） (b).liver of M.m albula（Bar=10μm）
(c).Kidney cortex of M.m albula（Bar=10μm）   (d).leaf of photinia scrrulata（Bar=10μm）

Fig. 2. Ultrasonic prepared specimens

4 Discussion and Conclusion

There have been a few reports about fast preparation, Coulter made use of diminishing sample bulk, reducing dehydration time and vacuum imbuing method. However, some steps had shortened time [1]. Robbins and G.Jentzsch used Epon812 to steep monolayer cell, used 3 times solvent of embed, every time costs 5 minutes, the whole press costs 4 days.[3][4][5][6] The scholars who have engaged in fleetness

preparation in homeland are also the same. The author is able to shorten preparation time, because ultrasonic is used to routine preparation procedure.

The author has done research on the applicability of this device, different processing method of different samples. Generally speaking it takes longer to process plant tissue than animal tissue, and it takes longer to process precise faction tissue than rare faction tissue. Meanwhile, the processing method is also suitable for scanning electron microscope specimen; however, it's difficult to process the primary embedded samples, because ultrasound can detach the primary embedded material from samples.

Ultrasonic is not only used for electron microscope biology sample preparation, but also may be used for organization slice up of the light microscope, some problems need further research. In hospital, frequency of the instrument for ultrasonic diagnosis and remedy in use is between 800 and 1000 KHz, while ultrasonic frequency used for electron microscope sample. Preparation is in 40KHz. could it be raised, or what is the extremity? The best frequency and amplitude (in short, strength), and the exact length of time to process need further research. Because ultrasonic strength is pretty important to biology sample preparation, using different strength will cause different results. If the strength doesn't exceed the limit, longer time of processing will not cause the impairment of cells and tissue. Otherwise, if the strength exceed extremely, it will cause impairment of tissue. Moreover, selection of conductive transmitter and the decreasing quantity of its vibrational frequency after transmitter flowing into sample bottle need to research further. The author suggests on that on the basis of not damaging cell structure, it is better to choose amplitude with low frequency for the purpose of fast preparation.

References

1. Coulter M D. J.:U1trastruct Res. 1967, 346-347.
2. Robbins G, Jentzsch J.:Histochem.Cytochem. 1967, 181-182.
3. Zheng R.:Practicality cytology technology. Beijing Scientific Press, 1980, 188-189.
4. Chen Shi, Peng Xueming: Biomedicine electron microscope technology. Social science Press of China, 1997.
5. Arturo González-Robles: Ultrastructure of trophozoites using fast freeze-fixation followed by freeze-substition J. of Electron Microscopy, 2001, 423-427.
6. Fu Honglan: Practical Electron Microscopy Beijing.Higher Education Press, 2004, 33-34.

A New Approach to Outlier Detection

Lancang Yang[1], Bing Shi[1], Xueqin Zhang[2], and Lei Qiao[1]

[1]School of Computer Science and Technology
Shandong University, Jinan 250061, P.R. China
`yanglancang@163.com`
[2]School of Information Science and Engineering
Jinan University, Jinan 250022, P.R. China
`zhangxueqin_2005@163.com`

Abstract. For many data mining applications, finding the rare instances or the outliers is more interesting than finding the common patterns. At present, many automated outlier detection methods are available, however, most of those are limited by assumptions of a distribution or require upper and lower predefined boundaries in which the data should exist. Whereas a distribution is often unknown, and enough information may not exist about a set of data to be able to determine reliable upper and lower boundaries. For these cases, a new dissimilarity function was defined, which can be viewed as fitness function of genetic algorithm, and a GA-based outlier detection method was formed in this paper. This method allows for detection of multiple outliers, not just one at a time. The illustrations show that the improved approach can automatically detect outliers, and performs better than GLOF approach.

1 Introduction

Outlier detection in large data sets is an active research field in data mining, it has many applications in all those domains that can lead to illegal or abnormal behavior, such as fraud detection[1], network intrusion detection, insurance fraud, medical diagnosis, marketing, or customer segmentation, etc. Outlier detection has become an important branch of data mining[2].

There exist a large number of outlier detection methods in the literature. Traditionally, these can be categorized into three approaches: the statistical approach, the distance-based approach[3], and the deviation-based approach. But many of those are limited by assumptions of a distribution or limited in being able to detect only single outliers. If there is a known distribution for the data, then using that distribution can aid in finding outliers. Often, a distribution is not known, or the experimenter does not want to make an assumption about a certain distribution[4].

Genetic Algorithm (GA) was introduced in the mid 1970s by John Holland and his colleagues and students at the University of Michigan. GA is inspired by the principles of genetics and evolution, and mimics the reproduction behavior observed in biological populations. GA employs the principal of "survival of the fittest" in its search process to select and generate individuals that are adapted to

their environment. Therefore, over a number of generations, desirable traits will evolve and remain in the genome composition of the population over traits with weaker undesirable characteristics. GA is well suited to and has been extensively applied to solve complex design optimization problems because it can handle both discrete and continuous variables and nonlinear objective and constrain functions without requiring gradient information[5].

In this paper, a new dissimilarity function had been defined, which can be viewed as the fitness function of genetic algorithm, and then genetic algorithm was used for outlier detection. This method can detect multiple outliers at a time, and what we should do is nothing but specifying the number of outliers we want. Extensive experiment results on synthetic and real data revealed that the GA-based outlier detection approach can detect outliers automatically and efficiently.

2   GA-Based Outlier Detection

2.1   Outlier Detection

Outlier mining can be described as: Given a set of n data points or objects, and k, the expected number of outliers, find the top k objects that are considerably dissimilar, exceptional, inconsistent with respect to the remaining data. The outlier mining problem can be viewed as two subproblems:

a. Define what data can be considered as inconsistent or exceptional in a given data set; and

b. Find an efficient method to mine the outliers so defined.

The computer-based outlier detection methods can be categorized into three approaches: statistical approach, distance-based approach, and deviation analysis approach. Notice also that many clustering algorithms discard outliers as noise. However, they can be modified to have outlier detection as a byproduct of their execution[6].

2.2   Genetic Algorithm

Genetic algorithm is a stochastic search technique that guides a population of solutions towards an optimum using the principles of evolution and natural genetics. In recent years, genetic algorithm has become a popular optimization tool for many areas of research, including the field of data mining.

The algorithm starts with a randomly generated initial population consisting of sets of "chromosomes" that represent the solution of the problem. These are evaluated for the fitness function or one of the objective functions, and then selected according to their fitness value[7]. To perform its optimization-like process, the GA employs three operators to propagate its population from one generation to another. The first operator is the selection operator,which mimics the principal of "Survival of the Fittest". The second operator is the crossover operator, which mimics mating in biological populations. The crossover operator

propagates features of good surviving designs from the current population into the future population, which will have better fitness value on average. The last operator is the mutation operator, which promotes diversity in population characteristics. The mutation operator allows for global search of the design space and prevents the algorithm from getting trapped in local minima[5].

2.3   Genetic Algorithm Operations

In this paper, for the given set of objects located in the space, genetic algorithm was used to detect the outliers. There are five primary elements in the genetic algorithm, and the parameter setting of genetic algorithm was shown as following in details:

In the approach, the number of outliers was specified firstly, and a random population of chromosomes was created representing the solution space. Each member of this random population represents a different possible solution for the genetic algorithm. The genetic algorithm proceeded to find the optimal solution through several generations.

A. Parameter Encoding
The population representing the solution space consists of many chromosomes. Each chromosome consists of k genes, where k is the number of outliers given. These genes represent the serial number of objects in the data set, which are viewed as outliers. A chromosome can have any combination of these gene values.

B. Fitness Function
The genes, which represent the serial number of outliers, are updated with each new population created. The random population is sorted based on the least fitness. The top chromosome with the least fitness is considered to be the elite chromosome within the population.

The fitness function used in the approach is the dissimilarity function, which can be any function that, if given a set of objects, returns a low value if the objects are similar to one another. The greater the dissimilarity among the objects, the higher the value returned by the function[6].

In our research, a new dissimilarity function was defined, which can be used to evaluate the degree of the outliers. According to the function, the lower the value returned after removing some objects, the greater the degree of these objects being outliers is.

Definition 1. Given a set S of n objects, S' is a subset of S, which contains k objects and denotes the set of outliers in S. Let S'' be the complement of S'. A dissimilarity function can be expressed as:

$$\frac{1}{n-k} \sum_{i=1}^{n-k} (x_i - \overline{x})^2 \tag{1}$$

Where n denotes the number of objects contained in set S, k denotes the number of objects contained in set S', namely, the number of outliers, x_i denotes the object in the set S'', and $\overline{x}$ denotes the mean value of all objects in the set S''.

C. Selection Operator

The Selection operator that mimics the principal of "Survival of the Fittest" selects the chromosomes with the least fitness as the elite chromosome within the population. Among many selection operators, stochastic tournament selection model is used in our approach.

D. Crossover Operator

The Crossover operator that mimics mating in biological populations propagates features of good surviving designs from the current population into the future population, which will have better fitness value on average. Among many crossover operators, two-point crossover model is used in our approach.

E. Mutation Operator

Mutation operator that promotes diversity in population characteristics allows for global search of the design space and prevents the algorithm from getting trapped in local minima. Among many mutation operators, what we used is basic mutation operator in our approach.

3   Experiments

A comprehensive performance study has been conducted to evaluate our algorithm. Our algorithm was implemented in VC++6.0. We ran our algorithm on some real life data sets (Wisconsin breast cancer data set and Boston housing data set) obtained from the UCI Machine Learning Repository[8], and demonstrated the effectiveness of our method against other algorithms. Experiment results are shown as follows.

3.1   Wisconsin Breast Cancer Data Set

The Wisconsin breast cancer data set has 699 instances with nine attributes. Each record is labeled as benign (458 or 65.5%) or malignant (241 or 34.5%). We followed the experimental technique of Harkins et a1.[9] by removing some of the malignant records to form a very unbalanced distribution, the resultant data

Table 1. Comparison between GLOF and our approach. Where N denotes the total number of "outliers" identified, $N1$ denotes the number of "true" outliers (malignant), $N2$ denotes the number of "pseudo" outliers (benign), and gen denotes the number of generations in genetic algorithm.

Approachs	Parameter	N	$N1$	$N2$
	$x_1=-1, x_2=1$	39	26	13
GLOF	$x_1=1, x_2=1$	39	26	13
$(|\xi - \mu| \geq 2 \bullet \sigma)$	$x_1=1, x_2=-1$	40	35	5
	$gen=2000$	39	31	8
OURS	$gen=3000$	39	33	6
$(k=39)$	$gen=4000$	39	35	4

Fig. 1. The test result on boston housing data

set had 39 (8%) malignant records and 444 (92%) benign records. With the data
set, we compared our approach with the GLOF approach[10]. The comparison
between two approaches is shown in Table 1.

3.2   Boston Housing Data Set

The Boston housing data set was taken from the StatLib library which is main-
tained at Carnegie Mellon University. This data set has 506 instances with 13
continuous attributes. For the convenience of observation, two attributes NOX
(nitric oxides concentration) and RM (average number of rooms per dwelling)
were extracted to form a test data set, and the number of outliers was specified
as 15. The test result is shown in Fig. 1.

4   Conclusions

In this paper, a new dissimilarity function was defined, which was viewed as the
fitness function of genetic algorithm, and then genetic algorithm was used for
outlier detection. In the approach, what we should do is nothing but specifying
the number of outliers we want. Extensive experiments on synthetic and real
data showed that the GA-based outlier detection approach can automatically
detect outliers, and that the improved approach performs better than GLOF
approach.

References

1. Park, L.J.: Learning of neural networks for fraud detection based on a partial area under curve. In: Advances in Neural Networks. Lecture Notes in Computer Science, Vol. 3497. Springer-Verlag, Heidelberg (2005) 922-927
2. Angiulli, F., Basta, S., Pizzuti, C.: Distance-Based Detection and Prediction of Outliers. IEEE Trans. Knowl. Data. Eng. 18 (2006) 145-160
3. Guha, R., Dutta, D., Jurs, P.C., Chen, T.: R-NN curves: An intuitive approach to outlier detection using a distance based method. J. Chem. Inf. Model. 46 (2006) 1713-1722
4. Amidan, B.G., Ferryman, T.A., Cooley, S.K.: Data Outlier Detection using the Chebyshev Theorem. In: Aerospace. IEEE AEROSPACE CONFERENCE PROCEEDINGS, IEEE, Piscataway NJ USA (2005) 3814 - 3819
5. Hassan, R., Cohanim, B., Weck, O., Venter, G.: A COMPARISON OF PARTICLE SWARM OPTIMIZATION AND THE GENETIC ALGORITHM. In: AIAA/ASME/ASCE/AHS/ASC Structures, Structural Dynamics and Materials. Collection of Technical Papers, Vol. 2. American Institute of Aeronautics and Astronautics, Reston (2005) 1138-1150
6. Han, J.W., Kamber, M.: Data Mining Concepts and Technique. San Francisco: Morgan Kaufmann, (2001)
7. Jerald, J., Asokan, P., Saravanan, R., Rani, A. Delphin Carolina : Simultaneous scheduling of parts and automated guided vehicles in an FMS environment using adaptive genetic algorithm. Int. J. Adv. Manuf.Technol. 29 (2006) 584-589
8. Merz C.J., Merphy P.: UCI repository of machine learning databases. URL: http://www.ics.uci.edu/mleaml MLRRepository.htm1. (1996)
9. Harkins, S., He, H., Willams, G.J., Baster, R.A.: Outlier detection using replicator neural networks. In: Kambayashi, Y., Winiwarter, W., Arikawa, M. (eds.): Data Warehousing and Knowledge Discovery. Lecture Notes in Computer Science, Vol. 2454. Springer-Verlag, Berlin (2002) 170-180
10. Jiang, S.Y., Li, Q.H., Li, K.L., Wang, H., Meng, Z.L.: GLOF: A NEW APPROACH FOR MINING LOCAL OUTLIER. In: Machine Learning and Cybernetics. Int. Conf. Mach. Learn. Cybern., Vol. 1. Institute of Electrical and Electronics Engineers Inc. (2003) 157-162

High-Dimensional Clustering Method for High Performance Data Mining*

Jae-Woo Chang and Hyun-Jo Lee

Research Center of Industrial Technology
Dept. of Computer Engineering, Chonbuk National University,
Chonju, Chonbuk, 561-756, South Korea
jwchang@chonbuk.ac.kr, hjlee@dblab.chonbuk.ac.kr

Abstract. Many clustering methods are not suitable as high-dimensional ones because of the so-called 'curse of dimensionality' and the limitation of available memory. In this paper, we propose a new high-dimensional clustering method for the high performance data mining. The proposed high-dimensional clustering method provides efficient cell creation and cell insertion algorithms using a space-partitioning technique, as well as makes use of a filtering-based index structure using an approximation technique. In addition, we compare the performance of our high-dimensional clustering method with the CLIQUE method which is well known as an efficient clustering method for high-dimensional data. The experimental results show that our high-dimensional clustering method achieves better performance on cluster construction time and retrieval time than the CLIQUE.

Keywords: High-Dimensional Clustering, Data Mining.

1 Introduction

Data mining is concerned with the extraction of interesting knowledge from a large amount data, i.e. rules, regularities, patterns, constraints. Clustering, one of the most important research topics in data mining, is the process of grouping data into classes or clusters, in such a way that objects within a cluster have high similarity to one another, but are very dissimilar to objects in other clusters [1]. The existing clustering methods have a critical drawback that they do not work well for clustering high-dimensional data because their retrieval performance is generally degraded as the number of dimension increases. In this paper, we propose an efficient high-dimensional clustering method for the high performance data mining. Our high-dimensional clustering method provides a cell creation algorithm to make cells by splitting each dimension into a set of partitions, and provides a cell insertion algorithm to construct clusters as cells with more density than a given threshold and insert them into an index structure. By using an approximation technique, we also propose a new filtering-based index structure to have fast accesses to the clusters.

The rest of this paper is organized as follows. The next section discusses related work on high-dimensional clustering methods. In Section 3, we propose a new high-dimensional clustering method. In Section 4, we analyze the performances of our high-dimensional clustering method. Finally, we draw our conclusion in Section 5.

2   Related Work

The existing high-dimensional clustering methods can be roughly classified into two groups, such as grid-based and partitioning [2]. CLIQUE[3] and MAFIA[4] belong to the grid-based approach while PROCLUS[5], FINDIT[6], and DOC[7] belong to the partitioning approach. In this section, we discuss the typical clustering methods for each approach. First, CLIQUE(CLustering In QUEst) was proposed as a density-based clustering method. CLIQUE automatically finds subspaces(grids) with high-density clusters. CLIQUE produces identical results irrespective of the order in which input records are presented, and it does not presume any canonical distribution of input data. Input parameters are the size of the grid and a global density threshold for clusters. Next, PROCLUS was the first top-down clustering method while CLIQUE scales linearly with the number of input records and it has good scalability as the number of dimensions in the data. PROCLUS samples the data, then selects a set of k medoids, and iteratively improves the clustering. PROCLUS is biased toward clusters that are hyper-spherical in space. While cluster may be found in differ subspaces, the subspaces must be of similar sizes since the user must input the average number of dimensions for the clusters.

3   An Efficient High-Dimensional Clustering Method

Since the existing clustering methods assume that a data set is resident in main memory, they are not efficient for handling large amounts of data. As the dimensionality of data is increased, the number of cells increases exponentially, thus causing the dramatic performance degradation. To remedy that effect, we propose an efficient high-dimensional clustering method for the high performance data mining. The overall architecture of our clustering method is shown in Figure 1.
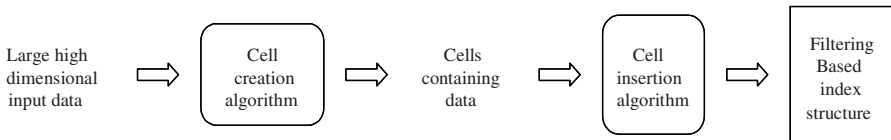
Fig. 1. Overall architecture of our clustering method

3.1   Cell Creation Algorithm

Our cell creation algorithm makes cells by splitting each dimension into a group of sections using a split index. Density based split index is used for creating split sections and is efficient for splitting multi-group data. Our cell creation algorithm first finds the optimal split section by repeatedly examining a value between the maximum

and the minimum in each dimension. The split index value is calculated by Eq. (1) before splitting and Eq. (2) after splitting. Using Eq. (1), we can determine the split index value for a data set S in three steps: i) divide S into C classes, ii) calculate the square value of the relative density (P_j) of each class, and iii) subtract from one all the square values of the densities of C classes. Using Eq. (2), we compute a split index value for S after S is divided into S_1 and S_2. Here the number of data in S is n and the number of data belonging to $S_1(S_2)$ is n_1 (n_2). If the split index value is larger than the previous value before splitting, we actually divide S into S_1 and S_2. Otherwise, we stop splitting. Secondly, our cell creation algorithm creates cells being made by the optimal split sections for n-dimensional data. As a result, our cell creation algorithm creates fewer cells than the existing clustering methods using equivalent intervals.

$$Split(S) = 1 - \sum_{j=1}^{C} P_j^{\,2} \qquad (1)$$

$$Split(S) = \frac{n_1}{n} Split(S_1) + \frac{n_2}{n} Split(S_2) \qquad (2)$$

If a data set has n dimensions and the number of the initial split sections in each dimension is m, the conventional cell creation algorithms make mn cells, but our cell creation algorithm makes only K1*K2*...*Kn cells (1 ≤K1, K2, .. ,Kn≤m).

3.2 Cell Insertion Algorithm

For cell insertion, we first obtain the cells created using the cell creation algorithm. Secondly, we construct clusters as the cells with more density than a given cell threshold and store them into a cluster information file. A record in the cluster information file consists of a cluster id and the number of data belonging to the cluster. The cluster information file for large, high-dimensional data is too large to reside in memory. Thirdly, we calculate the frequency of a section in all dimensions whose frequency is greater than a given section threshold. Finally, we set to '1' the bits corresponding to the sections with a high frequency in an approximation information file. We set to '0' the other bits for the remainder sections. We calculate the frequency of data in a cell. Finally, the cell threshold and the section threshold are shown in Eq. (3).

$$Section\ threshold = \begin{cases} \lambda = \dfrac{NR \times F}{NI} \\ NI : \text{the number of input data} \\ NR : \text{the number of sections per dimension} \\ F : \text{minimum section frequency being regarded as '1'} \end{cases} \qquad (3)$$

$Cell\ threshold\,(\tau) : \text{positive integer}$

3.3 Filtering-Based Index Structure

When the number of the created cells is very large due to large and high-dimensional data, it may take much time to answer users' queries. In order to reduce time to

respond to the queries, it is possible to construct a new filtering-based index scheme using the approximation information file. Figure 2 shows an example of a filtering-based index scheme containing both the approximation information file and cluster information file, assuming two-dimensional data. Let assume that K clusters are created by our cell-based clustering method and the numbers of split sections in X axis and Y axis are m and n, respectively. The following equation, Eq.(4), shows the retrieval times (C) when the approximation information file is used and when it is not used. We assume that is an average filtering ratio in the approximation information file. D is the number of dimensions of input data. P is the number of records per page. R is the average number of records in each dimension. When the approximation information file is used, the retrieval time decreases as decreases. For high-dimension data, our two-level index scheme using the approximation information file is an efficient scheme because the K value increases exponentially in proportion to dimension D. The size of the approximation information file is dependent on both the number of dimensions of data and the numbers of split sections in each dimension. Because we deal with high-dimensional data, we keep the approximation information file in disk, rather than in memory.

i) Retrieval time without the use of an approximation information file

$$C = \lceil K/P \rceil / 2 \quad \text{(Disk I/O accesses)}$$

ii) Retrieval time with the use of an approximation information file

$$C = \lceil (D*R)/P \rceil * \alpha + (1-\alpha) \lceil K/P \rceil / 2 \quad \text{(Disk I/O accesses)} \tag{4}$$

Figure 2 shows our filtering-based index scheme used to answer a query when a cell threshold and a section threshold are 1, respectively. For a query Q1, we determine 0.6 in X axis as the third section and 0.8 in Y axis as the fourth section. In the approximation information file, the value for the third section in X axis is '1' and the value for the 4-th section in Y axis is '0'. Because one of sections' values is '0', Q1 can be discarded without searching the corresponding cluster information file. For a query Q2, the value of 0.55 in X axis and the value of 0.7 in Y axis belong to the third section, respectively. Because the third bit for X axis and the third bit for Y axis have '1' in the approximation information file, we calculate a cell number and obtain its cell
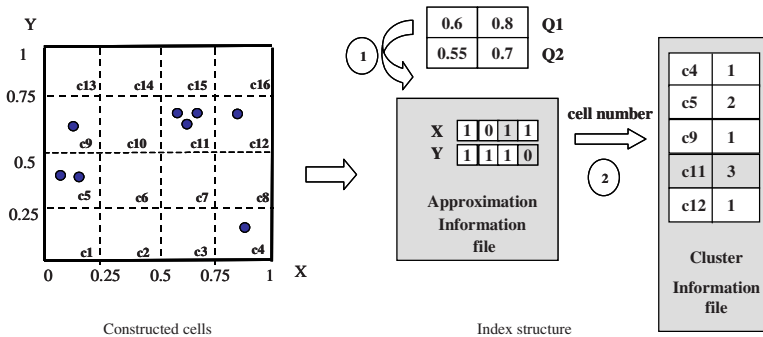
Fig. 2. Filtering-based index scheme

frequency by accessing the cluster information file. As a result, we obtain a cell number 11 and its frequency 3 for Q2.

4   Performance Analysis

For our performance analysis, we implemented our clustering method on Linux server with dual processors. We make use of one million data (16-dimensional one) created by Synthetic Data Generation Code for Classification in IBM Quest Data Mining Project [8]. A record in our experiment is composed of both numeric type attributes, like salary, commission, age, hvalue, hyears, loan, tax, interest, cyear, balance, and categorical type attributes, like level, zipcode, area, children, ctype, job. The factors of our performance analysis are cluster construction time, precision, and retrieval time. We compare our cell-based clustering method (CBCM) with the CLIQUE method, which is one of the most efficient high-dimensional clustering methods. For our experiment, we make use of three data sets, one with random distribution, one with standard normal distribution (variation=1), and one with normal distribution of

Table 1. Methods used for performance comparison (MI:Maximal Interval)

Methods	Description
CBCM-5R CLIQUE-5R	CBCM for data set with random distribution(MI = 5) CLIQUE for data set with random distribution (MI=5)
CBCM-10R CLIQUE-10R	CBCM for data set with random distribution (MI=10) CLIQUE for data set with random distribution (MI=10)
CBCM-5SND CLIQUE-5SND	CBCM with standard normal distribution (MI=5) CLIQUE with standard normal distribution (MI=5)
CBCM-10SND CLIQUE-10SND	CBCM with standard normal distribution (MI=10) CLIQUE with standard normal distribution (MI=10)
CBCM-5ND(0.5) CLIQUE-5ND(0.5)	CBCM with normal distribution of variation 0.5 (MI=5) CLIQUE with normal dist. of variation 0.5 (MI=5)
CBCM-10ND(0.5) CLIQUE-10ND(0.5)	CBCM with normal distribution of variation 0.5 (MI=10) CLIQUE with normal dist. of variation 0.5 (MI=10)
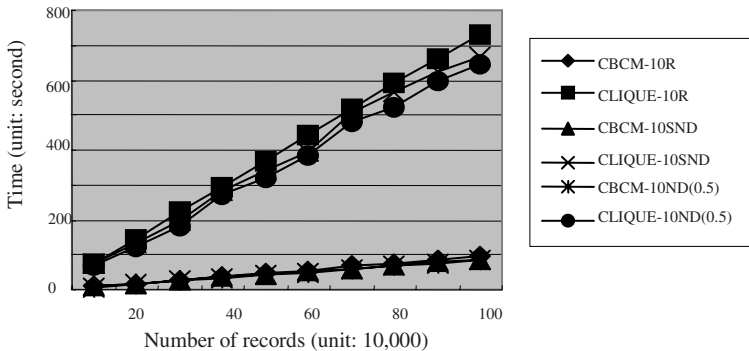
Fig. 3. Cluster Construction Time

variation 0.5. We also use 5 and 10 for the interval of numeric attributes. Table 1 shows methods used for performance comparison in our experiment.

Figure 3 shows the cluster construction time when the interval of numeric attributes equals 10. It is shown that the cluster construction time increases linearly in proportion to the amount of data. This result is applicable to large amounts of data. The experimental result shows that the CLIQUE requires about 700 seconds for one million items of data, while our CBCM needs only 100 seconds. Because our method creates smaller number of cells than the CLIQUE, our CBCM method leads to 85% decrease in cluster construction time. The experimental result with the maximal interval (MI)=5 is similar to that with MI=10.
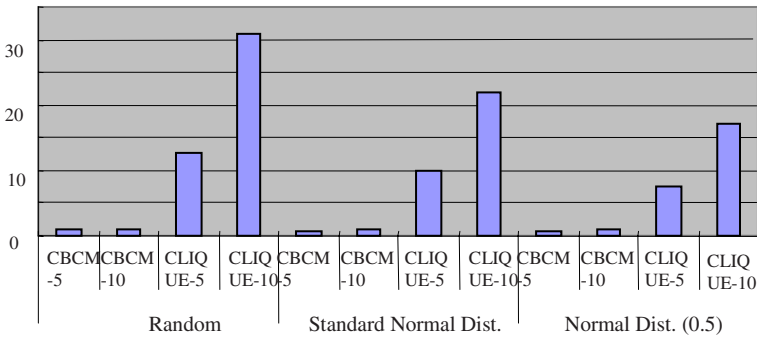
Fig. 4. Retrieval Time

Figure 4 shows average retrieval time for a given user query after clusters were constructed. When the interval of numeric attributes equals 10, the CLIQUE needs about 17-32 seconds, while our CBCM needs about 2 seconds. When the interval equals 5, the CLIQUE and our CBCM need about 8-13 seconds and 1 second, respectively. It is shown that our CBCM is much better on retrieval performance than the CLIQUE. This is because our method creates a small number of cells by using our cell creation algorithm, and achieves good filtering effect by using the approximation information file. It is also shown that the CLIQUE and our CMCM require long retrieval time when using a data set with random distribution , compared with normal distribution of variation 0.5. This is because as the variation of a data set decreases, the number of clusters decreases, leading to better retrieval performance.

Figure 5 shows the precision of the CLIQUE and that of our CBCM, assuming that the section threshold is assumed to be 0. The result shows that the CLIQUE achieves about 95% precision when the interval equals 10, and it achieves about 92% precision when the interval equals 5. Meanwhile, our CBCM achieve over 90% precision when the interval of numeric attributes equals 10 while it achieves about 80% precision when the interval equals 5. This is because the precision decreases as the number of clusters constructed increases.

Because both retrieval time and precision have a trade-off, we estimate a measure used to combine retrieval time and precision. To do this, we define a system efficiency measure in Eq. (5). Here E_{MD} is the system efficiency of methods (MD) shown in Table 1 and W_p and W_t are the weight of precision and that of retrieval time,
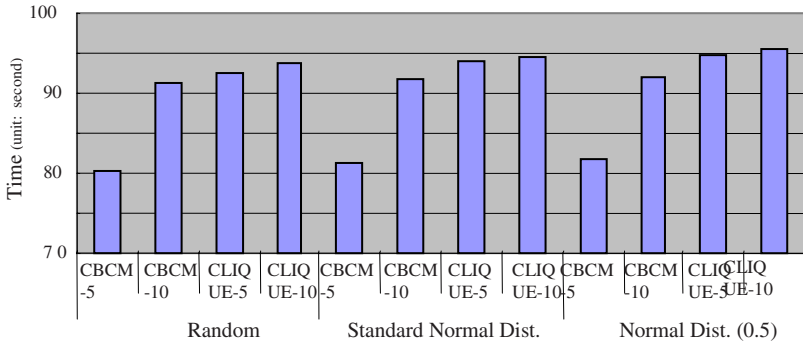
Fig. 5. Precision

respectively. P_{MD} and T_{MD} are the precision and the retrieval time of the methods (MD). P_{MAX} and T_{MIN} are the maximum precision and the minimum retrieval time, respectively, for all methods.

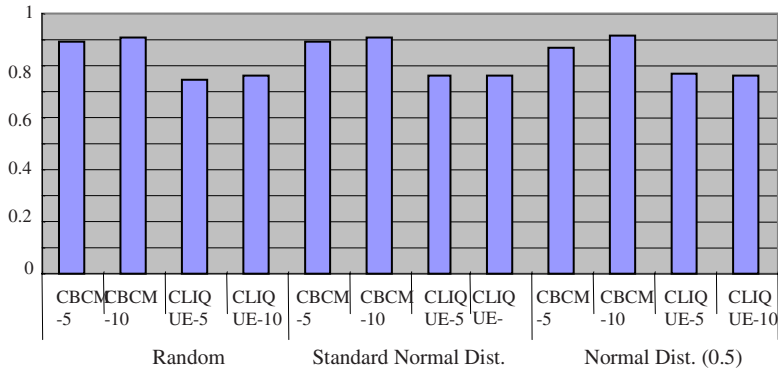$$E_{MD} = W_p \bullet \frac{P_{MD}}{P_{MAX}} + W_t \bullet \frac{1}{T_{MAX} / T_{MIN}} \tag{5}$$

Fig. 6. System efficiency

Figure 6 depicts the performance results of methods in terms of their system efficiency. The importance of the precision and that of the retrieval time depend on an application situation, but the precision is more important than the retrieval time in general. Thus, it is reasonable that we should set the weight of the precision to be three times greater than that of retrieval time, i.e., W_p=0.75, W_t =0.25. The performance result shows that our CBCM outperforms the CLIQUE with respect to the system efficiency, regardless of the data distribution of the data sets. Especially, the performance of our CBCM with MI=10 is the best.

5   Conclusion

The conventional clustering methods are not efficient for large, high-dimensional data. In order to overcome the difficulty, we proposed a new efficient clustering method with two features. The first one allows us to create the small number of cells for large, high-dimensional data. To do this, we calculate a section of each dimension through split index and create cells according to the overlapped area of each fixed section. The second one allows us to apply an approximation technique to our clustering method for the high performance data clustering. For this, we use a two-level index structure which consists of both an approximation information file and a cluster information file. For performance analysis, we compare our high-dimensional clustering method with the CLIQUE method. The performance analysis results show that our clustering method shows slightly lower precision, but it achieves good performance on retrieval time as well as cluster construction time. Finally, our high-dimensional clustering method shows a good performance on system efficiency which is a measure to combine both precision and retrieval time. As future work, it is required to study on the parallelism of our high-dimensional clustering method in order to achieve higher performance on retrieval.

References

1. Han, J., Kamber, M.: Data Mining: Concepts and Techniques. Morgan Kaufmann (2000).
2. Gan, G., Wu, J.: Subspace Clustering for High Dimensional Categorical Data. ACM SIGKDD Explorations networks, Vol. 6, Issue 2 (2004) 87-94.
3. Agrawal, R., Gehrke, J., Gunopulos, D., Raghavan, P.: Automatic Subspace Clustering of High Dimensional Data Mining Applications. Proc. of ACM SIGMOD (1998) 94-105.
4. Nagesh, H., Goil, S., Choudhary, A.: A Scalable Parallel Subspace Clustering Algorithm for Massive data Sets. Proc. of Int. Conf. on parallel Processing (2000) 477-486.
5. Aggrawal, C., Wolf, J., Yu, P., Procopiuc, C., Park, J.: Fast Algorithms for Projected Clustering. Proc. of ACM SIGMOD (1999) 61-72.
6. Woo, K., Lee, J.: FINDIT: A Fast and Intelligent Subspace Clustering Algorithm using Dimension Voting. PhD thesis, Korea Advanced Institute of Sci.&Tech, Dept. of CS (2002).
7. Procopiuc, C., Jones, M., Agrawal, P., Murali, T.: A More Carlo Algorithm for Fast Projective Clustering. Proc. of ACM SIGMOD (2002) 418-427.
8. http://www.almaden.ibm.com/cs/quest

Clustering Streaming Time Series Using CBC

Weimin Li, Liangxu Liu, and Jiajin Le

College of Computer Science and Technology of Donghua University, 1882 West Yan'an
Road, Shanghai, China, 200051
`108wml@mail.dhu.edu.cn`

Abstract. Clustering streaming time series is a difficult problem. Most traditional algorithms are too inefficient for large amounts of data and outliers in them. In this paper, we propose a new clustering method, which clusters Bi-clipped (CBC) stream data. It contains three phrases, namely, dimensionality reduction through piecewise aggregate approximation (PAA), Bi-clipped process that clipped the real valued series through bisecting the value field, and clustering. Through related experiments, we find that CBC gains higher quality solutions in less time compared with M-clipped method that clipped the real value series through the mean of them, and unclipped methods. This situation is especially distinct when streaming time series contain outliers.

1   Introduction

There are extensive studies on efficient algorithms that can manage large data sets [1, 2]. One of the popular data analyzing problems is data clustering. Clustering is an unsupervised learning method, because the data are assigned to the corrected cluster without knowing which cluster they belong to in the learning methods. Efficient and accurate clustering for data stream is a key problem, and many techniques have been proposed for clustering data stream [3, 4, 5].

In this paper, we investigate the clustering time series data streams, which is meaningful [6]. In some data sources, the generation rates of time series data streams have become faster than ever before. The rapid time series data streams have challenged the storage and computation time in our computing systems.

We propose a new approach that clusters on Bi-clipped (CBC) series. We first transform the time series data streams into the Piecewise Aggregate Approximation (PAA) representation, and then clip them into binary series (Bi-clipped) that is different from the process of clipping (M-clipped) in Anthony Bagnall et al. [7]. M-clipped method transforms the original series into a binary one with mean of them. However, mean is influenced by the outliers in original series. This is why we design the Bi-clipped method. Through CBC, we can find that our proposed method not only improves significantly space and time complexity, but also is better to diagnose outliers and have better cluster performance than M-clipped and unclipped series.

The remainder of this paper is organized as follows. In section 2, we briefly discuss related work. Section 3 outlines the proposed method CSC. In section 4, we discuss the advantages of CBC. An experimental evaluation of our method is given in section 5. Section 6 concludes the paper with a summary of the experiment results.

2   Related Work

Clustering streaming time series has attracted considerable interest recently. However, main memory and time tend to be a bottleneck. A better approximate representation would be considered for clustering streaming time series. According to this point, many methods including the Symbolic Aggregate Approximation (SAX) [8], M-clipped [7], Extend SAX [9], the Discrete Wavelet Transform (DWT) [10] and the Discrete Fourier Transform (DFT) [11] have been introduced.

Streaming time series is organized along with time axis and processed in a continuous way. However, there are continuous changes of their trends and it is the point to extract useful patterns in data mining research [12]. The Symbolic Aggregate Approximation (SAX) is a symbolic representation through a two-stage process of dimension reduction and discretization [8]. Extended SAX aims to realize efficient and accurate discovering of important patterns, necessary for financial applications [9]. M-clipped [7] transforms the real valued time series into a binary series through mean. Here we give a good representation for streaming time series. Bi-clipped method combined SAX and M-clipped, and improve the mean of M-clipped method influenced by outliers. Bi-clipped data can not only be more compactly represented and efficiently manipulated, but can it be robust to outliers.

3   Clustering on Bi-clipped Stream Data

The streaming time series consist of a set of multidimensional points $S_1 \ldots S_K \ldots$ arriving at time stamps $t_1 \ldots t_k \ldots$. Each data S_i is a multidimensional item containing m dimensions, marked by $S_K = (s_i^1 \ldots s_i^m)$. In this section, we combine the reduction technology with the clipped technology, and use it to cluster streaming time series. The clustering on Bi-clipped stream data (CBC) has three phrases, i.e., dimensionality reduction via piecewise aggregate approximation (PAA), Bi-clipped process of stream time series, and clustering the Bi-clipped data.

3.1   Dimensionality Reduction Via PAA

PAA has been proposed by Keogh et al. [13]. It is a simple dimensionality reduction technique to implement compared with more sophisticated techniques like Singular Value Decomposition (SVD), the Discrete Fourier Transform (DFT), and the Discrete Wavelets Transform (DWT).

As defined by Keogh et al. [13], a streaming data S of length n can be represented in a d-dimensional space by a vector D, and the ith element of D is calculated by the following equation:

$$d_i = \frac{d}{n} \sum_{j=\frac{n}{d}(i-1)+1}^{\frac{n}{d}i} s_j \tag{1}$$

To transform the streaming data from n dimensions to d dimensions, each sequence of streaming data is divided into d "frames" with equal sized and the mean value of each frame is used as a coordinate of a d-dimensional feature vector. This
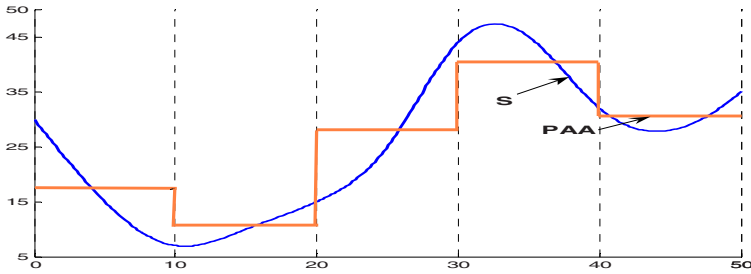
Fig. 1. A streaming data S is represented by PAA

data-reduced representation method is shown in Fig. 1, where the dimensionality is reduced from $n=50$ to $d=5$.

3.2 Bi-clipped Data

The dimensionality reduction through PAA is impossible too large, otherwise, more information may be lost. Streaming time series could be dimensionality reduction through PAA within measure. In this section, a new proposed streaming time series representation is described. It is different from the Symbolic Aggregate Approximation (SAX) [8] and M-clipped [7]. We transform PAA series into clipped data through the process of clipping. SAX and M-clipped transformation has similarities to our method. M-clipped transforms the real valued time series into a binary series through mean. However, when the streaming time series contains outliers, they would influence the mean value. Thus, we propose Bi-clipped method to overcome this shortcoming.

In this paper, clipping stream time series is transforming a PAA series D into a binary series Y. D is bisected into [min, a] and (a, max), and we called the whole process Bi-clipped. The elements in [min, a] are mapped to 0, otherwise they are mapped to 1. However, 'a' is not the mean value of D, but the value of the middle situation of the sorted D. In the same way, 'min' and 'max' represent the min and max place of the sorted D. For a time series, we can avoid the uncorrected mean influenced by outliers through using this method. Clipped data Y is produced from the following formula:

$$Y(t) = \begin{cases} 0 & if \quad D(t) \in [\min, a] \\ 1 & otherwise \end{cases} \tag{2}$$

3.3 Clustering the Bi-clipped Data

The problem of clustering is regularly defined as finding a partition of Y into k clusters. The cluster algorithm used in this paper is K-means clustering algorithm that classifies or groups given objects based on attributes into K numbers of group. It is one of the most popular and simple clustering algorithms. All cluster experiments performed in this study involve streaming time series of which the true clusters is not

known. The quality of a clustering model is measured by the sum of squared distances (SSQ) from each point to the cluster where it was assigned [14].

4   Advantages of CBC

4.1   Space and Time Improvements

The aim of using CBC and M-clipped methods is to pack them efficiently. We could gain better performance by analyzing the clipped data. And this reduction technology is effective for very long series like stream data. Because the stream data cannot store on disk, it is possible to analyze the Bi-clipped data of stream data in main memory.

The benefits of using CBC like M-clipped data could be packed efficiently in integer matrix and operated using bit operators, and they could provide a more significant time improvement than using unclipped data in bit operators. A series of doubles of length n using M-clipped method can be stored in an array of $n/64$ integers [7]. However, a Bi-clipped series of doubles of length n using PAA technology can be stored in an array of $d/64$. The average time taken to find clusters by different methods can be shown in section 5.2. In this paper, one aim of our study is to focus on improving the performance of clustering stream time series through using CBC.

4.2   Robust Performance to Outliers

When a reduction technology is adopted to deal with stream time series, it is crucial to maintain statistic information of stream time series. In this paper, we propose CBC method to hold the related information. A Bi-clipped series that convert from stream time series have the following properties: through analyzing Bi-clipped series of stream time series, we know that it is approximately a stationary series. We could gain the related information of stream time series from the Bi-clipped of it. In this aspect, CBC method is superior to M-clipped method.

CBC and M-clipped methods could eliminate outliers, but the fashion of them is different. M-clipped method uses the mean of original series to divide it into M-clipped data. However, our method applies PAA to dimensionality reduction and converts it to Bi-clipped through the number region of sorted stream time series, not the values of them. When the probability of outlier is higher, robust of the CBC method is superior to that of M-clipped in theory. Of cause, the robust of both methods absolutely exceed unclipped method.

5   Experiment

We performed a series of experiments to assess the performance of our method. To test the scalability of our method, we generate randomly 50 n-dimensional (n size from 5k to 25k points) datasets S. The data follow uniformly distributions. Through the Bi-clipped process, the data set S is converted to 50 n/d-dimensional points. In section 5.1, we compare the cluster results by using CBC, M-clipped and unclipped data. We find that the CBC method prior to the other methods in stream data that contain outlier. To measure the accuracy and quality of different clustering, we use

the SSQ described in Section 3. Next, another advantage in time complex is described in section 5.2.

5.1 Clustering Streaming Time Series

We perform experiments to analyze the ability of using CBC method compared with M-clipped and Unclipped. The Min/Average/Max SSQ value for K-means clustering using CBC, M-clipped and Unclipped data without outliers are shown in Table 1. Fig.2 shows the average value of SSQ. When the streaming time series do not contain outliers, the clustering quality of clipped series from CBC and M-clipped is

Table 1. Quality comparison without outliers

$N \times M$	CBC	M-clipped	Unclipped
	SSQ value (Min/Avg/Max×1.0E+05)		
20×5000	0.593/0.613/0.645	0.489/0.545/0.639	0.636/0.668/0.687
20×10000	1.091/1.180/1.293	0.987/1.103/1.191	1.186/1.263/1.389
20×15000	1.641/1.757/1.950	1.795/1.871/2.099	1.787/2.015/2.093
20×20000	2.191/2.26932.395	2.190/2.341/2.590	2.584/2.635/2.988
20×25000	2.735/2.892/3.236	2.479/2.699/2.731	3.223/3.255/3.475
20×30000	3.290/3.440/3.590	3.287/3.472/3.584	3.870/3.984/4.476

better than that of unclipped data. When the length of data becomes longer, the trend is more distinct. Compared with M-clipped, CBC does not have obvious advantages, but it is faster than the M-clipped method in finding cluster, and the related contents will be discussed in section 5.2.

Table 2 shows the Min/Average/Max SSQ value for K-means clustering using the three methods with outliers. The clustering quality of clipped series including CBC and M-clipped is better than that of unclipped data as above. However, CBC method
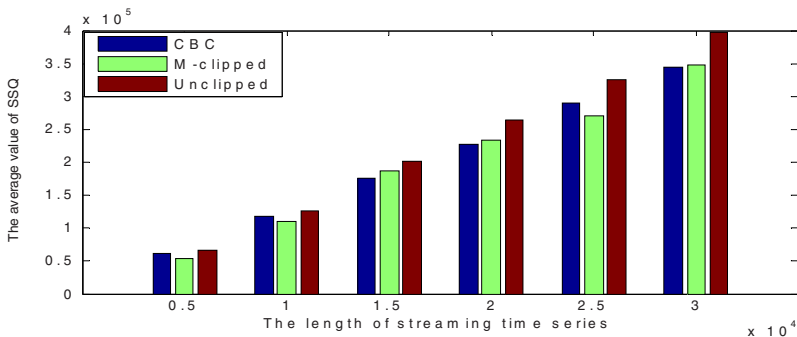
Fig. 2. The average value of SSQ without outliers

exceeds M-clipped method when the outliers exist. Fig.3 shows the average value of SSQ with outliers, which indicates that the Outliers significantly influence the clustering performance of Unclipped data. CBC method has better robust performance to outlier than M-clipped method. Therefore, when the streaming time series have outliers, the clustering quality of clipped series including CBC and M-clipped is better than that of unclipped data. Moreover, there are distinctly differences between CBC and M-clipped. CBC method has better robust performance than the other two methods. When the length of streaming time series is getting longer, CBC method has more distinct advantages than the other two methods in clustering performance. Therefore, CBC method gains better cluster results, which testify the thought about the benefit of CBC.

Table 2. Quality comparison with outliers

$N \times M$	CBC	M-clipped	Unclipped
	(Min/Avg/Max×1.0E+05)		
20×5000	2.453/2.598/2.703	2.245/2.644/2.952	2.630/2.633/2.641
20×10000	4.982/5.164/5.465	5.026/5.381/5.966	5.898/6.481/6.839
20×15000	8.157/8.181/8.208	7.589/8.388/8.993	8.789/9.238/10.940
20×20000	9.059/9.985/11.816	10.021/10.839/11.862	11.743/12.33/13.611
20×25000	12.486/12.540/12.564	12.532/13.731/14.899	14.747/15.190/15.928
20×30000	13.690/14.908/16.506	16.503/16.882/17.949	17.744/19.491/20.544
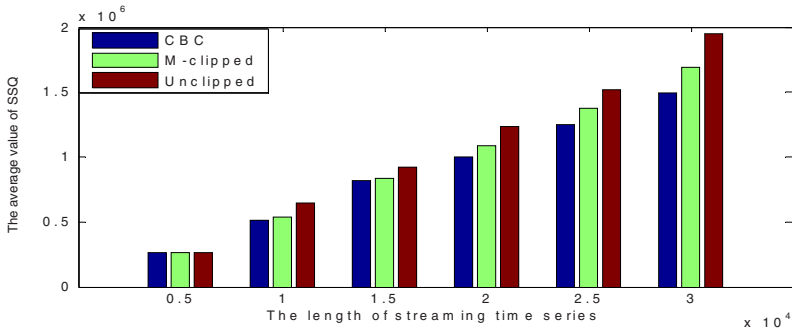
Fig. 3. The average value of SSQ with outliers

5.2   Time Complex

It is distinct that CBC and M-clipped methods could provide a more significant time improvement than using unclipped data in bit operators. In this section, we compare the average time of different means taken to find clusters. Fig.4 shows that with outliers. Each value in Fig.4 gives the time taken to find clusters in different data sets from 5k to 30k in length. The time to find cluster using CBC method is superior to the

other two methods. The time includes the process of clipped. When the length of streaming time series gets longer, it will take more time to find clusters. The ratio of time taken in CBC to that in the other methods is approximately a constant n/d. These results justify that our CBC method is a good dimensionality reduction and presentation method for clustering purposed.
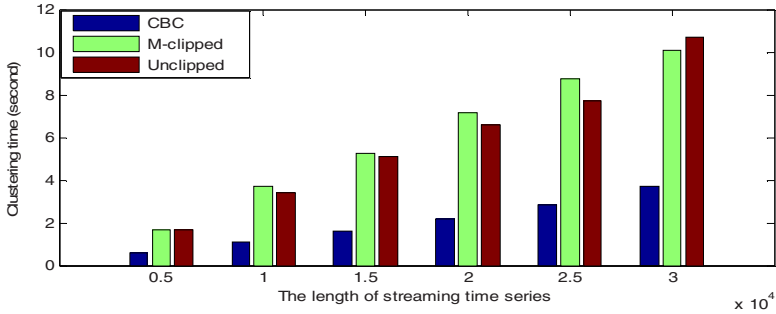
Fig. 4. Average time taken to find clusters with outliers

6   Conclusions

In this paper, considering the problem of clustering streaming time series mentioned above, we developed CBC techniques. Unlike existing methods such as M-clipped and SAX, CBC is based on PAA and Bi-clipped method. It contains dimensionality reduction process of PAA, Bi-clipped process of stream time series, and clustering the Bi-clipped data. The aim of using the CBC is to improve the performance of clustering and improve the time complex. Specific algorithms for binary series would improve time complexity [7]. According to our experiments, CBC performs much better than M-clipped and unclipped data in time complexity. A Bi-clipped series of doubles of length n can be stored in an array of $d/64$. Bi-clipped method allows for longer streaming time series to be stored in main memory. CBC gains better time complexity and space storage. The reduction technology with measure of CBC does not decrease the accuracy. When outliers exist in the streaming time series, CBC has better clustering performance than the other two methods.

References

1. Guha, S., Rastogi, R., Shim, K.: Cure: An efficient clustering algorithm for large databases. In ACM SIGMOD Conference (1998)
2. Zhang, T., Ramakrishnan, R., Livny, M.: Birch: An efficient data clustering method for very large databases. In ACM SIGMOD Conference (1996)
3. Aggarwal, C., Han, J., Wang, J., Yu, P. S.: A Framework for Clustering Evolving Data Streams, Proc. 2003 Int. Conf. on Very Large Data Bases (VLDB'03), Berlin, Germany (2003)

4. Guha, S., Mishra, N., Motwani, R., O'Callaghan, L.: Clustering data streams. In Proceedings of the Annual Symposium on Foundations of Computer Science. IEEE (2000)

5. Guha, S., Meyerson, A., Mishra, N., Motwani, R., O'Callaghan, L.: Clustering Data Streams: Theory and Practice TKDE special issue on clustering, Vol. 15 (2003)

6. Keogh, E., Lin, J., Truppel, W.: Clustering of time series subsequences is meaningless: Implications for previous and future research. In IEEE ICDE (2003) 115-122

7. Bagnall, A., Janacek, G.: Clustering time series with clipped data. Machine Learning 58(2-3) (2005) 151-178

8. Lin, J., Keogh, E., Lonardi, S., Chiu, B.: A symbolic representation of time series, with implications for streaming algorithms. In ACM SIGMOD Conference (2003) 2-11

9. Lkhagva, B., Suzuki, Y., Kawagoe, K.: Extended SAX: Extended of Symbolic Aggregate Approximation for Financial Time Series Data Representation. In DEWS2006.

10. Faloutsos, C., Ranganathan, M., Manolopoulos, Y.: Fast Subsequence Matching in Time-Series Databases. In ACM SIGMOD Conference (1994) 419-429

11. Chan, K., Fu, A. W.: Efficient Time Series Matching by Wavelets. In IEEE ICDE (1999) 126-133

12. Han, J., Kamber, M.: Data Mining- Concepts and Techniques, Morgan Kaufmannn, (2000)

13. Keogh, E., Chakrabarti, K., Pazzani, M., Mehrotra, S.: Dimensionality reduction for fast similarity search in large time series databases Journal of Knowledge and Information Systems (2000)

14. O'Callaghan, L., Mishra, N., Meyerson, A., Guha, S., Motwani, R.: Streaming-data algorithms for high quality clustering. In IEEE ICDE (2002)

Support Vector Machine Detection of Peer-to-Peer Traffic in High-Performance Routers with Packet Sampling: Nonlinear Kernel Approach

F.J. González-Castaño[1], P.S. Rodríguez-Hernández[1], R.P. Martínez-Álvarez[1], and A. Gómez-Tato[2]

[1] Departamento de Ingeniería Telemática, Univ. de Vigo, Spain
[2] CESGA, Spain
{javier,pedro,rmartinez}@det.uvigo.es,agomez@cesga.es

Abstract. In this paper, we apply nonlinear support vector machines to identify peer-to-peer (p2p) traffic in high-performance routers with packet sampling. Due to their high port rates, those routers cannot extract the headers of all the packets that traverse them, but only a sample. The results in this paper suggest that nonlinear support vector machines are highly successful and outperform recent approaches like [1,2].

Keywords: support vector machines, detection, p2p.

1 Introduction

In this paper, we apply nonlinear support vector machines [3,4] to detect peer-to-peer (p2p) traffic in high-performance routers with packet sampling. User behavior in research networks has changed radically with the advent of p2p multimedia file transfers: many users take advantage of the huge bandwidth to exchange movies and the like. This behavior may have a deep impact on research network utilization. We have identified similar concerns in other research networks (http://security.uchicago.edu/peer-to-peer/no_fileshare.shtml).

The increasing usage of p2p software in the last three years has raised the need of p2p detection tools. There are some related initiatives. Among them, in [5], the authors describe a methodology to identify p2p flows at the transport layer, based on connection patterns of p2p flows, regardless of packet payloads. The authors point that these patterns are more difficult to conceal than explicit flow-conveyed information. In [6], the authors propose to detect p2p traffic by identifying protocol-dependent signatures (key strings) in TCP packet payloads. This is unfeasible in high-performance routers that *sample* packet headers. However, it may be valid for low-to-medium performance routers. In [1], the authors present a Bayesian classifier of protocols. Although the mean classification accuracy (across all application types) is quite good, the results for p2p traffic are quite poor (an accuracy of 56%).

The MOLDEIP p2p detection tool we have developed fulfils the following goals: (i) it is independent from router performance, (ii) it is transparent to the users and (iii) it works with *sampled* packet headers[1]. It does not consider individual flows but the average activity of individual IP addresses. Consequently, there is no short-term technological dependence. Recent network activity is taken from CISCO *netflow* files, and thus we do not consider packet payloads (unlike the approach in [6]). As in [5], the system is transparent to network users because it does not scan their machines. It works with packet headers, and it does not check them all, but only a sample.

Off-line analysis is feasible because p2p traffic is a nuisance, but it does not disable the network. Thus, a 24-hour decision delay is acceptable.

MOLDEIP employs support vector machines (SVM). Reference [7] also uses SVMs to detect anomalous traffic, but it focuses on intrusion attacks instead of p2p traffic identification. In [2] we demonstrated that linear support vector machine detection of p2p traffic in high-performance routers with packet sampling is highly successful and outperforms recent approaches like [1]. In this paper we evaluate nonlinear support vector machines for the same purpose.

Specifically, we consider the problem of constructing SVM classifiers based on a given classification of m *training* vectors (*points*) in the n-dimensional space $I\!R^n$, represented by the $m \times n$ matrix D, given the membership of each IP point D_i, $i = 1, \ldots, m$ in one of two classes - "innocent" or "guilty"-. Each point $D_i \in I\!R^n$ is a vector representing an IP address within the Galician RECETGA network, whose components codify the behavior of that IP address.

For this problem, in [2] we followed the linear programming model in [10]:

$$
\begin{aligned}
\min_{w,z,\gamma,y} \quad & e'y + e'z \\
\text{such that } & C(Dw - e\gamma) + \tfrac{1}{\alpha}y \geq e \\
& -z \leq w \leq z, \ y \geq 0, \ z \geq 0,
\end{aligned}
\tag{1}
$$

where w is a vector of separator coefficients, y is a vector of slack variables, γ is an offset, α is an error penalty, C is a $m \times m$ diagonal matrix with plus ones or minus ones depending on the class of the points represented by D rows, and e stands for a vector of ones of appropriate dimension. This model allows us to employ state-of-the art linear programming solvers. If we compare (1) with the original quadratic model in [3], we see that it tries to minimize the 1-norm of the w parameters instead of their 2-norm (the 2-norm maximizes the margin $\frac{2}{w'w}$ between the bounding planes $x'w = \gamma \pm 1$ in the standard formulation).

We briefly comment our notation: Capital Latin letters are sets or matrices depending on the context. Lower case Latin letters denote vectors in $I\!R^n$, except for the range $i, \ldots, q$ that denotes integers. Lower case Greek letters are real scalars. Subindices are different components, i.e., x_i is the i-th component of the n-component vector x and $a'b$ is the inner product $\sum_{i=1}^n a_i b_i$. For any vector, a K subindex denotes a subvector whose components have indices belonging to the set K. For any matrix B, B_i is its i-th row, and B_K is the submatrix composed of all B_i such that $i \in K$. For any entity, a superindex is an iteration index.

We seek (*i*) a high classification accuracy, (*ii*) few nonzero classifier components (for fast operation and identification of statistically relevant information), (*iii*) few active constraints at the solution of problem (1). The corresponding set D_K of *support vectors* represents problem (1), i.e. the solution does not change if we drop the remaining vectors. When *updating* classifiers, it is interesting to add to the next problem as few representatives of previous training datasets as possible -i.e. their support vector sets-.

The rest of this paper is organized as follows: in section 2 we model p2p detection. In section 3 we evaluate detection with *full* monitoring of packet headers. In section 4 we evaluate detection from *sampled* packet headers, the main goal of this work. Finally, section 5 concludes the paper.

2   Problem Modeling

At the time this paper was written, all RECETGA network traffic of the Vigo Campus traversed *both* a CISCO 7206 router and a Juniper M10 router. The former produced binary netflow files comprising the headers of *all* traversing packets (origin and destination IP addresses, port identifiers, protocol identifiers, etc), whereas the latter only extracted the information of 0.1% packets.

We define a new problem each 24-hour slot, from a netflow data batch compiled in the previous slot. First, we convert the netflow files to ASCII format with *Flow-tools* (http://www.splintered.net/sw/flow-tools/). The resulting 24-hour files occupy 2 GB for the CISCO 7206 and 50 MB for the Juniper M10. Each line in these files corresponds to a single end-to-end transfer, with the following fields: *unix time*, *number of transferred packets*, *transfer size* in bytes, *origin IP address*, *destination IP address*, *origin port*, *destination port* and *transport protocol* (TCP or UDP).

Note that there is no flow nor session information: for a given IP address within RECETGA range, there may be thousands of end-to-end IP transfers that appear in the ASCII file as independent entries. Basically, our preprocessor generates a dataset with *a single entry* per RECETGA IP address.

Remark 1: The fields in each dataset entry match the current high-level metrics in RECETGA graphic analysis tools.

Previous analyses [11] have identified the block sizes and packet formats of most popular p2p protocols nowadays. However, We do not consider explicit p2p protocol information (which can be concealed or encrypted). Our parameters comprise different aggregation levels (day time, night time, 5-minute time slots and 1-hour time slots), to consider temporal behavior.

Let x be a RECETGA IP address. Its dataset entry has the following fields:

```
p1: number of different IP addresses x sets connections to, day time
p2: number of different IP addresses x admits connections from, day time
p3: number of different ports in x external IP addresses access, day time
p4: number of different ports x opens, day time
p5: total traffic x generates, day time (MB)
p6: total traffic x receives, day time (MB)
p7 - p12: same as p1-p6, night time
```

```
p13: average number of different IP addresses x sets connections to, day time, measured in
     5-minute slots
p14: same as p13, standard deviation
p15: same as p13, maximum
p16: average number of different IP addresses x admits connections from, day time, meas. in
     5-minute slots
p17: same as p16, standard deviation
p18: same as p16, maximum
p19: average number of different ports in x external IP addresses access, day time, meas. in
     5-minute slots
p20: same as p19, standard deviation
p21: same as p19, maximum
p22: average number of different ports x opens, day time, meas. in 5-minute slots
p23: same as p22, standard deviation
p24: same as p22, maximum
p25: average traffic x generates in a 5-minute slot, day time (MB)
p26: same as p25, standard deviation
p27: same as p25, maximum
p28: average traffic x receives in a 5-minute slot, day time (MB)
p29: same as p28, standard deviation
p30: same as p28, maximum
p31 − p48: same as p13-p30, night time
p49 − p66: same as p13-p30, 1-hour measurement slots
p67 − p84: same as p49-p66, night time
```

3   Performance Evaluation, CISCO 7206

We selected a representative netflow file for the evaluations in this section, corresponding to all RECETGA traffic March 28 2003. This file contained a typical RECETGA behavior without unusual events.

Remark 2: As previously said, at the time this paper was written, all Vigo Campus traffic traversed both the CISCO 7206 and the Juniper M10. Since the CISCO 7206 monitored all traffic, we analyzed its logs (i) to determine the effectiveness of SVMs for p2p off-line detection and (ii) to determine statistically relevant parameter classes. The main goal of this work is p2p detection from *sampled* data, as imposed by the Juniper M10. We study that case in section 4.

3.1   Training and Testing Sets

First, we applied two filters to the problem:

1. The preprocessor only generated entries for IP addresses belonging to *Universidad de Vigo*: 6141 IP addresses passed this filter.
2. The preprocessor only generated entries for IPs exchanging over 1000 KB/day (`threshold` parameter): 614 IP addresses passed both filters.

The preprocessing times on a Pentium IV (2.4 GHz, 512 MB DDR) are 17.5 hours for `p1-p12`, 1.25 hours for `p13-p48` and 7.25 hours for `p49-p84`. There are three types of parameters: *IP parameters*, such as `p1` and `p2`, *port parameters*, such as `p3` and `p4` and *traffic parameters*, such as `p5` and `p6`.

Once we obtained the dataset, we labeled it as follows to train the classifier:

1. *"Guilty" entries*: those satisfying any of the following conditions:
(1.1.) using TCP ports of well-known P2P protocols.
(1.2.) large night downloads: $p12 > 100 \times$ `threshold`

(1.3.) relatively large uploads: $((\texttt{p5} > 10 \times \texttt{threshold})$ AND $(\texttt{p5} > \texttt{p6}))$ OR $((\texttt{p11} > 10 \times \texttt{threshold})$ AND $(\texttt{p11} > \texttt{p12}))$

2. *"Innocent" entries*: otherwise.

Remark 3: RECETGA labeling criteria may vary with network regulations.

Remark 4: for further validation of labeling criteria 1-2, we checked the IP addresses in the dataset that established connections with well-known p2p servers. We detected 29 such addresses, which we had correctly labeled as "guilty" ones.

Finally, 456 "innocent" and 158 "guilty" IP addresses resulted. We divided the labeled dataset into one hundred random partitions of *training* and *testing* subsets (90% and 10% points, respectively). Let p be the percentage of "guilty" points (in this case, $p = 0.26$). Rather than applying the same factor $1/\alpha$ to all error variables in (1), we weighted them differently depending on point class: $1/p\alpha$ for "innocent" points and $1/(1-p)\alpha$ for "guilty" ones.

3.2 Parameter Options in SVM Training

We solved problem (1) on each training subset, and then tested the resulting classifier on the corresponding testing subset. Table 1 shows average results (across the 100 experiments) for parameter options **A** and **B** below (*note*: we tuned α in (1) in preliminary trials; N_w is the average number of nonzero classifier coefficients at the solution; N_{sv} is the average number of support vectors at the solution; a_g and a_i are average blind testing accuracies on the testing subsets for "guilty" and "innocent" IP addresses, respectively).

In option **A**, all parameters participate in the model. In option **B**, only day-time port parameters participate. This choice is motivated by three facts: first, malicious users may decide to hide behind the bulk of day-time traffic. Second, the parameters that depend on the number of IP addresses will be unfeasible with the advent of the huge IPv6 addressing range. Third, the size of "normal" data transfers keeps growing with the capacity of servers and links. For example, soon all p2p movie exchanges will consist of full DVD contents. Thus, traffic parameters have a strong short-term technological dependence. Note that the labeling criteria in section 3.1 are useless as *detection* criteria with option B.

Table 1. Average SVM results, options A and B, $\alpha = 10$

Option	N_w	N_{sv}	a_g	a_i
A	44	25%	74.1%	92.9%
B	11	42.4%	65.9%	93.4%

For option B, the testing accuracy for "guilty" points is low ($\sim 66\%$), and the testing accuracy for "innocent" points is high ($\sim$93%). However, the latter is less important for RECETGA managers than the performance for "guilty" points. As it could be expected, the number of points that support the classifier (N_{sv})

grows when limiting the number of parameters. In any case, even with option
B it is possible to discard 60% of them. The number of statistically significant
parameters is surprisingly low for option B, for a similar performance.

In general, option B seems better than option A. However, in principle, it is
not valid due to its low testing accuracy for "guilty" points. In the following
subsection we propose a first strategy to correct this problem.

3.3 γ Shift

In [2] we proposed a simple strategy to balance a_g and a_i. "Guilty" points tend
to form a "small" cloud at the edge of the "innocent" region in parameter space.
Consequently, once the classifier was available, we "tuned" it by shifting γ (we
refer the reader to [2] for an exact description of this procedure).

The resulting average accuracies of the tuned classifiers are well balanced. For
option A, a_g=90.2% and a_i=87.1%. For option B, a_g=79% and a_i=78.7%. We
observe that the testing accuracy for "guilty" points grows to $\sim$80% for option
B, which is much better than the results in [1].

For RECETGA managers, a high detection accuracy for "guilty" points is ex-
tremely important. In other networks, avoiding false positives may be preferable.
Note that γ-shift is a parameterizable process that can be adjusted accordingly.

3.4   Faster Preprocessing Stage

Solving (1) with CPLEX took few seconds in all tests, so preprocessing is domi-
nant in solution time. From the experience of RECETGA managers, port param-
eters are significant. Thus, in order to decrease preprocessing time, we defined
two new parameter options **C** and **D**. Option C consists of day-time port param-
eters, aggregation levels of 1 hour and 5 minutes. Option D consists of day-time
port parameters, aggregation level of 5 minutes.

Table 2. Average SVM results with γ shift, options B-D, $\alpha = 10$

Option	N_w	N_{sv}	a_g	a_i
B	11	42.4%	79%	78.7%
C	10	44.3%	78.3%	78.1%
D	6	47.2%	81.6%	81.4%

Table 2 shows the performance of trainer (1) with γ shift for these options.
We observe that, although the average number of support vectors grows slightly,
restricting parameters to 5-minute aggregation also yields the following:

1. Although all parameters in option D are significant, there are only 6 such
   parameters: p19-p24. In the training scenarios, these parameters appear fre-
   quently at the solution with nonzero weights: p19 in 100% scenarios, p20 in
   99%, p21 in 99%, p22 in 87%, p23 in 87% and p24 in 100%.

2. An average testing accuracy a_g of 81.6%. In other words, only 2-3 guilty IP addresses escape in each scenario, on average. Apparently, a 5-minute aggregation level captures the evolution of user behavior along the day.

If we preprocess the netflow files with the parameter options so far, the following preprocessing times result: 26 hours for option A, 7.75 hours for option B and 3.25 hours for option C. For option D, we only need ~34 min of Pentium IV CPU to preprocess 24 hours of RECETGA monitoring data.

3.5   Nonlinear Kernel Approach

Although γ-shift balances classification performance, it has no theoretical support. Therefore, we decided to apply a nonlinear kernel to the best scenario so far –option D– as follows: we extracted a kernel subset of 30 innocent and guilty points (15+15). From the original dataset in option D we generated a new one by applying the degree 9 polynomial kernel in [8] $K(u,v) = \frac{1}{512}(u/||u|| \cdot v/||v|| + 1)^9$, where u is an original point and v is a point in the kernel subset (both in $I\!R^6$). This polynomial kernel has been highly successful in text recognition. Therefore, each original point is mapped into a new one in $I\!R^{30}$. We only allow a subset of the original points in the kernel subset because this strategy produced good results in [9], for a low increase in computing load.

We ran 100 experiments (reserving 10% points in each case for testing) with $\alpha = 0.01$, and obtained the following results for option D: $N_w = 15$ (11 guilty points and 4 innocent points in the kernel subset), $N_{sv}=45.9\%$, $a_g=80.8\%$, $a_i=83.6\%$. Thus, the nonlinear support vector machine and the linear one with γ-shift behave similarly for the CISCO 7206.

4   Performance Evaluation, Juniper M10

In this section we evaluate the impact of packet sampling on p2p detection accuracy. The Juniper M10 (M10 in the sequel) cannot store all traversing packet headers. In RECETGA, the M10 samples 0.1% of them. As a result, we relaxed M10 labeling, by setting `threshold` to 1 KB/day.

Remark 5: this obvious change is the only design decision to admit sampled data, i.e. we use exactly the same programs and methodologies in section 3, but we feed them with the sampled headers of the M10.

Table 3 shows SVM detection performance March 28 2003, when RECETGA traffic traversed *both* the CISCO 7206 and the M10. Full preprocessing was much faster on M10 sampled data: it took less than 30 seconds. So there is no advantage in defining different aggregation levels, in terms of preprocessing time.

Note that the methodologies in section 3 improve on M10 data. If we apply γ-shift, for less significant port parameters (3 versus 6) and a comparable average number of support vectors, the average testing accuracy for "guilty" points is practically 90%. In all experiments, the three significant parameters in option D with γ-shift are p19, p21 and p24.

Table 3. Average SVM results. Option D, Juniper M10 dataset

Method	α	N_w	N_{sv}	a_g	a_i
Linear w. γ-shift	10	3	50.3%	89.3%	83.2%
Nonlinear	0.1	6	28.3%	91.6%	90.5%

If we apply the nonlinear kernel in section 3, only 6 points in the kernel subset are significant at the solution: 2 guilty points and 4 innocent points, on average. The average number of support vectors drops to 28% and the average testing accuracies (for innocent and guilty points) are well balanced and exceed 90%

5   Conclusions

High performance routers cannot monitor all the packet headers, due to their high line rates. As a consequence, techniques such as [5] are unfeasible. Nonlinear support vector machine detection of sampled p2p traffic achieves classification accuracies above 90%. It also outperforms the γ-shift procedure in [2] in average number of support vectors. The kernel in our experiments was quite small, with as few as six significant points.

References

1. Moore, A. W. and D. Zuev. Internet Traffic Classification Using Bayesian Analysis Techniques. In *Proc. ACM Sigmetrics 2005*.
2. González-Castaño, F.J., P.S. Rodríguez-Hernández, R. P. Martínez-Álvarez and A. Gómez-Tato. Support vector machine detection of peer-to-peer traffic in high-performance routers with packet sampling. In *Proc. ICANNGA 2007*.
3. Vapnik, V. N. *The nature of statistical learning theory*. Springer, New York, 1995.
4. Cristianini, N. and J. Shawe-Taylor. *An introduction to support vector machines*. Cambridge University Press, 2000.
5. Karagiannis, T., A. Broido, M. Faloutsos and K.C. Claffy. Transport Layer Identification of P2P Traffic. In *Proc. ACM IMC 2004*.
6. Sen, S., O. Spatscheck and D. Wang. Accurate, Scalable In-Network Identification of P2P Traffic Using Application Signatures. In *Proc. 13th International Conference on World Wide Web*, 2004.
7. Tran, Q.A., H. Duan and X. Li. One-Class Support Vector Machine for Anomaly Network Traffic Detection. 2nd Network Research Workshop, 18th APAN, 2004.
8. DeCoste, D. and B. Schoelkopf. Training Invariant Support Vector Machines. *Machine Learning*, 46:161-190, 2002.
9. González-Castaño, F.J., U. M. García Palomares and R. R. Meyer. Projection Support Vector Machine Generators. *Machine Learning*, 54-1:33-44, 2004
10. Bradley, P.S., O. L. Mangasarian and D. R. Musicant. Optimization Methods in Massive Datasets. In *Handbook of Massive Datasets*, J. Abello, P. M. Pardalos and M. G. C. Resende, Editors, Kluwer Publishing, 439-472, 2002.
11. Karagiannis, T., A. Broido, N. Brownlee, K.C. Claffy and M. Faloutsos. File-sharing in the Internet: A characterization of P2P traffic in the backbone. Technical report, Department of Computer Science, University of California, Riverside. *http://www.cs.ucr.edu/~tkarag/papers/tech.pdf*, 2003.

An Algorithm for Generating Classification Rules Based on Extended Function Dependency

Xiaoping Zhang, Fengzhan Tian, and Houkuan Huang

School of Computer & Information Technology,
Beijing Jiaotong University, Beijing 100044, P.R. China
xiao_ping_zhang@126.com,{fzhtian,hkhuang}@bjtu.edu.cn

Abstract. Classification is an important task in the fields of data mining and pattern recognition. Now there have been many algorithms for this task, while most of them do not focus on the application in databases. In this paper we extend the definition of function dependency, prove the properties of the extended function dependency, and on this basis propose an algorithm for classification. According to the two theorems in the paper, our algorithm is complete that means it can find all the classification rules from the database. At last, we demonstrate our algorithm by an example that shows the validity of our algorithm.

Keywords: Data mining, Classification, Function Dependency, Scope.

1   Introduction

Classification is an important task in the fields of data mining and pattern recognition[1,2] and there have been developed many algorithms used for this task[3] up to now. At present, the most used classification methods include decision tree method (such as C4.5[4], SLI algorithm[5] and SPRIN algorithm[6]), Bayesian classifiers (such as Naive Bayes[7], TAN[8,9] etc.), artificial neural network[10], classification algorithm based on association rules[11], rough set[12] and so on. Although these algorithms are used successfully in many problems, they all use the strategy of handling the dataset in main memory that is hard to integrate with database system. When the dataset is too large to be stored in memory, the above methods can't be applied. So it is very important to study classification techniques oriented to database system.

At present, classification algorithms oriented to database system mainly include MIND algorithm[13] and GAC-RDB algorithm[14]. MIND builds classifiers using decision tree method, compute the class distribution information of the datasets of non-leaf nodes using UDF method and partition the dataset. MIND algorithm is apt to integrate with database system, but the UDF is achieved by advanced program language that can't utilize the query optimization mechanism of the database system. So it is very complex to program and maintain UDF. In addition, the function achieved by SQL statements in MIND algorithm is very simple, but the way of using SQL statements is very complex. GAC-RDB is a kind of classification algorithm using SQL statements. Its advantage is to use the standard group aggregation

statements which can take advantage of the query processing function of database system so as to improve its efficiency and expandability. Also, the algorithm does not need to transform the dataset to the format of transaction database and to scan the dataset repeatedly. Furthermore the algorithm is apt to be programmed and integrated with database system. But the algorithm still needs to be improved in some aspects, such as how to determine automatically the parameters in the algorithm and how to improve the feature selection method etc.

In this paper, we use the idea of discernible matrix in rough set[15] and Granule calculating[16] for reference and extend the definition of function dependency. And then, we prove the properties of scope of the extended function dependency and on this basis propose a classification algorithm. Our algorithm has the following advantages. It can obtain the Boolean matrixes representing the function dependency relations by scanning database only once. Using logical operation 'Or' on Boolean matrixes, we can get all the classification rules. The algorithm is efficient because of the use of Boolean operations. In addition, the algorithm can generate all the classification rules without requiring manual input parameters. The two theorems in the paper guarantee the completeness of our algorithm. Finally, the generated classification rules are represented as the form of function dependency and easy to understand.

2   Function Dependency and Its Extension

2.1   The Definition of Function Dependency

Definition 1. Let R is a relational schema, $X, Y \subseteq R$, $X \rightarrow Y$ represents a function dependency, r is a relation of R. r fits function dependency $X \rightarrow Y$ if and only if $u_1[X] = u_2[X]$ implies $u_1[Y] = u_2[Y]$ for $\forall u_1, u_2 \in r$. An equivalent description is as follow: r fits function dependency $X \rightarrow Y$ if and only if for $\forall (u_1, u_2) \in r \times r$, $(u_1[X] = u_2[X]) \Rightarrow (u_1[Y] = u_2[Y])$ is true.

There are two conditions of $(u_1[X] = u_2[X]) \Rightarrow (u_1[Y] = u_2[Y])$ being true. One is $u_1[X] \neq u_2[X]$; the other is $u_1[X] = u_2[X]$ and $u_1[Y] = u_2[Y]$. Definition 1 shows that in classical relation theory, relation r fitting function dependency $X \rightarrow Y$ indicates that each pair (u_1, u_2) in $r \times r$ satisfies implication $(u_1[X] = u_2[X]) \Rightarrow (u_1[Y] = u_2[Y])$. Next we extend the above definition and allow part of pairs (u_1, u_2) in $r \times r$ to satisfy $(u_1[X] = u_2[X]) \Rightarrow (u_1[Y] = u_2[Y])$. We name the set of this part of pairs (u_1, u_2) as the scope of function dependency $X \rightarrow Y$.

2.2   The Definition of Extended Function Dependency

Definition 2. Let R is a relational schema, $r = \{u_1, ... u_n\}$ is a relation of R, $X, Y \subseteq R$, the scope of function dependency $X \rightarrow Y$ on relation r is denoted with $F_{X,Y}$, which is a subset of $r \times r$:

$$F_{X,Y} = \{(u_i, u_j) \mid u_i, u_j \in r \wedge ((u_i[X] = u_j[X]) \Rightarrow (u_i[Y] = u_j[Y]))\}$$

According to classical relation theory, if r fits $X \rightarrow Y$, then $F_{X,Y} = r \times r$, and if r does not fits $X \rightarrow Y$, then $F_{X,Y} \subset r \times r$.

Definition 3. Let R is a relational schema, $r = \{u_1, ... u_n\}$ is a relation of R, $X, Y \subseteq R$, the Boolean matrix T of function dependency $X \rightarrow Y$ on relation r is:

$$t_{ij} = \begin{cases} 1 & (u_i, u_j) \in F_{X,Y} \\ 0 & else \end{cases} \quad (i, j = 1, ..., n)$$

In Boolean matrix T, if all the values of a whole line are 1, we call this line as 'all 1 line'. And then we define the set of elements corresponding to the 'all 1 line' as scope of function dependency $X \rightarrow Y$.

For the analysis purpose, if we regard the table 1 as original database to generate classification rules and D as class attribute which are taken from the records in breast-cancer-wisconsin_data of UCI[17] and then the reduplicate record is removed , then we can regard $\{u_1, u_2, u_3\}$ as class one, $\{u_4, u_5, u_6\}$ as class two. We can extend function dependency to applications of classification.

Table 1. An example of a relation r

r	A (Clump thickness)	B (Uniformity of Cell Size)	C (Mitoses)	D (Class)
u_1	2	1	1	2
u_2	3	1	1	2
u_3	2	1	1	2
u_4	10	1	1	4
u_5	2	10	4	4
u_6	2	7	1	4

2.3   The Properties of the Scope of the Extended Function Dependency

Theorem 1. Let R is a relational schema, r is a relation of R, $X_1, X_2, Y \subseteq R$, then $F_{X_1 \cup X_2, Y} = F_{X_1, Y} \cup F_{X_2, Y}$.

Proof. We only need to prove the following two propositions：

(1) For $\forall (u_1, u_2) \in r \times r$, if $(u_i, u_j) \in F_{X_1 \cup X_2, Y}$, then $(u_i, u_j) \in F_{X_1, Y}$ or $(u_i, u_j) \in F_{X_2, Y}$, whose equivalent proposition is that if $(u_i, u_j) \notin F_{X_1, Y}$ and $(u_i, u_j) \notin F_{X_2, Y}$, then $(u_i, u_j) \notin F_{X_1 \cup X_2, Y}$.

(2) For $\forall (u_1, u_2) \in r \times r$, if $(u_i, u_j) \in F_{X_1, Y}$ or $(u_i, u_j) \in F_{X_2, Y}$, then $(u_i, u_j) \in F_{X_1 \cup X_2, Y}$.

The proof of the first proposition is as follows. According to $(u_i, u_j) \notin F_{X_1,Y}$ and the definition 2, we get $u_i[X_1] = u_j[X_1]$ and $u_i[Y] \neq u_j[Y]$. According to $(u_i, u_j) \notin F_{X_2,Y}$, we know $u_i[X_2] = u_j[X_2]$ and $u_i[Y] \neq u_j[Y]$. To sum up, we can infer that $u_i[X_1 \cup X_2] = u_j[X_1 \cup X_2]$ and $u_i[Y] \neq u_j[Y]$, that means $(u_i, u_j) \notin F_{X_1 \cup X_2,Y}$. So the first proposition is proved.

The proof of the second proposition is given as following. When there is $(u_i, u_j) \in F_{X_1,Y}$, according to the definition 2, there are two following cases. One case is $u_i[X_1] \neq u_j[X_1]$. Then there is $u_i[X_1 \cup X_2] \neq u_j[X_1 \cup X_2]$ and then we know $(u_i, u_j) \in F_{X_1 \cup X_2,Y}$ according to the definition 2. The other is $u_i[X_1] = u_j[X_1]$ and $u_i[Y] = u_j[Y]$, Whether $u_i[X_1 \cup X_2] = u_j[X_1 \cup X_2]$ or not, we can have $(u_i, u_j) \in F_{X_1 \cup X_2,Y}$.

When there is $(u_i, u_j) \in F_{X_2,Y}$, in the same way, we can prove $(u_i, u_j) \in F_{X_1 \cup X_2,Y}$. So we conclude that if $(u_i, u_j) \in F_{X_1,Y}$ or $(u_i, u_j) \in F_{X_2,Y}$, there is $(u_i, u_j) \in F_{X_1 \cup X_2,Y}$. The second proposition is proved. Therefore, the original proposition is proved.

Theorem 2. Let $R = \{A_1, \cdots, A_n, D\}$ is a relational schema, where $A_1, \cdots, A_n$ are conditional attributes and D is a class attribute, r is relation of R, $u \in r$, $X \subseteq R$. If for $\forall u_i \in r$, there is $(u, u_i) \in F_{X,D}$ and for each $X_1 \subset X$, there exist $u_i \in r$ which does not satisfy $(u, u_i) \in F_{X_1,D}$, then $(X = u[X]) \Rightarrow (D = u[D])$ is a classification rule.

Proof. For each $u_i \in r$, according to $(u, u_i) \in F_{X,D}$, we know $u[X] \neq u_i[X]$ or $u[X] = u_i[X]$ and $u[D] = u_i[D]$. That means for each element v whose value is $u[X]$ on X, there is $v[D] = u[D]$, namely $(X = u[X]) \Rightarrow (D = u[D])$. And because for each $X_1 \subset X$, there is $(X_1 = u[X_1]) \nRightarrow (D = u[D])$, so we know $(X = u[X]) \Rightarrow (D = u[D])$ is a classification rule.

3   An Algorithm for Generating Classification Rules Based on Scope of Extended Function Dependency

On the basis of Theorem 1 and Theorem 2, we propose an algorithm for generating classification rules based on scope of extended function dependency, whose procedure is as follows.

Input: Relational schema $R = \{A_1, \cdots, A_n, D\}$ and relation r of R, where $A_1, \cdots, A_n$ are conditional attributes and D is a class attribute
Output: A set of all classification rules S

Suppose the reduplicate records are removed before following step.

Step 1. For conditional attributes $A_1, \cdots, A_n$, calculate the Boolean matrixes of $F_{A_1,D}, \ldots, F_{A_n,D}$ in turn. For each matrix, each 'all 1 line' u can generate a classification rule, $(A_i = u[A_i]) \Rightarrow (D = u[D])$. Add it to set S.

Step 2. Let $i = 2$, $T = \{ F_{A_1,D} \}$.

Step 3. Let $T' = T \oplus F_{A_i,D}$, where

$$T \oplus F_{A_i,D} = \{ F_{X \cup \{A_i\},D} \mid F_{X \cup \{A_i\},D} = F_{X,D} \bigcup F_{A_i,D} \text{ and } F_{X,D} \in T \}$$

Step 4. Check the 'all 1 lines' of each $F_{X',D}$ in T' (here $X' = X \bigcup A_i$). If the line is included neither in T nor in $F_{A_i,D}$, then we call the line as a new 'all 1 line'. It can generate a classification rule, $(X' = u[X']) \Rightarrow (D = u[D])$. Add the rule to set S.

Step 5. Let $T = T \bigcup T' \bigcup \{ F_{A_i,D} \}$.

Step 6. Let $i = i + 1$. If $i \le n$, then go step 3; otherwise exit.

Suppose that the numbers of records and attributes in the database are m and n respectively. The Step 1 in the above procedure need to scan the database only once and then get $F_{A_1,D}, \ldots, F_{A_n,D}$, whose time complexity is O(m^2*n). The time complexity is also O(m^2*n) to find the 'all 1 lines' in $F_{A_i,D}$. In step 3, the time complexity of circling calculation of $T' = T \oplus F_{A_i,D}$ is O($2^n * m^2$). In step 4, the time complexity is O($2^n * m^2$) at worst case to check new 'all 1 lines' in each $F_{X',D}$ and then generate classification rules. So the time complexity of the whole procedure is O(m^2*n)+O($2^n * m^2$).

4   A Computation Example

Suppose $R = \{A, B, C, D\}$ and relation r of R is shown in Table 1. Assume D is a class attribute. According to the above algorithm, the steps to generate classification rules are as follows.

Step 1. Firstly generate the Boolean matrixes of function dependency $A \to D$, $B \to D$ and $C \to D$, which are denoted as table 2, table 3 and table 4 respectively. According to 'all 1 lines' in table 2, we know that $F_{A,D}$ contains u_2, u_4. So we have classification rules $(A = u_2[A]) \Rightarrow (D = u_2[D])$ and $(A = u_4[A]) \Rightarrow (D = u_4[D])$, which means $(A = 3) \Rightarrow (D = 2)$ and $(A = 10) \Rightarrow (D = 4)$. In the same way, we can get classification rule $(B = 10) \Rightarrow (D = 4)$ and $(B = 7) \Rightarrow (D = 4)$. And also according to the three 'all 1 lines' u_5 in table 4•we can get classification rule $(C = 4) \Rightarrow (D = 4)$. So, $S = \{ (A = 3) \Rightarrow (D = 2), (A = 10) \Rightarrow (D = 4), (B = 10) \Rightarrow (D = 4), (B = 7) \Rightarrow (D = 4), (C = 4) \Rightarrow (D = 4) \}$.

Step 2. Let $i = 2$, $T = \{ F_{A,D} \}$.

Step 3. Let $T' = T \oplus F_{B,D} = F_{AB,D}$, which is denoted as table 5, where all the new 'all 1 lines' are denoted by bold font.

Step 4. The new 'all 1 lines' in table 5 are u_1, u_3. So we have the following rules $(AB = \langle\, 2\, ,\, 1\, \rangle) \Rightarrow (D = 2)$. Therefore, $S = S \bigcup \{(AB = \langle\, 2\, ,\, 1\, \rangle) \Rightarrow (D = 2)\}$.

Step 5. Let $T = \{\, F_{A,D}, F_{AB,D}, F_{B,D}\, \}$.

Step 6. $i = i + 1 = 3$, go back to Step 3 of the algorithm and recalculate T and S, whose scope of function dependency are $F_{AC,D}$, $F_{BC,D}$ and $F_{ABC,D}$ respectively. The computation process is as same as the above, so we do not give the details here for the sake of space. At last, we get the following set of all the classification rules:

$$S = \{\quad (A = 3) \Rightarrow (D = 2) \quad , \quad (A = 10) \Rightarrow (D = 4) \quad , \quad (B = 10) \Rightarrow (D = 4) \quad , \quad (B = 7)$$
$$\Rightarrow (D = 4), (C = 4) \Rightarrow (D = 4), (AB = \langle\, 2\, ,\, 1\, \rangle) \Rightarrow (D = 2)\, \}.$$

Table 2. Boolean matrix of function dependency $A \to D$

$F_{A,D}$	u_1	u_2	u_3	u_4	u_5	u_6
u_1	1	1	1	1	0	0
u_2	1	1	1	1	1	1
u_3	1	1	1	1	0	0
u_4	1	1	1	1	1	1
u_5	0	1	0	1	1	1
u_6	0	1	0	1	1	1

Table 3. Boolean matrix of function dependency $B \to D$

$F_{B,D}$	u_1	u_2	u_3	u_4	u_5	u_6
u_1	1	1	1	0	1	1
u_2	1	1	1	0	1	1
u_3	1	1	1	0	1	1
u_4	0	0	0	1	1	1
u_5	1	1	1	1	1	1
u_6	1	1	1	1	1	1

Table 4. Boolean matrix of function dependency $C \to D$

$F_{B,D}$	u_1	u_2	u_3	u_4	u_5	u_6
u_1	1	1	1	0	1	0
u_2	1	1	1	0	1	0
u_3	1	1	1	0	1	0
u_4	0	0	0	1	1	1
u_5	1	1	1	1	1	1
u_6	0	0	0	1	1	1

Table 5. Boolean matrix of function dependency $AB{\to}D$

$F_{AB,D}$	u_1	u_2	u_3	u_4	u_5	u_6
$\boldsymbol{u_1}$	**1**	**1**	**1**	**1**	**1**	**1**
u_2	1	1	1	1	1	1
$\boldsymbol{u_3}$	**1**	**1**	**1**	**1**	**1**	**1**
u_4	1	1	1	1	1	1
u_5	1	1	1	1	1	1
u_6	1	1	1	1	1	1

5   Conclusion

In this paper, we extend the definition of function dependency, describe the concept of scope of function dependency and prove its properties. Based on the above properties, we put forward an algorithm for generating all the classification rules. In our algorithm, the dataset, Boolean matrixes and classification rules are all stored in database, so our algorithm can be applied to classification tasks in case of large-scale datasets. The algorithm is efficient because most of calculate is Boolean operation on Boolean matrixes. Our algorithm generates all the classification rules, but some classification rules are complex and are not typical. Next, we will do research on how to evaluate, merge and tailor the rule set to generate simple and effective rules. Our algorithm provides a new idea for research of classification method.

Acknowledgments

References

1. Han J. W., Fu Y. J., Wang W. et al.: DBMiner: A System for Mining Knowledge in Large Relational Database. In: Proceedings of the 2nd International Conference on Knowledge Discovery and Data Mining. CA, USA(1996) 250-255
2. Agrawal R., Mehta M., Shafer J. et al.: The Quest Data Mining System. In: Proceedings of the 2nd International Conference on Data Mining and Knowledge Discovery, Portland, Oregon (1996) 244-249
3. Liu H. Y.: Research and Implementation of a Fast and Scalable Classification System. Beijing: Tsinghua University(2000)
4. Quinlan J. R.: C4.5: Programs for Machine Learning. San Mateo. California: Morgan Kaufmann (1993)

5. Mehta M., Agrawal R., Rissanen J.: SLIQ: A fast scalable classifier for data mining. Lecture Notes in computer Science, Proc of the 5th International Conference on Extending Database Tech. Avignon. France(1996) l8–33
6. Shafer J. C., Agrawal R, Mehta M.: SPRINT: A scalable parallel classifier for data mining. Proc of the 22nd Int Conf on Very Large Databases. Mumbai Bombay.India(1996)
7. Elkan C.: Boosting and naïve bayesian learning. In Technical Report CS97-557, Dept. of Computer Science and Engineering, Univ. Calif. At San Diego(1997)
8. Friedman N. ,Geiger D. and Goldszmidt M.: Bayesian network classifier. Machine Learning. Vol. 29. (1997) l31–163
9. Meretakis D. and Wuthrich B.: Extending Naive Bayes classifiers using long itemsets. Chaudhuri S.Proceedings of 5th International Conference on Knowledge Discovery and Data Mining. USA: AAAI Press(l999)295-301
10. Weiss S. M. and Kulikowski C. A.: Computer Systems That Learn: Classification and Prediction Methods from Statistics. Neural Nets, Machine Learning, and Expert Systems. San Mateo, CA: Morgan Kaufmann(1991)
11. Liu B. Hsu W. Ma Y. : Integrating classification and association rule mining. Agrawal R Proc of the 4th Int Conf on Knowledge Discovery and Data Mining. NY.USA: AAAI Press(1998)80-86
12. Hu X. H.,Cercone N.:   Learing in relational database: a Rough Set approach. Computational Intelligence Vol 11. (1995) 323-338
13. WANG M., Iyer B., Vitter J. S.: Scalable mining for classification rules in relational databases. Eaglestone B. Desai B C, SHAO Jianhua.Proc of the 1998 Int Database Eng and Appl Syrup Cardiff,Wales.UK: IEEE Computer Society(1998) 58-67
14. Lu H. J. Liu H. Y.: Decision tables: scalable calssification exploring RDBMS capabilities. Proc 26th Int Conf on Very Large Databases. Cairo.Egypt (2000)373-384
15. Skowron A. ,Rauszer C.: The discernibility matrices and functions in information system. In : Slowinsk; Red. Intelligent Decision Support—Handbook of Applictions and Advances of the Rough Set Theory, Kluwer Academic Publishers(1992) 331-362
16. Liu Q. and Jiang S. L.: Reasoning about Information Granulaes Based on the Rough Logic. LNAI 2375, Springer(2002) 139-143
17. Bennett K. P., Mangasarian O. L.: Robust linear programming discrimination of two linearly inseparable sets, Optimization Methods and Software 1, Gordon & Breach Science Publishers(1992) 23-34

A Problem Oriented Approach to Data Mining in Distributed Spatio-temporal Database

Zhou Huang, Yu Fang, Xia Peng, Bin Chen, and Xuetong Xie

Institute of Remote Sensing & GIS, Peking University
Beijing, P.R. China 100871
`huangzhou@pku.edu.cn`

Abstract. Recently, a fast increment of spatio-temporal data volume has been achieved and more importantly the data might distribute everywhere. So, there is a need for spatio-temporal data mining systems that are able to support such distributed spatio-temporal query and analysis operations. Distributed spatio-temporal data mining technologies were discussed in this paper. After discussing the process of spatio-temporal data mining in distributed environment, one actual DSTDMS (Distributed Spatio-Temporal Data Mining System) was designed and then implemented. The system is based on data model of sequent snapshot and accomplished through spatio-temporal extension on PostgreSQL. Various spatio-temporal analyses and mining queries could be carried out in the system through simple SQL statements. By using the system, effective mining of distributed spatio-temporal data were achieved.

Keywords: Spatio-temporal data, Data mining, Distributed database, GIS.

1   Introduction

Along with the wide use of information technology, more and more attention is being paid on spatio-temporal data [1]. In GIS (Geographic Information System) research realm, how to discover useful knowledge among huge data distributed in network is one of the most concerned topics. There are many related researches now. Erwig [1] had a comparison and analysis among those common spatio-temporal data models, including sequent snapshot model, base state with amendment model, event based model, object oriented model and so on. Hamilton [2] concluded the architecture of distributed spatio-temporal database system and defined the concept of STDML (Spatio-Temporal Data Mining Language) and STDM (Spatio-Temporal Data Model) as well. Harms [3] researched on the architecture of knowledge discovery in spatio-temporal database. Pokrajac [4] indicated that a well approach to STDML would be achieved by extending SQL (Structured Query Language) for supporting spatio-temporal operations.

Existing researches mainly concentrate on STDM, STDML, Spatio-temporal mining algorithms, etc. However, a chief problem is that there is not one common and effective method for accomplishing a well-formed spatio-temporal data mining system, especially in the circumstance of distributed spatio-temporal database [5].

Complex characteristics of STDM and STDML, as well as lack of unified distributed spatio-temporal database architecture are the main reasons to that problem. So, it is necessary for us to provide a common and effective method for constructing DSTDMS. That is also a nature trend in GIS realm and of significance to promote the application based on spatio-temporal data.

Basing on key technologies of distributed spatio-temporal database, this paper concluded the structure model of DSTDMS (Distributed Spatio-Temporal Data Mining System). Then an instance of DSTDMS named SpatialMiningService was achieved based on that model. This paper accomplished the prototype by using PostgreSQL as the backend database and sequent snapshot as spatio-temporal data model. Running effect indicates that the system provides an effective way for the spatio-temporal data mining and analyses.

2   Structure Model of DSTDMS

Before discussing the data mining in distributed spatio-temporal database, the spatio-temporal data management should be referred firstly, which relates close with the data mining approach. Spatio-temporal data is unique for its spatial and temporal elements. The traditional method for GIS data management——combination of file and relation database——is not suitable for spatio-temporal data management [5]. And, object oriented database system is still a long way to actual applications. So, an appropriate approach is adopting ORDB (Object-Relation Database) to store and manipulate the spatio-temporal data [6]. Moreover, Spatio-temporal extension on ORDB is needed
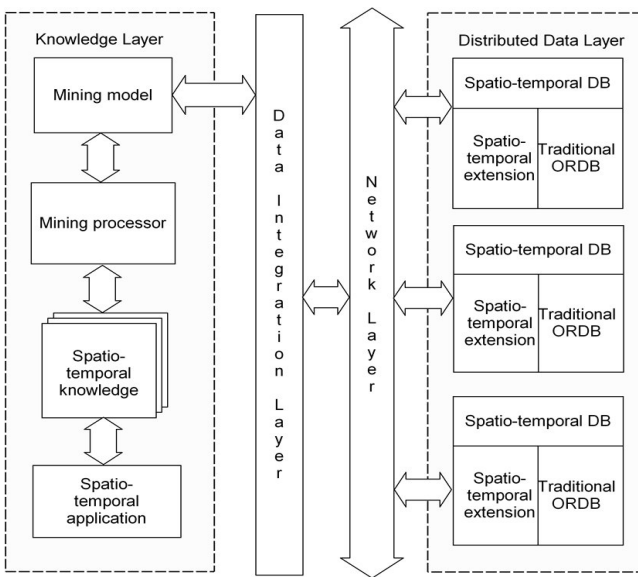
Fig. 1. Structure model of DSTDMS

for supporting operations on spatial and temporal elements and many mainstream ORDB products like Oracle, Informix and PostgreSQL all provide the mechanism of spatio-temporal extension. Thus, a typical and practical distributed spatio-temporal database is composed of a set of object-relation databases, on which spatio-temporal extension would be accomplished.

Based on the discussion above, the typical structure of DSTDMS based on ORDB backend is shown in Fig.1. Three layers, including knowledge layer, data integration layer and spatio-temporal database layer, construct a complete DSTDMS.

（1）Distributed data layer. The backend layer is composed of a set of separated spatio-temporal databases distributed on several data sites. This layer is used for spatio-temporal data storage and the data distribution could be redundant to obtain higher efficiency and stability [7]. Usually one common ORDB product like PostgreSQL or Oracle would be adopted. The capabilities of supporting spatio-temporal extension and SQL query are indispensable.

（2）Data integration layer. The middle layer in the model mainly refers to pre-selecting the data needed from separated data sites and integrating them into one complete view. This step is crucial for spatio-temporal discovery as it makes up of the data basis for further mining. This layer accepts global analysis query and translates it into a series of sub-queries, often in form of SQL statements. Then the sub-queries would be executed on selected sites and the final global data view is to be generated. Currently this topic is seldom referred in the researches of distributed spatio-temporal data mining, so this paper paid more attention on it and detailed distributed query processing algorithms were brought out and demonstrated in the system design section below.

（3）Knowledge layer. This layer is on the top of structure model and composed of various applications to abstract the specified knowledge from the spatio-temporal data, such as data visualization, classification, association, fitting, professional modeling, scientific computation, prediction and so on. The components of this layer mainly contain Mining processor and various spatio-temporal applications. The top layer is application oriented and various mining algorithms have been developed and discussed fitting to the specified spatio-temporal applications [8].

3   Design and Implementation

Based on the researches on distributed spatio-temporal data mining system model, the authors implemented an actual DSTDMS named SpatialMiningService. The system architecture was shown as Fig.2, in which the implementation could be concluded into two parts, including spatio-temporal data model, spatio-temporal extension and distributed query processing.

Query language this system used is adopted language compatible with SQL completely, so developers need not to do extra work as the system was extended on ORDB. Spatio-temporal extension should be done after adopting one suitable data
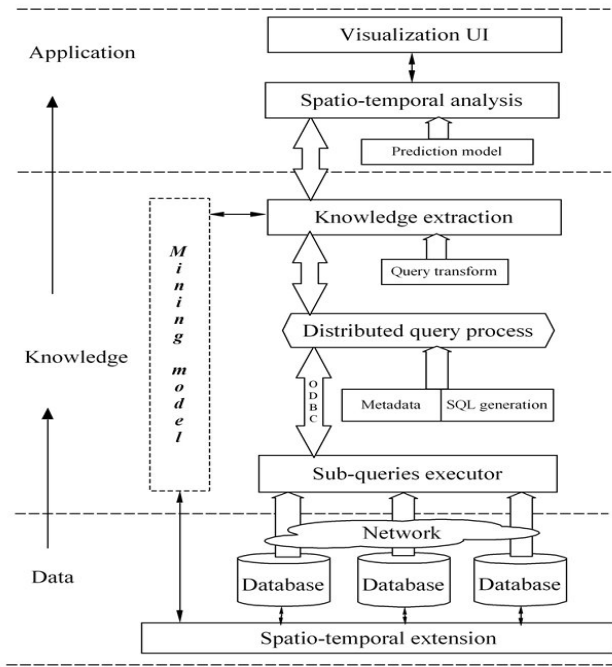
Fig. 2. System architecture of SpatialMiningService

model. SpatialMiningService uses sequent snapshot model and stores some corresponding sample data for test.

3.1 Sequent Snapshot Model

To describe the spatial objects two data models are often referred, vector model and raster model, which are also called feature model or domain model. The vector structure is used to express the discrete and separated objects while the raster structure are declined to describe the continuous phenomenon [9]. The raster model has a wide application on temperature, rainfall, pollution distribution, population evaluation, etc. Current raster model mainly refers to static model, which means it has no temporal dimension and could not express the spatio-temporal phenomenon. Considering it this paper adopted one model taking temporal dimension into account, which was called sequent snapshot model.

Sequent snapshot can be defined as $SSM = (M, S, T)$, where: S and T respsent the spatial and temporal variables. The spatial domain is partitioned into regularly rectangular grid, each of which has one value or intensity. The grids are represented by matrix. In temporal domain, a period was discretized according to a given size and divided into a series of moments. At every moment, the varying phenomenon was defined as a snapshot which was represented as a matrix with values. M is a 4-d array like $M[x, y, z, t]$, which consists of a group of matrixes in

temporal order, usually in the form of $m_1, m_2, \ldots, m_i, \ldots, m_n (1 \le i \le n)$, where $\{t_1, t_2, \ldots, t_i, \ldots, t_n\} \subset T$, m_i is the matrix snapshot at the moment t_i.

3.2 Spatio-temporal Extension

This paper extended sequent snapshot type and corresponding spatio-temporal operations based on PostgreSQL database. The type structure was shown in Table.1 and extra temporal type should be extended to record and represent the temporal variable.

Table 1. Demonstration of sequent snapshot type extension

```
Type SSM
{
    Box spatial_area;          //Spatial domain
    Time_type n_time;          // temporal domain, usually based on snapshot model
    Array IntensityValue[x,y,t]; //Intensity array
}
```

Mining model extension was accomplished in the system as well. Those mainly refer to extend spatio-temporal analysis functions between different spatio-temporal objects or data sources, such as spatial overlap function, spatial-temporal aggregation function, etc. Thus, mining process could be achieved through simple SQL statements, in which using the extended mining functions. So, the users only have to know the "problem" and submit one SQL statement and then the final knowledge would return. That's why the approach this paper brought up is called "problem oriented".

3.3 Distributed Query Processing

In SpatialMiningService, distributed query processing algorithm was combined the heuristic principles with the semi-join strategy. We concluded five basic heuristic rules in the distributed spatio-temporal query processing: (1)Execute the pre-select operations as soon as possible; (2)Execute the project operations as soon as possible; (3)Avoid only execute the Descartes accumulate but combination with selection and project operations; (4)Make the account of parallel operations most;   Select the strategy of less data transmission.

Based on the heuristic rules aforementioned and the characteristics of spatio-temporal query, the authors brought out one novel algorithm named HHOA (Hybrid Heuristic Optimization Algorithm), which is briefly described as follows.

Table 2. HHOA algorithm

Algorithm: SUBS_Generate(query)
Input: the global query string submitted by the user
Output: final result
{
   Step1(Build the query tree):
     Carry out the lexical and syntax analysis to build one query tree;
  Step2(Generate the pre-selection strategy):
   According to the components of the query tree, attract the separated conditions which
    could be executed firstly without need to data transmission;
  Step3(Generate the join strategy):
   Check if join operation appears in the global query
   {
    Case "True"
    Semi-join strategy is taken account, the less data transmission as the chief goal is the
     principle to select the optimization plan. The characteristic of huge spatial field and
     high dimensions were taken account into the selectivity factor calculation;
    break;
    Case "False"
     Skip to Step 4 directly;
   }
  Step4(Join the useful temporary results):
   The site with the most volume of temporary results is selected as the final result site,
    which means other useful temporary results would be sent to it;
  Step5(Confirm the final plan and execution):
   The execution plan mainly contains three steps (Step 2 to 4), execute them on the
    separated sites and get the final result.
}

---

4   Discussion

For demonstrating the application of SpatialMiningService the authors collected and input some sampling line and polygon data into the system, partitioning the complete data view into several ones according to the spatial domain and distributing them onto different sites (In fact, we used the railway and county data of China at different
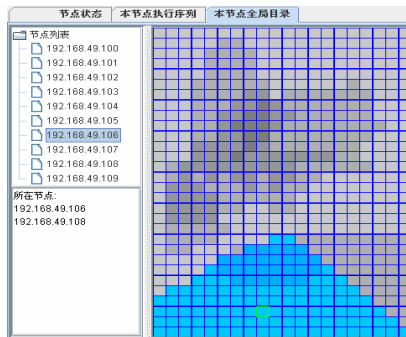
Fig. 3. The sampling data distribution

temporal points). The sampling data distribution could be shown as Fig.3 (Friendly visualization user interface was accomplished by the authors as well, through which the users could see the data distribution, knowledge visualization and even the status of the sub-queries in the execution plan).

Then the users could use simple SQL statement to model the discrete data or obtain advanced spatio-temporal knowledge. For example, we used this statement "*select county.name, county.geometry from county, rail where Overlap(rail.geometry, county.geometry) and rail.name='Zhegang Railway' and rail.time = '1997'*" to abstract the counties which the Zhegang Railway cross through at 1997. The returned result is graphically expressed as Fig.4. Also, clearly we obtained the complete data and knowledge view from the distributed spatio-temporal database according to the result.
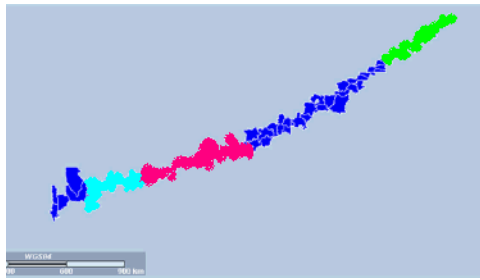
Fig. 4. The sample mining query result (different colors represent different data sites)

5   Conclusion

Spatio-temporal data mining system based on distributed database was implemented through the distributed query processing and spatio-temporal extension, mainly containing type, operation and mining model extension. This paper used the data model of sequent snapshot and constructed one actual DSTDMS named SpatialMiningService. Some experiments had been done and running effect indicates that the system provides ability for spatio-temporal manipulation and advanced analysis. Furthermore, more complex applications based on the system or this method should be experimented and more intelligent mining query language should be taken into account.

Acknowledgments

References

1. Erwig M., Schneider M. and Guting R.H.: Temporal Objects for Spatio-Temporal Data Models and a Comparison of Their Representations. Proceedings of the Workshops on Data Warehousing and Data Mining (1998)

2. Hamilton H.J. and Findlater L.: Looking Backward, Forward, and All Around: Temporal, Spatial, and Spatio-Temporal Data Mining. Proceedings of the Fifteenth International Florida Artificial Intelligence Research Society Conference (2002)
3. Harms S.K., Deogun J., Goddard S.: Building knowledge discovery into a geo-spatial decision support system. Proceedings of the 2003 ACM symposium on Applied computing (2003)
4. Pokrajac D., Hoskinson R.L., Obradovic Z.: Modeling spatial-temporal data with a short observation history. Knowledge and Information Systems. 5(3):86-95(2003)
5. Gudmundsson J., Kreveld M., Speckmann B.: Efficient detection of motion patterns in spatio-temporal data sets. Proceedings of the 12th annual ACM international workshop on Geographic information systems (2004)
6. Lin J., Keogh E., Lonardi S.: A symbolic representation of time series, with implications for streaming algorithms. Proceedings of the 8th ACM SIGMOD workshop on Research issues in data mining and knowledge discovery (2003)
7. Aggarwal C.C.: A framework for diagnosing changes in evolving data streams. Proceedings of the 2003 ACM SIGMOD international conference on Management of data (2003)
8. Kitamoto A.: Spatio-Temporal Data Mining for Typhoon Image Collection. Journal of Intelligent Information Systems. 19(1):19-26(2002)
9. Wang Y., Hijikata Y. and Nishida S.: A Study on a Spatio-Temporal Data Structure for Managing Video Data from Monitoring Cameras. Proceedings of the 17th International Conference on Advanced Information Networking and Applications (2003)

Data Set Homeomorphism Transformation Based Meta-clustering*

Xianchao Zhang, Yu Zong, He Jiang, and Xinyue Liu

School of Software, Dalian University of Technology, Dalian 116621, China
{xczhang, zongyu, jianghe, xyliu}@dlut.edu.cn

Abstract. Clustering analysis is an important data mining technique with a variety of applications. In this paper, the data set is treated in a dynamic way and a Data Set Homeomorphism Transformation Based Meta-Clustering algorithm (DSHTBMC) is proposed. DSHTBMC decomposes the task of clustering into multiple stages. It firstly constructs a series of homeomorphous data sets ranging from high regularity to low, and then iteratively clusters each homeomorphism data set based on the clustering result of the preceding homeomorphism data set. Since data sets of high regularities are easier to be clustered, and the clustering result of each homeomorphism data set can be used to induce high quality clusters in the following-up homeomorphism data set, in this way, the hardness of the problem is decreased. Two strategies (i.e., Displacement and Noising) for data set homeomorphism transformation are proposed, with classical hierarchical divisive method--Bisecting k-means as DSHTBMC's subordinate clustering algorithm, two new clustering algorithms---HD-DSHTBMC-D and HD-DSHTBMC-N are obtained. Experimental results indicate that the new clustering algorithms are remarkably better than Bisecting k-means algorithm in terms of clustering quality.

Keywords: Clustering Analysis, Meta-Clustering, Data Set Homeomorphism Transformation.

1 Introduction

Clustering analysis is an important data mining technique with a variety of applications in massive data statistic, network analysis and medicinal graph automatic detection, etc. Clustering divides the data set into different clusters according to the inherent characteristic of data, making data elements similar in the same cluster and dissimilar among different clusters. The recent study progress is proposed in [1-2]. Since the 1940's, a large number of clustering algorithms have been proposed, such as divisive method (k-means[3], CLARANS[4], FREM[5]) 、 hierarchical method (CHAMELEON[6], BRICH[7], PDDP[8,9]) 、 grid-based method (WaveCluster[10],

---

STING[11], CLIQUE[12]) and density-based method (DBSCAN[13], OPTICS[14]). These algorithms do not change the data set being processed, and they are here called static algorithms.

In this paper, a clustering strategy is proposed, which transforms data elements' positions in the data set and clusters the data set in different stages of the position transformation. Thus a Data Set Homeomorphism Transformation Based Meta-Clustering (DSHTBMC) is obtained. Different from traditional static clustering algorithms, DSHTBMC firstly adopts a data set homeomorphism transformation strategy to construct a series of homeomorphous data sets ranging from high regularity to low, and then, by iteratively calling a subordinate clustering algorithm, clusters each homeomorphism data set based on the clustering result of the preceding homeomorphism data set. Here regularity means the regular extent of data elements distribution. Since data sets of high regularity are easier to be clustered, and the clustering result of each homeomorphism data set can be viewed as a pre-clustering of the next homeomorphism data set, which induces high quality clusters in the latter one. In the end, a high quality clustering result is obtained in the original data set.

Two strategies for data set homeomorphism transformation are proposed in this paper. Displacement method views the extent of data elements closing to the barycenter of the data set as regularity, and constructs homeomorphism data sets by removing data elements from nearby barycenter to their initial positions gradually. Noising method views the even extent of data element distribution as regularity, and constructs homeomorphism data sets by adding random noises ranging from strong to weak to the original data set, where the noises are used reduce data elements' differences. Different transformation strategies lead to different DSHTBMCs and the DSHTBMCs adopting the above two strategies are called DSHTBMC-D and DSHTBMC-N respectively. The classical hierarchical divisive method--Bisecting k-means[15] is used as DSHTBMC's subordinate clustering algorithm, and two new clustering algorithms----HD-DSHTBMC-D (Hierarchical Divisive DSHTBMC Using Displacement) and HD-DSHTBMC-N (Hierarchical Divisive DSHTBMC Using Noises) are obtained. The performance differences among the new algorithms and the traditional algorithm Bisecting k-means are demonstrated with a series of experiments. Experimental results indicate that the new clustering algorithms are remarkably better than Bisecting k-means algorithm in terms of clustering quality.

This paper is organized as follows. In the next section, relevant notations and definitions are introduced. In section 3 the framework of Data Set Homeomorphism Transformation Based Meta-Clustering (DSHTBMC) and two homeomorphism transformation strategies are described. The principle and framework of hierarchical divisive DSHTBMC algorithm is discussed in Section 4. In the last section, experimental results and performance evaluations are demonstrated.

2   Preliminaries

Definition 1. For given **data set** $X = \{x_1, x_2, \cdots, x_n\}$, $\forall i \in \{1, 2, \cdots, n\}$, $x_i = (x_{i1}, x_{i2}, \ldots, x_{ip})$ is called a **data element** of X, and $\forall j \in \{1, 2, \cdots, p\}$, x_{ij} is an **attribute** of x_i.

Definition 2. For given data set X , **clustering** is a process of partitioning X into subsets $C=\{C_1,C_2,...,C_k\}$ according to inherent characteristic of data, subject to: $\forall i,j \in \{1,2,\cdots,k\}, C_i \neq \phi, C_j \neq \phi, C_i \cap C_j = \phi \ (i \neq j)$, and $\bigcup_{i=1}^{k} C_i = \{1,2,\cdots,n\}$. Where C_i is called a **cluster**, whose size is denoted by $|C_i|$.

Definition 3. For given data set $X=\{x_1,x_2,\cdots;x_n\}$, its **barycenter** is computed by $w^X =(w_1^X,w_2^X,...,w_p^X), \ \forall j \in \{1,2,...,p\}, \ w_j^X = \frac{1}{n}\sum_{i=1}^{n} x_{ij}$.

To assess the performance of clustering algorithms, two modes, external quality evaluation and internal quality evaluation are adopted at present. The former is to compare whether clustering result of an algorithm is consistent with the result obtained by professionals based on domain knowledge. The latter is mainly to compare the qualities of clustering results obtained by different algorithms. Since external quality evaluation is human dependent, most scholars adopt the mode of internal quality evaluation, so does this paper.

Sergio M.Savaresi etc.[16] proposed an internal quality evaluation, considering both similarity inside clusters and dissimilarity among clusters in accordance with the basic principles of clustering. The relevant definitions are as follows.

Assume that the clustering result is depicted as $C =\{C_1,C_2,...,C_k\}$, and the barycenter of C_i is denoted by w^{C_i} . Similarity inside a cluster is measured by **average discrete degree**. For a cluster C_i , its average discrete degree is computed as $e_i = 1/|C_i| \sum_{j \in C_i} \| x_j - w^{C_i} \|^2$. Dissimilarity among clusters is measured by **distance between clusters**, i.e., the minimum value of distances between the barycenters of a cluster C_i and the other clusters, denoted by $\hat{d}_i = \min_j (\| w^{C_i} - w^{C_j} \|)$.

With the above defined average discrete degree and distance, the internal quality can be computed by:

$$Q(C_1,C_2,...,C_k) = \sum_{i=1}^{k} |C_i| \, e_i \Big/ \hat{d}_i n \qquad (1)$$

The smaller the value $Q(C_1,C_2,...,C_k)$ is, the better quality of the obtained clustering result is[16].

Definition 4. [17] Assume $f : X \to Y$ is an one-one mapping, then f is called a **homeomorphism transformation** from X to Y . If such homeomorphism transformation f exists, then X and Y are called **homeomorphism equivalence**, denoted by $X \cong Y$. Data set X is called **original data set**, and Y is called a **homeomorphism data set** of X .

Homeomorphism is an important concept in Topology with a variety of applications in mathematics, biology and physics and so on.

3 Data Set Homeomorphism Transformation Based Meta-clustering

3.1 The Algorithm Framework

The underlying idea of data set homeomorphism transformation based meta-clustering is: constructing a series of homeomorphous data sets by transforming data positions, and clustering these homeomorphous data sets. The clustering of each homeomorphous uses the clustering result of the preceding data set as an initial solution. To The control the convergence of the algorithm, a homeomorphism factor is used, which reflects the regular degree of the data sets and can be used to. The algorithm terminates when homeomorphism factor reaches small enough.

The framework of DSHTBMC is described in algorithm 1.

Algorithm 1. DSHTBMC

Input: the original data set X, the data set homeomorphism transformation f, the
      initial value of homeomorphism factor α_0 and its threshold τ, step length λ.

Output: clustering result.

Begin

(1) $\alpha = \alpha_0$;

(2) perform homeomorphism transformation from X by calling f, and a homeomorphism data set Y is acquired;

(3) Y is clustered by calling the subroutine clustering algorithm , and clustering result C is obtained;

(4) while ($\alpha > \tau$)

    (4.1) $\alpha' = \alpha - \lambda$; $C'=\varnothing$;

    (4.2) the homeomrphism data set Y' of X is produced by calling f;

    (4.3) Y' is clustered by calling the subroutine clustering algorithm based on the initial solution C, and the clustering result C' is acquired;

    (4.4) $\alpha = \alpha'$, $C=C'$;

(5) return C;

End.

3.2 Data Set Homeomorphism Transformation Strategy

3.2.1 Displacement

The principle of displacement is that data elements of original data set X are diffused gradually from nearby barycenter to their original positions, thus a series of homeomorphism data set with different regularities are constructed. Algorithm 2 describes the framework of displacement. It can be observed from algorithm 2 that internal data difference of the obtained homeomorphism data set is largened gradually as the homeomorphism factor varies from big to small. When the homeomorphism factor equals 1, that is, $y_{ij} = x_{ij}$, the original data set is resumed.

Algorithm 2. Displacement
Input: homeomorphism factor $\alpha \geq 1$, original data set X and its barycenter w^X.
Output: homeomorphism data set.
Begin
(1) for each $x_i \in X$ do

　　for each x_{ij} do

　　if $x_{ij} \geq w_j^X$ then

　　$y_{ij} = w_j^X + (x_{ij} - w_j^X)^\alpha$;

　　else

　　$y_{ij} = w_j^X - (w_j^X - x_{ij})^\alpha$;

(2) return Y ;
End.

Power function transformation is adopted to transform position of data element x_{ij} in original data set X, so data of original data set should be normalized before data set homeomorphism transformation.

3.2.2 Noising

The essential idea of noising is to construct a series of homeomorphism data set with different regularities by adding noise from strong to weak to the original data set X. Algorithm 3 elaborates the framework of noising. During the course of the homeomorphism factor varying from big to small, the noise decreases gradually, and internal data elements differences of homeomorphism data set get largened little by little. When the homeomorphism factor equals 0, noise disappears, and then the original data set is resumed.

Algorithm 3. Noising
Input: original data set X, homeomorphism factor $\alpha \geq 0.0$.
Output: homeomorphism data set.
Begin
(1) for each x_{ij} do

　(1.1) generate a random number $R \in \{-1, 0, 1\}$;

　(1.2) $y_{ij} = x_{ij} \times (1 + R\alpha)$;

(2) return Y ;
End.

4　Hierarchical Divisive DSHTBMC

In this section, the classical hierarchical divisive method--Bisecting k-means is used as subordinate clustering algorithm of DSHTBMC, and a concrete algorithm is proposed.

4.1　Principle and Framework of the Algorithm

As an implementation DSHTBMC, we use the idea of hierarchical divisive clustering algorithm, and call this implementation as Hierarchical Divisive DSHTBMC (HD-DSHTBMC).

Hierarchical divisive clustering is a procedure of constructing hierarchical binary tree, where non-leaf nodes of binary tree denote mesne divisive clusters, and leaf nodes denote the clustering result. Correspondingly, HD-DSHTBMC performs clustering on a **homeomorphism data sets clustering tree**, which is a special hierarchical binary tree with the following features:

①The root of the tree corresponds to the initial homeomorphism data set with the highest regularity;

②The bottom layer corresponds to original data set, and each leaf node is a cluster;

③The rest layers correspond to the other homeomorphism data sets, and in each layer, a node is a cluster of the corresponding data set.

Note that each layer is more regular than the lower layers.

Algorithm 4 gives the framework of HD-DSHTBMC.

Algorithm 4. HD-DSHTBMC

Input: original data set X, the homeomorphism transformation f, the initial value of homeomorphism factor α_0 and its threshold value τ, step length λ.

Output: clustering result.

Begin

(1) $\alpha = \alpha_0$;

(2) call f to produce homeomorphism data set Y of original data set X;

(3) the initial cluster set $C = Y$;

(4) while($\alpha > \tau$) do

   (4.1) $\alpha' = \alpha - \lambda$; $C' = \varnothing$;

   (4.2) call f to produce new homeomorphism data set Y';

   (4.3) for each $C_i \in C$ do

      call Bisecting k-means algorithm to perform division operation for C_i, and insert the result into C';

  (4.4) $\alpha = \alpha'$; $C = C'$;

(5) return C;

End.

Different clustering algorithms are obtained by performing diverse strategies of data set homeomorphism transformation in the layers of the tree. The algorithms adopting displacement and noising are denoted by HD-DSHTBMC-D and HD-DSHTBMC-N, respectively.

5   Experimental Results

The contrasts of clustering quality, among Bisecting k-means, HD-DSHTBMC-D and HD-DSHTBMC-N, are shown in this section. The parameters used in HD-DSHTBMC-D algorithm are: $\alpha_0 = 1.0$, $\lambda = 1$, $\tau = 1$, and in HD-DSHTBMC-N: $\alpha_0 = 1.0$, $\lambda = 0.1$, $\tau = 0.0$.

Fig. 1 compares the qualities of the three algorithms for the same data set of different cluster numbers. The size of the data set is 15000. The three clustering

algorithms are run and the clustering results, with the number of clusters 4,6,8,10,12,14,16,18 and 20 are obtained. It can be observed from the figure that the clustering qualities of HD-DSHTBMC-D and HD-DSHTBMC-N are obviously better than Bisecting k-means method. The clustering qualities of HD-DSHTBMC-D and HD-DSHTBMC-N are very close, while HD-DSHTBMC-N is slightly better.

Fig. 2 compares the qualities of the three algorithms under the same cluster number on data sets of different sizes. The sizes of data sets are 1000, 3000, 5000, 7000, 9000, 11000, 13000, 15000. The three different clustering algorithms divide the data sets into 8 clusters. It can be concluded from the figure that the clustering qualities of HD-DSHTBMC-D and HD-DSHTBMC-N are remarkably better than Bisecting k-means method without reference to data size.
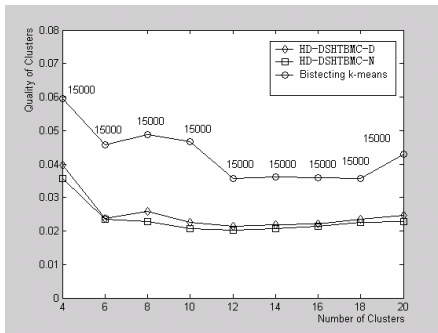
Fig. 1. Comparison of Cluster Quality of 3 Algorithms on the Same Data Set with Different Cluster Numbers
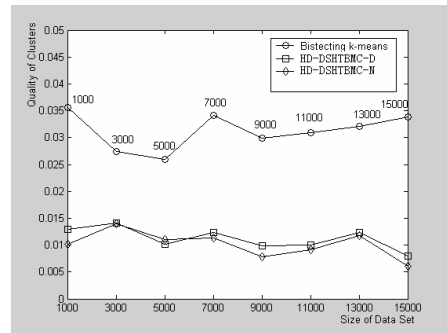
Fig. 2. Comparison of Cluster Quality of 3 Algorithms under the Same Cluster Number on Different Data Sets

6   Conclusion

Rather than concrete algorithms, the main contribution of this paper is that a novel idea of clustering, DSHTBMC, is proposed. Somehow like Shell-Sorting, which is a multi-stage sorting algorithm, DSHTBMC decomposes the task of clustering into multiple stages. Each stage is an easier clustering problem, and its solution can be used to induce solution of the next stage. In this way the initial clustering problem is eased. In contrast with traditional clustering algorithms through which the underlying data set remains changeless, homeomorphism transformation is employed in DSHTBMC. Two homeomorphism transformation strategies are introduced, and as an implementation of DSHTBMC, HD-DSHTBMC is proposed with Bisecting k-means as the subordinate algorithm. Experimental results show the effectiveness of DSHTBMC. Further works include designing diversified homeomorphism transformation strategies, diverse implementations of DSHTBMC, and employing various subordinate algorithms for different purposes.

References

1. Pavel Berkhin: Survey of Clustering Data Mining Techniques. Technical report, Accrue Software (2002)
2. Qian Wei-Ning, Zhou Ao-Ying: Analyzing Popular Clustering Algorithms from Different Viewpoints. Journal of Software (2002)1382-1394
3. Hartigan J, Wong M.: A K-means Clustering Algorithm. Applied Statistics (1979)100-108
4. Raymond T.Ng, Jiawei Han: Efficient and Effective Clustering Methods for Spatial Data Mining. Proceeding of the 20th VLDB Conference Santiago, Chile (1994)144-155
5. Ordonez C, Omiecinski E. FREM: Fast and Robust EM Clustering for Large Data Sets. In ACM CIKM Conference (2002)590-599. http://citeseer.ist.psu .edu/536108.html
6. Karypis G, Han EH, Kumar V. CHAMELEON: A Hierarchical Clustering Algorithm Using Dynamic Modeling. COMPUTER (1999)68-75
7. Zhang T, Ramakrishna R, Livny M. BIRCH: A New Data Clustering Algorithm and its Applications. Journal of Data Mining and Knowledge Discovery (1997)141-182
8. Boley DL.: Principal Direction Divisive Partitioning. Technical Report TR-97-056, Dept. of Computer Science, University of Minnesota, Minneapolis, to appear in Data Mining and Knowledge Discovery (1997)
9. Boley DL.: Principal Direction Divisive Partitioning. Data Mining and Knowledge Discovery (1998)325-344
10. Sheikholeslami G, Chatterjee S, Zhang A. WaveCluster: A Multi-resolution Clustering Approach for Very Large Spatial Databases. In .Proceedings of the 24th Conference on VLDB, New York, NY (1998)428-439
11. Wang W, Yang J, Muntz R. STING: A Statistical Information Grid Approach to Spatial Data Mining. In Proceedings of the 23rd Conference on VLDB, Athens, Greece (1997) 186-195
12. Agrawal R, Gehrke J, Gunopulos D, Raghavan P.: Automatic Subspace Clustering of High Dimensional Data for Data Mining Applications. In Proc.1998 ACM-SIGMOD Int. Conf. Management of Data (SIGMOD'98), Seattle, WA June (1998)94-105
13. Ester M, Kriegel HP, Sander J, Xu X.: A density-based algorithm for discovering clusters in large spatial database. In Proc.1996 Int. Conf.Knowledge Discovery and Data Mining (KDD'96), Portland, OR, Aug (1996)226-231
14. Ankerst M, Breunig M, Kriegel HP: Sander J. OPTICS: Ordering points to identify the clustering structure. In Proc.1999 ACM-SIGMOD Int.Conf Management of Data (SIGMOD'99), Philadelphia, PA, June (1999) 49-60
15. Sergio M. Savaresi, Daniel L. Boley. On Performance of Bisecting k-means and PDDP. In Proceedings of the 1st SIAM ICDM, Chicago, IL (2001)1-14
16. Sergio M. Savaresi etc. Choosing the Cluster to Split in Bisecting Divisive Clustering Algorithms. CSE Report TR 00-055, University of Minnesota (2000)
17. Jinkun Lin. Basic of Topology. Beijing: Science Press (2003)19-22

A Leave-One-Out Bound for $\nu-$Support Vector Regression*

Qin Ruxin[1], Chen Jing[1,$\star\star$], Deng Naiyang[1], and Tian Yingjie[2]

[1] College of Science, China Agricultural University, 100083, Beijing, China
jing_quchen@163.com
[2] Research Center on Data Technology & Knowledge Economy, Chinese Academy of
Sciences, 100080, Beijing, China

Abstract. An upper bound on the Leave-one-out (Loo) error for
$\nu-$support vector regression ($\nu-$SVR) is presented. This bound is based
on the geometrical concept of *span*. We can select the parameters of
$\nu-$SVR by minimizing this upper bound instead of the error itself, be-
cause the computation of the Loo error is extremely time consuming.
We also can estimate the generalization performance of $\nu-$SVR with the
help of the upper bound. It is shown that the bound presented herein
provide informative and efficient approximations of the generalization
behavior based on two data sets.

1 Introduction

Support Vector Machines (SVMs) have been proven to be powerful and robust
methodologies for learning from empirical data. They have been successfully
applied to many real-world problems, such as classification problem, regression
problem. It depends critically on the kernel and the parameters. One of the most
reasonable approaches is to select the kernel and the parameters by minimizing
the bound of Leave-one-out (Loo) error. However, the computation of the Loo
error is extremely time consuming. Therefore, an efficient strategy is to minimize
an upper bound of the Loo error, instead of the error itself. In fact, for Support
Vector Classification (SVC) and $\varepsilon-$support vector regression ($\varepsilon-$SVR), some
useful bounds have been proposed, see e.g. [1],[2],[3].

This paper is concerned with $\nu-$support vector regression ($\nu-$SVR). More
precisely, we will induce a bound for the standard $\nu-$SVR which corresponds
to the famous $\nu-$Support Vector Classification ($\nu-$SVC) algorithms. In our
experiments, the bound and their corresponding true Loo errors of some standard
benchmark are compared. The results show the validity of the approach proposed
in this paper.

This paper is organized as follows. In section 2, we propose the $\nu-$SVR algo-
rithm. In section 3, we induce Loo bound for $\nu-$SVR, and in section 4 experi-
ments are performed to verify the validity of our method.

** Corresponding author.

2 $\nu-$Support Vector Regression$(\nu - SVR)$

In this section, we propose the standard of $\nu - SVR$. Consider a regression problem with a training set

$$T = \{(x_1, y_1), \cdots, (x_l, y_l)\} \in (\mathcal{X} \times \mathcal{Y})^l, \tag{1}$$

where, $x_i \in \mathcal{X} = \mathbf{R}^n, y_i \in \mathcal{Y} = \mathbf{R}, i = 1, \cdots, l$. Suppose that the loss function is selected to be the $\varepsilon-$insensitive loss function.

$$c(x, y, f(x)) = |f(x - y)|_\varepsilon = max\{0, |y - f(x)| - \varepsilon\}. \tag{2}$$

In SVM framework, the input space is first mapped to a higher dimensional space $\mathcal{H}$ by

$$\mathrm{x} = \Phi(x), \tag{3}$$

and the training set T turns to be

$$\bar{T} = \{(\mathrm{x}_1, y_1), \cdots, (\mathrm{x}_l, y_l)\} \in (\mathcal{H} \times \mathcal{Y})^l, \tag{4}$$

where, $\mathrm{x}_i = \Phi(x_i) \in \mathcal{H} = \mathbf{R}^n, y_i \in \mathcal{Y} = \mathbf{R}, i = 1, \cdots, l$.

The dual optimization problem of standard $\nu-$SVR based on the training set T is

$$\max_{\boldsymbol{\alpha}^{(*)} \in \mathbf{R}^{2l}} W(\boldsymbol{\alpha}^{(*)}) = -\frac{1}{2} \sum_{i,j=1}^{l} (\alpha_i^* - \alpha_i)(\alpha_j^* - \alpha_j) K(x_i \cdot x_j) + \sum_{i=1}^{l} (\alpha_i^* - \alpha_i) y_i \tag{5}$$

$$\text{s.t.} \quad \sum_{i=1}^{l} (\alpha_i - \alpha_i^*) = 0 , \tag{6}$$

$$0 \leqslant \alpha_i^{(*)} \leqslant \frac{C}{l} , \ i = 1, \cdots, l , \tag{7}$$

$$\sum_{i=1}^{l} (\alpha_i + \alpha_i^*) \leqslant C \cdot \nu , \tag{8}$$

where $\alpha^{(*)} = (\alpha_1, \alpha_1^*, \cdots \alpha_l, \alpha_l^*)^T$, and $K(x_i, x_j) = (\mathrm{x}_i \cdot \mathrm{x}_j) = (\Phi(x_i) \cdot \Phi(x_j))$ is the kernel function. Thus, the algorithm can be established as follows:

Algorithm 1. $\nu-$Support Vector Regression$(\nu-$SVR)
1) Given a training set T defined in (1);
2) Select a kernel function $K(\cdot, \cdot)$ and parameters ν and C;
3) Solve problem (5)$\sim$(8) and get its solution $\alpha^0 = (\alpha_1^0, \alpha_1^{0*}, \cdots \alpha_l^0, \alpha_l^{0*})^T$;
4) Compute the threshold b^0 by KKT conditions(ref [4]), and construct the decision function as

$$f(x) = (\mathrm{w}^0 \cdot \mathrm{x}) + b^0 = \sum_{i=1}^{m} (\alpha_i^{0*} - \alpha_i^0) K(x_i, x) + b^0 \tag{9}$$

3   The LOO Bound

In this section, we give the definition of this error, and then estimate its bounds.

Definition 1. *Given a regression algorithm. Consider the training set* (11) *and the $\varepsilon-$insensitive loss function* (2)*. Let $f_{T|t}(x)$ be the decision function obtained by the algorithm from the training set $T|t = T \setminus \{x_t, y_t\}$, then the Loo error of the algorithm 1. with respect to the loss function and the training set T is defined as*

$$R_{Loo}(T) = \frac{1}{l}\sum_{t=1}^{l} d_t, \tag{10}$$

where,

$$d_t = \begin{cases} 0, & \text{if } c(x_t, y_t, f_{T|t}(x_t)) = 0, \\ 1, & \text{otherwise.} \end{cases} \tag{11}$$

Obviously, the Loo error is the proportion of $x_i (i = 1, \cdots, l)$ out of the $\varepsilon-$ zone. It is similar with the Loo error in [1],[2],[3], the computation cost of the Loo error is very expensive if l is large. In fact, for a training set including l numbers of training points, the computing of the Loo error implies l times of training. So finding a more easily computed approximation of the Loo error is necessary. An interesting approach is to estimate an upper bound of the Loo error, such that this bound can be computed through only one time of training. Next, we derive the bounds of the above algorithms respectively. In order to educe the Loo bound of $\nu - SVR$, we present the definition of $\nu-$span.

Definition 2. *The $\nu-$span for tth support vector is defined as*

$$S_\nu^2(t) := min\{\|\mathbf{x}_t - \hat{\mathbf{x}}_t\|_{\mathcal{F}}^2 | \hat{\mathbf{x}}_t \in \Lambda_t^\nu\} \tag{12}$$

where

$$\Lambda_t^\nu = \{ \sum_{i \in M_t(\alpha^0)}^n \lambda_i x_i : \sum_{i \in M_t(\alpha^0)}^n \lambda_i = 1, and \ \forall i \in M_t(\alpha^0), \alpha_i^{0(*)} + \alpha_t^{0(*)}\lambda_i \in [0, \frac{C}{l}]\}, \tag{13}$$

and $M_t(\alpha^0)$ is the margin support vector in the solution α^0.

Now we derive an upper bound of the Loo error for Algorithm 1. Obviously, its Loo bound is related with the training set $T|t = T \setminus \{x_t, y_t\}, t = 1, \cdots, l$. We label the solution of primal and dual problem as $\mathbf{w}^t, \boldsymbol{\xi}^{t(*)}, \varepsilon^t, b^t, \alpha^{t(*)}$.

According to (2), we say that an error is made in point $\mathbf{x}_l$ when

$$|f_{T|t}(\mathbf{x}_t) - y_t| \geq \varepsilon^t. \tag{14}$$

Obviously, $f_{T|t}(\mathbf{x}_t) = y_t$ when $\mathbf{x}_t$ is not support vector. So the error will only be occur on support vector. Next, we induce two inequalities which will be used.

The first inequality is

$$W(\alpha^t) \geq W(\alpha^0 - \delta), \tag{15}$$

where, α^t is the optimal solution of (5)~(8) based on the additional constraint

$$\alpha_t^{0(*)} = 0, \qquad (16)$$

and

$$\forall i \in M_t(\alpha^0): \ \delta_i^* = -\alpha_t^{0*}\lambda_i, \delta_i = -\alpha_t^0\lambda_i, \text{where} \sum_{i \in M_t(\alpha^0)}^{n} \lambda_i x_i \in \Lambda_t^\nu,$$

$$\forall i \notin M_t(\alpha^0) \cup \{t\}: \ \delta_i^* = 0, \delta_i = 0, \qquad (17)$$

$$\delta_t^* = \alpha_t^{0*}, \delta_t = \alpha_t^0.$$

This inequality (15) follows the solution α^t being the best legitimate solution for which $\alpha_t^{0(*)} = 0$, since $\alpha^0 - \delta$ represents a subset of the possible solutions with $\alpha_t^{0(*)} = 0$.

The second inequality is

$$W(\alpha^0) \geq W(\alpha^t + \gamma), \qquad (18)$$

where, α^0 is the optimal solution of (5)~(8), and the value of γ satisfied the follow conditions:

$$\gamma_i^{(*)} = 0, \ \text{if} \ \alpha_i^{t(*)} = 0 \text{ or } \frac{C}{l},$$

$$\gamma_t^* \gamma_t = 0, \gamma_t^* + \gamma_t \neq 0, \qquad (19)$$

and

$$\sum_{i \in M_t(\alpha^t)} (\gamma_i - \gamma_i^*) = 0, \ \sum_{i \in M_t(\alpha^t)} (\gamma_i - \gamma_i^*)y_i = 0, \ \sum_{i \in M_t(\alpha^t)} (\gamma_i + \gamma_i^*) \leq 0,$$

$$\alpha_i^t + \gamma_i \in [0, \frac{C}{l}], \alpha_i^{t*} + \gamma_i^* \in [0, \frac{C}{l}]. \qquad (20)$$

It is easy to prove the existence of γ satisfied (19)~(20).

Combining equations (15) and (18) yields

$$W(\alpha^0) - W(\alpha^0 - \delta) \geq W(\alpha^t + \gamma) - W(\alpha^t). \qquad (21)$$

To derive a bound from (21), we make use of the following lemma.

Lemma 1. *If the support vector x_t is left out, then $S_\nu^2(t)$ is defined, and*

$$W(\alpha^0) - W(\alpha^0 - \delta) = -\varepsilon|\alpha_t^{0*} - \alpha_t^0| + \frac{1}{2}(\alpha_t^{0*} - \alpha_t^0)^2 S_\nu^2(t), \qquad (22)$$

in which $S_\nu^2(t)$ is $\nu-span$.

Lemma 2. *If α^t misclassifies (x_t, y_t), it follows that*

$$W(\alpha^t + \gamma) - W(\alpha^t) \geq \Omega, \qquad (23)$$

where

$$\Omega = -\frac{C^2 D_t^2}{2l^2},\tag{24}$$

$$D_t^2 := max_{i\in\bar{T}|t}\|\mathrm{x}_t - \mathrm{x}_i\|.\tag{25}$$

For support vectors x_t misclassified by (w^t, b^t)(or α^t), we combine Lemma 1 and Lemma 2 and inequation (21) to obtain

Lemma 3. *If α^t misclassifies (x_t, y_t), it follows that*

$$-\varepsilon|\alpha_t^{0*} - \alpha_t^0| + \frac{1}{2}(\alpha_t^{0*} - \alpha_t^0)^2 S_\nu^2(t) \geq \Omega.\tag{26}$$

All the proof of the listed lemma are in the section of appendix.

4   Estimates of the LOO Error

We write $\mathcal{L}(T)$ as the number of errors made by the Loo procedure. Thus the Loo error becomes

$$e_{LOO} = \frac{\mathcal{L}(T)}{l}.\tag{27}$$

The result of Lemma 3 is a sufficient condition. That is to say, the inequality (26) may be occur when (x_t, y_t) is not misclassified. So we have the following theorem.

Theorem 1. *If the Λ_t^ν is nonempty, then the Loo error is bounded according to*

$$\frac{\mathcal{L}(T)}{l} \leq \frac{1}{l}card\{t : -\varepsilon|\alpha_t^{0*} - \alpha_t^0| + \frac{1}{2}(\alpha_t^{0*} - \alpha_t^0)^2 S_\nu^2(t) \geq \Omega\}.\tag{28}$$

where $card\{\cdot\}$ is the cardinality.
  The value of $\frac{1}{l}card\{t : -\varepsilon|\alpha_t^{0*} - \alpha_t^0| + \frac{1}{2}(\alpha_t^{0*} - \alpha_t^0)^2 S_\nu^2(t) \geq \Omega\}$ is the Loo bound for $\nu-$SVR.

5   Experiments

In this section, we will compare the Loo bound with the true Loo error. We consider two classical data bases - "Sinc" data set and "Boston Housing Data".

5.1   Results on Sinc Data Base

"Sinc" data is generated from function $sincx = \frac{sinx}{x}$ with added Gaussian noise and includes 100 instances uniformly distribute on $[-10, 10]$.
  Here we choose the Radial Basis Kernel

$$K(x, x') = exp(\frac{-\|x - x'\|^2}{\sigma^2}),\tag{29}$$

where σ is the kernel parameter, So the chose parameters in Algorithm 2.1 include C, ν, σ. and in our experiments, we choose the three parameters from the following sets:

$C \in P_1 = \{0.01, 0.1, 0.2, 0.5, 1, 2, 5, 10, 20, 50, 100, 200, 500, 1000\}$,
$\nu \in P_2 = \{0.05, 0.08, 0.1, 0.2, 0.3, 0.4, 0.5, 0.6, 0.7, 0.8, 0.9, 1\}$,
$\sigma \in P_3 = \{0.01, 0.1, 0.5, 1, 2, 3, 4, 5, 6, 10, 20, 50, 100, 200, 1000, 10000\}$.

We first describe the consequences of varying the C in S_1. We used $\nu = 0.5, \sigma = 2$ for our experiments. Applying these parameters in Algorithm 2.1 and using Definition 3.1, the Loo errors are computed. On the other hand, according to Theorem 4.1, the corresponding Loo error bounds are obtained. Both the Loo errors and the Loo error bounds are showed in Fig.1, where "$*$" denotes Loo error and "$\circ$" denotes Loo bound. To be clearly visible, the values of C are changed into $log(C)$.

Similarly, we chose $C = 1, \sigma = 2$ for our experiments with ν in S_2, the compared result is showed in Fig.2. We chose $C = 50, \nu = 0.3$ for our experiments with σ in S_3, the compared result is showed in Fig.3. To be clearly visible, the values of σ are changed into $log(\sigma)$.
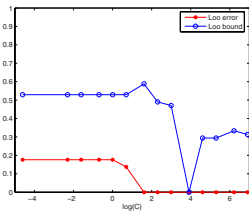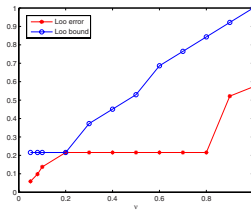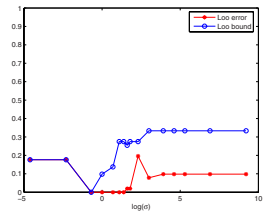
Fig. 1.   Fig. 2.   Fig. 3.

5.2   Results on Boston Housing Data

Boston Housing Data is a standard regression testing problem. This data set includes 506 instances, each of which has 13 attributes and a real-valued output. Here we randomly choose 100 instances for training, and the kernel function and parameters are all same to the experiment on Sinc Data. We choose the three parameters from the following sets:

$C \in S_1 = \{0.01, 0.1, 1, 2, 5, 8, 10, 20, 30, 50, 100, 200, 500, 1000, 10000\}$,
$\nu \in S_2 = \{0.05, 0.1, 0.15, 0.2, 0.25, 0.3, 0.4, 0.5, 0.55, 0.6, 0.7, 0.8, 0.85, 0.9\}$,
$\sigma \in S_3 = \{0.01, 0.1, 0.5, 1, 20, 50, 100, 200, 1000, 2000, 5000, 8000, 10000\}$.

We chose $\nu = 0.3, \sigma = 1$ for our experiments with C in P_1, the compared result is showed in Fig.4. The compared results of $C = 1000, \sigma = 5, \nu \in S_2$ and $C = 50, \nu = 0.3, \sigma \in P_3$ is respectively showed in Fig.5 and Fig.6.
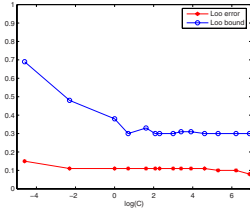
Fig. 4.
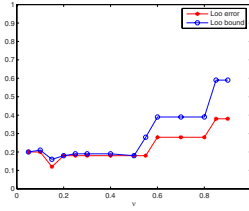
Fig. 5.
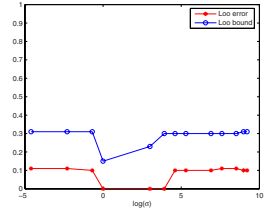
Fig. 6.

From the above figures, we can see that Loo bound which we proposed is really the upper bounds of the corresponding true Loo errors. Especially, they almost has the same trends with the corresponding true Loo errors according to variant parameters. So if we want to choose optimal parameters in Algorithm 2.1 for real problem, we only need to compute the proposed Loo bounds instead of Loo errors and it will cost much less time.

References

1. Joachims,T.: Estimating the generalization performance of an SVM efficiently[R]. In P.Langley, editor, Proceedings of the 17th International Conference on Machine Learning, 431-438, San Franscisco, California, MorganKaufmann (2000)
2. Vapnik, V., Chapelle, O.: Bounds on error expectation for support vector machines. Neural Computation[J], 12(9), (2000)
3. Tian, Y.J., Deng, N.Y.: Leave-one-out Bounds for Support Vector Regression[R]. IAWTIC. (2005)
4. Scholkopf, B., Smola, A.J.: Learning with Kernels- Support Vector Machines, Regularization, Optimization, and Beyond. The MIT Press, (2002)

Appendix

The Proof of Lemma 1
According to (17), we obtain

$$W(\alpha^0) - W(\alpha^0 - \delta) = (\alpha_t^{0*} - \alpha_t^0)(\sum_{i \in M_t(\alpha^0)} \lambda_i(f(\mathrm{x}_i) - y_i) + y_t - f(\mathrm{x}_t))$$

$$+\frac{1}{2}(\alpha_t^{0*} - \alpha_t^0)^2 \|\mathrm{x}_t - \sum_{i \in M_t(\alpha^0)} \lambda_i \mathrm{x}_i\|^2.$$

For *any* margin SVs x_i, if $\alpha_i^{0*} > 0$, $\alpha_i^0 = 0, \xi_i = 0, f(\mathrm{x}_i) - y_i = \varepsilon$; if $\alpha_i^0 > 0$, $\alpha_i^{0*} = 0, \xi_i^* = 0, y_i - f(\mathrm{x}_i) = \varepsilon$. So we yield

$$(\alpha_t^{0*} - \alpha_t^0)(\sum_{i \in M_t(\alpha^0)} \lambda_i(f(\mathrm{x}_i) - y_i) + y_t - f(\mathrm{x}_t)) = -\varepsilon|\alpha_t^{0*} - \alpha_t^0|. \qquad (30)$$

Finally, substituting in the definition of the $\nu-$span from equation (12) gives us

$$W(\alpha^0) - W(\alpha^0 - \delta) = -\varepsilon|\alpha_t^{0*} - \alpha_t^0| + \frac{1}{2}(\alpha_t^{0*} - \alpha_t^0)^2 S_\nu^2(t). \tag{31}$$

$\square$

The Proof of Lemma 2
From (19)∼(20), we obtain

$$W(\alpha^t + \gamma) - W(\alpha^t) = -\sum_{j=1}^{l}(\gamma_j^* - \gamma_j)f_{T|t}(\mathbf{x}_j) - \frac{1}{2}\|\sum_{i=1}^{l}(\gamma_i^* - \gamma_i)\mathbf{x}_i\|^2. \tag{32}$$

Based on (19),

$$\|\sum_{i=1}^{l}(\gamma_i^* - \gamma_i)\mathbf{x}_i\|^2 = (\gamma_t^* - \gamma_t)^2\|\mathbf{x}_t - \sum_{i \in M_t(\alpha^t)}\frac{\gamma_i - \gamma_i^*}{\gamma_t^* - \gamma_t}\mathbf{x}_i\|^2 \le (\gamma_t^* - \gamma_t)^2 D_t^2 \tag{33}$$

where D_t^2 is defined in (25).
By KKT condition,

$$\sum_{j=1}^{l}(\gamma_j^* - \gamma_j)f_{T|t}(\mathbf{x}_j) = \sum_{\alpha_j^{t*}>0, j\neq t}\gamma_j^*(y_j + \varepsilon^t) + \sum_{\alpha_j^t>0, j\neq t}(-\gamma_j)(y_j - \varepsilon^t) + (\gamma_t^* - \gamma_t)f_{T|t}(x_t)$$

$$= \sum_{j\neq t}(\gamma_j^* - \gamma_j)y_j + \varepsilon^t\sum_{j\neq t}(\gamma_j^* + \gamma_j) + (\gamma_t^* - \gamma_t)f_{T|t}(x_t). \tag{34}$$

According to (20),

$$\sum_{j\neq t}(\gamma_j^* - \gamma_j)y_j + \varepsilon^t\sum_{j\neq t}(\gamma_j^* + \gamma_j) \le -y_t(\gamma_t^* - \gamma_t) - \varepsilon^t(\gamma_t^* + \gamma_t). \tag{35}$$

When $\mathbf{x}_l$ is misclassified, according to (14),

$$f_{T|t}(x_t) > y_t + \varepsilon^t, \tag{36}$$

$$f_{T|t}(x_t) < y_t - \varepsilon^t. \tag{37}$$

When (36) or (37) occurs(i.e. this kind of error is occur), we let $\gamma_t > 0, \gamma_t^* = 0$ or $\gamma_t = 0, \gamma_t^* > 0$: according to (34), (35) and (36) or (37)

$$\sum_{j=1}^{l}(\gamma_j^* - \gamma_j)f_{T|t}(\mathbf{x}_j) \le -2\varepsilon^t\gamma_t^{(*)}. \tag{38}$$

Combining (32), (33) and (38),we obtain

$$W(\alpha^t + \gamma) - W(\alpha^t) \ge 2\varepsilon^t\gamma_t^* - \frac{1}{2}(\gamma_t^* - \gamma_t)^2 D_t^2 \ge \Omega, \tag{39}$$

where Ω is defined in (24).

A New Multi-class SVM Algorithm
Based on One-Class SVM

Xiao-Yuan Yang, Jia Liu, Min-Qing Zhang, and Ke Niu

Network and Information Security Key Laboratory,
Engineering College of the Armed Police Forces, Xi'an 710086, China
twinlj77@gmail.com

Abstract. Multi-class classification is an important and on-going research subject in machine learning and data mining. In this paper, we propose a new support vector algorithm, called OC-K-SVM, for multi-class classification based on one-class SVM. For k-class problem, this method constructs k classifiers, where each one is trained on data from one class. OC-K-SVM has parameters that enable us to control the number of support vectors and margin errors effectively, which is helpful in improving the accuracy of each classifier. We give some theoretical results concerning the significance of the parameters and show the robustness of classifiers. In addition, we have examined the proposed algorithm on several benchmark data sets, and our preliminary experiments confirm our theoretical conclusions.

Keywords: Machine learning, Multi-class SVM, One-class SVM.

1 Introduction

Support Vector Machines [1] (SVM) were originally designed for binary classification. How to effectively extend it for multi-class classification is still an on-going research issue. Currently there are two types of approaches for multi-class SVM. One is the "decomposition-reconstruction" architecture approach [2, 3, 4, 5] that makes direct use of binary SVMs to tackle the tasks of multi-class classification, while the other is by directly considering all data in one optimization formulation [6, 7, 8].

The first approach divides the multiple class problems into a number of binary classifications. The generalization step is based on a voting among the binary classifiers to derive the winning class. There are different transformations into binary problems [2, 3], being the most widely used: one-vs.-all (OVA), in which each class is compared with all the other classes considered as one [2]; and one-vs.-one (OVO), in which each class is individually compared with all the others [3]. They do not consider the full problem directly. Particularly, the one-vs.-all approach unbalances the training sets (if the classes are balanced, the negative class in each binary classifier will have far more samples than the positive class), and the one-vs.-one will be using only information from two classes, losing each classifier the information from all the remaining classes.

The second trend considers the multi-class problem directly as generalization of the binary classification scheme [6] and [7]. This formulation is very promising because it deals with all the samples and classes at the same time, without losing any relevant information for arriving to the best solution for each problem. Besides, the resulting machines need a lower number of support vectors [9] and achieve higher performances in the case where the training set is separable. However, if the working set selection is not good, its training speed may be slow when using a large parameter C [10].

In this paper, we propose a new algorithm for multi-class classification, called OC-K-SVM, with decomposition-reconstruction architecture. This method constructs k one-class SVM (OC-SVM) [11, 12, 13] classifiers where k is the number of classes.

The rest of this article is outlined as follows. We first give a brief account of one-class SVM in Section 2. In Section 3, we present OC-K-SVM algorithm and then show some theoretical results on OC-K-SVM. Numerical experiments are in Section 4, where we show the performance of OC-K-SVM. Finally we have some conclusions in Section 5.

2   One-Class Support Vector Machines

We first introduce terminology and notation conventions. Consider n training data points in a d-dimensional space denoted as $\{\vec{x}_1,...,\vec{x}_n\}$. An OC-SVM first projects these data into a higher, potentially infinite, dimensional space with the mapping:$\varphi: R^d \rightarrow F$ .In this space, a bounding hypersphere is computed that encompasses as much of the training data as possible while minimizing its volume. Shown in Figure 1 is an example where OC-SVM was trained on the black dots.
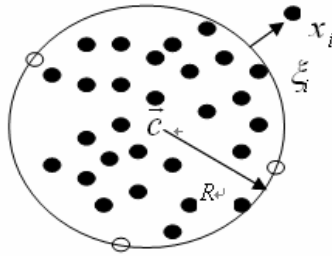
Fig. 1. The hypersphere contains the training data, described by the center $\vec{c}$ and radius R. Three white objects are on the boundary, the support vectors. One object x_i is outside and has $\xi_i > 0$.

The hypersphere center $\vec{c}$ and radius R are computed by minimizing:

$$\min_{\vec{c},R,\xi_1,...,\xi_n} R^2 + \frac{1}{n\nu}\sum_{i=1}^{n}\xi_i. \tag{1}$$

Where $v \in (0,1)$ is a parameterized constant that controls the fraction of training data that fall outside of the hypersphere, $\xi_i s$ are the "slack variables" whose values indicate how far these outliers deviate from the surface of the hypersphere. This minimization is subject to:

$$\left\| \phi(\vec{x}_i) - \vec{c} \right\| \leq R^2 + \xi_i, \quad \xi_i \geq 0, \quad i = 1,...,n. \tag{2}$$

Where $\|\cdot\|$ is the Euclidean norm. The objective function of Equation (1) embodies the requirement that the volume of the hypersphere is minimized, while simultaneously encompassing as much of the training data as possible. Equation (2) forces the training data to lie within the hyperspere.We can solve this optimization with Lagrangian multipliers.

In the following section we show how this basic framework can be extended to construct multi-class SVM with multiple hyperspheres.

3   OC-K-SVM

An OC-SVM with a single hypersphere, as described in the previous section, obviates the need for training classifiers on the other training sets. For k-class problem, we propose to cover the k-class training data sets with several hyperspheres, where each hypersphere encompasses one class subset of the training data. Shown in Figure 2 is a toy 2-D example where an OC-K-SVM was trained on three classes.
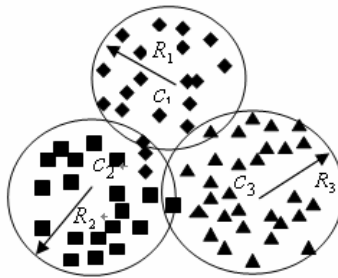
Fig. 2. Shown is a toy example of OC-K-SVM. The circles represent the OC-SVM classifiers. For example, The 2*th* one-class SVM are trained on only the black squares-notice that in the OC-K-SVM, the classifier is better able to generalize as both the black triangles and diamonds generally fall outside the support of the 2*th* bounding circle.

Note that, unlike the other multi-class SVM, an OC-K-SVM is trained on data from k classes by computing k bounding hyperspheres. We describe below the details behind the construction of such OC-K-SVM.

Given n_m training data $\left\{\vec{x}_1^m,...,\vec{x}_{n_m}^m\right\}$ for the mth class, $\vec{x}_i \in R^d$, $i=1,...,n_m$ where $m \in \{1,...,k\}$ is the class of $\vec{x}_i^m$, the OC-K-SVM solves the follows problems:

$$\min_{\vec{c}_m, R_m, \xi_i^m, \ldots, \xi_{n_m}^m} \quad R_m^2 + \frac{1}{n_m \nu_m} \sum_{i=1}^{n_m} \xi_i^m. \tag{3}$$

$$subject \quad to \quad \left\| \phi(\vec{x}_i^m) - \vec{c}_m \right\| \le R_m^2 + \xi_i^m. \tag{4}$$

$$\xi_i^m \ge 0, i = 1, \ldots, n_m, m = 1, \ldots k \tag{5}$$

where R_m and $\vec{c}_m$ are the radius and center of the mth hypersphere, $\nu_m \in (0,1)$ is a parameterized constant that controls the fraction of training data that fall outside of the mth hypersphere, the training data $\vec{x}_i^m$ are mapped to a higher dimensional space by the function ϕ and ξ_i^ms are the "slack variables".

To determine $\vec{c}_m$ and R_m, the quadratic programming problem of Equations (3) are transformed into their dual form:

$$\min_{a_1^m, \ldots, a_{n_m}^m} \sum_{i=1}^{n_m} \sum_{j=1}^{n_m} \alpha_i^m \alpha_j^m \phi(\vec{x}_i^m)^T \phi(\vec{x}_j^m) - \sum_{i=1}^{n_m} \alpha_i^m \phi(\vec{x}_i^m)^T \phi(\vec{x}_j^m). \tag{6}$$

$$subject \quad to \quad \sum_{i=1}^{n_m} \alpha_i^m = 1. \tag{7}$$

$$0 \le \alpha_i^m \le \frac{1}{n_m \nu_m}, \quad i = 1, \ldots, n_m, m = 1, \ldots, k. \tag{8}$$

Where α_i^m s are Lagrange multipliers. Standard techniques from quadratic programming can be used to solve for the unknown Lagrange multipliers. The centers of the hyperspheres are then given by:

$$\vec{c}_m = \sum_{i=1}^{n_m} \alpha_i^m \phi(\vec{x}_i^m), \quad m = 1, \ldots, k. \tag{9}$$

Similar to the above, R^2 is computed from such points, $\vec{x}_i$ with $0 < \alpha_i^m < 1/(n_m \nu_m)$. Any such data point $\vec{y}_m$ that lies on the surface of the mth optimal hypersphere satisfies the following:

$$R_m^2 = \left\| \phi(\vec{y}_m) - \vec{c}_m \right\|^2, \quad m = 1, \ldots, k. \tag{10}$$

Substituting the solution of Equation (9) into the above yields a solution for the hypersphere radius:

$$R_m^2 = \sum_{i=1}^{n_m} \sum_{j=1}^{n_m} \alpha_i^m \alpha_j^m \phi(\vec{x}_i^m)^T \phi(\vec{x}_j^m) - 2 \sum_{i=1}^{n} \alpha_i^m \phi(\vec{x}_i^m)^T \phi(\vec{y}_m) + \phi(\vec{y}_m)^T \phi(\vec{y}_m). \tag{11}$$

After solving (3), there are k decision functions:

$$f_m(\vec{x}) = R_m^2 - \|\phi(\vec{x}) - \vec{c}_m\|^2, \qquad m = 1,..,..., k.$$ (12)

Here we can say $\vec{x}$ is the class which has largest value of the decision function:

$$\arg\max_{m=1,...,k} \left(R_m^2 - \|\phi(\vec{x}) - \vec{c}_m\|^2 \right)$$ (13)

However, there are k hyperspheres with k radiuses and k centers, which makes large errors. So we redefine the decision function:

$$f_m(\vec{x}) = \frac{R_m^2 - \|\phi(\vec{x}) - \vec{c}_m\|^2}{R_m^2} = 1 - \frac{\|\phi(\vec{x}) - \vec{c}_m\|^2}{R_m^2}, \quad m=1,...,k.$$ (14)

$$\arg\max_{m=1,...,k} \left(1 - \frac{\|\phi(\vec{x}) - \vec{c}_m\|^2}{R_m^2} \right).$$ (15)

Substituting the solutions of Equation (9) and (11) into the above decision function (15) yields the decision function:

$$\arg\max_{m=1,...k} \left(1 - \frac{\sum_{i=1}^{n_m}\sum_{j=1}^{n_m} \alpha_i^m \alpha_j^m \phi(\vec{x}_i^m)^T \phi(\vec{x}_j^m) - 2\sum_{i=1}^{n_m} \alpha_i^m \phi(\vec{x}_i^m)^T \phi(\vec{x}) + \phi(\vec{x})^T \phi(\vec{x})}{\sum_{i=1}^{n_m}\sum_{j=1}^{n_m} \alpha_i^m \alpha_j^m \phi(\vec{x}_i^m)^T \phi(\vec{x}_j^m) - 2\sum_{i=1}^{n_m} \alpha_i^m \phi(\vec{x}_i^m)^T \phi(\vec{y}_m) + \phi(\vec{y}_m)^T \phi(\vec{y}_m)} \right).$$ (16)

If an appropriate kernel function is introduced, the re-formulated objective function takes the form:

$$\min_{\alpha_1^m,.....\alpha_n^m} \sum_{i=1}^{n_m}\sum_{j=1}^{n_m} \alpha_i^m \alpha_j^m k(\vec{x}_i^m, \vec{x}_j^m) - \sum_{i=1}^{n_m} \alpha_i^m k(\vec{x}_i^m, \vec{x}_j^m) \qquad m=1,..,..,k.$$ (17)

Then the class of point $\vec{x}$ is determined by the largest value of the decision function:

$$\arg\max_{m=1,...,k} \left(1 - \frac{\sum_{i=1}^{n_m}\sum_{j=1}^{n_m} \alpha_i^m \alpha_j^m k(\vec{x}_i^m, \vec{x}_j^m) - 2\sum_{i=1}^{n_m} \alpha_i^m k(\vec{x}_i^m, \vec{x}) + k(\vec{x}, \vec{x})}{\sum_{i=1}^{n_m}\sum_{j=1}^{n_m} \alpha_i^m \alpha_j^m k(\vec{x}_i^m, \vec{x}_j^m) - 2\sum_{i=1}^{n_m} \alpha_i^m k(\vec{x}_i^m, \vec{y}_m) + k(\vec{y}_m, \vec{y}_m)} \right)$$ (18)

Note that the idea is similar to the one-vs.-all approach. The one-vs.-all approach also constructs k one-class classifiers. The mth classifier constructs a hyperplane between one class and the k-1 other classes. However, for each classifier, the OC-SVM is trained on data from only one class by computing a bounding hypersphere (in the projected high-dimensional space) that encompasses as much of the training data as possible, while minimizing its volume.

The value $1/(v_m n_m)$ gives the upper boundary for the parameters α_i^m (see equation (8)) where $m \in \{1,...,k\}$. Similar to the statements in [12], the following statements hold:

i. v_m is an upper bound on the fraction of outliers, that is, training point outside the mth estimated region.

ii. v_m is lower bound on the fraction of support vectors.

iii. Suppose the data $\{\vec{x}_1,..., \vec{x}_{n_m}\}$ were generated independently from a distribution $P_m(\vec{x})$, which does not contain discrete components. Suppose, moreover, that the kernel is analytic and non-constant. With probability 1, asymptotically, v_m equals both the fraction of SVs and fraction of outliers.

4   Numerical Experiments

In this section we tested the proposed method on the benchmark data sets selected from the UCI data repository [14] and Statlog data collection. We scaled all the data to rage [-1, 1]. Table 1 summarizes the data sets used. Note that for problems glass and satimage, there is one missing class. That is, in the original application there is one more class but in the data set no examples are with this class.

Table 1. Benchmark datasets used for testing

Problem	Training data	testing data	class	attributes
Iris	150	0	3	4
Wine	178	0	3	13
glass	214	0	6	13
Segment	2310	0	7	19
Satimage	4435	2000	6	36
letter	15000	5000	26	16
shuttle	43500	14500	7	9

The most important criterion for evaluating the performance of this method is its accuracy rate. As a comparative approach, we also cite the result of comparing five methods which presents on [9] In order to reduce the search space of parameters, practically, we set parameters $v_1 = v_2 = ... = v_m = v$ for OC-K-SVM. We only trained the classifiers using the Radial Basis Function (RBF) kernel $k(\vec{x}_i, \vec{x}_j) = \exp(-\gamma \|\vec{x}_i - \vec{x}_j\|)$ with $\gamma = \{2^{-3}, 2^{-2}, ..., 2^3\}$ and $v = \{0.01, 0.05, 0.1, 0.15, 0.2\}$, where γ is the width parameter of RBF kernel and v is the penalty parameter. We use similar stopping criteria for our method. For each problem we stop the optimization algorithm if the KKT violation is less than 10^{-3}. We use two criteria to estimate the generalized accuracy. For data sets satimage, letter and shuttle where both training and testing sets are available, for each pair of (γ, v), the performance is measured by training the 80% of training set and testing the other 20% of the training set. Then we train the whole training set using the pair of

(γ, ν) that achieves the best validation rate and predict the test set. For the other four smaller datasets where test data may not be available, we simply conduct 5-fold cross-validation on the whole training data and report the best cross-validation rate.

We report best testing rate, training time, testing time and number of support vectors in Table 2. These experiments were carried out using LIBSVM [15] on Intel Pentium IV 2.00GHz PC with 256M RAM. However, LIBSVM did not provide one-class SVM algorithm based on hypersphere. We modified the program to output the radiuses and the value of decision function defined in our OC-K-SVM.

Table 2. The result of the numerical experiment. Measured: best rate, training time, testing time, and number of support vectors

problem	rate	training time	testing time	number of SVs
iris	90.67	0.0156	---	119
wine	54.49	0.0156	---	45
glass	71.03	0.0156	---	129
segment	98.57	0.0781	---	672
satimage	90.26	0.4063	4.35	949
Letter	90.00	0.5600	43.09	3584
shuttle	99.08	2.1820	7.37	1352

It can be observed that, for large problem, OC-K-SVM has a good performance. Comparing to earlier results listed in [9], the accuracy obtained by OC-K-SVM is competitive. Specifically, for the "segment" set, OC-K-SVM outperforms the others. For "shuttle" set, OC-K-SVM shows a similar performance to all the others. Unfortunately, we note that for smaller problems, the accuracy rate of the OC-K-SVM is lower than all the others. This is because one-class SVM is proposed in [11] as the data domain description problem. If the number of the objects is too small, it is likely that the data domain description has poor performance.

For the training time, our method is the best. This is due to that we only need to train k classifiers, each problem is smallest (only data from one class). Although one-vs.-one has to train as many as $k(k-1)/2$ classifiers, as each problem is smaller, the total training time is still less.

Regarding the testing time, the experience in [9] show that in general the testing time is still dominated by the kernel evaluations and is proportional to the number of support vectors. We also observe that among these methods, OC-K-SVM is really faster on the testing time.

We then discuss the number of support vectors. We can see that for larger problems, the methods from [6], [7] returns fewer support vectors than all three binary-based approaches. On the other hand, we cannot draw any conclusions about the OC-K-SVM method by us. Sometime it needs very few support vectors but sometimes the number is huge.

Finally we would like to draw some remarks about the implementation of our method. As can be seen in the Table 2, for the larger problems, the OC-K-SVM has smallest training and testing time. Moreover, the resulting accuracy is also acceptable. Therefore, if the training and testing time is very important, this method can be an option.

5   Conclusion and Future Work

In this paper, we propose a new algorithm, OC-K-SVM, for the multi-class classification based on one-class classification. This procedure has the advantage of providing solutions that are as good as the previously proposed schemes or better with a decrease in the training time. We have confirmed the established theoretical results and good behavior of algorithm through experiments on benchmark data sets.

It is worthwhile to investigate the proposed kernel with other efficient algorithms which can solve the one-class problems, e.g. The Nearest Point Algorithm or Successive Over-relaxation (SOR) algorithm. Future research subjects include more comprehensive testing of the algorithm and application to real-world problem.

References

1. C.cortes and V. Vapnik, J. (ed.): Support-vector network, Machine learning, Vol. 20, （1995）273-297.
2. L. Bottou, C. Cortes, and J. Denker, A.: Comparison of classifier methods: a case study in handwriting digit recognition, in Proc. of the International Conference on Pattern Recognition, IEEE Computer Society Press, Vol. 2. (1994) 77-87.
3. S. Knerr, L. Personnaz, and G. Dreyfus, In Fogelman-Soulie and Herault, (eds.): Single-layer learning revisited: a stepwise procedure for building and training a neural network. Neurocomputing: Algorithms, Architectures and Applications, Vol. F68 of NATO ASI Series. Springer-Verlag, Berlin Heidelberg New York (1990) 41-50.
4. J. C. Platt, N. Cristianini, and J. Shawe-Taylor, J. (ed.): Large margin DAGs for multi-class classification, Advances in Neural Information Processing Systems, Vol. 12. (2000)547-553.
5. Ping Zhong and Masao Fukushima, J. (ed.): A new multi-class support vector algorithm, Optimization Methods and Software, to appear.
6. V. Vapnik. Z.: Statistical Learning Theory, Wiley, New York, NY(1998).
7. J.Weston and C. Watkins, Multi-class support vector machines, Technical Report CSD-TR-98-04, Department of Computer Science, Royal Holloway, University of London, Egham, TW20 0EX, UK(1998).
8. Jeronimo, Arenas-Garcia, and Fernando Perez-Cruz, A: Multi-class support vector machines: a new approach. In: ICASSP, Hong Kong (2003) 6-10.
9. C. W. Hsu and C. J. Lin, B.C.: A comparison of methods for multi-class support vector machines, IEEE Transactions on Neural Networks, Vol. 13, no. 2.(2002)415-425.
10. C.-W. Hsu and C.-J. Lin, J. (ed.): A simple decomposition method for support vector machines, Machine Learning, Vol. 46. (2002)291-314.
11. Tax, D.M.J., and Duin, R.P.W, A: Data domain description by support vectors, Proceedings ESANN, Brussels: D Facto, (1999)251-256.
12. B. Scholkopf, J. Platt, J. Shawe-Taylor, A. J. Smola, and R. C. Williamson, J. (ed.): Estimating the support of a high-dimensional distribution, Neural Computation, Vol. 13, no. 7. (2001)1443-1471.
13. Siwei Lyu and Hany Farid, A: Steganalysis using color wavelet statistics and one-class support vector machines, in SPIE Symposium on Electronic Imaging, San Jose, CA(2004).
14. UCI-benchmark repository of artifical and real data sets, University of California Irvine, http://www.ics.uci.edu/~mlearn.
15. C.-C. Chang and C. J. Lin, LIBSVM: a library for support vector machines, software available at http://www.csie.ntu.edu.tw/~cjlin/libsvm, (2001).

Pushing Frequency Constraint to Utility Mining Model

Jing Wang, Ying Liu, Lin Zhou, Yong Shi, and Xingquan Zhu

Data Technology and Knowledge Economy Research Center, Chinese Academy of Sciences
Graduate University of Chinese Academy of Sciences
Beijing, China 100080
{jingw04, zhoulin05}@mails.gucas.ac.cn,
{yingliu, yshi}@gucas.ac.cn, xqzhu@cse.fau.edu

Abstract. Traditional association rules mining (ARM) only concerns the frequency of itemsets, which may not bring large amount of profit. Utility mining only focuses on itemsets with high utilities, but the number of rich-enough customers is limited. To overcome the weakness of the two models, we propose a novel model, called general utility mining, which takes both frequency and utility into consideration simultaneously. By adjusting the weight of the frequency factor or the utility factor, this model can meet the different preferences of different applications. It is flexible and practicable in a broad range of applications. We evaluate our proposed model on a real-world database. Experimental results demonstrate that the mining results are valuable in business decision making.

Keywords: general utility, utility mining, association rules mining, weighted association rules mining.

1 Introduction

Traditional association rules mining (ARM) [2] is to identify frequently occurring patterns of itemsets. ARM model treats all the items in the database equally by only considering if an item is present in a transaction or not. However, frequent itemsets may only contribute a small portion of the overall profit to the business and generate huge amount of inventory cost, labor cost, transportation cost.

In order to overcome the weakness of traditional association rules mining, utility mining model was proposed in [3]. Intuitively, utility is a quantitative measure of how "useful" (i. e. "profitable") an itemset is. The definition of utility of an itemset X, $u(X)$, is the sum of the utilities of X in all the transactions containing X.

Can we have a more general model which takes both frequency and utility into consideration simultaneously?

We propose a *general utility mining* model which is a linear combination of utility and frequency $gu(X)$: $\lambda \frac{\sup(X)}{S} + (1-\lambda) \frac{u(X)}{U}$, where $\frac{\sup(X)}{S}$ denotes the frequency of itemset X in the database, $\frac{u(X)}{U}$ denotes the fraction of the utility of itemset X out of total utility, λ is the weight of frequency, and $(1-\lambda)$ is the weight of

utility. A user specified threshold ε is used to measure the "usefulness" of itemset X. High utility itemsets with low supports may be filtered out by our model; popular itemsets that generate very low utility may also be filtered out.

Table 1 is an example transaction database where the total utility is 400. The number in each transaction in Table 1(a) is the sales volume of each item, and the subjective value of each item is listed in Table 1(b). For instance, let's set ε=15% and λ=0, $gu(\{B,C,E\}) = 0.18 > \varepsilon$, {B,C,E} is a high utility itemset. Although {B,C,E} generates $72 profit, it occurs only once in the database, which may potentially incur overstocking problem. If we set λ=0.4, $gu(\{B,C,E\}) = 0.148 < \varepsilon$, thus {B,C,E} is not interesting to the marketing professionals.

Table 1. A transaction database

(a) Transaction table.

ITEM TID	A	B	C	D	E
T_1	0	0	18	0	1
T_2	0	6	0	1	1
T_3	2	0	1	0	1
T_4	1	0	0	1	1
T_5	0	0	4	0	2
T_6	1	1	0	0	0
T_7	0	10	0	1	1
T_8	3	0	25	3	1
T_9	1	1	0	0	0
T_{10}	0	6	2	0	2

(c)The support and profit for all itemsets

Item-sets	Supp-ort	Profit ($)	Itemsets	Supp-ort	Profit ($)
A	5	24	BE	3	240
B	5	240	CD	1	43
C	5	50	CE	5	85
D	4	36	DE	4	56
E	4	50	ACD	1	52
AB	2	26	ACE	2	51
AC	2	41	ADE	2	46
AD	2	36	BCE	1	72
AE	3	33	BDE	2	182
BC	1	62	CDE	1	48
BD	2	172	ACDE	1	57

(b) Subjective value table. The right column displays the profit of each item per unit in dollars.

ITEM	PROFIT ($)(per unit)
A	3
B	10
C	1
D	6
E	5

(d)Transaction utility (TU) of the transaction database.

TID	TU	TID	TU
T_1	23	T_6	13
T_2	71	T_7	111
T_3	12	T_8	57
T_4	14	T_9	13
T_5	14	T_{10}	72

The difficulty of general utility mining is that the model does not follow "*downward closure property*" (*anti-monotone property*), that is, a high general utility itemset may consist of some low general utility sub-itemsets. Without this property, the number of candidates generated at each level increases exponentially. We push the frequency factor into Two-Phase algorithm proposed in [1], which maintains a *Transaction-weighted Downward Closure Property*. We apply our proposed general

utility mining model on a real world database and the observations demonstrate the significance of general utility mining.

The rest of this paper is organized as follows. Section 2 overviews the related work. In Section 3, we introduce the technical terms in utility mining model. In Section 4, we propose the *general utility mining model*. Section 5 presents the experimental results and we summarize our work in Section 6.

2   Related Work

A number of ARM algorithms and optimizations have been proposed in the past ten years. The common assumption is that each item in a database is equal in weight and the sales quantity is 0 or 1. These algorithms exploit the "downward closure property" as disclosed in Apriori [2] (all subsets of a frequent itemset must be frequent).

  Researches that assign different weights to items have been proposed in [4, 5, 6, 7]. These weighted ARM models are special cases of utility mining.

A utility mining algorithm is proposed in [9], which captures the semantic significance of itemsets at the transaction level. It focuses on mining the top-K high utility closed patterns that directly support a given business objective.

An alternative formal definition of utility mining and theoretical model was proposed in [3], where the utility is defined as the combination of objective information in each transaction and additional resources. Since this model cannot rely on "downward closure property" to restrict the number of itemsets to be examined, a heuristic is used to predict whether an itemset should be added to the candidate set.

An efficient utility mining algorithm, *Two-Phase algorithm* is proposed in [1]. It proposes the concept of "transaction-weighted utilization" and maintains "Transaction-weighted Downward Closure Property". *Two-Phase algorithm* finds out itemsets with high transaction-weighted utilization first, and then find out itemsets with high utility. It is scalable and the memory cost as well as the computation cost is efficiently reduced.

3   Utility Mining

We start with the definition of a set of terms that leads to the formal definition of utility mining problem. The same terms are given in [1].

- $I = \{i_1, i_2, \ldots, i_m\}$ is a set of items.
- $D = \{T_1, T_2, \ldots, T_n\}$ *is* a transaction database where each transaction $T_i \in D$ is a subset of I.
- $o(i_p, T_q)$, *objective value*, represents the value of item i_p in transaction T_q.
- $s(i_p)$, *subjective value,* is the specific value assigned by a user to express the user's preference.
- $u(i_p, T_q)$, *utility of an item i_p in transaction T_q,* is defined as $o(i_p, T_q) \times s(i_p)$.

- $u(X, T_q)$, *utility of an itemset X in transaction T_q, is defined as* $\sum_{ip \in X} u(i_p, T_q)$, *where X*
  = *{i_1, i_2, ..., i_k} is a k-itemset, $X \subseteq T_q$ and $1 \leq k \leq m$.*

- $u(X)$, *utility of an itemset X, is defined as* $\sum_{T_q \in D \wedge X \subseteq T_q} u(X, T_q)$.

- $tu(T_q)$, *the transaction utility of transaction T_q, is the sum of the utilities of all the items in T_q:* $tu(T_q) = \sum_{i_p \in T_q} u(i_p, T_q)$.

- $twu(X)$, *the transaction-weighted utilization of an itemset X, is the sum of the transaction utilities of all the transactions containing X:* $twu(X) = \sum_{X \subseteq T_q \in D} tu(T_q)$.

- $sup(X)$, *the support count of an itemset X, is the count of all the transactions containing X.*

- U, *the total utility of all the transactions:* $U = \sum_{T_q \in D} tu(T_q)$.

- S, *the total number of transactions.*

X *is a high utility itemset if* $u(X) \geq \varepsilon$, *where* $X \subseteq I$ *and* ε *is the minimum utility threshold, otherwise, it is a low utility itemset.* For example $u(\{A, D, E\}) = u(\{A, D, E\}, T_4) + u(\{A, D, E\}, T_8) = 46$. If $\varepsilon = 120$, $\{A, D, E\}$ is a low utility itemset.

4   General Utility Mining

In order to push frequency into utility mining model, we propose a general utility mining model which combines both frequency and utility linearly. We define *General Utility* and *General Transaction Utility*, and propose an extension to the Two-Phase algorithm in [1]. In addition, we discuss the universality and flexibility of this model.

4.1   Definitions and Theorems

Definition 1. (General Utility) The *General Utility of itemset X,* denoted as *gu(X),* is the linear combination of frequency and utility:

$$gu(X) = \lambda \frac{\sup(X)}{S} + (1 - \lambda) \frac{u(X)}{U} \quad (3.1)$$

where λ $(0 \leq \lambda \leq 1)$ is the weight assigned by users to adjust the contribution of frequency and utility. As $sup(X) \leq S$, $u(X) \leq U$, $0 \leq \frac{sup(X)}{S} \leq 1$, $0 \leq \frac{u(X)}{U} \leq 1$, so $0 \leq gu(X) \leq 1$.

Definition 2. (High General Utility Itemset) For a given itemset X, X is a high general utility itemset if $gu(X) \geq \varepsilon$, where ε $(0 \leq \varepsilon \leq 1)$ is the minimum threshold.

Definition 3. (General Transaction-weighted Utilization) The *general transaction -weighted utilization of itemset X,* denoted as *tgu(X),* is the combination of transaction -weighted utilization and frequency: $tgu(X) = \lambda \frac{\sup(X)}{S} + (1 - \lambda) \frac{twu(X)}{U}$ **(3.2)**

Definition 4. (High General Transaction-weighted Utilization Itemset) For a given itemset X, X is a *high general transaction-weighted utilization itemset* if $tgu(X) \geq \varepsilon'$, where ε' $(0 \leq \varepsilon' \leq 1)$ is the minimum threshold.

Theorem 1. (General Transaction-weighted Downward Closure Property) Let I^k be a k-itemset and I^{k-1} be a $(k-1)$-itemset such that $I^{k-1} \subset I^k$. If I^k is a high general transaction-weighted utilization itemset, I^{k-1} must be a high general transaction-weighted utilization itemset.

Proof: Let T_{I^k} be the collection of the transactions containing I^k and $T_{I^{k-1}}$ be the collection containing I^{k-1}. Since $I^{k-1} \subset I^k$, $T_{I^{k-1}}$ is a superset of T_{I^k}. According to definition of $twu(X)$ and $tu(X)$,

$$twu(I^{k-1}) = \sum_{I^{k-1} \subseteq T_q \in D} tu(T_q) \geq \sum_{I^k \subseteq T_p \in D} tu(T_p) = twu(I^k)$$

. And the itemsets that contain I^k must contain I^{k-1}, so $sup(I^{k-1}) \geq sup(I^k)$. Thus we can get $tgu(I^{k-1}) = \lambda \frac{\sup(I^{k-1})}{S} + (1-\lambda) \frac{twu(I^{k-1})}{U} \geq \lambda \frac{\sup(I^k)}{S} + (1-\lambda) \frac{twu(I^k)}{U} = tgu(I^k) \geq \varepsilon'$.

The *General Transaction-weighted Downward Closure Property* indicates that only the combinations of high *general transaction-weighted* utilization $(k-1)$-itemsets could be added into the candidate set C_k at each level.

Theorem 2. Let *HGTWU* be the collection of all high *general transaction-weighted utilization itemsets* in a transaction database D, and *HGU* be the collection of high *general utility itemsets* in D. If $\varepsilon' = \varepsilon$, then $HGU \subseteq HGTWU$.

Proof: $\forall X \in HGU$, if X is a high *general utility itemset*, then

$$\varepsilon' = \varepsilon \leq gu(X) = \lambda \frac{\sup(X)}{S} + (1-\lambda) \frac{u(X)}{U} = \lambda \frac{\sup(X)}{S} + (1-\lambda) \frac{\sum_{X \subseteq T_q} u(X, T_q)}{U}$$

$$= \lambda \frac{\sup(X)}{S} + (1-\lambda) \frac{\sum_{X \subseteq T_q} \sum_{i_p \in X} u(i_p, T_q)}{U} \leq \lambda \frac{\sup(X)}{S} + (1-\lambda) \frac{\sum_{X \subseteq T_q} \sum_{i_p \in T_q} u(i_p, T_q)}{U}$$

$$= \lambda \frac{\sup(X)}{S} + (1-\lambda) \frac{twu(X)}{U} = tgu(X)$$

Thus, X is a high *general transaction-weighted utilization itemset* and $X \in HGTWU$.

4.2 Two-Phase Algorithm

According to the above two theorems, we can utilize the *General Transaction-weighted Downward Closure Property* in general transaction-weighted utilization mining in Phase I, assuming $\varepsilon' = \varepsilon$, and prune those overestimated itemsets in Phase II. (Note we use the new term *transaction-weighted utilization* to distinguish it from *utility*. The focus of this paper is not to propose this term, but to utilize the property of *transaction-weighted utilization* to help reduce the searching space in general utility mining.)

Phase I

Let's use the sample database in Table 1 to show how *general transaction-weighted utilization mining* model works. Assume the transaction-weighted utilization threshold

ε' =0.4 and λ=0.5. At level 1, $HGTWU_1$ ={{B}, {C}, {D}, {E}} and C_2 ={{B, C}, {B, D}, {B, E}, {C, D}, {C, E}, {D, E}}. After the second scan of database, tgu ({B, C}) =0.24<ε', tgu ({B, D}) =0.3275<ε', tgu({B, E})=0.4675, tgu ({C, D}) = =0.12125 < ε', tgu ({C, E}) = 0.4725 and tgu ({D, E}) = 0.51625. Thus, $HGTWU_2$ ={{B, E}, {C, E}, {D, E}}, and then C_3 = Φ. Candidate generation stops after the second database scan. The efficient candidate generation process results from the *General Transaction-weighted Downward Closure Property*.

Phase II

Based on Theorem 2, if we let ε'=ε, the complete set of high general utility itemsets is a subset of the high general transaction-weighted utilization itemsets discovered in phase I. In the above example, by scanning the database another time, we finally get *high general utility itemsets HGU* = {{B}, {B, E}}. The other five itemsets obtained in Phase I are pruned. Only three database scans are incurred in the whole process of Phase I and II.

4.3   Model Universality and Flexibility

Traditional association rules mining (ARM) [2] and utility mining [1, 3] can be viewed as special cases of our proposed general high utility mining model. Utility mining focuses on zone I and IV in Figure 1. ARM focuses on zone III and IV in Figure 1. Our general model focuses on the region above the straight line in Figure 1. The line is actually the visualization of formula 3.1.
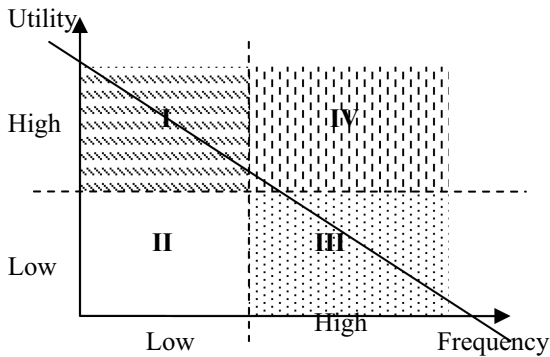
Fig. 1. High utility itemsets, frequent itemsets, high general utility itemsets

By adjusting λ, we can adjust the impact of frequency and utility in general utility. In Figure 1, when λ increases, frequency becomes more important in the application. When λ is 1, our model is the traditional association rules mining model. When λ decreases, utility becomes more important. When λ is 0, it is the utility mining model. By assigning different λ, users can mine different "useful" itemsets according to their own demands. For example, we set ε=0.4. When λ=0.2, u({B,E})=240, sup({B,E})=3, gu({B,E})=0.54>ε, {B,E} is a high general utility itemset; u({C,E})=85, sup({C,E})=5, gu({C,E})= 0.27<ε, {C,E} is not a high general utility itemset. However, if we set

λ=0.8, $gu(\{B,E\})$=0.36 < ε, it is not a high general utility itemset any more, but {C, E} becomes a high general utility itemset since $gu(\{C,E\})$= 0.4425 > ε.

5   Experimental Evaluation

We evaluate our general utility mining model by using a real-world market data from a major grocery chain store in California, USA. It contains products of various categories, such as food, health care, gifts, and others. There are 1,112,949 transactions and 46,086 items in the database, and the total utility is 26,388,499.8 dollars. Each transaction consists of the products and the sales volume of each product purchased by a customer at a time point. The utility table describes the profit of each item. The size of this database is 73MByte. The average transaction length is 7.2. The subjective value table, which is the profit table, describes the profit of each product.

Table 2. Top 10 itemsets and corresponding support, utility and general utility when varying λ (ε =0.075%)

λ=0 (Utility Mining)					λ=1 (ARM)			
Itemset	*Utility (%)*	*Support (%)*	*General Utility (%)*		*Itemset*	*Utility (%)*	*Support (%)*	*General Utility (%)*
39171, 39688	0.2435	0.3449	0.2435		16967, 16977	0.157	0.7009	0.7009
39690, 39692	0.1942	0.028	0.1942		13743, 16967	0.0623	0.4967	0.4967
39182, 39206	0.1714	0.016	0.1714		16967, 16975	0.0948	0.4033	0.4033
39143, 39182	0.1631	0.0128	0.1631		39430, 39432	0.031	0.399	0.399
5166, 16967	0.1606	0.227	0.1606		16967, 21738	0.1083	0.3893	0.3893
21283, 21308	0.1572	0.315	0.1572		3482, 3510	0.0763	0.382	0.382
16967, 16977	0.157	0.7009	0.157		16967, 16978	0.06	0.3784	0.3784
21308, 22900	0.1528	0.2946	0.1528		16967, 39684	0.0409	0.3733	0.3733
10481, 16967	0.1296	0.1461	0.1296		39171, 39688	0.2435	0.3449	0.3449
16967, 21738	0.1083	0.3893	0.1083		11780, 11783	0.0394	0.3404	0.3404

λ=0.1					λ=0.5			
Itemset	*Utility (%)*	*Support (%)*	*General Utility (%)*		*Itemset*	*Utility (%)*	*Support (%)*	*General Utility (%)*
39171, 39688	0.2435	0.3449	0.2536		16967, 16977	0.157	0.7009	0.429
16967, 16977	0.157	0.7009	0.2114		39171, 39688	0.2435	0.3449	0.2942
39690, 39692	0.1942	0.028	0.1776		13743, 16967	0.0623	0.4967	0.2795
21283, 21308	0.1572	0.315	0.173		16967, 16975	0.0948	0.4033	0.249
5166, 16967	0.1606	0.227	0.1672		16967, 21738	0.1083	0.3893	0.2488
21308, 22900	0.1528	0.2946	0.1669		21283, 21308	0.1572	0.315	0.2361
39182, 39206	0.1714	0.016	0.1559		3482, 3510	0.0763	0.382	0.2292
39143, 39182	0.1631	0.0128	0.1481		21308, 22900	0.1528	0.2946	0.2237
16967, 21738	0.1083	0.3893	0.1364		16967, 16978	0.06	0.3784	0.2192
10481, 16967	0.1296	0.1461	0.1312		39430, 39432	0.031	0.399	0.215

We compare the itemsets discovered from general utility algorithm, Apriori and utility mining by varying the value of λ and the threshold ε. Table 2 shows the top 10 itemsets when ε=0.075%. (We only show itemsets longer than 1.) From Table 2, we can observe different top 10 high general utility itemsets when varying λ. For example, itemset {39690, 39692} is in the top 10 high general utility itemsets when λ=0.1 (assigning more weight to the utility factor), but left out when λ=0.5 (assigning equal

weight to the utility and the frequency factor) due to its large utility 0.1942% but small support 0.028%. Itemset {39430, 39432} (utility = 0.031%, support = 0.399%) is just the opposite case. {21283, 21308} is in the top 10 itemsets when λ=0.5, but it is not in the top 10 frequent itemsets. It shows that the itemsets discovered by our proposed model are different with those by ARM or utility mining in many cases, more emphasizing the balance between frequency and utility.

6   Conclusions

General utility mining is a generalization of association rules mining (ARM) and utility mining. It balances the impact of frequency and utility by adjusting their weights, respectively. ARM and utility mining are two special cases of this model. General utility mining can overcome their weakness. It has a high universality and flexibility. We defined a term called *general utility* and *general transaction-weighted utilization* model which holds *Transaction-weighted Downward Closure Property*. We proposed a Two-Phase algorithm that can discover high general utility itemsets highly efficiently. A real data set from a chain grocery store was used to evaluate our proposed model and the experimental results showed that it could find itemsets that are missed by utility mining model and ARM. Our model can be applied in a broad range of applications, such as, business intelligence, web log mining, etc.

Acknowledgements

References

1. Ying Liu, Wei-keng Liao and Alok Choudhary: A Fast High Utility Itemsets Mining Algorithm. Utility-Based Data Mining Workshop with the 11th SIGKDD, 2005.
2. Agrawal and R. Srikant: Fast algorithms for mining association rules. 20th VLDB (1994)
3. Hong Yao, Howard J. Hamilton, and Cory J. Butz: A Foundational Approach to Mining Itemset Utilities from Databases. SDM (2004)
4. C.H. Cai, Ada W.C. Fu, C.H. Cheng, and W.W. Kwong: Mining Association Rules with Weighted Items. IDEAS (1998)
5. W. Wang, J. Yang, and P. Yu: Efficient Mining of Weighted Association Rules (WAR). 6th KDD (2000)
6. Feng Tao, Fionn Murtagh, and Mohsen Farid: Weighted Association Rule Mining using Weighted Support and Significance Framework. 9th KDD (2003)
7. S. Lu, H. Hu, and F. Li: Mining weighted association rules. Intelligent Data Analysis, 5(3) (2001), 211-225
8. B. Barber and H.J.Hamilton: Extracting share frequent itemsets with infrequent subsets. Data Mining and Knowledge Discovery, 7(2) (2003), 153-185
9. Raymond Chan, Qiang Yang, Yi-Dong Shen: Mining high utility Itemsets. ICDM (2003)
10. IBM data generator, http://www.almaden.ibm.com/software/quest/Resources/index.shtml

Feature Selection for VIP E-Mail Accounts Analysis

Zhan Zhang, Yingjie Tian[*], and Yong Shi

Research Center on Data Technology and Knowledge Economy of CAS,
Beijing 10080,
zhangzhan05@mails.gucas.ac.cn,
tianyingjie1213@163.com,
yshi@gucas.ac.cn,
www.dtke.ac.cn

Abstract. This paper introduces several feature selection methods on the VIP E-Mail account analysis, and then uses SVM to classify the users in order to maintain the ones who may leave in a short time. The websites hosting companies can follow the strategies, which are investigated in this paper, to reduce their labor cost and provide an attractive and simple registration for the users. The result shows that we can also reach the feasible predict accuracy.

Keywords: Support Vector Machine, Feature selection, VIP E-Mail.

1 Introduction

With the development of internet, E-Mail is becoming more and more popular and widely used. Because of its convenience and speediness, it is not only a tool for communication but also has its own commercial characteristics. Many websites hosting companies have developed the charged VIP E-Mail service to meet the demand of the certain persons. According to the statistics, as Chinese network advanced in the past few years, the total market of the Chinese VIP E-Mail service has reached 6.4 hundred million RMB by 2005, which has caused drastic competitions around the IT market. Meanwhile, the providers have to try their best to collect more information about the users and buy more memory to save them. The technical staffs have to face more and more data bases and log files. Therefore, it has become the most important problems for the service providers that how to look for the potential users, how to maintain the current users and how to analysis the behaviors of the users throughout the feature as few as possible.

Data mining means the nontrivial extraction of implicit, previously unknown, and potentially useful information from data. Feature selection is an important part of data mining. The number of features affects the classifier's speed that including a large number of features can result in long training and classification times.

The purpose of this paper is to apply several feature selection methods including Support Vector Machine (SVM), F-score method, and one-norm SVM to reduce the data scale and then use the SVM to deal with the classification on a famous Chinese

---

[*] Corresponding author.

website's VIP E-Mail data set. This paper is organized as follows. In Section 2 we introduce the SVM classifier; Section 3 focuses on the different methods that work on the feature selection; Section 4 introduces how to choose satisfying parameters with 10-fold cross validation; In Section 5, we show the experimental results during the development period of the competition; and the last part is the conclusion.

2   Support Vector Classification

The algorithm about SVM is originally established by Vapnik (1998). Since 1990s SVM has been a promising tool for data classification. Its basic idea is to map data into a high dimensional space and find a separating hyper plane with the maximal margin. SVM solves the following optimization problem:

$$\min_{w,b,\xi} \quad \frac{1}{2}w'w + C\sum_{k=1}^{m}\xi_k,$$

subject to

$$y_k(w^T \bullet \phi(x_k) + b) \geq 1 - \xi_k,$$
$$\xi_k \geq 0, k = 1,...,m,$$

Where training data are mapped to a higher dimensional space by the function ϕ, and C is a penalty parameter on the error. The decision function (predictor) is $f(x) = \text{sgn}(w^T\phi(x_k) + b)$.

The RBF kernel is used in our experiments: $k(x,x') = \exp(-\gamma \| x - x' \|^2)$. With the RBF kernel, there are two parameters to be determined in the SVM model i.e. C and γ.

3   Feature Selection Strategies

In this section, we will discuss three feature selection strategies respectively: SVM, F-score and one-norm SVM.

3.1   No Feature Selection: Direct SVM Strategy

Firstly, we use the SVM strategy directly without feature selection and choose the linear kernel function.

3.2   SVM Feature Selection Strategy

From 3.1, we can get the decision function (predictor): $f(x) = \text{sgn}(w^T x_k + b)$. If we scale the data by putting each feature to [0, 1], the coefficient |w| can be

considered as the weight of each feature. The larger the |w| is, the more discriminative this feature is. Therefore, we use this score as a feature selection criterion.

3.3 F-Score Feature Selection Strategy[3]

F-score is a simple technique which measures the discrimination of two sets of real numbers. Given training vectors x_k, k = 1… m, if the numbers of positive and negative instances are n_+ and n_-, respectively, then the F-score of the ith feature is defined as:

$$F(i) = \frac{(\overline{x}_i^{(+)} - \overline{x}_i)^2 + (\overline{x}_i^{(-)} - \overline{x}_i)^2}{\frac{1}{n_+ - 1}\sum_{k=1}^{n_+}(x_{k,i}^{(+)} - \overline{x}_i^{(+)})^2 + \frac{1}{n_- - 1}\sum_{k=1}^{n_-}(x_{k,i}^{(-)} - \overline{x}_i^{(-)})^2}$$

Where $\overline{x}_i$, $\overline{x}_i^{(+)}$, $\overline{x}_i^{(-)}$ are the average of the ith feature of the whole, positive, and negative data sets, respectively; $x_{k,i}^{(+)}$ is the ith feature of the kth positive instance, and $x_{k,i}^{(-)}$ is the ith feature of the kth negative instance. The numerator indicates the discrimination between the positive and negative sets, and the denominator indicates the one within each of the two sets. The larger the F-score is, the more discriminative this feature is. Therefore, we use this score as a feature selection criterion.

3.4 One-Norm SVM Feature Selection Strategy

According to SVM, we give the following linear program to calculate the coefficient w:

Given training vectors $x_k \in R^n$, k = 1… m, in two classes and a vector of labels $y \in R^m$ such that $y_k \in \{1, -1\}$, and we will solve the following linear program:

$$\min_{w,b,\xi,s} \quad \sum_{i=1}^{k} s_i + C\sum_{j}^{m} \xi_j,$$

$$subject \quad to$$

$$y_j((w \bullet x_j) + b) \geq 1 - \xi_j, j = 1,...,m,$$

$$-s_i \leq w_i \leq s_i, i = 1,...,k,$$

$$\xi_j \geq 0, j = 1,...,m.$$

Where C is a penalty parameter on the training errors.

Actually, the larger the |w| is, the more discriminative this feature is. Therefore, we use this score as a feature selection criterion.

4   K-Fold Cross Validation

When we have finished the feature selection, we use the SVM to do the classification. The cross validation will help to identify good parameters so that the classifier can accurately predict unknown data. In this paper, we use 10 fold cross validation to choose the penalty parameter C and γ in the SVM. When we get the nice arguments, we will use them to train model and do the final prediction.

5   Experimental Results

In this part, we use LIBSVM (Chang and Lin 2001) for SVM classification. Before doing the classification, we perform some data preprocessing. We choose 5499 positive records and 5498 negative records from the data set and then delete the non-numeric features, and scale each feature to [0,1].

Firstly, we use the SVM to do the classification without any feature selection. According to the 10-fold cross validation, we get the high accuracy as follows:

Table 1. Cross Validation with SVM on the Training Set

C	2^{-5}	2^{-4}	2^{-3}	2^{-2}	2^{-1}	2^{0}
Accuracy	80.53%	81.70%	83.11%	84.33%	85.16%	85.77%
C	2^{1}	2^{2}	2^{3}	2^{4}	2^{5}	2^{6}
Accuracy	86.35%	87.09%	87.55%	88.01%	88.42%	88.89%
C	2^{7}	2^{8}	2^{9}	2^{10}		
Accuracy	89.09%	89.21%	89.23%	89.25%		

Obviously, when C= 2^{10}, we get the highest accuracy 89.25%.

Then we will focus on the feature selection strategies mentioned in Section 3.2—3.4.

For the SVM feature selection strategy, after the above cross validation, with C equaling to 2^{10}, we can get the model $f(x) = \mathrm{sgn}(w^T x_k + b)$. Then we put the |w| in order, which stands for the weight of each feature. In fact, there are 226 features with |w|>0. In the experiment, we use the half-cut method to choose the features, which means every time we just maintain half features whose |w| are bigger than others. Using the same cross validation method we can select the optimized C, and the following table gives the top five accuracies with each half feature selected.

We find that only when there are still 113 features, the accuracy can be over 80%.

For the F-score feature selection strategy, as we have discussed in Section 3.3, first we calculate the F-score of each feature, and then put them in order, at last use the

half-cut method to choose the features. Using the same cross validation method we can select the optimized C, the following table gives the top five accuracies with half features selected.

Table 2. Cross Validation with SVM after SVM Feature Selection on the Training Set

C	Accuracy (3 features)	Accuracy (7 features)	Accuracy (14 features)	Accuracy (28 features)	Accuracy (56 features)	Accuracy (113 features)	Accuracy (all features)
2^8	66.04%	66.02%	67.26%	72.85%	73.20%	81.90%	89.21%
2^9	67.37%	66.35%	67.88%	73.28%	73.38%	81.91%	89.23%
2^{10}	66.81%	67.37%	68.25%	73.53%	73.84%	81.96%	89.25%

Table 3. Cross Validation with SVM after F-Score Feature Selection on the Training Set

C	Accuracy (3 features)	Accuracy (7 features)	Accuracy (14 features)	Accuracy (28 features)	Accuracy (56 features)	Accuracy (113 features)	Accuracy (all features)
2^8	70.08%	70.62%	78.86%	84.69%	86.20%	88.32%	89.21%
2^9	70.07%	70.62%	78.89%	84.86%	86.33%	88.52%	89.23%
2^{10}	70.07%	70.61%	78.94%	84.99%	86.47%	88.69%	89.25%

From the table we find that when we use the first 28 features, we can get a satisfying accuracy 84.99%.

For the one-norm SVM feature selection strategy, we can also get the |w| from the model the same as the SVM feature selection. In this experiment, we figure out that there are only 26 |w|>0, so with the same method, following table gives the top five accuracies with each half feature selected.

Table 4. Cross Validation with SVM after One-Norm Feature Selection on the Training Set

C	Accuracy (3 features)	Accuracy (7 features)	Accuracy (13 features)	Accuracy (26 features)	Accuracy (all features)
2^8	70.66%	74.01%	74.74%	80.97%	89.21%
2^9	70.66%	74.01%	74.74%	81.06%	89.23%
2^{10}	70.66%	74.01%	74.77%	81.12%	89.25%

All the above strategies are based on the hypothesis that the data set can be classified by a linear decision function. The following experiments are based on the hypothesis that the data set can not be classified by a linear function. As a result, we introduce the RBF kernel to the SVM.

When we use the SVM directly to choose the parameters C and γ, we get the graph as below:
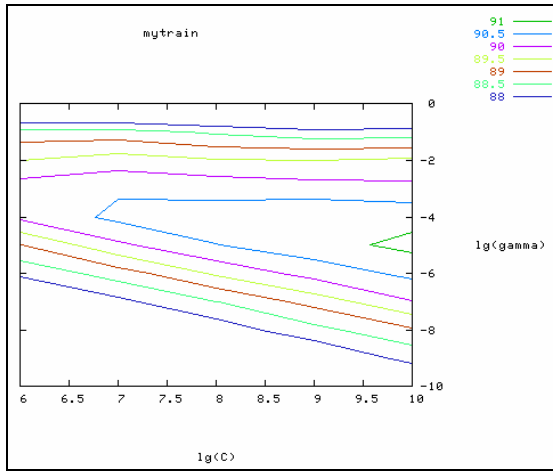
Fig. 1. Direct Use SVM with RBF Kernel on the Training Set

The following table gives the top five accuracies with all features.

Table 5. Cross Validation with RBF Kernel SVM on the Training Set

C γ	2^6	2^7	2^8	2^9	2^{10}
2^{-6}	88.11%	88.73%	89.58%	90.21%	90.62%
2^{-5}	88.99%	89.90%	90.49%	90.81%	91.14%
2^{-4}	90.11%	90.62%	90.76%	90.98%	90.84%
2^{-3}	90.27%	90.43%	90.33%	90.23%	90.15%
2^{-2}	89.50%	89.77%	89.56%	89.52%	89.63%

Compared with the other values of C, the value 2^{10} can always get the better accuracy; therefore, we just fix C at 2^{10} to choose the parameter γ. Based on the above three feature selection strategies, we still use the features selected respectively to do the RBF kernel SVM, we can get the following three tables for each strategy.

Table 6. Cross Validation with RBF Kernel SVM after SVM Feature Selection on the Training Set

γ	Accuracy (3features)	Accuracy (7features)	Accuracy (14features)	Accuracy (28features)	Accuracy (56features)	Accuracy (113features)	Accuracy (allfeatures)
2^{-6}	62.17%	62.51%	63.62%	70.64%	71.21%	80.74%	90.62%
2^{-5}	63.47%	63.57%	65.17%	71.38%	71.92%	81.00%	91.14%
2^{-4}	65.88%	65.83%	66.17%	72.44%	72.67%	83.59%	90.84%
2^{-3}	66.02%	66.04%	67.22%	72.91%	73.29%	84.50%	90.15%

Table 7. Cross Validation with RBF Kernel SVM after F-Score Feature Selection on the Training Set

γ	Accuracy (3features)	Accuracy (7features)	Accuracy (14features)	Accuracy (28features)	Accuracy (56features)	Accuracy (113features)	Accuracy (allfeatures)
2^{-6}	69.97%	76.00%	80.97%	86.76%	88.31%	89.33%	90.62%
2^{-5}	69.93%	77.49%	81.12%	87.22%	88.66%	89.71%	91.14%
2^{-4}	69.96%	77.64%	81.70%	88.29%	89.48%	90.20%	90.84%
2^{-3}	69.98%	77.98%	82.94%	88.85%	89.83%	89.71%	90.15%

Table 8. Cross Validation with RBF Kernel SVM after One-Norm SVM Feature Selection on the Training Set

γ	Accuracy (3 features)	Accuracy (7 features)	Accuracy (13 features)	Accuracy (26 features)	Accuracy (all features)
2^{-3}	72.93%	74.38%	75.60%	83.80%	89.97%
2^{-2}	72.92%	74.79%	74.98%	84.88%	90.62%
2^{-1}	72.92%	74.88%	75.56%	85.23%	91.14%

In table 1, it is obvious that the accuracy can be over 80% as long as the parameter C is bigger than 1 with all the 230 features, and also, in table 5, when we introduce the RBF kernel into SVM, the rate can be better than 90% with the proper parameters. In table 2, the accuracy could not be higher than 80% unless we maintain 113 features at least; with the same feature selection strategy, in table 6, we also have to leave no less than 113 features in the model to get the 80% accuracy; In table 3, we just need to keep only 28 features in order to get the accuracy better than 80% as well as 14 features in table 7; Meanwhile, in table 4 and table 8, we can get the 80% rate with 26 features.

6   Conclusion

In this paper, we experiment several feature selection strategies to work on the VIP E-Mail accounts data set. On the whole, the strategies with RBF kernel are better than the ones without it; the F-Score strategy and norm-SVM strategy are better than the SVM strategy. According to the result, the websites hosting companies can reduce the labor cost for information collection. On one hand, the engineers can be released from dealing with the massive log files; on the other hand, the users can get a quick and attractive registration without providing so much personal information.

References

1. Chang C.-C, Lin C.-J. LIBSVM: a library for support vector machines, (2001). Software available at http://www.csie.ntu.edu.tw/~cjlin/libsvm.
2. iResearch, China E-mail Market Research Report 2005 (Online). Available: http://www.iresearch.com.cn/html/email_service/detail_free_id_27497.html. (2005)
3. Chen Y.W., Lin C.J., Combining SVMs with various feature selection strategies. (2005)
4. Chapelle O., Vapnik V., Bousquet O., Mukherjee S.. Choosing kernel parameters for support vector machines. Machine Learning, Submitted. (2000)
5. Cortes C., Vapnik V.: Support-vector networks. Machine Learning, 20(3) (1995):273–297.

A Distributed Data Mining System for a Novel Ubiquitous Healthcare Framework

M. Viswanathan, T.K. Whangbo, K.J. Lee, and Y.K. Yang

College of Software, Kyungwon University, Seongnam-Si,
Kyunggi-Do, South Korea
{murli,,tkwhangbo,lkj9731,ykyang}@kyungwon.ac.kr

Abstract. Recent years have shown impressive growth in the development of ubiquitous healthcare (u-Healthcare) systems which aim for the next generation in e-Health services and associated research. Such systems are primarily being designed to provide emergency and preventive healthcare to citizens any-where/anytime using wired and wireless mobile technologies. Data mining is an indispensable aspect of such systems and represents the process of analyzing databases to extract hidden knowledge and relationships. This paper introduces and studies the development framework of a prototype ubiquitous healthcare system initiated by the South Korean government. Preliminary results with a distributed data mining system are presented in the context of a larger future integration with the ubiquitous healthcare framework.

Keywords: Distributed Data Mining, Ubiquitous Healthcare, Decision Supporting System, Healthcare Data, Data Classification.

1 Introduction

The increase in aging population in several countries has highlighted the need for efficient and preventive healthcare for the elderly. Ubiquitous healthcare is the next step in the integration of information technology with healthcare services and refers to the access to healthcare services at any time and any place for individual consumers through mobile computing technology. These u-Healthcare systems provide enhanced services including real-time patient data collection and monitoring for emergency care as well as preventive health recommendations. The vast amount of data collected from the distributed users of u-Health services results in a growing need for analyzing them across geographical lines using distributed and parallel systems. Implementations of data mining techniques on high-performance distributed computing platforms are moving away from centralized computing models for both technical and organizational reasons [11].

In this paper, we present and discuss the designed prototype for a ubiquitous healthcare system that will provide advanced patient monitoring and health services. Subsequently we introduce and present empirical analysis of a preliminary distributed data mining system. The integration of such a distributed mining system is studied in the context of the decision support framework for our ubiquitous healthcare system.

2   u-Healthcare Initiatives and Challenges

There are several ubiquitous challenges in the development of such healthcare frameworks and systems. These include:

- issues of security and privacy related to information transfer through unsecured infrastructure, potentially lost or stolen devices, legal enforcement and other scenarios;
- determining current context and user activity in real-time and locating context dependent information such as automatic discovery of services based on user health needs;
- development of low-power sensors to monitor user context and health condition;
- information management through development of techniques to collect, filter, analyze and store the potentially vast quantities of data from widespread patient monitoring and applying privacy preserving data mining at several levels;
- simple patient interaction systems to provide guidance, feedback and access to medical advice in acute situations;
- Adaptable network infrastructures to support large-scale monitoring, as well as real-time response from medical personnel or intelligent agents.;
- integration of specialized local u-Health architectures for unified data access and connection to National grids;

A growing number of ubiquitous healthcare projects are being pursued by large enterprises owning healthcare related companies and government bodies. MobiHealth project [2] is a mobile healthcare project supported by the EC with countries such as Netherlands, Germany, Spain and Sweden participating in it, and companies such as Philips and HP are providing technical support. EliteCare[3], is an elderly care system developed in the USA that monitors patients using various sensors and provides emergency and health information services. Tele-monitoring service[4] is being developed by the Philips Medical system, where centers analyze data that is collected from homes and transmitted by biomedical signal collection devices, and provide health management and related information. CodeBlue[5] is a sensor network based healthcare system being developed to treat and deal with emergencies, rehabilitation of stroke patients, and in general, to use health signal data in addition to hospital records in real time treatment decisions. The UbiMon[6] project which stands for Ubiquitous Monitoring Environment for Wearable and Implantable Sensors is studying mobile monitoring using sensors and real-time biomedical data collection for long time trend analyses. The Smart Medical Home[7] aims to develop a fully integrated personal health system with ubiquitous technology based on infrared and bio sensors, computers, video cameras and other devices. Sensor data is collected and transmitted to a center for further analysis and preventive care.

3   U-Healthcare System Framework

The components of the ubiquitous system prototype are summarized in this section. A system user in this paper refers to a patient who has a contract with a provider to use the ubiquitous healthcare services and regularly receives medical treatment at a hospital.

Fig. 1 shows an overview of the ubiquitous healthcare service framework as suggested in this paper.

The user wears a sensory device, provided by the hospital, on his wrist. The sensor regularly transmits collected data to a healthcare center through networking or mobile devices, and the transmitted data is stored at the u-healthcare center. In the center, monitoring staff are stationed to answer the user' queries, monitor his biomedical signals, and call an emergency service or visit the patient to check his status when an abnormal pattern is detected. The hospital monitors the collected data and judges the patient's status using the collected biomedical signals in his periodic checkup.
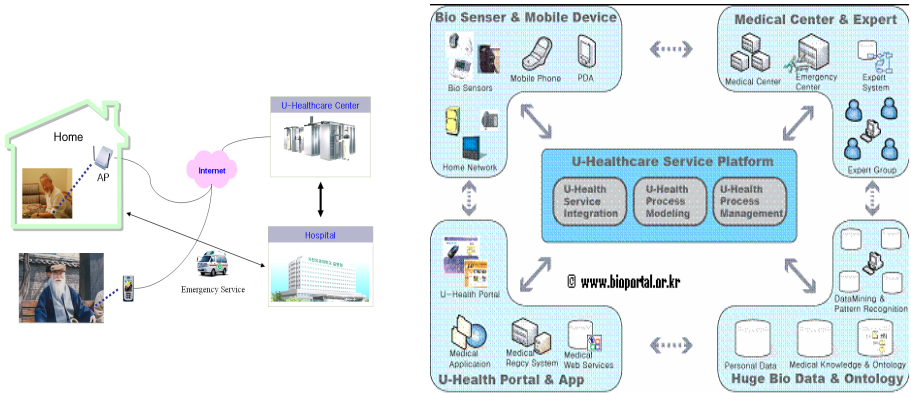
Fig. 1. Ubiquitous Healthcare Framework

3.1   Biomedical Signal Collection and Transmission

A sensor attached to a user's wrist collects data such as the user's blood pressure, pulse, and orientation and transmits the collected data to the user's mobile phone or access point (AP) at home using a wireless ZigBee device. Zigbee complements Bluetooth's weaknesses, provides multi hopping, and has low power consumption [8]. Biomedical signals can be collected while moving in and out of the user's residence. The data collected inside of the house is sent to the AP in the house using Zigbee module. The AP stores the collected data and sends it regularly to the data storage at the healthcare center. When the user is outside of the house, the sensor sends the collected data to the user's mobile phone and then using CDMA module of the mobile phone, transmits the data to the center.

3.2   Healthcare Center

The healthcare center has two primary roles. First, it provides storage and management for the biomedical data collected from the users, and second, it monitors the users' health status and takes appropriate emergency or preventive action when required. A database server in the healthcare center stores and manages data including the medical, personal, family and other information for all registered users as well as biomedical signals collected from them. This data is used for real-time monitoring of users in case

of emergencies and is also useful in periodic checkups. The healthcare center also includes personnel who are stationed to keep monitoring users' health status and provide health information as well.

3.3 CDSS (Clinical Decision Support System)

The CDSS supports long-term and short-term decision making processes by using models from distributed data mining, developing alternative plans and performing comparison analysis. In the short-term it assists in optimal planning to solve various decision making problems confronted in emergencies by utilizing the biomedical signals. The goal of this system is to provide an information system environment where a decision maker can solve problems easily, accurately and promptly such that users are benefited. The CDSS needs to be integrated with a distributed data mining system that can provide global models.

3.4 Emergency Response

Emergencies in a U-health framework require robust and quick recognition followed by an efficient emergency response. In this framework we employ a three pronged emergency recognition drive. Firstly, personnel monitoring the streaming biomedical data may detect abnormal signs and check user through phones or visits. Secondly, abnormal signs are also detected while mining the biomedical data collected over a period by the CDSS. Lastly, motion detectors mounted on sensors detect occurrence of falls and erratic movement.

The emergency management system uses a variety of hardware and software components that aim to improve emergency counteractions at the appropriate time and lower preventable deaths. This includes portable personal terminals comprising of RFID tags, portable RFID readers, an ambulance information system, a hospital information system and a healthcare information system. The efficiency of the treatment in emergency rooms is increased by using RFID tags and readers. Since the system is well integrated it also transfers patient information in real-time to hospitals, and therefore medical teams who will provide treatment during emergencies can be well-prepared.

3.5 Remote Monitoring System

With increasing urbanization, shrinking of living space and shifting concepts of the family, elderly people often tend to live alone without any assistance at home. In such cases prompt responses are most important when a medical emergency occurs. The remote monitoring system uses cameras for checking current situation when an abnormal sign is detected by sensory devices. There may be signals that cannot be detected even with motion detectors mounted on sensors, or false alarms may occur. In these cases, the situations can be checked using in-house video cameras. The remote monitoring system is not only a management system for patient monitoring but aims for general health improvement of consumers through prevention of diseases, early detection, and prognosis management [10].

4   Healthcare Decision Support with Data Mining

Table 1 presents the several levels of data mining applicable in such a healthcare framework. In this paper we consider the scenario [12] where a hospital needs to analyze a very large database with real-time patient sensor data. Due to processing and memory limits the database is partitioned and sent to individual machines to be processed. In this section we discuss how distributed data mining plays an important role within the CDSS component of the ubiquitous healthcare system.

Table 1. Levels of data mining

Low level	Sensor data mining for emergency detection Sensor data fusion for decision support
Hospital-Based	Periodic trend analysis & wellness recommendations Analysis of patient groups for drug effects, CRM and indirect factors Recovery analysis, drug interaction and other studies like allergy cause and detection
Global level	Clustering and classification analysis for epidemics and other implicit patterns

4.1   CDSS and DDM

In a ubiquitous healthcare framework DDM systems are required due to the large number of streams of data that have a very high data rate and are typically distributed. These need to be analyzed/mined in real-time to extract relevant information. Often such data come from wirelessly connected sources which have neither the computational resources to analyze them completely, nor enough bandwidth to transfer all the data to a central site for analysis. There is also another scenario where the data collected and stored at a center needs to be analyzed as a whole for creating the dynamic profiles. The preliminary empirical analysis with the prototype distributed data mining system discussed in this paper is suited towards this latter situation. The integration of the CDSS component of the ubiquitous healthcare framework with such a DDM is important.
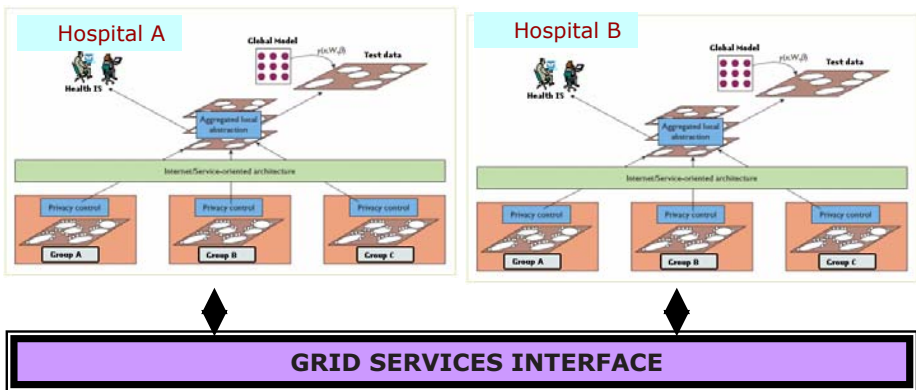
Fig. 2. Local to Global Mining

Data mining techniques used in the decision making system divide patients into groups. As a collection of patients have their own characteristics, they should be divided properly, and group properties are found through applying cluster analysis modeling techniques and searching created groups in the group analysis step. Secondly, causal models are developed for health patterns using mining techniques. Finally, a dynamic profile of the patient can be created using past history and domain knowledge in conjunction with sensory data. Each patient's risk rate is calculated by a system reflecting mining results, and administrators can see patients' risk rankings from the risk rates and give priority to patients with higher rates.

4.2   Distributed Data Mining Architecture

This section outlines a prototype system for DDM applicable in the scenario described above. For a detailed exposition of this system and results see [16]. The DDM system is built from various components as seen in figure 3. The DDM system takes collected biomedical hospital data and using SNOB [13], a mixture modeling tool, partitions it to clusters. The clusters get distributed over the LAN using MPI [14]. Data models are developed for each cluster dataset using the classification algorithm C4.5 [15].
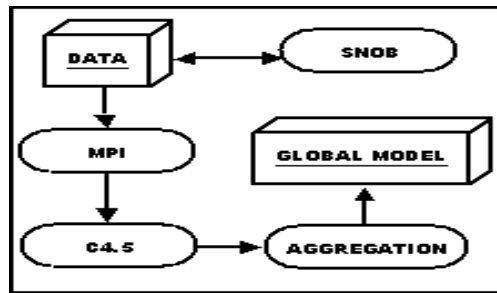
Fig. 3. DDM System Components

Finally the system uses a voting scheme to aggregate all the data models. The final global classification data model comprises of the top three rules for each class (where available). Note that MPI is used in conjunction with the known maximum number of hosts (line 4) to classify the clusters in parallel using the C4.5 classification algorithm. If the number of clusters exceeds the available number of hosts then some hosts will classify multiple clusters (using MPI). Also the aggregation model scans all Rule files (line 7) from all clusters and picks the best rules out of the union of all cluster rule sets. During the classification phase we have also classified the original dataset and produced rules modeling this data. To finally ascertain if our DDM system is efficient we compare our global model to this data model from the un-partitioned database. We compare the top three rules for each class from this model with our rules from the global model. If a global model is over 90% accurate in comparison to the data model from the original database we consider this as a useful result.

4.3 Preliminary Results

The DDM system was tested on a number of real world datasets in order to test the effectiveness of data mining and the predictive accuracy. Further empirical analysis can be studied from [16]. In this section we present the DDM system performance results on the 'Pima-Indians-Diabetes' dataset from the UCI KDD Archive [17]. In order to study the usefulness of the system we compare the top three rules for each class from the partition-derived classification rules and rules from the original dataset. The aim of this testing is to find out the effect of our clustering process in partitioning, to the efficiency of our classification model and its predictive accuracy. We apply an error threshold, average error rates of rules from partitions greater then 10% of that of the corresponding original rules is an undesirable result.

We can observe in figure 4 and other comparisons that the rules from partitions and original rules satisfy our error threshold. In general the distributed data mining system offers useful performance in the presence of a number of factors influencing the predictive accuracy. However many improvements and further research is needed in order to optimize the DDM system.

Fig. 4. Predictive Accuracy Comparison

5 Conclusions and Future Challenges

As the elderly population constitutes a larger proportion of the aging society, providing quality long term care becomes an increasingly critical issue over the world. Our research aims to enable a patient-centric ubiquitous healthcare environment instead of the existing hospital-centric approach. The use of traditional verification-based approaches to analysis is difficult when the data is massive, highly dimensional, distributed, and uncertain. Innovative discovery-based approaches to health care data analysis with the integration of distributed data mining techniques warrant further attention.

This paper commences by describing a ubiquitous healthcare framework designed to provide consumers with freedom from temporal and spatial restrictions in their access to professional and personalized healthcare services anytime and anywhere – even outside of the hospital. Components of the system framework are discussed in brief. A prototype distributed data mining system is introduced with results from preliminary

experiments on data. The plausibility of integrating such a DDM system with the clinical decision support component (CDSS) of the ubiquitous healthcare frameworks is highlighted.

References

1. United Nations Population Division Publications. UN World Population Ageing 1950~2050: http://www.un.org/esa/population/publications-/worldageing19502050 (2002)
2. MobileHealth: http://www.mobihealth.org/
3. EliteCare: http://www.elitecare.com/index.html
4. Tele-Monitoring: http://www.medical.philips.com
5. CodeBlue: http://www.eecs.harvard.edu/~mdw/proj/codeblue
6. Smart Medical Home. http://www.futurehealth.rochester.edu/smart_home/
7. J. Hill, M. Horton, R. Kling, L. Krishnamurthy: The Platforms enabling Wireless Sensor Netowrks. Communications of the ACM, Vol. 47 (2004) 41-46
8. Jardine, I. and Clough K.: The Impact of Telemedicine and Telecare on Healthcare. Journal of Telemedicine and Telecare, Vol. 5, Supplement 1 (1999) 127-128
9. Smithers C. R. and Hill N.: Options for Wireless Technology in Telemedicine and Telecare Applications. Journal of Telemedicine and Telecare, Vol. 5, Supplement 1 (1999) 138-139
10. Anup Kumar and Mehmed Kantardzic: Distributed Data Mining: Framework and Implementations, IEEE Internet Computing, vol. 10, no. 4 (2006) 15-17
11. Park B. H., Kargupta H.: Distributed data mining: Algorithms, systems, and applications. The Handbook of Data Mining.Nong Ye (ed) Lawrence Erlbaum, New Jersey (2003)
12. Wallace C. S., Dowe D. L.: MML clustering of multi-state, Poisson, von Mises circular and Gaussian distributions. Statistics and Computing, 10(1) (2000) 73-83
13. Message Passing Interface Forum: MPI: A message-passing interface standard. International Journal of Supercomputer Applications, 8(3/4) (1994) 165-414
14. Quinlan, J. R.: C4.5: Programs for machine learning. San Mateo, CA: Morgan Kaufmann (1993)
15. M. Viswanathan, Y. K. Yang, T. K. Whangbo: Distributed Data Mining on Clusters with Bayesian Mixture Modeling, Lecture Notes in Computer Science, Volume 3613 (2005) 1207 – 1216
16. Merz, C. and Murphy, P.: UCI repository of machine learning databases.A.B. Smith, C.D. Jones, and E.F. Roberts, "Article Title", Journal, Publisher, Location, Date (1998) 1-10

A Framework for Data Structure-Guided Extraction of XML Association Rules ⋆

Juryon Paik[1], Junghyun Nam[2], SeungCheol Lee[1], and Ung Mo Kim[1]

[1] Dept. of Computer Engineering, Sungkyunkwan University, Republic of Korea
`quasa277@gmail.com`, {`eddie,umkim`}`@ece.skku.ac.kr`
[2] Dept. of Computer Science, Konkuk University, Republic of Korea
`jhnam@kku.ac.kr`

Abstract. Because of the widespread interest and use of semi-structured data in XML format, the discovery of useful information from them is currently one of the main research topics on association rule extraction. Several encouraging approaches to developing methods for mining rules from XML data have been proposed. However, efficiency and simplicity are still barriers for further development due to the combinatorial explosion in the number of tree nodes. What is needed is a clear and simple methodology for extracting the knowledge that is hidden in the heterogeneous tree data. In this paper, we show that association rules can be unveiled and provided from any XML documents using a special data structure, called Simple and Effective Lists Structure (SELS), avoiding the computationally intractable problem in the number of nodes. SELS is flexible and powerful enough to represent both simple and complex structured association relationships in XML data.

Keywords: XML mining, Association rules, XML association rule, Tree structured data.

1 Introduction

Data Mining, one of the fast growing computer science fields, is used to extract *interesting* knowledge from rich sources of data stored in data repositories. As one of many ways to represent the knowledge, association rules [1] are effective in describing interesting relations in massive amounts of data.

Currently, XML [11] is being used to encode data virtually all areas of Internet applications. The ability to extract knowledge from them becomes increasingly important. Due to the inherent flexibilies of XML finding knowledge in XML data is more challenging than from traditional well-structured data. Hence, extracting association rules from the semi-structured XML data still remains a major problem, which was first introduced by Braga et al. [3].

Under the traditional framework for association rule, the basic unit of data to deal with is database record, and the construct unit of a discovered association rule is item having an atomic value [5]. However, since the structure of XML is a tree, it is required to have counterparts of record and item in association relationships. In the light of flexibility and hierarchy of tree, the construct unit of an XML association rule is usually generated by repeated tree joins which are performed by nodes combinations. The combinatorial time for unit generations becomes an inherent bottleneck of mining XML association rules.

In this paper,we define some fundamental concepts applied to the XML association rules. Furthermore, we present a clear and simple methodology for mining association rules from XML trees, which is guided by a special data structure, called Simple and Effective List Structure (SELS). The proposed structure not only reduces significantly the number of combinatorial times for obtaining desirable rules, but also simplifies greatly the extraction processes. To the best of our knowledge, this paper is the first attempt: 1) to define formally association rules from the tree-based data, 2) to provide a data structure model for uncovering XML association rules, and 3) to propose techniques for the data structure-guided extracting of association rules from large XML data.

2 Related Work

Since the problem of extracting association rules was first introduced in [1] upon retail databases, a large amount of work has been done in various directions. The famous Apriori algorithm for extracting association rules was published independently in [2] and in [9]. Then, a number of algorithms for extracting association rules from multivariate data have been proposed [6,8]. Because a huge part of the data available on the Internet is represented in XML, a couple of proposals to exploit XML within data mining have been suggested. Singh et al. [7] proposed to mine association rules that relate structural data values to concepts extracted from unstructured and/or semi-structured data. However, they do not seem suitable for discovering association rules from XML documents. Because their approach is not for the context of native XML documents and it considers just strict parent-child relations. Recently, tools for extracting association rules from XML documents have been proposed in [4,10], but both of them are approaching from the view point of a XML query language. This causes the problem of language-dependent association rules mining.

In this paper, we focus on rules detection from a collection of XML documents currently prevailed over the web. Each of XML documents corresponds to a database record, and possesses a tree structure. Accordingly, we extend the notion of associated item to an XML tree, and build up associations among trees rather than items.

3   Preliminaries

3.1   Association Rules for Traditional Data

Association rule is one of data mining technique to discover interesting rules or relationships among attributes in databases. It was first introduced by Agrawal et al. [1] to analyze customer habits in market basket transactions. It is an implication of the form $X \Rightarrow Y$, where the rule *body* X and *head* Y are subsets of the set $\mathcal{I}$ of *items* ($\mathcal{I} = \{I_1, I_2 \ldots I_n\}$) within a set of *transactions* $\mathcal{D}$ and $X \cap Y = \phi$. A rule $X \Rightarrow Y$ states that the transactions T ($T \in \mathcal{D}$) that contain the items in X ($X \subset T$) are likely to contain also the items in Y ($Y \subset T$). Association rules are characterized by two measures: the *support*, which measures the percentage of transactions in $\mathcal{D}$ that contain both items X and Y ($X \cup Y$); the *confidence*, which measures the percentage of transactions in $\mathcal{D}$ containing the items X that also contain the items Y. More formally, given the function $\texttt{freq}(X, \mathcal{D})$, which denotes the percentage of transactions in $\mathcal{D}$ containing X, we define: $\texttt{sup}(X \Rightarrow Y) = \texttt{freq}(X \cup Y, \mathcal{D})$, $\texttt{conf}(X \Rightarrow Y) = \frac{\texttt{freq}(X \cup Y, \mathcal{D})}{\texttt{freq}(X, \mathcal{D})}$. The problem of mining association rules from a set of transactions $\mathcal{D}$ consists of generating all the association rules that have support and confidence greater than two user-defined thresholds: minimum support (min_sup) and minimum confidence (min_conf).

3.2   Association Rules for Tree-Structured XML Data

XML represents data as trees, and makes no requirement that the trees be balanced. Indeed, XML is remarkably free-form, with the only requirements being that 1) the root is the unique node denoting a whole document, 2) the other internal nodes are labeled by tags, and 3) the leaves are labeled by contents or attributes of tags. Thus, XML tree is often called rooted labeled tree. For brevity, in the remaining of this paper, we call a rooted labeled tree as simply a tree. Let $T = (N, E)$ be a labeled rooted tree where N is a set of labeled nodes and E is a set of edges.

Definition 1. Given a tree $T = (N, E)$, we say that a tree $F = (N_F, E_F)$ is a *fragment* of T, denoted as $F \preceq T$, if and only if (i) $N_F \subseteq N$, (ii) for all edges $(u, v) \in E_F$, u is an ancestor of v in T, and (iii) the label of any node $v \in N_F$ is preserved in T.

Intuitively, as a fragment in this paper, any fragment F must not break the ancestor-descendant relationship among the nodes in a tree T.

Definition 2. The basic construct unit of XML association rule is referred to as *tree-structured item*, shortly *titem*. Any fragment is eligible for a titem because the whole XML document consists of several fragments and the structure of fragment is tree.

Assume that $\mathcal{D} = \{T_1, T_2 \ldots T_n\}$ is a collection of XML documents and $|\mathcal{D}|$ means the number of documents in $\mathcal{D}$. Let $\mathcal{F} = \{F_i, \ i > 0 \mid F_i \preceq T_j, \ for \ 0 < j \leq n\}$ be a total set of fragments and $\mathcal{I} = \{I_1, I_2 \ldots I_m\}$ be a set of titems, where $\mathcal{I} \subseteq \mathcal{F}$.

(a) A set of XML trees   (b) Possible XML association rules
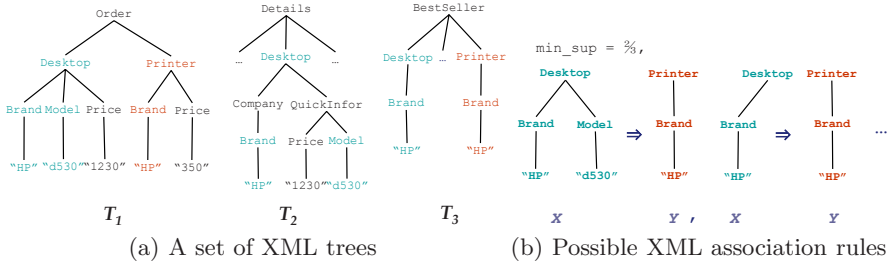
Fig. 1. Extraction of association rules from heterogeneous database $\mathcal{D}$

Definition 3. An *XML association rule* is an implication of the form $X \Rightarrow Y$, which satisfies following two conditions: (i) $X \in \mathcal{I}, Y \in \mathcal{I}$, (ii) $(X \nsubseteq Y) \wedge (Y \nsubseteq X)$.

Different from traditional association rules where associated items are usually denoted using simple tuple-based data, the items in XML association rules have hierarchical tree structures (titem), as indicated by the first clause of the definition. The second clause of the definition requires that titems are independent each other in an XML association rule.

Lemma 1. If one of X or Y $(X \Rightarrow Y)$ is assigned the entire tree T $(T \in \mathcal{D})$ as a titem, the other should be assigned among titems $\mathcal{I}'$ which is a subset of fragment $\mathcal{F}'$, where $\mathcal{F}' = \mathcal{F} - \{F_i, \quad i > 0 \mid F_i \preceq T\}$.

Proof. Let assume the body X is a tree T_2 in $\mathcal{D}$ and the head Y is F_{T_2}, one of fragments of T_2. The association rule $T_2 \Rightarrow F_{T_2}$, however, is against Definition 3. Since F_{T_2} is a fragment of T_2, it is included in T_2. Hence, they are not independent each other, which is the second condition of Definition 1. Therefore, any fragment of a tree T in $\mathcal{D}$ cannot be X or Y, if one of X or Y is a tree T.

Definition 4. Given $\mathcal{D}$, the *support* and *confidence* of an XML association rule $X \Rightarrow Y$ are defined as: $\texttt{sup}(X \Rightarrow Y) = \texttt{freq}(X \cup Y, \mathcal{D}) = \frac{|\mathcal{D}_{X \cup Y}|}{|\mathcal{D}|}, \texttt{conf}(X \Rightarrow Y) = \frac{\texttt{freq}(X \cup Y, \mathcal{D})}{\texttt{freq}(X, \mathcal{D})} = \frac{|\mathcal{D}_{X \cup Y}|}{|\mathcal{D}_X|}$, where $\mathcal{D}_{X \cup Y} = \{T_i \mid I_j \in (X \cup Y) \text{ and } I_j \preceq T_i, T_i \in \mathcal{D}\}$, and $\mathcal{D}_X = \{T_i \mid I_j \in X, \text{ and } I_j \preceq T_i, T_i \in \mathcal{D}\}$.

Let us consider three XML trees in Fig. 1(a), where each different information is provided from various data sources, e.g., ordering information (Order) and the detailed information of a product (Details). Consider the extraction of frequently occurring association rules in $\mathcal{D}$ that if a customer purchases HP Desktop, usually s/he is likely to buy HP Printer depicted in Fig. 1(b). The support of an association rule $\texttt{freq}(X \cup Y, \mathcal{D})$ is 0.66 because both titems X and Y appear together in T_1 and T_3 out of three, i.e., in 66% of the cases. Likewise, $\texttt{freq}(X, \mathcal{D})$ is 1 since the titem X is included in all of three trees, i.e., in 100% of the cases. Therefore, we can compute the confidence of XML association rule as: $\frac{\texttt{freq}(X \cup Y, \mathcal{D})}{\texttt{freq}(X, \mathcal{D})} = \frac{0.66}{1}$, which returns 0.66; it means HP Desktop is usually purchased at the rate of 66% in computer products together with HP Printer.

4   Extracting Association Rules Using SELS

4.1   Design and Construction of SELS

The flexibility of tree data comes from its hierarchical structure. The hierarchy, however, causes technical problems to exploit or extract some valuable partial data from the entire dataset. After some careful examination, we believe that the bottleneck of hierarchy is at fragments generation and titem tests. If one can only generate fragments which guarantee being proper titems, the rule mining performance can be substantially improved. Simple and Effective List Structure (SELS) is devised to enable avoiding useless fragments generation, reduce computational complexity and enhance fast extraction of desired fragments. It is a set of lists which includes all information of characteristics of trees, such as label, node id, tree id, and parent/ancestor relationships among nodes.

Definition 5. Given a tree database $\mathcal{D}$, node ids and tree ids are members of a single list under each unique node label. The list is operationally divided into two parts; one is for identifying list itself between a number of lists, and the other is for storing all relevant frequency information in a tree database. The former deals with a label of node and node ids being assigned the label. The latter is mostly about frequency of a label; tree id is kept, but there is a special filed for hierarchy of nodes assigned the label in trees; parent node ids are stored. Because complete single list is composed of finally node ids and tree ids, the list is called, *Node and Tree List* (*NaTL*). In addition, the leading part for distinguishing each NaTL is named *head of NaTL*, shortly ntl_{head} and the trailing part for counting frequency of each label is *body of NaTL*, ntl_{body}.

Every ntl_{head} consists of three fields in which a label, node ids assigned the label, and pointer to its corresponding ntl_{body} are included. As described in Definition 5, each ntl_{head} is unique due to the label in it thus, the label is called *key* of SELS for database $\mathcal{D}$. The corresponding ntl_{body} is a linkedlist of several elements. A single element is composed of one pointer field for next element and two id fields; one is for tree which contains node(s) assigned the label in ntl_{head} and the other is for parent nodes of the node(s) in the tree. The number of elements in a ntl_{body} means a total number of trees in $\mathcal{D}$ that assign the label to their node(s). In other words, the count of elements gives the information of the frequency of a label with respect to the database $\mathcal{D}$, and represents size of NaTL denoted as $|ntl|$. The size plays a key role to filter out some undesirable NaTLs from SELS.

4.2   Method of Refining SELS

Initially constructed SELS is composed of NaTLs of every unique node label. Therefore, it is highly possible that some NaTLs having not frequently occurred node labels are included in the SELS.

Definition 6. Given a min_sup, an NaTL is *frequent* if and only if size of its body $|\text{ntl}_{\text{body}}|$ is greater than or equal to $|\mathcal{D}| \times min\_sup$, otherwise *unfrequent*.

After filtering out unfrequent NaTLs, only frequent NaTLs whose body sizes satisfy the threshold are remained in SELS. This firstly filtered SELS is called *shallowly-frequent SELS*, shortly *sfS*. It is similar to having only frequent 1-size subtrees which have only one node labeled by a key of SELS. In traditional generate-and-test approaches, each frequent 1-size subtree is grown by joining of subtrees or enumeration of subtrees. In our approach, however, due to SELS, there is no need to grow subtrees. Instead, we verify each parent node in elements of ntl_{body} if it is unfrequent or not. Because all nodes composing a tree must be frequent in order the tree has to be frequent, as a first step to expand a single frequent node, the frequency of every parent node related to it should be considered. However, it is not guaranteed in sfS. This is the reason why the SELS is called shallowly-frequent after filtration of some NaTLs.

To refine sfS the unfrequent NaTLs are required. A *candidate_hash_table* is generated containing them, and it is built simultaneously with sfS. In the tabel, node ids are keys of table, a labeling function plays a role of hash function, node labels are indexes, and ntl_{body}s of unfrequent ntl_{head}s are records of indexes. Because every node is assigned only one label and it is not changed until artificial manipulation is performed, we assume that the labeling function is same as a hashing function. After finishing the refinement, the hash table is removed from the memory. The purpose of second refinement of SELS to deal with every parent node in elements and to make sfS contain all frequent nodes. We call this acquired SELS, *deeply-frequent SELS*, abbreviated *dfS*. To obtain dfS we proceed as follows: (1) a parent node in an element is verified by the candidate_hash_table to detect if the node is assigned by unfrequent label or not. (2) If so, the node is marked 'replace' and its record is retrieved to search a node id assigned by frequent node labels. (3) Step (1) and (2) continues until the node id assigned by any frequent node label is found. (4) The original parent node id is replaced by the found node which is actually an ancestor node of the original parent node. (5) Through step (1) to (3), if no any other nodes are frequent, the original parent node id is replaced by NULL. After applying above refining procedure over all parent nodes in elements, dfS holds only frequent node ids and associated labels (keys of dfS).

Given a dfS, both ntl_{head}s and ntl_{body}s are associated together depending on ancestor-descendant relationship. Note that every node id is only assigned by one of the keys of dfS. At least one big labeled tree [1] is derived from dfS. We call this derived tree as *Minimum Support Satisfying Trees* (MSST). During the construction of MSST, each edge has its own count which represents how much often it is occurred. If the frequency does not satisfy $\sigma \times |\mathcal{D}|$, the corresponding edge is deleted from MSST. After scanning all edges of MSST, tree(s) which is(are) satisfying min_sup is(are) derived. The stepwise refinement of $\text{SELS}_{\mathcal{D}}$ and its derived MSST are illustrated in Fig. 2. Due to the lack of space, we only show the prefix of labels in SELS and MSST; only heads of NaTLs and labels in MSST .

---

[1] To avoid derive graphs we duplicate nodes shared by different parents/ancestors.

(a) Initially constructed SELS

(b) sfS and dfS

(c) MSST before and after deleting some edges
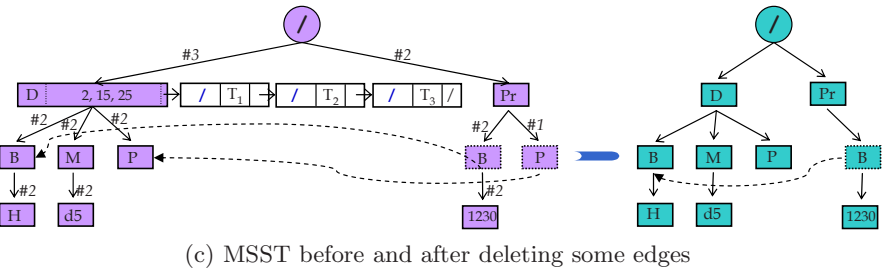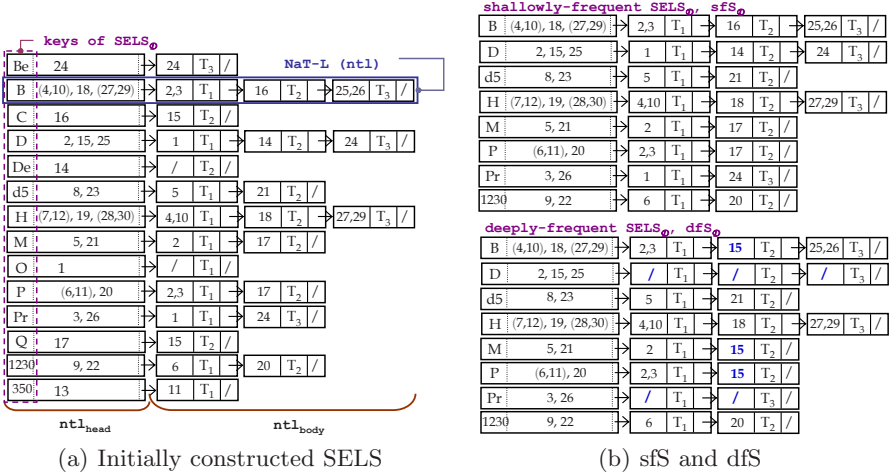
Fig. 2. Stepwise Refinement of SELS and Derived Trees

4.3 Correlating Concrete Contents with Structures

Let (h_i, e_{h_i}) and (h_j, e_{h_j}) be two NaTLs in MSST. The sizes of two elements, $|e_{h_i}|$ and $|e_{h_j}|$, are greater than $|\mathcal{D}| \times min\_sup$. Let t_i and t_j be the all tree indexes included in e_{h_i} and e_{h_j}, respectively. The sizes of each t_i and t_j are exactly same as the sizes of each e_{h_i} and e_{h_j}. We denote a path between them by $\mathcal{P}_{ij} = (h_i, h_j)$ where h_i is an ancestor of h_j by Definition 1. Let $\mathcal{I} = \{I_1, \ldots, I_m\}$ be a set of titems. Assume that $I_1 = \mathcal{P}_{ij} = (h_i, h_j)$ and $I_2 = \mathcal{P}_{pq} = (h_p, h_q)$ be titems. The confidence of $I_1 \Rightarrow I_2$ is computed as:

$$\mathtt{conf}(I_1 \Rightarrow I_2) = \frac{\mathtt{freq}(I_1 \cup I_2, \mathcal{D})}{\mathtt{freq}(I_1, \mathcal{D})} = \frac{|t_i \cap t_j \cap t_p \cap t_q|}{|t_i \cap t_j|} \tag{1}$$

Theorem 1. *Given a min_sup and MSST, all of XML association rules conforming to **any min_conf** are extracted.*

Proof. Let (h_i, e_{h_i}), (h_j, e_{h_j}) and (h_k, e_{h_k}) be three NaTLs in MSST. Assume that $|t_i \cap t_k| = \beta$, and $|t_i \cap t_j \cap t_k| = \gamma$. Given min_sup and min_conf are s_m and c_m, respectively, where $0 < s_m, c_m \leq 1$. Let x and y be a tree index in t_j and t_k, respectively, for $x \neq y$.

- **titem$_a$** ($x \in t_i \wedge y \notin t_i$): *The h_i and h_j forms $\mathcal{P}_{ij}$. It is a titem I_{ij}.* The support of titem$_a$ is definitely greater than or equal to s_m due to the characteristics of MSST.
- **titem$_b$** ($y \in t_i \wedge x \notin t_i$): *The h_i and h_k forms $\mathcal{P}_{ik}$. It is a titem I_{ik}.* The support of titem$_b$ is also greater than or equal to s_m.
- **Association Rule** The confidence of an implication of the form $I_{ij}(titem_a) \Rightarrow I_{ik}(titem_b)$ is computed by using the equation (1):

$$\mathtt{conf}(I_{ij} \Rightarrow I_{ik}) = \frac{\gamma}{\beta} = \begin{cases} \text{rules with confidence} \geq c_m \text{ if } \gamma \geq \beta \times c_m \ , \\ \text{rules with confidence} < c_m \text{ if } \gamma < \beta \times c_m. \end{cases}$$

5   Conclusion

This paper has presented a framework for data structure-guided association rules extraction from XML trees. We are currently finishing touches of practical algorithms for our approach and evaluating the performance results.

References

1. Agrawal, R., Imielinski, T., Swami, A. N.: Mining Association Rules between Sets of Items in Large Databases. Proc. of the ACM SIGMOD Intl. Conf. on Management of Data (1993) 207–216
2. Agrawal, R., Srikant, R.: Fast Algorithms for Mining Association Rules. Proc. of the 20th Intl. Conf. on VLDB (1994) 478–499
3. Braga, D., Campi, A., Klemettinen, M., Lanzi, P. L.: Mining Association Rules from XML Data. Lecture Notes in Computer Scienec, Vol. 2454. Springer-Verlag, Berlin Heidelberg New York (2002) 21–30
4. Braga, D., Campi, A., Ceri, S., Klemettinen, M., Lanzi, P. L.: A Tool for Extracing XML Association Rules. Proc. of the 14th IEEE Intl. Conf. on Tools with Artificial Intelligence (2002) 57–64
5. Feng, L., Dillon, T., Weigand, H., Chang, E.: An XML-Enabled Association Rule Framework. Lecture Notes in Computer Scienec, Vol. 2736. Springer-Verlag, Berlin Heidelberg New York (2003) 88–97
6. Han, J., Fu, Y.: Discovery of Multiple-Level Association Rules from Large Databases. Proc. of the 21st Intl. Conf. on VLDB (1995) 420–431
7. Singh, L., Scheuermann, P., Chen, B.: Generating Association Rules from Semi-Structured Documents Using an Extended Concept Hierarchy. Proc. of the 6th Intl. Conf. on Information and Knowledge Management (1997) 193–200
8. Srikant R., Agrawal, R.: Mining Generalized Association Rules. Proc. of the 21st Intl. Conf. on VLDB (1995) 409–419
9. Toivonen, H.: Sampling Large Databases for Association Rules. Proc. of the 22th Intl. Conf. on VLDB (1996) 43–52
10. Wan, J. W. W., Dobbie, G.: Extracting Association Rules from XML Documents Using XQuery. Proc. of the 5th ACM Intl. Workshop on Web Information and Data Management (2003) 94–97
11. The World Wide Web Consortium (W3C). Extensible Markup Language (XML) 1.0 (Third Edition) W3C Recommendation, http://www.w3.org/TR/2004/REC-xml-20040204/, 2004.

Online Burst Detection Over High Speed Short Text Streams

Zhijian Yuan[1], Yan Jia[2], and Shuqiang Yang[3]

Computer School, National University of Defense Technology, Changsha, China
yuan.georgie@gmail.com,
jiayanjy@vip.sina.com,
sqyang9999@126.com

Abstract. Burst detection is an inherent problem for data streams and it has attracted extensive attention in research community due to its broad applications. In this paper, an integrated approach is introduced to solve burst events detection problem over high speed short text streams. First, we simplify the requirement by considering burst event as a set of burst features, then the processing speed can be accelerated and multiple features can be identified simultaneously. Second, by using the ratio of the number of documents with specific feature and total number of documents during a period of time as the measurement, our solution adapts to any kind of data distribution. Then we propose two algorithms to maintain the ratio in the sliding window. Finally, we propose a burst detection algorithm based on Ratio Aggregation Pyramid (RAP) and Slope Pyramid (SP) data structure, which are extended from Aggregation Pyramid (AP). Our algorithm can detect burst in multiple window sizes simultaneously and is parameter-free. Theoretical analysis and experimental results verify the availability, efficiency and scalability of our method.

1 Introduction

Web and wireless applications such as BBS, forum, BLOG and SMS have brought massive text data, which occurred as high speed short text streams for its strong time sensitivity and short in length. One of the most important mining tasks is find the abrupt 'hot' events (also called burst events) from these data. Burst, means abnormal number of data (such as document related to a certain topic) emerge during a period of time. Finding burst occurring time and duration is our goal. Burst detection widely used in web topic mining, commercial information acquisition, astronomical observation, network monitoring, and fraud detection etc. Moreover, in many cases, multiply windows size should be monitored real time, simultaneously and distribution of text streams is not uniform, these take more challenge.

There already have some works deal with burst detection problem. Most of them are focused on numeric streams[1-4], [1] develop an efficient algorithm for detecting adaptive aggregation bursts in a data stream given a burst ratio. [2, 4] solve the elastic burst detection problem which allow identifying bursts in multiple window sizes simultaneously, [3] introduce Lasting Factor and Abrupt Factor in the general definition

of bursts. All of above works could not apply to text directly. There also have some works focused on text streams[5-7], [5] model text stream as an infinite-state automaton, and model bursts as state transitions, [7] proposed a feature-pivot clustering approach to detect bursty events based on the feature distributions. [5-7] don't deal with the performance and precision problem that can not solve our problem properly. All of the related works will be discussed detailed in section 2.

There are two kinds of method to find burst events in text streams; one is using clustering to group similar texts together, like K-Means, and identifies each cluster has burst or not, but no appropriate clustering algorithms can group short text streams fast and exactly. Another way is consider burst event as burst features for an event always show as a set of burst features. For example, the event "SARS" consists of the features "Outbreak", "Atypic", "Respire". Currently, it has no work can deal with multiple features and multiple window sizes simultaneously.

Our contributions can be summarized as follows:

1. We consider burst event as a set of burst features and give an integrated solution to detect bursts on multiple features simultaneously.
2. We adopt the ratio of the number of specific feature and total number of documents in a period of time as the measurement of the feature, so that our solution can adapts to any kind of data distribution density. We also propose two algorithms to maintain the ratio in the sliding window.
3. We propose a burst detection algorithm using Ratio Aggregation Pyramid and Slope Pyramid data structure, which extend Aggregation Pyramid data structure. Our algorithm can detect burst in multiple window sizes simultaneously and is parameter-free for each window.

2   Related Work

Burst Detection on data streams[8] and time serials has broad applications, including Gamma Ray[4], stock, Email[5], Blog[6, 9, 10], Instant Message, News[7] and so on. Many efficient algorithms have been developed.

[5]studied the bursty and hierarchical structure in temporal text streams to discover how high frequency words change over time. The text stream is modeled as an infinite-state automaton, where bursts are modeled as state transitions. Since the algorithm in [5] could not be applied to document streams where the distribution of documents was not uniform, [6]extended[5] algorithm and proposed a method to deal with Blog and BBS which do not exhibit uniform distribution. [5, 6] focused on modeling the bursty behaviors and our goal is finding an efficient solution to solve the burst detection problem in short text streams.[7] proposed a novel parameter-free probabilistic approach, called feature-pivot clustering. [7] tried to detect bursty events based on the feature distributions. [7] did not give the way to deal with multi-feature simultaneously. None of [5-7] can detect burst in multiple window sizes.

Detecting burst across multiple window sizes, the naive algorithm can only check each window size of interest once at a time. It requires $O(kN)$ time.(k is windows number, N is the length of sequence). [4] presented a general data structure called Shifted Binary Tree for detecting interesting aggregates over such elastic windows in nearly linear time. However, this algorithm is not efficient when the probability of bursts is

high frequency. As a result, [2] improved [4] 's data structure and algorithm, It included a family of data structures including Aggregation Pyramid, Shifted Aggregation Tree and a heuristic search algorithm to find an efficient structure when given the input. An aggregation pyramid is an N-level isosceles triangular-shaped data structure built over a time window of size N. Level 0 has N cells and is in one-to-one correspondence with the original time series. Level h has N-h cells, the ith cell stores the aggregate of the h+1 consecutive data in the original time series starting at time i. The problem in [4]and [2] is that they require many parameters - burst threshold for each window. Thus, it is difficult to find an effective way to tune these parameters. Our methods use ratio threshold for bursting measurement and only need two parameters.

[1]introduced a novel concept of adaptive aggregation burst to detect double-side relative bursts dynamically. [1] argued that ratio threshold for bursting measurement and adaptive window size was more suitable for data stream analysis applications. However, these methods can not deal with multiple window sizes and can not be applied to text streams directly while ours can.

3 Algorithms for Burst Detection

3.1 Problem Statement

Given a text stream $X_1, X_2, X_3 \ldots\ldots X_n$, an aggregation function F, S_t and S_t' are the latest two consecutive subsequences with the same length of t, $1 \leqslant t \leqslant n/2$. When X_n comes, $\forall j \in 1..i$, $\beta_1 > 1$, $if\ F(S_t) > \beta_1 F(S_t')$, then an increasing burst occurs on t-length window, $\forall j \in 1..i$, $0 < \beta_2 < 1$, $F(S_t) < \beta_2 F(S_t')$, then a decreasing burst occurs. β_1 is the increasing threshold and β_2 is the decreasing threshold. The problem of burst detection is finding the value pair (X_n, j), indicating that an increasing burst or a decreasing burst occurs in this window.

3.2 A Framework to Solve This Problem

As we discussed in section 1, using clustering to group short text streams is slow and inaccurate, so we adopt the second method. We use simplified vector to represent shot text data. Data stream is changing with time, so we should choose a relative value rather than an absolute term as a metric and algorithm could adapt to different data distribution density. In this paper, we use the ratio of the number of specific feature and total number of documents to measure the relative quantity of the feature.

Algorithms to judge whether there are bursts in data streams can be classified into two categories: one is based on the absolute value, called threshold value, namely if the aggregation value is beyond the scope, a burst is announced. This method is simple and intuitionist. However, the disadvantage is that it must assign a threshold to each window size. Another is based on the relative value, called ratio value, namely if the ratio of two neighboring windows is beyond the scope, a burst is announced. In this method, each window sizes and data distribution densities can use the unified parameter. Our work adopts the second method and eliminates the limitation of current algorithms, which cannot deal with multiple time-windows simultaneously.

Our framework is outlined in Fig. 1. There are three major steps:

1. Transforming text stream to simplified vector.
2. Aggregating multi-vectors to a single vector, which is the basic element of the sliding window.
3. Based on the above 2 steps, updating the Ratio Pyramid Aggregation and Slope Pyramid Aggregation data structure, and detecting burst for each feature.
   The follow sections will discuss each step in details.
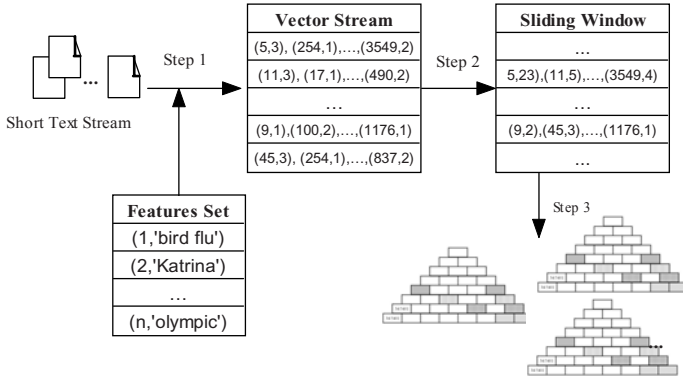
Fig. 1. The flow chart for solving the burst detection problem in short text streams

3.3 Forming Single Element in Sliding Window

Definition 1. Features set $H = \{(index, name) \mid 1 \leq index \leq N, name \in Vocabulary\}$, $N = |Vocabulary|$, *Vocabulary* is appointed by domain expert.

Definition 2. Text stream $D = \{D_1, D_2, D_3 \ldots\ldots D_t\}$, Document D_i could be denoted by $D_i = \{(index_m, count(index_m) \mid name_m \in Vocabulary(D_i)\}$.

After Splitting words, data cleaning, counting features and labeling, short text is transform to simplified vector. The length of vector is $|Vocabulary(D_i)|$.

It may improper to treat one document as basic element in sliding window for the high speed of text stream. We should specify a time period *T*. All the vectors in *T* are aggregated as one vector. As we know, data stream fluctuate with time. Therefore, choosing a relative value instead of an absolute value to measure the value of feature can make our algorithms suitable for different data distribution density. In this paper, we choose the ***Ratio*** as our metric, defined as:

$$Ratio(Feature) = \frac{Count(Feature)}{Count(Document)} \quad Feature \in H.Name$$

Obviously, These will increase the complexity from O(*n*) to O(*kn*), *k* is a constant.

There are two kinds of algorithms to compute *Ratio*: one is online algorithm. As soon as one vector comes, each item in this vector is analyzed. The other is batched process algorithm, which saves the coming element in *T* and processing together. The flow of these two algorithms list here:

Table 1. Online Processing Algorithm Vs Batched Processing Algorithm

Online Processing Algorithm	Batched Processing Algorithm
Input: text vector $D_1, D_2, D_3 \ldots\ldots D_n$ in time period T **Output:** result vector V 1: V←Φ; 2: **for** i←1 **to** n 3: **for each** (Item **in** D$_i$) **do** 4: **if** (Item.index **in** V.index) **then** 5: V[Item.index] = V[Item.index] + Item.count; 6: **else** 7: V.add(Item.index, Item.count); 8: **end if** 9: **end for** 10: **end for** 11: **for each** (Item **in** V) 12: V[Item.index] = V[Item.index]/n; 13: **return** V;	**Input:** text vector $D_1, D_2, D_3 \ldots\ldots D_n$ in time period T **Output:** result vector V 1: V←Φ; 2: **for** i←1 **to** n 3: Cursor(i)←1; 4: Item(i)←D$_i$(Cursor(i)); 5: **end for** 6: **repeat** 7: min←Min(Item(i). index), $1 \le i \le n$; 8: minCollection←{j |Item(j). index = min}; 9: count←0; 10: **for each** (m **in** minCollection) **do** 11: count←count +Item(m).count; 12: Cursor(m)←Cursor(m)+1; 13: Item (m)←D$_m$(Cursor(m)); 14: **end for** 15: V.add(MinIndex, tempCount); 16: **until** Cursor(i)=**EOF**(D$_i$) $1 \le i \le n$; 17: **return** V;

3.4 Data Structures and Algorithms for Burst Detection

Ratio Aggregation Pyramid
Our Algorithms for burst detection are based on the data structure called Ratio Aggregation Pyramid and Slope Pyramid. These two data structures are derived from Aggregation Pyramid, as we introduce above. In computing the cell's value of 1~*N*-1 level, an aggregation function *F* must be specified, commonly is **SUM**. Here, because the element in sliding window is *ratio*, we define an aggregation function F_R, which can be calculated as follows:

$$F_R (Ratio_1, Ratio_2) = \frac{Count(Term_1) + Count(Term_2)}{Count(Document_1) + Count(Document_2)}$$

We treat the value of this function as the basic element in the sliding window. We call the Aggregation Pyramid (AP) with aggregation function F_R as Ratio Aggregation Pyramid (RAP).

Fig. 2 is an example of AP and RAP. We suppose that the feature number in the sliding window is {1,4,0,3,2,3} and {1/105,4/354,0/98,3/209, 2/117,3/533}. We can calculate the value of the entire cell in AP and RAP.
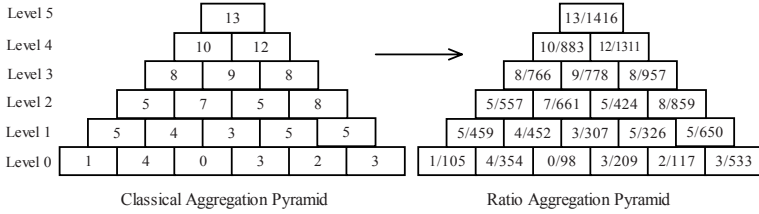
Fig. 2. Comparison of Classical Aggregation Pyramid and Ratio Aggregation Pyramid

Slope Pyramid

Algorithms to judge whether there are bursts in the aggregation tower are divided into two kinds: one kind uses absolute value, called threshold value, namely if cell value beyond the scope, then recognized this is a burst. This method is simple and direct-viewing and the shortcoming is that a threshold must be given to each window size (level). Another kind uses relative value, called ratio value, namely each time calculates the ratio of two neighboring windows, if the ratio beyond the scope, then recognized this as a burst. This ratio is equal to the slope. All windows size and data distribution density can use the unified parameter. This article uses the second method. The formula to compute Slope Pyramid is based on Ratio Aggregation Pyramid. It can be present as:

Slope(h) = cell(h,t)/cell(h,t-h-1)

Slope Pyramid only has one cell on one level. This cell stores the ratio of the latest two windows. Fig. 3 demonstrates how to compute the value of all the cell value in the Slope Pyramid.
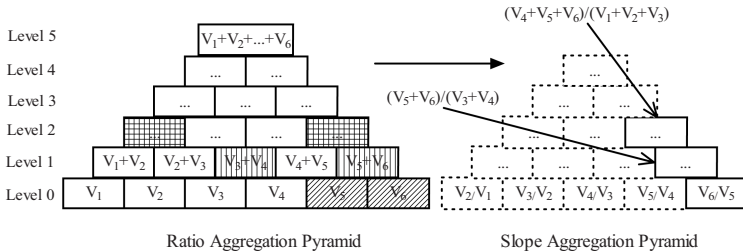
Fig. 3. Calculating Slope Pyramid through Ratio Aggregation Pyramid

Data Structure Updating and Burst Detection

When a new element is coming to sliding window, Ratio Aggregation Pyramid and Slope Pyramid update timely and identify if the value of the cell in Slope Pyramid is beyond the scope. If it is true, record the sliding window and the burst feature.

Formula for updating RAP is shown as following:

cell(h, t) = F_R(cell(h − 1, t − 1) , cell(0, t))

cell(h,t) means that the cell is in level h and in the end of time t.

After RAP has been updated, SP can be calculated and be checked if the value of the entire cell is in the normal scope. SP only needs to be calculated to level [t/2].

Fig. 4 demonstrates how to update RAP when a new element is coming.

cell(1,t)=cell(0,t-1)+cell(0,t)
cell(2,t)=cell(1,t-1)+cell(0,t)
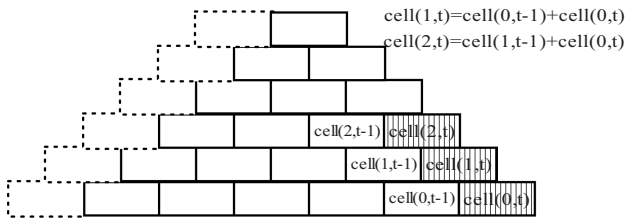
Fig. 4. Updating for Ratio Aggregation Pyramid

4   Experimental Evaluation

We have collected one-year (from 2005-01-01 to 2005-12-31) short documents (2,503,385 text items) containing news, forum and BBS from a web site. We implement our framework using Java^{TM} and Eclipse 3.0.1. Our experiments are performed on Inter Pentium4 2.4 HZ PC with 1.0G main memory. From all the features, we select eight burst features for demonstration, which is shown in Fig. 5.
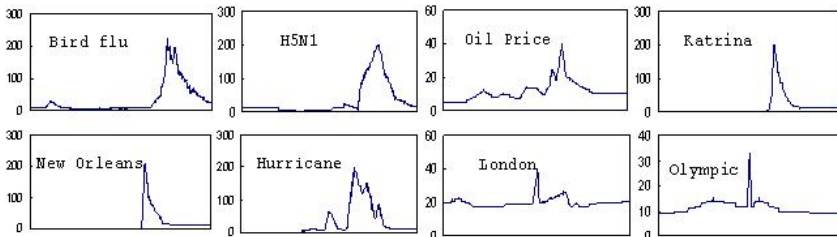
Fig. 5. The x-axis is the date starting from Jan. 1st, 2005 to Dec. 31st, 2005. The y-axis is the feature number in that day.

We first evaluate the efficiency of RAP. We have tested three groups of thresholds. The window size of each tested group is 4, 8, 12, 16 and 32. The experiment results are shown by Fig. 6. We can see that the burst number detected by RAP is only a little bit less than AP. This is because the fluctuation of the data distribution is small.
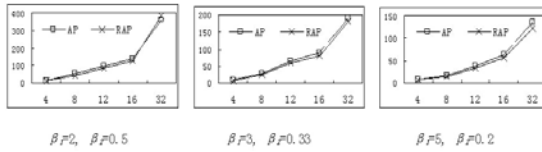
Fig. 6. Burst number detected based on AP and RAP with various thresholds

We also compare the executing time of RAP with AP. As is shown in Fig. 7, RAP need more time than AP. That is because RAP takes more time in updating ratio aggregation pyramid than that of AP does. Furthermore, RAP needs additional time to compute SP.

Finally, we evaluate the effects of thresholds to burst number. Fig. 8 reveals that increasing the *increasing threshold* and decreasing the *decreasing threshold* can reduce the number of the burst. For not all burst are significant, so users can adopt an appropriate threshold to get the demanding burst number.
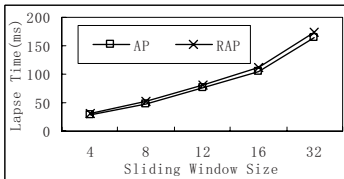
Fig. 7. processing time between AP and RAP
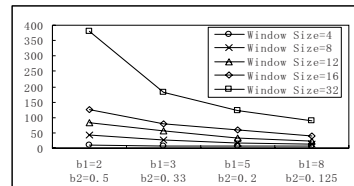
Fig. 8. Burst number detected with various thresholds and window sizes

5   Conclusion and Future Work

In this paper, we have proposed a simple but efficient solution for the burst events detection problem. Experimental results show that our algorithm is effective. It performs better when processing object is short text and distribution fluctuates greatly. However, many works can be improved. When generating simplified vector, we can establish the concept of semantic space models, giving synonymous with the terminology, so that the number of words and vector dimensions can be reduced, hence enhancing the efficiency and accuracy of algorithms. When the data stream flows are increasing, the usage of sampling and how to use the outline structure for high-speed data flows become open problems, which are left as our future work. In addition, burst forecasting and good visualization are also attractive.

References

1. Zhou Aoying, Qin Shouke, and Qian Weining. Adaptively Detecting Aggregation Bursts in Data Streams. in Lecture Notes in Computer Science. 2005.
2. Xin Zhang and Dennis Shasha. Better Burst Detection. in the 22nd International Conference on Data Engineering. 2006. Atlanta, Georgia, USA.

3. Tingting Chen, Yi Wang, Binxing Fang, and Jun Zheng. Detecting Lasting and Abrupt Bursts in Data Streams Using Two-Layered Wavelet Tree. in International Conference on Internet and Web Applications and Services/Advanced International Conference on Telecommunications. 2006.

4. Yunyue Zhu and Dennis Shasha. Efficient elastic burst detection in data streams. in Proceedings of the ninth ACM SIGKDD international conference on Knowledge discovery and data mining. 2003. Washington, D.C.: ACM Press.

5. Jon Kleinberg. Bursty and hierarchical structure in streams. in Proceedings of the eighth ACM SIGKDD international conference on Knowledge discovery and data mining. 2002. Edmonton, Alberta, Canada: ACM Press.

6. Toshiaki Fujiki, Tomoyuki Nanno, Yasuhiro Suzuki, and Manabu Okumura. Identification of Bursts in a Document Stream. in First International Workshop on Knowledge Discovery in Data Streams. 2004. Pisa, Italy.

7. Gabriel Pui Cheong Fung, Jeffrey Xu Yu, Philip S. Yu, and Hongjun Lu. Parameter free bursty events detection in text streams. in Proceedings of the 31st international conference on Very large data bases. 2005. Trondheim, Norway: VLDB Endowment.

8. Brian Babcock, Shivnath Babu, Mayur Datar, Rajeev Motwani, and Jennifer Widom, Models and issues in data stream systems, in Proceedings of the twenty-first ACM SIGMOD-SIGACT-SIGART symposium on Principles of database systems. 2002, ACM Press: Madison, Wisconsin.

9. Ravi Kumar, Jasmine Novak, Prabhakar Raghavan, and Andrew Tomkins. On the bursty evolution of blogspace. in Proceedings of the 12th international conference on World Wide Web. 2003. Budapest, Hungary: ACM Press.

10. Tomoyuki Nanno, Toshiaki Fujiki, Yasuhiro Suzuki, and Manabu Okumura, Automatically collecting, monitoring, and mining japanese weblogs, in Proceedings of the 13th international World Wide Web conference on Alternate track papers & posters. 2004, ACM Press: New York, NY, USA.

Parallel Computing of Kernel Density Estimates with MPI

Szymon Łukasik

Department of Automatic Control, Cracow University of Technology,
ul. Warszawska 24, 31-155 Cracow, Poland
Szymon.Lukasik@pk.edu.pl

Abstract. Kernel density estimation is nowadays a very popular tool for nonparametric probabilistic density estimation. One of its most important disadvantages is computational complexity of calculations needed, especially for data-based bandwidth selection and adaptation of bandwidth coefficient. The article presents parallel methods which can significantly improve calculation time. Results of using reference implementation based on *Message Passing Interface* standard in multicomputer environment are included as well as a discussion on effectiveness of parallelization.

Keywords: kernel density estimation, plug-in method, least squares cross-validation, adaptive bandwidth, parallel algorithms, MPI.

1 Introduction

Nonparametric methods find increasing number of applications in data mining problems. One of its main tools is kernel density estimation (KDE) introduced by Rosenblatt in 1956 [1] and Parzen in 1962 [2]. It has been successfully used in various applications like image processing [3], medical monitoring [4] and market analysis [5]. Theoretical and practical aspects of the estimation itself are covered in detail in numerous publications, e.g. popular monographs [6] and [7].

For n-dimensional probabilistic variable X with sample x_i of length m, kernel K and bandwidth h, the kernel density estimation evaluated for x is defined as a function:

$$\hat{f}(x) = \frac{1}{mh^n} \sum_{i=1}^{m} K\left(\frac{x - x_i}{h}\right) .$$

(1)

It can be seen that computation of KDE is of complexity $O(nm)$. Thus, long samples and large number of points p for which kernel density estimates are calculated can seriously influence the estimation time. The evaluation of density estimates can be made even more resource exhausting when one wishes to use bandwidth variation as suggested by Abramson [8]. Computational complexity of additional calculations is $O(nm^2)$ in this case.

Methods of data-based optimal bandwidth calculation have also high computational demands. Second order plug-in method [9], which involves estimating second derivative of density function from given sample, is of $O(nm^2)$ complexity. Also least squares cross-validation method (LSCV) [10,11], where selecting optimal bandwidth is based on minimizing objective function $g(h)$, has the same polynomial time complexity.

Few approximation techniques have been proposed to deal with the problem of time-consuming calculations of kernel density estimates. The first of them, proposed by Silverman [12], uses fast Fourier transform (FFT). The other one applies Fast Gauss Transform (FGT) as suggested by Elgammal [13].

An alternative to those methods could use parallel processing for obtaining density function estimates. The pioneer paper in this subject is due to Racine [14]. It proves the usability of parallel computations for kernel density estimation but covers in detail only the estimation itself. Parallelization is done by dividing set of points where estimator is to be evaluated. Each processor obtains the density function estimation for approximately $\frac{p}{c}$ points (where c denotes number of CPUs involved).

The aim of this paper is to verify how parallel processing can be applied for kernel estimation, bandwidth selection and adaptation. All presented algorithms have been implemented and tested in a multicomputer environment using *MPI (Message Passing Interface)* [16]. A possibility of parallelization at the sample level, by distributing the sample and calculating approximately $\frac{m}{c}$ sums in (1) separately on each of the c CPUs for every evaluated point x, is also discussed.

2 Parallelization Methods

Following subsections will briefly present routines for obtaining kernel density estimates using parallel processing. All algorithms will be included in the form of pseudo-code with group operations treated as collective ones.

In the presented code listings subsequent notation was used: *proc_rank* is current processor number (including 0 as a root/master processor), *proc_no* - overall number of processors involved c, *sample[k]* - k*th* sample element, *sample_length* - sample length m, *x_eval[k]* - k*th* evaluation point, *f[k]* - the estimator value for *x_eval[k]* and *ev_points* - the overall number of points p where estimator is to be evaluated.

2.1 Kernel Density Estimation

Parallelization of estimation process can be achieved either by dividing set of evaluation points or sample data. Both of suggested parallelization schemes were presented using code attached below:

Parallel KDE at evaluation level

```
Broadcast(sample);
shift:=proc_rank*ev_points/proc_no;
/* evaluation of KDE for x[k+shift] using all sample elements */
for k:=1 to ev_points/proc_no do
  f[k+shift]:=Compute_KDE(x[k+shift],sample,1,sample_length);
Gather_at_root(f);
return f;
```

Parallel KDE at sample level

```
Scatter(sample);
shift:=proc_rank*sample_length/proc_no + 1;
/* evaluation of KDE for x[k] using sample starting from element
sample[shift] to element indexed by shift+sample_length/proc_no */
for k:=1 to ev_points do
  f[k]:=Compute_KDE(x[k],sample,shift,shift+sample_length/proc_no);
Aggregate_at_root(f);
return f;
```

In the first case (presented already in [14]) whole sample should be distributed among processors taking part in calculations. In the end evaluated kernel estimator values should be gathered at the master machine. The alternative is to implement parallel model at the sample level - each CPU calculates all estimator values but considering only the part of a sample. Results are globally aggregated at the master machine. In this version of the algorithm there is no need to broadcast all sample points.

2.2 Bandwidth Selection Using Plug-In Method

Let us consider commonly used two-stage direct plug-in method of Sheather-Jones [7]. Proposed parallel algorithm for plug-in bandwidth selection with parallelization at the sample level is introduced below:

Parallel plug-in bandwidth selection

```
Broadcast(sample);
shift:=proc_rank*sample_length/proc_no + 1;
/* estimation of plug-in psi functional of order i using sample starting
from element sample[shift] of length sample_length/proc_no */
for i:=6 and 4 do
  psi[i]:=Compute_SJF(i,sample,shift,shift+sample_length/proc_no);
  Aggregate_at_all(psi[i]);
h=Select_Bandwidth_at_root();
return h;
```

2.3 Bandwidth Selection Using Least Squares Cross-Validation Method

The problem of minimizing score function *g(h)* can be approached using direct evaluation of the function in selected range with a required step or by applying

some optimization technique. Underlying evaluation of the score function can be easily parallelized at the sample level. Due to lack of space, only the algorithm of direct parallel minimization of $g(h)$ will be presented here. Experimental results were obtained using golden section rule [15].

Parallel LSCV bandwidth selection

```
Broadcast(sample);
shift:=proc_rank*sample_length/proc_no + 1;
g_min:=infinity, h_min:=0;
for h:=h_start to h_stop do
  /* calculation of g(h) using sample starting from
  element sample[shift] of length sample_length/proc_no */
  g:=Compute_G(h,sample,shift,shift+sample_length/proc_no);
  Aggregate_at_root(g);
  if g<g_min then g_min:=g, h_min:=h;
return h_min;
```

2.4   Adaptive Bandwidth

In order to reduce computational burden of bandwidth modifying coefficients calculation using Abramson method [8] parallel processing can be applied as presented below:

Parallel bandwidth adaptation

```
Broadcast(sample);
shift:=proc_rank*sample_length/proc_no;
/* first obtain unmodified estimates for sample points
taking into consideration all sample elements */
for k:=1 to sample_length/proc_no do
  f[k+shift]:=Compute_KDE(sample[k+shift],sample,1,sample_length);
Gather_at_all(f);
/* then calculate geometric mean of estimates using
sample_length/proc_no KDE values starting from f[1+shift] */
mean=Compute_Mean(f,1+shift,1+shift+sample_length/proc_no);
Product_at_all(mean);
/* obtain modifying coefficients */
for k:=1 to sample_length/proc_no do
  s[k+shift]:=(f[k+shift]/mean)^(-0.5);
Gather_at_all(s);
return s;
```

Modifying coefficients s_i can be easily incorporated into variable bandwidth parallel kernel density estimation (with $h_i = h \cdot s_i$) similarly as it was presented in Section 2.1.

3   Experimental Results

Reference implementation of proposed parallel algorithms was prepared to examine their efficiency. As a measure of parallelization performance following efficiency function was chosen:

$$E(c) = \frac{T(c)}{T(1)} \frac{1}{c} 100\% \, . \tag{2}$$

where: $T(c), T(1)$ are computation times for c CPUs and one CPU accordingly. Presented results were obtained for multiple execution of algorithms in Ethernet standard computer network of 6 Pentium®4 machines with MPICH-2 library used as a parallelization tool. The estimation was performed with radial normal kernel function for randomly generated one-dimensional samples. Some sample lengths correspond to those considered in [14], the others were chosen to create broader view on an average parallel estimation execution time (given in seconds). Due to space limitations only selected results were presented - full set can be obtained from author's web site (http://www.pk.edu.pl/~szymonl).

3.1 Parallel Kernel Density Estimation

First, the performance of two proposed parallelization schemes were tested for varying sample size and number of evaluation points. During the testing procedure $m = p$ was assumed (like in [14]). Obtained results (presented in Fig. 1) include, for reference, computation times for sequential ($c = 1$) version of the KDE.

It can be seen that results for small sample lengths are not encouraging, taking into consideration both calculation time and efficiency. The overhead, which include times of communication, synchronization and input/output operations, has a significant influence on effectiveness of multicomputer parallel system. Nevertheless, increasing problem size leads to speed-up which close to linear.

Parallelization at the evaluation level in most cases performs better than the scheme with distribution of sample elements. The time cost of global aggregation (using *MPI_Reduce*) in the multicomputer environment dominates the gain
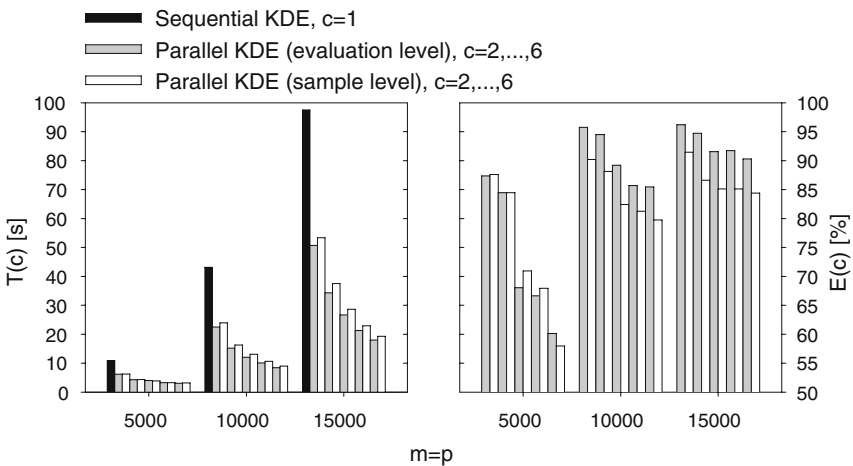
Fig. 1. Execution times and efficiency of parallel kernel density estimation methods

achieved by distributing smaller amount of data at the first phase of estimation. The proposed parallelization scheme can be applied successfully when $m \gg p$, though. The difference between performances of the presented methods is under these assumptions neglectable. For instance, if $m = 50000$, $p = 5000$ and $c = 3$ algorithm using parallelization at the sample level is only 0.3 s slower (which is a fraction of 107.8 s processing time for $c = 1$).

3.2   Parallel Bandwidth Selectors

Observing high computational complexity of data-based bandwidth selectors leads to preliminary conclusion, that parallel processing in the case of both plug-in and LSCV methods will give significant improvement in calculation time. Results of test performed for variable sample lengths presented in Fig. 2 confirm it. When ruling out cases where too many CPUs were assigned to a very small task, relatively high parallelization effectiveness can be also noticed. Advantage of using parallel processing is in case of least squares cross validation more considerable - it is a direct effect of substantial computational demands raised by this method.

3.3   Parallel Bandwidth Adaptation

Finally parallelized routine for bandwidth adaptation was under investigation. The test was conducted with $m = p$. Considered scheme of algorithm involved also parallelizing the density estimation itself at evaluation level. Results of the test are enclosed in Fig. 3.
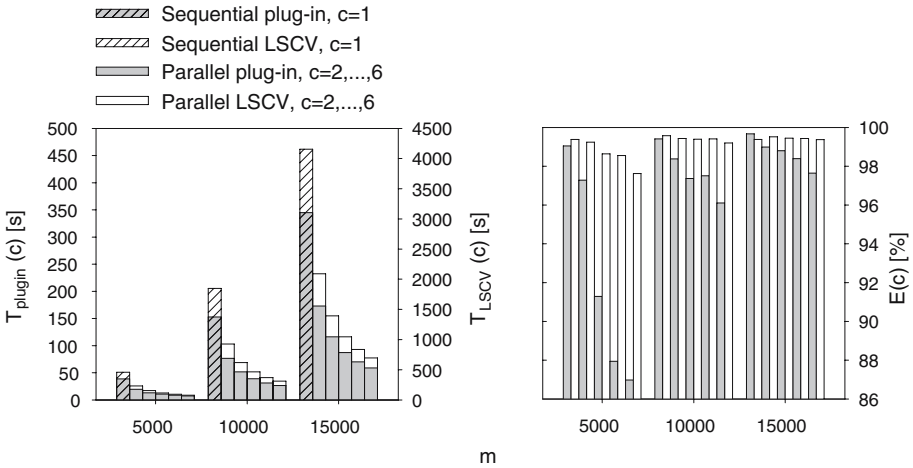
Fig. 2. Execution times and efficiency of parallel plug-in method and parallel least squares cross-validation
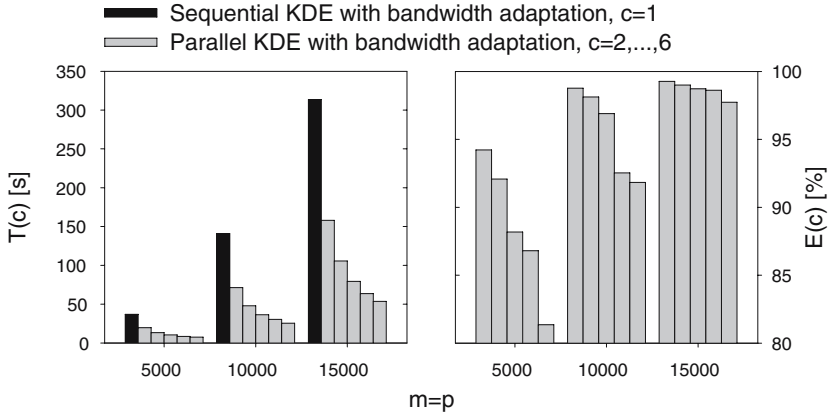
Fig. 3. Execution times and efficiency of parallel KDE with bandwidth adaptation

In contrast to parallel kernel estimation with fixed bandwidth, performing parallel bandwidth adaptation can be judged as highly effective, even when relatively small sample is under consideration. The obtained speed-up of computation, with increasing CPUs number, is in this case close to linear.

4   Conclusion

The article positively verifies the possibility of applying parallel algorithms for speeding up time-consuming process of kernel density estimation. Beneficial effects of parallelization, already proved for KDE [14] itself, were also confirmed for popular data dependent bandwidth selectors and bandwidth adaptation. Moreover, for fixed sample size, gain of using parallel calculation is in those cases more significant.

The option of using the alternative parallelization scheme for kernel density estimation - at the sample level - was also under consideration. Empirical studies proved that the proposed method is, in general case, not as effective as parallel evaluation of density estimates.

As in every parallel processing application it is important to note, that proper care has to be taken of granularity of calculation if one wishes to obtain effective use of engaged resources. Parallel bandwidth selectors and bandwidth adaptation involve substantial number of collective operations executed between calculation cycles so it would be also advisable to use load-balancing in order to eliminate overhead generated by MPI tasks synchronization routine (*MPI_Barrier*).

References

1. Rosenblatt, M.: Remarks on Some Nonparametric Estimates of a Density Function. Annals of Mathematical Statistics **27** (1956) 832–837
2. Parzen, E.: On Estimation of a Probability Density Function and Mode. Annals of Mathematical Statistics **33** (1962) 1065–1076
3. Mittal, A., Paragios, N.: Motion-Based Background Subtraction Using Adaptive Kernel Density Estimation. IEEE Computer Society Conference on Computer Vision and Pattern Recognition **2** (2004) 302–309
4. Cerrito, P.B., Barnes, G.R.: The Use of Kernel Density Estimators to Monitor Protocol Compliance. Proceedings of the Twenty-Fifth Annual SAS®Users Group International Conference **SUGI25** (2000) paper no. 273
5. Donthu N., Rust, R.T.: Estimating Geographic Customers Densities using Kernel Density Estimation. Marketing Science **8** (1989) 191–203
6. Silverman, B.W.: Density Estimation for Statistics and Data Analysis. Chapman and Hall, London (1986)
7. Wand, M.P., Jones, M.C.: Kernel Smoothing. Chapman and Hall, London (1995)
8. Abramson, I.: On Bandwidth Variation in Kernel Estimates - a Square Root Law. The Annals of Statistics **10** (1982) 1217-1223
9. Sheather, S.J., Jones, M.C.: A Reliable Data-Based Bandwidth Selection Method for Kernel Density Estimation. Journal of the Royal Statistical Society. Series B. Methodological **53/3** (1991) 683–690
10. Rudemo, M.: Empirical Choice of Histograms and Kernel Density Estimators. Scandinavian Journal of Statistics **9** (1982) 65-78
11. Bowman, A.W.: An Alternative Method of Cross-Validation for the Smoothing of Density Estimates. Biometrika **71** (1984) 353–360
12. Silverman, B.W.: Algorithm AS 176: Kernel Density Estimation Using the Fast Fourier Transform. Applied Statistics **31/1** (1982) 93–99
13. Elgammal, A., Duraiswami, R., Davis, L.S.: Efficient Kernel Density Estimation Using the Fast Gauss Transform with Applications to Color Modeling and Tracking. IEEE Transactions on Pattern Analysis and Machine Intelligence **25/11** (2003) 1499–1504
14. Racine, J.: Parallel distributed kernel estimation. Computational Statistics and Data Analysis **40/2** (2002) 293–302
15. Gill, P.E., Murray, W., Wright, M.H.: Practical Optimization. Academic Press, London (1981)
16. Snir, M., Otto, S., Huss-Lederman, S., Walker, D., Dongarra J.: MPI: The Complete Reference. The MIT Press, Cambridge (1996)

Quantization Error and Accuracy-Performance Tradeoffs for Embedded Data Mining Workloads

Ramanathan Narayanan, Berkin Özışıkyılmaz, Gokhan Memik,
Alok Choudhary, and Joseph Zambreno

Department of Electrical Engineering and Computer Science
Northwestern University
Evanston, IL 60208, USA
{ran310,boz283,memik,choudhar}@eecs.northwestern.edu

Abstract. Data mining is the process of automatically finding implicit, previously unknown and potentially useful information from large volumes of data. Embedded systems are increasingly used for sophisticated data mining algorithms to make intelligent decisions while storing and analyzing data. Since data mining applications are designed and implemented considering the resources available on a conventional computing platform, their performance degrades when executed on an embedded system. In this paper, we analyze the bottlenecks faced in implementing these algorithms in an embedded environment and explore their portability to the embedded systems domain. Particularly, we analyze the floating point computation in these applications and convert them into fixed point operations. Our results reveal that the execution time of five representative applications can be reduced by as much as 11.5× and 5.2× on average, without a significant impact on accuracy.

1 Introduction

Data mining algorithms have been successfully applied to predict trends in a variety of fields including marketing, biotechnology, multimedia, security, combinatorial chemistry, and remote sensing. As application-specific architectures become increasingly available, there is an urgent need to port data mining applications to embedded systems. The increased availability of embedded devices has led to a rapid increase in their usage in various fields. The level of intelligence demanded of these embedded systems require them to use complex and expensive data mining techniques. For example, a distributed traffic sensor system providing real-time information may consist of embedded devices with access to streaming data.

Data mining applications and algorithms are designed keeping in mind the ample computing power available on conventional systems. As a result, their performance on embedded systems is greatly hindered. In this paper, we study the amount of floating point calculations used by several data mining applications, and identify these as a major cause of poor performance of these algorithms on embedded environments. Further, we propose a solution to this problem by

replacing the floating point calculations with fixed point arithmetic. By doing so, we are sacrificing the high precision offered by floating point operations for the high implementation efficiency of fixed point computation. As data mining applications are used in critical sectors like healthcare and traffic sensors, it is imperative that we study the effects of our optimization techniques on the accuracy of these algorithms.

The remainder of this paper is organized as follows. In the following section, we present a brief overview of related work in this area. In Sect. 3, we present our methodology to convert a data mining application to use fixed point computations. A brief description of the data mining applications analyzed is provided in Sect. 4. The conversion procedure is described for each application in detail in Sect. 5, after which we provide the quantization and error analysis results. The paper is concluded in Sect. 6 with a look towards some planned future efforts.

2   Related Work

Our approach in this paper is similar to work done in the Digital Signal Processing [1,2] domain. In [2], the authors have used MATLAB to semi-automate conversion of floating point MATLAB programs into fixed point programs, to be mapped onto FPGA hardware. Currently our fixed point conversion is done manually. However, we support varying precisions and do not perform input scaling transformations. In [3], an implementation of sensory stream data mining using fixed point arithmetic has been described. The authors in [4] have used fixed point arithmetic with pre-scaling to obtain decent speedups for artificial neural networks used in natural language processing. Several data mining algorithms have been previously implemented on FPGAs [3,5,6]. In [5], the Apriori algorithm, which is nearly pure integer arithmetic, has been implemented on hardware. In [6], algorithmic transformations on K-Means clustering have been studied for reconfigurable logic.

3   Fixed Point Arithmetic

Fixed point representation uses a fixed number of digits to represent the integer and fractional parts of real numbers. We use the notation $Q.i.f$ to represent a fixed point variable of size $i + f$, with i digits used to represent the integer part and f digits used to represent the fractional part. The major stumbling blocks associated with fixed point arithmetic are *Overflow* and *Underflow*. Overflow occurs when a number is too large to be represented using the $Q.i.f$ format. The integer part of the fixed point number then wraps around and changes sign. Underflow, on the other hand, occurs when a number is too small to be represented using a fixed point notation, causing it to become zero.

3.1   Methodology

Our methodology for converting a data mining application using floating point arithmetic, to a fixed point application is described in Fig. 1. The first step in our
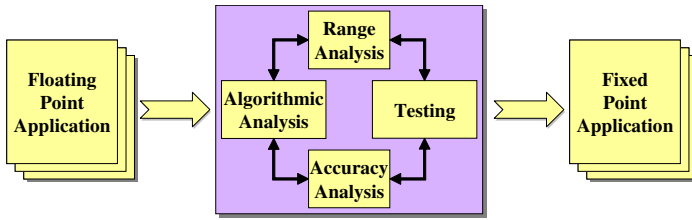
Fig. 1. Fixed Point Conversion Methodology

methodology is algorithmic analysis of the target application. In this step, we identify the functional blocks that are suitable for fixed point conversion. After a detailed algorithmic analysis and functional block identification, we apply a range analysis on the functional blocks. The purpose of range analysis is to determine the variables that may be susceptible to Overflow and Underflow errors. This step determines the various fixed point formats feasible and also identifies the various combinations of integer and fractional bits that are valid for the target application. In the accuracy analysis phase, we study the effects of differences between floating point operations and fixed point operations. We concentrate on the gradual loss of accuracy stemming from minor differences between fixed point and floating point operations. We may need to retain some of the critical components as floating point operations. In this phase, we may also have to reorder some of the calculations to optimize them with regard to fixed point calculations. This analysis procedure must be iterated several times until we obtain a fixed point representation that is *safe*, meaning that there are no critical errors. After the range and accuracy analysis are completed, we convert the data mining application to use fixed point operations.

4   Data Mining Applications

Data mining applications can be broadly classified into association rule mining, clustering, classification, sequence mining, similarity search, and text mining, among others. Each domain contains unique algorithmic features. In our study, we analyze applications belonging to four major domains: clustering, association rule mining, classification, and sequence mining. We have selected five applications from NU-MineBench, a data mining applications benchmark suite [7]. In our application selection, we have given priority to the applications that have the most floating point operations, since these are negatively affected while executing on embedded environments. Table 1 highlights the relative execution times on a conventional platform and an embedded system. The disparity in runtimes is due to the higher processor speed and dedicated hardware floating point unit available on the conventional (x86) platform (AMD Opteron, 2.4GHz), as compared to the embedded system (PowerPC). We also compute the fraction of floating point operations within the executed instructions [8], and surmise that there is significant scope for optimization by converting the

Table 1. Overview of the MineBench applications analyzed

Application	Inst Count (billions)	Floating Point Ops	Exec Time [x86] (s)	Exec Time [PPC] (s)
K-Means	53.77	19.87%	24.519	11145.89
Fuzzy	447.03	4.64%	443.7	57600.45
Utility	15.00	10.03%	9.506	482.21
ScalParC	5.47	9.61%	8.134	1553.82
PLSA	401.44	2.57%	136.67	2859.25

floating point operations to fixed point arithmetic. Detailed information about the K-Means, Fuzzy K-Means, Utility, ScalParC and PLSA applications and their corresponding datasets can be found in [7].

5   Conversion and Results

5.1   Experimental Setup

We performed our experiments on the Xilinx ML310, which is a Virtex-II Pro-based embedded development platform. It includes an XC2VP30 FPGA with two embedded PowerPC processors, DDR memory, PCI slots, ethernet, and standard I/O on an ATX board. We have 16KB separate, configurable, two-way set-associative instruction and data cache units. The operating frequency is 100MHz.

5.2   K-Means

Algorithmic analysis of `K-Means` reveals that a major fraction of floating point operations are due to Euclidean distance calculation. We performed a range analysis of the floating point operations, and determined the maximum and minimum values produced during computation. It is seen that at least 13 integer bits are required to avoid overflow, which generates negative values for distance and causes a critical error. Also, the input data requires precision of up to 10^{-3}, hence the binary representation of the number in fixed point notation must contain at least 12 fractional digits for accurate representation of the input data. Keeping this in mind, we find that the number of integer bits required by the fixed point representation for `K-Means` lies between 12 and 20.

The timing results for various fixed point implementation of `K-Means` are shown in Table 2. The results indicate that the fixed point versions run 9.1× to 11.6× faster than the floating point enabled version. The metric we use for accuracy analysis of `K-Means` is the 'membership' of each object to its cluster, as seen in Table 4. Here we study the percentage of points that change their cluster membership while varying the computation formats. The values obtained are well within reasonable error bounds for the `Q.16.16` and `Q.20.12` formats. The loss of precision is responsible for the larger error percentages in the `Q.24.8` case.

Table 2. Timing and speedup for K-Means

Type	Total
Floating point	11145.89s
Q16.16	9.06x
Q20.12	8.80x
Q24.8	11.59x

Table 3. Timing and speedup for Fuzzy

Type	Total
Floating point	3404.497s
Q12.20	1.46x
Q16.16	1.94x
Q20.12	3.19x
Q24.8	8.86x

Table 4. Relative error for K-Means

Num Clusters	Membership Error		
	Q16.16	Q20.12	Q24.8
5	1.52%	1.83%	2.44%
7	1.53%	1.58%	2.43%
9	1.55%	1.55%	2.09%
11	1.54%	1.62%	18.71%
13	1.61%	1.72%	4.65%

Table 5. Relative error for Fuzzy

Num Clusters	Membership			
	Q12.20	Q16.16	Q20.12	Q24.8
5	35.57%	1.69%	4.23%	4.85%
7	20.50%	0.35%	0.97%	1.87%
9	8.30%	0.17%	0.49%	1.18%
11	0.00%	0.12%	0.52%	3.33%
13	0.00%	0.08%	2.05%	2.89%

Considering various factors, it is seen that the Q.16.16 fixed point representation offers the best tradeoff between performance and accuracy. We also analyzed the difference in the cluster centers generated between the fixed point and floating point versions of the K-Means application. We notice that as the number of fractional bits increases from 8 to 16, the error in cluster centers decreases from 8% to 0.9%, for $k = 13$. In summary, K-Means can be executed using several fixed point representation formats to achieve significant speedups with minimal loss of accuracy.

5.3   Fuzzy K-Means

The major floating point computation intensive part in Fuzzy K-Means is the Euclidean distance calculation. Another important computation is that of the 'fuzzy membership' value and 'fuzzy validity' criterion. The Euclidean distance kernel discussed above, generates values that require 12 or more integer bits to avoid Overflow . The calculation of the 'fuzzy membership' value requires a fractional exponentiation computation, which is expensive to implement using fixed point computation. Hence, we make a design choice to compute this value using floating point variables. The choice of fractional bits for Fuzzy K-Means is slightly more flexible than the K-Means algorithm. Therefore the number of fractional bits needs only to be more than 10 in order to achieve reasonable results.

The timing results for Fuzzy K-Means, shown in Table 3, indicate significant speedups for the fixed point computation enabled versions. The speedup in execution time peaks at 8.86x for the $Q.24.8$ fixed point representation. To evaluate accuracy of the results, we analyze the percentage variation in the

Table 6. Timing and speedup for `Utility`

Support Value	Floating point	Q23.9	Q24.8
0.002	2863.02033s	1.27x	3.38x
0.004	1003.537s	1.18x	1.21x
0.008	571.711s	1.25x	1.32x
0.01	482.2119s	1.27x	1.59x
0.02	280.631s	1.38x	1.37x
0.03	367.3135s	1.37x	1.38x

Table 7. Average Relative Error for the total utility values of the points for various support values

Type/support	0.002	0.004	0.008	0.01	0.02	0.03
Q23.9	0.00147%	0.01100%	0.00314%	0.00314%	0%	N/A
Q24.8	0.02831%	0.02715%	0.00772%	0.00772%	1%	N/A

fuzzy-membership value. This value indicates the degree of membership of each object to its cluster. This value is shown in Table 5. We also analyze the differences in the cluster centers produced by the fixed point formats, and notice between 63% (for `Q.24.8`) and 0.73% (for `Q.12.20`) variation. Since the cluster centers are a derived attribute, we may compute them using higher precision floating point values. Therefore it can be seen that the optimum configuration for Fuzzy K-Means is the `Q.16.16` representation, which achieves significant speedup, with minimal loss of accuracy.

5.4   Utility Mining

Algorithmic analysis of `Utility mining` yields the calculation of 'Utility' value as the major floating point computation kernel. The range of Utility values generated using the dataset indicated that at least 23 integer bits would be required in the fixed point representation. Prevention of overflow is critical to the application and hence we are forced to choose fewer than 9 fractional bits. Fortunately, we have observed that other modules require accuracy of up to 10^{-2}, thus necessitating at least 8 fractional digits for successful termination of the algorithm. Consequently, we decided to use the `Q.23.9` or `Q.24.8` fixed point representation.

The speedup values for `Utility mining` shown in Table 6 reveal that a speed up of up to $3.38\times$ is possible using the valid fixed point representations determined in Sect. 5. To measure the accuracy of the results, we compared the utility itemsets generated by the algorithm, for various values of minimum utility support. The results show that for lower values of minimum utility support, the `Q.24.8` format produces only 10 of 25 utility itemsets, whereas the `Q.23.9` fixed point format produces all the utility itemsets generated by the floating point version. However, as the minimum utility support increases, there is 100% corre-

Table 8. Timing and speedup for ScalParC

Type	I/O	Comp.	Total
Floating	74.70s	1458.82s	1553.52s
Q4.28	0.98x	1.27x	1.25x
Q8.24	0.98x	1.27x	1.25x
Q12.20	0.99x	1.26x	1.24x

Table 9. Timing and speedup for PLSA

Type	Total
Floating point	2859.25s
Q2.30	1.003x
Q1.31	1.014x
Q0.32	1.003x

spondence in the utility itemsets generated. Another measure of accuracy is the 'total utility' value of each utility itemset (Table 7). Percentage variation over the total utility value over the valid fixed point representation formats shows there there is insignificant error due to fixed point conversion.

5.5   ScalParC

ScalParC has a large percentage of floating point operations (9.61%), thus hindering performance on embedded systems. All the expensive floating point operations are done in the 'Calculate Gini' module, which is the most compute intensive module of ScalParC. By using a fixed point variable to store the 'Gini' value and simple reordering of the computations, we were able to avoid significant floating point data type casting overheards.

The timing results for various fixed point implementation of ScalParC are shown in Table 8. The fixed point operations achieves a execution time speedup of 1.25x and 1.24x for the Q12.20 and Q4.28 configurations, respectively. We have also compared the accuracy of various implementations by examining the number of nodes in the generated decision tree at each level and discovered that with 20 fractional bits, one out of 697 splits was not performed. Our results reveal that the accuracy increases with increasing precision, however, the output changes for the ScalParC are in general negligible.

5.6   PLSA

We also analyzed and converted the PLSA application, which has a relatively low percentage of floating point operations. The main floating point operation lies in the area calculation module. Because of the large values of area, we can have only 0-2 fractional bits. The algorithm has been modified so that the implementation does not need any fractional bits, and a multiplication with 0.1 has been replaced by division by 10.

The timing results for various fixed point implementations of PLSA are shown in Table 9. In general, the performance improvement of the fixed point conversion is small. Higher speed-ups may be achieved when using larger data-sets, because there will be a higher fraction of floation point operations. To analyze the accuracy of the converted application, two metrics have been considered. The first one is the sequence alignments. The alignments are exactly the same in all the runs, which shows that the application has executed correctly. Another

metric is the total area of the blocks solved in the dynamic programming approach. Our analysis has shown that the difference between these values is also negligible.

6   Conclusions

In this paper, we have described a method for implementation of data mining algorithms on embedded systems. Data mining algorithms are designed and implemented for conventional computing systems, and show poor performance while executing on an embedded system. We applied our methodology to several representative data mining applications and have shown that significant speedups can be achieved. We also quantized the error in each case and determined the optimum configurations for fixed point implementation. Particularly, with our fixed point conversion methodology in 4 out of the 5 applications, we achieve significant speedups, as much as 11.5x and 5.2x on average, with minimal loss of accuracy. As embedded data mining assumes importance in various key fields, our methodology will serve as a starting step towards efficient implementations.

References

1. Menard, D., Chillet, D., Charot, F., Sentieys, O.: Automatic floating-point to fixed-point conversion for DSP code generation. In: Proceedings of International Conference on Compilers, Architecture and Synthesis for Embedded Systems (CASES). (October 2002)
2. Roy, S., Banerjee, P.: An algorithm for trading off quantization error with hardware resources for MATLAB-based FPGA design. IEEE Transactions on Computers **54**(7) (July 2005) 886–896
3. Cai, Y., Hu, Y.X.: Sensory steam data mining on chip. In: Second NASA Data Mining Workshop: Issues and Applications in Earth Science. (May 2006)
4. Ferrer, D., Gonzalez, R., Fleitas, R., Acle, J.P., Canetti, R.: NeuroFPGA - implementing artificial neural networks on programmable logic devices. In: Proceedings of Design, Automation and Test in Europe (DATE). (February 2004)
5. Baker, Z.K., Prasanna, V.P.: Efficient parallel data mining with the Apriori algorithm on FPGAs. In: Proceedings of IEEE Symposium on Field-Programmable Custom Computing Machines (FCCM). (April 2005)
6. Estlick, M., Leeser, M., Theiler, J., Szymanski, J.J.: Algorithmic transformations in the implementation of k-means clustering on reconfigurable hardware. In: Proceedings of the International Symposium on Field Programmable Gate Arrays (FPGA). (February 2001)
7. Narayanan, R., Ozisikyilmaz, B., Zambreno, J., Memik, G., Choudhary, A.: MineBench: A benchmark suite for data mining workloads. In: Proceedings of the International Symposium on Workload Characterization (IISWC). (October 2006)
8. Zambreno, J., Ozisikyilmaz, B., Pisharath, J., Memik, G., Choudhary, A.: Performance characterization of data mining applications using MineBench. In: Proceedings of the Workshop on Computer Architecture Evaluation using Commercial Workloads (CAECW). (February 2006)

Adaptive Mining the Approximate Skyline over Data Stream

Liang Su, Peng Zou, and Yan Jia

School of Computer Science National University of Defense Technology
Changsha 410073, China
suliangnudt@gmail.com, zpeng@nudt.edu.cn, jiayanjy@vip.sina.com

Abstract. Skyline queries, which return the objects that are better than or equal in all dimensions and better in at least one dimension, are useful in many decision making and monitor applications. With the number of dimensions increasing and continuous large volume data arriving, mining the approximate skylines over data stream under control of losing quality is a more meaningful problem. In this paper, firstly, we propose a novel concept, called *approximate skyline*. Then, an algorithm is developed which prunes the skyline objects within the acceptable difference and adopts correlation coefficient to adjust adaptively approximate query quality. Furthermore, our experiments show that the proposed methods are both efficient and effective.

Keywords: Approximate skyline, adaptive algorithm, data stream, data mining.

1 Introduction

For two objects $X=(x_1, x_2,...,x_d)$ and $Y=(y_1, y_2,...,y_d)$ in the d-dimensional space, X *dominates* Y if $x_i \leq y_i$ for $1 \leq i \leq d$. Skyline computing aims to find all objects that are not been dominated by other objects and roots in many decision making and monitor applications. B¨orzs¨onyi et al. [1] proposed first two algorithms for the skyline computation: the BNL (block nested loop) and DC (divide and conquer) algorithm. Subsequently, skyline problem and its variants [2,3,4,5] have been extensively studied, and a lot of algorithms have been developed. BBS [2] compute the skyline using nearest neighbor search. However, in [7], Bentley et al. proved that the average number of skyline objects is $O((lnN)^{d-1})$ (N is the size of the original objects) which is the cardinality bound most often cited and employed. In paper [3], Xuemin Lin et al. consider the problem of efficiently computing the skyline against the most recent N elements in a data stream, they had realized the algorism scalability and proposed approximate skyline problem. None of the algorithms referenced above was originally designed to support approximate skyline computation over data stream. These are the motivations of our research in the paper. To the best of our knowledge, there is no similar work existing in the literature in the context of adaptive approximate skyline computation over data stream.

The rest of the paper is organized as follows. Sections 2 provide our techniques for processing approximate skyline problem and algorithm. Results of comprehensive experimental studies are discussed in section 3. Section 4 concludes the paper.

2   Approximate Skyline Problem and Algorithms

To eliminate the number of skyline set and improve the manageability, intuitively, first we depict accurately how close the degree of two skyline objects is. We are naturedly aware of the geometry distance. Then we use an acceptable difference distance to prune some neighbor objects, and find the approximate skyline set. Behind of the paper we only use the Euclidian distance as the *dist* function.

Definition 1. (Approximate Skyline Set) Let Ω be the set of d-dimensional objects, and $\Omega_{skyline}$ be the skyline set on Ω. The acceptable difference distance is ε and obviously satisfies $\varepsilon \geq 0$. $\Omega_{Askyline}$ reprsents the approximate skyline set that satisfies:

1. $\forall X_i, X_j \in \Omega_{ASkyline}, X_i \neq X_j$, then $dist(X_i, X_j) \geq 2\varepsilon$

2. $\forall X_i \in \Omega_{Skyline}$, then $\exists X_j \in \Omega_{ASkyline}$, s.t. $dist(X_i, X_j) \leq \varepsilon$

Definition 2. (Strongly Dominating Relationship) An object $X_i \in \Omega$ strongly dominates another object $X_j \in \Omega$, noted as $X_i \rhd X_j$, if $X_i + \varepsilon \succ X_j$ ($X_i \succ X_j$ means X_i dominates X_j). That is to say: $\forall 1 \leq k \leq d, x_i^k + \varepsilon \leq x_j^k$, and $\exists 1 \leq t \leq d$, $x_i^t + \varepsilon < x_j^t$, reversely, X_j is a strongly dominated object by X_i.

Definition 3. (Correlation Coefficient) Given n d-dimensional objects, which $X_i = (x_i^1,...,x_i^d)$, $1 \leq i \leq n$, set matrix $A = (X_1,...,X_n)^T$ and $Y_j = (x_1^1,...,x_n^1)^T$,

then $A = \begin{pmatrix} x_1^1 & \cdots & x_1^d \\ \vdots & \ddots & \vdots \\ x_n^1 & \cdots & x_n^d \end{pmatrix} = (Y_1,...,Y_d)$, and $\rho(Y_i, Y_j) = \dfrac{E((Y_i - EY_i)(Y_j - EY_j))}{\sqrt{DY_i} \bullet \sqrt{DY_j}} = \dfrac{E(Y_i Y_j) - EY_i EY_j}{\sqrt{DY_i} \bullet \sqrt{DY_j}}$

is the correlation coefficient; $EY_i = \dfrac{1}{n} \sum_{k=1}^{n} x_k^i$ is the expectation of vector Y_i;

$DY_i = E(Y_i - EY_i)^2 = EY_i^2 - (EY_i)^2$ is the variance of vector Y_i. The correlation coefficient is between -1 and +1. We construct a translation function which is $\Phi(\rho) = \dfrac{a+b}{2} - \rho \dfrac{b-a}{2}$, $1 \leq a \leq b$ and choose $\varepsilon\Phi(\rho)$ as the bound of difference distance to adaptively mining the approximate skyline in data stream.

Theorem 1. Given a dataset $\Omega_{Skyline}$, if $X_i, X_j \in \Omega_{Skyline}$ and $dist(X_i, X_j) \leq \varepsilon$, then $\sum_{k=1}^{d} \left| x_i^k - x_j^k \right| \leq \varepsilon\sqrt{d}$.

2.1   Extended Micro-cluster Feature Tree Based Approximate Skyline Algorithm

To save the memory and run time, we partition the sliding window data into extended micro-cluster feature tree based on CF-tree [6] which only save the approximate

skyline set and the information of their close neighbors(two or more micro-clusters can build a larger one). The pseudo code of *EMCFTA* algorithm is showed below.

Definition 4. (Extended Micro-Cluster Feature Tree, EMCF-Tree) A extended micro-cluster feature tree for a set of *d*-dimensional objects $X_1, X_2, \ldots, X_n$ ($X_i = (x_i^1, \ldots, x_i^d)$), is defined as a $(3d+3+L(H_{skyline})+L(H_{dominated}))$-tuple ($\overline{ASF1}$, $\overline{ASF2}$, $\overline{ASF3}$, $K(X_{centriod})$, $X_{centriod}$, *Parent*, $H_{skyline}$, $H_{dominated}$). The definition of each of these entries is as follows, Figure 2 is the whole data structure:

- The *p*-th entry of $\overline{ASF1}$ is equal to $\sum_{j=1}^{n} x_j^p$;The *p*-th entry of $\overline{ASF2}$ is equal to $\sum_{j=1}^{n} (x_j^p)^2$;

- The *p*-th entry of $\overline{ASF3}$ is equal to $\min_{j=1}^{n}(x_j^p)$;$K(X_{centriod})$ is the ordinal of $X_{centriod}$;

- $X_{centriod}$ is belong to $\Omega_{ASkyline}$, which represents the centroid of its micro-cluster;
- *Parent* is pointer to its parent node, which is to trace back to modify its ancestors;
- $H_{skyline}$ is a heap to save the skyline objects within its micro-cluster; $H_{dominated}$ is a heap to save the dominated objects by $X_{centriod}$; *n* is the length of sliding window.
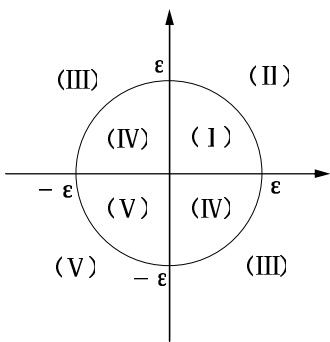
Fig. 1. Tree Micro-Cluster regions   **Fig. 2.** Extended Micro-Cluster Feather Tree
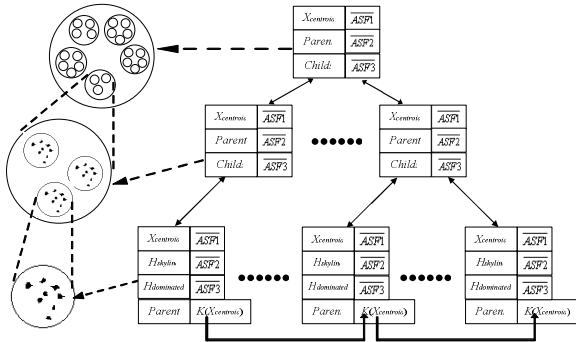
---

Algorithm *EMCFTA*(ε , Ω)

/*ε is the approximate skyline distance; input the original data objects in Ω; Output is the approximate skyline set $\Omega_{ASkyline}$. The X_{new} represents a new object from the data stream.*/

1   find the closest micro-cluster from the EMCF-Tree, that is MC_d which also is the leaf node;
2   if $X_{new} \succ X_{centriod}$, then X_{new} is located in region(Ⅴ) Fig 1, so $X_{centriod} := X_{new}$;
3   else if $X_{centriod} \succ X_{new}$
4   begin
5   if $K(X_{new})\text{-}K(X_{centriod}) \leq n\text{-}K(X_{centriod})\ mod\ n$, then no action;
6   else X_{new} is located in region(Ⅰ) Fig 1, so add X_{new} to $H_{dominated;}$
7   end;
8   else if dist(X_{new} , $X_{centriod}$) $\leq \varepsilon$, then X_{new} is located in region(Ⅳ) Fig 1, and add X_{new} to $H_{skyline;}$
10   else X_{new} is located in region (Ⅲ) Fig 1, create a new micro-cluster leaf node to MC_d's parent, and X_{new} is the centroid object.

3   Experiments

We use the three most popular synthetic benchmark data, *correlated*, *independent*, and *anti-correlated* [1,2,3,4,5] and implement them in C++. Experiments were performed on an Intel Pentium 4, CPU 2 GHZ, and RAM 512 MB, with Windows XP. All generated data value is between 0 and 1, the difference distance$\varepsilon \in [0,1]$ and dimension *d* is from 2 to 10.

Firstly, we compare $\Omega_{ASkyline}$ with $\Omega_{Skyline}$ in size at three data distributions. We observe that the result set produced by *EMCFTA* algorithm is between 30% and 55% of the basic skyline set with *d*=5 andε=0.1. Secondly, we would examine the quality of approximate skyline set. Because the number of basic skyline objects in the correlation distribution is fewer than other two distributions sharply, we only use the anti-correlation and independent distributions as next experiments. To measure the quality of approximate skyline set, We use the average distance in$\Omega_{Skyline}$ and$\Omega_{ASkyline}$ which is the average distance among the arbitrary two objects. These two formulas are as follows:

$$AvgDist_{Skyline} = \sum_{i=1}^{|\Omega_{Skyline}|} (\sum_{j=2 \wedge j \neq i}^{|\Omega_{Skyline}|} dist(X_i, X_j)) \Big/ (|\Omega_{Skyline}| \bullet (|\Omega_{Skyline}| - 1) \big/ 2) \qquad (1)$$

$$AvgDist_{ASkyline} = \sum_{i=1}^{|\Omega_{ASkyline}|} (\sum_{j=2 \wedge j \neq i}^{|\Omega_{ASkyline}|} dist(X_i, X_j)) \Big/ (|\Omega_{ASkyline}| \bullet (|\Omega_{ASkyline}| - 1) \big/ 2) \quad (2)$$

The average distance ratio (equals: 100*$AvgDist_{Skyline}$/ $AvgDist_{ASkyline}$) is between 90 and 99, the skyline objects have been reduced to almost 45% of basic skyline objects. So our algorithm is efficient which are meaningful for data stream mining.

4   Conclusions and Future Work

In this paper, we propose a novel concept and an efficient algorithm which can prune adaptively the skyline objects. In future, we plan to develop a parallel and distributed algorithm to meet more scalable and changeable data stream environment.

References

1. Stephan B¨orzs¨onyi, D.K., Konrad Stocker. The Skyline Operator. in ICDE (2001).
2. Dimitris Papadias, Y.T., Greg Fu, Bernhard Seeger. An Optimal and Progressive Algorithm for Skyline Queries. in SIGMOD (2003).
3. Xuemin Lin, Y.Y., Wei Wang, Hongjun Lu. Stabbing the Sky: Efficient Skyline Computation over Sliding Windows. in ICDE (2005).
4. Chee-Yong Chan, H.V.J.,et al. On High Dimensional Skylines. in EDBT (2006).
5. Y. Tao,et al. SUBSKY: Efficient Computation of Skylines in Subspaces. in ICDE (2006).
6. Tian Zhang, R.R., Miron Livny. BIRCH: An Efficient Data Clustering Method for Very Large Database. in *SIGMOD* (1996).
7. Bentley, J.L., Kung, H. T., Schkolnick, M., Thompson, C. D. On The Average Number of Maxima in a Set of Vectors and Applications. *JACM* (1978).

Generating Value from Textual Discovery

Peter Jackson

Chief Scientist, Thomson Corporation, 610 Opperman Drive, Eagan, MN 55123, USA
`peter.jackson@Thomson.com`

Abstract. Much of the information associated with legal, financial, medical and educational domains is stored in electronic document repositories and retrievable only by full text search. The ability of publishers to enhance such documents through traditional editorial processes struggles to keep pace with the volume and variety of textual data currently available in proprietary collections and on the Web. Fortunately, text mining tools that support the automatic classification, summarization, and linking of documents can be developed and deployed cost effectively. The outcome is a more flexible and dynamic approach to meta-data generation that does a better job of supporting the searching and browsing behaviors of information consumers. This paper describes the application of text and data mining techniques to legal information in a manner that enables powerful report generation and document recommendation services.

Keywords: Text Mining, Information Retrieval.

1 Introduction

Legal information is a primary example of a domain where language occupies a position of peculiar importance. Whether one thinks of the actual words of a statute, the exact phrasing of a judicial opinion, or the carefully constructed clauses of a contract, the linguistic details are extremely important, and constitute the true data of the document. Legal publishers such as Thomson West have traditionally been very scrupulous in the analysis, classification and annotation of documents, using highly qualified editors to read, sort and summarize them using a strict methodology.

As data volumes and document types proliferate, with everything from briefs to blogs being added to the mix, it is clear that the same care cannot be lavished upon the full range of information sources in a cost effective manner. Arguably, it ought to be possible for automation to aggregate, annotate and deliver documents of interest to users from myriad sources at a reasonable price. Furthermore, these processes should be able to support information services in addition to search, such as report generation and document recommendation.

There seem to two non-mutually exclusive views of what text mining is. To most writers, it is either (1) discovering novel patterns from text data, as data mining does for databases, or (2) a preliminary step to data mining, in which you first have to extract the relevant data from text sources. Here I propose a third view, namely that text mining technology can be used to create a 'metaverse' (a meta-data universe) that helps users perform their own acts of discovery and facilitates the implementation of discovery programs.

In support of this thesis, I describe two different applications of text mining technology that support very different information offerings, but draw upon a common set of tools that has been assembled at Thomson. The first is a service that generates reports concerning the litigation profile of a company; the second is a document recommendation system that enhances search results.

2 Mining People Data from the Law

In the past, legal publishers have concentrated upon the systematization of legal concepts and the documents that discuss them. Terms such as 'negligence', 'liability', and 'nuisance' have relatively precise legal meanings that are nonetheless subject to continuous exegesis and interpretation. Giving researchers access to the latest rulings and other writings that adhere to these concepts is one of the services that any quality publisher should provide.

Publishers have been less concerned with mining what I shall call 'the people side of the law': who has sued whom, who has represented whom, or who works for which law firm. Yet this orthogonal stream of legal data is of great utility in certain situations. Information about judges, attorneys and expert witnesses can be extremely helpful to litigators who are trying to formulate a winning strategy for their clients.

2.1 PeopleCite and Profiler

In 2000, we began text mining in a small way with a project called PeopleCite [2]. The idea was a very simple one, namely to consider the occurrence of a judge or an attorney's name in case law as a citation to that person's record in a legal gazetteer. Entity extraction programs identified such occurrences in the front matter of cases, and then Bayesian entity resolution programs matched those occurrences to the right database records and created links.

A few years later, we went further, by mining Jury Verdicts and Settlements to create the first comprehensive database of expert witnesses, called Profiler-EW. Expert witnesses play an important role in the resolution of many legal conflicts, but information about who testified at what trials and in which capacities exists only in textual form. To address this problem, we created a comprehensive expert witness database of 110,000 records using text mining techniques [3].

In our initial implementation of Profiler-EW, we extracted 290,000 references to expert witnesses from 300,000 trial case documents, using a part-of-speech tagger and a cascaded set of finite state transducers, which parsed expert name, geographical location, and field of expertise from the text. After the extraction of the reference records, we merged them together to create a file in which each particular expert is listed only once. Finally, we linked the profiles to professional license records, *medline* articles, and newspaper articles, as outlined in [4].

2.2 Firm360: Looking at Litigation History

Understanding the relationships that hold among cases, companies, and law firms can be important to the business of practicing law. For example, a legal counsel to some corporation might want to know which law firm they should engage to handle a difficult

intellectual property lawsuit, or a law firm might want to know what their chances are of engaging a large corporation as a new client. In such situations, it would be very useful to have access to a litigation history report that chronicles what cases a company has been involved in, either as a plaintiff or a defendant, which law firms have represented the company, and what kinds of cases they typically handle. Similarly, it would be good to know which attorney typically acts for a law firm on, say, intellectual property cases, and how many such cases this person has been involved in.

Firm360 is a product that can answer these questions, based on a litigation history database that covers over 50,000 companies. This database was created by (1) mining entities and their relationships out of case law documents, (2) resolving these entities by matching them against records for people and companies in various authority files, and (3) classifying cases to legal practice areas. Entity extraction was performed using cascaded finite automata and n-gram language models, entity resolution relied upon support vector machines and Bayesian record linkage, and cases were classified using a proprietary system called CaRE, which we describe later.

The text mining programs had access to a number of data resources in making their judgments. For example, attorney names were matched against the *West Legal Directory*, a database of some 500,000 law firms and solo practitioners. Features for matching included the Levenstein distance and cosine similarity between law firm names as well as information about geographic location, also mined from case law documents. A sister company, Thomson Financial, provided us with an authority file containing over 250,000 public, large private and pre-IPO companies. To ensure high precision with respect to company identifications, we applied a very high threshold to the *tf-idf* match score, and reviewed near misses by hand. To boost recall, we manually reviewed names that occurred more than 10 times in cases but did not match our company authority files, even though their n-gram language model scores indicated that they might be companies. Items that were judged to be actual companies were then added to the authority file.

Cases were classified to a cut-down version of West's *Key Number System*, called *KeySearch*, which contains roughly 10,000 legal topics. For the purposes of Firm360, we want a comparatively gross classification that tells us what practice area or sub-area a proceeding belongs to, so that we can identify both the nature of the suit and the specialism of the participating attorney. Our document categorization system, CaRE, is a highly scalable, multi-algorithm ensemble of programs that has performed well on taxonomies of up to 200,000 nodes (see Section 3).

The first release of Firm360 mined entities and relationships from 3 million case law opinions and 40 million dockets published between 1990 and 2006. 579,000 attorneys and 9,700 judges were linked to West Legal Directory, while 153,000 law firms and 58,000 companies were linked to authority files. Precision and recall on the identification of relationships ranged from 88% to 97%. Automatic text mining software was the only practical way to extract this amount of data cost effectively with a high degree of accuracy.

2.3 The Challenge of Event Extraction

Mining people data from case law is a non-trivial exercise, but this kind of entity extraction does not exhaust the potential of text mining in the legal domain. For

example, Jackson et al. [7] describe a multi-year research project, called History Assistant, on the extraction of rulings from court opinions and the determination of which prior cases are impacted by a new ruling. This is an extremely challenging task, but an essential one for any publisher, and one that would greatly benefit from some degree of automation.

History Assistant combined partial parsing techniques with domain knowledge and discourse analysis to extract information from the free text of court opinions. The same parser was also used to extract references to courts, dates, parties, and dockets for the purposes of determining the prior case or cases impacted by the opinion. This information was then used to generate a query that would return prior case candidates from a database of 7 million past cases.

Our editors insisted on near perfect recall, but were willing to tolerate precision in the 50% range. Our event extraction modules failed to achieve this recall goal, and at the time it seemed unlikely that further research would yield significant returns. (On the other hand, the prior case retrieval module achieved its stated goals and was been deemed worthy of further development.) It is worth asking why this problem is so hard, and what it would take to truly solve it.

A major limitation of current extraction technology is the fact that the information sought must be explicitly stated in the text. It cannot, for the most part, be merely implied by the text. This lack of an inferential capability can pose significant problems when extracting from real documents, where the writer expects the reader to be able to draw simple conclusions.

For example, some bankruptcy cases posed special problems for History Assistant. A debtor moves to convert from Chapter 7 to Chapter 13, and a creditor files a complaint to oppose this. The judge decides the case by 'finding for the plaintiff.' The program would have to perform a number of steps of reasoning to identify the outcome correctly as 'conversion denied', i.e., that the plaintiff is the creditor, that the creditor is asking for a denial of what the defendant (the debtor) is asking for, and that the Judge grants the denial.

This kind of inferential capability is still beyond the state of the art in text mining, and seems to require domain-specific representations of knowledge.

3   Content-Based Document Recommendation

In this section, we look at a different application, one that might not be thought of as involving text mining in the first instance. The primary technology employed in our document recommendation system involves text categorization, which is something that has been identified as not being text mining, *per se* [5]. However, we will argue that the use of categorization with other meta-data generation techniques does constitute an instance of what can be accomplished in this area.

The task of recommending documents to knowledge workers differs from the task of recommending products to consumers. Collaborative approaches [6], as applied to books, videos and the like, attempt to communicate patterns of shared taste or interest among the buying habits of individual shoppers. There are well-known problems with these approaches, e.g., when consumers temporarily shop for their children, but their effectiveness has been established in practice at many e-commerce sites.

Consumers of information typically rely upon more conventional classification schemes as an adjunct to search, such as browsing through tree-like structures, such as taxonomies and tables of contents, to narrow the application of queries. However, the problems with these approaches are also well known, primarily the inflexibility of purely taxonomical organizations of knowledge. Do the inheritance rights of children born out of wedlock belong under 'Wills' or under 'Infant Law', and how is the user supposed to know where to look in the tree?

Our approach to document recommendation leverages both user data and document meta-data. Legal researchers are typically confronted with an array of different sources: multiple document collections that are organized with respect to both document type and jurisdiction. When a user is searching a selected database, there are often relevant documents in other databases of which he or she may not be aware. Our document recommendation system, ResultsPlus, seeks to overcome this problem by matching the user's query, and other contextual information, against the indices and meta-data associated with such documents. Recommendations are then ranked by both relevance and popularity metrics based on user behavior.

3.1 Document Categorization for Content-Based Recommendations

The original version of ResultsPlus, released in 2002, used a blend of information retrieval and text categorization technologies to recommend secondary law materials to attorneys engaged in primary law research. Secondary materials include articles from legal encyclopedia, legal research papers, and law reviews. Primary law sources include cases, statutes, and regulations.

Research has long since demonstrated that superior automatic classification can be achieved through a combination of multiple classifiers. Both voting and averaging methods have been shown to improve performance. The rationale is that averaging reduces the classification score variance, which decreases the overlap between the scores of relevant and non-relevant documents, and therefore results in better classification. We decided to build a classification framework that allows the construction of multi-classifier systems that look at different document features along with custom meta-classifiers that determine how the results of multiple classifiers get combined and forwarded to a final decision making program. The resulting system, called CaRE (Classification and Recommendation Engine), is a generalization of CARP [1], a program that routed newly written case summaries to sections of American Law Reports for citation purposes. It has all necessary functionality for extracting features from documents, indexing category profiles, storing the profiles into databases, and retrieving them at run time for classification.

The ResultsPlus recommendation system relies on an innovative combination of traditional information retrieval, classification technologies, and editorial enhancements to generate recommendations. Candidate articles for recommendation are drawn from a pool of over 300 publications and document collections, representing over a million documents. All of these documents have been indexed by CaRE, and many of them reference, summarize or quote each other to form a web of legal facts and concepts.

Suggestions are generated in response to two different user actions on Westlaw:

1. The user searches a caselaw, analytical or statutes database.
2. The user views a specific document in the search result.

In the former case, the text of the search query is sent to ResultsPlus, along with meta-data from the top scoring search results. This is analogous to blind relevance feedback, where the initial search result is enhanced by another round of processing, except that we exploit meta-data from the first round of results, rather than just terms taken from these documents. In the second use case, the system uses selected text from the retrieved case or document as the ResultsPlus query text. In this case, we are using both text and meta-data to create an expanded query.

Since its release in 2002, ResultsPlus has been hailed as 'revolutionary' in the trade press and become a favorite of Westlaw users. It is powered wholly by machine learning technology, applied both to the content itself and to user behavior, as we shall see in the next section.

3.2 Optimizing Recommendations Based on User Behavior

The initial challenge for ResultsPlus was to provide a minimum number of relevant suggestions for a user's query. As the number of covered publications expanded and the pool of relevant documents for each query grew, the challenge evolved into presenting the best from among many good candidate suggestions in the limited real estate of the user's screen. We set out to leverage the significant amount of usage data collected daily to develop new ranking algorithms based on data mining approaches, and then test their performance on real users in controlled experiments.

In order to achieve this goal, we had to develop infrastructure that would perform the following essential tasks.

1. Collection of potentially useful data. The data mining algorithms we use depend on a rich data set that describes users, user groups, user sessions, and user actions.
2. Effective data mining. Our object was a system that discovers the relationships and features that drive optimal results, letting the data drive the tuning process.
3. Dynamic testing and rollout capability. To test each new ranking method, we use A/B split testing for a few days and compare the results to the current baseline.

The outcome of our experiments is a system that recommends a personalized list of the most relevant documents in response to each user's request, taking into account meta-data and click-through statistics about the user's historic usage of the system, preferences for particular content types, search context (e.g., jurisdictions and databases searched), and the recommended document's global click-through rate. The use of personalized ranking has significantly increased the click-through rates of ResultsPlus, driving both usage and revenues. Meanwhile, the daily implicit feedback mechanism continually modifies document rankings to improve relevance and enhances overall system utility for all users.

4 Conclusions and Forward Look

I will end by making some general remarks about the generation and further leverage of meta-data.

In Thomson, we often use the term 'meta-data' rather loosely, to encompass all extraneous data associated with documents, including hand-written summaries,

programmatically-generated classifications, or citation patterns within and across collections. But meta-data is really *machine-readable* data about data, and not all of the so-called meta-data types enumerated above are in fact machine-readable, in the sense of being fully interpretable by a program. After all, a hand-written summary may be no easier for a program to understand than the original text.

Furthermore, an external data source, such as an authority file, only counts as meta-data if you can systematically relate it to the underlying texts to which it is relevant. *West Legal Directory* used to be a marketing tool; it was only after we linked judge and attorney names to it (as described in Section 2) that it became a useful meta-data repository. Once we were able to generate authority files from scratch, as with our expert witness database, we reached another level in our ability to go from text to data and back again, systematically relating people and documents.

In the course of our experiments, we have made four broad discoveries about meta-data. One is that even meta-data that are not machine-readable, such as summaries, can still be extremely valuable to a text mining program. These ancillary data can serve several functions inside a machine learning regimen, e.g., as document surrogates, as sources of normalized language, as objects for clustering, and so on. Another is that almost any meta-data is better than none. For example, if we are classifying a pool of documents to a new taxonomy, and these documents are already classified to another quite different taxonomy, the latter classifications can still assist in the learning of the former. Thirdly, we have shown that quite strong transfer effects take place between document types if training takes place on good sources of meta-data. Thus we managed to train a document classifier to sort law firm documents successfully using case summaries as the input to the learner, even though these do not closely resemble the types of document found in a law firm.

Fourth and finally, we have found that, constructing upon a firm foundation, one can automatically build a 'pyramid' of meta-data layers that deliver more and more value to the end user. Thus, we were able to construct CaRE profiles for legal concepts on top of West's *Key Number System* that were applicable beyond the usual case law documents. Subsequently, we could use these profiles to supplement secondary law materials with case law references in a continuous and timely fashion. These meta-data associations were then used for a range of other tasks, such as classifying law firm documents, sorting attorneys into practice areas, and driving document recommendations.

I see 'discovery' in the context of text mining as being not so much about finding novel patterns in data, as one would in data mining, but about building a web of relationships among documents of diverse types in a way that dissolves the usual content silos that a user has to contend with. Thus, ResultsPlus does not care where you are searching on Westlaw, or what kind of document you are currently looking at; it only cares about the associative paths between documents that it can find dynamically in pursuit of relevant information. These pathways include explicit citations within the universe of documents, but do not depend upon them exclusively, leveraging instead a 'metaverse' of relationships contained in the meta-data layers we have built.

In summary, I think that publishers have the opportunity to move away from a world in which editorial intervention, hand-built taxonomies, and domain knowledge are required for every advance. We can still avail ourselves of topical classifications,

citations, summaries, and the like, but the patterns these make in the data can now be processed by machines that improve search, make connections, offer recommendations, and the like. The resulting applications can take into account all the information that would be available to an omniscient searcher who knew every feature of the portal and possessed a panoramic view of the document collections. To me, that is the kind of innovation that text mining has the power to unleash.

References

1. Al-Kofahi, K., Tyrrell, A., Vachher, A., Travers, T. & Jackson, P. Combining multiple classifiers for text categorization. In *Proceedings of the 10th International Conference on Information and Knowledge Manage Management (CIKM-2001).*, New York: ACM Press. (2001). 97-104

2. Dozier, C. & Haschart, R. Automatic extraction and linking of personal names in legal text. In *Proceedings of RIAO-2000 (Recherche d'Informations Assistée par Ordinateur)*, (2000). 1305-1321.

3. Dozier, C., Jackson, P., Guo, X., Chaudhary, M. & Arumainayagam, Y.. Creation of an expert witness database through text mining. In *Proceedings of the 9th International Conference on Artificial Intelligence and Law (ICAIL-2003)*, New York: ACM Press. (2003) 177-184

4. Dozier, C. & Jackson, P. Mining text for expert witnesses. *IEEE Software*, May/June, (2005). 94-100.

5. Hearst, M. A. Untangling text data mining. *Proceedings of the 37th Annual Meeting of the Association for Computational Linguistics*, (1999) 3-10.

6. Herlocker, J. L., Konstan, J. A., Terveen, L. G. & Riedl, J. T. Evaluating collaborative filtering recommender systems. *ACM Transactions on Information Systems*, 22(1), (2004) 5-53.

7. Jackson, P., Al-Kofahi, K., Tyrrell, A. & Vachher, A. Information extraction from case law and retrieval of prior cases. *Artificial Intelligence*, 150, (2003) 239-290.

A Flexible Image Retrieval Framework

Raoul Pascal Pein[1,2] and Zhongyu Lu[2]

[1] Multimedia Systems Laboratory (MMLab),
Faculty of Engineering and Computer Science,
Hamburg University of Applied Sciences,
Berliner Tor 7, 20099 Hamburg, Germany
[2] Department of Informatics,
School of Computing and Engineering, University of Huddersfield,
Queensgate, Huddersfield HD1 3DH, United Kingdom

Abstract. This paper discusses a framework for image retrieval. Most current systems are based on a single technique for feature extraction and similarity search. Each technique has its advantages and drawbacks concerning the result quality. Usually they cover one or two certain features of the image, e.g. histograms or shape information.

The proposed framework is designed to be highly flexible, even if performance may suffer. The aim is to give people a platform to implement almost any kind of retrieval issues very quickly, whether it is content based or somehing else. The second advantage of the framework is the possibility to change retrieval characteristics within the program completely. This allows users to configure the ranking process as needed.

Keywords: Content-based image retrieval (CBIR); retrieval framework; feature vectors; query image; combined retrieval; improved result quality.

1 Introduction

Most available programs which provide an image search have very limited possibilities. They lack a flexible design allowing to fine tune the software to the user's requirements. Often they are capable of searching based on only a few features. Especially the separation between common retrieval approaches and specialized Content based Image Retrieval (CBIR) is visible.

Based on this observation, a standard design for image retrieval systems has been developed, which can be implemented and extended as simple as possible. This paper presents a framework which is:

- platform independent
- extensible and capable of offering individual user interfaces
- based selectively on database or file system
- capable of ranking several features simultaneously
- useful locally and in the web
- allowing manual annotation to improve quality

The proposed framework is based on the system described in [12,13]. The emphasis is clearly placed on the properties mentioned above, rather than a high performance. Some design decisions are deliberately made to provide flexibility. The important background of CBIR systems can be found in several papers like the Northumbria report [4] and other related papers [15,14]. A standard design for CBIR is presented by Veltkamp and Tanase [17] which represents the direct background for this paper. A combined indexing approach exploiting multiple features is put on top of that design.

In Section 2 the basic types of image retrieval concepts are presented. Each type has specific advantages and disadvantages which the proposed design tries to exploit and overcome. Section 3 gives a brief overview of how the system is generally designed and how the single components interact. Section 4 describes a currently working implementation. The prototype is still under development aiming at a better result quality and a servlet based user interface.

2 Related Work

Most image retrieval systems are based on one or more of these four basic indexing techniques: *Keywords*, *Tags*, *Semantics* or *Content*. All these techniques have specific advantages and disadvantages.

The "classic" approach is the use of keywords. This technique clearly is based on a considerable amount of knowledge. Its advantage is that much previous research from different areas can be reused, as most retrieval work has been done on text based documents. The major drawback of this approach is the difficulty to extract useful keywords from images automatically. Current search engines used locally (i.e. Beagle[16], Google Desktop Search[7]) or in the World Wide Web usually understand textual queries.

A second approach is to use tags which are used to generate clusters of similar images. This approach makes searching very simple and straightforward. The query consists of one or more tags and the engine only needs to filter out the matches. Adding tags to an image can be done manually with a maintainable effort. As simple tags are valid for many similar images at once, they can be selected and tagged very quickly. The drawback is the bad accuracy of discrimination. If thousands of images are tagged with the same tags, the retrieval process is rendered quite useless. F-Spot [5] is a personal retrieval software using tags based on "Emblem Tags" in Gnome [2]. A much more ambitious project is the web based Flickr [6]. This program also allows to attach "geotags" enabling the user to find pictures taken dependent on their location.

To introduce high quality results, the semantics of files can be used for retrieval. This technique allows to find data based on very specific content, eliminating ambiguities in the natural language. Unfortunately, the research in semantics and semantic web is currently in a very early state and not even text based engines are working satisfactorily. Also the annotation has to be done very carefully and by experts to achieve significant improvements. An example for semantic image retrieval is the Ontogator project [8] or the approach by

Zhang and Izquierdo based on Bayesian Networks [18]. A more lightweight approach to semantics can be found in TopicSEEK [3], where less effort is put into mathematical correctness but in usability.

The fourth technique introduces image specific attributes. It concentrates on the actual content, represented by the pixels. This allows to use maths for extracting the relevant indexing data automatically. Ideally, there is no manual input required to build a large index. Many different algorithms are possible to extract features of many kinds. The difficulty is to analyse the real content of an image, as seen by a user. This would require a currently not available (and probably impossible to implement) recognition algorithm. In addition a special kind of user interface is required, as queries cannot be directly mapped to a string. Examples are given by QBIC [11] and Virage [1].

An approach combining content and semantics has recently been described by Lam and Singh [10].

3   Proposed Design

The proposed design (fig. 1) is based on similar projects as well as cognitions from the preceding prototype.
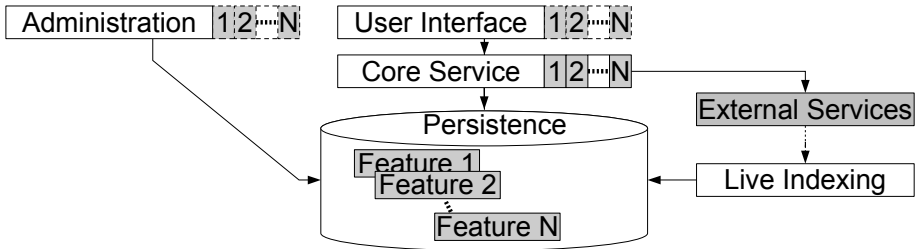
Fig. 1. The retrieval architecture consists of 6 basic modules. *Core Service* and *Persistence* can be enhanced by adding new features. Not content based features may also require an optional visualization in *User Interface* and *Administration*.

It is tried to model all components in the framework replaceable. Basically there are six different modules in the design: *Core Service*, *Persistence*, *User Interface*, *Administration*, *Live Indexing*, *External Services*.

Core Service. This module contains the whole retrieval logic, optimized on CBIR. For each single feature one separate index is created. Every feature needs to provide only two different algorithms: extraction of the binary (or else) feature from a pixel image and the calculation of similarity mapped to a range between 0 and 1. Based on these two algorithms, almost any feature can be supported directly. Queries containing more than a single feature are merged internally.

The most important function is to hand over a query to the server and to get a result set, which contains information about all relevant images. The query

should contain limitations where to cut off the ranking (minimal similarity, maximum result size) and some additional parameters to control each sub ranking for a single feature (especially CBIR related data). For each image x a combined and weighted ranking r_x is calculated based on the query. It is basically a weighted sum

$$r_x = \frac{1}{\sum_{f=1}^{n} w^f} * \sum_{f=1}^{n} w^f * r_x^f \qquad (1)$$

where w^f is the weight/importance of feature f. r_x^f is the partial ranking for image x using feature f. The optimal values for the feature weights depend on the users requirements. By altering these values the search characteristics of the engine can be changed completely. Alternative calculations (e.g. intersection of the results) may also be interesting for fine tuning.

Persistence. In the persistence layer all indexing data is stored. This can be a database, a file system or something completely different. There are only some basic requirements which are defined in the interface.

The basic access methods require opening and closing the source and read, update, delete and add of a single dataset. For searching, a sequential iteration over all datasets is required. To optimize the retrieval time, it may also be useful to have filtered access to a subset of an index.

User Interface. The user interface may vary widely. As well fat clients using a middleware as thin clients providing a web interface are possible. The interface of the core server is supposed to offer every service required, like searching and some information about the provided features. For manual annotation, writing feature data for an image directly to the repository needs to be offered.

Administration. A separate control instance is highly recommended to bar users from tinkering with important settings. This administration module needs direct access to the persistence module. It can be used to add new images into the repository and for setting basic properties for fine tuning the system.

Live Indexing. In order to provide live results which correspondent to locally available resources, a daemon process can be set up. This process monitors changes in the file system and adds new images automatically.

A web based service might use a similar program for automated updates. As the topology of the world wide web is different to a file system, a spider like program may be implemented.

External Services. Everything available from other retrieval services should be accessible. The core service is primarily designed to process image content, rather than textual queries. It is thought to exploit the techniques currently used in text based retrieval without re-implementing everything. A textual query can be used to get a list of relevant images which can be ranked with CBIR in the core system.

4   Implementation

A great deal of platform independence is already given by using a modern programming language like Java. Being aware of system specific properties like file names, the portability is reasonably high without much effort. Using further technologies requires also attention. To realize the prototype, components are chosen which are available on different platforms. For the underlying database, MySQL has been chosen, as it runs on most PCs. Further it is aimed not to use MySQL specific features to keep the migration effort to another data base low.

The current system is meant to be connected to an external engine to exploit existing text based search. The aim is to forward a search string from the user interface to this engine and get a list of matching files. This only requires a very simple interface, which will be realized as a small plug-in.

A promising engine seems to be the open-source project Beagle [16] which limits use of the extended image retrieval to Linux. The modular plugging of the external source allows to exchange the engine dependent on the user's needs.

To prove the design, support for a couple of different features is being implemented. Currently three different features are supported: keywords, histograms and spatially distributed histograms. Some other modules like a wavelet based one [9] and tags [2] are under development. Each module needs to implement two basic methods: *calculateFeatureVector(String fileName)* is required to extract the features from a file and *double calculateSimilarity(FeatureVector fv)* allows comparing two datasets. Optionally a specific GUI frame can be designed to provide a detailed query composition (e.g. entering keywords).

The realization of the histogram/wavelet based features provide gradual rankings anywhere between 0.0 and 1.0. Here a full scan over all datasets is adequate to achieve exact results, even if the required processing time is quite high. To improve speed, the index could also be put into a multi dimensional tree. In this case some otherwise good hits may be missing in the result set.

The text and tag based search is characterized for a much more distinctive ranking. Results may either be exactly 1.0 (hit) or exactly 0.0 (miss), slight differences may be realized with intermediate values. In the framework, these features are also easy to implement in the first place, especially for testing prototypes. Nevertheless a sequential search does not scale and the retrieval can be improved dramatically by adding an appropriate index structure (e.g. hashes, string based sorted trees) without losing any relevant result.

5   Results

The test data base contains information of 1709 images. To evaluate the efficiency of the combined ranking, the results of several queries are analyzed. The program combines three different result sets by using equation 1. As the *Keyword* component cannot handle query images, an additional query keyword is set. The query image shows a scene in Liverpool, therefore the query "liverpool" is passed to the engine.

This keyword represents the not content based queries in section 2. The search engine now has two independent views to calculate the final ranking. Figure 2 shows the resulting image set. The weighted ranking is displayed in figure 3 listing the detailed ranking for the first 125 images. To refine the result set, the weigths w^f for each of the three modules have been adjusted manually.

Fig. 2. The screenshot shows the top 20 results of a combined ranking. The query image (*upper left*) is ranked highest. Similarity decreases from left to right and top to bottom.
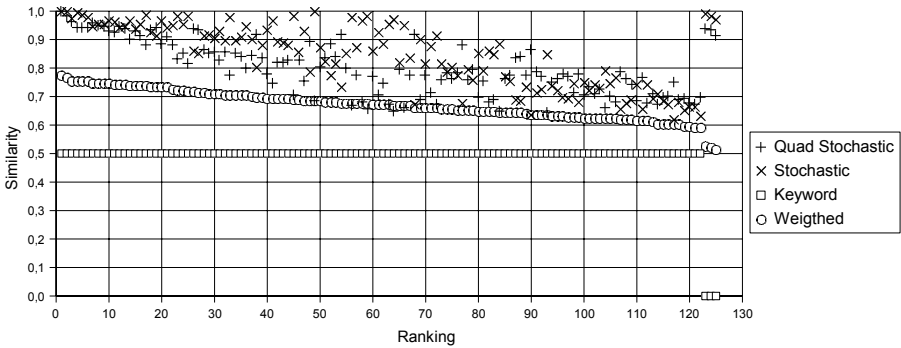
Fig. 3. The diagram visualizes details of the combined and weigthed ranking of fig. 2. The final ranking is based on the weighted similarity (*Weighted*).

6   Discussion and Analysis

The ranking generated by the retrieval service shows an eye-catching similarity between the first images in figure 2. A couple of brighter images with similar content got slightly higher ranks than some of the visually closer related images. This can easily be explained by the lossy compression of the histograms. An important fact is, that all results are somehow related to "liverpool". Queries without keyword restriction produce result sets containing several unrelated images in between the desired ones.

A way to overcome the drawbacks of each single indexing technique is to combine their strengths. Figure 3 shows the effect of combined retrieval. In this case, especially the *Keyword* module is a highly efficient filter to reject false

positives. At the lower end (rank 123-125) some images had a very high similarity (> 0.9) when only considering the content based modules. All 122 top ranked images all contain the specified keyword, while the similarity drops from 1.0 to about 0.6. All of the first 24 images show houses of Liverpool from above. Turning off the keyword search leads to a reatively high amount of images completely out of context, as the content based modules have no way to filter them out. If the user is only interested in visually similar images, disabling keywords helps to find images in less keyword-related regions of the repository.

7   Conclusion and Future Work

This paper shows a possible way to develop a flexible image retrieval system. The prototype design is a trade off between extensibility and high performance with an emphasis on extensibility. It is assumed that a combined retrieval can be used much more widely than a highly specialized one.

Achievements. The example query demonstrates the basic capabilities of the framework. It is possible to implement different feature modules supporting any of the types described in section 2. Tags and semantics are basically a special variation of keywords. The hard work with semantics need to be done in creating ontologies and adding certain values to an image, but this has nothing special to do with the framework itself.

Adding a new feature module can be done with minimal effort. There are only two important functions that need to be implemented plus some template-like ones for persistence issues (i.e. mapping from objects to low-level data types and back).

Future Work. The future work focuses on implementing new feature modules and web support including active user annotation. Further it is aimed to improve the text search by using specialized external search engines. A layer capable of building fast and scalable index structures is also under development.

As soon as multiple highly distinctive features are available, a detailed survey is planned. The objective is to evaluate whether the proposed combination of features leads to noticeable improvements in the result quality. The results of single features will be compared to combined features on a basis of several thousand images and many test persons to gain a significant representative sample.

References

1. J. Bach, C. Fuller, A. Gupta, A. Hampapur, B. Gorowitz, R. Humphrey, R. Jain, and C. Shu. Virage image search engine: an open framework for image management. In I. K. Sethi and R. C. Jain, editors, *SPIE, Storage and Retrieval for Image and Video Databases IV*, pages 76–87, February 1996.
2. James Barrett. Emblems and tagging in gnome, 2006. Available from: http://live.gnome.org/EmblemTags.

3. Andreas Christensen. Semantische Anreicherung von Suchanfragen auf Basis von Topic Maps., June 2005. Diplomarbeit.
4. J.P. Eakins and M.E. Graham. Content-based Image Retrieval. A Report to the JISC Technology Applications Programme. Technical report, University of Northumbria at Newcastle, January 1999. Available from: http://www.unn.ac.uk/iidr/VISOR.
5. Larry Ewing. F-spot - personal photo management, 2006. Available from: http://f-spot.org.
6. Flickr - Photo Sharing, 2006. Available from: http://www.flickr.com/.
7. Google desktop search, 2006. Available from: http://desktop.google.com.
8. Eero Hyvönen, Samppa Saarela, and Kim Viljanen. Intelligent image retrieval and browsing using semantic web techniques - a case study. Technical report, Helsinki Institute for Information Technology (HIIT) / University of Helsinki, 2003.
9. Charles E. Jacobs, Adam Finkelstein, and David H. Salesin. Fast multiresolution image querying. *Computer Graphics*, 29(Annual Conference Series):277–286, 1995. Available from: citeseer.ist.psu.edu/jacobs95fast.html.
10. Tony Lam and Rahul Singh. *Advances in Visual Computing*, volume 4292/2006 of *Lecture Notes in Computer Science*, chapter Semantically Relevant Image Retrieval by Combining Image and Linguistic Analysis, pages 770–779. Springer Berlin / Heidelberg, 2006.
11. W. Niblack, X. Zhu, J. Hafner, T. Breuel, D. Ponceleón, D. Petkovic, M. Flickner, E. Upfal, S. Nin, S. Sull, B. Dom, B.-L. Yeo, S. Srinivasan, D. Zivkovic, and M. Penner. Updates to the qbic system. *Retrieval for Image and Video Databases VI*, 3312:150–161, 1998.
12. Raoul Pascal Pein. Multi-Modal Image Retrieval, April 2005. Diplomarbeit.
13. Raoul Pascal Pein and Zhongyu (Joan) Lu. Content Based Image Retrieval by Combining Features and Query-By-Sketch. In Hamid R. Arabnia and Ray Hashemi, editors, *The 2006 International Conference on Information & Knowledge Engineering*, pages 49–55, 2006.
14. Monika Renz and Wolfgang Renz. Neue Verfahren im Bildretrieval. Perspektiven für die Anwendung. In R. Schmidt, editor, *Proceedings der 22. Online-Tagung der DGI*, pages 102–128, May 2000.
15. S. Shatford. Analyzing the Subject of a Picture: A Theoretical Approach. *Cataloging and Classification Quarterly*, 6:39–62, 1986.
16. Joe Shaw. Beagle desktop search, 2006. Available from: http://beagle-project.org/Main_Page.
17. Remco C. Veltkamp and Mirela Tanase. Content-Based Image Retrieval Systems: A Survey. Technical Report UU-CS-2000-34, Department of Computing Science, Utrecht University, October 2002.
18. Qianni Zhang and Ebroul Izquierdo. *Semantic Multimedia*, volume 4306/2006 of *Lecture Notes in Computer Science*, chapter A Bayesian Network Approach to Multi-feature Based Image Retrieval, pages 138–147. Springer Berlin / Heidelberg, 2006.

Privacy Preserving Data Mining Research: Current Status and Key Issues

Xiaodan Wu[1], Chao-Hsien Chu[2], Yunfeng Wang[1], Fengli Liu[1], and Dianmin Yue[1]

[1] School of Management, Hebei University of Technology, Tianjin 300130, China
`xwu@hebut.edu.cn`, `ywang@hebut.edu.cn`, `liufengli312@163.com`,
`dyue@hebut.edu.cn`
[2] College of Information Sciences and Technology, The Pennsylvania State University, 301K IST Building, University Park, PA 16802, USA
`chu@ist.psu.edu`

Abstract. Recent advances in the Internet, in data mining, and in security technologies have gave rise to a new stream of research, known as privacy preserving data mining (PPDM). PPDM technologies allow us to extract relevant knowledge from a large amount of data, while hide sensitive data or information from disclosure. Several research questions have often being asked: (1) what kind of option available for privacy preserving? (2) Which method is more popular? (3) how to measure the performance of these algorithms? And (4) how effective of these algorithms in preserving privacy? To help answer these questions, we conduct an extensive review of 29 recent references from years 2000 to 2006 for analysis.

Keywords: Privacy preserving; data mining.

1 Introduction

Data mining is a well-known technique for automatically and intelligently extracting information or knowledge from a large amount of data, which, however, can also disclosure sensitive information about individuals compromising the individual's right to privacy. Moreover, data mining techniques can reveal critical information about business transactions, compromising the free competition in a business setting [1]. Therefore, privacy preserving data mining (PPDM) has becoming an increasingly important field of study.

PPDM is a new era of research in data mining, where data mining algorithms are analyzed for possible infringement in privacy. PPDM research usually takes one of the three philosophical approaches: (1) data hiding, in which sensitive raw data like identifiers, name, addresses, etc. were altered, blocked, or trimmed out from the original database, in order for the users of the data not to be able to compromise another person's privacy; (2) rule hiding, in which sensitive knowledge extracted from the data mining process be excluded for use, because confidential information may be derived from the released knowledge; and (3) secure multiparty computation, where distributed data are encrypted before released or shared for computations; thus,

no party knows anything except its own inputs and the results. The ultimate goal of PPDM is to develop efficient algorithms that allow one to extract relevant knowledge from a large amount of data, while prevent sensitive data and information from disclosure or inference.

PPDM is a fast growing research area. Given the number of different algorithms have been developed over the past years, there is an emerging need of synthesizing literature to understand the nature of problems, identify potential research issues, standardize new research area, and evaluate the relative performance of different approaches [1] [28].

2   Related Work

Several researchers have attempted to synthesize the literature. Kantarcioglu and Clifton [7] suggested that adopting a common framework for discussing privacy preservation will enable next generation data mining technology to make substantial advances in alleviating privacy concerns. Verykios et al. [28] analyzed the state-of-the-art, classified the proposed algorithms from five different dimensions: data distribution, data modification, data mining algorithm, data or rule hiding, and privacy preservation. They also suggested a set of metrics for assessing PPDM performance. Bertino et al. [1] proposed a taxonomy for classifying existing PPDM algorithms. They also developed a framework and based upon which to evaluate the relative performance of selected heuristic-based hiding algorithms. In this paper, we propose to consolidate and simplify the taxonomy brought by [1]. We have also attempted to examine the relative performance of PPDM from individual component level instead of the complete PPDM algorithms.

3   Current Status

We present a simplified classification scheme, adopted from early studies, to guide the review process. The proposed taxonomy contains four levels (see Figure 1). This scheme differs from existing studies in two ways: (1) we treat data modification methods as part of privacy preserving techniques, and (2) we consider the purpose of hiding as a key classifier and place it before data mining task/algorithm level. The number appears below each category indicated its percentage of usage (popularity).

3.1   Data Distribution

The PPDM algorithms can be first divided into two major categories, centralized and distributed data, based on the distribution of data. In a centralized database (C-DB) environment, data are all stored in a single database; while, in a distributed database (D-DB) environment, data are stored in different databases [3]-[6] [13]-[22] [27] [29] [31]. Distributed data scenarios can be further classified into horizontal and vertical data distributions. Horizontal distributions refer to the cases where different records of the same data attributes are resided in different places [7] - [11] [26]; while in a vertical data distribution, different attributes of the same record of data are resided in different places [2] [23] [24] [25] [30] [33]. As can be seen, earlier research has been
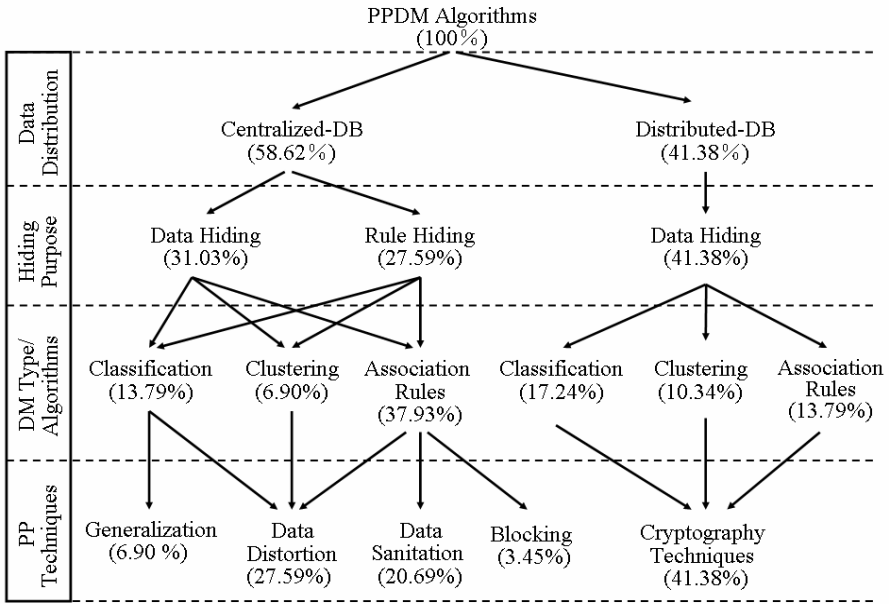
Fig. 1. Taxonomy of PPDM algorithms

predominately focused on dealing with privacy preservation in a centralized DB. The difficulties of applying PPDM algorithms to a distributed DB can be attributed to: first, the data owners have privacy concerns so they may not willing to release their own data for others; second, even if they are willing to share data, the communication cost between the sites is too expensive. However, in today's global digital environment, most data are often stored in different sites, so more attention and research should be focused on distributed PPDM algorithms.

3.2 Hiding Purposes

The PPDM algorithms can be further classified into two types, data hiding and rule hiding, according to the purposes of hiding. Data hiding refers to the cases where the sensitive data from original database like identity, name, and address that can be linked, directly or indirectly, to an individual person are hided. In contrast, in rule hiding, we remove the sensitive knowledge (rule) derived from original database after applying data mining algorithms. We summarize the related literature in Table 1. Majority of the PPDM algorithms used data hiding techniques. This is especially true in a distributed database environment, as the techniques can be used to prevent individual information from being discovered by other parties in the joint computational process. Please note that most PPDM algorithms hide sensitive patterns by modifying data. Also, at present, the rule hiding techniques is only being adopted by association rule mining for centralized DB. The reason for such a restriction is mainly due to its ease of implementation.

Table 1. Summary of the hiding purpose of PPDM

Purpose	References	
	Centralized DB	Distributed DB
Data hiding	[3] [4] [5] [6] [17] [18] [20] [29] [31]	[2] [7] [8] [9] 10] [11] [23] [24] [25] [27] [30] [33]
Rule hiding	[14] [15] [16] [19] [27] [21] [22]	None

3.3 Data Mining Tasks/Algorithms

Currently, the PPDM algorithms are mainly used on the tasks of classification, association rule and clustering. Association analysis involves the discovery of associated rules, showing attribute value and conditions that occur frequently in a given set of data. Classification is the process of finding a set of models (or functions) that describe and distinguish data classes or concepts, for the purpose of being able to use the model to predict the class of objects whose class label is unknown. Clustering Analysis concerns the problem of decomposing or partitioning a data set (usually multivariate) into groups so that the points in one group are similar to each other and are as different as possible from the points in other groups. We summarize the distribution of literature in Table 2. About 52% of the PPDM algorithms used association rule method for mining data, followed by classification, and then clustering. Compared with association rule mining, classification rule mining is more complicated to perform. Also, unlike association rules mining, which deals with existing data items, classification deals with attributes and its values. Moreover, instead of associating links between attribute values, it also needs to classify the attributes of each dataset.

Table 2. Summary of PPDM for data mining tasks

Data mining techniques	References	
	Centralized DB	Distributed DB
Classification	[3] [6] [13] [29]	[2] [8] [10] [25] [30]
Association Rules	[4] [5] [14] [15] [16] [20] [21] [22] [27] [31]	[7] [8] [25] [26]
Clustering	[17] [18]	[9] [11] [24]

3.4 Privacy Preservation Techniques

We can further divide PPDM algorithms according to privacy preservation techniques used. Four techniques – sanitation, blocking, distort, and generalization -- have been used to hide data items for a centralized data distribution. The idea behind data sanitation is to remove or modify items in a database to reduce the support of some frequently used itemsets such that sensitive patterns cannot be mined. The blocking approach replaces certain attributes of the data with a question mark. In this regard, the minimum support and confidence level will be altered into a minimum interval. As long as the support and/or the confidence of a sensitive rule lie below the middle in these two ranges, the confidentiality of data is expected to be protected. Also

known as data perturbation or data randomization, data distort protects privacy for individual data records through modification of its original data, in which the original distribution of the data is reconstructed from the randomized data. These techniques aim to design distortion methods after which the true value of any individual record is difficult to ascertain, but "global" properties of the data remain largely unchanged. Generalization transforms and replaces each record value with a corresponding generalized value.

The privacy preservation technique used in a distributed database is mainly based on cryptography techniques. SMC algorithms deal with computing any function on any input, in a distributed network where each participant holds one of the inputs, while ensuring that no more information is revealed to a participant in the computation than can be inferred from that participant's input and output. The distribution of the literature is given in Table 3. Data distort is the most popular method used in hiding data, followed by data sanitation and generalization. If one wants to obtain data mining results from different data sources, then the only method can be used is a cryptography technique. Since the parties who use SMC operators cannot reveal anything from others except final results, it can have benefits of both accuracy of data mining results and the privacy of the database.

Table 3. Summary for privacy preservation techniques

	PP Techniques	References
	Data Sanitation	[14] [15] [16] [19] [22] [27]
	Blocking	[21]
C-DB	Data Distort	[3] [4] [5] [6] [17] [18] [20] [31]
	Generalization	[13] [29]
D-DB	Cryptography Techniques	[2] [7] [8] [9] [10] [11] [23] [24] [24] [26] [30] [33]

3.5   Evaluation Criteria

The metrics commonly used in early research are:

1. *Efficiency*, which concerns the ability of an algorithm to execute with good performance in terms of all the resources implied by the algorithm; Performance is assessed, as usually, in terms of computational costs [14] [15] [18] [19] [21] [27], and in case of distributed algorithms, in terms of the communication costs incurred during information exchanges [2] [7] [8] [9] [10] [11] [23] [24] [25] [27] [30] [33].
2. *Effectiveness*, which considers both the capability of hiding sensitive information [3] [4] [5] [6] [13] [14] [15] [17] [18] [19] [20] [21] [22] [27] [29] [31] and accuracy of the data mining results [3] [4] [5] [6] [13] [14] [4] [16] [17] [18] [19] [20] [21] [27] [29] [31]. For example, the accuracy of data sanitation technique may be measured in terms of hiding failure, that is, the portion of sensitive information that is not hidden by the technique, and misses cost, that occurs when some legitimate patterns are hidden by accident.
3. *Scalability*, closely related to computational cost, concerns the size of problem the algorithm can solve within a reasonably acceptable timeframe. The higher the computational cost, the less chance the algorithms be used for solving larger size of problems.

3.6 Performance Assessment

Assessing the relative performance of PPDM algorithms is a very difficult task, as it is often the case that no single algorithm outperforms others on all possible criteria. Also, for maximum flexibility, we rate the relative merit of individual module that comprised by the PPDM algorithm. The rating is given in three different levels -- high, medium, and low. We summarize the results in Table 4, and discuss the general principles below.

Table 4. Relative performance of PPDM components

Elements	Computational Cost	Privacy Preserving	Accuracy of Mining	Scalability
Hiding Purpose:				
Data Hiding	Low	Contingent	Contingent	High
Rule Hiding	High	Contingent	Contingent	Low
Data Mining Tasks:				
Classification	Low	N/A	Contingent	High
Clustering	High	N/A	Contingent	Low
Association Rule	Low	N/A	Contingent	High
Privacy Preserving Technique:				
Sanitation	Medium	Medium	Medium	Low
Distortion	Low	High	Low	High
Blocking	Medium	Low	Medium	Low
Generalization	Low	High	Medium	High
Cryptography	High	High	High	Low

In term of computational efficiency, rule hiding is less efficient than data hiding, because one has to identify the items that contribute to the sensitive rule first and then hide the rule. For the privacy requirement, we think hiding rule is more critical than hiding data, because after the sensitive rules are found, more information is possible to be inferred. This is not to say that rule hiding is more accurate than data hiding. The selection of either hiding data or rule often depends on the goal of privacy preserving (hiding purpose) and data distribution. For instance, we can only hide data under a distributed database environment.

In general, clustering is more complex than classification (including association rules) because it often requires using an unsupervised learning algorithm. The algorithm used for association rule and classification can learn from known results, thus, they are more efficient. However, the preserving power and accuracy are highly dependent on hiding technique used or the algorithm used, not the data mining task. Assessing the performance of traditional data mining algorithms is out of the scope of this study.

The key idea behinds sanitization type of algorithms is to hide the set of frequent patterns from containing highly sensitive knowledge. The complexity of this type of algorithm is $O(n1*NlogN)$, where $n1$ is the number of restrictive patterns and N the number of transactions in the database [14]. Thus, comparing with other methods, the computational cost of sanitation type of algorithm is medium. Study has shown that the more sensitive patterns are hidden, the more legitimate patterns are missed, so it also degrades the accuracy of data mining results. Moreover, the optimal sanitization

is proved to be NP-hard in the context of association rule mining; therefore, it is computationally intensive as compared with a data perturbation approach.

The inherent mechanism of blocking and sanitization is basically similar. The former uses a '?' notation to replace selected items to be protected, while the latter deletes or modifies these items from viewing; thereby, their complexity are almost the same. However, the privacy preserving capability of blocking is lower than sanitization. Moreover, like sanitization, blocking technique is *NP-hard*. Therefore, these two modification methods cannot be used to solve larger size of problems.

Most existing studies which used distortion method focus on maintaining the level of privacy disclosure and knowledge discovery ability. It seems that efficiency and computational cost are not the issues for distortion method. In general, data distortion algorithms have good effectiveness in hiding data. However, these methods are not without faults. First, the distorting approach only works if one does not need to reconstruct the original data values. Thus, if the data mining task changed, new algorithms need to be developed to reconstruct the distributions. Second, this technique considers each attribute independently; as a result, when the number of attributes became large, the accuracy of data mining results will degrade significantly. Finally, there is a trade-off between accuracy of data mining results and data security using distortion methods. These methods may not be suitable for mining data in situations requiring both high accuracy and high security.

The generalization technique has been widely used in protecting individual privacy with the k-anonymity model in the past; however, it is relatively new to the data mining community. Since generalization has the advantage of not modifying the true value of attributes, it may have higher accuracy of data mining result than data distortion techniques. The complexity of this algorithm is O(k log k), where the constant in the big-O is less than 4. Although the runtime of this algorithm is exponential in k, its efficiency can be greatly enhanced as suggested by [12].

Cryptography-based SMC has the highest accuracy in data mining and good privacy preservation capability as well; however, it has strict usages as it is only applicable to a distributed data environment. Two models of SMC are available: semi-honest model and malicious model. The semi-honest models assume each party follows the protocol rules, but is free to later use what it sees during execution to compromise security; while the malicious model assumes parties can arbitrarily "cheat," and such cheating will not compromise either security or the results. How to prevent or detect malicious party in a computation process is an unsolved issue. Not to mention that SMC has the burden of high communicational cost, when the number of parties participated increased. Usually, the communicational cost increases at the exponential speed when data size increases linearly. Also, different problems need different protocols and the complexities vary naturally [30].

4 Key Issues

The following issues/directions were derived for future research. First, currently several groups of researchers have devoted effort in studying PPDM from different perspectives (e.g., statistics, database, data mining, knowledge discovery, and

information security), but they tend to use different terminology to describe similar or related practice. For instance, people have used data modification, data perturbation, data sanitation, data hiding, and preprocessing as possible methods for preserving privacy; however, all are in fact related to the use of some types of technique to modify original data so that private data and knowledge remain private even after the mining process. Lacking a common language for discussions will cause misunderstanding and slow down the research breakthrough. Therefore, there is an emerging need of standardizing the terminology and PPDM practice.

Second, although many machine learning methods have been used for classification, clustering, and other data mining tasks (e.g., diagnose, prediction, optimization), currently only the association rules method has been predominately used. It would be interesting to see how to extend the current technique and practice into other problem domains or data mining tasks. It may be also interesting in using different mining algorithms, especially the nature-based intelligent technologies such as genetic algorithms, neural networks, ant colony, and immune systems to mining and preserving privacy. Furthermore, it is important to find the privacy preserving technique that is independent of data mining task and algorithm so that after applying privacy preserving technique a database can be released without being constrained to the original task and mining algorithms.

Third, most prior PPDM algorithms were developed for use with data stored in a centralized database. However, in today's global digital environment, data is often stored in different sites. With recent advances in information and communication technologies, the distributed PPDM methodology may have a wider application, especially in medical, health care, banking, military and supply chain scenarios. In addition, current PPDM algorithms mainly focus on preserving tuples in the database. Fundamental questions such as where does privacy may happen, what kind of data, data attributes and data type need to preserve remain to be explored.

Fourth, data hiding techniques have been the dominated methods for protecting privacy of individual information. However, those algorithms do not pay full attention to data mining results, which may lead to sensitive rules leakages. While some algorithms are designed for preserving the rule liking with sensitive information, it may degrade the accuracy of other non-sensitive rules. Thus, further investigation, focusing on combining data and rule hiding, may be beneficial, specifically, when taking into account the interactive impact of sensitive and non-sensitive rules, the dependence relationship of the sensitive rules and problem-domain knowledge.

Fifth, various data distortion algorithms have been designed and developed for protecting privacy of individual information. However, those algorithms are usually limited to specialized type of data like integer and float numerical value. Further research could pay more attention to other types of data like character or hybrid type of data.

Finally, a framework for evaluating selected association rule hiding algorithms has been proposed by Bertino et al. [1]. Future research can consider testing the proposed evaluation framework for other privacy preservation algorithms, such as data distortion or cryptography methods.

5   Conclusions

PPDM has recently emerged as a new field of study. A portfolio of algorithms has been suggested for possible solutions. As a new comer, PPDM may offer a wide application prospect but at the same time it also brings us many issues / problems to be answered. In this study, we conduct a comprehensive survey of 29 prior studies to find out the current status of PPDM development. We propose a simplified taxonomy to help understand the problem and explore possible research issues. We also examine the strengths and weaknesses of different privacy preserving techniques and summarize general principles from early research to guide the selection of PPDM algorithms. As part of future work, we plan to formally test a complete spectrum of PPDM algorithms.

References

1. Bertino, E., Fovino, I., and Provenza, L.: A Framework for Evaluating Privacy Preserving Data Mining Algorithms. Data Mining and Knowledge Discovery 11: 2 (September 2005) 121-154
2. Du, W., and Zhan, Z.: Building Decision Tree Classifier on Private Data. In: Proc. Of the IEEE ICDM Workshop on Privacy, Security and Data Mining (PSDM'02), Maebashi City, Japan (Dec. 2002) 1-8
3. Du, W., and Zhan, Z.: Using Randomized Response Techniques for Privacy- Preserving Data Mining. In: Proc. of the Ninth ACM SIGKDD Int. Conf. on Knowledge Discovery and Data Mining, Washington, D.C. (Aug. 2003)
4. Evfimievski, A., Gehrke, J., and Srikant, R.: Limiting Privacy Breaches in Privacy Preserving Data Mining. In: Proc. of the Twenty-second ACM SIGMOD-SIGACTSIGART Symposium on Principles of Database Systems, San Diego, California (June 2003) 211-222
5. Evfimievski, A., Srikant, R., Agarwal, R., and Gehrke, J.: Privacy Preserving Mining of Association Rules. In: Proc. of the 8th ACM SIGKDD Int. Conf. on Knowledge Discovery in Databases and Data Mining (KDD'02), Edmonton, Alberta, Canada (July 2004) 217-228
6. Islam, M. Z., and Brankovic, L.: A Framework for Privacy Preserving Classification in Data Mining. In: Proc. of the 2nd workshop on Australasian information security, Data Mining and Web Intelligence, and Software Internationalization (AISW'04, AWDM&WI'04, AWSI'04), Dunedin, New Zealand (Jan. 2004) 163-168
7. Kantarcioglu, M., and Clifton, C.: Privacy-preserving Distributed Mining of Association Rules on Horizontally Partitioned Data. In: Proc. of ACM SIGMOD Workshop on Research Issues in Data Mining and Knowledge Discovery (DMKD) (June 2002)
8. Kantarcıoglu, M., and Clifton, C.: Assuring Privacy when Big Brother is Watching. In: Proc. of the 8th ACM SIGMOD Workshop on Research Issues in Data Mining and Knowledge Discovery, Privacy & Security (2003) 88-93
9. Klusch, M., Lodi, S., and Moro, G.: Distributed Clustering Based on Sampling Local Density Estimates. In: Proc. of the 18th Int. Joint Conf. on Artificial Intelligence (IJCAI'03), Acapulco, Mexico (Aug. 2003) 485-490
10. Lindell, Y., and Pinkas, B.: Privacy Preserving Data Mining. In: Advances in Cryptology – CRYPTO 2000, Springer-Verlag (Aug. 2000) 36–54

11. Merugu, S., and Ghosh, J.: Privacy-Preserving Distributed Clustering Using Generative Models. In: Proc. of the 3rd IEEE Int. Conf. on Data Mining (ICDM'03), Melbourne, FL, USA (Nov. 2003) 211-219

12. Meyerson, A. and Williamsy, R.: On the Complexity of Optimal K-Anonymity. In: Deutsch A, ed. Proc. of the 23rd ACM SIGACT- SIGMOD-SIGART Symposium on Principles of Database Systems (PODS 2004). New York: ACM (2004) 223-228

13. Natwichai1, J., Li, X., and Orlowska, M.: Hiding Classification Rules for Data Sharing With Privacy Preservation. In: Proc. of 7th International Conference on Data Warehousing and Knowledge Discovery (DaWaK'05), Copenhagen, Denmark (Aug. 2005) 468-477

14. Oliveira, S. R. M., and Zaïane, O. R.: Privacy Preserving Frequent Itemset Mining. In: Proc. of the IEEE international conference on Privacy, Security and Data Mining (PSDM'02), Maebashi City, Japan (Dec. 2002) 43-54

15. Oliveira, S. R. M., and Zaïane, O. R.: Algorithms for Balancing Privacy and Knowledge Discovery in Association Rule Mining. In: Pro. of the 7th Int. Database Engineering and Applications Symposium (IDEAS'03), Hong Kong, China (July 2003) 54-65

16. Oliveira, S. R. M., and Zaïane, O. R.: Protecting Sensitive Knowledge By Data Sanitization. In: Proc. of the 3rd IEEE Int. Conf. on Data Mining (ICDM'03), Melbourne, Florida, USA (Nov. 2003b) 613–616

17. Oliveira and, S. R. M., and Zaïane, O. R.: Privacy Preserving Clustering by Data Transformation. In: Pro. of the 18th Brazilian Symposium on Databases, Manaus, Amazonas, Brazil (Oct. 2003c) 304-318

18. Oliveira, S. R. M., and Zaïane, O. R.: Achieving Privacy Preservation When Sharing Data for Clustering. In: Pro. of the Int. Workshop on Secure Data Management in a Connected World (SDM'04), In Conjunction with the 30th Very Large Data Base Conference (VLDB'04), Toronto, Canada (Aug. 2004a) 76-82

19. Oliveira, S. R. M., Zaïane, O. R., and Saygin, Y.: Secure Association Rule Sharing. In: PAKDD 2004b 74-85

20. Rizvi, J., and Haritsa, R.: Maintaining Data Privacy in Association Rule Mining. In: Pro. of the 28th Very Large Data Base Conf. (VLDB'02), Hong Kong, China (Aug. 2002) 682-693

21. Saygin, Y., Verykios, V., and Clifton, C.: Using Un-knowns to Prevent Discovery of Association Rules. ACM SIGMOD Record 30: 4 (2001)

22. Saygin, Y., Verykios, V., and Elmagarmid, A.: Privacy Preserving Association Rule Mining. In: Proc. of 12th Int. Workshop on Research Issues in Data Engineering (RIDE) (Feb. 2002).

23. Vaidya, J., and Clifton, C.: Privacy Preserving Association Rule Mining in Vertically Partitioned Data. In: Proc. of the 8th ACM SIGKDD Int. Conf. on Knowledge Discovery and Data Mining (2002) 639–644

24. Vaidya, J., and Clifton, C.: Privacy-Preserving K-Means Clustering over Vertically Partitioned Data. In: Proc. of the 9th ACM SIGKDD Int. Conf. on Knowledge Discovery in Data (KDD'03), Washington D.C., USA (Aug. 2003) 206-215

25. Vaidya, J., and Clifton, C.: Privacy-Preserving Decision Trees over Vertically Partitioned Data. In: Proc. of the 19th Annual IFIP WG 11.3 Working Conf. on Data and Applications Security (DAS'05), Storrs, CT, USA (Aug. 2005) 139-152

26. Veloso, A., Meira, Jr., W., Parthasarathy, S., and de Carvalho, M.: Efficient, Accurate and Privacy-Preserving Data Mining for Frequent Itemsets in Distributed Databases. In: Proc. of the 18th Brazilian Symposium on Databases, Manaus, Amazonas, Brazil (Oct. 2003) 281-292

27. Verykios, S., Elmagarmid, K., Elisa, B., Saygin, Y. and Elena, D.: Association Rule Hiding. IEEE Transactions on Knowledge and Data Engineering (2003)
28. Verykios, S., Bertino, E., Fovino, I., Provenza, L., Saygin, Y., and Theodoridis, Y.: State-of-the-art in Privacy Preserving Data Mining. ACM SIGMOD Record 33: 1 (March 2004) 50-57
29. Wang, K., Yu, S., and Chakraborty, S.: Bottom-Up Generalization: A Data Mining Solution to Privacy Protection. In: Proc. the 4th IEEE Int. Conf. on Data Mining (ICDM'04), Brighton, United Kingdom (Nov. 2004) 249-256
30. Wenliang, D. and Zhijun, Z.: A Study of Several Practical Approach to Solve Secure Multiparty Computation Problems. In: Pro. of the Int. Conf. on Computer Networks and Mobile Computing (ICCNMC'03) (2003)
31. Xia, Y., Yang, Y., Chi, Y., and Muntz, R. R.: Mining Association Rules with Nonuniform Privacy Concerns. Technical Report CSD-TR No. 040015, University of California (March 2004)
32. Yang, Z., Zhong, S., Wright, R. N.: GrC. Privacy-Preserving Model Selection. In: Proc. of the IEEE Int. Conf. on Granular Computing (2006)
33. Zhan, J. Z., Matwin, S., and Chang, L.: Privacy-preserving Collaborative Association Rule Mining. DBSec (2005) 153-165

Combining Classifiers for Web Violent Content Detection and Filtering

Radhouane Guermazi[1], Mohamed Hammami[2], and Abdelmajid Ben Hamadou[1]

[1] Miracl-Isims, Route Mharza Km 1 BP 1030 Sfax Tunisie
[2] Miracl-Fss, Route Sokra Km 3 BP 802, 3018 Sfax Tunisie
rguermazi@laposte.net,
mohamed.hammami@fss.rnu.tn,
abdelmajid.benhamadou@isimsf.rnu.tn
http://www.isimsf.rnu.tn/

Abstract. Keeping people away from litigious information becomes one of the most important research area in network information security. Indeed, Web filtering is used to prevent access to undesirable Web pages. In this paper we review some existing solutions, then we propose a violent Web content detection and filtering system called "WebAngels filter" which uses textual and structural analysis. "WebAngels filter" has the advantage of combining several data-mining algorithms for Web site classification. We discuss how the combination learning based methods can improve filtering performances. Our preliminary results show that it can detect and filter violent content effectively.

Keywords: Web classification and categorization, data-mining, Web textual and structural content, violent website filtering.

1 Introduction

The growth of the Web and the increasing number of documents electronically available has been paralleled by the emergence of harmful Web pages content such as pornography, violence, racism, etc. This emergence involved the necessity of providing filtering systems designed to secure the internet access. Most of them process mainly the adult content and focus on blocking pornography. Whereas, the other litigious characters, in particular the violent one, are marginalized. In this paper, we propose a textual and structural content-based analysis using several major-data mining algorithms for automatic violent website classification and filtering. We focus our attention on the combination of classifiers, and we demonstrate that it can be applied to improve the filtering efficiency of violent web pages. The remainder of this paper is organized as follows. We overview related work according to web filtering in section 2. In the next section, we present our approach. The extraction of features vector is described, and the experimentation of each used algorithm is studied. In the fourth section, we show the efficiency of combining data-mining techniques to improve the filtering accuracy rate. In section 5 we describe the architecture and the functionalities of the

prototype "WebAngels filter" as well as its results compared to the most known software on the market. Finally section 6 presents some concluding remarks and future work directions.

2   Web Filtering: Related Works

Several litigious website filtering approaches were proposed. Among these approaches, we can quote (1) the Platform for Internet Content Selection (PICS)[1], (2) the exclusion filtering approach, which allows all access except to sites belonging to a manually constructed black-list, (3) the inclusion filtering approach, which only allows access to sites belonging to a manually constructed white-list and (4) the automated content filtering approach, designed to classify and filter Web sites and URLs automatically in order to reflect the highly dynamic evolution of the Web. In this approach, we can enumerate two types: (a) Keyword blocking where a list of prohibited words is used to identify undesirable Web pages. (b) Intelligent content Web filtering which falls in the general problem of automatic website categorization and uses machine learning. At least, three categories of intelligent content Web filtering can be distinguished : (i) textual content Web filtering [1], (ii) structural content Web filtering [2], [3] and (iii) Visual content Web filtering [4]. Other Web filtering solutions are based on an analysis of textual, structural and visual contents, of a Web page [5].

Litigious Web pages classification and filtering are diversified. However, the majority of these works treat particularity adult character. We propose in the following section our approach for the violent sites classification.

3   Our Approach to Violent Web Filtering

Black-lists and white-lists are hard to generate and maintain. Also filtering based on naive keyword-matching can be easily circumvented by deliberate mis-spelling of keywords. We propose to build an automatic violent content detection solution based on a machine learning approach using a set of manually classified sites, in order to produce a prediction model, which makes it possible to know which URLs are suspect and which are not. To classify the sites into two classes, we are based on the KDD process for extracting useful knowledge from volumes data [6]. The general principle of the approach of classification is the following: Let S be the population of samples to be classified. To each sample s of S one can associate a particular attribute, namely, its class label C. C takes its value in the class of labels(0 for violent, 1 for nonviolent)

$$C : S \rightarrow \Gamma = \{Violent, nonViolent\}$$
$$s \in S \mapsto C(s) \in \Gamma$$

Our study consists in building a means to predict the attribute class of each website. To do it three major steps are necessary: (a) selecting and pre-processing

---

step which consists on selecting the features which best discriminate classes and extracting the features from the training data set; (b) data-mining step which looks for a synthetic and generalizable model by the use of various algorithms; (c) evaluation and validation step which consists on assessing the quality of the learned model on the training data set and on the test data set.

3.1   Data Preparation

In this stage we identify exploitable information and check their quality and their effectiveness in order to build a two-dimensional table from our training corpus. Each table row represents a web page and each column represent a feature. in the last column, we save the web page class (0 or 1).

Construction of Training Set. The data-mining process for violent website classification requires a representative training data set consisting on a significant set of manually classified websites. We choused diversified websites according to their content, treated languages and structure. Our training data set is composed of 700 sites from which 350 are violent.

Textual and Structural Contents Analysis. The selection of features used in a machine learning process is a key step which directly affects the performance of a classifier. Our study of the state of the art and manual collection of our test data set helped us a lot to gain intuition on violent website characteristics and to understand discriminating features between violent web pages and inoffensive ones. These intuition and understanding suggested us to select both textual and structural content-based features for better discrimination purpose. We used in the calculation of these features a manually collected violent words vocabulary (or dictionary). The features used to classify the Web pages are n_v_words_page (total number of violent words in the current Web page), %v_words_page (frequency of the violent words of the page), n_v_words_url (total number of violent words in the URL), %v_words_url (frequency of violent words in the URL), n_v_words_title (total number of violent words which appear in the title tag), %v_words_title (frequency of violent words which appear in the title tag), n_v_words_body (number of violent words which appear in the body tag), %v_words_body (frequency of violent words which appear in the body tag), n_v_words_meta (number of violent words which appear in the meta tag), %v_words_meta (frequency of violent words which appear in the meta tag), n_links (total number of links), n_links_v (total number of links containing at least one violent word), %links_v (frequency of links containing at least a violent word), n_img (total number of images), n_img_v (total number of images whose name contains at least a violent word), n_v_img_src (total number of violent words in the attribute src of the img tag), n_v_img_alt (total number of violent words in the attribute alt of the img tag) and %img_v (frequency of the images containing a violent word). We took into serious consideration the construction of this dictionary and, unlike a lot of commercial filtering products, we built a multilingual dictionary.

3.2   Supervised Learning

In the literature, there are several techniques of supervised learning, each having its advantages and disadvantages. But the most important criterion for comparing classification techniques remains the classification accuracy rate. We have also considered another criterion which seems to us very important: the comprehensibility of the learned model. In our approach, we used the graphs of decision tree [7]. In a decision tree, we begin with a learning data set and look for the particular attribute which will produce the best partitioning by maximizing the variation of uncertainty $\Im_\lambda$ between the current partition and the previous one. As $I_\lambda(S_i)$ is a measure of entropy for partition S_i and $I_\lambda(S_{i+1})$ is the measure of entropy of the following partition S_{i+1}. The variation of uncertainty is:

$$\Im_\lambda = I_\lambda(S_i) - I_\lambda(S_{i+1}) \tag{1}$$

For $I_\lambda(S_i)$ we can make use the quadratic entropy (2) or Shannon entropy (3) according to the selected method:

$$I_\lambda(S_i) = \sum_{j=1}^{K} \frac{n_j}{n}(-\sum_{i=1}^{m} \frac{n_{ij}+\lambda}{n_i+m\lambda}(1-\frac{n_{ij}+\lambda}{n_i+m\lambda})) \tag{2}$$

$$I_\lambda(S_i) = \sum_{j=1}^{K} \frac{n_j}{n}(-\sum_{i=1}^{m} \frac{n_{ij}+\lambda}{n_i+m\lambda} \log_2 \frac{n_{ij}+\lambda}{n_i+m\lambda}) \tag{3}$$

Where n_{ij} is the number of elements of class i at the node S_j with $i \in \{c1, c2\}$; n_i is the total number of elements of the class i, $n_i = \sum_{j=1}^{K} n_{nj}$; n_j is the number of elements of the node S_j, $n_j = \sum_{i=1}^{2} n_{ij}$; n is the total number of elements, $n = \sum_{i=1}^{2} n_i$; $m = 2$ is the number of classes (c_1, c_2). λ is a variable controlling effectiveness of graph construction, it penalizes the nodes with insufficient effective.

In our work, four data-mining algorithms including ID3 [8], C4.5 [9], IMPROVED C4.5 [10], SIPINA [11] has been experimented.

3.3   Experiments

We present two series of experiments: in the first, we experimented with four data-mining techniques on the training data set and validate the quality of the learned models using random error rate techniques. Three measures have been used: *global error rate*, *a priori error rate* and *a posteriori error rate*. As global error rate is the complement of classification accuracy rate, while *a priori error rate* (respectively, *a posteriori error rate*) is the complement of the classical *recall rate* (respectively, *precision rate*). Figure 1 presents the obtained results by the four algorithms on the training data set. It shows that the best algorithm is SIPINA. These results can be explained by the fact that this algorithm tries to reduce the disadvantages of the arborescent methods (C4.5, Improved C4.5, ID3) on the one hand by the introduction of fusion operation and on the other

hand by the use of a measurement sensitive to effective. A good decision tree obtained by a data mining algorithm from the learning data set should not only produce classification performance on data already seen but also on unseen data as well. In the second experiments, in order to ensure the performance stability of our learned models from the learning data, we thus also tested the learned models on our test data set consisting of 300 Web sites from which 150 are violent. As we can see in the figure 2, all of four data-mining algorithms echoed
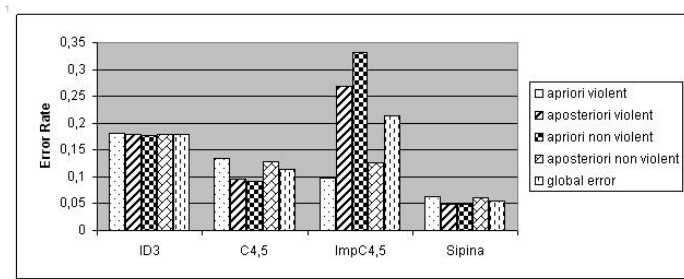
Fig. 1. Experimental results by the four algorithms on training data set

very similar performance. The strategy we choose consists on using the model which ensures a better compromise between the *recall* and the *precision*. For instance, when SIPINA displayed the best performance (taking into account both obtained results), we choose it as the best algorithm.
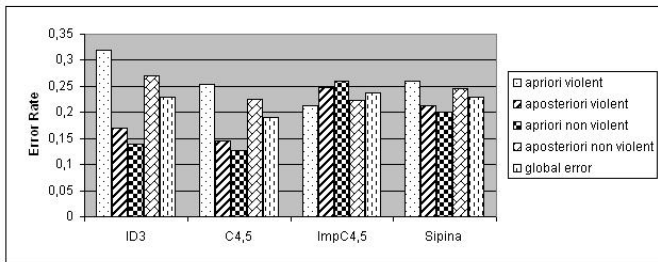
Fig. 2. Experimental results by the four algorithms on test data set

4   Classifier Combination

As shown figure 1 and figure 2, the four data-mining algorithms (ID3, C4.5, SIP-INA and Improved C4.5) displayed different performances on the various error rate. Although SIPINA gives the best results, Combining algorithms may provide better results. In our work, we experiment two combining classifier methods:

1. Majority voting: The page is considered violent if the majority of classifiers (SIPINA, C4.5, Improved C4.5, ID3) considered it as violent and in case of conflict votes, we consider the decision of SIPINA.
2. Scores Combination: we thus affect a weight associated to the score classification decision data-mining algorithm according to the formula (4):

$$Score_{page} = \sum_{i=1}^{4} \alpha_i S_i \tag{4}$$

Where S_i presents the score to be a violent web page according to $i - th$ data-mining algorithm ($i = 1 \ldots 4$). α_i presents the believe value we accord to the algorithm i. The score is calculated for each algorithm as follows: having the decision tree, we seek for each page the node that corresponds to the values of its characteristics vector. Once found the score is calculated as the ratio of pages judged as violent between S_i and S_{i+1}. The page is judged as violent if its score is greater than 0,5.

Figure 3 presents a comparison between the SIPINA predict model, the majority voting model and scores combination model on the test data set. The obtained
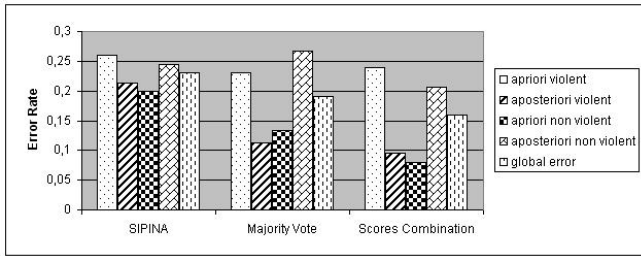
Fig. 3. Comparaison SIPINA model with combination approaches on test data set

results confirm the well interest to use the combining classifiers. Indeed, both majority voting and scores combination approaches provide better results than SIPINA. One clearly sees the reduction in the global error rate of 0.23 for SIPINA predict model to 0.19 by the majority voting and to 0.16 by the scores combination approach.

5   "WebAngels Filter" Tool

5.1   Architecture

The classifiers combination scores is used to propose an efficient violent Web filtering named "WebAngels filter" (figure 4). When a URL is launched, it carries out the following actions: (1) Block the Web page if the site is recorded on

the "black list" else load its HTML code source, (2) Analyze the textual and structural information code, (3) Decide if the access to the Web page is denied or allowed, (4) Update the black list, (5) Update the history of navigation, (6) Block the page if it is judged as violent.
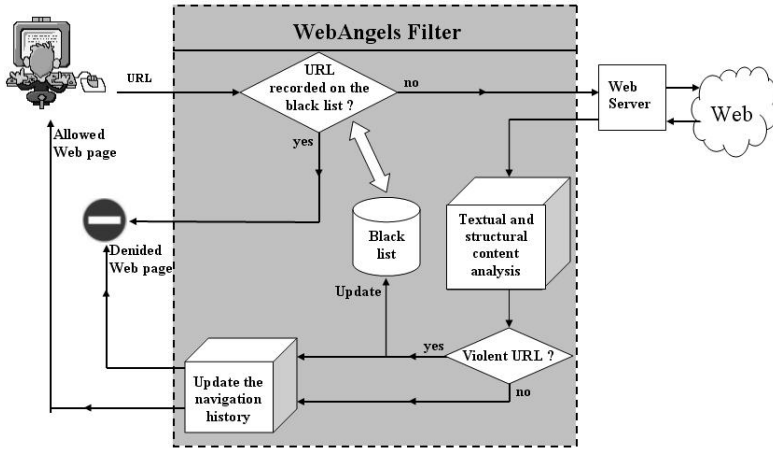
Fig. 4. "WebAngels filter" Architecture
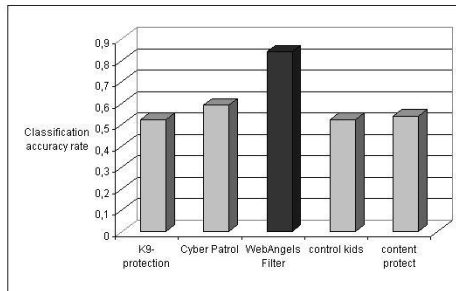
Fig. 5. Classification accuracy rate of "WebAngels filter" compared to some products

5.2 Comparison with Others Products

To evaluate our violent Web filtering tool, we carry out an experiment which compares, on the test data set , "WebAngels filter" with four litigious content detection and filtering systems, knowing, control kids[2] , content protect[3] , k9-webprotection[4] and Cyber patrol[5]. these tools were been parametric to filter violent Web Content.

[2] http://www.controlkids.com/fr
[3] http://www.contentwatch.com
[4] http://www.k9webprotection.com
[5] http://www.cyberpatrol.com

Figure 5 further highlights the performance of "WebAngels filter" compared to other violent content detection and filtering systems.

6   Conclusion

In this paper, we studied and highlighted a combination of several violent web classifiers based on a textual and structural content-based analysis for improving Web filtering through our tool "WebAngels filter". Our experimental evaluation shows the effectiveness of our approach in such systems. However, many future work directions can be considered. Actually, the elaboration of an indicative keywords vocabulary which play a big role in the improvement of the tool performances was manual, and a laborious automatic elaboration of this vocabulary can be one of the directions of our future work. Also, we must think to integrate the treatment of the visual content in the predict models in order to cure the difficulties in classifying violent Web sites which includes only images.

References

1. Caulkins, J.-P., Ding, W., Duncan, G., Krishnan, R., Nyberg, E.: A Method for Managing Access to Web Pages: Filtering by Statistical Classification (FSC) Applied to Text. Decision Support Systems (To apear)
2. Lee, P.Y., Hui,S.C., Fong, A.C.M.: Neural Networks for Web Content Filtering.IEEE Intelligent Systems (2002) 48–57
3. Ho, W.H., Watters, P.A.: Statistical and structural approaches to filtering Internet pornography.IEEE Conference on Systems, Man and Cybernetics (2004) 4792–4798
4. Arentz, W.-A.,Olstad, B.: Classifying offensive sites based on image content. Computer Vision and Image Understanding. Vol. 94. (2004) 295–310
5. Hammami, M.,Chahir, Y.,Chen, L.: A Web Filtering Engine Combining Textual, Structural, and Visual Content-Based Analysis.IEEE Transactions on Knowledge and Data Engineering (2006) 272–284
6. Fayyad, U., PIATETSKY-SHAPIRO, G., SMYTH, P.: The KDD process for extracting useful knowledge from volumes data. Communication of the ACM (1996) 27–34
7. Zighed, D.A., Rakotomalala, R.: Graphes d'Induction - Apprentissage et Data Mining. Hermes (2000)
8. Quinlan, J. R.:Induction of Decision Trees. Machine Learning. Induction of Decision Trees (1986) 81–106
9. Quinlan, J. R.:C4.5: Programs for Machine Learning.Morgan Kaufmann (1993)
10. Rakotomalala, R., Lallich, S.:Handling noise with generalized entropy of type beta in induction graphs algorithm. nternational Conference on Computer Science and Informatics (1998) 25–27
11. Zighed, D.A, Rakotomalala, R.:A method for non arborescent induction graphs. Technical report(1996).Loboratory ERIC, University of Lyon 2

Using WordNet to Disambiguate Word Senses for Text Classification

Ying Liu[1], Peter Scheuermann[2], Xingsen Li[1], and Xingquan Zhu[1]

[1] Data Technology and Knowledge Economy Research Center, Chinese Academy of Sciences
Graduate University of Chinese Academy of Sciences
100080, Beijing, China
`yingliu@gucas.ac.cn, lixingsen@126.com, xqzhu@cse.fau.edu`
[2] Department of Electrical and Computer Engineering
Northwestern University, Evanston, Illinois, USA, 60208
`peters@ece.northwestern.edu`

Abstract. In this paper, we propose an automatic text classification method based on word sense disambiguation. We use "hood" algorithm to remove the word ambiguity so that each word is replaced by its sense in the context. The nearest ancestors of the senses of all the non-stopwords in a give document are selected as the classes for the given document. We apply our algorithm to Brown Corpus. The effectiveness is evaluated by comparing the classification results with the classification results using manual disambiguation offered by Princeton University.

Keywords: disambiguation, word sense, text classification, WordNet.

1 Introduction

Text classification aims at automatically assigning a document to a pre-defined topic category. A number of machine learning algorithms have been investigated for text classification, such as K-Nearest Neighbor (KNN) [1], Centroid Classifier [2], Naïve Bayes [3], Decision Trees [4], Support Vector Machines (SVM) [4]. In such classifiers, each document is represented by a n-dimensional vector in a feature space, where each feature is a keyword in the given document. Then traditional classification algorithms can be applied to generate a classification model. To classify an unseen document, a feature vector is constructed by using the same set of n features and then passed to the model as the input. These methods suffer from the nature of text documents [6]. It is not feasible to organize a document into a fixed set of features because most text documents are semi-structured or completely not structured. An alternative type of approaches, keyword-based association analysis, has been proposed in [13,14,15]. Such classifiers proceed as follows: firstly, keywords and terms are extracted; secondly, concept hierarchies of keywords and terms are obtained by using WordNet, or expert knowledge, or some keyword classification systems. Documents in the training set can be classified into class hierarchies. A term association mining method is proposed to discover sets of associated terms that can be

used to distinguish one class from others. It derives a set of association rules associated with each document class. Such rules can be used to classify new documents.

However, word ambiguity is a severe problem in the keywords-based methods. For example, if 'bat' occurs several times in a document, should the file be classified to "sport" or "mammal"? A number of computer engineers tried to retrieve articles about "board", but a large number of Web pages about "board game" or "message board" were retrieved. Each word may have multiple senses (meanings), and multiple words may have the same sense. It is not trivial for a computer to know which sense the keyword is using in a given context. Extensive research has been done in word sense disambiguation [5,16,17,18]. However, to the best of our knowledge, disambiguation research is focused in retrieval or in query, not for text classification.

In this paper, we propose a text classification method based on sense disambiguation. In order to define an appropriate mid-level category for each sense, hood [5] is implemented on WordNet. Each keyword in a given document is mapped to the concept hierarchy where each sense maintains a counter. The hoods and the associated counters determine the intended sense of a given ambiguous word. Thirdly, the ancestors of the synsets of all the keywords are selected as the classes of a given document. We apply this algorithm to Brown Corpus. The effectiveness of our automatic text classification method is evaluated by comparing the classification results with the classification results using manual disambiguation offered by Princeton University.

The rest of this paper is organized as follows. Section 2 overviews the related work. Section 3 introduces WordNet. In Section 4, we present the sense disambiguation-based text classification algorithm. Section 5 presents our experiment results and discussion. We summarize our work in Section 6.

2   Related Work

Knowledge-based. In this category, disambiguation is carried out by using information from an explicit lexicon or knowledge base. The lexicon may be a machine readable dictionary, thesaurus or hand-crafted. [9,10,5] use WordNet as the knowledge base to disambiguate word senses, and [11] uses Roget's International Thesaurus.

Corpus-based. This category of approaches attempt to disambiguate words by using information gained from training on some corpus, rather than taking it directly from an explicit knowledge source [8]. Training can be carried out either on a disambiguated corpus or a raw corpus. In a disambiguated corpus, the semantics of each polysemous lexical item has been marked, while in a raw corpus, the semantics has not been marked yet.

Hybrid Approaches. A good example is Luk's system [12] which uses the textual definitions of senses from a machine readable dictionary to identify relations between senses. It then uses a corpus to calculate mutual information scores between the related senses in order to discover the most useful information. In this way, the amount of text needed in the training corpus is reduced.

3 WordNet

WordNet is a manually-constructed lexical system developed by George Miller at the Cognitive Science Laboratory at Princeton University [7]. It reflects how human beings organize their lexical memories. The basic building block of WordNet is synset consisting of all the words that express a given concept. Synsets, which senses are manually classified into, denote synonym sets. Within each synset, the senses, although from different keywords, denote the same meaning. For example, "*board*" has several senses, so does "*plank*". Both of them have a common sense "a stout
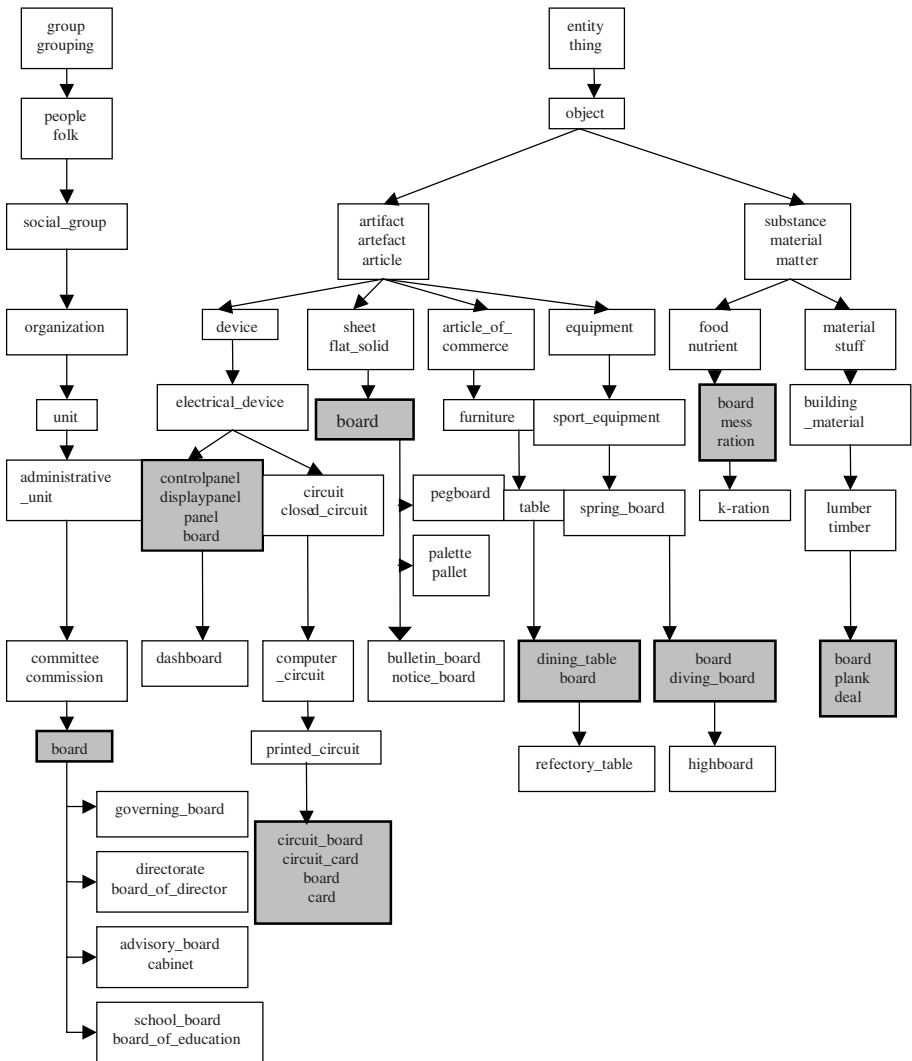
Fig. 1. The IS-A hierarchy for eight different senses of the noun "board"

length of sawn timber, made in a wide variety of sizes and used for many purposes". Thus, "*plank*" and "*board*" are synonymous in terms of this specific sense and form one synset. Because all synonymous senses are grouped into one synset and all different senses of the same word are separated into different synsets, there is no synonymous or polysemous synset separated into different synsets, there is no synonymous or polysemous synset. Hence, WordNet is a concept-based dictionary where every synset represents a lexicalized concept. WordNet consists of four divisions, nouns, verbs, adjectives and adverbs division. Within a division, synsets are organized by the lexical relations defined on them. We only use the noun division of WordNet in this study due to the page limitation. We use two lexical relations in the noun division, "IS-A" and "PART-OF".
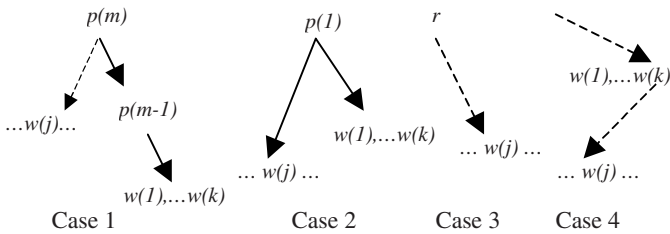
Fig. 2. Root of hoods of synset *s*

Figure 1 shows the hierarchy relating to the eight different senses of noun "*board*". The synsets with the heavy boundary are the actual senses of "*board*", and the remaining synsets are either ancestors or descendents of the senses. The synsets {*group, grouping*} and {*entity, thing*} are examples of heads of the hierarchies. WordNet 1.6 (2000) contains 94473 words and 116314 senses in the noun division. It is used as the framework of our proposed hierarchical text classification method.

4   Word Sense Disambiguation and Text Classification

In this section, we first present our implementation of "hood" proposed in [5] on WordNet. Hood is based on the idea that a set of words co-occurring in a document will determine the appropriate senses for one another word despite each individual word being multiply ambiguous. A common example of this effect is the set of nouns base, bat, glove and hit. Although each of them has several senses, when taken together, the intent is baseball game, clearly. To exploit this idea automatically, a set of categories representing the different senses of words needs to be defined. A counter is maintained in each category, which counts the number of words that have its associated senses. The sense of an ambiguous word is determined by the category with the largest counter. Then, the nearest ancestors of the senses of all the non-stopwords are selected as the classes of a given document.

4.1   Hood Construction

Using each separate hierarchy as a category is well defined but too coarse grained. For example, in Figure 1, 7 of 8 senses of "*board*" are in the {*entity, thing*} hierarchy.

Therefore, *hood* is intended to define an appropriate middle level category. To define the hood of a given synset, *s*, consider the synsets and the hyponymy links in WordNet as vertices and directed edges of a graph. Then, the hood of *s* is defined as the largest connected subgraph that contains *s*, containing only descendents of an ancestor of *s*, and containing no synset that has a descendent that includes another instance of a member of *s* as a member. A hood is represented by the root of the hood. Figure 2 illustrates the definition of hood, assuming synset *s* consists of *k* words w_1, w_2, $w_3...w_k$, and p_1, p_2, $p_3...p_n$ are *n* ancestors of *s*, where p_m is a father of p_{m-1}. p_m ($1 \leq m \leq n$) has a descendent synset which also includes w_j ($1 \leq j \leq k$) as a member. So, p_{m-1} is one of the roots of the hoods of *s*, as shown in Case 1. If *m* is 1, *s* itself is the root, shown in Case 2. If no such *m* is found, the root of WordNet hierarchy, *r,* is the root of the hood of *s*, as shown in Case 3. If *s* itself has a descendent synset that includes w_j as a member, there is no hood in WordNet for *s*, as shown in Case 4. Because some synsets have more than one parents, synsets can have more than one hoods. A synset has no hood if the same word is a member of both the synset and one of its descendents. For example, in Figure 1 the hood of synset "*committee sense*" of "*board*" is rooted at synset {*group, grouping*} (and thus the hood for that sense is the entire hierarchy where it occurs) because no other synset containing "*board*" in this hierarchy (case 3); the hood of "*circuit_board*" sense of "*board*" is rooted at {*circuit, closed_circuit*} because synset {*electrical_device*} has a descendent {*control_panel, display_panel, panel, board*} containing "*board*" (case 1), and the hood of "*panel*" sense of "*board*" is rooted at the synset itself because its direct parent {*electrical_device*} has a descendent synset {*circuit_board, circuit_card, board, card*} containing "*board*" (Case 2).

4.2   Word Sense Disambiguation

After the hoods for each synset in WordNet are constructed, they can be used to select the sense of an ambiguous word in a given text-document. The senses of the nouns in a text document in a given document collection are selected by using the following two-step process. A procedure, called *marking (w),* is fundamental to both of the steps. *Marking (w)* visits synsets and maintains a counter for each synset, which is increased by 1 whenever the synset is visited. Given a word *w*, what *marking (w)* does is to find all instances of *w* in WordNet, and then, for each identified synset *s*, follow the parent-child links up to the root of the hierarchy while incrementing the counter of each synset it visits. The first step of the two-step process is collection-oriented, that is, *marking (w)* is called for each occurrence of *w* in all the documents in the collection. The number of times *marking (w)* is called for each *w* is maintained by some counters. The first step produces a set of global counts (relative to this particular collection) at each synset. The second step is document-oriented, that is, *marking (w)* is called for each occurrence of *w* in an individual text document. Again the number of times *marking (w)* is called is maintained for the given individual document. The second step produces a set of local counts at the each synset. Given the local and global counts, a sense for a given ambiguous word *w* contained within a particular document is selected as follows:

$$difference = \frac{\# local\_visits}{\# local\_calls} - \frac{\# global\_visits}{\# global\_calls}$$

Difference is computed at the root of the hood for each sense of *w*. If a sense does not have a hood or if the local count at its hood root is less than 2, difference is set to 0. If a sense has multiple hoods, difference is set to the largest difference over the set of hoods. The sense corresponding to the hood root with the largest positive difference is selected as the sense of the word in the document. If no sense has a positive difference, no WordNet sense is chosen for this word.

The idea behind the disambiguation process is to select senses from the areas of the WordNet hierarchies where document-induced (local) activity is greater than the expected (global) activity. The hood construct is designed to provide a point of comparison that is broad enough to encompass markings from several different words yet narrow enough to distinguish among senses.

4.3 Text Document Classification

Assume that every word in each text document in a collection has been replaced by its senses after word sense disambiguation. In the classification phase, we actually work on senses of each word. The psuedo code is in Figure 3.

Procedure Classify (*t*: a text document)

For each *sense* of the words in *t* do
Locate the synset *s* in the hierarchy   //Find the synset *s* by searching the hierarchy
Mark *s*
End
Find the parents *p* of all the marked *s*   // Find the parents of all the marked synsets by
                                                            following the parent-child links in the
                                                            hierarchy
Return (*p*)

Fig. 3. Psuedo code of sense-based text classification

The advantages of our sense-based text classification algorithms are below:
1) The confusion incurred by ambiguation is reduced. All the keywords in a document help to determine the real sense in the context.
2) The class a given document classified into is all determined by itself, not disturbed by any user bias.
3) Since WordNet is an e-dictionary, the hierarchy of WordNet is easy to update. Therefore, the classes of all the documents are easy to update.
4) Each document may be classified in multiple classes.

5 Experimental Results

In our experiment, we use the part-of-speech tagged Brown Corpus. It consists of 1,014,312 words of running text of edited English prose printed in the United States during the calendar year 1961. This document set consists of 479 tagged documents. Each word is tagged with its certain linguistic category. It has been extensively used for natural language processing work. While the words in each grammatical class are used with a particular purpose, it can be argued that most of the semantics is carried

by noun words. Thus, nouns can be taken out through the elimination of verbs, adjectives, adverbs, connectives, articles and pronouns.

5.1   Flow of Experiment

Stemming. Stemming is a technique for reducing words to their grammatical roots. A stem is the portion of a word which is left after the removal of its affixes (i.e., prefixes and suffixes). A typical example of a stem is the word "*connect*" which is the stem for variants *connected, connecting, connection, and connections*. Stems are thought to be useful because they reduce variants of the same root word to a common concept.

Removing stopwords. Words which are too frequent among the documents are not good discriminators. In fact, a word which occurs in 80% of the documents in the document collection is useless for purpose of retrieval or classification. Such words are frequently referred to as stopwords and should be filtered out. Articles, prepositions and conjunctions are candidates for a list of stopwords, such as "an", "against", "and".

5.2   Experimental Result Analysis

We randomly choose 50 documents to classify. Since WordNet provides semantically tagged Brown Corpus files, we compare our results with the manually identified results. The accuracy rate of classification is 32%.

In order to find out the reason for the low classification accuracy, we investigate the effectiveness of word sense disambiguation of the 50 documents. Experimental results are shown in Table 1. Hit Rate is also defined.

$$Hit\_Rate = \frac{\#of\_words\_that\_are\_selected\_the\_same\_synset\_as\_manually\_identified}{\#\_of\_words\_in\_the\_stemmed\_file}$$

Table 1. Hit Rate of word sense disambiguation on Brown Corpus

Hit Rate	<15%	15%-20%	20%-25%	25%-30%	30%-35%	>40%
# docs getting the hit rate	1	7	12	16	14	0

From Table 1, we can see that the hit rate of word sense disambiguation is not as optimistic as expected. Most rates are between 15% and 35%. Therefore, the low hit rate resulted in the low classification accuracy of text documents.

Discussion

The reasons of the low hit rate of word sense disambiguation are as follows:

1) Although most of the semantics is carried by the noun words, verbs, adjectives, adverbs are important factors that can help determine appropriate senses for an ambiguous word. In order to improve the hit rate, WordNet for verbs, adjectives, adverbs cannot be ignored in further studies.

2) One word is possible to be used multiple times in one document, while each appearance may use different sense. In the current algorithm, multiple occurrences of

each word are ignored, and each word is mapped to a unique sense. Actually, an appropriate weight should be assigned to each non-stopword.

3) Part-of-speech tagger used for Brown Corpus separates words connected with underscore, such as school_board, which is an individual word while it is separated into two words "school" and "board" by the tagger. Thus, the sense of school or board will never hit the manually identified word sense of school_board. Therefore, it is also one of the factors that influence the accuracy.

6   Conclusions and Future Work

In this paper, we proposed a text classification method based on word sense disambiguation. In order to define an appropriate mid-level category for each sense, hood [5] was implemented on WordNet. Then, each non-stopword in a given document was mapped to the concept hierarchy where each synset maintains a counter. The hoods and the associated counters determined the intended sense of the ambiguous word. The nearest ancestors of the senses of all the non-stopwords were selected as the classes of a given document. We applied this algorithm to Brown Corpus. The effectiveness of our text classification method is evaluated by comparing the classification results with the classification results using manual disambiguation offered by Princeton University. We also discussed the weakness of our algorithm.

Our proposed sense-based text classification algorithm is an automatic technique to disambiguate word senses and then classify text documents. If this automatic technique can be applied in real applications, the classification of e-documents must be accelerated dramatically. It must be a great contribution to the management system of Web pages, e-books, digital libraries, etc.

In our future research, we will focus on the following aspects: 1) Build relational databases for verbs, adjectives, adverbs divisions of WordNet. Then, for each document, mapping all the non-stopwords including nouns, verbs, adjectives, adverbs to their senses. 2) Assign each non-stopword a weight which indicates its significance in a given document. For example, weight can be defined as the number of occurrence in a synset.

References

1. Yang, Y., Lin, X.: A re-examination of text categorization methods. SIGIR (1999) 42-49
2. Han, E., Karypis, G.: Centroid-Based Document Classification Analysis & Experimental Result. PKDD (2000)
3. McCallum, A., Nigam, K.: A Comparison of Event Models for Naïve Bayes Text Classification. AAAI/ICML, Workshop on Learning for Text Categorization (1998)
4. Sebastiani, F.: Machine learning in automated text categorization. ACM Computing Surveys. (2002) 34(1): 1-47

5. Voorhees, E.: Using WordNet to Disambiguate Word Senses for Text Retrieval. SIGIR (1993) 171-180
6. Wu, H., Phang, T., Liu, B., Li, X.: A Refinement Approach to Handling Model Misfit in Text Categorization. SIGKDD (2002) 207-216
7. Miller, G.: Special Issue, WordNet: An on-line lexical database. International Journal of Lexicography, 3(4) (1990)
8. Brown, P., Pietra, S., Pietra, V., Mercer, R.: Word sense disambiguation using statistical methods. Proc. of the 29th Meeting of the Association for Computational Linguistics (ACL-91), Berkley, C.A. (1991) 264-270
9. Agirre, E., Rigau, G.: Word sense disambiguation using conceptual density. Proc. of COLING (1996)
10. Richardson, R., Smeaton, A.: Using wordnet in a knowledge-based approach to information retrieval. Proc. of the BCS-IRSG Colloquium, Crewe (1995)
11. Yarowsky, D.: Word-sense disambiguation using statistical models of Roget's categories trained on large corpora. Proc. of the 14th International Conference on Computational Linguistics (COLING-92), Nantes, France (1992) 454-460
12. Luk, A.: Statistical sense disambiguation with relatively small corpora using dictionary definitions. Proc. of the 33rd Meetings of the Association for Computational Linguistics (ACL-95), Cambridge, M.A. (1995) 181-188
13. Feldman, R., Hirsh, H.: Finding associations in collections of text. Machine Learning and Data Mining: Methods and Applications, New York: John Wiley & Sons (1998) 223-240
14. Wang, K., Zhou, S., Liew, S.: Building hierarchical classification using class proximity. Proc. of Intl. Conf. Very Large Data Bases (1999) 363-374
15. Chakrabarti, S., Dom, B., Indyk, P.: Enhanced hypertext classification using hyper-links. Proc. of Intl. Conf. SIGMOD (1998) 307-318
16. Cowie, J., Guthrie, J., Guthrie, L.: Lexical disambiguation using simulated annealing. Proc. of COLING Conf. (1992) 359-365
17. Demetriou, GC.: Lexical disambiguation using constraint handling in Prolog (CHIP). Proc. of the European Chapter of the ACL, 6(1993) 431-436
18. Church, KW.: Using bilingual materials to develop word sense disambiguation methods. Proc. of ACM SIGIR Conference (1992) 315-350

Construction of Ontology-Based Software Repositories by Text Mining

Yan Wu, Harvey Siy, Mansour Zand, and Victor Winter

College of Information Science and Technology,
University of Nebraska at Omaha,
Omaha, Nebraska 68182, USA
{ywu,hsiy,mzand,vwinter}@mail.unomaha.edu

Abstract. Software document repositories store artifacts produced in the course of developing software products. But most repositories are simply archives of documents. It is not unusual to find projects where different software artifacts are scattered in unrelated repositories with varying levels of granularity and without a centralized management system. This makes the information available in existing repositories difficult to reuse. In this paper, a methodology for constructing an ontology-based repository of reusable knowledge is presented. The information in the repository is extracted from specification documents using text mining. Ontologies are used to guide the extraction process and organize the extracted information. The methodology is being used to develop a repository of recurring and crosscutting aspects in software specification documents.

Keywords: Software Repository, Early Aspects, Text Mining, Ontology.

1 Introduction

Efficient reuse requires software artifacts to be stored, presented and organized in such a way that makes them easy to retrieve and use. Potentially reusable artifacts include code (ranging in size from modules to applications), project documents, test cases, software architecture, design patterns, etc. Most existing software repositories are nothing more than archival storage of documents. In order to facilitate the storage and retrieval of reusable assets, the information in existing repositories need to be structured in a way that takes into account the meaning (semantics) of the documents.

In this paper, a framework to construct a searchable repository of crosscutting aspects in software specification documents is presented. The organization of this paper is as follows: Section 2 introduces the problem and existing techniques. Section 3 is the description of the framework that represents the structure and processes in constructing and retrieving, utilizing the early aspects repositories with the aid of other relevant technologies and some guidelines on how to realize this framework. Section 4 provides conclusions and discusses ongoing and future work.

2   Background

2.1   Software Repositories

Due to the effort and cost of developing new software, it is desirable to reuse existing artifacts from previous software development efforts [1]. Software repositories provide a potential source of reusable artifacts. Software repositories store artifacts used in the analysis, design, implementation, testing and maintenance of software systems. They provide mechanisms to organize and retrieve required artifacts.

A repository may store artifacts that belong to one project, or to several projects within a given application domain. We are interested in constructing domain-level repositories that use domain knowledge to organize and manage artifacts. Creating domain-specific repositories is a crucial factor for successful reuse of artifacts [2]. However, most artifacts are stored in scattered project-level repositories, which often contain overlapping information. Although the existence of scattered overlapping software repositories allows each repository to tailor its content and service [3], they are inefficient when searching for reusable artifacts.

Aside from scattered and overlapping repositories, a cursory examination of existing public software repositories uncovered several other problems. These include the the lack of systematic design of the software repository management system (especially for the representation model for the artifacts) and inadequate search and retrieval mechanisms.

2.2   Text Mining and Ontologies

Text Mining [4] focuses on the discovery of new or previously unknown information by automatically extracting information from different written resources. A key element is the integration of the extracted information to form new facts or new hypotheses to be explored further by conventional experimentation.

Ontology is a concept from philosophy for understanding reality. To explain simply, an ontology consists of concepts and the relationships between them.

We propose the application of text mining for clustering artifacts into domain-specific groups and for retrieving concepts and relationships from the groups of artifacts to construct ontologies to organize the structure of software repositories. It can also be applied to extract users search patterns.

2.3   Related Work

There are many techniques and tools for organizing reusable repositories. Most of them are geared towards code reuse. Among the ones that work with unstructured documents, we focus on several techniques based on text mining to construct ontologies for representing and classifying knowledge from these documents.

Seeling, et al. use text mining combined with metadata-based information brokering to discover and analyze metadata from weakly structured text documents

[5]. This approach uses a tool called DocMINER to cluster similar documents. Jiang, et al. constructed a system called Concept Relation Concept Tuple based Ontology Learning (CRCTOL) to mine semantic knowledge to construct ontology from domain-specific documents [6]. The ontology is constructed through natural language processing, where parsed text is analyzed using statistical and lexico-syntactic methods to accurately identify key concepts and semantic relationships.

3   A Framework for Constructing Ontology-Based Repositories Using Text Mining

In this section, the proposed framework and guidelines for constructing a domain-specific repository is presented. While the proposal can be applied to construct repositories for any artifact, we illustrate its use in creating repositories of specification documents and focus on the retrieval of *early aspects* from these documents.

Early aspects are crosscutting concerns identified in the early stage of software development such as requirement specifications and architecture [7]. The identification of these aspects enables them to be modularized. This makes specifications and architectures more maintainable through localizing changes. It also enables downstream activities such as design and implementation to localize components related to certain concerns.

The goal of early aspect repositories is to construct a flexible and maintainable repository that reflects current understanding of aspect oriented software development (AOSD), and to use this knowledge to predict and plan for future AOSD projects. Previous research in early aspects repositories mostly focus on the development of technologies and tools to support mining knowledge from them. Here we focus on the retrieval and reuse of early aspects stored in the repositories. A proposed framework is shown in Figure 1.

The intention of constructing this framework was to provide a knowledge base to help developers define and locate early aspects effectively and efficiently so that in future AOSD projects, crosscutting concerns can be identified as early as possible. And when developers analyze future requirements in certain domains, this knowledge base can provide clues to identify the possible aspects.

The rest of this section describes the framework. The input into this process is a collection of software requirements specification documents from different application domains.

Clustering stage divides requirement specifications collected from different software repositories into domain-specific groups. Beck et al. provides a useful tool named DocMINER (Document Maps for Information Elicitation and Retrieval) which produces a document map to represent the inter-document similarity for a document corpus [8]. In this research, domain-specific terms that appear in the requirements specifications are the links among them for the same domain. The important issue is that the classification according to the similarity largely depends on the quality of the requirements specifications. Large amount
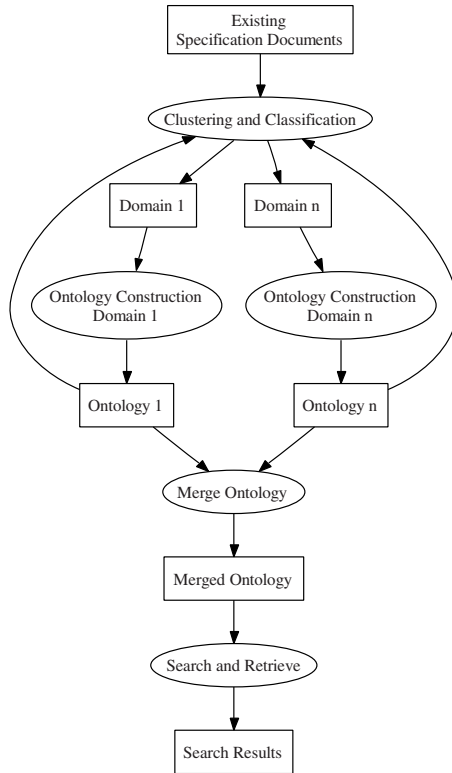
Fig. 1. Framework to manage and retrieve early aspects from requirements specification

of semantically domain rich terms can help differentiate the requirements clearly. The richer, the better, but at the same time the exactness and accuracy are important too. The other issue is that in the clustering process, a fuzzy cluster with some overlap will be a better choice than the exact cluster result.

Ontology construction is guided by domain experts. An ontology is constructed by defining concepts, properties, relationships, instances and axioms for a given domain. With ontology editors, domain experts can organize the domain knowledge and relationships well based on their knowledge. Morshed et al. concluded that in the three ontology construction tools they investigated, Protégé can be used to construct small-sized ontologies and OntoEdit, with its full functionality, can be used to develop medium to large-sized ontologies. Metis is good for enterprise architecture modeling [9].

Ontology construction consist of the following basic activities: first, the concepts, properties and relationships of any candidate early aspects from requirements specifications in a domain are identified using information retrieval

techniques with the help of domain experts; then a hierarchy is constructed to abstract the commonalities from clusters of similar early aspects into classes and subclasses. The commonalities, variabilities and relationships between different classes become the properties of the classes; then the concrete early aspects are represented by instances that belong to specific classes. Existing early aspects ontologies can also be added into this framework.

To construct ontologies that support the organization of early aspects repository, redundancy and overlap are necessary. As in the clustering activity, there will always be early aspects that cannot be clearly clustered into only one domain. For example, a security requirement can appear in different areas such as bank system, website design and so on. They have their own features but commonalities make them share information in the ontology construction. Hence, an aspect can be classified in several domains. This redudancy has the further advantage of being able to describe the aspect from different perspectives.

The constructed ontologies can be **merged** together. There can be intermediate ontologies between the upper ontologies such as SUMO and the low level domain-specific ontologies [10]. And for future use, concepts and relationships stored in the merged ontology and initial ontologies can be regarded as dictionaries to aid the clustering stage in a supervised manner. Subsequent clustering activities can improve their accuracy with the help of existing ontologies. Ontology is increasingly important in domain engineering with the development of domain analysis and design. The features of ontology such as the structure of knowledge and efficient retrieval are potentially useful in domain engineering.

The **search and retrieval interface** is designed to communicate with users to help them retrieve required early aspects from the merged early aspects repositories. According to the mismatch between the user's mental model and the system data model, a supervised retrieval method is recommended. There are ontology query languages such as HP's SPAQL for Jena which potentially can be the backbone of the search and retrieval interface. In addition to exact attribute match or wildcard match, natural language processing ability is a potentially useful aid for users to identify their real meanings. User usually cannot describe what they need exactly, so the search criteria should be allowed to have imprecision. These search criteria can be processed through natural language understanding to provide the alternative artifacts to choose. Even for the novices, a wizard that guides them to narrow down the requirement will be helpful.

3.1   Evolving and Refining the Repository

The basic framework presented can be extended in several ways in order to refine the ontologies in the repository.

Term addition. In practice, the mental model of the user will be different from that of the domain expert who designed the repository. This leads to a disparity between the user's understanding and the way the ontologies are organized. This makes it difficult for the user to retrieve the relevant early aspect. One solution is to allow users to evolve the ontology by adding their own concepts and terms. This had been applied in earlier reuse repositories such as [11]. This

is based on the idea that as programmers gain experience, their understanding of the knowledge in a particular domain gravitates toward a common structure [12]. The users will try their own keywords and feature descriptions to search for required early aspects, sometimes their words just do not fit the searchable terms that system defined but still useful to describe and locate the early aspects and could be more suitable for user's mental model.

Users are not domain experts, but from the perspective of system usage, users are people who really utilize the system to fit for their own requirement. Further, domain experts can make mistakes in identification of concepts and relationships among them. The other motivation for this stage is that the environment is dynamically changing and the terms and their relationships are changing. So the idea that let users to help us maintain the ontology structure is practical and useful. To get this capability, a database that records the usage scenarios of users is needed. User-defined terms and descriptions are emphasized and collected, analyzed to identify the suitable ones that could be added to the defined structures of existing ontology. The results are evaluated by the domain experts to decide whether or not revise the structure of the ontology to reflect the user's attitude and terms. A Bellcore study of people choosing terms to describe objects revealed that the probability of two people choosing the same keyword for these objects is between 10 and 20%, using 15 aliases will achieve 60-80% agreement, and 30 aliases can get up to 90% agreement [13]. Then revised ontologies with redundancy are used to facilitate the artifacts retrieval. This is an evolving process to help the system continuously improve performance and accuracy.

Trend detection. At the same time, the collected user terms can be used as the source for identifying the retrieval patterns of users with the help of text mining. The users' search criteria should be collected to construct the patterns of searching. The possible basis for this function is Google Zeitgeist[1] which pulls together search trends and patterns. It accumulates search statistics based on the millions of searches conducted on Google in a given period of time - weekly, monthly, and annually then produces a summary report. The trends and patterns identified in this stage could be used to guide the users' future search activities. Users' search terms will expose the retrieval habits of the users. For example, users who retrieve early aspects with feature set A also retrieve early aspects with feature set B. This kind of information can potentially provide user-specific intelligence to the retrieval stage.

3.2 Issues

Artifact representation. Creating suitable representations of the artifacts is essential to the overall management process. In this paper, the artifacts are early aspects with their containers – requirements specifications which are text documents in nature. But for some of other artifacts, the representation can be an issue. The accuracy and exactness of the representation may eliminate the need for clustering.

---

[1] http://www.google.com/press/zeitgeist.html

Repository structure. A scalable and credible structure of the software repository will always be the foundation of the whole system and till now it seems that ontologies provide the best choice.

Retrieval technology. Smart retrieval interfaces incorporating term addition and trend detection are good suggestions but there will be trade-offs between simplicity and cost. Also, the space to store the user-specific data will accumulate and could potentially become to the system. Therefore there might be some storage issues as well.

4   Conclusions and Future Work

In this paper, a framework and a series of guidelines for the specific early aspects repository management system with the help of text mining and ontology are provided. Although this is only a high level description of a specific kind of artifact, the benefits are still obvious: to guide the construction and organization of repositories of reusable artifacts which can be easily retrieved. When completed, a unified, standard software repository will greatly assist the domain-specific software system development and reuse process.

Our ongoing work consists of: a further refinement of the framework, an extension of this framework to other kinds of software artifacts, an implementation of this software repositories management system, and, an implementation and further refinement of the guidelines in practice.

Practically, we are working to accomplish the following tasks:

1. Obtain access to the software repositories.
2. Ensure the existence of unified description documents;
3. Ensure the reliability of the collected artifacts;
4. Choose the algorithm to classify the artifacts;
5. The efficiency and accuracy of user-defined terms.

References

1. Li, J.: A survey on reuse: Research fields and challenges (2003) Term paper for DIF8901.
2. Petro, J., Fotta, M., Weisman, D.: Model-based reuse repositories-concepts and experience. In: Proceedings, Seventh International Workshop on Computer-Aided Software Engineering. (July 10-14 1995) 60–69
3. Browne, S., Moore, J.: Reuse library interoperability and the world wide web. In: Proceedings of the 19th International Conference on Software Engineering. (1997) 684–691
4. Hearst, M.:   What is text mining? http://www.sims.berkeley.edu/~hearst/text-mining.html, updated Oct. 17, 2003, accessed Sept. 1, 2006.
5. Seeling, C., Becks, A.: Exploiting metadata for ontology-based visual exploration of weakly structured text documents. In: Proceedings of the Seventh International Conference on Information Visualization (IV'03). (2003)

6. Jiang, X., Tan, A.H.: Mining ontological knowledge from domain-specific text documents. In: Proceedings of the Fifth IEEE International Conference on Data Mining (ICDM'05). (2005)
7. Araújo, J., Baniassad, E., Clements, P., Moreira, A., Rashid, A., Tekinerdoğan, B.: Early aspects: The current landscape. Technical Report CMU-SEI-2005-TN-xxx, Carnegie Mellon University, Pittsburg, PA (2005)
8. Becks, A.: Visual knowledge management with adaptable document maps (2001) GMD research series 15.
9. Murshed, A., Singh, R.: Evaluation and ranking of ontology construction tools. Technical Report DIT-05-013, University of Trento (March 2005)
10. Niles, I., Pease, A.: Towards a standard upper ontology. In: Proceedings of the 2nd International Conference on Formal Ontology in Information Systems (FOIS'01). (Oct. 2001)
11. Henninger, S.: An evolutionary approach to constructing effective software reuse repositories. ACM Transactions on Software Engineering and Methodology **6**(2) (April 1997) 111–140
12. Curtis, B.: Cognitive issues in reusing software artifacts. In Biggerstaff, T., Perlis, A., eds.: Software Reusability, Vol. 2, Applications and Experience. Addison-Wesley, Reading, Mass. (1989) 269–287
13. Furnas, G., Landauer, T., Gomez, L., Dumais, S.: The vocabulary problem in human-system communication. Communications of the ACM **30**(11) (Nov. 1987) 964–971

Estimating the Change of Web Pages*

Sung Jin Kim[1] and Sang Ho Lee[2]

[1] Department of Computer Science, University of California, Los Angeles, USA
sjkim@cs.ucla.edu
[2] School of Computing, Soongsil University, Seoul, Korea
shlee@comp.ssu.ac.kr

Abstract. This paper presents the estimation methods computing the probabilities of how many times web pages are downloaded and modified, respectively, in the future crawls. The methods can make web database administrators avoid unnecessarily requesting undownloadable and unmodified web pages in a page group. We postulate that the change behavior of web pages is strongly related to the past change behavior. We gather the change histories of approximately three million web pages at two-day intervals for 100 days, and estimate the future change behavior of those pages. Our estimation, which was evaluated by actual change behavior of the pages, worked well.

Keywords: web page change estimation and web database administration.

1 Introduction

Many web applications, such as search engines, proxy servers, and so on, usually create web databases (collections of web pages) that enable users to retrieve web pages internally. As web pages on the web change actively, it is important that administrators update web databases effectively. To help administrators establish update policies, a number of researchers [1, 2, 3, 4, 5, 6, 7, 8] investigated the change behavior of web pages.

A good change estimation model certainly can help administrators manage the databases effectively. [2, 3] described the estimation method, based on a Poisson or memoryless process model (which assumes that changes of web pages are independent of the past changes). [1] also proposed the estimation method, using the change histories of web pages and the Poisson model together. [5] did not follow the Poisson process's change assumption, but did use only the change histories of web pages to make the databases keep the minimum number of obsolete pages. The previous researches for the estimation have directed their concern on the effective management of the entire databases and the contents modification of web pages.

In this paper, we describe simple estimation methods that can help administrators manage the set of web pages, which is a subset of the databases. In practice, administrators can divide web databases into a number of page groups in their own

way such as locality, domain, subject, and so on. Our estimation can help administrators manage each of the groups with different update policies on the basis of the aggregated change histories of all the pages in the corresponding group. Our main assumption is that the change behavior of web pages is strongly related to the past one. By the way, the previous studies simply ignored the fact that the downloadable states of web pages can change irregularly. However, we take into account not only the modification issue but also the download issue of web pages. The goal of our estimation is to help administrators avoid unnecessarily requesting undownloadable or unmodified web pages, in the situation where they have to manage the databases composed of many page groups, and where they feel that requests to undownloadable and unmodified pages are wasteful under a limited network bandwidth and a time.

We present the two estimation formulae: $P_{(Y=a,N=b}DR_{Y=c,N=d)}$ and $P_{(Y=a,N=b}DR_{Y=c,N=d)}$. The former denotes the probability that a page that was downloaded a times for $(a+b)$ download attempts will be downloaded c times for $(c+d)$ download attempts. The latter denotes the probability that a page is modified a times for $(a+b)$ successful downloads will be modified c times for $(c+d)$ successful downloads. We also define the two change metrics: the download rates and the modification rates. The download rate represents how consistently a web page is downloaded successfully. The modification rate represents how frequently a web page is modified. When the estimation formulae are used for a web page in a group, the distributions of download rates and modification rates of all the web pages in the group are used for the probability computation.

For the evaluation of our estimation methods, we first divide approximately 3 million web pages detected from 34,000 Korean sites into the two groups, named the famous sites and the random sites. We obtain the distributions of download rates and modification rates for each of the two groups, after monitoring those pages at two-day intervals for 100 days. We estimate the numbers of downloads and modifications of the selected URLs in the future five crawls, using the numbers of successful downloads and modifications in the past five crawls. Finally, the estimation was evaluated with the actual change behavior of the estimated pages. The evaluation results show our estimations work well.

The paper is organized as follows. Besides this introduction, we define the metrics for representing the change behavior of web pages in section 2. We gather the change histories of web pages in section 3. Section 4 presents our estimation methods to predict the change behavior of the web pages. Section 5 contains the closing remarks.

2   Metrics for Representing the Change of Web Pages

In this section, we describe the metrics for measuring the change of web pages in terms of download and modification issues. Fig. 1 represents a simple crawling example, where there are 16 crawls. A hyphen ("-") means that there is no download attempt since the URL is not available at that point. A black circle ("•") means that we fail to download the corresponding web page. The contents of a downloaded page is denoted as a circled character (here, ⓐ, ⓑ, etc.). For example, on the fourth crawl where three pages corresponding to URLs A, C, and D are detected, we download two pages whose contents are ⓓ and Ⓢ, respectively.

URL	Crawl number															
	1	2	3	4	5	6	7	8	9	10	11	12	13	14	15	16
A																
B	-	-	-	-		●		-	●	-	-	-	-	-	-	-
C	-	-			-	●			●	-	●	●	-	-	-	-
D	●		-	●					-		●			-	-	

Fig. 1. Crawling example

Definition 1. *The first detection number* and *the last detection number* are crawl numbers on which a URL (or a web page) is detected first and last, respectively. The *detection rate* of a page is defined as "*the number of detections* / (*the last detection number – the first detection number* + 1)"

For example, the page for URL B is detected on the 5th, 6th, 7th, and 9th crawls. The detection rate of the page is (4/(9-5+1)) = 0.8. Because the URLs with low detection rates are not informative enough to be studied, we should analyze the change behavior of web pages whose detection rates are higher than a given threshold.

Definition 2. The *download rate* of a page is defined as "*the number of successful downloads* / *the number of download requests*". The *download recall* of a page is defined as "*the number of download requests* / *the total number of crawls*". The download rate represents how consistently the corresponding web page has been downloaded. We accept the download rate of a page whose download recall is higher than a given threshold.

For example, the page for URL C is detected eight times, and the page is downloaded on the 3rd, 4th, 7th, and 8th crawls. The download rate is (4/8) = 0.5. Since there are eight attempts to download the page in 16 crawls, the download recall C is (8/16) = 0.5.

Definition 3. Suppose that a page of URL *u* is downloaded on the ith crawl, and that there is at least one download success with URL *u* prior to the ith crawl. The *current content* of the page on the ith crawl is defined as the content of a page that is downloaded on the ith crawl. The *previous content* of the page on the ith crawl is defined as the content of the page that is successfully downloaded latest prior to the ith crawl. If the current and previous contents of the page on the ith crawl are different from each other, the page of URL *u* is defined to be *modified* on the ith crawl.

Definition 4. The *modification rate* of a page is defined as "*the number of modifications* / (*the number of successful downloads* – 1)". The *modification recall* of a page is defined as "(*the number of successful downloads* – 1) / (*the total number of crawls* – 1)". The modification rate represents how frequently a web page changes in terms of the page contents. For the computation of the modification rate, the page should be downloaded at least twice. We accept the modification rate of a page whose modification recall is higher than a given threshold.

For example, the current content of the page for URL D on the 10th crawl is   and the previous content is Ⓥ. The page is modified on the 10th crawl. On the 12th crawl, the current and previous contents are of the same as Ⓦ. We say that the page is not modified on the 12th crawl. The page is downloaded nine times, which implies that eight comparisons take place. The page is modified twice on the 7th and 10th crawls. The modification rate and modification recall are $(2/(9-1)) = 0.25$ and $(8/15) = 0.53$, respectively.

3   Gathering the Change Histories of Web Pages

In this section, we obtain the distribution of download rates and the modification rates for our estimation. We monitored the 34,000 Korean sites at two-day intervals for 100 days (from January to March, 2004). Our robot [9] detected approximately 1.8 million URLs on each crawl and accumulated three million URLs after all 50 crawls. We regard each of those URLs as representing an individual web page. We grouped the monitored sites into the set of 4,000 famous sites and the set of 30,000 random sites in our own way. We gathered two kinds of change history sets: one for pages in the famous sites and the other for pages in the random sites. Because we visited a site every other day, we do not know if a page changes multiple times between our visiting intervals.

Table 1 shows the distribution of the download rates (DR) for the accumulated URLs satisfying the condition that the download recall is at least 0.2 and the detection rate is 0.9 or more. Table 2 shows the distribution of the modification rates (MR) of the pages in which the modification recalls were at least 0.2 and the detection rates were at least 0.9.

Table 1. Distribution of download rates

Famous sites				Random sites			
DR	Percent of URLs	DR	Percent of URLs	DR	Percent of URLs	DR	Percent of URLs
0	22.01%	0.50 ~ 0.59	0.07%	0	15.92%	0.50 ~ 0.59	0.03%
0.01 ~ 0.09	0.06%	0.60 ~ 0.69	0.07%	0.01 ~ 0.09	0.20%	0.60 ~ 0.69	0.08%
0.10 ~ 0.19	0.04%	0.70 ~ 0.79	0.09%	0.10 ~ 0.19	0.02%	0.70 ~ 0.79	0.07%
0.20 ~ 0.29	0.06%	0.80 ~ 0.89	0.33%	0.20 ~ 0.29	0.03%	0.80 ~ 0.89	0.35%
0.30 ~ 0.39	0.04%	0.90 ~ 0.99	9.53%	0.30 ~ 0.39	0.28%	0.90 ~ 0.99	7.34%
0.40 ~ 0.49	0.05%	1	67.66%	0.40 ~ 0.49	0.03%	1	75.65%
Total: 100.00%							Total: 100.00%

A number of contents comparison methods, such as the byte-wise comparison method, the document shingling method [6], the TF·IDF cosine distance methods [10], and so on, can be used to measure change of a web page. The byte-wise comparison method, which compares the contents of web pages character by character, is the strictest one. Therefore, even though any trivial changes take place on a web page, the method regards the page as being modified. We obtained

modification rates by means of the byte-wise comparison method. Our experiment shows the maximum level of modification rates. If having used some other comparison method, we could obtain lower modification rates than those we had.

Table 2. Distribution of modification rates

Famous sites				Random sites			
MR	Percent of URLs	MR	Percent of URLs	MR	Percent of URLs	MR	Percent of URLs
0	63.85%	0.50 ~ 0.59	1.04%	0	66.07%	0.50 ~ 0.59	0.40%
0.01 ~ 0.09	15.16%	0.60 ~ 0.69	0.49%	0.01 ~ 0.09	9.37%	0.60 ~ 0.69	0.17%
0.10 ~ 0.19	4.38%	0.70 ~ 0.79	0.86%	0.10 ~ 0.19	1.99%	0.70 ~ 0.79	0.19%
0.20 ~ 0.29	2.59%	0.80 ~ 0.89	0.98%	0.20 ~ 0.29	0.92%	0.80 ~ 0.89	0.19%
0.30 ~ 0.39	1.94%	0.90 ~ 0.99	1.28%	0.30 ~ 0.39	0.33%	0.90 ~ 0.99	0.44%
0.40 ~ 0.49	0.98%	1	6.46%	0.40 ~ 0.49	0.26%	1	3.23%
Total: 100.00%							Total: 100.00%

4 Estimating the Change of Web Pages

In this section, we present two estimation formulae computing the probabilities of how many times web pages in a group will be downloaded and modified in the future crawls, using the distributions of the download rates and the modification rates of all the web pages in the group. Our estimation postulates the following. First, the future change behavior of web pages is strongly related to the past change behavior of the web page. Second, history of downloadable states and history of modification are independent (even though that a web page is modified at a point means that the page is downloaded successfully at that point). Third, we hold sufficiently long period of the change histories. Possible estimation period of a page cannot exceed to the observation period of the page. Fourth, we hold appropriately recent period of the change histories. The change behavior of a web page is related equally to all the past change behaviors we hold. Fifth, we estimate the future change behavior of web pages at the same intervals as the observation.

Let $P(DR(x))$ of a URL denote the probability that a download rate value of the URL is x, where x is rounded to two decimals. Using Table 1, we can compute $P(DR(x))$ easily. For instance, $P(DR(0))$, the probability that the download rate of a page is 0, is 22.01%, and $P(DR(1))$ is 67.66%. In Table 1, we assume that instances are distributed uniformly in each range. Hence, we compute $P(DR(x))$ by dividing the percent corresponding to x by 9 when $0.01 \leq x \leq 0.09$, or 10 when $0.10 \leq x \leq 0.99$. For instance, $P(DR(0.55))$ is 0.07%/10 = 0.007%.

Let $P(_{Y=a,N=b}DR_{Y=c,N=d})$ of a URL denote the probability that a page that was downloaded a times for $(a+b)$ download attempts will be downloaded c times for $(c+d)$ download attempts. Before computing the probability, we have two preconditions. First, the sum of a, b, c, and d should be less than or equal to the total number of crawls (50 in this paper). Second, the intervals of $(a+b)$ and $(c+d)$

download attempts are the same as those of the monitoring interval (2 days in this paper). The probability is computed by the following formula:

$$P_{(Y=a,N=b}DR_{Y=c,N=d)} \;=\; \frac{P\!\left(DR\!\left(\dfrac{a+c}{a+b+c+d}\right)\right)}{\displaystyle\sum_{i=0}^{c+d} P\!\left(DR\!\left(\dfrac{a+i}{a+b+c+d}\right)\right)}$$

As an example, let us compute $P_{(Y=0,N=2}DR_{Y=0,N=3)}$, which is the probability that we will get three consecutive download failures when we have already failed to download the page twice in a row.

$$P_{(Y=0,N=2}DR_{Y=0,N=3)} \;=\; \frac{P(DR(0))}{P\!\left(DR\!\left(\dfrac{0}{5}\right)\right)+P\!\left(DR\!\left(\dfrac{1}{5}\right)\right)+P\!\left(DR\!\left(\dfrac{2}{5}\right)\right)+P\!\left(DR\!\left(\dfrac{3}{5}\right)\right)}$$

$$=\; \frac{22.01}{22.01+0.006+0.005+0.007} = 99.9\%$$

Now we intuitively explain the estimation formula. As a simple case, suppose that we have failed to download a page three times in a row. On the next crawl, if we download the page successfully, the download rate of the page becomes 0.25. If we fail to download the page again, the download rate of the URL becomes 0. Then, we estimate the probability that the page is downloaded successfully to be 'P(DR(0.25)) / (P(DR(0)) + P(DR(0.25)))'. The estimation formula above generalizes this idea.

Estimating modifications of a page is similar with estimating successful downloads. We use a table that shows the distribution of modification rates of web pages (see Table 2). Let $P(MR(x))$ of a page denote the probability that a modification rate value of the page is x. $P(MR(x))$ is computed similarly to $P(DR(x))$. Let $P_{(Y=a,N=b}MR_{Y=c,N=d)}$ of a page denote the probability that a page is modified a times for $(a+b)$ successful downloads will be modified c times for $(c+d)$ successful downloads. The probability is computed by the following formula:

$$P_{(Y=a,N=b}MR_{Y=c,N=d)} \;=\; \frac{P\!\left(MR\!\left(\dfrac{a+c}{a+b+c+d}\right)\right)}{\displaystyle\sum_{i=0}^{c+d} P\!\left(MR\!\left(\dfrac{a+i}{a+b+c+d}\right)\right)}$$

For the evaluation of $P_{(Y=a,N=b}DR_{Y=c,N=d)}$, we selected 581,608 pages from the famous sites and 838,035 pages from the random sites. The selected pages had been detected five times on the 46th to 50th crawl. With the number of successful downloads in the past five crawls, we estimate the number of successful downloads in the next five crawls. There are six possible cases such that a page will be downloaded 0, 1, 2, 3, 4, or 5 times, i.e., $P_{(Y=a,N=(5-a)}DR_{Y=0,N=5)}$, $P_{(Y=a,N=(5-a)}DR_{Y=1,N=4)}$, …, and $P_{(Y=a,N=(5-a)}DR_{Y=5,N=0)}$, respectively, where a is the number of successful downloads. And then, we actually have attempted to download the selected pages five times for 10 days at two-day intervals.

(a) in the famous sites   (b) in the random sites
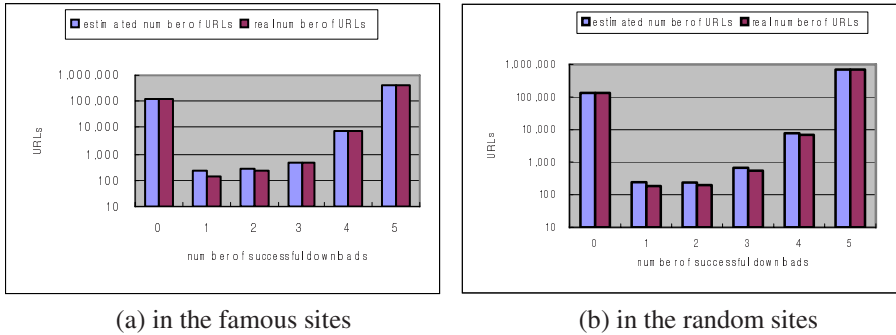
Fig. 2. Evaluation result of $P(_{Y=a,N=b}DR_{Y=c,N=d})$

Fig. 2 shows the evaluation results. The left bars represent the estimated numbers of successfully downloaded pages. The right bars represent how many pages were actually downloaded 0, 1, 2, 3, 4, or 5 times. In Fig. 2(a), the differences between the two bars in each case are 324, 86, 39, 64, 175, and 92, respectively. In Fig. 2(b), the differences are 129, 55, 35, 120, 732, and 813, respectively. Given the 581,608 pages in the famous sites and 694,583 pages in the random sites, the total number of the URLs that were incorrectly estimated is trivial (less than 0.07% and 0.11%).

(a) in the famous sites   (b) in the random sites
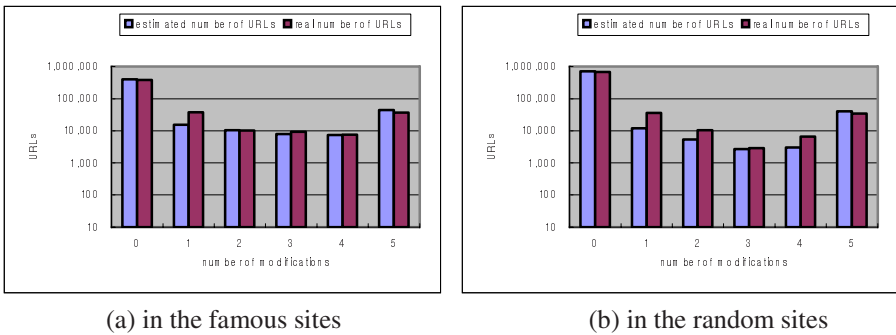
Fig. 3. Evaluation result of $P(_{Y=a,N=b}MR_{Y=c,N=d})$

For the evaluation of $P(_{Y=a,N=b}MR_{Y=c,N=d})$, we selected 483,603 pages and 766,328 pages, which had been downloaded web pages without any failures in the 44th to 50th crawl. We estimated the number of modifications of the web pages in the next five crawls. Fig. 3 shows the result of the evaluation result. Both the bars represent the estimated and the real numbers of modifications. In Fig. 3(a), the differences between the two bars in each case are 16,360, 22,057, 250, 1,347, 194, and 6,988 (the sum is 47,196 pages), respectively. In Fig. 3(b), the differences are 26,759, 24,659, 5,039, 191, 3,630, and 6,760, respectively. The modifications for 23,598 pages (4.8%) and 33,518 URLs (4.4%) were incorrectly estimated. Although the proportion of incorrectly estimated URLs is higher than the first evaluation, we believe that the

correctly estimated portion is acceptable enough (95.2% of the pages in the famous sites and 95.6% of the pages in the random sites) to avoid unnecessary requests for web pages that have not been changed.

5   Closing Remarks

We presented estimation methods computing the probabilities of how many times a page will be downloaded and modified on the future crawls. Our estimation postulates that the future change behavior of a web page is strongly related to the past changes. After observing the change histories of approximately three million web pages at two-day intervals for 100 days, we estimated the change behavior of those pages. The estimation was evaluated with the actual change behavior. As the results of download estimation, only 0.07% and 0.11% of the selected pages in the two page groups are incorrectly estimated. As the results of the modification estimation, 4.8% and 4.2% of the selected pages in the groups were incorrectly estimated. We believe that our estimation methods certainly help administrators manage their databases composed of a number of groups and avoid unnecessarily requesting undownloadable or unmodified web pages.

References

1. Brewington, B., Cybenko, G.: How Dynamic is the Web? the 9th World Wide Web Conference (2000) 257-276
2. Cho, J., Garcia-Molina, H.: The Evolution of the Web and Implications for an Incremental Crawler. the 26th VLDB Conference (2000) 200-209
3. Cho, J., Garcia-Molina, H. (2003): Effective Page Refresh Policies for Web crawlers. ACM Transactions on Database Systems. **28(4)** (2003) 390-426
4. Douglis, F., Feldmann, A., Krishnamurthy, B.: Rate of Change and Other Metrics: a Live Study of the World Wide Web. the 1st USENIX Symposium on Internetworking Technologies and System (1997) 147-158
5. Edwards, G., McCurley, K., Tomlin, J.: Adaptive Model from Optimizing Performance of an Incremental Web Crawler. the 10th World Wide Web Conference (2001) 106-113
6. Fetterly, D., Manasse, M., Najork, M., Wiener, J. L.: A large-scale study of the evolution of web pages. the 12th World Wide Web conference (2003) 669-678
7. Ntoulas, A., Cho, J., Olston, C.: What's New on the Web? The Evolution of the Web from a Search Engine Perspective. the 13th World Wide Web Conference (2004) 1-12
8. Toyoda, M., Kitsuregawa, M.: What's Really New on the Web? Identifying New Pages from a Series of Unstable Web Snapshots. the 15th World Wide Web Conference (2006) 233-241
9. Kim, S.J., Lee, S.H.: Implementation of a Web Robot and Statistics on the Korean Web. Springer-Verlag Lecture Notes in Computer Science **2713** (2003) 341-350
10. Salton, G., Mcgill, M.J.: Introduction to Modern Information Retrieval. McGraw-Hill (1983)
11. Dhyani, D., Ng, W.K., Bhowmick S.S.: A Survey of Web Metrics. ACM Computing Survey. **34(4)** (2002) 469-503
12. Huberman, B.A.. The Laws of the Web: Patterns in the Ecology of Information. MIT Press (2001)

Concept Level Web Search Via Semantic Clustering

Nian Yan and Deepak Khazanchi

College of Information Science and Technology,
University of Nebraska at Omaha, NE 68182, USA
`{nyan, khazanchi}@mail.unomaha.edu`

Abstract. Internet search engine techniques have evolved from simple web searching using categorization (e.g., Yahoo) to advanced page ranking algorithms (e.g., Google). However, the challenge for the next generation of search algorithms is not the quantity of search results, but identifying the most relevant pages based on a semantic understanding of user requirements. This notion of relevance is closely tied to the semantics associated with the term being searched. The ideal situation would be to represent results in an intuitive way that allows the user to view their search results in terms of concepts related to their search word or phrase rather than a list of ranked web pages. In this paper, we propose a semantic clustering approach that can be used to build a conceptual search engine.

Keywords: Conceptual Search, Search Engine, Document Clustering, Information Retrieval.

1 Introduction

Internet search engine techniques have evolved from simple web searching using categorization (e.g., Yahoo) to advanced page ranking algorithms (e.g., Google) [1]. However, one critical disadvantage of this approach is that ranking related information is not semantically grouped. That is, the results are not organized by concepts but by rank. For example, if one enters the term "Java" in Google, the search engine does not know what exactly this word means – is it "coffee Java", "Java programming" or even "island Java". Indeed, all three of these different results will show up in the search results. An added problem is that the phrase "Java programming" is so popular that it will dominate at least the first ten pages of the search results. Another related issue in traditional search engines is the use of Boolean operation. Internet users retrieve information from massively indexed data by inputting keywords followed by Boolean operations such as AND, OR and NOT as the representatives of the query. The major disadvantage of Boolean operations is that the search results have less relevance compared with what the user is actually looking for [2][3]. For example, a query for "Information System" returns results with key words "Information", "System" and "Information System", regardless of the associated meaning of the phrase. Besides Boolean operations, keyword searching has two major problems caused by synonymy and polysemy (multiple expressions of one thing or the same expression with multiple meanings).

The use of a "conceptual search engine" can provide clarity to users while accommodating the semantic content (and context) of a term or phrase being searched. The "concept" in a conceptual search is defined as "one overarching idea or topic present in a web page" [2]. An even broader view of conceptual search is to do what one does naturally in conversations with others. In human conversations, we are able to understand the meaning of specific text or media, including web pages, plain text, and any documents consist of text message. This characteristic should be mirrored in a conceptual search engine. Conceptual searching will look for patterns of relationships rather than for individual words. We are in some sense focused on the idea of understanding the "text" rather than just querying for the "text".

We define a "concept" as the abstract of one stream of topics that users are interested in. The results of "conceptual searching" should be to display relevant contents that are organized by meaningful concepts. Thus, in this paper we explore the possibility of developing a conceptual search engine using a semantic clustering approach.

2   Conceptual Searching

There are two general approaches that could be used to achieve the goal of conceptual searching. One is to index the documents obtained from the internet by keywords and concepts based on an ontology system. In [4], a goal-oriented search engine was proposed to achieve an improvement compared with Boolean search. An adaptive search engine was developed that uses natural language processing to parse a user's search goal and uses "common sense" reasoning to translate the user's goal into an effective query. In this project, an Open Mind knowledge base (obtained from network contributors) is regarded as the recourse of "common sense". Another conceptual search engine implementation retrieves documents based on a combination of keyword and conceptual matching [5]. The documents are indexed automatically using the Open Directory ontology (Open Directory Project, http://dmoz.org), a distributed database of web content classified by internet volunteers. This approach for information retrieval of internet documents requires the support of an ontology system. It is unrealistic to build a conceptual search engine based on an ontology system maintained by volunteers because a well defined global version of an ontology system has not been achievable. Moreover, the general purpose of constructing ontology system is only for specific domain knowledge, e.g. an ontology system for the field of health informatics. In most cases, internet users are interested in one specific domain rather than seeking for information within a global knowledge domain.

An alternative to the previous ontology based approaches is to build conceptual search engines that can take internet documents and self-organized them into individual concepts. This can be used to return highly relevant concepts based on users' requests.

3   Conceptual Searching Using Semantic Clustering

In this section we describe our proposed solution as an alternative to the algorithms used in classical search engines by improving upon Boolean search and incorporating

semantic clustering. In our solution, we assume that unstructured text data is preprocessed and then clustered. Fig. 1 illustrates the process we used in this paper to develop our proposed solution.
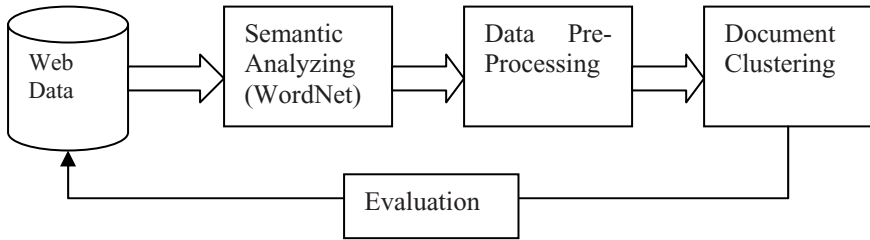
Fig. 1. Conceptual Searching by Semantic Clustering

3.1   Data Preprocessing

In order to analyze unstructured text data, preprocessing is implemented in three steps [6]: (1) Tokenization: dividing the documents into a set of index terms or keywords. (2) Stop-words: eliminating the most frequently used common English words, such as articles, prepositions, and conjunctions. (3) Stemming: prefixes and suffixes of the words are removed to reduce the redundancy of the same word in different phases. For example, "do", "doing", and "done" will be regarded as one word after stemming [7]. The documents are then processed by Vector Space Model [8] into a matrix with rows and columns representing documents and words respectively.

3.2   Data Sets

Google Search Data Set
This data source is directly collected from the internet. It aims to refine the search results of Google. Given a search term or phrase, Google's algorithm returns search results containing those key words ranked by a relevance score. It is necessary to design a query optimizer to extend the user's query to the range of key words derived from a thesaurus or even better lexical reference system, e.g. WordNet (http://wordnet.princeton.edu/). In this paper, the WordNet is used for semantically analyzing the user's input. The query optimizer then extends the original query, e.g. from term "Java" to "Java programming", "Java coffee" and "Java island" by referencing the thesaurus. We collected five cases from search results for each extended query. We use Google search API (http://code.google.com/apis/ajaxsearch/) to program and save the results.

UCI KDD Biomedical Data Set
This data set is part of the Syskill and Webert's web pages ranking data at UCI Machine Learning Repository (http://www.ics.uci.edu/~mlearn/MLRepository.html). We choose this dataset because many biomedical research applications used document clustering in, e.g. [6].

3.3 Semantic Clustering

In [9], a concept-driven search engine is designed and implemented (Carrot2, http://www.carrot2.org) based on clustering search results from traditional search engines, e,g, Google, Yahoo and etc. The search results from traditional search engines are preprocessed using Vector Space Model and latent semantic indexing technique and then clustered [9].

Document clustering varies in performance under different problem settings [10]. Certainly, developing high-performance clustering algorithms could improve document clustering. On the other hand, it is important to develop a good document modeling method for improving the performance of document clustering. In some situations, the lack of class-specific "core" words leads to the failure of correctly clustering the documents. In [11], the authors proposed a semantic smoothing method for document models for the process of clustering. A proper set of core words are selected semantically. As a result, for each document, general words can be discounted. We believe that document modeling plays a more important role compared with other aspects of document clustering. A semantic document model is proposed based on the Vector Space Model. Different from [11], we develop the core word list as illustrated in the algorithm in Fig. 2. We use k-means, the classical partitional clustering algorithm, to cluster the documents. However, the number of k in k-means is not easy to determine. We have to experiment within a range from $k = 2$, and $k < 8$. The reason k stops at seven is because of the inherent limitation of human beings to process no more than seven different concepts at the same time. Any more concepts will result in information overload and confusion in the mind of the user [12].

Step 1: Tokenizing

Step 2: Eliminating the stop words

Step 4: Stemming then generate word list $L = \{ x_1, ..., x_n \}$, porter stemming is used.

Step 5: Semantically Analyzing user's queries by WordNET, and generating initial core words list $C = \{t_0, ..., t_n\}$

Step 6: Adding more core words by analyzing the text sources, if

$t_i \subset \{x_j \mid f_{low} < tf_{x_j} < f_{high}, j = 1, ..., n\}, (i = 1, ..., m)$, where *tf* denotes term frequency

and f_{low}, f_{high} denotes the threshold of the word frequency which is regarded significant to the final core word list. Those two parameters are determined by the experienced threshold or analyze of the human experts.

Thus, the core word list is: $C = \{t_0, ..., t_n, t_{n+1}, ..., t_m\}$

Step 7: Applying Vector Space model (TF/IDF)

Step 8: Clustering the documents by k-means, k= $2, ..., 7$

Step 9: Evaluating the clusters by inter-distance. The longer the inter-distance is, the better the cluster will perform

Step 10: Presenting each cluster as an individual concept

Fig. 2. Semantic Clustering based on Vector Space Model

3.4 Simulations

The simulations are implemented in Java and the WVTools Java package (http://rapid-i.com/content/view/21/44/lang,en/) is used for data preprocessing.

Simulation 1: Clustering Google's Search Results
In this part, we design a pilot study on refining the Google's search into conceptual level. That is, using semantic cluster to identify the major streams in terms of concepts. For this case, we already know $k = 3$ because there are three different topics and for each one we collect five cases. We apply the algorithm in **Fig. 2**, clustering results are shown in Table 1. There is only one web page that belongs to cluster 3 but is clustered into cluster 2. Thus, the accuracy rate is 93.3%.

Table 1. Number of Cases in each Cluster

Cluster	Cases	Incorrectly clustered
1	5	0
2	6	1
3	4	0
Total Cases	15	

Simulation 2: Conceptual Search for UCI Biomedical Data Set
We used this data set to apply semantic clustering to identify the major streams in terms of concepts. In this case, after the step of stemming, the term frequency of each word is shown in Fig. 3. By a further human inspecting, we set $f_{low} = 2$, $f_{high} = 42$ and do the preprocessing again to get new core word list, after that there are 2051 words generated. By comparing the mean of inter-distance of the clusters under the different k (shown in Fig. 4), we found that when $k = 2$, the clustering performs best.
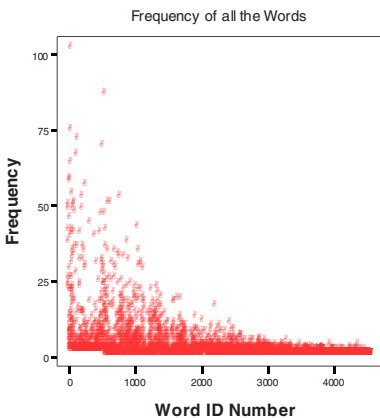
Fig. 3. Term Frequency
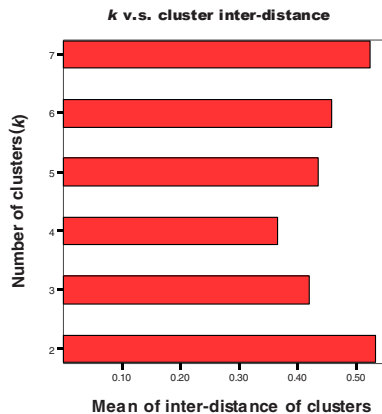
Fig. 4. Mean of inter-distance

When k =2, the two clusters have 4 and 132 pages, respectively. The contents of the clusters shows the fours are materials definitely not related to biomedical, e.g. networking, or invalid web pages. Thus we recommend $k = 7$, when the cluster performs little worse than $k = 2$ but more reasonable. The four cases are still in one cluster as well as when $k = 2$. The other six clusters are the representatives of the different topic streams. This result is shown in Table 2.

Table 2. Number of Cases in each Cluster

Cluster	1	**2**	3	4	5	6	**7**	Total Cases
Cases	46	18	4	11	13	30	14	136

4 Conclusions

In this paper, we developed a practical approach for implementing conceptual searching on the internet. The web documents obtained from a standard search are semantically modeled into vectors for clustering analysis. The simulation results show the effectiveness of this approach. For example, in simulation 1, the accuracy of correctly assigning a document to a given conceptual cluster is 93.3%. In this research, the identification of the topic for each cluster as the name of the concepts remains a good research topic in the future. For example, automatically creating a summary of the essential semantic content of a single web page for real time analysis without any other pre-processing, indexing and storing of the data from web needs to be further researched [2] [13]. Conceptual clustering techniques, such as COBWEB [14], contribute to creating the descriptions for clusters by incrementally creating hierarchical structure of the documents. Finally, the possible improvements that can be made in future research for this application is to analyze the document in phrases other than individual words (tokenization). Thus for example, the recognition of "software process improvement" as a phrase makes more sense for the Vector Space Model as compared with tokenization. The POS-tag [15] is a phrasing technique that can be used to make more sense of the data during pre-processing.

References

1. Page, L., Brin, S., Motwani, R., Winograd, T., The PageRank Citation Ranking: Bringing Order to the Web, Stanford University (1999)
2. Ramirez, P. and Mattmann, C., ACE: Improving Search Engines via Automatic Concept Extraction. Proceedings of the 2004 IEEE International Conference on Information Reuse and Integration (IEEE-IRI 2004), pp. 229-234. Las Vegas, Nevada, USA, November 8th-10th (2004)
3. Deniston, M., An Overview and Discussion of Concept Search Models and Technologies, Concept Searching Whitepaper, Fios Confidential (2003)
4. Liu, H., Lieberman, H., Selker, T., GOOSE: A Goal-Oriented Search Engine with Commonsense, Proceedings of the Second International Conference on Adaptive Hypermedia and Adaptive Web-Based Systems, pp. 253-263 (2002)

5. Gauch, S., Madrid, J., Induri, S., Ravindran, D. and Chadlavada, S., KeyConcept: A Conceptual Search Engine, Information and Telecommunication Technology Center, Technical Report: ITTC-FY2004-TR-8646-37, University of Kansas (2004)
6. Peng, Y., Yan, N., Kou, G., Chen, Z., Shi, Y., "Document Clustering in Antimicrobial Peptides Research", Proceedings of the Eleventh Americas Conference on Information Systems, August 11-14 (2005)
7. Baeza-Yates, R. and Ribeiro-Neto, B. Modern Information Retrieval. Addison-Wesley, Wokingham, UK (1999)
8. Porter, M.F., An algorithm for suffix stripping, Program, 14(3): 130-137 (1980)
9. Osinski, S, and Weiss, D., A Concept-Driven Algorithm for Clustering Search Results, IEEE Intelligent Systems ,vol. 20, no. 3, pp. 48-54, May/June (2005)
10. Zamir, O., Etzioni, O., Web document clustering: A feasibility demonstration. Proceedings of the 21st Annual International ACM Conference on Research and Development in Information Retrieval (SIGIR), 46-54 12 (1998)
11. Zhou, X., Zhang, X., and Hu, X., Semantic Smoothing of Document Models for Agglomerative Clustering, accepted in the Twentieth International Joint Conference on Artificial Intelligence (IJCAI 2007), Jan. 6-12, India (2007)
12. Miller, G. A., The Magical Number Seven, Plus or Minus Two: Some Limits on Our Capacity for Processing Information, The Psychological Review, vol. 63, pp. 81-97 (1956)
13. Michalski, R. S., "Knowledge acquisition through conceptual clustering: A theoretical framework and an algorithm for partitioning data into conjunctive concepts". International Journal of Policy Analysis and Information Systems 4: 219–244 (1980)
14. Fisher, D., "Knowledge acquisition via incremental conceptual clustering," Machine Learning, vol. 2, no. 2, pp. 139-172 (1987)
15. Hage, W., Rijke, M., and Marx, M., Information retrieval support for ontology construction and use, ISWC 2004: international semantic web conference, Hiroshima, Japan (2004)

An Efficient XML Index Structure with Bottom-Up Query Processing

Dong Min Seo, Jae Soo Yoo, and Ki Hyung Cho

Department of Computer and Communication Engineering, Chungbuk National University,
48 Gaesin-dong, Cheongju Chungbuk, Korea
{dmseo, yjs, khjoe}@chungbuk.ac.kr

Abstract. With the growing importance of XML in data exchange, much research has been done in proving flexible query mechanisms to extract data from structured XML documents. The semi-structured nature of XML data and the requirements on query flexibility pose unique challenges to database indexing methods. Recently, ViST that uses suffix tree and B+Tree was proposed to reduce the search time of the documents. However, it can cause a lot of unnecessary computation and I/O when processing structural join queries because the numbering scheme of ViST is not optimized. In this paper, we propose a novel index structure to solve the problems of ViST. Our index structure provides the bottom-up query processing method to efficiently process structural queries. Our experiments show that the proposed index structure is efficient in processing both single-path and branching queries with various wild-cards ('*' and '//').

Keywords: XML Index, XML Query, Bottom-Up Query Processing.

1 Introduction

XML provides a flexible way to define semi-structured data with the hierarchical structure. Because of such features of XML, XML is represented by a tree structure to process XML data [1]. Several query languages, including XPath, Quilt, XML-QL, and XQuery, have been proposed for semi-structured XML data. Also, path index methods that construct a graphical index on XML data to reduce query costs have been worked [2, 3].

Recently, many research papers on the structural join methods to efficiently process the XML queries involving the ancestor-descendant relationship have been done [4, 5, 6]. The structural join methods can answer simple queries efficiently. However, queries involving branching structures usually have to be disassembled into multiple subqueries. The results of these subqueries are then combined by expensive join operations to produce final answer.

To improve existing structural join methods, ViST that combines suffix tree and B+Tree was proposed [7]. The suffix tree with sequence matching matches structured queries against structured data to avoid many unnecessary structural join operations. B+Tree avoids a traversal of the whole XML document tree. However, the numbering

scheme used in suffix tree is not optimized because it regards element y that does not have ancestor-descendant relation with element x in XML data as the descendent of the element x. For the same reason, ViST can cause a lot of unnecessary computation and I/O when processing the queries.

In this paper, we propose an efficient index structure to solve problems of ViST and a novel query processing method suitable for proposed index structure. To verify the efficiency of our index structure, we compare the performance of our index structure with that of ViST.

The rest of this paper is organized as follows. In section 2, we review related works and describe the problems of ViST. In section 3, we present our proposed indexing technique. In section 4, we present the experimental results that compare our technique with ViST. Finally, conclusions and future works are discussed in section 5.

2   Related Work

2.1   Query Processing Methods Using Suffix Tree

Recently, query processing methods using suffix tree were proposed [8]. This methods use a sequential representation of both XML data and XML queries. Querying XML is equivalent to finding subsequence matches. Sequence matching matches structured queries against structured data as a whole without breaking down the queries into subqueries of paths or nodes and relying on join operations to combine their results. The purpose of modeling XML queries through sequence matching is to avoid as many unnecessary join operations as possible in query processing.

After both XML data and XML queries are converted to structure-encoded sequences in the suffix tree, it is straightforward to devise the naive algorithm to perform sequence matching. However, there are several difficulties. First, searching for the satisfied nodes is extremely costly since we need to traverse a large portion of the subtree for each match. Finally, suffix tree is main memory structure that is seldom used for disk resident data, and most commercial DBMSs do not have support for such structures [7].

2.2   The Problems of ViST

ViST improves the naive algorithm by eliminating costly suffix tree traversal. It uses a virtual suffix tree to organize structure-encoded sequences to speed up the matching process. ViST labels each suffix tree node x by a pair $<n_x, size_x>$, where n_x and $size_x$ are the prefix traversal order of x and the total number of descendants of x in suffix tree, respectively. Figure 1 shows the index structure of ViST. ViST consists of three parts such as the D-Ancestor B$^+$Tree, the S-Ancestor B$^+$Tree and the DocID B$^+$Tree. To construct the B$^+$Trees of ViST, it first inserts all suffix tree nodes into the D-Ancestor B$^+$Tree using their (*symbol*, *prefix*) as keys. For all nodes x inserted with the same (*symbol*, *prefix*), ViST indexes them by an S-Ancestor B$^+$Tree, using the n_x values of their labels as keys. In addition, ViST also builds a DocId B$^+$Tree, which stores for each node x (using n_x as key), the document IDs of those XML sequences that end up at node x when they are inserted into the suffix tree [7]. ViST simply

determines the ancestor-descendant relationship between two elements by the D-Ancestor B$^+$Tree and the S-Ancestor B$^+$Tree. If x and y are labeled $< n_x, size_x >$ and $< n_y, size_y >$ respectively, node x is the ancestor of node y iff $n_y \in (n_x, n_x+size_x]$. As a result, ViST no longer need to search the descendent of x to find such y.

(a) The suffix tree for *Doc1* and *Doc2*   (b) The structure of ViST
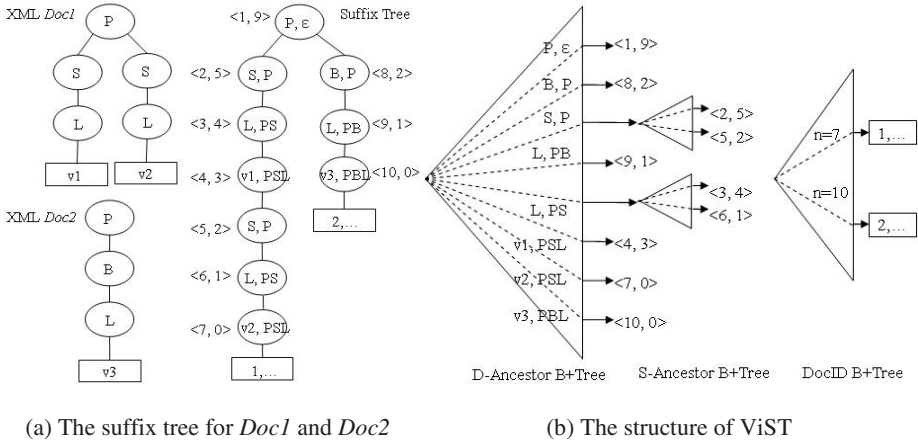
Fig. 1. The ViST index structure

Figure 2 shows the query processing method in ViST of Figure 1. If the query for "*/P/S/L/v1*" is requested, a structure-encoded sequence about this query is constructed. And it obtains the n_x and $size_x$ of the (P, ε) that is the first (*symbol, prefix*) of above structure-encoded paths by searching the D-Ancestor B$^+$Tree and the S-Ancestor B$^+$Tree of Figure 1.
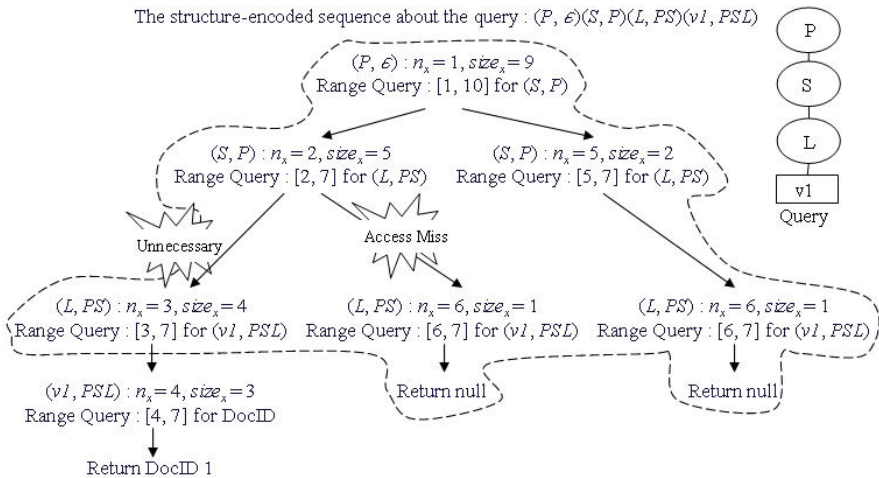
Fig. 2. The query processing in ViST

These values are used for range queries about the (*symbol*, *prefix*) of (S, P) involved in the (n_x, n_x+size_x) of the (P, ε). Then the range query about the (*symbol*, *prefix*) of the (L, PS) involved in the $<n_x, n_x+size_x>$ of the (S, P) and the (*symbol*, *prefix*) of the (*v1*, *PSL*) involved in the $<n_x, n_x+size_x>$ of the (L, PS) are executed with the set of above range query results, respectively. Finally, to obtain the documents corresponded to the query, the range query about the $[n_x, n_x+size_x]$ of the last (*symbol*, *prefix*) is executed in the DocID B⁺Tree.

As shown in Figure 2, the child node of the (S, P) with $n_x=2$ is only the (L, PS) with $n_x=3$ in the *Doc1* of Figure 1. However, when the range query about the (*symbol*, *prefix*) of the (L, PS) involved in above (S, P) is executed, the (L, PS) with $n_x=6$ is represented as the child of above (S, P). Moreover, because the characteristic that prefix of an element represents the path from the root element to itself is not used, the unnecessary nodes are accessed as shown in Figure 2. For example, with the *PSL* of the (*v1*, *PSL*), we estimate that the (*v1*, *PSL*) has the (L, PS) as its parent node, and the (P, ε) and (S, P) as its ancestor nodes. Therefore the range queries about the (P, ε), (S, P), and (L, PS) involving the (*v1*, *PSL*) are unnecessary. Also, because of noncontiguous subsequence matches, the branching query processing method of ViST triggers false alarms [9].

3   Our Proposed Index Structure

3.1   Our Proposed Index Structure

We use the *durable* numbering scheme [4] to solve the numbering scheme problem of ViST. Figure 3 shows our proposed index structure about the XML documents of Figure 1. The D-Ancestor B⁺Tree and the S-Ancestor B⁺Tree of our index structure are same as those of ViST. But our index structure inserts a pair *<order, size>* of the *durable* numbering scheme into the S-Ancestor B⁺Tree.
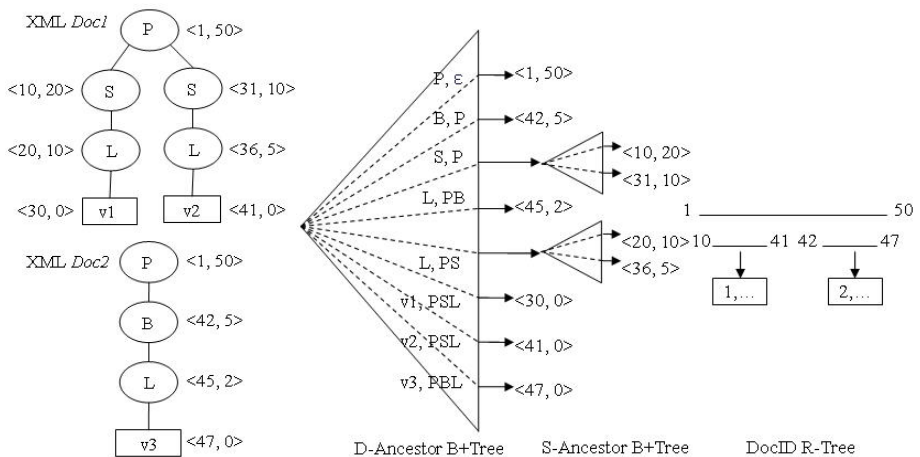
Fig. 3. Our proposed index structure

To directly find the documents involving the $<n_x, size_x>$ of the last node by the range query, we use the DocID R-Tree instead of the DocID B⁺Tree. The key of DocID R-Tree is assigned with a pair of numbers $<start, end>$. Element *start* is the minimum order and *end* is the maximum order in an XML document except for the root element.

3.2 Our Proposed Bottom-Up Query Processing Algorithm

Each prefix of nodes represents the path from the root node to each node. Therefore, when a query is executed, if we use the characteristic of the prefix, the query performance is significantly improved. We propose the bottom-up query processing method. Figure 4 shows the query processing methods in ViST and the proposed index structure. If the query of Figure 4(a) is executed by the top-down query processing method of ViST, ViST performs a range query to match (L, P^*) of the query sequence in the D-Ancestor B⁺Tree of Figure 1 after the search for the (P, ε). The search then continues on the S-Ancestor B⁺Tree with the results returned by the range query so the searches for the (L, PB) and the (L, PS) are executed. However, if the query is executed by our bottom-up processing method, our proposed index structure performs only a range query to match last element $(v1, P^*L)$ of the query sequence in the D-Ancestor B⁺Tree of Figure 3.

The structure-encoded sequence about the query : $(P, \varepsilon)(L, P^*)(v1, P^*L)$

Range Query : for (P, ε)

$(P, \varepsilon) : n_x = 1, size_x = 9$
Range Query : [1, 10] for (L, P^*)

$(L, PB) : n_x = 9, size_x = 1$
Range Query : [9, 10] for $(v1, PBL)$

$(L, PS) : n_x = 3, size_x = 4$
Range Query : [3, 7] for $(v1, PSL)$

$(L, PS) : n_x = 6, size_x = 1$
Range Query : [6, 7] for $(v1, PSL)$

Return null

$(v1, PSL) : n_x = 4, size_x = 3$
Range Query : [4, 7] for DocID

Return null

Return DocID 1

P

*

L

v1
Query

(a) By the top-down query processing in ViST

Range Query : for $(v1, P^*L)$

$(v1, PSL) : n_x = 30, size_x = 0$
Range Query : [30, 30] for DocID

Return DocID 1

(b) By the bottom-up query processing in our index structure

Fig. 4. The bottom-up wild-card query processing

As a result, in a single path query case, our method only executes the range query about last element of a query sequence. Moreover, as shown in Figure 4, our bottom-up query processing method is very efficient for wild-cards ('*' and '//') queries because node accesses for wild-cards in our bottom-up query processing method are smaller than that in ViST.

Figure 5 shows the branching query processing method in proposed index structure. First, to find (*v2*, *PSL*), our index structure performs the search in the D-Ancestor B⁺Tree and the S-Ancestor B⁺Tree of Figure 3. The search then continues on the D-Ancestor B⁺Tree and the S-Ancestor B⁺Tree to find (*L*, *PS*) involving $<n_x,$ $size_x>$ of (*v2*, *PSL*). The search then finds (*S*, *P*) involving $<n_x, size_x>$ of (*L*, *PS*) returned by the search for (*L*, *PS*). Then our index structure performs the search to find (*v1*, *PSL*) that is involved in $<n_x, size_x>$ of (*S*, *P*) and isn't involved in $<n_x, size_x>$ of (*L*, *PS*) that is the parent node of (*v2*, *PSL*). This processing method avoids unnecessary computation and I/O of the search to find (*P*, *ε*) and (*L*, *PS*) that are the parent nodes of (*v1*, *PSL*). In addition, our bottom-up query processing method for the branching query has no false alarm because it processes the branching query with a pair <*order*, *size*> of the *durable* numbering scheme. In Figure 5, our bottom-up query processing executes the range queries about (*S*, *P*) and (*L*, *PS*) to avoid false alarms.

The structure-encoded sequence about the query :
(*P*, *ε*)(*S*, *P*)(*L*, *PS*)(*v1*, *PSL*)(*L*, *PS*)(*v2*, *PSL*)
Range Query : for (*v2*, *PSL*)

(*v2*, *PSL*) : $n_x = 41$, $size_x = 0$
Range Query : [41, 41] for ⊏(*L*, *PS*)

(*L*, *PS*) : $n_x = 36$, $size_x = 5$
Range Query : [36, 41] for ⊏(*S*, *P*)

(*S*, *P*) : $n_x = 31$, $size_x = 10$
Range Query : NOT [41,41] and [31, 41] for (*v1*, *PSL*)

Return null
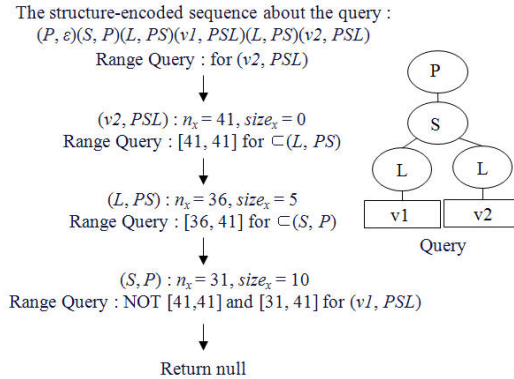
Fig. 5. The bottom-up branching query processing

4   Performance Evaluation

4.1   Experimental Setup

To determine the effectiveness of our index structure, we compare the performance of our index structure with that of ViST. Our results indicate that our index structure outperforms ViST. We implemented our XML indexing in C++. The implementation uses the B⁺Tree API provided by the Berkeley DB library [10]. All the experiments are carried out on a 3GHz Pentium   processor with 512 MB of RAM and Windows XP. We use the same set of queries for NIAGARA [11] with some slight changes on value predicates as shown in Table 1.

Table 1. Sample queries for the performance evaluation

No	Description
Q1	/W4F_DOC/Actor/Name/FirstName/Robert
Q2	/W4F_DOC/Actor/Name/*/Rebert
Q3	//Name/*/Robert
Q4	/W4F_DOC/Actor/Name[FirstName/Claudio]/LastName/Alfonsi
Q5	//*/Name[FirstName/Claudio]/LastName/Alfonsi

4.2 Performance Evaluation Results

The query processing performances of our index structure and ViST are illustrated in Figure 6.
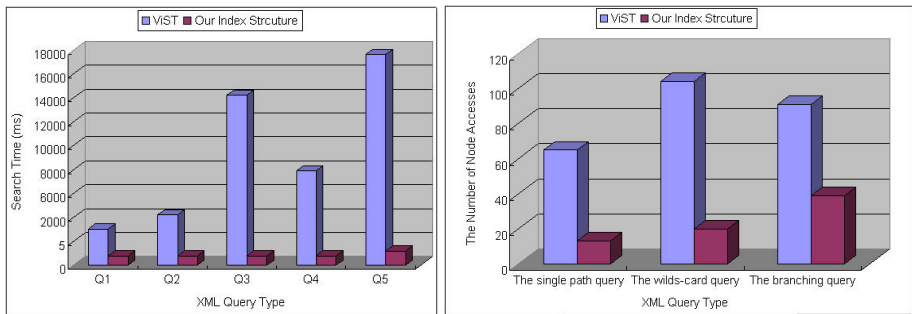
(a) The average query processing time   (b) The average number of node accesses

Fig. 6. The query processing performance about ViST and the proposed index structure

Figure 6(a) shows the average query processing time to process queries. *Q1* represents a single path query. *Q1* is evaluated with changing the depth of a query path. *Q2* represents the query with the wild-card '*' and *Q3* represents the query with wildcard '//'. *Q2* and *Q3* are evaluated with changing the appearance position and the number of wild-cards. *Q4* represents a multiple path query. *Q4* is evaluated with changing the number of the branches of queries. *Q5* represents a complex query that combines wild-cards '*' and '//'. Our index structure takes the same time in all cases because our bottom-up query processing method searches only last element of a query sequence. But, if the depth of the query path is longer, ViST takes longer time because it searches all elements of a query sequence. As a result, our index structure outperforms ViST because the proposed bottom-up query processing method avoids a lot of unnecessary computation and I/O of ViST.

Figure 6(b) shows the number of node accesses to process a query. This experiment is performed with single path queries, wild-cards queries and branching queries. Our index structure significantly outperforms ViST in all cases. In our index structure, the number of node accesses for a branching query is larger than that for a single path query and a wild-cards query. The reason is that our bottom-up query processing method for a branching query requires many range queries about elements in a query

sequence to avoid false alarms. As a result, our index structure is more efficient than ViST because our index structure has no false alarms.

5   Conclusion

In this paper, we have proposed a novel index structure for indexing XML data and processing XML queries. Our index structure provides the D-Ancestor B$^+$Tree and the S-Ancestor B$^+$Tree using the *durable* numbering scheme to efficiently determine structural relationship between any pair of element nodes and find all occurrences of structural relationships between two element sets. In addition, our index structure provides the bottom-up query processing to avoid a lot of unnecessary computation and I/O for structural join queries and has no false alarms. We have performed various experiments to evaluate the effectiveness of our index structure. Our studies show that our index structure significantly outperforms ViST for all the tested queries. In the future, we will study how to efficiently process the delimiters of the prefix schemes, to decrease the label size and to keep low label update costs.

References

1. T. Bray, J. Paoli, C. M. et. al., "Extensible Markup Language (XML) 1.0 3rd", http://www.-w3.org/TR/REC-xml (2004)
2. M. Fernandez and D. Suciu, "Optimizing regular path expressions using graph schemas", In -ICDE (1998) 14-23
3. C. W. Chung, J. K. Min, K. S. Shim, "APEX: An Adaptive Path Index for XML Data", In S-IGMOD (2002) 121-132
4. Q. Li and B. Moon, "Indexing and querying XML data for regular path expressions", In VL-DB (2001) 361-370
5. D. Srivastava, S. Al-Khalifa, H. V. Jagadish, N. Koudas, J. M. Patel, and Y. Wu, "Structural joins: A primitive for efficient XML query pattern matching", In ICDE (2002) 141-152
6. S, -Y, Chien, Z. Vagena, D. Zhang, V. Tsotras, and C. Zaniolo, "Efficient structural joins on indexed XML documents", In VLDB (2002) 263-274
7. H. Wang, S. Park, W. Fan, and P. S. Yu, "ViST: A Dynamic Index Method for Querying X-ML Data by Tree Structures", In SIGMOD (2003) 110-121
8. E. M. McCreight, "A space-economical suffix tree construction algorithm", Journal of the ACM (1976) 262-272
9. H. Wang and X. Meng, "On the Sequencing of Tree Structures for XML Indexing", In ICD-E (2005) 372-383
10. Sleepycat Software, "http://www.sleepycat.com", The Berkeley Database
11. The Niagara Project Group, "The Niagara Project Experimental Data", http://www.cs.wisc.-edu/niagara/data.html (2005)

Similarity Search Algorithm for Efficient Sub-trajectory Matching in Moving Databases

Eun-Cheon Lim and Choon-Bo Shim[*]

Division of Information & Communication Engineering, Sunchon National University,
Suncheon, 540-742, South Korea
`{eclim, cbsim}@sunchon.ac.kr`

Abstract. Similarity measure scheme on moving objects has become a topic of increasing in the area of moving databases. In this paper, we propose a new similarity search algorithm for efficient sub-trajectory matching. For measuring similarity between two sub-trajectories, we propose a new v(variable)-warping distance algorithm which enhances the existing time warping distance algorithm by permitting up to v replications for an arbitrary motion of a query trajectory. Our v-warping distance algorithm provides an approximate matching between two trajectories as well as an exact matching between them. Based on our v-warping distance algorithm, we also present a similarity measure scheme for the single trajectory in moving databases. Finally, we show that our scheme based on the v-warping distance achieves much better performance than other conventional schemes, such as Li's one (no-warping) and Shan's one (infinite-warping) in terms of precision and recall measures.

1 Introduction

The most striking difference between still images and videos stems from movement and variations. Retrieving moving objects, which requires both spatial and temporal knowledge, is part of content-based retrieval on moving databases. Typical applications are : automated surveillance systems, moving object monitoring, road traffic monitoring, video on demand etc. Modeling and similarity measure schemes based on moving objects has received some research attention recently [1-2], but it is certainly in its infancy. Most research in this area focuses on tracking the movement of a moving object, i.e., the trajectory of an object over a period of time, which is certainly very important.

In this paper, we propose a new similarity search algorithm for efficient sub-trajectory matching. For measuring similarity between two sub-trajectories, we propose a new v(variable)-warping distance algorithm which enhances the existing time warping distance algorithm by permitting up to v replications for an arbitrary motion of a query trajectory. Our v-warping distance algorithm provides an approximate matching between two trajectories as well as an exact matching between them. Especially in case of a large amount of moving objects, the approximate

---

[*] Corresponding author.

matching can improve the performance of retrieval on moving objects' trajectories, compared with the exact matching. Based on our v-warping distance algorithm, we also present a similarity measure scheme for a moving object's trajectory in moving databases. Finally, we show that our scheme based on proposed v-warping distance achieves much better performance than other conventional schemes, such as Li's one (no-warping) and Shan's one (infinite-warping) in terms of precision and recall measures.

2   Related Work

There have been two main researches on retrieval based on similar sub-trajectory by measuring the similarity between a given query trajectory and data trajectories, i.e., Li's scheme and Shan's scheme. First, Li et al. [2] represented the trajectory of a moving object as eight directions, such as North(NT), Northwest(NW), Northeast(NE), West(WT), Southwest(SW), East(ET), Southeast(SE), and Southwest(SW). They represented as (S_i, d_i, I_i) the trajectory of a moving object A over a given time interval I_i where S_i is the displacement of A and d_i is a direction. For a set of time interval $<I_1, I_2, \ldots, I_n>$, the trajectories of A can be represented as a list of motions, like $<(S_1, d_1, I_1), (S_2, d_2, I_2), \ldots, (S_n, d_n, I_n)>$. Based on the representation for moving objects' trajectories, they present a similarity measures to computes the similarity of spatio-temporal relationships between two moving object. Let $\{M_1, M_2, \ldots, M_m\}$ $(m \geq 1)$ be the trajectory of moving object A, $\{N_1, N_2, \ldots, N_n\}$ be the trajectory of moving object B, and $m \leq n$. The similarity measure between the trajectory of object A and that of object B, TrajSim(A, B), is computed by using the similarity distances of directional relations as follows. Here, minDiff(A, B) and maxDiff(A, B) are the smallest distance between A and B and the largest distance, respectively.

$$TrajSim(A, B) = \frac{\max Diff(A, B) - \min Diff(A, B)}{\max Diff(A, B)}$$

$$(\forall j, 0 \leq j \leq n - m)$$

Secondly, Shan and Lee [3] represented the trajectory of a moving object as a sequence of segments, each being expressed as the slope with real angle ranging from 0 to 360 degree for content-based retrieval. They also proposed two similarity measure algorithms, OCM (Optimal Consecutive Mapping) and OCMR (Optimal Consecutive Mapping with Replication), which can measure similarity between query trajectory and data trajectory. The OCM algorithm that supports exact matching measures the similarity for one-to-one segment mapping between query trajectory and data trajectory. Meanwhile, The OCMR algorithm supports approximation matching. In order to measure the similarity, each motion of query trajectory can be permitted to map with more than one motions of data trajectory.

3   Proposed Scheme Based on v-Warping Distance Algorithm

We first present three considerations for supporting efficient similar sub-trajectory retrieval on moving object's trajectory.

1. *The existing time warping transformation [4-5] used for a similar sub-sequence matching in sequence databases can allow the infinitive replication of a data sequence as well as a query sequence. However, for similar sub-trajectory retrieval in moving databases, it is necessary to allow the replication of only a query trajectory.*

2. *The time warping transformation for a similar sub-sequence matching can allow the infinitive replication of an arbitrary motion. However, for the similar sub-trajectory retrieval, it is necessary to support the replication of up to the variable dynamic number (v) of motions, so called v-warping distance.*

3. *For modeling motions being composed of the trajectory of a moving object, it is necessary to support multiple properties including angle, distance, and time, instead of the single property of angle.*

The consideration 1 is generally needed for supporting an approximation matching from similar sub-trajectory retrieval and the considerations 2 and 3 are needed for improving the effectiveness of the approximation matching. In addition, the considerations 2 and 3 are very sensitive, depending on application areas. The similar subsequence matching approach which is used for the existing time warping transformation does not satisfy all of the above three considerations. The reason is why the characteristic of data used in sequence database is different from that of trajectory data of moving objects in moving databases. Generally, the sequence data has a detailed and elaborate feature and the number of elements consisting of a sequence reaches scores or hundreds. On the other hand, the trajectory data of moving objects in moving databases are composed of motions over a time interval and the number of motions consisting of a trajectory is less than scores. Meanwhile, the Shan's OCMR scheme can satisfy the considerations 1, but it does not satisfy the considerations 2 and 3.

Therefore, we propose a new dynamic v-warping distance algorithm which can support an approximation matching and satisfy the above three considerations for similar sub-trajectory retrieval. In order to satisfy the consideration 3, we generally define the trajectory of moving objects as a collection of consecutive motions consisting of n-dimensional properties.

Definition 1. The trajectory of moving object S is defined as a set of consecutive motions, $S = (s[1], s[2], ..., s[|S|])$, where each motion $s[i]$ is composed of n-dimensional properties as follows:

$$s[i] = (s[i, 1], s[i, 2], …, s[i, n])$$

For measuring a similarity between two trajectories, we define a v-warping distance as follows, which is newly made by applying the concept of time warping distance[4-5] used for time-series databases to the trajectory data of moving objects in moving databases.

Definition 2. Given two trajectory of moving objects S and Q, the v-warping distance D_{vw} is defined recursively as follows:

$D_{vw}(0, 0) = 0, D_{vw}(S, 0) = D_{vw}(0, Q) = \infty$

$D_{vw}(S, Q) = D_{base}(S[1], Q[1]) + \min(\{D_{vw}((S[2+i:-], Q), 0 \leq i \leq v), D_{vw}(S[2:-], Q[2:-])\})$

$D_{base}(a, b) = d_{df}(a, b)$

Our v-warping distance algorithm is shown in Figure 1. It calculates a v-warping distance between a given query trajectory Q and a data trajectory S by permitting up to v(variable) replications for an arbitrary motion of a query trajectory Q. When the motions of a data trajectory and a query trajectory are represented by rows and columns in the cumulative table respectively, our a v-warping distance algorithm finds a minimum distance starting from the first column of the first row within the last column of the last row by replicating an arbitrary motion of a query trajectory up to v times. In addition, since a motion of a trajectory is modeled as both angle property and distance property, our algorithm measures a similarity between a data trajectory S and a query trajectory Q by considering both properties.

```
int v-warping_distance(S, Q, v)
{
  Input:
      S[]: Data Trajectory;
      Q[]: Query Trajectory;
      v: the variable number of warping(replication);
  Output:
      vw_dist:minimum distance acquired using v-warping;
  vwTbl[MAXSIZE];    // v-warping table;
  for i=0 to |S|-1 do
    for j=0 to |Q|-1 do
          vwTbl[j+i*|Q|] = 999.0f;
  for i=0 to |S|-|Q| do { // make v-warping table
    for n=0 to |Q|-1 do {
       y_p = i+n; x_p = n;
       vwTbl[x_p+(y_p*|Q|)] = d_df(S[y_p],Q[x_p]);
    } // end for n
    for j=0 to |Q|-1 do {
      for m=0 to v-1 do {
        for n=0 to |Q|-1 do {
          y_p = 1 + I + (j*v) + m + n;
          x_p = n;
          if((y_p>=|S|)||(y_p>x_p+(|S|-|Q|))) break;
          if(j == n)
             vwTbl[x_p+(y_p*|Q|)]=vwTbl[x_p+((y_p-1)*|Q|)] +
                     d_df(S[y_p],Q[x_p]);
          else
 vwTbl[x_p+(y_p*|Q|)]=d_df(S[y_p],Q[x_p])+ min(vwTbl[x_p+((y_p-1)*|Q|)],
                                 vwTbl[(x_p-1)+((y_p-1)*|Q|)]);
        } // end for n
      } // end for m
    } // end for j
 } // end for i
 vw_dist = 999.0f;  // initialize
    for i=0 to |S|-1 do{ // find the minimum v-warping dist.
    if(vw_dist > vwTbl[(|Q|-1)+(i*|Q|)]) {
       vw_dist = vwTbl[(|Q|-1)+(i*|Q|)];
       y = i; x = |Q|;
    }
  }
  return vw_dist;
}
```

Fig. 1. Dynamic v-warping distance algorithm
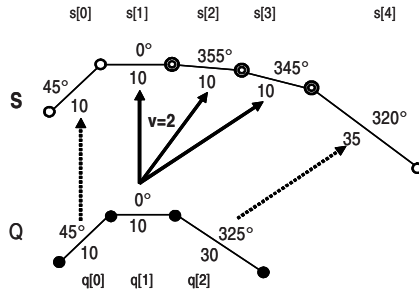
Fig. 2. Mapping of motions between S and Q when v=2

Figure 2 depicts an example of our v-warping distance algorithm which can calculate similarity between trajectory S and Q when v is 2. We can permit up to 2(=v) times replications for an arbitrary motion of only query trajectory Q. In the above example, we can obtain the minimum distance value, that is, the maximum similarity value, between S and Q when q[1] of trajectory Q is mapped to each s[1], s[2], and s[3] of trajectory S, instead of the exact matching, namely, one-to-one mapping between trajectory S and Q. Therefore, it is shown that the approximate matching is superior to the exact mating for calculating the similarity between trajectories in moving databases.

Based on our v-warping distance algorithm, we will define a similarity measure for a single trajectory. Since we measure a similarity between i-th motion in query trajectory Q and j-th motion in data trajectory S, we define a distance function between two motions, $d_{df}(q[i], s[j])$, as follows.

Definition 3. A distance function, $d_{df}(q[i], s[j])$, to measure the similarity between the arbitrary motion s[i] of a data trajectory S and the arbitrary motion q[j] of a query trajectory Q is defined as follows.

$$d_{dis}(s[i,2], q[j,2]) = | s[i, 2] - q[j, 2] |$$
if $| s[i, 1] - q[j, 1] | > 180$ then $d_{ang}(s[i, 1], q[j, 1]) = (360 - | s[i, 1] - q[j, 1] |)$
else $d_{ang}(s[i, 1], q[j, 1]) = | s[i, 1] - q[j, 1] |$
$$d_{df}(s[i], q[j]) = (((d_{ang} / 180) * \alpha) + ((d_{dis}/100) * \beta))$$

Here, d_{ang} is a distance function for the direction (angle) property for all the motions of a trajectory and d_{dis} is a distance function for the distance property. s[i, 1] and s[i, 2] are the direction and the distance value of the i-th motion in a trajectory S, respectively. α and β mean the weight of the direction and the distance, respectively, when $\alpha+\beta=1.0$.

For example, by using our v-warping distance algorithm, a similarity distance between a data trajectory S={(45,10), (0,10), (355,10), (345,10), (4,40), (325,45)} and a query trajectory Q={(45,10), (0,10), (325,10)} can be calculated in Figure 3. The value of the last column of the last row means the minimum distance 0.30 by permitting the infinitive replications of the query trajectory Q as shown in trajectory S1. In the case of v-warping distance, the motion of q[0] in the query trajectory Q corresponds to the s[0] in the data trajectory S, the motion of q[1] to the s[1], the motion of q[1] to the s[2], and the motion of q[2] to the s[3] respectively as shown in

trajectory S2. Finally, we can find a path starting from the first column of the first row within the last column of the last row, thus obtaining the minimum distance by permitting up to v(=2) replications. We can summarize the differences of distance between each motion of the query and the data trajectory on the path, that is, |q[0]-s[0]|+|q[1]-s[1]|+|q[1]-s[2]|+|q[2]-s[3]|= 0.00 + 0.00 + 0.02 + 0.07 = 0.09. This is a minimum distance value between the two trajectories by using our v-warping distance algorithm. Thus, the similarity degree between S and Q is 91%(=1-0.09) while the similarity degree based on Shan's OCMR(infinite warping) is 70%(=1-0.30). In conclusion, our similarity measure scheme based on the v-warping distance algorithm provides a better result than Shan's OCMR.
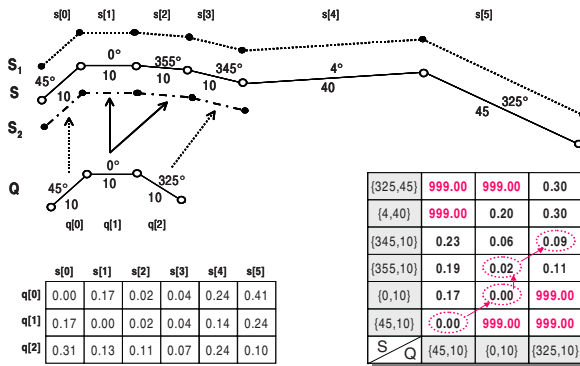
Fig. 3. Example of similarity measure between S and Q (v=2)

4   Experimental Results

In order to verify the usefulness of our representation scheme for moving object's trajectory, we do the performance analysis by using real soccer video data. Since soccer video data have many trajectories of soccer balls, i.e., salient objects, it is necessary to extract the trajectories of moving objects from the soccer ball. Most of video data, formatted as MPEG file, which are used in our experiment include a shot of 'getting a goal'. We extract the trajectories of a soccer ball by manually tracing the ball in a ground field. For our experiment, we make 50 query trajectories consisting of twenty in 'the right field' and twenty in 'the left field' from the half line of the ground field. The experimental data used for performance evaluation is as follows: (1) data domain : trajectory extracted from real soccer video data; (2) salient moving object : soccer ball; (3) data set : 1000; (4) the average number of motions for trajectory : 9.1; (5) the number of query : 50.

We implemented our similarity search algorithm under Windows 2003 Server O.S with Pentium Processor and 1 GB memory by using Microsoft Visual C++ compiler. We compare our representation scheme with the Li's and Shan's schemes in terms of retrieval effectiveness, that is, average precision and recall measures. Let RD (Relevant data in Database) be the number of video data relevant to a given query which are selected from the database, RQ (Retrieved data by Query) be the total

number of data retrieved by a given query, and RR (Relevant data that are Retrieved) be the number of relevant data retrieved by a given query. In order to obtain RD, we make a test panel which selects relevant data manually from the database. The precision is defined as the proportion of retrieved data being relevant and the recall is defined as the proportion of relevant data being retrieved as follows.

$$\text{Precision} = \frac{RR}{RQ} \qquad\qquad \text{Recall} = \frac{RR}{RD}$$

For our performance comparison, we adopt the 11-point measure [6], which is most widely used for measuring the precision and recall. For a moving object's trajectory, we consider the weight of angle (W_a) and the weight of distance (W_d) separately since we use both angle and distance for modeling the trajectory of moving objects. We also take into account the number of replications (v) since v is a very important parameter, depending on an application area. Here we do our experiment when v=0, 1, and 2 owing to the characteristics of the trajectory of the soccer ball in soccer video data. v=0 is exact matching and v=1 and 2 is approximate matching. We show from our experiment that there is no difference on retrieval effectiveness when v is greater than 2. Table 1 shows the retrieval effectiveness of our scheme, Li's scheme, and Shan's scheme. In case we do our performance analysis based on only the angle property (W_a=1.0 and W_d=0.0), it is shown that our scheme achieves about 10-15% higher precision than that of Li's and Shan's schemes while it holds about the same recall. In case we consider the weight of angle about two times greater than that of distance (W_a =0.7 and W_d=0.3), it is shown that our scheme achieves about 15-20% higher precision than that of Li's and Shan's schemes while it holds about the same recall.

Table 1. Experimental results

		Avg. Precision			Avg. Recall		
	# of warping	v = 0	v = 1	v = 2	v = 1	v = 1	v = 2
W_a:W_d= 1.0:0.0	Li's Scheme	0.25			0.45		
	Shan's Scheme	0.30			0.44		
	Our Scheme	0.34	0.38	0.40	0.51	0.48	0.47
W_a:W_d= 0.7:0.3	Li's Scheme	0.25			0.45		
	Shan's Scheme	0.30			0.44		
	Our Scheme	0.39	0.44	0.45	0.50	0.46	0.47
W_a:W_d= 0.5:0.5	Li's Scheme	0.25			0.45		
	Shan's Scheme	0.30			0.44		
	Our Scheme	0.33	0.34	0.38	0.51	0.50	0.51

From our experiment, we finally show that our similarity measure scheme based on our v-warping distance algorithm achieves better performance on average precision than Li's and Shan's schemes while it holds about the same recall in the moving object's trajectory. Particularly, the performance of our scheme is the best when the weight of angle is over two times than that of distance (W_a=0.7 and W_d=0.3).

5   Conclusions

In this paper, we propose a new similarity search algorithm for efficient sub-trajectory matching. For measuring similarity between two sub-trajectories, we propose a new v-warping distance algorithm which enhances the existing time warping distance algorithm by permitting up to v replications for an arbitrary motion of a query trajectory. Our v-warping distance algorithm provides an approximate matching between two trajectories as well as an exact matching between them. From our experiment, we showed that our similarity measure scheme based on the v-warping distance outperformed Li's and Shan's schemes in terms of precision and recall measures. The performance of our scheme achieves about 15-20% performance improvement against Li's one and Shan's one when the weight of angle is over two times greater than that of distance.

Acknowledgements

References

1. Forlizzi, L., Guting, R. H., Nardelli, E., Schneider, M.: A Data Model and Data Structures for Moving Objects Databases, Proc. of ACM SIGMOD Conf, (2000)319-330
2. Li, J., Ozsu, M. T., Szafron, D.: Modeling Video Temporal Relationships in an Object Database Management System," in Proceedings of Multimedia Computing and Networking(MMCN97), (1997)80-91
3. Shan, M., Lee, S. Y.,: Content-based Video Retrieval via Motion Trajectories, in Proceedings of SPIE Electronic Imaging and Multimedia System II, Vol. 3561, (1998)52-61
4. Yi, B., Lagadish, H. V., Faloutsos, C.: Efficient Retrieval of Similar Time Sequences Under Time Warping, In Proc. Int'l. Conf. on Data Engineering, IEEE,(1998)201-208
5. Park, S. H. et al.: Efficient Searches for Simialr Subsequence of Difference Lengths in Sequence Databases, In Proc. Int'l. Conf. on Data Engineering. IEEE, (2000)23-32
6. Salton, G., McGill, M.: An introduction to Modern Information Retrieval, McGraw-Hill, (1993)

Using Intrinsic Object Attributes for Incremental Content Based Image Retrieval with Histograms

Jongan Park, Seungjo Han, and Pankoo Kim

Dept of Information & Communications Engineering,
Chosun University, Gwangju, Korea
`japark@chosun.ac.kr`

Abstract. An incremental Content Based Image Retrieval (CBIR) method is proposed in this paper. This method is based on color histogram. Standard histograms, because of their efficiency and insensitivity to small changes, are widely used for content based image retrieval. We define an algorithm that utilizes the concept of Histogram Refinement [1] and we call it Color Refinement Method. Color Refinement method splits the pixels in a given bucket into several classes just like histogram refinement method. The classes are all related to colors and are based on color coherence vectors. After the calculation of clusters using color refinement method, inherent features of each of cluster is calculated. These inherent features are used for incremental CBIR.

1 Introduction

Content-based image retrieval (CBIR) is regarded as one of the most effective ways of accessing visual data. There are queries that require the comparing of the images on their overall appearance. In such cases, color histograms can be employed because they are very efficient regarding computations. Plus they offer insensitivity to small changes regarding camera position. But the main problem with color histograms is their coarse characterization of an image. That may itself result in same histograms for images with different appearances. We have also proposed color histogram in our algorithm. However, this paper is different because we try to exploit the colors of individual objects.

2 Related Work

Work by Arnold et. al. [2] is an excellent review of content based image retrieval till 2000. Hsu [3] exploits the degree of overlap between regions of the same color. They used a database of 260 images. Paisarn [4] proposed an unsupervised learning network to incorporate a self-learning capability into image retrieval systems. Smith & Chang's method also partitions the image. Histogram back-projection method [5] is used for back projecting set of colors onto the image.

Rickman and Stonham [6] provide a method based on small equilateral triangles with fixed sides. Djeraba [7] tried to add the generalization capability for indexing and retrieval. Stricker and Dimai [8] finds the first three moments of the color

distributions in an image. Huang et al. [9] method is called Color Correlogram and it captures the spatial correlation between colors. Pass and Zabih [1] method called Histogram Refinement partitions histogram bins by the spatial coherence of pixels. Jong-An, Bilal et al. [10] provided shape description based on histogram based chain codes. Choi et. al. [11] proposed SOM based R*-Tree as new indexing method for high dimensional features vector. Xin Huang et. al. [12] presented image retrieval methodology based on color and spatial feature.

3   Feature Extraction Algorithm

3.1   Pre-processing

At the pre-processing stage, the image is converted to grayscale image using threshold. The grayscale image is then quantized to 4 levels from 256 levels, in order to increase the computational speed. Hence, we get 4 bins (levels) after quantization. We used uniform quantization which provides us with 4 separate bins with equal range. The steps in the pre-processing stage can be observed from first 3 blocks in figure 1.

3.2   Features from Quantized Bins

We use color refinement method for feature extraction from the quantized bins based on histogram refinement [1] method. The histogram refinement method provides that the pixels within a given bucket be split into classes based upon some local property and these split histograms are then compared on bucket by bucket basis.

Color histogram buckets are partitioned based on spatial coherence just like computed by Pass and Zabih [1]. A pixel is coherent if it is a part of some sizable similar colored region, otherwise it is incoherent. So the pixels are classified as coherent or incoherent within each color bucket. If a pixel is part of a large group of pixels of the same color which form at least one percent of the image then that pixel is a coherent pixel. Otherwise it is incoherent pixel and the group is incoherent group or cluster.

Then two more properties are calculated for each bin. First the numbers of clusters are found for each case, i.e., coherent and incoherent case in each of the bin. Secondly, the average of each cluster is computed. So for each bin, there are six values: one each for percentage of coherent pixels and incoherent pixels, number of coherent clusters and incoherent clusters, average of coherent cluster and incoherent cluster. These values are calculated by computing the connected components. A connected component C is a maximal set of pixels such that for any two pixels p, $p' \in C$, there is a path in C between p and p'. A pixel is classified as coherent if it is part of a connected component whose size is equal to or greater than τ ($\tau = 5\%$ of the image size). Otherwise it is classified as incoherent.

For each discretized color j, let the number of coherent pixels as α_j, the number of coherent connected components as $C_{\alpha j}$ and the average of coherent connected component as $\mu_{\alpha j}$. Similarly, let the number of incoherent pixels as β_j, the number of incoherent connected components as $C_{\beta j}$ and the average of incoherent connected component as $\mu_{\beta j}$. For each discretized color j, the total number of pixels are $\alpha_j + \beta_j$ and the color histogram summarizes the image as $<\alpha_1 + \beta_1, \ldots, \alpha_n + \beta_n>$.

3.3 Features from Coherent Clusters

The additional features at this stage are based on the coherent clusters only. We select four features namely, Size of largest cluster in each bin; Size of median cluster in each bin; Size of smallest cluster in each bin; and Variance of clusters in each bin.

Let us denote the largest cluster in each bin as $L_{\alpha j}$, the median cluster in each bin as $M_{\alpha j}$, the smallest cluster in each bin as $S_{\alpha j}$ and variance of clusters in each bin as $V_{\alpha j}$. Since there are 4 bins, so we get additional 4 features for each bin. Therefore, a total of 40 additional features are considered for image retrieval. Considering section 3.2, initially 6 features per bin are selected for image retrieval and later 4 additional features per bin are considered in this section for refining result of image retrieval.

4 Incremental Image Retrieval Approach

Image retrieval is done in two stages hence the name incremental image retrieval approach. In the first stage, the features defined in section 3.2 are considered for retrieval while in stage 2; the features defined in section 3.3 are considered. The first stage gives us a coarse result while stage 2 refines the result obtained in stage 1. Therefore, result is relevant and accurate image retrieval from image databases.

4.1 First Level Retrieval

The features obtained in section 3.2 are used for retrieval at first level. We use the L_1 distance to compare two images I and I′.

$$\Delta_1 = \left| (\alpha_j\text{-}\alpha'_j) \right| + \left| (\beta_j\text{-}\beta'_j) \right| \tag{1}$$

$$\Delta_2 = \left| (C_{\alpha j}\text{-}C'_{\alpha j}) \right| + \left| (C_{\beta j}\text{-}C'_{\beta j}) \right| \tag{2}$$

$$\Delta_3 = \left| (\mu_{\alpha j}\text{-}\mu'_{\alpha j}) \right| + \left| (\mu_{\beta j}\text{-}\mu'_{\beta j}) \right| \tag{3}$$

In scheme [1], only equation (1) is used and following is used for comparison:

$$\Delta = \left| (\alpha_j+\beta_j) \right| - \left| (\alpha'_j+\beta'_j) \right| \tag{4}$$

4.2 Second Level Retrieval

This level of retrieval is used for further refining the result obtained in section 4.1. The additional features obtained in section 3.3 are used at this level of retrieval. Again we use the L_1 distance to compare two images I and I′. Using the L_1 distance, the jth bucket's contribution to the distance between I and I′ is:

$$\Delta_4 = \left| (L_{\alpha j} - L'_{\alpha j}) \right| \tag{5}$$

$$\Delta_5 = \left| (M_{\alpha j} - M'_{\alpha j}) \right| \tag{6}$$

$$\Delta_6 = \left| (S_{\alpha j} - S'_{\alpha j}) \right| \tag{7}$$

$$\Delta_7 = \left| (V_{\alpha j} - V'_{\alpha j}) \right| \tag{8}$$
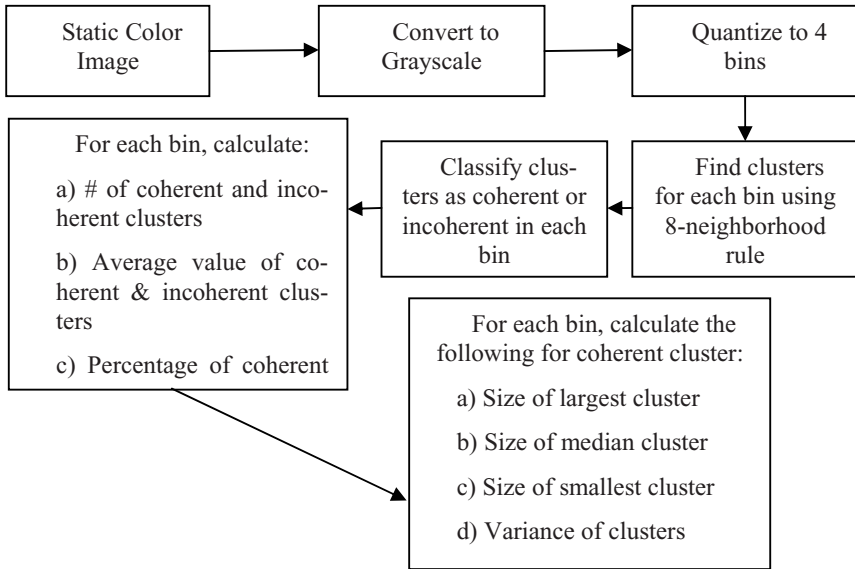
Fig. 1. Block diagram of the feature extraction algorithm

5   Results and Discussion

The proposed algorithm is tested with the database provided by James S. Wang et. al [14]. Ater theFirst the images were preprocessed and converted to grayscale images. Then the images were quantized and the features described in section 3.2 were calculated. Also, the features described in section 3.3 were calculated. These features were stored with each of the images. Figure 2 shows one of the image from the database, its corresponding grayscale image and then the corresponding quantized images.

Consider table 1. Table 1 provides the parameter values related with the incoherent clusters. The parameters include percentage of incoherent pixels (β_j), number of incoherent clusters (C_{β_j}) and average of incoherent cluster (μ_{β_j}) for each jth bucket or bin. As an example, we show the results for 4 bins of one of the images in table 1. Figure 3 shows the corresponding incoherent clusters.

Fig. 2. One of the image from the database, converted to grayscale & quantized

Table 1. Example of parameter values for Incoherent pixels

	β_i	$C_{\beta i}$	$\mu_{\beta i}$
Bin 1	0.78%	38	1.1053
Bin 2	7.02%	64	5.8438
Bin 3	31.02%	86	19.209
Bin 4	61.18%	105	31.048
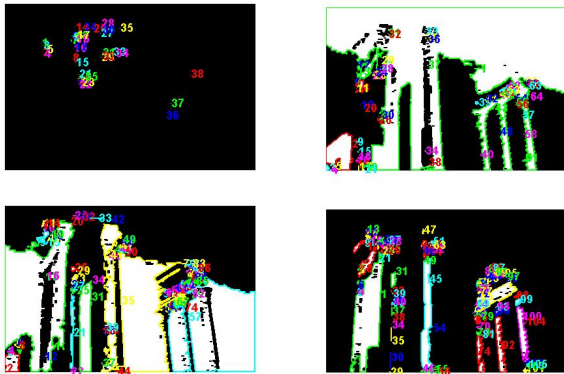
Fig. 3. Incoherent clusters in 4 different bins

Consider table 2. Table 2 provides the parameter values related with the coherent clusters. The parameters include percentage of coherent pixels (α_j), number of coherent clusters ($C_{\alpha j}$) and average of coherent cluster ($\mu_{\alpha j}$) for each jth bucket or bin. As an example, we show the results for 4 bins of one of the images in table 2.

Consider table 3. Table 3 provides the additional parameter values related with the coherent clusters. The parameters include size of largest cluster in each bin ($L_{\alpha j}$), size

Table 2. Example of parameter values for coherent pixels

	α_j	$C_{\alpha j}$	$\mu_{\alpha j}$
Bin 1	0	0	0
Bin 2	50.61%	2	26689
Bin 3	41.68%	4	10990
Bin 4	7.71%	3	2712

Table 3. Additional parameter values for coherent pixels

	$L_{\alpha j}$	$M_{\alpha j}$	$S_{\alpha j}$	$V_{\alpha j}$
Bin 1	0	0	0	0
Bin 2	51606	0	1772	1.24E+09
Bin 3	14553	12637	2340	34021226
Bin 4	4996	2025	1115	4119517

of median cluster in each bin ($M_{\alpha j}$), size of smallest cluster in each bin ($S_{\alpha j}$) and Variance of coherent clusters in each bin ($V_{\alpha j}$). As an example, we show the results for 4 bins of one of the images in table 3.

The results were compared with the L_1 distance as described in section 4. First, we used equation (1) to equation (3) for identifying the similarity between images. Then we used equation (5) to equation (8) to further refine the results.

The figure 4 shows the query images and the first 3 results obtained by using the above described algorithm. On inspection of all the images of the database, we found that this was the closest result. Similar query results were obtained for various query images.

(a) Query Image

(b) First Level Retrieval

(c) Second Level Retrieval

Fig. 4. Image Retrieval from the database

6   Conclusions

In this paper, we have proposed an algorithm that is based on color histogram. We have shown that the features obtained using this algorithm are quite useful for relevant image retrieval queries. The feature selection is based on the number, color and shape of objects present in the image. The grayscale values, mean, variance and various sizes of the objects are considered as appropriate features for retrieval. These

features are independent of image orientation. Color refinement method takes care of the color as well as the spatial relation feature. The shape features are extracted in section 3.3 from the color based features defined in section 3.2. This algorithm works well in space domain. We plan to extend it to the transform domain in future.

We have also presented a two stage approach for image retrieval. At first stage, initial set of features described in section 3.2 is used for image retrieval. At next stage, additional features described in section 3.3 are considered for retrieval. Hence, this approach is computationally efficient and provides refined result because of 2-stage retrieval. Results show algorithm presented provides relevant retrieval results.

References

1. Greg Pass and Ramin Zabih. Histogram Refinement for content–based image retrieval. In IEEE Workshop on Applications of Computer Vision, pages 96-102, December 1996.
2. Arnol W. M. Smeulders, Marcel Worring, Simone Santini, Amarnath Gupta, Ramesh Jain, "Content Based Image Retrieval at the end of the early years", IEEE Transactions on Pattern Analysis and Machine Intelligence, Vol 22, No. 12, pp 1349-1380, 2000.
3. Wynne Hsu, T. S. Chua and H. K. Pung. An integrated color-spatial approach to content based image retrieval. In ACM Multimedia Conference, pages 305-313, 1995.
4. Paisarn Muneesawang and Ling Guan, "Automatic machine interactions for content based image retrieval using a self organizing tree map architecture", IEEE Transactions on Neural Networks, Vol 13, No. 4, pp 821-834, 2002.
5. Michael Swain and Dana Ballard. Color indexing. International Journal of Computer Vision, 7(1):11-32, 1991.
6. Rick Rickman and John Stonham. Content based image retrieval using color tuple histograms. SPIE proceedings, 2670:2-7, February 1996.
7. Chabane Djeraba, "Association and content based retrival", IEEE Transactions on Knowledge and Data Engineering, Vol. 15, No. 1, pp 118-135, 2003.
8. Markus Stricker and Alexander Dima. Color indexing with weak spatial constraints. SPIE proceedings, 2670:29-40, February 1996.
9. Jing Huang, S. Ravi Kumar, Mandar Mitra, Wei-Jing Zhu, and Ramin Zabih. Image indexing using color correlograms. In IEEE Conference on Computer Vision and Pattern Recognition, pages 762-768, 1997.
10. Jong-An Park, Min-Hyuk Chang, Tae Sun Choi and Muhammad Bilal Ahmad, "Histogram based chain codes for shape description," IEICE Trans. On Communications, vol.E86-B, no.12, pp. 3662-3665, December 2003.
11. K.H.Choi, M.H.Shin, S.H.Bae, C.H.Kwon, I.H.Ra, "Similarity retrieval based on SOM-Based R*-Tree", LNCS 3038, International Conference on Computational Science (ICCS), pp 234-241, 2004.
12. Xin Huang, Shijia Zhang, Guoping Wang, Heng Wang, "Optimal matching of images using combined color feature and spatial feature", LNCS 3991, International Conference on Computational Science (ICCS), vol. 1, pp 411-418, 2006.
13. James Z. Wang, Jia Li, Gio Wiederhold, ``SIMPLIcity: Semantics-sensitive Integrated Matching for Picture LIbraries," IEEE Trans. on Pattern Analysis and Machine Intelligence, vol 23, no.9, pp. 947-963, 2001.

A Novel Method Providing Multimedia Contents According to Preference Clones in Mobile Environment*

Sanggil Kang[1] and Sungjoon Park[2,**]

[1] Computer Science and Engineering, INHA University, 253 Younhyun-dong, Nam-gu, Incheon, South Korea
sgkang@inha.ac.kr
[2] Department of Mobile Game, Kongju Communication and Arts College, Gongju, Chungnam 314-713, South Korea
sjpark@kcac.ac.kr

Abstract. We introduce a novel method of automatic providing multimedia content in mobile environment. With using our method, the problem of the limitation of resource of mobile devices can be solved. In this paper, we introduce a novel method of recommendation of personalized contents according to preference clones using a collaborative filtering technique in mobile environment. We divide the user group to two sub-groups by analyzing the match of preferences of members in the sub-groups. The division process recursively applies to each sub-group and place the sub-groups in a binary decision tree (BDT). From the binary decision tree, we identify the preference clones of each target user by matching the target user's consumption behavior to that of each sub-group in the BDT with a sequential manner. We also implemented our system based on Java Micro Edition platform.

Keywords: Binary decision tree, mobile devices, personalization, and preference clones.

1 Introduction

By the rapid spread of mobile devices such as cellular phone, PDA, and portable TV, user can enjoy many kinds of multimedia contents through mobile appliances anytime and anywhere. Especially, the population of Digital Multimedia Broadcasting (DMB) user increases drastically year by year since available as a commercial service from May 2005 in Korea. Also, DMB service has been at the center of developing issues in mobile environment. Because of significant increase of contents through mobile devices, user sometimes spends heavy effort and time for searching and downloading their preferred contents.

In order to solve the problem, we introduce a novel method of recommendation of personalized contents according to preference clones using a collaborative filtering

technique in mobile environment. In this paper the preference clone means a user whose consumption pattern is very similar to that of another user. We divide the user group to two sub-groups by analyzing the match of preferences of members in the sub-groups. The division process recursively applies to each sub-group and place the sub-groups in a binary decision tree (BDT). From the binary decision tree, we identify the preference clones of each target user by matching the target user's consumption behavior to that of each sub-group in the BDT with a sequential manner.

The remainder of this paper is organized as follows. Section 2 introduces related work. Section 3 overviews the overall architecture of the proposed system. In Section 4, we explain our proposed method. In Section 5, we design and implement the prototype of the proposed system and show the performance comparison between our method and a conventional method. We then conclude our paper in Section 6.

2   Related Work

Various personalization techniques can be classified into three possible categories such as the rule-based, inference method, and collaborative filtering. The rule-based recommendation is usually implemented by a predetermined rule, for instance, if - then rule. Kim et al. [1] proposed a marketing rule extraction technique for personalized recommendation on internet storefronts using tree induction method. As one of representative rule-based techniques, Aggrawall et al. [2] proposed a method to identify frequent item sets from the estimated frequency distribution using association-rule mining algorithm. The inference method is the technique that a user's content consumption behavior is predicted based on the history of personal content consumption behaviors. Lee [3] designed an interface agent to predict a user's resource usage in the UNIX domain by the probabilistic estimation of behavioral patterns from the user behavior history. Collaborative filtering (CF) technique recommends a target user the preferred content of the group whose content consumption mind is similar to that of the user. Because of the mature of the technique, CF has been attractive for predicting various preference problems such as net-news [4], e-commerce [5], digital TV [6], digital libraries [7], etc.

Several papers applied CF to mobile devices. Coster et al. [8] used a CF for predicting rating changes of movie data based on users' new or updated ratings in their system, MobiTip [9]. Also, Miller et al. [10] developed a recommender system for recommending video movie to occasionally connecting users through mobile devices. Tveit [11] applied a CF to mobile commerce based on using votes or opinions about products and services from similar customers using Peer-to-Peer. Zhang et al. [12] explored effective ways of delivering personalized content under the restrictions on wireless networks and mobile devices.

The literatures mentioned above do not consider recent implicit usage behavior for inferring users' preference. However, it can be a critical clue for predicting a target user's usage behavior near future. In this paper we use target user's implicit feedback by using binary decision technique. From the following section, we demonstrate our method in detail.

3   Architecture of Our System

Fig. 1 shows the overall architecture of our system in mobile environment. The architecture is composed of two parts: one is server side and the other is client side.
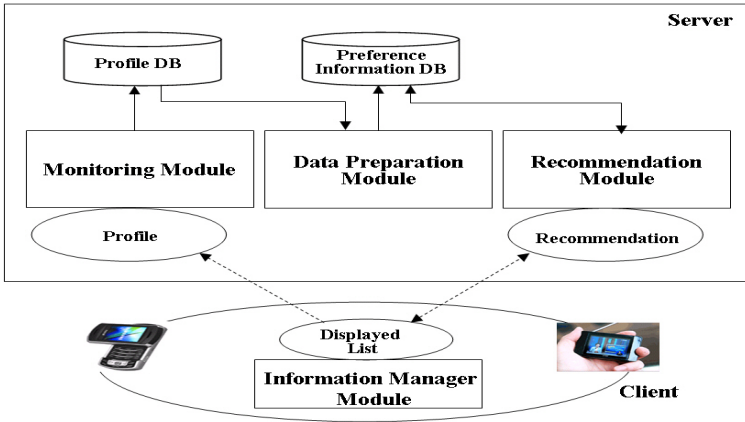
Fig. 1. Overall architecture of our system

The server side consists of three parts such as Monitoring Module (MM), Data Preparation Module (DPM), and Recommendation Module (MM). The MM records the log file such as user ID, gender, age, content consumption behavior (usage history), and store them into the Profile DB. The DPM eliminates nosy data from the collected usage history and makes groups according to users' age and gender. Also, it stores them into the Preference Information DB. The RM analyzes the preference of multimedia contents according to users' age and gender group using the proposed algorithm explained in detail from the following section. Then, it recommends preferred contents to each target user.

The client side has one module called Information Manager Module (IMM). The IMM displays recommendation list provided from the server side. Also, it records information of content consumed by the mobile user.

4   The Proposed Recommendation Algorithm

4.1   Group and Member Preference

In general the similarity of user preference can be characterized by age and gender. For instance, the documentary programs of DMB are usually popular favor for thirties and forties man, while the show programs are for teenagers and twenties. In each group, for each user, very similar or identical users to the user can exist, in the sense of consumption pattern. We call those similar or identical users "preference clones" in this paper. If preference clones for a new mobile user are founded, we recommend or provide the preferred contents of the preference clones to the new user, sometimes

called "target user." To recommend or provide preferred contents to target user, we first group existing users by age and gender as seen in (1).

$$U = [U_1, U_2, \cdots, U_i, \cdots U_L] \tag{1}$$

where, U_i (i = 1, 2, . . . L) is the ith age and gender group in the whole existing reference group, U. Also, the U_i includes J members as expressed in (2).

$$U_i = [u_1, u_2, \cdots, u_j, \cdots u_J] \tag{2}$$

where, u_j is the jth member in sub-reference group U_i. For U_i, the preference of contents can be computed and ordered by the frequency of the group's content consumption during predetermined time period. The overall preference order of contents for J members can be denoted as $Pref_{Ui}$. Also, for member u_j, the preference of contents can be computed and ordered from high preference to low preference by the frequency of the member's content consumption. The preference order of the contents can be denoted as $Pref_{uj}$. Using the preference order of each group and its corresponding members, the preference clones can be found by making sub-groups in binary decision tree (BDT).

4.2 Sub-reference Groups in Binary Decision Tree (BDT)

From any sub-reference group U_i, we can also decompose it into two sub-groups by matching between the first element of $Pref_{Ui}$, denoted as $Pref_{Ui}(1)$ and that of $Pref_{uj}$ of each member u_j, denoted as $Pref_{uj}$ (1), as seen in (3).

$$\begin{cases} u_j \rightarrow U_{i,p}, & \text{for} \qquad pref_{U_i}(1) = pref_{u_j}(1), \\ u_j \rightarrow U_{i,n}, & otherwise \end{cases} \tag{3}$$

where, $U_{i,p}$ and $U_{i,n}$ is called positive sub-reference group and negative sub-reference group of U_i, respectively. Also, j = 1, 2, . . ., J. With the same process, $U_{i,p}$ can also decompose two sub-reference groups. Let's say, if there are P members in the sub-reference group $U_{i,p}$ then the overall preference of contents consumed by the P members can be computed and ordered. The ordered preferences of the sub-reference group can be denoted as $Pref_{Ui,p}$. Also, for each member k in the sub-reference group, his/her ordered preference for the contents can be denoted as $Pref_{uk}$. The $U_{i,p}$ can be decomposed by matching between the second element of $Pref_{Ui,p}$, denoted as $Pref_{Ui,p}(2)$ and that of $Pref_{uk}$ of each member u_k, denoted as $Pref_{uk}(2)$, as seen in (4).

$$\begin{cases} u_k \rightarrow U_{i,p,p}, & \text{for} \qquad pref_{U_{i,p}}(2) = pref_{u_k}(2), \\ u_k \rightarrow U_{i,p,n}, & otherwise \end{cases} \tag{4}$$

where, $U_{i,p,p}$ and $U_{i,p,n}$ is called positive sub-reference group and negative sub-reference group of $U_{i,p}$, respectively. Also, k = 1, 2, . . ., K. For the same way, $U_{i,n}$ can also decomposed as seen in (5).

$$\begin{cases} u_k \rightarrow U_{i,n,p}, & \text{for} \qquad pref_{U_{i,n}}(2) = pref_{u_k}(2), \\ u_k \rightarrow U_{i,n,n}, & otherwise \end{cases} \tag{5}$$

Where, $U_{i,n,p}$ and $U_{i,n,n}$ is called positive sub-reference group and negative sub-reference group of $U_{i,n}$, respectively. Also, $k = 1, 2, . . ., J\text{-}K$. With the same process, each sub-reference group can be decomposed until each sub-reference group can not be decomposed anymore.

The accuracy of our method depends on the size of reference group. If the size is big then the accuracy will increase because the reference group has high possibility to contain more precise preference clones. In the following section, we compare the performance of our method with the typical Top-N recommendation method by varying the size of reference group.

5   Experiments

5.1   Experimental Environment

We implemented our system using CLDC/MIDP based on Java ME platform and Java SDK in the windowsXP environment. In order to test our method, J2ME Wireless Toolkit Emulator was used.

Due to difficulty in collecting users' contents in mobile environment until present time, we used 2000 TV viewers' watching history for executing our algorithm instead of the DMB programs. The data was provided by AC Nielsen Korea, one of the authorized market research companies, from January 1, 2003 to April 30, 2003. The watching history was collected by the Set-Top Box installed in the users' houses. The Set-Top Box also recorded viewers' profile information such as age and gender, and watched programs. In the data, there are around 100 programs. Thus, the multimedia content is considered the program in this experiment.

5.2   Demonstration of Our Method

Fig. 2 shows the demonstration of our method according to target user's watching behavior. We structured the binary decision tree (BDT) using 10 teenage boys' watching history collected during one month as explained in the previous chapter. When a target teenage user connected to the server, program P1 as seen in Fig. 3(a) is recommended through his mobile because P1 is the first ranked one in the teenage boy reference group as seen in the preference table. If the target user plays P1 by clicking the 'play' button on the mobile which implies positive feedback of our recommendation then we move to the left of the next level and recommend P5 at the next stage as seen in Fig. 3(b). The P5 is the second ranked program in the sub-reference group whose all members watched P1. If the target user skips the recommend program by clicking the 'skip' button which implies negative feedback, we move to the right of the next level and recommend P2 as seen in Fig 3(c). The P2 is the second ranked program in the sub-reference group whose all members did not watch P5. If the target user plays P2 then we move to the left of the next level and can find the preference clone u_1 of the target user. The programs the preference clone watched are automatically recommended to the target user in the future. Like this, our method dynamically recommends programs to the target user in a recursive manner.

Fig. 2. The BDT of the teenage boy group

| (a) The beginning stage | (b) The positive feedback stage | (c) The negative feedback stage |

Fig. 3. The examples of dynamical program providing through the target user's mobile device

5.3 Evaluation of Our Method

In this section, we compared the performance of our method with that of the conventional recommendation method, TOP-N [13]. The 2000 TV viewers' watching history was divided into reference data and target user data. Also, the reference data was grouped according to its members' age and gender such as teenage boys, teenage

girls, twenties man, twenties woman, thirties man, thirties woman, forties man, and forties woman. The performance was evaluated with the overall ratio of the number of match between recommended programs to target users' preference clones and watched programs by them. Also, we repeated the evaluation by varying the size of reference data such as 500, 1,000, and 1,500 members in the reference data and the collection period of usage history such as one month, two months, and three months. For the performance evaluation, the one next month data of the reference data was used.

From the table, it is shown that our method outperforms TOP-N method when the reference data size is relatively big. However, when the reference size is relatively small, TOP-N is little better than our method. For instance, for 500 reference members with one month collection period, the accuracy of our method and TOP-N are 65% and 68%, respectively. However, for 1,000 reference members, we have 73% for our method and 72% for TOP-N. For 1,500 reference members, we have 81% for our method and 73% for TOP-N. It is because the possibility that the preference clones of each target user are included in the reference data is low.

From the table, it is shown that the collection period does not much influence on the accuracy for both methods. For 1,500 reference data, the accuracies of our method for one month, two months, and three months are 81%, 82%, and 84%, respectively. Also, for TOP-N, we have 73%, 74%, and 75%. In general, user's preference trend for the multimedia content like TV program does not drastically change. That is the reason why the collection period does not give an impact on improving the performance for both our method and TOP-N method.

Table 1. Comparion of performances of our method and TOP-N method

Data collection period	Method	Reference Size		
		500	1,000	1,500
1 month	TOP-N	68%	72%	73%
	Our	**65%**	**73%**	**81%**
2 months	TOP-N	69%	74%	74%
	Our	**66%**	**74%**	**82%**
3 months	TOP-N	69%	75%	75%
	Our	**66%**	**76%**	**84%**

6   Conclusion

In this paper, we introduced a novel method of providing automatic multimedia contents through mobile devices. From the result of the performance comparison between our method and the conventional method, we can conclude that the performance of our method is better than that of the conventional method for relatively large reference data. However, for small reference data, our method is not appropriate for use.

The data (2,000 viewers) we used for evaluating our method and the conventional method is not big enough to confirm the accuracies. Therefore, we need to redo the

experiment with more data set. Also, we need to apply our method to other mobile multimedia contents such as music, mobile shopping mall, and mobile web service.

References

1. Kim, J.W., Lee, B.H., Shaw, M.J., Chang, H.L., Nelson, M.: Application of Decision-Tree Induction Techniques to Personalized Advertisements on Internet Storefronts. International Journal of Electronic Commerce, vol. 5, no. 3 (2001) 45-62
2. Aggrawall, R., Imielinski, T., Swami, A. : Mining Association Rules between Sets of Items in Large Databases. Proc. ACM SIGMOD Int'l Conference on Management of Data (1994) 207-216
3. Lee, J.J. : Case-based plan recognition in computing domains. Proc. The Fifth International Conference on User Modeling, (1996) 234-236
4. Resnick, P., Lacovou, N., Suchak, M., Bergstrom, P., Riedl, J. : GroupLens: An Open Architecture for Collaborative Filtering of Netnews. Internet Research Report, MIT Center for Coordination Science (1994) http://www-sloan.mit.edu/ccs/1994wp.html
5. Schafer, J.B., Konstan, J., Riedl, J. : Recommender systems in e-commerce. ACM Conference on Electronic Commerce (1999) 158-166
6. Cotter, P., Smyth, B. : Personalization Techniques for the Digital TV world. Proc. European Conference on Artificial Intelligence (2000) 701-705
7. Bollacker, K.D., Lawrence S., Giles, C.L.: A System for Automatic Personalized Tracking of Scientific Literature on the Web. Proc. ACM Conference on Digital Libraries (1999) 105-113
8. Coster, R., Svensson M. : Incremental Collaborative Filtering for Mobile Devices. Preeedings of the 2005 ACM Symposium on Applied Computing (2005) 1102-1106
9. Rudstrom, S., Svensson, M., Coster, R., Hook, K.: MobiTip: Using Bluetooth as a Mediator of Social Context. 6th International Conference of Ubiquitous Computing (2004)
10. Miller, B.N., Albert, I., Lam, S.K., Konstan, J.A., Riedl, J.: Movielens Unplugged: Experiences with an Occasionally Connected Recommender System. Proceedings of the 8th International Conference on Intelligent User Interfaces (2003) 263-266
11. Tveit, A.: Pear-to-peer based Recommendations for Mobile Commerce. Proceedings of the 1st International Workshop on Mobile Commerce (2001) 26-29
12. Zhang, D., Shijagurumayum, S.: Personalized Content Delivery to Mobile Devices. IEEE International Conference on Systems, Man and Cybernetics vol. 3 (2003) 2533-2538
13. Mukund D., George K.: Item-Based Top-N Recommendation Algorithms, ACM Transactions on Information System, vol. 22, Issue 1 (2004) 143-177

Belief Combination for Uncertainty Reduction in Microarray Gene Expression Pattern Analysis

Kajia Cao and Qiuming Zhu

Department of Computer Science, University of Nebraska
Omaha, Omaha, NE 68182
kcao@mail.unomaha.edu, qzhu@mail.unomaha.edu

Abstract. Many classification methods are used in microarray gene expression data analysis to identify genes that are predictive to clinical outcomes (survival/fatal) of certain diseases. However, the reliability of these methods is often not well established due to the imprecision of the method and uncertainty of the dataset. In this paper, a knowledge-based belief reasoning system (BRS) is proposed to solve the problem by dealing with the uncertainties inherent in the results of various classification methods. Through the belief combination process, we pursue a means to reduce the uncertainty and improve the reliability of classification so that the underlying features of gene behavior recorded in the microarray expression profiles could be convincingly revealed.

Keywords: uncertainty reasoning, belief reasoning system, Dempster Shafer Theory, microarray gene expression.

1 Introduction

Theories and techniques that dealt with incompleteness (but maybe precise) of information have been evolved in the development of non-monotonic logics, truth maintenance systems (TMSs), reason maintenance systems (RMSs), and other approaches [5]. Meanwhile, theories and techniques for reasoning uncertainty (but maybe complete) of information have also been attempted. For example, techniques adapted from fuzzy measurement and probability theories that accept non-realistic global assumptions have been studied [5, 6, and 11]. Specially, Dempster Shafer theory (DST) of belief projection provides a subtle and more thorough way of reasoning under uncertain and incomplete information which is easier to be referenced than the statistical confidence interval approach [3].

There are a number of methods discussed in the literature for identifying genes that are indicators of certain diseases, health disorders, or clinical treatment outcomes. Known as a classification problem, the identification process corresponds roughly to a clinical diagnosis process: given a set of known models based on prior knowledge, determine the correct model that best fit to the data obtained from measurement and observations [12].

In the expert systems, three distinct layers are defined: representation, inference, and control layers [5]. It is our claim that the treatment of uncertainty in Belief

Reasoning System (BRS) must address each of these layers. Most of researches in this area do not properly cover these issues. Some approaches lack clarity on representation paradigm. Others require unrealistic assumptions to provide uniform combining rules defining the plausible inferences. As we know that non-numerical approaches are inappropriate to represent measures of uncertainty. The numerical approaches need some restrictions on the observations (statistical information, or exclusiveness of hypotheses and so on). All the information that needs in numerical approaches should be precise and numerical. In this case, the input of whole reasoning procedure is complicated and restricted. We then propose a Belief Reasoning System for numerical approaches of reasoning with uncertainty, which organizes its description around the three-layer structure.

Representation Layer

There should be an explicit and consistent representation of the amount of evidence for supporting any given hypothesis on this layer. The presentation of the information about the evidence which is known as meta-information, such as the evidence source, the reasons for supporting a given hypothesis, should be given in an explicit way. Specially, all the evidence and its meta-information should be factual-based, but could be incomplete, in terms on the possibly limited observation on evidence. The representation of observation (evidence) should be available on discriminant information gathering which may be used to define the knowledge functions in inference layer. Multi-measurements that applied in the gene pattern classification are the inputs of the layer in this paper.

General approaches of classification include: (a) parametric methods where a model is often assumed prior the classification process, such as the principal component analysis (PCA) [7], independent component analysis (ICA), and separation correlation metric (SCM) [8], alternatively known as the Fisher's discrimination criterion (FDC) [1]; and (2) non-parametric methods where a model is often learned (formed) gradually during the classification process, such as the threshold number of misclassification (TNoM) [10], projection pursuit regression (PPR) [2], support vector machines (SVM) [11], and expectation maximization (EM) [13]. Each of these methods solves the uncertainty problem partially, from different aspect and at different levels, however. No single method of above can provide a completely certain and reliable solution to the classification problem of most real world applications, such as the microarray data analysis.

Inference Layer

The inference should be based on global assumptions of evidence independence and should not depend on any assumption on probability distribution or model of the propositions in terms of the objectivity of the reasoning [3]. For example, Triangular norms (T-norms) are presented to summarize and propagate the uncertain information previously [5]. T-norm is a binary function that satisfies the requirements of the conjunction and disjunction operators which should be monotonic, commutative, and associative.

Dempster Shafer Theory (DST) which proposed by Shafer which also satisfies all the assumptions is selected as the reasoning inference in this paper (section 2). Combination rules of evidence should also maintain the closure of the syntax and semantics of the representation of uncertainty, i.e., any knowledge functions that used

to propagate the uncertainty should have logically clear definition to allow the Control Layer to decide the most appropriate combination rule and making decision.

Control Layer

The appropriate uncertainty operator will be first decided in this layer, and then the related combination rule. It is important to measure the uncertainty of the information as well as the uncertainty of the measure itself. The aggregation and propagation of uncertainty through the reasoning process must be traceable to solve conflicts or contradictions that may be occurred in evidence and inference procedure. It should be possible to make pair-wise comparisons of uncertainty.

In this paper, the problem of reasoning uncertainty of multi-measurements based on belief reasoning system will be first generalized in section 2. Specifically, reasoning under uncertainty using Dempster Shafer Theory (DST) for identifying genes indicative to clinical survival outlook of DLBCL from gene profiling data analysis will be described. Experimental result and discussion are presented in section 3 and 4 respectively.

2   Uncertainty Reduction of Gene Pattern Analysis Based on Belief Reasoning System

2.1   Measurements Applied to DLBCL Gene Expression Profiling Data (Representation Layer)

Identifying genes that are predictive to clinical outcomes is one of the important goals in the analysis of gene expression profiling data from tumor samples. Two gene expression profiling studies of diffuse large B-cell lymphoma (DLBCL) have identified genes predictive of clinical outcomes [20, 21]. Rosenwald et al identify from functional (gene expression signature) groups of genes that are predictive of survival including genes that divide the tumor into distinct biologic subtypes [15]. Shipp et al applied supervised learning method on an expression profiling dataset of 7139 genes over 58 tumor specimens, and identified 13 genes that are highly predictive to the outcomes [14].

To create an outcome predictor that integrates a number of highly indicative genes, we concentrated on evaluating individual genes with respect to the expected outcome on Shipp's microarray dataset (www.genome.wi.mit.edu/MPR/lymphoma) applying multiple measurements [16]. The patient cases are pre-classified into two groups: *Group 0* (26 cases) as fatal cases and *Group 1* (32 cases) which represents survival cases. The measurements that applied to the dataset are Fisher's Discrimination Criterion (FDC) Cross-Projection (CP) and Discrete Partition (CP). FDC method is the parametric method identifying data attributes and their projections that are most likely to be separable among different classes. Cross-projection and Discrete Partition are proposed to fuse with the FDC in order to diminish the side effects of the outliers on FDC. All of these approaches are independent to each other. In Belief Reasoning System, the uncertainty and reliability of the three measurements: FDC, CP and DP will be discussed.

2.2 Dempster Shafer Theory as the Inference Layer

There are number of functions of measurements used in DST: the *basic probability assignment* (*bpa*) function (*m*), the *Belief* function (*Bel*), and the *Plausibility* function (*pl*). All these functions are related to each other in some ways. The basic probability assignment defines a mapping of the power set of independent variables to the interval between 0 and 1, *m: p(X) → [0, 1]*, which satisfies: $m(\varnothing) = 0$, $\sum_{A \in P(x)} m(A) = 1$.

Where *p(X)* represents the power set of a universal event set *X*, $\varnothing$ is the null set, and *A* is a subset in the power set [8]. The value of *m(A)* pertains only to the set *A* and makes no additional claims about any subsets of *A*. Any further evidence on the subsets of *A* would be represented by another bpa, i.e. $B \subset A$, where *m(B)* would be the bpa for the subset *B*.

Formally, for all sets *A* that are elements of the power set $A \in p(X)$, we have the following relations [8]:

$$Bel(A) = \sum_{B|B \subseteq A} m(B) \tag{1}$$

$$Pl(A) = \sum_{B|B \cap A \neq \varnothing} m(B) = 1 - Bel(\overline{A}) \tag{2}$$

where $\overline{A}$ is the classical complement of *A*.

Given two independent evidences which are expressed as two bpa's: m_1, and m_2, they can be combined into a single joined basic assignment m_{12} by applying Dempster's rule of combination, as shown in the following manner:

$$m_{12}(A) = \frac{\sum_{B \cap C = A} m_1(B)m_2(C)}{1 - \sum_{B \cap C = \varnothing} m_1(B)m_2(C)} \tag{3}$$

$$m_{12}(\varnothing) = 0 \tag{4}$$

where $1 - \sum_{B \cap C = \varnothing} m_1(B)m_2(C)$ is a normalization factor which is represented by letter *K* normally. When *K = 1*, it has the effect of completely ignoring conflict and attributing any probability mass associated with conflict to the null set [6].

2.3 Choice of Combination Rules of DST in Control Layer

There is no need to include page numbers. If your paper title is too long to serve as a running head, it will be shortened. Your suggestion as to how to shorten it would be most welcome.

Combination rules are the special types of aggregation methods for data obtained from multiple sources. Dempster's rule of combination is critical to the conception of belief projection in DST since the measures of Belief and Plausibility are derived from the combined basic assignments. There also derived several other combination

rules, for example, Yager's rule, Inagaki's rule, Zhang's rule etc., which may concern about other properties of the data that Dempster's rule of combination may not be applied.

In this paper, all the sources in the experiment (section 4) are independent to each other. This satisfies the request of Dempster's rule of DST: the Dempster's rule of combination is purely a conjunctive operation (AND), that is, the combination rule results in a belief function based on conjunctively pooled evidence [4].

To account for uncertainties, we choose several sets of candidate measurements, marked as S_1, S_2, …, S_n, respectively, in terms of their specific aspects merited to the problem of classification. All of these candidate measurements should be independent to each other according to the principle of belief projection [4].

For each set A of measurement objectives, we calculate the basic probability assignments (bpa) based on

$$m: p(X) \to [0, 1] \tag{5}$$

for each sample in our experimentation using:

$$m(A) = (m_1 \oplus m_2 \oplus m_3 \oplus ... \oplus m_n) = \sum_{\cap A_i = A} \prod_{1 \le i \le n} m_i(A_i) / K \tag{6}$$

where

$$K = 1 - \sum_{\cap A_i = \phi} \prod_{1 \le i \le n} m_i(A_i) = \sum_{\cap A_i \ne \phi} \prod_{1 \le i \le n} m_i(A_i) \tag{7}$$

A is the designated pattern (target); n is the number of measurements in each set of candidate measurements.

After the calculation, the belief function for each objectives $Bel(A)$ can be calculated by using formula (1).

3   Belief Projections of Multi-measurements on DLBCL

According to the multi-measurements (Fisher's Discrimination Criterion, Cross-Projection, and Discrete Partition) that mentioned above, one combinatorial set of candidate measurements is conducted. FDC and CP which are parametric methods perform maximum likelihood classification on gene dataset, while DP is the non-parametric method that calculates the minimum likelihood for each gene. It is possible that the result of FDC or CP is contradicted with DP result, that is, the statistics of the certain gene is not consistent with its geometrical display. The process of computation for belief projection using DST's rule of combination in gene pattern analysis is then described as follow:

1.   For each gene g_k
     //Measurements calculation
     1.1 Compute FDC, CP and DP value separately (see figure 1 through 3).
         The computation is given in [16].

1.2 Sort the results of FDC, CP and DP values separately. For the fairness of the experiments, pick up the first 400 genes (over 5% of whole 7129 genes) in the experiment result of FDC, CP and DP.

1.3 Present algorithmic fusion on the candidate lists and 15 genes are retrieved (see figure 4). We also do the ordinary overlapping on the 400 genes, and pick up the first 15 genes (see figure 5) as a comparison to 15 genes selected by algorithmic fusion.

//Calculate basic probability assignments

1.4 For the designated pattern A_k (from probability prospective, it is called "event") of the certain gene – "gene g_k is significantly expressed", the basic probability assignments (bpas) of FDC, CP and DP are projected into the interval [0, 1] by formula (5).

1.5 Because of the nature (possible contradiction) of input measurements, we would set the bpas which are shown in table 1.

1.6 Calculate the Belief function $m(\{A\})$ by formula (6) where normalization factor K could be calculated by formula (7).

2. Calculate *Bel(A)* by formula (1) for each contradicted or non-contradicted cases.

To compare the *belief(A)* on each gene list, we first sort the *belief(A)* in descending order on each list and draw the histogram for both, see figure 6.

Table 1. bpas of FDC, CP and DP

	A will happen	A will never happen	Uncertain
FDC	$m_{FDC}(\{A\})=bpa(FDC)$	$m_{FDC}(\{\neg A\})=0$	$m_{FDC}(\{A,\neg A\})=1-bpa(FDC)$
CP	$m_{CP}(\{A\})=bpa(CPI)$	$m_{CP}(\{\neg A\})=0$	$m_{CP}(\{A,\neg A\})=1-bpa(CPI)$
DP	$m_{DP}(\{A\})=0$	$m_{DP}(\{\neg A\})=bpa(DPI)$	$m_{FDC}(\{A,\neg A\})=1-bpa(DPI)$
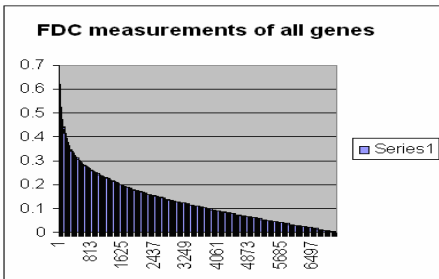
Fig. 1. FDC values of all genes   **Fig. 2.** CP values of all genes
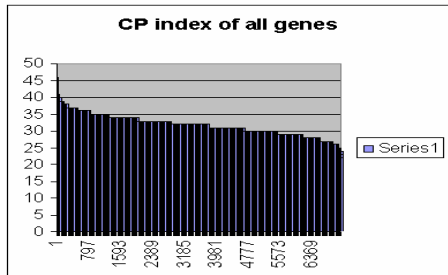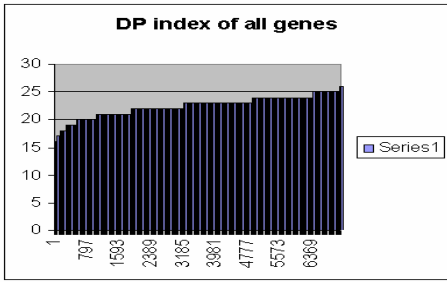
Fig. 3. DP values of all genes
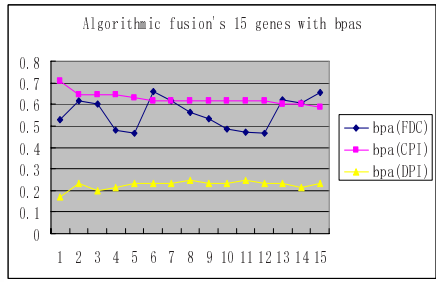
Fig. 4. Algorithmic fusion's 15 genes
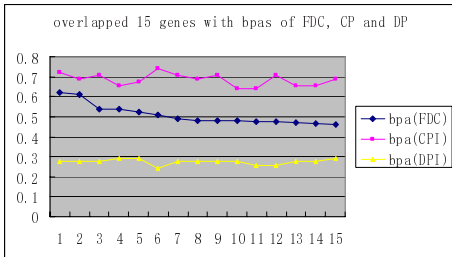
Fig. 5. Overlapped 15 genes
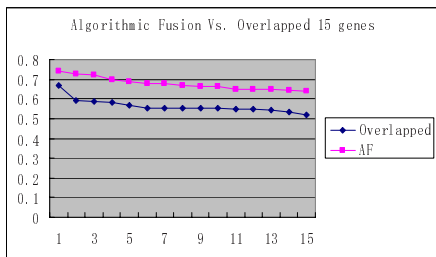
Fig. 6. Algorithmic Fusion Vs. 15 genes

4   Conclusion and Discussion

In this paper, we generated Belief Reasoning System and its application on DLBCL gene pattern analysis. We also adopted Demspter Shafer theory as numerical reasoning approach on testing the multi-sources during the reasoning procedure. From the experiments on DLBCL Microarray gene analysis, we found that BRS helps to build a modularized way which makes the multi-sources uncertainty reasoning procedure more organized and easy handling. In figure 5, it is intuitive that bpa of FDC varies significantly from the other two measurements while overlapped 15 genes in figure 6 shows more consistent relationship among the three measurements. But it is hard to say which list is trustable. After DST is applied on the measurements, the genes selected from algorithmic fusion outperformed highly the gene list picked from simply overlapped 15 genes in figure 7. So the conclusion can be made that the more comprehensive selection of genes is the more reliability can be guaranteed.

However, it needs to be pointed out that when the combination of measurements is large enough, the calculation of DST is too complex to be applied in real problem. For example, in the three measurements combination cases, six factors are needed to calculate normalization factor K, while in the four measurements combination cases, more than ten factors are needed on calculating K. Generally, DST could be used in microarray gene prediction, because three to four measurements are practically enough due to the similarity and relativity of parametric or non-parametric approaches.

References

1. Fisher, R. A. Sc. D., F. R. S.: The Use of Multiple Measurements In Taxonomic Problems, Reproduced from the Annals of Eugenics, Vol. 7 (1936) 179 – 188
2. Friedman, J. H., Tukey, J. W.: A Projection Pursuit Algorithm for Exploratory Data Analysis, IEEE Trans. of Computers, c-23(9), (1974) 881-890
3. Shafe, G. r: A Mathematical Theory of Evidence, Princeton University Press (1975)
4. Shafe, G. r: Probabiliy Judgement in Aritificial Intelligence, Uncertainty in Artificial Intelligence, L.N.Kanal and J.F. Lemmer, New York, Elsevier Science. 4 (1986)
5. Bonissone, P. P.: Summarizing and Propagating Uncertain Information with Triangular Norms, International Journal of Approximate Reasoning (1987) 1: 71 – 101
6. Yager, R.: On the Dempster-Shafer Framework and New Combination Rules, Information Sciences , 41 (1987) 93 – 137
7. Oja, E.: Principal Components, Minor Components, and Linear Neural Networks, Neural Networks, 5 (1992) 927-935
8. Klir,G. J., Wierman, M. J.: Uncertainty-Based Information: Elements of Generalized Information Theory, Heidelberg, Physica-Verlag (1998)
9. Wessels, L. F., Reinders, M. Baldocchi,J. R., Gray, J.: Statistical Analysis of Gene Expression Data, Proceedings of the Belgium-Netherlands Artificial Intelligence Conference (1999)
10. Ben-Dor, A., Fridman, N., Yakhini, Z.: Scoring Genes for Relevance, Technical report AGL-2000-13, Agilent Labs, Agilent Technologies (2000)
11. Brown, M., et. al.: Knowledge-Based Analysis of Microarray Gene Expression Data by Using Support Vector Machines, Proceedings of the National Academy of Sciences, USA, 97 (2000) 262 – 267
12. Slonim, D. K., Tamayo, P. J., Mesirov, P., Golub, T. R., LandeE, S. r: Class Prediction and Discovery Using Gene Expression Data, Proceedings of the fourth annual international conference on Computational molecular biology, Tokyo, Japan (2000) 263 - 272
13. Duda,R. O., Hart, P. E., Stork, D. G.: Pattern Classification, Second edition, John Wiley & Sons (2001)
14. Shipp, M. A., et. al.: Diffuse Large B-Cell Lymphoma Outcome Prediction by Gene Expression Profiling and Supervised Machine Learning, Vol. 8. Number 1, Nature Medicine (2002) 68-74
15. Rosenwald, A., Wright, G., Chan, W. , Connors, J., Campo, E., Fisher, R., Gascoyne, Muller-Hermelink, R. H., Smeland, E., Staudt, L.: The Use of Molecular Profiling to Predict Survival After Chemotherapy for Diffuse Large B-cell Lymphoma, The New England Journal of Medicine, Vol. 346, No. 25 (2002) 1937 – 1947
16. Zhu,Q., Cui, H., Cao, K., Chan,J.: Algorithmic Fusion of gene expression profiling for diffuse large B-cell lymphoma outcome prediction. IEEE Trans. on Information Technology in BioMedicine, Vol.8, June (2004) 79-88

Application of Classification Methods to Individual Disability Income Insurance Fraud Detection

Yi Peng[1], Gang Kou[1, 3,*], Alan Sabatka[2], Jeff Matza[2], Zhengxin Chen[1], Deepak Khazanchi[1], and Yong Shi[1]

[1] Peter Kiewit Institute of Information Science, Technology & Engineering, University of Nebraska, Omaha, NE 68182, USA
[2] Mutual of Omaha, Omaha, NE, USA
[3] Thomson Co., R&D, 610 Opperman Drive, Eagan, MN 55123, USA
Tel.: ++1 402 4030269
kougang@yahoo.com

Abstract. As the number of electronic insurance claims increases each year, it is difficult to detect insurance fraud in a timely manner by manual methods alone. The objective of this study is to use classification modeling techniques to identify suspicious policies to assist manual inspections. The predictive models can label high-risk policies and help investigators to focus on suspicious records and accelerate the claim-handling process.

The study uses health insurance data with some known suspicious and normal policies. These *known policies* are used to train the predictive models. Missing values and irrelevant variables are removed before building predictive models. Three predictive models: Naïve Bayes (NB), decision tree, and Multiple Criteria Linear Programming (MCLP), are trained using the claim data. Experimental study shows that NB outperformed decision tree and MCLP in terms of classification accuracy.

Keywords: Classification, Insurance Fraud Detection, Naïve Bayes (NB), decision tree, and Multiple Criteria Linear Programming (MCLP).

1 Introduction

Health care frauds cost private health insurance companies and public health insurance programs at least $51 billion in calendar year 2003 (The National Health Care Anti-Fraud Association, 2005). Traditional heuristic-rule based fraud detection techniques can not identify complex fraud schemes. Such a situation demands more sophisticated analytical methods and techniques that are capable of detecting fraud activities from large databases.

The objective of this study is to design, develop and test classification models to detect abnormal behaviors in disability income insurance data. The predictive models

---

* The corresponding author.

can label high-risk policies and help investigators to focus on suspicious records and accelerate the claim-handling process. To achieve the goal, this project studies the attributes; preprocesses dataset; and develops classification models using a three-step approach. The first step is model construction. A predictive model is constructed based on training dataset, which includes predefined class labels for each record. The second step is model validation. This step uses validation dataset to tune the model weights during estimation and assess the classification accuracy of the model. The third step is model usage. The classification model developed and validated in the first and second step is used to classify future unknown data into predefined classes. For comparison purposes, three classifiers: Naïve Bayes (NB), decision tree, and Multiple Criteria Linear Programming (MCLP), are constructed for the dataset. The resultant classification model(s) should provide acceptable classification accuracies and allow domain experts to use the classification model in future detection of abnormal behaviors.

This paper is organized as follows: The next section describes data and preprocessing steps, including feature selection and data transformation. The third section gives an overview of the three classification techniques. The fourth section presents the classification results and compares the three classifiers. The last section concludes the paper with future research direction.

2   Data Understanding and Data Preparation

The insurance data are from Mutual of Omaha insurance company (Mutual of Omaha, 2006). There are five datasets that provide information about policy types, claims, producers, and clients. The attributes include numeric, categorical, and date types. These datasets were combined into one dataset using a common unique key. The final dataset has over 18,000 records with 103 variables. A target attribute indicates the class of each record in the final dataset. These records belong to either Normal or Abnormal class.

Data preparation removes irrelevant variables and missing values; conducts correlation analysis to understand the relationship between attributes and the target attribute; selects attributes for classification modeling; and transforms attributes to appropriate forms for the three classifiers. If all instances of a variable are missing, this variable has no use in the classification and was removed.

Correlation analysis describes the relation between two or more variables. The goal of correlation analysis is to find out which variables are strongly associated with the target variable. Since many variables are categorical, Cramer's V, a popular chi-square-based measure of nominal association, was used. Cramer's V ranges from 0 to 1. The closer Cramer's V is to 0, the smaller association between the two variables. The closer V is to 1, the stronger association between the two variables. Attributes with V> 0.1 were selected for classification. As a result, the number of attributes was reduced from 103 to 20.

The software tools used in this study are base SAS, SAS Enterprise Miner (EM), and a C++ program for MCLP. Naïve Bayes (NB), decision tree, and MCLP require

different data types. The tree node of SAS EM handles the data transformation for decision tree method. NB requires attributes to be categorical while MCLP requires attributes to be numeric. Data transformation for NB and MCLP were carried out by base SAS and C++.

3   Classification Techniques

Based on the available data, three classification methods -- decision tree, Naïve Bayes, and Multiple Criteria Linear Programming (MCLP), were proposed. They classify data from different perspectives.

Decision tree is a machine learning technique that applies a divide-and-conquer method to recursively build a tree to classify data records. It is one of the most popular classification tools due to its high classification accuracy and easily interpretable results. From our previous experience, decision tree is efficient and superior to many other classifiers for different data sets. SAS EM provides tree nodes that compute decision tree solution.

Naïve Bayes (NB) classifier is a simple probabilistic classifier that computes the probabilities of instances belonging to each predefined class and assigns instances to the class that has the highest probability. NB is proposed for this project for two reasons. First, many variables selected by correlation analysis are categorical and NB is designed to classify categorical data. Second, despite its naïve design, NB works well in many real-world situations and outperforms some complex classifiers. In addition, NB takes approaches that are different from decision tree and MCLP to build classifier. NB function was implemented in base SAS.

MCLP is a mathematical-based classification approach that classifies records into distinct groups based on two or more objective functions. Previous experiences (Peng et al 2004; Kou et al 2005) proved that MCLP achieves comparable or superior classification results than other popular classification methods for various datasets. A self-developed C++ program (Kou et al 2003) was applied in this study to construct and solve the MCLP model.

4   Empirical Study

4.1   Decision Tree

The Tree node in SAS EM provides three criteria for tree splitting: chi-square test, entropy reduction, and gini reduction. Each criterion uses different techniques to split tree and establish a different decision tree model. Since each technique has its own bias, it may potentially provide a stronger solution if the results from three models are integrated. The method of integrating results from multiple models is called *ensemble* in machine learning. The following tables summarize the output of four decision tree models: chi-square test, entropy reduction, gini reduction, and ensemble. For each model, the confusion matrix is reported.

Table 1. Decision Tree Model using chi-square test

Confusion Matrix

Actual	Predicted		
	1	2	Total
1	18510	12	18522
2	316	37	353
Total	18826	49	18875

18510 (2nd row, 2nd column) is the correct predictions that a record is class 1 – Normal.

12 (2nd row, 3rd column) is the incorrect predictions that a record is class 2 - Abnormal.

316 (3rd row, 2nd column) is the incorrect predictions that a record is class 1 – Normal.

37 (3rd row, 3rd column) is the correct predictions that a record is class 2 - Abnormal.

Table 2. Decision Tree Model using entropy reduction

Confusion Matrix

Actual	Predicted		
	1	2	Total
1	18458	64	18522
2	102	251	353
Total	18560	315	18875

Table 3. Decision Tree Model using gini reduction

Confusion Matrix

Actual	Predicted		
	1	2	Total
1	18496	26	18522
2	213	140	353
Total	18709	166	18875

Table 4. Ensemble: chi-square, entropy reduction, and gini reduction

Confusion Matrix

Actual	Predicted		
	1	2	Total
1	18519	3	18522
2	227	126	353
Total	18746	129	18875

The ensemble node creates a new model by averaging the posterior probabilities from chi-square, entropy, and gini models.

All decision tree results, except the one using entropy reduction, have less than 50% classification accuracy for class 2 records. Since the prediction accuracy of class 2 (Abnormal class) is important in fraud detection, decision tree is not a satisfactory solution for this dataset.

Table 5. Naïve Bayes

Confusion Matrix
Training: 40%

Actual	Predicted		Total
	1	2	
1	7272	134	7406
2	1	143	144
Total	7273	277	7550

Test: 30%

Actual	Predicted		Total
	1	2	
1	4907	*656*	5563
2	42	58	100
Total	4949	714	5663

All data

Actual	Predicted		Total
	1	2	
1	17949	*573*	18522
2	2	351	353
Total	17951	924	18875

NB produces much higher class 2 classification accuracy than decision tree. For test data, NB achieves 99% classification accuracy for class 2 records, while the highest result of decision tree (using entropy reduction) is only 71%.

4.2 Multiple Criteria Linear Programming (MCLP)

MCLP requires all variables to be numeric, which is contrary to NB. The following tables illustrate the training and test results of MCLP. The overall classification accuracies for training and test are 59% and 57.95%, respectively.

The results of NB, Decision Tree, and MCLP indicate that probability-based methods, such as NB, outperform decision tree and MCLP for this dataset. The reason may be that many variables that are strongly associated with the target variable are categorical. When these variables were transformed into numerical types, part of the information is lost.

Table 6.

Training

	Predicted			
Actual	1	2	Total	Corr Rate
1	61	39	100	61%
2	43	57	100	57%
Total	104	96	200	59%

Test

	Predicted			
Actual	1	2	Total	Corr Rate
1	143	110	253	56.52%
2	7743	10679	18422	57.97%
Total	7886	10789	18675	57.95%

5 Directions for Future Projects

Based on the results of this project, we propose several future directions. The first direction is to further validate the classification classifier with new data. The second direction is to update the existing labeled data and classifiers. A fundamental job of a classifier is to identify patterns in unknown data that are similar to those in known data. The quality of known or training data determines the classification results. Labeled data need to be updated periodically because data patterns change over time. Accordingly, classifiers need to be trained periodically to catch the changes in the data. The third direction is to try different classification methods that can handle categorical data and compare the results with NB. The last suggestion is to try one-class classification algorithm. Normal classification needs two or more classes, while one-class classification only needs information of the target class. One-class classification is useful when labeled target class records are available. By concentrating on target class data, one-class classification may generate better results.

Acknowledgment

References

1. The National Health Care Anti-Fraud Association, available at: http://www.nhcaa.org/ (2005)
2. Kou, G., Liu, X., Peng, Y., Shi, Y., Wise, M., Xu, W.: Multiple Criteria Linear Programming to Data Mining: Models, Algorithm Designs and Software Developments *Optimization Methods and Software* 18 (4):, Part 2 AUG (2003) 453-473
3. Kou, G., Peng, Y., Shi, Y., Wise, M., Xu, W.: Discovering Credit Cardholders' Behavior by Multiple Criteria Linear Programming *Annals of Operations Research* 135 (1):, JAN (2005) 261-274
4. Mutual of Omaha Website: http://www.mutualofomaha.com/. (2006)
5. Peng, Y., Kou, G., Chen, Z. and Shi, Y.: Cross-validation and ensemble analyses on multiple-criteria linear programming classification for credit cardholder behavior in Bubak M et al, eds., ICCS 2004, LNCS 3039:, Krakow, POLAND, JUN 06-09, (2004) 931-939

A Bayesian Multilevel Modeling Approach for Data Query in Wireless Sensor Networks

Honggang Wang[1], Hua Fang[2], Kimberly Andrew Espy[2], Dongming Peng[1], and Hamid Sharif[1]

[1] Department of Computer and Electronics Engneering,University Of Nebraska Lincoln, Omaha, USA,68124
{hwang, dpeng, hsharif}unlnotes.unl.edu
[2] Office of Research, University of Nebraska Lincoln, Lincoln, USA,68588
{jfang2,kespy2}.unl.edu

Abstract. In power-limited Wireless Sensor Network (WSN), it is important to reduce the communication load in order to achieve energy savings. This paper applies a novel statistic method to estimate the parameters based on the real-time data measured by local sensors. Instead of transmitting large real-time data, we proposed to transmit the small amount of dynamic parameters by exploiting both temporal and spatial correlation within and between sensor clusters. The temporal correlation is built on the level-1 Bayesian model at each sensor to predict local readings. Each local sensor transmits their local parameters learned from historical measurement data to their cluster heads which account for the spatial correlation and summarize the regional parameters based on level-2 Bayesian model. Finally, the cluster heads transmit the regional parameters to the sink node. By utilizing this statistical method, the sink node can predict the sensor measurements within a specified period without directly communicating with local sensors. We show that this approach can dramatically reduce the amount of communication load in data query applications and achieve significant energy savings.

Keywords: Bayesian Multilevel Modeling, Wireless Sensor Network.

1 Introduction

In most WSN applications, the typical scenario is to collect and transmit the measured data from each sensor to the centralized sink where the data will be processed and analyzed. However, sensor nodes might be far away from the sink and have to send tremendous real-time data by multiple hops to the sink, which consume significant energy resources. Therefore, to save energy is to reasonably reduce the communication load from the local sensors to the sink.

Statistical modeling techniques have been applied to sensor network query systems [1-3]. However, these studies did not support data queries with specified error bound or clustering structure. Also, they undergo a heavyweight learning phase. Autoregressive multilevel Bayesian models have been widely used outside the

wireless sensor network domain as a way to approximate and summarize time series in many application domains such as finance, communication, weather prediction [14-15]. In this paper, we applied the multilevel Bayesian statistical model to predict sensor values based on multilevel clustering architecture instead of transmitting the real time data directly to sink by each sensor. These techniques take advantages of the recent historical readings to predict the most likely future values. It can drastically reduce the amount of communication from sensors to the sink, detect the abnormal data, and accommodate missing sensor data.

Clustering techniques have also been used in WSN. Many clustering techniques such as K-mean, C-mean, or hierarchical clustering [4-8] have been proposed to improve network performance and save energy in WSN. We propose a query-based two-level clustering structure with consideration of both temporal and spatial correlation, which matches the generic WSN topology. In the following sections, we first present two-level network architecture and discuss the data query in section II. A detailed multilevel Bayesian modeling approach to WSN data query is discussed in section III. We demonstrate the advantages of our approach by the simulation in section IV. Conclusions are reached in the last section.

2 Two Level Network Architecture and Data Query

Hierarchical (clustering) techniques can aid in reducing useful energy consumption [4]. In our proposed hierarchical network structure, the sensor with the highest number of neighbors was selected as the temporary cluster center. Other sensors within a defined radius are then removed and the algorithm looks for a new sensor with the highest number of neighbors. This continues until most sensors are clustered. In our algorithm, the sensor in the cluster with the highest remaining energy is selected as the cluster head. Once the selected cluster heads run out of battery, the new cluster heads will be selected. By this approach, the network is formed into a two-level network architecture. Each sensor joins a local cluster group, forming the level-1(i.e., the sensor level) structure; all the cluster heads form the second tier multi-hop network structure at the cluster level. In this two-level clustering-based network structure, the typical data query application scenario is described as follows: When users submit a query to the sink, each sensor at level-1 senses the local phenomena, sending the sample data to the cluster head. At level-2, the cluster heads summarize these local data, sending them to the sink by one hop or multiple hops. However, in our approach, local sensors and cluster heads only transmit Bayesian model parameters inferred from the historical data instead of transmitting the real-time readings to the sink. All user queries can be answered at the sink within the specified time interval.

Our two level WSN model consists of a dynamic set of sensors denoted by S, and one sink node. This set of sensors form different clusters $\{S_1, S_2......S_n\}$ and all clusters have dynamic cluster heads $\{C_{s1}, C_{s2}......C_{sn}\}$ by the algorithm we discussed above. Each sensor senses and performs readings on M physical phenomena metrics

$\{M_1, M_2, \ldots M_n\}$ over time. We assume that each sensor performs a reading on each M_i every T time units. Queries are executed at the sink. The typical query forms are designed as follows:

SELECT   Sensors WHERE R(M1,M2....Mn) ERROR X CONFIDENCE d% Where REGION = Re gion1

Where $R(M1, M2....Mn)$ predicted the values of $M1, M2....Mn$ based on the multilevel modeling. X represents an error bound required by the user in the query. The d% is confidence ratio that denotes at least of d% the readings should be within X of their true value, and REGION gives geographical location restrictions of sensor groups.

3   Bayesian Multilevel Modeling in WSN

In this paper, the Bayesian multilevel modeling approach is applied for this two-level generic WSN architecture. The time series measurement model is at level-1 and the Bayesian parameters are transmitted to its cluster head. All cluster heads collect these parameters, inferring the level-2 Bayesian parameters at the cluster level and transmitting them to the sink. When users submit a data query, the sink predictor can answer it within the specified time period.

The level-1 model is expressed as

$$Y_{tij}^{L1} = \beta_{0ij} + \beta_{1ij}T + \beta_{2ij}T^2 + e_{tij}, \quad e_{tij} \sim N(0, \Sigma) \tag{1}$$

where Y_{tij}^{L1} denotes the level-1 (L1) measurement outcomes (e.g., temperature or humidity) at time t for senor i in cluster j; β_{0ij} is the initial status of sensor i of cluster j; β_{1ij} and β_{2ij} denote the change rates and acceleration rates associated with time T and quadratic term T^2, respectively. The level-1 errors, e_{tij}, are normally distributed with mean of 0 and covariance matrix Σ under first-autoregressive assumption (AR(1)) which consists of variance, σ^2, and covariance of

$$Cov(e_{tij}, e_{t'ij}) = \sigma^2 \rho^{|t-t'|} \tag{2}$$

where $|t - t'|$ is the lag between two time points; ρ is the auto-correlation and σ^2 is the level-1 variance at each time point. In Bayesian notation, the observer data, Y are distributed according to $f(Y | B, \Sigma)$, where f is the normal density, B denotes the β parameters. The outcomes Y_{tij}^{L1} are assumed independently normally distributed with mean of

$$E(Y_{tij}^{L1} | B, \Sigma) = \beta_{0ij} + \beta_{1ij}T + \beta_{2ij}T^2 \tag{3}$$

and the covariance matrix Σ. The level-2 model is expressed as

$$B^{L2} = \begin{pmatrix} \beta_{0ij} \\ \beta_{1ij} \\ \beta_{2ij} \end{pmatrix} = \begin{pmatrix} \gamma_{00j} & \gamma_{01j} & \gamma_{02j} \cdots \gamma_{0qj} \\ \gamma_{10j} & \gamma_{11j} & \gamma_{12j} \cdots \gamma_{1qj} \\ \gamma_{20j} & \gamma_{21j} & \gamma_{22j} \cdots \gamma_{23j} \end{pmatrix} \begin{pmatrix} 1 \\ X_1 \\ X_2 \\ \cdots \\ X_q \end{pmatrix} + \begin{pmatrix} u_{0ij} \\ u_{1ij} \\ u_{2ij} \end{pmatrix} \tag{4}$$

In Bayesian notation, this specifies the prior $p(B^{L2} \mid \Lambda, G)$ where B^{L2} are the level-2 (L2) outcomes, containing the same β parameters (3×1) as shown in level-1 model, representing the initial status, linear change rate and acceleration (or deceleration) rate of individual sensor i of cluster j; Λ is a (3×q) matrix of γ parameters, representing the average initial status (e.g., the initial temperature or humidity) (γ_{00j}), linear change rates (γ_{10j}) and the acceleration rates (γ_{20j}) of cluster j, as well as other γ parameters associated with level-2 q×1 predictors (X), collected by cluster head j; u denotes level-2 random effects (or random errors), multivariately and normally distributed with a mean vector of 0 and G covariance matrix.

The Bayesian method requires to know the joint distribution of the data Y and unknown parameters, θ, which denotes both fixed coefficients γ and covariance matrix ψ (including G and Σ) in our study. The joint distribution can be written as:

$$P(Y, \theta) = P(\theta)P(Y \mid \theta) \tag{5}$$

where P (θ) is called the prior and P (Y| θ) is called the likelihood. As we observed the data Y, Bayes' Theorem was used to get the posterior distribution as follows:

$$P(\theta \mid Y) = \frac{P(\theta)P(Y \mid \theta)}{\int P(\theta)P(Y \mid \theta)d\theta} \tag{6}$$

specifically,

$$P(\gamma, \psi \mid Y) = \frac{f(Y \mid \gamma, \psi)P(\gamma \mid \psi)P(\psi)}{\int\int f(Y \mid \gamma, \psi)P(\gamma \mid \psi)P(\psi)d\gamma d\psi} \tag{7}$$

As the parameters γ are of primary interest, we have

$$P(\gamma \mid Y) = \int p(\gamma, \psi \mid Y)d\psi \tag{8}$$

In general, analytically performing the above integration has been a source of difficulty in application of Bayesian inference and often Markov Chain Monte Carlo (MCMC) simulation is one way to evaluate the integrals. In this study, we used one of MCMC procedures, Metropolis-Hastings sampling procedure, to implement this approximation [16-18].

4 Simulation and Analysis

We used SAS software [10] to simulate and test our approach. Our simulation was based on 50 random deployed sensors. With our clustering algorithm, all sensors form Cluster A and B. Cluster A has 20 sensors deployed while Cluster B has 30 sensors. The temperature data were collected at different clusters across different areas with a significant temperature difference. In our simulation, we used the first order radio model presented in [4]. In the specified radio model, the radio dissipates $E_{elec} = 50$ nJ/bit to run the transmitter or receiver circuitry and $E_{amp} = 100$ pJ/bit/m_2 for the transmit amplifier. To transmit a k-bit message a distance d meters, E_{Tx} was used by sensors. To receive a message, the sensors spent E_R.

$$E_{tx}(k,d) = E_{elec} \cdot k + E_{amp} \cdot k \cdot d^2 \tag{9}$$

$$E_{rx}(k,d) = E_{elec} \cdot k \tag{10}$$

After the clusters were formed and cluster heads were selected, the sink calculated the routing hops among cluster heads. In addition, an index matrix was created for time, area and sensor IDs. The two measured areas represented by the two sensor class heads were coded as 0 and 1, respectively. Individual sensors (IDs) were considered nested within each cluster represented by corresponding cluster heads, for instance, sensor IDs ranged from 1 to 20 for Class Head 1, and 21 to 50 for Class Head 2. Time started from 0 and extended to the assumed 14.5 hours with 0.5 hour interval. Based on Model (4), a univariate response vector of y_{ti} was created. For example, each sensor might have had 30 half-hour time points and one cluster had 20 sensors while the other had 30 sensors. The data generator [11-12] was validated with parameter estimates from Potthoff and Roy's data[13]. Table 1 presents partial local parameters generated by each sensor at level-1, to be transmitted to the cluster heads.

Table 1. Selected Model Parameters at Sensor Level

Parameters	Sensor ID	Estima tes	Parameters	Sensor ID	Estimates
Intercept	5	69.59662	Intercept	23	79.86074
Slope	5	0.307631	Slope	23	0.590479
Acceleration/ Deceleration	5	-0.00325	Acceleration/ Deceleration	23	-0.00355
Intercept	6	69.50935	Intercept	24	80.6984
Slope	6	0.403908	Slope	24	0.348969
Acceleration/ Deceleration	6	-0.00203	Acceleration/ Deceleration	24	-0.00375

...

Similarly, Table 2 shows the level-2 Bayesian model parameters based on the local colleted data, to be transmitted to the sink. The parameters β_0, β_s, and β_a represent the initial temperature, linear change rate and deceleration rate at the two areas, respectively. Based on these parameters, the sink predicts the next half hour temperature value.

Table 3 gives partial predicted temperatures at the sink with error bound and confidential interval, which responds to the queries submitted by the user at the sink.

Table 2. Model Parameters at Cluster Level

	Cluster Head 1			Cluster Head 2		
	β	SE	95% CI	β	SE	95% CI
β_0	69.980	0.128	(69.729, 70.231)	80.187	0.109	(79.973, 80.401)
β_s	0.307	0.025	(0.258, 0.356)	0.448	0.024	(0.401, 0.495)
β_a	-0.003	0.001	(-0.00496, -0.00104)	0.003	0.001	(0.001, 0.005)

Table 3. Selected Predicted Values with Error Bounds at Sink

Region	Time (hour)	Cluster	Predicted Temperature	SE	95% Confidence Interval	
					Lower Bound	Higher Bound
			...			
0	8	1	74.15	0.0773	74.00	74.30
0	8.5	1	74.30	0.1164	74.08	74.53
0	9	1	74.56	0.1432	74.28	74.84
0	9.5	1	74.65	0.1492	74.36	74.95
0	10	1	74.73	0.1578	74.42	75.04
			...			

Figure 1 (a) indicates the predicted temperature values of 20 sensors at each .5 hour in Cluster A and the solid red line represents the estimated temperature by Cluster Head A over 14.5 hours. Figure 1(b) presents the predicted temperature of each sensor and the green line is the temperature trajectory estimated at the corresponding cluster head in Cluster B within the same time interval. To show the significant temperature difference in the two areas, we compare the estimated temperature of the two areas in Figure 1 (c).

Figure 1(d) presents the residuals of the predicted values of each sensor. We found that all the predicted values were controlled within the ± 1.5 standard deviation. This simulation shows that our approach can satisfy the user controllable error bound requirements. We also compared the energy consumption with the general approach based on 50 random deployed sensors based on equation (9) and (10) within 14.5hours time interval. We compared the general data aggregation approach with our multilevel Bayesian approach in the same WSN topology and found that our approach has slightly higher energy consumption than General Data aggregation approach in the initial 1.5 hour time window. That is because the Bayesian model needs to

transmit more parameters than real temperature data at the beginning, however, with longer time period (1.5-14.5 hours), our approach has achieved significantly less energy consumption than the linear-increasing energy consumption of the General Data Aggregation approach when no parameters update is needed.

(a)

(b)

(c)

(d)
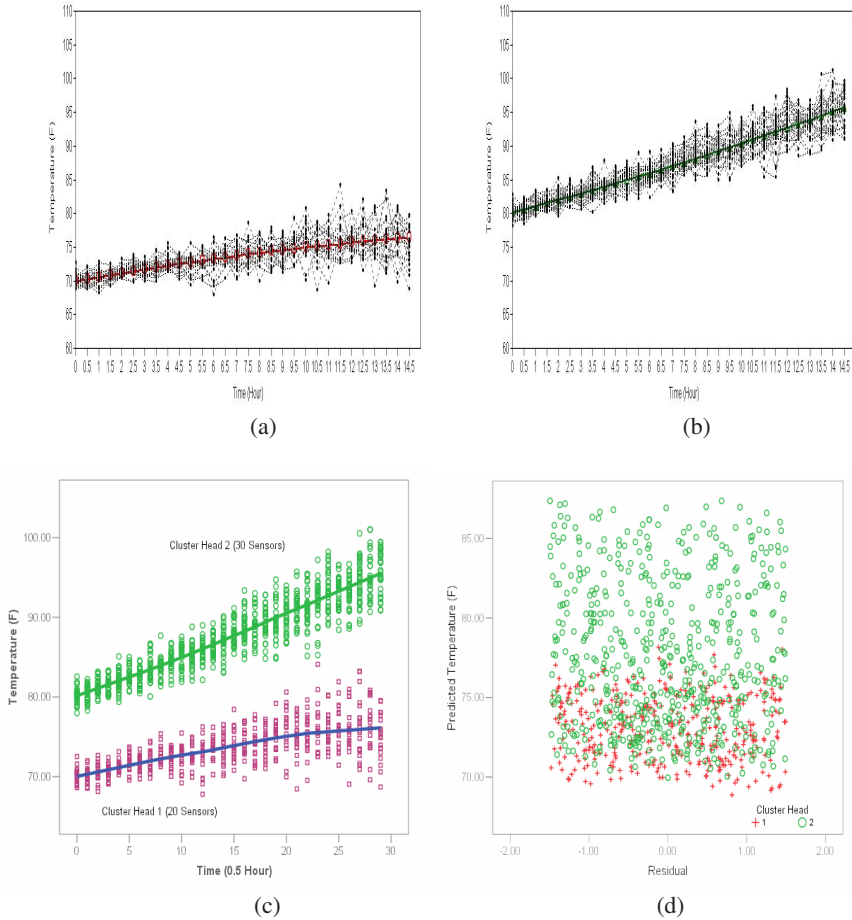
Fig. 1. Predicted values of each sensor against estimated value by each cluster head in two areas over 14.5 hours

5   Conclusions

In this paper, we proposed a multilevel Bayesian modeling approach to the query application in the WSN multilevel architecture, utilizing both temporal and spatial correlation to predict parameters at different levels. Our approach relies mostly on local Bayesian models computed and maintained at each sensor. In order to adapt the local model to variations in the data distribution, each sensor continuously maintains its local model, and notifies the sink only of significant changes. As we showed, our

approach can provide a significant reduction in communication load over the existing general data aggregation approach, and can also effectively predict future values with controllable error bounds. By using this approach, significant energy consumption is saved in typical data query applications.

References

1. Jain, A., E.Y., and Wanf, Y. Adaptive stream management using kalman filters. In SIGMOD, 2004.
2. Kotidis, Y., Snapshot queries: towards data-centric sensor networks. In Proc. Of the 21th Intl. Conf. on Data Engineering, April 2005.
3. Chu, D., Desphande, A., Hellerstein, J., and Hong, W. Approximate data collection in sensor networks using probabilistic models. In ICDE, April 2006.
4. Heinzelman, W. R., Chandrakasan, A., and Balakrishnan, H., An Application-Specific Protocol Architecture for Wireless Microsensor Networks, IEEE Transactions on Wireless Communications, vol. 1, no. 4, pp. 660¿C670, October 2002.
5. Lin, C.R., Gerla, M., Adaptive Clustering for Mobile Wireless Network, IEEE J. Select. Area Commun., vol15, pp. 1265-1275, Sept 1997.
6. Ryu, J.H., Song, S., Cho, D.H., Energy-Conserving Clustering Scheme for Multicasting in Two-tier Mobile Ad-Hoc Networks, Elec-tron. Lett., vol. 37, pp. 1253- 1255, Sept 2001.
7. Hou, T.C., Tsai, T.J., Distributed Clustering for Multimedia Support in Mobile Multihop Ad Hoc Network, IEICE Trans. Commun., vol. E84B, pp. 760-770, Apr 2001.
8. Han, J., Kamber, M., Data Mining: Concepts and Techniques, San Diego: Academy Press, 2001.
9. Productive Patterns Software Web site. http://www.predictivepatterns.com/docs/WebSiteDocs/ Clustering/Agglomerative_Hierarchical_Clustering_Overvie w.htm
10. SAS Institute Inc. (2003). SAS/STAT userí»s guide, version 9.1. Cary, NC: SAS Institute Inc..
11. Fang, H. (2006). %hlmdata and %hlmrmpower: Traditional repeated measures vs. HLM for multilevel longitudinal data analysis - power and type I error rate comparison. Proceedings of the Thirty-First Annual SAS Users Group Conference, SAS Institute Inc., Cary, NC.
12. Fang, H., Brooks, G. P., Rizzo, M. L., & Barcikowski, R. S. (2006). An empirical power analysis of multilevel linear model under three covariance structures in longitudinal data analysis. 2006 Proceedings of the Joint Statistical Meetings, American Statistical Association, Quality Industry and Technology Section [CD-ROM]. Seattle, Washington: American Statistical Association.
13. Potthoff, R. F., & Roy, S. N. (1964). A generalized multivariate analysis of variance model useful especially for growth curve problems. Biometrika, 51, 313-326.
14. Raudenbush S. W., & Bryk, A. S. (2002). Hierarchical linear models: Applications and data analysis methods. London: Sage publications, Inc..
15. McCulloch, C. E., & Searle, S. R. (2001). Generalized, linear, and mixed models. New York: John Wiley & Sons, Inc.
16. Carlin, B. P. & Louis, T. A.(2000). Bayes and Empirical Bayes Methods for Data Analysis. NY: Chapman & Hall/CRC.
17. Little, R.J., & Rubin, D.B. (2002). Statistical analysis with missing data (2nd edition). New York: John Wiley.
18. Ross, S. M. (2003). Introduction to probability models. San Diego, CA: Academic Press.

A Watermarking Method with a New SS technique

Kun Hua[1] and Liang Pu[2]

[1] Computer and Electronic Engineering Dept. University of Nebraska Lincoln,
1110 S 67th St. 68182, USA
[2] School of Energy and Power Engineering, Xi'an Jiaotong University
28 W Xianning Rd. Xi'an 710049 China
khua@unlnotes.unl.edu

Abstract. Among numerous techniques of information concealment, Spread spectrum watermarking (SSW) has proved to yield improved results when robustness against attack is at a premium. SSW hides information which is called watermark by spreading its spectrum and then adding them to a host image as a watermarked image. Spreading spectrum is done by a pseudo-noise (PN) sequence. But in standard SSW approaches, receiver must use a separate channel to achieve PN sequence used at the transmitter for detecting hidden information. The unique PN sequence must have a low cross correlation and thereby can be duplicated easily by hostile attackers. In this paper a novel approach based on the unconventional Random Encoding Spread Spectrum is proposed for recovering the spreading sequence of watermark signal without any information from the transmitter. It is contributed a higher secure feature by using of the time-varying random encoded spread spectrum.

Keywords: Data Mining, Spreading Spectrum Watermarking, Pseudo-noise.

1 Introduction

Nowadays, the digital watermarking technique is regarded as a promising means to address such problems as copyright protection, contention authentication, device control and signal multiplexing. The mostly important requirements for a digital watermarking system are the watermark transparency, robustness and security. Several kinds of digital watermarking techniques have been applied by industrial or academic approaches.

Spread spectrum technology is an important anti-interference technology in the watermarking. In traditional spread spectrum communications, short pseudo-noise (PN) codes are used broadly as spread spectrum sequences. For instance, m sequence and Gold sequence. PN codes have some noise-like characteristic. However it has certain periodicity and can be duplicated easily, which compromises the transmission security.

Recently, a lot of works have been done on hostile detecting by means of data mining [1]-[4]. Saeed raised a scheme based on Genetic Algorithm (GA) [5]. The approach is proposed for recovering PN sequence and detecting location with GA

optimization search, hence unauthorized users could detect hidden information from the watermarked signal. For example, by using of GA optimization search, a PN sequence with period of 63 chips and it's location can be detected by attackers in 70 seconds.

In order to improve the disadvantage of traditional spread spectrum, the theory of Random-Encoded Spread Spectrum (RESS) was presented in this paper, which avoids using the fixed spreading sequences. In this system, the spreading code is obtained from the transmission signal. To some extend, the dynamic variable spreading sequences assure the transmission security and low probability of detection (LPD) by attackers.

Comparing traditional spread spectrum, there are several advantages to exploit RESS into watermarking:

(1) RESS doesn't require a separate channel to transmit the spreading codes to the receiver. Watermarked signal is totally "white noise" to attackers.

(2) RESS can enhance watermarking transmission security by true random spreading sequence. Pseudo Noise sequence is just like random sequence.

(3) PN codes is fixed once they have been generated, so PN codes can be duplicated by unauthorized attackers. But in RESS, the spreading sequence is not only randomly generated and independent of the current symbol, but also dynamically changing form one symbol to the next. Also we can say it's time-varying random codes and is hard to be duplicated.

In this paper, we proposed a novel approach based on Random-Encoded Spread Spectrum for recovering PN sequence of watermark signal without any information from the transmitter. It is contributed a higher secure feature and LPD by using of the time-varying random encoded spread spectrum.

In section 2, we present the system model of the Random encoded spread spectrum system. The processing of RESS watermarking is described in section 3. The simulation parameters and results are presented in section 4. Conclusions of the paper are made in section 5.

2   Random Encoded Spread Spectrum

2.1   System Description

In the RESS system model, at the transmitter, delay registers are updated from N-tap delay of data where N is the code length. Delay registers generate the code chips that switch at N times the data rate for signal spreading. The random nature of the digital information source is assured by using data compression methods. The register contents at the transmitter and receiver should be identical initially. Differential coding (DC) is used in this system to avoid the error propagation among delay registers.

Our approach to improving the low probability of detection performance is to completely abandon the use of PN sequences. The random nature of the digital

information source is assured by applying appropriate data compression methods to remove any redundancy in the data stream, thereby maximizing its entropy. The binary data symbols can therefore be modeled as independent and identically distributed Bernoulli random variables. Symbol values of +1 and -1 occur equally likely with a probability of 1/2. As a result, the spreading sequence is not only randomly generated and independent of the current symbol, but also dynamically changing from one symbol to the next.

The random encoding operation at the transmitter is reversed at the receiver. The recovered data are fed back to the N-tap delay registers that provide an estimate of the transmitter's spreading codes required for signal de-spreading. Data recovery is by means of a correlation detector. As a result, random encoding makes unwanted detection of the data by an unintended receiver practically impossible. The security of the transmission can greatly be enhanced with this low probability of detection communication system.

3 Watermarking

3.1 Watermarking Embedding

Watermarking Embedding is performed in DCT domain. At first, we divide host image W into M non-overlapping 8×8 blocks[6]-[9],

$$W = \bigcup_{m=0}^{M-1} W_m(u,v), 1 \le u, v \le 8 \tag{1}$$

So there are M DCT coefficient $\tilde{W}(u,v)$ after DCT transformation for each block, and

$$\tilde{W} = \bigcup_{m=0}^{M-1} \tilde{W}_m(u,v) = \bigcup_{m=0}^{M-1} C_{DCT}[W_m(u,v)], 1 \le u, v \le 8 \tag{2}$$

Embed RESS watermarking data into 8 low frequency components of every 8×8 blocks of host image W, that is :

$$\tilde{W}_z = \bigcup_{m=0}^{M-1} \tilde{W}_{z_m}(u,v) = \bigcup_{m=0}^{M-1} C_{DCT}[W_m(u,v) + \alpha_m \bigcup_{i=8m}^{8m+7} Z_{s_i}] \tag{3}$$

The next step is to do IDCT to get the watermarked image W_Z,

$$W_Z = \bigcup_{m=0}^{M-1} C_{IDCT}^{-1}[W_m(u,v)] \tag{4}$$
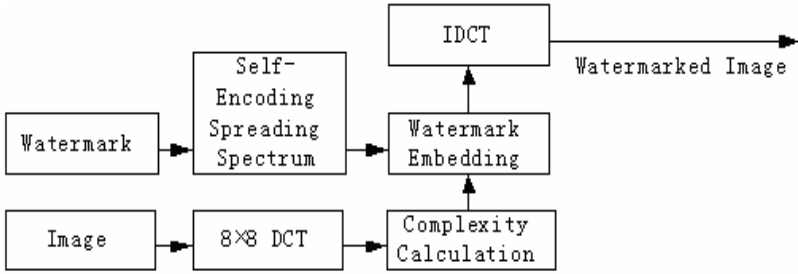
Fig. 1. RESS Watermarking Embedding Structure

3.2 Watermarking Extracting

To extract the watermark from the watermarked image, we first take 8×8 DCT and recover the watermark image by:

$$Z_s' = \{ \bigcup_{m=0}^{M-1} [\tilde{W}_{z_m}(u,v) - \tilde{W}_m(u,v)]/\alpha_m \} \tag{5}$$
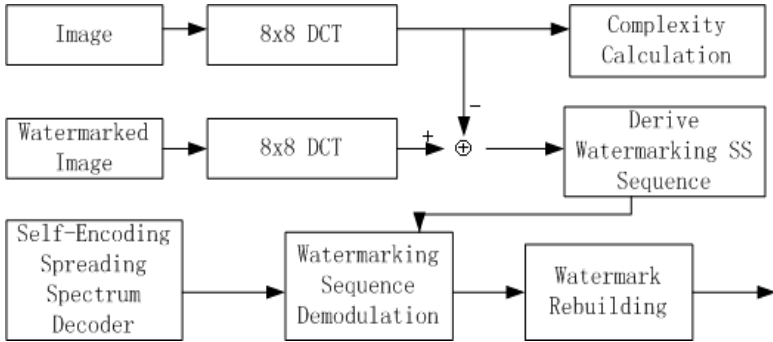
Fig. 2. RESS Watermarking Extracting Structure

The last step will be RESS decoding part. After this step, recovered watermark image Z' is extracted and will be compared with the original watermark image Z.

4 Experimental Results

4.1 Watermarking Results

In our simulation experiments, the original host image is taken as a gray testing image and the testing watermarking image is a 2-values image. In water marked image, we choose PSNR as 50dB and Gaussian Noise variance as 0.01. Spreading factor N=128. Delay register length m=7.

Fig.3 is the original host image and Fig.4 is the testing watermarking 2-values image. Fig.5 is the watermarked image and Fig.6 is the recovered watermark.

Fig.3-Fig.6 show that the watermark image is totally invisible in watermarked figure and can be recovered desirably. We can conclude that RESS can not only achieve a similar performance as conventional PN sequence spreading spectrum do, but also acquires higher secure feature and simpler structure without the separate channel for spreading sequence.

Fig. 3. Original Figure
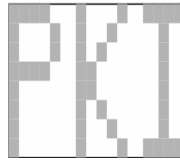
Fig. 4. Watermark image pattern

There was a shortage for regular spread spectrum watermarking algorithm: If the spreading sequence length is not long enough, the system can not achieve the ideal result. Thus, the original image must be very large which is hard to explore. But if we cut the image figure smaller, the spread spectrum sequence is also shorten, and the result is that the robustness of the whole system is influenced. But while Random-Encoded Spread Spectrum is introduced in this paper, any short sequence is still random.

What is more, we can now select much more spreading sequences than regular techniques[10]-[12]. This means for multi-users application in digital watermarking, more individual information can be sent in the same time without great interference comes from other information. This approach is still need to be proved by real experimental results.

Fig. 5. Watermarked Figure
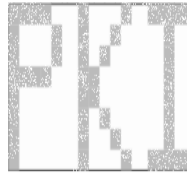
Fig. 6. Recovered Watermark

5   Conclusion

In this paper, a novel approach based on Random-Encoded Spread Spectrum is proposed for recovering spreading sequence of watermark signal without any information from the transmitter. It mainly contributed a higher secure feature by using of the time-varying random Random-encoded spread spectrum instead of the typical PN sequence. Random-Encoded Spread Spectrum can perform several advantages over PN sequences. The watermark detecting by the hostile unauthorized becomes almost impossible by developing the Random-Encoded Spread Spectrum Watermarking system. Such approach has been approved to be a better alternate data mining method which can be used in water marking technique easily. To some extend, the dynamic variable spreading sequences also assure the low probability of detection by attackers over the PN approach. Due to the random and dynamically changing, coded waveform, the techniques chart a completely different approach to spread spectrum techniques.

In multi-user application, we can select much more spreading sequences than regular PN techniques. This means for multi-users application in digital watermarking, more individual information can be sent in the same time without great interference comes from other information. Such approach is still need to be proved by real experimental results in the future.

References

1. Trivedi, S,Chandramouli, R.: Secret Key Estimation in Sequential Steganography, IEEE Transaction on signal processing, Volume 53, NO. 2, Feb. (2005)

2. Asghari, V. R. , Ardebilipour, M. : Spread Spectrum Code Estimation by Genetic Algorithm, International Journal of signal processing, VOL 1,Number 4, (2004).

3. Yen, K., Hanzo, L.: Genetic Algorithm Assisted Joint Multiuser Symbol Detection and Fading Channel Estimation for Synchronous CDMA Systems, IEEE Transaction on selected areas in communication, VOL. 19, NO. 6, JUNE (2001).

4. Asghari,V.R. , Ardebilipour ,M.: Spread Spectrum Code Estimation by Particle Swarm Algorithm, International Journal of Signal Processing, 2, No. 4, (2005) 268-272,

5. Sedghi, S. Mashhadi ,H. R, Khademi ,M. : Detecting Hidden Information from a Spread Spectrum Watermarked Signal by Genetic Algorithm 2006 IEEE Congress on Evolutionary Computation Sheraton Vancouver Wall Centre Hotel, Vancouver, BC, Canada July (2006) 16-21,

6. Gao,Q. Li, R. Wang, H. Dang, H, Liu, L.: Spread Spectrum Digital Watermarking Algorithm Using Gold Codes, Journal of xi'an jiaotong university, VOL 28, NO.2, Feb. (2004)

7. Marvel L M, Retter C T, Boncelet C GJ : Hiding information in images 1998 International Conference on Image Processing, Chicago , USA, (1998).

8. Ruanaidh J J K O, Csurka G :A Bayesian approach to spread spectrum watermark detection and secure copyright protection for digital image libraries IEEE Computer Society Conference on Computer Vison and Pattern Recognition, Fort Collins, USA, (1999).

9. Vassaux B, Bas P, Chassery J M. : A new CDMA technique for digital image watermarking, enhancing capacity of insertion and robustness 2001 International Corrence on Image Processing, Thessaloniki, Greece,(2001).

10. Peterson,R. L. Ziemer,R.E., Borth, D.E.: Introduction to Spread Spectrum Communications" Englewood Cliffs, NJ: Prentice Hall, (1995)

11. Dixon, R. C.: Spread Spectrum System New York, NY: John Wiley & sons, (1984)

12. Sarwate D. V., Pursley, M. B.: Crosscorrelation Properties of Pseudorandom and Related Sequences, Proceedings of IEEE, vol. 68, May (1980)593-619

epsilon-Support Vector and Large-Scale Data Mining Problems*

Gang Kou[1,2], Yi Peng[2,**], Yong Shi[2,3], and Zhengxin Chen[2]

[1] Thomson Co., R&D, 610 Opperman Drive, Eagan, MN 55123, USA
[2] College of Information Science & Technology, University of Nebraska at Omaha, Omaha, NE 68182, USA
`{gkou, ypeng, yshi, zchen}@mail.unomaha.edu`
[3] Chinese Academy of Sciences Research Center on Data Technology & Knowledge Economy, Graduate University of the Chinese Academy of Sciences, 100080, China
Tel.: ++1-402-4030269

Abstract. Data mining and knowledge discovery has made great progress during the last fifteen years. As one of the major tasks of data mining, classification has wide business and scientific applications. Among a variety of proposed methods, mathematical programming based approaches have been proven to be excellent in terms of classification accuracy, robustness, and efficiency. However, there are several difficult issues. Two of these issues are of particular interest of this research. The first issue is that it is challenging to find optimal solution for large-scale dataset in mathematical programming problems due to the computational complexity. The second issue is that many mathematical programming problems require specialized codes or programs such as CPLEX or LINGO. The objective of this study is to propose solutions for these two problems. This paper proposed and applied mathematical programming model to classification problems to address two aspects of data mining algorithm: speed and scalability.

Keywords: Data mining, Classification, Mathematical Programming, Multiple criteria decision making, Support Vector Machine.

1   Introduction

Over the years, optimization-based algorithms have shown their effectiveness in data mining classification (e.g., Bugera, Konno, and Uryasev, 2002) and Mathematical programming (MP) based algorithm is one of the optimization-based classification algorithms (e.g., Kou et al 2006). Nevertheless, due to the limitation of computation power and memory, it is difficult to apply the MP algorithm, or similar optimization algorithms, to huge datasets which may contain millions of observations. As the size

---

of today's databases is continuously increasing, it is highly important that data mining algorithms are able to perform their functions regardless of the sizes of datasets.

Develop mining algorithms that scale to real-life massive databases is the first research challenges proposed by Bradley, Fayyad, and Mangasarian in their overview of applying mathematical programming for data mining. They also pointed out that "approaches that assume that data can fit in main memory need to be revised or redesigned (Bradley, Fayyad, and Mangasarian 1998)." MP based algorithm is such an approach that requires the data to fit in main memory. This requirement comes from the fact that constraint matrix must be loaded into main memory in order to achieve an acceptable computation time and the size of constraint matrix is determined by the size of the training dataset. Therefore, as the size of dataset increases, the computation time increases and performance degraded.

The objectives of this research are: (1) to propose a new epsilon-support vector approach, and (2) to apply this approach to large scale data mining problem and analyze substantial datasets (size of $O(10^9)$). The results indicate that this new approach has the potential to handle arbitrary-size of datasets.

This paper is organized in three parts. The next section describes the epsilon-support vector for Multi-criteria Convex Quadratic programming (MCQP) two-group classification model. Section 3 presents the experimental results. The last section concludes the paper.

2 Epsilon-Support Vector (eSV) Approach

Each row of a $n \times r$ matrix $A = (A_1,...,A_n)^T$ is an vector $A_i = (a_{i1},...,a_{ir}) \in \Re^r$ which corresponds to one of the records in the training dataset of a binary classification problem, $i = 1,..., n$; n is the total number of records in the dataset. Two groups, G_1 and G_2, are predefined while $G_1 \cap G_2 = \Phi$ and $A_i \in \{G_1 \cup G_2\}$. A boundary scalar b can be selected to separate G_1 and G_2. Let $X = (x_1,...,x_r)^T \in \Re^r$ be a vector of real number to be determined. In the classification problem, $A_i X$ is the score for the ith data record. If all records are linear separable and an element A_i is correctly classified, then let β_i be the distance from A_i to b, and consider the linear system, $A_i X = b - \beta_i$, $\forall A_i \in G_1$ and $A_i X = b + \beta_i$, $\forall A_i \in G_2$. However, if we consider the case where the two groups are not linear separable because of mislabeled records, a "Soft Margin" and slack distance variable α_i need to be introduced. Previous equations now transforms to $A_i X = b + \alpha_i - \beta_i$, $\forall A_i \in G_1$ and $A_i X = b - \alpha_i + \beta_i$, $\forall A_i \in G_2$. To complete the definitions of β_i and α_i, let $\beta_i = 0$ for all misclassified elements and α_i equals to zero for all correctly classified elements. Incorporating the definitions of β_i and α_i, out classification models could be set as:

$$Minimize \ \frac{1}{2} \parallel X \parallel_2^2 + W_\alpha \sum_{i=1}^{n} \alpha_i^2 - W_\beta \sum_{i=1}^{n} \beta_i + \frac{W_b}{2} b^2$$

Subject to: $Y (<\!A\cdot X\!> - \text{eb}) = \delta' e - \alpha + \beta$

where Y is a given $n \times n$ diagonal matrix, $e=(1,1,...,1)^T$, $\alpha = (\alpha_1,...,\alpha_n)^T$, $\beta = (\beta_1,...,\beta_n)^T$, X and b are unrestricted.

The Lagrange function corresponding to Model 3 is

$$L(X,b,\eta,\theta) = \frac{1}{2} \parallel X \parallel_2^2 + \frac{W_\alpha}{2} \sum_{i=1}^{n} \eta_i^2 + W_\beta \sum_{i=1}^{n} \eta_i + \frac{W_b}{2} b^2 - \theta^T (Y(<\!A\cdot X\!> - \text{eb}) - e\delta' + \eta)$$

where $\theta = (\theta_1,...,\theta_n)^T$, $\eta = (\eta_1,...,\eta_n)^T$, $\theta_i, \eta_i \in \Re$.

According to Wolfe Dual Theorem, $\nabla_X L(X,b,\eta,\theta) = X - A^T Y\theta = 0$, $\nabla_b L(X,b,\eta,\theta) = W_b b + e^T Y\theta = 0$, $\nabla_\eta L(X,b,\eta,\theta) = W_\alpha \eta + W_\beta e - \theta = 0$. $\quad$ (3)

Introduce the above 3 equations to the constraints of Model 3, we can get:

$$Y((A\cdot A^T)Y\theta + \frac{1}{W_b} e(e^T Y\theta)) + \frac{1}{W_\alpha}(\theta - W_\beta e) = \delta' e$$

$$\Rightarrow \theta = \frac{(\delta' + \frac{W_\beta}{W_\alpha})e}{\frac{I}{W_\alpha} + Y((A\cdot A^T) + \frac{1}{W_b} ee^T)Y} \quad (4)$$

In algorithm, we describe how to use this model in a classification problem.

Algorithm

Input: a $n \times r$ matrix A as the training dataset, a $n \times n$ diagonal matrix Y labels the class of each record.

Output: classification accuracies for each group in the training dataset, score for every record, decision function $((X^* \cdot A_i) - b^*) \{ \begin{matrix} > 0, \Rightarrow A_i \in G_1 \\ \leq 0, \Rightarrow A_i \in G_2 \end{matrix}$

Step 1. compute $\theta^* = (\theta_1,...,\theta_n)^T$ by (5). W_β, W_α, W_b are chosen by cross validation.

Step 2. compute $X^* = A^T Y\theta^*$, $b^* = \frac{-1}{W_b} e^T Y\theta^*$.

Step 3. classify a incoming A_i by using decision function $((X^* \cdot A_i) - b^*) \{ \begin{matrix} > 0, \Rightarrow A_i \in G_1 \\ \leq 0, \Rightarrow A_i \in G_2 \end{matrix}$.

END

In existing SVM approaches (Boser et al 1992), the sparsity of the optimal α_i^* (many of $\alpha_i^* = 0$) is the key in solving large scale SVM problem and the support vectors ($\alpha_i^* = 0$) are the points at the hyperplane. Similarly, the support vector A_i of our models can be defined as $\alpha_i^* = \beta_i^* = 0$. Due to the formulation of the model objectives, almost none of the data points A_i lie on two adjusted bounding hyper planes $b \pm 1$. Thus most of the time α_i^* and β_i^* do not equal to zero simultaneously. A Karush-Kuhn-Tucker (KKT) condition that has been used in previous support vector approaches (Cristianini and Shawe-Taylor 2000, Schölkopf, and Smola 2002) can not be held any more because of the introduction of distance variable β_i in our model.

As a result, we need to establish another condition for those data points A_i whose corresponding $\left| \alpha_i^* - \beta_i^* \right| < \varepsilon$ to define the epsilon-support vectors (eSVs) such that the computation complexity can be reduced for large scale problems. ε is picked so that only a small part (e.g. 1%) of the records belongs to epsilon-support vectors. Generally, if $n < 1000000$, Model 2 can use the whole dataset; otherwise, a sample training set (e.g. 1% of the population) can be randomly generated from the original data. Using the sample set, we can find an optimal solution and epsilon-support vectors for the original dataset. All epsilon-support vectors are used to re-train the model repeatedly until the classification results meet certain criteria/threshold. A stratified random sampling approach is incorporated into our algorithm for large scale data mining problem ($>O(10^9)$).

Stratified Random Sampling

Since MP based algorithm requires training datasets to fit in main memory, the size of training dataset is limited by the capacity of main memory ($O(10^{6\sim8})$). One possible solution is to use only part of the training dataset when the dataset size is extremely huge ($>O(10^9)$). However, this approach may loss valuable information that exists in the unused part of the training dataset. In order to make the best use of the training dataset, we employ a revised stratified random sampling.

Let's briefly describe how standard stratified random sampling works. First, the dataset is partitioned into groups of data called strata. Each data belongs to one and only one stratum. Second, a sample is selected by some design within each stratum (Thompson 1992). As a sampling technique, the goal of stratified random sampling is to select a portion of a population that can be used as a "representation" of the population as a whole.

Algorithm

The following procedure summarized the whole process:

Algorithm 1

   Input: The training dataset A as the population, n is the number of observation in the population and is a huge number; m is the number of

subpopulations which can be fitted into main memory; The testing dataset A';
Algorithm Stop criteria.

Output: Average   classification   accuracies;   decision   scores   for   all
observations; decision function.

Step 1: A is evenly partitioned into m subpopulations or strata by random
selection.

Step 2: One random sample is drawn from each of m subpopulations and
formulate the first training set Tr.

Step 3: Compute $\theta^* = (\theta_1, \ldots, \theta_n)^T$ using Tr as input. W_β, W_α, W_b are
chosen by cross validation.

Step 4: Compute $X^* = A^T Y \theta^*$, $b^* = \dfrac{-1}{W_b} e^T Y \theta^*$. If the performance
measure meet pre-set criteria (accuracy, total computation time, etc) and
the iteration times > 10, stop; otherwise go to step 5.

Step 5: Compute $\left| \alpha_i^* - \beta_i^* \right|$ for all observations in A.

Step 6: Suppose we have n_1 observations (epsilon-support vectors (eSVs))
corresponding $\left| \alpha_i^* - \beta_i^* \right| < \varepsilon$ and n_2 observations (Non epsilon-
support vectors) which $\left| \alpha_i^* - \beta_i^* \right| > \varepsilon$. Formulate a new set with all n_1
eSVs and some (n_3, $n_3 \leq n_2$ and $n_3 \cong 10\% * n_1$) non eSVs. If ($n_3 + n_1$)
$\leq m$, the new set is the new training set, otherwise, random sample m
observations from the new set to formulate a train set. Go back to step
3.

END

* Iteration times must be greater than 10 to minimize the influence of the selection
of initial training dataset.

3 Experimental Results

The purpose of this research is to test the applicability of our algorithm in large scale
data mining problem $(>O(10^9))$, which is too large to be loaded into a typical PC
memory (512MB-4Gb) but can be saved in harddisk (40Gb-1Tb). Because we can't
find any real life data in such size, we use a Normally Distributed Clustered program
(NDC) (Musicant 1998) to generate datasets. Normally distributed cluster is a data
generator. NDC generates data points clustered to a series of random centers and all
points are multivariate normal distributed. All variables are integers for simplicity.
Then, NDC randomly generates a separating plane and assign a class for each random
center according to the random separating plane. NDC changes dataset separability by
changing the variances of the distributions. The percentage of separability is
calculated by counting how many points end up on the right and wrong side of the
separating plane. NDC will provide the percentage of linear separability.

The experimental study has two parts. The first one is to test the capability of the proposed algorithm in massive problem with low noises. The second test is to evaluate the performance of the proposed algorithm under high noises, large dataset.

Massive Dataset

The first experiment dataset consists of 100 million records and each record has 20 variables. It is balanced with 50% of the data in the first group and 50% of the data in the second group. The dataset is 95% linear separable (Musicant 1998).

Algorithm 2

Input: The input data set of 100 million records; Assume that at most 1 million records can be fitted into main memory.

Output: 10-fold cross validation average classification accuracies; computing time.

Step 1: The input data set is evenly partitioned into 10 subsets by stratified random sampling selection.

Step 2: A standard 10-fold cross-validation set of 10 sets of training dataset and testing dataset is stored by using one of the 10 subsets as the testing dataset and using the remaining 9 subsets as training dataset. Repeat the following steps for each of the 10 sets of training dataset and testing dataset

Step 3: $n=100$ million and $m=1$ million. Stop criteria: Prediction Accuracy > 94.8% or computing time > 1000 minutes. Apply algorithm 1.

END

Table 1. Massive dataset computing results

10-fold	training		time	testing	
	Class 1	Class 2	(seconds)	Class 1	Class 2
fold 1	94.93%	94.87%	631	94.91%	94.82%
fold 2	94.96%	94.82%	933	94.93%	94.82%
fold 3	94.85%	94.93%	378	94.87%	94.91%
fold 4	94.88%	94.89%	785	94.87%	94.90%
fold 5	94.84%	94.95%	655	94.82%	94.93%
fold 6	94.95%	94.93%	1217	94.89%	94.91%
fold 7	94.93%	94.93%	467	94.91%	94.86%
fold 8	94.98%	94.85%	632	94.92%	94.84%
fold 9	94.87%	94.94%	876	94.85%	94.83%
fold 10	94.83%	94.88%	539	94.84%	94.86%
average	94.90%	94.90%	711.3	94.88%	94.87%

Large Dataset with High Noise

The first experiment dataset consists of 2 million records and each record has 10 variables. It is balanced with 50% of the data in the first group and 50% of the data in the second group. The dataset is 75% linear separable.

Algorithm 3

   Input: The input data set of 2 million records; Assume that all records can
be fitted into main memory.
   Output: 10-fold   cross   validation   average   classification   accuracies;
computing time.
      Step 1: The input data set is evenly partitioned into 10 subsets by stratified
               random sampling selection.
      Step 2: A standard 10-fold cross-validation set of 10 sets of training dataset
               and testing dataset is stored by using one of the 10 subsets as the testing
               dataset and using the remaining 9 subsets as training dataset. Repeat the
               following steps for each of the 10 sets of training dataset and testing
               dataset
      Step 3: n=2 million and m=2 million. Stop criteria: Prediction Accuracy >
               70% or computing time > 1000 minutes. Apply algorithm 1.
   END

Table 2. High noise dataset computing results

10-fold	training		time	testing	
	Class 1	Class 2	(seconds)	Class 1	Class 2
fold 1	71.34%	74.33%	1279	70.25%	71.12%
fold 2	72.77%	74.13%	849	72.85%	72.47%
fold 3	74.79%	72.44%	1537	72.31%	71.23%
fold 4	70.94%	73.58%	2574	70.32%	72.09%
fold 5	74.11%	72.35%	742	72.57%	71.32%
fold 6	73.56%	74.33%	1380	73.24%	72.67%
fold 7	71.90%	70.38%	3546	70.39%	70.12%
fold 8	73.89%	72.48%	836	72.37%	72.23%
fold 9	72.37%	73.38%	711	71.56%	71.73%
fold 10	73.56%	72.84%	1207	72.40%	72.19%
average	72.92%	73.02%	1466.1	71.83%	71.72%

4   Conclusion

In this research, we proposed a new epsilon-support vector approach and conducted 2
experimental studies using computer generated large scale classification problem to
address two aspects of data mining algorithm: speed and scalability. The experimental
results indicate that the new approach is capable in solving large scale data mining
problems $(>O(10^9))$ and highly efficient (computing time complexity $O(n^{1.5 \sim 2})$). This
approach also has good performance when the dataset is highly noised (noises are
larger than 25% of the whole data).

References

 1. Boser, B. E., Guyon, I., Vapnik., V. N. : A training algorithm for optimal margin
    classifiers. Proceedings of the Fifth Annual Workshop on Computational Learning Theory,
    5:, (1992) 144--152

2. Bradley, P. : Mathematical Programming Approaches to Machine Learning and Data Mining. PhD thesis, University of Wisconsin, Computer Sciences Department, Madison, WI, USA, TR-98-11. (1998)

3. Bugera, V., Konno, H., Uryasev, S.: Credit Cards Scoring with Quadratic Utility Function. Journal of Multi-Criteria Decision Analysis 11 (2002) 197-211.

4. Cristianini, N. and J. Shawe-Taylor. An Introduction to Support Vector Machines. Cambridge University Press, Cambridge, UK, (2000)

5. Musicant, D. R. NDC: normally distributed clustered datasets,. www.cs.wisc.edu/_musicant/data/ndc/. (1998)

6. Kou, G., Peng, Y., Shi, Y., Wise, M., Xu, W.: Using Multi-objective Linear Programming to Classify Credit Cardholder Behavior, Optimization Methods and Software, Vol. 18, , (2003) 453-473

7. Kou, G., Peng, Y., Shi, Y., Wise, M., Xu, W.: Discovering Credit Cardholders' Behavior by Multiple Criteria Linear Programming, Annals of Operations Research 135 (1):, JAN (2005) 261-274

8. Schölkopf, B., Smola., A. J.: Learning with Kernels. MIT Press, (2002)

9. Smola, A., Bartlett, P., Schölkopf, B., Schuurmans, D. (eds).: Advances in Large Margin Classifiers. MIT Press, Cambridge, MA, (2000)

10. Thompson, Sampling, S.K., :A Wiley-Interscience Publication, New York. (1992)

11. Vapnik, V. N.,: The Nature of Statistical Learning Theory, Springer, New York. (1995)

Unsupervised and Semi-supervised Lagrangian Support Vector Machines *

Kun Zhao[1], Ying-Jie Tian[2], and Nai-Yang Deng[1],**

[1] College of Science
China Agricultural University
`piaopiao-zk@163.com,dengnaiyang@vip.163.com`
[2] Chinese Academy of Sciences
Research Center on Data Technology and Knowledge Economy
`tianyingjie1213@163.com`

Abstract. Support Vector Machines have been a dominant learning technique for almost ten years, moreover they have been applied to supervised learning problems. Recently two-class unsupervised and semi-supervised classification problems based on Bounded C-Support Vector Machines and Bounded ν-Support Vector Machines are relaxed to semidefinite programming[4][11]. In this paper we will present another version to unsupervised and semi-supervised classification problems based on Lagrangian Support Vector Machines, which trained by convex relaxation of the training criterion: find a labelling that yield a maximum margin on the training data. But the problems have difficulty to compute, we will find their semi-definite relaxations that can approximate them well. Experimental results show that our new unsupervised and semi-supervised classification algorithms often obtain almost the same accurate results as the unsupervised and semi-supervised methods [4][11], while considerably faster than them.

Keywords: Lagrangian Support Vector Machines, Semi-definite Programming, unsupervised learning, semi-supervised learning, margin.

1 Introduction

As an important branch in unsupervised learning, clustering analysis aims at partitioning a collection of objects into groups or clusters so that members within each cluster are more closely related to one another than objects assigned to different clusters[1]. Clustering algorithms provide automated tools to help identify a structure from an unlabelled set, in a variety of areas including bio-informatics, computer vision, information retrieval and data mining. There is a rich resource of prior works on this subject. The works reviewed below are most related to ours.

** The corresponding author.

Efficient convex optimization techniques have had a profound impact on the field of machine learning. Most of them have been used in applying quadratic programming techniques to Support Vector Machines (SVMs) and kernel machine training[2]. Semi-definite Programming (SDP) extends the toolbox of optimization methods used in machine learning, beyond the current unconstrained, linear and quadratic programming techniques.

Semi-definite Programming (SDP) has showed its utility in machine learning. Lanckreit *et al* show how the kernel matrix can be learned from data via semi-definite programming techniques[3]. De Bie and Cristanini develop a new method for two-class transduction problem based on semi-definite relaxation technique[5]. Xu *et al* based on[3][5] develop methods to two-class unsupervised and semi-supervised classification problems in virtue of relaxation to Semi-definite Programming[4]. Zhao *et al* present another version to unsupervised and semi-supervised classification problems based on Bounded ν-Support Vector Machines [11].

In this paper we provide a brief introduction to the application of Semi-definite Programming in machine learning[3][4][5][11] and construct other unsupervised and semi-supervised classification algorithms. They are based on Lagrangian Support Vector Machines (LSVMs), which obtain almost accurate results as other unsupervised and semi-supervised methods [4][11], while considerably faster than them.

We briefly outline the contents of the paper now. We review the Support Vector Machines and Semi-definite Programming in Section 2 . Section 3 will formulate new unsupervised and semi-supervised classification algorithms which are based on LSVMs. Experimental results will be showed in Section 4. In the last Section we will have a conclusion.

A word about our notation. All vectors will be column vectors unless transposed to a row vector by "T". The scalar (inner) product of two vectors x and y in the n-dimensional real space R^n will be denoted by $x^T y$. For an $l \times d$ matrix A, A_i will denote the ith row of A. The identity matrix in a real space of arbitrary dimension will be denoted by I, while a column vector of ones of arbitrary dimension will be denoted by e.

2   Preliminaries

Considering the supervised classification problem, we will assume the given labelled training examples $(x_1, y_1), \ldots, (x_n, y_n)$ where each example is assigned a binary $y_i \in \{-1, +1\}$. The goal of SVMs is to find the linear discriminant $f(x) = w^T \phi(x) + b$ that maximizes the minimum misclassification margin

$$\min_{w,b,\xi} \; \frac{1}{2}(\|w\|^2 + b^2) + \frac{C}{2}\sum_{i=1}^{n} \xi_i^2$$
$$\text{s.t. } y_i((w \cdot \phi(x_i)) - b) + \xi_i \geq 1 \;, i = 1, 2, \ldots, n \tag{1}$$

Let $\Phi = (\phi(x_1), \ldots, \phi(x_n))$, $K = \Phi^T \Phi$, then $K_{ij} = \phi(x_i)^T \phi(x_j)$, dual problem of (1) is

$$\max_{\alpha} \quad -\frac{1}{2} \sum_{i=1}^{n} \sum_{j=1}^{n} y_i y_j \alpha_i \alpha_j K_{ij} - \frac{1}{2} \sum_{i=1}^{n} \sum_{j=1}^{n} y_i y_j \alpha_i \alpha_j - \frac{1}{2C} \sum_{i=1}^{n} \alpha_i^2 + \sum_{i=1}^{n} \alpha_i \quad (2)$$

$$\text{s.t.} \quad \alpha_i \geq 0, i = 1, 2, \ldots, n$$

The problem (1) and (2) are primal and dual problem of Lagrangian Support Vector Machines (LSVMs) respectively [12].

Based on Bounded C-Support Vector Machines (BC-SVMs) [8] Xu *et al* get the optimization problem [4] that can solve unsupervised classification problem. Zhao *et al* based on Bounded ν-Support Vector Machines (Bν-SVMs)[7] get the optimization problem [11] that can solve unsupervised classification problem too. In this paper Lagrangian Support Vector Machines will be used to resolve unsupervised and semi-supervised classification problems.

Given $H \in \mathcal{M}^n$, $A_i \in \mathcal{M}^n$ and $b \in \mathcal{R}^m$, where $\mathcal{M}^n$ is the set of $n \times n$ symmetric matrix. The standard Semi-definite Programming problem is to find a matrix $X \in \mathcal{M}^n$ for the optimization problem

$$\min \quad H \bullet X$$
$$\text{(SDP)} \qquad \text{s.t.} \quad A_i \bullet X = b_i, i = 1, 2, \ldots, m$$
$$X \succeq 0$$

where the $\bullet$ operation is the matrix inner product $A \bullet B = tr A^T B$, the notation $X \succeq 0$ means that X is a positive semi-definite matrix. The dual problem to (SDP) can be written as:

$$\max \quad b^T \lambda$$
$$\text{(SDD)} \qquad \text{s.t.} \quad H - \sum_{i=1}^{m} \lambda_i A_i \succeq 0$$

Here $\lambda \in \mathcal{R}^m$. For Semi-definite Programming, interior point method has good effect, moreover there exists several softwares such as SeDuMi[10] and SDP3.

3   Unsupervised and Semi-supervised Classification Algorithms

A recent development of convex optimization theory is Semi-definite Programming, a branch of that fields aimed at optimizing over the cone of semi-positive definite matrices. One of its main attraction is that it has been proven successful in construct tight convex relaxation of NP-hard problem. Semi-definite Programming has showed its utility in machine learning too.

Lanckreit *et al* show how the kernel matrix can be learned from data via semi-definite programming techniques[3]. They presented new methods for learning a kernel matrix from labelled data set and transductive data set. Both methods

can relax the problem to Semi-definite Programming. For a transductive setting, using the labelled data one can learn a good embedding (kernel matrix), which can then be applied to the unlabelled part of the data. De Bie and Cristanini relax two-class transduction problem to semi-definite programming based on transductive Support Vector Machines[5].

Xu *et al* develop methods to two-class unsupervised and semi-supervised classification problems based on Support Vector Machines in virtue of relaxation to Semi-definite Programming[4] in the foundation of [5] [3]. Its purpose is to find a labelling which has the maximum margin not to find a large margin classifier. This leads to the method to cluster the data into two class, which subsequently run a SVM, and will obtain the maximum margin with all possible labelling. We should add constraint about class balance $-\varepsilon \leq \sum_{i=1}^{n} y_i \leq \varepsilon$, otherwise we can simply assign all the data to the same class and then get unbounded margin; moreover this can avoid noisy data's influence in some sense.

Using the method in [5] [3], Xu *et al* based on BC-SVMs get the optimization problem[4] that can solve unsupervised classification problem. Analogously Zhao *et al* based on Bν-SVMs get the optimization problem[11] that can solve unsupervised classification problem too, which the parameter ν in Bν-SVMs has quantitative meaning. However, the time consumed of both methods based on BC-SVMs and Bν-SVMs is too long. So it seems necessary to find a faster method, which has almost accurate results as above at least. The reason that unsupervised classification algorithms based on BC-SVMs and Bν-SVMs run slowly is their semi-definite relaxations have so many variables, concretely $n^2 + 2n + 1$ and $n^2 + 2n + 2$ variables respectively. In order to fasten the speed of algorithm, it seems better to find a qualified SVM which has fewer constraints, for the number of variables in semi-definite relaxation problem equals to sum of $n^2 + 1$ and number of constraints in SVM. Primal problems of BC-SVMs and Bν-SVMs have $2n$ and $2n+1$ constraints respectively, while primal problem of Lagrangian Support Vector Machines has n constraints. Therefore it seems better to use Lagrangian Support Vector Machines to resolve unsupervised classification problem.

We use the same method in [5] [3] to get the optimization problem based on LSVMs

$$\min_{y_i \in \{-1,+1\}^n} \quad \min_{w,b,\xi} \frac{1}{2}(\|w\|^2 + b^2) + \frac{C}{2} \sum_{i=1}^{n} \xi_i^2$$
$$\text{s.t.} \quad y_i((w \cdot \phi(x_i) - b) + \xi_i \geq 1 \tag{3}$$
$$-\varepsilon \leq \sum_{i=1}^{n} y_i \leq \varepsilon$$

It is difficult to solve Problem (3), so we will consider to get its approximate solutions. Since Semi-definite Programming can provide effective algorithms to cope with difficult computational problems and obtain high approximate solutions, it seems better to relax problem (3) to Semi-definite Programming. Let $y = (y_1, y_2, \ldots, y_n)^T$, $M = yy^T$, $\Phi = (\phi(x_1), \ldots, \phi(x_n))$ and $K = \Phi^T \Phi$,

moreover $A \circ B$ denotes componentwise matrix multiplication. Use the same method in [3], we obtain the Unsupervised Classification Algorithm.

Algorithm 3.1 (Unsupervised Classification Algorithm)

1.Given data set $D = \{x_1, \ldots, x_n\}$, where $x_i \in \mathcal{X} = \mathbf{R}^d$.
2.Select appropriate kernel $K(x, x')$, C and ε, then construct and solve the problem

$$
\begin{aligned}
\min_{M, \delta, u} \quad & \frac{1}{2}\delta \\
\text{s.t.} \quad & \begin{pmatrix} (K \circ M + M + \frac{1}{C}I) & (u + e) \\ (u + e)^T & \delta \end{pmatrix} \succeq 0 \\
& -\varepsilon e \leq Me \leq \varepsilon e \\
& M \succeq 0, diag(M) = e \\
& u \geq 0
\end{aligned}
\tag{4}
$$

Get the optimal solution M^*, δ^* and u^* with SeDuMi.
3.Construct label $y^* = sgn(t_1)$, where t_1 is eigenvector corresponding to the maximal eigenvalue of M^*.

It is easy to extend the unsupervised classification algorithm to semi-supervised classification algorithm. For semi-supervised SVMs training, we can assume $(x_1, y_1), \ldots, (x_n, y_n)$ have labelled by experts and $x_{n+1}, \ldots, x_{n+N}$ are not labelled. Only adding the constraints $M_{ij} = y_i y_j, i, j = 1, 2, \ldots, n$ to the problem (4)will obtain the Semi-Supervised Classification Algorithm.

4   Experimental Results

4.1   Results of Unsupervised Classification Algorithm

In order to evaluate the performance of unsupervised classification algorithm, we will compared our unsupervised classification algorithm (L-SDP)with (ν-SDP)[11] and maximum margin clustering algorithm (C-SDP)[4]. Firstly we consider four synthetic data sets including data set AI, Gaussian, circles and joined-circles, which every data set has sixty points. $\varepsilon = 2$, $C = 100$ and Gaussian kernel with appropriate parameter $\sigma = 1$ are selected. Results are showed in Table 1. The number is the misclassification percent. From Table 1 we can find that the result of L-SDP is better than that of C-SDP and ν-SDP, moreover the time consumed are showed in Table 2. The numbers are seconds of CPU. From Table 2

Table 1. Classification results about three algorithms on four synthetic data sets

Algorithm	AI	Gaussian	circles	joined-circles
L-SDP	9.84	0	0	8.19
C-SDP	9.84	1.67	11.67	28.33
ν-SDP	9.84	1.67	1.67	11.48

Table 2. Computation time about three algorithms on four synthetic data sets

Algorithm	AI	Gaussian	circles	joined-circles
L-SDP	1425	1328	1087.6	1261.8
C-SDP	2408.9	1954.9	2080.2	2284.8
ν-SDP	2621.8	1891	1837.1	2017.2
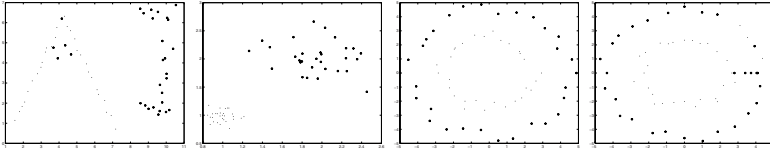
Fig. 1. Results by our unsupervised classification algorithm based on LSVMs on the four synthetic data sets including data set AI, Gaussian, circles and joined-circles

we can find that the speed of L-SDP is faster than those of C-SDP and ν-SDP, moreover almost half of the time consumed of others.

We also conduct our algorithm on the real data sets which can be obtained from http://www.cs.toronto.edu/ roweis/data.html, including Face and Digits data sets. As same to synthetic data sets, with thirty samples of every class of data sets. To evaluate clustering performance, a labelled data set was taken and the labels are removed , then run clustering algorithms, and labelled each of the resulting clusters with the majority class according to the original training labels, then measured the number of misclassification.The results are showed in Table 3 and the number is the misclassification percent. From Table 3 we

Table 3. Results about three algorithms on Face and Digits data sets

Algorithm	Digits32	Digits65	Digits71	Digits90	Face12	Face34	Face56	Face78
L-SDP	0	0	0	0	8.33	0	0	0
C-SDP	0	0	0	0	1.67	0	0	0
ν-SDP	0	0	0	0	1.67	0	0	0

can find that the result of L-SDP is almost same to C-SDP and ν-SDP except data set face12, but the time consumed are showed in Table 4. The numbers are seconds of CPU.

From Table 4 we can find that the speed of L-SDP is much faster than those of C-SDP and ν-SDP, moreover quarter of the time consumed of others at least.

4.2   Results of Semi-supervised Classification Algorithm

We test our algorithm to semi-supervised learning on the real data sets as same to section of unsupervised Classification Algorithm. As same to unsupervised classification algorithm, in order to evaluate the performance of semi-supervised

Table 4. Computation time about three algorithms on Face and Digits data sets

Algorithm	Digits32	Digits65	Digits71	Digits90	Face12	Face34	Face56	Face78
L-SDP	445.1	446.2	446.4	446.5	519.8	446.3	446.1	446
C-SDP	1951.8	1950.7	1951.6	1953.4	1954.5	1952.1	1950.3	1951
ν-SDP	1721.6	1721.5	1722.2	1722.8	1721.4	1722.1	1721	1719.7
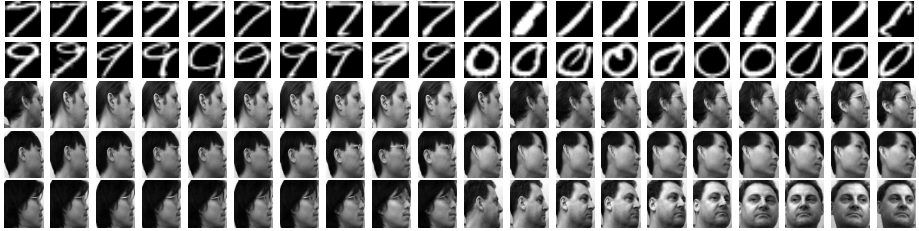
Fig. 2. Every row shows a random sampling of images from a data set, the first ten images are in one class, while the rest ten images are in another class by L-SDP.

classification algorithm, we will compared our semi-supervised classification algorithm (Semi-L-SDP)with (Semi-ν-SDP)[11] and maximum margin clustering algorithm (Semi-C-SDP)[4]. We separate the data into labelled and unlabelled parts, and get rid of the labels of the unlabelled portion, then run semi-supervised classification algorithms to reclassify the unlabelled examples in use of the learning results, eventually measured the misclassification error on the original labels. Thirty samples of every class of data sets will be used. The results will be showed in Table 5 and the number is the misclassification percent. From Table 5 we can find that the result of Semi-L-SDP is almost same to Semi-ν-SDP and better than Semi-C-SDP except data set face12, but time consumed of CPU is much less than those of others. Results are showed in Table 6. The numbers are seconds of CPU. From Table 6 we can find that the speed of Semi-L-SDP is much

Table 5. Results about three algorithms on Face and Digits data sets

Algorithm	Digits32	Digits65	Digits71	Digits90	Face12	Face34	Face56	Face78
Semi-L-SDP	5	5	5	5	11.67	5	5	5
Semi-C-SDP	25	28.3	28.3	28.3	16.67	28.3	28.3	28.3
Semi-ν-SDP	5	5	5	5	3.3	5	5	5

Table 6. Computation time about three algorithms on Face and Digits data sets

Algorithm	Digits32	Digits65	Digits71	Digits90	Face12	Face34	Face56	Face78
Semi-L-SDP	606.8	607.8	607.9	608.3	653.9	608.4	608	608.2
Semi-C-SDP	1034	1036	1035.6	1035.8	1094.7	1033.1	1035.1	1035.8
Semi-ν-SDP	734.8	735.5	735.7	735.9	810.6	734.4	735.5	736

faster than those of Semi-C-SDP and Semi-ν-SDP, moreover almost half of the time consumed of others.

5   Conclusion

We have proposed efficient algorithms for unsupervised and semi-supervised classification problems based on Semi-definite Programming. From Section of experimental results we can learn that unsupervised and semi-supervised classification algorithms based on Lagrangian Support Vector Machines is much faster than other methods based on Bounded C-Support Vector Machines and Bounded ν-Support Vector Machines, and classification results are better than them.

In the future we will continue to estimate the approximation of SDP relaxation and get an approximation ratio of the worst case.

References

1. J.A.Hartigan, *Clustering Algorithms*, John Wiley and Sons, 1975.
2. B.Schoelkopf and A.Smola, *Learning with kernels: Support Vector Machines, Regularization, Optimization,and Beyond*, MIT Press, 2002.
3. G.Lanckriet, N.Cristianini, P.Bartlett, L.Ghaoui and M.Jordan, Learning the kernel matrix with semidefinite programming,*Journal of Machine learning research*, 5, 2004.
4. L.Xu, J.Neufeld, B.Larson and D.Schuurmans, Maximum margin clustering, *Advances in Neural Information Processing Systems 17(NIPS-04)*, 2004.
5. T.De Bie and N.Crisrianini, Convex methods for transduction, *Advances in Neural Information Processing Systems 16(NIPS-03)*, 2003.
6. N.Y.Deng and Y.J.Tian, *A New Method of Data Mining: Support Vector Machines*, Science Press, 2004.
7. T.Friess, C.N.Christianini, C.Campbell, The kernel adatron algorithm: a fast and simple learning procedure for support vector machines, *Proceeding of 15th Intl. Con Machine Learning*, Morgan Kaufman Publishers, 1998.
8. O.L.Mangasarian and D.R.Musicant, Successive overrelaxation for support vector machines, *IEEE Trans. Neural Networks*, 5,1999(10),1032-1037.
9. Nello Cristianini and John Shawe-Taylor, *An Introduction to Support Vector Machines and Other Kernel-based Learning Methods*, Cambridge University Press, 2000.
10. Jos F.Sturm, Using SeDuMi1.02, A Matlab Toolbox for Optimization over Symmetric Cones, *Optimization Methods and Software*, 11-12, 1999, 625-653.
11. Kun Zhao, Ying-jie Tian and Nai-yang Deng, Unsupervised and Semi-supervised Two-class Support Vector Machines, to appear.
12. O.L.Mangasarian and David R.Musicant,Lagrangian Support Vector Machines, *Journal of Machine Learning Research*,1,2001,161-177.

A Security Specification Library
with a Schemaless Database

Shoichi Morimoto[1] and Jingde Cheng[2]

[1] School of Industrial Technology, Advanced Institute of Industrial Technology
1-10-40, Higashi-oi, Shinagawa-ku, Tokyo, 140-0011, Japan
`morimoto-syoichi@aiit.ac.jp`
[2] Department of Information and Computer Sciences, Saitama University
255, Shimo-okubo, Sakura-ku, Saitama, 338-8570, Japan
`cheng@aise.ics.saitama-u.ac.jp`

Abstract. In order to develop highly secure information systems, it is important to make a security specification of the systems, although it requires heavy labor. Thus database technologies have been applied to software engineering and information security engineering for practical reuse of security specifications. However, because the specifications do not have fixed layout, it is difficult to develop a flexible and useful library for the documents with conventional database technologies. Therefore, this paper proposes a security specification library with a schemaless native XML database. Users of the library can directly store and manage security specifications with any layout. Consequently, the library mitigates the labor for making security specifications.

Keywords: Common criteria, Digital pattern processing.

1 Introduction

Because quality of security specifications in development process are directly and closely related to security of information systems, it is desirable, but difficult, to develop a high quality security specification. Thus, we have developed a security requirement management database with a relational database, which supports development of secure information systems [1,4]. Users of the database can effectively manage and reuse security requirements in security specifications.

However, the specification documents severally have various styles and structures, because there are many software development processes and developers have to use the styles and structures suitable for each development process. Thus, it is difficult to develop a flexible and useful database for the purpose with relational or object-oriented databases that need to define fixed structure.

Therefore, in this paper we rebuild the security requirement management database with a schemaless native XML database. Users of the improved database can freely store security specifications without consideration to document structure after converting them into XML documents. Consequently, it mitigates labor making high quality security specifications and developing highly secure information systems.

2   The Security Requirement Management Database

The security requirement management database, named ISEDS, can manage data of specifications which are designed in conformity to ISO/IEC 15408 common criteria [1, 4]. The criteria define security functional requirements which should be applied to validate an information system [2]. Applicants who apply to obtain the evaluation of ISO/IEC 15408 have to describe and submit a security specification of their system. The security specification, called security target, must describe the category of the target system which is evaluated (target of evaluation, TOE for short), threats which are anticipated in the TOE, security objectives to oppose the threats, security functional requirements for achievement of the objectives, and security functions for implementation of the requirements. ISEDS implements the components of security targets and their interrelationships with a relational database.

3   Improvement of the Database

We reimplemented ISEDS with NeoCore XML Management System (XMS) [7], which is a native XML database and free for development only. Its advantage is high performance and low resource utilization because of its patented Digital Pattern Processing (DPP) technology. With DPP, XMS describes XML documents and their component contents in numeric finite-width fields. This ensures that performance remains unaffected by the length of tag names, element content, or document hierarchy. To further improve performance, DPP enables XMS to "index" every tag, element, and combination, ensuring extremely fast searches
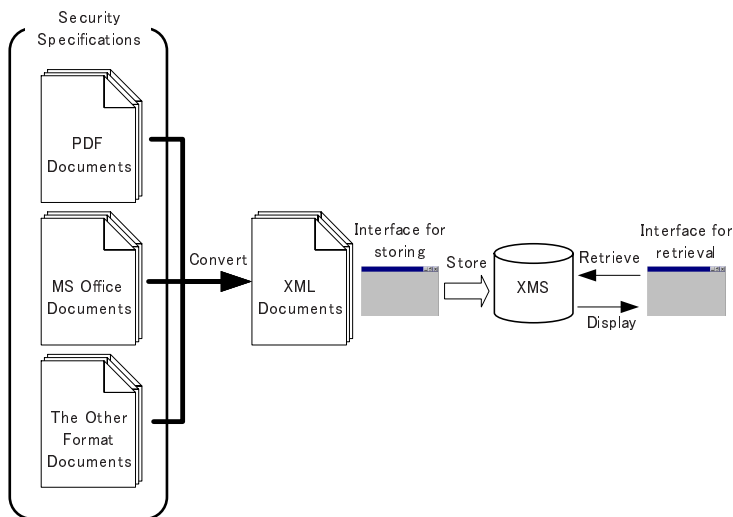
Fig. 1. The security requirement management database with XMS
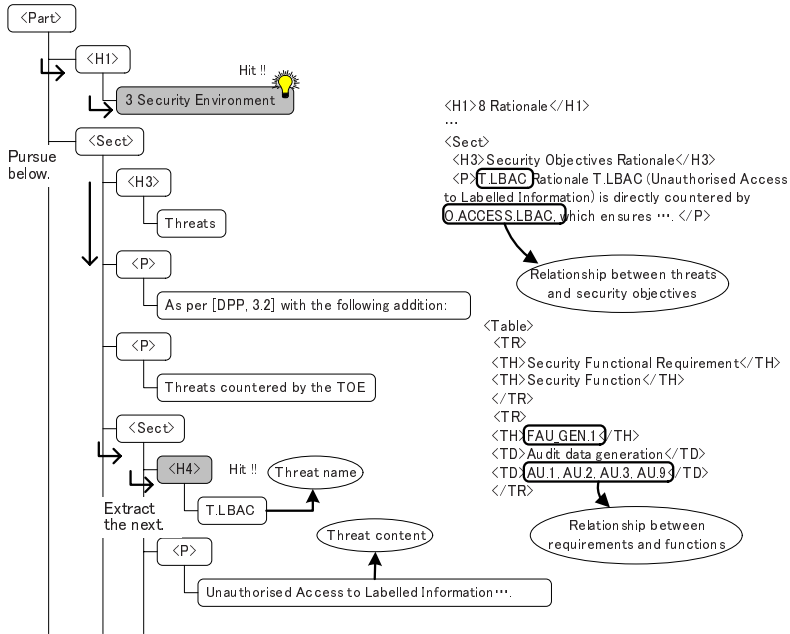
Fig. 2. The retrieval function behavior

on tags and data. The users of XMS can flexibly retrieve XML documents with XQuery, XPath, and FLWR expressions [6]. The most important merit is that XMS does not require defining a schema. That is, XMS can directly store XML documents without a schema. Because these advantages can solve the problem of ISEDS, we adopted XMS.

The improved ISEDS can store any layout and format document. Users must first convert security specifications into XML documents. Specifications, perhaps, are generally written by MS Word, Excel, OpenOffice, or PDF. Adobe Acrobat can convert PDF files into XML documents. Office documents can do likewise. Somehow the other format documents are also convertible into XML. After the conversion, the users can store them into ISEDS via the user interface. The interface appends metadata to the XML documents and stores them into XMS. The metadata record timestamps, modification times, source file passes, identifications, and tag names of document captions for retrieval. One can easily retrieve, update and delete the stored data via the other interface (Fig. 1). Because each XML document tree in ISEDS is different, there are no fixed passes for retrieval. Therefore, ISEDS retrieval function distinguishes each component in security specifications by caption names of security targets. For example, anticipated threats are described in the chapter "Security Environment." When retrieving threats, the function firstly searches for a tag which has the text "Security Environment" by utilizing the metadata. After finding the tag, it pursues the following tags and records the threat names and contents, cf., Fig. 2.

Similarly, the relationships are mentioned in the chapter "Rationale" by tables or texts. Security targets give each component an abbreviation, e.g., T.xxx, O.xxx. The prefix 'T.' denotes threats and the prefix 'O.' denotes security objectives. Thus, when retrieving relationships, the function records abbreviations of threats, security objectives, security requirements, and security functions beforehand. After the preparatory pursuit, the function reads relationships in the tables or texts leaning on the marks, i.e., each abbreviation name (Fig. 2).

Thus, the improved ISEDS can provide the functions equivalent to former all functions by XMS and the interfaces. Moreover, response performance of the retrieval was remarkably improved by the DPP technology of XMS.

4   Concluding Remarks

In order to apply effectively database technologies to information security engineering, we have redesigned and redeveloped the security requirement management database with a schemaless native XML database. Since users of the improved database do not need to define a schema, the former problem of the security requirement management database was solved and its performance was also improved. The users can collect, manage, and utilize security specifications with any layout, format, and structure. The specifications which are described with the database can be considered to be the security specification certified by ISO/IEC 15408. This fact is verifiable by our formal verification technique [3,5].

References

1. Horie, D., Morimoto, S., and Cheng, J.: A Web User Interface of the Security Requirement Management Database Based on ISO/IEC 15408, Proceedings of the International Conference on Computational Science (ICCS'06), Lecture Notes in Computer Science, Vol. 3994, Springer-Verlag (2006) 797–804
2. ISO/IEC 15408 standard: Information Technology - Security Techniques - Evaluation Criteria for IT Security (1999)
3. Morimoto, S. and Cheng, J.: Patterning Protection Profiles by UML for Security Specifications, Proceedings of the International Conference on Computational Intelligence for Modelling, Control and Automation and International Conference on Intelligent Agents, Web Technologies and Internet Commerce Vol-2 (CIMCA-IAWTIC'05), IEEE-CS (2005) 946–951
4. Morimoto, S., Horie, D., and Cheng, J.: A Security Requirement Management Database Based on ISO/IEC 15408, Proceedings of the International Conference on Computational Science and its Applications (ICCSA'06), Lecture Notes in Computer Science, Vol. 3982, Springer-Verlag (2006) 1–15
5. Morimoto, S., Shigematsu, S., Goto, Y., and Cheng, J.: Formal Verification of Security Specifications with Common Criteria, Proceedings of the 22nd Annual ACM Symposium on Applied Computing (SAC'07), ACM (2007) 1506–1512
6. World Wide Web Consortium: XQuery 1.0 and XPath 2.0 Formal Semantics, http://www.w3.org/TR/xquery-semantics/
7. Xpriori LLC: NeoCore XMS, http://www.xpriori.com/

Content-Based Image Retrieval
Using Shifted Histogram

Gi-Hyoung Yoo[1], Beob Kyun Kim[2], and Kang Soo You[3]

[1] Department of Computer Engineering, Chonbuk National University,
Jeonju, 561-756, Korea
`ghryoo@gmail.com`
[2] Korea Institute of science and technology Information, Daejeon, 350-806, korea
`Bkyun.kim@gmail.com`
[3] School of Liberal Arts, Jeonju University, Jeonju, 561-756, Korea
`kangsoo.you@gmail.com`

Abstract. This paper proposes the shifted histogram method (SHM), for histogram-based image retrieval based on the dominant colors in images. The histogram-based method is very suitable for color image retrieval because retrievals are unaffected by geometrical changes in images, such as translation and rotation. Images with the same visual information, but with shifted color intensity, may significantly degrade if the conventional histogram intersection method (HIM) is used. In order to solve this problem, we propose the shifted histogram method (SHM). Our experimental results show that the shifted histogram method

Keywords: Content-Based Image Retrieval, Color Histogram, Shift Histogram.

1 Introduction

Content-based image retrieval (CBIR) is a promising approach to search through an image database by means of image feature, such as appearance, color, texture, shape, pattern, or a combination these factors [1], [2], [3], [4]. In the Histogram intersection method (HIM) [5], [6] is the most common approach for using the intersected area of histograms acquired from image features.

Although the conventional color histogram method can describe the global color distribution of images in a straightforward manner, it only provides a very coarse characterization of images. There is no spatial information included in the color histogram. Thus, two completely different images may have very similar histograms. Also, the lighting conditions will alter the histogram of an image. Even two pictures with little difference in lighting conditions can not easily be matched.

In PWH (perceptually weighted histogram) by Lu *et al.* [7], each color from an image is represented by its 10 nearest similar colors. However, HIM still takes place of the full color-range (e.g. 256 colors) of the two images being compared. In MHM (merged histogram method), colors from individual images and between images are merged to form a dominant color set, instead of color components. The idea behind MHM is to retrieve images in a database of which the intensity has been changed by

light. However, this method requires greater processing capability to generate feature vectors.

In this paper, we propose a novel shifted histogram method (SHM), to overcome the disadvantages of the conventional histogram method.

2   Histogram-Based Color Image Retrieval

The histogram-based method is very suitable for color image retrieval, because this method is unaffected by geometrical information in images, such as translation and rotation. The histogram intersection method (HIM) [5],[6] measures the intersections between the two image histograms. These intersections are usually named query image for the query input and target image for the image database. An image histogram is an n-dimensional vector, in which each element represents the number of pixels of color in the n-color image.

Regardless of image size, each element is normalized before comparison. The similarity measure is then calculated by calculating the histogram intersection, as shown in equation (1).

$$I(T,Q) = \sum_{k=1}^{n} \min(T_k, Q_k) \tag{1}$$

The larger the value has, the more similar the image has in equation (1). Images can then be ranked from the image database.

3   Shifted Histogram Method (SHM)

In a more general mathematical sense, a histogram is simply a mapping that counts the number of observations that fall into various disjoint categories (known as bins), whereas the graph of a histogram is merely one way to represent a histogram. Thus, if we let the total number of observations be the total number of bins, the histogram meets the following conditions in figure 1.
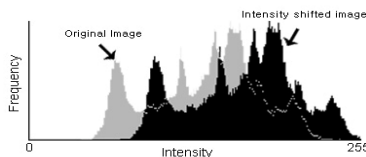
Fig. 1. Histogram of original image and shifted image by light change

The proposed SHM can be divided into 4 stages before similarity measurement. The process is as follows:

```
Comments : h(Q)-a histogram of query image,  h(T)-a
     histogram of image in database,   k-a histogram bin,
     n-the number of total bins,    Sim(T,Q)-Similarity
     between query image and image in database
   Step 1 :  Sim(T,Q) = 0, qk = 1, tk = 1
   Step 2 :   Make a histogram  h(Q)  and  h(T)
   Step 3 :  If  h_{qk}(Q) > Threshold  then go to Step 5,
                 otherwise, go to Step 4
   Step 4 :  If  qk < n  then  qk = qk +1 , go to Step3,
                 otherwise, go to Step 8
   Step 5 :  If  h_{tk}(T) > Threshold  then go to Step 7,
                 otherwise go to Step 6
   Step 6 :  If  tk < n  then  tk = tk +1 , go to Step 5,
                 otherwise go to Step 8
   Step 7 :  Sim(T,Q) = Sim(T,Q) + min(h_{qk}(Q), h_{tk}(T))
                 If  qk < n  and  tk < n  then  qk = qk +1 ,
                 tk = tk +1 , go to Step 3,
                 otherwise go to Step 8.
```

$$Step\ 8 :\quad Sim(T,Q) = \frac{Sim(T,Q)}{The\ Number\ of\ Pixel\ used\ in\ Query\ Image}$$

```
   Step 9 :   Return
```

4 Experiments

The analysis of histogram effectiveness in image discrimination is mainly used for the design of image retrieval systems. In order to test the performance of our method, we have implemented several groups of experiments. The testing image database includes images with a wide range of image content, such as nature scenes, flowers, animals, cars, trains, and so on.

The performance of the retrieval results is measured by Precision, Recall [8] and AVRR (AVerage Rank of Relevant images). Relevant images are referred to as images in the same class. In table 1 and table 2, the performance of SHM, MCH and CHM is compared in terms of precision, recall and AVRR.

Table 1. Result of the three methods in flowers

Method	Result	Recall	Precision	AVRR
SHM	7	0.78	0.67	4.2
MCH	6	0.59	0.61	4.0
CHM	4	0.47	0.51	3.5

Table 2. Result of the three methods in trains

Method	Result	Recall	Precision	AVRR
SHM	7	0.78	0.67	4.2
MCH	6	0.59	0.61	4.0
CHM	4	0.47	0.51	3.5

5   Conclusion

The shifted-color histogram method (SHM) is proposed for histogram-based image retrieval, and is based on the dominant colors in images. The histogram-based method is very suitable for color image retrieval because it is unaffected by geometrical changes in images, such as translation and rotation. However, images with similar visual information but with shifted color intensity, may result in a significant degradation in the similarity level, if the conventional histogram intersection method (HIM) is used. To solve the problem, the shifted histogram method (SHM) is proposed.

In comparison with other methods, our method is more straightforward. It doesn't haves special requirements or extra restrictions for images, for content-based image retrieval. Our experimental results show that the shifted histogram method has significantly higher retrieval effectiveness than the standard histogram method. In future study, the proposed retrieval method is expected to be applied to large scale image and video databases.

References

1. Flickner, M. *et al.*: Query by image and video content: The QBIC system. IEEE Computer, Vol. 28(9). (1995) 23–32
2. Swain, M.J., Ballard, D.H.: Color indexing. Int. J. Computer Vision, Vol. 7(1). (1991) 11–32.
3. Gagaudakis, G., Rosin, P.: Incoprerating shape into histograms for CBIR. Proc. Int. Conf. Image Processing, Thessaloniki, Greece, (2001) 7–10
4. Rui, Y., Huang, T., Chang, S.F.: Image Retrieval:Current Techniques, Promising Directions and Open Issues. J. Visual Communication and Image Representation, Vol. 10. (1999) 39–62
5. Wong, K.M., Cheung, C.H., Po, L.M.: Dominant Color Image Retrieval using Merged Histogram. Proc. the 2003 Int. Symposium, (2003)
6. Wong, K.M., Cheung, C.H., Po, L.M.: Merged-color histogram for color image retrieval. Proc. of the 2002 Int. Conference, (2002) 24–28
7. Seong, O.S., Choi, T.S.: Edge Color Histogram for Image Retrieval. IEEE ICIP 0–7803–7622–6/02/ (2000)
8. Muller, H., Muller, W., Squire D., Marchand, M.S., Pun, T.: Performance Evaluation in Content-Based Image Retrieval:Overview and Proposals. Pattern Recognition Letters, Vol. 22(5). (2001) 593–601

Image Segmentation by Nonparametric Color Clustering

Shukui Bo[1], Yongqiang Ma[2], and Chongguang Zhu[1]

[1] Institute of Remote Sensing Applications, Chinese Academy of Sciences,
P.O. Box 9718, 100101 Beijing, China
bsk586@163.com
[2] College of Computer Science & Technology, Henan Polytechnic University,
454000 Jiaozuo, China

Abstract. We present a color image segmentation scheme based on pixel color clustering. The proposed segmentation is based on mean shift clustering method, which is a powerful tool for the analysis of feature space. However, earlier clustering techniques based on mean shift use single scale over the entire feature space and are not feasible to analyze complex multi-modal feature spaces. In this paper, we present an adaptive mean shift method, in which the local scale information is involved. Actual regions in an image can be obtained by segmentation using the proposed clustering technique.

Keywords: image segmentation, clustering, mean shift.

1 Introduction

Image segmentation is a major step in shape feature extraction. Segmentation using clustering involves the search for image points that are similar enough to be grouped together. In the analysis of an image, K-means, ISODATA, and Fuzzy C-means are conventional clustering techniques. Conventional clustering techniques are always based on partitioning of the feature space. A usually used assumption in these methods is that the individual clusters obey multivariate normal distributions, i.e., the feature space can be modeled as a mixture of Gaussians. However, the assumption is not correct in many real data. Nonparametric methods in feature space analysis avoid the use of the normality assumption. Arbitrarily structured feature spaces can be analyzed only by nonparametric methods since these methods do not impose any assumptions. Mean shift (MS) algorithm is a nonparametric technique for feature space analysis. The mean shift theory was proposed in 1975 by Fukunaga and Hostetler [1]. The mean shift method and its applications have been discussed by a series of researchers [2,3,4,5,6]. In the related works, however, the local bandwidth (or local scale) and structure information of neighborhood around individual sample are not considered adequately. In [7], the algorithms only take into account the difference of local bandwidth. The other algorithms do not involve the information of both local bandwidth and the anisotropy of sample's neighborhood in the feature

space. Therefore, these methods are not effective when the real data has complex distribution in the feature space.

This paper introduces a segmentation technique based on the mean shift clustering, a simple nonparametric procedure for estimating density gradients. The clustering technique is improved by considering local scale information to avoid the drawbacks of the abovementioned techniques.

2   The Segmentation Algorithm

The mean shift procedure is a nonparametric analysis technique of feature space. To avoid the drawback of clustering using single scale for the whole feature space, we improve earlier mean shift algorithms by involving the neighborhood information of samples. The neighborhood of a point in feature space can be described using its K-nearest neighbor (KNN). The KNN query is a common type of query in databases. The nature of KNN tells the local density information, while the task of mean shift procedure is to find a local density maximum. Therefore, the combination of KNN and mean shift is an adaptive way to detect the exact local mode based on local density. The partition of the feature space is obtained by means of dividing all data points into groups centered on the modes. The improved method will do mean shift at suitable scales on different locations with various density, so clusters of contrasting sizes and densities could be detected correctly. As far as clusters of arbitrary shapes and structures are concerned, an idea of multi-center is considered, i.e., a cluster is represented by more than one "center" point (mode).

In the feature space, the volume covered by the K-nearest neighbor (KNN) of a point shows the density of its neighborhood. So embedding the KNN information will be a good choice to provide the local density parameter in clustering procedure. The KNN information can be obtained by performing K-nearest neighbor query to the points in the feature space. If the volume that the K-nearest neighbor of a sample holds is small in the feature space, the density around the sample is high because the number of nearest neighbors is fixed. That is to say the points in the neighborhood are close to each other. Therefore the appropriate local scale should be small and computed according to KNN information. On the other hand, if the volume is large, a relative large scale should be used in the mean shift procedure to locate the local mode.

However, clustering by means of the above method cannot be satisfactory in practical applications. The KNN query procedure is quite time consuming, since its computational complexity is $O(Kn^2)$ for a set of n data points and the data set of an image may be very large. So a subset can be randomly selected from the data because the points (pixels) in an image are spatially correlated to a great extent. In our program, a subset of m points ($m<<n$) is selected from the original data by a random tessellation of the image. The hyper-spheres centered on the m points will cover most of the data points, therefore, the quality of the density gradient estimate is not diminished by the use of sampling, while the computational complexity decreases to $O(Knm)$.

The above algorithm is called adaptive mean shift (AMS) in this paper. Involving the information of K-nearest neighbor in mean shift procedure makes the algorithm

adapt to regions of different density. After the mean shift procedures, m cluster center candidates are defined as the m convergent points. Although a cluster might be anisotropic in the feature space, it can be delineated by more than one point. If some of the m candidates belong to the same cluster, they will be close to each other after adaptive mean shift procedures. Then these close candidate points are assigned to a single cluster. So clusters of arbitrary shapes and structures can be described by several "centers" and the number of clusters is also determined automatically in this way.

3   Experiment and Analysis

In our experiment, a color image is used to test the proposed segmentation method. In both mean shift methods, we transform the RGB color space to the $L*u*v$ space, whose coordinates are related to the color values by nonlinear transformation [4]. All feature space computations are performed in the $L*u*v$ space measured by Euclidean distances. Note that all small regions less than 10 pixels are removed from the result images for the sake of visual effect.

The experiment uses part of the water lilies image to demonstrate the segmentation based on the adaptive mean shift clustering. Figure 1 shows the original image of water lilies. The main objects in the image are flowers, stems, and leaves. The background is composed of shadow and water.

Fig. 1. The water lilies image

Three methods: region growing, single scale mean shift and adaptive mean shift methods are performed on the experimental image individually. In the adaptive mean shift algorithm, the number of nearest neighbors K and the size of subset m were set to 10 and 1 percent of data size individually. This experiment well demonstrates the superiority of the adaptive mean shift algorithm over the other segmentation techniques. The results of segmentation are shown in figure 2.

As seen from the segmentation results, region-growing technique does not distinguish the image objects well. There are two segmented images by region growing method (figure2 (a) and (b)). The detailed segmentation result (figure2 (a)) cannot show the flowers in the straightforward way. The flowers are over-segmented, while the other objects are properly segmented. And in the coarse one, there are many sub-segmented objects such as the stem. Though the stem and leaves are un-segmented, the flowers are still shown in a complex way. The single scale mean shift also has the problem separating the flowers into many objects, like the region growing

method. Both of them cannot balance the over-segmented and sub-segmented regions in the image. However, the segmentation ability of the adaptive mean shift clustering is excellent. It has a powerful capability distinguishing objects in the image. The flowers are segmented clearly and simply, and the others are also appropriately separated as we can see from figure 2.

(a)   (b)   (c)   (d)
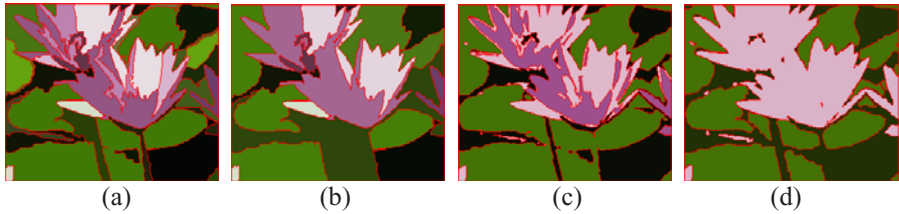
Fig. 2. The results of the image segmentation (a) region growing, detailed one, (b) region growing, coarse one, (c) single scale mean shift clustering, (d) the proposed method

4   Conclusions

In this paper, the goal of image segmentation is achieved by mean shift based clustering, a nonparametric clustering technique. Since earlier algorithms use single scale to the entire feature space, they have problems when the structures of clusters in the feature space are very different. The adaptive mean shift method is proposed by involving the local scale information. Clusters with various structures can be found in the procedure. It can be learned by the experiment that the proposed method has the advantage of segmentation quality over earlier methods.

References

1. Fukunaga, K, and Hostetler, LD. : The estimation of the gradient of a density function, with applications in pattern recognition. IEEE Trans Info Theory, 21(1975), 32-40
2. Comaniciu, D. and Meer, P.: Mean shift: A robust approach toward feature space analysis. IEEE Trans. on Pattern Analysis and Machine Intelligence, 24(2002), 603-619
3. Cheng, YZ. : Mean shift, mode seeking, and clustering. IEEE Trans. on Pattern Analysis and Machine Intelligence, 17(1995),790-799
4. Comaniciu, D. and Meer, P.: Robust analysis of feature spaces: Color image segmentation. In Proc. of the IEEE Conf. on Computer Vision and Pattern Recognition (CVPR), (1997) 750-755
5. Comaniciu, D. and Meer, P.:Mean shift analysis and applications. In Proc. of the IEEE Int'l Conf. on Computer Vision (ICCV), (1999)1197-1203
6. Comaniciu, D. and Meer, P.:, Distribution free decomposition of multivariate data. Pattern Analysis and Applications, 2(1999), 22-30
7. Comaniciu, D., Ramesh, and V., Meer, P.:The variable bandwidth mean shift and data-driven scale selection. In Proc. of the IEEE Int'l Conf. on Computer Vision (ICCV). (2001) 438-445

Similarity Measurement of XML Documents Based on Structure and Contents

Tae-Soon Kim[1], Ju-Hong Lee[1,*], Jae-Won Song[1], and Deok-Hwan Kim[2]

[1] Dept. of Computer Science & Information Engineering, Inha University, Incheon, Korea
[2] Dept. of Electronics Engineering, Inha University
{kts429, sjw}@datamining.inha.ac.kr,
{juhong, deokhwan}@inha.ac.kr

Abstract. Researches on the similarity measure between XML documents are being progressed in order to effectively control and retrieve various XML documents. Previous works mostly suggest similarity-measuring methods focusing only on the tag structure of XML documents. However, they have a problem of incorrectly calculating the semantic similarity of XML contents. In this paper, we propose a new similarity measurement method considering not only the structural information of tags in XML documents but also the semantic information of tags and text content information related with the tags. Our experiments demonstrate that our proposed method improves the accuracy of similarity, compared to the previous works.

1 Introduction

As the use of XML [2] is increased, many researches for calculating and controlling the similarity between XML documents are being actively progressed in order for efficient document organization, navigation and retrieval of a large amount of documents [1,5,6,9,12].

Lian et al. [5] summarized XML documents into an S-graph which reflects structural information. It is used to measure the similarity using only the tag structural information of XML documents. Patrick et al. [9] proposed a measure on the structural similarity among XML documents and DTDs, which is natural to understand and fast to calculate. Bergamashi et al. [1] proposed a method of calculating the similarity between DTDs or schemas of XML documents. These previous works presented the similarity measure using only the structural information of tags. Our preliminary work [3] proposed the vector model to reflect the structural information and semantic information of tags in XML documents.

In this paper, in order to increase the accuracy of semantic similarity between XML documents, we suggest the enhanced similarity measurement method using vector model which considers not only the structural information of tags but also the semantic information of tags and the text content information of XML documents

---

* Corresponding author.

since the semantic information of XML documents are included in tag structure and text content within tags.

This paper is organized as follows: Chapter 2 describes the vector model combining path term and content term and presents a new similarity measure for XML documents. Chapter 3 shows various experiments and result analysis. Finally, Chapter 4 concludes this work.

2 Vector Model for Similarity Between XML Documents

Our preliminary work proposed the vector model which considers the tag path as a term to reflect the structural information and semantic information of tags in XML documents simultaneously [3]. But, text contents of an XML document, differently from a general document, is included in a tag. Since the words in the text with the same frequency may have different importances depending on the tag in which they are, the weight of the word in the text must be reflected appropriately according to the importance of the related tags. As an example, in the XML document including some research paper, some tags such as title and abstract have relatively a few words, but the importance of the words within this tags are high. Some tags such as Introduction may have more words than others, but the importances of their words are relatively lower than those of words within *title* and *abstract* tags.

We call the text words within tags as ***content terms***. *CTW* (Content Term Weight) is a weight value of a content term in a XML document. The *CTW* is the product of *CTWF* (Content Term Weighted Frequency) and *CTIDF* (Content Term Inverse Document Frequency). CTW_{ij} of jth content term in i^{th} document is shown in equation (1).

$$CTW_{ij} = CTWF_{ij} \times CTIDF_j \tag{1}$$

$CTWF_{ij}$ is shown in equation (2).

$$CTWF_{ij} = \sum_{k=1}^{n} \left(cfreq_{ikj} \times \left(1 + \log \left(\frac{\#content\ term\ in\ i^{th} document}{\#content\ term\ in\ k^{th}\ tag} \right) \right) \right) \tag{2}$$

Where k is the index of tags in a document and $cfreq_{ikj}$ is the frequency of jth content term included in k^{th} tag of ith document. (1+log(#content term in i^{th} document / #content term in k^{th} tag)) is the formula to calculate the tag importance based on the number of included words. Note that the log function is used to lower the differences of values.

$CTIDF_j$ is shown in equation (3)

$$CTIDF_j = \log \frac{N}{DF_j} \tag{3}$$

Where N is the total number of documents, and DF_j is the number of documents in which the jth content term appears.

The similarity using *CTW* is called ***content term similarity(CTS).*** In vector model, the similarity measure between document d_i and document d_j can be quantified as the cosine value of adjacent angle between two vectors as shown in equation (4).

$$CTS(d_i, d_j) = \frac{D_i \cdot D_j}{|D_i| \times |D_j|} = \frac{\sum_{k=1}^{t} CTW_{ki} \times CTW_{kj}}{\sqrt{\sum_{k=1}^{t} CTW_{ki}^2} \times \sqrt{\sum_{k=1}^{t} CTW_{kj}^2}} \tag{4}$$

where t refers to the number of total terms within d_i and d_j, $D_i = (CTW_{1i}, CTW_{2i}, \ldots CTW_{ti})$, and $D_j = (CTW_{1j}, CTW_{2j}, \ldots CTW_{tj})$, respectively [10].

The similarity measure of the general vector model considers text content only. In the case of the XML document, however, we should consider the importance of tags to measure the similarity between XML documents. The overall similarity between XML documents is calculated as the weighted sum of path term similarity (*PTS*) and content term similarity (*CTS*) shown in equation (5). Here, the weights of *PTS* and the weights of *CTS* are represented as *pw* and *cw*, respectively.

$$\begin{cases} sim(d_1, d_2) = pw \times PTS(d_1, d_2) + cw \times CTS(d_1, d_2) \\ pw + cw = 1 \end{cases} \tag{5}$$

3 Test and Evaluation

In experiments, we used 1200 XML documents taken from SIGMOD [11], O'REILLY [8], and NIAGARA [7]. We applied the K-means algorithm using the similarity of general vector model, the similarity of S-graph based method, and the similarity of the proposed method. Table. 1 illustrates their purity values [4]. The experimental results demonstrate that the proposed method yields more accurate performance than S-graph based method and the general vector model.

Table 1. Performance comparison of various methods in terms of purity

	similarity of general vector model	S-graph	Proposed method
SIGMOD	0.4728	0.5055	0.6678
NIAGARA	0.5385	0.8154	0.8912
O'REILLY	0.4682	0.7533	0.8723

4 Conclusion

The previous methods are mostly based on graph since they considered only structural information of tags in XML documents. In order to measure more accurate semantic similarity, the semantic information of tags, and the text content information must be included in the similarity measure as well as the structural information of tags. In this paper, therefore, we introduce a new effective semantic similarity measure between

XML documents, which uses the vector model in order to reflect three kinds of information in the similarity measure simultaneously. This method undoubtedly can measure more accurate semantic similarity between XML documents because almost all information about semantic meaning of XML documents is reflected in the similarity measure.

Acknowledgement

References

1. Bergamashi, S., Castano, S.: Semantic Integration of Semistructured and Structured Data Sources. SIGMOD Record **28** (1999) pp. 54-59.
2. Brau, B., Bray, J.: Extensible Markup Language (XML) 1.0. W3C Recommendation, http://www.w3.org/Tr/Rec-xml
3. Kim, T.S., Lee, J.H.: Semantic Structural Similarity for Clustering XML documents. Inha University Technical Report (2006), http://webbase.inha.ac.kr/TechnicalReport/tech_04.pdf
4. Li, T., Ma, S.: Document Clustering via Adaptive Subspace Iteration. the 27th annual international ACM SIGIR conference on Research and development in information retrieval, Sheffield, United Kingdom (2004) pp. 218-225.
5. Lian, W. , Wai-lok, D.: An Efficient and Scalable Algorithm for Clustering XML Documents by Structure. IEEE Transactions on Knowledge and Data Engineering 16 (2004) pp. 82-96.
6. Marcos, C., Lozano, S.: A DTD for an XML-Based Mathematical Modeling Language. Lecture Notes in Computer Science, Springer-Verlag, Berlin Heidelberg **2660** (2003) pp. 968-977.
7. NIAGARA Experimental Data, http://www.cs.wisc.edu/niagara/data.html
8. O'REILLY XML Data, http://www.xml.com/pub/rg/Example_Files
9. Patrick, K.L., Ng, Vincent T.: Structural Similarity between XML Documents and DTDs. Lecture Notes in Computer Science, Springer-Verlag, Berlin Heidelberg **2659** (2003) pp. 412-241.
10. Salton, G., Buckley, C.: Term-weighting approaches in automatic text retrieval. Information processing and Management: an International journal **24** (1988) pp.513-524
11. SIGMOD Record data, http://www.acm.org/sigs/sigmod/record/xml
12. Young, K.N., Joseph G., Guilian W.: A Metadata Tool for Retrieval from Heterogeneous Distributed XML Documents. Lecture Notes in Computer Science, Springer-Verlag, Berlin Heidelberg **2660** (2003) pp. 1020-1029.

A Combined Web Mining Model and Its Application in Crisis Management

Xingsen Li[1,*], Lingling Zhang[1, 2], Maoliang Ding[4], Yong Shi[2, 3], and Jun Li[1]

[1] School of Management, Graduate University of the Chinese Academy of Sciences, Beijing, 100080
lixingsen@126.com
[2] The CAS Research Center on Data Technology & Knowledge Economy；Beijing, 100080
yshi@gucas.ac.cn, zll933@163.com
[3] Graduate University of the Chinese Academy of Sciences, Beijing, 100080
[4] Information center, Shandong Jinjing Group, Zibo, 255200
Jamesdingcn@msn.com

Abstract. Crisis management is an increasingly important activity of management. Organizations' critical crises can induce severe consequences or even disasters if wrong decisions are made. The World Wide Web provides an unprecedented freedom for the public to discuss one's opinions which impact much on the progress of the crisis. Based on the study of web mining and its relative techniques, a combined web mining model was presented. It consists of web mining, text mining, data mining and human experience knowledge. All knowledge from each part was saved in database through a knowledge management platform. Its application shows that utilizing the combined model for crisis management can improve the quality of decisions.

Keywords: Web Mining Model, Crisis Management, Data Mining, Knowledge Management.

1 Introduction

The World Wide Web has become a huge data source. Billions of pages are publicly available and it is still growing. The web provides an unprecedented freedom to discuss public issues, crisis events and politics etc. The general publics enjoy the right to speak on BBS, message board, self-owned sites and blogs. One can also take part in interactive actions online and even voting. Web Mining, that can discover knowledge from huge amounts of web pages, has become an urgent research area in computer science [1]. Crisis management is a relatively new field of management. Its activities include forecasting potential crises and planning how to deal with them, such as recover any damage to public image. Crisis management has many directions. Most research has relied heavily on case study methods yet often with rhetorical or even inconsistent suggestions [2]. The interactive features of the Web make crisis

---

* Corresponding author.

management become more complex, but also provide a great convenience to guide or steer public opinions for the management of crisis. Our goal in this paper is to present a novel application model combined with web mining, data mining and human experience knowledge sharing, and introduce its process in crisis management.

2   Framework of the Combined Web Mining Model

Web mining is powerful, but it also needs to combine with other technologies and management rules to enhance the business. Figure 1 shows a framework of combined web mining model:
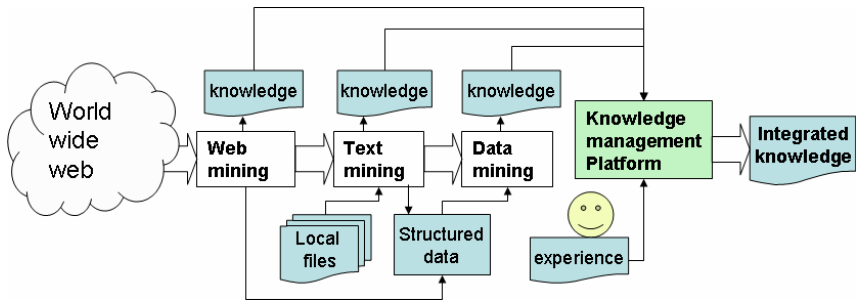
Fig. 1. Framework of the combined web mining model

Web mining extracts knowledge from web data, i.e. web content, web structure, and web usage data [1]. Web content mining is the process of extracting useful information from the contents of web documents. Web mining involves two main steps: Extracting the pages relevant to a query and ranking them according to their quality. Text mining deals with text documents in general, such as emails, letters, reports, and articles, that exist in both intranet and internet environment. Text mining is concerned with the analysis of very large document collections and the extraction of hidden knowledge include topic discovery and tracking, extracting association patterns or abstract, clustering of web documents and classification from text-based data.

Data mining has been used in many fields [3, 4]. During the process of web mining and text mining, statistic data such as visit-times, last-visit-date, browser numbers, weights, number of total words can be collected from mining software or by special software tools, these data sets are acted as training sets for data mining. We define two classes for this dataset using a label variable: The pages should be pay attention to (label = 1) and not (label = 0). After the classification model has been trained, the effect of new pages can be predicted by scoring in earlier time.

Finally, knowledge management is necessary for collecting experts' experience and compared with knowledge from data mining. Its working process is similar with the process presented in paper [5].

3   Working Process for the Aftermath of Crisis

In handling the aftermath of the crisis, the most important thing to do is to change the passive situation. Most organizations make decisions rely on experience of skilled persons [2]. How to guide managers to invoke corresponding reactions? We get the answers in a proper methodology based on web mining. The process has 7 main steps:
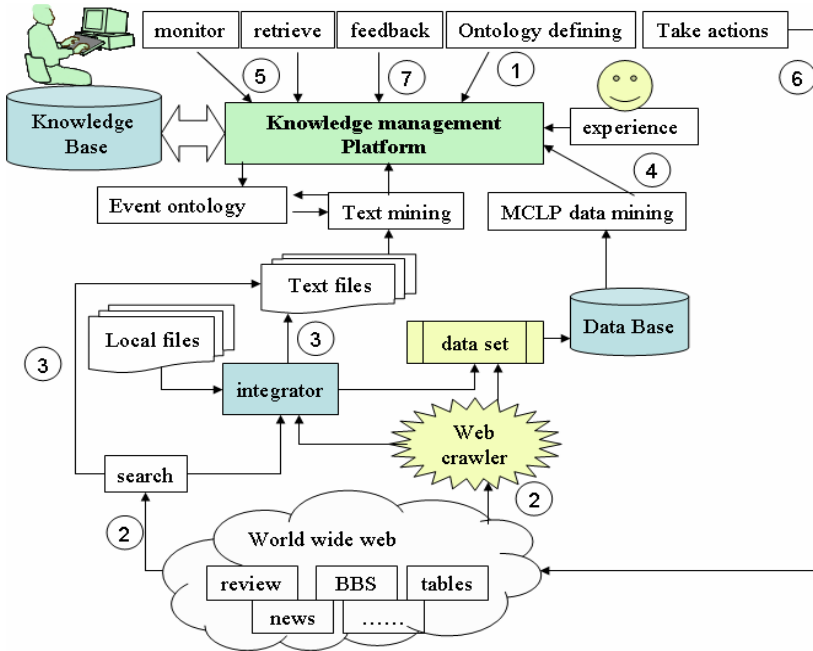
Fig. 2. The work process of the combined model

Step 1.   Define event ontology. Similar with the Personal Ontology concept [6] and the construction of ontology by mining the Semantic Web data [7], we put forward user defined event ontology in the dynamic environment.

Step 2.   Searching the web. Search information on the web manually or by web crawler tools. Useful pages and its web address are collected to software called integrator. Web crawler counts the information by statistic and transforms it into structured data set then stores into data base.

Step 3.   Files integration. Transfer web pages been searched into text or XML files and integrate some local files together by integrator. Noise on web pages should be cleaned before applying mining tasks to these files.

Step 4.   Mining. By web mining and text mining, we can discover interesting topics, extracting association patterns or abstract, clustering of web documents and classification. By data mining, we can get scoring knowledge and know which pages should pay more attention to and decide when to take actions combined with experience.

Step 5. Monitoring. Identifying communities of users and information sources [1] on the web. The communities play a more important role and can even identifying malicious competitions. Monitor all useful pages from mining and the new comments. OLAP or other visualization tolls can be used here to monitor efficiently, and redo step 2 to step 4 if necessary.

Step 6. Take actions. Since people are easily affected by the group consciousness. Proper actions can change the passive situation similarly, such as publish the true facts and guide browsers to see the positive side on the key websites, say the right words to invoke good corresponding reactions, advertisement on TV on the right time, communicating with customers or press conference, etc.

Step 7. Feeding back. After the actions been taken, the effect can be found by re-mining. At the same time, the experts' opinions can also be saved as text files or store in the knowledge base. This can make the future crisis management wiser and wiser.

This model had been implemented in a famous bedding company (Shumian) in Beijing, China. Its application shows that the model has a good effect.

4   Conclusions

We proposed a combined model based on web mining and described its working process. This approach gives a new tool to manage crisis problem and can also be applied to other fields, such as strategy, society security, web fraud, and advertisement etc. There are several issues need to be researched deeply, such as how to collect related pages efficiently by web crawler, how to mark the label of data set more precisely, how to mining other un-structured data. We also notice that the speed of the whole process should be increased and the Event Ontology needs to be updated by web mining results in the future study.

References

1. Srivastava, J., Desikan, P., Kumar, V.: Web Mining- Concepts, Applications and Research Directions, In Data Mining: Next Generation Challenges and Future Directions. AAAI/MIT Press, Boston, MA (2003)
2. Lin, Z.: Organizational Performance Under Critical Situations—Exploring the Role of Computer Modeling in Crisis Case Analyses, Computational & Mathematical Organization Theory, Springer Netherlands, Vol. 6, No. 3, (2000) 277–310
3. Kou, G., Y. Peng, etc.: Discovering Credit Cardholders' Behavior by Multiple Criteria Linear Programming, Annals of Operations Research Vol.135, (2005) 261–274

4. Kou, G., Peng, Y., Shi, Y., etc.: Network Intrusion Detection by Using Multiple-Criteria Linear Programming, Proceedings of 2004 International Conference on Service Systems and Service Management, Beijing, China (2004)
5. Li, X.S., Shi, Y., etc.: A Knowledge Management Platform for Optimization-based Data Mining，Sixth IEEE International Conference on Data Mining, Hong Kong, China, Dec. 18-22, (2006)
6. Nakayama, K., Hara, T., Nishio, S.: A Web Mining Method Based on Personal Ontology for Semi-structured RDF, Web information systems engineering. International workshop, New York NY, Vol. 3807, (2005) 227–234
7. Maedche, A., Staab, S.: Ontology Learning for the Semantic Web, IEEE Intelligent Systems, Vol. 16, No. 2, (2001) 72–79

A GM-Based Profitable Duration Prediction Model for Chinese Crude Oil Main Production District

Jinlou Zhao, Yuzhen Han, and Lixia Ke

Harbin Engineering University, Heilongjiang, China, 150001
zhaojinlou@sina.com

Abstract. In this paper, a grey model (GM) based profitable duration forecasting approach is proposed for Chinese crude oil main production district. In this methodology, the forecasting functions on electricity expenditure and crude oil sales revenue are first built via GM. Based on these two forecasting functions, the profitable duration of crude oil production under the restriction of the coefficient of limit electricity cost is then worked out. Finally, some ways to prolong the profitable duration are put forward in order to offer some valuable suggestions for the transformation of resource-based cities.

Keywords: GM, profitable duration, crude oil, china, forecasting.

1 Introduction

Besides the ocean oil-fields, there are 19 land oil-fields in China. Among them, the annual crude oil output of Daqing Oil Field occupies 1/4 of the Chinese land oil-fields' output, which make Daqing a 'weatherglass' of Chinese crude oil market. Therefore, the Daqing Oil Field is one of the main crude oil production districts in China.

As is known to us, crude oil is a non-renewable resource. Although Daqing Oil Field Company actively explore outer petroleum resources, the crude oil output in Daqing Oil Field decreases year by year with the continuous exploitation of crude oil. Along with the exploitation, the moisture content of crude oil increases continuously. It results in that the main variable costs of oil exploitation — electricity consumption increases continuously, and thus leading to the increase of unit electricity consumption cost for crude oil production. In such situations, some ideas are presented. For example, if crude oil output decreases year by year, but electricity consumption increases year by year, then there must be a certain year that the crude oil sales revenue cannot afford to electricity expenditure in the Chinese crude oil main production district. Therefore this time point is extremely important for the sustainable development of resource-based cities. As earlier noted, beyond this time point, the crude oil output of crude oil main production districts will be no meaningful because the oil output after this time point will not bring any profits.

As we know, the Chinese crude oil main production districts such as Daqing and Yumen are the common resource-based cities. In order to keep the sustainable development of these resource-based cities, it is necessary to forecast the profitable duration. With this profitable duration, we can provide time basis for the

resource-based cities' transformation and development strategies, which is the main motivation of this study.

The rest of this study is organized as follows. The next section describes the basic principle of calculating the profitable duration method. In Section 3, a practical example is given to present the computing process of the proposed methodology. Finally, some important ways to prolong the profitable duration and some valuable suggestions to the transformation-oriented resource-based cities are presented in Section 4.

2   Basic Principle for Profitable Duration Computation

Usually, the profitable duration of a main crude oil production district is defined as a time period that the crude oil sales revenues are larger than the electricity consumption expenditure for a certain crude oil production district. From this definition, our goal is to calculate the duration. For this purpose, we apply the limit electricity cost coefficient to arrive at this goal.

Generally, the limit electricity cost coefficient can be represented by

$$\frac{\text{Electricity expenditure}}{\text{Crude oil sales revenue}} = \text{Coefficient of limit electricity cost} \tag{1}$$

In the Equation (1), crude oil sales revenue and electricity expenditure are the future values and thus both oil sales revenue and electricity consumption expenditure are the function of time t. As Section 1 implied, the two functions are monotonic functions. Therefore, the time curves of the two functions may be intersected, the intersecting time is the non-profit time point. The time period covered from current to non-profit time point is the profitable duration. So far, our main task is to predict the non-profit time point.

From the above analysis, the key to the profitable duration is how to construct the crude oil sales revenue function and electricity consumption expenditure function regarding the time t. For this, we applied to grey model proposed by Deng [1] to construct the above two functions. For grey model, interested readers can refer to Deng [1] for more details.

The generic idea of calculating the profitable duration for crude oil main production district is composed of the following steps.

Step I: using grey forecasting model GM (1, 1) to obtain time function of annual crude oil output x and annual electricity consumption y : $x^{(0)}(k+1)$ and $y^{(0)}(k+1)$.

Step II: according to the statistical data, average oil unit price γ , unit industry electricity price β , and estimated value of limit electricity cost coefficient λ , are obtained.

Step III: Using the previous two monotonic functions $x^{(0)}(k+1)$ and $y^{(0)}(k+1)$ and some related parameters provided by Step II, electricity consumption expenditure

function can be represented by $\beta \times y^{(0)}(k+1)$ and the crude oil sales revenue function can be expressed as $\gamma \times x^{(0)}(k+1)$.

Step IV: In terms of Equation (1) and limit electricity cost coefficient λ, we can construct the following equation $\lambda \times \gamma \times x^{(0)}(k+1) = \beta \times y^{(0)}(k+1)$ to obtain the non-profit time point. Thus the profitable duration can be obtained.

For testing the effectiveness of the proposed procedure, we use Daqing Oil Field as a typical example to predict the profitable duration in the following section.

3 An Illustrative Example

In order to illustrate the above computational principle, we select Daqing Oil Field as a typical example to interpret the process of the calculating the profitable duration. Because Daqing Oil Field is the largest oil field of China and a main crude oil production district, selecting it as a representative is rather realistic. According to the current situation, we only collect the following data from Daqing Oil Field Co.Ltd [2], as shown in Table 1.

Table 1. The annual crude output and annual industry electricity consumption of Daqing Oil Field Co. Ltd. (2000-2005)

Year / Items	2000	2001	2002	2003	2004	2005
Annual crude output (ten thousand ton)	5,535	5,302	5,120	4,930	4,750	4,589
Annual electricity consumption (ten thousand KWh)	389,542	390,133	422,042	429,878	433,996	436,328

Due to the fact that the data are not enough and the existing data show monotonicity, the traditional statistical models are not used. To overcome the data shortage, this paper uses grey forecasting model GM(1,1), to fit forecast functions of annual crude output and annual electricity consumption respectively.

3.1 Annual Crude Oil Output Forecasting

According to the GM, the forecast differential equation of the annual crude oil output can be represented as:

$$\frac{dx^{(1)}}{dt} + ax^{(1)} = b \tag{2}$$

According to integral principle, Equation (2) can be transformed into the following form:

$$x^{(1)}(k+1) = (x^{(0)}(1) - \frac{b}{a})e^{-ak} + \frac{b}{a} \qquad (k = 1, 2 \cdots, n) \tag{3}$$

In term of least squares method, the coefficients of the Equation (3) are obtained:

$$a = 0.04583 \text{ , } b = 5613.26 \text{ , } x^{(0)}(1) = 5535$$

Thus the forecast equations of annual crude oil output can be expressed as:

$$x^{(1)}(k+1) = -116939e^{-0.04583k} + 122480 \tag{4}$$

$$x^{(0)}(k+1) = x^{(1)}(k+1) - x^{(1)}(k) \ (k = 1, 2\cdots, n) \tag{5}$$

Combining (4) and (5) , the final forecasting equation can be given as:

$$x^{(0)}(k+1) = -116939(e^{-0.04583k} - e^{-0.04583(k-1)}) \ (k = 1, 2\cdots, n) \tag{6}$$

After inspection, the mean relative error and the simulated relative error are as:

$$\bar{\Delta} = \frac{1}{6}\sum_{k=1}^{6}\Delta_k = 0.000581 = 0.0581\% < 0.01$$

$$\Delta_6 = 0.00087 = 0.087\% < 0.01$$

Therefore, the precision is realistic, and Equation (6) can be used to annual crude oil output prediction.

3.2 Annual Electricity Consumption Forecasting

Similar to Section 3.1, the Forecast differential equation of annual electricity consumption can be written as:

$$\frac{dy^{(1)}}{dt} + py^{(1)} = q \tag{7}$$

Through integral computation, the Equation (7) can be represented by:

$$y^{(1)}(k+1) = (y^{(0)}(1) - \frac{q}{p})e^{-pk} + \frac{q}{p} \quad (k = 1, 2\cdots, n) \tag{8}$$

Similarly, we can calculate the parameter values using least squares method:

$$p = -0.024330 \text{ , } q = 387808 \text{ , } y^{(0)}(1) = 389542$$

Using the parameter value, Equation (8) can be written as:

$$y^{(1)}(k+1) = 16329041e^{0.24330k} - 15939499 \tag{9}$$

$$y^{(0)}(k+1) = y^{(1)}(k+1) - y^{(1)}(k) \quad (k = 1, 2\cdots, n) \tag{10}$$

Integrating (9) and (10), we have the following form:

$$y^{(0)}(k+1) = 16329041(e^{0.24330k} - e^{0.24330(k-1)}) \quad (k = 1, 2 \cdots, n) \qquad (11)$$

After inspection, the mean relative error and the simulated relative error are as:

$$\bar{\Delta} = \frac{1}{6}\sum_{k=1}^{6}\Delta_k = 0.015232 = 1.15232\% < 0.05$$

$$\Delta_6 = 0.015899 = 1.5899\% < 0.05$$

Therefore, the precision is also realistic, and formula (11) can be used for annual electricity consumption prediction.

3.3 Presentation of the Average Industry Electricity Price, Average Oil Price and the Limit Electricity Cost Coefficient

Because the purpose of this paper is to forecast the profitable duration of the crude oil main production district in China, we directly give the average industry electricity price estimate function and average oil price estimate function according to the data provided by the Daqing Oil Field Co. Ltd [2] and Heilongjiang Electric Power Co., Ltd [3]:

$$\beta = 0.52 \times 1.046^k \quad (\text{RMB / KWh})$$

$$\gamma = 562.137 \times 0.09334^k \quad (\text{RMB /ton}) \quad (k = 1, 2 \cdots, n)$$

After consulting with financial staff in Daqing Oil-Field Company, maximum estimate value of limit electricity cost coefficient that electricity expenditure occupies the crude oil sales revenue: $\lambda = 1/3$ is offered.

3.4 Computation of Profitable Duration

From Section 2, the forecasting functions of the electricity consumption cost and crude oil sales revenue can be expressed by

$$E^{(0)}(k+1) = \beta \times y^{(0)}(k+1) \qquad (12)$$

$$Q^{(0)}(k+1) = \gamma \times x^{(0)}(k+1) \qquad (13)$$

According to Equation (1), one has

$$\lambda \times Q^{(0)}(k+1) = E^{(0)}(k+1) \qquad (14)$$

According to the previous work, we have the following form:

$$-116939(e^{-0.04583k} - e^{-0.04583(k-1)}) \times 562.137 \times 0.09334^k \times 1/3$$

$$= 0.52 \times 1.046^k \times 16329041 (e^{0.024330k} - e^{0.024330(k-1)}) \quad (k = 1, 2 \cdots, n) \qquad (15)$$
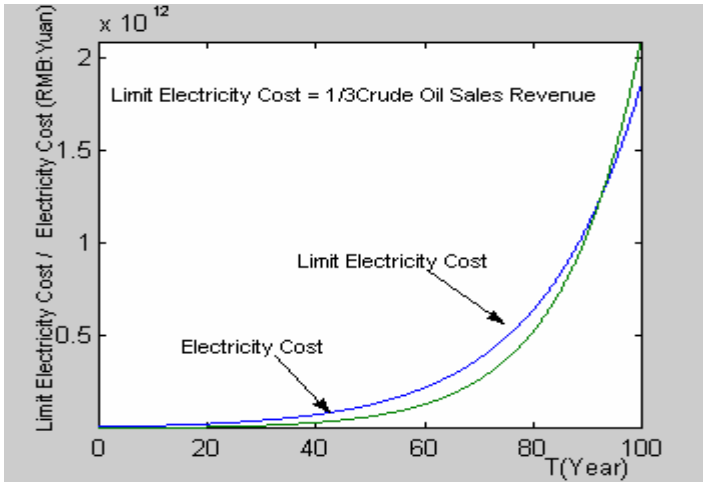
Fig. 1. The time changing of limit electricity cost and electricity cost of the crude oil main production district in China

Equation (15) can be solved by Matlab 6.5, the illustration of the two curves can be shown in Fig. 1.

From Matlab computation and Fig. 1, we can obtain that the intersecting point is $k \approx 93$. The forecast result shows that the profitable duration of Daqing Oil Field, one crude oil main production district in China, is about 93 years since 2000 if no actions are taken.

4   Concluding Remarks

In this study, we utilize GM-based model to predict the profitable duration of Chinese crude oil main production district and obtained a good result. As we know, the crude oil main production district in China takes oil industry as its leading industry. If the oil industry continues developing with the existing crude oil output and electricity consumption mode, it will be non-profitable for the crude oil output after hundreds of years, and thus it will also seriously influence and restrict the existence and development of resource-based cities. According to Equation (1), the key to prolong profitable duration is to increase crude oil output, reduce electricity consumption and decrease limit electricity cost coefficient. Through these ways, it can provide more transformation time for resource-based cities.

References

1. Deng J.L. Grey System. National Defence Industry Press. 2 (1985) 23-25.
2. Finance department of Daqing oil-field Co., Ltd. The "tenth five-year plan" financial reports of Daqing oil-field Co., Ltd. (confidential document). January 2006.
3. Heilongjiang Electric Power Co., Ltd. The electricity price form of Heilongjiang electric network 2006. September 2006.

A Hybrid ARCH-M and BP Neural Network Model For GSCI Futures Price Forecasting

Wen Bo[1], Wang Shouyang[1], and K.K. Lai[2]

[1] Institute of System Science, Academy of Mathematics and System Sciences Chinese Academy of Sciences, BeiJing, China
`wenbo@amss.ac.cn, sywang@amss.ac.cn`
[2] Department of Management Sciences, City University of Hong Kong
Tat Chee Avenue, Kowloon, Hong Kong
`mskklai@cityu.edu.cn`

Abstract. As a versatile investment tool in energy markets for speculators and hedgers, the Goldman Sachs Commodity Index (GSCI) futures are quite well known. Therefore, this paper proposes a hybrid model incorporating ARCH family models and ANN model to forecast GSCI futures price. Empirical results show that the hybrid ARCH(1)-M-ANN model is superior to ARIMA, ARCH(1)，GARCH(1,1), EGARCH(1,1) and ARIMA-ANN models on the RMSE, MAPE, Theil IC evaluation criteria.

Keywords: ARCH-M, ANN, GSCI, Commodity Index, Forecasting.

1 Introduction

Commodity index futures are a versatile tool for taking different forms of exposure to energy commodity markets. They provide investors with an instrument for taking leveraged exposure [1]. There are three famous commodity indices in energy markets which can serve as a surrogate for direct investment: Commodity Research Bureau (CRB) Index, Dow Jones-AIG (DJ-AIG) Commodity Index and Goldman Sachs Commodity Index (GSCI).

CRB index, which began trading on the New York Futures Exchange in 1986, is the oldest. DJ-AIG commodity index, which started in 1999, is rebalanced annually. It reduces return by about 1.5%, compared to monthly rebalancing [2]. GSCI, which started in July 1992 on the Chicago Mercantile Exchange, is a broad-based and production-weighted commodity index. Its volumes have generally exceeded those of CRB index. Lummer and Siegel (1993), who explored GSCI collateralized futures as an asset found that a collateralized position in GSCI futures is a good diversification for stocks and bonds. Paul D.Kaplan and Scott L.Lummer (1997) showed that GSCI collateralized futures were especially valuable to investors who seek diversification and protection against poor returns in other asset classes.

Therefore, we make a research effort covering the GSCI futures, especially the futures price forecasting. In the forecasting field, many researchers have created many successful models, such as ARIMA, ARCH etc... Recently, more hybrid forecasting

models have been developed that integrate time series model with artificial neural network model to improve prediction accuracy. Lean Yu and Shouyang Wang (2005) obtained a novel nonlinear ensemble forecasting model incorporating GLAR and ANN for foreign exchange rates. G.Peter Zhang (2003) also designed a time series forecasting model using a hybrid ARIMA and a neural networks model. In his paper, he argued that a hybrid methodology can take advantage of the unique strength of ARIMA and ANN models in linear and nonlinear modeling. So this paper proposes a hybrid model incorporating ARCH and ANN model to forecast GSCI futures price.

The rest of the paper is organized as follows. The next section presents a description of the GSCI. The hybrid model is introduced in detail in Section 3. A preliminary analysis and empirical results from the GSCI futures price data sets are reported in Section 4. Conclusions are obtained in Section 5.

2   Description of the GSCI

The GSCI is a world production-weighted commodity index comprising of liquid, exchange-traded futures contracts on energy products. It is designed to provide investors with a reliable benchmark for investment performance in energy commodity markets in a manner comparable to the S&P 500 Index for the stock markets.

The GSCI is world-production weighted; the quantity of each commodity in the index is determined by the average production in the last five years of available data. Such weighting provides the GSCI with significant advantages, both as an economic indicator and as a measure of investment performance. Currently, the GSCI contains 24 commodities from different commodity sectors: six energy products, five industrial metals, eight agricultural products, three livestock products and two precious metals. Table 1 displays a list of the 24 commodities with their dollar weights in the GSCI.

Table 1. GSCI Dollar Weights (%)

Commodity	Dollar Weights	Commodity	Dollar Weights	Commodity	Dollar Weight
Energy	**72.99**	**Industrial Metals**	**9.87**	**Agriculture**	**10.62**
Crude Oil	30.72	Aluminum	3.3	Wheat (CBOT)	2.52
Brent Crude oil	14.57	Copper	4.31	Wheat (KCBT)	1.05
Unleaded Gas	8.24	Lead	0.28	Corn	2.28
Heating Oil	8.21	Nickel	0.88	Soybeans	1.36
Gas Oil	4.5	Zinc	1.1	Cotton	0.77
Natural Gas	6.75	**Livestock**	**4.18**	Sugar	1.84
Precious Metals	**2.34**	Live Cattle	2.08	Coffee	0.62
Gold	2.07	Feeder Cattle	0.62	Cocoa	0.18
Silver	0.27	Lean Hogs	1.48		

Source: CME Equity Products: GSCI Components and Weights, 19 May 2006.

The GSCI futures are listed for all 12 calendar months. The contract value of each GSCI futures position is \$250 times the GSCI index. The minimum price fluctuation is 0.05 index points, equivalent to a value of \$12.5 per point. The last trading day of the GSCI futures is the eleventh business day of the contract month, and the position limits is 10,000 net long or short in all contract months combined. The final settlement price shall be the closing price of the GSCI futures price index on the eleventh business day of the contract month.

3   A Hybrid ARCH-M and BP Neural Network Model

3.1   ARCH Family Models

Following the introduction of autoregressive conditional heteroskedasticity (ARCH) model by Engle (1982), there are many extensions of ARCH model, such as GARCH, GARCH-M, EGACH etc.; we can call them ARCH family models. ARCH model can be expressed as follows

$$y_t = x_t' \beta + \varepsilon_t \tag{1}$$

$$\varepsilon_t = \sqrt{h_t} \cdot v_t \tag{2}$$

$$h_t = \alpha_0 + \alpha_1 \varepsilon_{t-1}^2 + \cdots + \alpha_q \varepsilon_{t-q}^2 \tag{3}$$

Where v_t i.i.d. , $E(v_t) = 0, D(v_t) = 1$ $\alpha_0 > 0, \alpha_i \geq 0$ $\sum_{i=1}^{q} \alpha_i < 1$

This model is also known as the linear ARCH(q) model. With financial data it captures the information from ε_t . Bollerslev(1986) proposed an alternative model, the GARCH(p,q) model. In his model, h_t was expressed as following:

$$h_t = \alpha_0 + \alpha_1 \varepsilon_{t-1}^2 + \cdots + \alpha_q \varepsilon_{t-q}^2 + \theta_1 h_{t-1} + \cdots + \theta_p h_{t-p} \tag{4}$$

Where v_t i.i.d. , $E(v_t) = 0, D(v_t) = 1$ $\alpha_0 > 0, \alpha_i \geq 0$ $\sum_{i=1}^{q} \alpha_i + \sum_{j=1}^{p} \theta_j < 1$

The ARCH-M model was introduced by Engle, Lilien, and Robins(1987). Since many theories in finance involve an explicit tradeoff between the risk and the expected return, this model is ideally suited to handling such questions in a time series context where the conditional variance may be time-varying. The model is given by

$$y_t = x_t' \beta + \gamma h_t + \varepsilon_t \tag{5}$$

$$h_t = \alpha_0 + \alpha_1 \varepsilon_{t-1}^2 + \cdots + \alpha_q \varepsilon_{t-q}^2 \tag{6}$$

Where v_t i.i.d. , $E(v_t) = 0, D(v_t) = 1$ $\alpha_0 > 0, \alpha_i \geq 0$ $\sum_{i=1}^{q} \alpha_i < 1$

Certainly, the ARCH-M model can also become the GARCH-M model if h_t fulfill the equation:

$$h_t = \alpha_0 + \sum_{i=1}^{q} \alpha_i \varepsilon_{t-i}^2 + \sum_{j=1}^{p} \theta_j h_{t-j} \tag{7}$$

People found the applications of the GARCH model limited since the conditional variance is only linked to past conditional variances. Then the EGARCH model was developed by Nelson (1991). In this class of ARCH models, the volatility depended not only on the magnitude of the past surprises in returns but also on their corresponding signs. EGARCH model is given as follows

$$\ln(h_t) = \alpha_0 + \sum_{j=1}^{p} \theta_j \ln(h_{t-j}) + \sum_{i=1}^{q} \alpha_i g(v_{t-i}) \tag{8}$$

$$g(v_t) = \varphi_i v_t + \left| \frac{\varepsilon_t}{\sqrt{h_t}} \right| - E \left| \frac{\varepsilon_t}{\sqrt{h_t}} \right| \tag{9}$$

To sum up, we can find that the ARCH family models focus on building the different models to dispose the variance ε_t in order to obtain more information from the time series data.

3.2   BP Neural Network Model

A neural network model takes an input vector X and produces output vector Y. The relationship between X and Y is determined by the network architecture. The neural network generally consists of at least three layers: one input layer, one output layer, and one or more hidden layers. It is widely accepted that a three-layer back propagation neural network with an identity transfer function in the output unit and logistic functions in the middle-layer units can approximate well any continuous function arbitrarily, given a sufficient amount of middle-layer units [3].

As Tam and Kiang (1992) reported, the back-propagation algorithm consists of two phases. Suppose we have s samples. Each is described by

$$x_i = (x_{i1}, x_{i2}, \cdots, x_{im}) \tag{10}$$

$$T_i = (t_{i1}, t_{i2}, \cdots, t_{in}) \tag{11}$$

Where X_i is an input vector, T_i is a target output vector and $1 \leq i \leq s$.

In the first phase (forward-propagation), X_i is fed into the input layer, and an output $Y_i = (y_{i1}, y_{i2}, \ldots, y_{in})$ is generated based on the current weight vector W. The objective is to minimize an error function E, which is defined as

$$E = \sum_{i=1}^{s} \sum_{j=1}^{n} \frac{(y_{ij} - t_{ij})^2}{2} \tag{12}$$

In the second phase (back-propagation), a gradient descent in the weight space, W, is performed to locate the optimal solution. The direction and magnitude change Δw_{ij} can be computed as

$$\Delta w_{ij} = -\frac{\partial E}{\partial w_{ij}} \varepsilon \tag{13}$$

Where $0 < \varepsilon < 1$ is a parameter controlling the algorithm's convergence rate.

3.3 A Hybrid Model

Since it is difficult to completely know the characteristics of the data in a real problem, hybrid methodology that has both linear and nonlinear capabilities can be a good strategy for practical use. According to the theory of ARCH model, we have the LM to test the GSCI data, and we find that the GSCI data have the ARCH effects. Therefore, we propose a hybrid model incorporating ARCH model and ANN model.

Considering a time series to be composed of a linear relation structure and a nonlinear component [4], the hybrid model is

$$\hat{Y}_t = \hat{L}_t + \hat{N}_t \tag{14}$$

Where $\hat{L}_t$ and $\hat{N}_t$ denote the linear and nonlinear components.

We first process the ARCH family model for the linear component, and then we obtain the residuals. The residual at time t is

$$e_t = y_t - \hat{L}_t \tag{15}$$

With the ANN model, the residual forecast value $\hat{N}_t$ will be

$$\hat{N}_t = f(e_{t-1}, e_{t-2}, \dots \dots e_{t-n}) + \xi_t \tag{16}$$

Where $f(\cdot)$ is a nonlinear function and ξ_t is the random error.

Thus, the combined forecast will be

$$\hat{Y}_t = \hat{L}_t + \hat{N}_t \tag{17}$$

3.4 Forecast Evaluation Criteria

Three criteria will be used to evaluate the model forecasting ability. The first is the root mean squared error (RMSE). The formula for RMSE is

$$\text{RMSE} = \sqrt{\frac{\sum (\hat{y}_t - y_t)^2}{n}} \tag{18}$$

Where $\hat{y}_t$ is the predicted value, y_t is the actual value.

The second is the mean absolute percent error (MAPE). It is a measure of average error in percentage terms for each point forecast. MAPE is given by

$$\text{MAPE} = \frac{1}{n}\sum\left|\frac{\hat{y}_t - y_t}{y_t} \times 100\right| \tag{19}$$

The third is the Theil Inequality Coefficient (Theil IC). Theil IC value is always between 0 and 1, and a smaller value indicates the error between the predicted value and the actual value is smaller. Theil IC is given by

$$\text{Theil IC} = \frac{\sqrt{\dfrac{\sum\left(\hat{y}_t - y_t\right)^2}{n}}}{\sqrt{\dfrac{\sum\hat{y}_t^2}{n}} + \sqrt{\dfrac{\sum y_t^2}{n}}} \tag{20}$$

4 Empirical Analysis

4.1 Data Description

The daily GSCI futures price data are obtained from Reuters Information System. The data span the period from 8 July 1996 to 26 May 2006 (2488 observations). We take data from 8 July 1996 to 25 May 2005 as in-sample data sets (2236 observations), and we take the data from 27 May 2005 to 26 May 2006 as out-of-sample data sets (252 observations) which are used to evaluate the performance of the predictions. Figure1 plots logarithm returns data series of GSCI futures price.
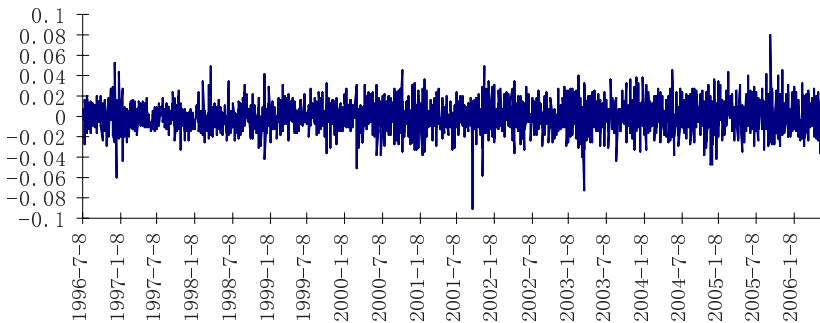
Fig. 1. Logarithm returns data series of GSCI futures price

4.2 Empirical Results

In this study, Arima and ARCH family models are implemented via the Eviews software, which is produced by Quantitative Micro Software Corporation. ANN model is built using the Matlab software, which is produced by Mathworks

Laboratory Corporation. The main equation is regression equation and Akaike's Information Criterion (AIC) rule is used to determine the lag lengths. Finally, we select 3 lags after testing many times. The residual equation we selected are ARCH (1), GARCH (1,1), ARCH (1)-M, GARCH (1,1)-M, EGARCH(1,1) for Bollerslev's (1988) idea, in most applications p=q=1 is found to suffice. On the other hand, the ANN model uses trial and error to determine the network architecture of 4-4-1 by minimizing the forecasting error [5].

First, we process the forecast using the ARCH family models. Table 2 gives the forecasting result. According to the forecast evaluating criteria, we can find that the ARCH(1)-M performs best.

Table 2. Forecast Result of ARCH Family Models

ARCH Family	RMSE	Rank	MAPE	Rank	Theil IC	Rank
Arima	7.3347	6	1.3650	5	0.008486	6
ARCH(1)	7.3303	3	1.3651	6	0.00848	3
GARCH(1,1)	7.3317	4	1.3649	4	0.008482	4
EGARCH(1,1)	7.3331	5	1.3648	3	0.008485	5
ARCH(1)-M	7.3241	1	1.3571	1	0.008476	1
GARCH(1,1)-M	7.3257	2	1.3620	2	0.008478	2

Therefore, we form the hybrid model using the best ARCH(1)-M model combined with the ANN model. Table 3 gives the forecasting results. Simultaneously, we also process the forecast using the ARIMA-ANN hybrid model. According to the forecast evaluation criteria, we can find that the ARCH(1)-M-ANN model performs better than the ARIMA-ANN model , and also performs the best in all the given models.

Table 3. Forecast Result of Hybrid Models

Hybrid Models	RMSE	Rank	MAPE	Rank	Theil IC	Rank
ARCH(1)-M-ANN	7.2347	1	1.3376	1	0.008371	1
Arima-ANN	7.3334	2	1.3593	2	0.008485	2

According to the NMSE, MAPE, Thiel IC evaluation criteria, we can find that the ARCH(1)-M-ANN hybrid model is superior to ARIMA, ARCH(1), GARCH(1,1), EGARCH(1,1) , ARCH(1)-M , GARCH(1,1)-M and ARIMA-ANN models for GSCI futures price forecasting.

5   Conclusions

Commodity index futures represent a useful investment vehicle for speculators and hedgers in energy markets. In this study, we propose a hybrid model combing ARCH-M model and ANN model to predict GSCI futures price. In terms of the empirical

results, we find that the model combining ARCH-M and ANN models performs the best on the selected criteria.

References

1. Wai Mun Fong, Kim Hock See. Modelling the conditional volatility of commodity index futures as a regime switching process. Journal of Applied Econometrics 2001; 16: pp. 133-163.
2. Commodity indexes overview and analysis. Seamans Capital Management. July 2003.
3. H. White. Connectionist nonparametric regression: multilayer feedforward networks can learn arbitrary mappings. Neural Networks, 1990, 3: pp. 535-549.
4. G.Peter Zhang. A time series forecasting using a hybrid ARIMA and neural network model. Neurocomputing. 2003; 50: pp.159-75.
5. Lean Yu, Shouyang Wang. A novle nonlinear ensemble forecasting model incorporating GLAR and ANN for foreign exchange rates. Computers & Operations Research 2005; 32.
6. Tim Bollerslev, Ray Y. Chou, Kenneth F. Kroner. ARCH modeling in finance. Journal of Econometrics 1992; 52: pp. 5-59.
7. Nowrouz Kohzadi, Milton S. Boydd. A comparison of artificial neural network and time series models for forecasting commodity prices. Neurocomputing 1996; 10:pp. 169-181.
8. G.E.P. Box. Time series analysis. Forecasting and Control.San Francisco, CA, 1970.
9. CME GSCI Futures and Options 2006 Information Guide. CME Equity Products.2006.
10. Sayantani Ghose. Downside risk in the DJ-AIG commodity index futures market. Working paper Submitted to European Journal of Finance. 2005.
11. Lummer, Siege.GSCI Collterized Futures: A hedging and diversification tool for institutional investors. Journal of Investing. 1993.
12. Engle, Robert F. Autoregressive conditional heteroskedasticity with estimates of variance of the U.K. inflation. Econometrica. 1982, 50: pp. 987-1008.
13. Paul D.Kaplan. GSCI collateralized futures as a hedging and diversification tool for institutional portfolios: an update. Forthcoming in the Journal of Investing 1997; 12.

Oil Price Forecasting with an EMD-Based Multiscale Neural Network Learning Paradigm

Lean Yu[1,2], Kin Keung Lai[2], Shouyang Wang[1], and Kaijian He[2]

[1] Institute of Systems Science, Academy of Mathematics and Systems Science,
Chinese Academy of Sciences, Beijing 100080, China
{yulean,sywang}@amss.ac.cn
[2] Department of Management Sciences, City University of Hong Kong,
Tat Chee Avenue, Kowloon, Hong Kong
{msyulean,mskklai,paulhekj}@cityu.edu.hk

Abstract. In this study, a multiscale neural network learning paradigm based on empirical mode decomposition (EMD) is proposed for crude oil price prediction. In this learning paradigm, the original price series are first decomposed into various independent intrinsic mode components (IMCs) with a range of frequency scales. Then the internal correlation structures of different IMCs are explored by neural network model. With the neural network weights, some important IMCs are selected as final neural network inputs and some unimportant IMCs that are of little use in the mapping of input to output are discarded. Finally, the selected IMCs are input into another neural network model for prediction purpose. For verification, the proposed multiscale neural network learning paradigm is applied to a typical crude oil price — West Texas Intermediate (WTI) crude oil spot price prediction.

Keywords: Crude oil price forecasting, artificial neural networks, empirical mode decomposition, multiscale learning paradigm.

1 Introduction

As is known to all, crude oil price forecasting is a rather challenging task due to high volatility and effects of irregular events. In the past practices, traditional statistical and econometric techniques are widely applied to crude oil price forecasting. For example, Huntington [1] applied a sophisticated econometric model to predict crude oil prices in the 1980s. Abramson and Finizza [2] utilized a probabilistic model for predicting oil prices, and Morana [3] suggested a semi-parametric statistical method for short-term oil prices forecasting. Usually, these models can provide good results when the time series under study is linear or near linear. However, in real-world crude oil price series, there is a great deal of highly nonlinearity and irregularity. Numerous experiments [4-5] have demonstrated that the performance might be very poor if one continued using these traditional statistical and econometric models. The main reason leading to this phenomenon is that the traditional statistical and econometric models are built on the linear assumptions and they cannot capture the nonlinear patterns hidden in the time series.

With the advent of artificial intelligence (AI), neural networks provide a powerful alternative solution to nonlinear time series prediction. In this situation, using neural network as a nonlinear modeling technique for nonlinear crude oil price forecasting has been a common practice in the past decades [6-7]. Unfortunately, the currently employed neural network learning process, both the training algorithms and preprocessing methods used, is essentially a single-scale learning procedure. That is, it is trained based on a pure time series. A possible drawback of such a conventional neural network learning process is that it is sometimes inadequate for complex and difficult problems [8], e.g., crude oil price forecasting problems, and often yields poor generalization performance. To alleviate the potential problem of the poor generalization, a multiscale neural network learning paradigm based on empirical mode decomposition (EMD) is proposed. In the multiscale learning paradigm, the original time series are first decomposed into various independent intrinsic mode components (IMCs) with a range of frequency scales. Then the internal correlation structures of different IMCs are explored by neural network. With the neural network weights, some important IMCs are selected as final neural network inputs and some unimportant IMCs that are of little use in the mapping of input to output are discarded. Finally, the selected IMCs are input into another neural network model for prediction purpose.

The rest of this study is organized as follows. Section 2 describes the building process of the proposed EMD-based multiscale neural network learning paradigm in detail. For verification, a typical crude oil price — West Texas Intermediate (WTI) crude oil spot price is used in Section 3. And Section 4 concludes the article.

2   Multiscale Neural Network Learning Paradigm

In this section, an overall formulation process of the EMD-based multiscale neural network learning paradigm is proposed for nonlinear time series prediction such as crude oil price forecasting. First of all, the EMD technique is briefly reviewed. Then the EMD-based multiscale neural network learning paradigm is proposed.

2.1   Empirical Mode Decomposition (EMD)

The empirical mode decomposition (EMD) method first proposed by Huang et al. [9] is a form of adaptive time series decomposition technique using spectral analysis via Hilbert transform for nonlinear and nonstationary time series data. Traditional forms of spectral analysis, like Fourier, assume that a time series (either linear or nonlinear) can be decomposed into a set of linear components. As the degree of nonlinearity and nonstationarity in a time series increases, the Fourier decomposition often produces large sets of physically meaningless harmonics when applied to nonlinear time series [10]. For wavelet analysis, it needs to select a filter function beforehand [11], which is difficult for some unknown time series. Naturally, a new spectrum analysis method, EMD based on Hilbert transform, is emerged.

The basic principle of EMD is to decompose a time series into a sum of intrinsic mode components (IMCs) with the following sifting procedure.

(1) Identify all the local extrema including local maxima and minima of $x(t)$,
(2) Connect all local extrema by a cubic spline line to generate its upper and lower envelopes $x_{up}(t)$ and $x_{low}(t)$.
(3) Compute the point-by-point envelope mean $m(t)$ from upper and lower envelopes, i.e., $m(t) = \left(x_{up}(t) + x_{low}(t) \right) / 2$.
(4) Extract the details, $d(t) = x(t) - m(t)$.
(5) Check the properties of $d(t)$: (i) if $d(t)$ meets the above two requirements, an IMC is derived and replace $x(t)$ with the residual $r(t) = x(t) - d(t)$; (ii) if $d(t)$ is not an IMC, replace $x(t)$ with $d(t)$.
(6) Repeat Step 1) – 5) until the residual satisfies the following stopping condition: $\sum_{t=1}^{T} \frac{\left[d_j(t) - d_{j+1}(t) \right]^2}{d_j^2(t)} < SC$, where $d_j(t)$ is the sifting result in the jth iteration, and SC is the stopping condition. Typically, it is usually set between 0.2 and 0.3.

The EMD extracts the next IMC by applying the above procedure to the residual term $r_1(t) = x(t) - c_1(t)$, where $c_1(t)$ denotes the first IMC. The decomposition process can be repeated until the last residue $r(t)$ only has at most one local extremum or becomes a monotonic function from which no more IMCs can be extracted. A typical sifting process can be represented by a tree graph, as illustrated in Fig. 1.
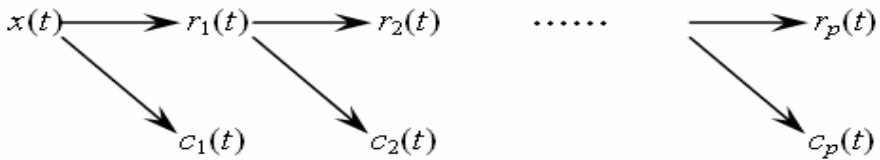
Fig. 1. The tree graph representation of the EMD sifting process

At the end of this sifting procedure, the time series $x(t)$ can be expressed by

$$x(t) = \sum_{j=1}^{p} c_j(t) + r_p(t) \tag{1}$$

where p is the number of IMCs, $r_p(t)$ is the final residue, which is the main trend of $x(t)$, and $c_j(t)$ ($j = 1, 2, \ldots, p$) are the IMCs, which are nearly orthogonal to each other, and all have nearly zero means. Thus, one can achieve a decomposition of the data series into m-empirical modes and a residue. The frequency components contained in each frequency band are different and they change with the variation of time series $x(t)$, while $r_p(t)$ represents the central tendency of time series $x(t)$. For later analysis, the residue has been seen as the $(p+1)$th IMC (i.e., c_{p+1}). Then the Eq. (1) can be re-written as

$$x(t) = \sum_{j=1}^{p+1} c_j(t) \tag{2}$$

2.2 EMD-Based Multiscale Neural Network Learning Paradigm

As we know, artificial neural networks (ANNs) are a new kind of intelligent learning algorithm and are widely used in some application domains. In this study, a standard three-layer feed-forward neural network (FNN) [12] is selected as a multiscale neural network learning tool for nonlinear time series prediction. The main reason of selecting FNN as a predictor is that an FNN is often viewed as a "universal approximator"[12]. However, a major challenge in neural network learning is how to make the trained networks possess good generalization ability, i.e., they can generalize well to cases that were not included in the training set. Some researchers argued to use the cross-validation technique for getting good generalization [13]. But in the cross validation technique, neural network learning is based on a single series representation for the entire training process. However, when the problem is very difficult and complex, single series representation for neural network learning may be inadequate [8]. For this reason, the EMD-based multiscale neural network learning is employed to decompose a time series and approximating it using decomposed components via a multi-variable analysis framework. Generally speaking, the EMD-based multiscale neural network learning paradigm consists of three different steps.

Step I: Decomposition. The original time series are decomposed into various independent intrinsic mode components (IMCs) with a range of frequency scales. These produced different IMCs can formulate the inputs of neural networks. Fig. 2 presents an illustrative decomposition example of a time series with p IMCs and one residue.
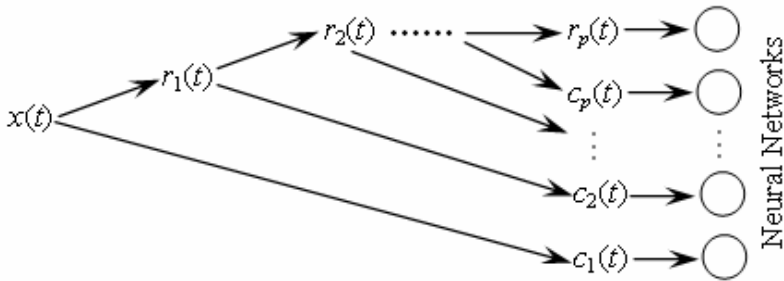
Fig. 2. The EMD decomposition to form the inputs of the neural networks

Step II: Selection. The IMCs produced by Step I are input into the neural networks for training. In the neural network learning process, the internal correlation structures of different IMCs should be explored. Using the explored internal relationships, some important IMCs are selected as final neural network inputs and some unimportant IMCs that are of little use in the mapping of input to output are discarded. The mapping is expected to be highly nonlinear and dependent on the characteristics of the individual time series data. In this study, we use the connection weights of neural networks as a selection criterion. Let

$$s_i = \sum_{j=1}^{q} \left| w_{ij} \right| \tag{3}$$

represent the importance of input c_i (e.g., IMC_i), where w_{ij} is the weight of input neuron i to hidden neuron j and q is the number of hidden nodes.

Subsequently, we use the following relative importance of input c_i (e.g., IMC_i) as a final selection criterion, i.e.,

$$\tilde{s}_i = s_i \Big/ \sum_{i=1}^{p} s_i \tag{4}$$

where $\tilde{s}_i$ represents the normalized input strength and p is the number of input nodes.

Usually, the input components (i.e., IMC_i) with small $\tilde{s}_i$ will be considered to be unimportant and may be discarded without affecting the prediction performance. Of course, as an alternative solution, principal component analysis (PCA) [14] can also be used to explore the relationships of different inputs, but it cannot effectively capture internal relationship between dependent variable and decomposed components.

Step III: Prediction. The final step is to use the selected IMCs with larger $\tilde{s}_i$ to train another neural network model for nonlinear time series prediction purpose.

It is interesting to examine the underlying idea of the multiscale learning paradigm. For a complex time series problem, a neural network is inadequate to approximate it due to lack of internal correlations. Through the EMD decomposition, the internal correlation structures at different scale levels that may be obscured in the original series are exposed by neural network learning. Usually, how well a network learns the internal correlation structure influences the degree of neural network generalization [8]. When the internal relationship is explicitly revealed to the neural networks, it can be more easily captured and learned.

3 Experiment

For evaluation and verification, a typical crude oil price series, West Texas Intermediate (WTI) crude oil spot price is chosen as the experiment sample data since the WTI price is most famous benchmark prices used widely as the basis of many crude oil price formulas. The WTI oil price data used here are daily data and are obtained from the website of Department of Energy (DOE) of US (http://www.eia.doe.gov/). We take the daily data from January 1, 1998 to October 30, 2006 excluding public holidays with a total of 2210 observations. Particularly, the data from January 1, 1998 till December 31, 2004 is used for training set (1751 observations) and the remainder is used as testing set (459 observations).

For performance comparison, the normalized mean squared error (*NMSE*) is used as the evaluation criterion, which can be represented by

$$NMSE = \frac{\sum_{i=1}^{N} \left(x_i - \hat{x}_i \right)^2}{\sum_{i=1}^{N} \left(x_i - \overline{x}_i \right)^2} = \frac{1}{\sigma^2} \frac{1}{N} \sum_{i=1}^{N} \left(x_i - \hat{x}_i \right)^2 \tag{5}$$

where σ^2 is the estimated variance of the testing data, x_i and $\hat{x}_i$ are the actual and predicted value, $\overline{x}_i$ being the mean, and N is the number of testing data. If the estimated mean of the data is used as predictor, *NMSE*=1.0 is obtained. The *NMSE* is

related to R^2 which measures the dependence between pairs of desired values and predictions by $NMSE = 1-R^2$. For comparison purpose, the conventional single-scale neural network learning paradigm is used as the benchmark model.

Following the multiscale learning paradigm, the WTI training data are decomposed into eight IMCs and one residue, as shown in Fig. 3. From this decomposition, a neural network model is used to select some important components for final multiscale learning. We use neural network with the architecture (9:15:1) to perform this selection task. That is, the neural network has nine inputs, fifteen hidden nodes and one
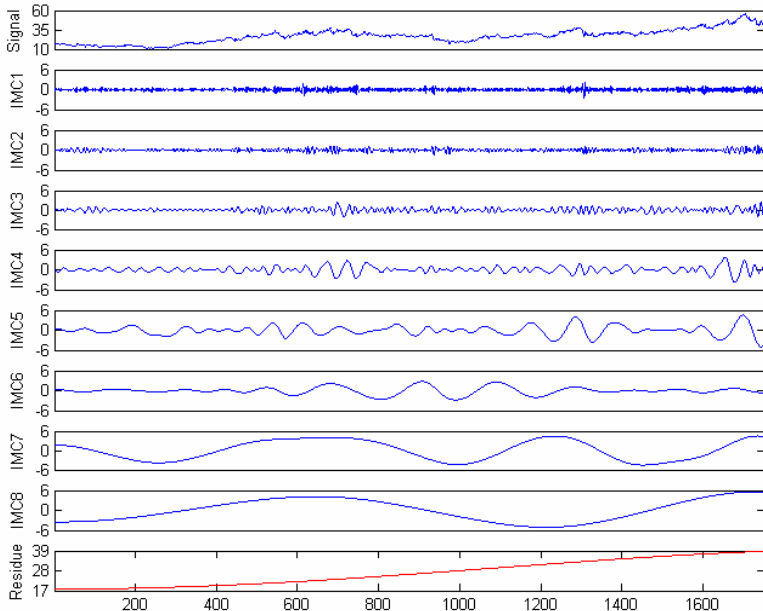
Fig. 3. The EMD decomposition of WTI crude oil spot price
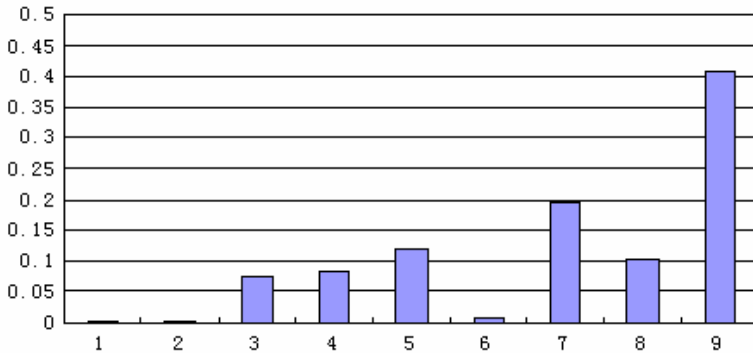
Fig. 4. The distribution of relative importance indicator of eleven IMCs

output neuron. Note that the number of hidden nodes is determined by trial and error and practical problems. Fig. 4 illustrates the normalized input strength or relative importance indicator of all decomposed components.

As can be seen from Fig. 4, it is not hard to find that the input components IMC1, IMC2 and IMC6 are consistently less important than other inputs. In this way, the remaining six IMC components are finally chosen as neural network inputs for final prediction purpose. With the decomposed IMCs, some simulations are re-implemented after these less important inputs are eliminated. This leads to a new neural network architecture (6:15:1). In this study, we represent the multiscale neural network by (6:15:1) = (9:15:1)-[1, 2, 6]. For consistency, we still use 15 hidden neurons. Table 1 shows the crude oil price prediction performance with different neural network learning paradigms.

Table 1. The out-of-sample prediction results for different neural network learning paradigms

Neural Network Model		Prediction Performance		
Architecture	Learning type	NMSE	Minimum	R^2
(9:15:1)	Single-scale	0.0712	0.0102	0.9288
	Multiscale	0.0143	0.0082	0.9767
(6:15:1)	Single-scale	0.0587	0.0095	0.9413
	Multiscale	0.0084	0.0008	0.9876

As can be revealed from Table 1, several interesting conclusions can be found. First of all, the multiscale learning generally performs better than the single scale learning in terms of different neural network architectures. Second, in the same network architecture, the performance of the multiscale learning is much better than that of the single scale learning. Third, when the network architecture is changed from (9:15:1) to (6:15:1), the single scale neural network learning model with architecture (6:15:1) can outperform another single scale neural network learning model with architecture (9:15:1). The main reason is that the crude oil prices are more dependent on some nearer crude oil price value. If we use some over-length lag term as neural network inputs, the performance may be worse because much redundancy is involved. Finally, after some less important inputs are eliminated, the multiscale neural network learning can show a more consistent performance for different weight initializations than the conventional single scale neural network learning.

4   Conclusions

In this study, an EMD-based multiscale neural network learning paradigm is proposed for complex nonlinear time series prediction problem. In this proposed multiscale learning paradigm, the original time series are first decomposed into various independent intrinsic mode components (IMCs) with different scales. Then these IMCs are input into neural network for exploring the internal correlation structures of different IMCs. Using the relative importance indicator, some important IMCs are selected as final neural network inputs and some unimportant IMCs that are of little use in the mapping of input to output are discarded. Finally, the retained IMCs are input into another neural network model for final prediction purpose. For verification

purpose, a typical crude oil price, WTI spot price series is used. Experimental results obtained confirm that the multiscale neural network learning paradigm can effectively improve the generalization capability, implying that the proposed multiscale neural network learning paradigm can be used as a promising tool for complex nonlinear time series prediction such as crude oil price forecasting problem.

Acknowledgements

References

1. Huntington, H.G.: Oil Price Forecasting in the 1980s: What Went Wrong? The Energy Journal 15(2) (1994) 1–22
2. Abramson, B., Finizza, A.: Probabilistic Forecasts from Probabilistic Models: A Case Study in the Oil Market. International Journal of Forecasting 11(1) (1995) 63–72
3. Morana, C.: A Semiparametric Approach to Short-term Oil Price Forecasting. Energy Economics 23(3) (2001) 325–338
4. Cichocki, A., Unbehauen, R.: Neural Networks for Optimization and Signal Processing. Wiley, New York (1993)
5. Weigend, A.S., Gershenfeld, N.A.: Time Series Prediction: Forecasting the Future and Understanding the Past. Addison-Wesley, Reading, MA (1994)
6. Wang, S.Y., Yu, L., Lai, K.K.: A Novel Hybrid AI System Framework for Crude Oil Price Forecasting. Lecture Notes in Artificial Intelligence 3327 (2004) 233-242
7. Wang, S.Y., Yu, L., Lai, K.K.: Crude Oil Price Forecasting with TEI@I Methodology. Journal of Systems Science and Complexity 18(2) (2005) 145-166
8. Liang, Y., Page, E.W.: Multiresolution Learning Paradigm and Signal Prediction. IEEE Transactions on Signal Processing 45 (1997) 2858-2864
9. Huang, N.E., Shen, Z., Long, S.R., Wu, M.C., Shih, H.H., Zheng, Q., Yen, N.C., Tung, C.C., Liu, H.H.: The Empirical Mode Decomposition and the Hilbert Spectrum for Nonlinear and Nonstationary Time Series Analysis. Proceedings of the Royal Society A: Mathematical, Physical & Engineering Sciences 454 (1998) 903-995
10. Huang, N.E., Shen, Z., Long, S.R.: A New View of Nonlinear Water Waves: The Hilbert Spectrum. Annual Review of Fluid Mechanics 31 (1999) 417-457
11. Li, X.: Temporal Structure of Neuronal Population Oscillations with Empirical Mode Decomposition. Physics Letters A 356 (2006) 237-241
12. Hornik, K., Stinchocombe, M., White, H.: Multilayer Feedforward Networks are Universal Approximators. Neural Networks 2 (1989) 359-366
13. Krogh, A., Vedelsby, J.: Neural Network Ensembles, Cross Validation, and Active Learning. In Tesauro, G., Touretzky, D., Leen, T. (eds.): Advances in Neural Information Processing Systems, Cambridge, MA, MIT Press 7 (1995) 231-238
14. Yu, L., Wang, S.Y., Lai, K.K.: A Novel Nonlinear Ensemble Forecasting Model Incorporating GLAR and ANN for Foreign Exchange Rates. Computers & Operations Research 32 (2005) 2523-2541

Crude Oil Price Prediction Based On Multi-scale Decomposition

Yejing Bao [1], Xun Zhang [1], Lean Yu [1], and Shouyang Wang[1, 2]

[1] Institute of Systems Science, Academy of Mathematics and Systems Science,
Chinese Academy of Sciences, Beijing 100080, China
[2] School of Management, Graduate School of Chinese Academy of Sciences,
Chinese Academy of Sciences, Beijing 100049, China
{baoyejing,zhangxun,yulean,sywang}@amss.ac.cn

Abstract. A synergetic model (DWT-LSSVM) is presented in this paper. First of all, the raw data is decomposed into approximate coefficients and the detail coefficients at different scales by discrete wavelet transforms (DWT). These coefficients obtained by previous phase are then used for prediction independently using least squares support vector machines (LSSVM). Finally, these predicted coefficients are combined into a final prediction. The proposed model is applied to oil price prediction. The simulation results show that the synergetic model has greater generalization ability and higher accuracy.

Keywords: crude oil price, wavelet transform, least squares vector machines.

1 Introduction

The forecasting of crude oil price as attracted many academic researchers and business practitioners, since the crude oil holds a strategic position in the international market. However the nonstationarity, nonlinearity and too many uncertain factors of crude oil price determination make its forecast an intractable task.

Traditional forecasting methods usually analyze the volatility of crude oil price under the framework of demand and supply or use data-driven model to fit the oil price series [1,2,3]. However, most of them failed to produce the consistently good results due to the nonlinear mechanism and intrinsic complexity of oil market. In the past the crude oil price was usually treated as a single series, the intrinsic complex modes involved in the price series are mixed and can not be explored deep.

Discrete wavelet transform (DWT) has outstanding scale separation ability. It could capture useful information on various resolution levels [4,5]. In this paper, DWT is used to decompose the original time series into separate components and each component is forecasted independently with least squares support vector machines (LSSVM) owing to its excellent forecasting performance [6,7]. Thus, a synergetic model based on multi-scale decomposition is presented. To validate the applicability of the proposed model, simulation experiments are conducted on crude oil spot price.

2 Multi-scale Based Forecasting

The forecasting framework is as follows (see Fig.1):

1 Decomposing the original series by DWT
A discrete wavelet transform can be computed with a fast filter bank algorithm called the `$a-trous$` algorithm. It is a non-decimated wavelet transform which produces smoother approximations of the signal [8].
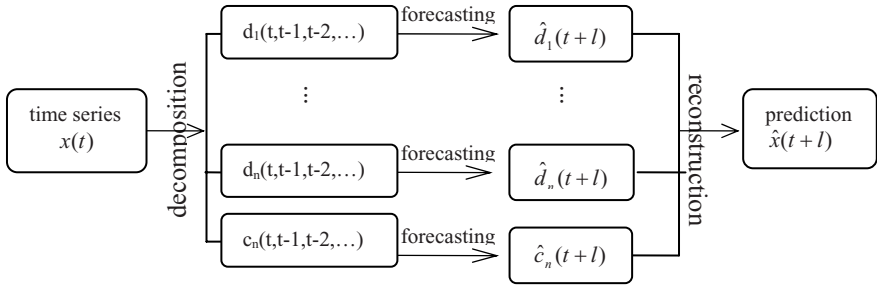
Fig. 1. The framework of prediction model

Given the time series of oil price $\{x(1), x(2),...,x(n)\}$, the scaling coefficients at different scales can be obtained by the `$a-trous$` wavelet transform. Then the original series could be expressed as the sum of the approximate coefficients c_J and the detail coefficients $d_j (j=1,2,...J)$:

$$x(t) = c_J + \sum_{j=1}^{J} d_j \tag{1}$$

2 Predicting the decomposed coefficients independently by LS-SVM
Instead of predicting the original series directly, we predict each decomposed coefficients by a separate LS-SVM:

$$\hat{c}_n(t+l) = f(c_n(t-1), c_n(t-2),...,c_n(t-m)) \tag{2}$$

$$\hat{d}_j(t+l) = f_j(d_j(t-1), d_j(t-2),...,d_j(t-n_j)) \tag{3}$$

Here m and n_j are referred as the embedding dimension. The l means l-th sample ahead prediction. For each value of l we train a separate forecasting architecture.

3 Reconstructing the predicted value
Using LS-SVM predictor, the predicted values of the approximate part and detail parts can be achieved. The reconstruction of predicted value can be expressed as:

$$\hat{x}(t+l) = \hat{c}_n(t+l) + \sum_{j=1}^{n} \hat{d}_j(t+l) \tag{4}$$

3   Material and Forecasting Results

3.1   Crude Oil Price Data

The data material consists of weekly and monthly WTI spot price ($/bbl). The original data material stems from the website of Energy Information Administration, US Department of Energy. The weekly data was divided into two parts, training sets (2004.01.02--2005.12.30) and testing sets (2006.01.06--2006.12.15). The monthly data was treated similarly (training sets: 1999.01-2004.12, testing sets: 2005.01-2006.11).

To test the model, the forecasting procedure is repeatedly applied to the testing samples. For every testing sample, we adopted moving window to intercept the training samples.

3.2   Simulation

For the decomposition of the weekly data, db5 wavelet is selected as the wavelet function and decomposition level is 4. The original series and the decomposed series are shown in Fig.2 (a). The original time series is shown in the first subfigure, following are approximate c4 and detail $d_j (j = 1,2,...4)$. The monthly data is dealt with the same processing and the results are shown in Fig.2 (b).
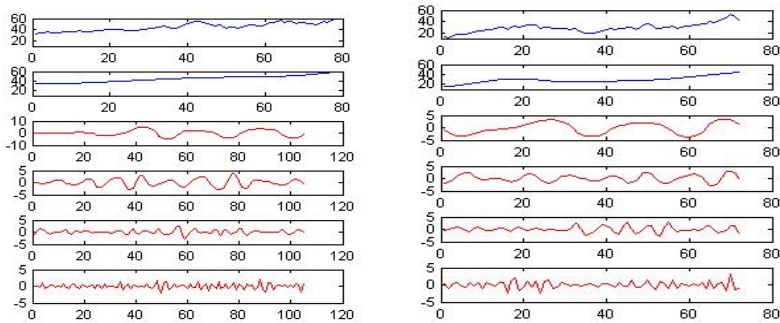
Fig. 2. (a) Decomposition results of weekly data   (b) Decomposition results of monthly data

By eq.(2,3,4), the prediction for 1,2,3 and 4-step ahead is obtained.

To estimate the prediction performance of the synergetic model, pure LS-SVM model is used for comparison. Three criterions are used to evaluate the performance of the prediction model: the mean absolute relative error (MARE), the normalized mean square error (NMSE) and the direction statistics (Dstat[1]). The results show in the table1. It can be obviously seen DWT-LS-SVM model outperforms the pure LS-SVM model.

---

[1] The direction statistics is defined as: $Dstat = \dfrac{1}{N} \sum\limits_{i=1}^{N} a_i$, here as $x_{i+1} - x_i)(\hat{x}_{i+1} - x_i) \leq 0$

then $a_i = 1$;otherwise $a_i = 0$.

Table 1. Comparison of DWT-LS-SVM model and LS-SVM model

Prediction depth	DWT-LS-SVM			LS-SVM		
	MARE	NMSE	Dstat	MARE	NMSE	Dstat
1-week	0.017	0.062	0.960	0.421	0.422	0.720
2-week	0.021	0.095	0.958	0.448	0.456	0.673
3 week	0.022	0.101	0.917	0.516	0.547	0.646
4-week	0.027	0.138	0.894	0.556	0.624	0.596
1-month	0.021	0.036	0.913	0.091	0.643	0.622
2-month	0.036	0.128	0.909	0.095	0.735	0.575
3-month	0.035	0.103	0.857	0.094	0.729	0.554
4-month	0.041	0.177	0.8	0.097	0.802	0.530

4 Conclusion

In this paper, we propose a synergetic prediction model (DWT-LSSVM) to predict the crude oil price. The simulations show the method outperforms the pure LS-SVM model. The decomposition methods separate complex series into several components which include less and much similar dynamics features based on time scale. The useful information on various scales would be easily captured. Therefore, wavelet transform improve the time series forecasting accuracy, especially for oil price.

References

1. Abramson, B., Finizza, A.: Probabilistic Forecasts from Probabilistic Models: A Case Study in the Oil Market. International Journal of Forecasting. 11(1) (1995), 63–72.
2. Abramson, B., Finizza, A.: Using Belief Networks to Forecast Oil Prices. International Journal of Forecasting. 7(3) (1991), 299–315.
3. Zamani, M.: An Econometrics Forecasting Model of Short Term Oil Spot Price. IIES Energy Economist. 6th IAEE European Conference (2004).
4. Murtagh, F., Starck, J.-L.: Image processing through multi-scale analysis and measurement noise modeling. Statistics and Computing, Vol. 10. (2000) 95–103
5. Percival DB, Walden AT.: Wavelet Methods for Time Series Analysis. Cambridge, MA: Cambridge University Press. (2000)
6. Suykens, J.A.K., Van Gestel, T., De Brabanter J., De Moor B., Vandewalle J.: Least Squares Support Vector Machines, World Scientific, Singapore, 2002
7. Vapnik, V.N.: The Nature of Statistical Learning Theory. Springer, Berlin. 1995
8. Shensa, M.J.: The Discrete Wavelet Transform: Wedding the `a Trous and Mallat Algorithms. IEEE Transactions on Signal Processing 40 (1992) 2464–2482.

An Improved CAViaR Model for Oil Price Risk

Dashan Huang[1], Baimin Yu[2], Lean Yu[2], Frank J. Fabozzi[3],
and Masao Fukushima[1]

[1] Department of Applied Mathematics and Physics, Graduate School of Informatics,
Kyoto University, Kyoto 606-8501, Japan
{dhuang,fuku}@amp.i.kyoto-u.ac.jp
[2] Academy of Mathematics and Systems Science, Chinese Academy of Sciences,
Beijing, 100080, China
{bmyu,yulean}@amss.ac.cn
[3] School of Management, Yale University, New Haven, CT06520, USA
{frank.fabozzi}@yale.edu

Abstract. As a benchmark for measuring market risk, Value-at-Risk
(VaR) reduces the risk associated with any kind of asset to just a num-
ber (amount in terms of a currency), which can be well understood by
regulators, board members, and other interested parties. This paper em-
ploys a new kind of VaR approach due to Engle and Manganelli [4] to
forecasting oil price risk. In doing so, we provide two original contribu-
tions: introducing a new exponentially weighted moving average CAViaR
model and developing a least squares regression model for multi-period
VaR prediction.

Keywords: CAViaR, oil price risk, exponentially weighted moving
average.

1 Introduction

Because of the key role of oil in the economies throughout the world, predicting
the future price of this commodity and managing the risks associated with fu-
ture oil prices are critical for central governments and businesses. Therefore oil
price prediction and its risk measurement has been a common research theme in
the last decades. Some examples of the oil price prediction are (1) a semipara-
metric approach to shot-term oil price forecasting developed by Morana [7], (2)
a hybrid artificial intelligence system framework for crude oil price forecasting
by integrating artificial neural networks and rule-based expert system with web-
based text mining techniques proposed by Wang et al. [10], and (3) a support
vector machine method (which is superior to the traditional ARIMA method and
the Wang et al. proposal) suggested by Xie et al. [11]. Our focus in this paper
is on oil price risk measurement. Previous work in this area includes (1) Cabedo
et al. [2] who proposed an ARMA historical simulation approach with Value-
at-Risk (VaR) ideology and (2) Kuper [6] who investigated (G)ARCH-based
volatility performance with different historical data. A good literature review on
oil price movements and their effects on economic and financial performance can
be referred to Sauter and Awerbuch [9].

Our motivation for concentrating on quantifying oil price risk are twofold. First, as noted by Sauter and Awerbuch [9], while most oil price movements from 1948-1985 were price increases, since 1986 the pattern has changed; more specifically, large price decreases are now commonplace, implying a rise in the volatility/risk of oil prices. Second, price risk in investments is more important than price level which determines whether to invest or not. Compared with the more developed financial market risk measures, however, oil price risk management is still in its infancy. This is because, being a physical asset, oil has some additional attributes that are not associated with traditional financial assets. For example, as Morana [7] points out, the price of oil is strongly influenced by transportation, inventory levels, weather, short-term demand and supply imbalances, and political issues. Thus, volatile oil price movements motivate consideration of how to quantify price risk. As a benchmark for measuring market risk, Value-at-Risk (VaR) reduces the risk associated with any kind of asset to just a number (amount in terms of a currency), which can be well understood by regulators, board members, and other interested parties.

The main objective of this paper is to investigate the predictive performance of various types of the conditional autoregressive value-at-risk (CAViaR) specifications for oil price risk prediction. The choice of this particular parametric method is motived by the fact that CAViaR does not require any assumption on the distribution of a time series and computes the VaR directly by quantile regression, implying that the model allows the time series to switch from one stochastic process to another. There are also two original theoretical contributions in this paper. First, we introduce a new exponentially weighted moving average CAViaR specification with only two parameters to be estimated, which in turn may reduce the model estimate risk. Second, we develop a least squares regression model for multi-period VaR prediction.

The rest of the paper is structured as follows. Section 2 briefly summarizes the CAViaR model and then proposes a new asymmetric CAViaR model. Section 3 provides some criteria for performance comparison. Section 4 presents some empirical results, followed by our concluding comments in Section 5.

2   Model

While the concept of VaR is intuitive, its modeling is a very challenging statistical problem. From a statistical point of view, VaR of a return series $\{r_t\}$, conditional on the information set $\mathcal{F}_{t-1}$, is defined as the negative θ-quantile, $q_t(\theta)$, for which $P(r_t \leq -q_t(\theta)|\mathcal{F}_{t-1}) = \theta$.

2.1   CAViaR

Building on the fact that the volatility of returns is highly autocorrelated (clustering), Engle and Manganelli [4] proposed the CAViaR model which computes $q_t(\theta)$ directly. In this paper, we will focus on the following four specifications:

Adaptive CAViaR: $q_t(\theta) = q_{t-1}(\theta) + \beta_1\{[1 + \exp(G[r_{t-1} + q_{t-1}(\theta)])]^{-1} - \theta\}$,
Symmetric CAViaR: $q_t(\theta) = \beta_0 + \beta_1 q_{t-1}(\theta) + \beta_2|r_{t-1}|$,
Asymmetric CAViaR: $q_t(\theta) = \beta_0 + \beta_1 q_{t-1}(\theta) + \beta_2(r_{t-1})^+ + \beta_3(r_{t-1})^-$,
GARCH(1,1) CAViaR: $q_t(\theta) = (\beta_0 + \beta_1 q_{t-1}^2(\theta) + \beta_2 r_{t-1}^2)^{1/2}$.

In the above, G is a positive number, and hence as $G \to \infty$, the adaptive CAViaR converges to $q_t(\theta) = q_{t-1}(\theta) + \beta_1[I(r_{t-1} \leq -q_{t-1}(\theta)) - \theta]$, where $I(\cdot)$ is the indicator function. As noted by Engle and Manganelli [4], the CAViaR specifications generalize the traditional GARCH-based VaR models by allowing for different stochastic processes in the tail of the return series, and can also deal with non-i.i.d. processes.

2.2 Improved CAViaR

Instead of estimating the entire distribution of a time series, the CAViaR model computes the conditional quantile directly, thereby exhibiting some theoretical advantages over the traditional VaR approach. However, in practice, CAViaR may face some implementation challenges. For example, to investigate the different effects of positive and negative returns on the prediction from a VaR model, Engle and Manganelli [4] suggested using the asymmetric CAViaR specification. This requires estimating four parameters in the optimization framework. Unfortunately, as an econometric model, more parameters may lead to more estimation error, which will in turn make the model unstable or unrobust.

Based on the exponentially weighted moving average volatility prediction idea, we propose a new asymmetric CAViaR model:

$$q_t(\theta) = \beta_0 q_{t-1}(\theta) + (1 - \beta_0)\left(\frac{v}{1 - \beta_1}I(r_{t-1} > 0) + \frac{v}{\beta_1}I(r_{t-1} \leq 0)\right)|r_{t-1} - \mu|,$$

where $v = \sqrt{\beta_1^2 + (1 - \beta_1)^2}$ $(0 < \beta_1 < 1)$ and μ is the sample mean. This CAViaR specification allows the VaR prediction to respond asymmetrically to positive and negative returns. For example, when $\beta_1 < 0.5$, negative returns have a larger influence on the VaR prediction. Moreover, in contrast to the asymmetric CAViaR model in [4], our model has only two parameters to be estimated. In Section 4, we show that our model can yield performance at least as good as the model of Engle and Manganelli (2004).

For parameter estimation, we follow Engle and Manganelli [4] and employ the linear and non-linear quantile techniques:

$$\hat{\beta}(\theta) = \text{argmin}_\beta\left\{\sum_{\{t:r_t \geq -q_t(\theta)\}} \theta|r_t + q_t(\theta)| + \sum_{\{t:r_t < -q_t(\theta)\}} (1 - \theta)|r_t + q_t(\theta)|\right\}.$$

This regression technique has a tractable property in that it does not require any assumption about the entire distribution of the error terms. Moreover, we can easily conduct various hypothesis tests on the quantile models [4,5].

2.3   Multi-period CAViaR

The simplest approach to generating multi-period VaR forecasts is to multiply the one step-ahead prediction by the square root of the holding period k, the procedure usually used in RiskMetrics [8]. However, this approach implicitly requires that the variance of the time series is constant in the holding period, thereby offsetting advantage that CAViaR can accommodate different stochastic processes in the holding period. But as a simple alternative, we provide an intuitive least squares regression model for multi-period VaR estimates:

$$q_{t+k}(\theta) = \alpha_0 + \alpha_1 q_t(\theta) + \alpha_2[I(r_t \leq -q_t(\theta)) - \theta],$$

where k is the holding period and the parameters α_0, α_1, and α_2 are estimated by the least squares regression. This regression model incorporates the following rules: When the time series follows a unique stochastic process in the holding period, α_1 will approach $\sqrt{k}$, and α_0 and α_2 will converge to 0. Moreover, in a similar spirit to the adaptive CAViaR model, whenever the loss exceeds VaR (underestimate), we increase it immediately, but when the loss does not exceed VaR (overestimate), we just decrease it slightly.

Note that while the multi-period VaR prediction approach examined here has two steps (estimate the one step-ahead VaR and estimate multi-period VaR) it may be combined into one step and thereby estimating all the parameters simultaneously.

3   Evaluation of Performance

To assess the predictive performance of the models investigated, in this section we employ tests designed for evaluating the predictive quantile performance as proposed by Bao et al. [1] and the references therein.

When assessing the accuracy of a VaR forecast model, there is always a general hypothesis required to be satisfied. That is,

$$E[H_t(\theta)|\mathcal{F}_{t-1}] = \theta, \tag{1}$$

where $H_t(\theta) = I(r_t < -q_t(\theta))$. Below we denote $H_t = H_t(\theta)$. If (1) holds, we say the VaR prediction is efficient with respect to $\mathcal{F}_{t-1}$. This means H_t is uncorrelated with any information in $\mathcal{F}_{t-1}$ up to time $t-1$. In this case, the forecast for VaR at time t and H_t cannot be improved. There are two implications in condition (1): correct unconditional coverage and independence of VaR forecasts.

With respect to the out-of-sample prediction, we split the sample into two parts, T_{in} and T_{out}, and use T_{in} to estimate the parameters and T_{out} for out-of-sample performance testing. Thus, we can compute the empirical coverage probability resulting from the VaR prediction series $\{\hat{q}_t(\theta)\}_{t \in T_{\text{out}}}$, that is,

$$\hat{\theta} = \frac{1}{|T_{\text{out}}|} \sum_{t \in T_{\text{out}}} \hat{H}_t,$$

Where $|T_{\text{out}}|$ denotes the cardinality of T_{out}. A VaR prediction model is preferred if its $\hat{\theta}$ is closer to the nominal value of θ.

3.1 Unconditional Coverage Test

Suppose VaR estimates are accurate. Then, the event of failure $\hat{H}_t = 1$ can be modeled as independent draws from a binomial distribution with a probability of occurrence equal to the significance level ($\hat{\theta} = \theta$). Thus, the likelihood-ratio test statistic (LR) is

$$\text{LR} = -2\ln[(1-\theta)^{|\text{T}_{\text{out}}|*(1-\hat{\theta})}\theta^{|\text{T}_{\text{out}}|*\hat{\theta}}] + 2\ln[(1-\hat{\theta})^{|\text{T}_{\text{out}}|*(1-\hat{\theta})}\hat{\theta}^{|\text{T}_{\text{out}}|*\hat{\theta}|}].$$

Under the null hypothesis, LR follows a χ^2 distribution with 1 degree of freedom.

3.2 Independence Test

A good VaR model must generate independent forecasts, i.e., violation ($\hat{H}_t = 1$) today has no effect on the probability of violation tomorrow.

In an approach similar to Engle and Manganelli [4], we investigate the regression of H_t on H_{t-i} ($i = 1, \cdots, M$) and $\hat{q}_t(\theta)$, that is,

$$H_t = \theta_0 + \sum_{i=1}^{M} w_i H_{t-i} + w_{M+1}\hat{q}_t(\theta) + u_t, \tag{2}$$

where w_i, $i = 1, \cdots, M + 1$, are regression parameters and

$$u_t = \begin{cases} -\theta, & \text{with probability } 1 - \theta, \\ 1 - \theta, & \text{with probability } \theta. \end{cases}$$

Under the null hypothesis, $\theta_0 = \theta$ and $w_i = 0$, $i = 1, \cdots, M + 1$. Denoting $w_0 = \theta_0 - \theta$, we rewrite (2) in vector notation as

$$\mathbf{H} - \theta\mathbf{1} = \mathbf{Xw} + \mathbf{u},$$

where $\mathbf{1}$ denotes the vector of ones. Thus, under the null hypothesis, $\Theta_0 : \mathbf{w} = 0$, Engle and Manganelli [4] proposed the following test statistic:

$$\text{DQ} = \frac{\hat{\mathbf{w}}'\mathbf{X}'\mathbf{X}\hat{\mathbf{w}}}{\theta(1-\theta)} \rightarrow \chi^2_{M+2} \text{ (asymptotically)}.$$

In the empirical application, we follow Engle and Manganelli (2004) to explore the dynamic quantile test: DQ in which $\mathbf{X}$ contains a constant, four lagged hits, $H_{t-1}, \cdots, H_{t-4}$, and a contemporaneous VaR estimate, $q_t(\theta)$.

4 Oil Price VaR

To implement the Engle and Manganelli approach and our proposed CAViaR model on real oil price risk forecasting, we took a sample of 2,475 daily data from Energy Information Administration for Brent and WTI spot prices, and computed the daily returns as 100 times the difference of the log of the prices,

Table 1. Performance of one-day-ahead VaR Prediction

		Adaptive	SCAV	ACAV	GARCH	Improved
1%	$\hat{\theta}$ Brent	0.0100	0.0100	0.0100	0.0080	0.0060
	WTI	0.0060	0.0040	0.0040	0.0040	0.0100
	p-value Brent	0.0016	0.9940	0.9694	0.9627	0.9908
	WTI	0.9907	0.8639	0.8636	0.9063	0.0002
5%	$\hat{\theta}$ Brent	0.0560	0.0440	0.0440	0.0420	0.0440
	WTI	0.0500	0.0360	0.0280	0.0320	0.0560
	p-value Brent	0.6001	0.9722	0.7462	0.8389	0.4582
	WTI	0.3393	0.7609	0.3035	0.5889	0.0481

Note: SCAV: symmetric CAViaR; ACAV: asymmetric CAViaR.

thereby generating 2,474 return scenarios. The samples range from November 29, 1996 to November 28, 2006. We used the first 1,974 observations for the estimation of the model parameters and the remaining 500 for out-of-sample testing. For the optimization routines, we employed a similar procedure to that described by Engle and Manganelli (2004). Because the objective function of the quantile regression model is designed to obtain the exact sample quantile with a given level, it is not surprising that the in-sample empirical coverage is quite precise (see Engle and Manganelli (2004) and Huang et al. (2006)). In this paper, we concentrated on the one-day-ahead and five-day-ahead out-of-sample VaR predictions. In the experiment, we use the empirical θ-quantile of the first 300 observations as the initialization to compute the VaR series.

For the one day-ahead VaR forecasting, in Table 1 we report the values of the empirical unconditional coverage probability and the p-value of the dynamic quantile test. As described in Section 3, the empirical coverage probability $\hat{\theta}$ represents the percentage of observations falling below the VaR predictions. Ideally, with a sufficiently large sample, the percentage should converge to θ. In this sense, all the models (the Engle and Manganelli model and our proposed model) pass the unconditional coverage test in general with only one exception (the confidence interval is [0.2%, 2%] at the 1% level and it is [3%, 7%] at the 5% level). Especially, all models perform well with Brent since the percentage of empirical coverage seems reasonably close to 1% or 5%. There is a surprising result that the asymmetric CAViaR specification does not pass the unconditional coverage test at the 5% level (the empirical coverage 0.028 is out of the confidence interval). This is in sharp contrast to the results reported by Engle and Manganelli (2004) which show that the asymmetric CAViaR model may do the best job.

With respect to the independence test, the adaptive model is rejected by Brent and the improved CAViaR is rejected by WTI at the 1% level. However, all the models survive in the independence test at the 5% level, producing rather large p-values.

Figure 1 plots the Brent return and one-day-ahead VaR forecast curves, which shows that although our proposed model has only two parameter, it can produce
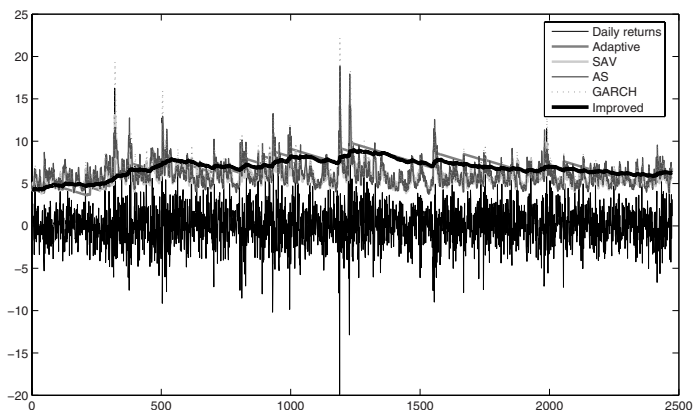
Fig. 1. Brent return and one-day-ahead estimated CAViaR plots at the 1% level

an estimate as good as the asymmetric CAViaR model with four parameters. Moreover, the superiority of our model will be more evident in the case of multi-period prediction.

In Table 2, for both Brent and WTI, we present the least squares regression parameters, α_0, α_1, and α_2, estimated for five-day-ahead VaR prediction. Interestingly, all the estimates of α_1 are far from $\sqrt{5}$, implying that both the Brent and WTI return processes do not follow a certain stochastic process in the holding period. Conversely, they may switch from one process to another; that is, the oil price process has structural breakpoints resulting from natural or politic events (Sauter and Awerbuch (2002) and Wang et al. (2004) identify important events affecting the price of oil). We also report the out-of-sample forecasting performance from the different models. The basic measure reported is the coef-

Table 2. Performance of five-day-ahead VaR Prediction at the 1&5% respective levels

		1%				5%			
		$\hat{\alpha}_0$	$\hat{\alpha}_1$	$\hat{\alpha}_2$	R^2	$\hat{\alpha}_0$	$\hat{\alpha}_1$	$\hat{\alpha}_2$	R^2
Adaptive	Brent	0.0806	0.9891	0.9341	0.9841	0.0687	0.9826	0.1771	0.9680
	WTI	0.1044	0.9871	0.9880	0.9823	0.1536	0.9636	0.4742	0.9313
SCAV	Brent	3.0473	0.4894	2.0959	0.2710	1.0678	0.7259	0.3763	0.5589
	WTI	4.9158	0.3476	1.5650	0.1301	2.3295	0.4049	0.3305	0.1820
ACAV	Brent	3.2865	0.4730	2.4061	0.2486	2.3161	0.3984	0.5588	0.1934
	WTI	4.8500	0.3585	1.6729	0.1383	2.4744	0.3772	0.3808	0.1614
GARCH	Brent	2.9499	0.5344	3.0928	0.3182	1.0172	0.7378	0.4619	0.5770
	WTI	5.9880	0.1595	0.5159	0.0263	1.6245	0.5942	0.4757	0.3767
Improved	Brent	0.0788	0.9896	0.2663	0.9939	0.0167	0.9959	0.0387	0.9947
	WTI	0.5929	0.9174	0.6988	0.8424	0.1461	0.9642	0.1300	0.9256

ficient of determination, R^2, from the least squares regression. The results show that both the adaptive and the proposed CAViaR specifications outperform the other three specifications (all the R^2 values exceed 0.9).

Acknowledgements

References

1. Bao, Y., Lee, T., Saltoğlu, B.: Evaluating the Predictive Performance of Value-at-Risk Models in Emerging Markets: A Reality Check. Journal of Forecasting, **25** (2006) 101-128
2. Cabedo, J.D., Moya, I.: Estimating Oil Price Value-at-Risk using the Historical Simulation Approach. Energy Economics, **25** (2003) 239–253
3. Energy Information Administration: //www.eia.doe.gov/
4. Engle, R.F., Manganelli, S.: CAViaR: Conditional Autoregressive Value at Risk by Regression Quantiles. Journal of Business and Economic Statistics, **22** (2004) 367-381
5. Huang, D., Yu, B., Lu, Z., Fabozzi, F.J., Fukushima, M.: Index-Exciting CAViaR: A New Empirical Time-Varying Risk Model. Working Paper, Kyoto University (2006)
6. Kuper, G.: Measuring Oil Price Volatility. CCSO Working Paper, No. 2002/08, Groningen University. http://www.eco.rug.nl/ccso/quarterly/2002q2.html (2002)
7. Morana, C.: A Semiparametric Approach to Short-Term Oil Price Forecasting. Energy Economics, **23**(3) (2001) 325-338
8. RiskMetrics: RiskMetrics^{TM} Technical Document. Fourth edition, J.P. Morgan/Reuters, (1996)
9. Sauter, R., Awerbuch, S.: Oil Price Volatility and Economic Activity: A Survey and Literature Review. IEA Research Paper, International Energy Agency, Paris, (2002)
10. Wang, S., Yu, L., Lai, K.K.: A Novel Hybrid AI System Framework for Crude Oil Price Forecasting. Lecture Notes in Computer Science, **3327** (2004) 233-242
11. Xie, W., Yu, L., Xu, S., Wang, S.: A New Method for Crude Oil Price Forecasting Based on Support Vector Machines. Lecture Notes in Computer Science, **3994** (2006) 444-451

The Portfolio Selection Model of Oil/Gas Projects Based on Real Option Theory

Zefu Lin[1] and Jianyue Ji[2]

[1] School of Management Science and Engineering, Central University of Finance and Economics, Beijing 100081, China
[2] School of Economics, Ocean University of China, Qingdao 266071, China
`linzf@cufe.edu.cn, jjx@ouc.edu.cn`

Abstract. Portfolio selection of oil/ gas projects is a fundamental subject of capital budgeting in the energy sector. In industry, strategic planning requires the selection of a portfolio of projects to advance the corporate goals. The term portfolio selection is more devoted to a set of financial assets that are easily traded and divisible. The principles and fundaments of portfolio selection can be used to compare strategies of investments, so that firms get maximum returns. In this paper, we discuss the oil/gas projects valuation methods first. Considering the characteristic of the oil/gas project, Real options method is more suitable for the oil/gas project than NPV method, and then a new model extended from the Black-Scholes model is built up. Finally, this paper put forward the portfolio selection model and gives a Computational case.

Keywords: Portfolio selection; Oil/gas projects; Real options theory.

1 Introduction

The decisions of committing limited resources to multiple uses can either strengthen or deteriorate their very financial foundation. On one end of the spectrum, capital budgeting procedures often employ traditional operations research (OR) techniques to guide and support decisions. On the other end, executives admit that selections come down to intuition. Typically, however, what is common is to build models that employ pro-forma plans centering on measures of the benefits of the investments – returns and risk.

Energy plays an important role in the global economy and politics. The decision about oil/ gas projects is also important for the industry and government. Developing an oil and/or gas field nowadays is subject to considerably larger investments in time, money, and technology. Furthermore, such large investments are almost always based on imperfect, scant, and uncertain information.

Extraction of oil (and/or gas) from a virgin field is undertaken in typically four stages: exploration and appraisal; development; production; and abandonment. This is a gross simplification, of course, for within each phase there are a multitude of technical, commercial, and operational considerations for the management to take optional action. Keeping one eye on real options, in their crudest form these phases can be briefly described as follows:

Exploration and Appraisal: Seismic data is obtained and a picture of the subsurface is then revealed. Coupled with geological knowledge, experience, and observations it is then possible to generate a more detailed depiction of a possible hydrocarbon-bearing zone. Seismic data cannot tell what fluids are present in the rock, so an exploratory well needs to be drilled to better establish the nature, size, and type of an oil and gas field.

Development: Once sufficient data has been obtained (from seismic or exploratory wells) to make an educated judgment on the size of the prize, we enter into the development phase. Here we decide upon the most commercially viable way for exploiting this new resource by engineering the number (and type) of producing wells, process facilities, and transportation. We must also establish if, at all, any pressure support is necessary.

Production: Depending on the size of the reserve, the engineer must manage this resource as carefully as any other valuable asset. Reservoir management (the manner and strategy in which we produce from a field) has become increasingly important over the past few years. Increasing the efficiency of our production from our reservoirs is now a crucial part of any engineering effort.

Abandonment: Once reserves have been depleted, the infrastructure can either be left to decay or – increasingly – it must be dismantled in an environmentally and economically efficient manner.

Portfolio selection of oil/ gas projects is a fundamental subject of capital budgeting in the energy sector. In industry, strategic planning requires the selection of a portfolio of projects to advance the corporate goals. The theory of financial portfolio is well developed and popular with the Markowitz' portfolio theory, which is based in the mean-variance optimization approach (Markowitz, 1959) .This theory, has tentatively been extended to real projects portfolio case, mainly in professional literature. However, although there are good papers showing that diversification principles remain valid (e.g., see Ball Jr. & Savage, 1999), the real projects case demands a richer portfolio theory in order to capture issues like synergy between real projects and the real options embedded into real projects such as the option to defer and learning options.

There are many challenges in implementing oil/gas portfolios. In particular, the risk and return of individual projects within the portfolio must be characterized in a consistent manner in order to achieve a minimum-risk and a maximum-return. Clearly, it is important to use economic evaluation techniques to characterize these risks and impacts on company performance and long-term value. Traditional methods based upon discounted cash flow (DCF) reported in the finance literature are always based upon static assumptions – no mention about the value of embodied managerial options.

For the case of mutually exclusive projects as those to develop oil and gas reserves, DCF rule tends to favor those with higher NPV values. However, in practice many managers overrule passive net present value (NPV) analysis by using intuition and executive judgment to take future managerial flexibility into assets values (Trigeorgis, 1996. There has been a move to use stochastic or dynamic methods in economic evaluations and portfolio management due to work of several researchers. Luehrman,

(1994), Copeland (1990) among others, suggest the use of option-based techniques to value implicit managerial flexibility in investment opportunities.

The valuation of projects and business opportunities using DCF and real option theory (ROT) is based on cost-benefit analysis, but they are different in the treatment of risk. Risk is the possibility of loss or gains since future values are dispersed around expected mean values so that the only way to measure risk is using probabilistic approach. Mathematical models for option valuation were firstly developed to price those on common stocks, exchange and interest rates, among others and later migrated to value real options on real assets from industrial projects. Volatility is not preset in DCF, but plays a remarkable role in option pricing.

Option theory methods for oil/ gas projects in the literature seem preoccupied with concern about the affect of future, uncertain oil and gas prices and, less so, on the non-financial options involved. Paddock, J., Siegel, D. and Smith, J. (1988) examine the options arising as better information through time reduces uncertainties in the exploitation of development assets. Luehrman, (1994) delves into the cost of foreclosing the option to develop an oil and gas asset; Lohrenz (1991) does so with respect to shut-in and abandonment of assets.

Obviously, oil/ gas projects give rise to different net cash flows. Each net cash flow has its own uncertainties and the market reacts to the perceived uncertainties. Jacoby and Margrabe (1978) give an option theory valuation methodology that considers each of the cost, net revenue, and tax cash flows and their unique uncertainties. The claimed advantage for their methodology is the ability to define the different risks associated through time for the investor and the taxing government.

2   Real Option Methods for Oil/Gas Project Valuation

Real options rest upon an analogy between real option value levers and financial option value levers. Luehrman (1994) established a mapping between project characteristics and financial option value drivers as depicted in table 1.

Table 1. Mapping between real option and financial option

Financial option Value	Variable	Real options Value
Exercise price	X	Investment cost
Stock price	A	Present value of expected cash flows
Time to expiry	T	Time to expiry
Risk-free interest rate	r_f	Risk-free interest rate
Uncertainty of stock price movements	σ	Volatility of expected cash flows

The investment cost is equivalent to the exercise price (X). When keeping the other real options levers constant, an increase in X will decrease the value of the project as X represents a negative cash flow.

The present value of the expected cash flows is analogous to the stock price (A). The higher the stock price the higher the value of the option. As a result, an increase in the present value of the expected cash flows will increase the overall value of the project.

The time to expiry is analogous to the time to maturity of a financial option (T). It is the maximum time period – expressed in years – which an investment can be deferred without losing the option to investment in the project. In an uncertain environment, the more time there is to learn about the uncertainty then the more insight will be gained of how to appropriately address the uncertainty. As a result, a longer time to expiry will increase the value of the project.

The risk-free rate (r_f) will increase (decrease) the value of a call (put) option because it will reduce the present value of the stock price (A). It will have the same effect when applied to a real options situation.

The volatility of expected cash flows (σ) is analogous to the volatility of stock price movements. Thus, a higher volatility will increase the value of the option.

Two fundamental methods for pricing financial options are the binomial tree model and the Black-Scholes model. In addition to the two models, and Margrabe (1978) put forward the pricing model which be used in exchange option pricing. These option-pricing models also can be used in the oil/gas projects. In the standard binomial tree model (Cox J., S. Ross and M. Rubinstein, 1979), Let C is the value of call option

Let A follow the binomial distribution, Starting at t_0, in one time period Δt, V may rise to uV with probability q or fall to dV with probability 1-q, where d<1, u>1 and d<r<u, with r being $1+r_f$.

So in the binomial tree model, under the assumption of risk-neutral, we can get:

$$p \equiv \frac{r_f - d}{u - d}, \quad u = e^{\sigma\sqrt{\Delta t}}, \quad d = e^{-\sigma\sqrt{\Delta t}}$$

$$C = \frac{pC_u + (1-p)C_d}{1+r_f} = \frac{pMax(0, uA - X) + (1-p)Max(0, dA - X)}{1+r_f} \tag{1}$$

This is the binomial tree pricing model of European call options that also can be used in oil/gas project valuation.

3   The Portfolio Selection Model Based on Real Option Theory

Based on characteristic of oil/gas project, we can extend the Black-Scholes (1973) as follows according to the previous research (Bjerksund & Stensland, 1993). The Variables in the model are listed in Table 2.

Table 2. Variables in the model

F: Unit value of non-developed reserve ;	I: Unit Investment cost;
Π: Unit profit	B: amount of developed reserve;
σ: Volatility of V (% per year)	T: total maturity period (years)
δ: Cash flow or "dividend yield" (%)	R: rate of return from developed reserves;
V: Unit value of developed reserve or underlying asset;	ω: Yearly production of the global reserve (%)
r: real risk free interest rate after tax (% per year)	τ: Time interval to expire the lease rights;
μ: Risk-adjusted discount rate or expected rate of return from V (%)	dz: Wiener's increment to add uncertain to the process;

The model assumes that production evolves over time as exponential decline curve as:

$$dB = -\omega B \, dt . \tag{2}$$

Here, B is the amount of oil and ω a fraction of the remained global reserve produced every year until economic depletion.

Then we can get the general for option valuation and similar to Black-Scholes equation.

$$\frac{1}{2}\sigma^2 V^2 \frac{\partial^2 F(V,t)}{\partial V^2} + (r - \delta)\frac{\partial F(V,t)}{\partial V} + r\frac{\partial F(V,t)}{\partial t} - rF = 0 \tag{3}$$

Considering the economic meaning, we can set certain boundary conditions for the equation. Then we can get the possible approximate solution for the Eq.(4) under certain boundary conditions is given by Bjerksund & Stensland (1993):

$$V^* = B_0 + (B_\infty - B_0)(1 - e^{h(T)}) \tag{4}$$

Where:

$$\beta = \frac{1}{2} - \frac{(r-\delta)}{\sigma^2} + \sqrt{\left[\frac{(r-\delta)}{\sigma^2} - \frac{1}{2}\right]^2 + \frac{2r}{\sigma^2}}$$

$$B_\infty = \frac{\beta}{\beta - 1}$$

$$B_0 = \max\left[I, \left(\frac{r}{r-\delta}\right)I\right]$$

$$h(T) = -((\rho - \delta)T + 2\sigma\sqrt{T}) * \left(\frac{B_0}{B_\infty - B_0}\right) . \tag{5}$$

When the firm exercises the option to develop the reserve, there is a exchange between investment and reserve value that may take place now or in the future. Then, a general expression for option valuation is of the form:

In a general case when the firm has n projects, the portfolio selection problem reduces to Maximize portfolio's NPV as:

$$Max \sum_{j=1}^{n} NPV_j x_j$$

$$S.t. \sum_{j=1}^{n} I_j x_j \leq I^* .$$

(6)

$$x_j = 0 \, or \, 1$$

Zero-one programming is better than the other portfolio selection methods such as index ranking etc. since it allows optimization of the full budget together with maximum NPV or other DCF's indicator. Considering the real option included in the petroleum projects, the portfolio selection model should reconsider the optimization objective as followed:

$$Max \sum_{j=1}^{N} V_j^* x_j$$

$$S.t. \sum_{j=1}^{n} I_j x_j \leq I^* .$$

(7)

$$x_j = 0 \, or \, 1$$

4   Computational Case

Firm L has 4 oil/gas projects to develop proved reserves under a constrained budget of US\$ 600 million. Table 3 shows the geological and financial aspects of all potential reserves. These reserves present little proportionality among many variables, especially in correlation to reserve's size.

Table 3. Data of the potential projects

Projects	A	B	C	D
Price (US$)	54	54	54	54
B (MMbbl)	500	600	850	620
$\delta(\%)$	2%	1.5%	1.2%	2%
T(year)	25	19	22	15
Investment (MM US$)	150	240	180	250

Considering that all projects present similar geological characteristics and comparable risk features, managers may be tempted to select project A, B, C according to the original decision model based on the NPV rule and the total NPV of the portfolio is 424. And the considering the uncertainty embodied in the oil/gas projects and the flexibility, the manager will select projects A, C, D from the portfolio based on Eq.(4),(5),(7)and the total value is 763 (see table 4).

Table 4. Results from NPV and real option analysis

Projects	A	B	C	D
NPV (M US$)	121	145	158	132
V* (M US $)	253	191	284	226

On the other hand, if these reserves do not reach their respective V*, which would happen because of price reduction or cost increase. In this case, the firm would develop immediately only reserve C, and save a large part of budget to be allocated in more profitable opportunities. Valuable option to wait leads firms to invest only at large positive NPV, the impact of competition drastically erodes the value of the option to wait and leads to investment at very near the NPV threshold. However, this is valid for competitive markets where firms don't have proprietary options, especially in projects of research and development (R&D), and not for proprietary options as the development of reserves, with embodied geological, operational, and financial uncertainties that enrich the option timing.

5   Conclusions

Portfolio selection of oil/ gas projects is a fundamental subject of capital budgeting in the energy sector. In industry, strategic planning requires the selection of a portfolio of projects to advance the corporate goals. In this paper, we discuss the oil/gas projects valuation methods first. Considering the characteristic of the oil/gas project, Real options method is more suitable for the oil/gas project than NPV method, and then a new model extended from the Black-Scholes model is built up. Finally, this paper put forward the portfolio selection model and gives a Computational case.

In this paper, we just discuss the single real option in the oil/gas projects. Actually, the decision-making may be different if option timing is not valuable or easily eroded by competitors. It is difficult if consider the compound option or the role of learning options and synergy between two or more real projects. The impact of sequential investment and active management on the value of a portfolio of real options also will increase the complexity of the problem. In following research, we will continue our research on the portfolio selection of the oil/gas project with compound option or the learning options and synergy between two or more real projects.

References

1. Markowitz, H.: Portfolio Selection, J. of Finance, (1952) 77-91.
2. Luehrman, T.A.: Extending the Influence of Real Options: Problems and Opportunities, paper SPE 71407, presented at the 2001 Annual Technical Conference and Exhibition, New Orleans, Louisiana, 2001.
3. Paddock, J., Siegel, D. and Smith, J.: Option Valuation of Claims on Physical Assets: The Case of Offshore Petroleum Leases, Quarterly Journal of Economics, 103 (1988): 479-508.
4. Trigeorgis L., Real Options: Managerial Flexibility and Strategy in Resource Allocation, MIT Press Cambridge, Massachusetts. 1996
5. Barone-Adesi G. and Whaley R.E. : Efficient Analytical Approximation of American Option Values, Journal of Finance, (1987)301-320
6. Cox J., S. Ross and M. Rubinstein: Option Pricing: A Simplified Approach, Journal of Financial Economics, (1979)229-263
7. Margrabe, W.: The Value of an Option to Exchange One Asset for Another, Journal of Finance, 33(1978) 177-186.
8. Dixit A.K. and Pindyck R.S. :Investment under Uncertainty, Princeton University Press, Princeton, NJ, 1994
9. Copeland T., Koller T. and Murrin J. Valuation: Measuring and Managing the Value of Companies, John Wiley and Sons, NY, 1990
10. Black F. and M. Scholes: The Pricing of Options and Corporate Liabilities, Journal of Political Economy, (1973)637-659
11. Luehrman, Timothy A.: Capital Projects as Real Options: An Introduction, Harvard Business School Technical Note, 1994
12. Dixit, A. K., R. S. Pindyck. Investment Under Uncertainty. Princeton University Press, Princeton, 1994

Fuzzy Real Option Analysis for IT Investment in Nuclear Power Station

Chen Tao, Zhang Jinlong, Liu Shan, and Yu Benhai

School of management, Huazhong University of Science and Technology,
Wuhan, 430074, China
chentaohust@yahoo.com.cn, jlzhang@mail.hust.edu.cn,
liushan@163.com, ybhai@163.com

Abstract. This paper develops a comprehensive but simple methodology to valuate information technology investment in a nuclear power station based on fuzzy risk analysis and real option approach. By linking the variability of expected payoffs to specific sources of risk factors, this method could help decision makers achieve a more reliable valuation of the target investment under multiple sources of risk, and avoid complex estimation tasks at the same time. The proposed approach can be easily adopted to value any irreversible investment subject to a high degree of uncertainty that is common in the field of energy economics.

Keywords: information technology investment, real options analysis, risk assessment, nuclear industry.

1 Introduction

Real options analysis (ROA) has been accepted as a modern approach for risk investment analysis. In recent years, this approach has been rapidly evolving, and is now spreading to the field of energy economics. It is ideally suited for the valuation of investments in tangible assets and infrastructure like energy generation plants that are subject to a high degree of uncertainty. Similar to energy investment, information technology (IT) investment is characterized by the nature of Long-time horizons, significant risks and irreversibility. Researchers propose to introduce ROA to IT investment decision-making. Benaroch and Kauffman illustrated the use of real options techniques in the context of a decision to expand a banking ATM network [1]. Taudes suggested that the value of IT investment can be defined as the sum of economic value and option value [2]. L. milder et al. use ROA to value an IT infrastructure investment in South Korea [3].

However, several challenging preliminary requirements has prevented the application of real options theory in practice. For example, Black–Scholes option pricing model requires the variance per period of rate of return on the asset must be estimated. In fact, obtaining such a reliable estimation of the variance is usually very difficult [1]. Furthermore, option pricing model generally assumes that the expected payoffs are characterized by certain probably distributions, geometric Brownian

motion, for instance. Unfortunately, there does not always exit an efficient market which could justify the assumption on stochastic phenomena. The use of assumption on purely stochastic phenomena may lead to improper investment valuation.

In this paper, we present a comprehensive but simple methodology to evaluate IT investment in a nuclear power station based on real options and fuzzy set theory. Fuzzy risk analysis is able to well formulate the uncertainty of the expected payoffs from an investment, moreover simplifies the real option model in certain degree. This approach will help investors acquire insights about the influence of risk factors on the expected payoff, and then make better valuation and justification of the target investment without complex mathematical calculation.

2   A Fuzzy Approach to Real Option Valuation

In this section, we present a new real option approach to value IT investment in nuclear industry. The investment valuation process consists of five stages. In what follows, we explain these steps in details.

Step 1: Risk identification

The first step is to identify the potential risk factors associated with IT investment, and then give a list of the most significant risks. There exist a great variety of risk factors that threaten the success of IT investment. Recently, Benaroch classified the IT investment risks identified by IS research stream into three categories, including firm-specific risks, competition risks and market risks [4].

Step 2: Estimate the risk factors

We assess risk factors largely employing the fuzzy evaluating method present by Ngai [5]. For simplicity of formulation, we adopt triangular fuzzy numbers to characterize the membership function of the linguistic terms. The triangular fuzzy numbers of each linguistic term are set as the same as Ngai does.

Step 3: fuzzy assessment aggregation

Our risk analysis methods allow more than one evaluator to assess the potential risk factors that affect the expected payoffs of an IT investment. After then, the fuzzy average operation is used to balance the deferent judgments from all evaluators. Supposing there are n evaluators and let $A_i = (a_1^{(i)}, a_M^{(i)}, a_2^{(i)})$ be the fuzzy numbers, i $=1,\ldots$, n. Then, we can get the triangular average mean:

$$A_{average} = (m_1, m_M, m_2,) = (\frac{1}{n}\sum_{i=1}^{n}a_1^{(i)}, \frac{1}{n}\sum_{i=1}^{n}a_M^{(i)}, \frac{1}{n}\sum_{i=1}^{n}a_2^{(i)}) \qquad (1)$$

After obtaining the fuzzy average of the likelihood and severity of each risk factor, we start to formulate the overall risk level of the IT investment under consideration. Fuzzy weighted average (FWA) is a commonly used operation in risk and decision analysis. To reduce the complexity of comparisons and arithmetic operation, we utilize an efficient fuzzy weighted average algorithm (EFWA) suggested by Lee and Park [6].

Step 4: determine expected payoffs and its standard deviation

The result of the calculated fuzzy weighted average is a fuzzy number, which represents the overall risk faced by IT investment under consideration. Since our purpose is to valuate the real option value of the investment, it's required to estimate the expected payoffs and its standard deviation. We calculate the expected payoffs using the following formula:

$$V = V^0 - E(V^0)\overline{R} \tag{2}$$

Where V^0 is the initial value of payoffs estimated by decision makers not considering risk factors, $E(V^0)$ denotes the possibilistic mean value of the initial estimation of payoffs. V is the revised expected payoffs taking into account the probable change range of payoffs caused by risk factors. $V^0 = (V^0_1, V^0_M, V^0_2)$, $\overline{R} = (\overline{R}_1, \overline{R}_M, \overline{R}_2)$ and $V = (V_1, V_M, V_2)$ are all fuzzy figures.

Supposing $A = (a_1, a_M, a_2)$ be a triangular fuzzy number then the possibilistic expected value of A is [7]

$$E(A) = \int_0^1 \gamma[a_1 + \gamma(a_M - a_1) + a_2 - \gamma(a_2 - a_M)] \, d\gamma = \frac{2}{3}a_M + \frac{1}{6}(a_1 + a_2) \tag{3}$$

Using the addition and scalar multiplication rules for arithmetic operations on triangular fuzzy numbers, we have

$$V = (V_1, V_M, V_2) = (V^0_1 - E(V^0)\overline{R}_2, V^0_M - E(V^0)\overline{R}_M, V^0_2 - E(V^0)\overline{R}_1) \tag{4}$$

[7] also introduced the possibilistic variance of fuzzy number V as

$$\sigma^2(V) = \frac{1}{2}\int_0^1 \gamma[(V_2 - V_1)(1 - \gamma)]^2 \, d\gamma = \frac{(V_2 - V_1)^2}{24} \tag{5}$$

Step 5: the real option valuation of the investment

In the last step, we can assess the real option value of the investment based on the result obtained above. For the purpose of simplicity, we assume that only the expected payoff is uncertain and utilize the Black-Scholes pricing model. Then the fuzzy real option value of an investment is [8]

$$FROV = VN(d_1) - X e^{-rT} N(d_2) \tag{6}$$

Where $d_1 = \dfrac{In(E(V)/X) + (r + \sigma^2/2)T}{\sigma\sqrt{T}}$, $d_2 = d_1 - \sigma\sqrt{T}$

Only V is fuzzy numbers. E(V) and σ represent respectively the possibilistic expected value and the standard deviation of fuzzy figure V. The computing result FROV is also a fuzzy number, representing the real option value of the investment under consideration.

3   Numerical Examples

The Daya Bay Nuclear Power Station, completed in 1996, is located on the coast of the Daya Bay in Guangdong Province, China. In order to maintain efficiency and competency, Daya Bay Nuclear Power Station utilizes information technology applications extensively. The company's Corporate Operation Management Information System (COMIS), has already become an indispensable management platform for its daily operation activities such as preventive maintenance, inventory management, procurement planning, et al.

Recently, the power station plan to establish a supplier relationship management (SRM) system to gain a more reliable supplying source of spares and services it uses. However, valuation of this investment is a challenging task because of uncertainties associated with the investment payoff and cost. In this section, we apply the fuzzy real option valuation approach introduced above to evaluate the SRM investment in Daya Bay Nuclear Power Station. Our purpose is to illustrate how the real option value of an investment could be calculated in fuzzy terms.

To valuate the real option value of the investment, it's required to estimate the expected payoffs and its standard deviation. Therefore, a series of interviews with senior managers in the power station are conducted. The expected payoff come from the SRM investment can be initially estimated as fuzzy triangular figure, which is $V^0 = (\ V^0{}_1, V^0{}_M, V^0{}_2) = $ (\$376000, \$387166, \$398332). Let $E(V^0)$ denote the possibilistic expected value of fuzzy figure V^0, then

$$E(V^0) = \frac{2}{3} \times 387166 + \frac{1}{6} \times (376000 + 398332) = \ \$387,166 \qquad (7)$$

Table 1. Mapping of the SRM investment risks and its assessment

Risk factors	Evaluator A		Evaluator B	
	Likelihood	Severity	Likelihood	Severity
Factor 1	Medium (0.25,0.5,0.75)	High (0.5,0.75,1)	Medium (0.25,0.5, 0.75)	Critical (0.75,1,1)
Factor 2	Medium (0.25,0.5,0.75)	Moderate (0.25,0.5,0.75)	Unlikely (0, 0.25, 0.5)	Moderate (0.25,0.5,0.75)
Factor 3	Unlikely (0, 0.25, 0.5)	Low (0, 0.25, 0.5)	Unlikely (0, 0.25, 0.5)	Low (0, 0.25, 0.5)
Factor 4	Medium (0.25,0.5,0.75)	Moderate (0.25,0.5,0.75)	Medium (0.25,0.5,0.75)	Moderate (0.25,0.5,0.75)

The time horizon of the investment is considered to be 3 years, and $400,000 is needed to develop the system. We use 50% to compute the investment opportunity. There may be a number of risk factors that affect the expected revenue and the deviation of revenues, such as incorrect requirements definition, unfavorable attitudes by users, insufficient experience among team members, or inadequate cooperation of suppliers. Since our purpose is to provide an illustration on calculating process, we simply assume the risks associated with the SRM investment could be mapped as table 1.

Table 2. Results of fuzzy average of all risk factors

Risk factors	Fuzzy average of likelihood(W_i)	Fuzzy average of severity(R_i)
Factor 1	(0.25,0.5,0.75)	(0.625,0.875,1)
Factor 2	(0.125,0.375,0.625)	(0.25,0.5,0.75)
Factor 3	(0, 0.25, 0.5)	(0, 0.25, 0.5)
Factor 4	(0.25,0.5,0.75)	(0.25,0.5,0.75)

The fuzzy averages of each risk factor are showed in table 2. And then, the EFWA algorithm can be used to calculate the overall risk level of the SRM investment. Following the computational procedure defined in EFWA algorithm, we can obtain the resulting membership function of the fuzzy weighted average as $\overline{R}$ = (0.2222, 0.5769, 0.9167). This triangular fuzzy figure represents the overall risk faced by the investment.

Consequently, the revised expected payoffs incorporating the overall risk level can be obtained:

$$V = V^0 - E(V^0)\overline{R} = (\$21085, \$163810, \$312304)$$
$$E(V) = \frac{2}{3} \times 163810 + \frac{1}{6} \times (21085 + 312304) = \$164,771.50 \tag{8}$$

The standard deviation of expected payoffs can be calculated as

$$\sigma(V) = \sqrt{\frac{(V_2 - V_1)^2}{24}} = \sqrt{\frac{(312304 - 21085)^2}{24}} = 59444.79 \tag{9}$$

i.e. $\sigma(V)$ = 36%. The last step is to valuate the investment using real option pricing model. We set the other parameters required by Black-Scholes formula as T = 3, X = $400,000, r = 7%. Then

$$FROV = VN(d_1) - X\,e^{-rT}N(d_2)$$

$$\text{Where } d_1 = \frac{In(164771.5/400000) + 3(0.07 + 0.36^2)}{0.36\sqrt{3}} \qquad (10)$$

$$d_2 = \text{-}0.77382\text{-}0.36\sqrt{3} = \text{-}1.39736$$

Thus, we can calculated that the fuzzy value of the real option is
FROV = ($21684, $9647, $42244).

4 Concluding Remarks

Real option analysis is a useful tool to formulate the investment decision in uncertain environment, the energy investment, for instance. However, several minor limitations of ROA has prevented its application in practice, even could lead to incorrect valuation. This paper developed a comprehensive but easy-to-use methodology to solve the complicated evaluation problem of ROA.

The valuation approach we present has incorporated fuzzy risk analysis and real option valuation. By utilizing risk analysis based on fuzzy set theory, decision makers could capture the effect of specific risk factors on the expected payoffs, thus obtain a more reliable estimation about parameters of the real option valuation model. It in turn provides a basis for a better evaluating and justifying of the target investment, and avoid complex estimation task at the same time. A numerical example, which involves an SRM investment in a nuclear power station, is presented to illustrate the proposed procedures. We are confident that this method is valuable to help managers produce a well-structured valuation process in information technology investment in nuclear industry. Besides, the approach can be easily applied in the fields of energy economic analyses, such as the evaluation of power plants, building transmission assets, or the adoption of energy efficient technologies.

References

1. Benaroch, M., Kauffman, R.J.: Justifying electronic banking network expansion using real options analysis. MIS Quarterly 24 (2000) 197–225
2. Taudes, A., Feurstein, M., Mild, A.: Options analysis of software platform decisions: a case study. MIS Quarterly 24 (2000) 227– 243
3. Miller, L., Choi, S.H., Park, C.S.: Using an options approach to evaluate Korean information technology infrastructure. The Engineering Economist 49 (2004) 199-219
4. Benaroch, M.: Managing Information Technology Investment Risk: A Real Options Perspective. Journal of Management Information Systems 19 (2002) 43-84

5. Ngai, E.W.T., Wat, F.K.T.: Fuzzy decision support system for risk analysis in e-commerce development. Decision Support Systems 40 (2005) 235-255
6. Lee, D.H., Park, D.: An efficient algorithm for fuzzy weighted average. Fuzzy Sets and Systems 87 (1997) 39–45
7. Carlsson, C., Fuller, R.: On possibilistic mean value and variance of fuzzy numbers. Fuzzy Sets and Systems 122 (2001) 315-326
8. Carlsson, C., Fuller, R.: A fuzzy approach to real option valuation. Fuzzy sets and systems 139 (2003) 297-312

A Variable Precision Fuzzy Rough Group Decision-making Model for IT Outsourcing Risk Evaluation in Nuclear Power Industry

Guodong Cong, Jinlong Zhang, and Benhai Yu

College of management, Huazhong University of Science and Technology
Luoyu road 1037, Wuhan, 430074, China
gd_cong@smail.hust.edu.cn, jlzhang@mail.hust.edu.cn,
ybhai@163.com

Abstract. Risks evaluation is critical for the success of IT outsourcing. It is especially important in nuclear industry due to high concerns about safety and service quality. This paper proposes a new integrated methodology, Variable Precision Fuzzy Rough Group Decision-making (VPFRGDM), to evaluate the risk in IT outsourcing. This method can improve fairness, flexibility and efficiency of risk evaluation, and is verified by a case in a large-scale nuclear power station.

Keywords: Risk evaluation VPFRGDM Nuclear industry.

1 Introduction

In China, nuclear industry is facing pressure of competition as the country's energy policy offers it no protection. Stations expect IT outsourcing to minimize costs and improve efficiency. However, they have experienced many failed and undesirable consequences, which are partially due to extremely high safety and service quality requirements. It is urgent for the stations to find an advanced and practical methodology to enhance competitive advantages with less cost and better IT service.

There have been many papers that have investigated IT outsourcing related risks. Validated measures of risk factors based on Transaction Cost Theory (TCT) [1], method to identify/assess risk [2]. However, papers mentioned above focus mainly on analyzing framework or prioritization of risk, yet further emphasis is needed on quantitative methodology. Additionally, the capability of handling potential error and the efficiency of the approaches need improvement.

This paper proposes a new model called Variable Precision Fuzzy Rough Group Decision-making (VPFRGDM) to evaluate IT outsourcing risk in the nuclear industry. Firstly, historical knowledge is represented in a fuzzy decision table(FDT) based on TCT; Then, based on VPFRS[3] and fuzzy TOPSIS approach[4], it evaluates the risk under a certain admissible inclusion error β and the whole error interval. The model further reduces the bias in fuzzy group decision-making (FGDM), improves the efficiency in IT outsourcing risk decision-making.

This paper is organized as follows: Section 2 describes the proposed model in detail. Section 3 provides a case of a synthetic evaluation of IT outsourcing risk. Section 4 then provides the final concluding remarks and future work required.

2 The VPFRGDM Model

Let U be a non-empty set of finite objects (the universe of discourse). Consider a fuzzy compatibility relation R, fuzzy set F and denote by X_i a compatibility class on U. With a given admissible inclusion error β, the mean rough fuzzy β-approximations $\mu_{\underline{R}_\beta}F(X_i)$ is defined in [3].

Assume that there are a total of m conditional features, denoted by C_i ($i=1, 2,..., m$), one decision feature, denoted by D; n evaluators and N possible alternatives. IT outsourcing risk evaluation will be dealt with Fuzzy TOPSIS [4]. The proposed model consists mainly of three steps:

Step 1: Calculate the weight of feature and evaluator
The weight of feature C_i will be:

$$W_{C_i}^\beta = \gamma_{C_i}^\beta(D) / \sum_i \gamma_{C_i}^\beta(D) \quad i = 1,2,...m \tag{1}$$

where $\gamma_{C_i}^\beta(D) = \sup_{X_j \in U/C_i} \sup_{F \in U/D} \{\mu_{\underline{R}_\beta}F(X_j)\}$.

Initially, each evaluator will give linguistic evaluation to each alternative and linguistic evaluation is turned into Triangular Fuzzy Number(TFN) [5]. Then the weight of each evaluator $W_{E_k}^\beta$ ($k=1,..., n$) will be calculated by mutual distance between TFN as shown in [6].

Step 2: Evaluate the risk of each alternative under a given β
Under a given β‹the distance of alternative i to fuzzy positive ideal solution and that to fuzzy positive ideal solution, the relative closeness to the ideal solution of alternative i ,denoted by $d^\beta(\tilde{A}_i, \tilde{A}^*)$, $d^\beta(\tilde{A}_i, \tilde{A}^-)$ and RC_i^β respectively, will be attained according to [4].

Step 3: Evaluate the risk on the whole admissible inclusion error interval $[0, \alpha]$

From the process, it is easy to know that $W_{C_i}^\beta$ and $W_{E_k}^\beta$ are linear functions of β ($\forall i \in [1,m], k \in [1,n]$). Consequently, function $d^\beta(\tilde{A}_i, \tilde{A}^*)$ and $d^\beta(\tilde{A}_i, \tilde{A}^-)$ are Riemann integral. Then the mean positive distance will be $\overline{d(\tilde{A}_i, \tilde{A}^*)} = \frac{1}{\alpha}\int_0^\alpha d^\beta(\tilde{A}_i, \tilde{A}^*)\,d\beta$ (2)

and similarly will be the mean negative distance $\overline{d(\tilde{A}_i, \tilde{A}')}$.

Thus, the mean risk of alternative i will be

$$RC_i = \overline{d(\widetilde{A}_i, \widetilde{A}^-)} \Big/ \left[\overline{d(\widetilde{A}_i, \widetilde{A}^-)} + \overline{d(\widetilde{A}_i, \widetilde{A}^*)} \right], \quad i = 1, 2, ..., N \tag{3}$$

3 A Numerical Case

The numerical case is from a famous nuclear power station in China, Nuclear Power Company (NPC). The IT staff established the index system and generated FDT, as shown in Table 1. In Table 1, 'L', 'M' and 'H' represents 'low', 'medium' and 'high' respectively. Data is the membership of an object belongs to the class.

Table 1. Fuzzy Decision Table of Risks in outsourcing IT operations

U	Transaction			Client			Supplier			Risk of decision		
	L	M	H	L	M	H	L	M	H	L	M	H
1	0.8	0.2	0	0	0.3	0.7	0.7	0.3	0	0.8	0.2	0
2	0.7	0.3	0	0.2	0.8	0	0.7	0.3	0	0.5	0.5	0
3	0.5	0.5	0	0.2	0.7	0.1	0.6	0.3	0.1	0.3	0.7	0
4	0.2	0.7	0.1	0.1	0.7	0.2	0.9	0.1	0	0.7	0.3	0
5	0.2	0.8	0	1	0	0	0.6	0.4	0	0.7	0.3	0
6	0	0.8	0.2	0	0.1	0.9	1	0	0	0.3	0.7	0
7	0.2	0.8	0	0.7	0.3	0	0.1	0.6	0.3	0.1	0.8	0.1
8	0	0.4	0.6	0.9	0.1	0	0.8	0.2	0	0.5	0.5	0

This time, NPC is about to choose the IT outsourcing service providers from four alternatives. Herein the threshold of inclusion error is $\alpha = 0.3$.

The evaluation results, under various β and the mean method, are shown in Table 2. According to Table 2, the final decision-making is to choose alternative 3

Table 2. The rating and ranking results

Alternative	$\beta \in [0,0.2)$		$\beta \in [0.2,0.25)$		$\beta \in [0.25,0.3]$		Mean	
	RC_i	Rank	RC_i	Rank	RC_i	Rank	RC_i	Rank
1	0.699	3	0.582	3	0.643	2	0.674	3
2	0.116	4	0.193	4	0.212	4	0.139	4
3	0.742	2	0.749	1	0.821	1	0.754	1
4	0.759	1	0.716	2	0.583	3	0.729	2

With the results in Table 2 compared, it is easy to see that the ranks of 1, 3, and 4 are varying. The reason of these variations is violent fluctuations in weights of features when β is small. When $\beta > 0.2$, the evaluation turns to be stable and more reasonable. It is evidence that the classification error and its associated negative influence are under better control. The final result is clear and convincing, which demonstrates the effectiveness of the mean method to eliminate bias.

4   Conclusion

This paper aims at facilitating evaluation of IT outsourcing risk in the nuclear industry, proposes a model to evaluate IT outsourcing risk. The model retains the advantages of FGDM and improves fairness, flexibility, versatility and efficiency in IT outsourcing risk measurement and decision-making, which is verified by the case of the company NPC.

The model could also be generalized to other risk domains and GDM methodology. Further research may be conducted in searching for fuzzy rules and fuzzy reasoning in risk knowledge discovery in order to optimize the risk decision-making.

Acknowledgement

References

1. Bahli, B., Rivard, S.: Validating Measures of Information Technology Outsourcing Risk Factors. Omega 33(2005) 175-187
2. Currie, W.L.: A Knowledge-based Risk Assessment Framework for Evaluating Web-enabled Application Outsourcing Projects. Int. J. Project Management 3(2003) 207-217
3. Mieszkowicz-Rolka, A., Rolka, L.: Variable Precision Fuzzy Rough Sets. In: James F. Peters - Andrzej Skowron (chief eds.): Transactions on Rough Sets I. Lecture Notes in Computer Science, vol. 3100. Springer Berlin / Heidelberg New York (2004) 144-160
4. Chen, C.T.: Extensions of the TOPSIS for Group Decision-making under Fuzzy Environment. Fuzzy Sets and Systems, 114(2000) 1-9
5. Laarhoven, P.J.M., Pedrycz, W.: A Fuzzy Extension of Saaty's Priority Theory. Fuzzy Sets and System 3(1983) 229-241
6. Xie,G., Zhang, J.L., Lai, K.K.: A Group Decision-Making Model of Risk Evasion in Software Project Bidding Based on VPRS. In: Dominik Slezak, JingTao Yao, James F. Peters, Wojciech Ziarko and Xiaohua Hu (eds.): Rough Sets, Fuzzy Sets, Data Mining, and Granular Computing Lecture Notes in Computer Science, vol. 3642. Springer Berlin / Heidelberg New York (2005) 530-538

A New Hybrid Approach for Analysis of Factors Affecting Crude Oil Price

Wei Xu[1], Jue Wang[2], Xun Zhang[2], Wen Zhang[1], and Shouyang Wang[1,2]

[1] School of Management, Graduate University of Chinese Academy of Sciences,
Chinese Academy of Sciences, Beijing, 100080, China
{xuw-06b1,zhangwen05}@mails.gucas.ac.cn
[2] Institute of Systems Science, Academy of Mathematics and Systems Science,
Chinese Academy of Sciences, Beijing, 100080, China
{wjue,zhangxun,sywang}@amss.ac.cn

Abstract. In this paper, a new hybrid approach is presented to analyze factors affecting crude oil price using rough set and wavelet neural network. Related factors that affect crude oil price are found using text mining technique and Brent oil price is chosen as the decision price because it plays an important role in world crude oil markets. The relevant subsets of the factors are discovered by rough set module and the main factors are got, and then the important degrees of these are measured using wavelet neural network. Based on the novel hybrid approach, the predictability of crude oil price is discussed.

Keywords: crude oil price, rough set, wavelet neural network, prediction.

1 Introduction

The high volatility and irregularity of crude oil market creates uncertainty, mainly because of the interaction of many factors in crude oil markets. How to analyze and use these factors to forecast the crude oil price has attracted increasing attention from academics and practitioners in the past decade. The literature on factors affecting crude oil price relates oil shocks either to the instability of the market structures or to the effect of the price elasticity of demand [1-4]. Mork [1] and Huntington [2] demonstrated the asymmetric relationship that a reduction in oil prices does not necessarily lead to noticeable output growth, while an increase can have a negative impact on output growth. The study of Ferderer points to the observation that disruptions in oil market not only give rise to higher prices, but also increase oil price volatility [3]. C.W.Yang [4] analyze factors affecting price volatility of the US oil market by examining the market structure of OPEC, the stable and unstable demand structure, and related elasticity of demand.

However, there are still several unsolved issues with the above methods. The first problem is that only a few factors, such as demand and supply, are taken into account in the researchers' models. In fact, many other factors have a combined effect on crude oil prices: economic, military, natural disasters and speculation, as well as people's expectations. These important factors can be hard to handle and they are not

included in the traditional models. The second problem is how to quantify the qualitative factors. Some qualitative variables, such as political variables, are not easy to quantify due to uncertainty. Furthermore, related data collection is very difficult. Thus, the above proposed models are not easy to operate or impractical. Therefore, it is important that new methods be developed for factors analysis.

Considering the discussed above, we present a new hybrid approach for factors affecting oil price analysis based on rough set (RS) and wavelet neural network (WNN). The related factors that affect oil price are found using text mining technique. The relevant subsets of the factors are discovered by rough set module and the main factors are got. The important degrees of these are measured using wavelet neural network. Based on the novel hybrid approach, the predictability of crude oil price is discussed. Finally, we draw the conclusions.

2   A Hybrid Approach Based on RS and WNN

2.1   Basic Concepts of Rough Set Theory

The theory of rough set (RS), proposed by Pawlak [5-6], has been proved to be a powerful tool for handling various types of data. Several models based on original rough set theory have been presented to solve different problems [7-8]. It has important applications to artificial intelligence and economic and financial prediction [9-10], as a tool for dealing with vagueness and uncertainty of facts, and in classification.

The set about objects is represented in the form of an information system. The rows of the information system are labeled by objects, whereas columns are labeled by attributes and entries of the information system are attribute values.

Formally, an information system (IS) is an quadruple $\varphi = (U, AT, V, f)$, where U is a finite nonempty set of objects and AT is a finite nonempty set of attributes, $V = \cup_{a \in AT} V_a$ and V_a is a domain of attribute a, f: $U \times AT \rightarrow V$ is a total function such that $f(x, a) \in V_a$ for every $x \in U$, $a \in AT$, called an information function. An IS can be seen as decision system assuming attributes concluding two part (AT D), and $AT \cap D = \phi$, where AT is called condition attributes and D contains decision attributes.

Let $R_A = \{(x, y) \in U \times U: f_a(x) = f_a(y), \forall a \in A\}$. The relation R_A thus partitions the universe of discourse U into disjoint subsets called equivalence classes, and the result is denoted by U/A which forms a partition of U. The equivalence class including x is denoted by $[x]_A$, that is, $[x]_A = \{y \in U: (x, y) \in R_A\}$. The sets in the partition U/A are referred to as A-elementary sets. Objects from $[x]_A$ are indiscernible with regard to their descriptors in the system. Given an arbitrary set $X \subseteq U$, it may be impossible to describe X precisely using the equivalence classes in U/A. In this case, one may characterize X by a pair of lower and upper approximations:

$$\underline{A}(X) = \left\{ x \in U : [x]_A \subseteq X \right\} \tag{1}$$

$$\overline{A}(X) = \left\{ x \in U : [x]_A \cap X \neq \phi \right\} \tag{2}$$

The lower approximation $\underline{A}(X)$ is the set of objects that belong to X with certainty, while the upper approximation $\overline{A}(X)$ is the set of objects that possibly belong to X.

In an IS, if $R_B = R_{AT}$, $B \subseteq AT$, then B is referred to as a consistent set of φ. If $B \subseteq AT$ is a consistent set of φ, and no proper subset of B is a consistent set of φ, then B is referred to as a reduction of φ. Similarly, In decision system, $\varphi = (U, AT, V, f, D)$, satisfying $R_{AT} \subseteq R_D$, if $R_B \subseteq R_D$, $B \subseteq AT$, then B is referred to as a consistent set of φ. If $B \subseteq AT$ is a consistent set of φ, and no proper subset of B is a consistent set of φ, then B is referred to as a reduction of φ.

2.2 Basic Concepts of Wavelet Neural Network

Wavelet neural network (WNN) is a novel approach towards the learning function [11]. Wavelet networks, which combine the wavelet theory and feed-forward neural networks, utilize wavelets as the basis function to construct a network. Wavelet function is a local function and influences the networks' output only in some local ranges. The wavelet neural network shows surprising effectiveness in solving the conventional problems of poor convergence or even divergence encountered in other kinds of neural networks [12]. The WNN consists of three layers: input layer, hidden layer and output layer. The connections between input-hidden units and hidden-output units are called weights u_{ti} and w_t, respectively. A Morlet mother function is used as node activation function for the hidden layer. The dilation and translation parameters, a_t and b_t, of the Morlet function for each node in the hidden layer are different and they need to be optimized. In the WNN, the gradient descend algorithm is employed and the error is minimized by adjusting u_{ti}, w_t, a_t and b_t parameters [13]. In the WNN, the following steps are carried out:

Step1. Initializing the dilation parameter a_t, translation parameter b_t and node connection weights u_{ti}, w_t to some random values. All those random values are limited in the interval (0, 1).

Step2. Inputting data $x_n(i)$ and corresponding output values v_n^T, where the superscript T represents the target output state.

Step3. Propagating the initial signal forward through the network:

$$v_n^T = \sum_{t=1}^{T} w_t h \left(\frac{\sum_{i=1}^{s} u_{ti} x_n(i) - b_t}{a_t} \right) \tag{3}$$

Where h is taken as a Morlet wavelet

$$h(t) = \cos(1.75t) \exp\left(-\frac{t^2}{2}\right) \tag{4}$$

Step4. Calculation of the WNN parameters: $\Delta w_t = -\eta \dfrac{\partial E}{\partial w_t} + \alpha \Delta w_t$, $\Delta u_{ti} = -\eta \dfrac{\partial E}{\partial u_{ti}} + \alpha \Delta u_{ti}$,

$\Delta a_t = -\eta \dfrac{\partial E}{\partial a_t} + \alpha \Delta a_t$, $\Delta b_t = -\eta \dfrac{\partial E}{\partial b_t} + \alpha \Delta b_t$, the error function E is taken as $E = \dfrac{1}{2}\sum_{n=1}^{N}\left(v_n^{\ T} - v_n\right)^2$, and $v_n^{\ T}$, v_n are the experimental and calculated values, respectively. N stands for the data number of training set, and η and α being the learning rate and the momentum term, respectively.

Step5. The WNN parameters were changed until the network output satisfies the error criteria.
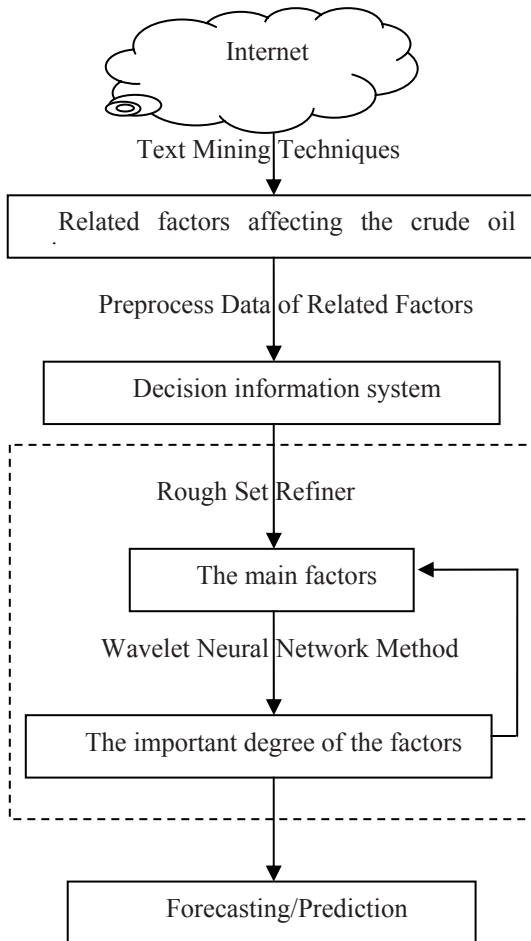
Fig. 1. The Main Process of the Proposed Hybrid Approach

2.3   A Hybrid Approach Based on RS and WNN

As revealed in previous two subsections, rough set theory is a powerful mathematical tool that handles vagueness and uncertainty. It can reduce the attributes from the large database and get the most important, but it can't find the important degree from the reduced attributes. However, wavelet neural network can did a good work on getting the important degree of the input, but its input variables are limited because of the algorithm's speed and astringency. In view of this point, a new hybrid approach— RSWNN approach— is proposed for factors affecting oil price analysis.

The proposed approach consists of three modules: the text mining module, the rough set module and the wavelet neural module. In the first module, as the preprocessing text mining techniques are used to mine the related factors affecting the oil price. The text mining theory is a powerful technique which draws on information retrieval, data mining, machine learning, statistics and computational linguistics [14-15]. The text mining process consists of four major stages: collecting documents, preprocessing documents, feature extraction, and metadata mining. The details have been given in Ref. [16]. In the second module, rough set theory is used as a refiner for the factors mining from the text mining technique. In the third module, WNN are used to measure the important degree of the factors getting from the rough set refiner. Based on the proposed approach, the predictability of crude oil price is discussed. Generally, the process of the proposed hybrid approach is illustrated in Fig. 1.

As can be seen from Fig. 1, the novel hybrid approach is actually an intelligent analysis system. Text mining techniques are used to mine the related factors affecting the crude oil price automatically. Decision information system is got through preprocessing the data of the related factors. And then as the main body the rough set refiner is used to find the main factors from a large number of factors affecting the crude oil price while the wavelet neural network are used to measure the important degree of the factors getting from the rough set refiner. Finally, based on the proposed approach, the predictability of crude oil price is discussed.

3   An Application of the Hybrid Approach

3.1   Presentation of the Text Mining Results and the Data

In Section 2.3, the text mining stages are described. In this section, the factors called attributes or metadata are presented in conjunction with crude oil price. Then "crude oil price, factor", "crude oil market, factor" and "crude oil volatility, factor" are used as keywords to search related data, including some numeric and textual data. We obtain the following factors affecting crude oil price, as shown in Table 1.

We select annual data of these attributes because of analyzing the long-run factors affecting oil price. The sources of these data are in the EIA, Reuters and IFS and the period of the data begin from 1970, and end of 2005. We choose Brent oil price as the decision attribute d because it plays an important role in world crude oil markets.

Table 1. The Factors Affecting Crude Oil Price

No	Factors	No	Factors	No	Factors
a_1	world total demand	a_{13}	Core OPEC production capacity	a_{25}	OPEC oil embargo
a_2	world total supply	a_{14}	Non-OPEC production	a_{26}	economic sanction to oil nations
a_3	China/U.S. foreign exchange rate	a_{15}	Non-OPEC production capacity	a_{27}	large oil company merger
a_4	Japan / U.S. foreign exchange rate	a_{16}	fuel switching capacity	a_{28}	rumors and false news
a_5	France / U.S. foreign exchange rate	a_{17}	OECD total stocks	a_{29}	oil worker strike
a_6	U.S. / U.K foreign exchange rate	a_{18}	world total reserves	a_{30}	hostage crisis
a_7	world economy growth	a_{19}	the distance in wells	a_{31}	terrorist attack
a_8	speculation	a_{20}	the number of drilling wells	a_{32}	political conflict in oil nations
a_9	OPEC market share	a_{21}	the number of oil wells	a_{33}	revolutions in oil countries
a_{10}	forward price of crude oil	a_{22}	gasoline tax rate	a_{34}	wars in oil countries
a_{11}	OPEC production	a_{23}	oil import fee	a_{35}	geopolitics
a_{12}	Core OPEC production	a_{24}	CO_2 limit	a_{36}	natural disasters related to oil

3.2 Presentation of the Rough Set Results

The above forms an information table $\varphi = (U, AT, V, f, D)$. The continuous attributes are discredited by setting norms dividing the original domains of the attributes into sub-intervals using equal frequency method.

The rough set analysis of the IS has been performed using an attribute reductions algorithm with genetic algorithm. 85 reductions were obtained based on the IS. They contain 5-8 attributes, which are considerably smaller than 36-the total number of attributes. This result gives the idea of reduction a strong support because each of the reductions contains fewer attributes, but, on the other hand, ensures the same value of quality of approximation as the whole set of attributes AT.

The proper reduction is selected among these reductions. The selection is based on two criteria: the reduction should contain as small a number of attributes as possible, and the reduction should not miss the attributes judged by the experts as the most significant factors. As a result, the reduction selected, as the main factors affecting the crude oil price, was the #31, which includes: a_1 (world total demand), a_2 (world total supply), a_4 (Japan / U.S. foreign exchange rate), a_6 (U.S. / U.K foreign exchange rate), a_7 (world economy growth) and a_{17} (OECD total stocks).

3.3   Presentation of the Wavelet Neural Network Results

In this subsection the important degree of the main factors - a_1 (world total demand), a_2 (world total supply), a_4 (Japan / U.S. foreign exchange rate), a_6 (U.S. / U.K foreign exchange rate), a_7 (world economy growth) and a_{17} (OECD total stocks) is got using wavelet neural network. In this module, the input variables are the data of these main factors and the output variable is the Brent oil price.

   The wavelet neural network is constructed based on these selected variables. In order to improve the algorithm stability and quicken the training, the input variables and the output variables are normalized respectively before training the WNN so that the data of learning samples are varied within small bound. The epoch is stopped when MSE satisfied the given error criterion. As a result, the selected input variables with their important degree in parentheses were world total demand (0.2021), world total supply (0.1745), Japan / U.S. foreign exchange rate (0.1953), U.S. / U.K foreign exchange rate (0.1011), world economy growth (0.1672) and OECD Total Stocks (0.1607). The important degree of the input variables describes the influence of these factors to the crude oil price.

   As can be seen above, world total demand and supply are the most important factors affecting crude oil price, and relatively demand is dominant. Crude oil stock can reduce the volatility of crude oil price. World economy growth and exchange rates also affect the crude oil price and increase the volatility of crude oil price.

3.4   The Predictability of the Proposed Approach

In this subsection, we discuss the predictability of the proposed approach. The annual data of these main factors and Brent oil price in 1970-2002 are used as training data, and the annual data in 2003-2005 are used as testing data. The result shows that MSE of the testing data is 2.94%. The hybrid approach can be used as a tool for crude oil price forecasting and improve the long-run prediction quality in view of empirical results.

4   Conclusions

In this paper, a new hybrid approach is presented to analyze factors affecting crude oil price using rough set and wavelet neural network. World total demand, world total supply, Japan / U.S. foreign exchange rate, U.S. / Euro foreign exchange rate, world economy growth and OECD total stocks are the main factors, and the important degree are found. In future work we will construct an intelligent system based on the proposed approach for forecasting crude oil price and compared with other models.

References

1. Mork K.A., Oil and the Macroeconomy When Prices Go Up and Down: an Extension of Hamilton's Results. Journal of Political Economy, 97 (1989) 740-744
2. Huntington H.G., Crude Oil Prices and US Economic Performance: Where Does The Asymmetry Reside? The Energy Journal, 19(4) (1998) 107-132

3. Ferderer J.P., Oil Price Volatility and the Macroeconomy: a Solution to the Asymmetry Puzzle. Journal of Macroeconomics, 18 (1996) 1-16
4. C.W. Yang, M.J. Hwang and B.N. Huang, An Analysis of Factors Affecting Price Volatility of the US Oil Market. Energy Economics, 24 (2002) 107-119
5. Pawlak Z., Rough Set. International Journal of Computer and Information Sciences, 11(5) (1982) 341-356
6. Pawlak Z., Rough Sets: Theoretical Aspects of Reasoning About Data. Kluwer Academic Publishers, Dordrecht (1991)
7. Yao Y.Y., Generalized Rough Set Model, In Rough Sets in Knowledge Discovery1: Methodology and Applications, L. Polkowski and A. Skowron (eds), Heidelberg: Physica-Verlag (1998)
8. Wezhi Wu, Wenxiu Zhang, Huaizu Li, Knowledge Acquisition in Incomplete Fuzzy Information Systems via the Rough Set Approach. Expert Systems, 20(5) (2003) 280-286
9. Slowinski R., Zopounidis C., Dimitras A., Prediction of Company Acquisition in Greece by Means of the Rough Set Approach. European Journal of Operational Research, 100 (1997) 1-15
10. Tay F.E. and Lixiang Shen, Economic and Financial Prediction Using Rough Sets Model. European Journal of Operational Research, 141 (2002) 641-659
11. Q. Zhang and A. Benveniste, Wavelet Networks. IEEE Trans. Neural Network, 3(6) (1992) 889–898
12. Zhang X, Qi J, Zhang R, Liu M, Hu Z, Xue H, et al. Prediction of Programmed-temperature Retention Values of Naphtha by Wavelet Neural Network. Computers and Chemistry, 25 (2) (2001) 125-133
13. Tabaraki R, Khayamian T, Ensafi A. A., Principle Component-wavelet Neural Networks as a New Multivariate Calibration Method. Analytical Letters, 38 (2005) 1-13
14. R. Chau, C.H. Yeh, A Multilingual Text Mining Approach to Web Cross-lingual Text Retrieval. Knowledge-Based Systems, 17, (5-6) (2004) 219-227
15. A. Gelbukh, Computational Linguistics and Intelligent Text Processing. Lecture Notes in Computer Science, Vol. 2004. Springer-Verlag, Berlin Heidelberg (2001)
16. Lean Yu, Shouyang Wang, K.K. Lai, A Rough-Set-Refined Text Mining Approach for Crude Oil Market Tendency Forecasting. International Journal of Knowledge and Systems Sciences, 2(1) (2005) 33-46

Investor Sentiment and Return Predictability in Chinese Fuel Oil Futures Markets[*]

Qian Zhao[1], Jianping Li[2,Ψ], and Shuping Wang[3]

[1] School of Economics, Renmin University of China, Beijing 100872, P.R. China
zqheropen@yahoo.com.cn
[2] Institute of Policy & Management, Chinese Academy of Sciences, Beijing 100080, China
ljp@casipm.ac.cn
[3] The College of Economics and Business Administration, North China University of
Technology, Beijing 100041, P.R. China
wangsp1@ruc.edu.cn

Abstract. We investigate the relation between investor sentiment and market returns in Chinese Fuel Oil Futures Markets by Vector Autoregressions（VAR）model. The sample period is from 5 September 2005 until 31 December 2006. Studies using daily datum on sentiments of professional advisors and individual investors suggest that past market returns are an important determinant of sentiment. Our evidence supports that not individual but professional sentiment has predictive power for returns. Extreme levels of sentiment do not possess any superiority in returns predictability with the exception of the individual bottom sentiment. For 1-week, 2-week and 4-week intervals, returns can weakly predict sentiment or changes. Individual sentiment severs as a contrary indicator of returns in the followed week, whereas we find no evidence for the other circumstance.

Keywords: Returns Predictability; Investor Sentiment; Vector Autoregressions.

1 Introduction

The sentiment-return relation is an important and extensively researched topic in the finance literature. Indirect（Market-based）[1], direct (survey-based) [2-4] or integrated measures [5,6] of sentiment are popularly used in order to find out whether sentiment follow or precede the stock markets. Several studies have also examined the causality in the futures markets with similar measures and the conclusions are mixed.

Simon *et al* [7] find that sentiment measures are able to predict returns on futures. Wang [8] shows that in the S&P 500 index futures market, large speculator sentiment is a price continuation indicator, whereas large hedger sentiment is a contrary indicator. Small trader sentiment can hardly forecast future market movements.

Moreover, extreme large trader sentiments and the combination of extreme large trader sentiments tend to provide more reliable forecasts. Chen *et al* [9] reveal that contrary sentiment indicators improve the forecasting accuracy and profits earning capability in S&P 500 futures. However, Dwight *et al* [10] demonstrate that the sentiment index displays only a sporadic and marginal ability to predict returns across 28 U.S. futures markets, and in those instances the pattern is one of return continuation—not reversals.

This study researches the causality in Chinese Fuel Oil Futures Markets. The primary focus is on the following two issues. Firstly, we test whether sentiment cause returns as predicted by the noise trader literature or sentiment simply responds to market behavior. Secondly, we examine whether extreme sentiment measures are useful for forecasting returns. Lastly, for robustness, we also test the causality with longer intervals.

2 Data and Sample Statistics

To empirically test our hypotheses, we use the results of a survey conducted by Jianzheng Future Brokerage Co. Ltd to measure the sentiment on a daily basis. The corporation gathers the opinions of above ten analysts, which form the professional advisers group. It also polls a random sample of its members each day, at the size of over one thousand, which represents the individual investors group. The sample period is from 5 September 2005 until 31 December 2006 for a total of 302 observations. The Bearish Sentiment Index at time t (BSI_t) is measured by the bull-bear spread,[1] the percentage of the bullish less that of the bearish.

A continuous series of futures return is created to match the sentiment data. The return (R_t) is measured as the percentage change in settlement prices (P_t) of the contract which is three months before the delivery date using a roll-over strategy, $\ln(P_t / P_{t-k})$. The data comes from Shanghai Futures Exchange.

It is necessary to examine the simple summary statistics to fully understand the datum and to motivate the time-series approach used in the analysis. Table 1 presents summary statistics for the datum. The results indicate that the average return is negative but not statistically different from zero. Sentiment is quite volatile, with large standard deviations and extreme values. The professional BSI ranges between 0.6 and -0.8 in our sample, and the individual, between 0.9598 and -0.6856. Individual investors are too optimistic with a mean sentiment level notably over a neutral value 0 (50-50), when compared with the zero-mean return. We conduct stationary tests in order to avoid spurious regressions. According to ADF test three series are all stationary. The last column of Table 1 displays the contemporaneous correlation coefficient between returns and sentiment: 0.56（significantly positive at the 1% level with two-tailed *t*-test）for the professional and -0.05（not significantly）for the individual. But correlation is not equivalent to causality for the reason that opinions collected may be affected by prices during the day, which may produce the fictitious causality.

---

[1] Some other measures are tested in the paper, such as the ratio of the proportion of bearish investors to the whole investors. Results are omitted for parsimony since they are resemble.

Table 1. Summary statistics of the sample datum

	Mean	Max	Min	S.D	Skew	Kurto	J-B	ADF	Corr.
BSIA	-2.28	60	-80	23.30	0.02	4.07	14.39***	-11.44***	0.56
BSIB	40.06	95.98	-68.6	34.59	-0.43	2.64	10.83***	-2.13**	-0.05
R	-0.02	4.02	-5.03	1.47	-0.46	3.70	16.77***	-17.45***	-

Remark. Variables are professional sentiment (BSIA), individual sentiment (BSIB) and returns.*, **, *** denote significance at the 10, 5, 1% levels, respectively.

3   Methodology and Results

3.1   Vector Autoregressions Model (VAR)

In order to see how sentiment and market returns interact and identify the (statistical) causality between sentiment and the market, we use a set of VAR models,[2] where Granger causality tests and impulse response functions are developed from.

The general model is

$$BSI_t = c + \sum_{i=1}^{p} a_i BSI_{t-i} + \sum_{j=1}^{q} b_j R_{t-j} + \varepsilon_t \tag{1}$$

$$R_t = k + \sum_{i=1}^{m} \alpha_i R_{t-i} + \sum_{j=1}^{n} \beta_j BSI_{t-j} + \eta_t \tag{2}$$

3.1.1   Granger Causality Tests

The bivariate Granger causality tests examine whether the lags of one variable enter the equation to determine the dependent variable, assuming that the two series (BSI_t and R_t) are covariance stationary and error items ε_t, η_t i. i. d. white noise errors.[3]

A significant slope coefficient of equation (1) suggests that returns can predict sentiment. In equation (2) a significant and positive slope coefficient shows that the sentiment is a straight buying or selling indicator, while a negative coefficient implies that the sentiment is a contrary indicator.

We estimate the models using both levels and changes(ΔBSI_t) in sentiment measures since it is not easy to determine which specification should reveal the primary effects of sentiment. For example, suppose investor sentiment decreases from very bullish to bullish. One might anticipate a positive return due to the still bullish

---

[2] Hedgers who are concerned about fundamental information tend to hold positions for longer horizons, whereas speculators likely adjust positions over shorter horizons in response to short-term information. In the survey most of the individual are speculators, which make it sound to test our hypothesis using VAR although with limit observations.

[3] This assumption is tested using White [11] standard errors correct for heteroskedasticity. A Lagrange multiplier test is used to verify that the residuals are serially uncorrelated. AIC, BIC and Likelihood ratio tests are used to choose the best lag length. The appropriate test for the parameter restrictions is a Wald Chi-squared test.

sentiment, but on the other hand, since sentiment has decreased it is also possible for someone to expect a reduction in the return.

Table 2 reports the results from estimating the daily sample using VAR for both professional and individual sentiment levels. The blocks of rows indicate the contribution of each lagged independent variable. As the first block of rows shows professional sentiment is strongly positively related to its past levels but less related to returns (significant only at the 5% level with a 3-day lag). The next column reveals that professional sentiment strongly predict returns. Individual sentiment is strongly positively related to its past levels and lagged returns according to the third column. However, in the last column, there is no evidence that the individual sentiment will predict returns.

These results confirm that both professional advisers and individual speculators are strongly swayed by recent market performance. Lagged levels of sentiment and market returns explain substantial variation in professional sentiment as indicated by the high R^2 of 0.155, and individual sentiment by 0.749. Besides, individual sentiment can not predict returns; but professional sentiment is a price-continuation indicator, probably due to their rational expectation of fundamental messages. We also find that individual sentiment is directed by professional sentiment (significant at the 10% level), but not vice versa.

Table 3 estimates the system using the changes in sentiments, showing that a change of either professional or individual sentiment is strongly related to its lagged levels and returns. Conversely, there is weak evidence that changes in the sentiment influence subsequent market returns, if any for the professional. The R^2 for each equation reveals that lagged sentiment changes and market returns explain roughly 30% of the professional sentiment and 8% of the individual sentiment, but less of the variability in the returns. Moreover, changes of the two sentiments have no causal relationship.

Table 2. Daily VAR-returns and professional-individual sentiment levels

Independent variable	Lag	Dependent variable		Independent variable	Lag	Dependent variable	
		BSIA	R			BSIB	R
BSIA	1	0.3341***	0.0118**	BSIB	1	0.7248***	-0.0068
	2	-0.0264	-0.0162***		2	0.1600***	0.0050
	3	0.2430***	00.0141***				
sum impact		0.5508***	-0.0828				-0.0019
R	1	-0.3990	-0.0828	R	1	1.4180**	-0.0176
	2	0.7616	-0.0044		2	1.4115**	-0.0948
	3	-2.1907**	-0.1101				
sum impact		-1.8281	-0.1973			2.8295***	-0.1124
constant		-1.580	0.0033			4.7823	0.0576
Block exogenity		5.356	19.110***			8.447**	2.155
$\overline{R}^2$		0.155	0.053			0.749	0.004

In summary, this section reveals that market returns are a strong predictor of subsequent sentiment for both professional advisors and individual investors. In contrast, there is no evidence that individual sentiment is useful in predicting future returns over short horizons, whereas professional sentiment is a price indicator.

Table 3. Daily VAR-returns and professional-individual sentiment changes

Independent variable	Lag	Dependent variable		Independent variable	Lag	Dependent variable	
		Δ BSIA	R			Δ BSIB	R
Δ BSIA	1	-0.4891***	0.0093**	Δ BSIB	1	-0.2452***	-0.0069
	2	-0.3822***	-0.0080		2	-0.1272**	-0.0048
	3	-0.0087	0.0067*				
sum impact		-0.8799***	0.0081			-0.3724***	-0.0117
R	1	-2.1346**	-0.0443	R	1	1.4417**	-0.0201
	2	-1.0101	-0.0013		2	1.5394**	-0.0183
	3	-4.1232***	-0.0970				
sum impact		-7.2678***	-0.1426			2.9810***	-0.1107
constant		-0.5121	-0.0198			0.2043	-0.0183
Block exogenity		0.0000***	0.0003***			0.0100***	0.2691
$\overline{R}^2$		0.285	0.053			0.074	0.006

Remark. Sum impact indicates the aggregate sign of causality of all lags of an explanatory variable, the null hypothesis that it equals zero is tested using a Chi-squared test. Block exogenity reports the value of an F-test that the coefficients on all lags of all independent variables (other than own-lags) are jointly zero. Variables are changes of professional sentiment (Δ BSIA) and individual sentiment (Δ BSIB) and returns.

3.1.2 Impulse Response Function

An impulse response function investigates the response of one variable to one standard deviation change of another variable by using the moving average representation of the shocks for vector autoregression. Fig. 1 provides the results revealing the time path of the dynamic interaction patterns between sentiment of the professional and returns, where the figure of the individual is omitted. It can be found that a shock in daily returns causes the greatest initial increase and then a steep decline in professional sentiment, whereas the individual sentiment responds much more slowly. Returns respond volatile to professional sentiment but insignificantly to individual sentiment. Furthermore, sentiment is strongly affected by its own lagged variable. On all accounts, the results are generally consistent with those obtained by Granger causality tests.

3.2 Extreme Levels of Sentiment and Returns

While the causality test results presented above do not indicate a consistent relationship between noise trader's sentiment and subsequent price movements, it

Response to Cholesky One S.D. Innovations ± 2 S.E.
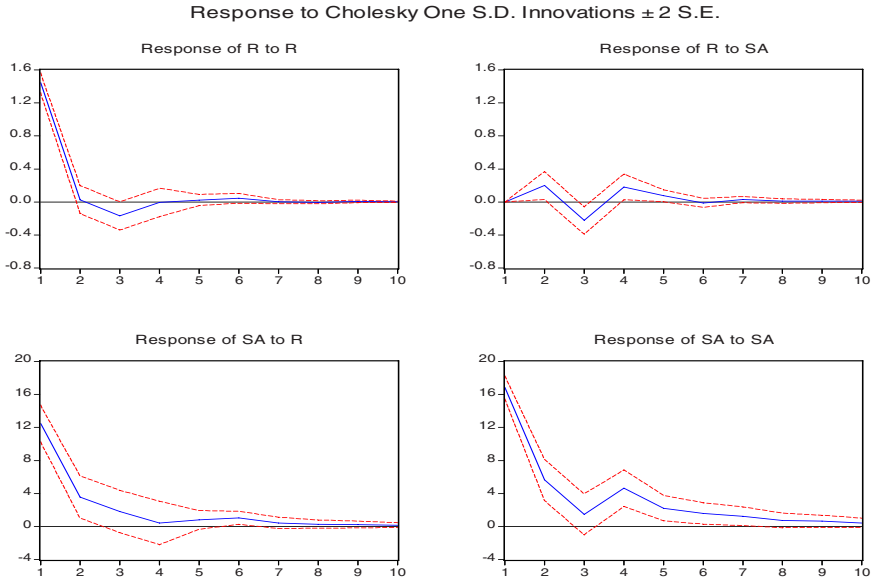
Fig. 1. Responses to Cholesky Innovations between professional sentiment and returns

may be possible that a relationship exists, but only at extreme levels of sentiment. The hypothesis is tested by forming two groups based on sentiment: the extremely bullish group (top 20%) and the extremely bearish group (bottom 20%). Results are shown in Table 4. The slope coefficients are insignificant at the 10% level by t test, with the exception of the individual bottom 20% sentiment since the equation is well fitted by t and F tests. This suggests that individual bottom sentiment severs as a contrary indicator of returns, and that other extreme sentiment levels could hardly predict returns.

Table 4. Regression results of returns on extreme levels of sentiment

Dependent variable	Group	Intercept	Slope coefficient	t value	R^2	Adj. R^2	F value
	Top	0.374	-0.003	-0.211	0.001	-0.021	0.045
BSIA	bottom	0.659	0.020	1.563	0.037	0.022	2.442
	Total	0.123	0.005	1.343	0.016	0.007	1.804
	Top	2.441	-0.029	-0.633	0.009	-0.013	0.400
BSIB	bottom	-0.007	-0.018	-2.295***	0.076	0.062	5.268
	Total	0.107	-0.003	-1.369	0.017	0.008	1.873

3.3 Robustness

We repeat the analysis using the data for 1-week, 2-week and 4-week intervals (Monday-Monday) , because it is possible that people's perception of risk will be changed over a longer interval than one day, and because it take some time for the

investing decisions to be carried out. Table 5 shows that professional sentiment and changes is respectively related to lag returns for the 1-week and 2-week horizon, both significant at the 10% level, however, individual sentiment is not affected by returns for any of the tested horizon. Table 6 shows that future returns is negatively related to changes of individual sentiment for the 1-week horizon (strongly significant at the 1% level) and the latter explains 16% of the returns, whereas the coefficients in the other circumstances are insignificant.

Table 5. The regression results of professional and individual sentiment on returns

Interval	Parameter	BSIA	Δ BSIA	BSIB	Δ BSIB	Observations
1-week	Coefficient.	1.144	-2.205*	0.484	-0.376	60
	Adj.R^2	0.008	0.068	-0.015	-0.015	
2-week	Coefficient.	1.651*	-0.990	0.336	-0.807	32
	Adj.R^2	0.086	-0.012	-0.033	-0.023	
4-week	Coefficient.	-0.513	-2.687	0.390	-0.716	16
	Adj.R^2	-0.066	0.127	-0.085	-0.079	

Table 6. The regression results of returns on professional and individual sentiment

Interval	Parameter	BSIA	Δ BSIA	BSIB	Δ BSIB	Observations
1-week	Coefficient	-0.008	0.0003	-0.015	-0.054***	60
	Adj.R^2	-0.013	-0.018	0.0006	0.160	
2-week	Coefficient	-0.0006	-0.015	0.013	-0.035	32
	Adj.R^2	-0.034	-0.027	-0.027	0.030	
4-week	Coefficient	-0.031	-0.025	0.076	0.064	16
	Adj.R^2	-0.070	-0.065	0.085	0.125	

Remark. Test statistics for individual coefficients is computed using White (1980) heteroskedasticity consistent standard errors. ***, **, and * denote significance at the 1, 5, and 10% levels, respectively.

4   Summary and Conclusions

In summary, we have demonstrated that survey-measuring investor sentiments are related to market returns. We find little evidence of short-run (1-day interval) predictability in returns for individual sentiment, but strong evidence for professional sentiment. Neither professional nor individual extreme sentiment could predict returns, with the exception of the individual bottom 20% sentiment. For 1-week, 2-week and 4-week intervals, sentiment and changes is weakly related to lag returns, which may be interpreted by the thing that individual investors make their decisions on short time market information. Individual sentiment can explains 16% of the returns a week later and it severs as a contrary indicator of returns, whereas the coefficients in the other circumstances are insignificant. We also reveal that professional sentiment is a predictor of individual sentiment, but not vice versa. Since the datum used in our tests are short, the findings might be improved by including more observations.

More work remains to be done in studying the determinants of investor sentiment and the value of forecast based on sentiment of different types of traders (arbitragers and speculators) in the futures markets. Some other sentiment measures may be constructed to test the robustness of our conclusions.

References

1. Parkinson, M. The extreme value method for estimating the variance of the rate of return. Journal of Business, 1992, (53): 61–65.
2. M.E. Solt, M. Statman, How useful is the sentiment index? Financial Analysts Journal, 44 (1988), 45-55.
3. K.L. Fisher, M. Statman, Investor sentiment and stock returns. Financial Analysts Journal, 56 (2000), 16-23.
4. W. B. Gregory, T. C. Michael, Investor sentiment and asset valuation. The Journal of Business, 78 (2005), 405-440.   monthly daily
5. G. W. Brown, M. T. Cliff, Investor sentiment and the near-term stock market. Journal of Empirical Finance, 11 (2004), 1-27.
6. Y. Wang, K. Aneel, J. T. Stephen, The relationships between sentiment, returns and volatility. International Journal of Forecasting, 22 (2006), 109-123.
7. D. P. Simon, R. A. Wiggins, S&P futures returns and contrary sentiment indicators. Journal of Futures Markets, 21 (2001), 447-462.
8. C. Wang, Investor sentiment and return predictability in agricultural futures markets. Journal of Futures Markets, 21 (2001), 929-952.
9. A. Chen, Y. Chang, Using extended classifier system to forecast S&P futures based on contrary sentiment indicators. Evolutionary Computation, 3 (2005), 2084- 2090.
10. R. S. Dwight, H. I. Scott, M. L. Raymond, The theory of contrary opinion: A test using sentiment indexes in futures markets. Journal of Agribusiness, 21 (2003), 39-64.
11. H. White, A heteroskedasticity-consistent covariance matrix estimator and a direct test for heteroskedasticity. Econometrica, 48 (1980), 817–838.

Energy, Economy, Population, and Climate's Influences on Environment in Anhui Province, China

Kai-ya Wu[1, 2], Lin Liu[2], and Ju-liang Jin[3]

[1] Innovation Base for Public Management and Public Policy, Fudan University, Shanghai, 200433, China
[2] School of Economics, Xiamen University, Xiamen, 361005, China
[3] College of Civil Engineering, Hefei University of Technology, Hefei, 230009, China
wuky2000@vip.sina.com

Abstract. Energy consumption, economic development level, population growth, and climate change and so on all have close relations with environment pollution. Based on the statistical data of Anhui province in China from 1987 to 2004, this paper analyzes the direct and indirect influences of energy consumption, total output value of industry, population, temperature and precipitation on environment pollution. The results show production pattern of industry and consumption of electric power are main reasons of environmental pollution.

Keywords: Energy consumption, Environment pollution, Multi-path analysis model, Anhui province.

1 Introduction

With society and economy developing, environment pollution becomes more and more serious, and, in some degree, begins to threaten economic development, human healthy and social security. Most of existing studies are about the influences of single social or economic factor on environment, and emphasize on the relationship between economic growth and environment pollution level, i.e. different expressive forms of Environmental Kuznets Curve, rarely relating to multi-factor influences on environment or direct and indirect influences on environment through effect factors. Since there are various factors which affect environment, such as the increase of energy consumption, the enhancement of industrialization, the growth of population, and the change of climate and so on, environment is a systematic engineering. Treating energy, economy, population, climate and environment as a whole, the multi-path analysis model is used in this paper to make a case study of Anhui province, China, analyzing direct and indirect influences of energy consumption, total output value of industry, population, temperature and precipitation on environment pollution as well as the interaction among each factor. The result of this paper can provide scientific foundation for coordination between regional economy and environment and policy-making of regional environment.

2   Methods

When there are many variables, one independent variable can act on dependent variable not only through direct effect, but also through indirect effect by acting on other dependent variables. Path analysis is combinational analysis of regression equation which is the supplement and development of correlation analysis [1]. It can reduce coefficients of simple correlation into many parts, and show both direct and indirect influences of independents on dependent [2].

Based on data coming from "Anhui statistics yearbook", "Anhui energy statistics yearbook" of 1988-2005 and other references [3], this paper will use path analysis model to analyze the direct and indirect influences on environment pollution in Anhui province from 1987 to 2004. Detailed processes and formulas which can be consulted in reference [4] are omitted.

In our calculation, dependent variables including total waste water discharge, industrial solid waste discharge and total waste gas discharge are used to show environment pollution situation. The following 7 indexes are used as independent variables which affected environment: quantity of population(X_1), consumption of electric power(X_2), consumption of petroleum(X_3), consumption of coal(X_4), total output value of industry(X_5), temperature(X_6) and precipitation(X_7).

3   Results

The main results can be observed from Table 1, Table 2 and Table 3, in which TII represents total indirect influence and PII represents proportion of indirect influence.

Table 1. Direct and indirect influence coefficient of influence factors acting on total wastewater discharge

	X_1	X_2	X_3	X_4	X_5	X_6	X_7	TII
X_1	-0.7575	0.5406	0.0332	0.2191	-0.8649	-0.0574	-0.0007	-0.1301
X_2	-0.7349	0.5572	0.0338	0.2300	-0.8892	-0.0537	-0.0003	-1.4143
X_3	-0.6771	0.5069	0.0371	0.2198	-0.8152	-0.0390	-0.0001	-0.8047
X_4	-0.6726	0.5912	0.0330	0.2468	-0.8564	-0.0491	0	-1.0259
X_5	-0.7166	0.5419	0.0331	0.2312	-0.9143	-0.0598	-0.0005	0.0293
X_6	-0.5105	0.3514	0.0170	0.1422	-0.6413	-0.0852	-0.0020	-0.6432
X_7	0.1159	-0.0382	-0.0006	0.0010	0.0969	0.0376	0.0046	0.2180

From our calculation, we find that consumption of three kinds of energy has a great influence on the pollution situation of atmosphere environment. Table 1 shows that the direct influence of total output value of industrial on waste water discharge is relatively high, and its path coefficient is -0.9143, very close to its correlation coefficients. The following is the quantity of population. Consumption of electric power and consumption of coal have the greatest indirect influences on waste water discharge through industry production and population quantity.

Table 2. Direct and indirect influence coefficient of influence factors acting on industrial solid waste discharge

	X_1	X_2	X_3	X_4	X_5	X_6	X_7	TII
X_1	0.0074	0.6776	-0.6091	0.4363	0.1943	0.1333	-0.0280	0.8044
X_2	0.0072	0.6984	-0.6200	0.4579	0.1998	0.1247	-0.0108	0.1588
X_3	0.0066	0.6354	-0.6815	0.4375	0.1831	0.0906	-0.0027	1.3505
X_4	0.0066	0.6508	-0.6068	0.4914	0.1924	0.1140	0.0008	0.3578
X_5	0.0070	0.6793	-0.6076	0.4603	0.2054	0.1387	-0.0194	0.6603
X_6	0.0050	0.4404	-0.3122	0.2831	0.1441	0.1978	-0.0808	0.4796
X_7	-0.0011	-0.0411	0.0102	0.0020	-0.0218	-0.0872	0.1832	-0.1390

Population quantity, consumption of electric power, consumption of petroleum, consumption of coal and total output value of industry all have great influences on industrial solid waste discharge, the coefficients are 0.8117, 0.8571, 0,6690, 0.8490 and 0.8636 respectively, all positive. Since quantity of population, consumption of petroleum and total output value of industry all have small direct influences on industrial solid waste discharge, with path coefficients 0.0074, -0.6815 and 0.2054 respectively(Table 2), their indirect influences on industrial solid waste discharge are great. The reason is that industrial solid waste discharge increases as the demand of electric power goes up which is caused by population growth, consumption of petroleum and industry production.

Table 3. Direct and indirect influence coefficient of influence factors acting on total waste gas discharge

	X_1	X_2	X_3	X_4	X_5	X_6	X_7	PII
X_1	-1.3508	1.4192	-0.1286	0.6557	0.0738	0.0815	0.0109	2.1125
X_2	-1.3105	1.4628	-0.1309	0.6881	0.0759	0.0763	0.0042	-0.5969
X_3	-1.2073	1.3309	-0.1439	0.6576	0.0695	0.0554	0.0011	0.9072
X_4	-1.1994	1.3630	-0.1281	0.7385	0.0731	0.0697	-0.0003	0.1830
X_5	-1.2779	1.4227	-0.1283	0.6918	0.0780	0.0849	0.0075	0.8007
X_6	-0.9103	0.9224	-0.0659	0.4255	0.0541	0.1210	0.0314	0.4578
X_7	0.2067	-0.0862	0.0022	0.0030	-0.0083	-0.0534	-0.0712	0.0640

In Table 3, the indirect influence of quantity of population and consumption of petroleum on waste gas discharge is high. Their correlation coefficients are all positive, and path coefficients are -1.3508 and -0.1439 respectively. Consumption of electric power has a great indirect influence on waste gas discharge, followed by consumption of coal. Coal is the main energy for economic development. Industry production, fire power station and daily life of residents all request large amount of coal, so consumption of coal is the main reason of air pollution in our country. Enhancing efficiency of energy utilization, developing clean coal technology, improving the process of waste gas treatment, exploring and adopting efficient waste gas treatment and comprehensive resource utilization technique is the fundamental solution for air pollution.

4   Conclusions

In this paper, multi-path analysis model is used to analyze direct and indirect influences of population, energy consumption, gross industrial output value, temperature and precipitation on environment pollution in Anhui province, China, from 1987 to 2004. The results show that production pattern of industry and electric power consumption are main reasons of environmental pollution in Anhui province.

As far as Anhui is concerned, quantity of population and total output value of industry all have high correlation degrees with waste water discharge and the direct influence of the later on waste water discharge is larger than the former. While population grows and industry develops, industry structure should be improved to enhance the technology of waste water disposal, and thereby boosts harmonious development.

While consumption of electric power has great direct influences on industrial solid waste discharge and waste gas discharge, quantity of population and consumption of petroleum all have great indirect influences on industrial solid waste discharge and waste gas discharge through consumption of electric power. With population growing, consumption of electric power will surely increase, leading to large amount discharge of waste gas and waste residue. Controlling population quantity, improving energy for generating electricity, exploring clean coal technology and increasing the rate of energy utilization, all can to some extent reduce environment pollution.

References

1. Li Chen, Shi-yun Zhang: Path Coefficient Analysis of Agricultural Growth of Anhui. Operations Research and Management Science, 13 (4) 126-130 (2004)
2. Heng-yun Ma: Path Analysis and Application in Economics Study. Statistical Research, (2) 52-54 (1995)
3. Kai-ya Wu, Xiao-jian Chen: Study on the Relationship between Economic Growth and Environmental Degradation of Anhui Province. Chongqing Environmental Sciences, 25(6) 9-11 (2003)
4. Yan Wang, Hong-rui wang, Wu-jiu Yan: Path Analysis of the Influence of Pollution, Energy and Economy Development on Environment in China. Journal of Anhui Normal University (Natural Science), 25(3) 277-280 (2002)

Optimization Models of Pricing Hydro-thermal Trade Based on Energy Economics

Guangjuan Chen, Zhongfu Tan, Jie Zhao, Jianxun Qi, and Li Li

Electricity Power Economics Institute, North China Electric Power University, Beijing, 102206, P.R. China
guangjuanchen@126.com, tanzhongfu@sina.com.cn

Abstract. An Optimization model of pricing hydro-thermal trade is presented in day-ahead market of electricity, which object is to maximize the social benefit increment. And an algorithm of the model is given using heuristics algorithm. Example indicates that the model and algorithm are feasible.

Keywords: Energy economics, Electricity market, Hydro-thermal trade.

1 Introduction

At present, the electric power industry of China is in the interim from planned economy to market economy. In China, some investments of electric power construction come from market but electricity market hasn't been come into being yet, which results that power enterprises are self-governed but the power grid is monopolized. On that condition, the government confirms the electricity price and quantity to grid of each power enterprise every year in order to ensure power enterprises' basic income. According to these data, the State Grid Corporation of China contracts with power enterprises. In this way, every enterprise has contract electric quantity, whatever hydropower or thermal, whatever efficient or inefficient. So it often appears that thermal power enterprises are consuming coal to generate electricity while some hydropower enterprises are spilling water [1].

Hydro-thermal trading is a measure to resolve this problem. Some experts also have already started the research working on the problem [2-5]. Lanbing L. and Chongqing K. *et al.* [2] presented the concept of generation right, whose emphasis was trade mode. Jiangang Y. *et al.* [3] researched the generation rights trade, but emphasized particularly on option. Yanling W. and Lizi Z. [4, 5] designed three kinds of forms of generation right trade. All of the papers didn't research the problem of pricing hydro-thermal trade.

Based on the object of energy economics, an optimization model of pricing hydro-thermal trading is bought forward aiming at day-ahead trade in the paper. And we put forward an algorithm of the model by heuristics algorithm and give an example.

2 Optimization Models of Pricing Hydro-thermal Trade

Suppose that there are n thermal power and m hydropower enterprises in one regional electric market. Each participant's goal is to maximize his profits increment. The day-ahead trade is carried out on the day before the electric dispatching center dispatches electric power (EDC) at the way of bidding. The EDC clears the uniform trading price and corresponding electric quantity at the object of maximizing the social profits increment.

2.1 Optimization Model of Day-Ahead Trade

In the day-ahead market, the model of maximizing the social profits increment is:

$$(P_3) \quad \max \Delta F_t = \sum_{t=1}^{l} \sum_{i=1}^{n} \sum_{j=1}^{m} (c_{fit} q_{ijt} - c_{ejt} q_{ijt}),$$

$$s.t. \quad q_{fit} = a_{fit} - b_{fit} p_{fit},$$

$$q_{ejt} = -a_{ejt} + b_{ejt} p_{fit},$$

$$p_{fit} = p_{ejt} = p_t,$$

$$\sum_{i=1}^{n} q_{fit} = \sum_{j=1}^{m} q_{ejt} = \sum_{i=1}^{n} \sum_{j=1}^{m} q_{ijt},$$

$$c_e < p_t < c_f,$$

$$q_{fit} \le Q_{fit},$$

$$W_{ejt} + q_{ejt} \le Q_{ejt},$$

(1)

where q_{fit} is the purchasing electric quantity, p_{fit} is the relevant price, a_{fit} and b_{fit} are coefficients of the demand function of thermal power enterprise i at t period of time. q_{ejt}, p_{ejt}, a_{ejt} and b_{ejt} are the parameters of hydro-power enterprise j at t period of time. q_{ijt} is the electric quantity that thermal power enterprise i purchases from hydropower enterprise j at the price pt at t period of time. c_{fit} is the average cost, q_{fit} is the contract electric quantity of thermal power enterprise i at t period of time. c_{ejt} is the variable cost and W_{ejt} is the contract electric quantity of hydropower enterprise j at t period of time. And Q_{ej} is the maximal electric quantity that hydropower enterprise j is able to produce at t period of time. l is the number of period of time. p_t and q_{ijt} are decision variables of (P_1). i=1,2,…,n. j=1,2,…,m. t=1,2,…,l.

2.2 Algorithm

The optimization model (P_1) is solved using heuristics algorithm and the flow of solving (P_1) is given in Fig. 1.
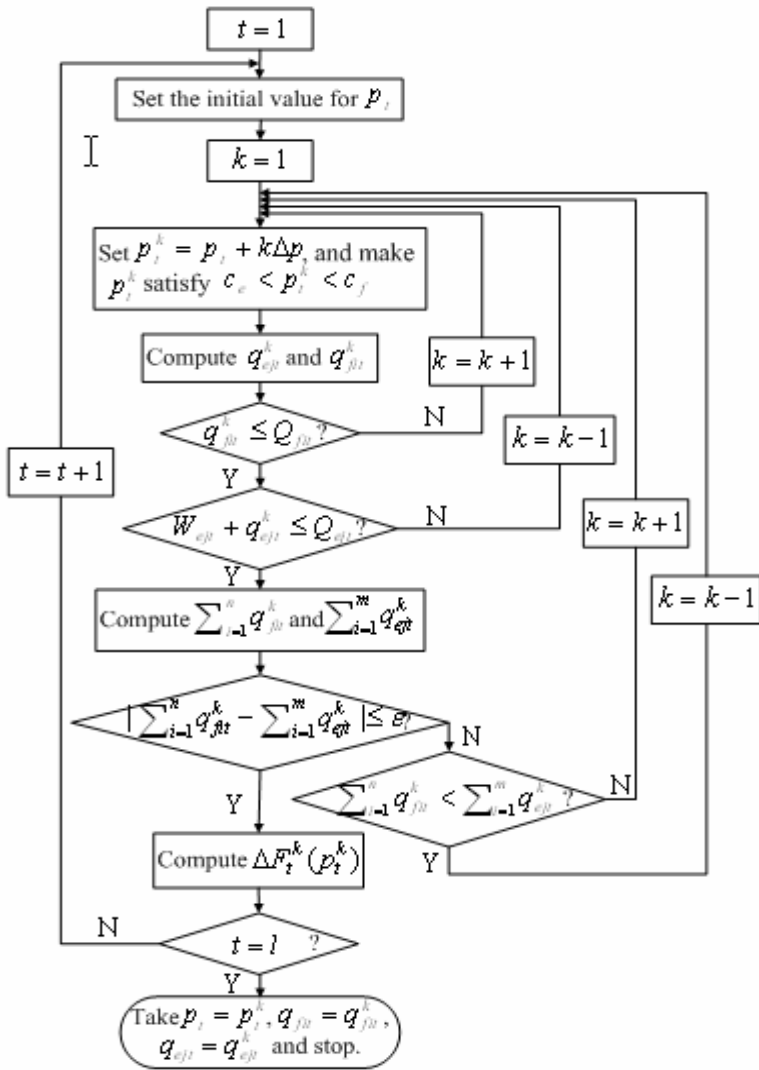
Fig. 1. The figure shows the flow of solving (P3) by using heuristics algorithm

3 Example

Suppose that there are three thermal power and two hydropower enterprises who will attend the hydro-thermal trade in one regional electricity market. We choose one period of time of one day to compute. The bidding information is offered in the Tab. 1. The trade results are given in the Tab. 2. From Table 2, we can see that the uniform clearing price is 62.176 Yuan/MWh and 270.46MWh electric quantity is exchanged.

Table 1. The bidding information of power enterprises in the day-ahead market

Enterprise	Trade Type	Average cost (Yuan/MWh)	Electric quantity (MWh)	Maximal quantity (MWh)	Bidding coefficient	
					a	b
Thermal a	Buy	100.00	156.25	208.33	90	0.80
Thermal b	Buy	98.00	156.25	197.92	110	0.90
Thermal c	Buy	91.00	166.67	218.75	100	0.95
Hydro a	Sell	36.00	156.25	208.33	150	3.20
Hydro b	Sell	41.50	166.67	260.42	150	3.80

Table 2. The results of the day-ahead trade

Enterprise	Trade Type	Price (Yuan/MWh)	Quantity (MWh)	The profits increment (Yuan)
Thermal a	Buy		40.26	1522.79424
Thermal b	Buy		54.04	1935.92896
Thermal c	Buy	62.176	40.93	1179.76632
Hydro a	Sell		48.96	1281.57696
Hydro b	Sell		86.27	1783.71852

4   Conclusion

The hydro-thermal trade can make thermal power and hydropower enterprises gain additional profits. And it can lessen water spill and decrease coal consume.

References

1. Quan W., Nianhua X.: Study on the spill electricity price of Central China Power Net. Automation of Electric Power Systems, 7 (2001) 48-51
2. Canbin L., Chongqing K., Qing X. et al: Generation rights trade and its mechanism. Automation of Electric Power Systems, Vol. 27, 6 (2003) 13-18
3. Jiangang Y., Qiliang Z., Jiaqi Z., Pan H.: Generation rights trade mode based on option theory. Proceeding of the CSEE, Vol. 25, 21 (2005) 76-81
4. Yanling W., Lizi Z., Yihan Y.: Adjustiong market of generation rights based on hydro-thermal exchange. Proceedings of the CSEE, Vol. 26, 5 (2006) 131-0136
5. Yanling W., Lizi Z.: Design trading market of generation rights. The 7th International Power Engineering Conference, Vol. 2 (2005) 842-847

Energy Efficiency and Productivity of China: Compared with Other Countries

X.P. Xu and L. Liang

School of Management, University of Science and Technology of China
He Fei, An Hui 230026, P.R. China
cicilj@mail.ustc.edu.cn, lliang@ustc.edu.cn

Abstract. Energy intensity(EI) is a commonly used index to estimate energy efficiency(EE) for countries, but it neglects the specific structure of energy consumption. We present a new index named weighted energy intensity(WEI), where weights are computed by a linear programming model named weighted energy intensity model(WEIM) and prove that it is equal to CCR model in DEA with one-output system. A comparison between WEI and EI is demonstrated. Results show that EI has underestimated EE of China and WEI is more accordant with real situation. We also use malmquist index(MI) to analyze changes of EE, frontier technology and total factor productivity of China over period 2000-2003.

Keywords: Weighted energy intensity, Energy productivity, Energy efficiency, DEA; Malmquist index.

1 Introduction

China has become the second greatest energy consumption country in the world. According to BP Statistical Review of World Energy, Chinese primary energy consumption increased by 15.1% in 2004. That's much higher than world primary energy consumption's 4.4%[1]. Energy intensity(EI) is a popular index to estimate energy efficiency(EE) for a country, which is defined as total energy consumption relative to total output(GDP or GNP)[2]. Using energy intensity, most researches support that EE of China is low. However, EI only considers simple-sum of energy consumption as single input to produce GDP neglecting structure of energy consumption. Usually, EI may overstate or understate energy efficiency. We present a new index named weighted energy intensity(WEI), where weights are computed by weighted energy intensity model(WEIM). We prove that WEIM is equal to CCR model in data envelopment analysis(DEA) and can easily overcome that shortage of EI. The same as CCR model, WEIM is a non-parametric approach that computes best practice efficient frontiers based on convex combinations of decision making units(DMUs) in the sample[3]. WEIM requires few assumptions and get results more objectively than EI.

Section 2 shows sample selection, inputs and output. Section 3 introduces WEI, WEIM, CCR and malmquist index(MI). WEIM is used to estimated EE of China among 49 countries and MI is used to analyze total factor productivity changes over the period 2000-2003 in section 4. Finally, we conclude.

2   Sample Selection, Inputs and Output

Two data sources are used, which are World Petroleum Yearbook[4] and International Statistical Yearbook[5]. Removing countries that didn't satisfy our sample selection criteria, we got 49 countries. They are United States, China, Russia Federation, Japan, India, and so on.

Most researches about the relationship between energy consumption and economic growth focus on how the latter impacts the former. However, experience has proved that it's very important for energy to drive economic growth[6]. We concentrate on production process where energy consumption is input and GDP is output. Main primary energy consumption concludes oil, natural gas, coal, nuclear energy and hydropower. Oil and natural gas consumption are incorporated as one input. Nuclear power and hydropower are also incorporated as another input. Coal is the third input. Gross Domestic Product (GDP) is the only output. Therefore, we have three input indexes(million tones oil equivalents) and one output index(100 million USD).

3   Methodology

Suppose that there are n countries to be evaluated. Each country consumes various amounts of m different energy inputs to produce GDP. Specifically, country j consumes amount x_{ij} of energy input i to produce amount y_j of GDP. We assume that $x_{ij} \geqslant 0$ and $y_j \geqslant 0$. WEI is defined as weighted energy consumption relative to total GDP. Weights are not selected subjectively, but through solving a linear programming model named WEIM, specific form of which is as follows.

$$\min \rho = \sum_{i=1}^{m} p_i x_{i0}/y_0 \quad subject\ to\ \sum_{i=1}^{m} p_i x_{ij}/y_j \geq 1(\forall j),\ p_i \geq 0(\forall i). \quad (1)$$

The target value of this model is WEI of country 0. p_i represents weight of input i. WEIM adopts a self-evaluation mechanism. Each country can get different combinations of p to maximize its WEI score.

Definition 1. *Country* 0 *is WEI efficient if there exists an optimal solution that* $\rho^* = 1$ *and* $p_i^* > 0(\forall i)$.

DEA is a relatively data oriented approach for evaluating performance of DMUs which convert multiple inputs into multiple outputs[3]. The following CCR model[7], one of DEA models, is corresponding model for our research.

$$\max \theta = uy_0/\sum_{i=1}^{m} v_i x_{i0}\ subject\ to\ uy_j/\sum_{i=1}^{m} v_i x_{ij} \leq 1(\forall j), u \geq 0, v_i \geq 0(\forall i). \quad (2)$$

Definition 2. *Country* 0 *is DEA efficient if there exists an optimal solution that* $\theta^* = 1$ *and* $u^* > 0, v_i^* > 0(\forall i)$.

Theorem 1. *WEIM is equal to CCR model, and* $\rho^* = 1/\theta^*, p_i^* = v_i^*/u^*(\forall i)$. *Proof. Take reciprocal of* θ *and let* $p_i = v_i/u(\forall i)$ *in CCR model, then CCR model can be easily turned into WEIM.*

MI is an index representing total factor productivity growth of a DMU under multiple inputs and multiple outputs framework. MI is defined as the product of "Catch-up" (CU) and "Frontier-shift" (FS) terms. CU relates to the degree that a DMU attains for improving its efficiency, while FS reflects the change in the efficient frontiers surrounding the DMU between the two time periods. $MI > 1$ indicates progress in total factor productivity, while $MI = 1$ and $MI < 1$ indicate respectively the status quo and decay in total factor productivity. CU and FS have similar explanations with MI[3].

4   Results

This paper primarily focuses on China and compares China with other countries. We use WEIM to compute energy efficiency for 49 countries and compare WEI with EI. To get a clear image of China, we just involve top five energy consumption countries among 49. Results are showed in Table 1. Using EI index, China is one of the lowest EE countries, of which rank is 43 and EI is 831.47 toe/10000 USD. EI of Russia Federation is lower than China, but EI of other three, including India, are higher than China. Main energy resource of China is coal, which makes up of nearly 70% of its energy consumption. Most other countries consume oil and natural gas. Usually, combustion efficiency of coal is lower than other kinds of energy. EI neglects this specific characteristic of different energy, but WEI can easily overcome this shortage. In WEIM, each country get different combinations of p to maximize its WEI score. Using WEI, rank of China is upgraded from 43 to 32. EE of Russia Federation is lower than China, while EE of United States and Japan are higher than China. Japan and United States are developed countries, after two oil crisis, they have made great efforts to improve their EE. India is a fast developing country like China and its WEI score is a little lower than China, which gives different result from EI. EI index has underestimated EE of China and WEI is more accordant with real situation.

Now let's examine the energy productivity changes of China over period 2000-2003. Results are showed in Table 2. From year 2000 to year 2001, MI of China is equal to 1.08, which implies slight progress in total factor productivity. The reason is high catch-up term of 1.20, which means great improvement in efficiency. Frontier-shift term is lower than 1, so the efficiency frontier has withdrew back. Not only for China, but also other four countries are confronted with regress

Table 1. Efficiency Scores and Rank by EI and WEI in 2003

Country	EI		WEI	
	EI	rank	ρ	rank
United States	209.87	16	1.90	21
China	831.47	43	3.19	32
Russia Federation	1549.55	46	15.70	47
Japan	117.37	3	1.09	5
India	575.09	38	3.24	33

Table 2. Catch-up, Frontier-shift and Malmquist Index Over Period 2000-2003

Country	2000 - 2001			2001 - 2002			2002 - 2003		
	CU	FS	MI	CU	FS	MI	CU	FS	MI
United States	1.12	0.93	1.05	0.96	1.05	1.01	0.85	1.24	1.06
China	1.20	0.90	1.08	1.01	1.01	1.02	0.81	1.22	0.99
Russia Federation	1.25	0.94	1.17	1.05	1.07	1.12	0.97	1.25	1.21
Japan	1	0.88	0.88	1	0.97	0.97	0.92	1.21	1.11
India	1.13	0.93	1.05	1.00	1.04	1.05	0.85	1.25	1.06

in the frontier technology. From year 2001 to year 2002, both catch-up and frontier-shift term of China are higher than 1, which means efficiency frontier moves upward and efficiency of China is improved, thus the MI is higher than 1. From year 2002 to year 2003, MI of China is lower than 1, showing slight regress in total factor productivity. Frontier-shift term is equal to 1.22, while catch-up term of China is equal to 0.81 and that is lower than other four countries.

5   Conclusion

This study has presented a index named WEI which overcomes one shortage of traditional energy intensity index and proved WEIM is equal to CCR model with one output in DEA. Energy efficiency in 2003 and productivity of China over period 2000-2003 were analyzed using WEIM and MI methods with a three-inputs and one-output system. Results showed that WEI were more accordant with the real situation than EI and EI underestimated energy efficiency of China. Using WEI, rank of China has been upgraded greatly. Evidences were also provided that total factor productivity of China increased over 2000-2002, decreased a little over 2002-2003, and increase rate over 2000-2002 was slow down.

Researches can be continued to do with this topic. This paper only considered total GDP as single output. Structure of GDP can be involved. Having evaluated the energy efficiency before, we can go on to forecast future efficiency trend.

References

[1] British Petroleum: 2005 Statistical Review of World Energy. http://www. bp.com.
[2] Ang, B.W.: Decomposition of industrial energy consumption: the energy intensity approach[J]. Energy Economics 16(1994), 163-174
[3] Willian W. Cooper, Lawrence M. Seiford and Joe Zhu: Handbook on Data Envelopment Analysis [M]. Kluwer Academic Publishers. (2004) 8-12, 203-207
[4] CPETRC: World Petroleum Yearbook[M]. Petroleum Industry Press.(2005)203-204
[5] NBSC: International Statistical Yearbook[M]. China Statistical Press. (2005)46-50
[6] International Energy Agency: World Energy Outlook[M]. Paris: OECD. (2004).
[7] Charnes, A., Cooper, W.W., Rhodes, E.: Measuring the efficiency of decision making units. European Journal of Operational Research 2 [J]. (1978)429-444

An Analysis About Market Efficiency in International Petroleum Markets: Evidence from Three Oil Commodities

Wang Shuping[1], Li Jianping[2], and Zhang Shulin[1]

[1] The College of Economics and Business Administration, North China University of Technology, Beijing 100041, P.R. China
wangsp1@ruc.edu.cn, cseec@sina.com
[2] Institute of Policy & Management, Chinese Academy of Sciences, Beijing 100080, P.R. China
ljp@casipm.ac.cn

Abstract. A modified model for testing market efficiency is presented, with introducing convenience yield and using lagged spot prices to adjust risk premium. Subsequently, an examination about market efficiency in international petroleum markets is given using the modified model for three widely traded oil commodities: WTI crude oil, unleaded gasoline, and heating oil. The main findings are that there have significant differences about market efficiency in different oil futures markets, and a nonlinear relationship among spot price, futures price, risk premium, and convenience yield is found in the crude oil market but not in refined oil markets. The nonlinear relationship can be eliminated through dividing the observed period into several stages. Meanwhile, the crude oil futures market is more and more efficient.

Keywords: International petroleum markets, Market efficiency, Futures price spot price, Risk premium, Convenience yield, Cointegration analysis.

1 Introduction

Today, oil is the world's most heavily exchanged commodity, with frequently fluctuation of its prices. Correspondingly, the oil futures markets play a more and more important role in the international oil markets. So the behavior about market efficiency in oil futures markets is arresting.

Several studies have examined this market efficiency in oil markets with mixed results. Bopp and Sitzer [1] argue that futures prices are good predictors of spot prices in the heating oil market. Ma [2] examines the existence of a risk premium for crude oil, heating oil, and leaded gasoline futures with maturities of 1, 2, 3, and 6-months. The results provide little evidence for a risk premium and there does not appear to be a systematic bias in the observed futures prices, supporting the simple efficiency hypothesis. Serletis and Banack [3] provide evidence that spot prices for crude oil, heating oil, and unleaded gasoline are cointegrated with their respective futures prices, but they do not explicitly test the joint restrictions implied by the unbiased hypothesis.

Using monthly observations of 30-day crude oil futures, Crowder and Hamed [4] test the simple efficiency hypothesis and the arbitrage condition, and obtain the conclusion supporting the former one. Roger and Mougoue [5] present some empirical results that the market efficiency hypothesis is supported by the data after the presence of nonlinear dependence using BDS test statistic and GARCH model. Recently, Joseph, Higgins and Miller [6] point out that oil futures prices do not predict well, and not also provide any easy way to predict the price of oil is headed. They attribute this result to convenience yield of oil storage.

So far, we can derive an elementary impression from above discussion that the market efficiency of oil futures markets is increasingly suspect due to frequent fluctuation of oil along with market speculation. Hence, further empirical testing is required to resolve, or at least to shed some light on, this issue as applied to the oil market.

The objective of this paper is to provide an empirical analysis about market efficiency in oil futures markets based on a modified testing model.

2 Models and Data

The efficiency of the futures markets in commodities or currency exchange has been extensively tested using the model

$$S_t = \alpha_0 + \alpha_1 F_{t-1} + \varepsilon_t \tag{1}$$

where S_t is the natural logarithm of the spot price in period t and F_{t-1} is the analogously defined futures price in period t-1 with the maturity period t, ε_t is stochastic error. In eq. (1), if $\alpha_0 = 0$, $\alpha_1 = 1$ and ε_t is white noise, then the futures market is weak form efficiency (see [7]). Weak form efficiency is also called as simple efficiency.

Subsequently, Brenner and Kroner [8] derive the conditions for market efficiency under the no arbitrage rule. Their model is

$$S_t = \alpha_0 + \alpha_1 F_{t-1} + \alpha_2 R_t + \varepsilon_t \tag{2}$$

where S_t, F_{t-1} and ε_t are defined as in eq. (1), R_t is the continuously compounded rate of return on the risk-free bond. A necessary condition for futures market efficiency is that there is a cointegration relationship among variables S_t, F_{t-1}, R_t, and the error term is serially uncorrelated as well as $\alpha_1 = \alpha_2 = 1$.

However, eq. (2) ignores two points. One point is the convenience yield of commodities storage. The other is how to calculate the risk premium. For oil commodities, first, it has a use option: if your refinery really needs input today, you can send your own oil to it. On the other hand, oil is easy to store in the ground, thus, you have some opportunities to obtain higher benefit when oil price rises. In addition, convenience yield comes often from oil shortage in a short future time.

In general, convenience yield is unobserved and uncertain. Gibson and Schwartz [9] estimate the convenience yield in the oil commodity market, and demonstrate that the convenience yield has significant mean reversion tendencies and conclude that it is a stationary process. We utilize this result to modify eq. (2).

Let y_t be convenience yield of oil commodity in period t, then y_t may be denoted as

$$y_t = \mu + u_t, \ h_t = h_0 + \sum_{i=1}^{q} \beta_i u_{t-i}^2 + \sum_{j=1}^{p} \theta_j h_{t-j} \tag{3}$$

where μ is the mean value of convenience yield and h_t is the conditional variance of the error u_t. Here, h_t is expressed as a generalized autoregressive conditional heteroscedasticity process, i.e. GARCH model. The investors perhaps hope to gain convenience yield from oil storage. Therefore, eq. (2) should comprise y_t, i.e.

$$S_t = \alpha_0 + \mu + \alpha_1 F_{t-1} + \alpha_2 R_t + u_t + \varepsilon_t. \tag{4}$$

Let $\alpha_0 + \mu = \mu_0$ and $u_t + \varepsilon_t = w_t$, then we obtain

$$S_t = \mu_0 + \alpha_1 F_{t-1} + \alpha_2 R_t + w_t, \ h_t = h_0 + \sum_{i=1}^{q} \beta_i w_{t-i}^2 + \sum_{j=1}^{p} \theta_j h_{t-j}. \tag{5}$$

where h_t is the conditional variance of the error w_t.

The second problem involves the calculation of the risk premium. We know that the investors only need to provide a small part of margin (about 5-10% of contract value) for buying or selling futures contracts. Therefore, the risk premium mainly concerns spot commodities but not futures contracts. According to this point, we adjust R_t in eq. (2) as follows

$$R_t = S_{t-1} r_t. \tag{6}$$

where S_{t-1} is the spot price in period $t-1$ and r_t is continuous compounding rate. Combines eq. (5) with eq. (6), we can obtain

$$S_t = \mu_0 + \alpha_1 F_{t-1} + \alpha_2 S_{t-1} r_t + w_t, \ h_t = h_0 + \sum_{i=1}^{q} \beta_i w_{t-i}^2 + \sum_{j=1}^{p} \theta_j h_{t-j}. \tag{7}$$

where all symbols in eq. (7) have the same definitions with eq. (5) and (6).

So far we argue the futures market is efficient if eq. (7) satisfies the conditions: (a) there is a cointegration relationship among variables S_t, F_{t-1} and $S_{t-1} r_t$; (b) $\alpha_1 = 1$ and $\alpha_2 = 1$; (c) w_t is serially uncorrelated and its mean value is zero.

The data used to test the efficiency of the oil futures markets are monthly observations from New York Mercantile Exchange (NYMEX), including three oil commodities: WTI crude oil, unleaded gasoline, and heating oil. The oil futures and spot prices series are available at http://www.eia.doe.gov. The observed period for WTI

is from Jan. 1986 to Dec. 2004, but for the latter two commodities is from Jun. 1986 to Dec. 2004. The futures price is defined as the closing price of a futures contract 30 days prior to the last day of trading on that contract. The future spot price is the cash price on the last trading day of the corresponding futures contract. The risk-free rate series is defined as the interest rate on the 3-month contract U.S. Treasury Bill that matures nearest to the last trading day of the relevant futures contract, and the data are available at http://www.economagic.com/. All variables are transformed into natural logarithm for eliminating in certain extent the heteroscedasticity of the error in eq. (7). The software we used is SAS 8.2.

3 Empirical Results

3.1 Stationarity Tests

The ADF unit root tests for the spot price, futures price and risk-free return of each oil product show that all these series are nonstationary. At the same time, all first differences are stationary, i.e., all these series are $I(1)$ (integration of order one).

3.2 Cointegration Analysis

3.2.1 A Linear Analysis

It is important to point out that the risk-free return $R_t = S_{t-1} r_t$ is quite little (less than 1 in general) in the real oil markets, so the natural logarithm of R_t is negative. Thus, it is needed to test the null hypothesis of market inefficiency (i.e. $\bar{\alpha}_2$ =-1) for risk premium in Table 1.

Table 1 gives the estimate results of long-run relationship among Spot price (S_t), lagged futures price (F_{t-1}), risk premium (R_t) and convenience yield (μ_0) for the three oil products. It should note that we do not adjust the error term using GARCH model. Table 2 reports the results of cointegration tests, and it indicates that there is a cointegration relationship among these variables for all three oil products.

Some results can be obtained from Table 1, as follows:

(a) For WTI crude oil and unleaded gasoline futures markets, it is significant at 0.05 level to reject the joint hypothesis: $\bar{\alpha}_1$ =1 and $\bar{\alpha}_2$ =-1 as well as the sole hypothesis: $\bar{\alpha}_1$ =1. This indicates that neither simple efficiency nor arbitrage equilibrium efficiency exist in the two markets. However, the futures prices have large forecasting function for the spot prices, and GDW tests imply the errors in eq. (7) are serially uncorrelated. In addition, there is convenience yield but not risk premium in the gasoline market, while the risk premium but not convenience yield exists in WTI crude oil market.

Table 1. Estimation of long-run relationship

	Parameters estimates			Testing statistics		
	$\bar{\mu}_0$	$\bar{\alpha}_1$	$\bar{\alpha}_2$	GDW	Q	LM
WTI crude Oil	0.07453 (0.346)	0.95213 (<0.0001)	-0.02919 (0.0323)	0.1798 0.2525 0.3400 0.0967 0.5132	0.0024 0.0080 0.0180 0.0343 0.0513	0.0060 0.0228 0.0533 0.1040 0.1670
	Test 1: $\bar{\alpha}_1$ =1 and $\bar{\alpha}_2$ =-1 [0.0001] Test 2: $\bar{\alpha}_1$ =1 [0.0423], Test 3: $\bar{\alpha}_2$ =-1 [0.0001]					
Unleaded gasoline	0.24960 (0.0342)	0.93514 (<0.0001)	-0.00567 (0.705)	0.1163 0.9244 0.0004 0.1299 0.0746	0.3133 0.5987 0.7930 0.3625 0.4387	0.3225 0.5983 0.7940 0.4450 0.4303
	Test 1: $\bar{\alpha}_1$ =1 and $\bar{\alpha}_2$ =-1 [0.0001] Test 2: $\bar{\alpha}_1$ =1 [0.0219], Test 3: $\bar{\alpha}_2$ =-1 [0.0001]					
Heating oil	0.12178 (0.2688)	0.96998 (<0.0001)	-0.00928 (0.5059)	0.3713 0.8493 0.0366 0.1407 0.1300	0.0108 0.0312 0.0649 0.1226 0.1661	0.0110 0.0215 0.0512 0.0999 0.1343
	Test 1: $\bar{\alpha}_1$ =1 and $\bar{\alpha}_2$ =-1 [0.0001] Test 2: $\bar{\alpha}_1$ =1[0.2614], Test 3: $\bar{\alpha}_2$ =-1 [0.0001]					

Remark. $\bar{\mu}_0$, $\bar{\alpha}_1$ and $\bar{\alpha}_2$ are the estimated values of the corresponding parameters in the regression: $S_t = \mu_0 + \alpha_1 F_{t-1} + \alpha_2 S_{t-1} r_t + w_t$; numbers in parentheses are significance probability for the *t*-statistic, while numbers in brackets are significance probability for the *F*-statistic; all the numbers below statistics GDW (generalized Durbin-Watson), Q (Portmanteau statistic) and LM (Lagrange Multiplier) represent significance probability for respective statistic, and the lagged orders are all from 1 to 5.

Table 2. Cointegration tests

	a	b	p	AEG
WTI crude oil	no	no	0	-15.07[*]
Unleaded gasoline	no	no	2	-7.15[*]
Heating oil	no	no	0	-14.26[*]

Remark. Use AEG statistic and the Augmented Dickey-Fuller regression: $\Delta \bar{w}_t = a + bt + \gamma \bar{w}_{t-1} + \sum_{i=1}^{p} \lambda_i \Delta \bar{w}_{t-i} + \varepsilon_t$ to test the null hypothesis of no cointegration (i.e. γ =0) among Spot price, futures price, risk premium and convenience yield, where $\bar{w}_t$ are the estimated residuals of the regression in Table 1; * indicates significance at 0.01.

(b) For heating oil market, it is significant at 0.05 level to reject the joint hypothesis: $\bar{\alpha}_1$ =1 and $\bar{\alpha}_2$ =-1, but not reject the two hypotheses $\bar{\alpha}_1$ =1 and $\bar{\mu}_0$ =0 at the significance of 0.2, respectively. This suggests the heating oil futures market is simple efficiency but not arbitrage equilibrium efficiency.

What could possibly explain above results? Why the three oil futures markets exhibit differences on market efficiency?

One possible explanation is that the crude oil prices fluctuate frequently from Jan 1986 to Dec 2004. In Table 1 Q and LM tests indicate that the errors have conditional heteroscedasticity for WTI crude oil in the observed period, so the structural relationship among spot price, lagged futures price, risk premium and convenience yield perhaps has changed. The changed structural relationship influences the accuracy of testing market efficiency. For gasoline and heating oil futures, they can utilize more information than crude oil market, for example, use crude oil futures price. Therefore, it does not have conditional heteroscedasticity of the errors in eq. (7) for the two oil products. Secondly, the speculative activities are more prevailing in the crude oil futures markets than refined oil markets. Hence, the risk premium is significant in WTI crude oil market but not in gasoline and heating oil markets. Finally, gasoline consumption is the largest in all of refined oil products in the world, so it comes easily forth shortage due to hoarding. Thus, gasoline storage possibly carries more convenience yield than the other two oil commodities for the holders.

Although the three oil futures markets present differences in the aspect of market efficiency, there is an identical point that the futures prices have large forecasting function for the spot prices.

3.2.2 A Nonlinear Analysis with GARCH Estimates
As the existence of conditional heteroscedasticity in WTI crude oil futures, we use eq. (7) to analyze the nonlinear relationship among these variables.

Table 3 gives the parameters estimates and relevant tests. Since the coefficient $\bar{\beta}_1$ is statistically significant at 0.05 level, the variance equation in eq. (7) is an ARCH(1) model. This implies the lagged errors impose a short-term influence to the conditional variance. The testing results in Table 3 do not support simple efficiency hypothesis or arbitrage equilibrium efficiency hypothesis.

Table 3. ARCH estimates for WTI crude oil

Parameters	$\bar{\mu}_0$	$\bar{\alpha}_1$	$\bar{\alpha}_2$	$\bar{h}_0$	$\bar{\beta}_1$
Estimates	0.0835	0.9463	-0.0324	0.008019	0.2303
	(0.1873)	(<0.0001)	(0.0080)	(<0.0001)	(0.0166)
Tests	Test 1: $\bar{\alpha}_1$ =1 and $\bar{\alpha}_2$ =-1 [0.0001], Test 2: $\bar{\alpha}_1$ =1 [0.0039]				

Remark. The estimated model is eq. (7); numbers in parentheses and brackets are significance probability for the *t*-statistic and *F*-statistic, respectively.

3.3 Analysis by Stages

Since the errors of eq. (7) have conditional heteroscedasticity for WTI crude oil in the observed period, in order to discuss effectively the market efficiency in the futures market, it is a good way to divide the observed period into several appropriate stages.

According to the movement characteristic of the residuals in Table 2, we try to divide the observed period into three stages: the first stage from Jan 1986 to Sep 1990, the second stage from Oct 1990 to Nov 2000, and the third stage from Dec 2000 to Dec 2004.

Table 4 reports the parameters estimates and relevant testing statistics for each of the three stages. Q and LM statistics tests indicate that there is no conditional heteroscedasticity longer in the error series for each stage. This further suggests the division of three stages is reasonable. Table 5 shows the results of AEG tests, and it indicates that there is a cointegration relationship among these variables (spot price, lagged futures price, risk premium and convenience yield) for all the three stages.

Table 4. Cointegration analysis by stages for WTI crude oil

	Parameters estimates			Testing statistics		
	$\bar{\mu}_0$	$\bar{\alpha}_1$	$\bar{\alpha}_2$	GDW	Q	LM
The first stage	1.12499 (0.1337)	0.69407 (0.0003)	0.10268 (0.3618)	0.0046 0.0722	0.0235 0.0577	0.0559 0.1587
	Test 1: $\bar{\alpha}_1$ =1 and $\bar{\alpha}_2$ =-1 [0.0001]			0.0630 0.0148 0.1974	0.1208 0.2042 0.2953	0.2960 0.4485 0.5937
	Test 2: $\bar{\alpha}_1$ =1 [0.0939], Test 3: $\bar{\alpha}_2$ =-1 [0.0001]					
The second stage	0.17903 (0.4867)	0.94259 (<0.0001)	0.00258 (0.9413)	0.2002 0.0749	0.6230 0.8196	0.5323 0.7993
	Test 1: $\bar{\alpha}_1$ =1 and $\bar{\alpha}_2$ =-1 [0.0001]			0.1918 0.3284 0.0944	0.9333 0.9747 0.9478	0.9262 0.9767 0.9772
	Test 2: $\bar{\alpha}_1$ =1 [0.3373], Test 3: $\bar{\alpha}_2$ =-1 [0.0001]					
The third stage	0.07892 (0.7464)	0.91932 (<0.0001)	-0.06460 (0.0215)	0.4983 0.3039	0.8152 0.9444	0.9697 0.7282
	Test 1: $\bar{\alpha}_1$ =1 and $\bar{\alpha}_2$ =-1 [0.0001]			0.1397 0.1485 0.3605	0.8975 0.9595 0.9865	0.5671 0.6551 0.7143
	Test 2: $\bar{\alpha}_1$ =1 [0.2295], Test 3: $\bar{\alpha}_2$ =-1 [0.0001]					

Remark. The meanings of the numbers in this table are analogous to Table 1.

Table 5. AEG tests by stages

	a	b	p	AEG
The first stage	no	no	0	-5.94[*]
The second stage	no	no	0	-10.49[*]
The third stage	no	no	0	-6.29[·]

Remark. The meanings of this table are analogous to Table 2.

Similarly, we can obtain some results about market efficiency in each stage from Table 4. The market efficiency is rather low in the WTI futures market in the first period, and the second stage supports simple efficiency hypothesis but not arbitrage equilibrium efficiency. However, the WTI futures market is semi-strong form efficiency (see [7]) in the third stage. These results imply that the market is more and more efficient and the speculators increasingly attach importance to risk premium.

4 Conclusions

In this paper, we present a modification for arbitrage equilibrium efficiency model, with introducing convenience yield and using lagged spot price to adjust risk premium. Empirical analysis indicates that there are significant differences about market efficiency in different oil futures markets: WTI and gasoline futures markets are neither simple efficiency nor arbitrage equilibrium efficiency, while heating oil futures market supports simple efficiency hypothesis. The analysis by stages for WTI futures market implies that the market is more and more efficient. Moreover, it is semi-strong form efficiency from Dec 2000 to Dec 2004.

Acknowledgements

References

1. Bopp, A. E., Sitzer, S. Are petroleum futures prices good predictors of cash value? The Journal of Futures Markets, 1987, (7): 705-719.
2. Ma, C. W. Forecasting efficiency of energy futures prices. The Journal of Futures Markets, 1989, (9): 393-419.
3. Serletis, A., Banack, D. Market efficiency and cointegration: An application to petroleum market. Review of Futures Markets, 1990, (9): 372-385.
4. Crowder, W. J., Hamed, A. A cointegration test for oil futures market efficiency. The Journal of Futures Markets, 1993, (13): 933-941.
5. Roger, A. F., Mougoue, M. Linear dependence, nonlinear dependence and petroleum futures market efficiency. The Journal of Futures Markets, 1997, 17, No. 1, 75-99.
6. Joseph, G. H., Higgins, P., Miller, J. Oil prices: Backward to the future? Economic Commentary (Federal Reserve Bank of Cleveland), Dec. 2004.
7. E. Fama. Efficient capital market: a review of theory and empirical work. Journal of Finance, 1970, Vol. 25, No. 2, 383-417.
8. Brenner, R., Kroner, K. Arbitrage, cointegration, and testing the unbiasedness hypothesis in financial markets. Journal of Financial and Quantitative Analysis, Mar. 1995, (30): 23-42.
9. Gibson, R., Schwartz, E. S. Stochastic convenience yield and the pricing of oil contingent claims. Journal of Finance, 1990, (45): 959-976.
10. Hansen, L., Hodrick, R. Forward exchange rates as optimal predictors of futures spot rates: An econometric analysis. Journal of Political Economy, 1980, (88): 829-853.

Model Integrating Fleet Design and Ship Routing Problems for Coal Shipping

Qingcheng Zeng and Zhongzhen Yang

Transport and Logistics College, Dalian Maritime University, 116026,Dalian, China
Qingcheng Zeng, Zhongzhen Yang, zqcheng2000@tom.com

Abstract. In this paper, an integrated optimization model is developed to improve the efficiency of coal shipping. The objective is (1) to determine the types of ships and the number of each type, (2) to optimize the ship routing, therefore, to minimize the total coal shipping cost. Meanwhile, an algorithm based on two-phase tabu search is designed to solve the model. Numerical tests show that the proposed method can decrease the unit shipping cost and the average ship delay, and improve the reliability of the coal shipping system.

Keywords: coal shipping, fleet design, ship routing, tabu search.

1 Introduction

Coal is one of the most important energy resources used in China. With the rapid economic development, the demand for coal is rapidly increasing in recent years. Due to the uneven distribution of coal sources, a large quantity of coal must be transported from west and north to east and south in China by railway and shipping. Therefore, optimization of shipping is the fundamental and key element to ensure the efficiency and reliability of coal transportation system. And significant improvement of fleet operation can be achieved by proper ship routing and scheduling.

In this paper, we will consider optimization of coal shipping from a set of outbound ports to demand ports. The problem involves determining the type of ships, the number of each type, and the optimal ship routing. Kim [1] developed a prototype optimization-based decision support system for the ship owner's scheduling problem in bulk trade. Fagerholt [2] developed a model to decide the optimal fleet size for liner shipping problem. Christiansen [3] studied a combined inventory management problem and a routing problem with time windows for ammonia transportation. Liua [4] studied the coal shipping and blending problems for an electric utility company. Fagerholt [5] considered a real ship scheduling problem as a multi-ship pickup and delivery problem with soft time windows. Persson [6] proposed an optimization model and a solution method to determine how to route a fleet of ships and the planning of which products to transport in these ships.

To ensure the integrated optimization, the ship routing and fleet design problems should be considered simultaneously. But most of the existing literatures studied the two problems respectively. In this paper, a model integrating fleet design and ship routing is developed. To solve the model, two-phase tabu search (TS) algorithm is

designed. And a real shipping planning problem is given as an example to illustrate the validity of the model and algorithm.

2 The Fleet Design and Ship Routing Problem

The background of this paper is a real problem that involves developing a new ocean shipping system for SEC (Shenhua Energy Company, the largest coal supply company in China). In the system, the coal produced by SEC is transported by railway to the outbound ports: Huanghua, Tianjin, and Qinhuangdao first, then by shipping to demand ports. Because of the natural constraints, the maximal ship capacity allowed by Huanghua port is 50,000 ton. Besides, Huanghua port is owned by SEC, to ensure the full utilization of the port, it is given priority in the ship routing. Therefore, if a ship's capacity exceeds 50,000 ton, it must be loaded at Huanghua port first, then reloaded at Tianjin or Qinhuandao, and discharged at demand ports lastly. Meanwhile, the type of ships used determines whether to reload or not and thus influences the ship routing. Therefore, optimization of coal shipping problem can be divided into two phases: the first phase is to determine the ship type; the second phase is to optimize the routing based on the ship type, and determine the reloading strategy.

Let P_T be the total set of ports and K, indexed by k, be set of available ship types to be routed and scheduled. $O \in P_T, D \in P_T$ denote the set of outbound and demand ports respectively, and s denote Huanghua port; Q_d is coal traffic destined for port d; c_{ijd}^k denotes the total unit shipping cost per ton from outbound port i to demand port d through reloading port j using ship type k; CAP^k is the capacity of ship type k, and CAP_i is the maximal ship that port i.

If coal demand of port d is transported by ship type k, $y_d^k = 1$, and 0, otherwise. $x_{ijd}^k = 1$ if ship of type k runs from port i to port d through reloading port j, and 0, otherwise. $x_{iid}^k = 1$ denotes that ships of type k run from port i to port d directly. Thus, the integrated model can be formulated as follows:

$$\text{Min} \sum_{i,j \in O, d \in D, k \in K} c_{ijd}^k Q_d y_d^k. \tag{1}$$

$$\text{s.t.} \sum_{k \in K} y_d^k = 1 \ \ \forall d \in D. \tag{2}$$

$$\sum_{j \in O} x_{ijd}^k = 1 \ \ \forall d \in D, \forall i \in O, \forall k \in K. \tag{3}$$

$$x_{sjd}^k = 1 \ \ \forall j \in O, \forall d \in D. \tag{4}$$

$$x_{isd}^k = 0 \ \ \forall i \in O, \forall d \in D. \tag{5}$$

$$x_{sjd}^k (CAP^k - CAP_s) \geq 0 \quad \forall k \in K, \forall d \in D, \forall j \in O .\tag{6}$$

$$y_d^k (CAP_d - CAP^k) \geq 0 \quad \forall k \in K, \forall d \in D .\tag{7}$$

$$x_{ijd}^k, y_d^k = 1, or\, 0 \quad \forall k \in K, \forall d \in D, \forall i, j \in O .\tag{8}$$

The objective function (1) is to minimize the total coal transportation cost. Constraints (2) ensure that every demand port is served by only one type of ship. Constraints (3) ensure that each ship is reloaded no more than once. Constraints (4) guarantee that all the ships must be loaded at Huanghua port first. Constraints (5) and (6) determine that reloading only happens on the condition that $CAP^k > CAP_s$. Constraints (7) ensure that the capacity of the ship served to demand port d does not exceed the maximal loaded ship the port allows. (8) is variable constraints.

3   Solution Procedures

To reflect the inter-relation between the fleet design and ship routing, a tabu search (TS) algorithm is designed to solve the model. Fig.1 shows the general process of this algorithm: The two-phase approach integrates two levels of decision making. In the first phase of the algorithm, one TS is performed to determine a good ship type design. For each ship type design obtained during the first phase, the other TS is ran to obtain the reloading scheme, then calculate objective function, namely, the total shipping cost, so as to influence the TS in the first phase. The feedback and reciprocity between the two phases form the optimization scheme.
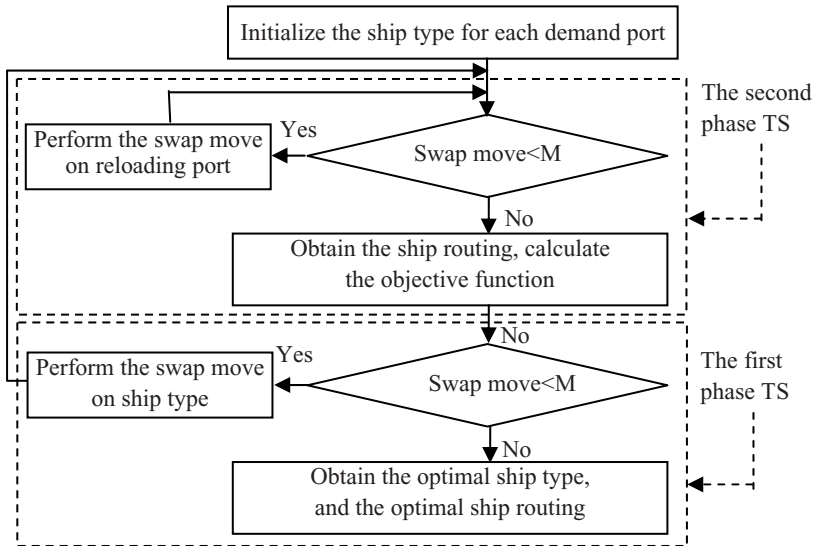
Fig. 1. Two-phase TS algorithm for coal shipping model

4   Numerical Tests

Numerical tests are used to illustrate the validity of the model and its algorithm. The maximal passing capacity of the three outbound ports is 100,000 ton; therefore, all the ship types we select are less than 100,000 ton. Results are shown as Table1. From Table1, we can compare the proposed method with the current status of SEC. We can find that the unit shipping cost decreases 21.01%, and the average ship capacity increases 37.39%. This indicates that the coal shipping cost can decrease by using larger ships. At the same time, the number of voyages decreases 34.4% due to the increase of the ship capacity. And also, the Average Delay in Huanghua Port decreases 26.87%, this is because the decrease of the ships berthing in Huanghua port.

Table 1. Comparison of the results by our method with the current status

Heading level	Our model(1)	Current status(2)	((1)-(2))/(2)
Unit cost (RMB/ton)	124	157	-0.2101
Average ship capacity (ton)	40,450	29,441	0.3739
The number of voyages	1,740	2,650	-0.3434
Average delay in Huanghua(hour)	49	67	-0.2687

5   Conclusions

In this paper, a model integrating fleet design and ship routing for coal shipping is developed. Numerical results indicate that the proposed method can decrease the unit shipping cost, reduce the ship delay in port, and improve the efficiency and reliability of the coal shipping system. For SEC, it can improve the coal shipping efficiency by large-scaled ships. However, this is restricted by the port passing capacity, especially the demand ports in south China. Therefore, for coal shipping system of China, the efficiency can be improved by reasonably planning the ports layout, and increasing the passing capacity of the demand ports.

References

1. Kim Si-Hwa, Lee Kyung-Keun: An optimization-based decision support system for ship scheuling. Computers & Industrial Engineering 33 (1997) 689–692.
2. Fagerholt Kjetil: Optimal fleet design in a ship routing problem. International Transactions in Operational Research. (1999) 453-464.
3. Christiansen Marielle: Decomposition of a combined inventory and time constrained ship routing problem. Transportation science 33, (1999) 3-16.
4. Liua Chiun-Ming, Sherali Hanif D. A coal shipping and blending problem for an electric utility company. Omega 28 (2000) 433-444.
5. Fagerholt Kjetil: Ship scheduling with soft time windows: An optimization based approach. European Journal of Operational Research 131(2001)559-571.
6. Persson Jan A: Shipment planning at oil refineries using column generation and valid inequalities. European Journal of Operational Research 163 (2005) 631-652.

Relative Entropy Method for Regional Allocation of Water Pollution Loading

Ju-liang Jin[1], Yi-ming Wei[2], Lin-yan Jing[1], and Yan Guo[1]

[1] College of Civil Engineering, Hefei University of Technology, Hefei, 230009, China
[2] Center for Energy and Environmental Policy Research, Institute of Policy and Management,
Chinese Academy of Sciences, Beijing 100080, China
JINJL66@126.com

Abstract. Regional allocation of water pollution loading is an important measure for achieving general quality and quantity control, which key problem is allocating right weights to sub-regions. Information entropy method (IEM) is proposed to mine the objective variation information of sub-regions and experience information of decision makers during the allocation process. The research results show that IEM is concise and universal, so it can be widely applied to theory and practice of various systems engineering applications.

Keywords: Allocation weighting, Analytic hierarchy process, Principle of minimum relative information entropy, Water pollution loads.

1 Introduction

Regional allocation of water pollution loading is important for achieving water controls, ensuring a sustainable utilization of a water-based environment, and supporting regional sustainable development [1]. Extant research methods are mostly based on the principle of economic optimization, the principle of equitableness, and the belief of both economic optimization and equitableness [2]. Using Delphi techniques and an Analytic Hierarchy Process (AHP), Li *et al.* argued for an allocation method of permissible regional water pollution loads [2], which key problem is how to conveniently determine allocation weights of sub-regions using objective information of sub-regions and experience information of decision-makers. Therefore, in this paper a method based on the relative information entropy principle (IEM) is discussed for allocating permissible polluted water at regional levels.

2 Relative Information Entropy Method for Regional Allocation of Water Pollution Loading

The establishment of IEM requires three steps, as follows.

Step 1: Establishing the hierarchy structure allocation model of region permissible water pollution loading. In order not to lose universality, the hierarchy structure

model is constituted of, from top-down, goal level A, criterion level B, index level C, and evaluated object level D.

Step 2: Determining the allocation weights of each sub-regions' permissible water pollution loading, y_k, $k=1$-n_d, where n_d is the number of sub-regions. Because the nine-point ratio-scale judgment matrix of AHP does not satisfy both linguistic and applied conventions, we use the fuzzy complementary judgment matrix that conforms to Chinese linguistic and cultural norms [3]. Evaluation is made of the importance of each element in B-D levels for upper levels, and to establish judgment matrixes of B, C and D level as follows: $A=\{a_{ij}|\ i,\ j=1$-$n_b\}$, $B^k=\{b_{ij}^k\ |\ i,\ j=1$-$n_c$•$k=1$-$n_b\}$, and $C^k=\{c_{ij}^k\ |\ i,$ $j=1$-$n_d;\ k=1$-$n_c\}$ respectively. Where n_b, n_c and n_d is the number of element B, C and D level, respectively. For brevity, A is described as an example to explain the process of computing weighting. According to Eq. (1), A can be changed into positive reciprocal judgment matrix E with nine-point ratio scale:

$$e_{ij} = \begin{cases} (b_m -1)(r_i - r_j)/(r_{max} - r_{min})+1, r_i \geq r_j \\ 1/[(b_m -1)(r_i - r_j)/(r_{max} - r_{min})+1], r_i < r_j \end{cases} \tag{1}$$

Where priority index $r_i = \sum_{j=1}^{n_b} a_{ij}$, $i=1$-n_b; r_{min} and r_{max} are the minimal and maximal value in $\{r_i\}$ respectively; $b_m=r_{max}/r_{min}$. Suppose the single priority weight value of each element of E is w_k, $k=1$-n_b. If E satisfies the consistency condition, then

$$\sum_{j=1}^{n_b} (e_{ij} w_j) / n_b = w_i \quad (i=1\text{-}n_b) \tag{2}$$

There is no general and precise scale to measure the priority of elements in the system, AHP only requires E to satisfy consistency in order to adapt to different complex useable systems. Therefore the left section of Eq. (2) can be considered as some prior probability distribution of the random variable which is relative to E, $\{w_k|k=1$-$n_b\}$ can be computed according to the relative entropy principle [4].

$$\min Q = \sum_{i=1}^{n_b} w_i [\ln w_i - \ln \sum_{j=1}^{n_b} (e_{ij} w_j / n_b)] \tag{3}$$

$$\text{s.t.} \sum_{i=1}^{n_b} w_i = 1, w_i > 0, i = 1 - n_b \tag{4}$$

Using the Lagrange multipliers method to solve Eq. (3) and Eq. (4), we obtain

$$w_i = \sum_{j=1}^{n_b} (e_{ij} w_j)/ \sum_{i=1}^{n_b} \sum_{j=1}^{n_b} (e_{ij} w_j) \quad (i=1\text{-}n_b) \tag{5}$$

So the iterative computing method can be used to compute w_i as follows:

$$w_i^t = \sum_{j=1}^{n_b} (e_{ij} w_j^{t-1}) / \sum_{i=1}^{n_b} \sum_{j=1}^{n_b} (e_{ij} w_j^{t-1}) \quad (i=1\text{-}n_b; \, t=1, 2, \ldots) \tag{6}$$

Where w_i^t is the tth iterative computed weight of the ith element. According to Eq. (2), Jin et al. defined the consistency index coefficient (*CIC*) of $\mathbf{E}$ as follows [5]

$$CIC(n_b) = \sum_{i=1}^{n_b} | \sum_{j=1}^{n_b} (e_{ij} w_j) - n_b w_i | / n_b \tag{7}$$

When *CIC*<0.10, $\mathbf{E}$ can be considered as satisfying consistency. In a similar way, we can calculate the weight of each element of each judgment matrix of C level w_j^i (j=1-n_c, i=1-n_b), and that of D level w_k^j (k=1-n_d, j=1-n_c), then find the total weight of each element of C level to the goal level A:

$$w_j^A = \sum_{i=1}^{n_b} w_i w_j^i \quad (j=1\text{-}n_c) \tag{8}$$

The allocation weight of permissible water pollution loads of each sub-region is

$$y_k = \sum_{j=1}^{n_c} \sum_{i=1}^{n_b} w_i w_j^i w_k^j \quad (k=1\text{-}n_d) \tag{9}$$

Step 3: Allocating reasonable regional permissible water pollution loading for each sub-region according to the allocation weights of each sub-region y_k..

3   Case Study

A river channel-type reservoir receives the domestic sewage and industrial wastewater from four cities in the drainage area. According to the goal of municipal water-quality planning, we know that the permissible total water pollution loading of chemical oxygen demanded organic pollutant (COD) of the water body is 35 000t/a [2]. The goal level A of the hierarchy structure model is the allocation goal. B_1, B_2, B_3 and B_4 is social, economic, environmental, and technological & managing criterion respectively. In the criterion level C, C_1 is the proportion of non-farm population, C_2 is the proportion of tertiary-industry employees, C_3 is the unemployment rate of urban workers and staff, C_4 is the medical and health condition level, C_5 is the social-culture level, C_6 is *per capita* gross domestic product, C_7 is *per capita* revenue of the local government, C_8 is the efficiency of social labor, C_9 is the area *per capita* income level, C_{10} is the area *per capita* consuming level, C_{11} is the utilization and protection ratio of water resource, C_{12} is the utilization ratio of carrying capacity of water environment, C_{13} is wastewater discharge of output of ten thousand yuan, C_{14} is COD discharge of output of ten thousand yuan, C_{15} is the urban sewage treatment rate, C_{16}

is the industrial wastewater increasing to the standard rate, C_{17} is the wastewater reuse rate, and C_{18} is advances in science and technology contribution rate. In the evaluated object level D, D_1 , D_2 , D_3 and D_4 are the cities, respectively. According to the Table 1 of reference [2], we obtain the fuzzy complementary judgment matrixes of Level B, C and D. Using IEM, we can get the weights from criteria 1 to criteria 4 of level B as 0.0625, 0.3125, 0.3125 and 0.3125 respectively, the total weight from C1 to C18 relative to the goal of level A as 0.0074, 0.0074, 0.0236, 0.0074, 0.0165, 0.1063, 0.1063, 0.0512, 0.0243, 0.0243, 0.1563, 0.1563, 0.0995, 0.0995, 0.0403, 0.0403, 0.0164 and 0.0164 respectively, the allocation weights from city 1 to city 4 as 0.178, 0.411, 0.186 and 0.225 respectively, and the permissible water pollution loading from city 1 to 4 as 6 230, 14 385, 6 510 and 7 875 t/a respectively. The above results are corresponds to those in [2]. According to the evaluated index values of each city in the Table 1 in [2], comparatively speaking, each index value of city 2 is clearly superior to that of the other three cities. Additionally, most of the indexes of city 4 are superior to those of city 1 and city 3. Each index value of city 1 is noticeably inferior to that of the other three cities.

References

1. Gren IM, Folmer H: Cooperation with Respect to Cleaning of an International Water Body with Stochastic Environmental Damage: the Case of the Baltic Sea. Ecological Economics, (47) 33-42 (2003)
2. Ru-zhong Li, Jia-quan Wang, Jia-zhong Qian: Delphi-AHP Method for Allocation of Waste Loads in a Region. Journal of Harbin of Technology, 37(1) 84-88 (2005)
3. Ming Yao: Fuzzy Information Processing Technology with Computer. Shanghai: Science and Technology Press of Shanghai (1999)
4. Xue-long Zhu: Foundation of Application Information Theory. Beijing: Tsinghua University Press (2001)
5. Ju-liang Jin, Yi-ming Wei, Qiang Fu, *et al*: Accelerating Genetic Algorithm for Computing Rank Weights in Analytic Hierarchy Process. Systems Engineering-Theory & Practice, 22(11) 39-43 (2002)

Using DEA and Grey Markovian Model to Measure the Goal Cost of Petroleum Enterprise

Jin-lan Liu, Meng-dong Wang, and Yin Bai

School of Management, Tianjin University, Tianjin 300072, China
liujinlan@tju.edu.cn, wmd1104@yahoo.com.cn, baiyin@tju.edu.cn

Abstract. With the longstanding development of Chinese petroleum enterprises, the control of discovery and exploitation goal cost is becoming a essential problem. Data Envelopment Analysis (DEA) is a linear programming method for measuring the relative efficiency of decision making units where the presence of multiple inputs and outputs makes comparisons difficult. Grey Markovian model has the merits of both grey model and Markov transition probability matrix model. In this paper, DEA and Grey Markovian model are combined to measure the discovery and exploitation goal cost of petroleum enterprise. This method is applied to the cost analysis of Huabei Oil Company of PetroChina, which gives strong support to the feasibility and availability of the study in this paper.

Keywords: Petroleum Enterprise Discovery Goal Cost, Exploitation Goal Cost, Data Envelopment Analysis (DEA), Grey Markovian Model.

1 Introduction

Petroleum as a kind of non-renewable natural resource is crucial for the development of economy. However, in accordance with the gradual decrease of resource, the discovery and exploitation cost is rising. Cost management should be used to optimize benefits. Most of the enterprises especially those with long history start to focus on cost control in China. Therefore, the study on how to measure and predict the cost accurately for the petroleum enterprise is quite important.

Data Envelopment Analysis (DEA) is a nonparametric linear programming-based method for measuring the relative efficiency of a decision making unit (DMU), which contains multiple inputs and multiple outputs [1]. The CCR model is the first DEA model and has been widely used in the frontier analysis. This model calculates the overall efficiency for each unit, where both technical efficiency and scale efficiency are aggregated into one value [2]. Grey Markovian model combining the grey model and Markov probability matrix model makes full use of historical data and improves the prediction accuracy of greatly fluctuating data sequences [3]. In this paper, we proposed a method to measure discovery and exploitation goal cost of petroleum enterprise by using DEA and Grey Markovian

model. Goal cost prediction of the Huabei Oil Company was taken to illustrate the proposed model.

2 Measuring Discovery and Exploitation Goal Cost

According to the principles of DEA and Grey Markovian model with taking into account the characteristics of the petroleum enterprise's operation style, the discovery and exploitation goal cost can be measured through following steps.

2.1 Calculating the Discovery and Exploitation Goal Cost Coefficients

We postulate that X_i is the discovery cost of the i th year; Y_i is the exploitation cost of the i th year; Q_i is the proved reserve of the i th year; W_i is the crude oil output of the i th year. we can evaluate the relative efficiencies of the discovery and exploitation cost first by using the CCR model of DEA,. Then X_i and Y_j are separately arranged in descending sequence according to their coefficients of relative efficiency and we can get two data sequences: $\{X_j\}$ and $\{Y_j\}$.

The discovery goal cost coefficient:

$$V_1 = \sum_{j=1}^{n/2} X_j \Big/ \sum_{j=1}^{n/2} Q_j \quad . \tag{1}$$

The exploitation goal cost coefficient:

$$V_2 = \sum_{j=1}^{n/2} Y_j \Big/ \sum_{j=1}^{n/2} W_j \quad . \tag{2}$$

Where in (1) and (2), if n is an odd number, let n=n+1.

2.2 Forecasting the Proved Reserve and the Crude Oil Output

Grey Markovian model constructing process can be divided into three steps. First, with GM (1, 1) model utilized, the stimulant sequence $X(k)$ and forecasting values can be got on the basis of the original data sequence. Then $X(k)$ is considered as the benchmark and divide the state into several areas with different curves paralleling to $X(k)$. Each area represents one state. Finally, through studying the state transition probability matrix, we can decide the grey area of the forecasting value and regard the midpoint of it as the most possible predictive value. Following the steps above, we can forecast the proved reserve Q^* and the crude oil output W^*.

2.3 Measuring the Discovery and Exploitation Goal Cost

Annual discovery goal cost:

$$X^* = V_1 * Q^* . \tag{3}$$

Annual exploitation goal cost:

$$Y^* = V_2 * W^* . \tag{4}$$

3 Illustrative Example

Huabei Oil Company of PetroChina has a long exploitation history. The decrease of oil production and the increase of cost result in the reduction of its profit year after year. The method mentioned above was applied to predict the goal cost of Huabei Oil Company.

We arrange the discovery cost of the i th year (X_i) from Table 1 in descending sequence according to its coefficients of relative efficiency shown in Table 2. The same method is used to arrange the exploitation cost of the i th year (Y_i). According to formula (1) and (2), the discovery goal cost coefficient (V_1) is 54.61 yuan/ton and the exploitation goal cost coefficient (V_2) is 730.00 yuan/ton.

From the result shown in Table 3 and through analyzing the state transition probability matrix, the forecasting value of proved reserve in 2006 (Q^*) is 2350.22 (10,000-ton). In the same way, the forecasting result of crude oil output in 2006 (W^*) is 468.14 (10,000-ton). According to formula (3) and (4), the discovery goal cost (X^*) and exploitation goal cost (Y^*) in 2006 can be predicted as 128345.51 (10,000-yuan) and 341742.20 (10,000-yuan) respectively.

Table 1. Historical Data

Year	Discovery Cost (10,000-yuan)	Exploitation input (10,000-yuan)	Proved Reserve (10,000-ton)	Exploitation Cost (10,000-yuan)	Oil wells	Crude Oil Output (10,000-ton)
1998	133,748.0	34,563	2,900	344,246	1,598	469
1999	139,278.0	35,245	2,780	340,112	1,780	464
2000	134,674.5	35,928	2,531	339,915	1,962	465
2001	167,764.6	36,521	2,858	340,180	2,161	466
2002	170,772.0	37,472	2,660	340,443	2,291	467
2003	208,570.3	37,886	2,436	340,236	2,525	468
2004	196,494.4	37,924	2,540	345,290	2,600	473
2005	203,427.3	38,041	2,513	341,112	2,836	466

Table 2. DEA Relative Efficiencies of Discovery Goal Cost

Number	DMU	θ^0	Results of Evaluation
1	1998	1.0000	efficient
2	1999	0.9401	inefficient
3	2000	0.8396	inefficient
4	2001	0.9327	inefficient
5	2002	0.8460	inefficient
6	2003	0.7663	inefficient
7	2004	0.7982	inefficient
8	2005	0.7873	inefficient

Table 3. Fitted Result of the Proved Reserve

Year	Original Value	Fitted Value
1999	2780	2747.51
2000	2531	2702.75
2001	2858	2658.71
2002	2660	2615.39
2003	2436	2572.78
2004	2540	2530.86
2005	2513	2489.63

4   Conclusion

Based on the DEA and Grey Markovian model, a forecasting model of discovery and exploitation goal cost in petroleum enterprise has been set up. From the predicting result of Huabei Oil Company, this model is convenient to apply in practice.

References

1. Nevera Stancheva, Vyara Angelova.: Measuring the Efficiency of University Libararies Using Data Envelopment Analysis. 10th Conference on Professional Information Resources (2004)
2. R. D. Banker, A. Charnes, W. W. Cooper. Some models for estimating technical and scale efficiencies in data envelopment analysis. Management Science, 30(9), (1984) 1078-1092
3. He Yong, Bao Yidan. Grey-Markov Forecasting Model and its Application. Systems Engineering Theory and Practice (1992)
4. A. Charnes, W. W. Cooper, E. Rhodes. Measuring the efficiency of decision making units European Journal of Operations Research, 2(6), (1978) 429-444
5. Sun Jihu. Forecasting Model of Coal Requirement Quantity Based on Grey System Theory. Journal of China University of Mining & Technology, 11(2), (2001) 192–195

A Novel DC Nodal Pricing Method Based on Linear Programming in Competitive Electricity Market

Bo Yang[1,3], Yun-ping Chen[1], Zun-lian Zhao[2], and Qi-ye Han[3]

[1] School of Electrical Engineering, Wuhan University, Wuhan 430072, China
`yangbo@ccpg.com.cn`
[2] State Grid Corporation of China, Beijing 100031, China
`zl-zhao@sgcc.com.cn`
[3] Central China Grid Company Limited, Wuhan 430077, China
`hanqy@ccpg.com.cn`

Abstract. AC based nodal pricing method makes market rule less transparent and affects market decisions on risk and opportunity in short-run and long-run periods. Therefore, AC based nodal pricing formulation is simplified into DC based nodal pricing formulation, which maximizes total social welfare with the condition of satisfying Kirchhoff's laws and other operational constraints in modified DC optimal power flow model. Then, a simple but practical linear programming based nodal pricing method, which can be applied to solve market clearing mode with piecewise constant supply and demand curves, is proposed. The proposed method is tested on IEEE 30 bus system. Test results show that it can avoid premature and divergent phenomenon, which always occurs in the solution of AC based nodal pricing formulation, and has potential application in competitive electricity market.

Keywords: nodal price, linear programming, constrained optimization, optimal power flow, electricity market.

1 Introduction

Nowadays, electricity industry is undergoing deregulation and reconstruction. Spot pricing [1], real-time pricing for active and reactive power [2], and reserve pricing [3] have been proposed to determine price of energy and ancillary services in competitive electricity market. These pricing methods above are mainly based on nodal pricing principle which is supported by marginal cost theory. Mathematically, nodal pricing formulation is a large-scale, nonlinear, multi-variable, and constrained optimization problem. Its objective function is to maximize social welfare on condition that supply and demand curves are given and operational constraints are satisfied. But it has following disadvantages: (1) optimal dispatch schedule including active power and reactive power makes market rule less transparent and hence affects market decisions on risk and opportunity in short-run and long-run periods; (2)optimal price-quantity pairs in supply and demand sides at each node may not be obtained because optimization algorithm is trapped into local optimum or even diverges; (3) two totally

different dispatch schedules may have the same or similar social welfare value, which violates initial intension of market designer and confuses market participants. Therefore, a novel linear programming based DC nodal pricing method is proposed in the paper.

2 Nodal Pricing Formulation

Nodal pricing problem can be formulated as follows:

$$\text{Max} \ B = \sum_{i=1}^{N} [\int_{0}^{S_i^d} p_i^d (S) dS - \int_{0}^{S_i^s} p_i^s (S) dS] \tag{1}$$

subject to:

$$P_i^s - P_i^d - \sum_{j \in N} |V_i| |V_j| |Y_{ij}| \cos(\theta_{ij} + \delta_j - \delta_i) = 0 \tag{2}$$

$$Q_i^s - Q_i^d - \sum_{j \in N} |V_i| |V_j| |Y_{ij}| \sin(\theta_{ij} + \delta_j - \delta_i) = 0 \tag{3}$$

$$P_{i,\min}^s \leq P_i^s \leq P_{i,\max}^s , \ Q_{i,\min}^s \leq Q_i^s \leq Q_{i,\max}^s \tag{4}$$

$$P_{i,\min}^d \leq P_i^d \leq P_{i,\max}^d , \ Q_{i,\min}^d \leq Q_i^d \leq Q_{i,\max}^d \tag{5}$$

$$P_{ij,\min} \leq P_{ij} \leq P_{ij,\max} , V_{i,\min} \leq V_i \leq V_{i,\max} \tag{6}$$

where S, P and Q are apparent power, active power, and reactive power, $Y_{ij} \angle \theta_{ij}$ and $V_i \angle \delta_i$ are the ijth element of bus admittance matrix and voltage at bus i, $p_i^d (S_i^d)$ and $p_i^s (S_i^s)$ are demand curve and supply curve at bus i, respectively. Superscripts d and s denote demand and supply, suffixes max and min denote upper and low limits, respectively. N is a bus set. P_{ij} is active power flow over $i \rightarrow j$.

3 LP-Based Method for DC Nodal Pricing

3.1 Modifications to Nodal Pricing Formulation

Given that branch resistances and charging capacitances are negligible, bus voltage magnitudes are close to 1 p.u., and voltage angle differences are small, AC based nodal pricing formulation can be modified into DC based nodal pricing formulation which is given as follows:

$$\text{Min } B = \sum_{i=1}^{N} [\int_{0}^{P_i^s} p_i^s(P)dP - \int_{0}^{P_i^d} p_i^d(P)dP] \tag{7}$$

subject to:

$$\sum_{i=1}^{N}(P_i^s - P_i^d) = 0 \ , \ P_{i,\min}^s \le P_i^s \le P_{i,\max}^s \ , \ P_{i,\min}^d \le P_i^d \le P_{i,\max}^d \ , \ P_{ij,\min} \le P_{ij} \le P_{ij,\max} \tag{8}$$

3.2 Nodal Price of Active Power

The Kuhn-Tucker conditions for the DC nodal pricing formulation can be solved to obtain nodal price of active power at each bus. λ , $\lambda_{i\max}^s$, $\lambda_{i\min}^s$, $\lambda_{i\max}^d$, $\lambda_{i\min}^d$, $\lambda_{ij\max}$ and $\lambda_{ij\min}$ are Lagrangian multipliers of corresponding constraints.

$$p_i^s(P_i^s) - \lambda + \lambda_{i\max}^s - \lambda_{i\min}^s + \sum_{i,j\in N} \lambda_{ij\max} \frac{\partial P_{ij}}{\partial P_i^s} - \sum_{i,j\in N} \lambda_{ij\min} \frac{\partial P_{ij}}{\partial P_i^s} = 0 \tag{9}$$

$$-p_i^d(P_i^d) + \lambda + \lambda_{i\max}^d - \lambda_{i\min}^d + \sum_{i,j\in N} \lambda_{ij\max} \frac{\partial P_{ij}}{\partial P_i^d} - \sum_{i,j\in N} \lambda_{ij\min} \frac{\partial P_{ij}}{\partial P_i^d} = 0 \tag{10}$$

$$\sum_{i=1}^{N}(P_i^s - P_i^d) = 0 \tag{11}$$

$$\lambda_{i\max}^s(P_{i\max}^s - P_i^s) = 0 \ , \ \lambda_{i\min}^s(P_i^s - P_{i\min}^s) = 0 \tag{12}$$

$$\lambda_{i\max}^d(P_{i\max}^d - P_i^d) = 0 \ , \ \lambda_{i\min}^d(P_i^d - P_{i\min}^d) = 0 \tag{13}$$

$$\lambda_{ij\max}(P_{ij\max} - P_{ij}) = 0 \ , \ \lambda_{ij\min}(P_{ij} - P_{ij\min}) = 0 \tag{14}$$

3.3 Solution Method

In many existing electricity markets, market rules set strict restrictions on the form of demand and supply curves. For example, demand and supply curves are required to be constant or piecewise constant functions. Since all constraints are linear in our proposed DC nodal pricing formulation, linear programming can be used to solve nodal price of active power at each bus if the restrictions above are imposed on demand and supply curves. It can avoid premature and divergent phenomenon, which always occurs in the solution of AC based nodal pricing formulation, and give certain price signal for market participants in competitive electricity market.

4   Simulation Results

To demonstrate the feasibility of the proposed method, we test it on IEEE 30 bus system [4]. In the experiment, demand price elasticity is zero and supply curve is piecewise constant function. Two cases are studied. In case 1, power flow limit over each transmission line is not attained; in case 2, power flow limits over transmission line $1 \rightarrow 2$ and $1 \rightarrow 3$ are decreased from 130 MW to 16MW. After computation by the proposed method, nodal price at each bus is 44.000$/MW in case 1, but is different in case 2. Nodal prices of case 2 are given in Fig. 1. Apparently, because of power flow limits over transmission line $1 \rightarrow 2$ and $1 \rightarrow 3$, nodal price dramatically decreases at bus 1, greatly increases at bus 2, slightly changes at bus 13,22,23 and 27. Besides, we can draw a conclusion that power flow transmission limit has greater influence on nodal price at neighboring bus than at remote bus.
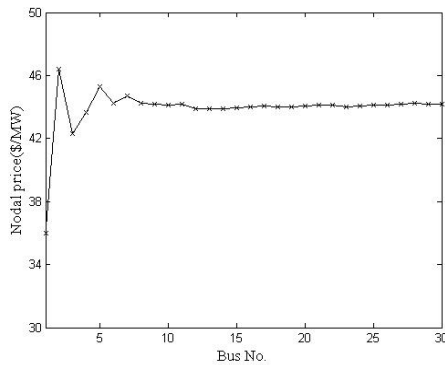
Fig. 1. Nodal price at each bus in case 2

5   Conclusions

A novel DC nodal pricing method based on linear programming is proposed in the paper. It can provide useful price signal for demand and supply sides. Because of its simplicity and practicability, it can be applied to day-ahead and balance markets.

References

1. F. C. Schweppe, M. C. Caramanis, R. D. Tabors and R. E. Bohn: Spot Pricing of Electricity. Kluwer Academic Publishers (1988)
2. M. L. Baughman and S. N. Siddiqi: Real-time Pricing of Reactive Power: Theory and Case Study Results. IEEE Trans on Power Systems. 1(6)(1991)23-29
3. E. H. Allen and M. D. Ilic: Reserve Markets for Power Systems Reliability. IEEE Trans on Power Systems. 1(15)(2000)228-233
4. R. W. Ferrero, S. M. Shahidehpour, V. C. Ramesh: Transaction analysis in deregulated power systems using game theory. IEEE Trans on Power Systems. 3(12)(1997) 1340-1347

Risk Analysis with Information Described in Natural Language

Chongfu Huang[1,2]

[1] Key Laboratory of Environmental Change and Natural Disaster
The Ministry of Education of China, Beijing Normal University
No.19 Xinjiekouwai Street Beijing 100875, China
[2] Research Center for System Simulation and Disaster Modeling
Academy of Disaster Reduction and Emergency Management
Ministry of Civil Affairs & Ministry of Education
hchongfu@bnu.edu.cn

Abstract. In this paper, we give a new definition of risk: a scene in the future associated with some adverse incident. The simplest scene is that, a stone is hooked over our head. When a wind comes, the stone would fall down on our head. In many cases, what can we do is to approximately represent risks. In this paper, we suggest an approach to infer risks with information described in natural language. With fuzzy logic, we give a sample to verify that the suggested approach is more flexible and effective.

Keywords: Risk Analysis; Natural Language; Fuzzy Logic.

1 Introduction

All goals of developing science and technology are specified three categorizations for daily life: (1) Producing high quality goods with low variable costs; (2) Exploring the mystery of the world; (3)Providing safety.

Five years ago, the world witnessed an unprecedented attack on the civilized world. The attacks of 9/11 shocked men and women everywhere, and images from that day remain etched in the minds of all of us who saw them. On that dreadful day, al-Qaida's hijack crews stole the future from nearly 3000 innocent people, devastating the lives of their families and friends.

Since then, the content of concept of safety is much relevant to homeland security and personal safety against terrorism. The aftermath of the attacks also clearly demonstrates the spirit of the civilized world and the enormous capacity of this world to unite; to coordinate efforts among civilized countries, organizations, as well as among private businesses, community groups, and individual citizens in response to a crisis; and to make the sacrifices necessary to respond both to these new threats and the consequences they entail.

Our challenge is to build upon a renewed purpose in ways that create both short- and long-term benefits and allow us to sustain our efforts. As a result, we must find the best ways to sustain our efforts over a significant time period and leverage our finite resources in ways that will have the greatest effects.

An effective framework to address these challenges will require a risk management approach to focus finite resources on areas of greatest need.

However, although the United States of America has the greatest number of high-technology tools, until now it does not have a comprehensive risk management approach [5] to help guiding federal programs for homeland security and apply their resources efficiently and to best effect. One of the main reasons why it is difficult to promote risk management in the new safety issue is that users have little confidence in the results of their risk analysis from incomplete data in a short time for a very complex system. In this paper, we will suggest an approach to study the information described in natural language for improving risk analysis.

This paper is organized as follows. In Section 2, we give a new definition of risk and a sample scene of risk. We outline of some methodologies for risk analysis and indicate their disadvantage in Section 3. We suggest an approach to infer risks with information described in natural language in Section 4. With fuzzy logic, in Section 5, we give a sample to verify that the suggested approach is more flexible and effective. We conclude the paper in Section 6.

2   A New Definition of Risk

Safety is the state of being certain that adverse effects will not be caused by some agent under defined conditions. The reciprocal of safety is risk.

There is no widely accepted definition of risk. Four items are found for risk in Webster Dictionary:

(1) Possibility of loss or injury;
(2) Someone or something that creates or suggests a hazard;
(3) a: The chance of loss or the perils to the subject matter of an insurance contract; *also*: the degree of probability of such loss.
    b: A person or thing that is a specified hazard to an insurer <a poor *risk* for insurance>.
    c: An insurance hazard from a specified cause or source <war *risk*>.
(4) The chance that an investment (as a stock or commodity) will lose value.

Obviously, the core of all definitions of risk is the same: risk exists when loss is possible and its financial impact is significant. This linguistic definition captures a property of risk that eludes definition in terms of mathematical formulas where risk had been defined as the probability per unit time of the occurrence of a unit cost burden [4].

But, what on earth is risk, anyway? Is it "loss"? "probability"? or "probability of loss"? No, they are not. They are at most features of risk. In fact, risk is a synthetic phenomenon that would be described in Definition 1.

Definition 1. *Risk is a scene in the future associated with some adverse incident.*

Scene means something seen by a viewer; a view or prospect. *Adverse* is contrary to one's interests or welfare; harmful or unfavorable.

A scene must be described with a system consisting of time, site and objects. The association would be measured with a metric space (such as probability). And, incident would be scaled with a magnitude (such as loss).

It is interesting to notice that, the concept of risk in Chinese is represented in two Chinese characters: "feng" and "xian," the former means "wind", and the latter "danger."

The risk meaning described in Chinese leads to a sample scene: a stone is hooked over our head. When a wind comes, the stone would fall down on our head. If the stone is small, or the hook can firmly hold the stone, any wind doesn't matter for us with respect to the stone. Otherwise, we have to take some prevention measure. Meanwhile, one day, the stone may fall down without any wind if the hook is made of wood. In the scene, there are three objects: stone, wind and our head. The wind would be replace by another force. For example, moth eats the wooden hook.

3   Outline of Some Methodologies for Risk Analysis

Risk management is the process of evaluating and, if necessary, controlling sources of exposure and risk. The culture, processes and structures that are directed towards the effective management of potential opportunities and adverse effects.

Risk evaluation is the process used to determine risk management priorities by comparing the level of risk against predetermined standards, target risk levels or other criteria.

Risk analysis is a systematic use of available information to determine how often specified events may occur and the magnitude of their consequences.

Risk assessment is the overall process of risk analysis and risk evaluation.

Strictly speaking, risk management covers the hazard identification and risk analysis, but focuses on executing, monitoring and controlling. On the other hand, risk analysts often divide risk analysis into these components: risk assessment, risk management and risk communication.

According to Definition 1, we know that the risk is a scene. Therefore, we refer to risk management as an appropriate activation so that our environment will become more safe, and refer to risk analysis as a scientifically description of a risk system so that the risk management will become more effective.

There have been appearing a lot of risk analysis methodologies. Among them, the following 11 methodologies are more popular.

(1) Failure Modes, Effects and Criticality Analysis (FMECA);
(2) Failure Mode and Effect Analysis (FMEA);
(3) Fault Tree Analysis (FTA);
(4) Hazard and Operability Analysis (HAZOP);
(5) Cause Consequence Analysis (CCA);
(6) Management Oversight Risk Tree (MORT);

(7) Safety Management Organization Review Technique (SMORT);
(8) Risk Analysis Bibliographies (RAB);
(9) Security/Survivability Systems Analysis (S/SSA);
(10) Cost-Effectiveness Analysis in Emergency Medicine, Computer (CEA);
(11) Cost Benefit Analysis (CAB)

Most of them involve the assumption that a risk system can be decomposed into several subsystems where the corresponding risks are known. For example, FTA is a deductive procedure for determining the various combinations of hardware and software failures, and human errors that could result in the occurrence of specified undesired events. Another example: one of basic steps in an FMEA is to enter the probability factor where a numerical weight should be assigned to each cause that indicates how likely that cause is (probability of the cause occurring).

In the cognitive viewpoint, there are four different types of societal risks [3]:

(T1) *Real risk* to an individual — eventually by future circumstances when they fully develop;
(T2) *Statistical risk* — determined by currently available data, typically measured actuarially for insurance premium and other purposes;
(T3) *Predicted risk* — predicted analytically from system models structured from historical studies;
(T4) *Perceived risk* — intuitively seen by individuals.

Therefore, the methodologies for risk analysis also can be specified four categorizations: (1) Investigating the current scene; (2) Statistically inferencing; (3) Modelling the future scene; (4) Evaluating with expert experiences.

Obviously, the core of risk analysis is not to combine the subsystems but to analyze the subsystems. The main disadvantage of these methodologies is that they depend on so much assumptions for subsystems, such as that we can find a statistical rule to show the risk phenomenon properly, or find some state equations to describe risk systems, or acquire expert experiences to understand the risk phenomenon. The real cases told us, it is difficult to verify if the assumptions are reasonable.

Beck [1] viewed the increasing focus on risk as the consciousness of a new stage of development in society. The return of uncertainty is the difference between an industrial society and a risk society. If it is barely possible to analyze risks in industrial societies with explicit assumptions, it will be impossible to analyze risks in post-modern societies with these assumptions. In many cases, only a few pieces of information in massive information are available; the environment is not clear and we are required to response quickly. We have to make a decision in an uncertain environment with fuzzy information as soon as possible. It is impossible to accurately analyze risks in complex systems. In the future, we would have to analyze risks by computing with words [7], or with images, in which we would process fuzzy information more efficiently. Fuzzy set theory is created to computing with words.

4   Inferring Risks with Information Described in Natural Language

Computation with information described in natural language, or NL-computation for short, is a problem of intrinsic importance because much of human knowledge is described in natural language [8]

Basically, NL-Computation is a system of computation in which the objects of computation are words and propositions drawn from a natural language. NL-Computation is reduced to computation with generalized constraints, that is, to generalized-constraint-based computation. NL-Computation is based on fuzzy logic. NL-Computation is closely related to Computing with Words (CW).

Here is an example of NL-Computation in risk analysis. A middle stone is hooked over our head with a wooden hook. If a storm comes, the stone would fall down on our head. It is called a stone-hook-wind system (SHW-system). Our task is to analyze what risk, with high possibility, we have to bear if we don't take any prevention measure?

Let E be risk in values: *yes* (the stone will fall down) or *no* , X be the features of the hook (strength and fastness), and Y be the features of the storm (force and frequency). X, Y are imprecisely described in natural language. Particularly, Y is a fuzzy random vector. The risk analysis is to calculate:

$$Prob(E = yes) \text{ with high possibility.} \tag{1}$$

In general, we are used to calculate $Prob(E = yes)$ by using observations based on some distribution assumptions or non-parametric method. However, now, we haven't any observation, but only information described in natural language about stone, hook and wind. It is impossible to directly calculate $Prob(E = yes)$ by using any traditional method.

The approach to NL-computation centers on what is referred to as generalized-constraint-based computation. A generalized constraint is expressed as "X is$r$ A," where X is the constrained variable, A is a constraining relation and r is an indexical variable which defines the way in which A constrains X.

NL-computation cannot be dealt with through the use of machinery of natural language processing. The problem is semantic imprecision of natural languages. More specifically, a natural language is basically a system for describing perceptions. Perceptions are intrinsically imprecise, reflecting the bounded ability of sensory organs, and ultimately the brain, to resolve detail and store information. Semantic imprecision of natural languages is a concomitant of imprecision of perceptions.

To a SHW-system, there is no loss of generality in assuming that "X isr_1 A" and "Y isr_2 B", where

$$X = \{X_1, X_2\} = \{strength, fastness\}, \tag{2}$$

$$Y = \{Y_1, Y_2\} = \{force, frequency\}, \tag{3}$$

$$r_1 = \{r_{11}, r_{12}\} = \{blank, blank\}, \tag{4}$$

$$r_2 = \{r_{21}, r_{22}\} = \{p, p\}, \tag{5}$$

where *blank* means the possibilistic constraint and p means the probabilistic constraint. Then,

$$\begin{aligned} &Prob(E = yes) \text{ with high possibility} \\ &= Prob(B|E = yes \text{ with high possibility determined by } A). \end{aligned} \tag{6}$$

5   A Calculation Case

The information for our case is that a middle stone is hooked over our head with a strong wooden hook *almost fast*. If the hook doesn't hold the stone *absolutely fast*, when a wind comes, the stone would fall down. The winds more than 40 km/h have been frequently observed in this region.

What risk do we face?

Let E be risk in values: 1 or 0 (down or not down). Let X be the fastness of that the hook holds the stone, with universe:

$$U = \{u_1, u_2, \cdots, u_{11}\} = \{0, 0.1, \cdots, 1\},$$

Y be the intensity (km/h) of a wind, with universe:

$$V = \{v_1, v_2, \cdots, v_{12}\} = \{0, 10, \cdots, 110\}.$$

From the information about the SHW-system, specifically described in natural language, we obtain:

$$X \text{ is } A$$

where

$$A \triangleq almost\ fast$$

with membership function

$$\mu_A(u) = \frac{0.3}{0.6} + \frac{0.6}{0.7} + \frac{1}{0.8} + \frac{0.6}{0.9} + \frac{0.3}{1}.$$

Suppose that, from information "If the hook doesn't hold the stone *absolutely fast*, when a wind comes, the stone would fall down," we obtain a falling table determined by u and v, shown in Table 1, where 1 means that the stone will fall down, and 0 means the hook can hold the stone.

We suppose that, the information "The winds more than 40 km/h have been frequently observed in this region" can be interpreted as that the average intensity of the wind is 40 km/h. Because the number of weak winds is much more than the number of strong winds, we suppose the probability distribution of the intensity is exponential.

Table 1. Falling table determined by the fastness and the intensity

Fastness	Intensity (km/h)											
	0	10	20	30	40	50	60	70	80	90	100	110
0	1	1	1	1	1	1	1	1	1	1	1	1
0.1	0	0.9	1	1	1	1	1	1	1	1	1	1
0.2	0	0.6	0.9	1	1	1	1	1	1	1	1	1
0.3	0	0.3	0.6	0.9	1	1	1	1	1	1	1	1
0.4	0	0	0.3	0.6	0.9	1	1	1	1	1	1	1
0.5	0	0	0	0.3	0.6	0.9	1	1	1	1	1	1
0.6	0	0	0	0	0.3	0.6	0.9	1	1	1	1	1
0.7	0	0	0	0	0	0.3	0.6	0.9	1	1	1	1
0.8	0	0	0	0	0	0	0.3	0.6	0.9	1	1	1
0.9	0	0	0	0	0	0	0	0.3	0.6	0.9	1	1
1	0	0	0	0	0	0	0	0	0	0	0	0

Then, we obtain a probability distribution of the intensity of a wind:

$$p(v) = 0.025e^{-0.025v}.$$

Table 1 can be regarded as a fuzzy relation matrix between fastness and intensity, constrained by falling phenomena. From input "almost fast", with the max-min composition [2], we obtain an output B, called *strong* wind, that makes the stone falls, with membership function:

$$\mu_B(v) = \frac{0.3}{40} + \frac{0.3}{50} + \frac{0.3}{60} + \frac{0.6}{70} + \frac{0.9}{80} + \frac{1}{90} + \frac{1}{100} + \frac{1}{110}.$$

The probability of the fuzzy event is [6]:

$$P(B) \approx \int_0^{110} \mu_B(v)p(v)dv$$

$$\approx 0.025(0.3\int_{35}^{65} e^{-0.025v}dv + 0.6\int_{65}^{75} e^{-0.025v}dv + 0.9\int_{75}^{85} e^{-0.025v}dv$$

$$+ \int_{85}^{110} e^{-0.025v}dv)$$

$$= 0.178154.$$

Therefore, we know that, the risk we face is

$$Prob(E = yes) \text{ with high possibility}$$

$$= Prob(B|E = 1 \text{ with high possibility determined by } A)$$

$$= Prob(B)$$

$$= 0.178154$$

i.e., the probability of that the stone falls is 0.178154 with high possibility. From the given information described in natural language, it is impossible to accurately calculate the probability of the falling of the stone. Here, the probability value 0.178154 is induced by using fuzzy logic. Because the inference is comparatively reliable, the value 0.178154 can be regarded one near real probability with high possibility.

6   Conclusion and Discussion

Risk is a scene in the future associated with some adverse incident. This linguistic definition can capture all properties of risk that eludes definition in terms of mathematical formulas.

It is possible to analyze risk with information described in natural language. The fuzzy logic can be used to quantify the information and infer the risk where computation with information described in natural language is reduced to computation with generalized constraints, that is, to generalized-constraint-based computation.

The basic condition to compute risk with information described in natural language is that we can understand the semantic in the information and change it into constraints. With the same information described in natural language, different experts would infer different risks due to different backgrounds. Therefore, any risk inferred from the natural language is soft. To limit the soft degree, it is necessary to form a set of kernel terms used to describe risk so that different experts have almost same understanding for each term in the set.

References

1. Beck, U.: Risk Society, Towards a New Modernity. Sage Publications, London (1992)
2. Huang, C.F., Shi, Y.: Towards Efficient Fuzzy Information Processing — Using the Principle of Information Diffusion. Physica-Verlag, Heidelberg (2002)
3. Sage, A.P., White, E.B.: Methodologies for Risk and Hazard Assessment: a Survey and Status Report. IEEE Trans. Systems, Man, and Cybernetics, **SMC-10**(8) (1980) 425–446
4. Starr, C., Whipple, C.: Risks of Risk Decisions. *Science*, **208**(4448) (1980) 1114–1119
5. United States General Accounting Office: Homeland Security: Challenges in Creating an Effective Acquisition Organization. GAO-06-1012T, Washington D.C., 2006
6. Zadeh, L.A.: Fuzzy Probabilities. Information Processing Management, **20**(3) (1984) 363–372
7. Zadeh, L.A.: Fuzzy Logic = Computing with Words. IEEE Trans. Fuzzy Systems, **4**(2) (1996) 103–111
8. Zadeh, L.A.: Computation with Information Described in Natural Language – The Concept of Generalized-Constraint-Based Computation. In: Ruan, D., D'hondt, P., Fantoni, P.F., De Cock, M., Nachtegael, M., Kerre, E.E. (eds.): Applied Artificial Intelligence. Proceedings of the 7th International FLINS Conference (Genova, Italy, August 29-31, 2006). World Scientific, Singapore (2006) 3–4

Risk Assessment Method Based on Business Process-Oriented Asset Evaluation for Information System Security⋆

Jung-Ho Eom, Seon-Ho Park, Young-Ju Han, and Tai-Myoung Chung

Internet Management Technology Laboratory,
Department of Computer Engineering,
School of Information and Communication Engineering,
Sungkyunkwan University,
300 Cheoncheon-dong, Jangan-gu,
Suwon-si, Gyeonggi-do, 440-746, Republic of Korea
{jheom,shpark,yjhan}@imtl.skku.ac.kr and tmchung@ece.skku.ac.kr

Abstract. We presented risk assessment methodology focused on business-process oriented asset evaluation and qualitative risk analysis method. The business process-oriented asset evaluation is to evaluate asset's value by the degree of asset contribution related to business process. Namely, asset's value is different according to the importance of department to which asset belongs, the contribution of asset's business, and security safeguard, etc. We proposed new asset's value evaluation applied to the weight of above factors. The weight is decided by evaluation matrix by Delphi team. We assess risk by qualitative method applied to the improved international standard method which is added the effectiveness of operating safeguard at information system. It reflects an assumption that they can reduce risk level when existent safeguards are established appropriately. Our model derives to practical risk assessment method than existent risk assessment method, and improves reliability of risk analysis.

1 Introduction

As information communication technology has developed steeply, business dependence on IT system is raising rapidly. As IT system has occupied important role in business, it begins to increase the concern of security on IT system. To protect IT system effectively, it firstly needs to analyze overall IT system risks. That is a risk assessment included the identification and valuation of assets, threat analysis, vulnerability analysis, the existing safeguards analysis and risk evaluation[1,4,5]. We have been studying on develop substantial risk assessment

method which could be evaluated risk level according to asset importance in organization. We focus on asset analysis reflected an organization's information system(IS) characteristics and environment for assessing risk effectively. So, we applied business process-oriented asset analysis which an asset's importance could be different in organization's business-process viewpoint, even if assets have same costs. Section 2 describes related work, section 3 presents our model and section 4 demonstrates application of our model. Finally, we conclude in section 5.

2   Related Works

2.1   Risk Assessment

Risk assessment is to assess a combination of the potential adverse business impacts of unwanted incidents and the levels of vulnerabilities and threats. The risk is a measure of the exposure to which an IS and the associated organization may be subjected. The risk assessment's goal is to identify and assess the risks to which the IS and its assets are exposed, in order to select appropriate and justified safeguards. Thus, the risk assessment is based on the values of the assets, the levels of threats and vulnerabilities and the existing/planned safeguards.

The risk assessment method has two types; qualitative and quantitative methods. The former uses the rating scale which is evaluated with asset, threat and vulnerability rating. The Delphi team decides rating scale with a degree of asset sensitivity, capability and motivation of threat and severity and exposure of vulnerability. The Table 1 is the method of rating scale in 'CSE Manuals ITSG-04' [8]. A degree of asset sensitivity is divided into 5 scales; little/no loss or injury (1), minor loss or injury (2), serious loss or business process could be negatively affected (3), very serious loss/injury, business process could fail (4), high loss or grave injury to an organization's or business process will fail (5).

Table 1. The matrix of risk assessment

	Scale of Threat	1					2					..
	Scale of Vulnerability	1	2	3	4	5	1	2	3	4	5	..
	1											
	2											
Asset	3											

Threat assessment is same as vulnerability assessment method. So, risk assessment is evaluated by combination with asset, vulnerability and threat scale.

The latter uses annual loss expectancy(ALE) in [12]. ALE defines damage that may be imposed to IT asset by monetary unit. ALE is used in quantitative analysis representatively since NIST proposed evaluation method by FIPS-65 document in 1979. ALE production method is as following.

$$ALE = Asset\ value(AV) \times Exposure\ factor(EF) \times Threat\ frequency(TF)$$

Asset value and threat frequency is computed in asset and threat analysis. Exposure factor(EF), which displays a degree of asset's exposure against threat, is computed from the ratio of the related safeguard/operating safeguard and non-establishing safeguard on the basis of the relation of asset and threats.

2.2   The Method of Asset Analysis

An asset is a component or part of a total information system to which an organization directly assigns value[7,9]. An asset analysis identifies all assets within a risk analysis boundary, classifies into the same kind of asset, and finally assesses value of each asset. An asset analysis' goal is to identify the most critical components of the organization so that they can be examined for vulnerabilities[5,7]. We observed an existent asset analysis method in the 3 viewpoints; classification, evaluation and level.

- ISO TR-13335 : This researches techniques for the successful management of IT security, and can be used to assess security requirements and risks [1,2,3].
  - Classification: Classify the boundaries of review into asset types such as information/data, hardware, software, equipment, documents, etc.
  - Evaluation: Evaluate by the cost of obtaining and maintaining the asset, and the potential adverse business impacts from loss of 3 security factors.
  - Evaluation Scale: negligible(0)-low(1)-medium(2)-high(3)-very high(4)

- CSE MG-3 : This expands on the standards stated in the Government Security Policy of Canada, provides specific guidance for risk assessment, and safeguards throughout the information technology system lifecycle [8].
  - Classification: Hardware, software, interfaces, personnel, supporting systems and utilities, and access control measures
  - Evaluation: Evaluate based on its replacement cost, its intrinsic value and the consequences, impact or injury resulting from asset compromise.
  - Evaluation Scale: negligible-low-medium-high-very

3   The Proposed Methodology

The proposed methodology is the business-process oriented risk assessment methodology. We assess IS asset with the relationship of business-process than asset's physical value such as purchase cost, annual maintenance expense and so on. We considered that they have a different value according to IS assets contribution to business process, even if they are same kind of asset. We focus on business process-oriented risk assessment methodology according to the contribution degree of asset in the organization's business.

3.1   Business Process-Oriented Asset Evaluation

We classify assets by asset 7 types in the general IS components such as H/W, S/W, network, information, application, user and environment. Then, we reclassify by a business-process oriented method [11].

The proposed asset evaluation considers that asset value could be different according to department utilization, business contribution, user position, etc., even if assets have same type. For example, it has a different value between financial and plan department, even if they are the same kind of PC. For example, it is Department A's server B, application D used with job C, data G, and user E. The examples of standards of specific factors for the business process-oriented evaluation method are as following:

- **Department Utilization(DU)** department's IT utilization according to the organization business
- **Business Contribution(BC)** Asset importance contributing to the organization on business
- **User Position(UP)** Task importance handling by user in the IS
- **Security Safeguard(SS)** Suitability of the safeguard that is established against risk

Table 2 shows an example of an improved asset classification which represents the relationship between the asset type and business-process oriented factors.

Table 2. An example of the proposed asset classification method

		ASSET				
		H/W		S/W		NETWORK
		Disk	Sever	MS Office	Security Program	Router	LAN
BUSINESS		USER.1					
CONTRI	DU	USER.2		**Asset.N**			
BUTION		USER.n					

We applied weight to analyze asset according to the scale of business process-oriented classification factors. Weight factors can be applied from 1 to n reflected an IS environment and business process. Also, weight is classified into five levels such as very low, low, medium, high, very high, and applied on a scale of $1-5$. We selected two business process-oriented classification factors such as department utilization and business contribution, but you can select more factors according to the organization's requirement and Delphi team's opinion.

We made up conversion table for converting quantitative asset cost into the qualitative value as like Table 4 . Delphi team has to create a conversion table based on an average between the organization's maximum and minimum quantitative asset value.

In this step, we have to evaluate the business process-oriented asset value(B-PAV). If the qualitative value is QV, the B-PAV formula is as follows;

Table 3. The evaluation standard of BU and DC

	Level	Scale	Standard
	Very low	1	do not use virtually IS; business weight is less than 20%
	Low	2	business dependence on IS is low; business weight is 20-40%
D	Medium	3	If using an IS, business is gone easy; business weight is 40-60%
U	High	4	Most business is achieved due to IS; business weight is 60-80%
	Very high	5	If an IS is not used, business is impossible; business weight is more than 80%
	Very low	1	don't use virtually IS; don't influence in operation
	Low	2	Business dependence on an IS is low; the most basic business
B	Medium	3	If using an IS, business is gone easy; business achieve certainly
C	High	4	Most business is achieved by IS; essential to the organization
	Very high	5	If not using an IS, business is impossible; critical business related to operation

$B - PAV = QV * W$

W is weight which uses a scale of business process-oriented classification factor.

$W = (W1 + W2 + W3 + + Wn)/n$

3.2 Risk Evaluation Method

We evaluate risk by such as asset value(AV), threat frequency(Tf), exposure degree(Ed) and effectiveness degree of safeguard(SED). AV is B-PAV. ED is evaluated by vulnerability assessment method in CSE Manuals ITSG-04. Delphi team can acquire Tf's rates through questionnaire or interview with system and security administrators or statistic log file of control systems directly. Risk evaluation formula is as following;

$R = B - PAV * Tf * Ed * SED$

SED influences in protection level according to implementation result(IR), and means different protection degree(PD) on each threat. Also, because there are various kinds of safeguard in a threat, each safeguard value should be reflected. And because effectiveness of safeguard is no actual 100%, The value of SED is;

$S = 1 - (S_{IR} * S_{PD})$.

So, $R = B - PAV * Tf * Ed * [1 - (S_{IR} * S_{PD})]$.

4 Application of Proposed Method

We take any enterprise as an example. The company has such departments as R&D, financial and plan departments, and uses router($350). It has only a firewall for protect IS.

Firstly, we have to convert physical cost into qualitative value by conversion table. Delphi team decides the weights with the evaluation standard of the business process-oriented classification factor. For example, the R&D department UNIX is more important than the Financial Departments. And the Financial

<div align="center">

Table 4. An example of conversion table

</div>

Qualitative value		Standard of the asset physical cost
Level	Scale	
Very low	1	The asset physical cost is less than $100
Low	2	The asset physical cost is $100-300.
Medium	3	The asset physical cost is $300-600.
High	4	The asset physical cost is $600-900.
Very high	5	The asset physical cost is $1,000.

Department's firewall is more important than the Plan Departments. If we perform like this method, we can decide weight value of each asset. If we evaluate the asset by the Table 4, each B-PAV value is as following Table 5.

<div align="center">

Table 5. The result of weights decision and B-PAV calculations

</div>

		weights decision						B-PAV calculations				
		R&D		Financial		Plan		R&D		Financial		Plan
Asset	QV	DU	BC	DU	BC	DU	DC	W	B-PAV	W	B-PAV	W	B-PAV
Router	3	2	2	5	4	4	2	2	6	4.5	13.5	3	9

Tf's values were derived by Delphi Team which combines experts in the arena of IS security and referred 'In the past 12 months, which of the following breaches have you experienced?' in InfoSecurity News May 1997. Tf is considered such 15 items as computer virus, accidental errors and abuse of access privileges and so on. Ed is evaluated by Delphi Team based on vulnerability assessment in CSE Manuals. S_{PD} was derived following Table 6 which represents according to ISO/IEC JTCI/SC27 IT security management guideline. S_{IR} was derived from safeguard list in [3]. It classified 5 levels according to implementation results.

We can calculate SED with Table 6. Router's SED value is 0.65 according to S_{PD} and S_{IR} is 0.5 and 0.7. Firewall has direct relation to the threat, and is enough to reflect security procedure. And Table 7 is risk assessment value.

If we compare international standard with the proposed method, we evaluate risk reflected organization's business process, and have more accurate risk assessment considered effectiveness of existent safeguard. As applying correct risk assessment's results, we can establish security policy and appropriate safeguard against risk. In here, we compare router's risk value in 3 viewpoints; international standard, method applied to only business process-oriented asset value and proposed method.

As you see Fig.1, if we assess router's risk at each department, its risk is same. But router's risk is different if applied to business process-oriented asset evaluation result or the proposed risk assessment method. As financial department takes charge of an organization's budget which handles business expanse and employee's salary, if information is leaked out or destructed from threat, an

Table 6. The values of Tf ,Ed , S_{PD} and S_{IR}

	Sever	UNIX	Router		Sever	UNIX	Router
Tf	7.3	5.1	3.7	**Ed**	4	3.5	2.5

	Value	Description
	0.0	No relation safeguard and the threat
	0.165	Safeguard has indirect relation to the threat
S_{PD}	0.5	Safeguard has direct relation to the threat
	0.865	Safeguard established for the threat
	0.1	No safeguard
	0.3	Identified risk, but no concrete safeguard and occasional protect
S_{IR}	0.5	set up protection procedure and start to implement safeguard
	0.7	Reflecting procedure and apply safeguard
	0.9	Perform the latest safeguard

Table 7. Risk value

		R&D	Financial	Plan
	B-PAV	6	13.5	9
	Tf	3.7	3.7	3.7
Router	Ed	2.5	2.5	2.5
	SED	0.65	0.65	0.65
	R	**36.08**	**81.17**	**54.11**
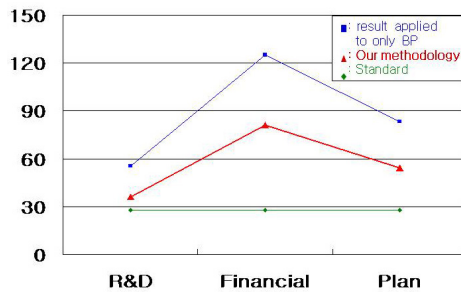
Fig. 1. The result of risk assessment for router

organization will be seriously impacted. So, in financial department viewpoint, router' value with business importance may be high, and risk level may be higher accordingly, and security safeguard may be established strongly.

5   Conclusion

We proposed risk assessment methodology based on business process-oriented asset evaluation and risk evaluation method. We have studied on our research in

2 aspects; business process-oriented asset analysis and concrete risk evaluation formula. The former focuses on asset value according to the importance of business process. Asset value depends on a business contribution of asset. The latter focuses on risk calculation. Our model applies international standard method to effectiveness of existent safeguard. It represents that risk value can be reduced by safeguard's fitness in information system. In future, we will apply our model to risk reduction method. We think that our model's result derives to select the suitable safeguard against risk.

References

1. ISO/IEC TR 13335(Part 1): Concepts and Models for IT Security, ISO/IEC JTC1/SC 27, 1996.
2. ISO/IEC TR 13335(Part 2): Managing and Planning IT Security, ISO/IEC JTC1/SC 27, 1997.
3. ISO/IEC TR 13335(Part 3): Techniques for the Management of IT Security, ISO/IEC JTC1/SC 27, 1997.
4. NIST Special Publication 800-30: Computer Security-Risk Management Guide, NIST, 2001.
5. B. D. Jenkins, 'Security risk analysis and management', Countermeasures Inc, 1998.
6. BS 7799: Guide to Risk Assessment and Risk management, BSI, 1998.
7. C. J. Alberts et al,'OCTAVE: Operationally Critical Threat, Asset, and Vulnerability Evaluation', Software Engineering Institute Carnegie Mellon, 1999.
8. CSE MG-3: A Guide to Risk Assessment and Safeguard Selection For Information Technology Systems, Communications Security Establishment, Jan. 1996.
9. Risk Analysis and Management Standards for Public Information Systems Security-Concepts and Models, TTA-Korea, 1998.
10. Risk Analysis and Management Standards for Public Information Systems Security-Risk Analysis, TTA-Korea, 2000.
11. Jung-Ho Eom, et. al, 'Two-Dimensional Qualitative Asset analysis Method based on Business Process-Oriented Asset Evaluation', Journal of KIPS, pp.79-85, Dec. 2005.
12. Kang Kim, et. al, 'A Risk Analysis Model For information System Security', journal of KIPS, pp.60-67, Sep. 2002.

Epidemic Alert & Response Framework and Technology Based on Spreading Dynamics Simulation

Chunhua Tian[1], Xun Zhang[2], Wei Ding[1], and Rongzeng Cao[1]

[1] IBM China Research Laboratory, Beijing, China
{chtian,dingw,caorongz}@cn.ibm.com
[2] China Academy of Science, Beijing, China
zhangx04@mails.gucas.ac.cn

Abstract. There have been many research works on epidemic spreading by mathematical or simulation methods. However, to make it practical as a decision support tool for policy maker, it should be combined with business operation of epidemic control. Thus, an alert and response framework covering outbreak detection, policy analysis and policy execution is proposed in this paper. Key technologies for such a framework at modeling, analysis and data collection aspects are discussed. Sensitivity analysis is proposed for model verification and confidence analysis. Critical point identification is another important topic for control policy making by network topology analysis. The importance and feasibility of these technologies are illustrated by the experiment on Beijing SARS (Severe Acute Respiratory Syndrome) data in 2003.

Keywords: Epidemics Simulation, Epidemic Alert & Response, Sensitivity Analysis, Critical Point Identification.

1 Introduction

Effective spreading control is an important approach in fighting with epidemics. At present, epidemics spreading control policy making is still heavily based on heuristic experience in past epidemic control. There is a big gap to be an effective control. On one hand, past experience is not always applicable to current cases due to diseases evolvement, social behavior change, transportation network improvement, and other social and environmental changes. On the other hand, effective epidemic control needs more precise estimations besides heuristic experience. So there is a great need of quantitative methods for policy maker in spreading control, such as spreading pattern analysis, critical control point through spreading and social network analysis, and policy comparison through what-if or scenario analysis. However, current research mostly focus on spreading process prediction by mathematical or simulation methods, which is not closely aligned with business operation of epidemic control. The purpose of this paper is to analysis the technology requirement and gap for the business operation and propose a technology framework for future work.

2 Literature Review

Bagni et al. [1] give an exhaustive review about the models and recent work in epidemics study. So only a brief review from model structure and research approach perspective is

presented here. Epidemics models can be distinguished from different perspectives: 1) continuous model where the total population can be partitioned infinitely, or discrete model with individual as the smallest grain, 2) pure temporary model, or spatial-temporary model, and 3) stochastic/determined model. SIR (Susceptible, Infective, and Recovered) model is the start point of many other continuous models for epidemic spreading, such as SIS, SEIR ('M' denotes 'Recovered'), MSEIR ('M' denotes "maternal antibody protection"), etc., All these models assume that the population is "well mixed" (i.e., either not distributed or geographically distributed in a uniform manner). With the application of computer simulation, more complicated models are proposed considering spatial dimension, traffic network, diversity of population and many other important factors. For example, global epidemics spreading model through air travel infrastructure is proposed by Colizza et al. [2].

As the complexity of the epidemic process, simulation becomes the trend in epidemiology study compared with traditional analytical approach. Epidemic simulation software is closely related with epidemic models. The first generation epidemic software (such as WinEpi, Vensim) provides fruitful mathematical models support. The second generation epidemic software enhances mapping and spatial analysis functions. The typical software include Epimap, HealthMapper, SIGEpi, etc. The third generation epidemic software has more considerations to the impact of social and environmental factors. EpiSims [3] is an agent-based modeling platform based on individuals everyday behaviors. A disadvantage of this approach is that it requires large amounts of computing resources even for small models. To avoid such disadvantage, STEM is developed by Ford et al. [4], whence continuous modeling is used for large areas while agent based model is applied in more specific areas.

3   Epidemic Alert & Response Framework and Technology

3.1   Alert & Response Framework

Most epidemic research just focus on epidemic spreading process prediction, without clear connection with business operation of epidemic spreading control. What policy maker really needs is a decision supporting tool in the whole lifecycle. Analytical mechanism is needed for early alert about epidemic outbreak. When there is an epidemics outbreak, policy makers often want to know what critical point for epidemics control is, what the effectiveness of different control policies is, what will happen if the real status is different from the reported scenarios, and etc. Besides policy making, the execution of policy is also very important. For example, how to effectively allocate healthcare workers and drugs to disaster areas.

Based on the business operations of epidemics spreading control, an Alert and Response framework shown in Fig. 1 is proposed which covers all three stages of epidemics control. Monitoring system acts a fundamental infrastructure for the analysis modules and GIS (Geographical Information System) display. Buckeridge et al. [5] gives a detailed summary about how to use spatial and other covariate information from disparate sources to improve the timeliness of outbreak detection. In operation research there have been lots of works on execution planner. So this paper focuses on the other 2 blocks: Policy/Scenario Analyzer and Epidemics Dynamics Simulation.
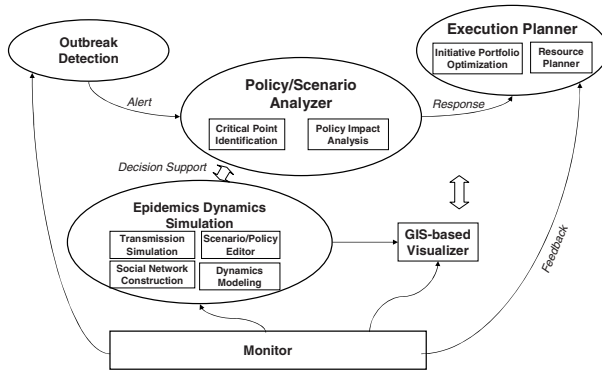
Fig. 1. Epidemic Alert & Response Framework

The technologies framework can be arranged into 4 layers: data, model, application, and representation layer, as illustrated in Fig. 2.

Fig. 2. Epidemic Simulation Technology

3.2 Data & Model Layer

Data is the fundamental layer to the whole framework. Unfortunately not all data are available from public channels or epidemics monitoring information system. Interview or other novel techniques for data collection/generation may be needed. For example, in EpiSims, the travel behaviors are generated by TRANSIS, which in turn relies on interview. Interview usually requires onerous effort. Some automatic approaches may be developed based on novel technologies. For example, cell-phone positioning technology is potential to be adopted in generating travel behavior or traffic flow data.

For modeling, a big challenge is how to obtain a precise estimation of model parameters. In epidemics spreading process, new epidemics data are continuously available with the development of disease. So the adaptive parameter estimation method is more desired. Furthermore, even if the monitoring system is full-scale, not all the states are observable, such as people exposed or in incubation period. State observer technology from control theory may be used to estimate the parameters or hidden states.

Another big challenge for modeling is social network construction, which is closely related with epidemics transmission mechanism. For example, some kinds of diseases (e.g., SARS) are diffused within one type of host (e.g., through human contact), traffic flow data may be enough to construct social network. While for the diseases (e.g., H5N1 Avian Influenza Virus) that diffused across hosts (e.g., through animal and human contact, rather than direct transmission through people), it is much harder to construct the social network.

3.3 Application Layer

3.3.1 Key Analysis Functions

Based on the model and data, various applications can be developed for decision support, such as epidemic spreading prediction, critical point identification, and policy/scenario analysis.

Epidemic spread prediction means predicting the trend and pattern of epidemic spread in the spatial and temporal dimension. However it is hard to have precise forecasting about number of each class, since quantitative model is an approximation to reality at the best, and the parameters are also not the exact number. For decision support purpose, spreading comparison under different scenarios and policies are more important instead.

Contact network is a key factor in epidemics spreading. There have been some researches on epidemiological process over complex network. Network property analysis (e.g., average clustering coefficient, characteristic path length) can provide some guidance (e.g., [3]) in critical point/approach identification for epidemic surveillance. Besides network analysis, rule-based or pattern matching technology may also be useful to help policy maker identify critical path in the large data source.

3.3.2 Sensitivity Analysis

Epidemic simulation often faces great challenge from policy makers about the confidence of simulation result, since epidemics model is an approximation to the real process, and parameters are just estimated value. There are fundamental technical difficulties in such model verification in philosophy just like most social studies. Control experiment is impossible, and spreading process is not replicable. So sensitivity analysis is proposed in this paper to analysis confidence level of the simulation result.

Sensitivity analysis investigates how model output changes as the result of the change of input parameters. Uncertainty in parameter estimation can be quantified under different assumptions (e.g., heterogeneity in variance, correlated errors, etc.). Sampling techniques (e.g., Latin hypercube, simple random sampling) are useful to explore the parameter space and assess the uncertainty of epidemiological quantities.

The real spreading process X^r over geography p and time t depends on initial state X_0^r (i.e., scenario). It can be expressed as the model with "optimal" parameter vector α^r with a un-modeled process ε, shown as

$$X^r(p,t) = f(p,t;X_0^r,\alpha^r) + \varepsilon(p,t). \tag{1}$$

$f(p, t; X_0^r, \alpha^r)$ is the best approximation of the spreading process according the given model. Before all the data are available, it is usually hard to obtain. A guess parameter to α^r, α^e and guess to initial states X_0^r, X_0^e are obtained according to partial epidemics data. Hence the result for the simulation model is expressed as

$$X^e(p, t) = f(p, t; X_0^e, \alpha^e). \tag{2}$$

Although it is impossible to obtain the real initial state and optimal parameter, it is still useful to know the sensitivity of spreading process $X(p, t)$ on these parameters. If the sensitivity is low, the simulation results are still believable.

Denote β as the joint vector of X_0 and α, i.e., $\beta = \lfloor X_0; \alpha \rfloor$. For $X_0 \in \delta(X_0^e)$ and $a \in \delta(a^e)$, calculate spreading process $X(p, t) = f(p, t; X_0, \alpha)$ by simulation. The confidence level of simulation result can be defined as

$$\lambda = 1 - \eta / (1 + \eta). \tag{3}$$

Whence, the variance of spreading process, η, is defined as

$$\eta = \max_{\beta \in \delta(\beta^e)} \| (X - X^e)./X^e \|. \tag{4}$$

$\|\cdot\|$ is a measure of function vector. Operator './' means the elementary division, i.e., for $a, b \in R^n$, $a./b = [a_1/b_1, \cdots, a_i/b_i, \cdots, a_n/b_n]^T \in R^n$.

The sensitivity of a parameter β_i in vector β around β^e can be defined as

$$S(\beta_i)|_{\beta^e} = \frac{\partial \| X - X^e \|}{\partial \beta_i}, \tag{5}$$

if such a partial differential exist. If it dose not exist, the sensitivity can still be evaluated by sampling difference calculation.

4   Experiment

In this section, SARS spreading in Beijing, 2003 from Chinese Minister of Health [6] is adopted to illustrate the importance of some key research topics in Section 3.

4.1   Model and Prototype

The BloComp(2,7) model proposed by Zhang et al. [7] is adopted here. The model has 2 types of environment according to contact rate: free environment and isolated environment. Besides the 4 states in SEIR model, 3 more states are extended, including "P" as Possible infectious, "D" as Diagnosed infectious and "H" as Health worker. A prototype based on Repast [8] is developed.

4.2   Parameter Estimation

The parameters and functions are given as the following formulas as [7], $\varepsilon = 0.04$, $d_{ep} = 0.16$, $d_{iq} = 1/3$, $d_{sp} = 0.027478$, $b_{sp} = 0.06341$, $d_{pq} = 0.12197$, $\gamma = 1/30$, $\alpha = \alpha_1 = 0.14/30$, $f(S, E, I, R) = \lambda_f(t)(0.1E + I)$, and $g(H, P, D) = \lambda_g(t)D$. However, in estimating $\lambda_f(t)$ and $\lambda_g(t)$, our approach differs a little from the approach of Zhang et al. [7], where they assume that today's number of new diagnosed equals to 8-day-ago's num of infective.

Let $\Delta d(t)$ denote the number of new diagnosed minus the number of new infected health care workers. Under the assumption that the average transition time from exposed class to the infective class is 5 days and that from infective class to the D-class is 3 days, the exposed at time t is the Δd from $t-5$ to $t-1$, and the number of infectious at time t is the Δd from t-8 to t-6. Thus $\lambda_f(t)$ can be estimated as

$$\lambda_f(t) = \frac{\Delta d(t)}{0.1 * \sum_{j=1}^{5} \Delta d(t-j) + \sum_{j=6}^{8} \Delta d(t-j)} \quad (t \geq 8). \tag{6}$$

$\lambda_g(t)$ can be also obtained in a similar way. Here a curve fitting method is adopted since it has more extensibility to other virus. Upon the observation of 16 days' data from Apr. 25th to May. 10th, Lorenz curve is selected which is given as

$$y(t) = y_0 + \frac{2A}{\pi} \cdot \frac{w}{(t - t_c)^2 + w^2}, \tag{7}$$

Whence, y_0, w, A and t_c are parameters to be estimated.
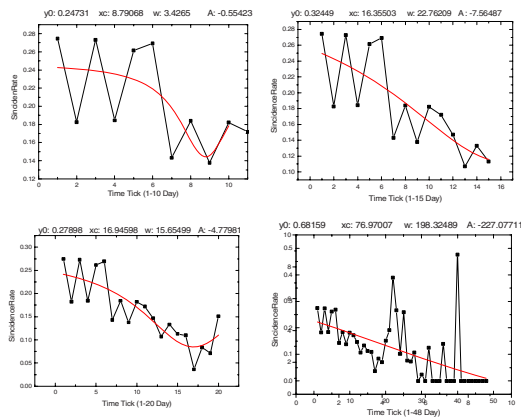
Fig. 3. Parameter Estimation with 10, 16, 20, and 50 Days' Historical Data

To study the impact of available data on the prediction precision, we use 10, 16, 20 and 50 days' data respectively to estimate the incident rate function $\lambda_f(t)$. The results are shown in Fig. 3. The estimation changes apparently with available data, which means that adaptive parameter estimation is usually necessary for real prediction.

Then, based on the estimation from 16 days' data, the simulation result about infectious healthcare worker and diagnosed class are shown in Fig. 4. These figures show that the simulation results have the same trend with the real data, however with significant error, especially around the jumping point such as April. 29 shown in Fig. 4(a). However these kinds of jumping points may be due to the imperfection of data reporting mechanism, which is also one key challenge for epidemics prediction.
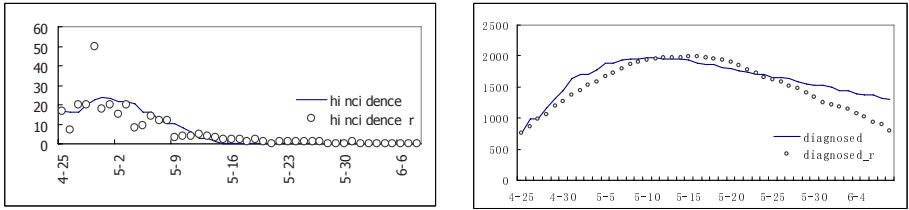
(a) Num of Incidence of Healthcare Workers   (b) Num of Diagnosed Class

Fig. 4. Simulation Result (solid curve) vs. Data from Chinese Minister of Health (dotted curve)

4.3   What-If Scenario Analysis

Fig. 5 shows the spreading process under three different scenarios. Scenario 1 is the simulated process based to the estimation from real data. Scenario 2 is the spreading process under lightly looser control measures with 3 times incidence of the original simulation. Scenario 3 is much looser with 10 times incidence of the original simulation. It clearly shows that quarantine policy does matter to the spreading process.
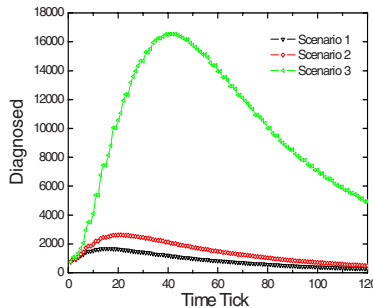
Fig. 5. Spreading Process under Three Control Policies

5   Conclusions

In a world reeling from the resurgence of old diseases and the emergence of new diseases, epidemic alert and response is very important. Current epidemics study need move from prediction to decision support. This paper proposes a research framework to identify the key analytical methods to fill such gaps. The experiment on 2003 Beijing SARS data proves the importance of those technologies. There are many interesting topics for future exploration, such as robust and adaptive parameter estimation method, critical control path identification algorithm, new data collection method, flexible simulation platform for general epidemics study, etc.

References

1. Bagni, R., Berchi, R., Cariello, P.: A comparison of simulation models applied to epidemics. Journal of Artificial Societies and Social Simulation. 3 (2002).
2. Colizza, V., Barrat, A., Barthélemy, M., Vespignani, A.: Prediction and predictability of global epidemics: the role of the airline transportation network. Proceedings of the National Academy of Science of the United States of America. 7 (2006) 2015-2020.
3. Eubank, S., Guclu, H., Anil Kumar, V. S., et al.: Modelling disease outbreaks in realistic urban social networks. Letters to Nature 429 (2004) 180-184.
4. Ford, D. A., Kaufman, J. H., Eiron, I: An extensible spatial and temporal epidemiological modeling system. International Journal of Health Geographics. 4 (2006).
5. Buckeridge, D. L., Burkom, H., Campbell, M., et al.. Algorithms for rapid outbreak detection: a research synthesis. Journal of Biomedical Informatics. 38 (2005) 99-113.
6. Chinese Minister of Health. <http://168.160.224.167>.
7. Zhang, J., Lou, J., Ma, Z., Wu, J. H.: A compartmental model for the analysis of SARS transmission patterns and outbreak control measures in China. Applied Mathematics and Computation. 162(2005) 909–924.
8. Repast Organization for Architecture and Development. (2003). http://repast. source-forge.net.

Quantitative Risk Analysis and Evaluation in Information Systems: A Case Study*

Young-Gab Kim and Jongin Lim

Graduate School of Information Management and Security,
Center for Information Security Technologies (CIST), Korea University,
1, 5-ga, Anam-dong, SungBuk-gu, 136-701, Seoul, Korea
{always, jilim}@korea.ac.kr

Abstract. The rapid growth of the Internet technology has encouraged organizations to protect their information assets. Furthermore, the need for risk analysis has become very important for organizations. However, the existing risk analysis just presents the guidelines that can be used to determine the security measures but do not support how to evaluate the risks quantitatively. Therefore, in this paper, the quantitative risk evaluation model based on the Markov process, especially for the case of interrelated threats, is proposed. In addition, in order to analyze the relationship between threats, the basic analysis method using the covariance and the correlation coefficient is presented.

1 Introduction

The Internet is growing in popularity exponentially due to its ease of use and the powerful ability to support information services. Furthermore, as dependency of network technology on large-scale critical infrastructure increases, the cyber attacks have also increased, targeted against vulnerable assets in information systems. Hence, in order to protect private information and computer resources, research relating to risk analysis is required. Risk analysis involves determining what you need to protect, what you need to protect it from, and how to protect it. It is the process of examining all of your risks, then ranking those risks by level of severity. This process involves making cost-effective decisions on what you want to protect [1]. Precise risk analysis provides several advantages such as supporting practical security policies for organizations by monitoring and effectively protecting the critical assets of the organization, and providing valuable analysis data for future estimation through the development of secure information management [2]. There is considerable research relating to risk analysis [3,4]. However, the existing risk analysis just presents the guidelines that can be used to determine the security measures but do not support how to evaluate the risks clearly. Furthermore, the existing risk propagation models are

---

inadequate in applying this to the analysis of attacks caused by diverse threats in information systems. That is, the existing models can only be applied to specific threats such as virus or worm. In addition, it is difficult to holistically analyze the risk propagation caused by these threats, using the relationship among the threats. Therefore, in our previous work [5], a probabilistic model for damage propagation based on the Markov process [6, 7], was proposed, based on historical data, occurring over several years. Using the proposed model, the occurrence probability and occurrence frequency for each threat in information systems can be predicted holistically, and applied to establish countermeasures against those threats. However, the previous work [5] only presented the approach method with a case study, and did not formulate a risk propagation model for the case of interrelated threats. Therefore, in this paper, the Markov process-based risk evaluation model, which can evaluate the occurrence probability and occurrence frequency of threats, especially in case a threat occurs related with other threats, is proposed. In addition, in order to analyze the relationship between threats, the basic analysis method using the covariance and the correlation coefficient is presented.

The subsequent sections of this paper are organized as follows: Section 2 presents the overview of security risk analysis model, and the Markov process-based risk analysis model. In Section 3, a case study to show the creation of the model, especially a threat occurs related with other threats, is presented. Finally, Section 4 concludes this paper.

2   Overview of Security Risk Analysis Model

Security analysis model presented in our previous work [2] is composed of 4 steps: Domain analysis, risk analysis, risk mitigation and effectiveness evaluation, and damage estimation and reporting results. In Step 1, the types of assets, threats, and vulnerabilities for the organization are analyzed. Step 2 evaluates the security risk of the system by summing up all the risks of system components with considering the existing threats in the core assets of the organization and the degree of vulnerabilities per threat. Step 3 is a process that shows the lists of current security countermeasure in the organization, and selects suitable mitigation methods against the threats, then show the effectiveness of the mitigation method. Finally, Step 4 summarizes the initial risks, the types and cost of the risk mitigation methods, the residual security risks, and their Return-On-Investment (ROI). In this paper, Step 2, risk analysis is focused, especially in case of evaluating security risk quantitatively. Therefore, in order to evaluate the risk, following equations are used:

$$RISK = Loss \times Probability \qquad (1)$$
$$LOSS = Asset\text{-}Value \times Damage \qquad (2)$$
$$DAMAGE = 1\text{-}((1\text{-}Threat\text{-}Rate) \times (1\text{-}Vulnerability\text{-}Rate)) \qquad (3)$$

RISK means a damage amount when assets are damaged by threats in a vulnerable system. It is calculated in Step 2. As a result, risk is calculated as multiplication of *LOSS*, which means the degree of shrinkage in the asset-value caused by threats, and the probability, which is the probability of threat-occurrence. An asset is a set of

items, which have economic value owned by an individual or organization in information systems. Examples are information or data, documents, hardwares, softwares, and so on. *DAMAGE* is a probability that is damaged by attacks. It is evaluated by threat-rate, which is potential probability of threat-occurrence, and vulnerability-rate, which is the degree of a weakness in an information system, system security procedures, internal controls, or implementation that could be exploited. The threat and vulnerability rate range from 0 to 1. In this paper, the focus is on calculating the probability in equation (1), and threat-occurrence, in particular, when threat occurs releated with other threats.

The Markov process-based risk propagation model proposed in the previous work [5] is composed of 4 steps: Threat-State Definition, Threat-state Transition Matrix, Initial Vector, and Risk Propagation Evaluation. In Step 1, all kinds of threat are examined, the threat-occurrence data are collected and analyzed in global systems, and finally the possible threat-states are defined. In Step 2, the threat-state transition matrix is calculated, which is a square matrix describing the probabilities of moving from one threat-state to another. In order to obtain the transition matrix, the following two tasks are performed. First, threat-states are listed by mapping the threat-occurrence data of each threat into the threat-state defined in the previous step. Second, the number from one threat-state to another is counted, allowing the matrix to finally be constructed. In Step 3, the initial probability is calculated against the occurrence of threat-state. Finally, in Step 4, the probability and frequency of threat-occurrence using the threat-state transition matrix and the initial vector calculated in the previous steps are estimated. A more detailed description of the Markov process-based, risk propagation model can be found in Kim et al. [5].

3   Case Study

In this section, a case study that presents how to make the risk propagation model, especially in case a threat occurs related with other threats, is presented. As in the previous work [5], in this case study, the statistics of hacking and virus published by the Korea Information Security Agency (KISA) [8] for 60 months is used from January 2001 to December 2005, for trust in the historical data.

First, threat-occurrence data is gathered and analyzed, and priority is given to threats. After this step, the frequency and statistics of threat for each month is obtained, as presented in Table 1, 2 and 3.

Table 1. Occurrence frequency of threat T_1

	Jan	Feb	Mar	Apr	May	Jun	Jul	Aug	Sep	Oct	Nov	Dec	Total
2001	85	125	70	89	85	64	65	495	268	77	51	97	1571
2002	401	119	82	59	286	417	313	298	210	465	472	990	4112
2003	1148	557	1132	934	306	450	185	544	119	137	129	96	5837
2004	154	148	118	1066	493	181	72	22	16	24	125	90	2509
2005	29	20	15	3	15	36	76	254	42	40	22	16	568

Table 2. Occurrence frequency of threat T_2

	Jan	Feb	Mar	Apr	May	Jun	Jul	Aug	Sep	Oct	Nov	Dec	Total
2001	1	1529	2429	625	684	520	6106	5965	10772	4795	4068	3024	40518
2002	2005	1384	1306	3165	2760	1774	1706	1458	1610	3566	3028	1684	25446
2003	1361	1320	2537	2350	3704	1854	1185	9748	19682	3999	11658	8949	68347
2004	4824	5750	9820	4233	19728	22767	15228	8132	3153	2658	2319	2117	100727
2005	1832	1205	1049	648	1302	1040	662	620	444	637	705	620	10764

Table 3. Occurrence frequency of threat T_3

	Jan	Feb	Mar	Apr	May	Jun	Jul	Aug	Sep	Oct	Nov	Dec	Total
2002	1665	1256	2080	2110	1776	1418	1177	1216	1601	2483	1596	1597	20335
2003	648	593	656	402	345	1489	469	4468	3120	3560	2201	315	14966
2004	2004	3389	10631	18546	11618	833	1591	1964	901	1794	2628	1381	57217

Threat T_1 is an Illegal intrusion using malicious applications such as Netbus and Subseven as one of the hacking threats in information system. This threat leaks information and interrupts the normal process in information systems. Threat T_2 is an Internet Worm as one of virus threats. The Internet worm is a self-replicating computer program or executable program with rapid propagation itself. Recently this threat occurs frequently, and much research relating to the propagation of the Internet worm is processing. Threat T_3 is a Network Eavesdrop as one of scanning detection. The network eavesdropping is an attack based on sniffing the network.

As mentioned previously, in this case study, a threat occurs related with other threats. Therefore the relationship between threats must be analyzed before estimation of risks. In order to analyze degree of the relationship, the covariance (Cov) [6, 9] and the correlation coefficient [6, 9] are used. Cov measures the degree of correlation between the random variables, and is defined by

$$Cov(X,Y) = E(XY) - E(X)E(Y) \tag{4}$$

where $E(X)$ is a expectation of the variable X. If $Cov(X,Y)$ is zero, this means that X and Y are uncorrelated. The correlation coefficient $\rho(X,Y)$ evaluates the coherence of relationship between X and Y as formula (5), and satisfies the formula (6).

$$\rho(X,Y) = \frac{Cov(X,Y)}{\sqrt{Var[X]Var[Y]}} = \frac{Cov(X,Y)}{\sigma_X \sigma_Y} \tag{5}$$

where $Var(X) = E(X^2) - \{E(X)\}^2$, $\sigma_X = \sqrt{Var[X]}$, $\sigma_Y = \sqrt{Var[Y]}$

$$-1 \le \rho(X,Y) \le 1 \tag{6}$$

$$\rho(X,Y) = \begin{cases} -1, & \text{if } X = -aY \, (a > 0) \\ 0, & \text{if } X \text{ and } Y \text{ are uncorrelat ed} \\ +1, & \text{if } X = aY \, (a > 0) \end{cases} \tag{7}$$

As presented formula (7), especially when the $\rho(X,Y)$ is zero, the variables X and Y are uncorrelated. In case $\rho(X,Y)$ is closed to -1, if X increases, Y decreases. Conversely, if $\rho(X,Y)$ is closed to 1, when X increases, Y also increases. In this case study, degree of the relationship among the threats T_1, T_2, and T_3 can be analyzed using formula (5) as follows:

$$\rho(T_1,T_2) = \frac{Cov(T_1,T_2)}{\sqrt{Var[T_1]Var[T_2]}} = \frac{Cov(T_1,T_2)}{\sigma_{T_1}\sigma_{T_2}} = 0.0070$$

$$\rho(T_1,T_3) = \frac{Cov(T_1,T_3)}{\sqrt{Var[T_1]Var[T_3]}} = \frac{Cov(T_1,T_3)}{\sigma_{T_1}\sigma_{T_3}} = 0.1998$$

$$\rho(T_2,T_3) = \frac{Cov(T_2,T_3)}{\sqrt{Var[T_2]Var[T_3]}} = \frac{Cov(T_2,T_3)}{\sigma_{T_2}\sigma_{T_3}} = 0.2572$$

From above results, it is sure that threats T_2 and T_3 have a closer relationship than others. That is, Internet worm T_2 can be sure to a little influence an occurrence of network eavesdrop T_3, and vice versa. On the contrary, threats T_1 and T_2 are uncorrelated. That is, illegal intrusion using malicious application T_1 give little influence an occurrence of Internet worm T_2, and vice versa. Although, in this paper, the relationship of only three threats T_1, T_2 and T_3 are analyzed, diverse threats in information systems can be analyzed and ranked using the Cov and correlation coefficient.

In order to evaluate the relationship among the threats, the threat-states should be created by a combination of a number of threat thresholds. In order to demonstrate this, the data depicted in Table 1 and 2 are used for T_1 and T_2. It is assumed that all threats have the same environments such as countermeasures, system resource and so on, whenever threats occur. In order to define threat-states, the thresholds of each threat are first defined using the analysis of the frequency data presented in Table 1 and 2. The thresholds of the each threat can be defined in the formulas (8) and (9):

- Thresholds of T_1 := H_1: 0~400, H_2: 401~800, H_3: 801~1200　　　(8)
- Thresholds of T_2 := W_1: 0~4000, W_2: 4001~8000, W_3: Over 8001　　(9)

As mentioned above, when a threat occurs that is related to other threats, the threat-states are defined as combination of thresholds of many threats. Therefore the nine number of threat-state as follows are defined:

$$S = \{S_1, S_2, S_3, S_4, S_5, S_6, S_7, S_8, S_9\} \qquad (10)$$

Where $S_1=(H_1, W_1)$, $S_2=(H_1, W_2)$, $S_3=(H_1, W_3)$, $S_4=(H_2, W_1)$, $S_5=(H_2, W_2)$, $S_6=(H_2, W_3)$, $S_7=(H_3, W_1)$, $S_8=(H_3, W_2)$, and $S_9=(H_3, W_3)$

In order to define the threat-state, a pair of threat-occurrence data of T_1 and T_2 presented in Table 1 and 2 is listed as follows:

(85, 1), (125, 1529), (70, 2429), (89, 684), (64, 520), (65, 6106), ... , (76, 662), (254, 620), (42, 444), (40, 637), (22, 705), (16, 620)

Next, the threat-occurrence pair is mapped into the thresholds of each threat defined in (8) and (9), and listed as follows:

(H$_1$, W$_1$), (H$_1$, W$_1$), (H$_1$, W$_1$), (H$_1$, W$_1$), (H$_1$, W$_1$), (H$_1$, W$_1$), ... , (H$_1$, W$_1$), (H$_1$, W$_1$), (H$_1$, W$_1$), (H$_1$, W$_1$), (H$_1$, W$_1$), (H$_1$, W$_1$)

Each pair of (H$_i$, W$_i$) is mapped into the threat-state defined in (10), and listed as follows:

S$_1$, S$_1$, S$_1$, S$_1$, S$_1$, S$_1$, S$_2$, S$_5$, S$_3$, S$_2$, S$_2$, S$_1$, S$_4$, S$_1$, S$_1$, S$_1$, S$_1$, S$_4$, S$_1$, S$_1$, S$_1$, S$_4$, S$_4$, S$_7$, S$_7$, S$_4$, S$_7$, S$_7$, S$_1$, S$_4$, S$_1$, S$_6$, S$_3$, S$_1$, S$_3$, S$_3$, S$_2$, S$_2$, S$_4$, S$_2$, S$_6$, S$_3$, S$_3$, S$_3$, S$_1$, S$_1$, S$_1$, S$_1$, S$_1$, S$_1$, S$_1$, S$_1$, S$_1$, S$_1$, S$_1$, S$_1$, S$_1$, S$_1$, S$_1$, S$_1$

From the above threat-states listing, the transition number from a threat (S$_1$~S$_9$) is counted for other threats, and the transition matrix is made as follows:

$$
\begin{array}{l}
S_1 \\ S_2 \\ S_3 \\ S_4 \\ S_5 \\ S_6 \\ S_7 \\ S_8 \\ S_9
\end{array}
\begin{bmatrix}
25 & 1 & 1 & 4 & 0 & 1 & 0 & 0 & 0 \\
1 & 2 & 0 & 1 & 1 & 1 & 0 & 0 & 0 \\
2 & 2 & 3 & 0 & 0 & 0 & 0 & 0 & 0 \\
3 & 1 & 0 & 1 & 0 & 0 & 1 & 0 & 0 \\
0 & 0 & 1 & 0 & 0 & 0 & 0 & 0 & 0 \\
0 & 0 & 2 & 0 & 0 & 0 & 0 & 0 & 0 \\
1 & 0 & 0 & 1 & 0 & 0 & 2 & 0 & 0 \\
0 & 0 & 0 & 0 & 0 & 0 & 0 & 0 & 0 \\
0 & 0 & 0 & 0 & 0 & 0 & 0 & 0 & 0
\end{bmatrix}
\begin{array}{l}
S_1 \\ S_2 \\ S_3 \\ S_4 \\ S_5 \\ S_6 \\ S_7 \\ S_8 \\ S_9
\end{array}
\begin{bmatrix}
0.78 & 0.03 & 0.03 & 0.13 & 0 & 0.03 & 0 & 0 & 0 \\
0.17 & 0.32 & 0 & 0.17 & 0.17 & 017 & 0 & 0 & 0 \\
0.29 & 0.29 & 0.42 & 0 & 0 & 0 & 0 & 0 & 0 \\
0.43 & 0.14 & 0 & 0.14 & 0 & 0 & 0.29 & 0 & 0 \\
0 & 0 & 1.00 & 0 & 0 & 0 & 0 & 0 & 0 \\
0 & 0 & 1.00 & 0 & 0 & 0 & 0 & 0 & 0 \\
0.25 & 0 & 0 & 0.25 & 0 & 0 & 0.50 & 0 & 0 \\
0 & 0 & 0 & 0 & 0 & 0 & 0 & 0 & 0 \\
0 & 0 & 0 & 0 & 0 & 0 & 0 & 0 & 0
\end{bmatrix}
\quad (11)
$$

From the threat-state transition matrix, and the entries of transition matrix, the transition from a threat-state to another, satisfy formula that the row of transition matrix adds to one. Furthermore, the threat-state transition matrix can be translated into a threat-state diagram, as depicted in Fig. 1.
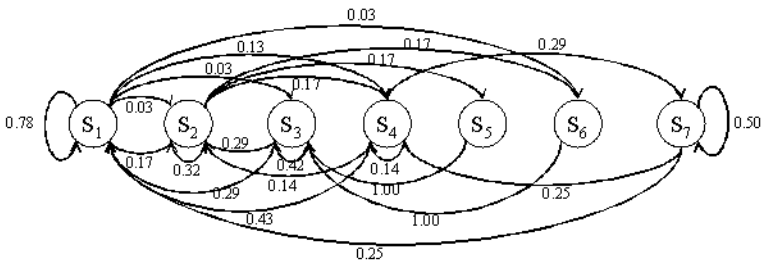
Fig. 1. Threat-State Diagram for T$_1$ and T$_2$

In order to calculate the initial probability for T_1 and T_2, the most recent data covering six months are used, from July 2005 to December 2005. Furthermore, the initial probability is calculated:

- Frequency: (76, 662), (254, 620), (42, 444), (40, 637), (22, 705), (16, 620)
  $= S_1, S_1, S_1, S_1, S_1, S_1$
- Initial Probability: $P(S_1 \ S_2 \ S_3 \ S_4 \ S_5 \ S_6 \ S_7 \ S_8 \ S_9)$

$$= P(1 \ \ 0 \ \ 0 \ \ 0 \ \ 0 \ \ 0 \ \ 0 \ \ 0 \ \ 0) \tag{12}$$

The probability of future threat-occurrence is estimated, using the transition matrix and initial probability, the formulas (11) and (12):

$$(1 \ 0 \ 0 \ 0 \ 0 \ 0 \ 0 \ 0 \ 0) \begin{bmatrix} 0.78 & 0.03 & 0.03 & 0.13 & 0 & 0.03 & 0 & 0 & 0 \\ 0.17 & 0.32 & 0 & 0.17 & 0.17 & 017 & 0 & 0 & 0 \\ 0.29 & 0.29 & 0.42 & 0 & 0 & 0 & 0 & 0 & 0 \\ 0.43 & 0.14 & 0 & 0.14 & 0 & 0 & 0.29 & 0 & 0 \\ 0 & 0 & 1.00 & 0 & 0 & 0 & 0 & 0 & 0 \\ 0 & 0 & 1.00 & 0 & 0 & 0 & 0 & 0 & 0 \\ 0.25 & 0 & 0 & 0.25 & 0 & 0 & 0.50 & 0 & 0 \\ 0 & 0 & 0 & 0 & 0 & 0 & 0 & 0 & 0 \\ 0 & 0 & 0 & 0 & 0 & 0 & 0 & 0 & 0 \end{bmatrix} \tag{13}$$

$$= (0.78 \ \ 0.03 \ \ 0.03 \ \ 0.13 \ \ 0 \ \ 0.03 \ \ 0 \ \ 0 \ \ 0)$$

From above result, the probability of threat-occurrence of T_1 and T_2 can be expected. That is, each threat-state from S_1 to S_9 can occur with the probability 0.78, 0.03, 0.03, 0.13, 0, 0.03, 0, 0, and 0 in good order. Consequently it can be conformed that the state S_1 (that is, a threshold of (H_1, W_1)) has the highest probability of threat-occurrence, that T_1 will occur with the number between 0 and 400, and T_2 will occur with the number between 0 and 4000. Furthermore, to estimate the exact frequency of threat-occurrence, which would occur in the future, the probability of threat-occurrence calculated in (13) is used and the medians $M(H_i)$ for T_1 and $M(W_i)$ for T_2. In this case study, in order to calculate the median, the frequency of threat-occurrence of the previous month is used. $M(H_i)$ and $M(W_i)$ can be calculated as follows:

- Median for T_1: $M(H_1)= 16$, $M(H_2)= 0$, $M(H_3)= 0$
- Median for T_2: $M(W_1)= 620$, $M(W_2)= 0$, $M(W_3)= 0$

Before the frequency of threat-occurrence is calculated, the probability of thresholds must be calculated against each threat as follows:

- Probability of threshold for T_1: $P(H_1)= 0.84$, $P(H_2)= 0.16$, $P(H_3)= 0$
- Probability of threshold for T_2: $P(W_1)= 0.91$, $P(W_2) = 0.03$, $P(W_3)= 0.06$

The Expected Frequency (*EF*) of threat-occurrence for each threat T_1 and T_2, can be calculated using formula (10) in [5], where n is 3 as follows:

$$EF \ of \ T_1 = \sum_{i=1}^{3} P(H_i)M(H_i) = 0.81 \times 16 \cong 14$$

$$EF \text{ of } T_2 = \sum_{i=1}^{3} P(W_i)M(W_i) = 0.88 \times 620 \cong 561$$

From the above result, the frequency of threat-occurrence of T_1 can be predicted at approximately 14 and that of T_2 is approximately 561.

4   Conclusion

In this paper, a probabilistic model of risk propagation based on the Markov process, which can estimate the spread of risk when attacks occur from not only virus or worms but also diverse threats, was presented briefly. Furthermore, a case study that especially a threat occurs related with other threats was presented using reliable historical data from the KISA, and the relationship among the threats was analyzed using the covariance and the correlation coefficient. The proposed model in this paper has different advantages from existing models: The proposed model estimates the probability or frequency of threat-occurrence unlike the worm or virus propagation model, which obtains the number of damaged systems, in particular, the number of infected computers in the system. This probabilistic approach can be applied to diverse kinds of threats in information systems. Therefore the threats can be analyzed synthetically with an analysis of the relationship among the threats.

References

1. M.P. Papazolou: Agent-Oriented Technology in Support of E-business, *Communication of the ACM*, Vol.44 No.4 (2001) 71-77
2. H. P. In, Y.-G. Kim, T. Lee, C.-J. Moon, Y.-J. Jung, I. Kim and D.-K. Baik: A Security Analysis Model for Information Systems. *Lecture Notes in Artificial Intelligence*, Vol.3398. Springer-Verlag, Berlin Heidelberg (2005) 505-513
3. G. Stoneburner, A. Goguen, and A. Feringa: Risk Management Guide for Information Technology Systems, NIST Special Publication 800-30, NIST (2002)
4. GAO: Information Security Risk Assetment-Practices of Leading Organizations. GAO/AIMD-00-33 (1999)
5. Y.-G Kim, T. Lee, H. P. In, Y.-J. Jung, I. Kim and D.-K. Baik: A Probabilistic Approach to Estimate the Damage Propagation of Cyber Attacks. *Lecture Note in Computer Science*, Vol. 3935. Springer-Verlag, Berlin Heidelberg (2006) 175-185
6. K. S. Trivedi: Probability and Statistics with Reliability, Queuing and Computer Science Applications. Second Edition, WILEY Interscience (2002)
7. R. D. Yates, and D. J. Goodman: Probability and Stochastic Process. Second Edition, WILEY International Edition (2003)
8. KISA: Statistics and Analysis on Hacking and Virus. http://www.krcert.or.kr
9. R.V. Hogg and A. T. Craig: Introduction to Mathematical Statics, Fifth Edition, Prentice-Hall (1995)

Ontology-Based Fraud Detection

Liu Fang, Ming Cai, Hao Fu, and Jinxiang Dong

College of Comupter Science and Technology, Zhejiang University,
Hangzhou 310027, China P.R.
`fangliuqq@gmail.com, cm@zju.edu.cn,`
`zjufuhao@gmail.com, djx@zju.edu.cn`

Abstract. One method for detecting fraud is to check for suspicious changes in user behavior. This paper proposes a novel method, built upon ontology and ontology instance similarity. Ontology is now widely used to enable knowledge sharing and reuse, so some personality ontologies can be easily used to present user behavior. By measure the similarity of ontology instances, we can determine whether an account is defrauded. This method lows the data model cost and make the system very adaptive to different applications.

Keywords: Fraud detection, ontology, ontology instance similarity, behavior, personality.

1 Introduction

According to Miniwatts Marketing Group [1], there are more than 1 billion Internet users now. Many wet sites ask suffers to online registration at the first visit and logon every other visit to offer complete service, such as recommendations, resource access control, especially in e-commerce system.

Many systems send the logon information to users to let them check whether someone others have logged in the system with their accounts, but we find that most of the users discard these messages. For complex system, this mechanism is not enough. During an invalid access, an invalid user may damage the system, although most of the system has a back up mechanism, its important to detect these invalid accesses as soon as possible.

People have their own usual practice when suffering. When a user logins to the system, his/her activities are logged and these activities are compared to those before, if the results are quite different, we can constrain his/her access or privileges, such as access prohibition or message post prohibition, which can be configured by system administrator.

In [2], the authors have discussed some fraudulent behavior, such as in areas of insurance, credit card, and telecommunications. And a brief description of the fraud detection method and applications is given.

The rest of the paper is organized into the following sections. Section 2 discusses related work, and section 3 presents the overview of our system. In section 4, we provide a discussion of how user's activity is colleted, classified, and presented. We give a method to measure the similarity of ontology instances in section 5. And finally, we show our experimental result and discuss some future work in section 6.

2   Related Works

One method for dealing with cloning fraud is to check for suspicious changes in user behavior. [3] describes the automatic design of user profiling methods for the purpose of fraud detection, using a series of data mining techniques. Specifically, they use a rule-learning program to uncover indicators of fraudulent behavior from a large database of customer transactions. Then the indicators are used to create a set of monitors, which profile legitimate customer behavior and indicate anomalies. Finally, the outputs of the monitors are used as features in a system that learns to combine evidence to generate high-confidence alarms. [4] presents a network intrusion detection models. They encode and compare the frequent patterns mined from the normal and intrusion datasets, and automatically construct statistical and temporal features that describe the anatomy and invariant behavior of the attacks.

In [5], they use activity monitoring to term a problem class which involves monitoring the behavior of a large population of entities for interesting events requiring action. They differentiate activity monitoring problems and present a framework within which each of the individual problems has a natural expression, as well as a methodology for evaluating performance of activity monitoring techniques.

From [2, 6], we can know the main idea of fraud detection now used is classification of feature patterns. But the classifier must be trained with examples and it may take many efforts to create these examples, for examples, in [3], they use thirty-day's record as the examples. Another problem is that the figures collected by the system may difficult for people to understand.

To prevention and early detection of fraudulent activity is an increasingly important goal for the EU and its Member States [7]. The FF POIROT (Financial Fraud Prevention Oriented Information Resources using Ontology Technology) project has developed legal core ontology, financial ontology and fraud ontology. They are at their beginning and focus on ontology building. For web applications, such as e-commerce, we can build the user behavior ontology using technology described in recommendation system [8]. In recommendation system, the personality of suffers can be extracted from users' behaviors and used to help the recommendation. We use the personality information to detect fraudulent activity. In the early stage of the application, we use the personality similarity as the judgments. We find that the result is quite attractive. Once there are enough examples to train the classifier, classifiers can be used to improve the fraud detection accuracy.

3   System Overview

Figure 1 presents framework of our detector. The users' activities will be tracked by the web server and then stored into the activity database. The activity database is an ontology instance database where each account has its according activities. Once there are certain new activities in the database for an account, the trigger in the database will start the ontology instance similarity computation component. If new ontology is added, first use similarity of ontology instances for detecting, after collecting enough examples, classifies will be started. So the system is very flexible to different applications. Now many applications have already building useful ontology which we can use for activity monitoring, and this is important for applications to use the fraud detection.
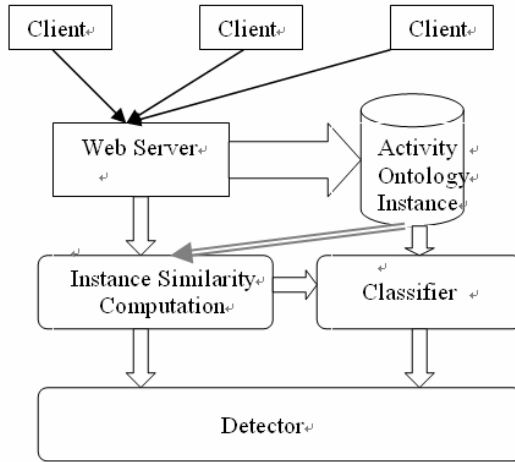
Fig. 1. System Architecture

If one ontology is little useful for detection, it will be easily removed from the system, and other ontology also can be added. In [3], they use rule-learning program to uncover indicator of fraudulent activities. If activities are added, the rule-learning program must be run again to generate the rules, because rules must be found from the all activities. For activity ontology, the activities are already clearly classified when the ontology is modeled. Some features will be removed from the ontology if they appear no usefulness to fraud detection.

The newly added ontology doesn't immediately be outputted to classifier, we should determine the newly added ontology is useful for fraud detection before adding the new ontology to the classifiers. So instance similarity computation component can help classifier to reduce noises.

4   Activity Ontology

4.1   Data Preparation

The Semantic Squirrel Special Interest Group (SSSIG) [9] is a group of researchers based at the University of Southampton who aim to automate the process of logging available raw data, (or 'nuts'), that can describe aspects of one's personal experience. A number of squirrels have been developed in this process, and an ethos of the group is to preserve this raw data in order to retain any unforeseen potentials for exploitation and transcend issues pertaining to platform and application restrictions. Applications can surely add their own data to the system.

4.2   Data Classification

This raw data forms the basis of the knowledge acquisition phase and then is parsed into RDF representations. Based on work of [10], we use following types of preliminary data:

■ Time Data:
Time Data includes the time when user logins to, leave the web site, such as MORNING, AFTERNOON, TWILIGHT, EVENING and NIGHT, and the time intervals, such as time a user spends on a web pages, the reading speeds and so on.

■ Geographical Data
Through uses' IP information, we can get the geographical data of users. Although many IPs can only indicate which city it belongs to, IP information is helpful for fraud detection if the user's IP is not dynamically allocated.

■ Navigation Habit Data
The Navigation Habit Data contains information about how user use bookmarks, how user use navigation history, and how user use back and forward button of the browser and so on. By virtue of its cross-platform nature, we have selected the Mozilla Firefox as our web-browser of choice. Firefox exposes the download information in RDF form and thus can be easily imported to the system. Scripts have been developed to parse the bookmarks and history data into RDF. The RDF model uses two namespaces taken from the mozilla developers centre.

■ Web Page Data
Web Page Data contains information about which types of web pages the user wants to browse, such as entertainment, political, sports and so on. We also extract some key words from text using natural language processing technology.
Other types of data are optional, such as email, music playcount statistics, and file system information.

4.3 Data Presentation

All the data we collected are presented in RDF. Each time the user login to the system, we create new ontology instances or update the statistical information of some ontology instances periodically. We add a new property {rev, acc, per, tim} for each RDF triples. The meaning of the 3 parameters is:

rev is the relevance value. It is a real number ranging from 0 to 1. It gives a measure of how much a concept characterizes a web resource be accessed by a user. A bigger value denotes higher relevance. For example, if a user accesses a web page and the rev is 0.9 to a concept "political news", we know that the web page is very relevant to political news.

acc is the access times for a web resource be accessed by a user in a certain time. It is a positive real number.

per is the time period in which the acc should to be updated, such as 1 minute, 10 minutes, half an hour and so on.

tim denotes the average time a user linger on a web resource. When computing it, we should take the content of the resource into consideration. For web pages, we divide the time by the number of words of the text.

Figure 2 is an example:
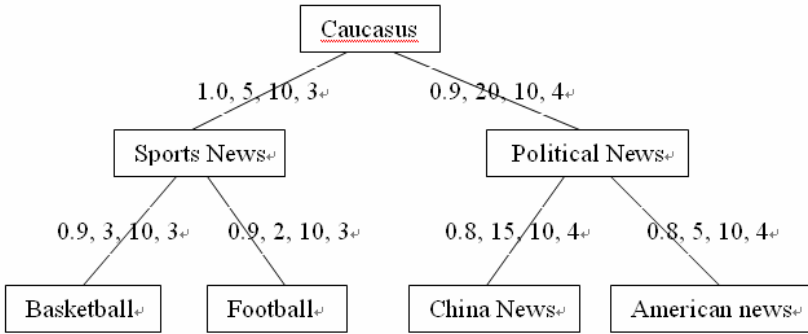
Fig. 2. Example of ontology instance

From the figure, we can know that a user called Caucasus has viewed 5 sports news in 10 minutes, and the average time of each news he linger on is 3 minutes.

5   Ontology Instance Similarity

Once a user login to a system, his/her new data is colleted and compared to the data stored in the database. If the similarity value between the new behaviors and the behaviors before for this account is below a threshold, we can say that the user may be defrauded.

In a RDF graph (ontology instance), the leaf node is a node that doesn't have an output edge. Since a RDF graph is not a tree, so it may be more than one path from the root node to a leaf node.

For each edge created in the new session (the data collected from the login), the similarity value with the corresponding edges (be stored in the database) is defined as following:

$$sim\_edg = (1-(rev\_new-rev\_old))*per/(acc\_new*tim\_new-acc\_old*tim\_old) \quad (1)$$

*_new and *_old denotes the newly colleted data and data in the database respectively. The time period should be the same for the two corresponding edges.

For a path from the root node to a leaf node, the similarity is defined as following:

$$sim\_path = (\sum(sim\_edg_n / ((rev\_new+rev\_old)/2))) /n \quad (2)$$

where th1 <= sim_edg / ((rev_new+rev_old)/2), and th1 is a threshold value. The edges with its sim_edg / ((rev_new+rev_old)/2) too little means that the edge can't well characterize a user's personality, so it won't be used for the fraud detection. For example, some events may change user's suffer interest, such as the holding of the Olympic Games, and the value of acc and tim may be much larger than the normal one.

The total similarity value of the two ontology instances is defined as following:

$$\text{sim\_inst} = (\sum(\text{sim\_path}_n))/n \tag{3}$$

the similarity value between the new instance and all the instances before:

$$\text{sim\_onto} = (\sum(\text{sim\_inst}_n))/n \tag{4}$$

and the similarity between the user's new behavior and before is:

$$\text{sim} = (\sum(w_n * \text{sim\_onto}_n))/n \tag{5}$$

w_n is the weight for an ontology, and this is an empirical value. A larger weight value means the ontology can better characterize the behavior of a user. If the value of sim is smaller than a threshold, then a warning may be delivered and some action may be taken, such as inhibiting the access or inhibiting the user from uploading files.

When using the classifier, the classifier may be trained by certain ontology instances and the new ontology instance is classified by the classifier.

6   Experiments and Future Work

We have applied our method to a BBS for experimental test. In the BBS, normal users can read and post articles or pictures, send messages or mails to each other, upload little attachment (<=1M), and so on. Board manager has some other privileges, such as modifying or deleting posts. In BBS, there is a friend list and user can add himself to the list, we have disabled this function for the users attend the test, we don't want the user to know whether they are be frauded so they won't change their activities.

40 students have been invited to do the test, among them, 5 are board managers. They have been asked to use the BBS as they do before and 6 random chosen users are asked to be the faker for some time. We use 3 ontologies for preliminary data (described in section 4.2) and a picture ontology. The geographical ontology is too helpful to be used in our experiment because most of the students only use computer when they are in laboratory or in their dorms, so we can easily detect the frauded accounts, but in other applications, the geographical data of a user may change frequently.

With a 30 days test, we have colleted these data, user use BBS 3 valid hours per day (many students stay in the BBS much longer than this, but the time period in which there are too few activities are omitted), and we created about 28800 ontology instances, including temporal instances, after selecting and merging, 8200 instances were stored in the database, (about 200 instances for each account, but not or the instances are used when computing similarity). Among them, 723 instances were created from the random chosen fakers, 674 instances have correctly indicated the fraud, and the accuracy is 93.2%. From the figure 3 of following, we can see, at the time of 2 minutes after the user' login, the accuracy for fraud detection is 70.60 (this
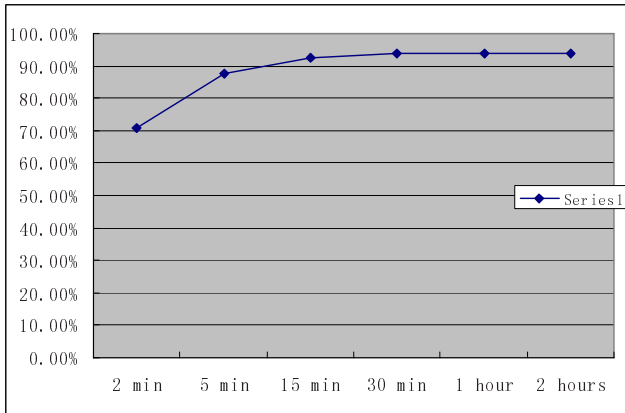
Fig. 3. Fraud detection accuracy

is for experiment, and not counted in former statistics), at the time of 5 minutes, the accuracy is 87.7%, at this time, an alarm may be delivered if fraud detected, after 30 minutes, the accuracy are mostly the same.

Compared to other experiments [2, 3], the accuracy has not be improved, we will explore more large scale test using better classifiers, and this will be one of our future work. Our contribution here is using the ontology to present the data, using the ontology instance similarity as the indicator of fraud detection for early stage of applications, when there are not enough examples to train the classifies. Ontology is now widely used and more and more domain will use ontology for the for the purpose of enabling knowledge sharing and reuse. Our system can easily be adapted to different applications. As far as we know, other methods for fraud detection should model the data for each applications, this will take a lots of work.

Our future work may take 2 directions, one is to choose or design better classifiers for ontology instances. And the other is to apply ontology extraction method to our system, because many ontologies are designed for other purpose and are not suit fraud detection very well.

References

1. http://www.internetworldstats.com/stats.htm
2. Clifton Phua, Damminda Alahakoon, and Vincent Lee: Minority Report in Fraud Detection: Classification of Skewed Data. ACM SIGKDD Explorations Newsletter. Volume 6, issue 1 (2004). 50-59.
3. Tom Fawcett, and Foster Provost: Adaptive fraud detection. Data Mining and Knowledge Discovery, (1997), 291-316.
4. Wenke Lee, Salvatore J. Stolfo, Kui W. Mok: Mining in a Data-flow Environmont: Experience in Network Intrusion Detection. Data Mining and Knowledge Discovery, (1999), 114-124.
5. Tom Fawcett, and Foster Provost: Activity Monitoring: Noticing interesting changes in behavior. Data Mining and Knowledge Discovery, (1999), 53-62.

6. Balaji Padmanabhan and Alexander Tuzhilin: On Characterization and Discovery of Minimal Unexpected Patterns in Rule Discovery. IEEE Transactions on Knowledge and Data Engineering, Vol. 18, No. 2, February 2006

7. John Kingston, Burkhardd Schafer, and Wim Vandenberghe: No Model Behavior: Ontologies for Fraud Detection. Law and the Semantic Web, LNCS 3369, (2005), 2 33-247.

8. Shuk Ying HO: An Exploratory Study of Using a User Remote Tracker to Examine Web users' Personality Traits. ICEC'05, 659-665.

9. http://www.semantic-squirrel.org/

10. Mischa M Tuffield, Antonis Loizou, David Dupplaw: The Semantic Logger: Supporting Service Building from Personal Context. CARPE'06, 55-63.

The Practical Application of Fuzzy Information Analysis in Flood Forecasting

Lihua Feng[1] and Weihu Hong[2]

[1] Department of Geography, Zhejiang Normal University, Jinhua 321004, China
[2] Department of Mathematics, Clayton College & State University, GA 30260, USA
fenglh@zjnu.cn

Abstract. The relationship between the peak stage and peak discharge is influenced by many factors in the flood system. Therefore, different peak discharges may occur under the same peak stage, while the same peak discharge may also occur under the different peak stages. If the peak stage set with similar peak discharges is taken as the fuzzy subset in the stage universe, then the membership function of these fuzzy subsets can be hypothesized to manifest a normal distribution graph. According to a_k and b_k, the mid-value of the universe element of the peak stage can be substituted into the normal distribution graph, and the fuzzy relational matrix can be obtained. Thus, the peak discharge can be calculated according to the peak stage using the fuzzy deduction theory. The relationship between the peak stage and peak discharge as $Q = f(H)$ has an important impact on the determination of the peak discharge during the high-water level period in the flood forecast. In this paper, the fuzzy information analysis method is used to forecast the peak discharge, with the result in accordance with the actual event. This method can be seen as a new and effective method of flood prediction and forecasting.

Keywords: fuzzy information analysis; universe; fuzzy relational matrix; flood forecast.

1 Introduction

Flooding is a common occurrence in China, and one that causes serious damage and harm. It is estimated that of the total economical loss caused by all kinds of disasters, 40% was due to flooding. Floods occur frequently, affect large areas of the community, and hence constitute a huge threat to human life and property. Flood damage has been aggravated by the rapid progress of the economy in recent years [1].

However, flood systems are complicated systems with strong indeterminacy [2-3]. Therefore, a method of recognition of flood systems using the fuzzy information analysis method [4] is devised and discussed in this paper.

2 Method of Fuzzy Information Analysis

Selection of a system model with higher reliability is difficult. A simple method is to directly construct a fuzzy relational matrix R without any transition through language variables and message net blocks [5-6].

Peak stage H and peak discharge Q are the most important parameters for the formation of flood damage. Unfortunately, at present the exact relationship between the two parameters as

$$Q = f(H) \tag{1}$$

cannot be found. In fact, there exists a fuzzy relationship between the two parameters. Therefore, the universe ranges of the peak stage and peak discharge need to be determined first. For the purpose of flood prevention, the range of the peak stage can be selected as m classes, and therefore the universe of the peak stage should be $U_H = \{H_1, H_2, \cdots, H_m\}$. The range of the peak discharge can also be selected as n classes and the corresponding universe of the peak discharge should be $U_Q = \{Q_1, Q_2, \cdots, Q_n\}$.

The method of determining the fuzzy relation through hypothesizing of the distribution form can only be performed upon analysis of the physical process. The relationship between the peak stage and peak discharge has been influenced by many factors in the flood system. If the peak stage set with similar peak discharges is taken as the fuzzy subset in the stage universe, then the membership function $\mu_k(H)$ of these fuzzy subsets can be hypothesized to manifest a normal distribution graph as follows:

$$\mu_k(H) = \exp\left[-\left(\frac{H - a_k}{b_k}\right)^2\right] \tag{2}$$

In the equation, k means the class of the peak discharge, with a_k and b_k as constants that can be obtained from the historical flood samples. Suppose the number of flood samples with the class of the peak discharge of k is N, then a_k and b_k can be calculated according to the following two equations:

$$a_k = \frac{1}{N} \sum_{j=1}^{N} H_j \tag{3}$$

$$b_k^2 = \frac{1}{N} \sum_{j=1}^{N} (H_j - a_k)^2 \tag{4}$$

In the equation H_j means the value of the peak stage of the jth sample.

According to a_k and b_k, the mid-value of the universe element H_i of the peak stage can be substituted into the equation (2), and the fuzzy relational matrix R can be obtained. If the mid-value of H_i is $\overline{H}_i$, then the element of R should be $r_{ik} = \mu_k(\overline{H}_i)$.

After determination of the fuzzy relational matrix R, the peak discharge Q can be calculated according to the peak stage H using the fuzzy deduction theory as follows:

$$Q = H \circ R \qquad (5)$$

The operator "$\circ$" means the combination operation in the equation.

As to the first forecast model, the relative fuzzy expression can be represented as $H = 1/H_i$ using the concept concerning language variables in fuzzy mathematics. Thus, the following expression can be constructed:

$$Q = (0, \cdots, 0, 1, 0, \cdots, 0) \circ \begin{bmatrix} r_{11} & r_{12} & \cdots & r_{1n} \\ r_{21} & r_{22} & \cdots & r_{2n} \\ \vdots & \vdots & & \vdots \\ r_{m1} & r_{m2} & \cdots & r_{mn} \end{bmatrix}$$

$$= \frac{r_{i1}}{Q_1} + \frac{r_{i2}}{Q_2} + \cdots + \frac{r_{in}}{Q_n} \qquad (6)$$

The above equation represents a fuzzy subset on the universe of the peak discharge. It is the result of the fuzzy recognition.

3   Application Illustration

The relationship between the peak stage and peak discharge as $Q = f(H)$ has an important impact on the determination of the peak discharge during the high-water level period in the flood forecast. Unfortunately, this relationship remains undetermined owing to the complexity of the factors that influence the flood. Therefore, different peak discharges may occur under the same peak stage, while the same peak discharge may also occur under the different peak stages. Table 1 lists data of the annual maximum peak stage H and annual maximum peak discharge Q surveyed in the Hankou hydrometric station of the Changjiang River of China. From the table it can be seen that the peak stage values H are about the same in 1948 and 1949 at the Hankou hydrometric station. Conversely, the two corresponding peak discharge values Q are different. In addition, the peak discharge values Q are about the same in 1935 and 1952, whilst the two corresponding peak stage values H are very different. Furthermore, a situation where the peak discharge value Q became even larger at a small peak stage value H was also observed.

Table 1. Data of the annual maximum peak stage H and annual maximum peak discharge Q in the Hankou hydrometric station of Changjiang River

Year	H (m)	Q (m³/s)	Year	H (m)	Q (m³/s)
1948	27.03	56000	1935	27.58	59300
1949	27.12	52700	1952	26.60	59500

In fact, a definite relationship can only exist within a certain range between the annual maximum peak stage H and annual maximum peak discharge Q, owing to the action of the factors that influence flooding. Therefore, flood data was selected for the

present discussion in a range from 1865 to 1970 at the Hankou hydrometric station of the Changjiang River. This area was scarcely influenced by human activity and so is less likely to be affected by extra factors, although the station was short of flood data for the period 1944-1945. The annual maximum peak stage H in the range was divided into nine classes. From this the universe of H should be $U_H = \{H_1, H_2, \cdots, H_9\}$ as shown in Table 3. The annual maximum peak discharge Q in the range was also divided into ten classes. From these classes, the universe of Q should be $U_Q = \{Q_1, Q_2, \cdots, Q_{10}\}$ as shown in Table 2. According to the calculation from equations (3) and (4), the values of a_k and b_k can be obtained (as listed in Table 2). As a result of the scarcity of the sample number of Q_8, Q_9 Q_{10}, several constants have been determined as $b_8^2 = b_9^2 = b_{10}^2 = 0.2$, which are just the average

Table 2. The range of the annual maximum peak discharge and its calculated results

U_Q	Range of peak discharge (m³/s)	Sample number	a_k	b_k^2
Q_1	29000-34000	2	22.05	0.2550
Q_2	34000-39000	9	23.34	0.0498
Q_3	39000-44000	16	24.36	0.0634
Q_4	44000-49000	33	25.12	0.3665
Q_5	49000-54000	24	26.13	0.1747
Q_6	54000-59000	11	26.63	0.1683
Q_7	59000-64000	7	27.21	0.3147
Q_8	64000-69000	1	27.36	0.2000
Q_9	69000-74000	0	28.55	0.2000
Q_{10}	74000-79000	1	29.73	0.2000

Table 3. The fuzzy relational matrix between the annual maximum peak stage H and annual maximum peak discharge Q

U_H	H(m)	Q_1	Q_2	Q_3	Q_4	Q_5	Q_6	Q_7	Q_8	Q_9	Q_{10}
H_1	21-22	0.31	0	0	0	0	0	0	0	0	0
H_2	22-23	0.44	0	0	0	0	0	0	0	0	0
H_3	23-24	0	0.58	0	0	0	0	0	0	0	0
H_4	24-25	0	0	0.74	0.34	0	0	0	0	0	0
H_5	25-26	0	0	0	0.67	0.10	0	0	0	0	0
H_6	26-27	0	0	0	0	0.45	0.90	0.20	0.02	0	0
H_7	27-28	0	0	0	0	0	0.01	0.76	0.90	0	0
H_8	28-29	0	0	0	0	0	0	0	0	0.98	0
H_9	29-30	0	0	0	0	0	0	0	0	0.01	0.76

values of $b_1^2 \sim b_7^2$. Afterwards, the mid-value $\overline{H}_i$ of the universe of the annual maximum peak stage was substituted into the equation (2). From this the fuzzy relational matrix R between H and Q can be obtained, as shown in Table 3.

With the help of the fuzzy relational matrix R, the annual maximum peak discharge Q can be obtained according to equation (5). The fit rate of the calculated result for the flood data from 1865 to 1970 in the Hankou hydrometric station is satisfactory at a rate of 73%.

Thus, the annual maximum peak discharge in the Hankou hydrometric station can be predicted according to the present fuzzy relational matrix R. For example, the annual maximum peak stage in 1971 in the Hankou hydrometric station is 24.21m. At this time the value of H can satisfy the relation as $H = 1/24.21 = 1/H_4$. Therefore, fuzzy deduction can be performed according to equation (5) and the result can be represented as follows:

$$Q = \frac{0.74}{Q_3} = \frac{0.34}{Q_4}$$

Table 4. The forecast of the annual maximum peak discharge Q in the Hankou hydrometric station and its fit conditions

Year	H(m)	U_H	U_Q	Range of peak discharge (m³/s)	Q (m³/s)	Fit Conditions
1971	24.21	H_4	Q_3	39000-44000	43700	√
1972	22.15	H_2	Q_1	29000-34000	36400	×
1973	26.85	H_6	Q_6	54000-59000	54300	√
1974	26.19	H_6	Q_6	54000-59000	54900	√
1975	25.00	H_4	Q_3	39000-44000	43800	√
1976	26.50	H_6	Q_6	54000-59000	58400	√

If taking the value of Q with the highest probability as the forecasted value, then the annual maximum peak discharge in 1971 can be forecasted in a range between 39000m³/s and 44000m³/s. In fact, the actual value of the annual maximum peak discharge in 1971 is Q=43700m³/s, an exact forecasted value. The annual maximum peak discharges from 1971 to 1976 in the Hankou hydrometric station were also forecasted, as listed in Table 4. The forecasted values within those five years are in accordance with the actual situations with the exception of 1972.

4   Conclusion

The relationship between the peak stage and peak discharge is hard to determine due to the complexity of the factors which can influence flooding. In fact, there exists a fuzzy relationship between the two terms. Therefore, the fuzzy information analysis method can be used to study the exact relationship between the above two terms. The

method can also be used to forecast the corresponding peak stage or peak discharge and precipitation runoff between the hydrometric stations in the upper and lower reaches of the same river. Although the result of the flood forecast is always within a certain range, the forecast can satisfy the demands of most situations. In conclusion, flood forecasting using the fuzzy information analysis technology is effective.

References

1. Feng, L.H., Chen, L.R.: Three Large Floods Along the Yangtze River in the 20th Century. Journal of Natural Disasters 1 (2001) 8-11
2. Fan, Z.P., Ma, J., Zhang, Q.: An Approach to Multiple Attribute Decision Making Based on Fuzzy Preference Information on Alternatives. Fuzzy Sets and Systems 1 (2002) 101-106
3. Cordon, O., Moya, F., Zarco, C.: A New Evolutionary Algorithm Combining Simulated Annealing and Genetic Programming for Relevance Feedback in Fuzzy Information Retrieval Systems. Soft Computing 5 (2002) 308-319
4. Huang, C.H., Wang, J.D.: Analysis of Fuzzy Information and Its Application. Beijing Normal University Publisher (1992) 177-182
5. Nils, H., Peter, S.: Precautionary Saving and Fuzzy Information. Economics Letters 1 (2001) 107-114
6. Isabelle, B., Thierry, G.: Representation and Fusion of Heterogeneous Fuzzy Information in the 3D Space for Model-Based Structural Recognition--Application to 3D Brain Imaging. Artificial Intelligence 1-2 (2003) 141-175

A Fuzzy Comprehensive Evaluation Method on Firms' Credit Sale Risk*

Guoqiang Liu[1], Zongfang Zhou[1], Xinmin Song[1], and Yong Shi[2]

[1] School of Management, University of Electronic Science & Technology of China,
P.R. China, 610054
zhouzf@uestc.edu.cn
[2] College of Information Science & Technology, University of Nebraska at Omaha, Omaha,
NE 68182, U.S.A
itdmeditor@yahoo.com.cn

Abstract. This paper utilizes the fuzzy comprehensive evaluation method (FCEM) to evaluate firm's credit sale risk, and provide the credit line and time limit of a credit sale according to the grades of firm's credit sale risk. Finally, we also present an example to validate the feasibility of this method. The result will greatly benefit in enhancing the firm's credit sale risk management.

Keywords: Credit sale risk, FCEM, credit sale grades.

1 Introduction

Market economy, characterized with openness and competition, will no doubt lead to the formation of buyers' market, and then Chinese market will be a highly developed credit market, which brings risks and costs to the firms as well as benefits. The credit sale is adding the risk of bad debts, additional financing cost, managing cost, which may lower the firms' capacity of earning profits.

Firms in our country have little consciousness of credit. Lack of scientific risk management system and perfect credit sale management measurements within the business has made great bad debts losses to the firms. Some even said that credit sales are going to die but no credit sales are waiting to die. So, enhance the credit management system and establish the evaluation grade system of client credit has been a burning question of all the firms.

Client's credit risk is credit sale risk, that is, the client unable to or unwilling to repay the credit sale on schedule. Because it should consider many aspects and involves a great deal of quantitative and qualitative indicators to make an analysis of customer's credit risk, including three phases of a trade. The present research on firms' credit risk mostly concentrates on the whole assessment of firm's credit [6][7][8], and mainly adopts the accounting method. They seldom carry on a systemic study on credit sale risk [7], not to say to combine client's credit level with the credit line and credit time limit.

---

* National Natural Science Foundation of China (No. 70671017).

This paper uses the fuzzy comprehensive evaluation method to give a quantitative analysis of clients' credit risk and to evaluate the clients' risk degree, and the credit line the firms may offer, and then determine the credit time limit. The result will be an important reference for the firms' credit sale policy-making.

2 Indictors of the Firms' Credit Sale Risk

The firms mostly gets the information of clients through the front line staff, however, it's hard for them to get clients' financial information. According to the characteristics of clients' credit risk, this paper builds the indictor system of accessing firms' client credit risk on the basis of the credit grade indictor of the firms and the characteristic of clients' credit (Fig. 1). In my opinion, in order to avoid overly affecting the formulation of fiems' credit policy by a client's past credit sales situation, only the credit situation during some period T need to be evaluated by firms (Time T can be confirmed by the industry environment of the firms).

Firm's client credit sale risk U should include the following indictors: previous transaction U_1, business status U_2, management and profit level U_3, developing potential U_4, financial analysis U_5.

(1) Previous transaction U_1 includes: ordering quantity U_{11}, repayment and payment attitude U_{12}, goodwill U_{13}.

(2) Business status U_2 includes: leader's quality U_{21}, employ's quality U_{22}, technical level U_{23}, product sales income U_{24}, gross profit U_{25}, capitalization U_{26}, business environment $U_{27.}$

(3) Management and profit level U_3 includes: market share U_{31}, major business and funds status U_{32}, total profit growth rate U_{33}, products sale growth rate U_{34}, capital preserves value growth rate $U_{35.}$

(4) Developing potential U_4 includes: market prospect U_{41}, major products potential U_{42}, industry position U_{43}.

(5) Financial analysis U_5 includes: liability and net assets ratio U_{51}, short-term liability and net asset ratio U_{52}, quick ratio U_{53}, working capital U_{54}, receivable accounts turnover U_{55}.

3 The Application of FCEM

3.1 Evaluation of the indictor weights

This paper uses AHP method to determine the weight of firms' client credit sale risk, and the calculation procedure is as follows:

(1) Use scale 1-9 to construct Judgment Matrix A

Element a_{ij} in matrix A refers to the relative importance of U_{ij} pairwise. An expert panel generally constructs the judgment matrix. Certainly firms may also choose experienced sellers, financial personnel.
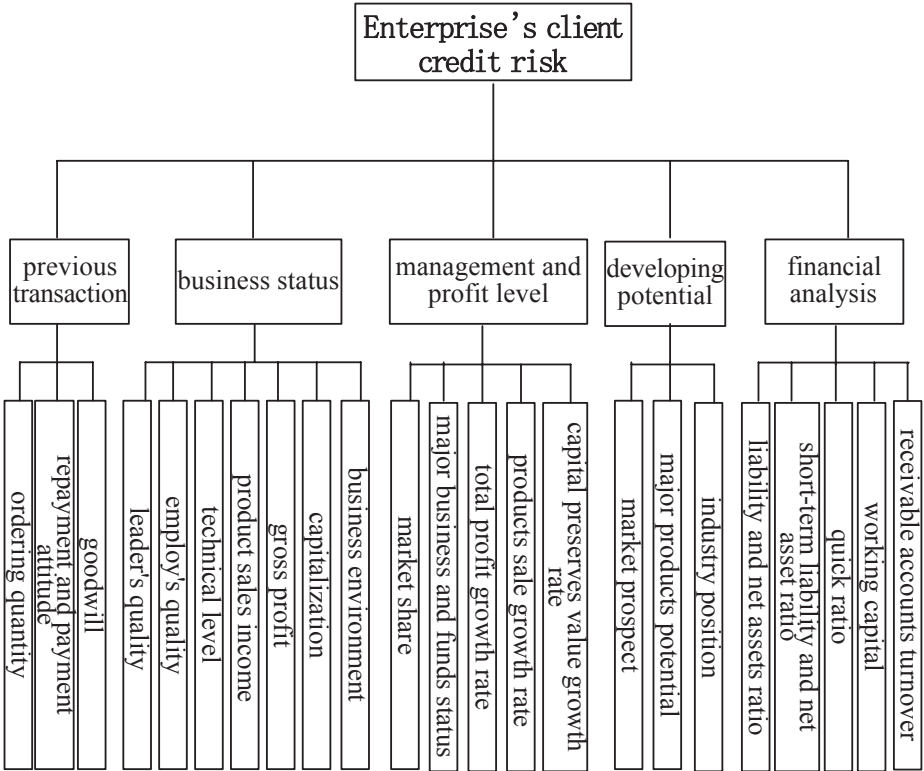
Fig. 1. Indicator system of client's credit sale risk

Table 1. Scale 1－9

Scale	Meaning
1	Indicates two indicators are of equal importance;
3	Indicates the former indicator is weakly more important than the latter one;
5	Indicates the former indicator is strongly more important than the latter one;
7	Indicates the former indicator is very strongly more important than the latter one;
9	Indicates the former indicator is absolutely more important than the latter one;
2, 4, 6, 8	Intermediate values;
Reciprocal	If the importance ratio of indicator i to j is a_{ij}, then this ratio of indicator j to i is $a_{ji} = 1/a_{ij}$;

(2) Using maximum eigenvalue to calculate the weight:

$$A\omega = \lambda_{\max}\omega \tag{1}$$

Where $\lambda_{\max}$ is the maximum eigenvalue in matrix A, ω is corresponding characteristic vector. It can be regarded as the weight vector behind the normalization of ω.

(3) Consistency test

Consistency test is used to validate whether the judgment matrix has a consistency. If not, we have to adjust the matrix by the steps follows:

I.   Consistency index:

$$C.I. = \frac{\lambda_{\max} - n}{n-1} \tag{2}$$

II.   Finding the corresponding average random consistency ： $R.I.$
III. Consistency ratio：

$$C.R. = \frac{C.I.}{R.I.} \tag{3}$$

If $C.R. < 0.1$, it is acceptable that the matrix is consistent; otherwise, the judgment matrix would need some modification.

(4) Calculate combined weights

Relative weight of the indicator should be calculated from one level to another. Supposing the weight of the second level indicator to the indicator of client's credit risk was $\varpi = (\omega_1, \omega_2, \ldots\ldots, \omega_k)^T$, and the weight of the third level indicator to the second level was $\varpi_i = (\omega_{1i}, \omega_{2i}, \ldots\ldots, \omega_{ni})^T$, $i = 1,2,\ldots\ldots, k$. Then the combined weight of the third level indicator to client's credit risk should be $V = (v_1, v_2, \ldots\ldots, v_n)^T$, and $v_i = \sum_{j=1}^{k} \omega_j \omega_{ij}$, $i = 1,2,\ldots\ldots, n$.

3.2 Clients' Credit Sale Risk Grades

Client's credit sale risk is related directly to the firms' credit sale policy to this client. This paper grouped client's credit sale risk into six rates, each with corresponding credit line.

(1) Membership degree of quantitative index

There are so many kinds of membership functions that the judgment of its belongingness is very subjective.

Whereas in the practical situation, belonging to which membership function can be decided, according to the specific situation of firms' clients. We will apply membership function: $\mu v_i(u) = e^{-a(u-c)^b}$. In this formula, there are some instructions: u stands for the actual value of the indicator; $\mu v_i(u)$ means the

Table 2. Firms' client credit sale risk and corresponding credit line

Rate	Definition	Annotation / note
1	For the client with very good credit, firms could provide the most affordable credit risk.	$a > b > c > d$
2	For the client with better credit, firms could provide credit provide under a%.	Firms could adjust rate and credit indicator
3	For the client with average credit, firms could provide credit risk under b%.	accordingly, plus with some measures
4	For the client with bad credit, firms could provide credit risk under c%.	if necessary.
5	For the client with worse credit, firms could provide credit risk under d%.	
6	For the client with most terrible credit, firms would provide no credit risk. Only can be conducted the transaction by cash.	

membership degree of u to v_i, $a > 0, b$ is plus even number, a and b are unallocated constants, and c is the constant when it is applied to membership degree of v_i level $\mu v_i (u) = 1$.

(2) Membership degree of qualitative indicator

When choosing senior marketing personnel, financial personnel and business management personnel, we should classify all the evaluative elements into groups according to the already designated evaluation standard. And then calculate the frequency M_{ij} of each evaluate elements divided by level v_i. At last the membership degree would become clear:

$$\mu_{ij} = M_{ij} / n \tag{4}$$

From above membership function we can make out the degree r_{ijt} of U_i's indicator u_{ij} devised by the evaluation number t, the U_i's fuzzy comprehensive evaluation matrix:

$$R_i = \begin{bmatrix} r_{i11} & r_{i12} & \cdots & r_{i1m} \\ r_{i21} & r_{i22} & \cdots & r_{i2m} \\ \cdots & \cdots & \cdots & \cdots \\ r_{in1} & r_{in2} & \cdots & r_{inm} \end{bmatrix} \tag{5}$$

In this matrix, i is the quota's number of each categorical element, that is, $U_1, U_2, \ldots, U_5$; where n: the number of each evaluation indicator in U_i; m: the evaluation number of vector's evaluation set. By the formula $U_i = \omega_i \bullet R_i$, we can get the fuzzy comprehensive evaluation set of all indicators in

level U and $U_i = (b_{i1}, b_{i2}, ..., b_{im})$, ω_i stands for proportion vector of each U_i evaluation indicator, b_{it} is get from $M(\bullet, \oplus)$ operator, that is,

$$b_{it} = \omega_{i1} \bullet r_{i1t} \oplus \omega_{i2} \bullet r_{i2t} \oplus ... \oplus \omega_{in} \bullet r_{int} \tag{6}$$

This operator has to take all the elements' weight into consideration, which fulfill firms' need of taking the whole synthesized indicator of client's credit risk into consideration.

3.3   The Credit Sale Time Limit

Credit sale time limit usually means the period from the time when clients buy the commodity to the time of payment. Too long a period will cause some indefinite elements and the corresponding cost. Too short a period would cause clients lose interest, thus lose its function. Therefore, firms should set an appropriate credit sale time limit for each would-be client.

Supposing all the clients would pay credit loan on time, and according to Capital-Time-Value Principle and the fact that credit profit will always be larger than credit cost, together with credit line, firms will get the credit sale time limit to its clients.

$$\text{[credit loan} /(1+R)^{CT} - \text{sales cost} - \text{credit sales cost}] / \text{total cost} \geq R \tag{7}$$

In this formula, credit sale cost includes bad debts cost (credit loan×bad debts rate), opportunity cost ((profit rate + loan interest) ×CT) and management cost (the additional fee of receivable account). R stands for standard financial rate of return; CT shows the credit sale time limit.

If clients want to extend credit sale time limit, firms can use the same method to test whether the cost is equal to or larger than firm's interest rate. If the answer is positive, then the request is acceptable; otherwise, it would be refused.

4   Illustration

Suppose there is a company, its credit management department is evaluating a client's credit risk. Consulting its senior marketing personnel and management personnel, the company works out a comparative evaluation matrix. Each indicator's weight would be clear by power method:

Indicator weights of U: (0.4185, 0.0973, 0.1599, 0.0618, 0.2625);
Indicator weights of U_1: (0.1007, 0.6738, 0.2255);
Indicator weights of U_2: (0.0667, 0.0260, 0.1099, 0.3648, 0.1958, 0.0410);
Indicator weights of U_3: (0.1441, 0.4699, 0.0792, 0.2619, 0.0448);
Indicator weights of U_4: (0.1172, 0.6144, 0.2684);
Indicator weights of U_5: (0.0901, 0.3466, 0.1668, 0.3466, 0.0500).

According to the membership function with a normal distribution and suggestions from senior marketing personnel, financial personnel and management personnel, client's membership degree to each level should be:

$$U=(0.0885,\ 0.1178,\ 0.2730,\ 0.2124,\ 0.2008,\ 0.1075)$$

The conclusion is that the credit sale risk of this firm's clients belongs to the third rate and the credit line is 15% at the most. Through the formula (7), we can get that the time limit available to the client is no more than 23 days.

5   Conclusion

This paper illustrates a systematic research of an firms' credit sale policy and evaluation on its client's credit risk. There are three parts of this process: evaluating clients' credit risk by the fuzzy comprehensive evaluation method, working out clients' credit line with the consideration of clients' credit rate, and calculating the time limit of credit sale. Besides, the evaluation system also includes recovering the money, result evaluation of credit department, etc., we will devote ourselves to these researches in the future.

References

1. Wang Lianfen, Xu Shubai, Theory of Analytic Hierarchy Process (in Chinese), RENMIN University of China Press, 1990.
2. Yang Lunbiao, Gao Yingyi, Fuzzy Mathematics Theory and Application (in Chinese), South China University of Technology Press, 2003.
3. Peng Zuzeng, Sun Wenyu, Fuzzy Mathematics and its Application (in Chinese), Wuhan University Press, 2002.
4. Zhou Zongfang, Tang Xiaowo, The Research on Ordering Structure of Credit[J].Journal of Systems Science and Information, 2004,3（2）:531-534
5. Zhou Zongfang, Tang Xiaowo. Research on Targets Evaluation for Customers Credit[J].Journal of Systems Science and Information, 2003,4（1）:635-638
6. Zhou Wenxin, Wang Jiancheng, The Fuzzy Comprehensive Evaluation Method of the Credit Level of Firms Rating (in Chinese) [J], Systems Engineering, vol19 no4, pp72-75, July 2001.
7. Lin Hanchuan, Xia Minren, Firms Rating Theory and Practice (in Chinese), University of International Business and Economics Press, pp133-160, 2003.
8. Pu Xiaolei, Han Jiaping, Firms Credit Management paragon, China International Business and Economics Press (China Commerce and Trade Press), 2001.

Flood Disaster Risk Analysis for Songhua River Basin Based on Theory of Information Diffusion

Chang Yi, Chongfu Huang, and Yaozhong Pan

College of Resources Science and Technology, Beijing Normal University,
100875 Beijing, China
yichang531@ires.cn

Abstract. Flood disaster risk analysis, the essential of which is to estimate the probability distribution of flood disaster loss, is an important nonstructural measure for flood control and disaster reduction. In the paper, a frequency analysis method of flood disaster loss based on fuzzy mathematics theory of information diffusion with short time series of flood disaster samples is suggested for flood disaster risk analysis. With the support of historic disaster data, the method has been applied to flood disaster risk analysis for Songhua River Basin and turned out to be effective and practical.

Keywords: Information Diffusion, Flood Disaster, Risk Analysis, Songhua River Basin.

1 Introduction

In recent years, flood disaster loss has been sharply increasing with the rapid social-economic development. More and more attention has been paid to flood disaster risk analysis, an important nonstructural measure of flood prevention and disaster reduction [1, 2]. Predominating flood disaster risk is an important basis for decisions on flood control and flood insurance. When the historic flood data is sufficient, the results of risk evaluation can be obtained with considerable satisfaction generally by probability and statistics. However, in fact, the phenomenon of lack of experimental flood data occurs frequently, resulting in fewer samples that can only provide us with finite and incomplete knowledge to understand risk. In this case, it is inappropriate to take risk analysis by means of probability and statistics with a small sample, the sample size of which is usually less than 30, as the great fuzziness and uncertainty of the activity can sometimes lead to very unstable results that may even depart quite far from the real situation. Actually, one sample in a small sample set can not be treated as a specific observation due to its fuzziness and uncertainty, but a representation of the samples or a set-value sample as well as an observation sample of a fuzzy set. In this paper, fuzzy mathematics theory of information diffusion is used to establish the flood risk evaluation model with a small number of experimental samples. The model is then applied to flood risk analysis for Songhua River Basin in North-East China.

2   Definition of Flood Risk

The definition of Flood Risk is the basis of study on flood risk. The majority of researchers believe that risk is the occurrence probability of adverse events and the seriousness of their possible aftereffects. Flood disaster denotes the disaster situation that forms when the hazard, flood, acts on disaster-affected bodies in certain disaster-formative environment. Based on the definition of risk mentioned above, it can be deduced that adverse event of flood risk is flood, and the aftereffect is flood loss, namely disaster situation. Therefore, flood risk refers to the occurrence probability of flood at different intensity and the flood loss possibly caused, which is actually threefold: (1) *flood*, measurement of characteristics and magnitude of the flood, such as the highest water level, the flood peak discharge, the grade of flood volume in interval and the condition for flood happening, etc; (2) *probability*, the occurrence probability of flood event mainly denotes the occurrence frequency and the recurrence interval of those flood events that exceed certain grade or numerical value; (3) *loss*, the loss possibly caused by the occurrence of flood event basically includes flood disaster economic loss, personnel casualties, environment pollution, social influence, etc. Flood risk analysis is just to study on the probability distribution of flood loss (or of disaster situation).

3   Flood Disaster Risk Analysis Based on Information Diffusion

Flood risk analysis utilizing historic disaster data mostly adopts the method of flood disaster loss frequency analysis. Flood frequency analysis has got widely application in hydrology, but fewer frequency analyses have been done on flood disaster loss (disaster situation). Most scholars believe that flood disaster loss (disaster situation) data fall short of the requirement of frequency analysis for data consistency. Indeed, with respect to flood disaster economic loss (currency measurement), its gradual increase with the development of society leads to the non-conformity to the requirement for data consistency, however, certain disaster indicators like disaster-affected rate of arable land, in certain period, can be considered as a random variable whose frequency can be analyzed on.

   In the statistical risk based on probability and statistics, the uncertainty involved in risk is relevant to the similitude degree to some standard mode, which can be depicted by fuzzy sets membership in mathematics theory. Information diffusion is just a fuzzy mathematic set-value method for samples, considering optimizing the use of fuzzy information of samples in order to offset the information deficiency. The method can turn an observed sample into a fuzzy set, that is, turn a single point sample into a set-value sample [3]. The simplest model of information diffusion is normal diffusion model.

   Suppose X is the natural disaster indicator, and the transcendental frequency distribution of X in T years can be defined as disaster risk. Concretely, X is given as economic loss indicator which consists of some specific quantitative values, noted as

$X = \{x_1, x_2, ..., x_n\}$. And suppose the probability for loss transcending x_i is $p_i(x \geq x_i)$, i =1, 2, 3,…,n, then the probability distribution is $P = \{p_1, p_2, ..., p_n\}$, which can be named as loss risk caused by disaster, or disaster risk.

If the actual records of the natural disaster indicator in some region during the past n years are $y_1, y_2, ..., y_n$ respectively, then the observed sample set is $Y = \{y_1, y_2, ..., y_m\}$, in which, y_j, (j =1, 2,…,m) is named as disaster sample.

Suppose that the universe discourse of disaster indicator is $V = \{v_1, v_2, ..., v_n\}$. Usually, the natural disaster indicator X is taken as the universe discourse V, and each x in X is taken as corresponding element in the universe discourse V.

A single point observed sample y can diffuse the information it takes to every v_i according to $R(v_i)$, $R(v_i) = \dfrac{1}{\eta\sqrt{2\pi}}\exp[-\dfrac{(y-v_i)^2}{2\eta^2}]$, in which η is the diffusion coefficient. $\eta = \alpha(b-a)/(m-1)$ can be typically determined by the maximum value - b, the minimum value - a, and the number of samples - m, of the sample set, in which α is the parameter relevant to the sample size as shown in equation (1).

$$\eta = \begin{cases} 1.6987(b-a)/(m-1)..............1 < m \leq 5 \\ 1.43416(b-a)/(m-1).........5 \leq m \leq 10 \\ 1.4208(b-a)/(m-1)................10 \leq m \end{cases} \quad (1)$$

Thus, the single point sample y has been turned into the fuzzy set y^* which takes $\mu_y(v_i)$ as its membership function.

During risk evaluation, in order to maintain the status of each set-value sample the same, every sample y_j should be diffused according to equation $R(v_i)$, that is,

$$R_j(v_i) = \frac{1}{\eta\sqrt{2\pi}}\exp[-\frac{(y_j-v_i)^2}{2\eta^2}] \quad (2)$$

The membership function of corresponding fuzzy sets is

$$\mu_{y_j}(v_i) = \frac{R_j(v_i)}{\sum\limits_{i=1}^{n} R_j(v_i)}. \quad (3)$$

The $\mu_{y_j}(v_i)$ is called as the normalized information distribution of sample y_j.

Suppose that the number of samples, whose observation value is v_i, deduced by information diffusion is

$$l(v_i) = \sum\limits_{j=1}^{m} \mu_{y_j}(v_i) \quad (4)$$

Then, the frequency value of a sample falling at v_i is

$$P(v_i) = \frac{l(v_i)}{\sum_{i=1}^{n} l(v_i)}. \tag{5}$$

The frequency value can be taken as the estimation value for probability. Apparently, the probability value of transcending v_i should be

$$p(v_i) = \sum_{k=i}^{n} p(v_k) . \tag{6}$$

The $p(v_i)$ is the very risk estimation value needed to be calculated.

4   Flood Disaster Risk Analysis—Taking Songhua River Basin for Example

Songhua River is the largest branch river of Heilongjiang Basin in China. After the confluence of the upper reaches-Nen River and the second Songhua River-at Sanchahe, Fuyu County, Jilin Province, the main stream of Songhua River runs to meet Heilong River at Tongjiang County. In history, Songhua River had repeatedly suffered from attacks of flood. During the 240 years from 1746 to 1985, 104 times of flood disasters had happened in Songhua River Basin altogether, among which 15 were extraordinary ones[4].

To analyze the spatial characteristics of flood risk in Songhua River Basin, and according to the historic disaster data having been collected so far, the paper divides Songhua River Basin into three sub-basins respectively, that is, Nen River sub-basin, the main stream of Songhua River sub-basin and the second Songhua River sub-basin. Afterwards, in terms of the different provinces these sub-basins belong to, Nen River sub-basin is divided further into Heilonjiang district, Neimenggu district and Jilin district; the main stream of Songhua River sub-basin is divided further into Heilongjiang district and Jilin district; and the Second Songhua River sub-basin mainly lies in Jilin Province.

Disaster-affected rate has been chosen as the disaster indicator in flood risk analysis. In a certain time period, disaster-affected rate commonly has quite fine consistency. Disaster-affected rate means the ratio of disaster-affected area to crop area. In practical calculation, it is so difficult to collect the crop area in every region year by year that the arable land area is taken as a substitute. Then, calculate the disaster-affected rate[1] of each district in Songhua River Basin for the 25 years from 1965 to 1989 year by year, the result of which is shown in Table 1.

---

[1] The disaster-affected area data was provided by Songhua River and Liaohe River Conservancy Commission, and the arable land area data was acquired by measuring from the electronic 1:4,000,000 land use map.

Table 1. The disaster-affected rate of each district in Songhua River Basin year by year

Dist Year	The main stream of Songhua River		The second Songhua River	Nen River		
	Jilin	Heilongjiang	Jilin	Jilin	Heilongjiang	Neimenggu
1965	2.259077769	1.015268	0.925307	1.381932	0.691327	1.787675
1966	0	0.411851	0.11615	0.028548	0.141697	0.079912
1967	0	0.048061	0.04391	0	0.171606	0
1968	0	0.057183	0.030985	0	0.500109	0
1969	0.219576086	0.267162	0.174934	0.071613	2.404771	2.345648
1970	0	0.031505	0.495763	0	0.397145	0
1971	0.75515585	0.189877	0.89804	0.604837	0.26934	1.802717
1972	0	1.325423	0.145011	0	0.524133	0
1973	0.305547675	1.530334	1.518452	0	0.262802	0.188028
1974	0.066221359	0.999304	0.071886	0.181451	0.052299	0.06581
1975	0.101074706	0.401715	1.209662	0.558869	0.346807	0.00282
1976	0	0.093672	0	0	0.025332	0
1977	0	0.881982	0.402276	0.140322	0.92945	2.749908
1978	0	0.805626	0.057898	0	0.170952	0
1979	0	0.313196	0.313039	0	0.193343	0.296144
1980	0.644786918	0.431109	0.227166	0	1.773751	1.41491
1981	5.088588648	7.406639	1.925509	1.075642	2.686695	1.354271
1982	0.108626265	0.566168	0.110661	0	0.027457	0.288623
1983	2.038920794	4.881731	1.905501	2.533541	3.354814	2.842982
1984	1.067674194	4.369283	1.210725	1.694028	4.586944	2.101212
1985	5.769390691	7.780818	9.782116	7.028206	2.58128	2.326375
1986	9.726407343	3.819079	8.38247	12.41077	2.624753	6.26932
1987	0.411269493	8.870246	2.185253	5.180308	1.505556	3.866324
1988	4.173688292	10.65009	1.361047	6.365305	6.362329	10.74203
1989	5.424342557	3.027896	2.323713	0	1.884396	5.739551

Suppose that S_j ($j = 1, 2, ...25$) are the disaster-affected area in the period of the 25 years respectively, and S_j' is the crop area of the corresponding year, then the disaster-affected rate can be expressed as

$$I_j = \frac{S_j}{S_j'} \times 100\% \ (j=1,2,...25) .$$
(7)

Based on equation (7), the disaster-affected rates of the 25 samples can be calculated out, that is, the observed sample set $I = \{I_1, I_2,..., I_{25}\}$ .In view of both convenience and accuracy of the computer-aided calculation, the universe discourse of disaster-affected rate is taken as $V = \{v_1, v_2,..., v_{71}\} = \{0, 0.002, 0.004,..., 0.140\}$. The normalized information distribution of each I_j , that is, $\mu_{I_j}(v_i)$, can be obtained according to equation (2) and (3). Then, based on equation (4), (5) and (6), the flood risk estimation value $P(v_i)$, that is, disaster-affected risk probability, of each district in Songhua River Basin can be worked out, as shown in table 2.

Table 2. The flood disaster risk evaluation values of each district in Songhua River Basin

Dist	The main stream of Songhua River		The second Songhua River	Nen River		
$P(v_i)$	Jilin	Heilongjiang	Jilin	Jilin	Heilongjiang	Neimenggu
0.000	1.000000	1.000000	1.000000	1.000000	1.000000	1.000000
0.002	0.860689	0.919120	0.893011	0.875254	0.883896	0.900566
0.004	0.720842	0.829189	0.779280	0.750705	0.748927	0.801654
0.006	0.594220	0.736548	0.668676	0.634099	0.622752	0.711202
0.008	0.490093	0.647643	0.568698	0.531315	0.525449	0.634224
0.010	0.411498	0.567664	0.482775	0.445509	0.460861	0.571848
0.012	0.356112	0.499791	0.410570	0.377105	0.420676	0.521880
0.014	0.318592	0.445143	0.349633	0.324440	0.392956	0.480364
0.016	0.292944	0.403203	0.297178	0.284728	0.368197	0.443287
0.018	0.274120	0.372388	0.251184	0.254942	0.341847	0.407742
0.020	0.258722	0.350553	0.210706	0.232409	0.313480	0.372332
0.022	0.245061	0.335359	0.175669	0.215067	0.283484	0.336989
0.024	0.232767	0.324545	0.146439	0.201478	0.250857	0.302507
0.026	0.222180	0.316142	0.123352	0.190709	0.215064	0.270046
0.028	0.213715	0.308624	0.106343	0.182171	0.178988	0.240714
0.030	0.207430	0.300966	0.094790	0.175483	0.147662	0.215284
0.032	0.202903	0.292601	0.087622	0.170355	0.123933	0.194038
0.034	0.199356	0.283297	0.083585	0.166518	0.107040	0.176776
0.036	0.195902	0.273014	0.081532	0.163681	0.095094	0.162954
0.038	0.191781	0.261811	0.080593	0.161519	0.086960	0.151906
0.040	0.186512	0.249814	0.080207	0.159684	0.081591	0.143034
0.042	0.179904	0.237233	0.080065	0.157829	0.077113	0.135899
0.044	0.171945	0.224398	0.080018	0.155638	0.071438	0.130178
0.046	0.162630	0.211760	0.080005	0.152860	0.063748	0.125551
0.048	0.151853	0.199851	0.080001	0.149334	0.055211	0.121600
0.050	0.139473	0.189203	0.080000	0.145004	0.047964	0.117781
0.052	0.125521	0.180235	0.080000	0.139904	0.043312	0.113493
0.054	0.110412	0.173169	0.080000	0.134124	0.041005	0.108206
0.056	0.095000	0.167977	0.080000	0.127763	0.039875	0.101606
0.058	0.080407	0.164400	0.080000	0.120891	0.038574	0.093700
0.060	0.067706	0.162008	0.080000	0.113541	0.035762	0.084832
0.062	0.057608	0.160269	0.079999	0.105740	0.030418	0.075610
0.064	0.050308	0.158609	0.079994	0.097545	0.022670	0.066753
0.066	0.045529	0.156440	0.079978	0.089097	0.014205	0.058911
0.068	0.042704	0.153203	0.079930	0.080632	0.007245	0.052517
0.070	0.041200	0.148439	0.079798	0.072464	0.002938	0.047724
0.072	0.040482	0.141894	0.079479	0.064930	0.000932	0.044427
0.074	0.040174	0.133616	0.078794	0.058326	0.000229	0.042348
0.076	0.040055	0.123982	0.077486	0.052847	0.000043	0.041148
0.078	0.040009	0.113608	0.075269	0.048561	0.000006	0.040517
0.080	0.039976	0.103167	0.071931	0.045406	0.000001	0.040213
0.082	0.039910	0.093190	0.067451	0.043226	0.000000	0.040080
0.084	0.039745	0.083957	0.062075	0.041816	0.000000	0.040026
0.086	0.039354	0.075528	0.056247	0.040961	0.000000	0.040001
0.088	0.038536	0.067865	0.050425	0.040478	0.000000	0.039977
0.090	0.037017	0.060954	0.044866	0.040223	0.000000	0.039928
0.092	0.034516	0.054843	0.039531	0.040097	0.000000	0.039810

Table 2. (*Continued*)

0.094	0.030866	0.049580	0.034171	0.040039	0.000000	0.039544
0.096	0.026146	0.045101	0.028561	0.040014	0.000000	0.039003
0.098	0.020735	0.041166	0.022711	0.040001	0.000000	0.038002
0.100	0.015237	0.037399	0.016927	0.039990	0.000000	0.036327
0.102	0.010286	0.033404	0.011681	0.039968	0.000000	0.033786
0.104	0.006334	0.028929	0.007393	0.039920	0.000000	0.030296
0.106	0.003538	0.023975	0.004261	0.039816	0.000000	0.025953
0.108	0.001785	0.018799	0.002224	0.039606	0.000000	0.021058
0.110	0.000810	0.013818	0.001048	0.039209	0.000000	0.016060
0.112	0.000330	0.009453	0.000444	0.038514	0.000000	0.011437
0.114	0.000120	0.005985	0.000169	0.037385	0.000000	0.007565
0.116	0.000039	0.003491	0.000057	0.035681	0.000000	0.004627
0.118	0.000011	0.001870	0.000017	0.033293	0.000000	0.002607
0.120	0.000003	0.000917	0.000005	0.030185	0.000000	0.001349
0.122	0.000001	0.000411	0.000001	0.026430	0.000000	0.000640
0.124	0.000000	0.000168	0.000000	0.022217	0.000000	0.000278
0.126	0.000000	0.000062	0.000000	0.017828	0.000000	0.000110
0.128	0.000000	0.000021	0.000000	0.013581	0.000000	0.000040
0.130	0.000000	0.000007	0.000000	0.009765	0.000000	0.000013

Table 2 has shown the general situation of overall risk level for each district that Heilongjiang district of the main stream of Songhua River and Jilin district of Nen River are the two districts suffering from the flood disaster risk most, while Heilongjiang district in Nen River endures the lowest level of risk. According to the risk evaluation results shown above, it can be summed up that the disaster-affected rates of each district at different probability levels are as follows in table 3:

Table 3. The disaster-affected rates of each district in Songhua River Basin at different probability levels

Dist	The main stream of Songhua River		The second Songhua River	Nen River		
Probability	Jilin	Heilongjiang	Jilin	Jilin	Heilongjiang	Neimenggu
0.01	10.2	11.2	10.2	13.0	6.6	11.2
0.02	9.8	10.6	9.8	12.4	6.4	10.8
0.05	6.4	9.4	8.8	7.6	5.0	6.8
0.10	5.4	8.0	3.0	6.4	3.6	5.6
0.20	3.2	4.8	2.0	2.4	2.6	3.0

It can be learned from table 3 that when a flood disaster encountered once in a hundred years happens, almost 10.2% arable land in Jilin district of the main stream of Songhua River, 11.2% around arable land in Heilongjiang district of the main stream of Songhua River and about 13.0% arable land in Jilin district of Nen River will be affected; likewise, when a flood disaster encountered once in five years happens, nearly 3.2% arable land in Jilin district of the main stream of Songhua River, and almost 4.8% arable land in Heilongjiang district of the main stream of Songhua

River will be affected, etc. Concerning disaster-affected rate of arable land, the flood disaster risk lying in Songhua River Basin is relatively low.

5   Conclusion and Discussion

In this paper, based on the short time series of flood disaster historic data, the flood disaster risk estimation in Songhua River Basin has been done divisionally through flood disaster loss probability distribution estimation using information diffusion method, which is superior to the traditional statistic model. It is worth to mention that the division for Songhua River Basin in this paper is comparatively cursory, so that the analysis results can not yet completely reflect the spatial differences of flood disaster risk. More accurate division will definitely help to understand the spatial characteristics of flood disaster risk of Songhua River Basin, but the collection of historic disaster data is extremely difficult. In view of the facts that the theoretic system of flood risk evaluation has not been perfect enough so far, and the observed series of flood disaster are quite short or even unavailable, the method based on information diffusion adopted in the paper is indisputably an effective and practical method. However, when it comes to the form and adaptive condition of diffusion function and the determination of diffusion coefficients, further in-depth research should be conducted in the future, in order to ensure the estimation probability values get much closer to the real happening values.

References

1. Shifeng Huang, Chenghu Zhou, Qing Wan: Primary Analysis on Flood Disaster Risk Evaluation. Geographical Research, Vol. 17. (Supplement) (1998) 71–77
2. Chenghu Zhou, Qing Wan, Shifeng Huang, Deqing Chen: A GIS-based Approach to Flood Risk Zonation. Acta Geographica Sinica, Vol. 55. (2000) 15–24
3. Chongfu Huang and Yong Shi: Towards Efficient Fuzzy Information Processing--Using the Principle of Information Diffusion. Physica-Verlag (Springer), Heidelberg, Germany, (2002)
4. Dianying, Zhu: History of Drought and Flood in the Past 240 Years in Heilongjiang Province. Heilongjiang Technology, Harbin, China (1991)

A Novel Situation Awareness Model for Network Systems' Security

Guosheng Zhao[1,2], Huiqiang Wang[1], Jian Wang[1], and Linshan Shen[1]

[1] Institute of Computer Science and Technology, Harbin Engineer
University, Harbin 150001, China
[2] Center of Computer Network and Information, Harbin Normal
University, Harbin 150001, China
gs.zhao@yahoo.com.cn

Abstract. Building and maintaining the information superiority is the basis of the principle of active defense, integrated guarding in the cyberspace. In this paper, a novel method based on grey verhulst model was introduced to forecast the network system's security situation. Starting with unequal interval original risk data series, the proposed method choosed grey verhulst model or its inverse function to forecast the future risk value of network system, ant then it could modify the forecasting precision based on multilevel residual error. Simulation results reveal that the presented model not only gains the intuitionistic curve graph of network security situation, but also can achieve satisfactory precision. At the same time, it is simple in use and deserves further study to fully explore its potential for evaluation issues.

Keywords: non-equal interval, grey verhulst model, residual error revision, situation awareness.

1 Introduction

The situation awareness[1,2] is to analyze or comprehend various elements' behavior in time and space in active or autonomic way, as well as its evolutive tendency, attempt and prospective developments situation. It is an indispensably credible technology for safe precaution system.

Because the influencing factors of network security is complex and uncertain, so it is difficult to construct an appropriate forecasting model for security situation of network system. At present the various proposed frames[2,3,4] of cyberspace situation awareness cannot mostly provide practically useful situation information, cannot help manager make the right decision-making in the system actual security condition. According to the theory of grey system pioneered by Professor Deng[5], a system that lacks adequate information can be considered as a grey system. In this case, the network system can be view as a grey system. Considering the non-linearity of the risk data sequence, the grey verhulst model is selected and employed, which may discover the system's developmental principles and may scientifically make the quantitative forecast for future system's security situation. The verhulst model is

suitable to model for non-monotonous swings sequence or the saturated 'S' shape sequence very much, just as figure 1 demonstrated. This kind of curves can be divided into three segments as a whole: in I segment, the rate of curve slow increases; in II segment, the rate of curve is close to the linearity; in III segment, the rate of curve tends to steady value. Due to the original sequence is generally non-equal interval, so this paper chooses the non-equal interval grey verhulst model with residual error revision to carry out the modeling of the network system's security situation.
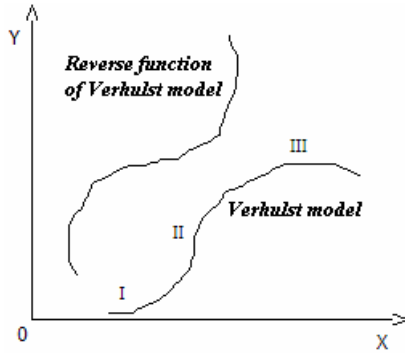
Fig. 1. The curves of verhulst model and its reverse function

This paper proposes a first-time application of mathematics based grey verhulst model for the forecasting of network system's security situation. Following contents are arranged as follows: section 1, 2 introduced the proposed model and its residual error revision method in detail; section 3 validates the model through simulation experiments; section 4 was a conclusion, which pointed out the future possible studies.

2 Modeling Process

2.1 The Processing Method of Non-equal Interval Data Sequence

Referring to the literature's processing method[6], we suppose the original sampling risk data sequence is $X^{(0)} = \{x^{(0)}(t_k), k = 1, 2, ..., n\}$, where $t_{i+1} - t_i > 0$. Due to the data sequence t_k is non-equal interval, and the difference $dt = t_{k+1} - t_k$ is not bigger, we may use the least squares method to construct the equal interval data sequence t'_k. According to the equation $t'_k = m_0 + m_1 \cdot k$, we can obtain the group of equations $T' = AM$, where $A^T = \begin{pmatrix} 1 & 1 & \cdots & 1 \\ 1 & 2 & \cdots & n \end{pmatrix}$, $M = \begin{pmatrix} m_0 \\ m_1 \end{pmatrix}$. In order to make $(dt)^T dt$ minimum, let $\dfrac{\partial (dt)^T dt}{\partial M} = 0$, thus we can deduce $A^T AM - A^T T = 0$, namely,

$$M = \left(A^T A \right)^{-1} A^T T \tag{1}$$

Then, we can gain T' using $t'_k = m_0 + m_1 k$ .Finally, we uses *Langrange* method to obtain the equal interval data sequence $X^{(0)}(T')$ again.

2.2 The Establishment of Non-equal Interval Verhulst Model

After the processing of equal interval, we can obtain equal interval data sequence, and then we may use the verhulst model to carry out modeling and forecasting. Let the original data sequence be $X^{(0)} = \{x^{(0)}(t) \mid t = 1,2,...,n\}$, then the *AGO* (accumulated generation operation) of $X^{(0)}$ is $X^{(1)} = \{x^{(1)}(t) \mid t = 1,2,...,n\}$, where $x^{(1)}(t) = \sum_{i=1}^{k} x^{(0)}(i)$, $t = 1,2,...,n$, and let $x^{(1)}(1) = x^{(0)}(1)$,   the nonlinear differential equation of $X^{(1)}(t)$ can be synthesized as follows:

$$\frac{dX^{(1)}(t)}{dt} = aX^{(1)}(t) - b(X^{(1)}(t))^2 \tag{2}$$

where a denotes the development coefficient, whose size and sign reflect the development situation of $X^{(0)}$; b denotes the system's input and its value presents some kind of grey information. These coefficients a , b can be identified by the least squares method as follows:

$$[a,b]^T = [B^T B]^{-1} B^T Y \tag{3}$$

where $B = \begin{pmatrix} \frac{1}{2}(x^{(1)}(1) + x^{(1)}(2)) & -\frac{1}{4}(x^{(1)}(1) + x^{(1)}(2))^2 \\ \frac{1}{2}(x^{(1)}(2) + x^{(1)}(3)) & -\frac{1}{4}(x^{(1)}(2) + x^{(1)}(3))^2 \\ \vdots & \vdots \\ \frac{1}{2}(x^{(1)}(n-1) + x^{(1)}(n)) & -\frac{1}{4}(x^{(1)}(n-1) + x^{(1)}(n))^2 \end{pmatrix}$, $Y_N = [x^{(0)}(2), x^{(0)}(3),...,x^{(0)}(n)]^T$.

Consequently, from Eq. (2), $\hat{X}^{(1)}(t)$ can be observed as

$$\hat{X}^{(1)}(t) = \frac{\dfrac{a}{b}}{1 + (\dfrac{a}{b} \cdot \dfrac{1}{X^{(0)}(1)} - 1)e^{-a(t-1)}} \tag{4}$$

Furthermore, from Eq. (4), can acquire the forecasted value as

$$\hat{X}^{(0)}(t) = \hat{X}^{(1)}(t) - \hat{X}^{(1)}(t-1) \tag{5}$$

Thus, the above equation from Eq. (2-5) is the non-equal interval Verhulst model.

2.3 Inverse Function Model of Grey Verhulst Model

The actual risk-time curve of network security situation frequently takes on the shape of reverse "S", which is similar to the curve of Verhulst model's inverse function. This kind of curves can be also divided into three segments as a whole: in I segment,

the rate of curve linearly increases; in II segment, the rate of curve slow grows; in III segment, the movements fast goes up, and finally tend to peak value. Therefore, we may use the inverse function model of non-equal interval grey verhulst model to analyze the reverse "S" characters of security situation curve.

Through solving Eq. (4) for a reverse function solution of $\hat{X}^{(1)}(t)$, we obtain the following inverse function model of grey verhulst:

$$\hat{X}^{(1)}(t) = \frac{1}{a}\ln\frac{(a-bt_0)t}{at_0-bt_0t} + \hat{X}^{(0)}(t) \tag{6}$$

In above equation, t denotes a time: a, b represents the coefficient of expression. Thus, using the Eq. (5) to regress, we may obtain the forecast value of the original data sequence.

3 Model's Residual Error Revision

Definition 1. Suppose $\varepsilon^{(0)} = (\varepsilon^{(0)}(1), \varepsilon^{(0)}(2),...,\varepsilon^{(0)}(n))$ is the residual error sequence, where $\varepsilon^{(0)}(k) = x^{(1)}(k) - \hat{x}^{(1)}(k)$ is the residual error sequence of $X^{(1)}$. If $\exists k_0$, make $\varepsilon^{(0)}(k_0) < 0$, where $\forall k, k \neq k_0$, has $\varepsilon^{(0)}(k_0) \leq \varepsilon^{(0)}(k)$, and then let E be constant, make $E > |\varepsilon^{(0)}(k_0)|$, call $(\varepsilon^{(0)}(1)+E, \varepsilon^{(0)}(2)+E,...,\varepsilon^{(0)}(n)+E)$ be the modeling residual error sequence, still marks $(\varepsilon^{(0)}(1), \varepsilon^{(0)}(2),...,\varepsilon^{(0)}(n))$.

Definition 2. Suppose the residual error sequence $\varepsilon^{(0)}$ is the original data sequence's one-order AGO sequence, then the time response expression of grey GM (1, 1) model can be obtained.

$$\hat{\varepsilon}^{(1)}(k+1) = (\varepsilon^{(0)}(k_0) - \frac{b_\varepsilon}{a_\varepsilon})\exp[-a_\varepsilon(k-k_0)] + \frac{b_\varepsilon}{a_\varepsilon}, \quad k \geq k_0 \tag{7}$$

Let $\hat{e}^{(0)} = (\hat{e}^{(0)}(k_0), \hat{e}^{(0)}(k_0+1),...,\hat{e}^{(0)}(n))$ as the simulation sequence of $\hat{e}^{(0)}$, where $\hat{\varepsilon}^{(0)}(k+1) = (-a_\varepsilon)(\varepsilon^{(0)}(k_0) - \frac{b_\varepsilon}{a_\varepsilon})\exp[-a_\varepsilon(k-k_0)] - E$, $k \geq k_0$.

Definition 3. If we revise $\hat{X}^{(1)}$ with $\hat{e}^{(0)}$, then the time response of expression amended is:

$$\hat{X}^{(1)}(k+1) = \begin{cases} \dfrac{\dfrac{a}{b}}{1+(\dfrac{a}{b}\cdot\dfrac{1}{X^{(0)}(1)}-1)e^{-a(t-1)}}, \varepsilon^{(0)}(k) \notin \varepsilon^{(0)} \\ \\ \dfrac{\dfrac{a}{b}}{1+(\dfrac{a}{b}\cdot\dfrac{1}{X^{(0)}(1)}-1)e^{-a(t-1)}} + \hat{\varepsilon}^{(0)}(k+1), \varepsilon^{(0)}(k) \in \varepsilon^{(0)} \end{cases} \tag{8}$$

we call the Eq. (8) as the residual error revision model of grey verhulst.

If the forecasted precision has not been good once, we may also establish the multilevel residual error revision. The so-called multilevel residual error is the difference of the forecast value and the original accumulation value after many times revising. For instance, if the forecasted value revised k times is $\hat{X}^{(1)}(t,k)$, the kth times residual error is $\varepsilon^{(0)}(t,k)$, where $\varepsilon^{(0)}(t,k) = x^{(1)}(t) - \hat{x}^{(1)}(t,k)$ and $\hat{x}^{(1)}(k,0) = \hat{x}^{(1)}(k)$, we thus have $\hat{x}^{(1)}(t,k) = \hat{x}^{(1)}(t,0) + \sum_{i=0}^{k-1} \varepsilon^{(0)}(t,i)$.

A model can't be applied to predict, unless it is tested well. Generally, when we predict, whether the value of prediction and actual value is consistent or not is more important than the predicted value itself. Here, we uses the backward error-detection test method[7] to carry out the measure, furthermore the model's precision can be depicted together by backward error-detection ratio C and small error probability P (see Table 1).

Table 1. The test standard of model precision

Forecasting Precision	Good	Qualification	Reluctant Qualification	Disqualification
P	>0.95	0.95-0.80	0.80-0.70	<0.70
C	<0.35	0.35-0.50	0.50-0.65	>0.65

4 Simulations

By taking the attack data collected by network security organize - HoneyNet[8] in November as test data , we continued the tracing of security situation of network system in this month following the proposed approach. Using the method[9] to process the test data first, we can obtain the initial non-equal interval generating series shown in the following table 2, namely $X^{(0)}(t_i) = \{18.5, 5.0, 3.7, 8.2, 16.4, 12.0, 6.6, 12.1\}$, where $(i = 1,2,...,8)$, $T = \{0,2,5,10,14,17,19,22\}$. After being processed, having $M = \begin{pmatrix} m_0 \\ m_1 \end{pmatrix} = \begin{pmatrix} -3 \\ 4 \end{pmatrix}$, $t_i' = m_0 + m_1 \cdot i$, $(i = 1,2,...,8)$, and the equal interval time series are $T' = \{1,5,9,13,17,21,25,29\}$. Let T and $X^{(0)}(T)$ be the raw data, we use the interpolation method to get the equal interval data series, namely, $X^{(0)}(T') = \{17.9, 3.7, 7.5, 14.6, 12.0, 8.3, 4.4, 11.8\}$.

Table 2. The initialized non-equal interval generating series

Number	1	2	3	4	5	6	7	8
Date	11-08	11-10	11-13	11-18	11-22	11-25	11-27	11-30
Risk value	18.5	5.0	3.7	8.2	16.4	12.0	6.6	12.1

Accumulating $X^{(0)}(T')$ by AGO, we can get $X^{(1)}(T')$, whose value is $\{17.9, 21.6, 29.1, 43.7, 55.7, 64.0, 68.4, 80.2\}$ .Because the curve slope of AGO series rapidly increase in II section, so we adopted the Verhulst model to directly modeling. Due to Eq. (2)-Eq. (6),the forecast model can be list as table 3 shown.

Table 3. The non-equal interval Verhulst model

Number	1	2	3	4	5	6	7	8
Date	11-08	11-10	11-13	11-18	11-22	11-25	11-27	11-30
$X^{(0)}$	17.9	3.7	7.5	14.6	12.0	8.3	4.4	11.8
$X^{(1)}$	17.9	21.6	29.1	43.7	55.7	64.0	68.4	80.2
$\hat{X}^{(1)}$	17.9000	25.0104	33.7789	43.8182	54.3800	64.5471	73.5311	80.8884
ε	0.0000	3.4104	4.6789	0.1182	-1.3199	0.5471	5.1311	0.6884
Model	$X^{(1)}(k+1) = \dfrac{1}{(0.01003 + 0.045836 * \exp(-0.42542k))}$							

The above model's precision is good, where $C = \dfrac{se}{sx} = \dfrac{2.2478}{21.6376} = 0.1037 < 0.35$, $P = \{|\varepsilon(k) - \bar{\varepsilon}| < 0.6745 sx\} = 1 > 0.95$. However, the individual residual error is obviously bigger, we need carry out the revision of residual error. Let $\{\varepsilon^{(0)}(2), \varepsilon^{(0)}(3), \varepsilon^{(0)}(5), \varepsilon^{(0)}(7)\}$ be a raw residual error sequence, thus the time response expression of $\hat{\varepsilon}^{(1)}(k+1)$ can be obtained as $\hat{\varepsilon}^{(1)}(k+1) = 56.53987 \exp(-0.075903 * k) - 51.129497$ .After regressed to the former model, the final results shows in table 4.

Table 4. The non-equal interval Verhulst model with residue error revision

Number	1	2	3	4	5	6	7	8
$X^{(1)}$	17.9	21.6	29.1	43.7	55.7	64.0	68.4	80.2
$\hat{X}^{(1)}$	17.9000	22.3503	30.7515	43.8182	50.5276	64.5471	68.7178	80.8884
ε'	0.0000	0.7503	1.6515	0.1182	5.1724	0.5471	0.3178	0.6884
Model	$\dfrac{1}{(0.01003 + 0.045838 * \exp(-0.42542 * k))} + 4.321603 \exp[-0.075903 * k] - 2$							

After being checked by the backward error-detection test method, the above model's precision is good and the size of each residual error is less. For $\hat{X}^{(0)}(T')$, it can be obtained from Eq. [7], and then let $\hat{X}^{(0)}(T')$ and T' be the raw data, so we can

get $X^{(0)}(T)$ using the interpolation method. Thus, we obtained the new model with the residual error revision.

Now, we use the new model with the residual error revision and the model without the residual error revision to forecast the security situation of network system from December 1 to December 5 respectively, the sampled data is randomly choosed in different time span of every day. The curve fitting between the forecasted result and the actual value can be seen from figure 2.
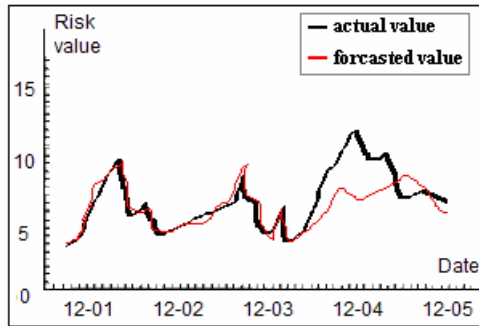
(a) The model without residual error revision
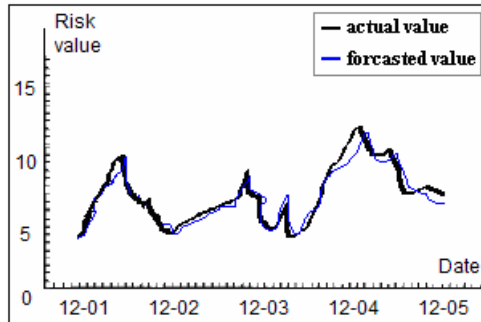
(b) The model with residual error revision

Fig. 2. The evolutive curve of network system's security situation

Seen from figure 2(a), the forecasted error is smaller during the initial three days, but along with days passing, the forecasted error has the tendency of increase and the forecasted precision gradually drop, which accords with the verhulst model itself shortcoming. Moreover, the situation curves in figure 2(b) was revised time and again, which may be obviously seen that the precision greatly enhances, the curve fitting between the forecasted result and the actual value are really satisfied. The above-mentioned results indicated that the non-equal interval grey verhulst model with residual error revision can effectively forecast the relative long-term security situation of network system.

5 Conclusions

This paper proposed a non-equal interval grey verhulst model with residual error revision to predict network system security's development situation for the first time. The experimental results show the model effectively overcome the discrete traits of original data, can obtain the reasonable network security development tendency even if in uncertain or lack information, and has certain practical value. Although the proposed method has done some work in the realization aspect of network security situation awareness, there are still many important problems not been considered, such as the suitable question of massive samples, the selection way of residual error sequence, as well as model's time and spatial complexity and so on, which waits for further research.

References

1. Mark, L. H., Olga, S., Karen, A. H.: On-line situation assessment for unmanned air vehicles. Proceedings Fourteenth International Florida Artificial Intelligence Research Society Conference. Florida: Key West, FL(2001)44-48
2. Tim, B.: Intrusion systems and multisensor data fusion: creating cyberspace situational awareness. Communications of the ACM.43(4) (2000)99-105
3. Adam, X. M., Greg, L. Z., Kao, S.P.: A Computational Situation Assessment Model for Nuclear Power Plant Operations. IEEE Transactions on Systems, Man and Cybernetics. 27(6)(1997)728-742
4. Sandeep, M., Rinkus, G., Illgen, C., et al.: OLIPSA: On-line intelligent situation awareness in the tactical air processor for situation assessment.Second Annual Symposium and Exhibition on Environment. Patuxent River, MD(1997)
5. Deng, J.L.: Grey system theory .Huhan: Huazhong University of Science and Technology Press(2002)
6. Zhu, H.J.,Ma, S.J. :Application of Non-equal Interval Gray Model to Forecast of Building Subsidence. Engineering of Surveying and Mapping.10(4) (2001)39~41
7. Deng, J.L., Properties of the grey forecasting model of GM (1,1),grey system, China Ocean Press, Beijing.(1988)79-90
8. Honeynet Project. Know your enemy: statistics. http://www.HoneyNet.org/papers/stats/, 2001-07-22
9. Chen, X.Z.,Zheng, Q.H.,Guan X.H.: Study on Evaluation for Security Situation of Networked Systems, Journal of Xi'an JiaoTong University.38(4)(2004)404-408

Parallel Preconditioning Methods with Selective Fill-Ins and Selective Overlapping for Ill-Conditioned Problems in Finite-Element Methods

Kengo Nakajima

Department of Earth and Planetary Science, The University of Tokyo
7-3-1 Hongo, Bunkyo-ku, Tokyo 112-0002, Japan
nakajima@eps.s.u-tokyo.ac.jp
http://www-solid.eps.s.u-tokyo.ac.jp/~nakajima

Abstract. In the present paper, parallel preconditioning methods with selective fill-ins and selective overlapping for contact problems have been developed and evaluated on PC clusters with 64 cores. The proposed methods provide robust convergence with efficiency. Finally, the proposed methods have been applied to ill-conditioned problems with heterogeneity and robustness, and their efficiency has been evaluated on TSUBAME super-cluster with up to 512 cores.

1 Introduction

Contact phenomenon is one of the most important and critical issues in various types of science and engineering applications. The author has been developing preconditioning methods for contact problems in geophysics, in which stress accumulation on plate boundaries (faults) is computed for estimating the earthquake generation cycle [1,2]. In [1,2], the augmented Lagrangian method (ALM) and the penalty method are implemented, and a large penalty number λ is introduced for constraint conditions around faults. The nonlinear process is solved iteratively by the Newton-Raphson (NR) method. A large λ ($\sim 10^4$) can provide an accurate solution and fast nonlinear convergence for NR processes, but the condition number of the coefficient matrices for linear equations is large, and several iterations are required for the convergence of iterative solvers. Therefore, a robust preconditioning method is essential for such ill-conditioned problems.
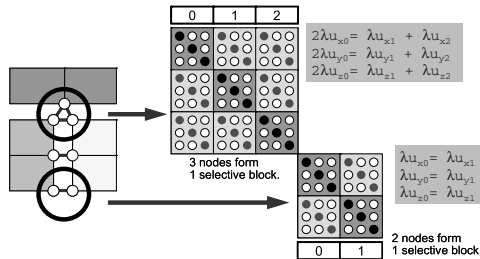
Fig. 1. Matrix operation of nodes in contact group for *selective blocking* preconditioning

Selective blocking is a special preconditioning method developed for this type of application by the author [1]. In this method, finite element nodes in the same contact group coupled through penalty constraints are placed into a large block (selective block or super node) (Fig. 1). For symmetric positive definite matrices, preconditioning with *block* incomplete Cholesky factorization *using selective blocking* (SB-BIC) shows excellent performance and robustness [1, 2]. In previous studies [1, 2], the number and location of nodes on both sides of the contact surface are identical. This is not flexible and cannot be applied to fault contact simulations with large slip/deformation, in which the number and location of nodes in contact groups might be inconsistent.

In the present study, new parallel preconditioning methods for this type of general contact problem have been developed. One remedy is a preconditioning method with *selective fill-ins*, in which *fill-ins* of higher order are introduced only for nodes connected to special elements for contact conditions [1, 2]. Another remedy is extension of overlapped elements between domains. In the present study, the *selective overlapping* method has been proposed, which extends the layers of overlapped elements according to the information of the special elements for contact conditions. Both methods are based on the idea of *selective blocking*, but are more general and flexible.

In the remainder of this paper, algorithms of parallel preconditioning methods with *selective fill-ins* and *selective overlapping* will be described, and the results of example problems with contact conditions are shown. Finally, the developed methods are applied to general ill-conditioned problems with the heterogeneous material property, and parallel performance up to 512 cores is evaluated.

2   Parallel Preconditioning Methods

2.1   Selective Fill-Ins

The *selective blocking* preconditioning method [1, 2] is a very robust and efficient preconditioning method for contact problems. However, it can be applied to a very limited number of situations. **ILU(p)** (Incomplete LU factorization with p-th-order fill-ins) preconditioning methods are widely used for various types of applications [3]. If the order of fill-ins (**p**) is higher, the preconditioner is more robust, but is usually more expensive. The required memory for coefficient matrices increases by a factor of from 2 to 5, if the order of fill-ins (**p**) increases from 0 to 1 or from 1 to 2 [1, 2].
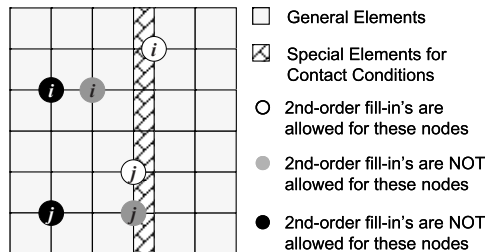
Fig. 2. Example of **ILU(1+)**

In the present study, new preconditioning methods for general contact problems have been developed. The first approach is a preconditioning method with *selective fill-ins*, called **ILU(p+)**. Figure 2 describes the idea of **ILU(p+)**. In **ILU(p+)**, (p+1)-th order fill-ins are allowed for m_{ij}, which represents the component of preconditioned matrices, if both the *i-th* and *j-th* nodes are connected to special elements for contact conditions, such as *master-slave* type elements [2]. In Fig. 2, second-order fill-ins can be allowed for all three *i-j* pairs, according to graphical connectivity information. However, only the white circles are allowed to generate second-order fill-ins.

This approach is very similar to that of *selective blocking*, in which full LU factorization is applied to nodes in contact groups, but is much more general and flexible. Since the constraint conditions through penalty terms are applied to the nodes that are connected to special elements, *selective* ILU factorization with higher order fill-ins for these nodes is expected to provide robust convergence with efficiency. In [4], a preconditioning method with block ILU factorization is proposed for coupled equations of incompressible fluid flow and solid structure. Different orders of fill-ins are applied to velocity and pressure components for generating block ILU factorization of coefficient matrices. **ILU(p+)** is very similar to this idea.

2.2 Selective Overlapping

Another approach is the extension of overlapped zones between domains for parallel computing. In previous studies [1, 2], the *GeoFEM* local data structure has been applied. This data structure is node-based with a single layer of overlapped elements(the depth of overlapping is 1) and is appropriate for parallel iterative solvers with block Jacobi-type localized preconditioning methods [1, 2]. Figure 3 shows an example of the local data for contact problems, in which the depth of overlapping is 1.
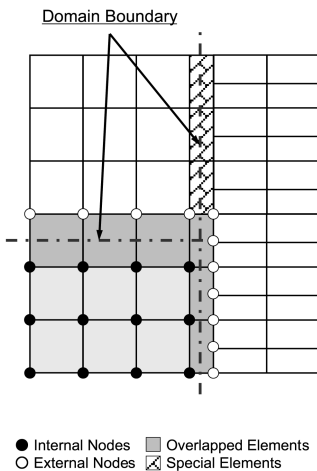
Fig. 3. Example of GeoFEM local data structure for contact problems
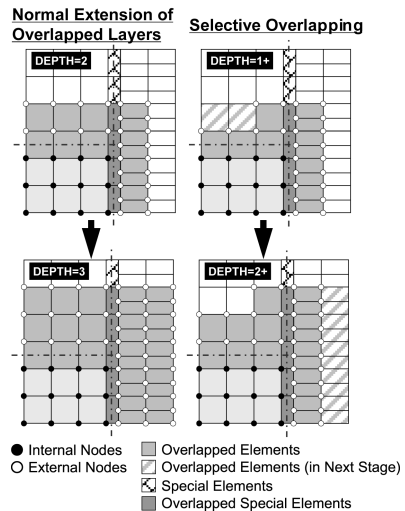
Fig. 4. Example of *selective overlapping*. Precedence for extensions of overlapped layers is taken over nodes connected to special elements for contact conditions

In the present study, a greater number of layers of overlapped elements are considered for the robustness of parallel preconditioners. Generally speaking, a larger depth of overlapped layers provides faster convergence in block Jacobi-type localized preconditioning methods, but the cost for computation and communications is more expensive [1,2,5].

In the present study, the *selective overlapping* method is proposed. This method provides priority over nodes connected to special elements for contact conditions, when extensions of overlapped layers are applied, as shown in Fig. 4. In *selective overlapping*, extension of overlapping for nodes that are *not* connected to special elements for contact conditions is *delayed*. *Hatched* elements in Fig. 4 are to be included as extended overlapped elements in normal extension cases. However, in selective overlapping, extension of overlapping for these elements is performed in the next stage of overlapping. Thus, the increase in cost for computation and communication by extension of overlapped elements is suppressed.

This idea is also an extension of the idea of *selective blocking*, and is also based on the idea of special partitioning strategy for contact problems, developed in [1, 2]. The convergence rate of parallel iterative solvers with block Jacobi-type localized preconditioning is generally bad, because the *edge-cut* may occur at inter-domain boundary edges that are included in contact groups [1, 2]. All nodes in the same contact group should be in the same domain in order to avoid such edge-cuts [1, 2]. Because the constraint conditions through penalty terms are applied to those nodes that are connected to special elements, *selective* extension of overlapping for these nodes is expected to provide robust convergence with efficiency.

3   Examples

3.1   Problem Description

Figure 5 describes the model for validation of the developed preconditioning methods. This problem simulates general contact conditions, in which the positions and number of nodes on contact surfaces are inconsistent. There are four blocks with elastic material that are discretized into cubic tri-linear type finite-elements. Each block is connected through elastic truss elements generated at each node on contact surfaces. Truss elements are in the form of a cross, as shown in Fig. 5. In this case, the elastic coefficient of the truss elements is set to 10^4 times that of the solid elements, which corresponds to the coefficient λ (=10^4) for constraint conditions of the augmented Lagrangian method (ALM). Poisson's ratio for cubic elements is set to 0.25.
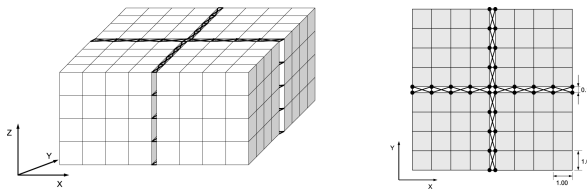
Fig. 5. Elastic blocks connected through truss elements

Symmetric boundary conditions are applied to x = 0 and y = 0 surfaces, and the Dirichlet fixed condition for deformation in the direction of the z-axis is applied to z = 0 surfaces. Finally, a uniform distributed load in the direction of the z-axis is applied to z = Z_{max} surfaces. This problem is linear-elastic, but the coefficient matrices are very ill-conditioned and simulate those for nonlinear contact problems very well [2].

3.2 Serial Cases with a Single CPU

Each chart in Fig. 6 shows the results of linear-elastic computation on the model in Fig. 5 using a single core of AMD Opteron 275 (2.2 GHz) with PGI compiler. Each block in Fig. 5 has 8,192 (=16×16×32) cubes, where the total problem size is 117,708 DOF (=degrees of freedom) (38,148 cubes, 39,236 nodes). GPBi-CG (Generalized Product-type methods based on Bi-CG) [6] for general coefficient matrices have been applied as an iterative method, although the coefficient matrices of this problems are positive indefinite. Each node has three DOF in each axis in 3D solid mechanics; therefore, **block ILU (BILU)** type preconditioning [1,2] has been applied.

BILU(1+), in which additional *selective fill-ins* have been applied for nodes connected to special elements (elastic truss elements in Fig. 5) to **BILU(1)**, provides the most robust and efficient convergence. **BILU(p)** provides faster convergence if p is larger, as shown in Fig. 6, but the cost for computation is more expensive. **BILU(1)** and **BILU(1+)** are competitive, but **BILU(1+)** provides a better convergence rate.

| (a) Computation time | (b) Iterations for convergence (320 for BILU(0)) | (c) Off-diagonal component # of preconditioned matrix |

Fig. 6. Results of linear-elastic problem in Fig.5 with a single core of AMD Opteron 275 (2.2 GHz) with PGI compiler. 117,708 DOF (38,148 cubes, 39,236 nodes)

3.3 Parallel Cases with Multiple CPU's

Each chart in Fig. 7 shows the results of linear-elastic computation on the model shown in Fig. 5 using 64 cores of AMD Opteron 275 cluster with PGI compiler and MPICH connected through Infiniband network. Each block in Fig. 5 has 250,000 (=50×50×100) cubes, where the total problem size is 3,152,412 DOF (1,000,000 cubes, 1,050,804 nodes). The effect of the extension of overlapping is evaluated for **BILU(1)**, **BILU(1+)**, and **BILU(2)**, respectively. **BILU(p)-(d)** means **BILU(p)** preconditioning, where the depth of overlapping is equal to **d**. Partitioning was applied in an RCB (recursive coordinate bisection) manner [2].

Generally speaking, the convergence rate is improved by the extension of overlapping (Fig. 7(a)). This is significant, when the depth of overlapping (**d**) is increased from (**d = 1**) to (**d = 1+**) because *edge-cuts* may occur at truss elements for contact

conditions, if the depth of overlapping is 1. However, the decrease in the number of iterations for convergence is very slight if the depth of overlapping is greater than 2.

The number of off-diagonal components of preconditioned matrices increases, as the depth of overlapping is larger (Fig. 7(c)). Finally, computation with a larger depth of overlapping is more expensive. Therefore, the computation time increases, because the depth of overlapping is greater than 2 (Fig. 7(a)). **BILU(1)-(1+)** and **BILU(1+)-(1+)** are the best cases and they are competitive.

(a) Computation time   (b) Iterations for convergence   (c) Off-diagonal component # of precond. mat. per core
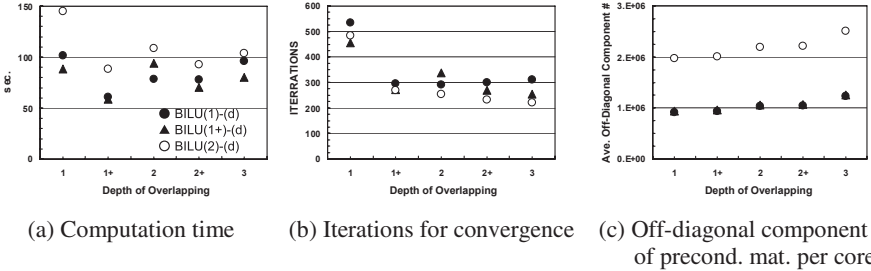
Fig. 7. Results of linear-elastic problem in Fig.5 with 64 cores of AMD Opteron 275 (2.2 GHz) cluster. 3,152,412 DOF (1,000,000 cubes, 1,050,804 nodes)

4   Applications to Problems with Heterogeneous Material Property

Parallel preconditioning methods with selective fill-ins and selective overlapping (**BILU(p)-(d)** approach), which are developed in the present study, provide robust and efficient convergence in ill-conditioned problems with contact conditions. In this section, this **BILU(p)-(d)** is extended to **BILU(p+,ω)-(d+,α)** for ill-conditioned problems with heterogeneous material property, where ω and α are threshold parameters for the extension of fill-ins and overlapping. In applications for a heterogeneous distribution of material property, coefficient matrices for linear solvers are generally ill-conditioned and the rate of convergence is poor.

In this section, linear-elastic problems for simple cube geometries with heterogeneity are solved. Poisson's ratio is set to 0.25 for all elements, and the heterogeneous distribution of Young's modulus in each tri-linear element is calculated by a sequential Gauss algorithm, which is widely used in the area of geo-statistics [7]. The minimum and maximum values of Young's modulus are 10^{-2} and 10^{2}, respectively, where the average value is 1.0. Boundary conditions in Section 3.1 have been applied. Each chart of Fig. 8 shows the results of linear-elastic computation on the model with heterogeneity using 64 cores of AMD Opteron 275 cluster. The total problem size is 3,090,903 DOF (1,000,000 cubes). In **BILU(p+,ω)-(d+,α)**, (p+1)-th-order fill-ins are allowed for pairs of nodes if both nodes are connected to elements for which the Young's modulus is greater than ω, and *selective overlapping* is applied to nodes if the nodes are connected to elements for which the Young's modulus is greater than α. In this case, **BILU(1)** generally requires more iterations for convergence than **BILU(1+,ω)** and **BILU(2)**. **BILU(1+,5)** and **BILU(1+,10)** are competitive, but **BILU(1+,5)-(1+,10)** ($\omega = 5$, $\alpha = 10$) provides the best performance. In **BILU(2)** and

BILU(1+,ω), the effect of the convergence rate by selective overlapping is similar to that in the previous cases for contact problems. Finally, the parallel performance of **BILU(1+,5)-(1+,10)** has been evaluated using between 32 and 512 cores of TSUBAME super-cluster [8] at the Tokyo Institute of Technology. In this evaluation, a *strong scaling test* has been applied, where the entire problem size is fixed as 3,090,903 DOF (1,000,000 cubes). Figure 9 shows parallel performance. Usually, the convergence rate for block Jacobi-type localized parallel preconditioning in strong scaling cases becomes worse as the number of domains increases [1,2]. However, selective overlapping provides an almost constant number of iterations up to 512 cores, as shown in Fig. 9(a), and excellent parallel performance, as shown in Fig. 9(b).

(a) Computation time   (b) Iterations for convergence
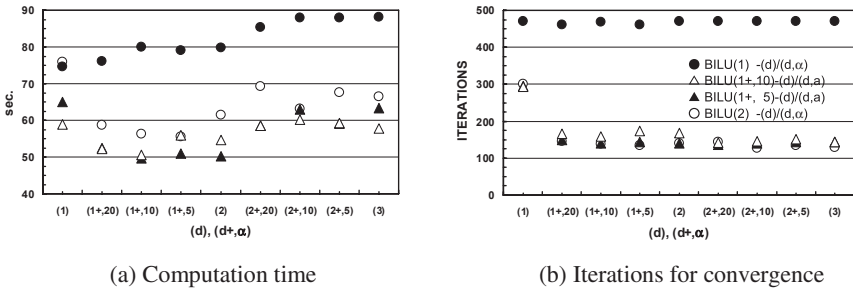
Fig. 8. Results of linear-elastic problem with heterogeneity using 64 cores of AMD Opteron 275 (2.2 GHz) cluster. 3,090,903 DOF (1,000,000 cubes, 1,030,301 nodes)

(a) Iterations for convergence   (b) Parallel Speed-Up
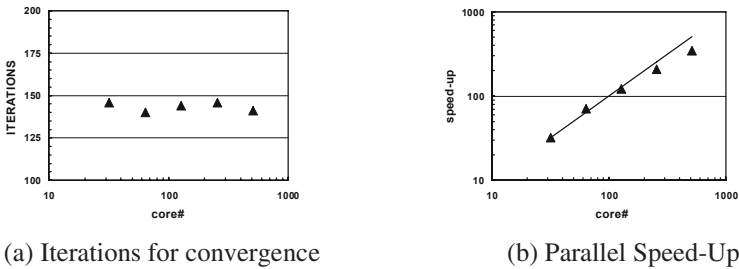
Fig. 9. Parallel performance of BILU(1+,5)-(1+,10) for linear-elastic problem with heterogeneity using TSUBAME super-cluster using up to 512 cores (3,152,412 DOF)
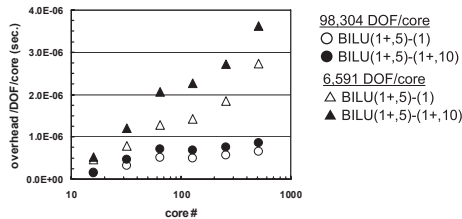
Fig. 10. Overhead for weak scaling test on TSBUME cluster using **BILU(1,+5)**

Figure 10 shows the results of the *weak scaling test*, in which the problem size per core is fixed. The obtained results correspond to the overhead by communications and additional computations per iteration divided by the problem size per core. If the problem size per each core is sufficiently large, the additional overhead by *selective overlapping* (**(d=1)** and **(d+,α)= (1+,10)**) is negligible.

5   Concluding Remarks

In the present paper, parallel preconditioning methods with *selective fill-ins* and s*elective overlapping* for contact problems have been developed and evaluated on PC clusters. The proposed methods are based on the concept of *selective blocking* in previous studies, but are much more flexible and provide robust convergence with efficiency. The proposed methods have also been applied to ill-conditioned problems with heterogeneity and were found to be robust and efficient on TSUBAME super-cluster with up to 512 cores. Generally speaking, **BILU(1+)-(1+)** or **BILU(1+,ω)-(1+,α)**, with selective fill-in **(p = 1+)** and selective overlapping **(d = 1+)**, provides the best performance with robustness. The effect of *selective overlapping* is very significant, if the depth of overlapping increases from **(d = 1)** to **(d = 1+)**. In future studies, the proposed methods will be evaluated in various types of real applications with different parameters on massively parallel computers.

Acknowledgements

References

1. Nakajima, K. (2003), Parallel Iterative Solvers of GeoFEM with Selective Blocking Preconditioning for Nonlinear Contact Problems on the Earth Simulator, ACM/IEEE Proceedings of SC2003.
2. http://geofem.tokyo.rist.or.jp/
3. Saad, Y. (2003), Iterative Methods for Sparse Linear Systems (2nd Edition), SIAM.
4. Washio, T., Hisada, T., Watanabe, H., and Tezduyar, T.E. (2005), A Robust and Efficient Iterative Linear Solver for Strongly Coupled Fluid-Structure Interaction Problems, Computer Methods in Applied Mechanics and Engineering, 194, 4027-4047.
5. Smith, B., Bjϕrstad, P. and Gropp, W. (1996), Domain Decomposition: Parallel Multilevel Methods for Elliptic Partial Differential Equations, Cambridge University Press.
6. Zhang, S.L. (1997), GPBi-CG: Generalized Product-type methods based on Bi-CG for solving nonsymmetric linear systems, SIAM Journal of Scientific Computing, 18, 537-551.
7. Deutsch, C.V. and Journel, A.G. (1998), GSLIB Geostatistical Software Library and User's Guide, Second Edition, Oxford University Press.
8. http://www.gsic.titech.ac.jp/

An R-Minimum Strategy for Finite Element Modeling of Non-linear Deformation Behaviours of Rate-Dependent Materials

H. L. Xing and J. Zhang

Earth Systems Science Computational Centre (ESSCC), The University of Queensland,
St. Lucia, Brisbane, QLD 4072, Australia
`xing@esscc.uq.edu.au`

Abstract. An R-minimum strategy, which was proposed and successfully applied to analyse the non-linear finite deformation behaviours of elasto-plastic materials (e.g. [1] [2]), is extended and applied here to simulate the deformation behaviours of the rate-dependent materials. It involves no iterations, thus belongs to the static-explicit algorithm and avoids the convergence problem resulting from nonlinearities. The R-minimum strategy based adaptive control scheme of the time step size is proposed and applied to the analysis of both time-dependent and -independent viscous materials and verified through the comparison with the others to demonstrate the stability, efficiency and usefulness of this algorithm.

Keywords: R-minimum Strategy, Finite Element, Rate-Dependent Materials, Non-linear Deformation, Static-Explicit Algorithm.

1 Introduction

In the current finite element analysis of non-linear deformation behaviours of a several of materials (including the rate-dependent/-independent materials), the static-implicit algorithm is widely applied. Usually, it employs the iterative scheme, such as the Newton-Raphson and the modified Newton-Raphson, to treat the governing equations as a system of non-linear equations and attempt to solve them by applying the unbalanced forces, computing the corresponding displacement increments, and iterating until the drift from the equilibrium state is under the prescribed small value. One major disadvantage of the Newton-Raphson family of algorithms is that the iterations may not converge, particularly when the behaviour is strongly non-linear. Although many efforts have been made, there still exist problems to be overcome.

A so-called R-minimum strategy was proposed and extended to analyze the non-linear deformation behaviours (including the thermal-mechanical coupling and frictional contact) of elasto-plastic materials (e.g. [1-2]). The R-minimum strategy belongs to the static-explicit algorithm involving no iterations and could avoid the related convergence problems as mentioned above. One common problem for the explicit algorithm is that it trends to drift from the equilibrium state as the solution proceeds. This effect can be minimized by using the R-minimum to limit the size of

this increment step. The R-minimum strategy has been successfully applied for elasto-plastic materials in the industry-strength finite element code and validated through simulating sheet metal forming processes etc.(e.g. [3] and references thereafter), and the in-house finite element code for frictional contact between deformation bodies and successfully applied to simulate the structure assembling, stick-slip frictional instability and earthquakes etc. (e.g. [4] and references thereafter). This paper will focus on extending and applying the so-called R-minimum strategy to simulate the non-linear deformation behaviours of rate-dependent materials,..

2   Constitutive Equations of Rate-Dependent Materials

Rate-dependent phenomena have been observed and described in certain science and practical application fields, such as the Earth sciences and deformation/creep behaviours of the metals/polymers at the high temperature. For simplicity and focusing on the key point of this paper, i.e. to study the non-linear deformation behaviours of rate-dependent materials using R-minimum strategy, a simple Voigt typed visco-elastic material model is taken as an example to be studied here. It includes two basic elements, the elastic and the viscous, being parallel connected. The total stress σ_{ij} is [e.g. 5]

$$\sigma_{ij} = \sigma_{ij}^{e} + \sigma_{ij}^{\eta} \tag{1}$$

where σ_{ij}^{e} and σ_{ij}^{η}, the elastic and creep/viscous stress components of the Voigt model, are given respectively by

$$\sigma_{ij}^{e} = C_{ijkl}^{e}\varepsilon_{kl}, \ \ \sigma_{ij}^{\eta} = \eta_{ijkl}\dot{\varepsilon}_{kl} \tag{2}$$

Summing up the contributions from equations (2) to equation (1), we have

$$\sigma_{ij} = C_{ijkl}^{e}\varepsilon_{kl} + \eta_{ijkl}\dot{\varepsilon}_{kl} \tag{3}$$

where C_{ijkl}^{e} and η_{ijkl} are the Hooke's elasticity and the viscosity matrix, respectively.

The linearilized form of equation (4) can be described as

$$\dot{\sigma}_{ij} = C_{ijkl}^{e}\dot{\varepsilon}_{kl} + \eta_{ijkl}\ddot{\varepsilon}_{kl} \tag{4}$$

Assuming $\ddot{\varepsilon}$ of equation (4) remains constant in a sufficient short time increment Δt, we have

$$\dot{\sigma}_{ij} = C_{ijkl}^{e\eta}D_{kl} + \dot{\sigma}_{ij}^{*} \tag{5}$$

Where

$$C_{ijkl}^{e\eta} = C_{ijkl}^{e} + \eta_{ijkl}\big/\Delta t, \ \ \dot{\sigma}_{ij}^{*} = -\eta_{ijkl}D_{tkl}\big/\Delta t \tag{6}$$

D_{kl} and D_{rkl} are the deformation rates at the current and the previous time step, respectively. Thus $\overset{*}{\dot{\sigma}}_{ij}$ is known at the current configuration once the current time step size Δt is defined.

3 Governing Equations

3.1 Finite Element Discretization

The updated Lagrangian rate formulation is employed to describe the nonlinear deformation problem. The rate type equilibrium equation and the boundary at the current configuration are equivalently expressed by a principle of virtual velocity of the form

$$\int_V (\overset{\circ}{\tau}_{ij} - D_{ik}\sigma_{kj} + \sigma_{ik}D_{jk} - \sigma_{ik}D_{kj})\delta L_{ij}dV = \int_S \dot{F}_i\delta v_i dS \tag{7}$$

where V and S denote respectively the reference domains occupied by the body B and its boundary at time t; S_F is a part of the boundary of S on which the rate of nominal traction $\dot{F}_i$ is prescribed; δv is the virtual velocity field which satisfies the condition $\delta v = 0$ on the velocity boundary; $\overset{\circ}{\tau}_{ij}$ is the Jaumann rate of Kirchhoff stress; L is the velocity gradient tensor, $L = \partial v / \partial x$.

Substituting equation (5) into equation (7) leads to the final form of the virtual velocity principle as

$$\int_V (C^*_{ijkl}L_{kl} + \overset{*}{\dot{\sigma}}_{ij})\delta L_{ij}dV = \int_{S_F} \dot{F}_i\delta v_i dS \tag{8}$$

where $C^*_{ijkl} = C^{e\eta}_{ijkl} + S_{ijkl}$, $S_{ijkl} = \frac{1}{2}(\sigma_{jl}\delta_{ik} - \sigma_{ik}\delta_{jl} - \sigma_{il}\delta_{jk} - \sigma_{jk}\delta_{il})$.

The eight-node hexahedron element is adopted here. The selective reduced integration (SRI) algorithm, i.e. the $\overline{B}$-method proposed by Hughes [6], is employed to calculate equation (8). For an element E, the left side of equation (8) can be rewritten as

$$Q^E = \sum_\alpha \delta v_{\alpha i}\sum_\beta [\overline{K}_{\alpha\beta}]_{ik}v_{\beta k} + \sum_\alpha \delta v_{\alpha i}[\overline{F}^t_\alpha]_i \tag{9}$$

where the elemental stiffness matrices for the selective reduced integration

$$[\overline{K}_{\alpha\beta}]_{ik} = (\int_{V^E} N_{\alpha,j}C^*_{ijkl}N_{\beta,l} + N_{\alpha,j}(3k\delta_{ij} - \sigma_{ij})a_{\beta k} + a_{\alpha i}(3k\delta_{kl} - \sigma_{kl})N_{\beta,l} \\ + a_{\alpha i}(3k\delta_{kl} - \sigma_{kl})N_{\beta,l} \tag{10}$$

and the loading matrices from the viscous term for the selective reduced integration

$$[\overline{F}^t_\alpha]_i = \int_{V^E} (N_{\alpha,j}\overset{*}{\dot{\sigma}}_{ij} + a_{\alpha i}\overset{*}{\dot{\sigma}}_{mm})dV \tag{11}$$

are evaluated at all the Gauss interpolation points. In equation (10) and (11), N is the shape function and α, β are nodal numbers; and $N_{\alpha,j}$ is the differentiation of N_{α} with respect to the natural coordinate.

3.2 Time Integration Algorithm

The time integration method is one of key issues to formulate a nonlinear finite element method. It is well known that the fully implicit method is often subjected to bad convergence problems for a non-linear deformation. In order to avoid this, we employ an explicit time integration procedure as follows. It is assumed that under a sufficiently small time increment all rates in equation (7) can be considered constant within the increment from t to $t + \Delta t$ as long as there are no drastic changes of states and deformation takes place. The R-minimum strategy is extended and used here to choose the step size to avoid such a drastic change within an incremental step. Thus all the rate quantities used to derive equation (7) are simply replaced as

$$\Delta \boldsymbol{u} = \boldsymbol{v} \Delta t \;\; \text{and} \;\; \Delta \boldsymbol{\tau} = \overset{\circ}{\boldsymbol{\tau}} \Delta t \tag{12}$$

Finally equation (8) can be rewritten as

$$(\boldsymbol{K} + \boldsymbol{K}_{\eta}) \Delta \boldsymbol{u} = \Delta \boldsymbol{F} + \Delta \boldsymbol{F}_{\eta} \tag{13}$$

Here $\boldsymbol{K}$ is the standard stiffness matrix; $\Delta \boldsymbol{F}$ is the external force increment; $\Delta \boldsymbol{u}$ is the nodal displacement increment; $\boldsymbol{K}_{\eta}$ and $\Delta \boldsymbol{F}_{\eta}$ are the contributions to the stiffness matrix and force increment from the influence of the viscous terms.

4 Time Step Size Control

As described above, the R-minimum strategy was originally proposed and successfully applied to analyze the non-linear deformation behaviours (including the thermal coupling and frictional contact) of elastic/elasto-plastic materials [1-4], i.e. the rate-independent materials. To ensure the stability and accuracy of the solution due to the nonlinearity resulted from the rate-dependent effects in the model, the R-minimum strategy is extended here to control the time step size. Here we take

$$\text{R-minimum} = \Delta t / T_{total} \tag{14}$$

where T_{total} is the total deformation time prescribed. Thus, the key problem in the following is how to define the R-minimum to control the step size to minimize the drift from the real solution. Considering a given non-linear deformation time T_{total}, one simple choice for the solution is to divide the total deformation process into the smaller enough time steps with the same size. The smaller time step size is, the more accurate result is. The sufficiently accurate result can be achieved with a small enough time step size, but it requires more calculation steps and thus more computing time cost. To improve the efficiency, i.e. to get the more accurate results with less

computation steps, an R-minimum strategy based adaptive algorithm for controlling the variable time step size automatically is proposed and applied as following steps for the visco-elastic materials. It keeps the similar idea as what we proposed for solving the nonlinear problems of the elasto-plastic (i.e. rate-independent material) materials [2-4]. (1). Let the prescribed total deformation time be T_{total}. For the first calculation step, it can have the following two choices in the code: one is the pure elastic deformation Δu is firstly calculated subject to the boundary conditions, i.e. $K_\eta = 0$ and $\Delta F_\eta = 0$ in the stiffness equation (13); the other is that visco-elastic deformation Δu is calculated with a given small enough time step size Δt_1, here $\Delta F_\eta = 0$, but $K_\eta \neq 0$ in equation (13). Afterwards, the maximum deformation rate D_{max} at the integration points can be obtained to calculate the R-minimum value as

$$\text{R-minimum} = \frac{ES}{D_{max} T_{total}},$$ and then the time step size Δt_2 for the second step can be

decided from equation (14) as $\Delta t_2 = \text{R-minimum} \times T_{total}$, here ES is the maximum allowable deformation increment per time step. Then the visco-elastic or viscous only deformation in the further time steps can be defined as follows; (2). If the sum of the deformation time $\sum \Delta t_j \geq T_{total}$, go to step 4; otherwise the time step size for the $i+1$

step can be calculated as $\Delta t_{i+1} = \text{R-minimum}^{(i)} \times T_{total}$, here $\text{R-minimum}^{(i)} = ES/D_{max}^{(i)} T_{total}$, $D_{max}^{(i)}$ is the maximum deformation rate at the integration points calculated with the known solution Δu_i at the time step i; If

$\sum_{j=1}^{i+1} \Delta t_j > T_{total}$, the R-minimum value is reduced to $\text{R-minimum} = 1 - \sum_{j=1}^{i} \Delta t_j \Big/ T_{total}$.

Thus, the time size Δt_{i+1} is finally defined by $\Delta t_{i+1} = \text{R-minimum}^{(i)} \times T_{total}$ and then applied to the stiffness equation (13) for the solution Δu_{i+1} at the time step of $i+1$; (3). Repeat the step 2; (4). The total deformation process is over, and the total displacement $u_{total} = \sum \Delta u_j$.

5 Application Examples

A beam with the quadrate cross-section of $2mm \times 2mm$ and the length of $20mm$ is taken as an example to be analyzed here. It is fixed along all the directions at the left end and loaded by the axial tensile nodal force of 800N to the elastic beam at the other end firstly, and then keeps the above loading condition for the further creep deformation for 1000 seconds. Two cases for the visco-elastic materials with the time-independent and -dependent viscosity are investigated as follows.

5.1   Time Independent Viscosity Case

The following material parameters are used in this paper if not otherwise specified: Young's modulus $E = 10000 MPa$, Poisson's ratio $v = 0.25$, the viscosity $\eta_K = 10000 MPa$ and $\eta_G = 2000 MPa$. Different results of deformation processes are obtained corresponding to the different prescribed *ES* values and compared with each other. Fig. 1 shows the displacement at the end of the beam. The smaller prescribed *ES* value is, the closer to accurate result is, but the more time steps are required; and when the *ES* value decreases to a certain value, its further decrease has almost no effects on improving the accuracy of the results, although it takes more time steps to complete. Take both the computing time cost and the accuracy issues together into account, let $ES = 2 \times 10^{-5}$ as the safe strain increment value here.
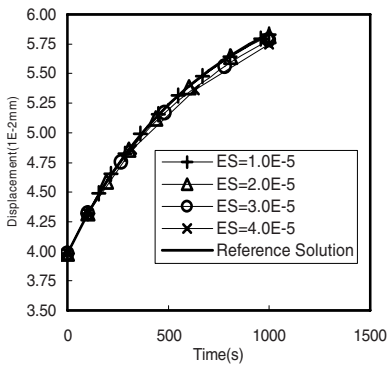
Fig. 1. The calculated results of displacement for the visco-elastic materials with the time-independent constant viscosity using the R-minimum strategy based time step size control scheme with the different *ES* values
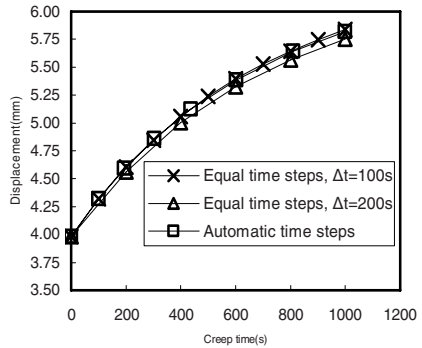
Fig. 2. Comparison of displacement res ults and time steps for the visco-elastic materials with the time-independent viscosity using the R-minimum strategy based time step size control scheme with those using the equal time increment step scheme

The R-minimum strategy has also been compared with the equal time steps scheme as shown in Fig. 2. For $ES = 2 \times 10^{-5}$, it automatically takes the smaller step size (similar as $\Delta t = 100s$) due to the higher nonlinearity at the beginning deformation stage, but gradually gets to the larger step size (similar as $\Delta t = 200s$) in the later deformation stage. This makes it get the similar accuracy as that with the equal time step $\Delta t = 100s$, but use 3 time steps less in total (The R-minimum strategy based case takes 7 steps, while that with the equal time step size of $\Delta t = 100s$ takes 10 steps as shown in Fig. 2). Although the case of equal time step size $\Delta t = 200s$ takes 2 steps less than the R-minimum strategy based case, it drifts more and more from the real solution as the deformation proceeds. This demonstrates that the R-minimum strategy based automatic control scheme of the time step size can keep sufficient accuracy of the solution for the rate-dependent materials with the constant viscosity during the whole deformation process with the less computational time cost.

5.2 Time Dependent Viscosity Case

Refer to the Backofen equation ($\bar{\sigma} = K\dot{\bar{\varepsilon}}^{m}$), which are widely applied to describe the rate-dependent superplastic deformation (e.g. [7]), and keep the same structure of the constitutive equation as above, here let both the time-dependent bulk and shear modulus of viscosity be as follows,

$$\eta_K = \frac{K_K}{3}\dot{\bar{\varepsilon}}^{m-1}, \quad \eta_G = \frac{K_G}{3}\dot{\bar{\varepsilon}}^{m-1} \tag{15}$$

where m is the strain rate sensitivity index; K_K and K_G are the material constants; $\dot{\bar{\varepsilon}}$, the equivalent strain rate, is calculated using the known values of the last time step.

The same model as that in section 5.1 is calculated here but with the time-dependent viscosity defined as above. Here, let $m=0.5$, $K_K =5000MPa$, $K_G =1000MPa$. The calculation results (as shown in Fig. 3) indicate that the smaller prescribed ES value is, the closer to accurate result is, but the more time steps are required; and when the ES value decreases to a certain value, its further decrease has almost no influence on improving the accuracy of the results, although it takes more time steps to complete.
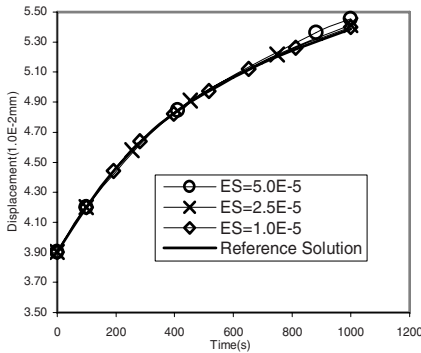
Fig. 3. The calculated results of displacement for the visco-elastic materials with the time-dependent viscosity using the R-minimum strategy based time step size control scheme with the different ES values
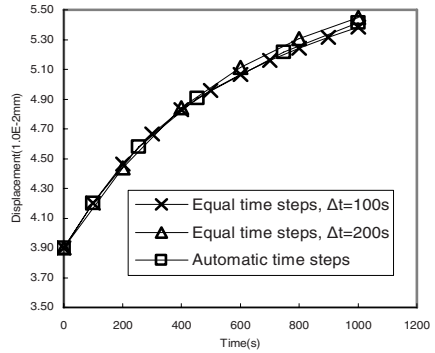
Fig. 4. Comparison of the calculated results of the displacement and time steps for the visco-elastic materials with the time-dependent viscosity using the R-minimum strategy based time step size control scheme with those using the equal time increment step scheme

The R-minimum strategy for $ES = 2.5\times10^{-5}$ has also been compared with the equal time step scheme as shown in Fig. 4. It demonstrates that the R-minimum strategy based automatic control scheme of the time step size can keep sufficient accuracy of the solution for the rate-dependent materials with the time-dependent viscosity during the whole deformation process with the less computational time cost. The same conclusion was drawn from the above time-independent viscosity case.

6 Conclusions

A three-dimensional finite element computational model and code have been developed to simulate the non-linear deformation behaviours of the rate-dependent materials using the so-called R-minimum strategy. The R-minimum strategy, which was proposed and successfully applied to analyse the non-linear deformation behaviours of rate-independent elasto-plastic materials, is extended and applied here to limit the size of increment time step in the finite element analysis of the non-linear deformation behaviours of rate-dependent materials. The procedures to determine the R-minimum (i.e. the time step size) for the rate-independent and the rate-dependent materials are different, but it all involves no iterations, thus belongs to the static-explicit algorithm and avoids the convergence problem resulting from nonlinearities. A beam of visco-elastic materials is calculated with both the time-independent and the time-dependent viscosity using the R-minimum strategy (i.e. an adaptive control scheme of the time step size) and compared with the those using the equal time step size scheme. The analysis results show that the R-minimum strategy based automatic control scheme of the time step size can keep sufficient accuracy of the solution for the visco-elastic materials with the time-independent and -dependent viscosity during the whole deformation process with the reasonable computational time cost.

References

1. Yamada, Y, N. Yoshimura and T. Sakurai: Plastic stress-strain matrix and its application for the solution of elastic-plastic problems by finite element method, Int. J. Mech. Sci., 10 (1991) 343–354
2. Xing, H.L., Makinouchi, A.: Three dimensional finite element modelling of thermomechanical frictional contact between finite deformation bodies using R-minimum strategy, Computer Methods in Applied Mechanics and Engineering, 191 (2002) 4193–4214
3. Xing, H.L., Makinouchi, A.: Numerical analysis and design for tubular hydroforming, Int. J. Mech. Sci., 43 (2001) 1009–1026
4. Xing, H. L., Mora, P., Makinouchi, A.: An unified friction description and its application to simulation of frictional instability using finite element method. Philosophy Magazine (2005; in press)
5. Gong, X. N: Constitutive Equations of Engineering Materials, Architecture and Building Press, Beijing, (1995)
6. Hughes, T. J. R.: Generalization of selective integration procedures to anisotropic and nonlinear materials, Int. J. Num. Methods Eng., 15 (1980) 1413–1418
7. Xing, H. L., K. F. Zhang and Wang, Z. R.: Recent development of mechanics of superplasticity and its applications, J. Mater. Proc. Tech., 151 (2004) 196–202

Nonlinear Analysis on Single Pile by Meshfree Local Petrov-Garlerkin Method (MLPG)

Ming-hua Zhao, Wei He, and You Wang

Geotechnial Institute, Civil engineering department, Hunan university, ChangSha,
410082, China
`Mhzhaohd@21cn.com`

Abstract. The Meshfree Local Petrov-Garlerkin Method (MLPG) was introduced to study the behavior of extra-long and large-diameter piles. The nonlinear behavior of the soil and pile shaft materials was firstly analyzed, based on these, the solving steps of MLPG was put forward involving the elastic-plastic model of soil and pile shaft reinforcement. Then a testing example was analyzed in contrast to the Finite Element Method (FEM), and the results indicated that the MLPG was of higher accuracy. Lastly, the MLPG was applied to analyze the data of static test on a full scale extra-long pile to study the behavior of pile.

Keywords: Pile foundation; Nonlinear; extra-long; MLPG method.

1 Introduction

For the past few years, the extra-long pile with large-diameter was more and more applied in the engineering practice. Although it takes higher bearing capacity, the fully exertion of it involved larger displacement. So it is important to study on the calculating method of settlement [1]. The finite element method (FEM) is the most highly developed tools to analyze mechanical problems, but its shape function is constructed based on the element, when analyzing the problems such as the large deflection and the contact, the serious distortion of element in FEM will cause the method unworkable. Recent years, a new numerical method termed "Meshfree Method" was put forward, in which the shape function is based on the nodes, can conquer some of the shortcomings in FEM. There are a number of meshfree methods, such as the element free Galerkin (EFG) method, the meshless local Petrov-Galerkin (MLPG) method [2], meshless point collocation method, PCM and so on. Herein, the MLPG is studied with the method considering elastic-plastic property of the material.

2 Basic Equation of MLPG

In MLPG, MLS approximation is employed to create shape functions for field variable approximation, and penalty method is introduced herein to enforce the essential boundary condition. The weak form for a node, say, node I, based on the local weighted residual method can be stated as [2]:

$$\int_{\Omega} (\boldsymbol{\sigma}_{ij,j} + \mathbf{b}_i) \mathbf{W}_I d\Omega - \alpha \int_{\Gamma_u} (\mathbf{u}_i - \bar{\mathbf{u}}_i) \mathbf{W}_I d\Gamma = 0 \cdot \tag{1}$$

Where $\mathbf{W}_I$ is the weight or test function, and we use the same weight function for all equations involved. The $\boldsymbol{\sigma}_{ij,j}$ is the tensor of stress, $\mathbf{b}_i$ is the tensor of external body force, $\mathbf{u}_i$ is the test displacement on the boundary, $\bar{\mathbf{u}}_i$ is the real displacement of the node i on the boundary. α is the penalty factor.

Using the divergence theorem, we obtain:

$$\int_{\Gamma_s} \sigma_{ij} n_j \mathbf{W}_I d\Gamma_s - \int_{\Omega_s} \sigma_{ij} \mathbf{W}_{I,j} d\Omega_s + \int_{\Omega_s} \mathbf{b}_i \mathbf{W}_I d\Omega_s - \alpha \int_{\Gamma_{us}} (\mathbf{u}_i - \bar{\mathbf{u}}_i) \mathbf{W}_I d\Gamma_{us} = 0 \tag{2}$$

Where $\Gamma_s = L_s \bigcup \Gamma_{us} \bigcup \Gamma_{ut}$.

Then the formula (2) can be transformed to:

$$\int_{\Omega_s} \boldsymbol{\sigma}_{ij} \mathbf{W}_{I,j} d\Omega_s + \alpha \int_{\Gamma_{us}} \mathbf{u}_i \mathbf{W}_I d\Gamma_{us} - \int_{\Gamma_{su}} \sigma_{ij} \mathbf{n}_j \mathbf{W}_I d\Gamma_{su} - \int_{L_s} \sigma_{ij} \mathbf{n}_j \mathbf{W}_I dL_s$$
$$= \int_{\Gamma_{st}} \boldsymbol{\sigma}_{ij} \mathbf{n}_j \mathbf{W}_I d\Gamma_{st} + \int_{\Omega_s} \mathbf{b}_i \mathbf{W}_I d\Omega_s + \alpha \int_{\Gamma_{us}} \bar{\mathbf{u}}_i \mathbf{W}_I d\Gamma_{us} \tag{3}$$

When the calculating domain is located entirely in the problem domain, integrals related to Γ_{us} and Γ_{ut} vanish, and the formula (3) can be simplified as:

$$\int_{\Omega_s} \boldsymbol{\sigma}_{ij} \mathbf{W}_{I,j} d\Omega_s = \int_{\Omega_s} \mathbf{b}_i \mathbf{W}_I d\Omega_s \tag{4}$$

3   Elastic-Plastic Models of Soil and Reinforcement Concrete

3.1   Elastic-Plastic Model for Soil

The yield rule can be described as the function of stress in the soil. That is:

$$f^*(\sigma_{ij}) = k_f \tag{5}$$

Where $f^*(\sigma_{ij})$ is the function of stress, can use a certain form of stress invariant as independent variable.

The rule put forward by Drucker and Prager is a form of the general Mises rule [3]:

$$\alpha I_1 + \sqrt{J_2} = k \tag{6}$$

Where J_2 is the second stress invariant, it is

$$J_2 = \frac{1}{6}\left[(\sigma_1 - \sigma_2)^2 + (\sigma_2 - \sigma_3)^2 + (\sigma_3 - \sigma_1)^2\right] \tag{7}$$

Drucker and Prager also got the parameter in planar stress conditions:

$$\alpha = \frac{\sin\varphi}{\sqrt{3}\sqrt{3 + \sin^2\varphi}} \qquad k = \frac{\sqrt{3}c\cos\varphi}{\sqrt{3 + \sin^2\varphi}} \tag{8}$$

Where the c and φ is the cohesion and inner friction angle. When $\varphi = 0$, the formula (6) turns to be Mises rule.

3.2 Elastic-Plastic Model for Pile Shaft Reinforcement Concrete

The behavior of reinforcement concrete is quite different from the soil, and the Japanese scholar Noguchi [4] advised that the α and k can be got as:

$$\alpha = 0.07 \ , k = -\frac{0.88}{\sqrt{3}}\left|f_c'\right| \tag{9}$$

Where the f_c' is the compression strength of prism shape concrete.

4 Testing Example

The cantilever beam acted by a vertical fixate was analyzed by MLPG, FEM and elastic solution[5]. The beam is pictured in Fig. 1, and the result is shown in Table 1.
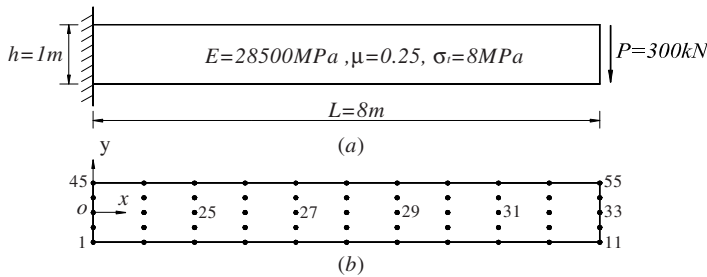
Fig. 1. Calculating model of vertical loaded beam

Table 1. The displacement of y direction at each node by three method

No.	Elastic Solution	Marc	Difference	Precise	MLPG	Difference	Precise
23	0.000	0.000	—	—	0	—	—
24	0.296	0.251	-0.044	-0.15	0.321	0.026	0.09
25	1.205	0.975	-0.230	-0.19	1.257	0.052	0.04
26	2.632	2.107	-0.525	-0.20	2.727	0.095	0.04
27	4.511	3.599	-0.913	-0.20	4.673	0.161	0.04
28	6.779	5.398	-1.381	-0.20	7.003	0.224	0.03
29	9.370	7.454	-1.915	-0.20	9.697	0.327	0.03
30	12.219	9.716	-2.504	-0.20	12.658	0.439	0.04
31	15.263	12.131	-3.132	-0.21	15.816	0.553	0.04
32	18.436	14.649	-3.787	-0.21	19.108	0.672	0.04
33	21.674	17.221	-4.453	-0.21	22.469	0.795	0.04

5 Analysis on a Test Pile by MLPG Method

A test pile[6], which was 60 meters long, and the calculating domain could be determined as a rectangle domain which was 120 meters high and 120 meters long.

Because of the large slenderness ratio, the domain had to be represented by huge number of scattered nodes, 26225 nodes were used here. The contour map of the calculating domain can be got by MLPG, and due to the limit of the space, only principal strain ε_1 is shown in Fig.2
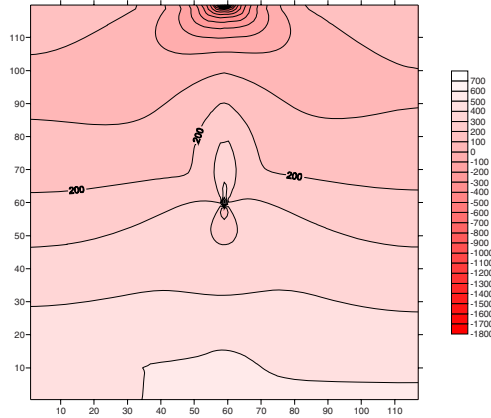
Fig. 2. Contour map of principal strain ε_1

6   Conclusions

The conclusion can be drawn as follows:

1. The basic equation of MLPG was deduced by weighted residual method, and the nonlinear behavior of the soil and pile were studied.

2. The cantilever beam, was analyzed by MLPG, FEM and elastic solution. The results of these three methods showed that the MLPG had better accuracy than FEM.

3. A test pile was analyzed by MLPG, and contour maps of strain in the problem domain could be got.

References

1. Zhao Minghua. Calculating and Detecting for Pile Foundations of Bridges [M]. Beijing: China Communications Press, 2000. (in Chinese)
2. Atluri SN, Zhu T. A new meshless local Petrov-Galerkin (MLPG) approach in computational mechanics. Comput. Mech., 1998, 22:117-127
3. Qian Jiahuan, Yin Zongze. Principle and calculation of soil (The 2nd edition) [M]. Beijing: China water conservancy and electrical power press，1995 (in Chinese)
4. Lv Xilin, Jin Guofang, Wu Xiaohan. Nonlinear theory and application of FEM for reinforcement concrete. Shanghai: Tongji university press, 1997 (in Chinese)
5. Xu Zhilun. Abecedarium for elastic mechanics. Beijing: High education press. 1983 (in Chinese)
6. Zhao Ming-hua, Zou Xin-jun, Liu Qi-jian. Research on the axial bearing capacity of super-long and large diameter bored piles in Dongting Lakeland by loading test [J]. China civil engineering journal. 2004,37(10): 63-67 (in Chinese)

Stabilized Procedures for Finite Element Analysis in Saturated Soils Under Cyclic Loading

Maosong Huang[1], Ming Liu[1], and O.C. Zienkiewicz[2]

[1] Department of Geotechnical Engineering, Tongji University, 200092 Shanghai, China
[2] Institute for Numerical Methods in Engineering, University of Wales Swansea,
Swansea SA2 8PP, U.K.
`mshuang@mail..tongji.edu.cn`

Abstract. Conventional finite element procedures with equal order interpolations for saturated soil dynamic $u - p$ formulation have been experiencing numerical difficulties for the problems concerning with small permeability and neglectable compressibility of pore-fluid. Such difficulties can be avoided by the staggered implicit-implicit algorithm and the direct α-method which were introduced by Huang *et al.* (2004). Several numerical examples for surface step loadings were given to demonstrate the performance of the proposed methods. Since the numerical examples for the step loadings are not typical for dynamic problems, which usually show the relatively strong oscillation nature of dynamic behaviors. Due to the necessity to show the effectiveness of the proposed stabilization techniques for cyclic loading problems, two numerical examples regarding saturated soils subject to a surface cyclic loading are presented in this paper. Discussion on uniform and non-uniform mesh configuration is also given.

Keywords: Saturated soils; Cyclic loading; u-p formulation; Incompressible behavior; Stabilization procedures.

1   Introduction

Extensive research has been devoted during the past few decades to coupled dynamic analysis of soil - pore fluid interaction problems due to its application to the problems subjected to earthquake or other types of cyclic loadings. Verification exercises assisted by the VELACS (VErification of Liquefaction Analysis by Centrifuge Studies) project of the US National Science Foundation have demonstrated the importance of the full two-phase, numerical analysis for saturated soil dynamic problems. The problems are generally formulated in terms of the displacement of the solid phase u and the pore-water pressure p under certain assumptions [1-2]. The numerical solution procedure for solving such a $u - p$ formulation with a general direct implicit time-stepping algorithm was discussed fully in Ref. [3]. It requires that the interpolation functions for u and p in the finite element discretization must fulfill the Babuska-Brezzi conditions or the much simpler Zienkiewicz-Taylor patch test in the limit of nearly incompressible pore fluid and small permeability. Only certain combinations of shape functions for u and p variables are permissible for the mixed

formulation. In particular, when both the permeability and compressibility of the pore fluid tend to zero, the solution will 'lock' or oscillate wildly unless the displacements are interpolated from their nodal values by polynomials one order higher than those used for the pressure. The problem here is identical to that encountered in solid mechanics or fluid mechanics. The restriction of mixed formulation will complicate the finite element coding and preclude the use of otherwise useful element types. Therefore, it is necessary to introduce simple stabilization techniques which permit continuous and equal interpolation to be used for u and p.

Three classes of the stabilization methods have been introduced in the literature so far. The first of them is referred to as the fractional step method or operator-splitting method, which can be realized in either semi-explicit form or staggered implicit-implicit form [4-5]. Advantages of the introduction of the staggered implicit-implicit form over the semi-explicit form are not just its unconditional stability. Meanwhile, optimal solutions can be achieved with the staggered implicit-implicit form. As already explained in Ref. [6], the proposed fractional step method (or staggered algorithm) may experience difficulties due to the time-stepping stability requirement. Such difficulties can be partially overcome with the introduction of the second class of the stabilization techniques, which is so-called direct α -method [6]. As an alternative, Mira et al. [7] presented a new formulation in which stabilization was achieved through an approach based on the enhanced strain element. However, only the problems of quasi-static consolidation were discussed in Ref. [7]. Further research the application of the proposed method into saturated soil dynamic problems is obviously required. Indeed, the analysis of examples with surface step loadings used by the authors in Ref. [6] is not quite typical for dynamic problems, since numerical errors caused by numerical stability problems may be gradually accumulated for the examples with cyclic loadings. Therefore, in this paper several numerical examples subjected to cyclic loadings are provided to demonstrate numerical stability of the previously proposed techniques for dynamic problems.

2   Governing Equations and Stabilized Procedures

Here the staggered implicit-implicit algorithm and the direct α -method proposed by the authors [5-6] are briefly reviewed. As described in Ref. [6], the governing total momentum equilibrium and conservation equation of pore-fluid flow for $u – p$ formulation can be written as

$$S^T(\sigma' - mp) + \rho b - \rho \ddot{u} = 0 \cdot \tag{1}$$

$$m^T S\dot{u} - \nabla^T \bar{k} \nabla p + \frac{n}{K_f} \dot{p} + \nabla^T \bar{k} \rho_f b = 0 \cdot \tag{2}$$

where u is the vector of displacement, p is the pore-pressure, b is the body force vector, ρ is the total density of the mixture, ρ_f is the density of the fluid, n is the porosity, $\bar{k} = k/(\rho_f g)$, k is the permeability coefficient generally used in soil mechanics, g is the gravity acceleration, K_f is the bulk modulus of the pore fluid. σ' is the vector form of the effective stress defined as $\sigma' = \sigma - mp$ where σ is the

total stress, ∇ is the gradient operator, S is the strain operator and the vector m in the 2D case take the forms $m^T = \begin{bmatrix} 1 & 1 & 0 \end{bmatrix}$. The equations have to be supplemented by a constitutive law for the soil skeleton linking σ' and the strain $\varepsilon = Su$. For a rate-independent material, it can be expressed as $d\sigma' = D_T d\varepsilon$.

We now approximate the governing equations in time using the generalized Newmark scheme[8], i.e. applications of GN22 to the displacement and GN11 to the pore-pressure. Thus, the total momentum balance equation is written at $t = t_{n+1}$ as

$$S^T[\sigma'_{n+1} - m(p^p_{n+1} + \dot{p}_{n+1}\theta\Delta t)] + \rho b_{n+1} - \rho \ddot{u}_{n+1} = 0 \ . \tag{3}$$

where $p^p_{n+1} = p_n + (1-\theta)\Delta t\dot{p}_n$. The staggered algorithm (or operator-splitting method) can be performed using an intermediate acceleration $\ddot{u}^*_{n+1}$. Thus, equation (3) is approximated with the predicted value $S^T\sigma'^p_{n+1}$ and can be split into two parts as

$$\rho \ddot{u}^*_{n+1} = S^T\sigma'^p_{n+1} - S^T m[p_n + (1-\delta)\Delta t\dot{p}_n] + \rho b_{n+1} \ . \tag{4}$$

and

$$\rho \ddot{u}_{n+1} = \rho \ddot{u}^*_{n+1} - S^T m[(\delta-\theta)\Delta t\dot{p}_n + \dot{p}_{n+1}\theta\Delta t] \ . \tag{5}$$

Similarly, the conservation equation of pore-fluid flow is written at $t = t_{n+1}$ as

$$m^T S(\dot{u}^p_{n+1} + \ddot{u}_{n+1}\gamma\Delta t) - \nabla^T \bar{k}\nabla(p^p_{n+1} + \dot{p}_{n+1}\theta\Delta t) + \frac{n}{K_f}\dot{p}_{n+1} + \nabla^T \bar{k}\rho_f b_{n+1} = 0 \ . \tag{6}$$

Substituting equation (5) into equation (6) leads to

$$m^T S\{\dot{u}^p_{n+1} + \ddot{u}^*_{n+1}\gamma\Delta t - \frac{1}{\rho}S^T m[(\delta-\theta)\Delta t\dot{p}_n + \dot{p}_{n+1}\theta\Delta t]\gamma\Delta t\}$$

$$-\nabla^T \bar{k}\nabla(p^p_{n+1} + \dot{p}_{n+1}\theta\Delta t) + \frac{n}{K_f}\dot{p}_{n+1} + \nabla^T \bar{k}\rho_f b_{n+1} = 0 \ . \tag{7}$$

Performing the spatial discretisation and applying the standard Galerkin procedure to equations (4), (7) and (3) result to the following algebraic equations (for a linear elastic problem)

$$M\ddot{\bar{u}}^*_{n+1} = (f^*_s)_{n+1} - K\bar{u}^p_{n+1} + Q[\bar{p}_n + (1-\delta)\Delta t\dot{\bar{p}}_n] \ . \tag{8}$$

$$(C + H\theta\Delta t + H^*\theta\gamma\Delta t^2)\dot{\bar{p}}_{n+1} = (f_p)_{n+1} - H^*(\delta-\theta)\gamma\Delta t^2\dot{\bar{p}}_n - Q^T(\dot{\bar{u}}^p_{n+1} + \ddot{\bar{u}}^*_{n+1}\gamma\Delta t) - H\bar{p}^p_{n+1} \ . \tag{9}$$

$$(M + K\beta\Delta t^2)\ddot{\bar{u}}_{n+1} = (f_s)_{n+1} - K\bar{u}^p_{n+1} + Q(\bar{p}^p_{n+1} + \theta\Delta t\dot{\bar{p}}_{n+1}) \ . \tag{10}$$

where

$$H^* = \int_\Omega (\nabla N_p)^T \frac{1}{\rho}(\nabla N_p)d\Omega$$

As already explained in Ref. [6], the optimal elemental values of the splitting factor δ can be determined by $\delta = \delta_0 (\frac{\Delta t_{crit}}{\Delta t})^2$ ($0 < \delta \leq 1.0$, $1/2 \leq \delta_0 \leq 1.0$), where Δt_{crit} is the critical time step length for the direct explicit-implicit algorithm [6].

The so-called direct α-method is referred to as direct modification resulting in steady state approximation which avoids mixed form restriction. Considering the presence of the pore pressure variable in first order, the divergence of the time derivative of the momentum equation should be added to the conservation equation of pore-fluid flow. The momentum balance equation (1) and its discrete form will remain unchanged. However, the conservation equation of pore-fluid flow (2) is now modified by the addition of a proportion α of the divergence of the time derivative of the momentum balance equation. We write thus

$$\mathbf{m}^T \mathbf{S} \dot{\mathbf{u}} - \nabla^T \bar{k} \nabla p + \frac{n}{K_f} \dot{p} + \nabla^T \bar{k} \rho_f \mathbf{b} + \alpha \nabla^T \frac{d}{dt}[\mathbf{S}^T(\boldsymbol{\sigma}' - \mathbf{m}p) + \rho\mathbf{b} - \rho\ddot{\mathbf{u}}] = 0 \quad \cdot \tag{11}$$

Applying equation (2) into equation (11), and neglecting the time derivative of the body force and the second-order time derivatives of pressure, we obtain

$$\mathbf{m}^T \mathbf{S} \dot{\mathbf{u}} - \nabla^T \bar{k} \nabla p + \frac{n}{K_f} \dot{p} + \nabla^T \bar{k} \rho_f \mathbf{b} + \alpha \nabla^T (\mathbf{S}^T \dot{\boldsymbol{\sigma}}') - \alpha \nabla^T \nabla \dot{p} = 0 \quad \cdot \tag{12}$$

After the spatial Galerkin discretization, the total momentum balance equation and equations (12) become (for linear elasticity)

$$M\ddot{\bar{u}} + K\bar{u} - Q\bar{p} = f_s \quad \cdot \tag{13}$$

$$(C + \tilde{H}^*)\dot{\bar{p}} + H\bar{p} + Q^T \dot{\bar{u}} - L\ddot{\bar{u}} = \tilde{f}_p \quad \cdot \tag{14}$$

where

$$\tilde{H}^* = \int_\Omega (\nabla N_p)^T \alpha (\nabla N_p) d\Omega \qquad L = \int_\Omega (\nabla N_p)^T \alpha \mathbf{S}^T DB d\Omega$$

Again as already demonstrated in Ref. [6], the best solutions can be obtained with the selection of α value from $\alpha = \alpha_0 \Delta t_{crit}^2 / \rho$ ($1/4 \leq \alpha_0 \leq 1/2$).

3   Numerical Examples

Several examples were given in Ref. [6] concerning with the solution of transient problems as well as of the final steady states obtained by the staggered implicit-implicit algorithm and direct α-method. Those were mainly used for modeling elastic porous media on uniform and non-uniform meshes subjected to a surface step loading. The space does not permit here the full description of the performance of the proposed stabilization method in all numerical examples. Due to the significance of the success of the proposed procedures for the cases with cyclic loading, two numerical examples are presented here for a soil column and a soil foundation under a surface cyclic loading.

3.1   Example 1: An Elastic Soil Column Subjected to a Surface Cyclic Loading

First, a simple example is presented to demonstrate the performance of the proposed stabilization techniques described in Section 2. This is a soil column subjected to a surface cyclic loading given by $q = 1.0 + 0.5\sin(2.0t)$ kPa. Boundary conditions are sketched in Fig. 1. The material has been assumed isotropically elastic, with the following properties: $E = 2.0 \times 10^7 \, N/m^2$, $\nu = 0.2$, $\rho_s = 2.0 \times 10^3 \, kg/m^3$, $\rho_f = 1.0 \times 10^3 \, kg/m^3$, $K_f = \infty$, $n = 0.3$. Three different permeabilities of $k = 0.0$, $k = 1.0 \times 10^{-6} \, m/s$ and $k = 1.0 \times 10^{-4} \, m/s$ are considered. For each permeability, five analyses are carried out by using various algorithms as the following: 1 – direct implicit algorithm, 10 4/4 node elements; 2 – direct implicit algorithm, 10 8/4 noded elements; 3 – staggered implicit-implicit algorithm, 10 4/4 nodded elements; 4 – direct α-method, 10 4/4 noded elements; 5 – direct implicit algorithm, 100 8/4 noded elements. Elements with non-uniform interpolation, i.e. biquadratic for u and bilinear for p (8/4 noded elements) are considered to be acceptable. The computed results obtained using such elements can be used as the basis of comparison.
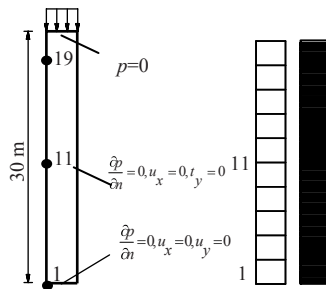
Fig. 1. A soil column subjected to a surface cyclic loading
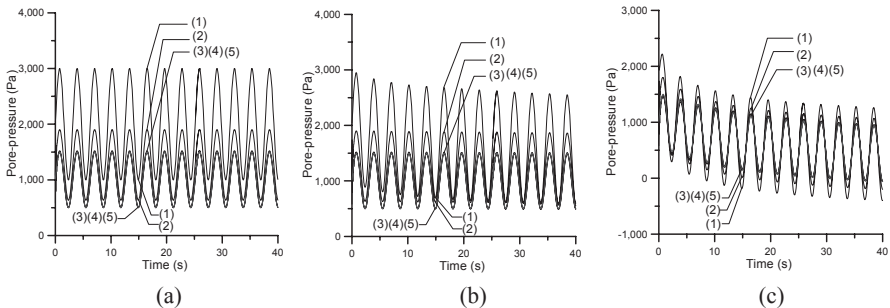
Fig. 2. Solutions for example 1 using various algorithms (Node 19): (a) $k = 0.0$; (b) $k = 1.0 \times 10^{-6} \, m/s$; (c) $k = 1.0 \times 10^{-4} \, m/s$

It is observed from Fig. 2(a), (b) and (c) that the solutions obtained by using direct implicit algorithm with equal interpolation (i.e. 4/4 noded element) overestimate the initial pore-pressure significantly, especially for the cases of low permeability. The results can be improved when the proposed direct α-method is introduced. As far as the results of pore-pressure are concerned, the proposed procedure performs even better than mixed elements with non-uniform interpolation (i.e. 8/4 noded element) for a mesh composed of 10 elements. In fact, the computational results of pore-pressure obtained by using the stabilization α-method and the staggered implicit-implicit algorithm agree well with those from 100 8/4 noded elements.

3.2   Example 2: An Elastic Soil Foundation Subjected to a Surface Cyclic Loading

Next, to further demonstrate the performance of the proposed stabilization methods, numerical investigations of a real two-dimensional example with uniform and non-uniform meshes are carried out. This is an elastic foundation again with a surface cyclic loading same as that in example 1. The boundary conditions are sketched in the Fig. 3(a). The material properties are identical to those in example 1.
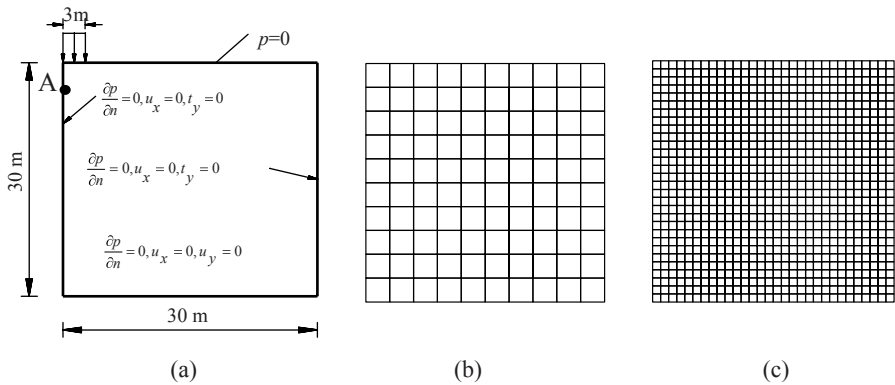
Fig. 3. A soil foundation subjected to a surface cyclic loading: (a) geometry and boundary conditions; (b) uniform mesh - 100 elements; (c) uniform mesh - 900 elements

3.2.1   Uniform Meshes (Fig. 3b, 3c)

Two uniform meshes used in the analyses consist of 100 or 900 quadrilateral elements as depicted in Fig. 3(b) and Fig. 3(c). Again, three different permeabilities are studied with comparisons of five different algorithms similar to those already mentioned in example 1, except 100 elements used for the algorithm Nos. 1, 2, 3, 4 and 900 elements used for the algorithm No. 5. The numerical results obtained by using various algorithms are shown in Figs. 4(a), (b) and (c). As expected, similar conclusions can be made with the excellent performance of the proposed stabilization method.
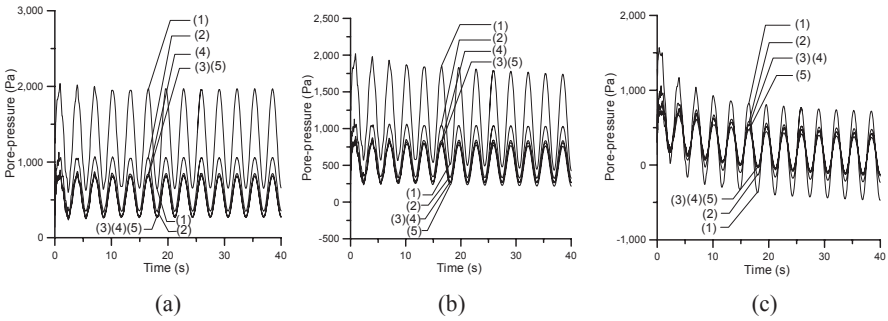
Fig. 4. Solutions for example 2 using various algorithms with uniform meshes (Node A): (a) $k = 0.0$; (b) $k = 1.0 \times 10^{-6} m/s$; (c) $k = 1.0 \times 10^{-4} m/s$

3.2.2   Non-uniform Mesh (Fig. 5)

As already demonstrated in Ref. [6], the staggered implicit-implicit algorithm with a global splitting factor δ gives us a significant oscillation for non-uniform mesh since only global time step can be used for transient problems. The computed results of pore-pressure can be improved when local splitting factors δ are introduced. The non-uniform mesh used for the analysis is shown in Fig. 5 and it consists of only 4/4
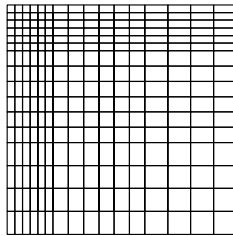
Fig. 5. A non-uniform mesh used for example 2
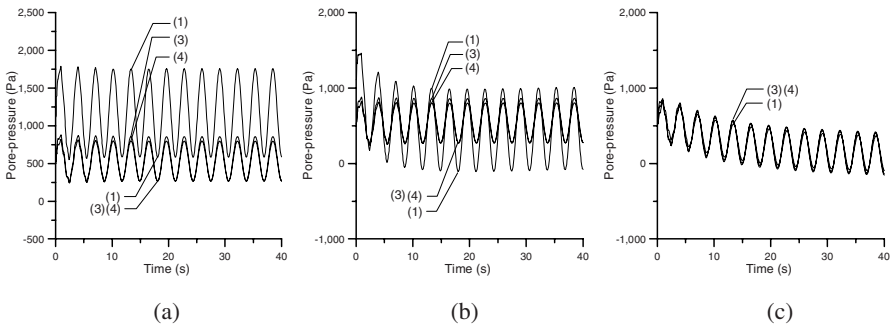
Fig. 6. Solutions for example 2 using various algorithms with non-uniform mesh (Node A): (a) $k = 0.0$; (b) $k = 1.0 \times 10^{-6} m/s$; (c) $k = 1.0 \times 10^{-4} m/s$

noded elements. Fig. 6(a), 6(b) and 6(c) present the comparisons of the computed pore-pressure obtained by using three different algorithms (1 – direct implicit algorithm; 3 – staggered implicit-implicit algorithm with local δ ; 4 – direct α - method). Again, the results of pore-pressure can be improved when the proposed stabilization method is introduced, especially for the cases with low permeabilities.

4   Conclusions

In this paper, two classes of the stabilization methods proposed previously by the authors for saturated soil dynamics in the limit of nearly incompressible pore-fluid and small permeability has been briefly reviewed. Attention is then paid to the performance of the proposed procedures in the problems subjected to cyclic loading, and two numerical examples have been presented. The numerical results have shown a good performance of the proposed procedures. It must be pointed out here that the extension of the stabilized procedures to the elasto-plastic problems is of significantly importance for practical purpose. Further research in the elasto-plastic analysis with a more complicated constitutive model based on the concept of bounding-surface plasticity is currently underway. It must be pointed out that the success in elasto-plastic problems is due to not only the introduction of the proposed stabilization method but also the use of adaptive remeshing or other suitable techniques such as the assumed strain method, etc. The incompressible-undrained issue can be solved using the proposed stabilization method with the elements of equal linear interpolation. However, such elements still behave poorly for the bending dominated problems, which are important in the calculations involving strain localization. It must be emphasized that the difficulties remaining for the elasto-plastic problems should not underestimate the importance in the determination of stabilization parameters. Optimal elemental parameters can provide the best solutions for the pore-pressure, which are obviously essential to the success not only in elastic problems but also for elasto-plastic cases.

References

1. Zienkiewicz OC, Chang CT, Bettess P. Drained, undrained, consolidating and dynamic behaviour assumptions in soils; Limits of validity. *Geotechnique*, 1980, 30:385-395.
2. Zienkiewicz OC, Shiomi T. Dynamic behaviour of saturated porous media: the generalised Biot formulation and Its numerical solution. *Int J Numer Analyt Meth Geomech*, 1984, 8:71-96.
3. Zienkiewicz OC, Chan AHC, Pastor M, Paul DK, Shiomi T. Static and dynamic behaviour of soils: a rational approach to quantitative solutions, Part I: Fully saturated problems. *Proc R Soc London*, 1990, A429:285-309.
4. Zienkiewicz OC, Huang M, Wu J, Wu S. A new algorithm for coupled soil-pore fluid problem. *Shock and Vibration*, 1993, 1:3-14.

5. Huang M, Wu S, Zienkiewicz OC. Incompressible or nearly incompressible soil dynamic behaviour - a new staggered algorithm to circumvent restrictions of mixed formulation. *Soil Dynamics and Earthquake Engineering*, 2001, 21:169-179.
6. Huang M, Yue ZQ, Tham LG, Zienkiewicz OC. On the stable finite element procedures for dynamic problems of saturated porous media. *Int J Numer Meth Engng*, 2004, 61:1421-1450.
7. Mira P, Pastor M, Li T, Liu X. A new stabilized enhanced strain element with equal order of interpolation for soil consolidation problems. *Comput Methods Appl Mech Engrg*, 2003, 192:4257-4277.
8. Zienkiewicz O C, Taylor R L. The Finite Element Method, 5th Edition. Oxford: Butterworth Heinemann, 2000.

Numerical Study on the Effect of Grouting on Long-Term Settlement of Tunnels in Clay

Dong-Mei Zhang, Hong-Wei Huang, and Jian-Ming Wang

Department of Geotechnical Engineering, Tongji University, Shanghai 200092, China
dmzhang@mail.tongji.edu.cn

Abstract. The long-term settlements over tunnels can be rather significant, particularly when tunnels are embedded in soft and compressible soils. The influence of grouting on the evolution of long-term surface settlement, as well as ground loss, is simulated by imposing prescribed volumetric strain on the disturbed area around the tunnel due to shield tunneling. The volumetric strain could be detected from the grouting ratio of grouting volume and the volume of the physical gap of shield tunnel. Finally, some conclusions are drawn from the numerical simulations.

Keywords: Grouting, Tunnel, Long-term settlement, Prescribed volumetric strain.

1 Introduction

Many field observations on long-term settlements of tunnels have indicated that the long-term settlements can be significant when tunnels are embedded in soft and compressible soils regardless of the tunneling methods ([1], [2], [3], [4], [5], [6]). [7] reported that this kind of long-term settlement might last two or more years in saturated soft ground even without any surface loading for Shanghai urban subway tunnel. The surface settlement of Shanghai metro tunnel line 2 almost doubled in three months after the tunnel construction ([2]). Based on comprehensive field data, [4] concluded that typically the increase in settlements over long-term is of the order of 30%-90% of the total settlement. This is confirmed, for example, by the observed settlements over a period of 11 years reported by [6] for a 3m diameter tunnel constructed in normally consolidated silty clay in Grimsby, England. The final equilibrium of settlement was achieved after about 10 years.

[1] concluded that the major factors influencing the development of post-construction settlements above tunnels could be attributed to the followings. 1.The magnitude and distribution of excess pore pressure due to shield tunneling; 2.The compressibility and permeability of the soil; 3.The drained conditions of the tunnel lining relative to the permeability of the surrounding soils; 4.The initial pore pressure distribution prior to the tunnel construction;

These four factors indicate that the long-term behaviour is, to some extend, the extension of the short-term behaviour of the tunnel in terms of ground movements due to tunneling. In all the related studies with regard to the long-term behaviour of

tunnels, the effect of grouting on the development of long-term behaviour is omitted for simplification. However, [4] pointed out that the effects of grouting around tunnel linings deserves more attention than it has generally been given and its influence on settlement must be taken into account when the detailed long-term behaviour of tunnel is studied numerically. The field-based measurement from Shanghai metro tunnel line-2 also confirms that the effect of grouting on the excess pore pressure is quite remarkable and not reasonable for neglecting ([2]). [9] studied the effectiveness of grouting on tunnels in clay during long-term through field trial, laboratory test combined with numerical simulations. However, only settlements over tunnels were considered.

Consequently, the influence of grouting on the long-term behaviour of tunnels in clay is simulated using FEM code of Plaxis in terms of the development of surface settlement and ground loss, which are usually used to predict the influence of the shield tunneling on the surrounding environment.

2 Numerical Modelling

The numerical modelling is carried out based on Shanghai No.2 metro tunnel. The tunnel lining is simulated using linear elastic model and is simplified as elastic beam in numerical modelling. Elasto-plastic model of Mohr-Coulomb is adopted for soft soils. The numerical simulation is performed with 15-node isoparametric finite elements under the assumption of plane strain conditions. The tunnel lining for Shanghai metro line No.2 is 6.2m in external diameter and 5.5m in internal diameter. The average depth to the center-line of the tunnel is about 1.8D (D is the tunnel diameter). The tunnel was excavated by EPB shield machine. The shield body is 6.24m long with 6.34m in diameter. Correspondingly, the clearance between the external diameters of shield body and the tunnel, which is usually named physical gap G_p according to the definition of [2], will reach 140mm. Correspondingly, the FEM mesh of the tunnel is shown in Fig.1 combined with soils distribution. The symmetry of the model is considered in the simulation. The width of the numerical model is 40m, which is 6.5 times as wide as the external diameter of the tunnel. The vertical dimension is 36m, which is about 3 times the depth of the external diameter of the tunnel.

2.1 Simulation of Grouting

The grouting in shield tunnel plays a very important role to decrease the closure of the tail void and the surface settlement over tunnels in result. The influence of grouting is usually simulated by exerting a uniform pressure on the tunnel lining in references. However, it is quite difficult to determine the magnitude and distribution of the grouting pressure since their fluctuations during construction. Meanwhile, the volume of the grouting is stable and very easy to obtain. The volume of grouting denoted as V_{grout} could be defined in terms of grouting ratio R and the volume of physical gap V_{gap} shown as equation (1).

$$V_{grout} = R \cdot V_{gap} .$$

(1)

Here, V_{grout} is the volume of grouting during shield tunneling. V_{gap} means the volume of physical gap. The volume of physical gap studied in this paper is $1.38 m^3 / m$. R represents the grouting ratio.

Actually, the grouting will inevitably result in the expansion of the soils in a disturbed area around the tunnel when R is larger than 1.0. As a result, the effect of grouting could be simulated by imposing a prescribed volumetric strain on the disturbed area around the tunnel. The disturbed area is assumed to be a homocentric circle with the tunnel, which is of 10m in diameter based on the in-situ observation. Then the disturbed area V_{dis} reaches $48.32 m^3 / m$. Correspondingly, the prescribed volumetric strain could be presented by equation (2).

$$\varepsilon_v = (R-1) \cdot V_{gap} / V_{dis} = 2.85 \cdot (R-1)(\%) . \qquad (2)$$
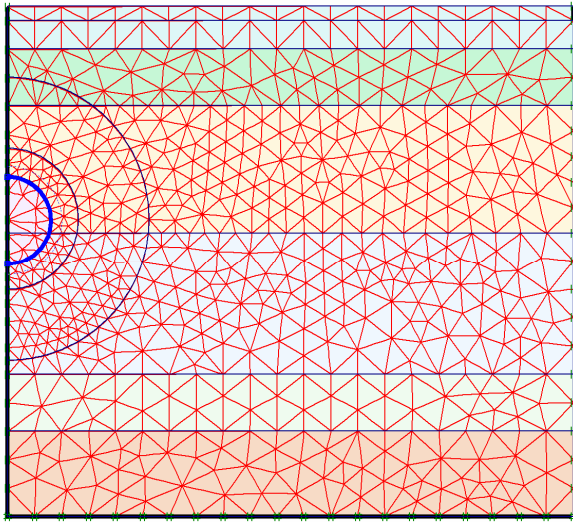
Fig. 1. FEM mesh in numerical simulation

2.2 Boundary Conditions

The boundary conditions in the numerical simulation contain the following two types, one is the displacement boundary condition, and the other is the drainage condition. A free displacement boundary condition is adopted at the ground surface. It is assumed that no horizontal nor vertical displacement takes place at the lower boundary, for it is beyond the influence of tunnel construction. The lateral displacements at left- and right-hand boundary are both fixed as zero. The left-hand boundary is the line of symmetry. The drainage condition at the ground surface is assumed to be free; meanwhile the lower boundary as well as the left-hand boundary condition is considered to be impermeable, in order to prevent the pore pressure dissipation across

the boundary during the settlement development. However, the right-hand boundary is taken as permeable during the long-term settlement.

The initial effective stresses and hydrostatic pore pressure are calculated based on the weight of the soil and the underground water condition.

2.3 Parameters Used in Numerical Modeling

The parameters involved in the numerical analysis are listed in Table 1and Table 2

Table 1. Characteristics of soils of Shanghai

Depth (m)	Young's modulus E (MPa)	Poisson's ratio V	Bulk density γ (kN/m³)	Cohesion c (kPa)	Friction angle φ (°)
0~3	2.395	0.35	18.7	13	14.8
3~7	2.032	0.35	18.0	7	18.7
7~16	1.293	0.35	17.0	10	9.8
16~26	3.000	0.35	18.3	10	19.1
26~30	4.216	0.35	19.9	30	12.8
30~36	6.560	0.35	20.1	6	26.3

Table 2. Parameters of tunnel lining

EA (kN/m)	EI (kN·m²/m)	Poisson's ratio V
1.2e7	1.2e5	0.15

2.4 Numerical Simulation Procedure

The influence of grouting on the long-term settlement was simulated using 4 consecutive steps. The 4 consecutive steps correspond to different stages of the development of surface settlement over tunnels. STEP 0 means the initial state of the ground before taking account of the influence of tunneling. STEP 1 represents the tunnel construction. The effect of grouting is modeled in STEP 2 by imposing the prescribed volumetric strain on the disturbed area. STEP 3 is the final case in the simulation, where the long-term settlement occurs due to the consolidation of the soil. The numerical results for each step are the initial state of the next step since the 4 steps are consecutive both in time and stress state.

The prescribed volumetric strains adopted in STEP2 are 0%, 0.5%,1%，2%，3% and 4%. They are corresponding to the grouting ratios of 1, 1.17, 1.35, 1.7, 2.05 and 2.4 respectively. The volume of grouting is usually much larger than that of physical gap considering the over-excavation during shield tunneling. Correspondingly, the grouting ratios R with a scale of 1 to 2.4 are adopted in the numerical simulation.

3   Influence of Grouting on the Long-Term Settlements

The evolutions of long-term surface settlements over tunnels with 6 different grouting ratios are presented in Fig.2 and Fig.3. The surface settlement in Fig.2 involves the short-term settlement and therefore is the total settlement.
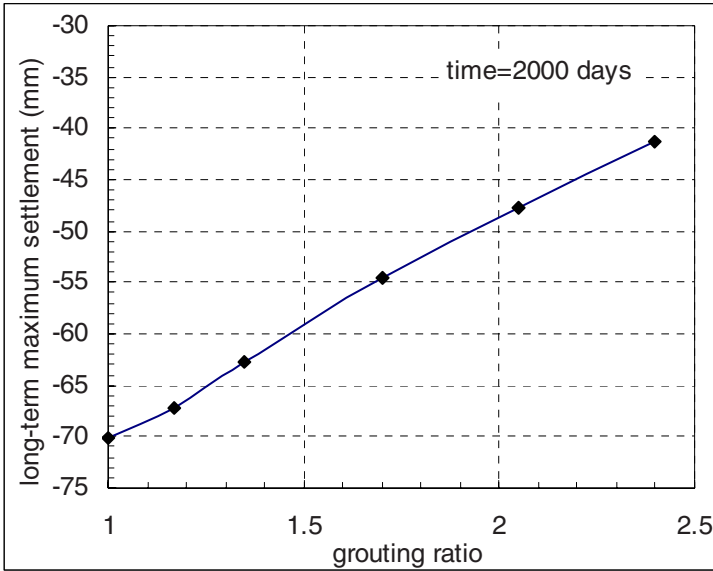
Fig. 2. Development of long-term maximum surface settlement with grouting ratio
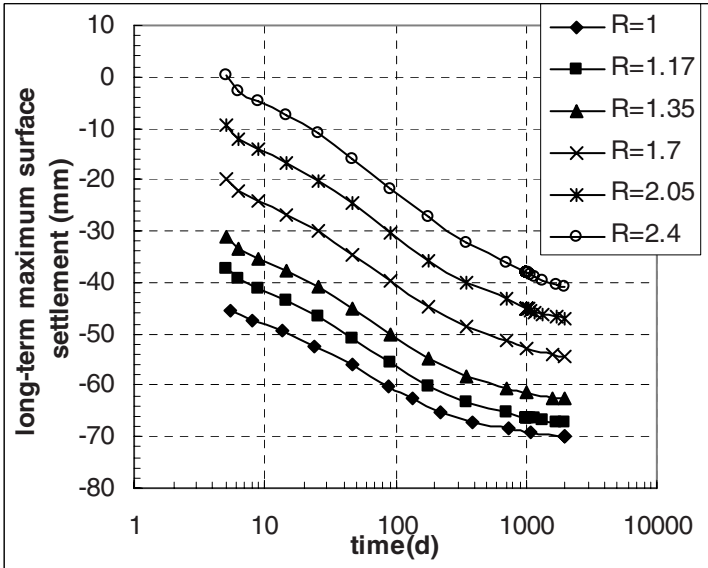
Fig. 3. Evolution of long-term maximum surface settlement with different grouting ratios

Fig.2 and Fig.3 reveal that the magnitude of maximum surface settlement is smaller at any time with a higher grouting ratio. The maximum long-term settlement almost decreases 42% with the grouting ratios increase from 1 to 2.4 at 2000 days

after grouting. However, it could be found that higher grouting ratio results in higher post-grouting settlements from the different slopes of the curves in Fig.3 due to the higher pore pressure caused by grouting. Therefore, it takes more time for the long-term settlement to reach the stability for the case with higher grouting ratios.

The development of ground loss normalized to the area of the cross section of tunnel with grouting ratio is presented in Fig. 4. The normalized ground loss can be described by equation (3).

$$V/V_t = \sqrt{2\pi} i S_{max} / \pi r^2 \ (\%) \ . \tag{3}$$

Here S_{max} means the maximum surface settlement, r is the external diameter of shield machine. i is the width of surface settlement trough and could be determined by Peck's empirical formulation (equation 4) ([8]).

$$S(x) = S_{max} \exp(-x^2/2i^2) \ . \tag{4}$$

Here, x is the distance from studied point to the tunnel centre.
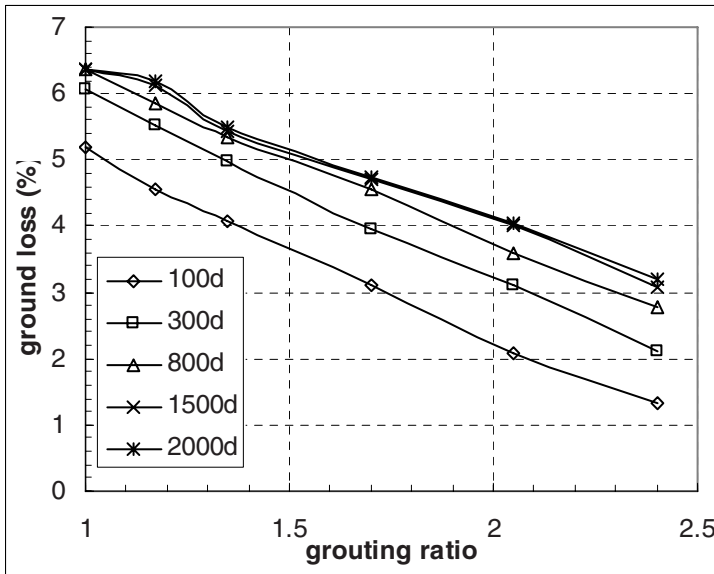
Fig. 4. Evolution of ground loss with grouting ratio

It can be clearly found from Fig.4 and Fig.5 that ground loss continuously decrease with grouting ratio and increases with time until it reaches the stability. The evolution of ground loss with time corresponding to different grouting ratio is similar with that of the long-term maximum surface settlement.
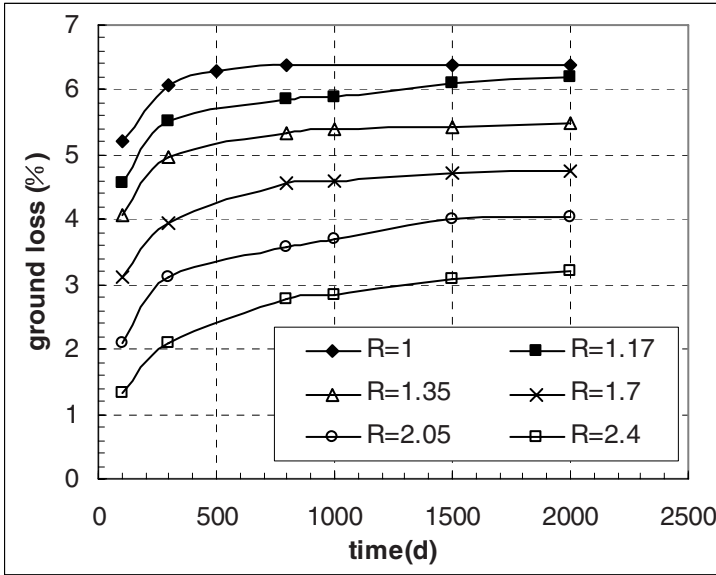
Fig. 5. Evolution of ground loss with time

4   Conclusions

The grouting effect is simulated by imposing prescribed volumetric strain on the disturbed soils around the tunnel. The evolution of long-term settlement of tunnels in clays is studied and the following conclusions are obtained.

1. It is feasible and reasonable to simulate the grouting effect with the prescribed volumetric strain of the disturbed area. However, there is a lack of in-situ measurement to validate the numerical simulation.

2. The long-term settlement as well as the ground loss decreases significantly with grouting. While the post-grouting settlement and ground loss increase with the grouting ratio due to the higher pore pressure caused by the higher grouting ratios.

3. The evolution of surface settlement and ground loss with time is remarkable regardless of the grouting ratios.

References

1. Mair, R. J., Taylor, R. N.: Theme lecture: Bored tunneling in the urban environment. Proceedings of the Fourteenth International Conference on Soil Mechanics and Foundation Engineering, (1997) 2353-2385
2. Lee, K. M., Ji, H. W., Shen, C. K., Liu, J. H., Bai, T. H. : Ground Response to the Construction of Shanghai Metro Tunnel-Line 2. Soils and Foundations, 39(3). (1998) 113-134

3. Shirlaw, J. N.: Pore pressure around tunnels in clay: 1 Discussion. Canadian Geotechnical Journal 30, (1993) 1044-1046
4. Shirlaw, J. N.: Observed and calculated pore pressures and deformations induced by an earth balance shield: Discussion 1. Canadian Geotechnical Journal 32, (1995) 181-189
5. Cooper, M. L., Chapman, D. N., Rogers, C. D. and Chan, A. H.: Movements in the Piccadilly Line tunnels due to the Heathrow Express construction. Géotechnique, 52(4). (2002) 243-257
6. O'Reilly, M. P., Mair, R. J., Alderman, G. H.: Long-term settlements over tunnels: an eleven-year study at Grimsby. Proceedings of Conference Tunneling, London, Institution of Mining and Metallurgy, (1991) 55-64
7. Hou, X., and Zhou, Z.: Saturated ground movement due to shield tunneling. Proceedings of the International Conference of International Tunneling Association, Madrid, Spain. (1988) 351-356
8. Peck, R. B.: Deep excavation and tunneling in soft ground. Proceeding 7th International Conference on Soil Mechanics and Foundation Engineering, 3. (1969) 1469-1472
9. Komiya, K. Soga, K. Akagi, H. Jafari, M.R. and Bolton, M.D.: Soil consolidation asssociated with grouting during shield tunneling in soft clayed ground. Geotechnique, 51(10). (2001) 835-846

Large Scale Three-Dimensional Boundary Element Simulation of Subduction

Gabriele Morra[1], Philippe Chatelain[2],
Paul Tackley[1], and Petros Koumoutsakos[2]

[1] Geophysical Fluid Dynamics, ETH Zurich
Einsteinstr. 1, Zurich CH-80XX, Switzerland
`http://www.gfd.ethz.ch`
[2] Computational Science and Engineering Laboratory, ETH Zurich
Universitaetstr. 6, Zurich CH-8092, Switzerland
`http://www.cse-lab.ethz.ch`

Abstract. We present a novel approach for modeling subduction using a Multipole-accelerated Boundary Element Method (BEM). The present approach allows large-scale modeling with a reduced number of elements and scales linearly with the problem size. For the first time the BEM has been applied to a subduction model in a spherical planet with an upper-lower mantle discontinuity, in conjunction with a free-surface mesh algorithm.

Keywords: Boundary Elements, Subduction, Fluid Dynamics, Fast Multipole, Global Earth Model.

1 Introduction

Geodynamics at the planetary scale is an inherently multiscale problem exhibiting very large variations in viscosity and spatial scales. In a nearly isoviscous system, convection occurs through finger-like, cylindrically symmetric Rayleigh-Taylor instabilities [1]. In contrast, highly viscous plates do not sink, but drift laterally and sink asymmetrically at zones known as subduction zones. This subduction process is the driving mechanism of plate tectonics. A self-consistent model of plate tectonics involves flows at planetary scales (the pacific plate is over 10000km wide) strongly coupled to small scale dynamics, such as trench fault lubrication (lithospheric shear-zones are thought to be 100m to 1km thick [2]).

Recent numerical results [3,4] have shown that the potential energy of the sinking plate is mostly dissipated through the interaction of the plate and the upper mantle. Accordingly a dynamic interaction between distinct slabs and the sharp viscosity transition at 660km depth could be caused by mantle back flow. There is a debate as to whether, for example, these processes modify the kinematics, shape and stress state of the trenches of the ring of fire around the Pacific plate, or whether each subduction system can be considered independently.

The present work introduces a novel numerical approach based on a Fast Multipole (FM) extension of the Boundary Element Method(BEM). The resulting

technique is much more efficient than the classical Finite Element (FE) or Finite Difference (FD) methods usually employed in geodynamics. We apply the present method to the simulation of subduction at the planetary scale.

This paper is structured as follows. In Sect. 2, we summarize our approach and present several resolution and scaling tests on a Beowulf cluster with up to 64 processors. In Sect. 3 then, we show how the Boundary Element Method for the solution of viscous flows can be adapted to subduction modeling. The results of models at the global scale are shown in Sect. 4.

2   Simulation of Stokes Flow

2.1   Governing Equations

We consider the Stokes equation for a steady, highly viscous flow

$$\nabla \cdot \sigma + \rho \mathbf{b} = 0 \tag{1}$$

where $\sigma = -\nabla P + \mu \nabla^2 \mathbf{u}$ is the stress tensor; $\mathbf{b}$, the body force; P, the pressure; $\mathbf{u}$, the velocity field and μ, the dynamic viscosity.

The Stokes equation can be recast into a variety of integral equations. We follow here the formulation of [5], to which we refer for further details. We denote as D is the domain where (1) holds and we write

$$u_i(\mathbf{x}_o) = \frac{1}{8\pi\mu} \int_D \sigma_{ik}(\mathbf{x}) n_k G_{ij}(\mathbf{x}, \mathbf{x}_o) dS(\mathbf{x}) + \frac{1}{8\pi} \int_D u_i(\mathbf{x}) n_k T_{ijk}(\mathbf{x}, \mathbf{x}_o) dS(\mathbf{x}) \tag{2}$$

where G_{ij} and T_{ijk} are the steady, Green's functions for velocity and stress respectively, also known as the *Stokeslet* and the *Stresslet*

$$G_{ij}(\mathbf{x} - \mathbf{x}_o) = \frac{\delta_{ij}}{r} + \frac{\hat{x}_i \hat{x}_j}{r^3}; \ \hat{\mathbf{x}} = \mathbf{x} - \mathbf{x}_o \text{ and } r = |\hat{\mathbf{x}}| \tag{3}$$

$$T_{ijk}(\mathbf{x} - \mathbf{x}_o) = -6\frac{\hat{x}_i \hat{x}_j \hat{x}_k}{r^5} \ . \tag{4}$$

In turn, (2) is cast into a form more appropriate for quasi-steady multiphase flows in the presence of a gravity field. Hence for $\mathbf{x} \in S_i$ we obtain

$$\frac{1 + \lambda_i}{2} \mathbf{u}(\mathbf{x}) - \sum_{j}^{N} \frac{1 - \lambda_j}{8\pi} \int_{S_j}^{PV} \mathbf{n} \cdot \mathsf{T} \cdot \mathbf{u} \, dS = -\frac{1}{8\pi\mu_0} \sum_{j}^{N} \int_{S_j} \mathsf{G} \cdot \Delta \mathbf{f} \, dS \ , \tag{5}$$

where PV denotes the principal value of the integral, μ_0 is the viscosity of the mantle, taken as a reference and $\lambda_i = \mu_i/\mu_0$ *and* $\Delta\mathbf{f}$ is a normal stress jump that accounts for gravity

$$\Delta\mathbf{f} = \Delta\rho\mathbf{b} \cdot \mathbf{xn} \ . \tag{6}$$

2.2   Numerical Method

The surfaces S_i and the supported quantities $\mathbf{u}$, $\Delta\mathbf{f}$,... are discretized with panels. The boundary integral equation (5) thus becomes a linear system

$$((1+\lambda)/2 + \mathsf{T})\,\mathbf{U} = \mathbf{F}\,. \tag{7}$$

Many approaches rely to the construction of the matrix; this scales as N_{panels}^2 both memory- and computation time-wise though, making it impractical for large systems.

We use a fast multipole method (FMM)[6,7,8] for the evaluation of the integrals in (5). The FMM scales as $N \log(N)$, which is far more tractable and still allows the use of a Generalized Minimized Residual method (GMRES) or any Krylov space based method that does not rely on the storage of the full matrix.

A multipole method exploits the decay of the kernel to convolve and makes a controlled approximation. More explicitly, let us compute

$$u(\mathbf{x}_o) = \int_D G(\mathbf{x}_o - \mathbf{x})\rho(\mathbf{x})dV(\mathbf{x})\,. \tag{8}$$

We consider the contribution from D_i, a part of D that is far *enough* from our evaluation point $\mathbf{x}_o$ and proceed with a Taylor expansion of the kernel G about $\mathbf{x}_c \in D_i$

$$
\begin{aligned}
u(\mathbf{x}_o) &= \int_{D_i} G(\mathbf{x}_o - \mathbf{x})\rho(\mathbf{x})dV(\mathbf{x}) \\
&\simeq \int_{D_i} (G(\mathbf{x}_o - \mathbf{x}_c) - \nabla G(\mathbf{x}_o - \mathbf{x}_c)\cdot(\mathbf{x}_o - \mathbf{x}_c) + \ldots)\,\rho(\mathbf{x})dV(\mathbf{x}) \\
&\simeq G(\mathbf{x}_o - \mathbf{x}_c)\int_{D_i} \rho(\mathbf{x})dV(\mathbf{x}) \\
&\quad -\nabla G(\mathbf{x}_o - \mathbf{x}_c)\cdot\int_{D_i}(\mathbf{x}_o - \mathbf{x}_c)\rho(\mathbf{x})dV(\mathbf{x}) + \ldots
\end{aligned} \tag{9}
$$

We note that the equation involves successive moments of the ρ distribution in D_i . The FMM algorithm thus sorts the sources in a tree structure whose cells contain the moment integrals–or multipoles– and carries out a field evaluation through a tree traversal. The refinement of the interactions is determined by a tree traversal stopping criterion based on a prescribed tolerance. The reader is referred to [6,7,8] for further details.

The present FMM code can handle convolutions with the Green's functions for the Poisson equation, the Stokeslet or the Stresslet. It employs up to the second order moments of the source distributions (quadrupoles).

2.3   Performances

The FMM-BEM drastically improves the computational cost of the method. Figure 1(a) shows the computation time of a time step for a viscous sphere

(a) Complexity (b) Parallel efficiency
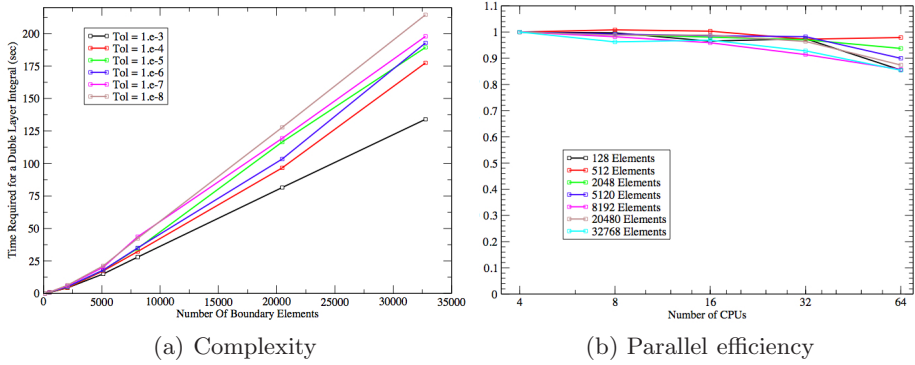
Fig. 1. Fast Multipole Method: performance plots

under gravity for several tolerances and resolutions. For the coarse resolutions, the method displays the nominal N^2 scaling of a direct interaction code. This is attributed to the relatively few elements and tree cells. The scaling then quickly approaches a nearly linear one ($N \log(N)$) for the finer resolutions.

The FMM-BEM has been parallelized using MPI. Figure 1(b) shows the parallel efficiency tested on a Opteron cluster with Quadrics connections. The scaling is very good up to 64 CPUS, still keeping 90% of efficiency. In its current implementation the FMM-BEM uses a shared tree, thus reducing the communication load at the expense of memory requirements.

3   Modeling Subduction with FMM-BEM

Subduction is the process through which a highly viscous ($O(10^2)\mu_{UM}$) and heavier plate ($1 - 3\%$) enters into the earth. Analytical and numerical models [9,10] have shown that the process is mainly controlled by the interaction of the lithosphere with the surface and is one-sided, characterized by an unsubducted plate overlapping the subducting plate. We assume that three fundamental forces control the subduction process: the lithosphere-mantle-air/water buoyancy difference, the viscous resistance of the mantle to the plate motion and the resistance to bending and stretching of the lithosphere itself.

Buoyancy difference arises from the density difference between the bottom and the top of the plate, of the mantle and air/water, respectively. This property is critical in subduction as it prevents the unsubducted plate from sinking straight down [11].

The drag force exerted by the less viscous (μ_{UM}) mantle on the lithosphere dissipates most of the energy [3,4] and controls the speed of the process. Consequently intraplate interaction might be mostly controlled by induced mantle flow.

The resistance to bending and stretching of the lithosphere itself is controlled by its very diverse and complex inner rheology. Simplified models of the internal distribution of strength of an oceanic lithosphere display a peak at 30-40km

depth, triggering the concept of lithospheric strength controlled by a stiff core [12,2,3]. In this work, the overall resistance to bending and stretching will be parameterized by an effective uniform layer with a viscosity two orders of magnitude higher than the mantle and an effective thickness of $80km$.

In order to appropriately model subduction, we have implemented a novel adaptive mesh algorithm which modifies the shape of the earth surface directly on top of the lithosphere. More explicitly, the algorithm adapts this free-surface to the lithospheric topography up to to a depth of half of the lithospheric thickness. The results of Sect. 4 show that this method automatically creates a physically consistent buoyancy force. The density difference between the mantle and ocean self-consistently sustains the unsubducted lithosphere as on the Earth but lets the upper surface of the lithosphere free to deform in a full free surface setting. Numerically, the method requires only one parameter, the critical distance h_{crit} between the boundary elements of the Earth surface and of the lithosphere surface. If the distance is too low, instabilities arises during the computation and if it is too high the uplifting force is not properly calculated. Tests have shown that the critical distance h_{crit} has to be no less than half of the element size of the Earth surface, but not more than 20% of the lithosphere thickness. The method is therefore more effective at a relatively high resolution, which is made affordable by the FMM-BEM.

4   Results

The simplest implementation of subduction at the global scale in a uniform Earth is obtained using only two surfaces, one delimiting the Earth surface and the second the lithosphere-mantle boundary. A slightly more sophisticated model, employing three surfaces, allows modeling the interaction with the 660km discontinuity. We use the boundary integral form of (5), usually employed for solving the interaction between immersed distinct bodies, translating this setting to a bounded problem by orienting the normal of the Planet surface inwards, as sketched in Fig. 2.

The reference viscosity μ_0 of (5) is the upper mantle effective viscosity μ_{UM}; $\lambda_1 = \mu_{Ocean}/\mu_{UM}$ is virtually null, being the ratio between the viscosities of
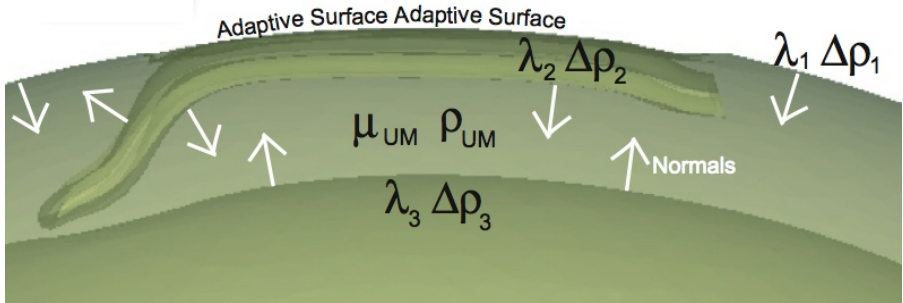
Fig. 2. Subduction model: geometry and parameters
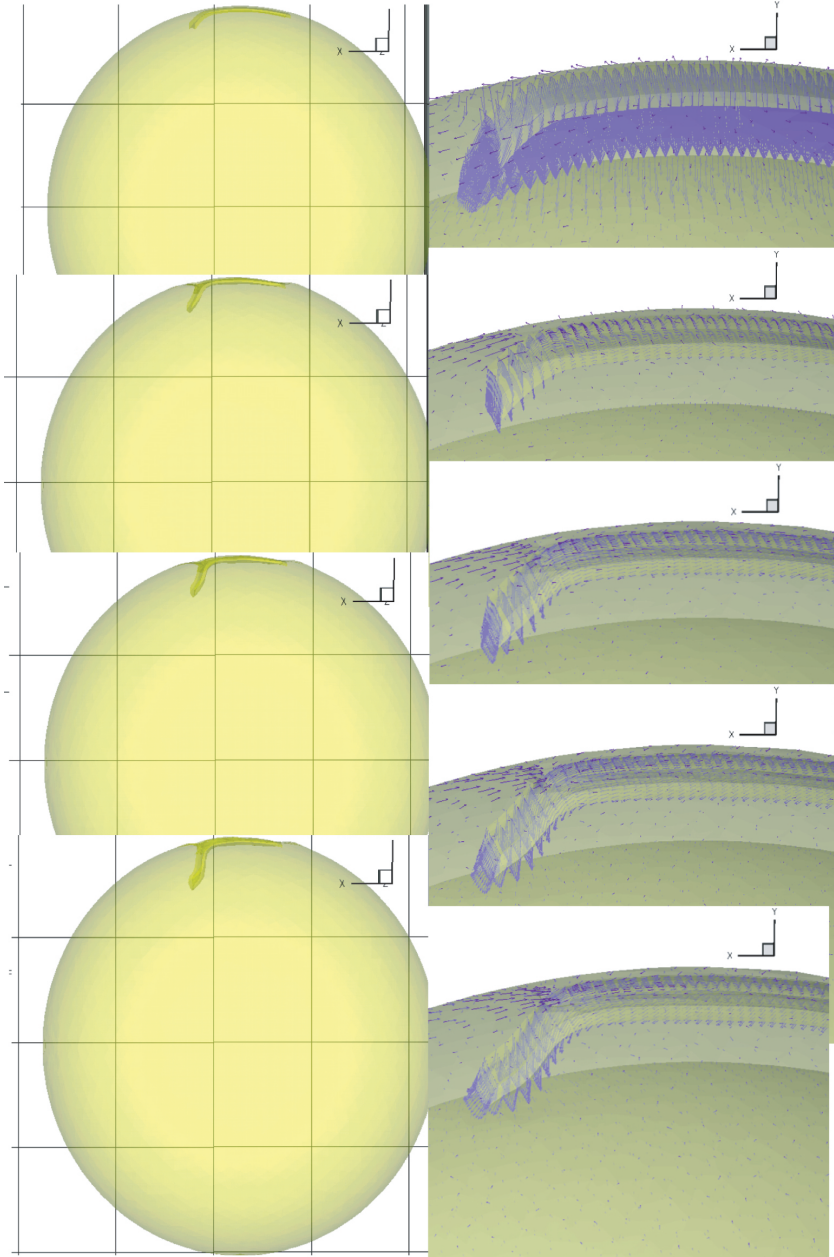
Fig. 3. Left: subduction of a plate 20 times more viscous then the mantle. Right: subduction of a plate 100 time more viscous then the mantle and interacting with a sharp viscous discontinuity at 660km, arrows represent the velocity vector.

ocean (water) and the upper mantle; $\lambda_2 = \mu_{\mathrm{Litho}}/\mu_{\mathrm{UM}}$ is the ratio between the lithosphere and upper mantle viscosities; $\lambda_3 = \mu_{\mathrm{LM}}/\mu_{\mathrm{UM}}$ is the ratio between the lower and upper mantle viscosities. We define $\Delta\mathbf{f}$ on surfaces 1, 2 and 3 in the same fashion; they are respectively equal to the difference between ocean (water) and upper mantle densities, the difference between the lithosphere and upper mantle densities and the difference between lower and upper mantle densities

$$\Delta\mathbf{f}_1 = (\rho_{\mathrm{Ocean}} - \rho_{\mathrm{UM}})\, g\, r\, \mathbf{n}$$
$$\Delta\mathbf{f}_2 = (\rho_{\mathrm{Litho}} - \rho_{\mathrm{UM}})\, g\, r\, \mathbf{n}$$
$$\Delta\mathbf{f}_3 = (\rho_{\mathrm{LM}} - \rho_{\mathrm{UM}})\, g\, r\, \mathbf{n}$$

where r is the length of $\mathbf{x}$, g is the gravity acceleration ($10m^2/s$) and gravity is assumed constant and radial $\mathbf{b} = -g\,\mathbf{x}/r$.

The solution of equation 5 with the parameters described above is shown in Fig. 3. In the left column, four frames of the time evolution of subduction for a lithosphere 3% heavier and 20 times more viscous than the mantle are shown. Surface topography is amplified by a factor of 10 in order to better show the efficiency of the adaptive mesh algorithm to embed the buyancy force and self-consistently let the planetary surface deform. Buoyancy sustains the lithosphere but allows the trench to freely migrate and the plate to freely move horizontally. At the beginning a 45 degrees dip is set, then the model evolves toward an almost vertical slab subduction, the dynamics accelerates, the trench retreat diminishes and the horizontal migration of the plate accelerates. Other models not shown here have been performed for two and more lithospheres just adding a new surface for each of them to equation 5.

The right column of Fig. 3 shows four frames of the evolution of a lithosphere 100 times more viscous than the upper mantle subducting in an Earth with the 660km (UM-LM) discontinuity. As for the first case, the plate is free to change shape and migrate horizontally and the trench evolves freely. Confirming results of laboratory experiments, the higher viscosity ratio and the presence of the upper-lower mantle discontinuity causes a lower subduction velocity but a much larger trench retreat than the first case. The arrows represent velocities, showing a slight forward motion for the plate while wedge velocities are much stronger. Finally, we note that the poloidal components of the velocities are dominant.

5   Conclusions

We have presented a novel computational approach for modeling subduction using a fast multipole acceleration of the boundary elements method. We have shown that the code scales linearly with the problem size for large sizes (more than 10^3 elements) and shows a very good parallel behavior that is promising for larger systems. An adaptive mesh algorithm has been developed for reproducing the buoyancy force, within a free surface setting. Exploiting this innovation, for the first time FMM-BEM has been employed for modeling subduction at the planetary scale. Finally, illustrative examples have been presented for subduction

in a viscously uniform Earth and in an Earth with the upper lower mantle viscosity discontinuity. Future work includes a comprehensive investigation of the roles played by the plate geometry, the lithosphere-mantle and upper-lower mantle differential properties and the study of the interaction of subducting plates.

References

1. Tackley, P.: Self-consistent generation of tectonic plates in time- dependent, three-dimensional mantle convection simulations, 1. Pseudoplastic yielding. In: G3, Geochemistry Geophysics Geophysics (2000) Volume 1 Number 23
2. Regenauer-Lieb, K. and Yuen, D.A.: Modeling shear zones in geological and planetary sciences: solid- and fluid-thermal-mechanical approaches. In: Earth-Science Reviews (2003), Volume 63, 295-349
3. Capitanio, F.A., Morra G. and Goes, S.: Dynamic controls on subduction kinematics: The role of the downgoing lithosphere and passive mantle flow In: Earth and Planetary Science Letters, 2007 (now submitted)
4. Stegman, D.R., Freeman, J., Schellart, W. P., Moresi, L. and May, D.: Influence of trench width on subduction hinge retreat rates in 3-D models of slab rollback.
5. Pozrikidis, C.: Boundary Integral and Singularity Methods for Linearized Viscous Flow (1992).
6. Barnes, J. and Hut. P., A hierarchical O(N log N) force-calculation algorithm, Nature (1986), 324
7. Greengard, L. and Rokhlin, V.: A Fast Algorithm for Particle Simulations. In: Journal of Computational Physics A (1987), Volume 73, 325-348
8. Warren, M.S. and Salmon, J.K.: A parallel hashed Oct-Tree N-body algorithm. In: Supercomputing, 1993, Pages 12-21
9. Jacoby W.R.: Model Experiment of Plate Movements. In: Nature-Physical Science (1973), Volume 242, Number 122, 130-134
10. Christensen, U. R.: The influence of trench migration on slab penetration into the lower mantle. In: Earth and Planetary Science Letters (1996), Volume 1996, 27-39
11. Funiciello, F., Morra, G., Regenauer-Lieb, K. and Giardini, D.: Dynamics of retreating slabs (part 1): Insights from 2-D numerical experiments. In: Journal of Geophysical Research (2003), Volume 108(B4)
12. Regenauer-Lieb, K., Yuen, D. and Branlund, J.: The Initiation of Subduction: Criticality by Addition of water? In: Science (2001), Volume 294, 578-580 In: G3, Geochemistry Geophysics Geophysics (2006) Volume 7 Number 3

An Homogenization-Based Nonlocal Damage Model for Brittle Materials and Applications

Zhu Qizhi, Djimedo Kondo, and Shao Jian-fu⋆

Laboratory of Mechanics of Lille, URA CRNRS 8107, University of Lille,
Cité Scientifique, 59655 Villeneuve d'Ascq, France
`jian-fu.shao@polytech-lille.fr`

Abstract. A micromechanics-based constitutive damage model with clear physical grounds and few parameters is presented, in which the Ponte-Castaneda and Willis estimate (PCW estimate) is adopted and applied to solid matrix weaken by penny-shaped microcracks. The basic idea is to integrate the homogenization procedure into the standard thermodynamics framework. An energy release rate-based damage criterion is proposed in which the interaction effects between different cracks families are involved. The proposed constitutive model is then extended to an orientation-based nonlocal version. Finally, this model has been implemented into a finite element code and the numerical results obtained for 2D problems show its predictive capacity and mesh independent characteristics.

Keywords: Homogenization, damage, crack interaction, nonlocal.

1 Introduction

Nonlinear behavioral characteristics in brittle materials such as concrete and some rocks are commonly considered as the consequence of the nucleation and growth of microcracks [1] [2]. The modelling of the behaviors due to microcracking processes in brittle materials is a topic of great concern in many fields of civil engineering. Various material models have been developed, among which continuum damage mechanics based on the thermodynamics irreversible processes is widely used for investigation of materiral deteriorating phenomena by using one or several internal state-dependent variables [3] [4] [5]. In spite of the efficiency of model implementations and the advantages in application to engineering analysis, some of the concepts and parameters involved in these models are not clearly related to physical mechanisms [6].

For two decades, several micromechanical models have been developed for concrete and rocks [7] [8] [9], which provide a promising tool for more physically based descriptions of damage induced anisotropy and of material degradation. However, these models are often limited to dilute distribution of microcracks without consideration of interactions between microcracks. Further, most of

---

⋆ Corresponding author.

these models are not based on a rigorous upscaling method to define macroscopic properties of homogenized material. Moreover, these models without characteristic length leads to serious mesh dependency due to strain localization.

In this paper, materials weaken by microcracks are considered as a matrix-inclusions (cracks) system [10]. The physically-based homogenization scheme developed by Ponte-Castaneda and Willis is adopted, in which the inclusions' geometry and the spatial distribution can be simultaneously taken into account by means of different functions [11]. The PCW estimate is then applied to penny-shaped microcracks and integrated into the standard thermodynamics framework. In addition, a strain energy release rate based damage criterion is used to determine the damage evolution in which interactions between microcracks are involved. In order to overcome the consequences due to the strain localization, a nonlocal formulation with material length is proposed. Finally, this model is implemented into a finite element code. The numerical results obtained from 2D problems show its predictive capacity and mesh independent characteristics.

2 Model Formulations

2.1 Basic Principles of Upscaling Methods

Consider the representative elementary volume (r.e.v.), occupying a domain Ω and having a boundary surface $\partial\Omega$, as a matrix-inclusion system, solid matrix with the elasticity tensor $\mathbb{C}^s$ and inclusions with $\mathbb{C}^{c,r}, r = 1, \ldots, N$. The local behavior is assumed to be linear elastic: $\boldsymbol{\sigma}(\underline{z}) = \mathbb{C}^c(\underline{z}) : \boldsymbol{\varepsilon}(\underline{z})$ ($\forall \underline{z} \in \Omega$) with $\boldsymbol{\sigma}(\underline{z})$ and $\boldsymbol{\varepsilon}(\underline{z})$ as the local stress and strain fields, respectively. By using the superposition principle and taking the average of the local strain over Ω, the general effective (homogenized) elasticity tensor is expressed as follows:

$$\mathbb{C}^{\text{hom}} = \mathbb{C}^s + \sum_{r=1}^{N} \varphi^r (\mathbb{C}^{c,r} - \mathbb{C}^s) : \mathbb{A}^{c,r} \tag{1}$$

where φ^r is the volume fraction representing the concentration of the inclusion family r. $\mathbb{A}^{c,r}$ is so-called strain concentration tensor which relates in a linear way the local strain $\boldsymbol{\varepsilon}$ to the macroscopic uniform strain $\boldsymbol{E}$.

The determination of Eq.(1) is then summarized in determining the fourth order concentration tensor $\mathbb{A}^{c,r}$ for which we can benefit from the basic solution to the matrix-inclusion system of Eshelby's problem. For many engineering materials, it is useful to take into account both the influences of the shape of inclusions and those of its spatial distribution. For this purpose, we are interested in the homogenization scheme developed by Ponte-Castaneda and Willis in which two independent tensorial functions $\mathbb{P}^r_\epsilon$ (so-called Hill's tensor) and $\mathbb{P}_d$ are introduced to take into account the influences of the shape form of inclusions and of its spatial distribution on the material effective properties [11]. The corresponding effective (homogenized) stiffness tensor reads:

$$\mathbb{C}^{\text{hom}} = \mathbb{C}^s - \mathbb{C}^d : \left(\mathbb{I} + \mathbb{P}_d : \mathbb{C}^d\right)^{-1} \tag{2}$$

where we have in the Eshelby tensor-based form ($\mathbb{S}_\epsilon = \mathbb{P}_\epsilon : \mathbb{C}^s$):

$$\mathbb{C}^d = \sum_{j=1}^{N} \varphi^j (\mathbb{C}^s - \mathbb{C}^{c,j}) : \left[\mathbb{I} - \mathbb{S}_\epsilon^j : (\mathbb{I} - \mathbb{S}^s : \mathbb{C}^{c,j}) \right]^{-1}. \tag{3}$$

For simplicity, we adopt in this study a spherical distribution for all cracks families, which returns in considering an isotropic form for $\mathbb{P}_d$ as follows:

$$\mathbb{P}_d = \frac{\alpha}{3k^s} \mathbb{J} + \frac{\beta}{2\mu^s} \mathbb{K}; \quad \text{with} \quad \alpha = \frac{3k^s}{3k^s + 4\mu^s}; \quad \beta = \frac{6(k^s + 2\mu^s)}{5(3k^s + 4\mu^s)}. \tag{4}$$

2.2   Application to Cracked Mediums

We are now interested in microcracked materials. A family of cracks supposed to be penny-shaped in this work can be approximated as flat ellipsoids characterized by its unit normal vector (orientation) $\underline{n}$ and the aspect ratio $\frac{c}{a}$, noted ϵ, with a as the radius of the circular crack and c as the half-length of the small axis. In addition, it is possible do express the volume fraction φ^r of the rth cracks family in the form:

$$\varphi^r = \frac{4}{3} \pi a_r^2 c_r \mathcal{N}_r = \frac{4}{3} \pi \epsilon d^r \tag{5}$$

where $\mathcal{N}_r$ denotes the cracks density (number of cracks per unit volume) of the family r, and $d^r = \mathcal{N}_r a_r^3$ is the crack damage parameter widely used as internal variables in micromechanical analysis [12].

The elasticity tensor $\mathbb{C}^c$ for open cracks is classically defined by $\mathbb{C}^c = 0$ to account for the cancellation of the stress on the crack faces. On the basis of the definition for damage parameters, the forth order tensor $\mathbb{C}^d$ in (3) is rewritten in the following form:

$$\mathbb{C}^d = \sum_{j=1}^{N} d^r \mathbb{T}^r \tag{6}$$

where, considering the assumption of small aspect ratio ($\epsilon \ll 1$), $\mathbb{T}^r$ reads for open cracks

$$\mathbb{T}^r = \frac{4}{3} \pi \mathbb{C}^s : \lim_{\epsilon \to 0} \epsilon (\mathbb{I} - \mathbb{S}_\epsilon^r)^{-1}. \tag{7}$$

The expression of $\mathbb{T}^r$ in the Walpose's base are given in [13]. For simplifying later formulations, it is convenient to rewrite Eq.(2) in the form:

$$\mathbb{C}^{\text{hom}} = \mathbb{C}^s - \mathbb{C}^d + \mathbb{C}^d : \mathbb{B} : \mathbb{C}^d \tag{8}$$

in which we put $\mathbb{B} = \left(\mathbb{I} + \mathbb{P}_d : \mathbb{C}^d \right)^{-1} : \mathbb{P}_d$. The macrosocpic stress-strain relation is then given by derivation of the macroscopic free energy $W (= \frac{1}{2} \boldsymbol{E} : \mathbb{C}^{\text{hom}} : \boldsymbol{E})$ with respect to $\boldsymbol{E}$:

$$\boldsymbol{\Sigma} = \frac{\partial W}{\partial \boldsymbol{E}} = \mathbb{C}^{\text{hom}} : \boldsymbol{E}. \tag{9}$$

The conjugate thermodynamic force associated with any damage variable d^r is defined by:

$$F^{d^r} = \frac{1}{2}\boldsymbol{E} : \mathbb{T}^r : \boldsymbol{E} - \frac{1}{2}\boldsymbol{E} : (\mathbb{T}^r : \mathbb{B} : \mathbb{C}^d + \mathbb{C}^d : \mathbb{B} : \mathbb{T}^r) : \boldsymbol{E}$$
$$+ \frac{1}{2}\boldsymbol{E} : \mathbb{C}^d : \mathbb{B} : \mathbb{T}^r : \mathbb{B} : \mathbb{C}^d : \boldsymbol{E}. \quad (10)$$

2.3   Damage Criterion and Evolution Law

In the framework of thermodynamics, the damage criterion should be determined as a function of the conjugate force F^{d^r} on the basis of experimental evidences. However the determination of such a criterion is usually not easy. Note that the expression of F^{d^r} contains two linear terms in $\mathbb{T}^r$, $\mathbb{C}^d$ and $\mathbb{B}$, and one high order term. For the sake of simplification, only the two linear terms are used in damage driving force.

Denoting $\tilde{F}^{d^r}$ the first two terms of (10)

$$\tilde{F}^{d^r} = \frac{1}{2}\boldsymbol{E} : \mathbb{T}^r : \boldsymbol{E} - \frac{1}{2}\boldsymbol{E} : (\mathbb{T}^r : \mathbb{B} : \mathbb{C}^d + \mathbb{C}^d : \mathbb{B} : \mathbb{T}^r) : \boldsymbol{E}, \quad (11)$$

the following simple damage criterion is proposed:

$$f(\tilde{F}^{d^r}, \underline{d}) = \tilde{F}^{d^r} - \mathcal{R}(d^r) \leq 0 \quad (12)$$

where $\mathcal{R}(d^r)$ is the local resistance against the damage propagation. $\mathcal{R}(d^i) = c_0 + c_1 d^r$ is adopted in this work, with c_0 and c_1 being two material constants.

Following the theoretical framework of generalized standard materials, we adopt the normality rule in determination of damage evolutions:

$$\dot{d}^r = \dot{\lambda}^{d^r} \frac{\partial f^r(\tilde{F}^{d^r}, d^r)}{\partial \tilde{F}^{d^i}} = \dot{\lambda}^{d^r} \quad ; \quad \dot{\lambda}^{d^r} \geq 0 \quad (13)$$

where the damage multiplier $\dot{\lambda}^{d^r}$ is determined by the consistency conditions $\dot{f}^r = 0$, $r = 1, \ldots, N$ for all considered families [13].

3   Nonlocal Formulation

It is commonly recognized that the strain softening or damage-induced strength degradation can be localized into a band of zero thickness with paradoxical consequences of structural failure with zero energy dissipation. In order to overcome this shortcoming in continuum models without characteristic length, the so-called non local approaches are widely used. The basic idea consists in replacing the local damage force $\tilde{F}^{d^r}$ for all considered families with its average over a representative volume V of the material centered at a given point [14]. The damage variable d^r is then function of the non local driving force $\overline{\tilde{F}^{d^r}}$ which will be defined as:

$$\overline{\tilde{F}^{d^r}}(x) = \int_V \varpi(x, y)\tilde{F}^{d^r}(y)dV(y). \quad (14)$$

In Eq.(14), $\varpi(x,y)$ is a space weight function which describes the mutual nonlocal interactions and depends only on the distance between the source point x and the receiver point y. Mathematically, the normalization condition $\int_V \varpi(x,y)dV = 1$ is required for a uniform field. In this study, we adopt the following Gauss-type weighting function,

$$\varpi(x,y) = \left(\frac{1}{l\sqrt{2\pi}}\right)^{N_{dim}} \exp\left(-\frac{\|x-y\|^2}{2l^2}\right) \tag{15}$$

where N_{dim} is the number of spatial dimensions and l is a material characteristic length which defines the size of interaction zone for failure processes. The factor $\left(\frac{1}{l\sqrt{2\pi}}\right)^{N_{dim}}$ is used to satisfy the normalization condition.

4   Numerical Applications

4.1   3-Point Bending Test

Three-point bending test represents a structural case which may emphasize more practical issues in terms of complexity and size when it comes to industrial structures. The geometry and the loading condition of this test are shown in Fig. 1. The parameters used in the analysis are as follows: $E^s = 3.7 \times 10^4$MPa, $c_0 = 1. \times 10^{-3} J.m^{-2}$ and $c_1 = 5. \times 10^{-4} J.m^{-2}$. The structure is discretesized respectively by 560 and 990 rectangle elements with 320 and 504 elements in the zone $|x| \leq 50mm$, respectively. The force-displacement relations and the global damage distribution diagrams for the two meshes are shown and compared respectively in Fig. 2 and Fig. 3, from which mesh independent properties are observed. This kind of result is in agreement with most experimental data reported in literature.
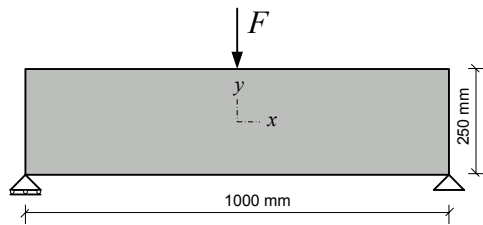
Fig. 1. Geometry and loading condition of the 3-point bending test

4.2   Hassanzadeh's Direct Tension Test

The second numerical application of the proposed model concerns a direct traction test performed by Hassanzadeh on a four-side notched concrete sample [15]. The geometric description of the notched sample and the loading condition are
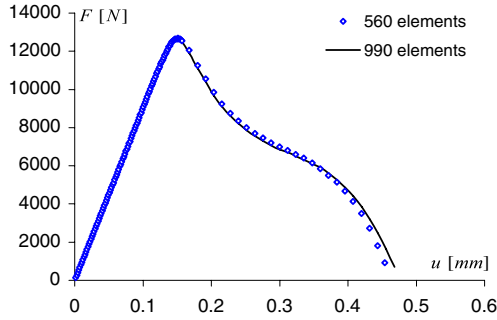
Fig. 2. Comparisons of the force-displacement response curves
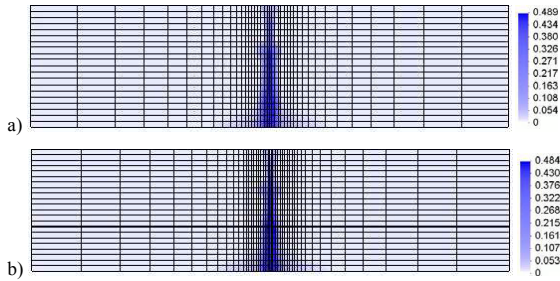
Fig. 3. Final global damage distributions for the two meshes: a) 560 meshes and b) 990 meshes
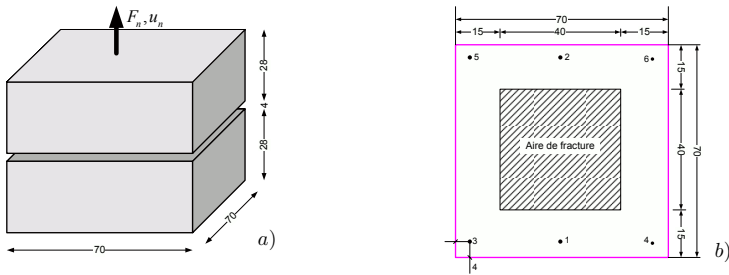
Fig. 4. Geometry (in mm) and loading condition of the Hassanzadeh test: a) geometry of the structure; b) geometry of the notches

indicated in Fig. 4. The hypothesis of plane strain condition is adopted for the numerical analysis.

In order to study the mesh sensitivity of the proposed nonlocal micromechanics based model, two different meshes are considered: the first discretization with 960 rectangular elements and the second one with 1512 elements which is obtained by refining the discretization in the central fracture zone. The material
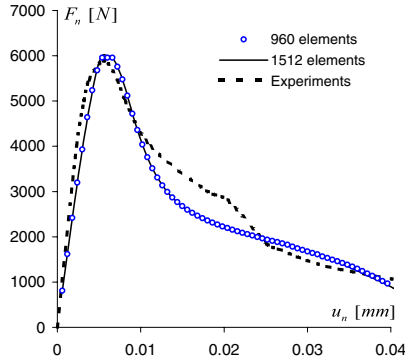
Fig. 5. Force-displacement response curves and comparisons to the experimental data reported in [15]
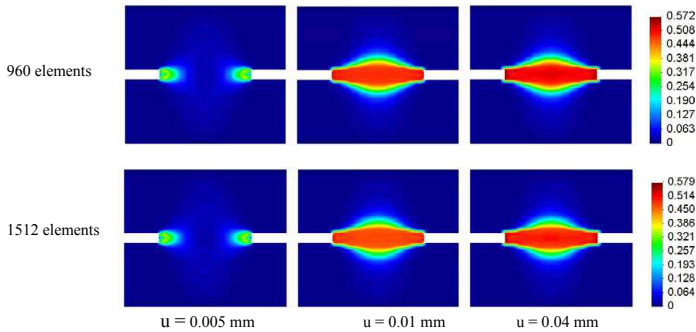
Fig. 6. Distributions of the global damage at three displacement levels for the two meshes

constants and model parameters are: $E^s = 3.6 \times 10^4 \text{MPa}$, $c_0 = 7.5 \times 10^{-4} J.m^{-2}$ and $c_1 = 1. \times 10^{-3} J.m^{-2}$.

Fig. 5 shows the force-displacement curves for the two meshes which are compared to the experimental data reported by Hassanzadeh [15]. The global damage distributions at three different values of imposed displacements are presented and compared for the considered meshes in Fig. 6. It can be seen a good agreement between the numerical results and experimental data. Further, the mesh independency of numerical prediction is again observed.

5   Conclusions

In this study, we present a new homogenization-based damage model with few parameters. The micromechanical grounds provide the proposed model the capacity of dealing with main physical aspects such as unilateral effects related to cracks closures, the crack spatial distribution and interaction effects between mi-

crocracks, which are generally neglected in widely-used macroscopic models. The constitutive model is extended to the nonlocal version and implemented into a finite element program. The numerical applications to concrete structures show that the proposed micromechanics based model provides a promising tool to further capture and model the complex mechanical behaviors and failure process in quasi brittle materials.

References

1. Kranz, R.L.: . Microcracks in rocks: a review, Tectonophysics, 100(1983) 449-480
2. Zhao, Y.: Crack pattern evolution and a fractal damage constitutive model for rock. International Journal of Rock Mechanics and Mining Sciences, 35(1998) 349-366 W
3. Murakami, S., Kamiya,K.: . Constitutive and damage evolution equations of elastic brittle materials based on irreversible thermodynamics. International Journal of Mechanical Science. 39(1996) 473-486
4. Halm, D., Dragon, A.: A model of anisotropic damage by mesocrack growth: unilateral effect. Int. J. Damage Mech. 5(1996) 384-402
5. Swoboda, G., Yang, Q.: An energy-based damage model of geomaterials I and II: deduction of damage evolution laws. Int. J. Solids Structures. 36(1999) 1735-1755
6. Dragon, A., Halm, D.: Damage Mechanics. Some modelling challenges. Institute of Fundamental Technological Research, Polysh Academy of Science, Editeur: IPPT PAN, Warsaw, Poland. (2004)
7. Andrieux, S., Bamberger, Y., Marigo, J.J.: Un modèle de matériau microfissuré pour les roches et les bétons. Journal de mécanique théorique et appliquée. 5(1986) 471-513
8. Gambarotta, L., Lagomarsino, S.: A microcrak damage model for brittle materials. International Journal of Solids and Structures. 30(1993) 177-198
9. Pensée, V., Kondo, D., Dormieux, L.: Micromechanical analysis of anisotropic damage in brittle materials. Journal of Engineering Mechanics, ASCE. 128(2002) 889-897
10. Eshelby, J.D.: The determination of the elastic field of an ellipsoidal inclusion and related problems. Proc. R. Soc. Lond. A. 241(1957) 375-396
11. Ponte-Castaneda, P., Willis, J.R.: The effect of spatial distribution on the behavior of composite materials and cracked media. Journal of the Mechanics and Physics of Solids. 43(1995) 1919-1951
12. Budiansky, B., O'Connel, J.R.: Elastic moduli of a cracked solid. International Journal of Solids and Structures. 12(1976) 81-97
13. Zhu, Q.Z.: Applications des approches d'homogénéisation à la modélisation tridimensionnelle de l'endommagement des matériaux quasi fragile : Formulation, validation et implémentation numérique. Ph.D. Thesis (in French), University of Lille I, France. (2006)
14. Pijaudier-Cabot, G., Bazant, Z.P.: Nonlocal Damage Theory. Journal of Engineering Mechanics. 113(1987) 1512-1533
15. Hassanzadeh, M.: Behavior of fracture process zones in concrete influenced by simultaneously applied normal and shear displacements, Ph.D. Thesis Lund Institute of Technology, Lund. (1991)

An Elastoplastic Hydro-mechanical Model for Unsaturated Soils

De'an Sun and Li Xiang

Department of Civil Engineering, Shanghai University, 149 Yanchang Road,
Shanghai 200072, China
`Sundean06@163.com`

Abstract. This paper presents a coupled elastoplastic constitutive model for predicting the hydraulic and stress-strain-strength behaviour of unsaturated soils. Hydraulic hysteresis in the water-retention behaviour is modeled as an elastoplastic process with the elastic region of the saturation degree. The effect of change in degree of saturation on the stress-strain-strength behaviour and the effect of change in void ratio on the water-retention behaviour are taken into consideration in the model, in addition to the effect of suction on the hydraulic and mechanical behaviour. Model predictions of the stress-strain and water-retention behaviour are compared with those obtained from triaxial tests on unsaturated soil along isotropic compression, triaxial stress paths with or without variation in suction.

Keywords: Unsaturated soil, elastoplastic model, water-retention curve, suction, triaxial test.

1 Introduction

Since the model was proposed by Alonso et al. [1], several elastoplastic constitutive models for unsaturated soils have been proposed, on both the experimental and theoretical studies. In the early models, the stress state variables employed in most models for unsaturated soils are the net stress (the difference between total stress and pore-air pressure) and the suction (the difference between pore-air pressure and pore-water pressure). In these models, the influence of unsaturation on the soil behaviour is considered through the variable of suction and the degree of saturation is computed from the suction using the soil-water characteristic curve. Hydraulic hysteresis which accounts for irreversible behaviour between the suction and the saturation is usually not considered in these constitutive models. Another shortcoming of these models is related to their implementation into existing finite element codes for saturated soils where constitutive relations are always described in terms of effective stresses. As discussed by Sheng et al [4], using the average skeleton stress and the suction as the stress variables leads to a convenient implementation of unsaturated soil models into finite element codes working with effective stresses, whereas using the net stress and the suction is more appropriate for finite element codes working with total stress.

In recent years, some conceptual models incorporating hydraulic hysteresis of unsaturated soils have been proposed [2][4][7]. However, most of these models can only describe the coupled hydro-mechanical behaviour in qualitative terms or are only formulated for isotropic stress conditions. This paper presents a complete mathematical formulation of an elastoplastic model for the hydraulic and mechanical behaviour of unsaturated soils, especially incorporating the effect of the deformation on the water-retention behaviour. The model performance is then validated quantitatively by experimental results obtained from suction-controlled triaxial tests on unsaturated compacted soil along various stress paths.

2   Coupled Hydro-mechanical Model for Unsaturated Soils

2.1   Stress-State Variable for Unsaturated Soils

To identify the hydraulic and mechanical behaviour of unsaturated soils properly, the stress-state variables employed in the model are the average skeleton stress σ'_{ij} and the suction s. The average skeleton stress σ'_{ij} is defined as:

$$\sigma'_{ij} = \sigma_{ij} - u_a \delta_{ij} + S_r s \delta_{ij} \ . \tag{1}$$

where σ_{ij} is the total stress tensor, S_r is the saturation degree, u_a is the pore-air pressure, and δ_{ij} is the Kronecker delta. Eq. (1) is similar to the effective stress proposed by Bishop [2], with S_r taking the place of the weighting factor χ. The average skeleton stress and the suction are not independent variables, but their work-conjugate strains (soil skeleton strains and the degree of saturation) are independent variables [4]. The average skeleton stress and suction variables adopted in the present study permit a general form of hydraulic behaviour to be represented and also provide a smooth transition between the saturated and unsaturated states.

2.2   Formulation of the Elastoplastic Model for Isotropic Stress States

In previous work, the author developed a so-called 'load-collapse' (LC) yield curve in the p-s plane for the isotropic stress [6]. A similar form is adopted in the following equation, except that the average skeleton stress is new defined as per Eq. (1).

$$p'_y = p'_n \left(\frac{p_{0y}}{p'_n} \right)^{\frac{\lambda(0)-\kappa}{\lambda(s)-\kappa}} \ . \tag{2}$$

where p_{0y} and p'_y are the yield stresses for saturated soil and unsaturated soil with suction s; p'_n is an isotropic stress at which no collapse occurs when the suction is decreased; κ is a swelling index for unsaturated soils (including saturated soil in the e-ln p' plane); and $\lambda(0)$ and $\lambda(s)$ are the slopes of the normal compression lines of

saturated soil and unsaturated soil with suction s in the e-ln p$^{'}$ plane. The quantity $\lambda(s)$ is assumed as:

$$\lambda(s) = \lambda(0) + \frac{\lambda_s s}{s + p_a} \quad .$$

(3)

where λ_s is a material parameter for identifying the change of $\lambda(s)$ with suction s. $\lambda(s)$ in Eq.(3) has the following feature: when $s \to \infty$, $\lambda(s) = \lambda(0) + \lambda_s$.
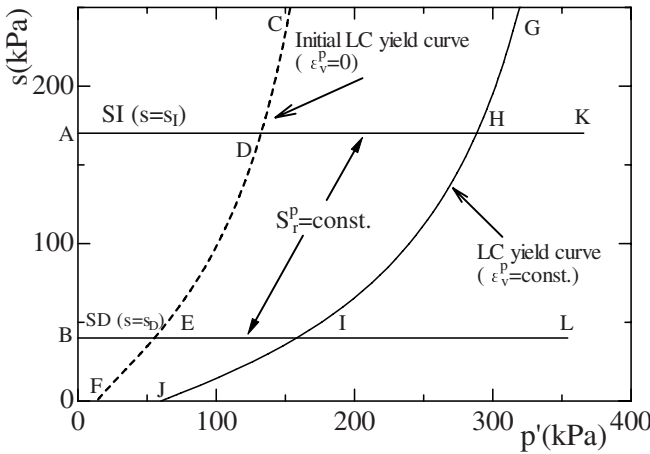
Fig. 1. LC yield curve, SI and SD yield curves for compacted Pearl-clay under isotropic stress states

The initial LC yield curve CDEF and the subsequent LC yield curve GHIJ in Fig. 1 are depicted using Eqs (2) and (3), and values of the model parameters and the initial state for compacted Pearl-clay, which are given later. When the stress state ($p^{'}$, s) is on the left side of CDEF, there is only elastic deformation occurring during the stress change.

From Eq. (2) we have

$$dp_y^{'} = \frac{\partial p_y^{'}}{\partial p_{0y}} dp_{0y} + \frac{\partial p_y^{'}}{\partial s} ds \, .$$

(4)

When the stress state is inside the LC yield curve, the elastic volumetric strain increment is given by:

$$d\varepsilon_v^e = \frac{\kappa dp^{'}}{(1+e)p^{'}} \, .$$

(5)

When the stress state is on the LC yield curve and its increment vector points to the right side of the LC yield curve, the plastic volumetric strain increment is given by:

$$d\varepsilon_v^p = \frac{(\lambda(0)-\kappa)dp_{0y}}{(1+e)p_{0y}} \quad . \tag{6}$$

Or, from Eqs (4) and (6):

$$d\varepsilon_v^p = \frac{\lambda(0)-\kappa}{(1+e)p_{0y}}(dp_y' - \frac{\partial p_y'}{\partial s}ds)/\frac{\partial p_y'}{\partial p_{0y}} . \tag{7}$$

In addition to the LC yield curve, two more yield curves are needed to model hydraulic behaviour as an elastoplastic process, as shown in Fig. 1. The water-retention behaviour is represented by a suction increase (SI) yield curve and a suction decrease (SD) yield curve. The water-retention curve is assumed as Fig. 2.
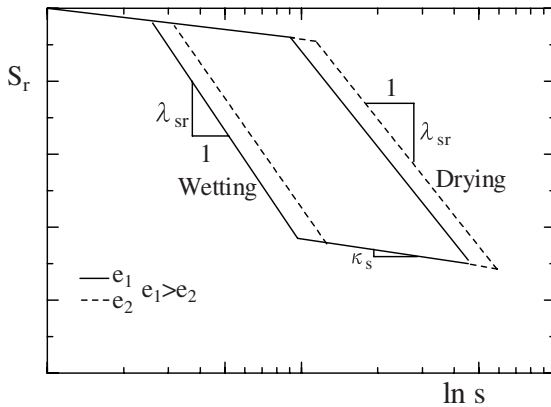
Fig. 2. Model for water retention behaviour at diffferent void ratios

The change in the degree of saturation due to the change in void ratio is attributed to the elastic part of the increment of the degree of saturation. When the change in the degree of saturation is elastic, i.e. along the scanning curves, the elastic increment of the degree of saturation can be derived from Eq. (1) as follows:

$$dS_r^e = -\lambda_{se}de - k_s\frac{ds}{s} . \tag{8}$$

The plastic change in the degree of saturation can expressed as:

$$dS_r^p = dS - dS_r^e = (\lambda_{sr} - k_s)\frac{ds}{s} . \tag{9}$$

From the condition $dS_r^p = 0$ we can obtain the following SI and SD yield curves as

$$f_{SI} = \ln(s_1) + c_1 . \text{ (for SI)} \tag{10}$$

$$f_{SD} = \ln(s_D) + c_2 . \text{ (for SD)} \tag{11}$$

where c_1 and c_2 are integration constants.

For a given plastic change in S_r, the SI and SD curves can be drawn as shown in Fig. 1. The SI curve AK is stems from Eq. (12), while the SD curve BL follows from Eq. (13). The plastic volumetric strain ε_v^p is equivalent along the same LC yield curve, with the plastic change in S_r being equivalent along the same SI curve or the same SD curve. Therefore, as shown in Fig. 1, there are six zones with different yielding characteristics for ε_v^p and dS_r^p.

2.3   Formulation of the Elastoplastic Model for General Stress States

The Modified Cam-clay model has been used extensively for saturated soils, and gives reasonably good predictions for clays. This model is adopted here because it is simple. Assuming an associated flow rule, the yield function (*f*) and the plastic potential function (*g*) are proposed to have the following form:

$$f = g = q'^2 + M^2 p'(p' - p_y') = 0 . \tag{12}$$

The associated flow rule is obeyed in the 'effective stress' space; that is:

$$d\varepsilon_{ij}^p = \Lambda \frac{\partial f}{\partial \sigma_{ij}'} . \tag{13}$$

where the proportionality constant Λ can be determined from the consistency condition. Eq. (12) can be rewritten as $f = f(p', q', p_y') = 0$, leading to:

$$df = \frac{\partial f}{\partial p'} dp' + \frac{\partial f}{\partial q'} dq' + \frac{\partial f}{\partial p_y'} dp_y' = 0 . \tag{14}$$

Substituting Eq. (4) into Eq. (14) and re-arranging gives:

$$df = \frac{\partial f}{\partial p'} dp' + \frac{\partial f}{\partial q'} dq' + \frac{\partial f}{\partial p_y'} \frac{\partial p_y'}{\partial p_{0y}} dp_{0y} + \frac{\partial f}{\partial p_y'} \frac{\partial p_y'}{\partial s} ds . \tag{15}$$

where the isotropic yielding stress p_{0y} for saturated soil is related to the volumetric strain ε_v^p and is the same as that used in the traditional Cam-clay model. Because the plastic volumetric strain ε_v^p is a hardening parameter in the present model, the

volumetric plastic strains $d\varepsilon_v^p$ caused by dp_{0y} in a saturated soil are the same as those in an unsaturated soil which are caused by $dp_y^{'}$ and/or ds . Allowing for Eq. (13), the following is obtained:

$$dp_{0y} = \frac{1+e}{\lambda(0)-\kappa} p_{0y} d\varepsilon_v^p = \frac{1+e}{\lambda(0)-\kappa} p_{0y} \Lambda \frac{\partial f}{\partial p'}. \tag{16}$$

Substituting Eq. (16) into Eq. (15) and solving for Λ gives:

$$\Lambda = -\frac{\dfrac{\partial f}{\partial p'} dp' + \dfrac{\partial f}{\partial q'} dq' + \dfrac{\partial f}{\partial p_y^{'}} \dfrac{\partial p_y^{'}}{\partial s} ds}{\dfrac{\partial f}{\partial p_y^{'}} \dfrac{\partial p_y}{\partial p_{0y}} p_{0y} \dfrac{1+e}{\lambda(0)-\kappa} \dfrac{\partial f}{\partial p'}}. \tag{17}$$

From Eqs (13) and (17), it is possible to calculate the plastic strain increments caused by the increment in the 'effective stress' and/or the decrement in suction.

Following the formulation in plasticity, the plastic increment of S_r is written as

$$dS_r^p = \Lambda_\alpha \frac{\partial f_\alpha}{\partial s}. \ (\alpha = SI, SD) \tag{18}$$

where Λ_α are plastic multipliers. From Eqs (11) and (12), we have

$$\frac{\partial f_{SI}}{\partial s} = \frac{1}{s_I} ; \ \frac{\partial f_{SD}}{\partial s} = \frac{1}{s_D} \tag{19}$$

Substituting Eq (19) into Eq (18) and then comparing with Eq (9) gives

$$\Lambda_{SI} = \Lambda_{SD} = (\lambda_{sr} - \kappa_s) ds \tag{20}$$

3 Model Predictions Versus Experimental Results

The model requires five parameters to describe the stress-strain behaviour ($\lambda(0), \lambda_s, \kappa, p_n^{'}$ and M) and three parameters to describe the water-retention behaviour (λ_{sr}, κ_s and λ_{se}).

We have performed a series of triaxial tests on unsaturated Pearl clay with suction control. Details of the Pearl clay properties, specimen preparation, and testing procedure can be found in the previous works of Sun et al. [5], which provides information about the stress-strain behaviour of Pearl clay, but do not give details of the measured water-retention behaviour. These are given below together with the model predictions. The model parameters for compacted Pearl clay are as follows: $\lambda(0) = 0.12, \kappa = 0.03, \lambda_s = 0.12, p_n^{'} = 2MPa, M = 1.15$ and $\lambda_{se} = 0.35, \lambda_{sr} = 0.1, \kappa_s = 0.01$.

(a) Stress-strain response

(b) Deformation and hydraulic response
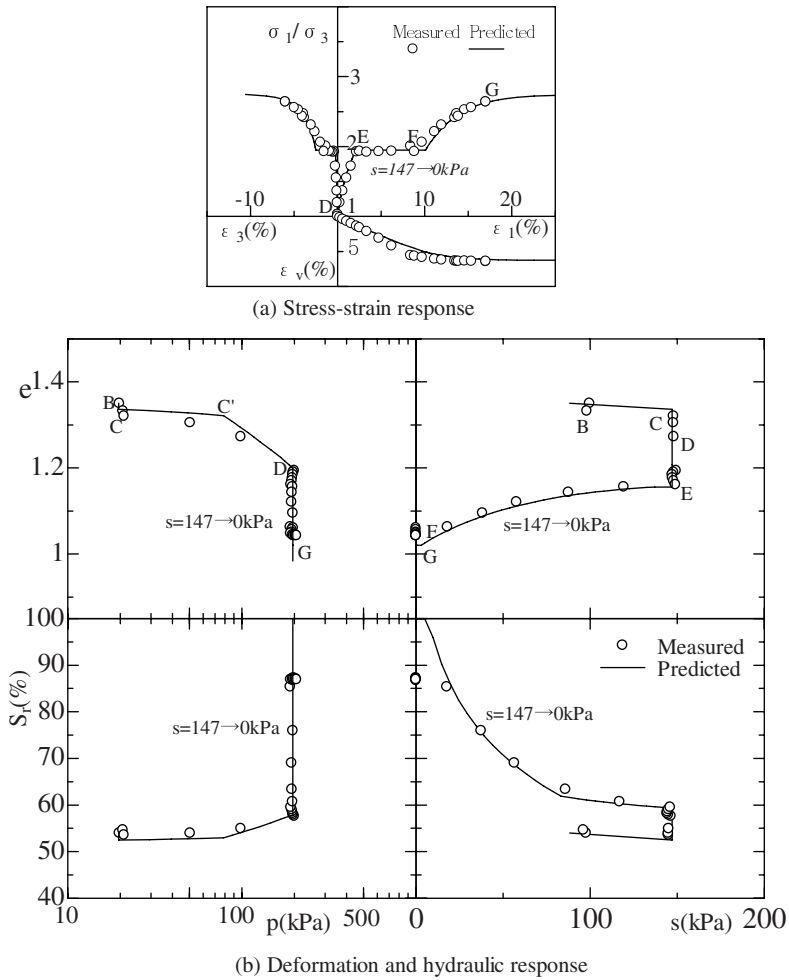
Fig. 3. Predicted and measured results of triaxial compression test under s=147kPa, wetting (s=147kPa→0kPa) and zero suction (s=0kPa) and p=196kPa

Figure 3 shows predicted and measured results of isotropic compression, triaxial shear and wetting tests. The stress paths consist of CC'D (isotropic compression with constant suction s of 147kPa), DE (triaxial compression with constant mean net stress p of 196kPa and s=147kPa), EF (wetting from s=147kPa to 0kPa under p=196kPa and principal stress ratio of 2.0), and FG (triaxial compression under p=196kPa and s=0kPa). It can be seen the model predicts well not only the stress-strain relationship but also hydraulic characteristics of unsaturated compacted clay.

Figure 4 shows predicted and measured results of triaxial tests on unsaturated compacted Pearl clay with almost the same initial void ratio but different degrees of
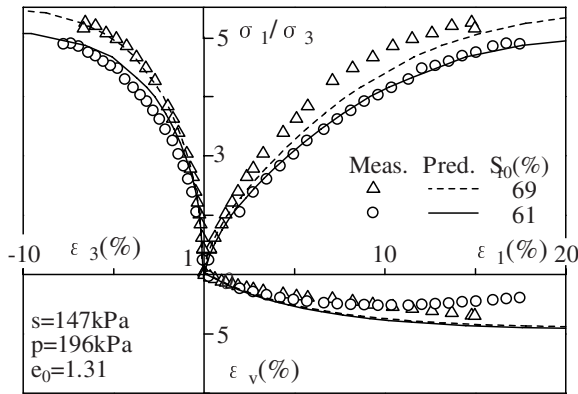
Fig. 4. Predicted and measured results of triaxial compression tests with different degrees of saturation

saturation (S_{r0}) at the beginning of triaxial shear tests. The measured stress-strain relationship and strength are different due to different degrees of saturation before loading even if the initial density and imposed net stress path and suction are the same. Hence, the mechanical behaviour of unsaturated soils depend not only the net stress and suction but also the degree of saturation. It can be seen from Fig. 4 that our model can predict the unsaturated soil behaviour.

4   Concluding Remarks

A coupled elastoplastic constitutive model is proposed for predicting the hydraulic and stress-strain-strength behaviour of unsaturated soils, and the predicted and measured results of triaxial tests were compared to validate the model.

References

1. Alonso F.E., Gens A., Josa A.: A constitutive model for partially saturated soils, Geotechnique 1990; 40(3): 405-430.
2. Bishop A. W. : The principal of effective stress, Teknisk Ukeblad, 1959, 39, 859-863.
3. Buisson M.S.R., Wheeler S.J.: Inclusion of hydraulic hysteresis in a new elastoplastic framework for unsaturated soils. In: Tarantino A. and Mancuso C. (eds): Experimental Evidence and Theoretical Approaches in Unsaturated Soils, Balkema (2000) 109-1119.
4. Sheng D.C., Sloan S.W., Gens A.: A constitutive model for unsaturated soils: thermomechanical and algorithmic aspects. Computational Mechanics 2004; 33: 453-465.
5. Sun D.A., Matsuoka H, Xu Y.F.: Collapse behavior of compacted clays by suction-controlled triaxial tests. ASTM Geotechnical Testing Journal 2004; 27(4): 1-9.
6. Sun D.A., Matsuoka H., Yao Y.P., Ichihara W.: An elastoplastic model for unsaturated soil in three-dimensional stresses. Soils and Foundations 2000; 40(3): 17-28.
7. Wheeler S.J., Sharma R.S., Buisson M.S.R.: Coupling of hydraulic hysteresis and stress-strain behaviour in unsaturated soils, Geotechnique 2003; 53(1):41-54.

An Elastoplastic Model Considering Sand Crushing

Yangping Yao[1], Naidong Wang[1], Haruyuki Yamamoto[2], and Huilin Xing[3]

Department of Civil Engineering, Beihang University,
Beijing 100083, P.R. China
ypyao@buaa.edu.cn,wangnd@ce.buaa.edu.cn
Graduate School for International Development and Cooperation, Hiroshima University,
Higashi-Hiroshima 739-8529, Japan
yamamoto@idec.hiroshima-u.ac.jp
Earth Systems Science Computational Center, University of Queensland,
St Lucia, Brisbane, QLD 4072, Australia
xing@esscc.uq.edu.au

Abstract. The behavior of sand crushing will appear when the confining pressure is up to a certain value, which results in disappearing of the positive dilatancy of sand. Adopting a new hardening parameter with the crushing stress, an elastoplastic constitutive model considering sand crushing is proposed. Comparing the conventional triaxial compression test results with the model prediction, it shows that the proposed model can reasonably describe the dilatancy of sand from positive to negative.

Keywords: Crushing, Elastoplastic model, Hardening, Sand, Dilatancy.

1 Introduction

Many triaxial experiments[1,2] indicate that sand presents crushing at a high confining stress, which results in positive dilatancy at low confining stress and negative dilatancy at high confining stress. The peak strength of sand also decreases with the confining stress increasing. Therefore, it is necessary to develop an elastoplastic constitutive model to describe the mechanical behavior of sand crushing.

2 The Model Considering Sand Crushing

Referencing the work by Sun et al.[3], Nakai[4], Yao and Luo[5], the relationship between the elastoplastic volumetric strain ε_v^p (or ε_v^e) and the mean stress p under isotropic consolidation condition could be assumed as Eqs.(1) and (2):

$$\varepsilon_v^e = C^e \left[\left(p/p_a \right)^m - \left(p_0/p_a \right)^m \right] \tag{1}$$

$$\varepsilon_v^p = \left(C^{ep} - C^e \right) \left[\left(p/p_a \right)^m - \left(p_0/p_a \right)^m \right] \tag{2}$$

where p_0 is the initial mean stress, p_a is the atmospheric pressure, C^{ep} is the compression index, C^e is the swelling index and m is a coefficient for sand. There are two examples shown as Fig.1.
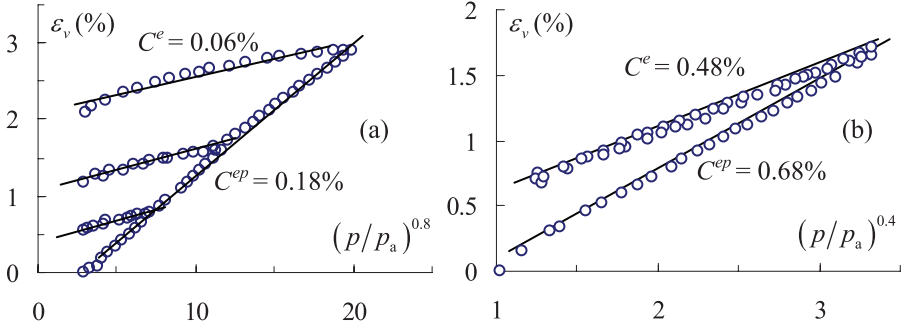
Fig. 1. The loading-unloading tests of isotropic compression, which of cement sand is shown in panel(a), Toyoura sand in panel(b)

Revising the hardening parameter[6,7] developed by Yao et al. as

$$H = \int dH = \int \Theta d\varepsilon_v^p = \int \frac{M_{pt}^4}{M_f^4} \frac{M_f^4 - \eta^4}{M_{pt}^4 - \eta^4} d\varepsilon_v^p \tag{3}$$

$$M_f = M\left(p/p_c\right)^{-n} \tag{4}$$

$$M_{pt} = M\left(p/p_c\right)^{n} \tag{5}$$

in which M_{pt} is the stress ratio at characteristic point, M_f the stress ratio at shear failure, M the stress ratio at critical state, η the stress ratio($\eta=q/p$), p_c the crushing stress, n a material parameter of sand ($0<n<1$). The parameters of proposed model are M, p_c and n. In the proposed model, the equations of the yield locus and plastic potential are similar to the modified Cam-clay model's[8,9] on the p-q plane. Adopt the revised hardening parameter H with crushing stress p_c to replace the plastic volumetric strain ε_v^p in Cam-clay model. The yield function is given as

$$\left(C^{ep} - C^e\right)\left(\frac{p_0}{p_a}\right)^m \left[\left(\frac{p}{p_0} + \frac{q^2}{M^2 p p_0}\right)^m - 1\right] - H = 0 \tag{6}$$

The stress-dilatancy equation is expressed as

$$d\varepsilon_v^p / d\varepsilon_d^p = (M_{pt}^2 - \eta^2)/2\eta \tag{7}$$

3   Prediction Versus Experiments

The following seven soil parameters used in the proposed model: C^e, C^{ep}, m, M, p_c, n and the poisson coefficient v, all of which can be determined via TC tests. The parameters C^e, C^{ep} and m are confirmed at isotropic consolidation conditions as in Fig.1. The parameters M, p_c and n are determined by drained triaxial compression tests at different initial stresses. The model parameters for Toyoura sand are listed in Tab.1 and the value of atmospheric pressure p_a is given as 0.1MPa.

Table 1. There are seven parameters required for the proposed model

Isotropic consolidation	Triaxial compression	Elastic poisson
C^e = 0.0046 C^{ep} = 0.0068 m = 0.4	M = 1.35 p_c = 5.9MPa n = 0.103	v = 0.3
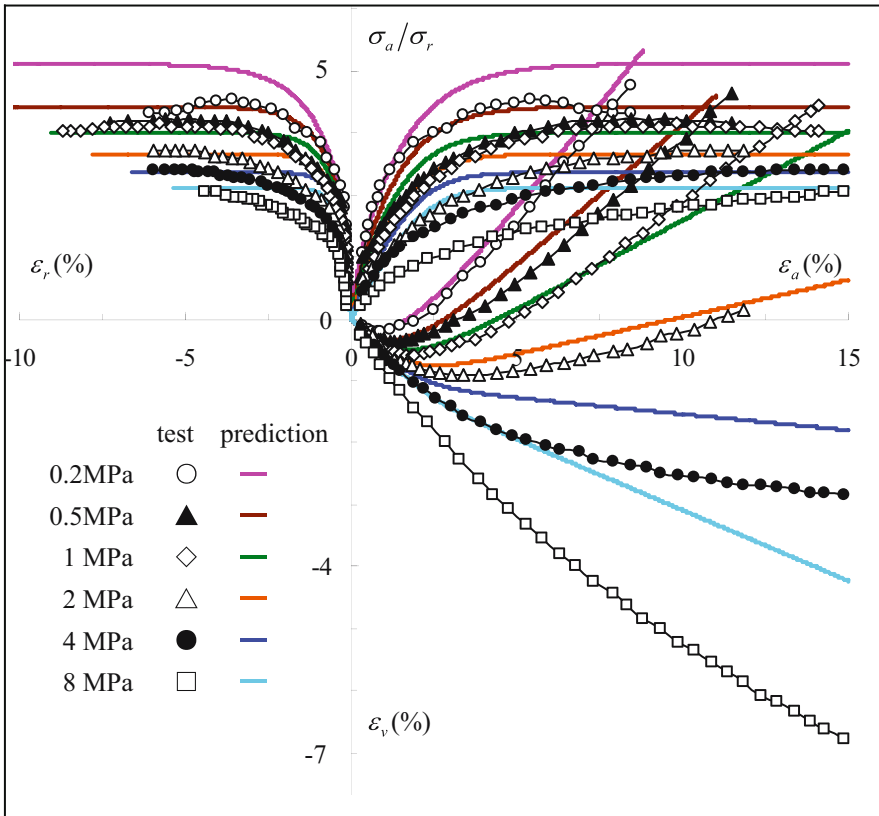
Fig. 2. The test results (data after Sun et al.[10]) and the predicted stress-stain curves by proposed models in this paper

The test results and the predicted relationships between axial strain ε_a, radial strain ε_r, volumetric strain ε_v and principal stress radio σ_a / σ_r are shown in Fig.2.

Analyzing the prediction results as shown in Fig.2, it can be seen that: ①The predicted curves by the proposed model agree well with the test results for Toyoura sand under conventional triaxial compression conditions except the ε_a-ε_v curves at p=4, 8MPa. ②When the confining stress of sand rises, the strength (peak principal stress ratio) decreases. ③When the confining stress of sand rises, the volumetric dilatant degree of sand decreases.

4   Conclusions

(1)Because of the behavior of sand crushing, the peak principal stress ratio and the degree of positive dilatancy for conventional triaxial compression tests both decrease when the confining stress rises. The dilatancy will disappear when the confining stress is larger than the crushing stress.

(2)The proposed elastoplastic constitutive model, adopting the new hardening parameter revised by the crushing stress, can reasonably describe the stress-strain behavior and the dilatancy of sand.

Acknowledgements

References

1. Daouadji, A., Hicher, P.Y., Rahma, A.: An elastoplastic model for granular materials taking into account grain breakage, Eur.J. Mech. A/Solids 20(2001)113-137
2. Fukumoto, T.: Particle breakage characteristics of granular soils, Soils and Foundations, 1992,32(1):26-40
3. Sun, D.A., Matsuoka, H., Yao, Y.P., Ichimura, M.: A transformed stress based on extended SMP criterion and its application to elastoplastic model for geomaterials, Proc. of JSCE, 2001, No.680/III-55: 211-224 (in Japanese)
4. Nakai, T.: An isotropic hardening elastoplastic model considering the stress path dependency in three-dimensional stresses, Soil and Foundations,1989, 29(1):119-139
5. Yao, Y.P., Luo, T.: New transformed stress space and its application, Proc. of 7th Numerical Calculation and Analysis on Geomechanics, Dalian: Dalian University of Technology Press, 2001, 16-22(in Chinese)
6. Matsuoka, H., Yao, Y.P., Sun, D.A.: The Cam-clay models revised by the SMP criterion, Soils and Foundations, 1999,39(1):81-95
7. Yao, Y.P., Luo, T., Sun, D.A., Matsuoka, H.: A simple 3-D constitutive model for both clay and sand, Chinese Journal of Geotechnical Engineering, 2002, 24(2):240-246
8. Roscoe, K.H., Burland, J.B.: On the generalized stress-strain behavior of 'wet' clay. Heyman J, Leckie F A. Engineering Plasticity. Cambrige: Cambrige University Press, 1968. 535-609

9. Wroth, C.P., Houlsby, G.T.: Soil mechanics-property characterization and analysis procedures. Proceedings of the 11th International Conference on Soil Mechanics and Foundations Engineering, San Francisco, 1985. 1:1-55
10. Sun, D.A., Huang, W.X., Sheng, D.C., Yamamoto, H.: An elastoplastic model for granular materials exhibiting particle crushing, Key Engineering Materials, 2007, Vol.341, 1273-1278

Modeling of Thermo-Mechanical Behavior of Saturated Clays

E.L. Liu[1,2] and H.L. Xing[2]

[1] School of Mechanics & Civil Engineering, China University of Mining & Technology, Beijing, P.R. China
`lel02@mails.tsinghua.edu.cn`
[2] Quakes, University of Queensland, St.Lucia, Brisbane, QLD 4072, Australia

Abstract. A new thermo-elasto-plastic constitutive model of saturated clay is proposed here based on the double hardening model for clays and available experimental results, which describes the effects of temperature and over consolidation ratio on the mechanical properties of saturated clays by introducing the two hardening parameters - σ_c' & α. Finally, the proposed model is applied to model the related important features of saturated clays under the different temperatures and loadings and compared with the available experimental results to demonstrate its accuracy.

Keywords: Thermo-mechanical behavior, Saturated clay, Constitutive model.

1 Introduction

Recently more attention has been focused on researching the mechanical response of soils to the combined effects of stress and temperature which is important in many geotechnical engineering applications. A number of experiments were carried out to investigate the influence of temperature on the behaviors of soils [1][2]. To study the effects of temperature on clays, a few of constitutive models were proposed to describe the thermo-elasto-plastic behavior of the solid skeleton [3][4]. Most of the above models mainly focused on modeling the thermal-mechanical behaviors of saturated soils under the constant loading, but without considering the different over-consolidated ratio (OCR) effects under the isothermal triaxial drained conditions. In this paper, we propose a new thermo-elasto-plastic constitutive model to describe the combined effects of the temperature and the OCR on the mechanical properties of saturated clays and verify it with the available experimental results.

2 Thermo-Mechanical Constitutive Equations of Saturated Clay

2.1 The Formulation of the Constitutive Equations

Based on the above experimental results, a thermo-elastic-plastic constitutive equation is deduced in the following. Let

$$\sigma'_m = \frac{1}{3}\sigma'_{kk} \; ; \sigma_s = \sqrt{\frac{3}{2}s_{ij}s_{ij}} \; , s_{ij} = \sigma'_{ij} - \sigma'_{kk}\delta_{ij} \; ; \varepsilon_v = \varepsilon_{kk} \; ; \varepsilon_s = \sqrt{\frac{2}{3}e_{ij}e_{ij}} \; , e_{ij} = \varepsilon_{ij} - \frac{1}{3}\varepsilon_{kk}\delta_{ij} \tag{1}$$

The thermo-elastic strain tensor ε^{Te} is the superposition of a reversible thermal induced strain ε^{T} and a mechanical elastic strain ε^{e} under adiabatic conditions. In incremental form we have

$$d\varepsilon^{Te} = d\varepsilon^{T} + d\varepsilon^{e} \tag{2}$$

The elastic shear strain is assumed as purely mechanical, so we have

$$d\varepsilon_v^{Te} = \frac{d\sigma'_m}{K} + \beta'_s dT \quad \text{and} \quad d\varepsilon_s^{e} = \frac{d\sigma_s}{3G} \tag{3}$$

where $d\varepsilon_v^{Te}$ is the volumetric thermo-elastic strain increment, $d\varepsilon_s^{e}$ is the shear strain increment, $d\sigma'_m$ is the mean effective stress increment , $d\sigma_s$ is the shear stress increment, dT is the temperature increment, β'_s is the isotropic thermal expansion coefficient of the solid skeleton, K is bulk elastic modulus and G is shear elastic modulus.

The thermal-plastic strain depends on deformation and temperature history, and in general cannot be uniquely expressed through effective stress and temperature. Based on the double hardening model for clays [5] under the isothermal temperature condition, the irreversible thermal effects are introduced using the dependence of yield surface, flow rule and internal variables on temperature. The yield surface is assumed to be a function of stress, plastic volumetric strain and plastic shear strain and temperature variation dT (referring to an environmental temperature T_o),

$$F = \frac{\sigma'_m}{1 - \left(\dfrac{\eta}{\alpha}\right)^n} - \sigma'_c = 0 \tag{4}$$

where $\eta = \sigma_s / \sigma'_m$; σ'_c and α are hardening parameters,

$$\sigma'_c = \sigma'_c(T)\exp(\beta\varepsilon_v^p) = \sigma'_c(T_o)\exp(\beta\varepsilon_v^p)\{1 - \gamma\log[T/T_o]\} \tag{5}$$

$$\alpha = \alpha(\varepsilon_s^p, T) = \alpha_c(T)\left[\alpha_m - (\alpha_m - \alpha_o)\exp(\frac{\varepsilon_s^p}{c_a})\right] \tag{6}$$

In which
$$\varepsilon_v^p = \varepsilon_{kk}^p \; , \; \varepsilon_s^p = \sqrt{\frac{2}{3}e_{ij}^p e_{ij}^p} \; , e_{ij}^p = \varepsilon_{ij}^p - \frac{1}{3}\varepsilon_{kk}^p\delta_{ij} \; ;$$

$\sigma'_c(T)$ and $\sigma'_c(T_o)$ are the pre-consolidation stress at a given temperature T and T_o , respectively; $\alpha_c(T)$ represents the effect of temperature on the hardening parameter α ; $\gamma, \beta, \alpha_m, \alpha_o$ and c_a are constant for a certain soil.

The incremental thermal-plastic strain can be formulated as the following equations

$$d\varepsilon_{ij}^{p} = d\lambda \frac{\partial g\left(\sigma_{ij}', \varepsilon_{ij}^{p}, \Delta T\right)}{\partial \sigma_{ij}'} \text{ or } d\varepsilon_{v}^{p} = d\lambda \frac{\partial g}{\partial \sigma_{m}'} \quad d\varepsilon_{s}^{p} = \frac{3}{2} d\lambda \frac{\partial g}{\partial \sigma_{s}} \tag{7}$$

where g is a plastic potential,

$$g = g\left(\sigma_{m}', \sigma_{s}, \varepsilon_{v}^{p}, \varepsilon_{s}^{p}, \Delta T\right) \tag{8}$$

And $d\lambda$ is the plastic multiplier, which can be derived from the consistency conditions,

$$\frac{\partial F}{\partial \sigma_{ij}'} d\sigma_{ij}' + \frac{\partial F}{\partial \varepsilon_{v}^{p}} d\varepsilon_{v}^{p} + \frac{\partial F}{\partial \varepsilon_{s}^{p}} d\varepsilon_{s}^{p} + \frac{\partial F}{\partial T} dT = 0 \tag{9}$$

Substituting for the plastic volumetric strain increment $d\varepsilon_{v}^{p}$ and the plastic shear strain $d\varepsilon_{s}^{p}$ from the equations (7), $d\lambda$ can be described as,

$$d\lambda = \frac{\frac{\partial F}{\partial \sigma_{ij}'} d\sigma_{ij}' + \left[\frac{\partial F}{\partial \sigma_{c}'} \frac{\partial \sigma_{c}'}{\partial T} + \frac{\partial F}{\partial \alpha} \frac{\partial \alpha}{\partial T}\right] dT}{H} \tag{10}$$

where H is thermo-plastic hardening modulus, and

$$H = \frac{3}{2} \frac{n \sigma_{m}' \eta^{n}}{\alpha^{n+1}\left[1 - \left(\frac{\eta}{\alpha}\right)^{n}\right]^{2}} \frac{1}{c_{a}}\left[\alpha - \alpha_{c}(T)\alpha_{m}\right] \frac{\partial g}{\partial \sigma_{s}} + \beta \sigma_{c}' \frac{\partial g}{\partial \sigma_{m}'} \tag{11}$$

The total volume strain increment $d\varepsilon_{v}$ and shear strain increment $d\varepsilon_{s}$ are assumed as,

$$d\varepsilon_{v} = d\varepsilon_{v}^{Te} + d\varepsilon_{v}^{p}, d\varepsilon_{s} = d\varepsilon_{s}^{e} + d\varepsilon_{s}^{p} \tag{12}$$

Combining equations (7), (10), (11) with (12), the incremental form of stress-strain-temperature equations can be described finally as,

$$d\sigma_{m}' = C_{mv} d\varepsilon_{v} + C_{ms} d\varepsilon_{s} + B_{Tv} dT, d\sigma_{s} = C_{sv} d\varepsilon_{v} + C_{ss} d\varepsilon_{s} + B_{Ts} dT \tag{13}$$

Where $C_{mv} = \frac{1}{M}\left[\frac{1}{3G} + \frac{3}{2} \frac{1}{H} \frac{\partial F}{\partial \sigma_{s}} \frac{\partial g}{\partial \sigma_{s}}\right]$, $C_{ms} = -\frac{1}{M} \frac{1}{H} \frac{\partial F}{\partial \sigma_{s}} \frac{\partial g}{\partial \sigma_{m}'}$, $C_{sv} = -\frac{3}{2} \frac{1}{M} \frac{1}{H} \frac{\partial F}{\partial \sigma_{m}'} \frac{\partial g}{\partial \sigma_{s}}$,

$$C_{ss} = \frac{1}{M}\left[\frac{1}{K} + \frac{1}{H} \frac{\partial F}{\partial \sigma_{m}'} \frac{\partial g}{\partial \sigma_{m}'}\right], M = \frac{1}{3KG} + \frac{1}{3GH} \frac{\partial F}{\partial \sigma_{m}'} \frac{\partial g}{\partial \sigma_{m}'} + \frac{3}{2KH} \frac{\partial F}{\partial \sigma_{s}} \frac{\partial g}{\partial \sigma_{s}},$$

$$B_{Tv} = -\frac{1}{M}\left[\frac{1}{3G}\beta_{s}' + \frac{3}{2} \frac{1}{H} \frac{\partial F}{\partial \sigma_{s}} \frac{\partial g}{\partial \sigma_{s}} \beta_{s}' + \frac{1}{3GH}\left(\frac{\partial F}{\partial \sigma_{c}'} \frac{\partial \sigma_{c}'}{\partial T} + \frac{1}{H} \frac{\partial F}{\partial \alpha} \frac{\partial \alpha}{\partial T}\right) \frac{\partial g}{\partial \sigma_{m}'}\right]$$

$$+\frac{1}{M}\left[\frac{3}{2} \frac{1}{H^{2}}(1-\frac{1}{H}) \frac{\partial F}{\partial \sigma_{s}} \frac{\partial F}{\partial \alpha} \frac{\partial \alpha}{\partial T} \frac{\partial g}{\partial \sigma_{m}'} \frac{\partial g}{\partial \sigma_{s}}\right],$$

$$B_{Ts} = -\frac{1}{M}\left[\frac{3}{2HK}\left(\frac{\partial F}{\partial \sigma_{c}'} \frac{\partial \sigma_{c}'}{\partial T} + \frac{\partial F}{\partial \alpha} \frac{\partial \alpha}{\partial T}\right) \frac{\partial g}{\partial \sigma_{s}} + \frac{3}{2} \frac{1}{H^{2}}(1-\frac{1}{H}) \frac{\partial F}{\partial \sigma_{m}'} \frac{\partial F}{\partial \alpha} \frac{\partial \alpha}{\partial T} \frac{\partial g}{\partial \sigma_{m}'} \frac{\partial g}{\partial \sigma_{s}}\right]$$

$$+\frac{1}{M}\left[\frac{3}{2} \frac{1}{H} \frac{\partial F}{\partial \sigma_{m}'} \frac{\partial g}{\partial \sigma_{s}} \beta_{s}'\right].$$

2.2 The Determination of the Model Parameters

For the thermo-elastic case, the three sets of parameters K, G and β'_s, can be determined in this paper as follows,

$$K = K_{ref}\left(\frac{\sigma'_m}{P_a}\right)^m \quad G = G_{ref}\left(\frac{\sigma'_m}{P_a}\right)^m \tag{14}$$

where K_{ref} and G_{ref} are the bulk and shear modulus at a reference pressure; $P_a = 0.104$ MPa, and $m = a_1(\sigma_c/\sigma_o) + b_1$, a_1, b_1 are constants, σ_c is consolidated pressure, σ_o is unit pressure and OCR is the over-consolidation ratio.

$$\beta'_s = \beta'_{so}(3.5 - 0.2(OCR))(1 + \varsigma T)(OCR) \tag{15}$$

In which β'_{so} is the volumetric thermal expansion coefficient at the reference temperature, and ς corresponds to the slope of the variation of β'_s with respect to present temperature T.

While for the thermo-plastic parameters, due to the lack of experimental results, the thermo-plastic potential function is assumed to be the same as the yield function

$$g = F \text{ and } \alpha_c(T) = \alpha_c(T_o) + N_s(T - T_o) \tag{16}$$

Where $\alpha_c(T_o)$ is the reference value at the reference temperature T_o, N_s is a constant. Other parameters in equation (7) can be determined as follows: $\alpha_m = \sqrt[n]{1 + n}\sin\varphi_r$ and φ_r is residual frictional angle; $n = a_2(\sigma_c/\sigma_o) + b_2$, a_2, b_2, α_o and c_a are constants.

3 Validation of the Proposed Model

The validation tests were conducted on CM clay (Kaolin) under triaxial shear conditions with different temperatures [6]. These comparisons were made at two different temperatures for two over-consolidation ratios (OCR=1.2 and 3). Figure 1 and Figure 2 show the results for the isothermal triaxial cases conducted at 22 °C and 90 °C, respectively. The model parameters used are: $\sigma'_c(T_o) = 0.6$ MPa, $\beta'_{so} = -1.3\times10^{-5}(°C^{-1})$, $\varsigma = -0.003$, $\beta = 5.2$, $\gamma = 0.17$, $K_{ref} = 1.65$ MPa, $G_{ref} = 0.92$ MPa, $C_a = 0.5$, $\varphi_r = 23°$, $\alpha_o = \alpha_m$, $\alpha_c(T_o) = 2.52$, $N_s = -0.03$, $a_1 = 1.33$, $b_1 = 0.835$, $a_2 = 2.33$, $b_2 = 0.035$. All the above results demonstrated that the proposed model can reproduce the major aspects of the temperature influence on mechanical behavior of saturated clays and agrees well with the experimental results.
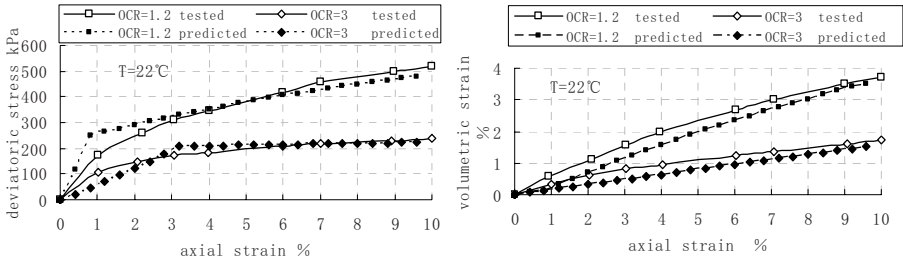
Fig. 1. Comparison results on drained triaxial case at 22℃ for two OCR values
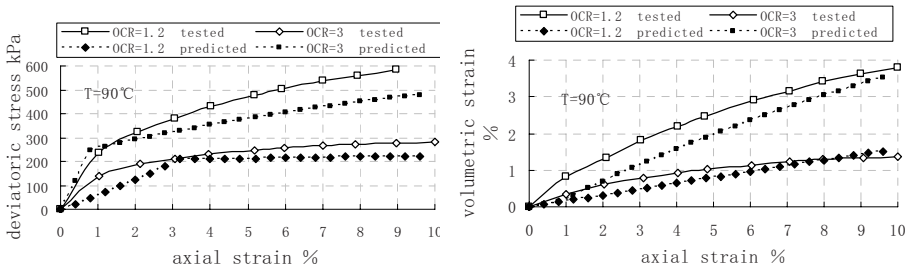
Fig. 2. Comparison results on drained triaxial case at 90℃ for two OCR values

4 Conclusions

The effects of both the temperature and the over consolidation ratio (OCR) on the mechanical properties of saturated clays are described by introducing two hardening parameters. The proposed model has been applied to compare with the experimental results, which demonstrated that the new model may describe many important thermo-elastic-plastic features of saturated clays well.

References

1. Baldi, G., Theckel, T., Pellegrini, R.: Thermal Volume Changes of The Mineral-water System in Low-porosity Clay Soils. Can. Geo. J. 25 (1988) 807-825
2. Sultant, N.,Delage,P.,Cui,Y.J.: Temperature Effects on The Volume Change Behavior of Boom Clay. Engineering Geology 64 (2002) 135-145
3. Hueckel, T., Borsetto, M.: Thermo-plasticity of Saturated Soils and Shales : Constitutive Equations. J. of Geo. Engineering 12 (1990) 1765-1777
4. Cui, Y.J.,Sultan, N., Delage, P.: A Thermo-mechanical Model for Saturated Clays. Can. Geo. J. 37 (2000) 607-620
5. Shen, Z.J.: A Double Hardening Model for Clays. Rock and Soil Mechanics 1 (1995)1-8 (in Chinese)
6. Cekerevac, C., Laloui, L.: Experimental Study of Thermal Effects on The Mechanical Behavior of A Clay. Int.J. for Num. and Anal. Met. in Geo. 28 (2004) 209-228

Analytical and Numerical Investigation of Fracture Dominated Thermo-Fluid Flow in Geothermal Reservoir

H.H. Xu[1,2], H.L. Xing[1,3], D. Wyborn[4], and P. Mora[1,3]

[1] ESSCC, The University of Queensland, St. Lucia, QLD 4072, Australia
[2] South China Sea Institute of Oceanology, CAS, Guangzhou 510301, China
[3] ACcESS, Major National Research Facility
[4] Geodynamics Limitedd, Suite 6, Level 1, 19 Lang Parade, Milton, Brisbane, QLD 4064, Australia

Abstract. Fluid flow in most of geothermal reservoirs is dominated by fractures and their distribution. In this study, the following process of cold water injection into a fractured geothermal reservoir is considered: the cold water from a injection well advances along the fractures and gradually extract heat from the adjacent rock matrix, and eventually arrives at a production well. Both analytical and finite element based numerical models are developed and applied to investigate the temperature and/or pressure evolution in the above process, and compared with each other.

Keywords: Fracture, analytical, Finite element, thermal-fluid flow.

1 Introduction

Fluid flow in most HDR/HFR geothermal reservoirs is dominated by fractures and their distribution. How the fractures affect the heat transfer between the fluid and the rock mass during injection process must be critically addressed. Several related researches have been reported [1,2]. The existing analytical model discussed by Bodvarsson [2,3] did not include the effect of conduction in fracture. In this paper, a model is proposed that includes the effect of conduction in the fracture. To investigate the advancement of the thermal fluid during the injection process into the fractured reservoir system, both the analytical and the finite element based numerical methods are developed and verified as follows through a simplified reservoir system consisting of a horizontal fracture intersecting an injection well and a production well.

2 Analytical Solution

The analytical model considers an injection well penetrating a reservoir with equally spaced horizontal fractures. Here, we assume the constant aperture H along the fractured zone, the constant injection rate q and an impermeable rock matrix (see Fig. 1). The

differential equation governing the fluid temperature in the fracture can be derived by satisfying the energy conservation in the fracture zone as

$$\rho_a c_a \frac{\partial T_a}{\partial t} = \kappa_a \frac{\partial^2 T_a}{\partial x^2} - \frac{\rho_w c_w q}{H} \frac{\partial T_a}{\partial x} + \frac{2\kappa_1}{H} \frac{\partial T_1}{\partial z}\bigg|_{z=0} \tag{1}$$

where T_a and T_1 are the temperatures of fluid in the fracture and of the rock matrix, respectively. The temperature of the rock matrix is governed by the heat conduction equation as

$$\rho_1 c_1 \frac{\partial T_1}{\partial t} = \kappa_1 \frac{\partial^2 T_1}{\partial z^2} \tag{2}$$

The simultaneous solution of the equations using the Laplace transformation is derived. In the Laplace domain, the solutions for the fracture and the rock temperature are
Fracture zone

$$u = \frac{1}{s} \exp[(\frac{1}{2\delta} - \sqrt{\frac{1}{4\delta^2} + \frac{\lambda}{\delta}})\xi] \tag{3}$$

Rock matrix

$$v = \frac{1}{s} \exp[(\frac{1}{2\delta} - \sqrt{\frac{1}{4\delta^2} + \frac{\lambda}{\delta}})\xi](\cosh \sqrt{s}\eta - \sinh \sqrt{s}\eta \tanh \sqrt{s}) \tag{4}$$

$$\lambda = \theta s + 2\sqrt{s} \tanh \sqrt{s} \tag{5}$$

where s is the Laplace parameter and u, v is temperature variable in Laplace transform. Equation (3) and (4) are impossible to be inverted analytically from the Laplace domain, so a numerical inverter by Stehfest [4] is used here.

3   Finite Element Based Numerical Equations

From the above, the analytical solution is limited to the simplified ideal case. For simulating the practical complicated geothermal reservoir system, the finite element based numerical method is also developed. Numerical modeling of flow in porous/fractured media requires the coupling of various processes associated with the complex geological and hydrological setting of geothermal systems. For an example, the processes in the reservoir involve transport of fluid, heat and chemical species. In this research, the modeling will focus on coupling of fluid transport and heat transfer. The general conservation of mass for fluid is given by

$$S_s \frac{\partial p}{\partial t} = \nabla \cdot [\frac{k}{\mu}(\nabla p + \rho g \nabla z)] \tag{6}$$

$$S_s = \rho g(\alpha + \phi\beta) \tag{7}$$

From the energy conservation, the heat conductive-convective heat transfer in rock mass can be described as

$$c\rho\,\frac{dT}{dt} = \nabla \cdot (\kappa\nabla T) - c_w\,\rho_w\,q\,\nabla T \tag{8}$$

$$q = -\frac{k}{\mu}(\nabla p + \rho g\nabla z) \tag{9}$$

Generally, the Galerkin's finite element method is applied to solve the above equation to simulate the conventional thermo-fluid flow in the porous media. It is feasible because the fluid flow in the conventional porous media is usually slow and thus the Pelect number ($Pe = \dfrac{qh}{k}$ with h being a characteristic length) is less then 1. However, if convection is dominant, such as in the fracture zone of a fracture dominated system, the Pelect number is normally much larger than 1, and the above Galerkin formulation may suffer from spurious oscillations. So the Taylor-Galerkin formulation [5] is utilized here.

The thermo-fluid flow coupling is governed by the Eqs.(6), (8) and (9), which affect each other. The staggered method is applied here to treat this coupled problem [6,7]. Considering the above boundary conditions, the finite element formulation for fluid extra-pressure analysis can be deduced from Eq. (6) as

$$\left(\frac{M}{\Delta t} + \frac{K}{2}\right)P_{t+\Delta t} = \left(\frac{M}{\Delta t} - \frac{K}{2}\right)P_t + Q \tag{10}$$

where

$$M_{ij} = \int_V \rho S_s N_i N_j dV \quad K_{ij} = \int_V \rho\frac{k}{\mu}\frac{\partial N_i}{\partial x_k}\frac{\partial N_j}{\partial x_k}dV \tag{11}$$

$$Q_i = \int_V \rho^2 g\frac{k}{\mu}\frac{\partial N_i}{\partial x_3}dV$$

While, from Eqs. (8) and (9), the finite element formulation for heat transfers analysis can be rewritten as

$$\left(\frac{M}{\Delta t} + \frac{K_d}{2}\right)T_{t+\Delta t} = \left(\frac{M}{\Delta t} - \frac{K_d}{2} - (K_a + K_{bd})\right)T_t + Q_t \tag{12}$$

Where

$$M_{ij} = \int_V \rho c N_i N_j dV \qquad K_{d\,ij} = \int_V k\frac{\partial N_i}{\partial x_k}\frac{\partial N_j}{\partial x_k}dV \tag{13}$$

$$K_{a\,ij} = \int_V \rho c q_k N_i \frac{\partial N_j}{\partial x_k} dV \qquad K_{bd\,ij} = \frac{\Delta t}{2} \int_V \rho c q^2 \frac{\partial N_i}{\partial x_k} \frac{\partial N_j}{\partial x_k} dV$$

The above algorithm has been implemented to the existing finite element code for heat transfer analysis; the implicit algorithm is applied to solve the above equations (10) and (12) [6,7].

4 Practical Example

Geothermal energy manifests itself in spectacular fashion in many places on the earth's surface and has been widely recognized as a renewable green energy in the world. Several countries have started the related projects for developing the Hot Dry Rock (HDR) geothermal system which has been renamed as Hot Fractured Rock (HFR) in Australia. The Cooper Basin is entirely covered by the Mesozoic Eromanga Basin, where the measured surface heat flow is over 100mW/m^2. Geodynamics Limited is developing the first Australian HFR geothermal reservoir system there for electricity generation. From the analysis of the microseismicity recorded during the hydraulic stimulation through the drilled well Habanero 1, the geothermal reservoir being developed in the Cooper Basin is determined as fracture dominated. The fracture zone is estimated to spans 30m thickness along the vertical direction and is composed of a main fracture and a high permeability rock mass, which is further simplified as the following model (Figure 1) to be analysed by both the analytical and finite element methods, in which the permeability of the 30m thick (D=15m) fracture zone is taken as 10 microDarcy, while the transmissibility of the main fracture with the aperture H=0.01m down the middle of the fracture zone is 1 Darcy metre; and the temperature of injected fluid is 90℃, the initial temperature of rock matrix is 260 ℃.

4.1 The Analytical Result

Figure 1 illustrates a schematic picture of the basic model for the analytical study. The following conditions are assumed here: Let the temperature in the vertical direction of the main fracture be uniform; the rock matrix be impermeable; horizontal conduction be neglected, and no heat flow along both the top and the bottom surfaces.
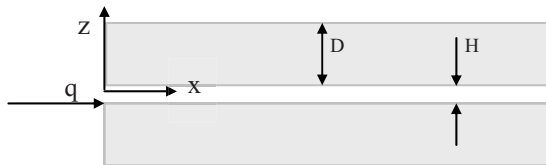
Fig. 1. Schematic of analystical model

Fig 2-5 show the analytical results with the parameters listed in table 1. From the results of temperature variation during 30 to 70 years at X=400m and 500m (i.e. the distance of from the injection well) respectively shown in Figs 2 and 3 , we see the

temperature of fluid in the fracture is almost the same as that of rock matrix after 30 years due to thermal conduction. Figs 4 and 5 show the fluid temperature variation at different distances and times. After 70 years the temperature has decreased from 260℃ to 150℃ at the production point 500m away (Fig 5).

Table 1. Parameters used in analytical study

	Fracture	Rock Matrix
Thermal conductivity (J/ms℃)	2.8	3.0
Density (kg/m³)	1000	2650
Specific heat (J/kg℃)	1000	800
Injection rate (m²/s)	1.7E-5	0
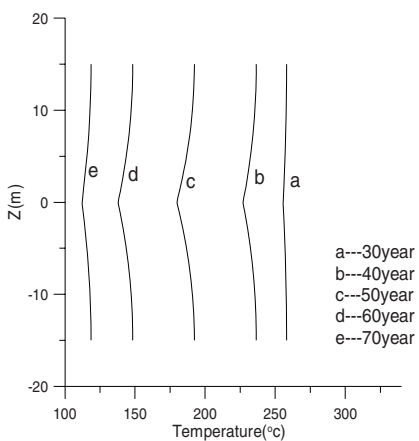
Fig. 2. Temperature variation at X=400m   **Fig. 3.** Temperature variation at X=500m
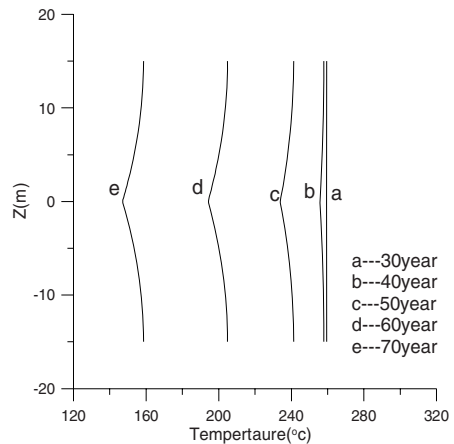
4.2 Finite Element Based Numerical Analysis

Most of the assumptions in the analytical case are not necessary for the numerical analysis. The aperture H of the fracture is constant but the fluid flow rate q is not constant, and the rock matrix is permeable, which is governed by Darcy equation. Similar to the analytical model, a 500mx30mx1m 3D model with the main fracture of H=0.01m in the middle is constructured and discretised into 20,000 8-node hexahedral elements. The initial and boundary temperature conditions are the same as for the analytical study. 70Mpa is set for the injection well and the pressure difference between the injection and production well is 7Mpa. No thermal flow is assumed along the other boundaries. All the parameters used here are listed in Table 2.
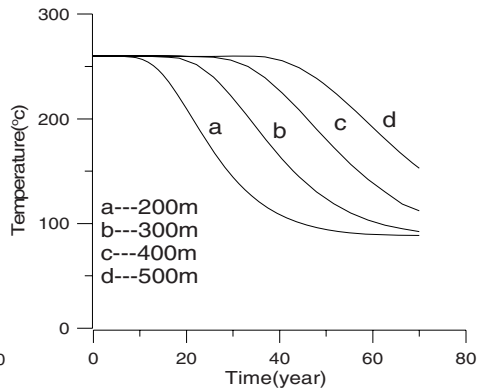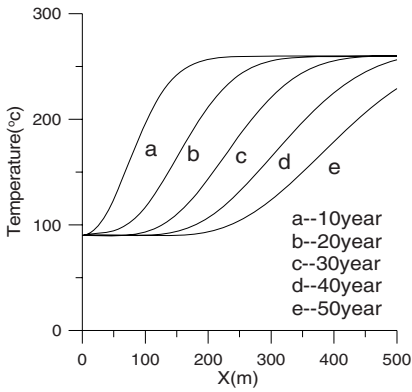
Fig. 4. Temperature evolution in fracture   **Fig. 5.** Temperature distribute in different points

Table 2. Parameters used in numerical study

	Fracture	Rock matrix
Thermal conductivity (J/m s℃)	2.5	3.0
Density (kg/m³)	1000	2650
Specific heat (J/kg℃)	4200	1000
Porosity	1	0.01
Permeability (m²)	1.0e-10	1.0e-14
Compressibility (Pa⁻¹)	5.0e-10	5.0e-10
Viscosity (kg/m s)	8.5e-3	8.5e-3
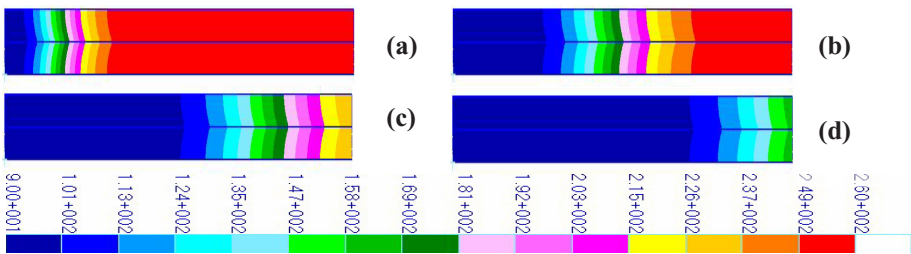
Fig. 6. Temperature evolution (years)(a -10 ,b- 30 ,c -50 d-,70)

Figure 7 shows the pressure evolution at different times. The pressure varies drastically at the beginning stage around the injecting well, but reaches a stable state much more quickly than the temperature in Fig. 6, and then remains constant after about 50 hours.

This can also be seen from the curves of fluid flow velocity vs time in Figure 10, where the fluid velocity reaches a constant along the whole fracture at 50 hours. Figures 8 and 9 show the fluid temperature of in fracture zone evolution at different

positions and time. Around the production well, the temperature remains above 150 ℃ after 50 years(Fig. 8). Assuming an allowable maximum temperature decrease of 40℃ at the projection well, it will last up to 40 years as shown in Fig.9
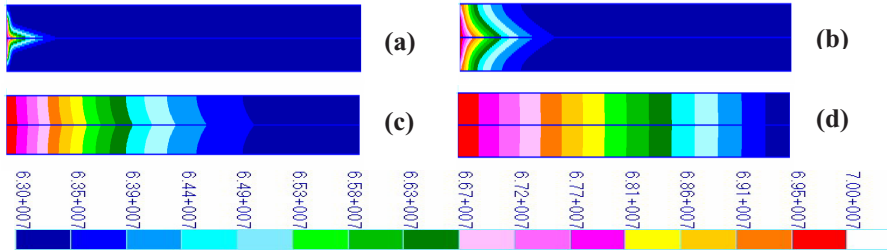
Fig. 7. Pressure evolution(a-0.1 hours ,b-1 hour, c -10hours, d -50 hours)
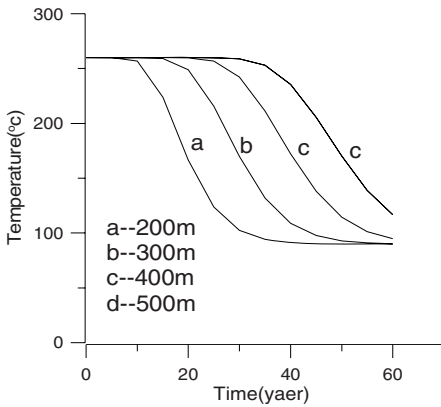
Fig. 8. Temperature at different point
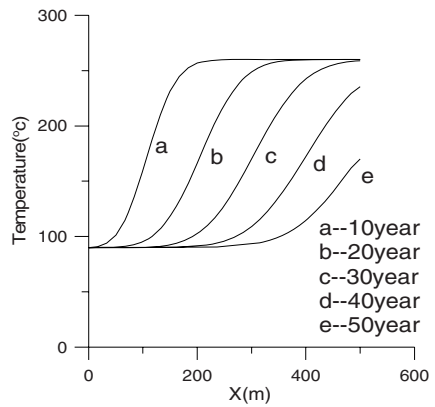
Fig. 9. Temperature at different time
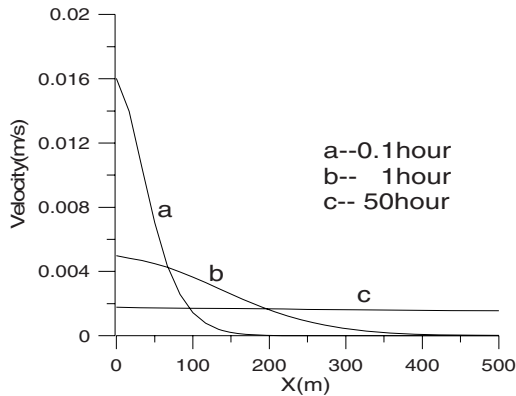
Fig. 10. The fluid velocity distribute in fracture

5 Discussions and Conclusion

From the comparison of the above results from the analytical and the numerical solutions, the temperature evolution is almost the same at the different time and positions as shown in Figs 4 and 9, 5 and 8; the trend of both results is the same, but the temperature decrease is faster in the numerical solution than in analytical. In the analytical work, the assumption of an impermeable rock matrix was made and in the numerical solution the rock is permeable, the fluid in porous can take over heat of rock matrix. This demonstrates that (1) the assumptions made for the analytical solution, such as constant flow, are correct for such a long term case, because the fluid pressure/velocity reaches to a steady state in a very short time (about two days, Figs 7 and 10); (2) the numerical algorithm proposed here for the thermo-fluid coupling analysis works well; (3) The analytical solution is more suitable for a long term analysis, but not applicable for transient and/or complicated fault geometry, while the finite element based numerical analysis does well for the all the cases and may also be applicable to transient complicated analysis.

References

1. Gringarten, A.C., Witherspoon, P.A., and Ohnishi, A., Theory of heat extraction from aquifers with uniform regional flow, J. Geophys. Res., 80(8), (1975), 1120-1124.
2. Bodvarsson, G.S and Tsang, C.F., Injection and thermal breakthrough in fractured geothermal reservoirs, J. Geophys. Res., 87(2),(1982), 1031-1048
3. Bodvarsson, G.S., On the temperature of water flowing through fracture, J. Geophys. Res., 74(8), (1969), 1987-1992
4. Stefest, H., Numerical inversion of Laplace transforms, Commun. ACM, 13, (1979), 44-49.
5. Donea, J., A Taylor-Galerkin method of convective transport problem, Int. J, Num. Meth. Engg, 20, (1984), 101-119.
6. Xing, H.L., and Makinouchi, A., Three dimensional finite element modelling of thermomechanical frictional contact between finite deformation bodies using R-minimum strategy, Computer Methods in Applied Mechanics and Engineering, 191, (2002), 4193-4214
7. Xing, H.L., and Makinouchi, A., FE modelling of thermo-elasto-plastic finite deformation and its application in sheet warm forming, Engineering Computations – Int. J. Computer-Aided Engineering and Software, 19,(2002), 392-410

Three-Dimensional Numerical Modeling of a Deep Excavation Adjacent to Shanghai Metro Tunnels

Y.M. Hou, J.H. Wang, and L.L. Zhang

Civil Engineering Department, Shanghai Jiaotong University, 1954 Hua Shan Road,
Shanghai, China
{ymhou, wjh417, lulu_zhang}@sjtu.edu.cn

Abstract. Due to rapid construction and limited urban area in Shanghai, some deep excavations are very close to the existing metro tunnels or sensitive superstructures. Therefore the safety of the adjacent tunnels and surrounding structures become an important issue during design and construction of these deep excavations. This paper presents a 3D finite-element modeling using the finite element analysis program ABAQUS for an oversize deep excavation in Shanghai soft deposits. The excavation is the excavation of the north square underground shopping center of Shanghai South Railway Station. Two cases of numerical analyses assuming anisotropic and isotropic soil stiffness respectively are conducted. The estimated wall deflection and ground movements are compared with the field monitoring results. It is found that soil stiffness anisotropy has a significant effect on the accuracy of prediction of the diaphragm wall deflection and the ground movement around excavation for the oversize excavation in Shanghai soft deposits. The calculated ground movements of the anisotropic case agree well with the field measurements.

Keywords: numerical modeling, excavation, ground movement, anisotropic stiffness.

1 Introduction

To meet the increasing demand for economic growth, extensive underground structures and metro systems have been rapidly constructed in Shanghai. Some of these excavations are very close to the existing metro tunnels or sensitive superstructures. The safety of the adjacent tunnels and surrounding structures may be affected by the ground movement induced by the excavation. The excavation of the north square underground shopping center of Shanghai South Railway Station is one of the deep excavations under complicated conditions in the urban area of Shanghai. The site is located in the south of the city. It was only about 3 m away from the existing tunnels of Shanghai Metro Lines No.1 and No.3. The minimum distance between the excavation and the tunnels of the new route of Shanghai Metro Line No.1 was only 2 m. In addition, the excavation of the interchange station of Metro Lines No.1 and No.3 was

located besides this excavation in northwest and was constructed before this excavation. The retaining structures of the two excavations were shared. Therefore, it is important to predict the ground movement accurately in order to assess the impact of the excavation on the metro tunnels and the existing excavation nearby.

Finite-element analyses have been used to study the performance of excavations as the soil stress-strain behaviors can be considered and the construction sequences can be modeled in the numerical modeling [3, 4, 6, 8, 10]. The constitutive models of soils are most important in numerical analyses. Researchers showed that anisotropic stress-strain strength of soft clays and nonlinear stiffness properties at small shear strains have significant effect on the predicted wall deflections and soil movements [7]. Generally, soils in Shanghai are sedimentary soils which are deposited through the process of sedimentation followed by consolidation under accumulative overburden pressures. Therefore, it may improve the prediction of ground movements induced by excavation if considering the soils as anisotropic materials. In this paper, the excavation of the North Square of Shanghai South Railway Station is studied by a three-dimensional finite element modeling. Numerical analyses are conducted to study the effect of anisotropic stiffness of soils on the computed ground deformation around the excavation. The wall deflection and ground settlement for an isotropic case and an anisotropic case are presented and compared with the field monitoring measurements.

2   Site Description and Ground Conditions

The site in this paper is the excavation site of the north square underground shopping center of Shanghai South Railway Station, which is located in the south of Shanghai. Fig. 1 shows the layout of the excavation. The area of the site was about 40,000 m^2. The excavation was only about 3 m away from the existing tunnels of Shanghai Metro Line No. 1 and No. 3, which were in the northwest and northeast side of the excavation, respectively. The new route of Shanghai Metro Line No. 1 was in the east of the site. The minimum distance between the excavation and the tunnels was only 2 m.
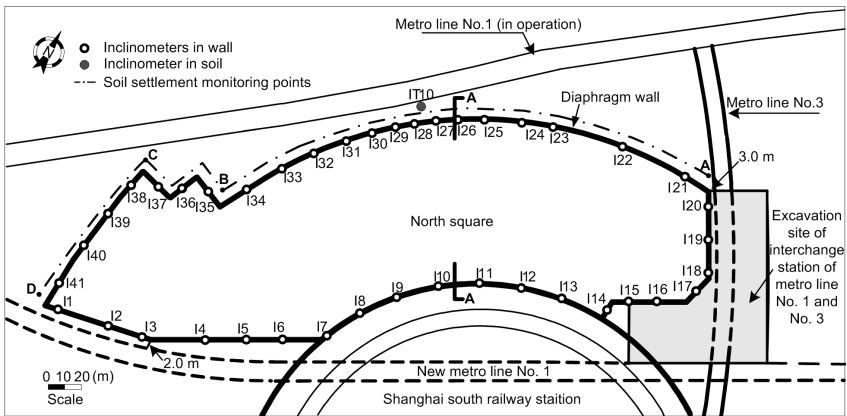
Fig. 1. The location and instrumentation of the excavation site
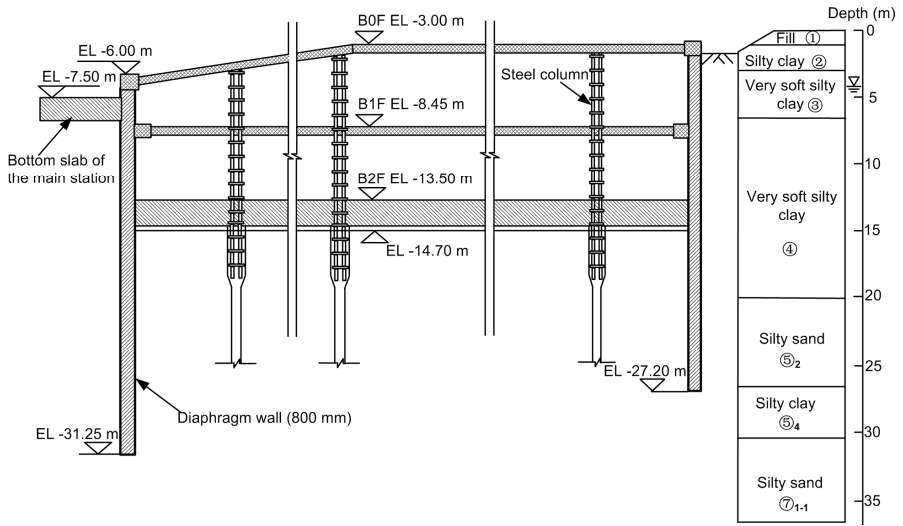
Fig. 2. Cross Section A-A of the excavation
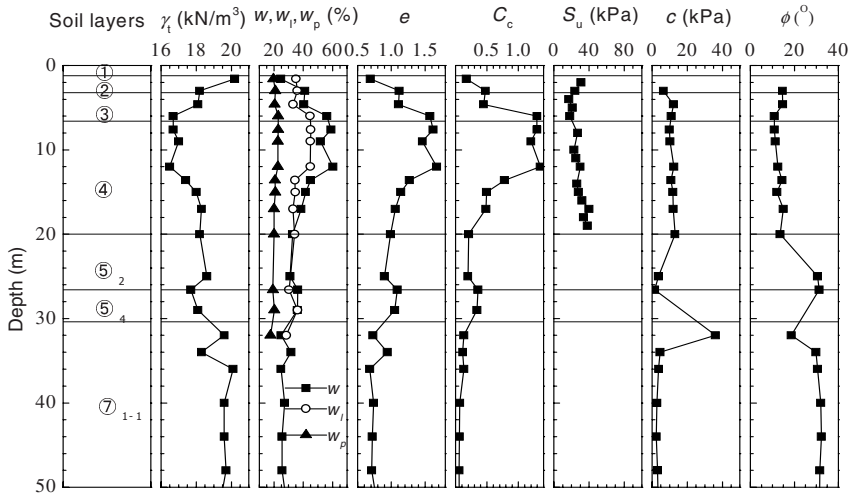
Fig. 3. Soil profiles and variation of soil properties with depth

To monitor the performance of the excavation, a comprehensive monitoring system was installed on site. As shown in Fig. 1, forty one inclinometers I1~I41 were installed in the diaphragm walls to measure the rotation and deflections of the walls. The inclinometer IT10 was installed adjacent to Line No. 1 to monitor the lateral displacement induced by the excavation in the soil. Thirty one surface settlement points were installed along the west boundary of the excavation (from point A to B to C to D). The excavation was 12.5 m deep with two basement levels as shown in Fig. 2

and was constructed using the top-down method. The concrete floor slabs were located at elevations of -3 m, -8.45 m and -14.7 m, respectively. The excavation was supported by a 0.8 m thick concrete diaphragm wall. The depths of the walls were 24 m to 27.85 m. The site of the interchange station of Metro Line No. 1 and No. 3 was adjacent to the excavation site and the retaining structures between the two excavations were diaphragm walls.

The site is underlain by thick, relatively soft Quaternary alluvial and marine deposits. Fig. 3 illustrates the succession of soil layers and the variation of soil properties with depth. The soil properties include total unit weight, water contents, void ratio, compression index, field vane shear strength, cohesion and friction angle.

3   Numerical Modeling of the Excavation

3.1   Finite Element Mesh and Boundary Conditions

In this paper, the finite element analysis program ABAQUS is used to conduct numerical modeling. The meshes of the entire 3D-finite element model (1200 m $\times$ 500 m $\times$ 80 m) and the retaining structures are shown in Fig. 4. The three-dimensional solid elements were used for soil layers. The columns and girders of the structure are simulated by beam elements. The diaphragm walls and concrete floor slabs are modeled using shell elements. The entire 3-D model consists of 178,162 nodes and 155,160 elements. The four side boundary surfaces are fixed along the vertical direction and the direction perpendicular to each surface. The bottom boundary is fixed in all x, y and z directions.

(a)   plan view of the mesh in the x-y plane

(b) 3D mesh of the excavation   (c) mesh of retaining structures
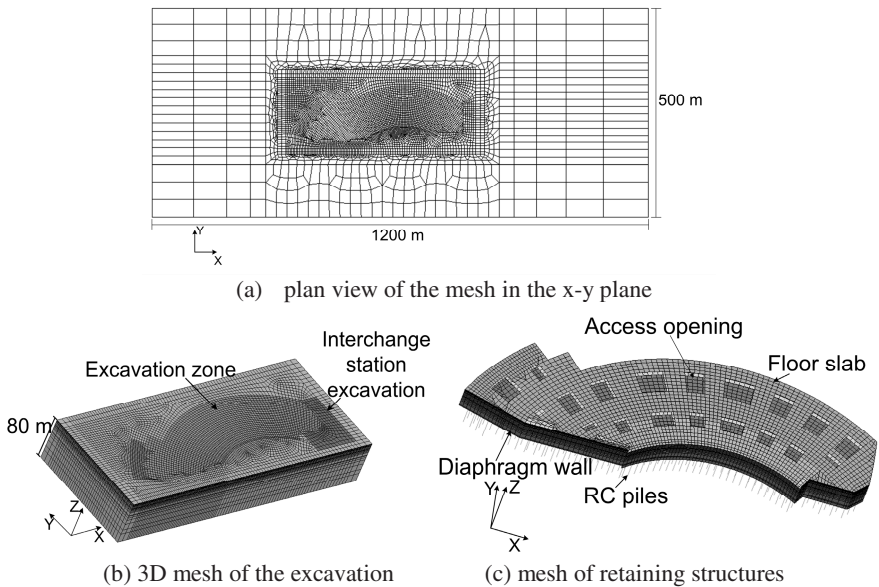
Fig. 4. Mesh of the 3D finite-element model

3.2 Soil Model and Parameters

In the numerical analyses, the diaphragm walls, the steel columns, the RC piles of the foundation and the floor slabs are assumed to be linear-elastic materials with the Young's modulus of 30 GPa and the Poisson's ratio of 0.2.

The numerical modeling includes establishment of the 3-D finite element mesh of the complex shaped excavation with foundation piles and the detailed construction process such as installing piles and retaining structures and zoned excavation is also needed to be modeled. Therefore, it is reasonable to model soils as elastic materials considering the complication and difficulties of modeling and the cost of computation time. As the soils in the site are generally Quaternary alluvial and marine soils deposited through the process of sedimentation followed by consolidation in horizontal layers, two cases with isotropic and anisotropic soil properties are conducted to study the effect of soil stiffness anisotropy. In the anisotropic case, it is assumed that the soils are cross-anisotropic, in which the inherent anisotropy is considered but the stress-induced anisotropy of the soil and the changes of the degree of anisotropy due to excavation are ignored. For an idealized cross-anisotropic elastic material, the stress-strain behavior is governed by five independent elastic parameters: E_h, E_v, G_{vh}, v_{vh} and v_{hh}, where E_h and E_v are the Young's moduli in the horizontal and vertical directions, respectively; G_{vh} is the shear modulus in any vertical plane; v_{hh} is the Poisson's ratio for the effect of horizontal strain on the complementary horizontal strain; and v_{vh} is the Poisson's ratio for the effect of vertical strain on horizontal strain. As the stress paths of the soil around the deep excavation correspond approximately to triaxial extension, the extension moduli of the soils should be used in the numerical analyses of excavation.

Table 1. Soil parameters used in numerical analysis

Layer No.	γ_t (kN/m³)	K_0	E_c (kPa)	E_h (kPa)	E_v (kPa)	G_{vh} (kPa)	v_{vh}	v_{hh}
①	19.1	0.50	5530	13270	22120	6194	0.33	0.35
②	19.5	0.50	3870	9280	15480	4024	0.29	0.30
③	17.8	0.55	3040	7290	12160	3162	0.33	0.35
④	17.0	0.64	2090	5000	8360	2174	0.37	0.42
⑤₂	18.5	0.52	13750	33000	55000	14300	0.29	0.30
⑤₄	24.3	0.43	20250	48600	81000	21060	0.29	0.30
⑦₁₋₁	19.3	0.43	--	120000	200000	520000	0.29	0.30

Becker [1] summarized undrained anisotropic elastic parameters for various clays. The ratio of E_h/E_v ranges from 0.5 to 2.4, and the ratio of G_{vh}/E_v ranges from 0.23 to 0.44. Ng [9] compared compression modulus and extension modulus under drained and undrained conditions. It shows the ratio of E_v/E_v' ranges from 0.26 to 0.54, in which E_v is the Young's modulus of compression condition and E_v' is the Young's modulus of extension condition. Lee [5] proposed that G_{vh}/E_v should be 40%-100% of the value of G/E under isotropic condition. Large numbers of back analyses for the excavations in Shanghai soft deposits indicate the vertical Young's modulus E_v can be

taken as $4E_c$, in which E_c is the modulus of compressibility. The modulus of compressibility in this study (Table 1) is adopted from the ground investigation report of the site. The ratios of E_h/E_v and G_{vh}/E_v of the soils in this study are assumed to be 0.6 and 0.26, respectively. For the isotropic case, the Young's modulus E is equal to E_v and the Poisson's ratio v is equal to v_{hh} in Table 1.

Table 2. Construction sequence of the excavation

Stage	Construction operation
1	Construction of diaphragm walls and RC piles
2	Excavation of the interchange station
3	Excavation of Shanghai South Railway Station
4	Excavate to -3.75 m
5	Construct the first floor slab and excavate to -7.5 m
6	Construct the second floor slab and excavate to -13.0 m
7	Excavate to -14.7 m and construct the bottom floor slab

3.3   Results and Discussion

The deformation of the soil adjacent to Metro tunnels may induce significant effects on the Metro tunnels. Therefore, the soil deformation and structure displacement near the Metro tunnels are studied here in detail.

Fig. 5(a) and 5(b) illustrate the calculated and field measured deformation at Stage 7 for the inclinometers I29 and IT10, respectively. The two inclinometers are very close to the Metro Line No. 1. The maximum wall deflection occurs near the bottom of the excavation. It shows that the wall deflection increases significantly with the anisotropic soil stiffness parameters. The maximum computed wall deflection of the anisotropic case is 37.5 mm, which is about 50% greater than that of the isotropic case. The maximum difference between measurements and the computed wall deflection of the anisotropic case is only 8%, while the maximum difference between the measured and the computed deformation with the isotropic soil model is about 30%. The calculated ratio of maximum measured lateral wall deflection to the excavation depth for the inclinometer I29 is 0.25%, which is within the range of the reported values in [2]. For the anisotropic case and the isotropic case, the ratios of maximum wall deflection to the excavation depth are 0.25% and 0.18%, respectively. It shows that the anisotropy of soil properties should be considered for a more accurate prediction of wall deflection.

The maximum value of the observed horizontal soil movement by IT10 is about 18 mm, which is much smaller than the maximum wall deflection of the inclinometer I29. Therefore, the retaining structures of the excavation reduce the ground movement and the deformation of the operating tunnels of Metro Line No. 1 is well controlled. The computed maximum ground movement of the anisotropic case is 18.4 mm, while the computed maximum ground movement of the isotropic case is only 14.7 mm. It shows the numerical analysis with anisotropic soil parameters yield a more accurate estimation of the lateral ground movement.

Fig. 6 presents the measured and calculated ground surface settlement along ABCD near the Metro Line No. 1 at Stage 7. The measured settlement is 10.8 mm to 16.75 mm. The ground settlements near the corners of the excavation are generally larger than the settlement at other locations. This is probably due to the arching effect of the corner. The predicted ground settlement of the anisotropic case is slightly smaller than the observed settlement. However, the maximum difference between the computed settlement of the isotropic case and the measured values is approximately 50%. It shows that the soil models with anisotropic stiffness could improve the accuracy of the prediction of the soil settlement around the excavation. The adopted soil parameters for the anisotropic elastic model are shown to be reasonable for Shanghai soils.

(a)   (b)
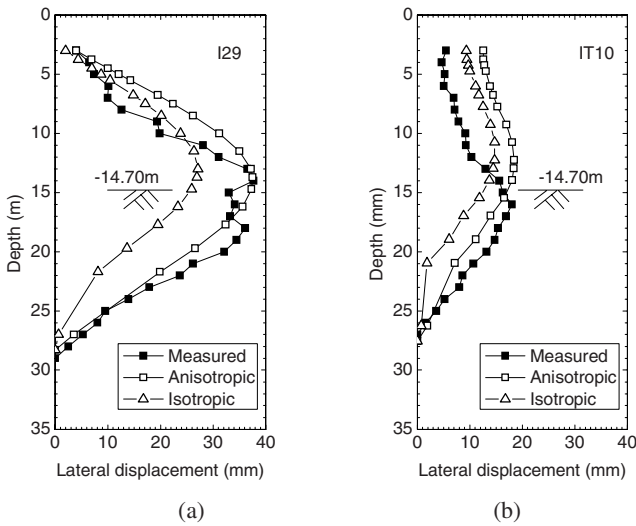
Fig. 5. Measured and calculated wall deflection and soil lateral displacement at Stage 7
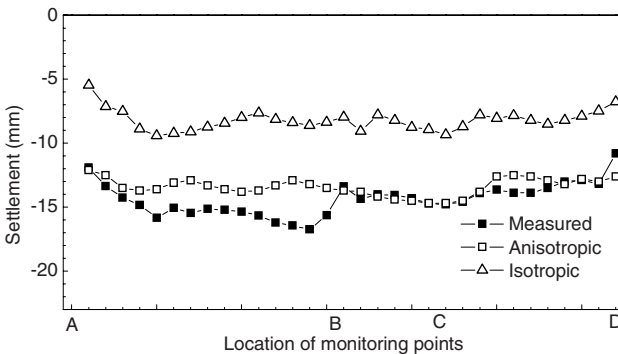
Fig. 6. Measured and calculated ground surface settlements at Stage 7

4   Conclusions

In this paper, a three-dimensional finite-element modeling is conducted to study the performance and soil deformation of the excavation for the north square of Shanghai South Railway Station. Two cases of numerical analyses with isotropic and anisotropic soil stiffness parameters are conducted to study the effects of anisotropic stiffness. It shows the anisotropic stiffness has significant effects on the computed wall deflection and ground deformation induced by the excavation. The wall deflection and ground lateral movement of the anisotropic case are significantly larger than those obtained in the isotropic case. The use of the anisotropic soil model greatly improves the accuracy of the estimated wall deflection and soil deformation around excavation. The adopted soil parameters for the anisotropic elastic model in the numerical modeling are shown to be reasonable for Shanghai soils.

References

1. Becker, D. E.: Settlement Analysis of Intermittently-loaded Structures Founded on Clay Sub-soils. PhD thesis, University of Western Ontario (1981).
2. Clough, G. W., and O'Rourke, T. D.: Construction-induced Movements of In-situ Walls. In: Design and Performance of Earth Retaining Structures. Geotechnical Special Publication No. 25. ASCE. (1990) 439-470.
3. Clough, G. W., Weber, P. R., and Lamont, J.: Design and Observation of Excavation Support Systems by Iterative Design. In: Proc. ASCE Spec. Conf. on Perf. of Earth and Earth-supported Struct., ASCE, New York, N.Y. Vol. 1 (1972), 1367-1390.
4. Finno, R. J., and Harahap, I. S.: Finite Element Analysis of HDR-4 Excavation. Journal of Geotechnical Engineering, ASCE, 117(10) (1991), 1590-1609.
5. Lee, K.M., and Rowe, R. K.: Deformations Caused by Surface Loading and Tunneling: The Role of Elastic Anisotropy. Geotechnique, 39(1) (1989), 125-140.
6. Mana, A. I., and Clough, G. W.: Prediction of Movement for Braced Cut in Clay. Journal of Geotechnical Engineering, ASCE, 107(8) (1981), 759-777.
7. Ng, C. W. W., Leung, E. H. Y., and Lau, C. K.: Inherent Anisotropic Stiffness of Weathered Geomaterial and Its Influence on Ground Deformations around Deep Excavations. Canadian Geotechnical Journal, 41 (2004), 12-24.
8. Ng, C. W. W., Lings, M. L.: Effects of Modeling Soil Non-linearity and Wall installation on Back-analysis of Deep Excavation in Stiff Clay. Journal of Geotechnical & Geoenvironmental Engineering, ASCE, 121(10) (1995), 687-695.
9. Ng, R. M. C.: Ground Reaction and Behaviour of Tunnels in Soft Clays. PhD thesis, University of Western Ontario (1984).
10. Ou, C. Y., Shiau, B. Y., and Wang, I. W.: Three-dimensional Deformation Behavior of The Taipei National Enterprise Center (TNEC) Excavation Case History. Canadian Geotechnical Journal, 37 (2000), 438-448.

Analytical Solution to Settlement of Cast-In-Situ Thin-Wall Concrete Pipe Pile Composite Foundation

Han-long Liu[1,2], An Deng[1,2], and Shi-qing Wen[1,2]

[1] Key Laboratory for Geotechnical Engineering of Ministry of Water Resource,
Hohai University, Nanjing 210098, P.R. China
[2] Geotechnical Research Institute, Hohai University, Nanjing 210098, P.R. China
{hliu,a_deng,sqw}@hhu.edu.cn

Abstract. The cast-in-situ thin-wall concrete pipe pile (PCC pile) is increasingly employed as a soft soil improvement technique in China. The formed composite foundation by using PCC pile renders a competitive advantage compared to conventional comparable soft soil treatment techniques. To calculate the settlement of PCC composite foundation helps better design a soil improvement scenario and understand the mechanism of PCC composite foundation. In this study, an elastic analytical solution to deformation modulus of PCC composite foundation was developed based upon the pile-soil-cushion interaction system and model analyses. Using the calculated modulus, formula presenting pile-soil stress ratio and composite foundation settlement were derived. A case study was conducted to verify the calculations. It is indicated that calculated settlements are in consistency with fielding monitoring data.

Keywords: PCC pile, composite foundation, deformation modulus, pile-soil stress ratio, settlement.

1 Introduction

As the drastic developments along the east China areas, a number of infrastructure works, e.g. ports, highway, bridges and warehouses, are constructed or planned. One of the obstacles in constructions is the poor bearing capacity of soft ground, which widely exists in east China, in particular in the vicinities of sea, rivers and lakes. Soil treatment has to be applied to improve the bearing capacity and decrease the settlement of soft soil foundations. The cast-in-situ, thin-wall, concrete pipe pile (PCC pile), a patented technique for soft soil improvement,[1, 2] has been extensively employed to address the soft soil concerns.

The PCC pile is a cast-in-situ, thin-wall, concrete pipe pile. The external diameter varies from 1000 to 1500 mm, and the wall thickness is in the range of 150 to 200 mm. The length of PCC pile is decided by ground properties and engineering goals, generally ranging from several meters to tens of meters. PCC piles can either be driven into ground fully as a composite foundation, or be driven partially with embedded reinforcement to set as a retaining structure. Fresh concrete is cast and vibrated at continuous steps to form the pile body. Using PCC composite foundation to improve soft soils has advantages spanning multiple aspects, i.e. concept, construction, performance, and economics. In concept, it maximizes the utilization of

shaft frictions through both inside and outside soil masses. It also minimizes concrete consumption by converting a solid pile into an economical annular cross section. The dimensions of PCC pile are adjustable, which makes PCC suitable for various soil properties and engineering goals. A steel pipe mold is driven into the soil mass to form an annular-shape room and the fresh concrete is poured. In this manner, the completeness and continuity of pile body is ensured. Since the shaft friction resistance is basically doubled, and the inner and outer soils may co-work together with PCC piles, the bearing capacity of PCC composite foundation is increased in a more effective way than other conventional techniques, e.g. deep-soil-mixing columns.

Mechanical mechanism of PCC composite foundation has not been clearly recognized. As a newly patented technique, the soil-pile interaction and composite foundation settlement are not yet understood. The primary settlement of composite foundation is not easy to estimate. Current applications are basically fulfilled at an empirical basis. Lack of deeper technical knowledge about PCC composite foundation barriers its optimization in designs. To upgrade this technique is also delayed without knowing its mechanical mechanism. This paper presents the establishment of a theoretical frame and computing methods regarding the deformation modulus, the pile-soil stress ratio and the settlement the composite foundation. A case study is conducted to verify the reliability of the derivation and computation.

2 Method and Analyses

2.1 Composite Foundation Model

A PCC composite foundation model, the pile-soil-cushion unit, is demonstrated in Fig. 1. The upper load P is uniformly applied over the cushion. The cushion is constructed with the thickness of h_c and modulus of E_c. The pile length is h, with its outer diameter D and inner diameter d. The pile body has elastic modulus E_p. The elastic modulus of soil layer i within the improvement area is E_{si}. After the adjustment of layer, the uniform load on PCC pile is P_s. The total soil compression is composed of two parts: S_1 for h thick improved deposit and S_2 for underlying soil deposits. The pile compression is S_3. The settlement of pile tip is δ_p. It is known that δ_p is equal to the addition of S_1, S_2 and S_3.

Assumptions are made with respect to the PCC composite foundation. It is assumed that the composite foundation is an elastic semi-infinite body, ignoring the boundary conditions. The replacement ratio of PCC composite foundation is m. PCC piles are arranged at the same spacing. The contact stresses upon cushions, pile heads and soil surface are uniformly distributed. Inner soils' bearing capacity is ignored. Soil-pile composite foundation is homogeneously layered. The underlying soil layers are compressible homogenous elastic body conforming to Hooker's law. The elastic soil layer, outside and inside PCC piles, has identical compression modulus E_S and shaft frictional resistance coefficient K. When the pile-soil relative displacement δ is less than the ultimate displacement δ_u, the frictional resistance is the product of relative displacement δ and frictional resistance coefficient K. Otherwise, when relative displacement δ exceeds the ultimate displacement δ_u, the frictional resistance is the product of δ_u and K.
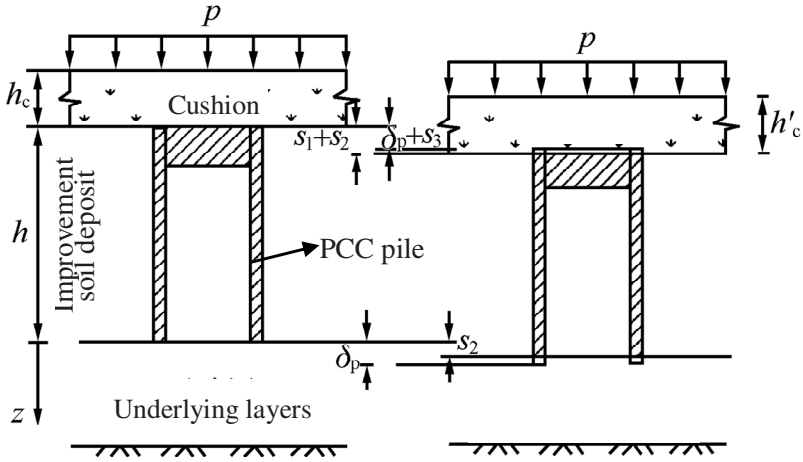
Fig. 1. PCC composite foundation loads and displacements model

2.2 Model Analyses

The upper load P on cushion is transferred to pile at P_p and soil at P_s, respectively, and quantified by Eq. 1 according to the pile-soil replacement ratio m.[3]

$$p = mP_p + (1-m)P_s .$$ (1)

The cushion deformation above pile tip due to P_p is expressed as $h_c - [h_c' - (S_1 + S_2 - S_3 - \delta_P)]$ according to Fig. 1. Thus, the pile load P_p is computed using Eq. 2.

$$P_p = E_c \frac{h_c - [h_c' - (S_1 + S_2 - S_3 - \delta_P)]}{h_c} .$$ (2)

On the other hand, the cushion deformation above soil due to P_s is expressed as $h_c - h_c'$. The load on soil, P_s, is shown in Eq. 3.

$$P_S = E_c \frac{h_c - h_c'}{h_c} .$$ (3)

The stress transferring model of PCC pile in a linear elastic condition is presented in Fig. 2 as recommended for a conventional pile.[4, 5] The pile is divided into a number of identical small units. Because all units follow deformation and stress coordination, Eq. 4 is derived and converted into Eq. 5.

$$N_z = N_z + \frac{dN_z}{dz} dz + (f_{z1}c_1 + f_{z2}c_2)dz .$$ (4)

$$\frac{dN_z}{dz} + (f_{z1}c_1 + f_{z2}c_2) = 0 .$$ (5)
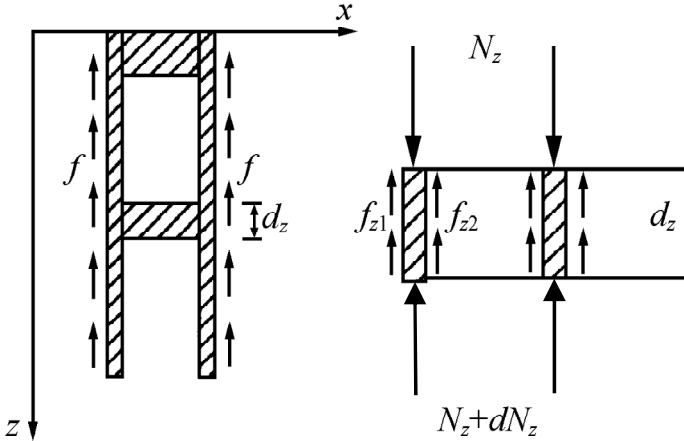
Fig. 2. Linear elastic stress transferring model of PCC pile

where, f_{z1} indicates the outer friction resistance of a unit; c_1 indicates pile outer perimeter; fz_2 is the inner friction resistance of a unit; c_2 is pile inner perimeter.

As it is assumed that soil-pile composite foundation is homogeneously layered, the compression of improved soil deposit, S_1, can be calculated by using layer-wise summation method as shown in Eq. 6.

$$S_1 = \sum_{i=1}^{n} \frac{P_{si}}{E_{si}} h_i = \varphi P_s .$$ (6)

where, n is the total layer number of improved soil deposit. The additional stress for layer i is P_{si}. The thickness of layer i is h_i. The composite modulus of layer i is E_{si}. φ represents the equivalent compression coefficient of improved deposit.

Pile may punch into cushion and underlying layer at deep S_h and S_l, respectively.[6] The pile punching effect and displacement coordination between pile and soil are taken in consideration to calculate the composite foundation modulus $\overline{E}_c$ as shown in Eq. 7.

$$\overline{E}_c \overline{\varepsilon}_c = m \varepsilon_p E_p + (1-m) E_s \varepsilon_s .$$ (7)

where, $\overline{\varepsilon}_c = \varepsilon_s = S_1 / h$, $\varepsilon_p = [S_1 - (S_h + S_l)] / h \times \varepsilon_p$. ε_p and ε_s represent the vertical strains of pile and soil, respectively. $\overline{\varepsilon}_c$ is the vertical strain of composite foundation. S_h, the depth of upper pile punching, is equal to ($S_1 + S_2 - \delta_P - S_3$); S_l, the depth of lower punching, is equal to ($\delta_p - S_2$). Eq. 7 is further converted into Eq. 8.

$$\overline{E}_c = m[1 - (S_h + S_l) / S_1] E_p + (1-m) E_s = u_p m E_P + (1-m) E .$$ (8)

where, $u_p = 1 - (S_h + S_l)/S_1 = S_3/S_1$, which indicates the performance coefficient of the pile modulus. Its value can be obtained by using iteration method.

The compression of underlying layers, S_2, can be calculated by using layer-wise summation method as shown in Eq. 9.

$$S_2 = \sum_{j=1}^{k} \frac{P_{sj}}{E_{sj}} h_j.$$ (9)

where, k is the total number of compressible underlying layers; P_{sj} is the additional stress for underlying layer j; h_j is the thickness of underlying layer j; E_{sj} is the compression modulus of underlying layer j. P_{sj} can be calculated by using stress diffusion method.[3]

The total amount of PCC pile compression is relatively small, which can be approximately calculated using Eq. 10.

$$S_3 = (P_P A_1)/(E_P A) = G P_P.$$ (10)

where, $A_1 = \pi D^2$, indicating pile-soil section area; $A = \pi (D^2 - d^2)$, indicating PCC pile annular area; $G = (A_1 h)/(E_P A)$.

Under elastic conditions, the pile-soil displacement is relatively small. Suppose the compression curve of improved deposit is linear, and the compression of rigid piles varies linearly with depth, the outer shaft friction resistance of the pile is expressed using Eq. 11.

$$f_{z1} = K[\delta_p - (S_1 + S_2 - S_3) + (z/h)(S_1 - S_3)].$$ (11)

Similarly, suppose the compression curve of the inner soil is linear, the inner shaft friction resistance at point Z is expressed in Eq. 12.

$$f_{z2} = K(z/h)[\delta_p + S_3(1 - z/h) - S_2].$$ (12)

By applying Eqs. 11 and 12 to Eq. 5, Eq. 13 is obtained.

$$\frac{dN_Z}{dZ} = -Kc_1 \frac{S_1 - S_3}{h} z - Kc_1 \delta_p + Kc_1(S_1 + S_2 - S_3) - Kc_2 \frac{z}{h}(\delta_p + S_3 - S_2) + Kc_2 S_3 \frac{z^2}{h^2}.$$ (13)

Given the boundary condition at pile cap, $N_z = P_p A_1$, as shown in Fig. 2, Eq. 13 is integrated into Eq. 14.

$$N_z = \frac{1}{3} Kc_2 S_3 \frac{z^2}{h_2} - \frac{1}{2} Kc_1 \frac{S_1 - S_3}{h} z^2 - \frac{1}{2} Kc_2 \frac{z^2}{h}(\delta_p + S_3 - S_2) - Kc_1 \delta_p z$$
$$+ Kc_1(S_1 + S_2 - S_3)z + P_p A$$ (14)

It is supposed that the pile tip foundation conforms to Winkler's Law.[7] Therefore, when point Z reaches to depth h in Fig. 2, the axial stress of pile tip, N_z, is $k_s A(\delta_P - \delta_2)$. K_s is the coefficient of subgrade reaction for the pile tip bearing layer. Apply it to Eq. 14, Eq. 15 is obtained.

$$\frac{1}{2}Kc_1h(S_1 - S_3) - \frac{1}{6}Kc_2hS_3 - \alpha\delta_P + \alpha S_2 + P_pA_1 = 0. \tag{15}$$

where, $\alpha = k_sA + Kc_1h + \frac{1}{2}Kc_2h$.

Combining Eqs. 1 to 3, 6, 10 and 15, pile load P_p, soil load P_s, and compressed cushion thickness h'_c are computed as shown in Eqs. 16, 17 and 18, respectively.

$$P_p = \frac{P[(1-m)\theta\varphi + \alpha\beta]}{m\alpha\beta + (1-m)(\theta G + \alpha\beta + A_1 - \frac{1}{6}Kc_2hG)}. \tag{16}$$

$$P_s = \frac{P(\theta G + \alpha\beta + A_1 - \frac{1}{6}Kc_1hG - m\theta\varphi}{m\alpha\beta + (1-m)(\theta G + \alpha\beta + A_1 - \frac{1}{6}Kc_2hG)}. \tag{17}$$

$$h_c = \left(1 - \frac{P_s}{E_c}\right)h_c = h_c - P_s\beta. \tag{18}$$

where, $\beta = h_c/E_c$, $\theta = k_sA + \frac{1}{2}Kc_1h + \frac{1}{2}Kc_2h + \frac{1}{2}Kc_2h$.

Thus, the total deformation of the composite foundation is shown in Eq. 19.

$$S = S_1 + S_2 + h_c - h'_c = \varphi P + \beta P_s + S_2. \tag{19}$$

The pile-soil stress ratio is shown in Eq. 20.

$$N = \frac{P_p}{P_o} = \frac{(1-m)\theta\varphi + \beta\alpha}{\theta G + \alpha\beta + A_1 - \frac{1}{6}Kc_2hG - m\theta\varphi}. \tag{20}$$

Parameter u_p can also be calculated using Eq. 21.

$$u_P = \frac{S_1}{S_3} = \frac{G}{\varphi}\frac{(1-m)\theta\varphi + \alpha\beta}{m\alpha\beta + (1-m)(\theta G + \alpha\beta + A_1 - \frac{1}{6}Kc_2hG)}. \tag{21}$$

In Eq. 21, because φ is related to u_p, value of u_p cannot be calculated directly. Iteration method may provide an analytical value of u_p by following procedures.

First, suppose a relatively small value of u_{p1} and run the calculations to obtain the value of φ and a new value u_{p2}. Secondly, run a comparison between calculated u_{p2} and supposed value u_{p1}. If u_{p2} is larger than u_{p1}, increase supposed u_{p1} in a proper addition to u_{p3}, re-run the calculations. Repeat the procedures until u_{pi} and

$u_{p(i-1)}$ are identical. Final value u_{pi} is the performance coefficient of pile modulus. Based on the iteratively inferred u_{pi} value, the pile-soil stress ratio and the PCC composite foundation settlement are obtained. A program can be coded to run the iterative computations according to design data of PCC composite foundation.

3   Case Study

A case study was conducted to verify the analytical solution developed in this study. Hang-Ning Highway links Hangzhou and Nanjing and crosses most soft ground zones. The PCC composite foundation was applied for improving soils at Changxing section of the highway.

   The PCC pile spacing is 2.5 m. The outer diameter D and inner diameter d of the pile is 1.0 and 0.76 m, respectively. The pile length h is 16 m. The composite foundation displacement ratio m is 0.053. The cushion, composed of gravels and sands, is 0.5 m thick with E_c being 31 MPa.[8] The coefficient subgrade reaction K_s is 20 MPa.[8] The embankment filling height is 4.5 m. After iterative computations, U_p is calculated as 5.6%; pile-soil stress ratio is 12.2; the settlement of improvement deposit S_1 is 21.5 mm; the settlement of underlying layers S_2 is 104.3 mm; the total settlement of composite foundation is 125 mm. Field monitoring data indicate that the maximum pile-soil stress ratio is 16, and the composite foundation settlement is 141 mm. Calculated results are less than but close to monitored data. Therefore, analytical solution is validated.

4   Concluding Remarks

Analytical solutions are derived regarding the composite modulus, the pile-soil stress ratio, and the settlement of PCC composite foundation, based on the displacement coordination of pile-soil-cushion unit model. The analytical solutions help understand the pile-soil interaction mechanism, optimize PCC composite foundation design, and predict foundation's future primary settlement. Monitored data in a highway project using PCC composite foundation present good agreement with calculated data according to analytical solutions, and thus the derived solutions are verified.

References

1. Liu, H. L., Fei, K., Ma, X. H.: Field Pour Concrete Cased Pile with Vibrated and Steel Tube Mould Technology and its Application I: Development and Design Theory. Rock Soil Mech. 24 (2003) 164-168
2. Liu, H. L., Hao X. Y., Fei, K.: Field Pour Concrete Cased Pile with Vibrated Steel Tube Mould Technology and its Application II: Application and in-situ Test. Rock Soil Mech. 24 (2003) 372-375

3. Gong, X. N.: The Theory and Practice of Composite Foundation. China Architecture Building Press, Beijing (2001)
4. Zhang, S. N.: Pile-Soil Stress Ratio Study of Mixing Pile Composite Foundation. Foundation Treatment, 6 (1995) 9-14
5. Ronald Y. S. P., Feng, J.: Rational Mechanical of Axial Soil-Pile Interaction. J. Eng. Mech. 119 (1993) 813-831
6. Mao, Q., Gong, X. N.: Research on the Properties of Cushion of the Composite Ground. Rock Soil Mech. 19 (1998) 67-73
7. Fu, J. H., Song, E. X.: Analysis of Rigid Pile Composite Foundation Working Performance. Rock Soil Mech. 21 (2000) 335-339
8. Zhou, J. X., Wang H. J., Yu, S. M.: Foundation Construction. Tsinghua University Press, Beijing (1996)

Numerical Analysis and Risk Assessment on Face Stability of Large-Diameter Tunnels

Qunfang Hu[1] and Hongwei Huang[2]

[1] Shanghai Institute of Disaster Prevention and Relief, Tongji University, Shanghai, China
huqunf@mail.tongji.edu.cn
[2] Department of Geotechnical Engineering, Tongji University, Shanghai, China
huanghw@mail.tongji.edu.cn

Abstract. For the two types of shield tunneling such as Slurry and EPB shield the stability of tunnel face depends on the prevailing support pressure. The support pressure at the tunnel face has to be applied to a value that gives as well sufficient safety against a collapse of the tunnel face as the against uplifting. The paper aims at a better understanding of the mechanics of face failure for those lager-diameter tunnels. And some different determination methods of the applied support pressure are compared and given a risk assessment, which are illustrated their application by numerical analysis in the Yangtze River Tunnel of Shanghai.

Keywords: face stability, risk assessment, numerical analysis, large-diameter tunnel.

1 Introduction

With underground excavations and construction works progress into much larger diameter tunnels and more complex geological environments, Slurry shield and EPB tunneling have been successfully applied worldwide in recent years, which allow the control the surface settlement and limit the risk of tunnel face failure through the continuous support the face. However, face instabilities may occur under extremely unfavorable geological conditions, especially some lager-diameter tunnels like the Yangtze River Tunnel of Shanghai whose outside diameter is about 15.0m.

As is known, Peck [1] introduced the one of main issues to be addresses for the design and construction of tunnels: stability of the opening during construction with particular attention to the tunnel face stability. The stability of tunnel face is of paramount importance for construction the lager-diameter tunnel works. Several approaches have been developed to analyze and calculate the support pressure of tunnel face over the past thirty years. Early works on face stability were concerned with tunnels constructed in clays (Broms and Bennermark [2]; Peck [1]). Then a more theoretical approach based on limit analysis was presented for clays by Davis et al [3]. Within the framework of limit analysis, some lower bound solutions were presented to analyze tunneling in sandy ground by Muelhaus [4], Leca and Panet [5] and Leca and Dormieux [6]. And the approaches were checked against model tests performed with Fontainebleau sand in the centrifuge of the Laboratoire Central des Ponts et Chaussées (LCPC) in Nantes, France (Chambon and Corté [7,8]). Another approach,

taking full account of the 3-dimensional geometry at the tunnel face, was proposed by Anagnostou and Kovári [9, 10, 11], using limit equilibrium principles based on the Horn [12] (see figure 1) model. Recent developments allowed the computational methods of tunnel face support pressure were proposed and performed by many researchers, Chen Z.L. [13], W. Broere [14], Vermeer P.A.& Ruse N. [15].

There are so many methods for calculating the support pressure of tunnel face, and it is not easily to select the best one for design and construction large-diameter tunnel. The paper aims at a better understanding of the mechanics of face failure for those large-diameter tunnels by 3-Dimensional numerical simulation. And some different determination methods of the applied support pressure are compared here and given a risk assessment, which are illustrated their application by numerical analysis in the Yangtze River Tunnel of Shanghai.

2   Different Computational Methods on Support Pressure of Tunnel Face

In order to analyze the mechanics of face failure for those large-diameter tunnels by 3-D numerical simulation, 6 different computational methods were introduced as follows.

(1) The computational model of passive earth pressure [16]
(2) The computational model of earth pressure at rest [16]
(3) The computational model of active earth pressure [16]
(4) The computational model of Chen Z.L. [13]

$$p_z = (0.6 \sim 0.7) \tan^2(\frac{\pi}{4} - \frac{\phi'}{2})(\sigma_v - u) + u \tag{1}$$

Where u is the pore water pressure, and φ' is soil effective friction angle.

(5) The computational model of Ruse. N. [15]

$$p_R = -c' \cot \varphi' + \gamma D \left(\frac{1}{9 \tan \varphi'} - 0.05 \right) \tag{2}$$

Where c' and φ' are soil effective cohesion and soil effective friction angle respectively, γ is the unit soil weight at the depth of tunnel axis, and D is tunnel diameter.

(6) The computational method of the minimal support pressure based on the Multilayered Wedge model

To construct a wedge stability model, as sketched in Fig.1, which could handle heterogeneous soil conditions by Anagnostou and Kovári [9, 10, 11], the horizontal slice model described by Walz [17] for slurry-filled trenches might serve as a starting point. The failure wedge is subdivided in N smaller bodies by W. Broere [14], see Fig. 2, possibly of different thickness, inside each of which the soil conditions are homogeneous. The soil conditions would vary between these slices, as may the wedge angle θ_i between the i th slice's slanted failure plane and the horizontal. The conditions of horizontal and vertical equilibrium could lead to calculate the minimal support pressure as follows.
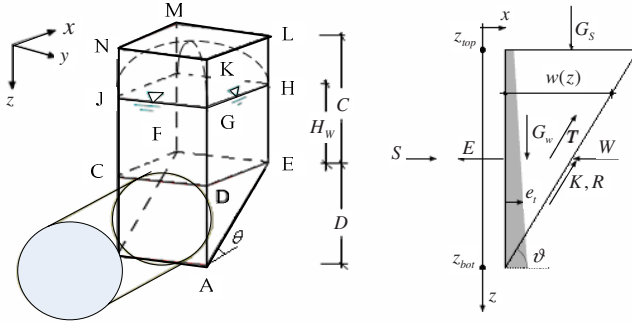
Fig. 1. Wedge-loaded model of three-dimensional tunnel face failure mechanism by soil silo

Each slice i is loaded by the resulting forces from the slice above $(i-1)$ and below $(i+1)$, $Q_a^{(i)}$ and Q_b^i respectively, the effective weight of the slice itself G_w^i and an overburden force G_s^i. At the slanted failure plane there is a cohesive force $K^{(i)}$ acting parallel to the plane, as well as a friction force $R^{(i)}$, which results from the normal force $N^{(i)}$, working perpendicular to the failure plane. The side faces of the wedge are each assumed to be loaded by the shear force $T^{(i)}$, which act in the same direction as $K^{(i)}$, against the deformation direction of the wedge. Force equilibrium will yield the effective earth force $E^{(i)}$ at the face which, combined with the water force $W^{(i)}$, is equal to the support force $S^{(i)}$.
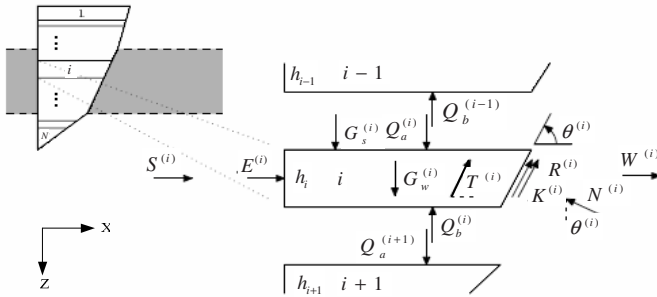
Fig. 2. Multilayered Wedge model of three-dimensional tunnel face failure for calculating the minimal support pressure

$$p_{\min} = 4 \cdot S /(\pi \cdot D^2), \ S = E + W \tag{3}$$

$$E = -\frac{\xi'_-}{\xi'_+}[G_S + G_w + \sum_{i=1}^{N} \frac{1}{\xi^{(i)}_-}(2T^{(i)} + K^{(i)})], \ \frac{\xi'_+}{\xi'_-} = \frac{1}{N}\sum_{i=1}^{N}\frac{\xi^{(i)}_+}{\xi^{(i)}_-} \tag{4}$$

Where all computational parameters are given in Fig. 2, and some functions were explained [14] and [16].

3   Numerical Analysis Model and Risk Assessment

3.1   The Model of Numerical Analysis

According to all above computational methods of support pressure of tunnel face, some different support pressure of tunnel face may be calculated. When large-diameter tunnels were designed and constructed, the factual support pressure at the tunnel face had to be applied to a value that gives as well sufficient safety against a collapse of the tunnel face as the against uplifting. So the appropriate support pressure should be selected through analyzing the mechanics of face failure for large-diameter tunnel. In order to analyze the mechanics of tunnel face failure through numerical simulation, there were some problems which needed to be considered in advance.

(1) The method of numerical analysis. There are so many softwares such as ANSYS, ABAQUS, Plaxis and FLAC3D etc., which could be used to simulate and analyze the process of tunneling. Because the method of numerical analysis aimed at a better understanding and simulating of the mechanics of face failure for those lager-diameter tunnels, the selected software should calculate the 3-D tunnel built of soil that undergo large deformation, plastic flow and face collapse. As is known, FLAC3D offers an ideal analysis tool for solution of 3-D problems in geotechnical engineering. And it could accord with the requirement of numerical analysis for engineering mechanics computation of tunnel face instability.

(2) The criterion to judge the face failure of tunnel. The key problem is to establish a criterion for judging the plastic or collapse condition of tunnel face. There are two criteria [18], one is to set the non-convergence of force and displacement of tunnel face as a judgment of numerical analysis; and the other is to set the plastic flow or the yield stress state as determining the face failure condition. After considered that the distribution of plastic zone was influenced by many factors such as Poisson's ratio, flow rule, etc, non-convergence of displacement in numerical analysis program could be taken as a suitable evaluating criterion for estimating the tunnel face failure.

(3) How to apply the support pressure to tunnel face. When tunnel face was excavating by slurry shield or EPB, the force distribution of in-suit tunnel face was trapeziform from the top to bottom of tunnel. So how to apply the support pressure to balance the in-suit earth pressure is a big problem. There are two application modes, one is to apply the support pressure to balance the earth pressure of tunnel face at the center of tunnel axis, and the other is to apply the support pressure to balance the earth pressure of tunnel face at the point of composition forces of tunnel face. Because the numerical simulation was to analyze the face stability of large-diameter tunnel, the latter mode was selected as a application mode of support pressure.

3.2   Risk Assessment

During the excavation of tunnel face, the distribution of earth pressure would change with tunneling. The face stability was a dynamic condition (see Fig.3). That is, the face stability would be undergone from a stable state to limit equilibrium and to instability even face collapse. So the risk about face stability of large-diameter tunnel

could be assessed through the criterion for judging the face failure with the ratio of support pressure to vertical earth pressure at the centre of tunnel face.

$$\lambda = p / \sigma_v \tag{5}$$

Where p is the support pressure at tunnel face, and σ_v is the vertical earth pressure at the centre of tunnel face.
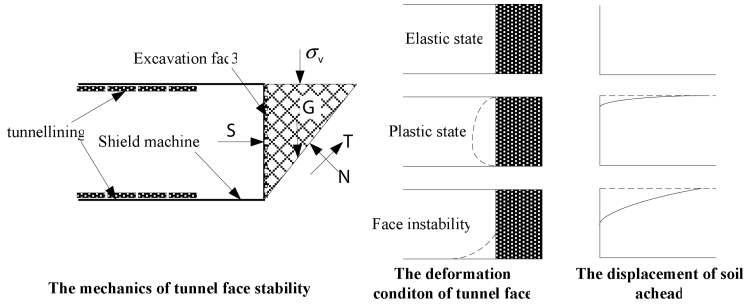
Fig. 3. The face stability condition and displacement of tunneling when the support pressure was decreased gradually

3.3 Case Study

Yangtze River tunnel is the south crossing way from Pudong to Changxing Island in Shanghai. This tunnel has about a 7.5km in length and 15m in outside diameter. In order to illustrate the method of numerical analysis and risk assessment, the tunnel alignment pile K0+589 was studied [16]. Based on the geology investigation data and tunnel structure design, the computational parameters of soil and tunnel at No K0+589 are shown in Table 1.

Table 1. The computational parameters of soil at Pile No. K0+589

Soil type	thickness m	γ kN/m^3	c kPa	φ	c' kPa	φ'	q_u kPa	E_s MPa	K_0
②₃	4	18.7	8	27	-	-	-	10.84	-
③₁	3.5	17.5	13	12.5	8	30.3	43	3.27	0.57
③₂	2.5	18.3	7	28.5	-	-	-	9.06	-
④	16.5	16.9	14	10.5	10	26.8	52	2.62	0.63
⑤₁	1.2	17.3	16	12	15	25.2	58	3.19	0.61
⑤₂	17.3	18	12	22	-	-	-	5.99	0.38
⑦₁₋₂	10.45	18.2	12	24	-	-	-	5.86	0.37

The different support pressures of large-diameter tunnel face were calculated by all above methods. And the deformation of the large-diameter tunnel could be studied by the different support pressure using the software Flac3D. And the risk assessment [19] could be given by the ratio of support pressure to vertical earth pressure at the centre of tunnel face shown as Table 2.

Table 2. Risk assessment of different support prrssure applied on the tunnel face

Support pressure	p_p	p_0	p_a	p_z	p_R	p_{min}
p/kPa	473.356	202.891	197.519	91.417	65.804	51.75
$\lambda = p/\sigma_v$	1.56	0.67	0.65	0.30	0.22	0.17
Risk class	serious	insignificant	considerable	serious	serious	severe

(a) the relation of displacement and support pressure of tunnel face

(b) the relation of displacement velocity and support pressure of tunnel face
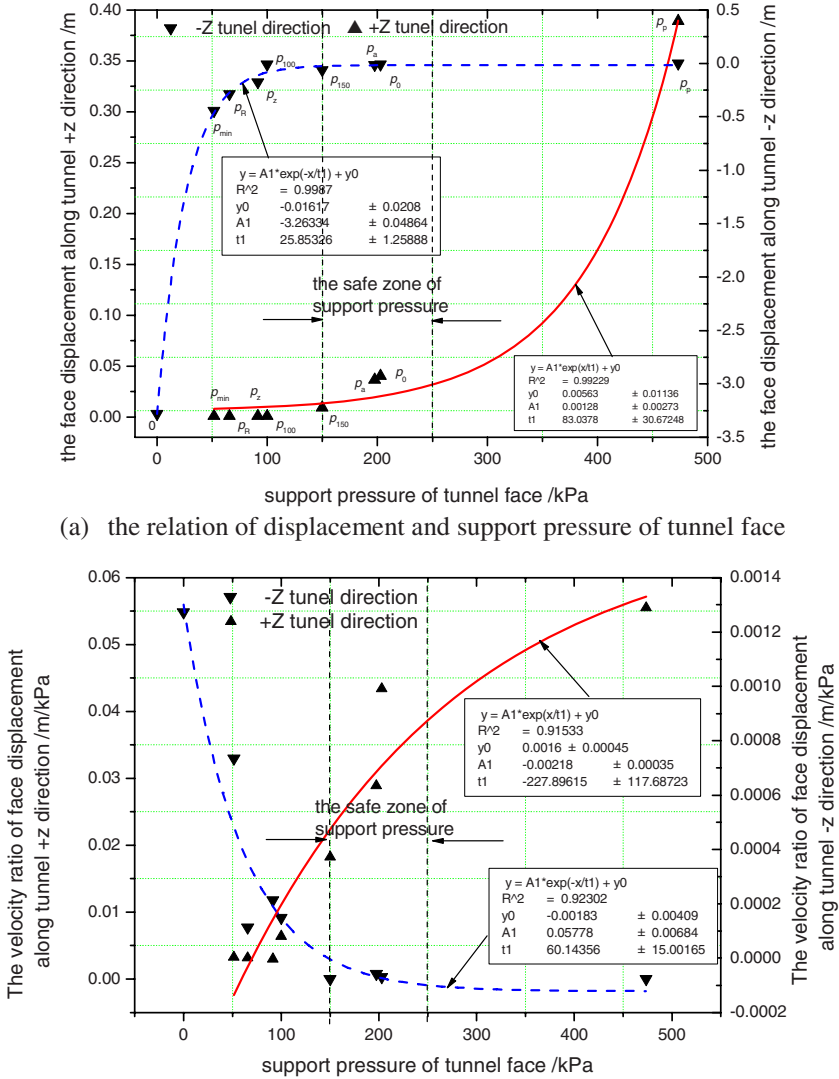
Fig. 4. The relation of displacement and support pressure of tunnel face

As the support pressure of tunnel face was decreased from p_p to p_0, the +z direction displacement along tunnel alignment was also decreased, otherwise, the -z direction displacement along tunnel alignment was increased (See Fig.4 (a)). When the support pressure was decreased from p_0 to p_{min}, the +z direction displacement along tunnel alignment was still reduced to 0m, simultaneity, the -z direction displacement along tunnel alignment was increased the maximum, that is face collapse or instability when support pressure was null. The relation of displacement velocity and support pressure of tunnel face was shown in Fig.4 (b).

When the large-diameter was excavated by shield machine, the safety support pressure could be estimated by the displacement velocity of tunnel face to which was applied different support pressure. And the safe zone of support pressure of pile No.K0+589 was shown in Fig.5 (a) and Fig.5 (b).

4   Conclusions

(1) There were so many method which could be used to calculate the support pressure of large-diameter, and the actual support pressure was a value that gave as well sufficient safety against a collapse of the tunnel face as the against uplifting. So it is essential that the mechanics of face stability should be studied before the design and construction. And the method of numerical analysis and risk assessment could provide a new approach to determinate the safe support pressure.

(2) The face stability of tunnel was a dynamic process when the support pressure was changed during shield tunneling. The numerical analysis could give an elaborate simulation of the displacement process while the support pressure was decreased gradually. Compared the displacement and displacement velocity of different support pressure, the risk of tunnel face stability may be assessed simultaneity. And the risk management of tunnel construction should also be paid much attention to consider and adopt when the large-diameter tunnel was excavating.

References

1. Peck, R.B.: Deep excavations and tunneling in soft ground. Proceedings 7th International Conference Soil Mechanics and Foundation Engineering, Mexico, State-of-the-Art Volume (1969) 225-290
2. Broms, B.B. (ed.): Stability of Clay at Vertical Openings. ASCE Journal of the Soil Mechanics and Foundation Division, SM1 (1967) 71-94
3. E. H. Davis (ed.): The stability of shallow tunnels and underground openings in cohesive material, Geotechnique, Vol.30, No.4 (1980)397-416
4. H. B. Muelhaus: Lower bound solutions for circular tunnels in two or three dimensions, Rock Mech. Rock Engng., Vol.18 (1985) 37-52

5. Leca, E. and Panet, M: Application du calcul à la rupture à la stabilité du front de tailled'un tunnel. Revue Française de Géotechnique (1988) 5-19

6. Leca, E. (ed.): Upper and lower bound solutions for the face stability of shallow circular tunnels in frictional material. Géotechnique, Vol. 40, No.4 (1990) 581-606

7. Chambon, P. and Corté, J.F.: Stabilité du front de taille d'un tunnel faiblement enterré:modélisation en centrifugeuse. Proc. Int. Conf. Tunnelling and Microtunnelling in Soft Ground:From field to theory, Paris (1989) 307-315

8. Chambon, P. and Corté, J.F.: Shallow tunnels in cohesionless soil: stability of tunnel face. ASCE Journal of Geotechnical Engineering, Vol.120, No.7 (1994)1148-1165

9. Anagnostou, G.: A Model for Swelling Rock in Tunnelling. Rock Mechanics and Rock Engineering, Vol. 26, No. 4 (1993) 307-311

10. Anagnostou, G. and Kovàri, K.: Face Stability in Slurry and EPB Shield Tunneling. Proceedings International Symposium Geotechnical Aspects of Underground Construction in Soft Ground, London, 15-17 April 1996, R.J. Mair & R.N. Taylor Eds. (1996a) 453-458

11. Anagnostou, G. and Kovàri, K.: Face Stability Conditions with Earth-Pressure-Balanced Shields. Tunnelling and Underground Space Technology, Vol. 11, No. 2 (1996b) 165-173

12. Horn, M. Alagutak homlokbiztositására ható vizszintes földnyomásvizsgálat néhány erdménye. Landeskonferenz der ungarischen Tiefbauindustrie,Budapest (1961)

13. Chen Z.L., (ed.): Experimental study on stability of tunnel excavation surface in sand foundation by slurry shield method, Vol. 18, No.5 (2001)53-55

14. W. Broere. Tunnel Face Stability & New CPT Applications. PhD thesis, Delft University of Technology, Delft (2001)

15. Vermeer P.A., (ed.): Tunneling heading stability in drained ground. Felsbau (2002) 8-18

16. Q.F.Hu. Risk Analysis and Its Application for Tunnel Works based on Research of Stratum and Soil Spatial Variability. PhD thesis, Tongji University, China (2001)

17. B. Walz, J. (ed.): Berechnung und Ausfˈuhrung. Technical report, Bergische Universitˈat Gesamthochschule Wuppertal (1983)

18. ZHAO Shang-yi (ed.): Slope safety factor analysis by strength reduction FEM. Chinese Journal of Geotechnical Engineering, Vol.24, No. 3 (2002) 343-346

19. D.E. Søren (ed.): Guidelines for the Tunneling Risk Management [J]. Tunneling and Underground Space Technology, Vol. 19, Issue 3, May (2004) 217-237

Torsional Pile Subjected to Transient Loading in Viscoelastic Poroelastic Medium

Yuanqiang Cai, Gang Chen, and Feiyu Liu

College of Civil Engineering and Architecture, Zhejiang university, Hangzhou 310027, China

Abstract. Considering viscoelastic saturated soil, The transient dynamic response of an elastic pile is studied. The pile-soil system is divided into thin layers, the control equations of the soil are solved respectively by using Laplace transform. Considering the mixed boundary-value conditions at the interface of pile and soil, expression is derived to describe the relationship between the inner force and the displacement of the pile segment. Then the expressions of all pile segments are integrated to form the stiffness matrix of pile. Considering the transient torsional loading at the pile head, the pile displacement in time domain is calculated by numerical method, with the result showing the influence of various pile parameters.

Keywords: poroelastic medium; viscidity; elastic pile; transient dynamic response.

Wide attention has been paid to the research on the dynamic response of pile foundations. Novak [1, 2] has studied pile's torsional vibration and revealed the fundamental characteristics of the interaction between the pile and the surrounding soil. Zeng [3], Jin [4] and Cai[5] have studied the time harmonic response of elastic pile embedded in a poroelastic half-space with axial, lateral and torsional loading respectively. The analysis of pile foundation subjected to transient dynamic loading is a complex task. Militano [6] have studied the dynamic response of an elastic pile subjected to transient torsional and axial loading. It should be noted that no work on transient torsional response of a pile embedded in poroelastic soil has been reported in literature. The main objective of this paper is to present the dynamic response of an elastic pile embedded in saturated soil under transient torsional loading (Fig. 1), and the viscidity of soil is considered too. The influence of parameters of pile and soil is clarified from the numerical computation results.
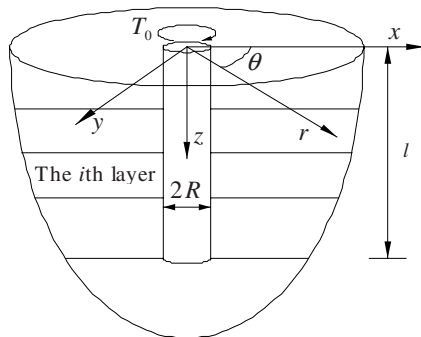
Fig. 1. Elastic pile embedded in a saturated soil

1 Basic Equations and Solution

The soil is divided into k thin layers, and the equilibrium equation of the soil layer corresponding to torsional loading can be expressed as:

$$\frac{\partial \sigma_{r\theta}}{\partial r}+\frac{\partial \sigma_{\theta z}}{\partial z}+2\frac{\sigma_{r\theta}}{r}=\rho\frac{\partial^2 u_\theta}{\partial t^2}+\rho_w\frac{\partial^2 w_\theta}{\partial t^2} \tag{1}$$

where $\sigma_{r\theta}$, $\sigma_{\theta z}$ are shear stresses of soil; $\rho=(1-n)\rho_s+n\rho_w$, ρ_s, ρ_w signify the densities of the solid phase and the fluid phase respectively; u_θ, w_θ denote the displacements of the solid phase and the fluid phase in the θ-direction respectively.

The Voigt-Kelvin model is adopted to describe the viscidity of soil. The constitutive equations are:

$$\sigma_{r\theta}=G\varepsilon_{r\theta}+G'\dot{\varepsilon}_{r\theta} \tag{2}$$

$$\sigma_{\theta z}=G\varepsilon_{\theta z}+G'\dot{\varepsilon}_{\theta z} \tag{3}$$

where G' denote the viscous parameter of the medium. $\varepsilon_{r\theta}=\frac{1}{r}\frac{\partial u_r}{\partial \theta}+\frac{\partial u_\theta}{\partial r}-\frac{u_\theta}{r}$,

$\varepsilon_{\theta z}=\frac{\partial u_z}{\partial r}+\frac{\partial u_r}{\partial z}$, $\dot{\varepsilon}=\frac{\partial \varepsilon}{\partial t}$.

The equilibrium equation of the fluid can be expressed as follows:

$$\frac{\rho_w g}{k_d}\frac{\partial w_\theta}{\partial t}+\rho_w\frac{\partial^2 u_\theta}{\partial t^2}+\frac{\rho_w}{n}\frac{\partial^2 w_\theta}{\partial t^2}=-\frac{1}{r}\frac{\partial p_w}{\partial \theta}=0 \tag{4}$$

where k_d is the dynamic permeability coefficient containing the viscidity of liquid; g denotes the gravitational acceleration; p_w is the excess pore fluid pressure.

Militano [6] studied the transient torsional response of a pile embedded in elastic soil by neglecting the gradient of $\sigma_{r\theta}$ in the vertical direction. Following a similar assumption and considering the viscidity of soil, Equation (1) can be expressed in terms of $u_\theta(r,t)$ as:

$$G\left(\frac{\partial^2 u_\theta}{\partial r^2}+\frac{1}{r}\frac{\partial u_\theta}{\partial r}-\frac{u_\theta}{r^2}\right)+G'\frac{\partial}{\partial t}\left(\frac{\partial^2 u_\theta}{\partial r^2}+\frac{1}{r}\frac{\partial u_\theta}{\partial r}-\frac{u_\theta}{r^2}\right)=\rho\frac{\partial^2 u_\theta}{\partial t^2}+\rho_w\frac{\partial^2 w_\theta}{\partial t^2} \tag{5}$$

The Laplace transform is introduced and its definition is given by:

$$\hat{f}(r,p)=\int_0^\infty f(r,t)e^{-pt}dt \tag{6}$$

where p is the Laplace transform parameter.

Considering Equation (4), after introducing the dimensionless constants and variables, the government equation can be expressed in the Laplace transform space:

$$\frac{\partial^2 \hat{\bar{u}}_\theta}{\partial \bar{r}^2}+\frac{1}{\bar{r}}\frac{\partial \hat{\bar{u}}_\theta}{\partial \bar{r}}-\left(s^2+\frac{1}{\bar{r}^2}\right)\hat{\bar{u}}_\theta=0 \tag{7}$$

where $s^2 = \dfrac{1}{1+p\eta}\left(1+\dfrac{n\overline{k}_d}{n+p\overline{k}_d}\overline{\rho}_w p\right)p^2$, $\eta = \dfrac{G'}{G}$, $\overline{u}_\theta = \dfrac{u_\theta}{R}$, $\overline{w}_\theta = \dfrac{w_\theta}{R}$, $\overline{r} = \dfrac{r}{R}$,

$\overline{\rho}_w = \dfrac{\rho_w}{\rho}$, $\overline{t} = \dfrac{t}{R}\sqrt{\dfrac{G}{\rho}}$, $\overline{k}_d = \dfrac{k_d}{Rg}\sqrt{\dfrac{G}{\rho}}$.

The general solutions of Equation (7) can be expressed as:

$$\hat{\overline{u}}_\theta\left(\overline{r},p\right) = AI_1\left(s\overline{r}\right) + BK_1\left(s\overline{r}\right) \tag{8}$$

where I_n , K_n are modified Bessel functions of the first and second kind respectively. $A(p)$, $B(p)$ are arbitrary functions.

The soil is assumed to be infinite in the radial direction, with the displacement and stress of soil tending to be zero as $r \to \infty$. Considering the characters of the first and second kind Bessel functions, $A(p) \equiv 0$ can be identified. The displacement and stress can be expressed as:

$$\hat{\overline{u}}_\theta\left(\overline{r},p\right) = BK_1\left(s\overline{r}\right) \tag{9}$$

$$\hat{\overline{\tau}}_{r\theta}\left(\overline{r},p\right) = \dfrac{\partial \hat{\overline{u}}_\theta}{\partial \overline{r}} = -(1+p\eta)BsK_2\left(s\overline{r}\right) \tag{10}$$

The relationship between $\hat{\overline{u}}_\theta$ and $\hat{\overline{\tau}}_{r\theta}$ can be deduced:

$$\hat{\overline{u}}\left(\overline{r},p\right) = -\dfrac{K_1\left(s\overline{r}\right)}{s(1+p\eta)K_2\left(s\overline{r}\right)}\hat{\overline{\tau}}_{r\theta}\left(\overline{r},p\right) \tag{11}$$

2   Impedance of Pile Segments and the Whole Pile

Fig.2 shows a typical pile segment subjected to torsional loading. The dynamic response of the ith pile segment is described as follows:

$$G_p\dfrac{\partial^2\varphi}{\partial z^2} + 4\dfrac{\tau_\theta}{R^2} = \rho_p\dfrac{\partial^2\varphi}{\partial t^2} \tag{12}$$

where G_p and ρ_p denote the shear modulus and mass density of pile, τ_θ is the contact stress between soil and pile.

After introducing the dimensionless groups $\overline{z} = \dfrac{z}{R}$,

$\overline{G} = \dfrac{G_p}{G}$, $\overline{\tau}_\theta = \dfrac{\tau_\theta}{G}$, $\overline{\rho}_p = \dfrac{\rho_p}{\rho}$, Equation (12) can be

expressed in the Laplace transform domain as:
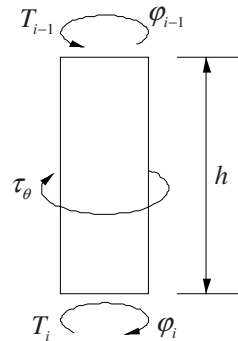
Fig. 2. Pile segment discreted

$$\overline{G}_P \frac{\partial^2 \hat{\overline{\varphi}}}{\partial \overline{z}^2} + 4\hat{\overline{\tau}}_\theta = \overline{\rho}_P \left(p^2 \hat{\overline{\varphi}} - pa_{i0} - \varphi_{i0} \right) \tag{13}$$

where a_{i0} and φ_{i0} denote the initial values of rotational and angular velocities of the ith pile segment, and are assumed to be zero. $\hat{\overline{\tau}}_\theta$ can be substituted by $\hat{\overline{\tau}}_{r\theta}\big|_{r=1}$ of soil,

and is equal to $-\dfrac{sK_2(s\overline{r})}{K_1(s\overline{r})} \hat{\overline{u}}_\theta(\overline{r}, p)\bigg|_{r=R}$. Therefore, the general solution of Equation (12)

can be given as:

$$\hat{\overline{\varphi}}(\overline{z}, p) = C \exp(-\omega\overline{z}) + D \exp(\omega\overline{z}) \tag{14}$$

where $\omega = \left\{ \dfrac{4sK_2(s)}{\overline{G}_P K_1(s)} + \dfrac{\overline{\rho}_P p^2}{\overline{G}_P} \right\}^{\frac{1}{2}}$; $C(p)$ and $D(p)$ are arbitrary functions to be

determined from the boundary conditions.

The relationship between the inner force and displacement of elastic pile can be

expressed as $T(z) = \dfrac{G_P \pi R^4}{2} \dfrac{\partial \varphi}{\partial z}$, with the application of the Laplace transform

resulting in:

$$\hat{\overline{T}}(z, p) = \frac{\overline{G}_P \pi}{2} \frac{\partial \hat{\overline{\varphi}}}{\partial \overline{z}} = \frac{\overline{G}_P \pi \omega}{2} \left[-C \exp(-\omega\overline{z}) + D \exp(\omega\overline{z}) \right] \tag{15}$$

In the Laplace transform space, the inner forces and displacements at the segment

top and bottom of the ith segment are denoted as $\hat{\overline{T}}_{i-1}$, $\hat{\overline{T}}_i$, $\hat{\overline{\varphi}}_{i-1}$, $\hat{\overline{\varphi}}_i$. The substitution

of the boundary condition in Equation (14) yields:

$$\left\{ \begin{matrix} C \\ D \end{matrix} \right\} = \frac{1}{\exp(\omega\overline{h}) - \exp(-\omega\overline{h})} \left[\begin{matrix} \exp(\omega\overline{h}) & -1 \\ -\exp(-\omega\overline{h}) & 1 \end{matrix} \right] \left\{ \begin{matrix} \hat{\overline{\varphi}}_{i-1} \\ \hat{\overline{\varphi}}_i \end{matrix} \right\} \tag{16}$$

Integrating Equations (15) and (16) yields the following relationship for the pile

segment:

$$\left\{ \begin{matrix} \hat{\overline{T}}_{i-1} \\ \hat{\overline{T}}_i \end{matrix} \right\} = \alpha \left[\begin{matrix} -\beta & 2 \\ -2 & \beta \end{matrix} \right] \left\{ \begin{matrix} \hat{\overline{\varphi}}_{i-1} \\ \hat{\overline{\varphi}}_i \end{matrix} \right\} \tag{17}$$

where $\alpha = \dfrac{\overline{G}_P \pi \omega}{2 \left[\exp(\omega\overline{h}) - \exp(-\omega\overline{h}) \right]}$, $\beta = \exp(\omega\overline{h}) + \exp(-\omega\overline{h})$.

The whole pile has been discreted into k segments, with Equation (17) describing the impedance of the ith segment. Combining the impendance equations of all segments, the stiffness matrix in the Laplace transform domain is deduced as:

$$\widehat{\overline{H}} = K\widehat{\overline{\Phi}} \tag{18}$$

where $\widehat{\overline{H}} = \left\{ \widehat{\overline{T}}_0, 0, 0, \cdots, 0, \widehat{\overline{T}}_k \right\}^T$,

$\widehat{\overline{\Phi}} = \left\{ \widehat{\overline{\Phi}}_0, \widehat{\overline{\Phi}}_1, \widehat{\overline{\Phi}}_2, \cdots, \widehat{\overline{\Phi}}_k \right\}^T$,

$$K = \alpha \begin{bmatrix} -\beta & 2 & & & \\ -2 & 2\beta & -2 & & \\ & \ddots & \ddots & \ddots & \\ & & -2 & 2\beta & -2 \\ & & & -2 & \beta \end{bmatrix}_{(k+1)\times(k+1)}$$

In Equation (18), $\widehat{\overline{T}}_0$ is the dimensionless loading in Laplace transform domain. $\widehat{\overline{T}}_k$ is the moment extended by soil at the bottom of the pile, and is assumed to be equal to the static stiffness corresponding to a rigid disk of radius R attached to the surface of an elastic half space. Considering the viscidity of soil, the base stiffness of the pile can be expressed as $\widehat{\overline{T}}_k = \frac{16}{3}(1 + p\eta)\widehat{\varphi}_k$ in Laplace transform domain.

Equation (18) can be solved numerically.

3   Numerical Results and Discussions

The solving process is carried in the Laplace transform domain. And the numerical inverse transform should be used to achieve the final result in the time domain. The numerical Laplace inversion transform method proposed by Durbin[7] is adopted in this paper:

$$f(t) = \frac{4e^{at}}{S}\left[-\frac{1}{2}\mathrm{Re}\left\{\widehat{f}(a)\right\} + \sum_{k=1}^{NSUM} \mathrm{Re}\left\{\widehat{f}\left(a + ik\frac{2\pi}{S}\right)\right\}\cos k\frac{2\pi}{S}t \right] \tag{19}$$

where S, a, $NSUM$ are transform parameters. The values: $S = 20$, $a = 0.75$, $NSUM = 50$ are accurate enough.

Two types of loading are adopted in the numerical procedure as shown as Fig. 3, one is the rectangular pulse and the other is the triangular pulse. The non-dimensional twist angles $\varphi'(z) = \varphi(z)G/T_0$ are calculated to illustrate the influence of various factors. Some properties of poroelastic material and pile are $n = 0.4$, $\rho_s = 2650 \text{ kg/m}^3$, $\rho_w = 1000 \text{ kg/m}^3$, $\overline{\rho}_b = 1.3$, $\overline{t}_0 = 2$.

Fig. 4($l/R = 15$, $k_d = 10^{-7}$ m/s, $\eta = 0$) shows the displacement of the pile head in the time domain, part (a) and part (b) show the dynamic responses of elastic pile with different $\overline{G}_p$ under the rectangular pulse and the triangular pulse respectively (φ'_0 denotes the non-dimensional displacement of the pile head). The results indicate

(a) rectangular pulse   (b) triangular pulse

Fig. 3. Transient load typses

(a) Response under rectangular pulse   (b) Response under triangular pulse
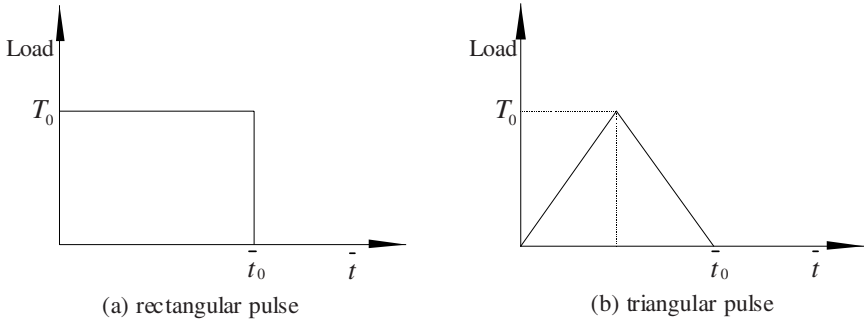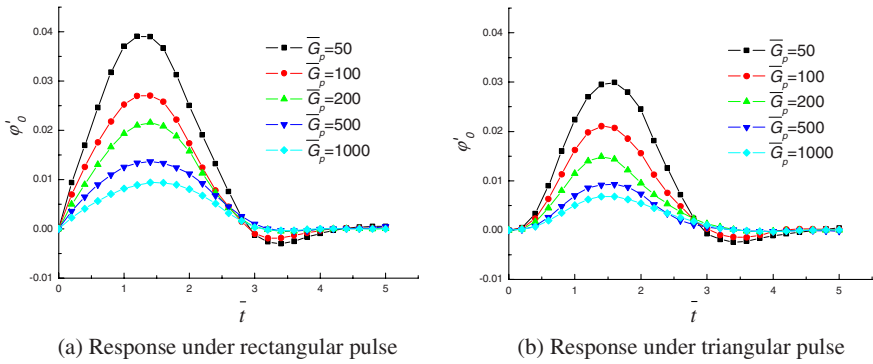
Fig. 4. Time histories of the non-dimensional twist angle of the pile head with different shear modulus

that the displacement is oscillating in the time domain, and is close to zero finally. Each curve has an obvious peak value varying with different $\overline{G}_p$. The pile head displacement increases with the reduction of the pile's Young's modulus. Under two types of loading, the response curves are alike. But the pile head displacement is small under triangular pulse, and the trends are different at the initial stages.

The displacement responses of the surrounding soil for different shear modulus of pile are also taken into consideration. Time histories of the non-dimensional displacement of soil around the pile are depicted in Fig.5. ($k_d = 10^{-7}$ m/s, $\eta = 0$). It's found that a flexible pile ($\overline{G}_p = 100$) causes larger soil responses than a stiffer pile ($\overline{G}_p = 500$). And for a stiffer pile, the generated surface wave can not propagate as far as that of a flexible pile.

By changing the soil viscidity, computation results of the non-dimensional twist angle at the pile head are presented in Fig. 6 and Fig. 7 ($k_d = 10^{-7}$ m/s) for $\overline{G}_p$ with

(a) Response with $\overline{G}_p = 100$ (b) Response with $\overline{G}_p = 500$
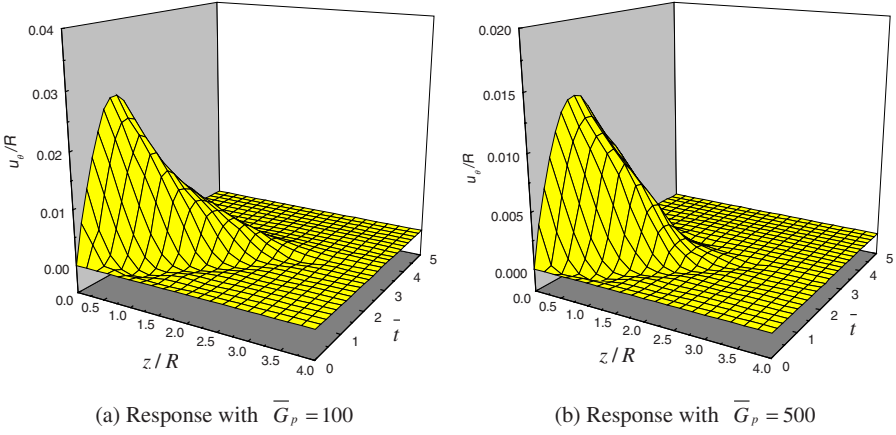
Fig. 5. Time histories of the non-dimensional displacement of soil around the pile

(a) $l/R=10$ (b) $l/R=30$

(c) $l/R=50$
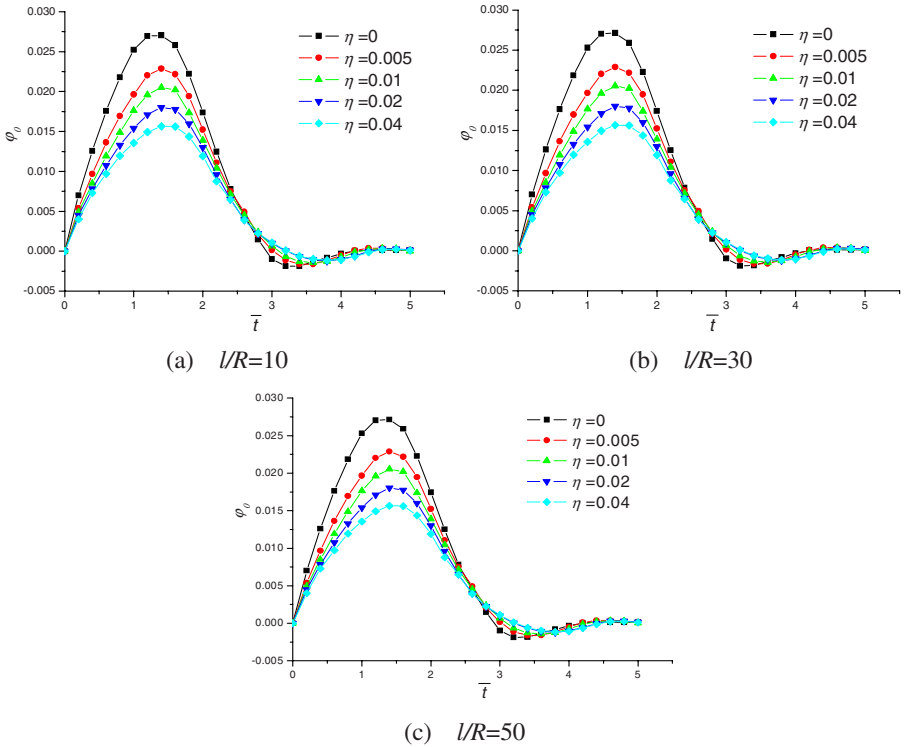
Fig. 6. Time histories of the non-dimensional twist angle of the pile head with different viscidity($\overline{G}_p = 100$)

(a) *l/R*=10

(b) *l/R*=30

(c) *l/R*=50
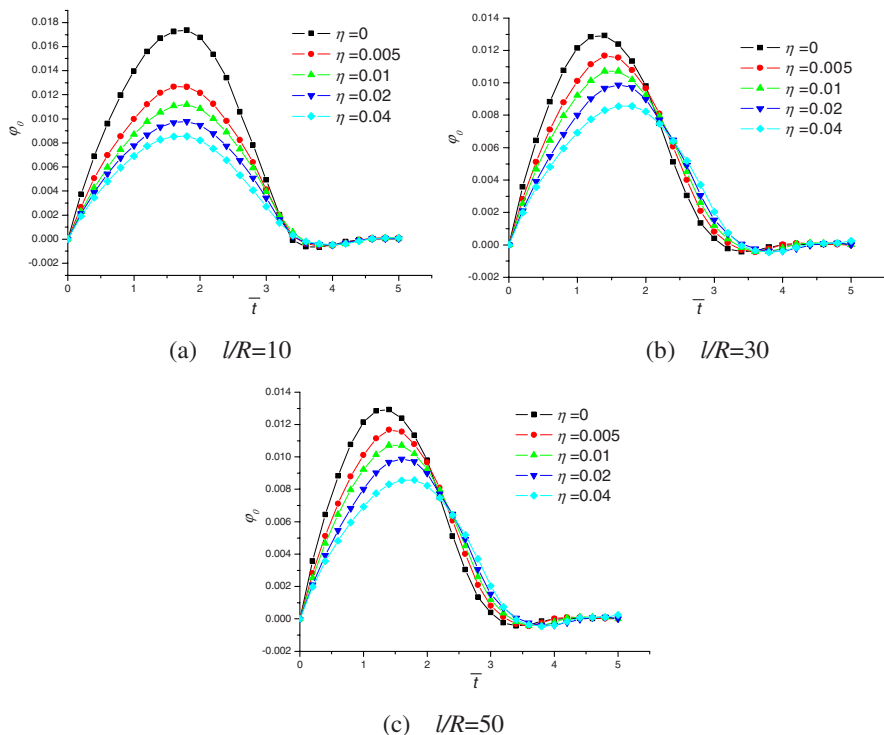
Fig. 7. Time histories of the non-dimensional twist angle of the pile head with different viscidity ($\overline{G}_p = 500$)

values of 100 and 500 respectively. The results show that the soil viscidity remarkably affects the response amplitudes at the pile head, and the bigger value of η leads to the smaller amplitude of twist angle. Also, it is found that the increasing of the soil viscidity causes a time lag for the occurrences of response peaks at pile head. In the range of η taken into account, only when the pile is stiff ($\overline{G}_p = 500$) the change of slenderness ratio of pile will cause a difference in the response that can be noticed.

4   Conclusion

Analytical method was developed to study the transient dynamic response of an elastic pile embedded in a homogeneous poroelastic medium and subjected to transient torsional loading. Numerical method was used to calculate the elastic pile twist angle, and the conclusions were obtained as follows:

1) Compared with the triangular load, the rectangular step torque causes larger pile displacement.
2) The non-dimensional shear modulus affects substantially the pile transient response, the peak twist angle of pile decreases with the increasing of pile stiffness.

3) The flexible pile contributes more to the surrounding surface soil than the stiffer pile.

4) The bigger value of η leads to the smaller amplitude of twist angle, and the increasing of soil viscidity causes a time lag for the occurrences of response peaks at the pile head.

Acknowledgements

References

1. M. Novak and J.F. Howell, Torsional Vibration of Pile Foundations. Journal of the Engineering Mechanics Division, 103. (1977) 271-285
2. M. Novak and J.F. Howell, Dynamic Response of Pile Foundations. Journal of the Engineering Mechanics Division, 104. (1978) 535-552
3. Zeng and R.K.N.D. Rajapakse, Dynamic Axial Load Transfer from Elastic Bar to Proelastic Medium. Journal of the Engineering Mechanics Division, 125. (1999) 1048-1055
4. B. Jin, D. Zhou and Z. Zhong, Lateral Dynamic Compliance of Pile Embedded in Poroelastic Half-Space. Soil Dynamics and Earthquake Engineering, 21. (2001) 519-525
5. Y.Q. Cai, G. Chen and C.J. Xu et. al, Torsional response of pile embedded in a poroelastic medium. Soil Dynamic and Earthquake Engineering, 26. (2006) 1143-1148
6. G. Militano and R.K.N.D. Rajapakse, Dynamic Response of a Pile in a Multi-layered Soil to Transient Torsional and Axial Loading. Geotechnique, 49. (1999) 91-109
7. F. Durbin, Numerical inversion of Laplace transforms: an efficient improvement to Dubner and Abate's method. The Computer Journal, 17. (1974) 371-376

Reliability Analysis on Vertical Bearing Capacity of Bored Pile Determined by CPT Test

Chun-feng Zhao[1,2], Chao Xu[1,2], and Chun-mao Jiao[1,2]

[1] Key Laboratory of Geotechnical Engineering, Tongji University, Shanghai 200092, China
[2] Department of Geotechnical Engineering, School of Civil Engineering, Tongji University, Shanghai 200092, China

Abstract. Based on the random field theory and reliability theory, the statistical methods used in the research on the probabilistic features of parameters,P_s,f_i,P_{sb} had been studied. In addition, the problems with the correlation distance, pile cross section dimensions and the range of pile tip resistance, which would be used in the reliability analysis, were discussed in this paper. The reliability analyses were made on seventeen (17) construction sites based on forty-six (46) CPT test curves in Shanghai area, China. The reliability indices were obtained and the probabilistic characteristics of reliability indices were derived accordingly.The study shows that: (1) generally, the reliability index of large pile in diameter is greater than that of small pile for either prefabricated pile or cast-in-place pile, and the coefficient of variation of reliability index of prefabricated pile is less than that of cast-in-place pile; and (2) For bored piles, the variation coefficient of reliability index is less for big pile in diameter (or dimensions) than that for small pile in diameter (or dimensions). . . .

Keywords: Random field, Correlation distance, Reliability, CPT, Vertical bearing capacity of pile.

1 Introduction

Traditionally, the safety factor, K, is used to express whether the design of pile bearing capacity is risk or conservative. Apparently, if K is larger, the design is safer, but it is not in fact. The reliability analysis with consideration of the variation of variables has become one of the hot points in the civil engineering area in the past twenty years. The researchers in the geotechinical engineering community are still facing challenges to apply the reliability analysis in their design since the nature of the variety of the soil and rock properties is difficult to recognize and the failure mode for geotechnical engineering objects is much vague. Nevertheless, the endeavor is continuing internationally. Many scholars in China have done a lot of research work to find a way to transit the traditional foundation design code,which is based on the deterministic design method, to a new foundation design code based on the reliability analysis. In this paper,the

authors will present such research results with the vertical pile bearing capacity for prefabricated piles and the bored piles.

2   Formulae for Determining Limit Bearing Capacity of Pile

As the scenario of bored pile is much complex and it is still a technical challenge to make clear the borehole cross section dimensions, the slurry thickness and their functions influencing the bearing capacity of bored pile, seldom foundation design codes and guidelines recommend the formulae to determine the limit bearing capacity of bored pile by means of CPT. However, the extensive usage of bored pile in many area around the world and the CPT technology is widely used to estimate the soil engineering properties, it is necessary to explore the possibility to evaluate the bearing capacity for bored pile using the CPT results. Some scholars including the authors have done limited researches in this area (Zhao etc., 1999; Chen etc., 1994). The formula adopted for studying the reliability of evaluating the bearing capacity of bored pile by means of the specific penetration resistance of CPT is apparently same with equation (1), but the methods for evaluating the variables involved in equation (2) are different, i.e.,

$$Q_u = \sum_{i=1}^{n} f_i U_i l_i + a_b P_{sb} A_p \qquad (1)$$

Where Q_u is the bearing capacity of single pile (kN), f_i is the standard value of ultimate friction resistance for the i-th soil layer by means of the specific penetration resistance of CPT (kPa); U_i and l_i represent the average perimeter of pile and the thickness for the i-th soil layer respectively; a_b is the modified coefficient for pile end resistance; P_{sb} is the average specific penetration resistance of CPT near the pile end (kPa); A_p is the cross section area of pile end (m2); n is the number of soil layer that pile penetrates.

3   Calculation Methods of the Probabilistic Features of the Specific Penetration Resistance P_s

For the standard values of the ultimate friction resistance and ultimate end resistance are evaluated based on the specific penetration resistance P_s of CPT according to empirical formulae, their probabilistic characteristics will depend on the statistical methods, i.e., how to get the parameter of P_s. The P_s value of CPT varies continuously along with the penetration depth, so the question that how the P_s value is calculated based on the CPT test curve for a foundation soil layer arises. As there is autocorrelation of soil parameters, and the independence of choosing individual P_s value should be guaranteed. The probabilistic properties (variance and variation coefficient) of P_s value should be evaluated taking the correlation distance of typical soil layer in shanghai area into consideration.

The calculated variance is so called 'point variance', and the variation coefficient based on point variance can be gotten. Then authors obtain the variation coefficient for a soil layer based on one-dimensional random field theory (Vanmarcke, 1977), i.e.,

$$V_i = V_i' \sqrt{\frac{\delta_{i,0}}{l_i}} \tag{2}$$

Where V_i' represents the variation coefficient derived from the point variance for the i -th soil layer of a CPT hole, V_i is the variation coefficient derived from one-dimensional random field theory for the i-th soil layer of the CPT hole, $\delta_{i,0}$ is the correlation distance for the i-th soil layer, l_i refers to the thickness for the i-th soil layer.

Preceding discussion only considers the soil parameter variation along depth; the variability in horizontal direction also needs to be taken into account. For there are only a few CPT holes and the distances between holes of CPT are relatively large in a construction site, the random variable theory was adopted to calculate spatial average variance of a site approximately. The spatial variation coefficient V_{hi} is evaluated by Equation (3):

$$V_i = V_h' \frac{1}{\sqrt{m}} \tag{3}$$

Where V_h' is the variation coefficient for a site, which is calculated based on the point variance; m is the number of the hole of CPT.

3.1   The Method for Evaluating P_s in a Site

While calculating the statistical properties of the CPT specific resistance, P_s, by means of random field theory, very probably, the thickness of soil layer cannot be divided by the correlation distance neatly. For solving the question, the practical thickness is divided by correlation distance, then round off to the nearest whole number, the real thickness of soil layer is replaced by the multiplication of the correlation distance and the round number. As shown in Fig.1, where h_{il}' is thickness of the CPT hole for the i-th soil layer, h_{il} is the soil layer thickness used in the calculation. Here i represents the serial number of soil layer, $i = 1, \cdots, n$; l refers to the serial number of CPT hole in one site, $l = 1, \cdots, m$. The process of evaluating the statistical properties of P_s is as followed.

(1) Rounding $\left[\frac{h_{il}'}{\delta_{i,0}}\right]$ to a nearest whole number, N, then replacing the real soil layer thickness by $h_{il} = N \cdot \delta_{i,0}$.
(2) Averaging P_s in the range of h_{il} to obtain $\overline{P}_{sil}$, calculating the standard point variance σ_{sil}' and the point variation coefficient V_{sil}' of P_s.
(3) Calculating the average standard variance σ_{sil} and average variation coefficient V_{sil} of P_{sil} in the range of h_{il} , i.e.,

$$\sigma_{sil} = \sigma_{sil} \sqrt{\frac{\delta_{i,0}}{h_{il}}}, \quad V_{Sil} = V_{Sil} \sqrt{\frac{\delta_{i,0}}{h_{il}}} \tag{4}$$
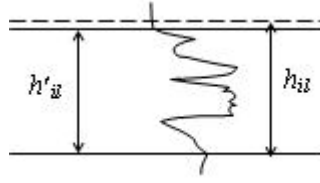
Fig. 1. The profile for i-th soil layer in l-th CPT hole

(4) Averaging the variation coefficient V_{sil} of the i th soil layer along the depth for a site, i.e.,

$$\overline{V}_{si} = \frac{1}{m} \sum_{i=1}^{n} V_{sil} \tag{5}$$

(5) Averaging the mean value of the specific resistance, $\overline{P}_{sil}$ of the i-th soil layer for a site and calculating the field variation coefficient V_{hi} across the site, i.e.

$$\overline{P}_{si} = \frac{1}{m} \sum_{i=1}^{m} \overline{P}_{sil} \quad V_{hi} = \frac{\left[\frac{1}{m-1} \sum_{i=1}^{m} \left(\overline{P}_{sil} - \overline{P}_{si} \right)^2 \right]^{\frac{1}{2}}}{\overline{P}_{si}} \tag{6}$$

(6) Calculating the spatial variation coefficient V_i for the i-th soil layer and the average standard variance $\sigma_{P_{si}}$, i.e.,

$$V_i = \left(\overline{V}_{Si}^2 + \frac{1}{m} V_{hi}^2 \right)^{\frac{1}{2}}, \quad \sigma_{P_{si}} = \overline{P}_{si} \cdot V_i \tag{7}$$

4   The Methods for Evaluating the Friction Resistance f_i

In the case of bored pile, as the pile diameter is influenced by several factors, such as the soil properties, the construction process and quality, it is still a difficult task in the civil engineering community to get the statistical properties of the diameter of bored pile. One thing is clear, whether for a single soil layer or for the total soil layers along the pile shaft, the shaft friction resistance calculated according to the estimated pile diameter should be equivalent to the practical friction resistance. The author has made attempt to deal with the problem (Zhao, 1998). In this paper, the diameter of the bored pile is assumed as the design diameter for lacking test data. For the bored pile, the side friction resistance f_i of the i-th soil layer can be written as,

$$f_i = a + bP_{si} + cP_{si}^2 \tag{8}$$

Where a,b,c are coefficients, which can be evaluated based on the soil properties.
(1) For shallow topsoil (the depth is not beyond 6m),

$$a = 15 kPa \qquad b = c = 0 \tag{9}$$

(2) For clay, whose average specific resistance satisfies $\overline{P}_{sl} \leq 5000kPa$,

$$a = 8.775kPa \qquad b = 0.029 \qquad c = -2.551 \times 10^{-6} \qquad (10)$$

(3) For clay, whose average specific resistance satisfies $\overline{P}_{sl} \geq 5000kPa$

$$a = 90kPa \qquad b = c = 0 \qquad (11)$$

(4) For clay $(\overline{P}_{sl} \geq 15000kPa)$, sandy silt, and sand,

$$a = 18.705kPa \qquad b = 0.010 \qquad c = -3.498 \qquad (12)$$

(5) For clay $(\overline{P}_{sl} \geq 000kPa)$, sandy silt, and sand,

$$a = 90kPa \qquad b = c = 0 \qquad (13)$$

While bearing stratum is sand or silt and the pile end penetrates into this layer less than 10 d (d represents the design pile diameter), the side friction resistance in the range of 4 d above the pile end should be modified as follow,

$$f_i^* = \eta f_i, \quad (\eta = 0.5) \qquad (14)$$

Supposing P_{si} subject to normal distribution, the statistical properties of side friction resistance, f_i, for the bored pile can be derived based on Equation (8) and the error propagation theory, viz.,

$$\overline{f}_i = a + b\overline{P}_{si} + c\left(\overline{P}_{si}^2 + \sigma_{P_{si}}^2\right) \qquad (15)$$

$$\sigma_{P_{si}}^2 (f_i) = b^2 \sigma_{P_{si}}^2 + 4bc\overline{P}_{si}\sigma^2 + 4c^2\overline{P}_{si}^2 2\sigma_{P_{si}}^2 + 2c^2\sigma_{P_{si}}^4 \qquad (16)$$

$$V_{f_i} = \frac{\sigma_{P_{si}} \left[\left(b + 2c\overline{P}_{si}\right)^2 + 2c^2\sigma_{P_{si}}^2 \right]^{\frac{1}{2}}}{a + b\overline{P}_{si} + c\left(\overline{P}_{si}^2 + \sigma_{P_{si}}^2\right)} \qquad (17)$$

5   The Methods for Evaluating the Pile Tip Resistance P_{sb}

The evaluating methods of statistic property of the tip resistance P_{sb} for bored pile are similar to the methods for the prefabricated pile, but the calculating range for the bored pile is different, it includes 4D (D refers to the diameter of the bored pile) above the pile end and 1D under the pile end, as showed in fig. 2 (Chen Qianghua, etc., 1994). The methods for evaluating the statistic properties of the tip resistance P_{sb} for the bored pile are briefly discussed as followed.
(1) As the same reason to consider the factor of correlation distance, and the ratios of $\frac{2d}{\delta_{i,0}}$, $\frac{4d}{\delta_{i,0}}$ and $\frac{6d}{\delta_{i-1,0}}$ may not the integer(s), authors take the same strategies to round the ratios to whole numbers. After these manipulations, the integer
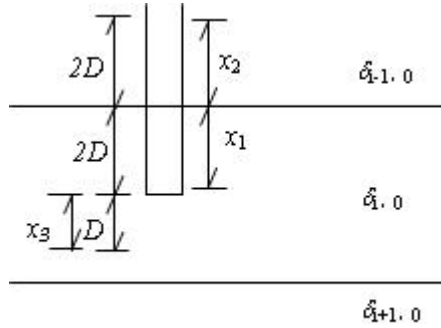
Fig. 2. The skeleton for the pile tip resistance analysis of the bored pile

parts of $\frac{2d}{\delta_{i,0}}$, $\frac{4d}{\delta_{i,0}}$ and $\frac{6d}{\delta_{i-1,0}}$ are expressed by n_1 , n_2 and n_3 and the corresponding thickness are x_1 , x_2 and x_3 , respectively. (2) The thickness weighted average specific penetration resistance, $\overline{P}_{il1}$ and the average variation coefficient, V_{il} , in the range of $x_1 + x_2$ for the l-th CPT hole are evaluated by equation (18).

$$V_{il1} = \frac{x_2 V_{si-1l2} + x_1 V_{sil1}}{x_1 + x_2} \tag{18a}$$

$$\overline{P}_{il1} = \frac{x_2 \overline{P}_{si-1l2} + x_1 \overline{P}_{sil1}}{x_1 + x_2} \tag{18b}$$

(3) The variation coefficient, V_{il} and the average specific penetration resistance, $\overline{P}_{il}$ in the range of $x_1 + x_2$ for the i -th soil layer in a site are obtained as followed.

$$V_{il} = \frac{1}{m} \sum_{l=1}^{m} V_{il1}, \quad \overline{P}_{il} = \frac{1}{m} \sum_{l=1}^{m} \overline{P}_{il1} \tag{19}$$

(4) In the same way, we can obtain the average specific penetration resistance, $\overline{P}_{sil3}$, in the rang of x_3 , and the average variation coefficient, V_{sil3} , for i-th soil layer in the l-th CPT hole and the variation coefficient, V_{i2} , for i-th soil layer in a site.

$$V_{sil3} = 0 \qquad (n_3 = 1)$$

$$V_{sil3} = V'_{sil3} \sqrt{\frac{1}{n_3}} \quad (n_3 \geq 2)$$

$$V_{i2} = \frac{1}{m} \sum_{l=1}^{m} V_{sil3} \tag{20}$$

(5) The average specific penetration resistance, $\overline{P}_{i2}$, in the range of x_3 within the territory of a site is easily obtained by equation (21).

$$\overline{P}_{i2} = \frac{1}{m} \sum_{l=1}^{m} P_{il3} \tag{21}$$

(6) The field variation coefficients of above the pile end and under the pile end for the i-th soil layer are calculated by equations (22), respectively.

$$V_{hil} = \frac{\left[\frac{1}{m-1}\sum_{i=1}^{m}\left(P_{il1} - \overline{P}_{i1}\right)^2\right]^{\frac{1}{2}}}{\overline{P}_{i1}}, \quad V_{hi2} = \frac{\left[\frac{1}{m-1}\sum_{i=1}^{m}\left(P_{sil3} - \overline{P}_{i2}\right)^2\right]^{\frac{1}{2}}}{\overline{P}_{i2}} \tag{22}$$

(7) The total variation coefficient of above the pile end and under the pile end for the i-th soil layer are calculated by equations (23).

$$V_{P1} = \left(\frac{1}{m}V_{hil}^2 + V_{il}^2\right)^{\frac{1}{2}}, \quad V_{P2} = \left(\frac{1}{m}V_{hi2}^2 + V_{i2}^2\right)^{\frac{1}{2}} \tag{23}$$

(8) The average pile tip resistance for bored pile, P_{sb}, and the variation coefficient V_{sb} are determined by equation (24).

$$P_{sb} = \frac{\overline{P}_{i1} + \overline{P}_{i2}}{2}, \quad V_{sb} = \frac{\left(V_{P1}^2\overline{P}_{i2}^2 + a^2V_{P2}^2\overline{P}_{i2}^2\right)^{\frac{1}{2}}}{\overline{P}_{i1} + \overline{P}_{i2}} \tag{24}$$

6   Reliability Analysis and the Results

The limit state equation of the pile bearing capacity failure model for the bored pile can be written as,

$$\sum_{i=1}^{n} f_i U_i l_i + a_b P_{sb} A_p - Q_G - Q_L = 0 \tag{25}$$

This is a linear equation, which contains $n + 3$ variables. That all these basic variables are subject to normal distribution is presumed herein, the reliability index,β, can be calculated on equation (37).

$$\beta = \frac{m_{P_{sb}}a_b A_P + U_P\sum_{i=1}^{n}m_{f_i}l_i - m_{Q_G} - m_{Q_L}}{\left(a_b^2 A_P^2\sigma_{P_{sb}}^2 + U_P^2\sum_{i=1}^{n}\sigma_{f_i}^2 l_i^2 + \sigma_{Q_G}^2 + \sigma_{Q_L}^2\right)^{\frac{1}{2}}} \tag{26}$$

Where $m_{P_{sb}}m_{f_i}, m_{Q_G}, m_{Q_L}$ are the average of corresponding variables, $\sigma_{P_{sb}}, \sigma_{f_i}$, $\sigma_{Q_G}, \sigma_{Q_L}$ are the standard variance of corresponding variables.

The results of reliability on the bored pile in seventeen (17) construction sites in Shanghai area are presented in table 3. In the calculation of the reliability index, β, based on JC method, the safety factor $K = 2$ is assumed, the bored piles with different diameters (650mm and 800mm) are considered, and the different load ratios (0.2 and 0.5) are set in the computation.

It should be noted that the variation of the analysis mode and the bored pile diameter weren't taken into account in the above reliability analyses. If these factors were considered, the reliability indexes would decrease in theory. These problems definitely need further research work.

Table 1. The statistical properties of the reliability index β for bored piles

Pile diameter	650mm		800mm	
Load ratios	0.2	0.5	0.2	0.5
Average	4.889	4.573	4.940	4.618
Standard variance	0.576	0.475	0.489	0.398
Variation coefficient	0.118	0.104	0.099	0.086

7   Conclusions

(1)The reliability index is larger for big pile in diameter (or dimensions) than that for small pile in diameter (or dimensions).

(2) The variation coefficient of reliability index is less for big pile in diameter (or dimensions) than that for small pile in diameter (or dimensions).

(3) The results in tables 3 show that the reliability indexes are very large, which indicates that the method to estimate the limit bearing capacity of pile by using the specific penetration resistance based on equation (1).

References

1. Shanghai Standard: Foundation design code **S** DBJ08-11-1999
2. China National Code: Architecture pile foundation technology standard **S** JGJ 94–94
3. Zhao Chunfeng, Ye Guanbao: Reliability analysis on the bearing capacity of bored pile evaluated by CPT. Rock and Soil Mechanics, **20**1999 65–68
4. Cheng Qianghua:the bearing capacity of single bored pile evaluated by CPT. China architecture and building press, Proceedings of the 7th Conference on Soil Mechanics and Foundation Engineering.1994:373–376
5. Zhao Chunfeng: reliability analysis on pile foundation in Shanghai region, the thesis for degree of doctor of Tongji University, 1998 96–99
6. Vanmarcke, E.H.: Probabilistic modeling of soil profile. ASCE, GT11,**103** 1977 1227–1246
7. Zhao Chunfeng: Research on partial factors of recommended limit bearing capacity formula of precast pile in Shanghai Foundation Design Code,Engineering Mechanics,**20** 2003:141–144
8. Zhao Chunfeng: Research on partial factors of vertical bearing capacity of cast-in-place pile, Engineering Mechanics,**23** 2006:126–130

Can Tsunami Waves in the South China Sea Be Modeled with Linear Theory?

Yingchun Liu[1,2], Yaolin Shi[2], Hailing Liu[1],
Shuo M. Wang[4], David A. Yuen[3,4], and Hui Lin Xing[5]

[1] South China Sea Institute of Oceanology, Chinese Academy of Sciences, Guangzhou, China
[2] Graduate University of Chinese Academy of Sciences, Beijing, China
spring.yingch@gmail.com, shiyl@gucas.ac.cn
[3] Minnesota Supercomputing Institute, University of Minnesota, Minneapolis, USA
[4] Department of Geology and Geophysics, University of Minnesota, Minneapolis, USA
[5] ESSCC, University of Queensland, Australia

Abstract. We have compared the results from linear and nonlinear theories of the shallow-water equations applied to the South China Sea. Our results indicate that tsunami waves in the South China Sea can be modeled with linear theory. There is little difference in the probability predicted by nonlinear theory and that forecasted by linear treatment on tall waves, more than two meters high, which may impinge on Hong Kong, Macau and Taiwan. This probability is estimated to be 10% in the next century.

Keywords: Tsunami, Shallow-water equation, Numerical computation, South China Sea.

1 Introduction

The recent Pingtung earthquake occurred on December 26, 2006 in southern Taiwan has called our attention to possible tsunami hazards along the Chinese coast from large earthquakes from Taiwan in the north to the Manila trench in the south. Numerical simulation based on linear theory with the shallow-water equations is a good candidate for timely prediction due to much smaller amount of computation involved. The South China Sea (SCS) (Fig. 1), together with Taiwan to its east and the Philippine arc-trench, form complicated channel-basin structural system. The majority of earthquakes in South China Sea region are distributed around South Taiwan and Philippine (Fig. 1), especially along the Manila trench fault, which is the region most likely to generate tsunamis in the South China Sea. Historical seismic tsunami catalog shows that tsunamis have occurred close to Taiwan and Manila trench.

2 Comparison of Linear and Non-linear Modeling

The initial condition of the linear shallow water equation is computed according to Okada's work [3], which numerically predicts the water level changes due to earthquake faulting. Rectangular 2-D fault and half-space elastic models are adopted to represent major seismic faults for calculating the earthquake induced tsunamis. The earthquake
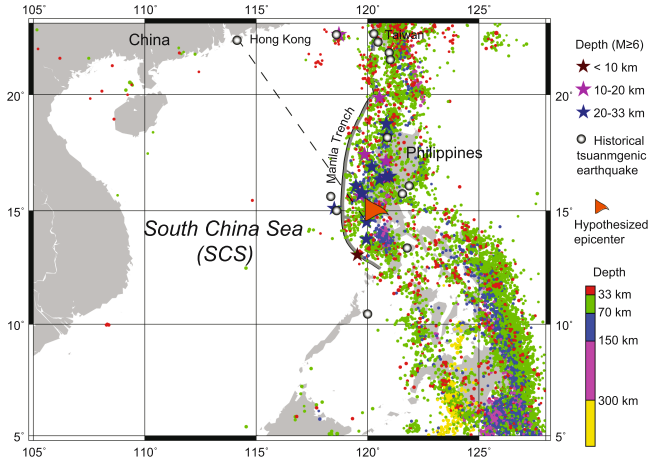
Fig. 1. Earthquake distribution with the epicenter depth in South China Sea and its adjacent regions. Database comes from NEIC. Major shallow earthquakes with magnitude over 6 are marked with star symbol. Grey balls represent the historical seismic tsunamis catalog from NGDC/NOAA. The marked hypothesized epicenter is used in Fig.3 and 4. A total of 31 receivers are placed on a straight line from epicenter to Hong Kong.

magnitude is set to be 8.0. In the rupture models, source parameters (rupture length L, width W, and the average slip D) are derived from theoretical and empirical relationships [5]. The fault dips and strikes from the composite fault plane solutions come from the average dip of the fault segments according to the Harvard catalog. The following linear shallow-water equations (1) are employed:

$$\frac{\partial \eta}{\partial t} + \frac{\partial M}{\partial x} + \frac{\partial N}{\partial y} = 0; \frac{\partial M}{\partial t} + gD\frac{\partial \eta}{\partial x} = 0; \frac{\partial N}{\partial t} + gD\frac{\partial \eta}{\partial y} = 0. \tag{1}$$

Due to the existence of the shallow water regions, for comparison, we also apply the non-linear shallow-water model. Here we include the effect of the friction coefficient on the wave height. The non-linear equations (2) are given by:

$$\frac{\partial \eta}{\partial t} + \frac{\partial M}{\partial x} + \frac{\partial N}{\partial y} = 0$$
$$\frac{\partial M}{\partial t} + \frac{\partial}{\partial x}\left(\frac{M^2}{D}\right) + \frac{\partial}{\partial y}\left(\frac{MN}{D}\right) + gD\frac{\partial \eta}{\partial x} + \frac{n^2}{D^{7/3}}M\sqrt{M^2 + N^2} = 0 \tag{2}$$
$$\frac{\partial N}{\partial t} + \frac{\partial}{\partial x}\left(\frac{MN}{D}\right) + \frac{\partial}{\partial y}\left(\frac{N^2}{D}\right) + gD\frac{\partial \eta}{\partial y} + \frac{n^2}{D^{7/3}}N\sqrt{M^2 + N^2} = 0.$$

In both models where η is the water height, t is time, x and y are the horizontal coordinates, M and N are the discharge fluxes in the horizontal plane along x and y coordinates, $h(x,y)$ is the undisturbed basin depth, $D = h(x,y) + \eta$ is the total water depth, g is the gravity acceleration, and n is the Manning roughness.

We have employed in our simulations the linear tsunami propagation model Tunami-N1 and nonlinear model Tunami-N2, that were developed in Tohoku University (Japan) and provided through the Tsunami Inundation Modeling Exchange (Time) program [1]. These models solve the governing equations by the finite-difference technique with a leap-frog scheme [1]. We use open boundary condition in these models, which permits
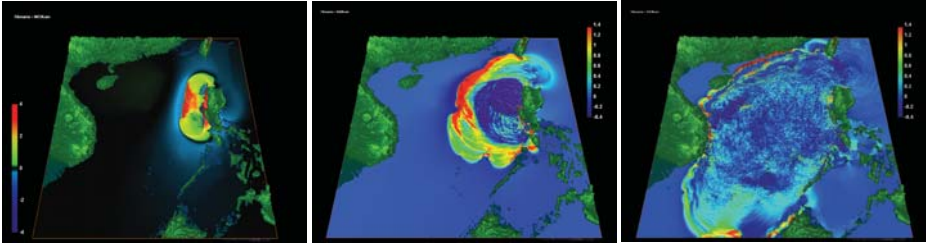
Fig. 2. Visualization of the tsunami wave propagation at three different times: 12 minutes, 72 minutes, and 479 minutes. Four meters represent the maximum height shown.
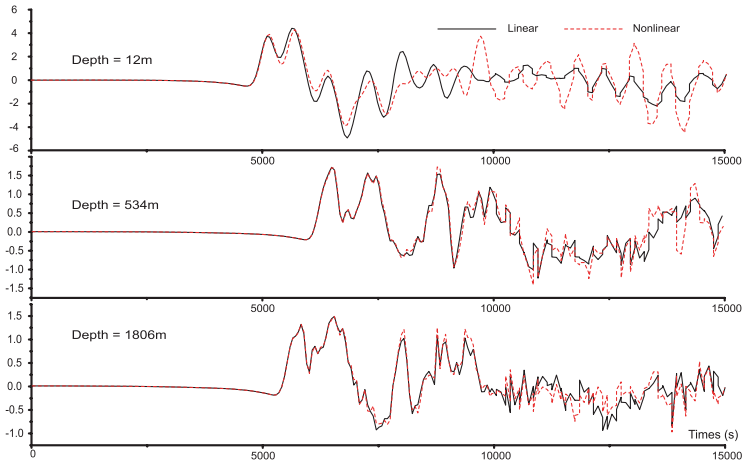
Fig. 3. Comparison of water heights in time histories with linear and nonlinear models in various water depths: 12.0m, 534.0m, 1806.0m. These waves are taken at the receivers located in s straight line between the epicenter (marked in Fig.1) and Hong Kong.

free outward passage of the wave at the open sea boundaries. The bathymetry of the South China Sea was obtained from global seafloor topography (Etopo2) with grid resolution of nearly 3.7 km. The total number of grid points in the computational domain is $361,201$, which is 601×601 points. The time steps in both models are selected to be 1 second to satisfy the temporal stability condition.

We have visualized in Fig. 2 one set of simulated tsunami wave propagations with the nonlinear model. The duration of wave propagation is 6.0 hours. This hypothesized seismic tsunami occurs southwest to Philippines ($14.5°N, 119.2°E$), with a magnitude of 8.0. For comparison between the linear and nonlinear models, we perform our simulations under the condition of $n = 0.025$ as the bottom friction coefficient in this application [1]. Tsunamis occurring at this location are furthest to the coast of mainland China. Due to the longest propagation time and very strong wave energy of this tsunami,

strong oscillations, reflection, and interference characteristics of tsunami waves can be well observed near the islands.

To further validate the wave propagation process in linear and nonlinear models, we place 31 receivers along the straight line between the epicenter in the Philippines and Hong Kong, as shown in Fig. 1. It has been found in our simulation that, there is one critical region with depth between 400 and 500 meters. The nonlinear character dominates the wave with small wavelengths. Above this depth, both linear and nonlinear models generate similar wave shapes and wave magnitudes. In other words, with the ratio of wave height to water depth smaller than 0.01, wave propagation can be modeled by linear theory with reasonable accuracy. We select three receivers (Fig. 3) at different water depths.

3   Probabilities of Potential Tsunami Hazard of SCS

In South China Sea, over three-fourth of this area is deeper than 500 meters. Due to dominance of the deep region, the linear model is expected to perform well. Here we will compute the probabilities of the tsunami hazard in the South China Sea area by using both linear and non-linear models. In the nonlinear model, the Manning roughness is 0.025 for the natural channels in good condition which is suitable for the South China Sea. The probability of seismic studies for the South China Sea and the adjacent areas was based on the Gutenberg-Richter (G-R) relationship [2]. The number of earthquakes is computed from the probability of seismic evaluation [6]. Earthquakes are sampled with the epicenter randomized according to a modified G-R distribution [4]. To estimate precisely the probability of tsunami hazard, 13 seismic tsunami models with magnitudes ranging from 6.5 to 8.0 are computed. We record the maximum positive amplitudes of the tsunami over a sufficiently long period of time.

Our probability for tsunami wave occurrence is computed from the probability of earthquake occurrence and the probability of maximum wave height of all seismic tsunami induced by such earthquakes. The tsunami wave with heights of [1.0m, 2.0m] and heights over 2.0 meters are considered for the hazard prediction. We forecast that the probability for tsunami wave with more than 2.0 meters to hit within the next 100 years is 10.12% for Hong Kong and Macau, 3.40% for Kaoxiong, and 13.34% for Shantou with the linear model. With the nonlinear model, the probability is the same for the same tsunami wave height at Hong Kong and Macau, and Kaoxiong, while a lower probability at Shantou of 10.12% is found. In general, the probabilities for most coastal cities do not change with the usage of nonlinear theory.

Acknowledgement

References

1. Goto, C., Ogawa, Y., Shuto, N., and Imamura, N.: Numerical method of tsunami simulation with the leap-frog scheme (IUGG/IOC Time Project), IOC Manual, UNESCO, No. **35** (1997)
2. Gutenberg, B. and Richter, C. F.: Seismicity of the Earth and Associated Phenomena, Princeton Univ. Press, Princeton (1949)
3. Okada, Y.: Surface deformation due to shear and tensile faults in a half-space, Bull. Seism. Soc. America **75** (1985) 1135–1154
4. Reiter, L.: Earthquake Hazard Analysis: Issues and Insights, Columbia Univ. Press, New York (1990)
5. Wells, D., Coppersmith, K.: New empirical relationships among magnitude, rupture length, rupture area, and surface displacement. Bull. Seismol. Soc. Am. **84** (1994) 974–1002
6. Liu, Yingchun, *et al*.: Tsunami Hazards From Potential Earthquakes along South China Coast. submitted to Physics of the Earth and Planetary Interiors (PEPI), Elsevier, 2007

A Coupled Chemo-Thermo-Hydro-Mechanical Constitutive Model for Porous Media

Zejia Liu[1], Xikui Li[2], and Liqun Tang[1]

[1] College of Traffic and Communications, South China University of Technology,
Guangzhou, 510641, P.R. China
`zjliu@scut.edu.cn`

[2] The State key Laboratory for Structural Analysis of Industrial Equipment,
Dalian University of Technology, Dalian, 116024,P.R. China

Abstract. Basing on the existing thermo-hydro-mechanical constitutive model presented in reference[1], and the chemo-mechanical constitutive model presented in reference[2], a coupled chemo-thermo-hydro-mechanical(CTHM) constitutive model of porous media is developed in the present paper. The chemoplastic and thermoplastic coupling behavior is considered in the present constitutive model. The present coupled CTHM constitutive model has been integrated into the coupled thermo-hydro-mechanical mathematical model including contaminant translation in porous media. The numerical results are illustrated to particularly emphasize the effects of the contaminant concentration and temperature to the coupled CTHM system in porous media.

Keywords: porous media, chemo-thermo-hydro-mechanical, constitutive model, coupling.

1 Introduction

In the recent years, the coupled chemo-thermo-hydro-mechanical(CTHM) behavior of porous media has attracted comprehensive attentions in engineering practice.

The thermo-plasticity of clay is charactered with the thermo-softening on cohesion and pre-consolidation pressure in the constitutive model. Wu[1] developed a THM constitutive model for unsaturated clay. The concept of chemical softening was suggested by Hueckel[2] to describe the chemo-plastic response of clay. Liu[3] developed this model into a couple chemo-hydro-mechanical constitutive model of unsaturated clay.

The present CTHM constitutive model is developed on the basis of the CAP model for unsaturated porous media with integration of the thermal and chemical effects on the hydro-mechanical behavior into the model.

2 The Constitutive Model and the Consistence Algorithm

This model is composed of four yield surfaces: The State Boundary Surface[1,4], The Critical State Line[1,4], The Suction Increase Curve [1,4] and The Traction Model[1]:

$$f_1 = q^2 + m^2 \left(p - 3p_s\left(\bar{\varepsilon}^p, s, T, c\right)\right)\left(p + 3p_{0c}\left(\varepsilon_v^p, s, T, c\right)\right) = 0 \tag{1}$$

$$f_2 = q + m\left(p - 3p_s\left(\bar{\varepsilon}^p, s, T, c\right)\right) = 0 \tag{2}$$

$$f_3 = s - \left[s_0 + \langle Se \rangle^{k1}\left(s_I\left(\varepsilon_v^p, \Delta T\right) - s_0\right)\right] = 0 \tag{3}$$

$$f_4 = p - 3\sigma_t = 0 \tag{4}$$

The cohesion is written in the form:

$$p_s\left(\bar{\varepsilon}^p, s, c\right) = p_s\left(0, T_r\right) + h_p \bar{\varepsilon}^p + k_{ps} s + k_{pc} c \tag{5}$$

where $p_s(0, T_r)$ is the cohesion with $s=0$, $c=0$ and $T=T_r$. h_p, k_{ps}, k_{pc} are the material parameters. The pre-consolidation pressure defines as:

$$p_{0c}\left(\varepsilon_v^p, s, T, c\right) = p_0\left(\varepsilon_v^p, s, T\right)\exp\left(-\alpha_c c\right) \tag{6}$$

where α_c is a chemical-softening parameter. The preconsolidation pressure $p_0(\varepsilon_v^p, s, T)$ with $c=0$ is still described in format of Loading-Collapse(LC) curve[1,4].

The strain rate is written as:

$$\dot{\varepsilon}_{ij} = \dot{\varepsilon}_{ij}^p + \dot{\varepsilon}_{ij}^{m,e} + \dot{\varepsilon}_{ij}^{s,e} + \dot{\varepsilon}_{ij}^{T,e} + \dot{\varepsilon}_{ij}^{c,e} \tag{7}$$

The elastic strains[1,2] are given by:

$$\tag{8}$$

κ is elastic stiffness parameter for changes in suction, α_2 is the thermal expansion parameter. The chemical expansion coefficient is written in positive form[2,3]:

$$\beta = F_0 \beta_0 \exp\left[\beta_0\left(1 - c + \ln c\right)\right]\left(1/c - 1\right) \tag{9}$$

The plastic potential function g has the same form of yield function with dilated angle. The plastic strain rate vector is defined by the non-associated flow rule:

$$\dot{\varepsilon}_{ij}^p = \dot{\lambda}^p \frac{\partial g}{\partial \sigma_{ij}} \tag{10}$$

For a specific yield surface, the consistent condition can be written as:

$$\dot{f} = \frac{\partial f}{\partial \sigma_{ij}}\dot{\sigma}_{ij} + \frac{\partial f}{\partial \xi}\dot{\xi} = 0 \tag{11}$$

The evolution of the internal variable is described by a hardening/softening law:

$$\dot{\xi} = \frac{\partial \xi}{\partial \varepsilon}\dot{\varepsilon}^p + \frac{\partial \xi}{\partial s}\dot{s} + \frac{\partial \xi}{\partial T}\dot{T} + \frac{\partial \xi}{\partial c}\dot{c} \tag{12}$$

To derive the general form of the constitutive equations, the stress can be written as:

$$\dot{\sigma}_{kl} = C^e_{klij}\left[\dot{\varepsilon}_{ij} - \left(\lambda^p\frac{\partial g}{\partial\sigma_{ij}} + h_{ij}\dot{s} + T_{ij}\dot{T} + D^c_{ij}\dot{c}\right)\right] \tag{13}$$

The plastic multiplier is obtained by introducing the equation (12),(13) into (11):

$$
\begin{aligned}
\dot{\lambda}^p =& \left[\frac{\partial f}{\partial\sigma_{kl}}C^e_{klij}\frac{\partial g}{\partial\sigma_{ij}} - \left(\frac{\partial f}{\partial\xi}\frac{\partial\xi}{\partial\varepsilon^p_{ij}}\right)\frac{\partial g}{\partial\sigma_{ij}}\right]^{-1}\left[\left(\frac{\partial f}{\partial\xi}\frac{\partial\xi}{\partial s}\right)\dot{s} + \left(\frac{\partial f}{\partial\xi}\frac{\partial\xi}{\partial T}\right)\dot{T}\right.\\
&+ \left.\left(\frac{\partial f}{\partial\xi}\frac{\partial\xi}{\partial c}\right)\dot{c} + \frac{\partial f}{\partial\sigma_{kl}}C^e_{klij}\left[\dot{\varepsilon}_{ij} - \left(h_{ij}\dot{s} + + T_{ij}\dot{T} + D^c_{ij}\dot{c}\right)\right]\right]
\end{aligned}
\tag{14}
$$

The rate constitutive equations can be derived from equation (13),(14).

3   Numerical Results

We consider a circular tunnel of 5m diameter at 220m depth excavated in unsaturated clay[3]. F_0=0.04. The other parameters can be found in reference [1], [3].

Two cases are analyzed p_0^*=1000Mpa and p_0^*=2MPa. Let us consider the state of the clay at time t=3*10^8s. The results around the tunnel are plotted (Fig. 2-7). These distributions are quite axisymmetrical in the region around the tunnel subjected to coupling effects. In fact, the influence of the variation of in situ stresses due to gravity is much smaller than the coupling influence and is negligible on the resulting stress and strain distributions. Figure 4 indicates that the coupling effects induce an expansion of the clay, whereas neglected volume change observed without the effect of c,T (Fig. 5). Regarding shear strains, the coupling effects are quite similar in both cases, inducing a significant increase of shear strains close to the tunnel (Fig. 6,7).
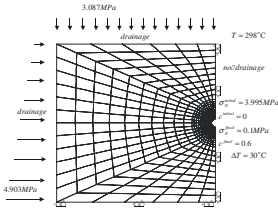
Fig. 1. The description of the problem   **Fig. 2.** Concentration   **Fig. 3.** Temperature
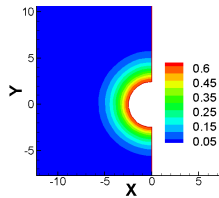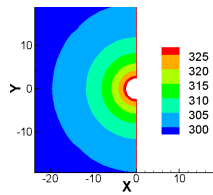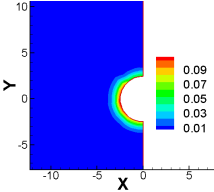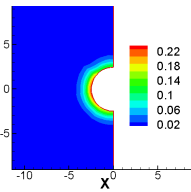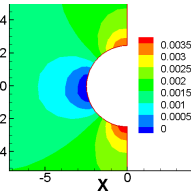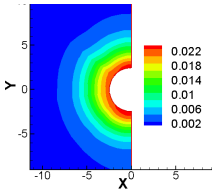
Fig. 4. ε_v (p_0^*=2MPa)   **Fig. 5.** ε_v (without c,T)   **Fig. 6.** ε_{eq} (p_0^*=2MPa)   **Fig. 7.** ε_{eq} (p_0^*=1000Mpa)

4 Conclusions and Discussion

The numerical results show the influence of coupling effect on the behavior around the tunnel during excavation. It is concluded that environmental load plays an important role in generating response and needs to be clearly articulated in the formulation of the problem. The proposed model may be a useful tool in designing this type of experiment, or as a matter of fact, field studies.

References

1. Wu W., et al: A thermo-hydro-mechanical constitutive model and its numerical modelling for unsaturated soils [J]. Computers and Geotechnics, 31(2)(2004) 155-167
2. Hueckel T: Chemo-plasticity of clays subjected to stress and flow of a single contaminant [J]. Int. J. Numer. Anal. Meth. in Geomech., 21(1997) 43-72
3. Liu Z., et al: Modelling chemo-hydro-mechanical behaviour of unsaturated clays: a feasibility study, Int. J. Numer. Anal. Meth. in Geomech, 29 (2005) 919-940
4. Alonso EE, Gens A, Josa A. A constitutive model for partially saturated soils [J]. Geotechnique, 40(3)(1990) 405-430

DEM in 3D Simulation of Influencing Factors of Deformation Properties and p-y Curves of a Laterally Loaded Pile

Xiao Zhao-ran[1] and Wang Junlin[2]

[1] School of Civil Engineering and Architecture, Henan University of Tecnology, Zhengzhou
[2] School of Environmental and Water conservancy, Zhengzhou University, Zhengzhou

Abstract. Based on structural similarity principles, a scale model of a laterally loaded pile was established to numerically simulate and study the problem of lateral soil-pile interaction by distinct element method in 3 dimensions. Level displacements of the pile and soil resistance around the pile related to the factors of the pile's diameter, the pile's rigidities and soil properties. According to the above distinction classification method, the factors of the pile's diameter, the pile's material rigidities and internal frictional coefficient of soil around the pile were analyzed in detail to find different quantity influences on the mechanics characters of horizontal displacements of the pile and the p-y curve.

Keywords: laterally loaded pile; p-y curves; distinct element method; reduced-scale model.

1 Introduction

Piles of buildings mainly withstand vertical axial loads in general foundation engineering, but piles in river ports, bridges, high buildings, offshore oil extraction platforms, shoring buildings and aseismatic buildings also simultaneously withstand horizontal loads of wind force, wave force, ship impacting force, earth pressure, seismic force and so on. In the oceanic engineering, the problems of piles and their stabilities are concerned mostly by design apartments currently, since 40% ~ 50% of a oceanic engineering's cost is focused on groundwork[1]. At present, the horizontal ultimate bearing and the bearing behavior of a laterally loaded pile are taken seriously but not settled well in geological engineering, because of laterally loaded piles' wide application. Level distortion of the pile and the p-y curve relate to the factors of the pile's diameter, the pile's rigidities (material) and soil conditions. In order to determine bearing capacity of the pile, it is necessary to numerically analyze scientifically and reasonably different quantity influences by the factors of the pile's diameter, the pile's rigidities (material) and soil conditions on the mechanics characters of horizontal displacements of the pile and the p-y curve.

The horizontal bearing properties of a pile largely depend on deformation characteristics of soil around the pile, and its capabilities of bearing horizontal loads

greatly relate to microscopic mechanical properties and the relation between microscopic structure and macroscopic mechanical phenomenon of soil[2]. With the aid of distinct element theory's special advantage in simulating mechanical problems of dispersed medium, the microscopic structure of soil around a pile has been simulated and analyzed with distinct element method while the pile is bearing lateral loads in the article. The above influent factors could be reasonably considered according to the rules of the lateral deformation of the pile and the p-y curve, in order that the design scheme was chose reasonably and the property of bearing lateral loads of the pile-soil system were enhanced.

2   Model Establishments

2.1   Establishing the Reduced-Scale Model

The loads and stresses of the pile-soil system were mainly produced by its own weight, and they also controlled the distortion and the destruction of the structure. But a less sizes model could not reappear the characteristic of the prototype, since its gravity was much lower than the prototype. The only way of solving this problem was enhancing the gravity of the reduced-scale model so as to equal the prototype's gravity. So the stress-strain relationship of the model was the same as that of prototype.

A 1/n (n was the reduced ratio) pile-soil reduced-scale model has been simulated in distinct element method under a condition of the acceleration of ng (g is gravity acceleration) or the density gravity of $n\gamma$ (γ is density gravity of the raw material). Since it was absolutely equivalent between the gravitational fields of the model and the prototype, the model had equal stress and strain, similar distortion and same destructive mechanism with the prototype. Therefore, the reduced-scale model could reappear the characteristics of the prototype. At the same time, soil was divided into inner layer soil near the pile and outer layer soil far away the pile in order not to destroy the pile-soil constitutive relationship. The grain diameter of the former soil was close to grain diameter of middle sand, and the grain diameter of the latter soil was slightly bigger than the former. Partial reduced-scale factors of the reduced-scale model relative to its prototype were listed in Table 1[4].

Table 1. Reduced-scale factors of a reduced-scale model relative to its prototype

Measure	Prototype	Reduced-scale model (gravitational acceleration of ng)
Length	1	$1/n$
Area	1	$1/n^2$
Volume	1	$1/n^3$
Quality	1	$1/n^3$
Density	1	1
Acceleration	1	n
Force	1	$1/n^2$
Stress	1	1
Strain	1	1

2.2   Choice of Calculation Parameters

According to experiment conditions in reference [4], the size of the model box was 45.7cm (length) ×25.7cm (width) ×25.7cm (high). The pile diameters of the model piles were 0.6cm, 1.2cm and 2.4cm, and the length was 16.8cm. Under the acceleration of 50g (n=50), the diameters of prototype piles corresponding to that of the model piles were 0.3m, 0.6m and 1.2m, and the length was 8.4m.

Sand in the model box was formed by rigid granules, and the box was made from walls. There were normal and tangential distortion rigidities and frictional coefficients among granules and walls. The tangential and normal rigidities of walls were equal. The rigidities of four peripheral walls were10 times of the rigidities of sand, and the rigidities of the bottom wall were 10 times of peripheral walls. Parameters of the model were listed in Table 2. It is necessary to point out that the parameters of soil and pile foundation were user-defined in the DEM numerical simulation, and they were not their own real physical indexes. The model constitution was shown in Fig. 1. The formed granules were balanced under their own gravity (The acceleration of gravity was 50g). The granule aggregate was about 16.8cm high, the porosity percent of soil was 38.9%, and the porosity ratio of soil was 0.637 after being balanced.

2.3   Loading Manner of the Model

The loading mode of continuous classification that was the same as the single pile experiment of vertical static loads was adopted in the model formed under itself gravity, i.e. the result documents were saved after the pile-soil system was balanced fully under every level load, and then next load was forced. The simulation loads of the model were divided into ten levels, and the ordinal steps were 20N, 28N, 36N, 44N, 52N, 60N, 68N, 72N, 76N and 80N. On the base of the reduced-scale parameters in Table 1, external loads
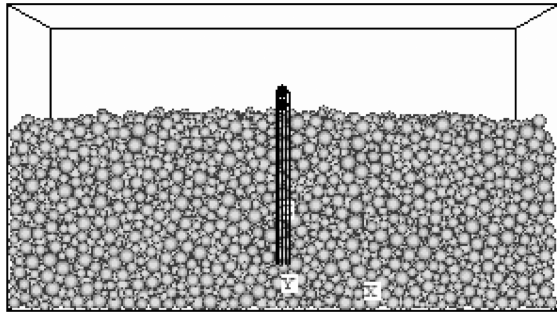
Fig. 1. The distinct element model in 3D of a laterally loaded pile

forced on the model were 50kN, 70kN, 90kN, 110kN, 130kN, 150kN, 170kN, 180kN, 190kN and 200kN in turn from the point of view of the prototype.

3   Results Analysis of Numerical Simulation

In order to reduce the dimension effect of the reduced-scale model, partial coordinates used dimensionless form. In figures y was the lateral displacement on top of the pile,

Table 2. The collection table of basic factors of the distinct element model in 3D

Types	ρ	R	M	K_s	K_n	μ
Sand	2650	1.3~3.0	1.85	1.0e4	1.0e4	0.6/0.8/1.0
Pile	3000	6.0/12.0/24.0		5.0e4/5.0e5/5.0e6	5.0e4/5.0e5/5.0e6	0.7

Note: ρ —density of granules ($kg \cdot m^{-3}$); R—radius of granules (mm); M—magnification factor of granule radius; K_s —Tangential rigidity ($N \cdot m^{-1}$); K_n —normal rigidity ($N \cdot m^{-1}$); μ —frictional coefficient.

z represented the distance from some position to the head of the pile, D was the diameter of the model pile, and H was the length of the model pile.

3.1   Effect Analysis of Diameter of the Pile

The normal and tangential stiffness of the pile was supposed to be $500\, kN \cdot m^{-1}$, diameters of 0.3m, 0.6m and 1.2m of the pile were chose to calculate and analyze.

3.1.1   Effect of Diameter of the Pile on the Flex Displacement of the Pile

Fig. 2 told us that the pile size had notable effect on the flex curve of lateral displacement of the pile. The pile diameter was the bigger, the lateral displacement of the single pile was the smaller under the same lateral load. The lateral displacement on top of the pile increased by 55% when the pile diameter reduced from 0.6m to its half; the lateral displacement on top of the pile reduced by 87% when the pile diameter increased from 0.6m to its two times. Besides, the model pile gradually became from an elastic pile to a rigid pile with increasing the pile diameter.   Therefore, enlarging the pile diameter could obviously control the lateral displacement of the pile.
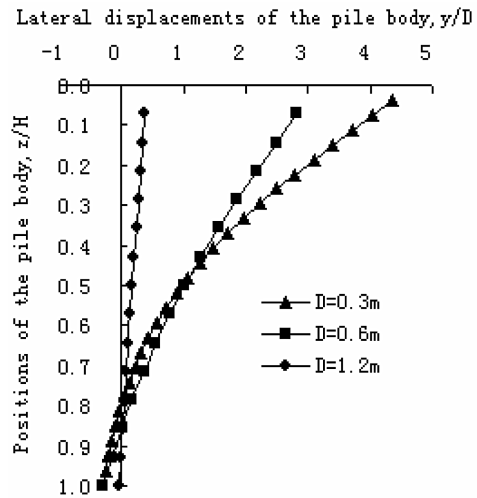
Fig. 2. Effect of diameter of the pile on flex displacement distribution of the pile

3.1.2 Effects of Diameter of the Pile on the p-y Curve the Pile

The following p-y curves were chose at the positions of distances 0.31L, 0.46L and 0.62L from the top of the pile. The diameter (or width) of the pile was one of the effect parameters to analyze the p-y curve.

(a) Distance from the top of the pile was

(b) Distance from the top of the pile was 0.46L

(c) Distance from the top of the pile was 0.62L
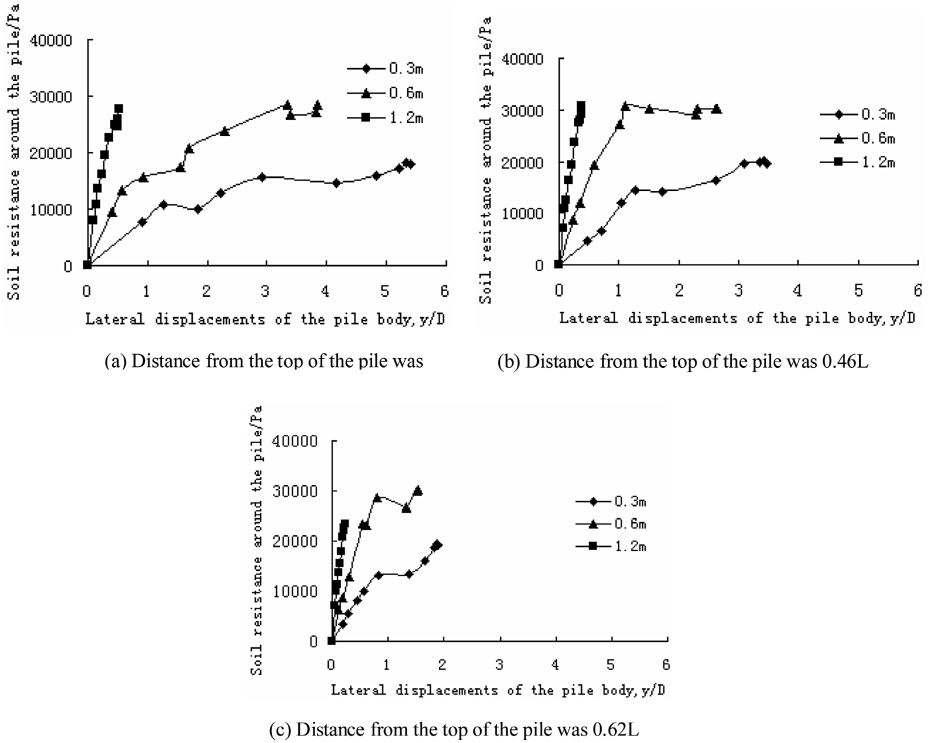
Fig. 3. Effect of diameter of the single pile on the p-y curves of the pile

The pile diameter was the bigger; soil resistance p was the bigger under definite situations in Fig. 3. The relationship between the ultimate soil resistance around the pile and the pile diameter was roughly linear. The emulational results of the model pile comparatively approached the Broms's viewpoints [5].

3.2 Effect Analysis of Connected Stiffness of the Pile

The bearing force of the pile was relevant to its elastic modulus, and the elastic modulus was corresponding to the connected stiffness of the model pile. The pile diameter was unchangeable and while analyzing the effect of the pile connected stiffness on laterally loaded properties of the pile, i.e. D=0.6m, but the normal stiffness and tangential stiffness in the connected pile model were variational. The connected stiffness of the pile was listed in Table 3.

3.2.1 Effect of Connected Stiffness of the Pile on the Flex Displacement of the Pile

The simulation result of Fig. 4 indicated that the flexibility of the pile and the displacement along the pile in the lateral load direction were the bigger while the connected stiffness of the pile were the smaller. But the pile displacement was not sensitive to its connected stiffness, which it may be relevant to being more rigid of the pile.

3.2.2 Effect of Connected Stiffness of the Pile on the p-y Curve of the Pile

It was supposed that the p-y curve of the laterally loaded pile was not relevant to the pile stiffness in references of [6, 7]. But the analysis results of Briaud[8] and others indicated stiffness of the pile had some effect on the p-y curve of the single pile in the shallow soil.

Simulation results were shown in Fig. 5.

Fig. 4. Effect of connected stiffness of the pile on flex displacement distribution of the pile

The analytical results indicated the p-y curve of the laterally loaded single pile was not sensitive to the material modulus, i.e. connected stiffness. This conclusion was consistent with that in reference [9]. But the connected stiffness was the bigger, the lateral resistance of soil would be developed deeper, so the transform point of the resistance moved down, and the lateral resistance of below soil increased, which was beneficial to enhancing the lateral bearing capacity of the pile.

3.3 Effect Analysis of Internal Frictional Coefficient of Soil

The mainly parameters of soil were water content, density, void ratio, plastic index, liquid index, compression coefficient, compression modulus, internal frictional angle and so on. Only the internal frictional coefficient of soil was considered while simulating in the article. In order to analyze the effect of internal frictional angle of

Table 3. The normal stiffness and tangential stiffness of the pile

Number	1	2	3
$K_s / kN \cdot m^{-1}$	50	500	5000
$K_n / kN \cdot m^{-1}$	50	500	5000
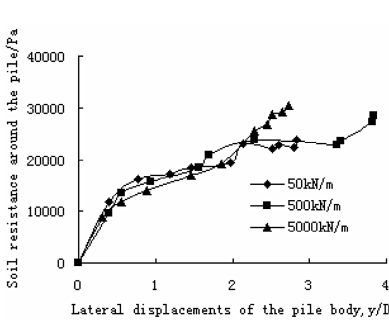
(a) Distance from the top of the pile was 0.31L
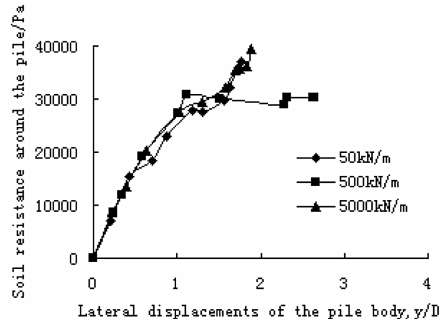
(b) Distance from the top of the pile was 0.46L
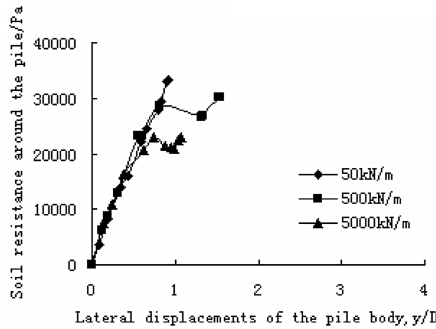
(c) Distance from the top of the pile was 0.62L

Fig. 5. Effect of connected stiffness of the single pile on the p-y curves of the pile

Table 4. Parameters of internal frictional coefficients of soil

Number	1	2	3
Internal frictional coefficients μ	0.6	0.8	1.0

soil on the lateral bearing character of the pile, normal stiffness and tangential stiffness were supposed to be $500\,kN \cdot m^{-1}$, and the diameter of the pile was 0.6m. Three selective internal frictional coefficients were listed in Table 4.

3.3.1 Effect of Internal Frictional Coefficient of Soil on the Flex Displacement of the Pile

The effect of the character of the soil around the pile on the flex displacement distribution of the pile was little. The lateral displacement of the pile did not reduce notably when the internal frictional coefficient of soil gradually increased, which was shown as in Fig. 6.
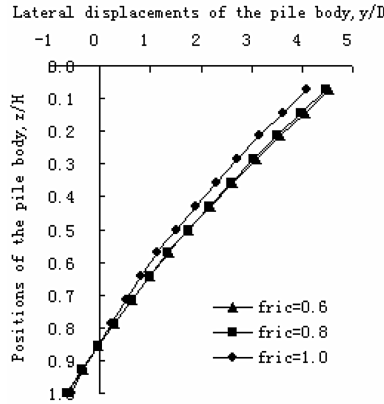
Fig. 6. Effect of internal frictional coefficient of soil on flex displacement distribution of the pile

3.3.2   Effect of Internal Frictional Coefficient of Soil on the p-y Curve of the Pile
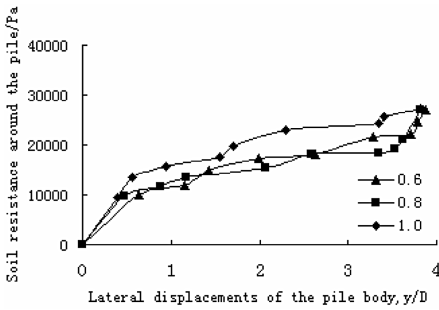
(a) Distance from the top of the pile was 0.31L   (b) Distance from the top of the pile was 0.46L
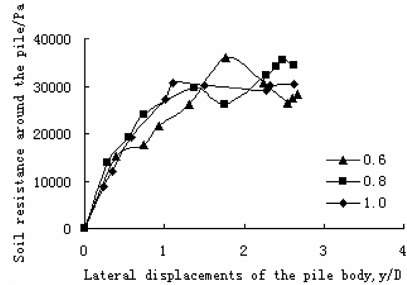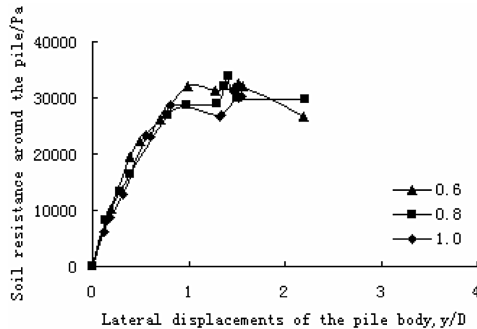
(c) Distance from the top of the pile was 0.62L

Fig. 7. Effect of internal frictional coefficient of soil on the p-y curves of the pile

4 Conclusions

Compared with other numerical simulation methods, the superiority of distinct element method in 3D was that it was only necessary to assign some microscopic basic parameters (such as contact rigidities and frictional coefficient and so on) between granules when it was used to cope with the problem of pile-soil interaction under lateral loads. The constitutive relationship of the pile-soil system could formed automatically, thus choosing the constitutive relationship and determining the corresponding parameters could be avoided, and the simulation results tended to being realer. In addition, on the base of similitude between the reduced-scale model and the prototype, the gravitational field of the model absolutely equaled that of the prototype. The analysis results indicated that the reduced-scale model could basically reappeared properties of stress, strain, distortion and so on.

The factors of the pile's diameter, the pile's material rigidities and internal frictional coefficient μ of soil around the pile were analyzed in detail to find different quantity influences on the mechanics characters of horizontal displacements of the pile and the p-y curve in the article. Based on the similarity of the reduced-scale model to the prototype, the numerical simulation results indicated that the connection of microscopic structural change with macroscopic mechanical action, the bearing behavior of the laterally loaded pile, and microscopic structural response could be simulated well by 3D DEM. However, since it was ambiguous of the corresponding relationships between microscopic parameters and macroscopic model parameters, only qualitative and semi-quantitative researches of the model have been done, but it was difficult to contrast with the theoretical calculation results in detail, which was the further study when distinct element procedure was applied.

References

[1] Wu Hengli. Solutions of laterally loaded piles by composite stiffness principle with biparameter method (second edition). Beijing: People transportation press, 2000.
[2] Liu Wenbai. Experimental study and particle flow code numerical simulation of extended foundation with aeolian sand under the action of uplift loading. Shanghai: Doctoral dissertation. Tongji University, 2003.
[3] Cundall P A, Strack O D L. A discrete numerical model for granular assembles[J]. Geotechnique, 1979, 29(1): 47-65.
[4] Ricard Ramos. Centrifuge Study of Bending Response of Pile Foundation to a Lateral Spread Including Restraining Effect of Superstructure [D]. New York: Doctor of Philosophy. Rensselaer Polytechnic Institute Troy, New York,1999.
[5] Broms BB. Lateral resistance of piles in cohesionless soils. J Soil Mech Found Div – ASCE 1964;90(3):123–56.
[6] O'Neill MW, Murchison JM. An evaluation of p–y relationships in sands. Research Report No. GT-DF02-83, Department of Civil Engineering, University of Houston; 1983.
[7] Reese LC, Cox WR, Koop FD. Analysis of laterally loaded pile in sand. In: Proceedings of the Sixth annual offshore technology conference, Houston (TX). Paper no. 2080; 1974.
[8] Briaud JL, Smith TD, Meyer BJ. Using the pressuremeter curve to design laterally loaded piles. In: Proceedings of the fifteenth annual offshore technology conference. Houston, (TX). Paper no. 4501; 1983.
[9] Chia-Cheng Fan, James H.Long. Assessment of existing methods for predicting soil response of laterally loaded piles in sand. Computers and Geotechnics, 2005, 32:274-289.

Calculation of Dynamic Pore Pressure in Stone Column Composite Foundation*

H.R. Zhang[1] and Y.M. Zhang[1,2]

[1] School of Civil Engineering and Architecture, Beijing Jiaotong University, Beijing 10044, China
[2] School of Storage and Transportation Engineering, China University of Petroleum - East China, Dongying City, Shandong Province, Shandong 257061, China
hrzhang@163.com

Abstract. For typical initial and boundary conditions, a group of general solutions for the generation and dissipation of excess pore water pressure in stone column composite foundation under coupling action of dynamic and static loads have been developed by separation of variables and Green functions to the control differential equations. In the control equation, the pore pressure increasing ratio is expressed as the function of depth and time. A special solution is obtained to zero initial condition and upper boundary pervious, based on an existing dynamic pore pressure calculation model. The numerical example shows that the effect of seepage of the stone column is prominent.

Keywords: Stone Column; Pore Pressure; Dynamic; Drain; Liquefaction.

1 Introduction

The liquefaction of saturated sand generated by earthquake loading does tremendous damage to engineering structures. As one of anti-liquefaction reinforcement methods, stone column composite foundation has been widely used in engineering practice. In some cases, it may be the unique choice of foundation reinforcement strategy.

In order to understand the behavior of stone column composite foundation during earthquake, it is important to investigate the production, growth and dissipation of the pore water pressure in the sand deposit under the action of dynamic loads. The ordinary approach to deal with this problem is to adopt the Terzaghi's or Biot's consolidation theory, combined with a selected dynamic pore pressure models. For most of these approaches, numerical discretization is usually required in engineering applications. This may cost a great deal of computational effort. The alternative consideration is to seek analytical or semi-numerical computational methods. Some researchers have contributed to this problem.

Seed & Booker (1976) [1, 2] proposed a analytical solution for the dynamic pore water pressure formula to an asymmetric saturated sand model by combining Terzaghi's consolidation equations and a nonlinear increase model for pore water pressure induced by vibrations. The dissipation of water happens only in horizontal direction.

Xu (1985) [3] proposed a analytical solution to dynamic pore water pressure in saturated sand improved by stone columns, where the drainage occurs only in the radius direction. In 1992, Xu [4] extended his solutions to the situations where dissipation appears in both the horizontal (radius) and vertical directions and found that the vertical dissipation contributes a tremendous part in saturated sand during earthquake action.

Huang (1992) [5] proposed a simplified analytical solution in uniform strain condition with ignoring the well resistance of stone columns to the seepage.

In this paper, the solutions are extended to generalize pore water pressure model.

2   Equations and Solutions

It is assumed that the seepage of the porous water through sand is governed by the Darcy's law and the porous water is incompressible. The coefficient of permeability and the coefficient of compression of sand keep constant. The coefficient of permeability of stone column is large enough to neglect its resistance to seepage.

By the continuous condition of porous water flow, the control differential equation can be written in cylindrical coordinate system as following:

$$\frac{\partial u}{\partial t} = C_{vr} \left(\frac{\partial^2 u}{\partial r^2} + \frac{1}{r} \frac{\partial u}{\partial r} \right) + C_v \frac{\partial^2 u}{\partial z^2} + \frac{\partial u_g}{\partial t}. \tag{1}$$

Where u is the excess pore pressure. r is the distance from the center of stone column. u_g is the dynamic pore pressure generated by vibrations. C_{vr} and C_v are the horizontal and vertical consolidation coefficients.

General solutions can be obtained by solving equation (1) by variable separation method and Green functions. When the initial pore water pressure is zero and only the upper boundary is free of drainage, the solutions for the generation and dissipation of excess pore water pressure in sand deposit improved by stone column can be expressed as following:

$$u(r,z,t) = \sum_{n=0}^{\infty} \sum_{m=1}^{\infty} D_{mn} \sin \frac{(2n+1)\pi}{2H} z \left[J_0(v_m r) - \frac{J_0(v_m a)}{N_0(v_m a)} N_0(v_m r) \right] e^{-C_v \lambda_{mn} t}. \tag{2}$$

In which, v_m is the mth root of the following equation:

$$J_1(vb) N_0(va) - J_0(va) N_1(vb) = 0. \tag{3}$$

Where, $J_0(va)$ and $J_1(va)$ are the Bessel functions of the 1st kind of order zero and 1st. $N_0(va)$ and $N_1(vb)$ are the Bessel functions of the 2nd kind of order zero and 1st.

$$D_{mn} = \int_0^t \int_0^H \frac{\partial u_g}{\partial t} \frac{2\pi J_1^2(v_m b) N_0(v_m a) \sin\frac{(2n+1)\pi}{2H} \eta}{H\left[J_1^2(v_m b) - J_0^2(v_m a)\right]} e^{C_v \lambda_{mn} \tau} d\eta d\tau. \tag{4}$$

$$\lambda_{mn} = \frac{(2n+1)^2 \pi^2}{4H^2} + \frac{C_{vr}}{C_v} v_m^2, \quad n = 1,2\cdots \;; \; m = 1,2\cdots. \tag{5}$$

It can be found that the solution form depends on the dynamic pore water pressure model of u_g. To illustrate the principal behavior of stone columns, the following dynamic pore water pressure model [6] is adopted:

$$u_g = u_f \left[\frac{1}{2}(1 - \cos\pi\frac{t}{t_f})\right]^B = A_0 \gamma' z \left[\frac{1}{2}(1 - \cos\pi\frac{t}{t_f})\right]^B. \tag{6}$$

In which, u_f is the possible maximum pore pressure. t_f is the time to reach u_f. B and A_0 are parameters.

3   Numerical Example

A site is composed of silty sand of 8m thick. The diameter and space of the stone column are 0.6m and 2.0m separately. The other parameters are shown in Table 1.

Table 1. Parameters

Parameter	γ (kN/m^3)	k_h (m/s)	k_v (m/s)	m_v (kPa^{-1})	K_0	ϕ' (°)	B	A_0
Value	19.0	10^{-5}	4×10^{-6}	1.5×10^{-4}	0.5	36.6	2	1.25

Substituting equation (6) into (5), special solution can be obtained and the numerical results are shown in Fig. 1 to Fig. 4.

It is shown from these figures that the maximum pore pressure occurs in the intermediate depth (Fig. 1). The pore pressure decreases with closing to the column in depth of 1m and 5m (Fig.2 and 3). The effect of stone column decreases with depth in the conditions that only upper boundary is free of drainage (Fig.4).
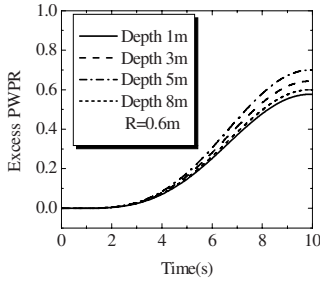
Fig. 1. The Pore pressure development in sand deposit with stone column drainage
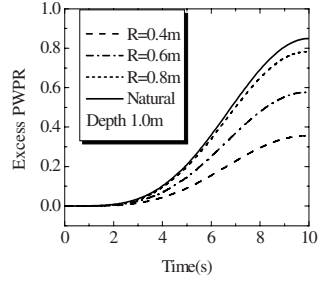
Fig. 2. The Pore pressure ratio change with distance from the stone column at depth 1.0m.
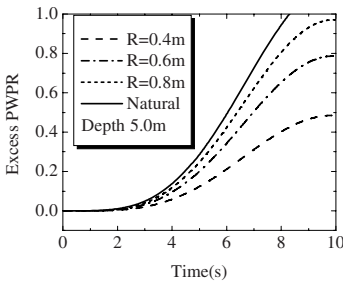
Fig. 3. The Pore water pressure ratio change with distance from the stone column at depth 5.0m.
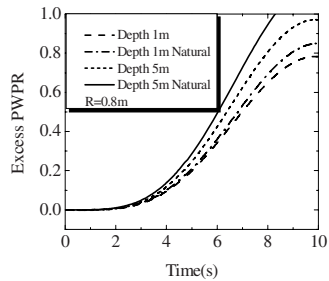
Fig. 4. The Pore water pressure ratio change with depth at distance 0.8m

4   Conclusions

The effect of seepage of the stone column is prominent. The maximum pore pressure occurs in the intermediate depth. The excess pore pressure increases with the distance to the stone column. The effects of stone column decrease with depth when the lower boundary is impervious.

References

1. Seed, H. B. & Booker, J. R.: Stabilization of Potentially Liquefiable Sand Deposits Using Gravel Drains Systems. Report No. EERC 76-10, University of California, Berkeley. (1976)
2. Seed, H.B. & Booker, J. R.: Stabilization of Potentially Liquefiable Sand Deposits Using Gravel Drains. J. of Geotechnical Engineering Division, ASCE, 103(GT7) (1977) 757-768
3. Xu, Z. Y.: Anti-liquefaction Analysis and Calculation of Sand Deposits Using Gravel Drains, Survey Science and Technology, 1 (1985)1-7
4. Xu, Z. Y.: Calculation of Pore Pressure of Liquefiable Sand Deposits Using Gravel Drains, Earthquake Engineering and Engineering Vibration, Vol. 12, No. 4 (1992)88-93

5. Huang, M. S., Wu, S. M. & Zhao, Z. Z.: Liquefaction Analysis of Subsoil Strengthen by Vibro-flotion Stone Pile Method and Vibro-compaction Sand Pile Method, Journal of Zhejiang University, Vol. 26, No. 2 (1992) 165-171
6. Zhang, J. M. & Xie, D. Y.: A Practical Calculation Method for the Growth of Vibration Induced Pore Pressure in Saturated Sand. Journal of Hydraulics, 8 (1989)45-51

Dynamic Responses of an Infinite Beam on a Layered Water-Saturated Poroelastic Foundation Under Moving Loads

B. Xu[1,2], J.F. Lu[3], and J.H. Wang[1]

[1] Department of Civil Engineer, Shanghai Jiao Tong University, 1954 Hua Shan Road, Shanghai, China
[2] Department of Civil Engineering, Nanchang Institute of Technology, 209 Beijing East Road, Nanchang, Jianxi, China
[3] Department of Civil Engineering, Jiangsu University, Zhenjiang, Jiangsu, China
{xubin1,wjh417}@sjtu.edu.cn, ljfdoctor@yahoo.com

Abstract. Based on the Biot's dynamic equation and the dynamic theory of elastic beam, the dynamic responses of an infinite beam resting on a layered water-saturated poroelastic foundation subjected to moving loads is investigated by the transmission and reflection matrices (TRM) method in this study. Applying the triple Fourier transformation, the general solutions for the water-saturated poroelastic foundation and the beam in the transformed domain are derived. Utilizing the continuity conditions between each layer and boundary condition at the surface of the half space, the equivalent stiffness of the layered water-saturated poroelastic foundation is obtained. Time-space domain solutions are obtained by means of IFFT arithmetic. The present methodology was validated by comparing present solutions with some known results. According to numerical results, it can be seen that the occurrence of a softer middle layer enhances the deformation of the beam.

Keywords: Moving loads, layered poroelastic foundation, Biot's theory, infinite beam, TRM method.

1 Introduction

The dynamic response of an infinite beam resting on a foundation under moving loads has been a hot topic for engineers for a long time, as the model can be conveniently used to simulate the railway subjected to moving train loads and pavements used as roadways. Also, it has been found that most of foundations may consist of one or more layers at some depth under the surface. Thus, a layered half-space is an appropriate approximation for the inhomogeneous soils. The steady-state vibration of a beam supported on an elastic half-space under a moving load has been studied in [1]. The response of an elastic beam on a visco-elastic layer to a moving constant load is investigated in [2]. A review of the literature about solving of a layered half-space is given in [3]. It should be noticed that the transmission and reflection matrix (TRM) method established by Luco and Apsel [4] is a very important method for solving

dynamic problems of a layered half space. The advantage of the method is that the mismatched exponential terms are eliminated in all the terms of the TRM. However, most research has been mainly treated subsoil as elastic or a layered elastic foundation. The investigation about the layered water-saturated porous medium is in a preliminary stage. It is well known that a saturated soil is two-phase material consisting of soil frame and pore water. Consequently, for a saturated soil, the saturated porous medium model is more realistic than the linear elastic or visco-elastic one. To the best of the authors' knowledge, Jin[5] investigate the dynamic responses of an infinite beam on a poroelastic half space produced by a moving periodic load using a rigorous analytical method.

In this paper, the response of an infinite beam on a layered poroelastic foundation subjected to moving load is studied. Timoshenko beam theory is used to describe the beam, while Biot's theory[6] is adopted to characterize the layered poroelastic soil. Biot's dynamic equations are solved by the Fourier transform method to establish the general solutions of the displacements, the stresses and the pore pressure for the layered soil. Based on the transmission and reflection matrices (TRM) method, the equivalent stiffness of the layered porous foundation is obtained by using the continuity condition between the beam and the layered foundation as well as the continuity conditions at each layer interface. The solutions for the beam and the layered poroelastic foundation are derived in the frequency-wave number domain. By means of the inverse Fourier transform, the time domain solutions of the beam and the poroelastic soil are retrieved from the frequency-wave number solutions. When reduced to some special cases, our solutions agree very well with some known results.

2 Biot's Equations and Corresponding General Solutions

The constitutive relations for the porous medium have the form [6]

$$\left.\begin{aligned}
\sigma_{ij} &= \lambda \delta_{ij}\theta + \mu \varepsilon_{ij} - \alpha \delta_{ij} p \\
p &= -\alpha M \theta + M e \\
e &= w_{i,i} \\
\theta &= u_{i,i}
\end{aligned}\right\} \tag{1a-b}$$

where u_i and w_i (i=1, 2, 3) are the displacement of solid matrix and the infiltration displacement of the pore fluid, respectively; σ_{ij} is the stress of the bulk material; p is the pore pressure; ε_{ij} and θ is the strain tensor and the dilatation of the solid skeleton; e is the volume of fluid injection into unit volume of bulk material; δ_{ij} is the Kronecher delta; λ and μ are Lame constants; α and M are Biot's parameters accounting for compressibility of the two-phased material.

The equations of motion for the bulk porous medium and the pore fluid have the form

$$\left.\begin{aligned}
\mu u_{i,jj} + (\lambda + \alpha^2 M + \mu)u_{j,ji} - \alpha M w_{j,ji} &= \rho_b \ddot{u}_i + \rho_f \ddot{w}_i \\
\alpha M u_{j,ji} + M w_{j,ji} &= \rho_f \ddot{u}_i + m\ddot{w}_i + b\dot{w}_i
\end{aligned}\right\} \tag{2a-b}$$

where ρ_b and ρ_f are mass densities of the bulk material and the pore fluid, ρ_b=(1-f)ρ_s+$f\rho_s$, ρ_s is the density of solid skeleton and f is the porosity of porous medium; m=a$_\infty\rho_f$/f and a$_\infty$ is tortuosity; b is a parameter account for the viscosity of the pore fluid and the permeability of the porous medium.

In order to solve Biot's governing equations, two kinds of Fourier transform are involved: the Fourier transform with respect to time and the Fourier transform with respect to horizontal coordinates. In this paper, the Fourier transform for time and the two horizontal coordinates are defined as follows:

$$\left.\begin{aligned}
&\hat{f}(\omega)=\int_{-\infty}^{\infty} f(t)e^{-i\omega t}dt, \quad f(t)=\frac{1}{2\pi}\int_{-\infty}^{\infty}\hat{f}(\omega)e^{i\omega t}d\omega \\
&\bar{f}(\xi)=\int_{-\infty}^{\infty} f(x)e^{-i\xi x}dx, \quad f(x)=\frac{1}{2\pi}\int_{-\infty}^{\infty}\bar{f}(\xi)e^{i\xi x}d\xi \\
&\tilde{f}(\eta)=\int_{-\infty}^{\infty} f(y)e^{-i\eta y}dy, \quad f(y)=\frac{1}{2\pi}\int_{-\infty}^{\infty}\tilde{f}(\eta)e^{i\eta y}d\eta
\end{aligned}\right\}
\tag{3}$$

In this paper, the superimposed symbol $\wedge\ -\ \sim$ above a variable denotes the Fourier transform with respect to time t, x- and y-directions, respectively.

Performing Fourier transform on Eqs. (1) and (2) and following the procedures as in ref.[5], the general solutions for the homogeneous poroelastic foundation were obtained

$$\left.\begin{aligned}
&i\xi\hat{\bar{\tilde{u}}}_x=v_1(Ae^{\gamma_1 z}+Be^{-\gamma_1 z})+v_2(Ce^{\gamma_2 z}+De^{-\gamma_2 z})-\gamma_3(Ee^{\gamma_3 z}-Fe^{-\gamma_3 z})-i\eta(Ge^{\gamma_3 z}+He^{-\gamma_3 z}) \\
&\hat{\bar{\tilde{u}}}_z=-\gamma_1 a_1(Ae^{\gamma_1 z}-Be^{-\gamma_1 z})-\gamma_2 a_2(Ce^{\gamma_2 z}-De^{-\gamma_2 z})+Ee^{\gamma_3 z}+Fe^{-\gamma_3 z} \\
&\hat{\bar{\tilde{u}}}_y=-i\eta[a_1(Ae^{\gamma_1 z}+Be^{-\gamma_1 z})+a_2(Ce^{\gamma_2 z}+De^{-\gamma_2 z})]+Ge^{\gamma_3 z}+He^{-\gamma_3 z} \\
&\hat{\bar{\tilde{w}}}_z=\gamma_1(a_1\vartheta+\rho_f\omega^2/\vartheta)(Ae^{\gamma_1 z}-Be^{-\gamma_1 z})+\gamma_2(a_2\vartheta+\rho_f\omega^2/\vartheta)(Ce^{\gamma_2 z}-De^{-\gamma_2 z})-\vartheta(Ee^{\gamma_3 z}+Fe^{-\gamma_3 z}) \\
&\hat{\bar{\tilde{\sigma}}}_{zz}=\tau_1(Ae^{\eta z}+Be^{-\eta z})+\tau_2(Ce^{\gamma_2 z}+De^{-\gamma_2 z})+2\mu\gamma_3(Ee^{\gamma_3 z}-Fe^{-\gamma_3 z}) \\
&i\xi\hat{\bar{\tilde{\sigma}}}_{xz}=-g_1(Ae^{\eta z}-Be^{-\eta z})-g_2(Ce^{\gamma_2 z}-De^{-\gamma_2 z})-(\xi^2+\gamma_3^2)(Ee^{\gamma_3 z}+Fe^{-\gamma_3 z})-i\gamma_3\eta(Ge^{\gamma_3 z}-He^{-\gamma_3 z}) \\
&\hat{\bar{\tilde{\sigma}}}_{yz}=-2i\eta\gamma_1 a_1(Ae^{\eta z}-Be^{-\eta z})-2i\eta\gamma_2 a_2(Ce^{\gamma_2 z}-De^{-\gamma_2 z})+i\eta(Ee^{\gamma_3 z}+Fe^{-\gamma_3 z})+\gamma_3(Ge^{\gamma_3 z}-He^{-\gamma_3 z}) \\
&\hat{\bar{\tilde{p}}}=Ae^{\gamma_1 z}+Be^{-\gamma_1 z}+Ce^{\gamma_2 z}+De^{-\gamma_2 z}
\end{aligned}\right\}
\tag{4}$$

where $\vartheta=\rho_f\omega^2/(m\omega^2-ib\omega)$, $\beta_1=[(m\omega^2\text{-}ib\omega)(\lambda+\alpha^2 M+2\mu)+\rho\omega^2 M-2\alpha M\rho_f\omega^2]/[(\lambda+2\mu)M]$,

$\beta_2=[(m\omega^2\text{-}ib\omega)\rho\omega^2 M-\rho_f^2\omega^4]/[(\lambda+2\mu)M]$, $S^2=(-\rho_f\vartheta+\rho)\omega^2/\mu$, $L_1^2=\frac{1}{2}(\beta_1-\sqrt{\beta_1^2-4\beta_2})$,

$L_2^2=\frac{1}{2}(\beta_1+\sqrt{\beta_1^2-4\beta_2})$, $\gamma_j=\sqrt{\xi^2+\eta^2-L_j^2}$, $\gamma_3=\sqrt{\xi^2+\eta^2-S^2}$, $\tau_i=\lambda(\chi_j-2\mu a_j\gamma_j^2)$,

$a_j=[\lambda(\chi_j+\mu)-\alpha+\vartheta]/[(S^2-L_j^2)\mu]$, $\chi_j=[\vartheta ML_j^2-\rho_f\omega^2]/[\rho_f\omega^2(\alpha-\vartheta)M]$, $g_j=\chi_j+a_j(\gamma_j^2-\eta^2)$,

$v_j=-\gamma_j(\chi_j+a_j(\gamma_j^2+\xi^2-\eta^2))$ ($j=1, 2$).

Note that symbol A, B, C, ……, H are arbitrary functions of ξ, η and ω. The radicals $\gamma_i (i=1, 2, 3)$ are selected such that $\text{Re}(\gamma_i)\geq 0$. In addition, L_1 and L_2 are the complex wave numbers for the first kind (fast wave) and the second kind (slow wave) dilatational wave, respectively.

3 The Model and the Equivalent Stiffness for a Beam Resting on a Layered Poroelastic Soil

The model for an infinite beam resting on N horizontal porous layers overlying a porous half-space subjected to a moving load with a constant velocity c is illustrated in Fig. 1. The j-th porous layer is denoted by the symbol M_j and the bottom layer is denoted by the symbol M_{N+1}. The thickness of the j-th layer is $h_j=z_j-z_{j-1}$ and z_j, z_{j-1} denote the depth of the upper and lower boundary of the j-th layer.

The following assumptions are made for the beam and the load: (a) The beam is an infinite Timoshenko elastic beam with width $2a$; (b) The deformation of the beam is small; (b) Both the load and the normal stresses are uniformly distributed over the width of the beam; (c) The contact between the beam and the foundation is smooth.
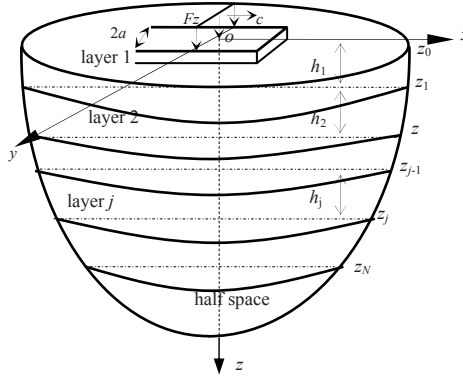
Fig. 1. Model for an infinite beam resting on a layered poroelastic soil

According to Timoshenko beam theory, the equation of motion for the beam is as follows

$$EI_z \frac{\partial^4 w_b(x,t)}{\partial^4 x} + m_b \frac{\partial^2 w_b(x,t)}{\partial^2 t} = F(x,t) - q(x,t) \tag{5}$$

where $w_b(x, t)$ is the deflection of the beam, E the Young's modulus of the beam, I_z the second moment of the area of the beam cross section about its neutral axis, $q(x, t)$ the interaction force between the beam and the surface of the soil, $F(x, t)$ the applied moving load, x the horizontal coordinate along the length of the beam.

The surface load $F(x, t)$ is a line load moving with a constant velocity c and given by the following expression

$$F(x,t) = F_z \delta(x - ct) \tag{6}$$

where F_z is the magnitude of the force, $\delta(\ldots)$ is the Dirac delta function.

According to the assumptions concerning the beam, the stress, ''open pore'' boundary conditions for the surface of the layered soil are as follows[7]

$$\left. \begin{array}{l} 2a\sigma_{zz}(x,y,0,t) = q(x,t)H(a - |y|) \\ \sigma_{xz}(x,y,0,t) = 0, \quad \sigma_{yz}(x,y,0,t) = 0, \quad p(x,y,0,t) = 0 \end{array} \right\} \tag{7}$$

where $H(\ldots)$ is the unit step function.

Assuming that the centerline of the beam and the surface of the foundation are always in contact, then, the compatibility condition has the form

$$u_z(x,0,0,t) = w_b(x,t) \tag{8}$$

To analyze the problem, the concept of the "equivalent stiffness" [2] is introduced. According to this concept, to solve the proposed problem, the equivalent stiffness of the

layered foundation has to be determined in advance. The equivalent stiffness method allows an exact reduction of an original 3-D problem to a 1-D problem by introducing a frequency and wave number dependent complex stiffness χ_{eq}^{layer} for the layered foundation. In order to determine the equivalent stiffness of the layered porous soil via the TRM method, for the j-th porous layer M_j, extracting all the positive and negative exponential term $e^{\pm\gamma_i z}(i=1,2,3)$ from general solution for displacement, pore pressure and stress(Eqs.(3)) and combining them with the arbitrary functions $A(\xi, \eta, \omega)$, ...,

$H(\xi, \eta, \omega)$ which are replaced by $a^j(\xi,\eta,\omega)e^{-\gamma_1^j z_j}$, $b^j(\xi,\eta,\omega)e^{\gamma_1^j z_{j-1}}$, $c^j(\xi,\eta,\omega)e^{-\gamma_2^j z_j}$, $d^j(\xi,\eta,\omega)e^{\gamma_2^j z_{j-1}}$, $e^j(\xi,\eta,\omega)e^{-\gamma_3^j z_j}$, $f^j(\xi,\eta,\omega)e^{\gamma_3^j z_{j-1}}$, $g^j(\xi,\eta,\omega)e^{-\gamma_3^j z_j}$,

$h^j(\xi,\eta,\omega)e^{-\gamma_3^j z_{j-1}}$, the expressions for the displacements, the stresses and the pore pressure of the j-th porous layer in the transformation domain are recast as follows

$$
\left.\begin{aligned}
\boldsymbol{\Psi}^j(\xi,\eta,\omega,z)_{8\times1} &= \begin{bmatrix} \boldsymbol{D}_d^j(\xi,\eta,\omega) & \boldsymbol{D}_u^j(\xi,\eta,\omega) \\ \boldsymbol{S}_d^j(\xi,\eta,\omega) & \boldsymbol{S}_u^j(\xi,\eta,\omega) \end{bmatrix} \begin{bmatrix} \boldsymbol{W}_d^j(\xi,\eta,\omega,z)^T & \boldsymbol{W}_u^j(\xi,\eta,\omega,z)^T \end{bmatrix}^T \\
\boldsymbol{\Psi}^j(\xi,\eta,\omega,z)_{8\times1} &= \begin{bmatrix} i\xi\hat{\bar{u}}_x^j & \hat{\bar{u}}_y^j & \hat{\bar{u}}_z^j & \hat{\bar{w}}_z^j & i\xi\hat{\bar{\sigma}}_{xz}^j & \hat{\bar{\sigma}}_{yz}^j & \hat{\bar{\sigma}}_{zz}^j & \hat{\bar{p}}^j \end{bmatrix}^T \\
\boldsymbol{W}_d^j(\xi,\eta,\omega,z) &= \begin{bmatrix} b^j e^{-\gamma_1(z-z_{j-1})} & d^j e^{-\gamma_2(z-z_{j-1})} & f^j e^{-\gamma_3(z-z_{j-1})} & h^j e^{-\gamma_3(z-z_{j-1})} \end{bmatrix}^T \\
\boldsymbol{W}_u^j(\xi,\eta,\omega,z) &= \begin{bmatrix} a^j e^{-\gamma_1(z_j-z)} & c^j e^{-\gamma_2(z_j-z)} & e^j e^{-\gamma_3(z_j-z)} & g^j e^{-\gamma_3(z_j-z)} \end{bmatrix}^T
\end{aligned}\right\} \quad (9)
$$

where the superscript j denotes the j-th porous layer. The vectors $\boldsymbol{W}_d^j(\xi,\eta,z,\omega)$, $\boldsymbol{W}_u^j(\xi,\eta,z,\omega)$ are termed as down-going and up-going wave vector.

In terms of Eq.(9), the down-going and up-going wave vectors are recasted in the following form

$$
\left.\begin{aligned}
\boldsymbol{W}_d^j(\xi,\eta,z,\omega) &= \boldsymbol{E}^j(z-z_{j-1})\boldsymbol{W}_d^j(\xi,\eta,z_{j-1},\omega) \\
\boldsymbol{W}_u^j(\xi,\eta,z,\omega) &= \boldsymbol{E}^j(z_j-z)\boldsymbol{W}_u^j(\xi,\eta,z_j,\omega)
\end{aligned}\right\} \quad (10)
$$

where $\boldsymbol{E}^j(\hbar)$ is a 4×4 identity matrix, $E_{ii}^j = e^{-\gamma_i^j \hbar}$ $(i=1,2,3)$, $E_{44}^j = e^{-\gamma_3^j \hbar}$, $E_{kq}^j = 0$ $(k,q=1,2,3,4)$.

According to Deresiewicz and Skalak[7], displacements, the pore pressure, stresses should be continuous at the interfaces. In terms of Eq.(9) and the continuity condition for the j-th interface, one has the follows

$$
\begin{bmatrix} \boldsymbol{W}_d^{j+1}(\xi, \eta, \omega, z_j) \\ \boldsymbol{W}_u^j(\xi, \eta, \omega, z_j) \end{bmatrix} = \begin{bmatrix} \boldsymbol{T}_d^j & \boldsymbol{R}_u^j \\ \boldsymbol{R}_d^j & \boldsymbol{T}_u^j \end{bmatrix} \begin{bmatrix} \boldsymbol{W}_d^j(\xi, \eta, \omega, z_j) \\ \boldsymbol{W}_u^{j+1}(\xi, \eta, \omega, z_j) \end{bmatrix} \quad (11)
$$

$$
\begin{bmatrix} \boldsymbol{T}_d^j & \boldsymbol{R}_u^j \\ \boldsymbol{R}_d^j & \boldsymbol{T}_u^j \end{bmatrix} = \begin{bmatrix} -\boldsymbol{D}_d^{j+1} & \boldsymbol{D}_u^j \\ -\boldsymbol{S}_d^{j+1} & \boldsymbol{S}_u^j \end{bmatrix}^{-1} \begin{bmatrix} -\boldsymbol{D}_d^j & \boldsymbol{D}_u^{j+1} \\ -\boldsymbol{S}_d^j & -\boldsymbol{S}_u^{j+1} \end{bmatrix} \quad (12)
$$

The 4×4 matrix $\boldsymbol{R}_u^j(\xi,\eta,\omega)$ and $\boldsymbol{R}_d^j(\xi,\eta,\omega)$ in Eq.(11) represent reflection matrices for up-going and down-going P_1, P_2, S waves incident on the j-th interface, while $\boldsymbol{T}_u^j(\xi,\eta,\omega)$, $\boldsymbol{T}_d^j(\xi,\eta,\omega)$ denote the transmission matrices for the up-going and down-going P_1, P_2, S waves incident on the j-th interface. For the bottom half space porous medium, one has

$$W_d^{N+1}(\xi, \eta, \omega, z_N) = T_d^N W_d^N(\xi, \eta, \omega, z_N) \Big\}$$
$$W_u^N(\xi, \eta, \omega, z_N) = R_d^N W_d^N(\xi, \eta, \omega, z_N) \Big\} \quad (13\text{a-b})$$

According to the continuity condition on the interface between the M_N-th layer and the M_{N-1}-th layer, the following relation is obtained

$$W_d^N(\xi, \eta, z_{N-1}, \omega) = T_d^{N-1} W_d^{N-1}(\xi, \eta, z_{N-1}, \omega) + R_u^{N-1} W_u^N(\xi, \eta, z_{N-1}, \omega) \Big\}$$
$$W_u^{N-1}(\xi, \eta, z_{N-1}, \omega) = R_d^{N-1} W_d^{N-1}(\xi, \eta, z_{N-1}, \omega) + T_u^{N-1} W_u^N(\xi, \eta, z_{N-1}, \omega) \Big\} \quad (14)$$

Combination of Eq. (13a) and Eq.(14a) together with the utilization of Eq.(10) yields the generalized transmission matrix for the down-going in the M_N-th layer incident on the M_{N-1}-th interface($j=N-1$)

$$W_d^N(\xi, \eta, z_{N-1}, \omega) = T_d^{gN-1} W_d^{N-1}(\xi, \eta, z_{N-1}, \omega) \Big\}$$
$$T_d^{gN-1} = (I - R_u^{N-1} E(z_{N-1}) R_d^N E(z_N))^{-1} T_d^{N-1} \Big\} \quad (15)$$

Note that in Eqs.(14) and (15), the wave vectors $W_d^N(\xi, z_{N-1}, \omega)$, $W_u^N(\xi, z_{N-1}, \omega)$ at the M_N-th layer have been expressed in terms of the down-going wave vector $W_d^{N-1}(\xi, z_{N-1}, \omega)$ at the M_{N-1}-th layer. Similarly, the up-going and down-going wave vectors at the j-th porous layer can also be obtained in terms of the down-going wave vector at the first layer

$$W_d^j(\xi, \eta, z_{j-1}, \omega) = T_{de}^{g\,j-1} T_{de}^{g\,j-2} ... T_{de}^{g2} T_d^{g1} W_d^1(\xi, \eta, z_1, \omega) \Big\}$$
$$W_u^j(\xi, \eta, z_j, \omega) = R_d^{g\,j} W_d^j(\xi, \eta, z_j, \omega)$$
$$R_d^{g\,j} = R_d^j + T_{ue}^j R_{de}^{j+1} T_d^{g\,j}$$
$$T_{de}^{g\,j} = (I - R_{ue}^j R_{de}^{g\,j+1})^{-1} T_{de}^j \qquad j = 2,3........N \Big\} \quad (16)$$

In terms of the surface boundary conditions Eq.(7) and according to Eq. (16), the down-going wave vector for the first layer is obtained

$$W_d^1(\xi, \eta, z_0, \omega) = [S_d^1 + S_u^1 E^1(h_1) R_{de}^{g\,1}]^{-1} \hat{\tilde{Q}}(\xi, \eta, \omega) \quad (17)$$

where $R_{de}^{g\,1}$ can be obtained by Eqs.(16) and $\hat{\tilde{Q}}(\xi, \eta, \omega) = \begin{bmatrix} 0 & 0 & q(\xi, \omega)\dfrac{\sin(\eta a)}{\eta a} & 0 \end{bmatrix}^T$.

After the wave vectors in the first layer are determined, it is straightforward to obtain all the variables in the first layer. Also, the vertical displacement of the first layer is obtained by using Eq.(16) and Eq.(17)

$$\hat{\tilde{u}}_z(\xi, \eta, z_0, \omega) = \frac{\sin(\eta a)}{\eta a} \phi(\xi, \eta, z_0, \omega) \hat{\tilde{q}}_z(\xi, \omega) \quad (18)$$

$$\phi(\xi, \eta, z_0, \omega) = -\gamma_1^1 a_1^1 (A^1 e^{-\gamma_1^1 h_1} - B^1) - \gamma_2^1 a_2^1 (C^1 e^{-\gamma_2^1 h_1} - D) + E^1 e^{-\gamma_3^1 h_1} + F^1 \quad (19)$$

To implement the compatibility condition (8) and perform a one-dimensional inverse Fourier transform $\eta \rightarrow y$, one has the following equation for the beam in the Fourier transformed domain

$$\hat{\bar{w}}_b(\xi, \omega)[-m_b \omega^2 + EI\xi^4 + \chi_{eq}^{layer}(\xi, \omega)] = -2\pi F_z \delta(\omega + \xi c) \quad (20)$$

where $\chi_{eq}^{layer}(\xi,\omega)=2\pi/\int_{-\infty}^{-\infty}\phi(\xi,\eta,z_0,\omega)[\sin(\eta a)/(\eta a)]d\eta$ is the equivalent stiffness of the layered foundation. As mentioned above, the equivalent stiffness of the layered foundation is a function of the frequency ω and the wave number ξ.

Applying the two-dimensional inverse Fourier transformation on Eq.(20) and using the property of the Dirac's delta function in the integral, the following equation is obtained

$$w_b(x,t)=\frac{F_z}{2\pi}\int_{-\infty}^{\infty}\frac{\delta(\omega+\xi c)e^{i\xi x}}{EI\xi^4-m_b\omega^2+\chi_{eq}^{layer}(\xi,\omega)}d\xi \tag{21}$$

It also should be noted that the real ξ–axis and η–axis is free of any singularities for a multi-layered poroelastic medium if the parameter b representing internal friction between the solid and the pore fluid does not vanish. Thus, the infinite integration in Eq.(20, 21) with respect to the horizontal wave number ξ and η are free of any singularities in the path of integration. In this paper, the FFT method is adopted to perform the inverse Fourier transformation [8]. To computer the inverse transform accurately with the discrete Fourier transform, the integrals must be truncated appropriately to avoid aliasing. We found that an FFT over a grid of 2048 points by 2048 and a range of $-16\leq\xi$, $\eta\geq16$ satisfied both these requirements.

4   Numerical Results and Discussions

When the material parameters for each layer are assumed the same values, then, the layered poroelastic half space is reduced to a homogeneous poroelastic half-space. The material parameters for the porous medium are chosen as follows: $\mu=2.0\times10^7N/m^2$, $\lambda=4.0\times10^7N/m^2$, $\rho_s=2000kg/m^3$, $f=0.3$, $\alpha=0.97$, $M=2.4\times10^8N/m^2$, $b=1.94\times10^6$ kg/m^{3}s, $m=1990$ kg/m^3. The parameters for the beam are as follows: $EI_z=1.28\times10^9N/m^2$, $m_b=7350kg/m$, $a=2.0m$, $F_z=150kN$, respectively. Fig. 2 show the beam displacement curves versus the load velocity for the load at the origin of the coordinate system. In order to validate our method, the solutions of Jin [5] are also shown in Fig.2. From Figure, it shows a very good agreement between our result and that of [5].
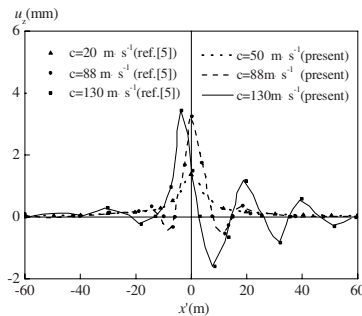
Fig. 2. Comparison of present result with results obtained by ref. [5]
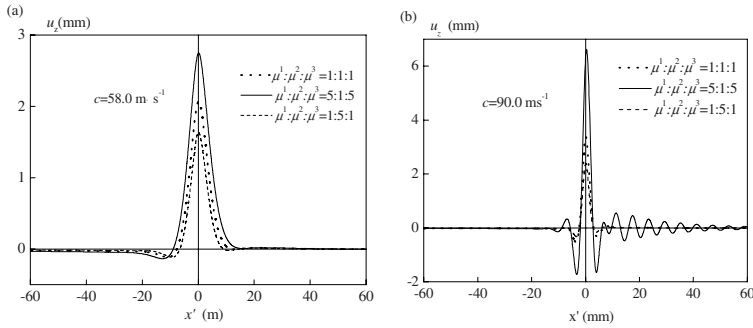
Fig. 3. The deflection of beam subject to moving load on three-layer poroelastic foundation (a) velocity c=50m/s; (b) velocity c=90m/s

In the second example, the soil is a three layered poroelastic medium: two porous layers and an underlying porous half space. The thicknesses of the two layers are $h^1=h^2=2.0$m. The following three cases are calculated: A) $\mu^1: \mu^2: \mu^3=1:5:1$; B) $\mu^1: \mu^2: \mu^3=5:1:5$; C) $\mu^1: \mu^2: \mu^3=1:1:1$, where $\mu^3=2.0\times10^7$N/m^2. The load moves along the positive x-axis. The remaining parameters for each layer and the reference values assume the same values as those in the first example. The load moves with velocities c=50m/s and c=90m/s along the positive x-direction. The deflections of the beam for the three cases are showed in Figs. 3(a-b), respectively.

It follows from Figs 3(a-b) that the occurrence of a softer middle layer inside the layered foundation leads to a considerable increment of the vertical displacement. Moreover, Fig. 3b indicates that the response of the layered medium also exhibits an oscillatory nature.

5   Conclusions

The dynamic response of an infinite beam resting on a layered poroelastic foundation subjected to moving loads is addressed in this study. The equivalent stiffness of the layered porous foundation is derived by means of the reflection transmission matrices (TRM) method. Since the TRM solution is free of any mismatched exponential functions, the method can be used in the calculation of the layered porous soil with arbitrary number of layers and arbitrary thickness. The new method was validated by comparing present solutions with some known results. Our calculation indicates that the response of a multi-layered foundation tends to contain higher frequency components and exhibits larger magnitude compared with a homogeneous one.

References

1. Madshus C., Kaynia A.M. High-speed railway lines on soft ground: dynamic behaviour at critical train speed. J. Sound Vib.. Vol. 3. (2000) 689–701.
2. Metrikine A.V., Popp K. Steady-state response of an elastic beam on a visco-elastic layer under moving load. Arch. Appl. Mech. Vol. 70. (2000) 399-408.
3. Lu J.F., Hanyga A. Fundamental solution for a layered porous half space subject to a vertical point force or a point fluid source. Comput. Mech. Vol.35(5). (2005) 376-391.
4. Luco J.E., Apsel R.J. On the Green's functions for a layered half-space: Part I. Bull. Seism. Soc. Am. Vol. 73. (1983) 909–929.
5. Jin B. Dynamic displacement of an infinite beam on a poroelastic half space due to a moving oscillating load. Arch. Appl. Mech.. Vol. 74. (2004) 277-287.
6. Biot MA. Mechanics of deformation and acoustic propagation in porous media. J. Appl. Phys.Vol. 33 (1962) 1482–1498.
7. Deresiewicz H., Skalak R. On the uniquness in dynamic poroelasticity. Bull. Seism. Soc. Am. Vol. 53.(1963) 783–788.
8. Oppenheim A.V., Schafer R.W. Discrete-time signal processing. Prentice-Hall, Inc., Englewood Cliffs, NJ.(1999)

Author Index